



Provided by the author(s) and University of Galway in accordance with publisher policies. Please cite the published version when available.

Title	A chemical kinetic computational toolkit for computational modelling and estimation of fuel thermodynamic properties
Author(s)	Sánchez Martínez, Sergio Enrique
Publication Date	2023-03-27
Publisher	NUI Galway
Item record	http://hdl.handle.net/10379/17710

Downloaded 2024-04-20T03:52:17Z

Some rights reserved. For more information, please see the item record link above.



**A chemical kinetic computational toolkit for
computational modelling and estimation of fuel
thermodynamic properties**

Sergio Enrique Sánchez Martínez
(MSc, BSc)

Submitted in fulfilment of the requirements for the
degree of
Doctor of Philosophy

School of Biological and Chemical Sciences

University of Galway



Supervisor: Prof. Henry J. Curran
Head of School: Prof. Olivier Thomas

Submitted September 2022

Abstract

It is undeniable that, due to human activity, global warming is one of the most challenging environmental issues of our time. It is well known that the main source of greenhouse gases (GHG) is due to the burning of fossil fuels, particularly those used for electricity, heat, and transportation purposes. These GHG emissions are mostly composed of carbon dioxide (CO₂), unburned hydrocarbons (UHC), nitrous oxides (NO_x), soot, and industrial gases. Reducing these emissions can be achieved by improving the efficiency of the combustion systems. Therein lies the importance of the development of reliable chemical kinetic mechanisms. Undoubtedly, as chemical kinetic mechanisms become more detailed so does our understanding of the chemistry controlling fuel oxidation. For this reason, chemical kinetic modelling is an essential tool to helping to increase the efficiency and reduce emissions from combustion systems. However, the complexity and laboriousness of developing and modelling real fuels make the process challenging. In this thesis chemical kinetic computational codes have been developed to help automate the development of reliable chemical kinetic mechanisms. These codes reduce considerably the time of simulation, the human error, and allows the user to run multiple simulations at the same time. These can include different types of reactors, such as shock tubes (STs), rapid compression machines (RCMs), jet-stirred reactors (JSRs), and flow reactors (FRs), along with flame speed (FS) measurements. Moreover, the user can validate a full database formed from hundreds to thousands of experimental points in a short period of time, gathering, plotting, and printing out in a user-friendly way all of the simulated data for sensible interpretation. These simulations can be performed in a server-cluster or on a single supercomputer with high performance computing (HPC) with 100s to 1000s of cores, rather than in local machines with a limited number of expensive licenses. These tools are developed using python language and using open-source libraries including numpy, pandas, scipy, sundials, matplotlib, and Cantera. Cantera is widely used to solve problems involving chemical kinetics, thermodynamics, and transport processes. These tools are widely used in the data science and combustion modelling communities, and the current suite of tools were designed with licencing and scalability of HPC clusters in mind.

These chemical computational tools are divided into three types; thermochemistry, kinetic and post-processing codes to make the development of chemical kinetic mechanisms easier. In all cases, the codes are designed to run automatically. The thermochemistry code, used for gas phase fuels, calculates the thermodynamic properties including heat capacity, enthalpy and entropy and generates a file with the thermochemistry data that is essential to run any kinetic

mechanism and validate it against kinetic properties such as ignition delay times (IDTs), and speciation profiles (SPs). The kinetic code oversees the running of every simulation based on the experimental conditions from either individual conditions or a large number of them. The post-processing code allows the user to generate graphs of the experimental data compared against one, or multiple simulation results, and produces a LaTeX document that converts into a .pdf file with all results in a formal report format.

To validate the toolkit proposed in this work, a reliable chemical kinetic mechanism was developed to describe the oxidation of $C_1 - C_3$ blends of gaseous hydrocarbons including methane, ethane, ethylene, and propane for binary, ternary, and quaternary mixtures. This mechanism was validated against the IDT of the next experimental conditions: $T = 666 - 2615$ K, $p = 0.54 - 91.5$ atm, and equivalence ratios (ϕ) = 0.5 – 2.0, from the University of Galway (UG) and the physico-chemical fundamentals of combustion (PCFC) experimental database which was collected in low-pressure/high pressure shock tubes (LP/HPST), and RCMs. Not only this, but these codes have also been used widely within the context of C_3 by other members of the combustion chemistry centre (C^3) thus supporting the continued optimisation of gasoline and diesel fuels, amongst others. The application of these mechanisms extends far beyond the subset of $C_1 - C_3$ fuels presented here. Furthermore, the complete validation of the C^3 database used to take a number of days, but with the application of these codes this time frame has been reduced to a few hours using HPC servers. Finally, future work should aim to further develop these tools in a number of ways; (i) in the further deployment on HPC clusters, and (ii) the addition of further modules for other applications within the wider combustion landscape, such as automatic rate rule development.

Declaration

This is to certify that:

- (1) This thesis is my original work which is in fulfilment for the degree of Doctor of Philosophy. Work that is not my original work is indicated appropriately.
- (2) All other literature material used has been appropriately cited.

A handwritten signature in black ink, consisting of a large, stylized initial 'A' followed by a vertical line and the letters 'te.' and 'mz' written below it.

*To Mam and my siblings:
Enriqueta, Severino, Pedro, Jorge y Miriam
¡Gracias por todo!
Los llevo en el corazón.*

“So, remember to look up at the stars and not down at your feet. Try to make sense of what you see and hold on to that childlike wonder about what makes the universe exist.” — Stephen Hawking

Acknowledgements

I would like to thank my supervisor Prof. Henry Curran for giving me the opportunity to carry out my PhD in the C³ group, as well as for all the opportunities to present my research at conferences (nationally and internationally), to show my research presenting posters, giving talks, and by the publication of my papers. Thanks for everything.

A huge Thank you! to the ex-members of the C³ group Ultan Burke, Kieran Patrick Somers, Vaibhav Patel, Jennifer Power, Colin Banyon, Gavin Kenny, David McKay, Pat Meier, Yanjin Sun, Mohammadreza Baigmohammadi, Amrit Sahu, Snehasish Panigrahy, Shashank Nagaraja, Nitin Lokachari, and Shijun Dong, and all the visitors and people passing by, for not only the good times but we learnt from each other and always tried to be the best version of ourselves. Thanks to the current members of C³, Manik Ghosh, Ahmed Mohamed, Hamdy Mohamed, Pengzhi, and Yijun. A special thanks to Kieran, Yannick, and Vaibhav for so many adventures and good talks; we did it lads, we did it! Also, a special thanks to the girls of the gang, Jennifer, Caroline, Helen, Fiona, and Marta, we had fun gals. As well to all the lovely people in the school of chemistry. I also must show my gratitude to this beautiful country, I learnt so much from your Irish people, and I found out we are more alike than I thought, Mexicans and Irish, with one heart. I learnt here that “Like so many things in life, a well-poured pint of Guinness is worth waiting for”, and I will always treasure my time here. Thank you!

To my family, Mamá, Severino, Pedro, Jorge, y Miriam – agradecido con la vida y con el universo, por haberme puesto aquí, exactamente al mismo tiempo que todos ustedes, y que fuesen ustedes mi familia. Quiero que sepan que siempre tengo presentes las memorias vividas juntos, los buenos y malos momentos, y quiero decirles que los amo mucho a todos y que si tuviera que escoger de nuevo no dudaría en escogerlos una vez más. Gracias por todo su apoyo y amor, siempre están en mi corazón. Gracias mama, Enriqueta, no sólo lo hiciste muy bien al educarnos, pero también hiciste lo mejor que pudiste, y eso para mí fue más que suficiente. Siempre estarás en un lugar especial en mi corazón madre mía, te amo. A mi hermana Cinthia, gracias por todos esos buenos momentos compartidos en familia. Este trabajo es para ustedes, mi familia, porque sin ustedes no valdría la pena todo este sacrificio y esfuerzo. Thank you, this is for you, guys!

Me gustaría agradecer a mi familia materna, los Martínez, a mis tíos, tías, y primos. La vida no es fácil para nadie, pero con ustedes de mi lado, nunca se me hizo imposible lograrlo, gracias a todos, presentes y ausentes, siempre están conmigo. Thank you to my friends in Mexico that always believed in me: Alex, Alvaro, Chilis, Tello, Inge, and Benja, gracias Pavon por todo.

Javier, Irving, Miguel, el amigo, Rogelio, y tantos más. My physicists' friends: Pablo, Ismael, Diego, Mary Carmen, Vero, Sarah, Paulina, Lupita, el bulto and so many other beautiful people I have met in this journey. Also, after thanking my Mexican family is time to thank my Irish one, I would like to thank the Walsh Family, John and Ann, James, John, Marion, Aoibheann and Dave, thanks for open your family to me and take me in as your own, thank you for everything, God bless you guys. Finally, I would like to express my gratitude with all that people I could not name here but they reside in my memory, you always travel with me, Thanks for everything. ¡Hasta siempre!

Publications

- (1) **S. Martinez**, M. K. Ghosh, H.J. Curran, “THERM23: A Thermodynamic Property Estimator for Gas Phase Species using the Group Additivity Method”, *paper in preparation*.
- (2) **S. Martinez**, M. Baigmohammadi, V. Patel, S. Panigrahy, A. B. Sahu, S. Nagaraja, A. Ramalingam, K.A. Heufer, A. Pekalski, H.J. Curran, “A comprehensive experimental and modeling study of the ignition delay time characteristics of ternary and quaternary blends of methane, ethane, ethylene, and propane over a wide range of temperature, pressure, equivalence ratio, and dilution”, *Combustion and Flame* 234 (2021) 111626.
- (3) **S. Martinez**, M. Baigmohammadi, V. Patel, S. Panigrahy, A.B. Sahu, S.S. Nagaraja, A. Ramalingam, A. Abd El-Sabor Mohamed, K.P. Somers, K.A. Heufer, A. Pekalski, H.J. Curran, “An experimental and kinetic modeling study of the ignition delay characteristics of binary blends of ethane/propane and ethylene/propane in multiple shock tubes and rapid compression machines over a wide range of temperature, pressure, equivalence ratio, and dilution”, *Combustion and Flame* 228 (2021) 401–414.

Other Publications

- (1) M. Baigmohammadi, V. Patel, S. Nagaraja, A. Ramalingam, **S. Martinez**, S. Panigrahy, A. A. El-Sabor Mohamed, K. P. Somers, U. Burke, K. A. Heufer, A. Pekalski, and H. J. Curran, “Comprehensive Experimental and Simulation Study of the Ignition Delay Time Characteristics of Binary Blended Methane, Ethane, and Ethylene over a Wide Range of Temperature, Pressure, Equivalence Ratio, and Dilution”, *Energy and Fuels* 34(7) (2020) 8808–8823.
- (2) M. Baigmohammadi, V. Patel, **S. Martinez**, S. Panigrahy, A. Ramalingam, U. Burke, K. P. Somers, K. A. Heufer, A. Pekalski, and H. J. Curran, “A Comprehensive Experimental and Simulation Study of Ignition Delay Time Characteristics of Single Fuel C₁–C₂ Hydrocarbons over a Wide Range of Temperatures, Pressures, Equivalence Ratios, and Dilutions”, *Energy and Fuels* 34(3) (2020) 3755–3771.
- (3) Q-D. Wang, S. Panigrahy, S. Yang, **S. Martinez**, J. Liang, and H. J. Curran, “Development of Multipurpose Skeletal Core Combustion Chemical Kinetic Mechanisms”, *Energy and Fuels* 35(8) (2021) 6921–6927.

Conferences, Short–Papers and/or Posters

- (1) Poster, “A thermodynamic property estimator for gas phase hydrocarbons using the group additivity method”, MaREI Symposium, 26th and 27th May 2022.
- (2) Poster and video, “Ignition delay time characteristics of Binary Blends of Ethane/Propane and Ethylene/Propane Combustion Chemistry”, MaREI Symposium, 23rd–27th November 2020.
- (3) M. Baigmohammadi, **S. Martinez**, H. J. Curran, A. Pekalski, “A comprehensive modelling study of ignition delay time characteristics of C₁–C₃ gaseous hydrocarbon mixtures over a wide range of pressures, temperatures, equivalence ratios, and dilutions”, 17th International Conference on Numerical Combustion, Aachen Germany, 6–8th May 2019.
- (4) **S. Martinez**, M. Baigmohammadi, K. P. Somers, H. J. Curran, A. Pekalski, “Modelling study of ignition delay time characteristics of ultra-rich C₁/C₂ mixtures in a constant volume reactor at low-pressure”, 9th European Combustion Meeting (ECM 2019), Lisbon Portugal, 14th–17th April 2019. Short–paper and poster.

Table of Contents

Chapter 1: General introduction	1
1.1 Energy scenario.....	1
1.2 The foundations of thermochemistry and kinetics	4
1.2.1 Thermodynamics.....	4
1.2.2 Chemical kinetics.....	8
1.3 Group additivity in combustion chemistry.....	10
1.3.1 Experimental and theoretical methods.....	11
1.3.2 Benson’s group additivity method	15
Chapter 2: Tools for chemical kinetic modelling	21
2.1 Local automation of chemical kinetic simulations in python	21
2.1.1 Database management.....	22
2.1.2 Chemical kinetic simulations in python.....	24
2.2 Server automation of chemical kinetic simulations in python	28
Chapter 3: THERM23: A thermodynamic property estimator for gas phase species using the group additivity method	31
3.1 Introduction.....	33
3.2 Overview of THERM23.....	35
3.2.1 GAVs notation	36
3.2.2 Updated GAVs.....	37
3.2.3 Estimation of group additivity values	40
3.2.4 Operation procedure of THERM23	41
3.2.4.1 Example calculations	44
3.3 Conclusions.....	52
Chapter 4: A comprehensive experimental and modelling study of the ignition delay time characteristics of ternary and quaternary blends of methane, ethane, ethylene, and propane over a wide range of temperature, pressure, equivalence ratio and dilution	57
4.1 Introduction.....	59
4.2 Design of experiments and experimental approach	61
4.2.1 Uncertainty analysis.....	64
4.3 Computational modelling.....	64
4.4 Results and discussions.....	65
4.4.1 Performance of NUIGMech1.2 and the correlations versus experimental data.....	65
4.4.2 Effect of blending on ignition	68
4.4.3 Effect of pressure on ignition.....	79
4.4.4 Correlation analysis.....	81
4.5 Conclusions.....	84
Chapter 5: An experimental and kinetic modelling study of the ignition delay characteristics of binary blends of ethane/propane and ethylene/propane in multiple shock tubes and rapid compression machines over a wide range of temperature, pressure, equivalence ratio and dilution	89
5.1 Introduction.....	91
5.2 Design of experiments and experimental approaches	93
5.3 Computational modelling.....	96

5.4	Results and discussion	97
5.4.1	Ethylene/propane and ethane/propane blends	97
5.4.2	Synergistic/antagonistic effect of blends	100
5.4.3	Effect of pressure on ignition.....	107
5.4.4	Effect of equivalence ratio on ignition.....	110
5.4.5	Regression analysis.....	111
5.5	Conclusions.....	112
Chapter 6: Comprehensive experimental and simulation study of the ignition delay time characteristics of binary blended methane, ethane, and ethylene over a wide range of temperature, pressure, equivalence ratio, and dilution.....		121
6.1	Introduction.....	123
6.2	Design of experiments and experimental approach	125
6.2.1	Set-up and procedure	126
6.2.2	Uncertainty analysis.....	127
6.3	Computational modelling.....	127
6.4	Results and discussion	128
6.4.1	General performance of the NUIG mechanism and the correlations versus experimental data	128
6.4.2	Individual effect of the studied parameters on IDT	129
6.4.3	Correlations and their performances	142
6.5	Conclusions.....	147
Chapter 7: A comprehensive experimental and simulation study of ignition delay time characteristics of single fuel C₁ – C₂ hydrocarbons over a wide range of temperatures, pressures, equivalence ratios, and dilutions.....		151
7.1	Introduction.....	153
7.2	Design of experiments and experimental approaches.....	155
7.2.1	Setup and procedure.....	157
7.2.2	Uncertainty analysis.....	157
7.3	Computational modelling.....	158
7.4	Results and discussion	158
7.4.1	General performance of NUIG mechanism and the correlations versus experimental data	158
7.4.2	Individual and combined effects of the studied parameters on IDT	163
7.4.3	Correlations and their performances	176
7.5	Conclusions.....	180
Chapter 8: Performance of NUIGMech models.....		185
8.1	Statistical analyses of mechanism performance.....	185
8.1.1	Results and discussion	188
8.2	Chemistry updates in NUIGMech core mechanisms	194
Chapter 9: Conclusions and future work		205
9.1	General conclusions	205
9.2	Future work and recommendations.....	207
Appendix A		209
(Supplementary material for Chapter 2)		209
1.	Figures codes	209

2.	Python code for STcreator.py	218
3.	Python code for RCMcreator.py	221
4.	Python code for p2v_converter.py	224
4.1.	python runner.py	224
4.2.	python converter.py	225
5.	Python code for Shock Tube (ST).....	227
6.	Python code for Rapid Compression Machine (RCM)	234
7.	Python code for Laminar Burning Velocity (LBV)	243
8.	Python code for Flow Reactor (FR).....	251
9.	Python code for Jet Stirred Reactor (JSR)	258
10.	Python code for SA bruteforce.....	286
11.	Python code for RP (fluxes).....	294
12.	Python code for Plots and LaTeX-PDF generator	296
12.1.	Plotters	296
12.2.	LaTeX to pdf generator.....	323
13.	Python main subroutine code for Unix-Slurm servers	328
Appendix B		337
(Supplementary material for Chapter 4)		337
1.	Design of experiments	337
2.	Applied gases for making the mixtures.....	338
3.	Low-pressure shock tube	339
4.	High-pressure shock tube.....	340
5.	Rapid compression machine	342
5.1.	NUIG-RCM	342
5.2.	PCFC-RCM.....	344
6.	Data acquisition system	345
7.	Uncertainty analysis.....	346
7.1.	Equivalence ratio.....	346
7.2.	Diluent concentration.....	347
7.3.	IDTs in Shock tube	347
7.4.	Rapid compression machine	349
8.	Pressure profiles of the applied rapid compression machines (RCMs)	351
9.	Performances of different chemical mechanisms	359
10.	Correlation analyses.....	377
11.	Rate constant graphs and sensitivity analyses.....	382
12.	References.....	384
Appendix C		389
(Supplementary material for Chapter 5)		389
1.	Design of experiments	389
2.	Facilities.....	389
2.1.	Low-/High-pressure shock-tube.....	389
2.2.	NUIG/PCFC-RCM.....	392
3.	NUIG/PCFC-RCM pressure vs. time traces.....	394
4.	Correlation parameters.....	400
5.	Statistical analyses	401
6.	References.....	410
Appendix D		415

(Supplementary material for Chapter 6)	415
1. Design of experiments	415
2. Applied gases for making the mixtures.....	415
3. Low–pressure shock tube.....	416
4. High–pressure shock–tube	417
5. Rapid compression machine	418
5.1. NUIG-RCM	419
5.2. PCFC–RCM.....	420
6. Data acquisition system	421
7. Uncertainty analysis.....	421
7.1. Equivalence ratio.....	422
7.2. Diluent concentration.....	422
7.3. IDTs in Shock tube	423
7.4. Rapid compression machine	425
8. Pressure profiles of the applied rapid compression machines (RCMs)	426
9. Comparing the performances of NUIGMech1.0 versus other available mechanisms	432
10. Chemical kinetics development	443
11. References.....	446
Appendix E	451
(Supplementary material for Chapter 7)	451
1. Motivation for taking new experimental data	451
2. Performance of the other kinetic models	452
3. Design of experiments	458
4. Applied gases for making the mixtures.....	460
5. High–pressure shock–tube	460
6. Rapid compression machine	463
6.1. NUIG–RCM.....	464
6.2. PCFC–RCM.....	465
7. Data acquisition system	466
8. Uncertainty analysis.....	467
8.1. Equivalence ratio.....	467
8.2. Diluent concentration.....	469
8.3. IDTs in Shock–tube	470
8.4. Rapid compression machine	477
9. NUIG Rapid Compression Machine Traces	480
10. Performance of NUIGMech0.9 under high pressure–low temperature regime	512
11. Complementary analyses	513
11.1. Ignition delay time	513
11.2. Laminar burning velocity.....	515
11.3. Speciation (JSR): Ethylene	517
11.4. Individual and combined effects of the studied parameters on IDTs.....	518
11.5. Chemical kinetics development analyses.....	520
12. Correlations.....	539
Appendix F	547
(Supplementary material for Chapter 8)	547
1. Chemical kinetic report: Exp data vs NUIGMechs.....	547

List of Figures

Figure 1-1. Graph of energy consumption by fuel in the left, and consumption by sector in the right [1].	2
Figure 1-2. Light-duty vehicle sales by technology or fuel [1].	2
Figure 1-3. Graph of indexed delivered energy by end-use sector in the left and indexed delivered energy across end-use sectors in the right [1].	3
Figure 1-4. Graph of energy-related CO ₂ emissions by fuel source in the left, and the U.S. energy-related CO ₂ emissions in the right [1].	4
Figure 1-5 (a) Constant-volume calorimeter or bomb calorimeter, (b) constant-pressure calorimeter or coffee-cup calorimeter [16].	12
Figure 1-6 Schematical representation of the BGA method of 2-methylnonane. The molecule of interest is first broken down in groups with corresponding GAVs. Then these GAVs [37].	16
Figure 2-1. K&SS python subroutine flowchart showing the automation of the simulations of different types of reactors (ST, RCM, JSR, FR, LBV) for the validation of chemical kinetic mechanisms under development.	26
Figure 2-2. Python flowchart showing the automation of the simulations of different types of reactors (ST, RCM, LBV) and sensitivity analyses brute-force (SA) for the validation of chemical kinetic mechanisms under development.	29
Figure 3-1. Screenshot of the five different options available in THERM23 to calculate thermochemical properties and graphical representations. Option 1 – interactive mode; Option 1 – automatic mode; Option 3 – recalculate mode; Option 4 – thermo plotter; Option 5 – thermo fitter.	43
Figure 3-2. Flowchart of the group additivity method employed by THERM23.	44
Figure 3-3. Name, molecular formula, structural formula, GAVs, number of rotors, and symmetry number of ethane (C ₂ H ₆), propane (C ₃ H ₈), 2-methyl-butane (iC ₅ H ₁₂), 2,2,4-trimethyl-pentane (iC ₈ H ₁₈), phenol (C ₆ H ₅ OH), and phenoxy radical (C ₆ H ₅ O).	46
Figure 3-4 The .DOC file contain line by line shows the specie name, elemental formula, units, linearity, number of different GAVs considered, GAVs identification (ID), estimated thermochemical properties, and C _p at infinite temperature (CPINF), the number of rotors, the symmetry number, and the creation date.	47
Figure 3-5. Group definitions of 2,2-dimethylbutane (C ₆ H ₁₄ 22) and it's corresponding radicals.	48
Figure 3-6 Content of the .DAT file format. It contains the 14 coefficients of the NASA polynomials for every specie calculated.	50
Figure 3-7 Heat capacities (C _p) comparison for ethane (C ₂ H ₆), propane (C ₃ H ₈), and phenol (C ₆ H ₅ OH). From the literature, in black symbols C ₂ H ₆ data reported by Gurvich et al. [44], in red symbols C ₃ H ₈ data reported by Chao et al. [45], and in blue symbols the C ₆ H ₅ OH data presented by Kudchadker et al. [46]. Solid lines represent THERM23 in this work, and dashed lines represent RMG [18] estimations.	51
Figure 4-1. Experimental tests performed in the current study for % vol. composition of (a) ternary (CH ₄ /C ₂ H ₄ /C ₂ H ₆) blends represented in solid symbols and quaternary (CH ₄ /C ₂ H ₄ /C ₂ H ₆ /C ₃ H ₈) blends represented in half solid symbols, and (b) the input conditions for C ₁ – C ₃ blends studied in the current work at various equivalence ratios (x-axis), pressures (y-axis) and dilution levels (z-axis).	62
Figure 4-2. Definition for measuring IDT in the NUIG-RCM using Kistler pressure trace and PMT-CH* trace mounted on the side wall of the reaction chamber.	63
Figure 4-3. Experimental and simulated IDT data of CH ₄ /C ₂ H ₄ /C ₂ H ₆ mixtures. (a) 90% CH ₄ /5% C ₂ H ₄ /5% C ₂ H ₆ blend at 75% N ₂ (black square symbols/lines), 75% N ₂ +10% Ar (red circle symbols/lines), and 75% N ₂ +15% Ar (blue triangle symbols/lines), (b) 75% CH ₄ /12.5% C ₂ H ₄ /12.5% C ₂ H ₆ blend at 75% N ₂ +10% Ar (black square symbols/lines), 75% N ₂ +15% Ar (red circle symbols/lines), and 75% N ₂ (blue triangle symbols/lines), (c) 60% CH ₄ /20% C ₂ H ₄ /20% C ₂ H ₆ blend at 75% N ₂ +15% Ar (black square symbols/lines), 75% N ₂ (red circle symbols/lines), and 75% N ₂ +10% Ar (blue triangle symbols/lines), (d) 90% CH ₄ /5% C ₂ H ₄ /5% C ₂ H ₆ blend at 90 bar with 67.8% N ₂ +7.5% Ar (orange square symbols/lines), 68.3% N ₂ +17% Ar (olive green circle symbols/lines), and at 135 bar with 68.3% N ₂ +17% Ar (magenta triangle symbols/lines). Solid lines: NUIGMech1.2; dashed lines: derived correlations; and dotted lines: CV – low-temperature simulations.	67
Figure 4-4. Experimental and simulated IDT data for CH ₄ /C ₂ H ₄ /C ₂ H ₆ /C ₃ H ₈ mixtures. (a) 80% CH ₄ /5% C ₂ H ₄ /10% C ₂ H ₆ /5% C ₃ H ₈ blend at 75% N ₂ (black square symbols/lines), 85% N ₂ (red circle symbols/lines), and 90% N ₂ (blue triangle symbols/lines), (b) 70% CH ₄ /10% C ₂ H ₄ /10% C ₂ H ₆ /10% C ₃ H ₈ blend at 75% N ₂ +10% Ar (black square symbols/lines), 90% N ₂ (red circle symbols/lines), and 75% N ₂ (blue triangle symbols/lines), (c) 60% CH ₄ /15% C ₂ H ₄ /15% C ₂ H ₆ /10% C ₃ H ₈ blend at 75% N ₂ +15% Ar (black square symbols/lines), 75% N ₂ (red circle symbols/lines), and 85% N ₂ (blue triangle symbols/lines), (d) 80% CH ₄ /5% C ₂ H ₄ /10% C ₂ H ₆ /5% C ₃ H ₈ blend at 90 bar with 68.1% N ₂ +7.5% Ar (orange square symbols/lines), 68.5% N ₂ +17.1% Ar (olive green circle symbols/lines), and at 135 bar with 68.5% N ₂ +17.1% Ar (magenta triangle symbols/lines).	

Solid lines: NUIGMech1.2; dashed lines: derived correlations; and dotted lines: CV – low-temperature simulations.....	68
Figure 4-5. (a) Comparisons of IDT predictions for various single, binary, ternary, and quaternary fuels in air at $p_C = 40$ atm and $\varphi = 1.0$, and (b) the predictions of their corresponding correlations (dotted lines).	69
Figure 4-6. Flux analyses of pure CH ₄ (black), 50% CH ₄ /50% C ₂ H ₆ blend (magenta), 50% CH ₄ /25% C ₂ H ₄ /25% C ₂ H ₆ blend (red), and 50% CH ₄ /16.66% C ₂ H ₄ /16.66% C ₂ H ₆ /16.66% C ₃ H ₈ (blue) mixtures at $p_C = 40$ atm and $\varphi = 1.0$, at the time of 20% fuel consumed for (a) $T_C = 800$ K and (b) $T_C = 1450$ K.....	72
Figure 4-7. Sensitivity analyses to IDTs for pure CH ₄ , 50% CH ₄ /50% C ₂ H ₆ blend, 50% CH ₄ /25% C ₂ H ₄ /25% C ₂ H ₆ blend, and 50% CH ₄ /16.66% C ₂ H ₄ /16.66% C ₂ H ₆ /16.66% C ₃ H ₈ mixtures in ‘air’ at $p_C = 40$ atm, $\varphi = 1.0$, for (a) $T_C = 800$ K and (b) $T_C = 1450$ K.	73
Figure 4-8. (a) Effects of addition of CH ₃ Ö ₂ ↔ CH ₂ O + ÖH reaction and updated $\dot{C}H_3 + \dot{C}H_3 (+M) \leftrightarrow C_2H_6 (+M)$ rate constant on the IDTs for 4.9% CH ₄ at $\varphi = 0.5$ [36] and 9.5% CH ₄ at $\varphi = 1.0$ [36]; -----, NUIGMech1.1; - • - •, NUIGMech1.1 plus CH ₃ Ö ₂ ↔ CH ₂ O + ÖH [35]; —, NUIGMech1.2 which includes CH ₃ Ö ₂ ↔ CH ₂ O + ÖH [35] reaction as well as an updated rate constant for $\dot{C}H_3 + \dot{C}H_3 (+M) \leftrightarrow C_2H_6 (+M)$. (b) Comparisons of the rate constants for $\dot{C}H_3 + \dot{C}H_3 (+M) \leftrightarrow C_2H_6 (+M)$ [37-42].....	74
Figure 4-9. Effect of pressure over the IDT predictions of (a) 50% CH ₄ /25% C ₂ H ₄ /25% C ₂ H ₆ blend (solid lines), and (b) 50% CH ₄ /16.66% C ₂ H ₄ /16.66% C ₂ H ₆ /16.66% C ₃ H ₈ blend (solid lines), pure CH ₄ (dashed lines), and corresponding correlations (dotted lines) for fuel in air at $\varphi = 1.0$	80
Figure 4-10. Flux analyses as function of pressure of 1 atm, 40 atm and 80 atm (black, blue, and magenta percentages respectively), at $T_C = 800$ K, $\varphi = 1.0$, for (a) 50% CH ₄ /25% C ₂ H ₄ /25% C ₂ H ₆ , and (b) 50% CH ₄ /16.66% C ₂ H ₄ /16.66% C ₂ H ₆ /16.66% C ₃ H ₈ in air.	81
Figure 5-1. Experimental Taguchi [36] L9 matrix of conditions. For 90%/10%, 70%/30%, and 50%/50% ratios (a) red: binary C ₂ H ₄ /C ₃ H ₈ blends, blue: binary C ₂ H ₆ /C ₃ H ₈ blends; and (b) pressure, equivalence ratio, and dilution parameters.	94
Figure 5-2. Comparisons of experimental ST (□) and RCM (■) data against model predictions using NUIGMech1.1 (solid lines) and AramcoMech3.0 (dashed lines) for; (a) a 50% C ₂ H ₄ /50% C ₃ H ₈ blend at 75% N ₂ (black symbols/lines), 75% N ₂ + 10% Ar (red symbols/lines), and 75% N ₂ + 15% Ar (blue symbols/lines); (b) a 70% C ₂ H ₄ /30% C ₃ H ₈ blend at 75% N ₂ + 10% Ar (black symbols/lines), 75% N ₂ + 15% Ar (red symbols/lines), and 75% N ₂ (blue symbols/lines); and (c) a 90% C ₂ H ₄ /10% C ₃ H ₈ blend at 75% N ₂ + 15% Ar (black symbols/lines), 75% N ₂ (red symbols/lines), and 75% N ₂ + 10% Ar (blue symbols/lines).....	99
Figure 5-3. Comparisons of experimental ST (□) and RCM (■) data against model predictions using NUIGMech1.1 (solid lines) and AramcoMech3.0 (dashed lines), for; (a) a 50% C ₂ H ₆ /50% C ₃ H ₈ blend at 75% N ₂ (black symbols/lines), 75% N ₂ + 10% Ar (red symbols/lines), and 75% N ₂ + 15% Ar (blue symbols/lines); (b) a 70% C ₂ H ₆ /30% C ₃ H ₈ blend at 75% N ₂ + 10% Ar (black symbols/lines), 75% N ₂ + 15% Ar (red symbols/lines), and 75% N ₂ (blue symbols/lines); (c) a 90% C ₂ H ₆ /10% C ₃ H ₈ blend at 75% N ₂ + 15% Ar (black symbols/lines), 75% N ₂ (red symbols/lines), and 75% N ₂ + 10% Ar (blue symbols/lines); and (d) a 90% C ₂ H ₆ /10% C ₃ H ₈ blend at 45.2% N ₂ + 45.2% Ar (magenta symbols/lines), 76.8% N ₂ (green symbols/lines), and 65.4% N ₂ + 25% Ar (orange symbols/lines).	100
Figure 5-4. IDT predictions of pure fuels, 90% C ₂ H ₄ /10% C ₃ H ₈ and 90% C ₂ H ₆ /10% C ₃ H ₈ binary blend in air. The corresponding derived correlation predictions are marked as dotted lines for pure fuels and dotted-dashed for binary blends.	101
Figure 5-5. Flux analyses of pure (a) C ₂ H ₄ , (b) C ₂ H ₆ , and (c) C ₃ H ₈ fuel ignition for $T_C = 1430$ K, $p = 40$ bar and $\varphi = 0.5$, at the time of 15% fuel consumption.	101
Figure 5-6. Comparisons for experimental and theoretical determinations for (a) the total reaction rate constant of C ₂ H ₄ + Ö [58, 60-68] and (b) product pathways for the reaction C ₂ H ₄ + Ö.	102
Figure 5-7. Sensitivity analyses to IDT at 790 K, 40 atm, and $\varphi = 0.5$, for; (a) C ₂ H ₄ and 90% C ₂ H ₄ /10% C ₃ H ₈ , in air; and (b) C ₂ H ₆ and 90% C ₂ H ₆ /10% C ₃ H ₈ in air.....	104
Figure 5-8. Flux analyses for; (a) pure C ₂ H ₄ (black) and 90% C ₂ H ₄ /10% C ₃ H ₈ (red); and (b) pure C ₂ H ₆ (black) and 90% C ₂ H ₆ /10% C ₃ H ₈ (red) mixtures ignition for 790 K and at 40 atm, and $\varphi = 0.5$	105
Figure 5-9. (a) Effect of changing the rate constant for C ₂ H ₄ + HÖ ₂ ↔ C ₂ H ₄ O1-2 + ÖH and Ö ₂ C ₂ H ₄ OH → products on IDT predictions for 90% C ₂ H ₄ /10% C ₃ H ₈ mixtures, — NUIGMech1.1, ----- AramcoMech3.0, — — — AramcoMech3.0 plus updated rate constant [76] for C ₂ H ₄ + HÖ ₂ ↔ C ₂ H ₄ O1-2 + ÖH, — AramcoMech3.0 plus updated rate constant for C ₂ H ₄ + HÖ ₂ ↔ C ₂ H ₄ O1-2 + ÖH and Ö ₂ C ₂ H ₄ OH → products [77]; and (b) Comparison of current rate constant [75] for C ₂ H ₄ + HÖ ₂ ↔ C ₂ H ₄ O1-2 + ÖH against the study by Zsély et al. [11] and Zádor et al. [78].	106
Figure 5-10. Effect of pressure for; (a) 50% C ₂ H ₄ /50% C ₃ H ₈ (solid lines) binary blend and pure ethylene (dashed lines); and (b) 50% C ₂ H ₆ /50% C ₃ H ₈ (solid lines) binary blend and pure ethane (dashed lines). The derived correlation predictions for binary blends are represented by dotted lines.	107

Figure 5-11. Sensitivity analyses to IDT predictions as function of pressure at $\phi = 0.5$, 50% C ₂ H ₄ /50% C ₃ H ₈ ; (a) 800 K; and (b) 1600 K.	108
Figure 5-12. Flux analyses at 800 K, $\phi = 0.5$, $p = 1$ (black), and 40 atm (red), with 75% N ₂ as diluent for; (a) 50% C ₂ H ₄ /50% C ₃ H ₈ ; and (b) 50% C ₂ H ₆ /50% C ₃ H ₈	109
Figure 5-13. Effect of equivalence ratio in (a) 50% C ₂ H ₄ /50% C ₃ H ₈ (solid lines) binary blend and pure ethylene (dashed lines); and (b) 50% C ₂ H ₆ /50% C ₃ H ₈ (solid lines) binary blend and pure ethane (dashed lines). The derived correlation predictions for binary blends are represented by dotted lines.	110
Figure 6-1. Extracted data from the studied literature (squares); new experimental tests defined in the current study (spheres); blue spheres/squares: fuel-lean mixtures; black spheres/squares: stoichiometric mixtures; red spheres/squares: fuel-rich mixtures.	125
Figure 6-2. Experimental and simulation data of methane/ethylene's IDT values: (a) 2.08% CH ₄ , 2.08% C ₂ H ₄ , 20.83% O ₂ , ($\phi = 0.5$) in 75% N ₂ at $p_C = 1$ bar, P5C1; (b) 2.143% CH ₄ , 2.143% C ₂ H ₄ , 10.71% O ₂ , ($\phi = 1.0$) in 75% N ₂ , 10% Ar, $p_C = 20$ bar, P5C2; (c) 2.22% CH ₄ , 2.22% C ₂ H ₄ , 5.55% O ₂ , ($\phi = 2.0$) in 75% N ₂ , 15% Ar, $p_C = 40$ bar, P5C3; (d) 5.303% CH ₄ , 2.273% C ₂ H ₄ , 17.424% O ₂ , ($\phi = 1.0$) in 75% N ₂ , $p_C = 40$ bar, P5C4; (e) 4.88% CH ₄ , 2.09% C ₂ H ₄ , 8.02% O ₂ , ($\phi = 2.0$) in 75% N ₂ , 10% Ar, $p_C = 1$ bar, P5C5; (f) 1.25% CH ₄ , 0.54% C ₂ H ₄ , 8.2% O ₂ ($\phi = 0.5$) in 75% N ₂ , 15% Ar at $p_C = 20$ bar, P5C6; (g) 10.976% CH ₄ , 1.22% C ₂ H ₄ , 12.805% O ₂ , ($\phi = 2.0$) in 75% N ₂ , $p_C = 20$ bar, P5C7; (h) 2.596% CH ₄ , 0.288% C ₂ H ₄ , 12.115% O ₂ ($\phi = 0.5$) in 75% N ₂ , 10% Ar at $p_C = 40$ bar, P5C8; (i) 2.9% CH ₄ , 0.32% C ₂ H ₄ , 6.77% O ₂ , ($\phi = 2.0$) in 75% N ₂ , 15% Ar, $p_C = 1$ bar, P5C9. (solid line: NUIGMech1.0, dashed-line: derived correlations (Section 6.4.3)).	130
Figure 6-3. Available experimental and simulated data of methane/ethane's IDT values at: (a) 0.15% CH ₄ , 0.15% C ₂ H ₆ , 1.7% O ₂ , ($\phi = 0.5$) in 98% Ar, $p_C = 1.46$ bar, P6C1; (b) 0.67% CH ₄ , 0.67% C ₂ H ₆ , 3.67% O ₂ , ($\phi = 1.0$) in 95% Ar, $p_C = 32.02$ bar, P6C2; (c) 3.16% CH ₄ , 3.16% C ₂ H ₆ , 8.68% O ₂ , ($\phi = 2.0$) in 85% Ar, $p_C = 15.44$ bar, P6C3; (d) 0.91% CH ₄ , 2.73% C ₂ H ₆ , 11.36% O ₂ , ($\phi = 1.0$) and 85% Ar, $p_C = 31.42$ bar, P6C4; (e) 5.14% CH ₄ , 1.71% C ₂ H ₆ , 8.14% O ₂ , ($\phi = 2.0$) in 85% Ar, $p_C = 29.03$ bar, P6C5; (f) 2.28% CH ₄ , 1.23% C ₂ H ₆ , 20.15% O ₂ , ($\phi = 0.5$ [5] and 0.6 [8]) in 75.74% N ₂ , $p_C = 22.26$ bar [5] and 9.62 bar [8], P5C6; (g) 4.19% CH ₄ , 0.47% C ₂ H ₆ , 20.03% O ₂ , ($\phi = 0.5$) in 75.31% N ₂ , $p_C = 22.71$ bar, P5C7; (h) 8.01% [3]/7.66% [7] CH ₄ , 0.89% [3]/0.85% [7] C ₂ H ₆ , 19.13% [3]/18.3% [7] O ₂ , ($\phi = 1.0$) in 71.97% N ₂ [3]/30% N ₂ +43.2% Ar [7], $p_C = 40$ bar; P6C8; (i) 0.12% CH ₄ , 0.36% C ₂ H ₆ , 1.52% O ₂ , ($\phi = 1.0$) and 98% Ar, $p_C = 1.36$ bar, P6C9. (solid line: NUIGMech1.0, dashed line: derived correlations (Section 6.4.3)).	131
Figure 6-4. Experimental and simulation data for ethane/ethylene oxidation at: (a) 1.67% C ₂ H ₆ , 1.67% C ₂ H ₄ , 21.67% O ₂ ($\phi = 0.5$), 75% N ₂ , $p_C = 1$ bar, P8C1; (b) 1.765% C ₂ H ₆ , 1.765% C ₂ H ₄ , 11.471% O ₂ ($\phi = 1.0$), 75% N ₂ , 10% Ar, $p_C = 20$ bar, P8C2; (c) 1.9% C ₂ H ₆ , 1.9% C ₂ H ₄ , 6.19% O ₂ ($\phi = 2.0$), 75% N ₂ , 15% Ar, $p_C = 40$ bar, P8C3; (d) 4.023% C ₂ H ₆ , 1.724% C ₂ H ₄ , 19.253% O ₂ ($\phi = 1.0$), 75% N ₂ , $p_C = 40$ bar, P8C4; (e) 3.92% C ₂ H ₆ , 1.68% C ₂ H ₄ , 9.39% O ₂ ($\phi = 2.0$), 75% N ₂ , 10% Ar, $p_C = 1$ bar, P8C5; (f) 0.91% C ₂ H ₆ , 0.39% C ₂ H ₄ , 8.7% O ₂ ($\phi = 0.5$), 75% N ₂ , 15% Ar, $p_C = 20$ bar, P8C6; (g) 8.26% C ₂ H ₆ , 0.92% C ₂ H ₄ , 15.83% O ₂ ($\phi = 2.0$), 75% N ₂ , $p_C = 20$ bar, P8C7; (h) 1.71% C ₂ H ₆ , 0.19% C ₂ H ₄ , 13.10% O ₂ ($\phi = 0.5$), 75% N ₂ , 10% Ar, $p_C = 40$ bar, P8C8; (i) 2.02% C ₂ H ₆ , 0.22% C ₂ H ₄ , 7.75% O ₂ ($\phi = 1.0$), 75% N ₂ , 15% Ar, $p_C = 1$ bar, P8C9. (solid line: NUIGMech1.0, dashed line: derived correlations (Section 6.4.3)).	132
Figure 6-5. Individual effects of the studied parameters on methane/ethylene and ethane/ethylene IDTs: (a) effect of blending composition; (b) effect of dilution level; (c) effect of equivalence ratio; and (d) effect of pressure.	134
Figure 6-6. Sensitivity analysis of IDT corresponding to the temperature of 1200 K (0.833) in Fig. 6-5(a).	135
Figure 6-7. Experimental and simulation data for ethane/ethylene oxidation concerning Fig. 6-5(b). The magenta dashed line refers to the turning point temperature (0.909) in Fig. 6-5(b).	137
Figure 6-8. Sensitivity analysis of IDT corresponding to the temperature 1100 K (0.91) in Fig. 6-5(b).	138
Figure 6-9. Sensitivity analysis of IDT corresponding to the temperature 1200 K (0.833) in Fig. 6-5(c).	140
Figure 6-10. Sensitivity analysis of IDT corresponding to the temperature 1200 K (0.833) in Fig. 6-5(d).	142
Figure 6-11. Performance of the derived correlation under an over-pressure (> 50 bar) condition [11].	147
Figure 7-1. Extracted data from the studied literature (black spheres); the literature data used in the study (Table 7-1) (blue spheres); and new experimental tests defined in the current study (red spheres); T_C : the compressed gas mixture temperature.	155
Figure 7-2. Available experimental and simulation data of methane's IDT values for average compressed reactive mixture pressure (p_C): (a) $\phi = 0.5$, 75% Ar, 0.85 bar, P1C1; (b) $\phi = 1.0$, 71.48% Ar, 24.32 bar, P1C2; (c) $\phi = 2.0$, 66.7% Ar, 40.53 bar, P1C3; (d) $\phi = 0.5$, 75% N ₂ , 24.3 bar, P1C4; (e) $\phi = 1.0$, 71.57% N ₂ , 43.23 bar, P1C5; (f) $\phi = 2.0$, 98% Ar, 0.85 bar, P1C6; (g) $\phi = 0.5$, 75.05% N ₂ , 44.53 bar, P1C7; (h) $\phi = 1.0$, 98% Ar, 0.93 bar, P1C8; (i) $\phi = 2.0$, 65.2% Ar, 24.32 bar, P1C9.	160
Figure 7-3. Available experimental and simulated data of ethylene's IDT values at (a) $\phi = 0.5$, 76.32% N ₂ , 1.025 bar, P2C1; (b) $\phi = 1.0$, 75.0% N ₂ , 20 bar, P2C2; (c) $\phi = 2.0$, 75% N ₂ , 40 bar, P2C3; (d) (ST) $\phi = 0.5$, 76.32% N ₂ , 23.24 bar, (RCM) $\phi = 0.5$, 37% Ar + 48% N ₂ , 20 bar, P2C4; (e) $\phi = 1.0$, 10% Ar + 75% N ₂ , 40 bar,	

P2C5; (f) $\phi = 2.0$, 69.29% N₂, 1.1 bar, P2C6; (g) $\phi = 0.5$, 15% Ar + 75% N₂, 40 bar, P2C7; (h) $\phi = 1.0$, 98% Ar, 1.16 bar; P2C8; (i) (ST) $\phi = 3.0$, 93% Ar, 18.75 bar, (RCM) $\phi = 2.0$, 45% Ar + 45% N₂, 20 bar, P2C9. 161

Figure 7-4. Available experimental and constant volume simulation data for ethane oxidation at (a) $\phi = 0.5$, 75% Ar, 1.31 bar, P3C1; (b) $\phi = 1.0$, 75% N₂, 20 bar, P3C2; (c) $\phi = 2.0$, 75% N₂, 40 bar, P3C3; (d) $\phi = 0.5$, 75% N₂, 10% Ar, 20 bar, P3C4; (e) $\phi = 1.0$, 75% N₂, 10% Ar, 40 bar, P3C5; (f) $\phi = 2.0$, 97.25% Ar, 0.98 bar, P3C6; (g) $\phi = 0.5$, 75% N₂, 15% Ar, 40 bar, P3C7; (h) $\phi = 1.0$, 97.75% Ar, 1.17 bar, P3C8; (i) $\phi = 2.0$, 75% N₂, 15% Ar, 20 bar, P3C9; (j) $\phi = 0.5$, 38.35% Ar, 38.35% N₂, 80 bar, P3C10; (k) $\phi = 1.0$, 80 bar, P3C11. 162

Figure 7-5. Experimental and simulation (NUIGMech0.9) IDT data. (a, b) Ethylene: (P2C2) $\phi = 1.0$, 75% N₂, 20 bar; (P2C3) $\phi = 2.0$, 75% N₂, 40 bar; (P2C4) $\phi = 0.5$, 37% Ar + 48% N₂, 20 bar; (P2C5) $\phi = 1.0$, 10% Ar + 75% N₂, 40 bar; (P2C7) $\phi = 0.5$, 15% Ar + 75% N₂, 40 bar; (P2C9) $\phi = 2.0$, 45% Ar + 45% N₂, 20 bar. (c, d) Ethane: (P3C2) $\phi = 1.0$, 75% N₂, 20 bar; (P3C3) $\phi = 2.0$, 75% N₂, 40 bar; (P3C4) $\phi = 0.5$, 75% N₂ + 10% Ar, 20 bar; (P3C5) $\phi = 1.0$, 75% N₂ + 10% Ar, 40 bar; (P3C7) $\phi = 0.5$, 75% N₂ + 15% Ar, 40 bar; (P3C9) $\phi = 2.0$, 75% N₂ + 15% Ar, 20 bar; (P3C10) $\phi = 0.5$, 38.35% Ar + 38.35% N₂, 80 bar; (P3C11) $\phi = 1.0$, 80 bar. 165

Figure 7-6. Constant volume adiabatic simulations of individual and combined effects of pressure, equivalence ratio, and dilution on variations of IDTs for ethylene (Eqn. 7-1) (y-axis is in log₂ scale); dashed line (1): 1700 K, dashed line (2): 1370 K, and dashed line (3): 1177 K (1112 K at Fig. 7-6(d)). 167

Figure 7-7. Normalized flux analysis (based on the flux analysis of P2C2 base case when 20% of ethylene is consumed) of some important reactions corresponding to Fig. 7-6(d). Blue lines: case (1), $T_C = 1700$ K. Black lines: case (2), $T_C = 1370$ K. Red lines: case (3), $T_C = 1112$ K. Red numbers: effect of dilution. Black numbers: effect of pressure. Magenta numbers: effect of equivalence ratio. Blue numbers: combined effects. 171

Figure 7-8. Constant volume adiabatic simulation of individual and combined effects of pressure, equivalence ratio, and dilution on variations IDTs for ethane (Eqn. 7-1) (y-axis is in log₂ scale). Dashed line (1): 1700 K. Dashed line (2): 1112 K. Dashed line (3): 750 K. 172

Figure 7-9. Normalized flux analysis (based on the flux analysis of P3C2 base case when 20% of ethane (fuel) is consumed) of some important reactions shown in Figs. ES99 – ES102 corresponding to Fig. 7-8(b). Blue line: case (1), $T_C = 1700$ K. Red line: case (2), $T_C = 1112$ K. Red numbers: effect of equivalence ratio. Black number: effect of dilution. Blue number: combined effects (P3C4). 176

Figure 7-10. (a) Populated experimental points using the Taguchi approach, “Exp” refers to targeted experimental conditions derived from the L9 Taguchi matrix (“x” is 1 – 3). (b) Populated simulation points inside the studied cube. “Sim” refers to simulations performed over the designed cube using the NUIGMech0.9 mechanism for deriving the correlations in accordance to the applied fuels. 178

Figure 8-1. Graphical example of the experimental data (■), against model predictions (— NUIGMech0.9, NUIGMech1.0, ----- NUIGMech1.1, ——— NUIGMech1.2). The left plot covers the high-temperature range (ST), and the right one the low-temperature range (RCM). Appendix F includes the chemical kinetic report based on the total of samples used in these analyses, and it can be consulted there. 187

Figure 8-2. Histograms for high temperature presenting the total sample size taken (n), mean of the sample (μ), and the standard deviation ($2 \times \sigma$) for each mechanism. The occurrence of each specific % error is plotted as a function of individual relative percentage errors (RPE) for (a) NUIGMech0.9, (b) NUIGMech1.0, (c) NUIGMech1.1, and (d) NUIGMech1.2, respectively. 189

Figure 8-3. Histograms for low temperature presenting the total sample size taken (n), mean of the sample (μ), and the standard deviation ($2 \times \sigma$) for each mechanism. The occurrence of each specific % error is plotted as a function of individual relative percentage errors (RPE) for (a) NUIGMech0.9, (b) NIGMech1.0, (c) NUIGMech1.1, and (d) NUIGMech1.2. 193

List of Tables

Table 2-1. Comparison between IDT_C ₁ –C ₃ database and the whole C ³ database for ST and RCM input data. It shows how IDT_C ₁ –C ₃ conforms to only ~12% of the total ST data, and ~18% of the total RCM data of the corresponding whole C ³ database.	23
Table 3-1. Optimized GAVs for the enthalpies of formation, H_f^0 (kcal mol ⁻¹); entropies, S_0 (cal K ⁻¹ mol ⁻¹) and heat capacities, C_p (cal K ⁻¹ mol ⁻¹) of stable non-oxygenated species.	37
Table 3-2. Optimized GAVs for the enthalpies of formation, H_f^0 (kcal mol ⁻¹); entropies, S_0 (cal K ⁻¹ mol ⁻¹) and heat capacities, C_p (cal K ⁻¹ mol ⁻¹) of stable oxygenated species.	37
Table 3-3. Optimized GAVs for the enthalpies of formation, H_f^0 (kcal mol ⁻¹); entropies, S_0 (cal K ⁻¹ mol ⁻¹) and heat capacities, C_p (cal K ⁻¹ mol ⁻¹) of bond dissociation groups.	38
Table 3-4. Optimized GAVs for the enthalpies of formation, H_f^0 (kcal mol ⁻¹); entropies, S_0 (cal K ⁻¹ mol ⁻¹) and heat capacities, C_p (cal K ⁻¹ mol ⁻¹) of correction groups.	39
Table 3-5. Comparison of enthalpies of formation from THERM23 and literature, ΔH_f^0 (kcal mol ⁻¹).	45
Table 3-6 The standard heats of formation (kcal mol ⁻¹) for 2-methylbutane and its corresponding radicals from the ab-initio calculations and group additivity method at 298.15 K.	49
Table 4-1. CH ₄ /C ₂ H ₄ /C ₂ H ₆ and CH ₄ /C ₂ H ₄ /C ₂ H ₆ /C ₃ H ₈ mixture compositions in % mole volume in the current study. Where keywords LPST, HPST and RCM.	63
Table 5-1. IDTs for C ₂ H ₄ , C ₂ H ₆ , C ₃ H ₈ , and binary blends from the literature.	93
Table 5-2. C ₂ H ₄ /C ₃ H ₈ and C ₂ H ₆ /C ₃ H ₈ mixture compositions in % mole volume in the current study. Where keywords NUIG refers to ST/RCM facilities at C ³ -NUIGalway, and PCFC refers to RCM facility at PCFC-RWTH Aachen University, respectively.	95
Table 6-1. Test conditions defined in the current study.	126
Table 6-2. Average uncertainties for compressed mixture temperature (T_c or T_s) and measured IDTs.	127
Table 6-3. Evaluated coefficients for correlation of the simulated IDTs for methane + ethylene mixtures.	145
Table 6-4. Evaluated coefficients for correlation of the simulated IDTs for methane + ethane mixtures.	145
Table 6-5. Evaluated coefficients for correlation of the simulated IDTs for ethane + ethylene mixtures.	146
Table 6-6. Performance of the methane/ethylene correlations versus the experimental data shown in Fig. 6-2.	146
Table 6-7. Performance of the methane/ethane correlations versus the experimental data shown in Fig. 6-3.	146
Table 6-8. Performance of the ethane/ethylene correlations versus the experimental data shown in Fig. 6-4.	146
Table 7-1. Test conditions defined in the current study.	156
Table 7-2. Average uncertainties for compressed mixture temperature (T_c or T_s) and measured IDTs.	158
Table 8-1. Overall statistical analyses parameters for the different mechanism versions of NUIGMech in the current study for high temperature, $\sim 1000 \leq T \leq \sim 2000$	190
Table 8-2. Overall statistical analyses parameters for the different mechanism versions of NUIGMech in the current study for low temperature, $\sim 700 \leq T \leq \sim 1000$	193
Table 8-3. Rate constants from the C ₀ chemistry for the development of (a) NUIGMech0.9, (b) NUIGMech1.0, (c) NUIGMech1.1, and (d) NUIGMech1.2 that have had an upgrade, any change, a refit or simply were aggregated as new reactions. Rate constants are presented in the form of $k = A T^n \exp(-Ea/RT)$ with units of first and second-order reactions are s ⁻¹ and cm ³ mol ⁻¹ s ⁻¹ , and cal mol ⁻¹ for activation energy.	196
Table 8-4. Rate constants from the C ₁ chemistry for the development of (a) NUIGMech0.9, (b) NUIGMech1.0, (c) NUIGMech1.1, and (d) NUIGMech1.2 that have had an upgrade, any change, a refit or simply were aggregated as new reactions. Rate constants are presented in the form of $k = A T^n \exp(-Ea/RT)$ with units of first and second-order reactions are s ⁻¹ and cm ³ mol ⁻¹ s ⁻¹ , and cal mol ⁻¹ for activation energy.	198
Table 8-5. Rate constants from the C ₂ chemistry for the development of (a) NUIGMech0.9, (b) NUIGMech1.0, (c) NUIGMech1.1, and (d) NUIGMech1.2 that have had an upgrade, any change, a refit or simply were aggregated as new reactions. Rate constants are presented in the form of $k = A T^n \exp(-Ea/RT)$ with units of first and second-order reactions are s ⁻¹ and cm ³ mol ⁻¹ s ⁻¹ , and cal mol ⁻¹ for activation energy.	200
Table 8-6. Rate constants from the C ₃ chemistry for the development of (a) NUIGMech0.9, (b) NUIGMech1.0, (c) NUIGMech1.1, and (d) NUIGMech1.2 that have had an upgrade, any change, a refit or simply were aggregated as new reactions. Rate constants are presented in the form of $k = A T^n \exp(-Ea/RT)$ with units of first and second-order reactions are s ⁻¹ and cm ³ mol ⁻¹ s ⁻¹ , and cal mol ⁻¹ for activation energy.	201

Chapter 1: General introduction

1.1 Energy scenario

Energy is a fundamental requirement for sustaining human life and in the development of societies and economies. In the last century, with a growing global population and society's growing motorization and reliance on technology, the demand for energy has increased drastically. To satisfy this growth of energy demand society has heavily relied on fossil fuels. These fossil fuels originate from geologic deposits of organic material, which over millennia have been converted into crude oil, coal, natural gas, and peat. Fossil fuels are undeniably a very versatile and energy dense source of energy, as a result, are being used to supply up to ~84% of the world's energy consumption [1].

The United States of America (USA) ranks eleventh in the world for the highest reserves of oil and is also the number one consumer [1, 2] with global consumption of ~ 20% of the world share. Therefore, based on the U.S. Energy Information Administration (EIA) report from 2022 [1], the British Petroleum statistical review of world energy 2022 (BP) [2], and the World Energy Outlook 2021 from the International Energy Agency (IEA) [3], with projections out to 2050 petroleum and natural gas will remain the main sources of energy consumption, with renewable energies being the fastest growing energy source. Moreover, gasoline will remain the most prevalent transportation fuel despite the electric vehicles gaining market share, as shown in Fig. 1-1. It is reported that gasoline remains the dominant fuel for light-duty vehicles (LDV). However, it is expected that the levels of consumption will not recover to those of the pre-pandemic period, mainly due to the gradual introduction of different types of electric vehicles (EV), Fig. 1-1. The predictions indicate that the share of LDVs will decrease from 54% to 51% from 2021 to 2050. This reduction will lead a decrease in the consumption of fossil fuels because of the increasing introduction of battery-electric vehicles (BEVs), hybrid-electric vehicles (HEVs), and plug-in hybrid-electric vehicles (PHEVs).

Furthermore, the predictions show that the sales of internal combustion engines (ICE) LDV which includes vehicles powered by gasoline, diesel, flex-fuel, natural gas, and propane powertrains, will decrease from 92% to 79% because of growth in sales of BEVs, PHEVs, and HEVs, as presented in Fig. 1-2. This can simply be explained by the fact that, as ICE-LVDs become old they will be replaced by EV, with the type of EV depending on the application. This leads to a projected increase in EV stock from 3% to 13% in the period from 2021 to 2050. Thereafter, a gradual increase in the EV fleet will lead to the production of millions of EVs. Hence, a growth from 1.31 million to 2.21

million EVs is expected in that timeframe. Finally, this increases not only in stock but also in the number of vehicles will increase the consumption of electricity from less than 0.5% to 2% of total energy consumption in the transportation sector.

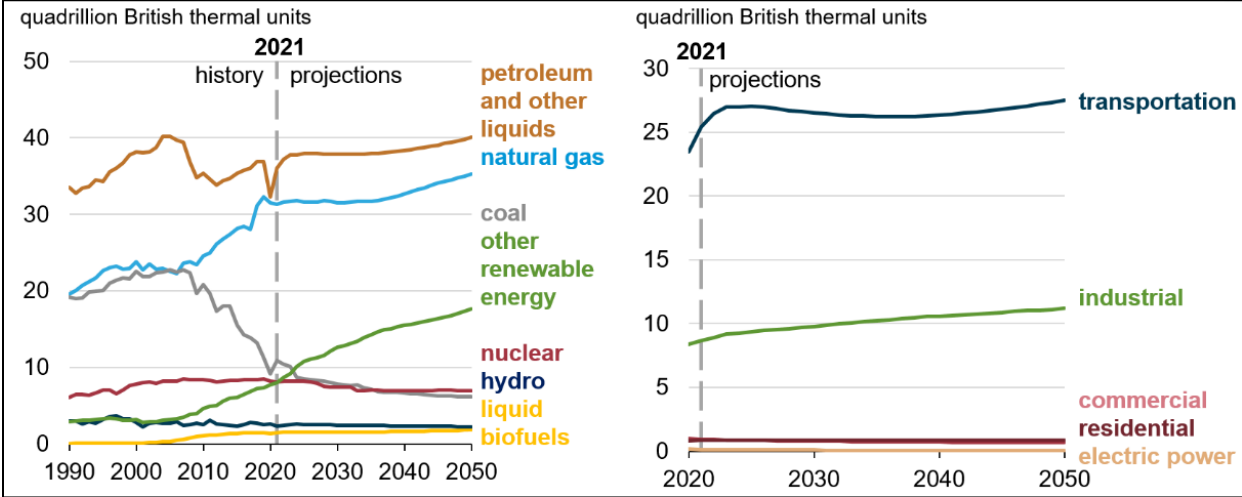


Figure 1-1. Graph of energy consumption by fuel in the left, and consumption by sector in the right [1].

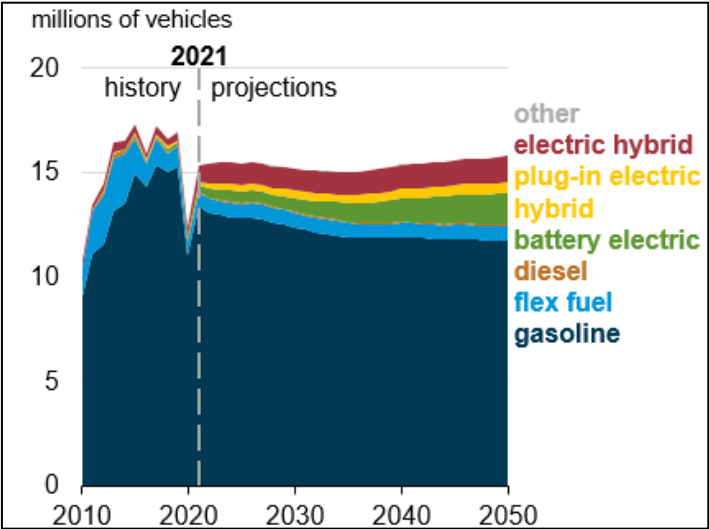


Figure 1-2. Light-duty vehicle sales by technology or fuel [1].

Vehicles and industry remain the main consumers of petroleum and other liquids. Gasoline, diesel and distillate fuel oil are mostly consumed by the transportation sector. The current fuel economy remains constant after 2026 and 2027 for the LDV and heavy-duty vehicles (HDV), respectively. It is worth noting that in the reference case it is generally assumed that current laws and regulations that affect the energy sector will remain unchanged throughout the projection period.

Based on this reference case, it is expected that the consumption of renewable energy increases at a steady pace after 2026, with natural gas also being predicted to fill a large part of the market, with a continuous decrease in the use of coal as an energy source.

It is well known that economy, energy, and pollution are closely related. Hence, it is not strange that the energy scenario presented here depends on economic growth; as economies grow, energy consumption increases. Moreover, energy consumption is projected to increase through 2050 as population and economic growth outweigh efficiency gains, Fig. 1-3. It is anticipated that renewable energy will be the fastest growing sector through 2050. Additionally, new technologies will lower the installation costs associated with wind, and solar energy generation. Moreover, for the reference case starting from the early 2020s, the industrial sector has the largest share of natural gas consumption.

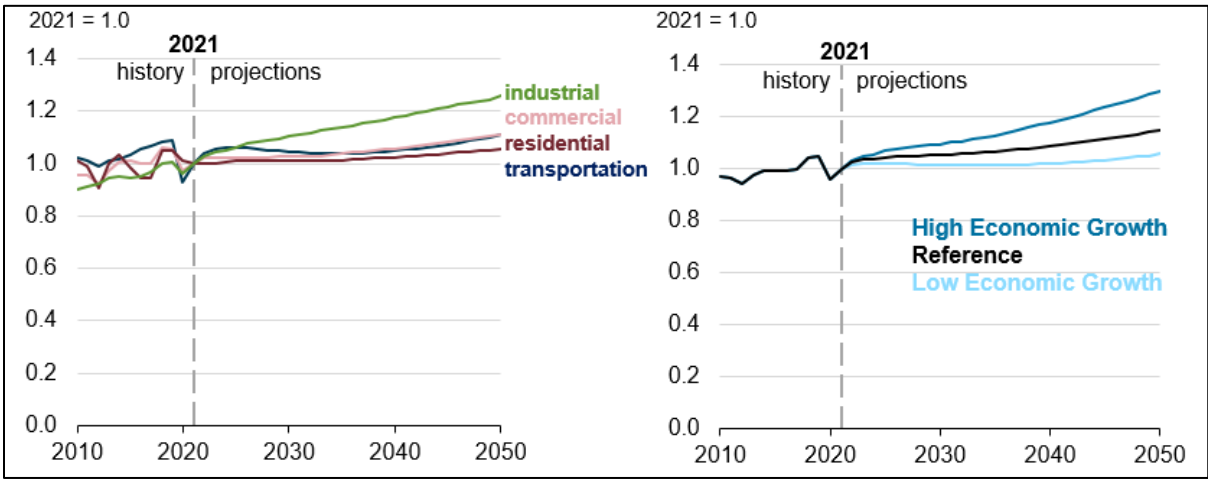


Figure 1-3. Graph of indexed delivered energy by end-use sector in the left and indexed delivered energy across end-use sectors in the right [1].

One of the primary energy challenges modern society faces is energy-related greenhouse gas (GHG) emissions, particularly carbon dioxide (CO₂). Emissions of CO₂ are expected to decrease in time from 2022 – 2037 because of the transition from carbon-intense coal to less carbon-intense natural gas and renewable energy for electricity generation. After this period, CO₂ emissions are expected to have an upward trend corresponding to increasing energy consumption due to population and economic growth. After 2021, CO₂ emissions are projected to peak around 2050 but are expected to remain below the peaks of previous levels in the years before 2021, Fig. 1-4.

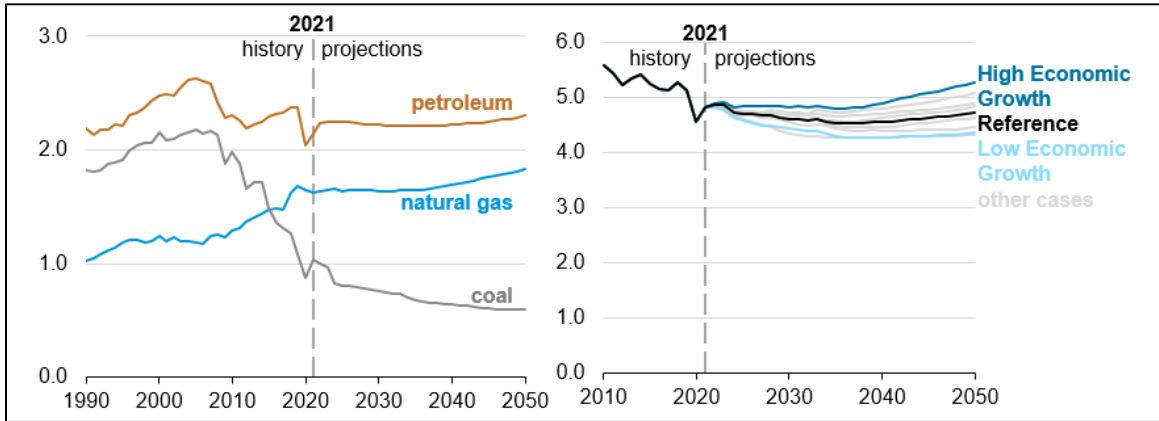


Figure 1-4. Graph of energy-related CO₂ emissions by fuel source in the left, and the U.S. energy-related CO₂ emissions in the right [1].

Hence, the combustion community has as one of its primary goals a desire to improve the efficiency of fuels and to decrease GHG emissions through optimal combustor design and operation. In this regard, decarbonizing future sources of energy is required, and therefore a greater understanding of the chemistry involved in the combustion of alternative non-carbon fuels is required. Combustion researchers can contribute to this goal by developing accurate detailed chemical kinetic mechanisms to describe alternative fuel combustion. This thesis provides details of the development of detailed chemical kinetic mechanisms and associated software to describe the combustion of small hydrocarbons including methane, ethane, ethylene and propane.

1.2 The foundations of thermochemistry and kinetics

To succeed in improving the efficiency of fuel combustion a detailed chemical kinetic model is needed that can describe its oxidation characteristics over a wide range of temperature (T), pressure (p), equivalence ratio (ϕ) and dilution (D). A chemical kinetic model is generated by including elementary reactions with their corresponding rate constants (kinetics) and reaction species thermodynamics (thermo) and transport data. This section is intended to provide the reader with the basic fundamental concepts for the chemical kinetic modeling. Whereas kinetics is the main subject explored during the development of chemical kinetic mechanisms, the thermodynamics properties also have an important role in this process.

1.2.1 Thermodynamics

The branch of physical chemistry that studies the transformation of energy from heat into work is called thermodynamics. Thermodynamics provides useful relations between observable properties of the bulk matter and the properties of atoms and molecules. This important connection is possible through statistical thermodynamics. Furthermore, thermodynamics has many branches, one of the most significant branches of thermodynamics is that which deals with the heat output of chemical reactions [4-7]. At the end of this Section, we will understand that thermodynamics and kinetics are inter-related and that to be able to predict and understand the pyrolysis and combustion of fuels we need both.

There are three fundamental thermodynamic properties of our interest which are essential in chemical kinetic modeling development, namely the enthalpy (H), entropy (S), and heat capacity (C_p , C_V) of every chemical species. Henceforth, the units we will use for any property related to energy will be either $\text{kJ}\cdot\text{mol}^{-1}$ for enthalpy and $\text{J K}^{-1}\text{ mol}^{-1}$ for entropy and heat capacity. Thus, from the internal energy (ΔU):

$$\Delta U = q + w \quad (1.1)$$

q is the energy transferred to the system as heat, and w is the energy transferred to the system as work. The ΔU is then the sum of all of the kinetic and potential energy contributions. Taking the expression from the ideal gas equation:

$$pV = nRT \quad (1.2)$$

where p is the pressure of the gas, V is the corresponding volume, n as the number of moles of gas, R is the molar gas constant, and T is the gas temperature. This ideal gas law is the most useful expression because it ties the number of moles of gas to its pressure, volume, and temperature. Then, taking the expression for the enthalpy [4-7]:

$$\Delta H = \Delta U + p\Delta V \quad (1.3)$$

thus, replacing Eqn. 1.2 in Eqn. 1.3 we can rewrite this expression as:

$$\Delta H = \Delta U + \Delta nRT \quad (1.4)$$

where ΔU is the kinetic and potential energy stored in the atoms or molecules of a system, and the second term is the difference between the enthalpy and the internal energy. By definition, the standard enthalpy of formation ($\Delta_f H^\theta$) is the change in enthalpy when one mole of a substance in the standard state (1 atm of pressure, and 298.15 K) is formed from its pure elements under the same conditions.

Due to their nature, both U and H , are state functions, which means that they do not depend on the trajectory or path but only on the initial and final states. Indeed, the determination of the most basic properties related to the oxidation of fuels is strongly related to these properties, and not only that but in the end, a proper estimation of enthalpy perhaps leads a chemical kineticist in the direction to speculate about which reactions would be important for the development of the corresponding model. For example, the enthalpy of reaction ($\Delta_r H^0$) can readily be determined from the $\Delta_f H^0$ of the products and reactants for that reaction via:

$$\Delta_r H = \sum \Delta_f H^0(\text{products}) - \sum \Delta_f H^0(\text{reactants}) \quad (1.5)$$

this Eqn. 1.5 basically states that the standard enthalpy of formation is equal to the sum of the standard enthalpies of formation of the products minus the sum of the standard enthalpies of formation of the reactants.

The next important thermodynamic property concerns the degree of disorder of the system. Thus, the measure of the disorder of matter and energy used in thermodynamics is called entropy (S). Some of the physical and chemical phenomena tend to occur in a natural direction, which implies without outside intervention, spontaneously. For instance, a hot object will, in time, tend to cool to the temperature gradient of its surroundings. Also, we can think of ice melting, at the beginning, the individual molecules are fixed and ordered in the solid state, but when ice melts the molecules become freer to move, and therefore become disordered. Thereafter it can become a gas, and the molecules are freer than before to move independently through space. We must remember that spontaneous changes happen only in the direction that leads to equilibrium [7].

These examples help to illustrate the concept of spontaneous change. It is worth noting that, for all spontaneous processes, no outside intervention is required for the state of the system tends towards disorder or dispersion, but non-spontaneous processes are ones where work must be done to make the system more ordered. All of these spontaneous changes can be quantified via entropy change, ΔS . The common units of S^0 are $\text{J} \cdot \text{K}^{-1} \text{mol}^{-1}$, where a positive value indicates an increase in entropy, while a negative value denotes a decrease in the entropy of a system. Hence, we can write the entropy change in a chemical reaction ($\Delta_r S$) as the sum of the entropies of the products minus the sum of the entropies of the reactants:

$$\Delta_r S = \sum \Delta S^0(\text{products}) - \sum \Delta S^0(\text{reactants}) \quad (1.6)$$

The heat capacity (C_p or C_v) is the final thermodynamic quantity we need to consider. Eqn. 1.1 shows that the internal energy can change by either heat or work. Zemansky [6] stated that it is easier to generate heat from combustion or electricity passing through a resistor than it is to produce work from falling weights or by compressing strings. At this level it is important to clarify a common misunderstanding regarding the term “heat capacity”. It is usual to interpret it as the heat a substance can hold, which is not correct. Heat itself is not a function of the thermodynamic state of a system. Therefore, the proper term would be internal energy capacity. However, the oxymoron “*heat capacity*” is commonly used. In this work we will also use this term. Its SI unit is J/K and is a measure of the heat energy required to change the temperature of a quantity of substance (in this case 1 mole) by a defined amount.

From the state functions U , H , and S , and using the expression for $\Delta S = \Delta q_{rev}/T$, we can derive the heat capacity expression we are looking for, but first, the expression should be rearranged as follows:

$$q_{rev} = T\Delta S \quad (1.7)$$

At constant volume no work is done to the system and $\Delta U = \Delta q_{rev}$, so the relationship for heat capacity at constant volume (C_v) is:

$$\Delta U = C_v\Delta T \quad (1.8)$$

and from the enthalpy equation at constant pressure $\Delta q_{rev} = \Delta H$, so the relation for the heat capacity at constant pressure (C_p) is:

$$\Delta H = C_p\Delta T \quad (1.9)$$

Heat capacity is essential in the thermodynamic description of any physical reactor containing an arbitrary number of chemical components and it can be defined in terms of either constant pressure (C_p) or volume (C_v) processes, with these two values related by R for the special case of an ideal gas. Using Eqns. 1.8 and 1.9 we can write both expressions in the equation:

$$C_p - C_v = R \quad (1.10)$$

In fact, the relation of S and C_p (or C_v) is similar to that for U and H . Moreover, the C_p and C_v expressions have utility in the extrapolation of standard thermodynamic quantities. Indeed, the enthalpy and entropy can be written in terms of the initial (T_i) and final (T_f) temperatures, plus the integral of the heat capacity at constant pressure (C_p) from T_i to T_f . These equations directly depend

on the temperature of the system as follows, from Eqns. 1.5 and 1.6 we can re-formulate the next relations:

$$\Delta_f H(T_f) = \Delta_f H(T_i) + \int_{T_i}^{T_f} \Delta C_p dT \quad (1.11)$$

$$\Delta S(T_f) = \Delta S(T_i) + \int_{T_i}^{T_f} \frac{\Delta C_p}{T} dT \quad (1.12)$$

For a detailed derivation of all these equations and further information regarding these topics the reader is referred to Atkins [4, 5], Zemansky [6], and Kotz [7].

1.2.2 Chemical kinetics

Chemical kinetics is the study of the rates of chemical reactions and the mechanisms by which they take place. Chemical kinetics introduces the time variable in the study of chemical reactions and studies the path that reactants follow to become products. Kinetics can be applied to process optimization, for example, in organic chemistry synthesis, analytical reactions, and chemical manufacturing. The three main application fields are the environment, food, and pharmacology. Also, it has multiple applications in material corrosion, ageing, and deterioration of products, from medical applications to drug design, development, and manufacturing to ensure the stability of such drugs, to mention a few.

In the study of rate constants, the following concepts and short discussion can be easily found in the following references [4, 5, 8-12] which comprise chemical kinetics, and physical chemistry. An elementary unimolecular reaction is the simplest type of reaction which occurs in a single step with a single transition state and no intermediates. This involves the conversion of a single reactant to a single or multiple products in a single-step process. Some examples of this range from radioactive decay to cis-trans isomerization, thermal decomposition, or ring-opening [13]. Considering that an irreversible reaction can be written as $aA \rightarrow bB$, here the capital A is an arbitrary reactant but with a stoichiometric coefficient, a , and the capital B is a single product with its stoichiometric coefficient represented by b . Thus, we know that the rate at which a particular reactant A is getting consumed in the reaction can be illustrated by $-d[A]/dt$, it must be proportional to its concentration, $[A]$ (amount per unit volume), and it is raised to the power of its corresponding stoichiometric coefficient, a , as shown:

$$-\frac{d[A]}{dt} \propto [A]^a \quad (1.13)$$

This mathematical relationship of reaction rate with reactant concentrations is known as the rate law. Similarly, the rate at which a particular product B is getting produced is the rate of formation of the product B :

$$+\frac{d[B]}{dt} \propto [A]^a \quad (1.14)$$

It is important to realize that Eqns. 1.13 and 1.14 have a *proportionality* (\propto) sign not an equality sign. To complete the equality, it is required to introduce a proportionality constant (k) which is called rate constant, and it is the center of the field of chemical kinetic modelling [14]. But why is this proportionality constant (k) so important? This rate constant is the fundamental link between the concentration of a specific species and the rate at which that species reacts.

$$-\frac{d[A]}{dt} = +\frac{d[B]}{dt} = k[A]^a \quad (1.15)$$

from 2.15 where the coefficients a and b are equal to 1, then the rate law for this elementary reaction is defined as:

$$-\frac{d[A]}{dt} = k[A]^1 \quad (1.16)$$

this reaction is a first-order reaction in A where the order is defined as the power of A , in this case, equal to 1. The molecularity of the reaction, which refers to the number of reactant particles involved in the reaction, is also equal to 1 because, during the reaction, it only consumes a single molecule (A). Now, in a different but similar case, for the bimolecular reaction $aA + bB \rightarrow products$, the corresponding rate law will be:

$$-\frac{d[A]}{dt} = -\frac{d[B]}{dt} = k[A]^a[B]^b \quad (1.17)$$

following the same logic than before, the reaction is a^{th} order in A , b^{th} order in B and the overall order is $a + b$. Thus, we can re-write 2.17 as follows:

$$-\frac{d[A]}{dt} = -\frac{d[B]}{dt} = k[A]^1[B]^1 \quad (1.18)$$

In this brief, we have considered uniquely elementary reactions for the simple explanation of the rate laws. However, that does not mean these are the only ones that a kineticist will encounter, for a further explanation of temperature and pressure dependencies the reader should refer to the

literature [9-11, 13, 14]. Regarding these rate laws we have already shown in Eqns. 1.16 and 1.18 which govern first, and second order reactions are the type to be considered during the construction of chemical kinetic mechanisms, as shown by:

For $A \rightarrow \text{products}$,

$$-\frac{d[A]}{dt} = k[A] \quad (1.19)$$

For $A + B \rightarrow \text{products}$,

$$-\frac{d[A]}{dt} = -\frac{d[B]}{dt} = k[A][B] \quad (1.20)$$

During the process of the development of chemical kinetic mechanisms, the main objective is not only to provide the combustion community with a collection of the most important reactions and their corresponding thermodynamic properties but a detailed chemical kinetic mechanism. In this regard, a detailed chemical kinetic mechanism should contain all of the possible reactions for all the possible paths such as it can be used to extract from it a variety of sub-mechanisms for a wide range of conditions.

In summary, thermodynamics will tell us what can occur during a process, while kinetics tells us what exactly occurs. Thus, thermodynamics focuses on the energetics of the products and the reactants, whereas kinetics focuses on the pathway from reactants to products. Now we need the proper tools to use these definitions and be able to construct a detailed chemical kinetic mechanism. Unequivocally, in the Combustion Chemistry Centre (C³) the main goal is the development of accurate detailed chemical kinetic mechanisms.

1.3 Group additivity in combustion chemistry

To accurately describe fuel pyrolysis and combustion a reliable chemical kinetic mechanism is required. This typically includes three files: (1) the chem file which lists all of the species and their elementary reactions and associated rate constants; (2) the therm file which is a list of the thermochemistry, in NASA polynomial format, associated with all of the species involved in the reactions; and (3) the trans file which lists the transport data associated with each species, which need to be considered for experiments which involve convection, diffusion, or conduction.

As explained earlier, the main thermodynamic properties of interest are enthalpy (H), entropy (S), and heat capacity (C_p , C_v). These properties can be obtained experimentally, by calorimetry for

example, or computationally, via ab initio quantum chemistry calculations. However, these methods are time-consuming and expensive. An alternative, known as Benson's group additivity method [15], has become widely used as it is relatively cheap, convenient, and quick. This section provides further explanation of Benson's group additivity method, following a brief overview of the experimental and theoretical methods commonly used to calculate these properties.

1.3.1 Experimental and theoretical methods

Typically, calorimetry is used to determine heat capacities, enthalpy, and internal energy. This technique is based on thermometric methods that are performed in a specialized device called a calorimeter, which uses a known volume of liquid. There are two types of settings for this calorimeter: constant-volume and constant-pressure calorimetry.

The constant-volume calorimeter is used to measure the change in internal energy (ΔU) of a combustion reaction. In this technique, a sample is burned at constant volume in a device called a bomb calorimeter, as shown in Fig. 1-5(a). The sample is burned in pure oxygen in the bomb, which is inside a water-filled container. The energy transferred as heat from the reaction warms the bomb and the water that surrounds it. By measuring the increase in temperature, the total energy transferred as heat during the reaction can be determined [16]. The bomb calorimeter is a widely used method in thermochemistry due to its simplicity and accuracy. Constant-pressure calorimetry is used to measure the change in enthalpy (ΔH) of a physical or chemical process. In this technique, the experiment is carried out in a solution using a coffee cup calorimeter, an inexpensive device composed of two Styrofoam cups, as presented in Fig. 1-5(b). The chemical reaction produces a change in the temperature of the solution in the calorimeter. Then, the change in temperature of the solution is measured, and knowing the mass and specific heat capacity of the solution and the temperature change, the enthalpy change for the reaction can be calculated. The Styrofoam container is very effective in preventing any transfer of energy in the form of heat between the solution and the surroundings. Furthermore, because the cup is open to the atmosphere, this is a constant-pressure measurement [16]. This calorimeter is very simple and inexpensive and widely used in undergraduate lab experiments.

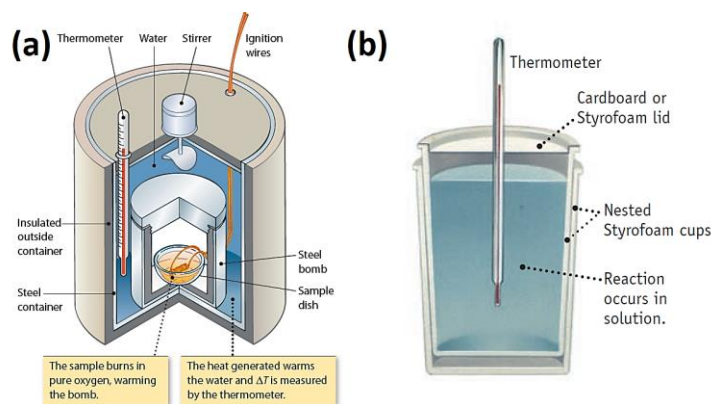


Figure 1-5 (a) Constant-volume calorimeter or bomb calorimeter, (b) constant-pressure calorimeter or coffee-cup calorimeter [16].

One limitation of calorimetry is that it is not always possible to measure heat capacities, enthalpy, and internal energy of all types of substances. For example, gases and liquids are relatively easy to measure, but solids are much more difficult. Additionally, some substances may not be suitable for calorimetry due to their high reactivity or volatility. Another limitation of calorimetry is that it is not always possible to measure the heat capacities, enthalpy, and internal energy of a substance at all conditions. For example, some substances may only be measurable at high temperatures or pressures, which can be difficult to achieve or maintain. Additionally, the measurement of enthalpy may require the use of a constant-pressure calorimeter, which can be more complex and expensive than a constant-volume calorimeter.

Additionally, calorimetry measurements are not always precise and accurate, the precision of the calorimeter can be affected by factors such as the quality of the thermometer, the calibration of the instrument, and the skill of the operator. The accuracy of the calorimeter is also affected by the quality of the sample and the purity of the reactants.

Finally, some chemical reactions may be too fast or too slow to be measured by calorimetry or may not be feasible to be performed in a calorimeter, this can be a limitation for certain kinds of reactions, like detonations or explosions for example. In summary, calorimetry is a widely used technique used to measure heat capacities, enthalpy, and internal energy of a substance, but it also has some limitations such as the types of substances that can be measured, the conditions under which measurements can be made, and the precision and accuracy of the measurements. Further information regarding calorimeter settings, modern approaches, and different versions of this and other technique can be found in the references [16-18].

On the other hand, theoretical methods based on quantum mechanics (QM) and usually called electronic structure methods, are used to calculate the properties of molecules and materials. These methods can be divided into three main categories: semi-empirical, density functional theory (DFT) and ab initio. Semi-empirical methods use approximations and parameters from empirical data to solve the Schrödinger equation, which describes the behavior of electrons in a system but only considers the valence electrons, which reduces the computational cost. DFT methods determine properties based on calculations made on the electron density of a system, which reduces the computational cost compared to ab initio methods. Ab initio methods solve the Schrödinger equation directly, without using any empirical data, which makes them more accurate but also more computationally expensive [19-21]. Each method has its advantages and limitations, and the choice of method depends on the specific system being studied and the level of accuracy required [22].

Ab initio methods are widely used in the combustion chemistry field to study the thermodynamics, kinetics, and mechanism of various combustion reactions. These methods can provide detailed information about the electronic structure, bond dissociation energies, and reaction pathways of different species involved in the combustion process. One of the main advantages of ab initio methods is that they do not require any experimental data or empirical parameters, making them particularly useful for studying complex systems and reactions that are difficult to measure experimentally. They can also provide a deeper understanding of the underlying chemical and physical processes that govern combustion reactions. These QM calculations are extremely rigorous and therefore the size of the molecular systems that can be studied using these methods is limited. High-level QM methods, such as Møller-Plesset (MP) methods, can account for electron-correlation effects, which enables them to represent London dispersion interactions [23]. However, due to their computational intensity, they can only be applied to systems composed of a dozen or so atoms. Less rigorous QM methods, such as Density Functional Theory (DFT) methods, can be used for larger systems involving hundreds of atoms. However, DFT methods generally do not account for electron-correlation effects, which can be important depending on the molecular system being studied. Therefore, these methods often require the addition of specific empirical parameters to accurately represent the molecular behavior of a designated system. The current limitations in the size of molecular systems that can be handled with QM methods make them largely unsuitable for direct application in simulating protein-surface interactions [24]. Despite these limitations, QM methods

are highly valuable and widely used to establish parameter values for empirical force fields for classical molecular dynamics (MD) simulations [25].

The most important ab initio quantum mechanical (QM) methods used are Hartree-Fock (HF) method, Møller-Plesset perturbation theory (MPn), Configuration Interaction (CI), Coupled Cluster (CC), and Multi-Configurational Self-Consistent Field (MCSCF) including Complete Active Space Self-Consistent Field (CASSCF) and Restricted Active Space Self-Consistent Field (RASSCF) [26]. The HF method is the simplest approach to ab initio calculations. It assumes that the problem of many particles can be replaced by a one-electron problem, considering this electron is moving in an effective static potential field. This method is relatively fast and easy to implement, but it does not account for electron correlation effects [27]. Møller-Plesset perturbation theory (MPn) is a post-HF method that adds electron correlation effects through Rayleigh-Schrödinger perturbation theory (RS-PT) to second (MP2), third (MP3), or fourth (MP4) order [28]. This method improves the accuracy of the results but at the cost of increased computational intensity. Configuration interaction (CI) is a method where the wave function is represented as a linear combination of different configurations, or electronic states, that are obtained from the HF method. This method allows for the inclusion of electron correlation effects but requires a large number of configurations to obtain accurate results.

Additionally, Coupled Cluster (CC) methods are based on the idea of building up a wavefunction through the excitation of electrons from occupied to virtual orbitals. These methods are considered to be the most accurate, but they are also the most computationally expensive. The most widely used coupled-cluster method is CCSD(T) which is based on the Coupled-Cluster Singles and Doubles (CCSD) method and includes perturbative corrections for triple excitations. Multi-configurational self-consistent field (MCSCF) methods are used to account for electron correlation effects in molecules. These methods are based on the idea of representing the wave function of a system as a linear combination of different electronic configurations, or states, that are obtained from the HF method. The basic idea behind the MCSCF method is to use a set of spatial orbitals that are optimized to represent the electronic structure of a system. These orbitals are determined by a self-consistent procedure, in which the electronic density is calculated using the current set of orbitals, and the orbitals are then adjusted to better represent this density. This process is repeated until the orbitals converge to a stable solution [29]. The MCSCF method can be further divided into two different categories, complete active space self-consistent field (CASSCF) and Restricted active space self-consistent field (RASSCF) methods. In CASSCF methods, all electrons and all orbitals are

treated as active, while in RASSCF methods, only a subset of the electrons and orbitals are treated as active. One of the main advantages of the MCSCF method is that it allows for the inclusion of electron correlation effects without the need for a large number of configurations as in Configuration Interaction (CI) method. However, it is still a computationally intensive method, and it is typically limited to small to medium-sized molecules [30].

Although it is true that ab initio methods are a powerful tool to calculate the properties of molecules and materials, they also have some limitations that should be considered. One limitation is that they are computationally expensive, which makes them impractical for large and complex systems. The cost of the calculation increases rapidly with the size of the system and the level of accuracy required. This makes it difficult to apply ab initio methods to study large biomolecules, for example, or to perform extensive optimization and sampling of potential energy surfaces. Another limitation is that they require a high level of expertise to set up and run the calculations and interpret the results. The methods are based on fundamental principles of quantum mechanics and require a deep understanding of the underlying theory to use effectively. Additionally, the accuracy of the results depends on the level of theory used and the quality of the basis set. It's also important to consider that ab initio methods are based on the assumption that the electronic wave functions are represented by a linear combination of a basis functions, which could limit the accuracy of the results for certain systems. Further details about semi-empirical, ab initio and DFT methods can be found in the next references [31-34].

1.3.2 Benson's group additivity method

Benson's group additivity (BGA) method was proposed by Benson et al. [35-38] in 1958. This method is used to estimate the thermochemical properties of organic molecules by breaking them down into smaller, well-characterized units called group additivity values (GAVs), usually based on the heavy atoms in a molecule. These groups are assigned heat of formation, entropy and heat capacity values based on available experimental or ab initio calculations. The thermochemical properties of the entire molecule can be predicted by summing the thermochemical values of the individual groups. BGA method is often used in conjunction with ab initio calculations because it permits a more efficient prediction of thermochemical properties by reducing the number of calculations required for a given molecule. Ab initio methods, on the other hand, can provide highly

accurate results, but they are computationally expensive. By combining BGA with ab initio methods, the computational cost can be reduced while still maintaining a high level of accuracy for the predicted thermochemical properties.

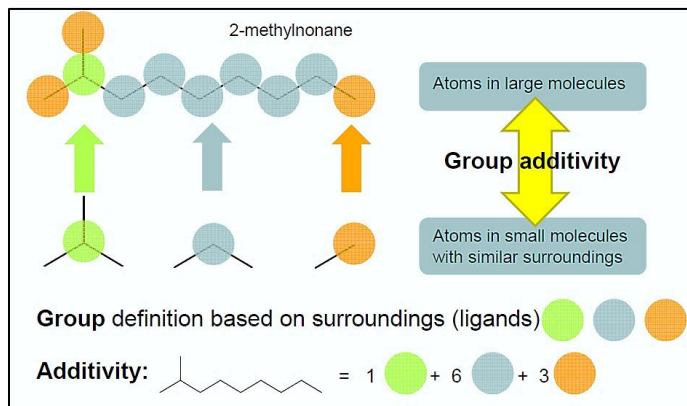


Figure 1-6 Schematic representation of the BGA method of 2-methylnonane. The molecule of interest is first broken down in groups with corresponding GAVs. Then these GAVs [37].

The BGA method has some limitations that should be considered. It relies on the availability of experimental data or ab initio calculations to derive the thermochemical properties of the individual groups. If data is not available for certain groups, the predicted thermochemical properties of the entire molecule will be inaccurate. Additionally, the method may not be able to predict the thermochemical properties of large and complex molecules accurately. Furthermore, there is a dependency of the results on the specific set of groups chosen to represent a molecule, which could lead to different results when using different group sets. Therefore, it is important to be aware of these limitations when using BGA and to validate the results with experimental data or other theoretical methods where possible.

To show how to use the BGA method to estimate the heat of formation (ΔH_f^0), consider the case of the compound 2-methylnonane ($C_{10}H_{22}$). The molecule can be broken down into three groups (GAVs): a methyl group ($-CH_3$), a methylene group ($-CH_2$) and a methine group ($-CH$). The thermochemical values for these groups, such as their (ΔH_f^0), can then be used to estimate the $\Delta H_{f-C_{10}H_{22}}^0$ by summing the heat of the formation of each group. In this case, from the NIST webbook, the experimental $\Delta H_{f-C_{10}H_{22}}^0 = -62.18$ kcal/mol [38]. Thus, by summing the heat of the formation of the three methyl groups ($\Delta H_{f-CH_3}^0$), six methylene groups ($\Delta H_{f-CH_2}^0$), and one methine group (ΔH_{f-CH}^0) as shown in Fig.1-6, $\Delta H_{f-C_{10}H_{22}}^0 = (\Delta H_{f-CH_3}^0 \times 3) + (\Delta H_{f-CH_2}^0 \times 6) + (\Delta H_{f-CH}^0 \times 1)$. Taking the GAVs

from Gosh et al [39], we have $\Delta H_{f_C_{10}H_{22}}^0(\text{BGA}) = -(10.16 \times 3) - (4.91 \times 6) - (1.68 \times 1) = -30.48 - 29.46 - 1.68 = -61.62$ kcal/mol. In this case, the deviation will be about -0.56 kcal/mol which is under the unit, and an acceptable deviation from experimental values based on BGA estimations.

As mentioned early, it is essential to note that the BGA method requires a set of carefully chosen groups that should be able to represent as much as possible the chemical behaviour of the molecule, which will be used to predict the thermochemical properties of the entire molecule. From there, the significance of using ab initio methods is to calculate the data as accurately as possible for the corresponding GAVs. For more detail about the complexity of these GAVs, and their forms and their justification please refer to [34-36].

Recently, a total of 58 GAVs from Gosh et al [39], and 101 GAVs from Zhu et al. [40] were reported to have very good agreements between the traditional group additivity estimations (GAE) against the GAVs calculated and optimized by these QM methods. To make more precise the GAE, the corresponding GAVs are required to be as accurate as possible.

Moreover, Gosh et al. [39] has calculated the heats of formation based on CCSD(T)-F12/cc-pVTZ-F12//B2PLYPD3/cc-pVTZ level of theory with an estimated 2σ uncertainties of ± 1.0 kcal/mol. The CCSD(T)-F12/cc-pVTZ-F12 method is a highly accurate computational method for determining the electronic structure of molecules. The CCSD(T) stands for Coupled-Cluster with Single and Double substitutions, and inclusion of a perturbative treatment for triples excitations. F12 denotes the use of the F12 correlation method, which is a variant of the traditional Coupled Cluster method that includes electron correlation effects beyond traditional CCSD. The cc-pVTZ-F12 basis set is a large and accurate basis set that is used to represent the molecular orbitals. The B2PLYPD3 is a density functional method for the calculation of non-covalent interactions. The cc-pVTZ basis set is an accurate basis set that is used to represent the molecular orbitals of the atoms in the molecule. Therefore, CCSD(T)-F12/cc-pVTZ-F12//B2PLYPD3/cc-pVTZ is a high level of theory that is able to accurately calculate the electronic structure of the molecule and the non-covalent interactions in order to determine the heats of formation with high accuracy.

Additionally, Zhu et al. [40], has estimated the structural and vibrational properties of the molecules using geometry optimizations, and vibrational frequency calculations conducted at the M06-2X/6-311++G(d,p) level of theory. The M06-X/6-311++G(d,p) level of theory is a computational method that combines the M06-X density functional method with the 6-311++G(d,p) basis set. This level of theory is considered to be a good balance between accuracy and computational

cost for geometry optimization and vibrational frequency calculations. It is also useful for large molecules and heavy atoms calculations.

These studies show that instead of calculating hundreds and hundreds of species with ab initio methods, which may be time-consuming and with high computational cost, to guarantee accuracy, it is possible to train the GA method to improve the estimations. In Chapter 3 of this thesis, THERM23 a paper in preparation, can be consulted for further information about how complex these GAVs can become, and for more details about the BGA method and its application when trained by ab initio GAVs.

References

- [1] U.S. Energy Information Administration, Annual Energy Outlook 2022 (AEO2022) with projections to 2050, (2022).
- [2] British Petroleum Company, BP statistical review of world energy. London: British Petroleum Co., (1981).
- [3] International Energy Agency, World Energy Outlook 2021, IEA, . Licence: Creative Commons Attribution CC BY-NC-SA 3.0 IGO, (2021).
- [4] P. Atkins, Atkins's the elements of physical chemistry, third ed., Oxford University Press, (2001).
- [5] P. Atkins, J. de Paula, Atkins' physical chemistry, seventh ed., Oxford University Press, (2002).
- [6] M.W. Zemansky, R.H. Dittman, Heat and thermodynamics: an intermediate book, seventh ed., McGraw-Hill, (1997).
- [7] J.C. Kotz, P.M. Treichel, J.R. Townsend, Chemistry and chemical reactivity, seventh ed., Thomson, (2009).
- [8] E.S. Swinbourne, Analysis of kinetic data: studies in modern chemistry, Nelson, (1971).
- [9] K.A. Holbrooke, M.J. Pilling, S.H. Robertson, Unimolecular reactions, John Wiley & Sons, Baffins Lane, Chichester, West Sussex PO19 1UD, England, (1996).
- [10] M.J. Pilling, I.W.M. Smith, Modern gas kinetics: theory, experiment and application, Blackwell Scientific Publications, (1987).
- [11] M.J. Pilling, P.W. Seakins, Reaction kinetics, Oxford University Press, Great Clarendon Street, Oxford OX2 6D. UK, (1995).
- [12] R.D. Levine, R.B. Bernstein, Molecular reaction dynamics and chemical reactivity, Oxford University Press, (1987).
- [13] R. Chang, Physical chemistry for the biosciences, University Science Books, U.S., Sausalito, United States, (2005).
- [14] J.H. Espenson, Chemical kinetics and reaction mechanisms, McGraw-Hill Book Company, New York, (1974).
- [15] S.W. Benson, J.H. Buss, Additivity rules for the estimation of molecular properties. Thermodynamic properties, J. Chem. Phys. 29 (1958) 546-572.
- [16] J.C. Kotz, P.M. Treichel, J.R. Townsend, and D.A. Treichel, Chemistry and chemical reactivity 10th Ed., Cengage Learning, Boston U.S.A. (2019).
- [17] W. Hemminger, and G. Hoehne, Calorimetry. Germany, (1984).
- [18] A. Navrotsky, Progress and New Directions in Calorimetry: A 2014 Perspective. J. Am. Ceram. Soc., (2014) 97[11] 3349–3359.

- [19] R.G. Parr, On the genesis of a theory, *Int. J. Quantum Chem.* (1990) 37 (4): 327–347.
- [20] R.A. Friesner, Ab initio quantum chemistry: Methodology and applications, *PNAS* vol. 102, no 19, (2005) 102 (19) 6648-6653.
- [21] F. Jensen, *Introduction to Computational Chemistry*, Chichester, England: John Wiley and Sons. (2007), 80-81.
- [22] R.A. Latour, Molecular simulation methods to investigate protein adsorption behavior at the atomic level, *Comprehensive Biomaterials*, Volume 3, (2011), 171-192.
- [23] C. Møller and M.S. Plesset, Note on an approximation treatment for many-electron systems, *Phys. Rev.* 46(1934), 618.
- [24] M. Ozboyaci, D.B. Kokh, S. Corni, and R.C. Wade, *Modeling and simulation of protein surface interactions: achievements and challenges*, Cambridge University Press, (2016).
- [25] C.J. Cramer, *Essentials of Computational Chemistry: Theories and Models*, 2nd Ed. Wiley, (2004).
- [26] J.W. Park, R. Al-Saadon, M.K. MacLeod, T. Shiozaki, and B. Vlaisavljevich, Multireference electron correlation methods: journeys along potential energy surfaces, *Chem. Rev.*, 120(2020), 13, 5878-5909.
- [27] J.C. Slater, A simplification of the Hartree-Fock method, *Phys. Rev.* 81 (1951) 385.
- [28] C. Møller and M.S. Plesset, Note on an approximation treatment for many-electron systems, *Phys. Rev.* 46(1934), 618.
- [29] A.C. Wahl, and G. Das, The multiconfiguration self-consistent field method. In: Schaefer, H.F. (eds) *Methods of Electronic Structure Theory. Modern Theoretical Chemistry*, vol 3(1977). Springer, Boston, MA. https://doi.org/10.1007/978-1-4757-0887-5_3.
- [30] C.J. Cramer, *Essentials of computational chemistry*, Chichester: John Wiley & Sons, Ltd. 191-232 (2002).
- [31] J.N. Murrell, S.F.A. Kettle, J.M. Tedder, *The chemical bond*, 2nd Ed. John Wiley & Sons (1985).
- [32] I.N. Levine, *Quantum chemistry*, 5th Ed. Prentice-Hall Inc., New York, (2000).
- [33] J.B. Foresman, and A. Frisch, *Exploring chemistry with electronic structure methods*, 2nd Ed. Gaussian Inc. (1993).
- [34] S.W. Benson, *Thermochemical kinetics*, Wiley (1976).
- [35] S.W. Benson, F. Cruickshank, D. Golden, G.R. Haugen, H. O'Neal, A. Rodgers, R. Shaw, R. Walsh, Additivity rules for the estimation of thermochemical properties, *Chem. Rev.* 69 (1969) 279-324.
- [36] S.W. Benson, *The foundations of chemical kinetics*, McGraw-Hill, New York (1960).
- [37] M. Liu, A.G. Dana, M.S. Johnson, M.J. Goldman, A. Jocher, A.M. Payne, C.A. Grambow, K. Han, N.W. Yee, E.J. Mazeau, K. Blondal, R.H. West, C.F. Goldsmith, W.H. Green, Reaction mechanism generator v3.0: advances in automatic mechanism generation, *J. Chem. Inf. Model.* 61 (2021) 2686-2696.
- [38] G.E. Moore, M.L. Renquist, G.S. Parks, Thermal data on organic compounds. XX. Modern combustion data for two methylnonanes, methyl ethyl ketone, thiophene and six cycloparaffins, *J. Am. Chem. Soc.*, 62 (1940) 1505-1507.

- [39] M.K. Ghosh, S.N. Elliott, K.P. Somers, S.J. Klippenstein, H.J. Curran, Group additivity values for the heat of formation of C₂–C₈ alkanes, alkyl hydroperoxides, and their radicals, *Combust. Flame* (2023), 112492.
- [40] S. Zhu, Z. Xiong, and C-W Zhou, An extensive theoretical study on the thermochemistry of aromatic compounds: from electronic structure to group additivity values, *Phys. Chem. Chem. Phys.* 24 (2022) 18582-18599.

Chapter 2: Tools for chemical kinetic modelling

Computational chemistry tools use available computing technology to solve the numerical problems related to thermodynamics and kinetics. These tools allow the automation and optimization of the processes involved in developing chemical kinetic mechanisms and are essential for fast and accurate simulations. The mechanisms are validated using experimental data as simulation targets. Thus, the main goal in developing reliable chemical kinetic mechanisms is to predict the fundamental combustion properties of fuels such as ignition delay times (IDTs), laminar burning velocities (LBVs), and speciation profiles (SP), to name a few. These properties can then be used to characterize the different types of fuels, and blends, for both safety and to optimize their efficiency and reduce combustion pollutant products.

The following sub-sections are intended to explain simply and succinctly how the codes work and several flowcharts are included to help in understanding them. All of the codes developed in this work are new or are adaptations of previous codes. The development itself has been carried out during the duration of my doctorate. This includes writing and automating them along with building a database. A detailed authorship is provided with each code. It is worth noting that all codes included here have been developed and written in python and use a third-party module Cantera [1-3] in order to use the proper solvers for every different type of simulation target.

2.1 Local automation of chemical kinetic simulations in python

To describe all of the codes developed in python [4] for use by local computers at the Combustion Chemistry Centre (C³) it is necessary to explain by the type of code, such as the type of reactor, and the type of analyses that the code performs. A total of twelve codes are presented. These codes relate to the type of reactor considered in this work including shock tubes (STs), rapid compression machines (RCMs), jet-stirred reactors (JSRs), flow reactor (FRs), and laminar burning velocities (LBVs). Together with these codes that have been developed to simulate a specific reactor, we find the *K&SS* subroutine which can control all of these codes as a unity and automate the process, this is explained in more detail in Section 2.1.2. Moreover, six of the python codes were developed for pre/post-processing analyses along with the main kinetic ones. Such analyses are Excel file to input file creator (*STcreatorTest*, *STcreatorTest*), pressure to volume converter (p2v), sensitivity analyses (brute force SA), flux analyses or reaction pathway (RP), and plotters in general.

Finally, as presented in Chapter 3, a work is in preparation that includes a python code to calculate the thermodynamic properties of fuels using the Benson group additivity method. This python code only requires a few dependencies to execute specific modules, such as NumPy, Pandas, Matplotlib, SciPy, SymPy, and Cython. It can be executed either on computers using either Windows or Linux operating systems. It has been developed to calculate either manually or automatically, and re-calculates thermodynamical properties including enthalpy, entropy and heat capacities with a valid Wilhoit extrapolation method in the temperature range 300–5000 K. Additionally, this code can plot the results and also generate the data in NASA polynomial format which is used ubiquitously in the simulation of combustion experiments. Below is a discussion of the large database created, updated, and managed for these projects and in general for every validation for every chemical kinetic mechanism that is commonly needed.

2.1.1 Database management

Before explaining the codes one by one, it is necessary to introduce the corresponding input files for each type of reactor. For this purpose, the C³ database is introduced, which contains experimental data in input file format from different types of reactors. These experimental data have been collected either in the C³ facilities or gathered from the literature. Each input file refers to the source of the experiments. C³ has four experimental facilities. It has two ST facilities, one for low-pressure measurements (LPST), and one for high-pressure measurements (HPST). It also has two RCM facilities, one the red RCM and the other the blue RCM, both equipped with a dual-piston system. For more information regarding the physical facilities available at C³, please refer to the literature [5-8].

For the special case of the C³ experimental data collected from ST and RCM, corresponding to Chapters 4-7 of this work, the data is usually gathered by the experimentalist performing the experiments in an excel file, as shown in Fig. A1 of appendix A.1. Once the excel file is properly completed, the experimentalist can then use a python code. This python code allows the experimentalist to generate an input file based on the information gathered in the corresponding excel file. The code that has been developed to manipulate excel files and convert them into input files work for both ST and RCM experiments. An example of these codes, named *STcreatorTest* and *RCMcreatorTest* respectively is presented in Fig. A2 of appendix A.1.

Moreover, for the RCM experimental data, a proper p2v python code will manipulate the experimental pressure traces recorded for non-reactive mixtures where O₂ is replaced by N₂ in the mixture and reduce the amount of data from millions of points to only 100 – 200 points using the minimum square error (MSE) method. Furthermore down-sampling is applied, and the mixture composition is also used to generate the volume-time profile input file which is used to simulate RCM facility effects in simulations, Fig. A3 of appendix A.1.

This database corresponds to the work presented in Chapters 3-6. This data was collected either at UG, at PCFC-RWTH Aachen University, or from available literature. The name IDT_C1 – C3 is used, this data was generated in a project sponsored by Shell Research Ltd. Hence, this IDT_C1 – C3 database was collected for ST and RCM only. The database contains a total of 99 ST input files with 1208 experimental points, and a total of 71 RCM input files with 926 experimental points. The entire C³ database also includes JSR and FR data, with a total of 811 ST input files with 9102 experimental ST points, a total of 386 RCM input files with 5472 experimental RCM points, a total of 110 JSR input files with 1439 experimental JSR points, and a total of 105 FR input files with 2053 experimental FR points. Table 2-1 shows the comparison between both databases, IDT_C1–C3 against C³ database. This comparison shows the number of input files and the number of total simulation points for ST and RCM reactors that a kineticist usually must perform to validate every model before its release.

Table 2-1. Comparison between IDT_C1–C3 database and the whole C³ database for ST and RCM input data. It shows how IDT_C1–C3 conforms to only ~12% of the total ST data, and ~18% of the total RCM data of the corresponding whole C³ database.

IDT_C1–C3		C ³ DATABASE		(ST _{C1–C3} *100)/ST _{database}	(RCM _{C1–C3} *100)/RCM _{database}
ST	RCM	ST	RCM	%	%
99	71	811	386	12.20	18.39
1208	926	9102	5472	13.27	16.92

Moreover, it is worth noting that before the development of these codes that will be presented in the next sub-section, the validation of a chemical kinetic mechanism used to take weeks. This time has been reduced considerably to a couple of days to hours depending on the size of the database and the mechanism used. Now that we have seen the format of the ST and RCM input files, we can introduce the corresponding input files for JSR and FR. As shown in Fig. A4 of appendix A.1, on the

left side, the JSR input files, and on the right side, the FR input file is presented. These input files are quite similar but with small differences. The most significant difference is in the way the experimental data is presented. In a JSR simulation the temperature, pressure and residence time are included, while in a FR usually only the time is given. However, for both JSR and FR simulations any species of interest is provided as species concentrations are dependent on temperature and/or time.

Finally, a sample LBV input file is presented in Fig. A5 of appendix A.1. This file should usually contain, not only the author information, but also a list of the corresponding experimental conditions including, pressure, temperature, equivalence ratio (ϕ), experimental LBV, and the mixture composition.

2.1.2 Chemical kinetic simulations in python

Now, that we know the input file formats we can introduce the corresponding python codes for each type of simulation. These codes already discussed (*STcreatorTest.py*, *RCMcreatorTest.py*, and *p2v_converter.py*) are included as part of the appendix A for a reader interested in exploring the coding lines. In Fig. A6 of appendix A.1, the content of the folder REACTORS is shown. This directory contains the corresponding python codes listed by reactor name; *ST.py*, *RCM.py*, *LBV.py*, *JSR.py*, and *FR.py*. These codes have a coding line size of 375 lines for *ST.py*, 450 lines in *RCM.py*, 427 for the *LBV.py* code, 1430 lines in the *JSR.py*, and 330 lines for the *FR.py* code. These code dependencies are similar to the code presented in Chapter 2, plus the addition of the module called Cantera.

To execute these codes and collect the desired simulated results we need a database, in this case, the database is located in “*C:\DKM\DATA*”, the corresponding mechanism to simulate with is in “*C:\DKM\MODELS*”, and the result will be stored in “*C:\DKM\OUTPUTDATA*”. In Fig. A7 of appendix A.1 are shown the corresponding directories for this example of database.

Hence, to run the simulations we have two options, either run them one by one or run in automatic mode with the *K&SS* subroutine. Here and now, they are run one by one, and thereafter a flowchart of *K&SS* automation and how it works is provided. Thus, to run these codes we need to generate corresponding .bat executable files. This can be done easily by opening any terminal in Windows, for our purpose we will use PowerShell. In PowerShell and located in the “*C:*” directory of our hard drive, we should run the following commands:

```
>python DirTools.py ST
```

```
>python DirTools.py RCM
>python DirTools.py LBV
>python DirTools.py JSR
>python DirTools.py FR
```

as shown in Fig. A8 of appendix A.1, the screen should display a résumé of the content of the DATA folder, this is the working path, the number of directories, the number of files found, and a list with the number of input files found for the ST, RCM, LBV, JSR, and FR simulations.

Furthermore, these instructions will generate four .bat files corresponding to each reactor as shown in Fig. A9 of appendix A.1. From bottom to top; tasksST4.bat, tasksST3.bat, tasksST2.bat, tasksST1.bat, tasksRCM4.bat, and so on for the rest. The format of these .bat files is shown in Fig A10 of appendix A.1.

Moreover, Fig. A11 of appendix A.1 presents the content of the “*OUTPUTDATA*” with all the simulated data. From left to right, the content of the folder “*DATABASE*” shows folders with the name of the different fuels that have been simulated. Thereafter, the *CH4* folder indicates that there is another level of data included which is sorted by type of reactor in the folder’s name. In the third position, the picture shows that inside each reactor folder there are folders with the name of the author, for example, “*PETERSEN*”. Finally, the last image shows the content of the author’s folder which is more folder, but this time named after the experimental condition that was simulated by the code.

Furthermore, in Fig. A12 of appendix A.1 the content of those folders with the experimental case as names for different reactors is shown. From the left to the right a ST output file with extension ST_IDT is included. Next is the RCM data is simulated with extension RCM_IDT and for the JSR the extension is txt and only for these cases the graph is generated automatically, and the last one for FR with extension PFR_EXP.

Also, in Fig. A13 of appendix A.1 the format of those output files is shown. In this case, only ST and RCM output files are presented. For the ST file we can see listed the initial pressure, initial temperature, the IDT in seconds, $1000/T$ in K, again the IDT but now in μs , followed by the mixture composition, etc.

The main difference with the RCM data is that an initial temperature and pressure needs to be provided in addition to the compressed gas temperature (T_C) and pressure (p_C), followed by the IDT measured in seconds using the pressure rise. Finally, in the case of the JSR, and FR output files

the species profiles are presented as a function of temperature, time, or both. For instance, the format of the output files for the JSR and FR are presented in Fig. A14 of appendix A.1. For JSR at constant time and in the function of temperature can be seen on the left side of Fig. A14 of appendix A.1, whereas for FR at constant temperature and in the function of time is shown on the right side of Fig. A14 of appendix A.1.

In addition, the *K&SS* subroutine is a collection of ST, RCM, JSR, FR, and LBV python codes controlled by the main file called TBD driver. This driver is in charge of administrating the resources to run automatically either one or all of the reactors simultaneously. The options are almost endless. However, the limitations will be set by the local computer capabilities. To benefit of the maximum capabilities of this subroutine it is recommended to use a computer superior to the average, with at least 8 virtual processors and 4 cores, 18 to 32 GB of RAM, and in the case of required plots, to prepare enough hard drive space to allocate the results along with the plots. The main flowchart of *K&SS* is shown in Fig. 2-1.

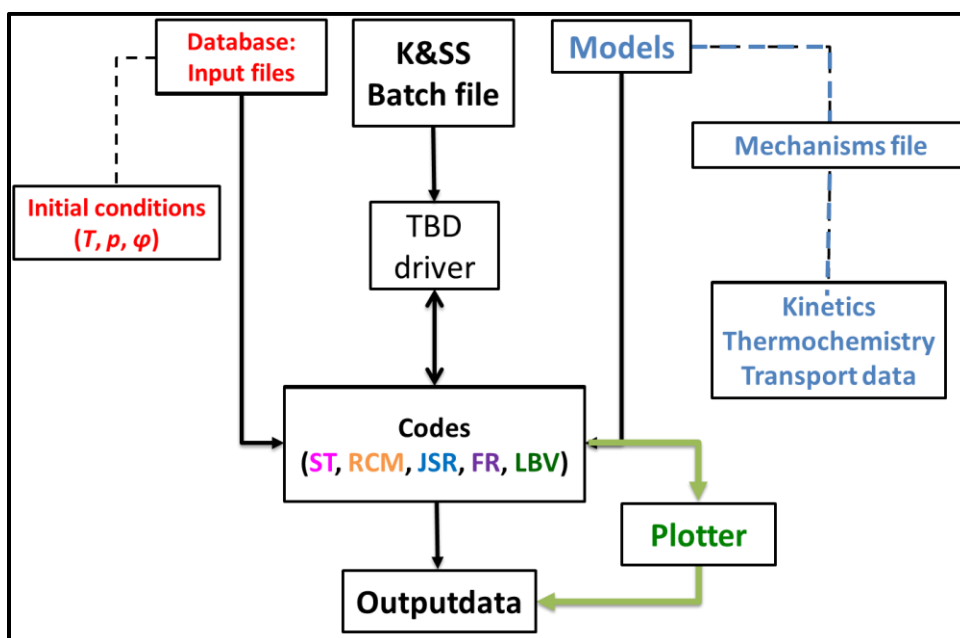


Figure 2-1. *K&SS* python subroutine flowchart showing the automation of the simulations of different types of reactors (ST, RCM, JSR, FR, LBV) for the validation of chemical kinetic mechanisms under development.

Using the *K&SS* through TBD will require the corresponding initial conditions for the experimental points to simulate using input files. Once TBD identifies and sorts the input files it will run either reactor by reactor, file by file, or simultaneously depending on the user's instructions. As

K&SS is generating simulated results the code itself starts generating plots also allocated in the same folder where the corresponding result is.

The brute force sensitivity analyses (SA), reaction paths (RP), and plotters, in general, are shown in Figs. A15–A17 of appendix A.1. In the case of the brute force SA code is used to identify the controlling chemistry both promoting and inhibiting reactivity in the system and thus their effect on IDT predictions, the definition of the sensitivity coefficient (S) is as follows:

$$S = \frac{\ln(\tau_+/\tau_-)}{\ln(k_+/k_-)} = \frac{\ln(\tau_+/\tau_-)}{\ln(2.0/0.5)} \quad (2.21)$$

this sensitivity coefficient is calculated for every reaction included in the chemical kinetic mechanism. It acts as a perturbation directly over the rate constant affecting the IDT (τ) in the pre-exponential factor in the Arrhenius equation. This coefficient S can be either positive or negative, a positive value means a reaction that inhibits reactivity giving longer IDTs and a negative coefficient means a reaction which promotes the reactivity, decreasing the IDTs.

The reaction paths (RP) code is useful to acquire a visual representation of the connecting reactions that form or deplete chemical species. As the brute force SA, the RP is a complementary tool to determine the chemical paths a species is following just before the ignition with a specific amount of fuel consumed. For our RPs the fuel consumption is fixed to 20% of the initial amount for the specific condition.

To finalize this sub-section, the plots generated by the plotters were developed to complete the codes that simulate the experimental data. There are two ways to generate this type of graph, either using these codes uniquely developed for that purpose or using the *K&SS* subroutine and asking to plot the results. Indeed, those plots generated by the plotter codes are nicer and are better formatted for formal documentation.

The last plot, Fig. A18 of appendix A.1, shows a LaTeX [9, 10] report in .pdf format that can be generated by the plotter codes at the end of the plotting process if the user indicates it. The code will compile and collect all of the plots generated in the database to organize them in a LaTeX file to convert later into .pdf format. The code has been adapted to work with output from either Cantera [1-3] or Chemkin [11].

2.2 Server automation of chemical kinetic simulations in python

The University of Galway (UG) has access to computing time for the KAY supercomputer located in Dublin. The KAY supercomputer belongs to the Irish Centre for High-End Computing (ICHEC) [12]. This server has a Unix/Linux Operative System (OS) environment connected through the shell interface either by Bourne Again Shell (BASH) or by C Shell (CSH). A BASH code automates all of the simulations using SLURM. SLURM is an open-source scalable cluster management and job scheduling system for large and small Linux clusters. The codes used to simulate the ST and RCM reactors and SA analyses have all been automated for the server. These codes have been already discussed in detail above, but it is important to consider that all of them are now linked to a SLURM code written in BASH SHELL for Unix/Linux Clusters.

This SLURM manager is used to generate proper and optimized control files and to submit the corresponding simulations automatically to the supercomputer. The KAY supercomputer cluster has four nodes available as a minimum setting, with each node corresponding to 40 processors which means that $40 \times 4 = 160$ different conditions can be simulated at the same time. Assuming for a reasonable size model taking 1 s per simulated point, running a target validation of all our C³ databases for all the reactors, a total of 7,696 experimental points for ST, RCM, JSR, and FR, it will take ~2.1 h to complete. On local computers this would take one day approximately, and with the old system before these codes, it would take approximately a week.

Along with this simple math, in Fig. 2-2 the flowchart corresponding to the KAY server and how this is connected to the SLURM manager is shown. First, the code will need input files specifying the initial conditions to be simulated. Secondly, a mechanism/model is required, this one should include the chemistry and thermodynamics files. It should also include the transport data if the user wants to simulate LBVs.

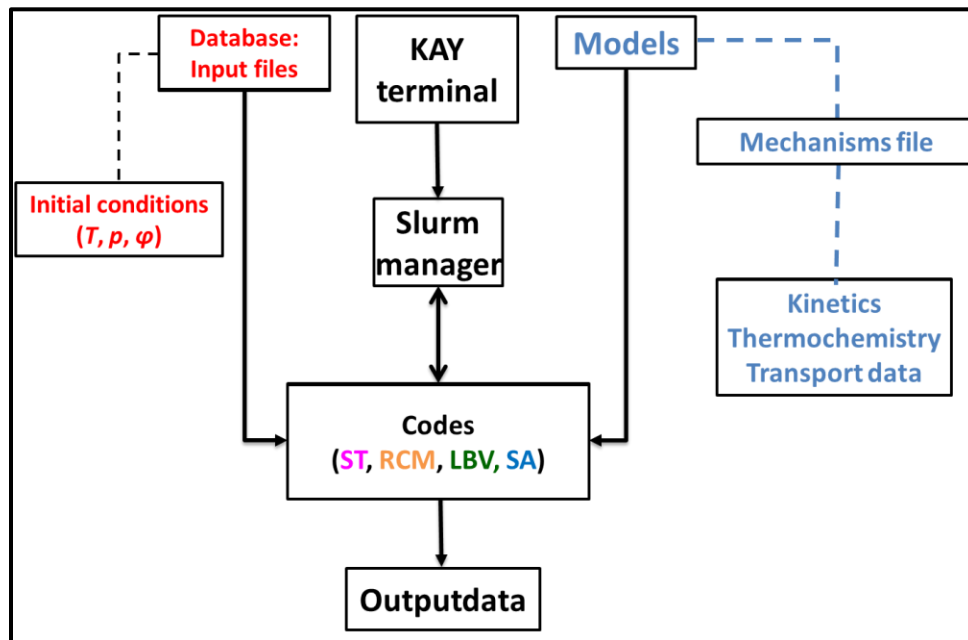


Figure 2-2. Python flowchart showing the automation of the simulations of different types of reactors (ST, RCM, LBV) and sensitivity analyses brute-force (SA) for the validation of chemical kinetic mechanisms under development.

Once these initial requirements are fulfilled, SLURM can gather the information that is needed to proceed to submit the jobs to the KAY cluster. After that, it is just a matter of time to collect the results in the “*OUTPUTDATA*” directory.

Due to the numerous codes that are required to run every experimental condition, generating adequate thermodynamic data, input file creation, output file data extraction, and file management comprise an arduous task for a kineticist. In this regard, a tools suite has therefore been developed to automate the development of chemical kinetic mechanisms which are used in C^3 , and by extension, in this Thesis. The codes are described in detail such that future members of C^3 can benefit from their efficiency and continue with their development and enhancement into the future. Also, the reactor codes (ST, RCM, LBV, FR, and JSR), codes for analyses (SA_bruteforce.py, RP.py), codes used for plotting, and the control code for Unix-Servers (DirTools.py) mentioned in this Thesis are included as part of the appendix A for future consultation.

References

[1] D.G. Goodwin, H.K. Moffat, R.L. Speth, Cantera: An object-oriented software toolkit for chemical kinetics, thermodynamics, and transport processes, Caltech, Pasadena, CA 124 (2009).

- [2] D.G. Goodwin, H.K. Moffat, R.L. Speth, Cantera: An object-oriented software toolkit for chemical kinetics, thermodynamics, and transport processes, version 2.2. 1, Cantera Developers, Warrenville, IL, (2017).
- [3] D.G. Goodwin, R.L. Speth, H.K. Moffat, B.W. Weber, Cantera: an object-oriented software toolkit for chemical kinetics, thermodynamics, and transport processes, <https://www.cantera.org>, (2018). doi:10.5281/zenodo.170284.
- [4] V. Rossum G, Drake F.L. Python 3 Reference Manual. Scotts Valley, CA: CreateSpace; (2009).
- [5] M. Baigmohammadi, V. Patel, S. Nagaraja, A. Ramalingam, S. Martinez, S. Panigrahy, A.A. El-Sabor Mohamed, K.P. Somers, U. Burke, K.A. Heufer, A. Pekalski, H.J. Curran, Comprehensive experimental and simulation study of the ignition delay time characteristics of binary blended methane, ethane, and ethylene over a wide range of temperature, pressure, equivalence ratio, and dilution, *Energy Fuels* 34 (7) (2020) 8808-8823.
- [6] L. Brett, J. Macnamara, P. Musch, J.M. Simmie, Brief communication: simulation of methane autoignition in a rapid compression machine with creviced pistons, *Combustion and Flame* 124 (2001) 326–329.
- [7] E.L. Petersen, M. Röhrig, D.F. Davidson, R.K. Hanson, C.T. Bowman, High-pressure methane oxidation behind reflected shock waves, *Symposium (International) on Combustion* 26 (1996) 799-806.
- [8] C. Lee, S. Vranckx, K.A. Heufer, S.V. Khomik, Y. Uygun, H. Olivier, R.X. Fernandez, On the chemical kinetics of ethanol oxidation: shock tube, rapid compression machine and detailed modeling study, *Z. Phys. Chem.* (2012), 226(1), 1-28.
- [9] A. Borbón, W.M. Flores, *LaTeX 2017*, 2016.
- [10] D. Kotz, *LaTeX and the Gnuplot plotting program*, (2006).
- [11] *Reaction-Design, CHEMKIN-PRO 18.2*, San Diego, 2013.
- [12] Irish Centre for High-End Computing (ICHEC) <https://www.ichec.ie/>.

Chapter 3: THERM23: A thermodynamic property estimator for gas phase species using the group additivity method

Publication in preparation.

Author Contributions

1) Sergio Martinez (University of Galway, Ireland)

Contribution: Python code developer, performed thermodynamic calculations, and manuscript preparation.

2) Manik Kumer Ghosh (University of Galway, Ireland)

Contribution: Provided optimized group values and reviewed the manuscript.

3) Henry J. Curran (University of Galway, Ireland)

Contribution: Managed the project, reviewed the project and manuscript throughout.

Abstract

The development of reliable chemical kinetic mechanisms relies on accurate thermodynamic data, rate constants and transport properties. To calculate accurate thermodynamic data for the species present in chemical kinetic mechanisms reliable methods are needed. In this regard, Benson's group additivity method has proven to be useful in calculating reasonably accurate data for a large number (sometimes thousands) of species. THERM23 is an open-source code written in Python and developed at the Combustion Chemistry Centre (C³). This software is designed to work with either Windows or Linux operating systems and can be used to calculate, modify and/or record thermodynamic parameters such as heat of formation (H_f^0), entropy (S^0) and heat capacities (C_p) of any combustion related species, i.e., hydrocarbons, oxygenated hydrocarbons, NO_x species, and associated to their radicals in NASA polynomial format with 14 coefficients. This data is compatible with kinetic modelling and fluid dynamics simulation software, including but not limited to CHEMKIN and Cantera. In addition, the Wilhoit extrapolation method is used to generate polynomials in the temperature range of 300 – 5000 K. This code preserves the classic parent molecule system for radical species employed in THERM. The corresponding group additivity values (GAVs) used in this software are determined from experimental and/or optimization methods and are available together with the software and are editable. THERM23 offers a traditional and an advanced way to calculate thermochemical properties and offers interactive, automatic, recalculation, and graphical options to the user in a user-friendly interface.

Keywords: THERM, thermochemistry, group additivity, NASA polynomials, python.

3.1 Introduction

Based on the Energy Outlook report 2022 [1] with projections out to 2050, global energy use will remain dependent on combustion. This is expected to be true for the production of electricity and heat, and energy use for transportation. This continued use of fossil fuels in producing harmful emissions of greenhouse gases (GHG) [1] and other species. To help with the reduction of such emissions, combustion researchers are developing reliable chemical kinetic mechanisms to improve fuel combustors, making them cleaner and more efficient. To accomplish this, it is essential to have accurate thermochemistry data, rate constants, and transport data. This thermochemical data can be obtained by experimentally, theoretical calculations or group additivity (GA) method. In practice, group additivity method, developed by Benson and co-workers [2-4], is widely used to estimate these

thermochemical properties including enthalpy of formation, entropy, and heat capacities as a function of temperature.

Benson's group additivity (GA) method has proven to be reliable for the estimation of thermodynamic properties [2-10]. The GA method considers thermodynamic properties to be the sum of individual contributions from each heavy atom or "group" comprising the species of interest. A group is defined as a polyvalent atom in a molecule together with all of its ligands and is denoted as $X-(A)_i(B)_j(C)_k(D)_l$ with X the central atom surrounded by i ligands A, j ligands B, etc. Each heavy atom contributes to the thermodynamic properties depending on its local environment, e.g., a sp^3 hybridized carbon atom bonded to another sp^3 hybridized carbon atom and three hydrogen atoms is labelled as a C/C/H3 group. Group additivity is referred to as a second order method because it not only takes into account the contributions from chemical bonds, but it also includes corrections such as gauche and 1,5 hydrogen atom interactions where appropriate. Different order methods such as zero-, first- and secondorder were discussed by Hoffman [11] and Reid [12].

Several programs have been developed based on Benson's GA method such as THERM [13, 14], CHETAH [15], THERGAS [16], NIST structures and properties [17] and RMG [18]. In this work we present an open-source code written in Python named as THERM23 that can emulate THERM developed by Ritter and Bozzelli [13, 14]. However, THERM23 does not pretend to compete with these codes, but offers additional functionality based on the GA method. THERM is an executable software that calculates thermodynamic properties using Benson's GA method [2-4], and it requires a third-party program called DOSBox to emulate a DOS environment to run properly. By contrast, THERM23 does not need any other dependencies than those contained in the Python language, including numpy, scipy, and pandas. The complete list of dependencies is discussed in Section 2.3. We have retained most of the features already present in THERM. These include the manual input options, the re-calculation option, an interpreter to fit and obtain NASA polynomials from .LST files, and the output file formats including the .DOC, .DAT, and .LST files. Finally, the python source code is made available and is fully editable so that a user can either extend or improve upon the capabilities of the software.

THERM23 is designed to offer a more intuitive interface with various options to efficiently calculate thermochemical properties. It also allows the user to plot the results for easier interpretation and analysis of the data. The software can be used manually or automatically by processing pre-prepared input files or multiple input files. Additionally, users can input the InChI string of the

species, and THERM23 will return the corresponding GAVs, facilitating the estimation of thermodynamic properties. In the following section, further instructions on how to use THERM23, including tables featuring newly optimized GAVs and software-generated documentation, will be provided. The purpose of THERM23 is not to compete with other online software, but rather to complement them with multi-functional capabilities, automation, and plotting. The code includes many optimized groups from recent literature studies [19, 20].

The thermochemistry of a radical species is calculated based on the thermochemistry of the parent molecule by adding the bond dissociation (BD) group, called the hydrogen bond increment (HBI) approach which is implemented in THERM [13, 14], originally proposed by Lay et al. [21]. Therefore, THERM is not able to calculate the thermochemistry of a radical species as long as the thermochemistry of the corresponding parent molecule is not stored in the system. Very recently, Ghosh et al. [19] derived a set of 58 GAV terms from an extensive and accurate database of 192 *ab initio* thermochemical values [22]. Among the 58 GAV terms, 40 are refinements of previously reported and 18 are newly developed. These new GAV terms are mainly non-next-neighbour interactions (NNI) and β -corrections which are mostly present in the radicals rather than in parent molecules. As THERM calculate the thermochemistry of radical species from their parents, it cannot capture these additional corrections during the calculations which are present only in the radicals but not in their parents. Therefore, this work also aims to calculate the thermochemistry of radical species either independently or from the parent by adding/removing/modifying groups.

3.2 Overview of THERM23

This software aims to generate reasonably accurate (≤ 2 kcal mol⁻¹ in the heat of formation for relatively small species: $\leq C_9$) thermochemical properties for large numbers of species in a quick and easy way. The code provides an output file which contains enthalpy of formation (H_f^0), entropy (S^0) and heat capacities (C_p) at 300 – 2500 K. In addition, it provides an output file of 14 NASA polynomial coefficients which is compatible with kinetic modeling and fluid dynamics simulation software, including CHEMKIN [23] and Cantera [24-26]. It includes a plotter to better interpret the values calculated. At first glance, the functionality included in THERM23 is very similar to other traditional software developed to calculate thermodynamic properties. However, THERM23 offers more than the traditional manual input option to calculate the properties based on the input typed by

the user. The following discussion is intended to explain the functionality of THERM23. Tables 3-1 – 3-4 explicitly provide the new GAVs that are used in this software.

3.2.1 GAVs notation

In THERM23, we maintain the use of the group additivity value (GAV) notation established in THERM [13]. To gain a better understanding of this notation, readers are advised to consult Benson et al. [2-4] and Ritter and Bozzelli [13, 14]. To demonstrate the GAV notation, we have included a range of species, ranging from those that can be calculated using simple groups to those that require more complex corrections, such as radical (HBI/ β) or GAUSS/NNI/OI group corrections. To further illustrate, we have provided three examples of Benson's notation and its equivalent in THERM/THERM23. Ethane (C_2H_6) has two methyl groups, and thus two heavy atoms each with the same local environment, namely an sp^3 hybridized carbon atom bonded to one other carbon atom and three hydrogen atoms, which are represented by the C/C/H3 group in THERM [13] and THERM23. Similar to ethane, propane (C_3H_8) has two terminal methyl groups, and one methylene group which is an sp^3 hybridized carbon atom bonded to two sp^3 hybridized carbon atoms and two hydrogen atoms, with that group represented by C/C2/H2 in both THERM [13] and THERM23. Thus, two different GAVs are required for propane, namely $2 \times C/C/H3$ groups and $1 \times C/C2/H2$ group. Furthermore, phenol (C_6H_5OH) has a total of seven groups, five are benzene ring carbon atoms bonded to a hydrogen atom, namely $5 \times CB/H$, one benzene ring carbon atom bonded to an oxygen atom, $1 \times CB/O$, and one oxygen atom bonded to a benzene ring carbon atom and a hydrogen atom, $1 \times O/CB/H$. Moreover, in the case of a radical species, e.g., phenoxy radical ($C_6H_5\dot{O}$), one must first estimate the thermochemistry of the parent phenol molecule and then calculate the radical based on this parent considering the hydrogen bond dissociation (HBD) energy. Thus, to estimate a phenoxy radical we include $5 \times CB/H$, $1 \times CB/O$, $1 \times O/CB/H$, and $1 \times PHENOXY$, this procedure is required only in interactive option and is explained in Section 2.3. It is crucial to keep in mind that THERM can only estimate the thermochemistry of radical species based on their parent molecule, similar to THERM23 in its interactive mode. However, THERM23 offers an advantage over THERM in that it doesn't require the calculation of the parent molecule for estimating radical species in its automatic/re-calculation option. This difference is thoroughly explained in the manual provided as supplementary material (SM).

3.2.2 Updated GAVs

In this work, we present a collection of new GAVs from the literature and provide them as part of the THERM23 software. These GAVs are allocated in group files with the extension ‘grp’ which comes along with the code. Further information about these group files is provided in Section 2.1 of the supplementary material. Tables 3-1 – 3-4 comprise all of the new GAVs for stable non-oxygenated species (HC.grp), stable oxygenated species (HCO.grp), bond dissociation groups (BD.grp), and correction groups (INT.grp), respectively. For all of the remaining GAVs that are not mentioned here, a discussion of their origin is included in Ritter and Bozzelli [13].

Table 3-1. Optimized GAVs for the enthalpies of formation, H_f^0 (kcal mol⁻¹); entropies, S^0 (cal K⁻¹ mol⁻¹) and heat capacities, C_p (cal K⁻¹ mol⁻¹) of stable non-oxygenated species.

Type of GAVs: stable non-oxygenated species									
Source file: HC.grp									
Group ID	H_f^0	S^0	C_p						
			300	400	500	600	800	1000	1500
^a C/C/H3	-10.16	30.28	6.01	7.68	9.24	10.51	12.69	14.45	17.28
^a C/C2/H2	-4.91	9.76	5.63	7.05	8.38	9.56	11.35	12.60	14.47
^a C/C3/H	-1.68	-11.98	5.28	7.03	8.41	9.59	10.95	11.52	12.03
^a C/C4	0.14	-33.15	4.38	6.16	7.53	8.71	9.76	9.85	9.37
^b CB/H	3.30	11.53	3.24	4.44	5.46	6.30	7.54	8.41	9.73
^b C/CB/H3	-10.15	30.13	5.86	7.57	9.35	10.96	12.86	14.48	16.85
^b C/CB/C/H2	-5.11	9.56	5.24	6.81	8.41	9.78	11.09	12.21	13.71
^b C/C2/CB/H	-1.70	-11.73	5.04	6.60	7.94	8.93	9.56	10.07	10.63
^b CD/CB/H	7.27	6.27	3.20	4.77	6.21	7.39	8.31	9.03	9.95
^b CD/C/CB	10.07	-17.33	4.28	6.02	7.41	8.44	9.13	9.65	10.19
^b CT/CB	26.93	5.12	2.42	3.31	4.07	4.63	4.89	5.13	5.41
^b C/CB/CD/H2	-5.08	12.64	3.88	5.07	6.30	7.41	8.31	9.15	10.21
^b C/C/CB/CD/H	-1.39	-9.16	3.97	4.77	5.67	6.48	6.80	7.09	7.21
^b C/CB/CT/H2	-3.57	9.43	4.66	6.49	8.20	9.63	11.02	12.22	12.81
^b C/C/CB/CT/H	-0.37	-12.16	5.22	6.88	8.19	9.16	9.76	10.27	9.81
^b C/CB/CD2/H	-0.80	-2.38	4.12	4.20	4.32	4.53	4.18	4.08	3.70
^b C/CB/CD/CT/H	0.46	-9.05	3.35	4.67	5.74	6.56	6.76	7.07	6.23
^b C/CB/CT2/H	5.40	-11.37	3.48	5.54	7.16	8.38	9.22	9.95	8.75
^b CD/CB/CD	9.41	-14.09	3.86	4.63	5.36	5.99	6.17	6.43	6.61
^b CD/CB/CT	8.81	-14.22	2.69	3.77	5.42	5.18	5.64	6.07	6.37
^b CB/CB	4.57	-9.21	3.47	4.04	4.69	5.23	5.53	5.75	5.70

^a Ghosh et al. [19], ^b Zhu et al. [20]

Table 3-2. Optimized GAVs for the enthalpies of formation, H_f^0 (kcal mol⁻¹); entropies, S^0 (cal K⁻¹ mol⁻¹) and heat capacities, C_p (cal K⁻¹ mol⁻¹) of stable oxygenated species.

Type of GAVs: stable oxygenated species									
Source file: HCO.grp									
Group ID	H_f^0	S^0	C_p						
			300	400	500	600	800	1000	1500
^a C/H3/OO	-9.01	29.65	7.31	8.53	9.67	10.65	12.22	13.39	15.24

^a C/C/H2/OO	-8.23	6.67	7.34	8.40	9.41	10.23	11.56	12.49	13.84
^a C/C2/H/OO	-6.97	-15.13	7.11	8.38	9.23	9.98	10.96	11.64	12.44
^a C/C3/OO	-6.91	-34.62	7.13	8.40	9.40	10.16	10.82	11.02	11.13
^a OO/ME/H	-21.38	37.48	7.31	8.53	9.67	10.65	12.22	13.39	15.24
^a OO/CP/H	-20.49	39.81	7.34	8.40	9.41	10.23	11.56	12.49	13.84
^a OO/CS/H	-19.74	40.43	7.11	8.38	9.23	9.98	10.96	11.64	12.44
^a OO/CT/H	-19.02	38.54	7.13	8.40	9.40	10.16	10.82	11.02	11.13
^b O/CB/H	-37.54	29.12	4.70	4.69	4.97	5.43	5.83	6.34	6.70
^b O/CB/O	0.58	11.04	2.60	2.22	2.33	2.62	3.03	3.39	3.26
^b O/CB/C	-22.73	8.19	3.13	2.80	2.88	3.21	3.29	3.54	3.30
^b O/CB/CD	-25.73	59.61	7.36	8.36	9.97	11.84	14.40	16.62	19.54
^b O/CB/CT	-17.92	10.00	2.43	2.19	2.36	2.26	2.84	3.32	0.00
^b O/CB/CO	-36.78	7.06	2.50	2.89	3.37	3.79	3.82	3.85	3.18
^b CO/CB/H	-32.64	33.20	7.23	8.30	9.40	10.49	11.84	12.66	0.00
^b CO/CB/O	-36.39	13.72	6.92	7.61	8.45	9.43	10.50	11.22	0.00
^b CO/CB/C	-33.35	13.02	6.68	7.49	8.28	9.24	10.00	10.35	0.00
^b CO/CB/CD	-32.18	11.20	1.83	2.42	3.02	3.62	3.94	4.03	0.00
^b C/CB/O/H2	-6.63	7.69	6.19	7.94	9.40	10.47	11.21	11.96	12.25
^b C/CB/C/H/O	-6.45	-14.47	7.29	8.80	9.76	10.27	10.16	10.15	9.35
^b C/CB/C2/O	-5.34	-36.11	5.78	7.72	8.92	9.44	8.76	8.22	6.39
^b C/CB/CO/O/H	-6.46	-19.09	6.31	9.54	11.93	13.21	13.17	12.66	24.70
^b C/CB/CO/H2	-4.82	9.70	5.02	6.76	8.35	9.50	10.73	11.71	27.30
^b C/CB/CO/H/C	-1.85	-13.61	7.23	8.49	9.17	9.43	9.64	9.81	24.33
^b C/CB/CO/CD/H	-0.52	-10.83	6.25	6.98	7.39	7.49	7.13	6.97	20.91
^b C/CB/CO/CT/H	1.28	-13.47	6.68	8.29	9.33	9.83	9.99	10.16	23.58
^b CD/CO/CB	10.43	-14.86	3.18	4.10	5.06	5.84	6.20	6.66	0.00
^b C/OO/CB/H2	-6.96	7.06	4.79	5.63	7.30	8.20	9.55	10.60	0.00
^b C/OO/CB/C/H	-6.76	-15.70	6.09	6.59	7.84	8.28	8.72	9.00	0.00
^b C/OO/CB/C2	-5.51	-38.46	6.73	7.64	8.69	8.64	8.10	7.54	0.00

^a Ghosh et al. [19], ^b Zhu et al. [20]

Table 3-3. Optimized GAVs for the enthalpies of formation, H_f^0 (kcal mol⁻¹); entropies, S^0 (cal K⁻¹ mol⁻¹) and heat capacities, C_p (cal K⁻¹ mol⁻¹) of bond dissociation groups.

Type of GAVs: bond dissociation groups									
Source file: BD.grp									
Group ID	H_f^0	S^0	C_p						
			300	400	500	600	800	1000	1500
^a P	101.00	2.10	-0.54	-0.83	-1.40	-1.90	-2.70	-3.36	-4.57
^a S	98.28	3.14	-1.30	-1.80	-2.33	-2.76	-3.43	-3.96	-4.82
^a T	96.51	9.89	-0.92	-3.23	-4.77	-5.24	-5.91	-6.52	-6.67
^a P/QOOH	100.46	0.59	0.67	0.01	-0.46	-0.89	-2.00	-2.96	-4.40
^a S/QOOH	98.20	1.86	0.34	-0.99	-1.32	-1.70	-2.64	-4.08	-5.23
^a T/QOOH	95.12	4.76	-0.03	-2.32	-2.62	-3.56	-4.18	-5.80	-5.91
^a C2H5	101.10	2.16	-0.17	-0.57	-1.27	-1.66	-2.42	-3.14	-4.29
^a IC4H9	101.81	2.94	-0.20	-1.08	-1.94	-2.52	-3.44	-4.06	-4.86
^a TC4H9	96.68	7.48	-1.35	-3.18	-4.27	-4.73	-5.13	-5.26	-5.42
^a NEO-C5	102.71	0.58	-0.18	-0.31	-1.16	-1.79	-2.83	-3.64	-4.69
^a CC.C	98.15	4.51	-1.22	-2.09	-2.71	-2.99	-3.47	-3.90	-4.71
^a CJCOOH	103.75	2.99	-0.78	-1.20	-1.75	-2.13	-3.09	-3.83	-4.85
^a C2JCOOH	102.71	1.27	1.39	0.17	-0.52	-1.00	-2.16	-3.21	-4.48
^a C3JCOOH	103.22	2.88	1.43	0.56	-0.17	-0.85	-1.04	-1.98	-3.90
^a CCJCOOH	101.21	6.60	-0.71	-1.31	-1.91	-2.35	-3.23	-3.86	-4.69
^a CCCJCOOH	101.91	2.77	2.68	1.03	-0.07	-0.71	-1.36	-1.86	-4.21

^a C2CJCOOH	99.66	9.31	-0.88	-2.34	-3.37	-4.29	-5.36	-5.85	-5.96
^a MEPEROX	85.45	-0.47	-2.59	-2.93	-3.13	-3.26	-3.48	-3.69	-4.12
^a ALPEROX/P	85.16	-0.12	-2.98	-3.14	-3.43	-3.21	-3.74	-4.18	-4.72
^a ALPEROX/S	84.45	-0.12	-2.41	-2.99	-3.43	-3.46	-3.64	-4.11	-4.59
^a ALPEROX/T	84.03	-1.78	-1.89	-2.50	-3.27	-3.50	-4.10	-4.45	-4.93
^b DSUALLYLT	79.31	-1.20	-1.19	-0.90	-1.00	-1.25	-1.77	-2.32	-3.48
^b TSUALLYLT	73.36	-6.85	-0.34	0.36	0.73	0.74	-0.08	-0.92	-2.69
^b BENZYL P	90.42	-1.62	1.08	0.93	0.44	-0.14	-1.13	-1.93	-3.24
^b C*CCJOH	83.62	-2.20	0.48	0.41	0.11	-0.30	-1.20	-1.92	-3.16
^b BENZYL S	87.95	-0.69	-0.20	-0.49	-0.91	-1.32	-1.94	-2.49	-3.52
^b BENZYL T	87.41	1.75	-1.36	-2.00	-2.41	-2.68	-3.03	-3.35	-4.08
^b DSUALLYLS	78.81	-4.29	0.23	0.65	0.78	0.67	-0.04	-0.80	-2.44
^b PHI	113.47	1.09	-0.50	-1.08	-1.67	-2.19	-2.94	-3.53	-4.48
^b PHENOXY	87.85	-0.98	-1.81	-2.26	-2.54	-2.71	-2.93	-3.14	-3.66

^a Ghosh et al. [19], ^b Zhu et al. [20]

Table 3-4. Optimized GAVs for the enthalpies of formation, H_f^0 (kcal mol⁻¹); entropies, S^0 (cal K⁻¹ mol⁻¹) and heat capacities, C_p (cal K⁻¹ mol⁻¹) of correction groups.

Type of GAVs: correction groups									
Source file: INT.grp									
Group ID	H_f^0	S^0	C_p						
			300	400	500	600	800	1000	1500
^a P/BETA	0.45	0.20	0.34	0.23	0.19	0.16	0.10	0.02	0.01
^a S/BETA	0.31	3.14	-0.10	-0.08	-0.06	-0.04	-0.02	-0.02	-0.02
^a T/BETA	0.41	-2.23	-0.44	-0.15	0.11	0.10	0.21	0.25	0.31
^a P/QOOH/C-BETA	0.70	0.85	-0.02	-0.03	-0.04	-0.05	-0.10	-0.16	-0.08
^a S/QOOH/C-BETA	0.13	1.06	-0.46	-0.09	0.00	0.00	0.05	0.20	0.25
^a S/QOOH/O-BETA	2.38	1.01	0.65	0.55	0.24	0.10	0.09	0.19	0.21
^a T/QOOH/C-BETA	0.67	1.47	-0.05	-0.04	-0.03	-0.01	0.11	0.20	0.17
^a T/QOOH/O-BETA	3.02	0.54	0.00	0.06	0.08	0.10	0.12	0.17	0.22
^a AG	0.82	-1.11	0.15	0.10	0.03	-0.02	-0.10	-0.13	-0.05
^a RG1	0.40	0.02	-0.11	-0.16	-0.21	-0.24	-0.28	-0.20	-0.03
^a RG2	0.29	-0.89	0.08	-0.02	-0.20	-0.51	-0.72	-0.57	-0.26
^a G/COOH	1.21	-1.15	0.72	0.67	0.65	0.64	0.63	0.61	0.57
^a RG1/COOH	1.40	-0.78	0.88	0.52	0.24	0.18	0.13	0.06	0.01
^a RG2/COOH	0.74	-0.43	-0.50	-0.40	-0.31	-0.26	-0.22	-0.20	-0.12
^a G/OOH	0.65	-0.04	0.74	0.55	0.38	0.25	0.07	-0.03	-0.07
^a RG1/OOH	-0.96	-1.52	-0.38	-0.25	-0.16	-0.09	-0.06	-0.04	-0.08
^a RG2/OOH	0.80	-0.39	0.70	0.50	0.20	0.10	0.10	0.11	0.12
^a G/OOJ	0.43	-0.72	0.42	0.38	0.28	0.21	0.14	0.16	0.10
^a G/OH	-0.12	-0.94	0.03	0.03	0.02	0.02	0.02	0.01	0.01
^a RG2/OH	-0.15	-1.05	0.25	0.24	0.23	0.15	0.09	0.03	0.02
^a G/OJ	-0.09	-0.11	0.08	0.06	0.04	0.05	0.07	0.11	0.19
^a H/REPEL/15	1.47	-0.58	-0.23	-0.21	-0.08	0.12	0.51	0.74	0.69
^a H/15/1J	0.92	-1.44	0.74	0.87	1.03	1.19	1.44	1.45	0.90
^a H/15/3J	-0.21	-1.87	-0.28	0.22	0.42	0.75	1.02	1.09	0.76
^a H/15/4J	-0.01	-5.56	2.66	2.42	1.95	1.4	0.65	0.15	-0.27

^a Ghosh et al. [19]

3.2.3 Estimation of group additivity values

The standard enthalpy of formation and entropy at 298.15 K and the heat capacities at a set of discrete temperatures (300–2500 K) are calculated based on group additivity values. For a species I , the thermochemical species values φ_i ($\varphi_i = \Delta H_{f,i}^{298}, S_{int,i}^{298}, C_{p,i}^T$) are thus determined on the values ψ_i of the underlying groups ($\psi_j = \Delta H_{f,j}^{298}, S_j^{298}, C_{p,j}^T$) as

$$\varphi_i(\psi) = \sum_{j=1}^m a_{ij} \psi_j \quad (1)$$

where a_{ij} is the number of groups j in species i and $S_{int,i}^{298}$ is the intrinsic standard entropy [27]. The standard entropy is influenced by molecular symmetry and optical isomerism, which are non-local effects. Therefore, the standard entropy is calculated from the intrinsic-symmetry dependent entropy, $S_{int,i}^{298}$ and symmetry and optical isomerism effects also need to be considered separately.

$$S_i^{298} = S_{int,i}^{298} - R \ln(\sigma_i / n_{OI,i}) \quad (2)$$

where $n_{OI,i}$ is the number of optical isomers of species i . The contribution of optical isomer(s) is included with the addition of an entropy group value of $R \times \ln(2)$ for every chiral centre in the species which is already implemented in THERM as an ‘‘OI’’ group. Therefore, the OI group has a fixed value and is not included in the optimization. σ_i is the global symmetry number, i.e., the product of the internal (σ_{int}) and external (σ_{ext}) symmetry numbers:

$$\sigma_i = \left(\prod_k \sigma_{int,k} \right) \sigma_{ext} \quad (3)$$

The thermochemistry of a radical is calculated using separate groups for radical-centred and radical-adjacent atoms instead of using the groups from the parent molecule [4]. Alternatively, Lay et al. [21] proposed a method called the hydrogen bond increment (HBI) approach which is implemented in THERM [13, 28]. This approach does not work when new corrections, that are not required to represent the parent, are introduced for radicals. Therefore, we used a modified HBI approach which is implemented in THERM23. The following equation is used in the determination of the heat of formation of a radical species:

$$\begin{aligned}
\Delta H_{f,i}^{298}(\text{radical}) &= \Delta H_{f,i}^{298}(\text{parent}) + \Delta H_{f,i}^{298}(\text{BD}) - \Delta H_f^{298}(\dot{H}) \\
&+ \left(\Delta H_{f,i}^{298}(CG_{\text{radical}}) - \Delta H_{f,i}^{298}(CG_{\text{parent}}) \right) \quad (4)
\end{aligned}$$

where CG_{parent} and CG_{radical} are the group corrections present in the parent and radical species, respectively. The heat of formation of hydrogen atom, $H_f^{298}(\dot{H}) = 52.01 \text{ kcal mol}^{-1}$ (at 298.15 K) is used in this work [29]. The following equation is used in the determination of the heat capacities of a radical species:

$$\begin{aligned}
C_{p,i}^T(\text{radical}) &= C_{p,i}^T(\text{parent}) + C_{p,i}^T(\text{BD}) \\
&+ \left(C_{p,i}^T(CG_{\text{radical}}) - C_{p,i}^T(CG_{\text{parent}}) \right) \quad (5)
\end{aligned}$$

Heat capacities are determined over a wide range of temperature from 300 K to infinity. The heat capacity at “infinite” temperature is approximated in terms of the vibrations and torsions of the molecule as:

$$C_p(\infty) = (3N - 2 - n/2)R \quad (6)$$

where N is the number of atoms and n is the number of rotors in the species. Since entropy is influenced by molecular symmetry and optical isomerism, the following equation is used in the determination of the entropy of a radical species:

$$\begin{aligned}
S_i^{298}(\text{radical}) &= S_{\text{int},i}^{298}(\text{parent}) + S_i^{298}(\text{BD}) - R \ln(\sigma_i^{\text{radical}} / \sigma_i^{\text{parent}}) \\
&- R \ln(n_{\text{OI},i}^{\text{parent}} / n_{\text{OI},i}^{\text{radical}}) + \left(S_i^{298}(CG_{\text{radical}}) - S_i^{298}(CG_{\text{parent}}) \right) \quad (7)
\end{aligned}$$

3.2.4 Operation procedure of THERM23

THERM23 is written in Python language and so Python is needed to execute and run the code. The ‘THERM23’ folder contains the source code and other folders, and the files can be placed in any directory on user’s computer. A user needs to ensure that the numpy, matplotlib, pandas, scipy, sympy and cython modules are installed in the local python environment. Those who are not familiar with programming languages and/or installation of software please refer to the THERM23 manual which is included with the code and is available as SM. THERM23 comes with a total of five different options, three of which calculate thermochemical properties, the fourth one is used to plot results, and the fifth one for fitting the thermochemistry data to NASA polynomials. Figure 3-1 presents the “Main menu:” in a screenshot of the main user interface. *Option 1* runs the code in interactive mode

where the user can type each parameter needed to calculate the thermochemistry of a specie. *Option 2* enables the user to run the code automatically performing calculations based on a pre-existing .INP files. *Option 3* enables the user to re-run their own .DOC/.RERUN files through the software if/when group values are updated. *Option 4* permits the user to graphically plot the thermochemical data from a .DAT file(s) or compare two or more different sources of thermochemical data on the same graph. Finally, *Option 5* takes the data provided from any .LST file and generates a corresponding .DAT file. In this work we will focus our attention on the most important of these output files, the .DOC, and .DAT files. A more detailed explanation of the options and content of the other output files can be found in the THERM23 manual provided with the code in SM.

To better understand how THERM23 works, we have added a simple flowchart depicting how the thermochemical properties and corrections are applied, as shown in Fig. 3-2. The code first prompts the user to enter the species name and chemical formula. It then identifies if the species is a stable molecule or a radical. If the species is a stable molecule, then it progresses to apply ring/NNI/OI corrections before applying a symmetry correction leading to the final estimation of the thermodynamic parameters. If the species entered is a radical, a hydrogen bond dissociation energy (HBD), and a β -correction is applied, if needed. The code then proceeds in the same way as per a stable species in applying ring/gauche and symmetry corrections to generate the thermochemistry from 300 – 1500 K. Additionally, once the code has the values for 300 – 1500 K it can extrapolate using the Wilhoit function from 1000 – 5000 K. The calculated data can then be saved in either .DOC or .LST file format. Finally, the code checks if the previous specie thermochemistry calculated was the last one to calculate, otherwise start over again the cycle with the next specie provided. All the parameters in the code required for the calculations can be provided by the user manually or through an input file.

```

C:\WINDOWS\system32\cmd.exe
C:\Users\Sergio\Desktop\FILES_02-01-2023\Work_04-11-2022\Corrections_2022-THESIS_SM\24_10_2022_THERM22\WINDOWS
THERM23>python Therm23.py
-----
                        Welcome
                        to
                        THERM23
-----
                A Thermodynamic Property Estimator for Gas Phase Hydrocarbon Radicals and
                Molecules Based on Benson's Group Additivity Method
-----
> Version of this software: THERM23
> Combustion Chemistry Centre (C3)
> National University of Ireland Galway (NUIG), IE
> Sergio Martinez
> Prof. Henry Curran
> 11/01/2023
> s.martinez3@nuigalway.ie; sergioesmartinez@gmail.com
> henry.curran@nuigalway.ie
-----
Directory for output files:           '\THERM23\OutputsDir\' already exists!
Reading GAVs from:                   '\THERM23\GroupsDir\' directory folder
-----
There are 8 file(s) that content GAVs in such directory folder
The next is the list of file(s) with valid GAVs:
BD.grp - CDOT.grp - CLC.grp - CYCH.grp - HC.grp - HCN.grp - HCO.grp - INT.grp
-----
Type 'END/end or quit/Q/q' to exit this program at any time
-----
Main menu:
1.- Interactive                       (User needs to type all inputs)
2.- Automatic                         (The code uses THERM23.inp/any *.inp file as input)
3.- Re-calculate                      (The code uses rerun/DOC files to recalculate properties)
4.- Thermo Plotter                   (H, S and Cp are plotted on single or multiple graphs)
5.- Thermo fitter                     (H, S and Cp are fitted and saved in a dat file)
-----
Type an option number:

```

Figure 3-1. Screenshot of the five different options available in THERM23 to calculate thermochemical properties and graphical representations. Option 1 – interactive mode; Option 1 – automatic mode; Option 3 – re-calculate mode; Option 4 – thermo plotter; Option 5 – thermo fitter.

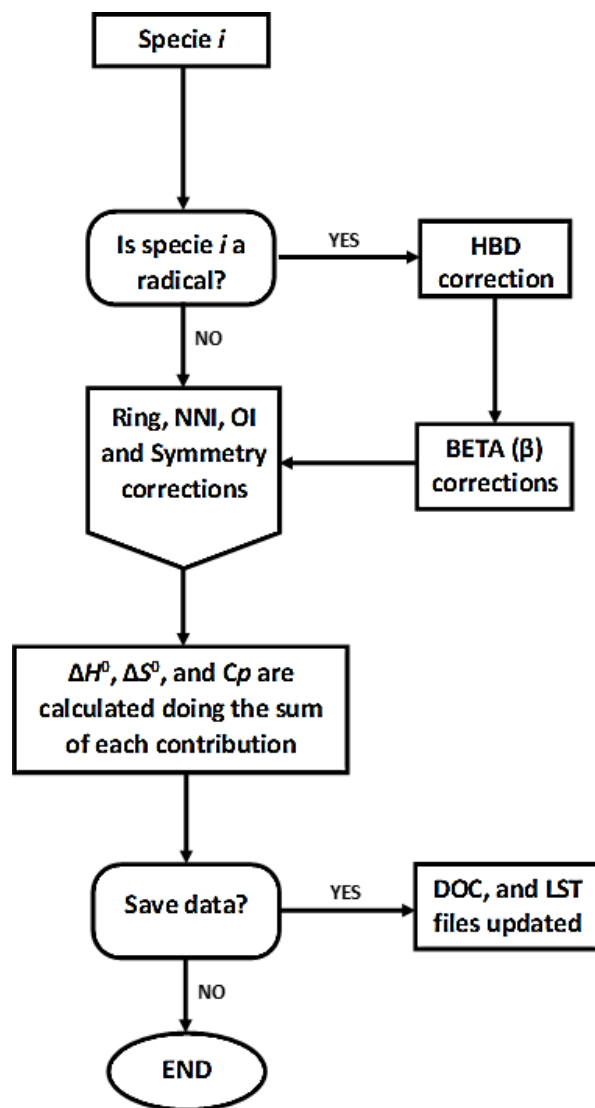


Figure 3-2. Flowchart of the group additivity method employed by THERM23.

3.2.4.1 Example calculations

Calculations can be performed using either *option 1* or *option 2* in the THERM23 software. Table 3-5 presents a list of enthalpies of formation, ΔH_f^0 from THERM23 compared with the literature values for eight different species. These species have been chosen to illustrate the reliability of the GAV method in a wide range of different size and type of species. These include small alkanes, such as ethane (C_2H_6), propane (C_3H_8), and 2-methyl-butane (iC_5H_{12}), an aromatic species, phenol (C_6H_5OH) and its associated phenoxy ($C_6H_5\dot{O}$) radical, to bigger species including 2,2,4-trimethylpentane (iC_8H_{18}), bi-phenoxy ($C_{12}H_{10}$), and *n*-tetradecane ($C_{14}H_{30}$). Note that *n*-tetradecane is not a limit but is used as a reference regarding the size of species that are becoming more common

fuels present in chemical kinetic models. In fact, the software can calculate fuel molecules as large as desired.

Table 3-5. Comparison of enthalpies of formation from THERM23 and literature, ΔH_f^0 (kcal mol⁻¹).

Formula	Species name	THERM23	Experiment	% Error
C ₂ H ₆	ethane	-20.32	-20.08 ^a , -20.03 ^b , -20.24 ^c	-0.24, -0.29, -0.08
C ₃ H ₈	propane	-25.23	-25.02 ^b , -24.80 ^c	-0.21, -0.43
iC ₅ H ₁₂	2-methyl-butane	-36.25	-36.73 ^d , -36.80 ^e , -36.92 ^c	0.48, 0.55, 0.67
C ₆ H ₅ OH	phenol	-22.30	-23.03 ^f , -23.04 ^g	0.73, 0.74
C ₆ H ₅ Ö	phenoxy	12.10	12.90 ^h	-0.8
iC ₈ H ₁₈	2,2,4-trimethylpentane	-53.32	-53.56 ^c	0.24
C ₁₂ H ₁₀	biphenyl	42.92	43.09 ⁱ , 43.49 ^j , 43.52 ^k	-0.17, -0.57, -0.6
C ₁₄ H ₃₀	<i>n</i> -tetradecane	-79.24	-79.37 ^c	0.13

^a Manion et al [31], ^b Pittam and Pilcher [32], ^c Prosen and Rossini [33], ^d Good [34], ^e Pilcher and Chadwick [35], ^f Cox [36], ^g Andon et al [37], ^h Tsang [38], ⁱ Roux et al [39], ^j Chirico et al [40], and ^k Coleman and Pilcher [41].

Figure 3-3 shows the name, molecular formula, structural formula, GAVs, number of rotors, and symmetry number of ethane (C₂H₆), propane (C₃H₈), 2-methylbutane (iC₅H₁₂), 2,2,4-trimethylpentane (iC₈H₁₈), phenol (C₆H₅OH), and phenoxy radical (C₆H₅Ö). The enthalpy of formation for ethane (C₂H₆) is estimated in THERM23 as -20.32 kcal mol⁻¹, while experimental values reported as -20.08, -20.03 and -20.24 kcal mol⁻¹ by Manion et al. [31], Pittam et al. [32], and Prosen et al. [33], with a deviation of -0.24, -0.29, and -0.08 kcal mol⁻¹, respectively. For propane (C₃H₈), the value is estimated in THERM23 to be -25.23 kcal mol⁻¹ where the reported experimental values are -25.02 and -24.08 kcal mol⁻¹ by Pittman [32], and Prosen [33], with a deviation of -0.21, and -0.43, respectively. Also, the higher order hydrocarbons i.e., 2,2,4-trimethylpentane (iC₈H₁₈) and *n*-tetradecane (C₁₄H₃₀) show a deviation of 0.24, and 0.13 from the experimental measurements but both phenol (C₆H₅OH) and phenoxy radical (C₆H₅Ö) show deviations slightly higher as 0.73, 0.74, and -0.8 from the experimental measurements. These higher errors may be due to using the groups involving to the aromatic species from Zhu et al. [20], where the groups were optimized based on the *ab-initio* calculations indicating that the further modification and updated groups are necessary. In their calculations, the 0 K energies are calculated using a combination of G3 [42] and G4 [43] compound methods and vibrational frequencies and 1-D internal rotational potential barriers are calculated M06-2X/6-31G level of theory. By contrast, other species show maximum deviations of -0.17 which are used the groups recently optimized by Ghosh et al. [19] based on very high-level STAR-1D [22] calculations.

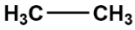
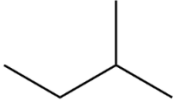
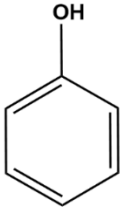
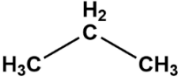
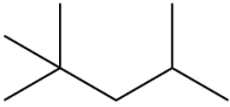
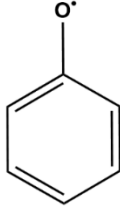
ethane	2-methyl-butane	phenol
C_2H_6	iC_5H_{12}	C_6H_5OH
		
C/C/H3 × 2 Rotor 1 Symmetry 18	C/C/H3 × 3 C/C2/H2 × 1 C/C3/H × 1 AG × 1 Rotor 4 Symmetry 27	CB/H × 5 CB/O × 1 O/CB/H × 1 Rotor 1 Symmetry 2
propane	2,2,4-trimethyl-pentane	phenoxy
C_3H_8	C_8H_{18}	$C_6H_5O^\bullet$
		
C/C/H3 × 2 C/C2/H2 × 1 Rotor 2 Symmetry 18	C/C/H3 × 5 C/C2/H2 × 1 C/C3/H × 1 C/C4 × 1 AG × 3 H/REPEL/15 × 1 Rotor 7 Symmetry 729	CB/H × 5 CB/O × 1 O/CB/H × 1 PHENOXY × 1 Rotor 0 Symmetry 2

Figure 3-3. Name, molecular formula, structural formula, GAVs, number of rotors, and symmetry number of ethane (C_2H_6), propane (C_3H_8), 2-methyl-butane (iC_5H_{12}), 2,2,4-trimethyl-pentane (iC_8H_{18}), phenol (C_6H_5OH), and phenoxy radical ($C_6H_5O^\bullet$).

All of these species have been previously explained in terms of GAVs. However, as an example of calculation and documentation produced by THERM23, we take the case of 2-methylbutane, or *iso*-pentane (iC_5H_{12}) as shown in Fig. 3-3. By using the updated and modified GAV terms, the ΔH_f^0 (298 K) is calculated both in THERM and THERM23 as ΔH_f^0 (298 K) = (C/C/H3 × 3) +

$(C/C2/H2 \times 1) + (C/C3/H \times 1) + (AG \times 1) = (-10.16 \times 3) + (-4.91 \times 1) + (-1.68 \times 1) + (+0.82 \times 1)$
 $= -36.25 \text{ kcal mol}^{-1}$ which is in excellent agreement with the STAR-1D value of $-36.60 \text{ kcal mol}^{-1}$ [22]. In addition, the information of symmetry, rotors and optical isomerism (OI) are needed to calculate the entropy and heat capacities at the function of temperature. Once all of this information is provided into the system, it will generate a .DOC file contain a number of information as shown in Fig. 3-4. The .DOC file contain the species name (for this example 2-methylbutane); the chemical formula (iC_5H_{12}); the units used for these calculations; the information whether the specie is a linear or non-linear molecule; the GAVs identification (ID) names and the number of different GAVs present in this species (in this case: $C/C/H3 \times 3$, $C/C2/H2 \times 1$, $C/C3/H \times 1$, and $AG \times 1$); the thermodynamic properties, i.e. $H_f^0(298 \text{ K})$, $S^0(298 \text{ K})$, and C_p at 300–1500 K. It also shows CPINF (C_p at ∞ temperature); the total number of rotors; symmetry number of the species; and the creation date.

```

SPECIES
IC5H12
Thermo estimation for molecule
IC5H12                                C5H12
UNITS:  K,kcal - NONLINEAR SPECIE
GROUPS  4
      Gr  #   Group ID  Quantity
          1   -   C/C/H3    -     3
          2   -   C/C2/H2   -     1
          3   -   C/C3/H    -     1
          4   -   AG         -     1
      Hf   S      CP300 CP400 CP500 CP600 CP800 CP1000 CP1500
      -36.25 80.96 29.09 37.22 44.54 50.66 60.27 67.34 78.29
              CPINF = 94.05
Number of rotors:4
Symmetry: 27
Creation date: 30/08/2022
ENDSPECIES
  
```

Figure 3-4 The .DOC file contain line by line shows the specie name, elemental formula, units, linearity, number of different GAVs considered, GAVs identification (ID), estimated thermochemical properties, and C_p at infinite temperature (CPINF), the number of rotors, the symmetry number, and the creation date.

One of the most important features of THERM23 is to calculate radical species more accurately than that of the calculation from THERM. As we previously mentioned that THERM calculate the radical species from the thermochemistry of their parent molecules by adding the BD group and subtracting the enthalpy of formation of hydrogen atom as follows:

$$\Delta_f H^0(\text{radical}) = \Delta_f H^0(\text{parent}) + \Delta_f H^0(\text{BD}) - \Delta_f H^0(\dot{H})$$

Similarly, for the radical standard entropy and heat capacity, the BD group values are simply added to the parent molecule's value, i.e.

$$S^0(\text{radical}) = S^0(\text{parent}) + S^0(\text{BD}) \quad (9)$$

$$C_p(\text{radical})(T) = C_p(\text{parent})(T) + C_p(\text{BD})(T) \quad (10)$$

Note that symmetry number and number of optical isomers may be different for a radical and its parent molecule, which has to be considered for calculation of the radical entropy. Therefore, if a radical species has different GAV terms from the parent, THERM cannot

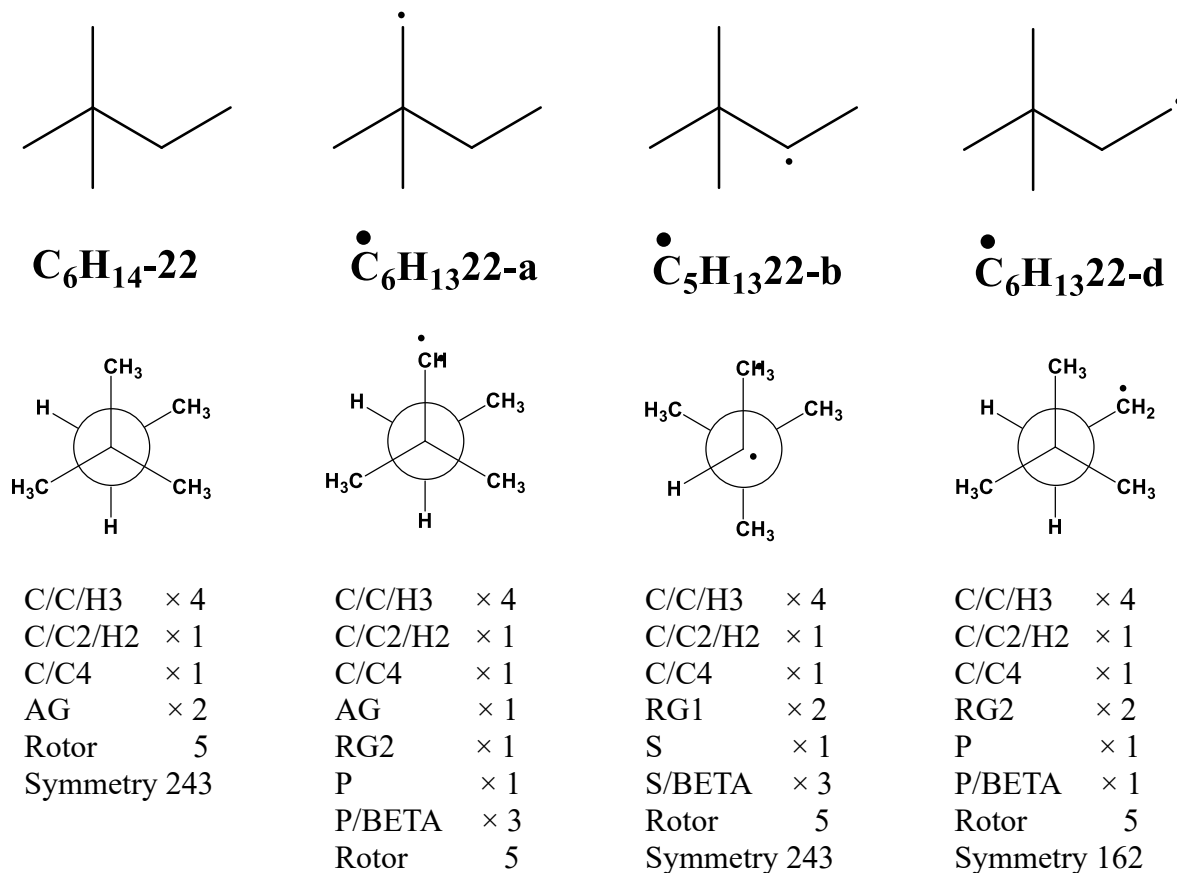


Figure 3-5. Group definitions of 2,2-dimethylbutane ($\text{C}_6\text{H}_{14}\text{22}$) and its corresponding radicals. in Fig.

3-5 and the calculated enthalpies of formation are compared in Table 3-6. In Fig. 3-5, it can be seen that the 1,4-gauche interactions are different in radicals than that of parent. In addition, there are β -corrections in the radicals which are absent in the parent molecule. Those contributions could influence on the predictions of enthalpies of formation for these radicals. For example, the enthalpy of formation for 2,2-dimethylbutane ($\text{C}_6\text{H}_{14}\text{22}$) is calculated as $\Delta H_f^0(\text{C}_6\text{H}_{14}\text{22}) = (\text{C/C/H3} \times 4) + (\text{C/C2/H2} \times 1) + (\text{C/C4} \times 1) + (\text{AG} \times 1) = (-10.16 \times 4) + (-4.91 \times 1) + (0.14 \times 1) + (+0.82 \times 2) = -$

43.77 kcal mol⁻¹ by both THERM and THERM23 which is in good agreement with the STAR-1D value of -44.02 kcal mol⁻¹ as shown in Table 3-6. Therefore, $\dot{C}_6H_{13}22$ -a radical is calculated by THERM as $\Delta_f H_f^0(\dot{C}_6H_{13}22\text{-a}) = \Delta_f H_f^0(C_6H_{14}22) + \Delta_f H^0(P) - \Delta_f H^0(\dot{H}) = (-43.77) + (+101.00) - (+52.10) = 5.13$ kcal mol⁻¹. By contrast, THERM23 calculate this value as $\Delta_f H_f^0(\dot{C}_6H_{13}22\text{-a}) = (C/C/H3 \times 4) + (C/C2/H2 \times 1) + (C/C4 \times 1) + (AG \times 1) + (RG2 \times 1) + (P/BETA \times 3) + \Delta_f H^0(P) - \Delta_f H^0(\dot{H}) = (-10.16 \times 4) + (-4.91 \times 1) + (0.14 \times 1) + (+0.82 \times 1) + (0.29 \times 1) + (0.45 \times 3) + (+101.00) - (+52.10) = 5.95$ kcal mol⁻¹ which is in excellent agreement with the STAR-1D value of 6.00 kcal mol⁻¹. The comparison of the enthalpies of formation for other radicals of 2,2-dimethylbutane are also presented in Table 3-6 and shows that by including the corrections, THERM23 can significantly improve the predictions. It should be noted that the calculation in THERM could show higher errors if the updated group values are not used.

Table 3-6. The standard heats of formation (kcal mol⁻¹) for 2-methylbutane and its corresponding radicals from the ab-initio calculations and group additivity method at 298.15 K.

Species	QM ^a (STAR-1D)	Group additivity ^b		Deviations from QM ^d	
		THERM23	THERM ^c	THERM23	THERM
C ₆ H ₁₄ -22	-44.02	-43.77	-43.77	0.25	0.25
$\dot{C}_6H_{14}22$ -a	6.00	5.95	5.13	-0.05	-0.87
$\dot{C}_6H_{14}22$ -c	2.75	2.50	2.41	-0.25	-0.34
$\dot{C}_6H_{14}22$ -d	4.57	4.52	5.13	-0.05	0.56

^a Reference [29]. ^b the updated GAVs [20] are used in both THERM and THERM23. ^cReference [5, 6]. ^d $\Delta = \Delta_f H^0(GA) - \Delta_f H^0(QM)$.

Furthermore, THERM23 will provide the user with a .DAT file which contain the NASA polynomials to be used in any software compatible such as Chemkin [23], Cantera [25]. This NASA polynomials are in a format of 14 coefficients and are valid over the temperature range of 300–5000 K. The example of this file is presented in Fig. 3-6 which includes all the species listed in Fig. 3-3. For each species, the first line contains the total number of C, H, O and N atoms in the species, phase representation (G), lowest (300 K) and highest (5000 K) temperature limits, and the breaking point (BP) of the polynomials. The first seven coefficients listed are used to calculate the thermochemistry properties over the BP temperature (BP–5000 K) and the second set of seven coefficients are used for the low temperature, which means under the BP temperature (300 K–BP). This BP is calculated as the tangential point of both polynomial fits, the accuracy of absolute tolerance for this point ideally would be 0.005%, while the slope of dCp/dT will have the same tolerance of 0.005%. This method

has been widely discussed by Ritter and Bozzelli [13, 14]. With this definition of BP every specie will have a different BP, then the polynomials are not forced to fit a fix temperature, and both polynomials will share the best point to fit.

Another important feature of THERM23 is to create a plot from the results of NASA polynomials which appeared in the .DAT files. Option 4 can plot the data for every species in the .DAT file and generates individual graphs for C_p , H, and S. This option also allows the user to plot two .DAT files at the same time that will generate a double C_p , H, and S graphs for the same species from different source file for comparison. Further detail regarding the options of THERM23, how to use them, what to expect, and common bugs, can be found in its manual along with the source code.

The image shows a screenshot of a text file named 'PaperTHERM22.dat'. The file contains a list of species and their corresponding NASA polynomial coefficients. The data is organized into columns: species name, chemical formula, number of atoms, and 14 coefficients. The species listed include ETHANE, Propane, 2-methyl-butane, C6H5OH, C6H5O, and 224-trimethyl-pentane.

Line	Species	Chemical Formula	Atoms	Coefficients	Order
1	THERMO				
2				300.00 1000.00 5000.00	
3	ETHANE	C 2H 6	0 OG	300.000 5000.000 830.000	1
4				1.81442090E+00 1.88659943E-02-7.46507535E-06 1.36953940E-09-9.53331483E-14	2
5				-1.16782463E+04 1.16731264E+01-9.37052998E-01 2.88181620E-02-2.15147540E-05	3
6				1.05879823E-08-2.41480728E-12-1.10557388E+04 2.52642670E+01	4
7	Propane	C 3H 8	0 OG	300.000 5000.000 908.000	1
8				3.28881919E+00 2.64648815E-02-1.07486877E-05 2.00849717E-09-1.41806037E-13	2
9				-1.50406354E+04 5.71965456E+00-5.53379835E-01 3.72162723E-02-2.11060060E-05	3
10				5.95149119E-09-6.31230403E-13-1.40090824E+04 2.54964108E+01	4
11	2-methyl-butane	C 5H 12	0 OG	300.000 5000.000 1000.000	1
12				1.28265536E+01 3.05418958E-02-1.11262630E-05 1.81379311E-09-1.14082337E-13	2
13				-2.47967525E+04-4.46728684E+01-1.97796480E+00 6.60643671E-02-3.94941066E-05	3
14				9.58032703E-09-2.30657721E-13-2.02158403E+04 3.36948717E+01	4
15	C6H5OH	C 6H 6O	1 OG	300.000 5000.000 1102.000	1
16				1.46057496E+01 1.88747069E-02-6.39867978E-06 1.03436617E-09-6.57315810E-14	2
17				-1.79842070E+04-5.44390724E+01-5.15503845E+00 7.59160817E-02-6.82287003E-05	3
18				3.08845521E-08-5.46296145E-12-1.25129076E+04 4.73406595E+01	4
19	C6H5O	C 6H 5O	1 OG	300.000 5000.000 1000.000	1
20				1.35207210E+01 1.79009799E-02-6.11882248E-06 9.99205750E-10-6.41570585E-14	2
21				-1.90411713E+02-4.70745907E+01-3.75441953E+00 6.44769520E-02-5.13245370E-05	3
22				1.94765679E-08-2.63661413E-12 4.76046513E+03 4.27687312E+01	4
23	224-trimethyl-pentane	C 8H 18	0 OG	300.000 5000.000 1000.000	1
24				2.20331088E+01 4.61644273E-02-1.76356785E-05 3.07687926E-09-2.04537980E-13	2
25				-3.77860886E+04-9.40522799E+01-4.29758202E+00 1.08595024E-01-6.52251596E-05	3
26				1.36387590E-08 7.23039389E-13-2.96335212E+04 4.54453117E+01	4

Figure 3-6 Content of the .DAT file format. It contains the 14 coefficients of the NASA polynomials for every specie calculated.

Figure 3-7 shows the C_p s comparison of C_2H_6 , C_3H_8 , and C_6H_5OH . This data was collected from the literature, from Gurvich et al. [44] for C_2H_6 data, from Chao et al. [45] for C_3H_8 , and from Kudchadker et al. [46] for C_6H_5OH . This work estimation is represented by the solid lines, and dashed lines represent RMG [18] estimations. As expected, for the low-temperature range to intermediate (≤ 1500 K) both THERM23 and RMG agree on the overall predictions by a maximum percentage error of $\sim 0.7\%$. RMG is able to predict in this range of temperature experimental data with a maximum percentage error of $\sim 0.57\%$, THERM23 has only a maximum percentage error of $\sim 0.41\%$ for the

same range. Once this temperature has been surpassed, then RMG extrapolations continue to increase when THERM23 predictions tend to a constant value, this C_p limit has already been explained during the section. Especially in the case of ethane, where experimental data exhibit a trend corresponding more to THERM23 extrapolations.

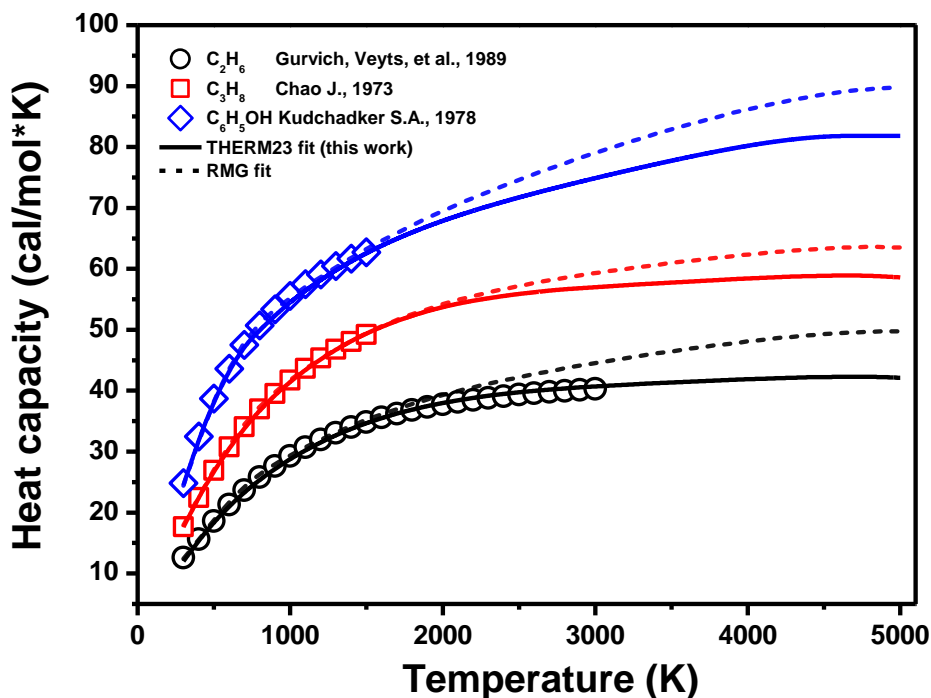


Figure 3-7 Heat capacities (C_p) comparison for ethane (C_2H_6), propane (C_3H_8), and phenol (C_6H_5OH). From the literature, in black symbols C_2H_6 data reported by Gurvich et al. [44], in red symbols C_3H_8 data reported by Chao et al. [45], and in blue symbols the C_6H_5OH data presented by Kudchadker et al. [46]. Solid lines represent THERM23 in this work, and dashed lines represent RMG [18] estimations.

We have obtained an excellent agreement with other software, THERM [13], RMG [18], and literature data [44-46]. Finally, it is worth to mention that *Option 5* in the THERM23 menu can calculate missing C_p 's and fit .LST files data to NASA polynomial and generates the corresponding .DAT output file. All of these capabilities make THERM23 a flexible and practical thermochemistry tool. Furthermore, due to the continuous expansion of experimental, theoretical, and estimation databases, THERM23 has an easy way to add/update the GAVs using the grp format to make it possible to generate new files containing new thermochemistry massively. Subsequently allowing the user a better interpretation of the data generated, with the final goal of the obtention of as accurate as possible thermochemistry for the chemical modelling of fuels.

3.3 Conclusions

We have created THERM23, a software written in Python that can be used on both Windows and Linux operating systems. This software helps calculate, recalculate, and plot the thermochemical properties of species involved in combustion in a gas phase. It utilizes Benson's group additivity method to estimate these properties and offer valid extrapolations for temperatures ranging from 300 – 5000 K. THERM23 provides NASA polynomials in a convenient format and allows users to plot these results individually or side by side for comparison. One of the keys features of THERM23 is its flexibility and editability, as it maintains many of the original features of THERM while improving accuracy. The software can calculate the properties of species including radicals, regardless of any information about the parent molecule. It is also designed to accommodate new groups or corrections as they become available in the future.

This software is available in the combustion chemistry centre (C³) website [48] in a single open-source package. The program comes in executable format with a bat executable file along with the python files which can be executed directly from any terminal i.e., PowerShell, CMD, Unix shell and so on.

Acknowledgments

The authors acknowledge funding from Science Foundation Ireland (SFI) via project number 16/SP/3829. We also acknowledge use of computing resources from the Irish Centre for High-End Computing (ICHEC). The authors would like to express their gratitude to Vaibhav Patel and Kieran P. Somers for their useful advice.

References

- [1] U.S. Energy Information Administration, Annual energy outlook 2022 (AEO2022) with projections to 2050, IEO2019, 2022. (2022).
- [2] S.W. Benson, Thermochemical kinetics, Wiley (1976).
- [3] S.W. Benson, J.H. Buss, Additivity rules for the estimation of molecular properties. Thermodynamic properties, J. Chem. Phys. 29 (1958) 546-572.
- [4] S.W. Benson, F. Cruickshank, D. Golden, G.R. Haugen, H. O'neal, A. Rodgers, R. Shaw, R. Walsh, Additivity rules for the estimation of thermochemical properties, Chem. Rev. 69 (1969) 279-324.
- [5] N. Cohen, Aerospace report No. ATR-88(7073)2, aerospace corporation, El Segundo, California, (1988).
- [6] S. Stein, D. Golden, S.W. Benson, Predictive scheme for thermochemical properties of polycyclic aromatic hydrocarbons, J. Phys. Chem. 81 (1977) 314-317.

- [7] S.E. Stein, A. Fahr, High-temperature stabilities of hydrocarbons, *J. Phys. Chem.* 89 (1985) 3714-3725.
- [8] R. Shaw, D.M. Golden, S.W. Benson, Thermochemistry of some six-membered cyclic and polycyclic compounds related to coal, *J. Phys. Chem.* 81 (1977) 1716-1729.
- [9] H.K. Eigenmann, D.M. Golden, S.W. Benson, Revised group additivity parameters for the enthalpies of formation of oxygen-containing organic compounds, *J. Phys. Chem.* 77 (1973) 1687-1691.
- [10] E.S. Domalski, E.D. Hearing, Estimation of the thermodynamic properties of hydrocarbons at 298.15 K, *J. Phys. Chem. Ref. Data* 17 (1988) 1637-1678.
- [11] M.J. Hofmann, Process hazard review in a chemical research environment, *Chemical Process Hazard Review*, Am. Chem. Soc. (1985), 7-15.
- [12] R. Reid, J. Prausnitz, T. Sherwood, *The properties of gases and liquids*, McGraw-Hill, New York, (1977) 560.
- [13] E.R. Ritter, J.W. Bozzelli, THERM: Thermodynamic property estimation for gas phase radicals and molecules, *Int. J. Chem. Kinet.* 23 (1991) 767-778.
- [14] E.R. Ritter, THERM: A computer code for estimating thermodynamic properties for species important to combustion and reaction modeling, *J. Chem. Inf. Comput. Sci.* 31 (1991) 400-408.
- [15] W.H. Seaton, CHETAH-The ASTM chemical thermodynamic and energy release evaluation program, American Soc. for Testing and Materials 1974.
- [16] C. Muller, V. Michel, G. Scacchi, G.-M. Côme, THERGAS: a computer program for the evaluation of thermochemical data of molecules and free radicals in the gas phase, *J. Chim. Phys.* 92 (1995) 1154-1178.
- [17] S.E. Stein, J.M. Rukkers, R.L. Brown, NIST Structures&Properties Database and Estimation Program, NIST, Gaithersburg, MD, (1991).
- [18] M. Liu, A.G. Dana, M.S. Johnson, M.J. Goldman, A. Jocher, A.M. Payne, C.A. Grambow, K. Han, N.W. Yee, E.J. Mazeau, K. Blondal, R.H. West, C.F. Goldsmith, W.H. Green, Reaction Mechanism Generator v3.0: Advances in Automatic Mechanism Generation, *J. Chem. Inf. Model.* (2021), 61, 2686–2696.
- [19] M.K. Ghosh, S.N. Elliott, K.P. Somers, S.J. Klippenstein, H.J. Curran, Group additivity values for the heat of formations of C₂ – C₈ alkanes, alkyl hydroperoxides, and their radicals, *Combust. Flame*, (2022) 112492. <https://doi.org/10.1016/j.combustflame.2022.112492>.
- [20] S. Zhu, Z. Xiong, C.-W. Zhou, An extensive theoretical study on the thermochemistry of aromatic compounds: from electronic structure to group additivity values, *Phys. Chem. Chem. Phys.*, (2022), 24, 18582-18599.
- [21] T.H. Lay, J.W. Bozzelli, A.M. Dean, E.R. Ritter, Hydrogen atom bond increments for calculation of thermodynamic properties of hydrocarbon radical species, *J. Phys. Chem.* 99 (1995) 14514-14527.
- [22] S.N. Elliott, K.B. Moore III, A.V. Copan, Y. Georgievskii, M. Keçeli, K.P. Somers, M.K. Ghosh, H.J. Curran, S.J. Klippenstein, Systematically derived thermodynamic properties for alkane oxidation, *Combust. Flame*, (2023) 112487. <https://doi.org/10.1016/j.combustflame.2022.112487>.
- [23] C.-P. Reaction-Design, San Diego, (2013).
- [24] D.G. Goodwin, R.L. Speth, H.K. Moffat, B.W. Weber, Cantera: an object-oriented software toolkit for chemical kinetics, thermodynamics, and transport processes, <https://www.cantera.org>, doi:10.5281/zenodo.170284, (2018). doi: 10.5281/zenodo.170284.
- [25] D.G. Goodwin, H.K. Moffat, R.L. Speth, Cantera: An object-oriented software toolkit for chemical kinetics, thermodynamics, and transport processes, Caltech, Pasadena, CA 124 (2009).

- [26] D.G. Goodwin, H.K. Moffat, R.L. Speth, Cantera: An object-oriented software toolkit for chemical kinetics, thermodynamics, and transport processes, version 2.2. 1, Cantera Developers, Warrenville, IL, (2017).
- [27] N. Cohen, S.W. Benson, The thermochemistry of alkanes and cycloalkanes, *Alkanes and Cycloalkanes 1992*, 215-287.
- [28] E.R. Ritter, THERM: a computer code for estimating thermodynamic properties for species important to combustion and reaction modeling, *J. Chem. Inf. Model.* 31 (1991) 400-408.
- [29] J. Cox, D. Wagman, V. Medvedev, CODATA Key Values for Thermodynamics, Hemisphere Publishing Corp, New York, (1989).
- [30] S.N. Elliott, M. Keçeli, M.K. Ghosh, K.P. Somers, H.J. Curran, S.J. Klippenstein, High accuracy heats of formation for alkane oxidation: from small to large via the CBH-ANL method, *J. Phys. Chem. A* (2023), 127, 6, 1512–1531. <https://doi.org/10.1021/acs.jpca.2c07248>.
- [31] J.A. Manion, Evaluated enthalpies of formation of the stable closed shell C₁ and C₂ chlorinated hydrocarbons, *J. Phys. Chem. Ref. Data* 31 (2002) 123-172.
- [32] D.A. Pittam, G. Pilcher, Measurements of heats of combustion by flame calorimetry. Part 8. methane, ethane, propane, n-butane and 2-methylpropane, *J. Chem. Soc., Faraday Trans. 1* 68 (1972) 2224.
- [33] E.J. Prosen, F.D. Rossini, Heats of combustion and formation of the paraffin hydrocarbons at 25 degrees c., *J. Res. Natl. Bur. Stand.* 263 (1945) 34.
- [34] W. Good, The enthalpies of combustion and formation of the isomeric pentanes, *J. Chem. Thermodyn.* 2 (1970) 237-244.
- [35] G. Pilcher, J. Chadwick, Measurements of heats of combustion by flame calorimetry. Part 4. n-Pentane, isopentane, neopentane, *Trans. Faraday Soc.* 63 (1967) 2357-2361.
- [36] J. Cox, The heats of combustion of phenol and the three cresols, *Pure Appl. Chem.* 2 (1961) 125-128.
- [37] R.J.L. Andon, D.P. Biddiscombe, J.D. Cox, R. Handley, D. Harrop, E.F.G. Herington, J.F. Martin, 1009. Thermodynamic properties of organic oxygen compounds. part I. preparation and physical properties of pure phenol, cresols, and xylenols, *J. Chem. Soc.*, (1960) 5246-5254.
- [38] W. Tsang, Heats of formation of organic free radicals by kinetic methods, *Energetics of organic free radicals*, Springer, (1996), 22-58.
- [39] M.V. Roux, M. Temprado, J.S. Chickos, Y. Nagano, Critically evaluated thermochemical properties of polycyclic aromatic hydrocarbons, *J. Phys. Chem. Ref. Data* 37 (2008) 1855-1996.
- [40] R. Chirico, S. Knipmeyer, A. Nguyen, W. Steele, The thermodynamic properties of biphenyl, *J. Chem. Thermodyn.* 21 (1989) 1307-1331.
- [41] D. Coleman, G. Pilcher, Heats of combustion of biphenyl, bibenzyl, naphthalene, anthracene and phenanthrene, *Trans. Faraday Soc.* 62 (1966) 821-827.
- [42] L.A. Curtiss, K. Raghavachari, P.C. Redfern, V. Rassolov, J.A. Pople, Gaussian-3 (G3) theory for molecules containing first and second-row atoms, *J. Chem. Phys.* 109 (1998) 7764-7776.
- [43] L.A. Curtiss, P.C. Redfern, K. Raghavachari, Gaussian-4 theory, *J. Chem. Phys.* 126 (2007) 084108.
- [44] L.V. Gurvich, I. Veyts, Thermodynamic properties of individual substances: elements and compounds, Vol. 2. CRC press, (1990).
- [45] J. Chao, R.C. Wilhoit, B.J. Zwolinski, Ideal gas thermodynamic properties of ethane and propane, *J. Phys. Chem. Ref. Data* 2 (1973) 427-438.
- [46] S.A. Kudchadker, A.P. Kudchadker, R. Wilhoit, B.J. Zwolinski, Ideal gas thermodynamic properties of phenol and cresols, *J. Phys. Chem. Ref. Data* 7 (1978) 417-423.

- [47] C.W. Gao, J.W. Allen, W.H. Green, R.H. West, Reaction mechanism generator: automatic construction of chemical kinetic mechanisms, *Comput. Phys. Commun.*, (2016). doi:<https://doi.org/10.1016/j.cpc.2016.02.013>(2016) 212-225.
- [48] <https://www.nuigalway.ie/combustionchemistrycentre/softwaredownloads/>.

Chapter 4: A comprehensive experimental and modelling study of the ignition delay time characteristics of ternary and quaternary blends of methane, ethane, ethylene, and propane over a wide range of temperature, pressure, equivalence ratio and dilution

Published in: Combustion and Flame, Volume 234, July 2021, 111626.

DOI : <https://doi.org/10.1016/j.combustflame.2021.111626>

Author Contributions

- 1) Sergio Martinez (National University of Ireland, Galway, Ireland)
Contribution: Performed calculations, chemical kinetic modelling, and manuscript preparation.
- 2) Mohammadreza Baigmohammadi (National University of Ireland, Galway, Ireland)
Contribution: High pressure shock tube experiments and reviewed the manuscript.
- 3) Vaibhav Patel (National University of Ireland, Galway, Ireland)
Contribution: Rapid compression machine experiments.
- 4) Snehasish Panigrahy (National University of Ireland, Galway, Ireland)
Contribution: Chemical kinetic modelling and reviewed the manuscript.
- 5) Amrit B. Sahu (National University of Ireland, Galway, Ireland)
Contribution: Chemical kinetic modelling.
- 6) Shashank Nagaraja (National University of Ireland, Galway, Ireland)
Contribution: Low pressure shock tube experiments.
- 7) Ajoy Ramalingam (PCFC, RWTH Aachen, Germany)
Contribution: Rapid compression machine experiments.
- 8) Karl A. Heufer (PCFC, RWTH Aachen, Germany)
Contribution: Managed the project and reviewed the manuscript.
- 9) Andrzej Pekalski (Shell research limited, Shell Centre London)
Contribution: Project management as industrial sponsor and manuscript review.
- 10) Henry J. Curran (National University of Ireland, Galway, Ireland)
Contribution: Managed the project, made technical contributions, and reviewed the project and manuscript throughout.

Abstract

The ignition delay time (IDT) characteristics of ternary and quaternary blended $C_1 - C_3$ gaseous hydrocarbons, including methane/ethane/ethylene and methane/ethane/ethylene/propane, are studied over a wide range of mixture composition, temperature ($\sim 800 - 2000$ K), pressure ($\sim 1 - 135$ bar), equivalence ratio ($\sim 0.5 - 2.0$), and dilution ($\sim 75 - 90\%$) using both experimental data and kinetic modelling tools. All of the experimental tests were designed using the Taguchi approach (L_9) to fulfil the experimental matrix required to generate a comprehensive set necessary to validate a detailed chemical kinetic model. High- and low-temperature IDTs were recorded using low/high-pressure shock tubes (L/HPST) and rapid compression machines (RCM), respectively. The model predictions using NUIGMech1.2 are evaluated versus all of the newly recorded experimental data. Moreover, the individual effects on IDT predictions of the parameters studied, including mixture composition and pressure, are investigated over the temperature range. The results show that NUIGMech1.2 can reasonably reproduce the experimental IDTs over the wide range of the conditions studied. The constant-volume simulations using the chemical kinetic mechanism reveal the synergistic/antagonistic effect of blending on IDTs over the studied temperature range so that IDTs in certain temperature ranges are very sensitive to even small changes in mixture composition.

Keywords: methane, ethane, ethylene, propane, shock tube, RCM, ignition delay time.

4.1 Introduction

The combustion of low-carbon fuels ($C_1 - C_3$) for energy and power generation is a very promising step towards future low-to-zero emission energy production. Thus, gaining a deep understanding of the combustion chemistry of such fuels and their blends is important. Hence, the development of high-fidelity chemical mechanisms which can satisfactorily explain the oxidation and pyrolytic characteristics of low-carbon fuels is demanding. Together with speciation and laminar burning velocity techniques, ignition delay times (IDTs) are important in the validation of chemical kinetic mechanisms [1, 2]. Developing a comprehensive experimental IDT database that can stochastically and unbiasedly cover a wide range of operating conditions, including pressure, temperature, equivalence ratio, and dilution, is essential in this regard. Such a database can efficiently support the development of high-fidelity chemical kinetics, which can be validated against all available experimental IDT data. To do so, Baigmohammadi et al. [2] studied the IDT characteristics

of $C_1 - C_2$ pure hydrocarbons including methane (CH_4), ethane (C_2H_6), and ethylene (C_2H_4) fuels [2] as well as their binary blends [3]. Subsequently S. Martinez et al. [4] extended this work to higher hydrocarbons by investigating the IDTs of binary blends of C_2H_4 /propane (C_3H_8) and C_2H_6 / C_3H_8 mixtures in a shock tube (ST) and in a rapid compression machine (RCM) over a wide range of temperatures, pressures, equivalence ratios, and dilutions conditions. As these previous works focused on the IDT studies of single and binary blended fuel mixtures, this paper intends to examine the IDT behaviours of ternary and quaternary blends of $C_1 - C_3$ hydrocarbons with relevance for engine and gas turbine applications. Furthermore, although there is enough data recorded in the literature for the IDT characteristics of $C_1 - C_3$ alkane blended fuels and natural gas mixtures (NG) [3-11], evidence of the effect of adding olefin to $C_1 - C_3$ alkane blends on IDTs has not been reported to date. Thus, towards developing a comprehensive IDT database, we have designed a set of IDT experiments to cover this void over a wide range of pressure, temperature, equivalence ratio, and dilution (Figs. 4-1). The new experimental data sets are designed to explore the IDT characteristics of ternary and quaternary blends of $CH_4/C_2H_4/C_2H_6$ and $CH_4/C_2H_4/C_2H_6/C_3H_8$ mixtures.

Furthermore, providing stochastically and unbiasedly distributed experimental IDTs over a wide range of pressure, temperature, equivalence ratio, dilution with varying ethylene concentrations can help researchers develop more sophisticated and higher fidelity chemical kinetics. It can also lead to a valuable database capable of resembling the IDT characteristics of modified NG mixtures for a wide range of applications such as industrial furnaces and internal/external combustion engines working under homogenous charge compression ignition (HCCI), exhaust gas recirculation (EGR), and moderate or intense low oxygen dilution combustion regimes.

To achieve this, the current experimental and simulation study was defined, and the number of desired IDT experiments were optimised, covering the target operating conditions discussed above using the Taguchi [5] design of experiments (DOE) approach as shown in Fig. 4-1. However, high-pressure (> 40 bar) tests were added to the Taguchi matrix to develop the database further. As shown in Fig. 4-1(a), the composition of the blends is distributed diagonally to cover the target fuel compositions. Figure 4-1(b) demonstrates how using the Taguchi approach, we can reasonably populate the physical conditions in the desired cube so that a wide range of conditions can be covered without performing an overwhelming number of IDT experiments. The designed experiments encapsulate equivalence ratios of 0.5, 1.0, and 2.0 in 'air', at pressures (p_5 and p_C) of 1, 20, 40, 90, and 135 bar, for diluent (N_2 and Ar) concentrations of 75%, 85%, and 90% of reactive mixtures in

the temperature (T_5 and T_C) range of $\sim 800 - 2000$ K. The detailed kinetic mechanism NUIGMech1.2 is used to evaluate all of the newly measured experimental data, and the important reactions are identified to determine the synergistic/antagonistic effects of various blending effects on the IDTs.

The current study is organized in three stages, including (i) the design of new experiments over a wide range of operating conditions using the Taguchi approach; (ii) experimental measurements; and (iii) simulations using NUIGMech1.2 mechanism. Comprehensive Supplementary material files containing non-reactive traces for RCM simulations, the original spreadsheets of experimental tests, L/HPST oscilloscope traces, and the combined figures of reactive, non-reactive, and modelling pressure traces are provided as Appendix B. Moreover, the general information about the gases (fuel/oxygen/argon/nitrogen), experimental facilities, and data acquisition systems are also accessible in Appendix B.

4.2 Design of experiments and experimental approach

As mentioned above, all of the new IDT experiments were designed using an L_9 Taguchi matrix to optimally reduce the number of experiments and time required. The Taguchi approach can tackle the issue using a specific design of orthogonal arrays which permits a comprehensive experimental investigation by doing a minimal number of experimental tests. In this regard, the minimum number of experiments is determined as follows:

$$N_{\text{Taguchi}} = 1 + NF(L - 1) \quad (4-1)$$

where, N_{Taguchi} , NF , and L are the number of experiments, number of factors, and number of levels, respectively. According to the Taguchi approach, its performance is optimal when there are limited interactions between the desired variables. To use the Taguchi method, it is essential to define the controlling factors and levels. According to the factors and levels, several design of experiments (DOE) matrices are derived and are included as Supplementary material in Appendix B. The DOE process was followed for four parameters of ternary and quaternary fuel combinations, pressure, equivalence ratio, and dilution at three levels, where the details are shown in Fig. 4-1 and Table 4-1. As previously discussed by Baigmohammadi et al. [2, 3], the new IDT experimental data presented in Table 4-1 were collected using low- and high-pressure shock tubes (L/HPST) and RCMs refers to the low pressure shock tube, the high pressure shock tube and the (red) rapid compression machine

facilities at C³-NUI Galway, respectively, and PCFC refers to the RCM facility at PCFC RWTH Aachen University.

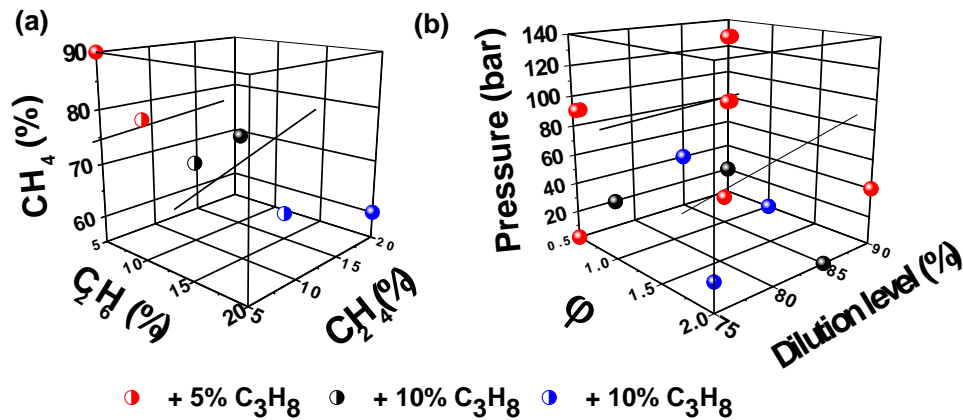


Figure 4-1. Experimental tests performed in the current study for % vol. composition of (a) ternary (CH₄/C₂H₄/C₂H₆) blends represented in solid symbols and quaternary (CH₄/C₂H₄/C₂H₆/C₃H₈) blends represented in half solid symbols, and (b) the input conditions for C₁ – C₃ blends studied in the current work at various equivalence ratios (x-axis), pressures (y-axis) and dilution levels (z-axis).

In the RCM facilities, the IDT of the normal studied mixtures (diluent concentration = 75%) and the pressure/time histories of their relevant non-reactive mixtures were recorded using a Kistler 6045A transducer mounted in the reaction chamber wall. However, the IDTs of mixtures at 85% and 90% dilution and at post-compression pressures of 20 and 40 bar were recorded using both the Kistler pressure record and light emission using a photomultiplier (PMT) equipped with a CH* filter due to the weak pressure signal observed at these diluted conditions. Therefore, as shown in the figure below, the IDT is defined as the maximum gradient in pressure or CH* after compressing the studied mixtures. The following figure illustrates the IDT definition for experiments and simulations of the RCM data measured in the current work. More detailed information of the LPST, HPST, NUIG-RCM and PCFC-RCM data is included in Sections 3 – 5 of Appendix B.

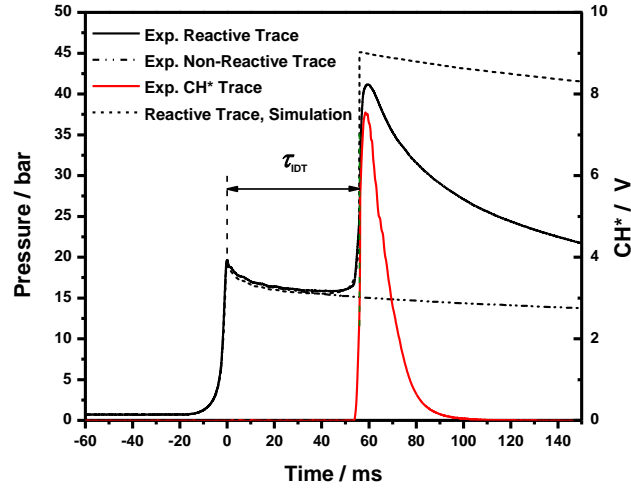


Figure 4-2. Definition for measuring IDT in the NUIG-RCM using Kistler pressure trace and PMT-CH* trace mounted on the side wall of the reaction chamber.

Table 4-1. CH₄/C₂H₄/C₂H₆ and CH₄/C₂H₄/C₂H₆/C₃H₈ mixture compositions in % mole volume in the current study. Where keywords LPST, HPST and RCM.

	No	% CH ₄	% C ₂ H ₄	% C ₂ H ₆	% C ₃ H ₈	% O ₂	% N ₂ + % Ar	ϕ	T _c (K)	p _c (bar)	Facility
CH ₄ /C ₂ H ₄ /C ₂ H ₆ 90%/5%/5%	1	4.29	0.24	0.24	0.0	20.24	75+0	0.5	1396–1874	1	LPST NUIG
	2	4.32	0.24	0.24	0.0	10.20	75+10	1.0	967–1797	20	HPST
	3	4.40	0.20	0.20	0.0	5.20	75+15	2.0	960–2033	40	RCM
	4	5.70	0.90	0.90	0.0	17.50	75+0	1.0	885–1536	40	NUIG
CH ₄ /75.3% C ₂ H ₄ /C ₂ H ₆ 75%/12.5%/12.5%	5	5.22	0.87	0.87	0.0	8.04	75+10	2.0	1432–1951	1	LPST NUIG
	6	1.33	0.22	0.22	0.0	8.22	75+15	0.5	996–2001	20	HPST
	7	6.67	2.22	2.22	0.0	13.89	75+0	2.0	911–1604	20	RCM
CH ₄ /C ₂ H ₄ /C ₂ H ₆ 60%/20%/20%	8	1.5	0.50	0.50	0.0	12.50	75+10	0.5	914–1484	40	NUIG
	9	1.71	0.57	0.57	0.0	7.14	75+15	1.0	1311–2032	1	LPST NUIG
CH ₄ /C ₂ H ₄ /C ₂ H ₆ 90%/5%/5%	10	4.24	0.24	0.24	0.0	20	67.8+7.5	0.5	877–987	90	RCM
	11	4.24	0.24	0.24	0.0	10	68.3+17	1.0	885–976	135	PCFC
	12	4.24	0.24	0.24	0.0	10	68.3+17	1.0	911–1015	90	
CH ₄ /C ₂ H ₄ /C ₂ H ₆ /C ₃ H ₈ 80%/5%/10%/5%	13	3.51	0.22	0.44	0.22	20.61	75+0	0.5	1259–2002	1	LPST NUIG
	14	3.58	0.22	0.45	0.22	10.50	85+0	1.0	941–1717	20	HPST
	15	3.68	0.23	0.46	0.23	5.40	90+0	2.0	908–2049	40	RCM
	16	4.93	0.70	0.70	0.70	17.96	75+0	1.0	826–1561	40	NUIG
CH ₄ /C ₂ H ₄ /C ₂ H ₆ /C ₃ H ₈ 70%/10%/10%/10%	17	4.62	0.66	0.66	0.66	8.41	75+10	2.0	1379–2062	1	LPST NUIG
	18	1.15	0.16	0.16	0.16	8.36	90+0	0.5	977–2024	20	HPST
CH ₄ /C ₂ H ₄ /C ₂ H ₆ /C ₃ H ₈	19	6.42	1.60	1.60	1.07	14.30	75+0	2.0	890–1668	20	RCM

60%/15%/15%/10%	2	1.41	0.35	0.35	0.24	12.64	85+0	0.5	891–1560	40	NUIG
	0										
	2										
CH ₄ /C ₂ H ₄ /C ₂ H ₆ /C ₃ H ₈	2	1.63	0.41	0.41	0.27	7.28	75+15	1.0	1290–1987	1	LPST NUIG
	1										
	2										
	2										
	2										
80%/5%/10%/5%	2	3.42	0.21	0.43	0.21	20.10	68.1+7.5	0.5	871–948	90	RCM
	3										
	4										
80%/5%/10%/5%	2	3.43	0.21	0.43	0.21	10.08	68.5+17.1	1.0	857–941	135	PCFC
	3										
	4										

4.2.1 Uncertainty analysis

The details of the uncertainty analysis are provided as Supplementary Material in the Appendix B. However, a synopsis is presented here. The presented uncertainty analysis is adopted based on the methods applied by Petersen et al. [6] and Weber et al. [7]. According to our analyses [2, 3], the average uncertainties in the compressed mixture temperatures (T_5 or T_C) and measured IDTs (σ_{IDT} %) in the NUIG STs and RCM are estimated to be approximately ± 20 K and $\pm 25\%$ (in the H/LPSTs) and $\pm 5 - 15$ K and $\pm 20\%$ (in the RCM), respectively over the entire range of cases studied. The uncertainty in the PCFC RCM is estimated using the methods described in Ramalingam et al. [8], and for the compressed temperature, the uncertainty is estimated to be within ± 5 K, with a measurement uncertainty of ± 0.15 bar for the compressed pressure and variation of $\pm 15\%$ for the IDTs.

4.3 Computational modelling

NUIGMech1.2 is developed as a further development/refinement of NUIGMech1.1 with the addition and modification of several important reactions which are discussed in more detail in Section 4.4.2 below. This mechanism includes 2746 species and 11279 reactions and reproduces similar good results as those previously published using NUIGMech1.1 for the oxidation of C₁–C₆ species [9-14]. These experimental and theoretical studies include natural gas mixtures [10], propane/propene blends [14], propyne [11], and the auto-ignition and pyrolysis studies of C₂–C₆ alkenes [12, 13]. All of the simulations are conducted using a Python script based on the CANTERA [15] library for the ST simulation and CHEMKIN-Pro 18.2 [16] software for the RCM simulations. Details of these simulations have already been published [2, 3, 8, 17-20]. The effect of surface reactions on IDTs is ignored in our simulations [2, 3]. The definition of IDT is taken to be the maximum gradient of CH* specie $\left. \frac{dCH^*}{dt} \right|_{max}$ or the maximum gradient of pressure $\left. \frac{dp}{dt} \right|_{max}$ for the ST simulations. For the RCM

simulations, the facility effects are included using the volume-time profiles derived from the non-reactive experimental pressure-time traces in which O₂ is replaced by N₂ in the mixture [18, 21].

To identify the controlling chemistry both promoting and inhibiting the reactivity of the system and thus their effect on IDT predictions, we present sensitivity analyses based on the brute force definition, with the definition of sensitivity coefficient (S) in Eqn. 4-2 [22] being:

$$S = \frac{\ln(\tau_+/\tau_-)}{\ln(k_+/k_-)} = \frac{\ln(\tau_+/\tau_-)}{\ln(2.0/0.5)} \quad (4-2)$$

This sensitivity coefficient is calculated for every reaction included in the chemical kinetic mechanism of interest. The IDT (τ) is perturbed through direct changes in the pre-exponential factor in the Arrhenius equation. S can be either positive or negative, with a positive value corresponding to a reaction that inhibits reactivity giving longer IDTs and vice versa. Moreover, the flux analyses presented in this work are based on rate of production (ROP) analyses performed to track the consumption of the main components in the different mixture compositions as their intermediates species.

A global analysis of regressions implemented to correlate simulated IDTs assuming constant volume conditions using NUIGMech1.2 is presented in Section 4.4.4. Moreover, the respective correlation equations and their coefficient values for specific conditions, based on various temperatures, pressure, equivalence ratios, and different fuel mixtures composition, are also provided. General correlations are intended to be a practical engineering tool to quickly and accurately calculate IDTs at the required condition. A more complete and fully detailed Tables BS12–BS15 of correlation values, standard errors, and performance are in Appendix B.

4.4 Results and discussions

A comprehensive comparison between the experimental IDTs (Table 4-1) and those predicted using NUIGMech1.2 is presented below.

4.4.1 Performance of NUIGMech1.2 and the correlations versus experimental data

The performance of NUIGMech1.2 compared to the new experimental ST and RCM IDT data for various ternary and quaternary blends of CH₄/C₂H₄/C₂H₆ and CH₄/C₂H₄/C₂H₆/C₃H₈ fuels, Table 4-1, is shown in Figs. 4-3 and 4-4. The symbols refer to the experimental data, with the solid lines

from NUIGMech1.2 simulations and the dashed lines representing the correlation equation results. These correlations are derived over well-defined conditions, as discussed in Section 4.4.4.

Figures 4-3 and 4-4 show that NUIGMech1.2 can reasonably reproduce all of the measured IDTs over the stochastically distributed conditions studied. It not only reproduces the effects of mixture composition and temperature on IDTs, but it can also reliably predict the effects of pressure, equivalence ratio, and the effect of dilution except at very high-pressures (≥ 90 bar) where the model under-predicts the IDTs for the ternary blends of the $\text{CH}_4/\text{C}_2\text{H}_4/\text{C}_2\text{H}_6$ mixtures. A detailed comparison between the performance of NUIGMech1.2 and other available mechanisms is provided in Section 9 of Appendix B. Considering similar comparisons of $\text{C}_1 - \text{C}_3$ pure and binary fuels mixtures, including methane, ethane, ethylene, and propane, over the wide range of physical and chemical conditions presented previously by the authors [2-4], NUIGMech1.2 better reproduces the oxidation behavior of small hydrocarbon species compared to the other similar available mechanisms [23-32].

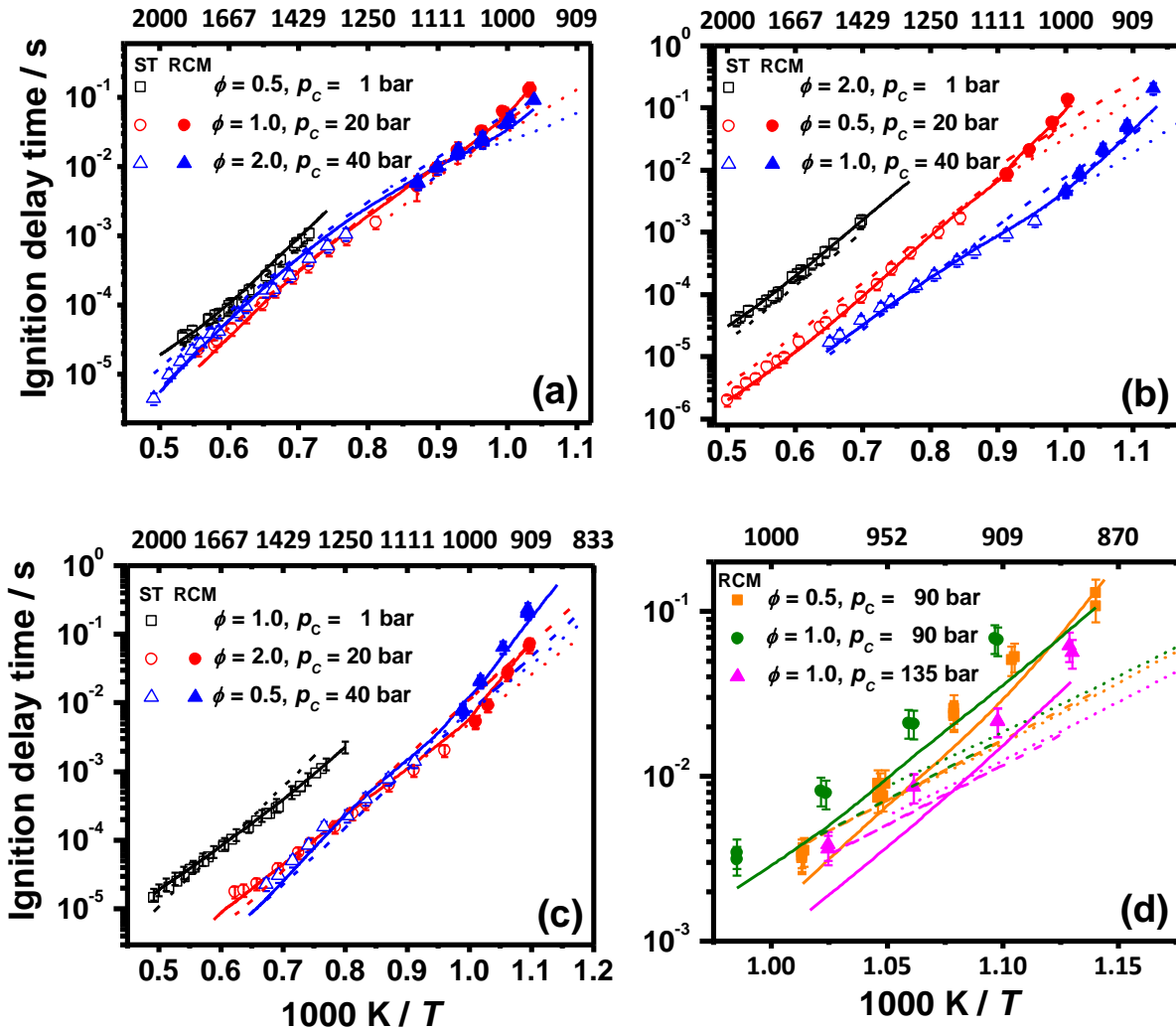


Figure 4-3. Experimental and simulated IDT data of CH₄/C₂H₄/C₂H₆ mixtures. (a) 90% CH₄/5% C₂H₄/5% C₂H₆ blend at 75% N₂ (black square symbols/lines), 75% N₂+10% Ar (red circle symbols/lines), and 75% N₂+15% Ar (blue triangle symbols/lines), (b) 75% CH₄/12.5% C₂H₄/12.5% C₂H₆ blend at 75% N₂+10% Ar (black square symbols/lines), 75% N₂+15% Ar (red circle symbols/lines), and 75% N₂ (blue triangle symbols/lines), (c) 60% CH₄/20% C₂H₄/20% C₂H₆ blend at 75% N₂+15% Ar (black square symbols/lines), 75% N₂ (red circle symbols/lines), and 75% N₂+10% Ar (blue triangle symbols/lines), (d) 90% CH₄/5% C₂H₄/5% C₂H₆ blend at 90 bar with 67.8% N₂+7.5% Ar (orange square symbols/lines), 68.3% N₂+17% Ar (olive green circle symbols/lines), and at 135 bar with 68.3% N₂+17% Ar (magenta triangle symbols/lines). Solid lines: NUIGMech1.2; dashed lines: derived correlations; and dotted lines: CV – low-temperature simulations.

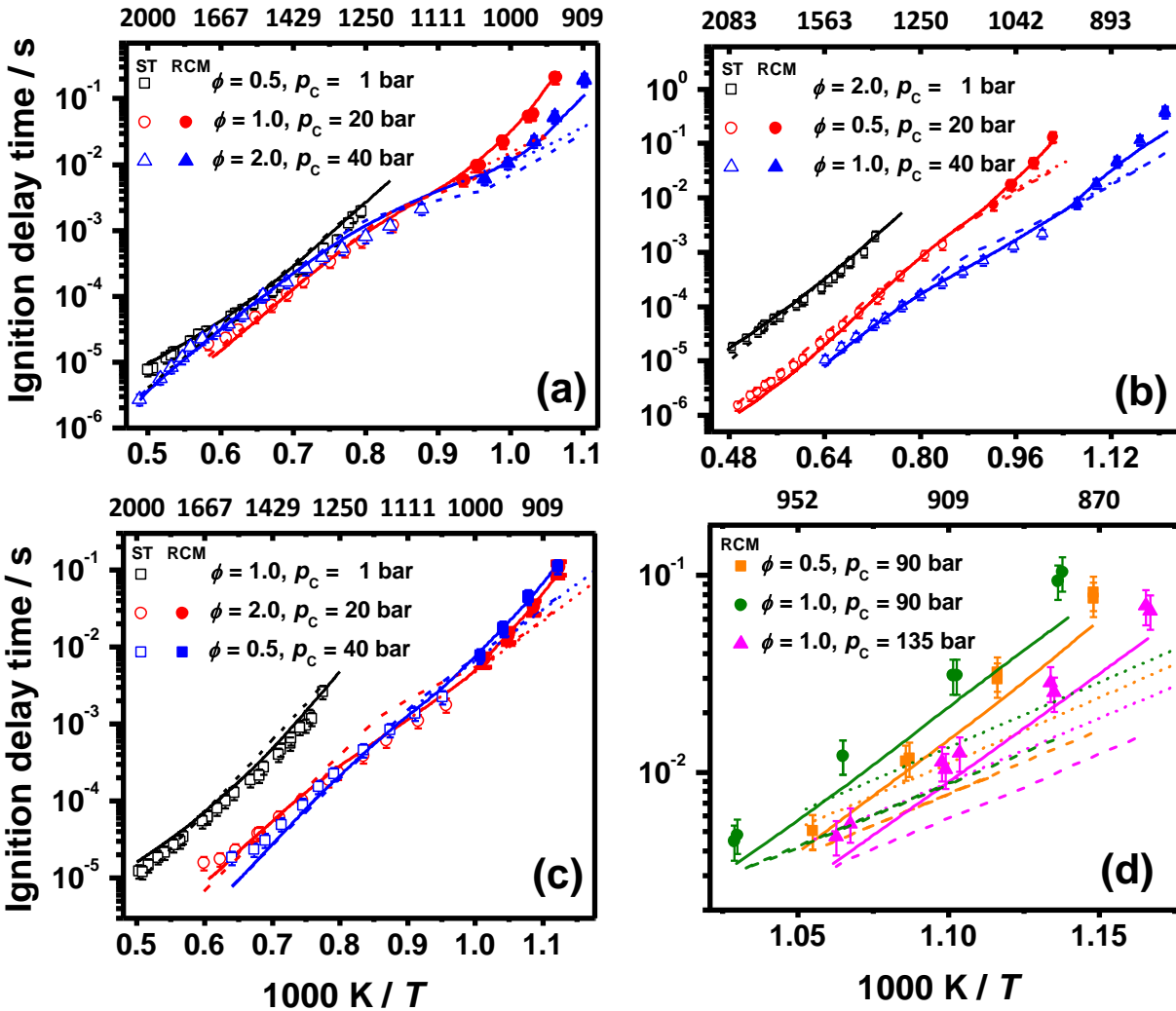


Figure 4-4. Experimental and simulated IDT data for $\text{CH}_4/\text{C}_2\text{H}_4/\text{C}_2\text{H}_6/\text{C}_3\text{H}_8$ mixtures. (a) 80% $\text{CH}_4/5\%$ $\text{C}_2\text{H}_4/10\%$ $\text{C}_2\text{H}_6/5\%$ C_3H_8 blend at 75% N_2 (black square symbols/lines), 85% N_2 (red circle symbols/lines), and 90% N_2 (blue triangle symbols/lines), (b) 70% $\text{CH}_4/10\%$ $\text{C}_2\text{H}_4/10\%$ $\text{C}_2\text{H}_6/10\%$ C_3H_8 blend at 75% $\text{N}_2+10\%$ Ar (black square symbols/lines), 90% N_2 (red circle symbols/lines), and 75% N_2 (blue triangle symbols/lines), (c) 60% $\text{CH}_4/15\%$ $\text{C}_2\text{H}_4/15\%$ $\text{C}_2\text{H}_6/10\%$ C_3H_8 blend at 75% $\text{N}_2+15\%$ Ar (black square symbols/lines), 75% N_2 (red circle symbols/lines), and 85% N_2 (blue triangle symbols/lines), (d) 80% $\text{CH}_4/5\%$ $\text{C}_2\text{H}_4/10\%$ $\text{C}_2\text{H}_6/5\%$ C_3H_8 blend at 90 bar with 68.1% $\text{N}_2+7.5\%$ Ar (orange square symbols/lines), 68.5% $\text{N}_2+17.1\%$ Ar (olive green circle symbols/lines), and at 135 bar with 68.5% $\text{N}_2+17.1\%$ Ar (magenta triangle symbols/lines). Solid lines: NUIGMech1.2; dashed lines: derived correlations; and dotted lines: CV – low-temperature simulations.

4.4.2 Effect of blending on ignition

To determine the chemistry controlling ignition times of $\text{CH}_4/\text{C}_2\text{H}_4/\text{C}_2\text{H}_6/\text{'air'}$ and $\text{CH}_4/\text{C}_2\text{H}_4/\text{C}_2\text{H}_6/\text{C}_3\text{H}_8/\text{'air'}$ blends, Fig. 4-5(a) depicts the IDTs of single fuel mixtures of $\text{CH}_4/\text{'air'}$, $\text{C}_2\text{H}_4/\text{'air'}$, $\text{C}_2\text{H}_6/\text{'air'}$, $\text{C}_3\text{H}_8/\text{'air'}$, while binary mixtures of $\text{CH}_4/\text{C}_2\text{H}_6/\text{'air'}$ are depicted together with

the ternary and quaternary blends at fuel-stoichiometric condition, at a pressure of 40 atm and temperatures in the range 714–1667 K.

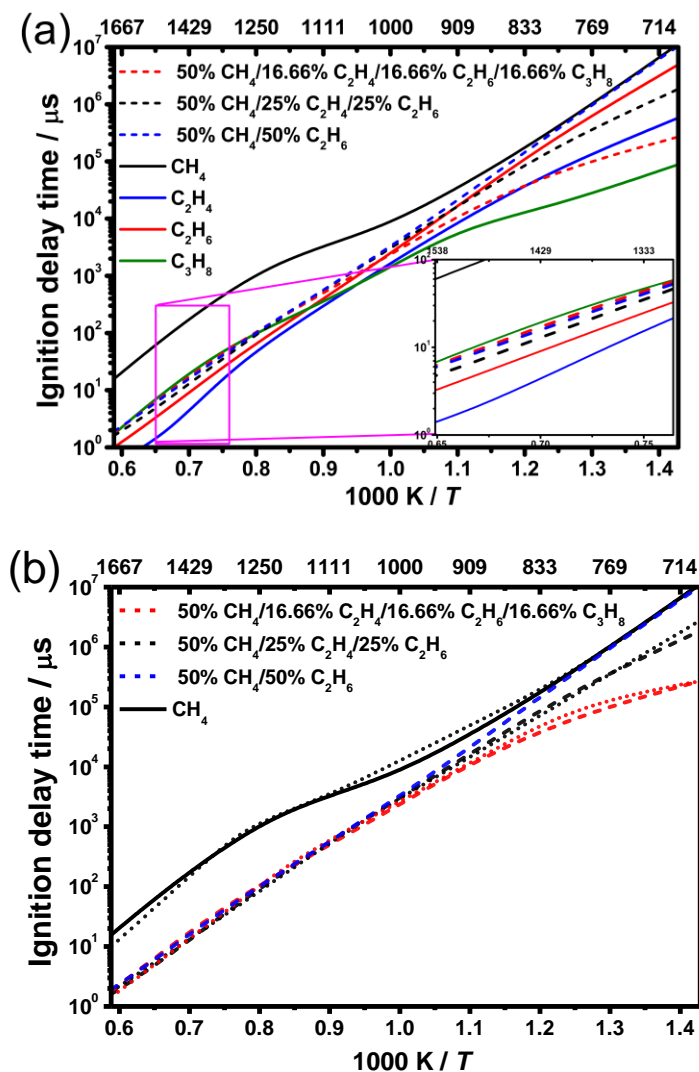


Figure 4-5. (a) Comparisons of IDT predictions for various single, binary, ternary, and quaternary fuels in air at $p_C = 40$ atm and $\phi = 1.0$, and (b) the predictions of their corresponding correlations (dotted lines).

At first glance, in Fig. 4-5(a), the CH_4 /'air' mixture is the slowest to ignite over the entire temperature range studied in this work, while the C_2H_6 /'air' is the next slowest in the low-temperature regime (< 900 K), being $\sim 25\%$ faster than CH_4 . However, C_2H_6 /'air' becomes the second-fastest mixture to ignite, after ethylene, by inverting its trend at $\sim T_C = 1100$ K. Overall, C_2H_6 /'air' mixtures are approximately an order of magnitude faster to ignite than CH_4 and are $\sim 50\%$ faster compared to the C_3H_8 /'air' mixtures, but are slower by a factor of ~ 1.5 when compared to C_2H_4 /'air' mixtures at

temperatures higher than 1150 K. The C_2H_4 /'air' mixtures are the fastest to ignite at high-temperatures, but exhibit shorter IDTs compared to the C_3H_8 /'air' mixtures at the temperature below ~ 1050 K, with propane being the fastest fuel to ignite in the low-temperature regime.

To determine the chemistry controlling the reactivities of various fuel/'air' mixtures, reaction pathways based on multiple rate of production (ROP) analyses are illustrated in Fig. 4-6 for (i) the pure fuels in 'air', (ii) the 50% CH_4 /50% C_2H_6 binary mixtures, (iii) the 50% CH_4 /25% C_2H_4 /25% C_2H_6 / ternary mixtures, and (iv) the 50% CH_4 /16.66% C_2H_4 /16.66% C_2H_6 /16.66% C_3H_8 quaternary mixtures at $p_C = 40$ atm, $\phi = 1.0$, for (a) $T_C = 800$ K and (b) $T_C = 1450$ K. The ROP analyses are implemented following a standardized elemental carbon balance. The normalised values above the arrow denote the fractions of the parent fuel proceeding via various reaction pathways. Moreover, sensitivity analyses are performed at $p_C = 40$ atm, $\phi = 1.0$, for (a) $T_C = 800$ K and (b) $T_C = 1450$ K to interpret the most sensitive reactions to IDTs and are presented in Fig. 4-7.

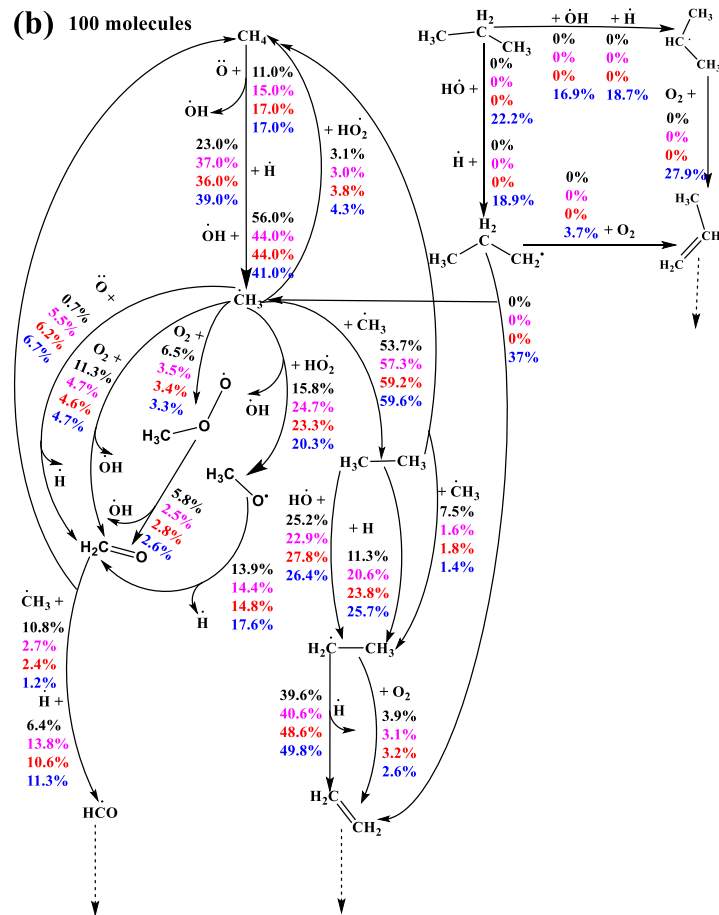


Figure 4-6. Flux analyses of pure CH_4 (black), 50% CH_4 /50% C_2H_6 blend (magenta), 50% CH_4 /25% C_2H_4 /25% C_2H_6 blend (red), and 50% CH_4 /16.66% C_2H_4 /16.66% C_2H_6 /16.66% C_3H_8 (blue) mixtures at $p_c = 40$ atm and $\varphi = 1.0$, at the time of 20% fuel consumed for (a) $T_c = 800$ K and (b) $T_c = 1450$ K.

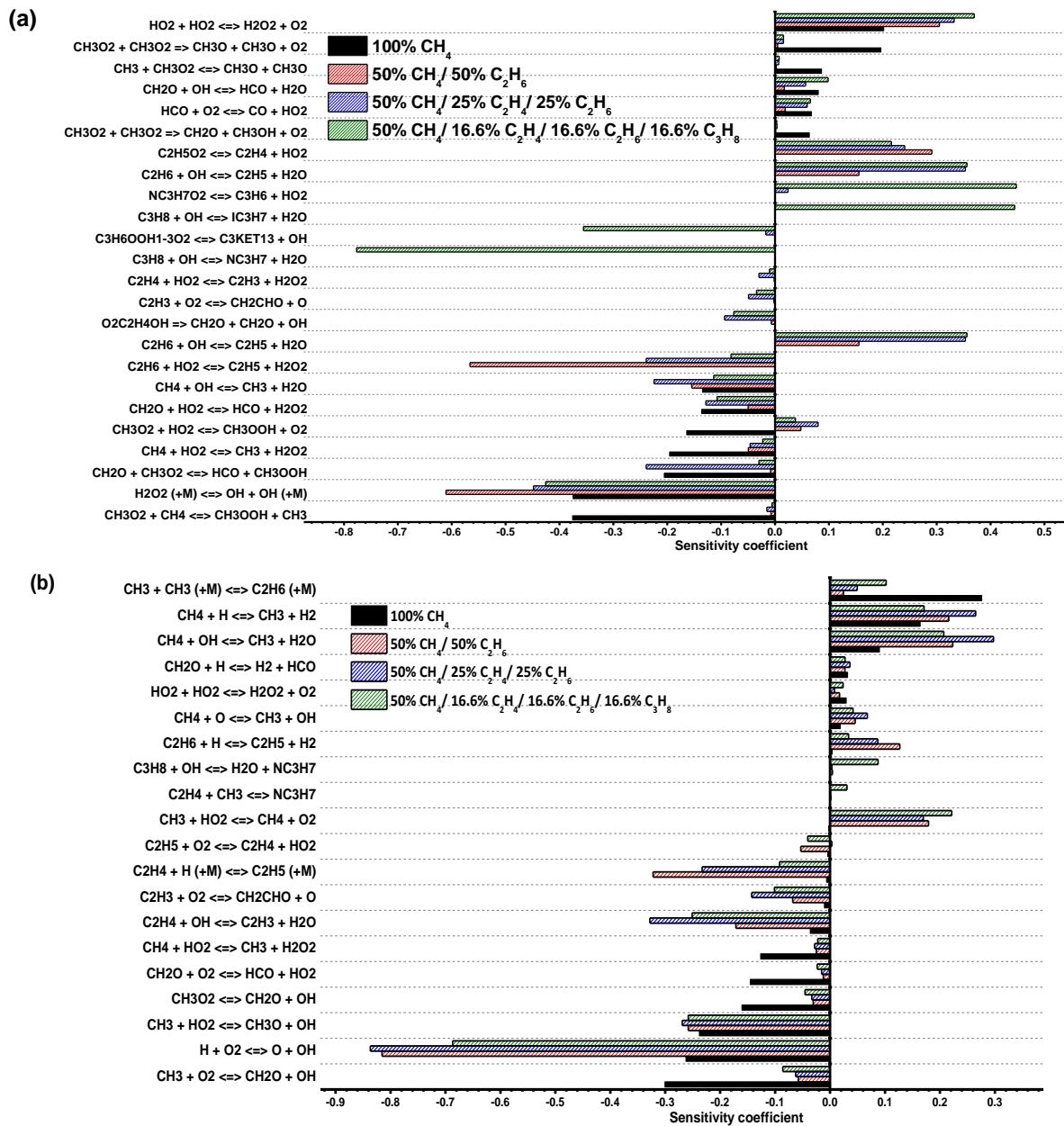


Figure 4-7. Sensitivity analyses to IDTs for pure CH_4 , 50% CH_4 /50% C_2H_6 blend, 50% CH_4 /25% C_2H_4 /25% C_2H_6 blend, and 50% CH_4 /16.66% C_2H_4 /16.66% C_2H_6 /16.66% C_3H_8 mixtures in ‘air’ at $p_C = 40$ atm, $\phi = 1.0$, for (a) $T_C = 800$ K and (b) $T_C = 1450$ K.

Figure 4-7(b) shows that, at 1450 K, the chain branching reaction $\dot{\text{H}} + \text{O}_2 \leftrightarrow \ddot{\text{O}} + \dot{\text{O}}\text{H}$ governs and promotes the ignition of the fuel/‘air’ mixtures, the rate of which depends on the amount of hydrogen atoms and molecular oxygen available in the mixtures. However, for the CH_4 /‘air’ mixture, methyl ($\dot{\text{C}}\text{H}_3$) radicals rather than $\dot{\text{H}}$ atoms dominate the ignition behaviour, with $\dot{\text{C}}\text{H}_3 + \text{H}\dot{\text{O}}_2 \leftrightarrow \text{CH}_3\dot{\text{O}}$

+ $\dot{\text{O}}\text{H}$ and $\dot{\text{C}}\text{H}_3 + \dot{\text{O}}_2 \leftrightarrow \text{CH}_2\text{O} + \dot{\text{O}}\text{H}$ being the most sensitive reactions promoting reactivity, and $\dot{\text{C}}\text{H}_3 + \dot{\text{C}}\text{H}_3 (+\text{M}) \leftrightarrow \text{C}_2\text{H}_6 (+\text{M})$ is the most sensitive reaction inhibiting reactivity, as illustrated in Fig. 4-7(b). At 1450 K, CH_4 is mostly consumed by H-atom abstraction by $\dot{\text{H}}$, $\dot{\text{O}}$ and $\dot{\text{O}}\text{H}$ radicals producing methyl ($\dot{\text{C}}\text{H}_3$) radicals, Fig. 4-6(b). Approximately 11% of these $\dot{\text{C}}\text{H}_3$ radicals react with O_2 through $\dot{\text{C}}\text{H}_3 + \text{O}_2 \leftrightarrow \text{CH}_2\text{O} + \dot{\text{O}}\text{H}$ to generate formaldehyde (CH_2O) and $\dot{\text{O}}\text{H}$ radicals in a reaction that greatly promotes the reactivity of the mixture, as seen by the sensitivity analysis presented in Fig. 4-7(b). The CH_2O then reacts with $\dot{\text{C}}\text{H}_3$ radical and leads to the formation of CH_4 and formyl ($\dot{\text{H}}\text{C}\dot{\text{O}}$) radical. Another pathway contributing to the consumption of the $\dot{\text{C}}\text{H}_3$ radicals (15.8%) is the chain branching reaction $\dot{\text{C}}\text{H}_3 + \dot{\text{H}}\text{O}_2 \leftrightarrow \text{CH}_3\dot{\text{O}} + \dot{\text{O}}\text{H}$, which produces methoxy ($\text{CH}_3\dot{\text{O}}$) and $\dot{\text{O}}\text{H}$ radicals, significantly promoting reactivity, Figs. 4-6(b) and 4-7(b). The current mechanism employs the rate coefficients for $\dot{\text{C}}\text{H}_3 + \dot{\text{H}}\text{O}_2 \leftrightarrow \text{CH}_3\dot{\text{O}} + \dot{\text{O}}\text{H}$ from the theoretical calculation by Jasper et al. [33]. This reaction channel directly competes against the chain-terminating reaction $\dot{\text{C}}\text{H}_3 + \dot{\text{H}}\text{O}_2 \leftrightarrow \text{CH}_4 + \text{O}_2$ for the hydroperoxyl ($\dot{\text{H}}\text{O}_2$) radicals, as shown in Fig. 4-7(b), and the current mechanism utilizes the rate constant from Zhu et al. [34] for this inhibiting pathway. At the high temperature of 1450 K, ~7% of methyl ($\dot{\text{C}}\text{H}_3$) radicals react with O_2 to form methyl peroxy ($\text{CH}_3\dot{\text{O}}_2$) radicals via $\dot{\text{C}}\text{H}_3 + \text{O}_2 \leftrightarrow \text{CH}_3\dot{\text{O}}_2$. These radicals further dissociate to CH_2O and $\dot{\text{O}}\text{H}$ radicals, promoting reactivity as illustrated in Fig. 4-7(b). This direct dissociation of $\text{CH}_3\dot{\text{O}}_2$ radicals was not incorporated in the previous mechanism, and in NUIGMech1.2, the rate constant for this reaction is adopted based on an extensive study of rate rules by Villano et al. [35] derived using electronic structure calculations.

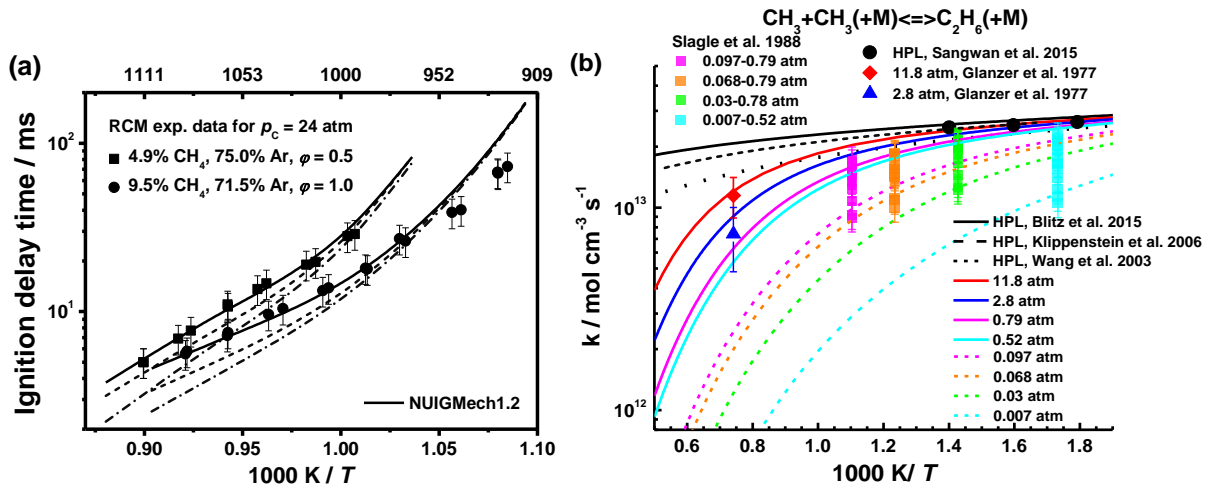


Figure 4-8. (a) Effects of addition of $\text{CH}_3\dot{\text{O}}_2 \leftrightarrow \text{CH}_2\text{O} + \dot{\text{O}}\text{H}$ reaction and updated $\dot{\text{C}}\text{H}_3 + \dot{\text{C}}\text{H}_3 (+\text{M}) \leftrightarrow \text{C}_2\text{H}_6 (+\text{M})$ rate constant on the IDTs for 4.9% CH_4 at $\varphi = 0.5$ [36] and 9.5% CH_4 at $\varphi = 1.0$ [36]; -----, NUIGMech1.1; - · - ·, NUIGMech1.1 plus $\text{CH}_3\dot{\text{O}}_2 \leftrightarrow \text{CH}_2\text{O} + \dot{\text{O}}\text{H}$ [35]; —, NUIGMech1.2 which includes $\text{CH}_3\dot{\text{O}}_2 \leftrightarrow$

$\text{CH}_2\text{O} + \dot{\text{O}}\text{H}$ [35] reaction as well as an updated rate constant for $\dot{\text{C}}\text{H}_3 + \dot{\text{C}}\text{H}_3 (+\text{M}) \leftrightarrow \text{C}_2\text{H}_6 (+\text{M})$. (b) Comparisons of the rate constants for $\dot{\text{C}}\text{H}_3 + \dot{\text{C}}\text{H}_3 (+\text{M}) \leftrightarrow \text{C}_2\text{H}_6 (+\text{M})$ [37-42].

Figure 4-8(a) shows the importance of the addition of the $\text{CH}_3\dot{\text{O}}_2$ dissociation channel and the updated rate constant for $\dot{\text{C}}\text{H}_3 + \dot{\text{C}}\text{H}_3 (+\text{M}) \leftrightarrow \text{C}_2\text{H}_6 (+\text{M})$ on the IDT predictions using NUIGMech1.2 compared to NUIGMech1.1, which slightly under-predicts the IDTs in the intermediate temperature range of 1000 – 1100 K at $p_C = 24$ atm, and for both $\phi = 0.5$ and 1.0. The addition of the $\text{CH}_3\dot{\text{O}}_2 \leftrightarrow \text{CH}_2\text{O} + \dot{\text{O}}\text{H}$ reaction channel results in a decrease in predicted IDTs represented by dashed-dotted lines in Fig. 4-8(a). Nonetheless, an excellent improvement in IDT prediction is achieved by updating the $\dot{\text{C}}\text{H}_3 + \dot{\text{C}}\text{H}_3 (+\text{M}) \leftrightarrow \text{C}_2\text{H}_6 (+\text{M})$ rate constants together with the inclusion of $\text{CH}_3\dot{\text{O}}_2$ dissociation reaction ($\text{CH}_3\dot{\text{O}}_2 \leftrightarrow \text{CH}_2\text{O} + \dot{\text{O}}\text{H}$) in NUIGMech1.2, as depicted by the solid lines in Fig. 4-8(a).

According to the ROP and the sensitivity analysis of CH_4 /'air' mixtures, at high temperatures (1450 K) a significant quantity (~55%) of the methyl radicals undergo self-recombination to form C_2H_6 making methane the slowest fuel to ignite compared to the other single fuels. The self-recombination reaction of methyl radicals has been widely studied in the literature. Comparisons of pressure-dependent rate constants and various experimental measurements for $\dot{\text{C}}\text{H}_3 + \dot{\text{C}}\text{H}_3 (+\text{M}) \leftrightarrow \text{C}_2\text{H}_6 (+\text{M})$ from the literature [37-42] are shown in Fig. 4-8(b). NUIGMech1.1 employed a rate constant from the experimental and theoretical study of Wang et al. [41] for this reaction. Here NUIGMech1.2 uses the fit derived from a comprehensive experimental review by Blitz et al. [40] for the high-pressure limit rate constant. We have chosen this rate constant as the revised high-pressure limit is in good agreement with the recent experimental study by Sangwan et al. [38] in the temperature range 292 – 714 K as well as with the high-level theoretical calculation by Klippenstein et al. [42]. Figure 4-8(b) shows that the high-pressure limit reported by Wang et al. [41] is ~17% slower than that measured by Sangwan et al. [38] at 714 K. In NUIGMech1.2 the low-pressure limit and the fall-off parameters are taken from Wang et al. [41], as this satisfactory match the experimental measurements from Slagle et al. [37] and Glanzer et al. [39] in the pressure-dependent fall-off regime, Fig. 4-8(b).

In Fig. 4-6(a), the ROP analysis of the pure CH_4 /'air' mixture at 800 K shows that ~50% of $\dot{\text{C}}\text{H}_3$ radicals react with $\text{H}\dot{\text{O}}_2$ forming methoxy ($\text{CH}_3\dot{\text{O}}$) radicals by $\dot{\text{C}}\text{H}_3 + \text{H}\dot{\text{O}}_2 \leftrightarrow \text{CH}_3\dot{\text{O}} + \dot{\text{O}}\text{H}$, which further decomposes through $\text{CH}_3\dot{\text{O}} (+\text{M}) \leftrightarrow \text{CH}_2\text{O} + \dot{\text{H}} (+\text{M})$ to produce formaldehyde (CH_2O) and $\dot{\text{H}}$ atoms. A significant quantity of $\dot{\text{C}}\text{H}_3$ (30%) reacts with O_2 to form methyl peroxy radicals through $\dot{\text{C}}\text{H}_3 + \text{O}_2 \leftrightarrow \text{CH}_3\dot{\text{O}}_2$. Approximately ~11% of $\text{CH}_3\dot{\text{O}}_2$ is consumed by its reaction with $\text{H}\dot{\text{O}}_2$, via $\text{CH}_3\dot{\text{O}}_2$

+ $\dot{\text{H}}\text{O}_2 \leftrightarrow \text{CH}_3\text{OOH} + \text{O}_2$ followed by rapid dissociation of the methyl hydroperoxide (CH_3OOH) into methoxy ($\text{CH}_3\dot{\text{O}}$) and $\dot{\text{O}}\text{H}$ radicals, thus significantly enhancing reactivity. Furthermore, considerable amounts of CH_3OOH can be produced from $\text{CH}_3\dot{\text{O}}_2$ by $\text{CH}_3\dot{\text{O}}_2 + \text{CH}_4 \leftrightarrow \text{CH}_3\text{OOH} + \dot{\text{C}}\text{H}_3$ and $\text{CH}_2\text{O} + \text{CH}_3\dot{\text{O}}_2 \leftrightarrow \text{HCO} + \text{CH}_3\text{OOH}$ reactions promoting methane ignition at low temperatures, as can be seen in Fig. 4-7(a). The ROP analysis shows that ~17% of $\text{CH}_3\dot{\text{O}}_2$ radicals further react with $\dot{\text{C}}\text{H}_3$ to produce two methoxy radicals through $\text{CH}_3\dot{\text{O}}_2 + \dot{\text{C}}\text{H}_3 \leftrightarrow \text{CH}_3\dot{\text{O}} + \text{CH}_3\dot{\text{O}}$. Figure 4-7(a) also shows that this reaction along with $\text{CH}_3\dot{\text{O}}_2 + \text{CH}_3\dot{\text{O}}_2 \leftrightarrow \text{CH}_3\dot{\text{O}} + \text{CH}_3\dot{\text{O}} + \text{O}_2$ competes for $\text{CH}_3\dot{\text{O}}_2$ radicals with the chain propagating reactions $\text{CH}_4 + \text{CH}_3\dot{\text{O}}_2 \leftrightarrow \text{CH}_3\text{OOH} + \dot{\text{C}}\text{H}_3$ and $\text{CH}_2\text{O} + \text{CH}_3\dot{\text{O}}_2 \leftrightarrow \text{HCO} + \text{CH}_3\text{OOH}$ producing methyl hydroperoxide, thus decreasing the reactivity of the CH_4 /'air' mixture. NUIGMech1.2 utilizes the rate constant recommended by Lightfoot et al. [43] for $\text{CH}_3\dot{\text{O}}_2 + \text{CH}_3\dot{\text{O}}_2 \leftrightarrow \text{CH}_3\dot{\text{O}} + \text{CH}_3\dot{\text{O}} + \text{O}_2$ based on flash photolysis measurements at atmospheric and low temperatures conditions, as shown in Fig. BS51. For $\text{CH}_3\dot{\text{O}}_2 + \dot{\text{C}}\text{H}_3 \leftrightarrow \text{CH}_3\dot{\text{O}} + \text{CH}_3\dot{\text{O}}$, the rate coefficients are adopted from the work of Keiffer et al. [44], as shown in Fig. BS52. However, further research is recommended in the study of the rate constant of this reaction. Finally, at 800 K, the remaining 12% of $\dot{\text{C}}\text{H}_3$ radicals react through the self-recombination reaction $\dot{\text{C}}\text{H}_3 + \dot{\text{C}}\text{H}_3 (+\text{M}) \leftrightarrow \text{C}_2\text{H}_6 (+\text{M})$, thus activating the C_2H_6 chemistry.

Unlike the case for CH_4 /'air' mixtures, the most important reaction promoting the reactivity at high temperatures for the binary, ternary and quaternary blends is the chain branching reaction $\dot{\text{H}} + \text{O}_2 \leftrightarrow \dot{\text{O}} + \dot{\text{O}}\text{H}$. This is because C_2H_4 , C_2H_6 , and C_3H_8 mixtures generate larger concentrations of $\dot{\text{H}}$ atoms compared to CH_4 /'air' mixtures and consequently increases the fuel reactivities of the blended mixtures at the high-temperature conditions, as shown in Fig. 4-5. In a previous study [4], the important reactions, as well as the choice of their rate constants governing the oxidation behavior of C_2H_4 /'air', C_2H_6 /'air', C_3H_8 /'air' mixtures and their binary blends, were discussed in detail. Thus, in this work, particular emphasis is placed on understanding the synergistic and antagonistic effects of ethane/ethylene/propane fuels on the ignition of methane/fuel mixtures.

The consumption of C_2H_6 is initiated by H-atom abstraction, mainly by $\dot{\text{O}}\text{H}$ radicals and $\dot{\text{H}}$ atoms producing ethyl radicals ($\dot{\text{C}}_2\text{H}_5$), through $\text{C}_2\text{H}_6 + \dot{\text{H}}/\dot{\text{O}}\text{H} \leftrightarrow \dot{\text{C}}_2\text{H}_5 + \text{H}_2/\text{H}_2\text{O}$. Most ethyl radicals decompose to C_2H_4 and $\dot{\text{H}}$ atoms via $\dot{\text{C}}_2\text{H}_5 (+\text{M}) \leftrightarrow \text{C}_2\text{H}_4 + \dot{\text{H}} (+\text{M})$. Ethylene can further undergo H-atom abstraction reactions to form vinyl radicals ($\dot{\text{C}}_2\text{H}_3$) which are responsible for the generation of a substantial amount of $\dot{\text{H}}$ atoms by their reaction with O_2 via $\dot{\text{C}}_2\text{H}_3 + \text{O}_2 \leftrightarrow \dot{\text{C}}\text{H}_2\text{CHO} + \dot{\text{O}}$ and $\text{CH}_2\text{CHO} \leftrightarrow \text{CH}_2\text{CO} + \dot{\text{H}}$, ultimately leading to the faster ignition of C_2H_6 /air mixtures compared to

CH₄/air mixtures, as shown in Fig. 4-5(a). The remaining \dot{C}_2H_5 radicals react with O₂ to produce ethylene through $\dot{C}_2H_5 + O_2 \leftrightarrow C_2H_4 + \dot{H}O_2$, which directly competes with $\dot{C}_2H_5 (+M) \leftrightarrow C_2H_4 + \dot{H} (+M)$, resulting in a shorter IDT for C₂H₆/air mixture compared to C₂H₄/air mixture. The effect on IDTs of the addition of ethane to CH₄/air mixtures is presented in Fig. 4-5(a). The reactivity of the mixture increases significantly for the 50% CH₄/50% C₂H₆ binary blend at high temperatures (> 1000 K) compared to the pure methane mixture. In Fig. 4-6(b), the magenta-bold percentages represent the ROP for 50% CH₄/50% C₂H₆ binary mixtures at 40 atm, $\varphi = 1.0$ and $T_C = 1450$ K. Flux analyses show that the addition of C₂H₆ to CH₄/air mixtures does not alter the main reaction pathways corresponding to the pure CH₄ chemistry; however, it leads to increased production of \dot{H} atoms which increases the sensitivity coefficients of $\dot{H} + O_2 \leftrightarrow \ddot{O} + \dot{O}H$ and $C_2H_4 + \dot{O}H \leftrightarrow \dot{C}_2H_3 + \dot{H}O_2$ for the 50% CH₄/50% C₂H₆ binary mixtures, Fig. 4-7(b). On the contrary, the reactions $CH_4 + \dot{H} \leftrightarrow \dot{C}H_3 + H_2$ and $CH_4 + \dot{O}H \leftrightarrow \dot{C}H_3 + H_2O$ compete for the available \dot{H} atoms and $\dot{O}H$ radicals which exhibit higher positive sensitive coefficients for the C₂H₆-blended mixtures in comparison to the pure CH₄ case.

At low temperatures, pure C₂H₆/air mixture is still faster to ignite than pure CH₄/'air' mixture, but the difference between the two IDTs decreases with a decrease in temperature, Fig. 4-5(a). Furthermore, for the 50% CH₄/50% C₂H₆ binary blend, the IDT predictions overlap with the pure CH₄ ones at low-temperature conditions. The sensitivity analysis shows that the sensitivities of $H_2O_2 (+M) \leftrightarrow \dot{O}H + \dot{O}H (+M)$ and $\dot{H}O_2 + \dot{H}O_2 \leftrightarrow H_2O_2 + O_2$ are strengthened by the addition of 50% C₂H₆ to CH₄/air mixtures. This is because, compared to the pure CH₄ case, H-atom abstraction from C₂H₆ by $\dot{H}O_2$ radicals exhibits a relatively larger negative sensitivity coefficient promoting reactivity, which is attributed to the higher rate constant of $C_2H_6 + \dot{H}O_2 \leftrightarrow \dot{C}_2H_5 + H_2O_2$, which is approximately an order of magnitude faster than that of $CH_4 + \dot{H}O_2 \leftrightarrow \dot{C}H_3 + H_2O_2$. However, most of the \dot{C}_2H_5 radicals formed add to O₂ producing ethylperoxy (C₂H₅ \dot{O}_2) radicals, followed by the concerted elimination reaction $C_2H_5\dot{O}_2 \leftrightarrow C_2H_4 + \dot{H}O_2$, which plays an important role in inhibiting the ignition of the C₂H₆ blended mixtures at low temperatures, Fig. 4-7(a).

C₂H₄ is an essential intermediate of C₂H₆ chemistry and is the fastest fuel to ignite compared to the other single fuels at high temperatures. The effect on IDT predictions of the addition of C₂H₄ to a CH₄/C₂H₆/'air' mixture is presented in Fig. 4-5(a). The reactivity of the 50% CH₄/25% C₂H₆/25% C₃H₈ ternary blend is ~15% faster than the CH₄/C₂H₆ binary blend at high temperatures (> 1000 K). Moreover, at low temperatures, the ternary blend is ~80% faster than the binary blend. The main reason for the increased reactivity of C₂H₄ blended mixtures at high temperatures is attributed to the

substantial formation of \dot{H} atoms due to the reaction sequence, $C_2H_4 + \ddot{O} \leftrightarrow \dot{C}H_2CHO + \dot{H}$, and $C_2H_4 + \ddot{O} \leftrightarrow \dot{C}H_2 + CH_2O$, followed by $\dot{C}H_2 + O_2 \leftrightarrow CO_2 + \dot{H} + \dot{H}$ [4], thus increasing the importance of the $\dot{H} + O_2 \leftrightarrow \ddot{O} + \dot{O}H$ and $C_2H_4 + \dot{O}H \leftrightarrow \dot{C}_2H_3 + H\dot{O}_2$ reactions for the ternary blend compared to the binary blend mixtures, Fig. 4-7(b). On the other hand, at low temperatures (< 1000 K), C_2H_4 is primarily consumed by the addition of $\dot{O}H$ radicals producing hydroxyl-ethyl (\dot{C}_2H_4OH) radicals which add to molecular oxygen to form hydroxyethylene-peroxy ($\dot{O}_2C_2H_4OH$) radicals. The dissociation of $\dot{O}_2C_2H_4OH$ radicals ultimately increases the reactivity of the ethylene blended mixtures at low temperatures by generating two molecules of formaldehyde and $\dot{O}H$ radicals. For the ternary mixtures, $\dot{O}H$ radicals are also formed through the reaction $C_2H_4 + H\dot{O}_2 \leftrightarrow C_2H_4O1-2$ (oxirane) + $\dot{O}H$, further promoting reactivity.

Propane/‘air’ oxidation at high temperatures (> 900 K) is mainly dominated by H-atom abstraction by $\dot{O}H$ radicals and \dot{H} atoms, leading to the formation of n-propyl ($n\dot{C}_3H_7$) and iso-propyl ($i\dot{C}_3H_7$) radicals. Most $n\dot{C}_3H_7$ radicals decompose via β -scission $n\dot{C}_3H_7 \leftrightarrow C_2H_4 + \dot{C}H_3$. The methyl radicals so formed can react with hydroperoxyl radicals either via $\dot{C}H_3 + H\dot{O}_2 \leftrightarrow CH_3\dot{O} + \dot{O}H$, which promotes reactivity, or $\dot{C}H_3 + H\dot{O}_2 \leftrightarrow CH_4 + O_2$, which inhibits reactivity. Methyl radicals also self-react to form C_2H_6 , further reducing the reactivity of the propane/air mixtures. The effect on IDTs of adding C_3H_8 to $CH_4/C_2H_6/C_2H_4$ /‘air’ mixtures is shown in Fig. 4-5(a). At high temperatures, the 50% $CH_4/16.66\%$ $C_2H_6/16.66\%$ $C_2H_4/16.66\%$ C_3H_8 quaternary blend is ~15% slower than the 50% $CH_4/25\%$ $C_2H_6/25\%$ C_3H_8 ternary mixtures, Fig. 4-5(a). The sensitivity analysis, Fig. 4-7(b), shows that at 1450 K, the main chain branching reaction $\dot{H} + O_2 \leftrightarrow \ddot{O} + \dot{O}H$ is relatively less sensitive to the IDT of the quaternary blends compared to the ternary blends leading to a lower reactivity of the 50% $CH_4/16.66\%$ $C_2H_6/16.66\%$ $C_2H_4/16.66\%$ C_3H_8 /air mixtures. Fig. 4-6(b) shows that the addition of pure C_3H_8 to $CH_4/C_2H_6/C_2H_4$ ternary blends becomes an important source of methyl radicals produced from the β -scission of $n\dot{C}_3H_7$ radicals, is responsible for the slower reactivity of the quaternary blends compared to the ternary blends at higher temperatures.

Figure 4-7(a) shows that at lower temperature the reactivity of the quaternary blends is governed by $C_3H_8 + \dot{O}H \leftrightarrow n\dot{C}_3H_7 + H_2O$ being the most reactivity promoting channel, while the most sensitive reactions inhibiting the reactivity are $C_3H_8 + \dot{O}H \leftrightarrow i\dot{C}_3H_7 + H_2O$ and $n\dot{C}_3H_7O_2 \leftrightarrow C_3H_6 + H\dot{O}_2$. At $T_C < 900$ K, $n\dot{C}_3H_7$ radicals add to molecular oxygen producing n-propyl-peroxy ($nC_3H_7\dot{O}_2$) radicals, which then isomerize to hydroperoxyl-propyl ($\dot{C}_3H_6OOH1-3$) radicals that can add to molecular oxygen generating hydroperoxyl-propyl-peroxy ($C_3H_6OOH1-3\dot{O}_2$) radicals. The

$C_3H_6OOH-3\dot{O}_2$ radicals can further isomerize and generate carbonyl hydroperoxide and $\dot{O}H$ radicals. Finally, the carbonyl hydroperoxide undergoes $RO-OH$ bond cleavage, producing a second $\dot{O}H$ radical and a carbonyl-alkoxy ($R\dot{O}$) radical in a chain branching process that increases the reactivity of propane at low temperatures, Fig. 4-6(a). The addition of propane to the ternary blends significantly increases the reactivity of the 50% $CH_4/16.66\% C_2H_6/16.66\% C_2H_4/16.66\% C_3H_8$ quaternary blends, this being just less reactive than the pure C_3H_8 /'air' mixture at lower temperatures (< 900 K), Fig. 4-5(a).

4.4.3 Effect of pressure on ignition

Figure 4-9 illustrates the effect of the pressure on IDTs for 50% $CH_4/25\% C_2H_4/25\% C_2H_6$ blend, 50% $CH_4/16.66\% C_2H_4/16.66\% C_2H_6/16.66\% C_3H_8$ blend along with pure methane at $\phi = 1.0$. Figure 4-9 indicates that the reactivity of the mixtures increases at high-pressure conditions due to the corresponding increase in concentration with pressure. Furthermore, it is observed that at lower temperatures (< 830 K), the addition of C_2H_4/C_2H_6 and $C_2H_4/C_2H_6/C_3H_8$ fuels to pure methane for the ternary and quaternary blends results in faster IDTs at high-pressure conditions (20, 40 and 80 atm) compared to the 1 atm case. Figures 4-10(a) and 4-10(b) illustrate the effect of pressure on IDTs based on reaction path analyses depicted by black numbers for the 1 atm case and blue numbers for the 40 atm case at 800 K for the 50% $CH_4/25\% C_2H_4/25\% C_2H_6$ and 50% $CH_4/16.66\% C_2H_4/16.66\% C_2H_6/16.66\% C_3H_8$ blends, respectively. The flux analyses presented in Figs. 4-10(a) and 4-10(b) show that for the ternary and quaternary blends, the total fluxes going through the ignition promoting pathways $\dot{C}H_3 + O_2 \leftrightarrow CH_3\dot{O}_2$ and $\dot{C}H_3 + H\dot{O}_2 \leftrightarrow CH_3\dot{O} + \dot{O}H$ are around two times higher at 40 and 80 atm compared to 1 atm, while $\sim 32\%$ less flux goes through the methyl radical recombination reaction $\dot{C}H_3 + \dot{C}H_3 (+M) \leftrightarrow C_2H_6 (+M)$ at 40 and 80 atm compared to 1 atm, thus increasing the overall reactivity of the blends at high pressure and low-temperature conditions. Moreover, for the ternary blend, as pressure rises, the carbon fluxes going through the channels generating hydroxyl-ethyl (\dot{C}_2H_4OH) radicals from $C_2H_4 + \dot{O}H$ followed by the O_2 addition and the subsequent dissociation of $O_2\dot{C}_2H_4OH$ leading to two formaldehyde and a hydroxyl radical increase, as seen in Fig. 4-10(a). These formaldehyde molecules react with $H\dot{O}_2$ radicals to generate H_2O_2 , which more strongly promotes the reactivity through the thermal dissociation reaction $H_2O_2 (+M) \leftrightarrow \dot{O}H + \dot{O}H (+M)$ at the high-pressure condition of 40 and 80 atm compared to 1 atm, as shown in Fig. BS53.

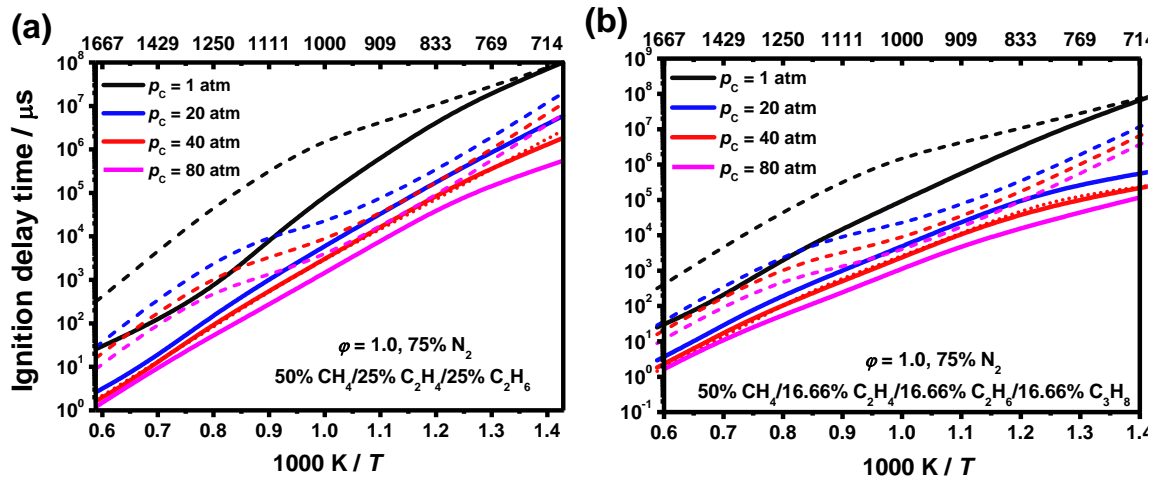


Figure 4-9. Effect of pressure over the IDT predictions of (a) 50% CH₄/25% C₂H₄/25% C₂H₆ blend (solid lines), and (b) 50% CH₄/16.66% C₂H₄/16.66% C₂H₆/16.66% C₃H₈ blend (solid lines), pure CH₄ (dashed lines), and corresponding correlations (dotted lines) for fuel in air at $\phi = 1.0$.

For the 50% CH₄/16.66% C₂H₄/16.66% C₂H₆ /16.66% C₃H₈ quaternary blend, at 1 atm, a considerable amount of nC₃H₇ (21.7%) undergoes β -scission, via nC₃H₇ \leftrightarrow CH₃ + C₂H₄, while for 40 atm, the percentage contribution through this channel reduces significantly accounting only 0.4% of the total flux. Whereas, at 40 atm ~34% more flux goes through the nC₃H₇ + O₂ \leftrightarrow nC₃H₇O₂ pathway compared to 1 atm condition increasing the reactivity for the quaternary blend at high pressures and low temperatures through the generation of two reactive OH radicals, as discussed in Section 4.4.2.

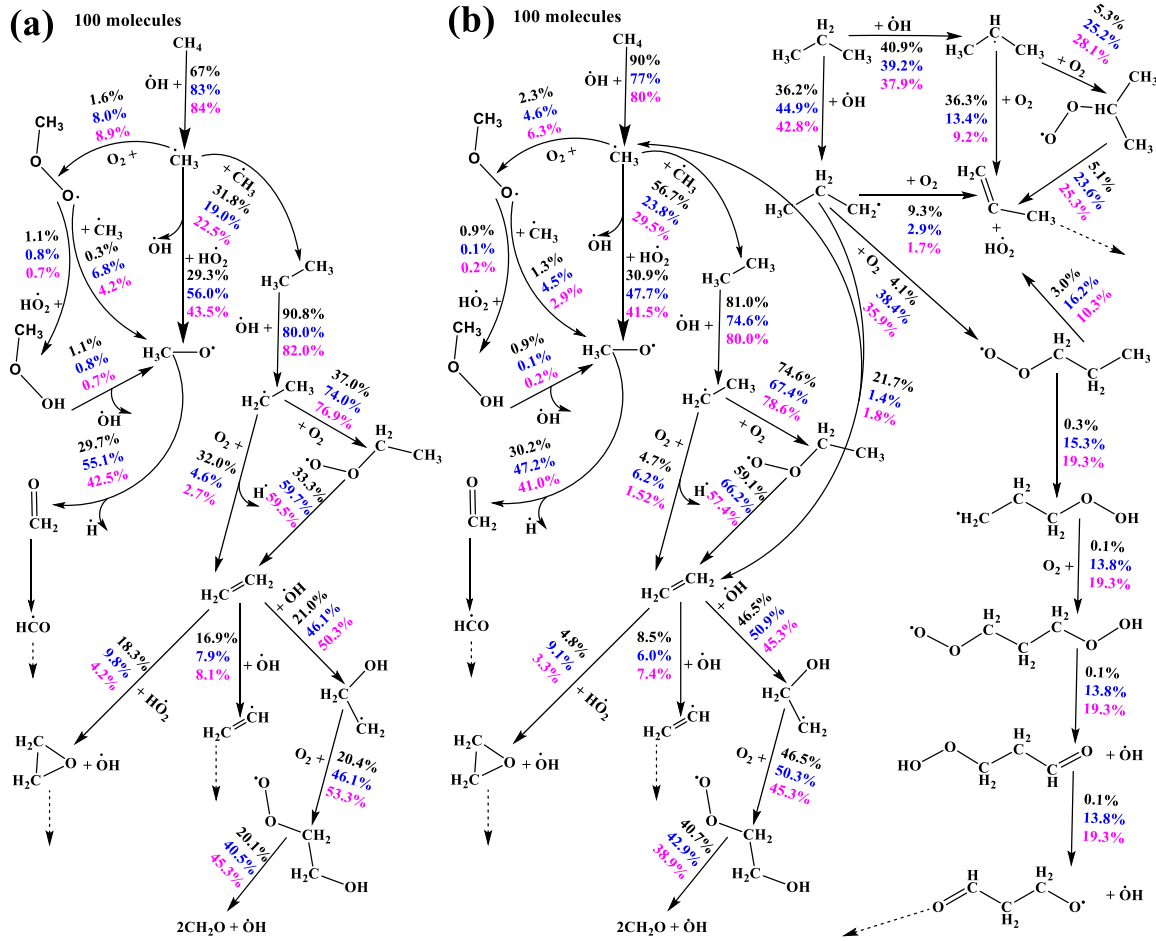


Figure 4-10. Flux analyses as function of pressure of 1 atm, 40 atm and 80 atm (black, blue, and magenta percentages respectively), at $T_C = 800$ K, $\phi = 1.0$, for (a) 50% CH₄/25% C₂H₄/25% C₂H₆, and (b) 50% CH₄/16.66% C₂H₄/16.66% C₂H₆/16.66% C₃H₈ in air.

4.4.4 Correlation analysis

Reliable global correlations that can accurately reproduce experimental measurements are desirable tools for analytical, semi-empirical, or computational fluid dynamics (CFD) calculations of reactive flows. Such correlations are versatile tools that can predict a mixture's sensitivity to any change in the correlated parameters. As discussed previously [2, 3], these correlations significantly reduce the required simulation time in response to any change in the chemical system, a critical parameter in real-time combustion controlling and monitoring systems. A simple form of the correlations applied here follows those previously published [2, 3] and is expressed in Eqn. 4-3. As previously shown, this type of correlation can reasonably explain the IDT characteristics of single and binary blended C₁ – C₃ hydrocarbons over a wide range of conditions [2, 3]. Here, it should be

noted that Eqn. 4-3 explains the general form of the correlations used in the study so that the “F” variable is zero for the tertiary blended C₁–C₂ fuels where no propane is present.

$$\tau_{\text{corr}} = 10^A \exp\left(\frac{B}{T_C}\right) [\text{CH}_4]^C [\text{C}_2\text{H}_4]^D [\text{C}_2\text{H}_6]^E [\text{C}_3\text{H}_8]^F [\text{oxygen}]^G [\text{diluent}]^H \quad (4-3)$$

where A represents the pre-exponential factor coefficient, B represents the activation energy divided by universal gas constant, and C–H represent coefficients for methane, ethylene, ethane, propane, oxidizer, and dilution, respectively.

All of the correlations were derived using NUIGMech1.2 based on thousands of adiabatic constant volume simulations, and their corresponding correlation coefficients are presented below and in Tables BS12–BS15 of Appendix B. The correlation coefficients were calculated using a non-linear curve fitting routine available in OriginPro 8.5 [45] which provides linear regressions together with residuals, R², χ^2 and standard errors for every coefficient value. Some of the examples of these conditions are presented in Fig. 4-5(b) and Fig. 4-9. However, according to the simple form of Eqn. 4-3, the correlations are derived over ranges where the dependency of the IDT on the various parameters does not become highly non-linear. Moreover, for relatively long IDTs (> 10 ms) measured using the RCM, the correlation results derived using the adiabatic constant volume calculations differs significantly from the simulations including heat loss effects for the facility. We have already discussed this effect in detail [2, 4].

For $1100 \leq T_C \leq 2000$ K:

$$\tau_{\text{corr}} = 10^{-10.94} \exp\left(\frac{21208}{T_C}\right) [\text{CH}_4]^{1.004} [\text{C}_2\text{H}_4]^{-0.888} [\text{C}_2\text{H}_6]^{-0.041} [\text{C}_3\text{H}_8]^{0.0} [\text{oxygen}]^{-1.399} [\text{diluent}]^{0.666} \quad (4-4)$$

$$\tau_{\text{corr}} = 10^{-10.36} \exp\left(\frac{21320}{T_C}\right) [\text{CH}_4]^{0.834} [\text{C}_2\text{H}_4]^{-0.222} [\text{C}_2\text{H}_6]^{-0.186} [\text{C}_3\text{H}_8]^{-0.165} [\text{oxygen}]^{-1.496} [\text{diluent}]^{0.48} \quad (4-5)$$

For $800 \leq T_C \leq 1100$ K:

$$\tau_{\text{corr}} = 10^{-8.049} \exp\left(\frac{16817}{T_C}\right) [\text{CH}_4]^{0.31} [\text{C}_2\text{H}_4]^{-0.722} [\text{C}_2\text{H}_6]^{-0.138} [\text{C}_3\text{H}_8]^{0.0} [\text{oxygen}]^{-0.398} [\text{diluent}]^{-0.162} \quad (4-6)$$

$$\tau_{\text{corr}} = 10^{-8.011} \exp\left(\frac{15826}{T_C}\right) [\text{CH}_4]^{0.133} [\text{C}_2\text{H}_4]^{-0.257} [\text{C}_2\text{H}_6]^{-0.105} [\text{C}_3\text{H}_8]^{-0.5} [\text{oxygen}]^{-0.292} [\text{diluent}]^{-0.089} \quad (4-7)$$

At high temperatures (1100 – 2000 K), the coefficient associated with CH₄ in both blends (CH₄/C₂H₄/C₂H₆/‘air’ and CH₄/C₂H₄/C₂H₆/C₃H₈/‘air’) is strongly positive, while those for C₂H₄,

C_2H_6 , and C_3H_8 are negative. CH_4 produces high concentrations of $\dot{C}H_3$ radicals, which are relatively less reactive compared to \dot{H} atoms produced in the oxidation of C_2H_4 , C_2H_6 , and C_3H_8 . Thus, increasing the CH_4 concentration in the ternary and quaternary blends will increase IDT, and increasing C_2H_4 , C_2H_6 , and C_3H_8 concentrations will decrease the mixture IDT. Moreover, the coefficient associated with C_3H_8 in the quaternary ($CH_4/C_2H_4/C_2H_6/C_3H_8$ /'air') blend is smaller than the coefficients for C_2H_4 and C_2H_6 . This is because, at high temperatures, C_3H_8 produces $\dot{C}H_3$ radicals and C_2H_4 molecules from $n\dot{C}_3H_7$ radicals that decompose via β -scission reaction by $n\dot{C}_3H_7 \leftrightarrow C_2H_4 + \dot{C}H_3$, whereas C_2H_4 and C_2H_6 oxidation produces higher amounts of \dot{H} atoms, thus more effectively enhancing the reactivity of the C_2H_4 or C_2H_6 blended mixtures than those of the C_3H_8 blended ones. Therefore, although increasing the concentrations of C_2H_4 and C_3H_8 relative to CH_4 will increase mixture reactivity, the former will dominate the latter.

Furthermore, at high temperatures, the coefficient corresponding to the oxidizer is significantly higher than other coefficients showing the strong sensitivity of oxygen concentrations under the respective conditions. For the low-temperature range, 800 – 1100 K, the coefficients for C_2H_4 and C_3H_8 become strongly negative. This is because, in this temperature range, C_2H_4 and C_3H_8 greatly enhance reactivity by producing higher concentrations of highly active $\dot{O}H$ radicals compared to the CH_4 and C_2H_6 fuels. Moreover, the coefficient corresponding to the oxidizer in Eqns. 4-6 and 4-7 is comparable to other coefficients showing less importance on oxygen concentrations under these specific conditions. A more detailed correlation table is included for all conditions studied in this work in Appendix B, which includes the coefficients, standard errors related to coefficients R^2 , and χ^2 . For both, low and high temperatures, the corresponding R^2 and χ^2 parameters are ranging from 0.985 – 0.999 and 1.53×10^{-4} – 1.02×10^{-11} , respectively.

Figures BS51 and BS52 in Appendix B compare the predictions of the quaternary correlations derived in this study with our prior published experimental IDTs of binary blends for C_2H_4/C_3H_8 and C_2H_6/C_3H_8 mixtures at high temperature and high-pressure conditions [4]. The present correlations are also compared with the IDT predictions calculated using the binary correlations derived in our previous work [4]. It can be seen that the global correlation of the quaternary blend is unable to accurately predict the IDTs of the C_2H_4/C_3H_8 and C_2H_6/C_3H_8 binary blends. This is attributed to the fact that the present correlations were derived from simulations of quaternary mixtures with CH_4 as the major fuel component. Eqn. 4-5 shows that, for quaternary mixtures, the coefficient associated with CH_4 is strongly positive compared to the other fuel components in the blend and thus CH_4

dominates the predicted reactivity of the fuel mixture. Since our previously published [4] binary blends did not include CH₄ as an additive component, the predictions of the present correlations differ significantly from those calculated using the binary mixture correlations [4].

4.5 Conclusions

In the current study, a detailed experimental and kinetic modelling study of the IDT characteristics of C₁ – C₃ novel ternary and quaternary blends of CH₄/C₂H₄/C₂H₆ and CH₄/C₂H₄/C₂H₆/C₃H₈ mixtures was performed over a wide range of experimental conditions, temperature (~750 – 2000 K), pressure (1 – 135 bar), equivalence ratio ($0.5 \leq \varphi \leq 2.0$), and dilution (~75 – 90%). 24 new IDT datasets, including approximately 360 data points were measured, which were not already available in the literature. Low- and high-temperature IDT characteristics of CH₄/C₂H₄/C₂H₆ and CH₄/C₂H₄/C₂H₆/C₃H₈ combinations were investigated using the ST and RCM facilities at NUIG and PCFC RWTH Aachen University. The results showed that NUIGMech1.2 could predict the IDT characteristics of the blends studied with high fidelity over the wide range of conditions studied here.

Therefore, NUIGMech1.2 was used to perform studies on the blending and pressure effect on ignition. It was observed that for all blends used in this work, as the temperature and the pressure increase, the IDTs decrease. For high temperatures ($T > 1100$ K), CH₄ exhibit the slowest reactivity because its chemistry is mainly driven by methyl chemistry, $\dot{\text{C}}\text{H}_3 + \text{H}\dot{\text{O}}_2 \leftrightarrow \text{CH}_4 + \text{O}_2$, and $\dot{\text{C}}\text{H}_3 + \dot{\text{C}}\text{H}_3 (+\text{M}) \leftrightarrow \text{C}_2\text{H}_6 (+\text{M})$; these reaction pathways are responsible for the very slow ignition on pure CH₄ and the ternary and quaternary blends at this temperature. C₂H₆ is the second-fastest mixture to ignite, and this is because the pressure dependent reaction from ethyl radical enhances the reactivity $\dot{\text{C}}_2\text{H}_5 (+\text{M}) \leftrightarrow \text{C}_2\text{H}_4 + \dot{\text{H}} (+\text{M})$ at the same time, competition with the concerted elimination reaction $\dot{\text{C}}_2\text{H}_5 + \text{O}_2 \leftrightarrow \text{C}_2\text{H}_4 + \text{H}\dot{\text{O}}_2$ slow down the ignition making C₂H₆ slower than C₂H₄. Ethylene mixtures show the fastest reactivity due to the vinyl ($\dot{\text{C}}_2\text{H}_3$) chemistry that makes C₂H₄ the fastest fuel to ignite. Furthermore, C₃H₈ is much slower than C₂H₄ due to the high amount of methyl ($\dot{\text{C}}\text{H}_3$) radicals produced from n $\dot{\text{C}}_3\text{H}_7$ channels.

It was observed that for low temperatures ($T < 1100$ K), methyl chemistry is still responsible for the slow ignition exhibited by CH₄. This is because of the large amount of $\dot{\text{C}}\text{H}_3$ radicals reacting with O₂ to form methyl peroxy radicals $\dot{\text{C}}\text{H}_3 + \text{O}_2 \leftrightarrow \text{CH}_3\dot{\text{O}}_2$, which further react through $\text{CH}_3\dot{\text{O}}_2 + \text{CH}_3\dot{\text{O}}_2 \leftrightarrow \text{CH}_3\dot{\text{O}} + \text{CH}_3\dot{\text{O}} + \text{O}_2$ to inhibit the reactivity. However, here C₂H₆ is the second slowest due to the concerted elimination reaction, $\text{C}_2\text{H}_5\dot{\text{O}}_2 \leftrightarrow \text{C}_2\text{H}_4 + \text{H}\dot{\text{O}}_2$, which becomes very important at this

temperature. Additionally, C_2H_4 is the second-fastest in igniting due to hydroxy-ethyl-peroxy ($\dot{O}_2C_2H_4OH$) and oxirane ($C_2H_4O_{1-2}$) channels that enhance the reactivity. Moreover, C_3H_8 exhibits the fastest ignition at this temperature due to the considerable amount of $\dot{O}H$ radicals generated by the addition of n-propyl ($n\dot{C}_3H_7$) radicals to O_2 and going to chain branching reactions.

Finally, several correlations were derived from mimicking the performance of NUIGMech1.2 in predicting the IDT characteristics of the blended fuels over a wide range of pressure, temperature, equivalence ratio, fuel composition, and dilution. The results demonstrated that the derived correlations could be depended upon as agile, fast, and reasonably reliable tools to predict the IDTs of the blends studied over their validity range of pressure, temperature, and mixture composition.

Acknowledgements

The authors would like to express their gratitude to Shell Research Ltd. and Science Foundation Ireland (SFI) for funding via project numbers 15/IA/3177 and 16/SP/3829, and KAY-ICHEC via the project ngche079c. The authors from PCFC, RWTH Aachen University, would like to recognize the funding support from the German Research Foundation (Deutsche Forschungsgemeinschaft, DFG) through project number – 322460823 (HE7599/2-1).

References

- [1] C.J. Aul, W.K. Metcalfe, S.M. Burke, H.J. Curran, E.L. Petersen, Ignition and kinetic modeling of methane and ethane fuel blends with oxygen: a design of experiments approach, *Combust. Flame* 160 (2013) 1153-1167.
- [2] M. Baigmohammadi, V. Patel, S. Martinez, S. Panigrahy, A. Ramalingam, U. Burke, K.P. Somers, K.A. Heufer, A. Pekalski, H.J. Curran, A comprehensive experimental and simulation study of ignition delay time characteristics of single fuel $C_1 - C_2$ hydrocarbons over a wide range of temperatures, pressures, equivalence ratios, and dilutions, *Energy Fuels* 34(3) (2020) 3755-3771.
- [3] M. Baigmohammadi, V. Patel, S. Nagaraja, A. Ramalingam, S. Martinez, S. Panigrahy, A.A. El-Sabor Mohamed, K.P. Somers, U. Burke, K.A. Heufer, A. Pekalski, H.J. Curran, Comprehensive experimental and simulation study of the ignition delay time characteristics of binary blended methane, ethane, and ethylene over a wide range of temperature, pressure, equivalence ratio, and dilution, *Energy Fuels* 34(7) (2020) 8808-8823.
- [4] S. Martinez, M. Baigmohammadi, V. Patel, S. Panigrahy, A.B. Sahu, S.S. Nagaraja, A. Ramalingam, A.A. El-Sabor Mohamed, K.P. Somers, K.A. Heufer, A. Pekalski, H.J. Curran, An experimental and kinetic modeling study of the ignition delay characteristics of binary blends of ethane/propane and ethylene/propane in multiple shock tubes and rapid compression machines over a wide range of temperature, pressure, equivalence ratio, and dilution, *Combust. Flame* 228 (2021) 401-414.

- [5] P.J. Ross, Taguchi techniques for quality engineering, McGraw-Hill, New York, 1988.
- [6] E.L. Petersen, M.J.A. Rickard, M.W. Crofton, E.D. Abbey, M.J. Traum, D.M. Kalitan, A facility for gas- and condensed-phase measurements behind shock waves, *Meas Sci Technol* 16 (2005) 1716-1729.
- [7] B.W. Weber, C.-J. Sung, M.W. Renfro, On the uncertainty of temperature estimation in a rapid compression machine, *Combust. Flame* 162 (2015) 2518-2528.
- [8] A. Ramalingam, K. Zhang, A. Dhongde, L. Virnich, H. Sankhla, H. Curran, A. Heufer, An RCM experimental and modeling study on CH₄ and CH₄/C₂H₆ oxidation at pressures up to 160 bar, *Fuel* 206 (2017) 325-333.
- [9] A.A. El-Sabor Mohamed, S. Panigrahy, A. Sahu, G. Bourque, H.J. Curran, An experimental and modeling study of the auto-ignition of natural gas blends containing C₁ – C₇ n-alkanes, *Proc. Combust. Inst.* 38 (2021) 365-373.
- [10] S.S. Nagaraja, J. Power, G. Kukkadapu, S. Dong, S.W. Wangon, W.J. Pitz, H.J. Curran, A single pulse shock tube study of pentene isomer pyrolysis, *Proc. Combust. Inst.* 38 (2021) 881-889.
- [11] S. Panigrahy, J. Liang, S. Nagaraja, Z. Zuo, G. Kim, T. MacDougall, S.S. Vasu, H.J. Curran, A comprehensive experimental and improved kinetic modeling study on the pyrolysis and oxidation of propyne, *Proc. Combust. Inst.* 38 (2021) 479-488.
- [12] S. Dong, K. Zhang, P.K. Senecal, G. Kukkadapu, S.W. Wagnon, S. Barrett, N. Lokachari, S. Panigrahy, W.J. Pitz, H.J. Curran, A comparative reactivity study of 1-alkene fuels from ethylene to 1-heptene, *Proc. Combust. Inst.* 38 (2021) 611-619.
- [13] S.S. Nagaraja, J. Liang, S. Dong, S. Panigrahy, A. Sahu, G. Kukkadapu, S.W. Wagnon, W.J. Pitz, H.J. Curran, A hierarchical single-pulse shock tube pyrolysis study of C₂ – C₆ 1-alkenes, *Combust. Flame* 219 (2020) 456-466.
- [14] A. Ramalingam, S. Panigrahy, Y. Fenard, H. Curran, K.A. Heufer, A chemical kinetic perspective on the low-temperature oxidation of propane/propene mixtures through experiments and kinetic analyses, *Combust. Flame* 223 (2021) 361-375.
- [15] D.G. Goodwin, R.L. Speth, H.K. Moffat, B.W. Weber, Cantera: An object-oriented software toolkit for chemical kinetics, thermodynamics, and transport processes, <https://www.cantera.org>, (2018). Version 2.4.0. doi:10.5281/zenodo.170284.
- [16] Reaction-Design, CHEMKIN-PRO 18.2, San Diego, 2013.
- [17] C.-J. Sung, H.J. Curran, Using rapid compression machines for chemical kinetics studies, *Prog. Energy Combust.* 44 (2014) 1-18.
- [18] S.S. Goldsborough, S. Hochgreb, G. Vanhove, M.S. Wooldridge, H.J. Curran, C.J. Sung, Advances in rapid compression machine studies of low- and intermediate-temperature autoignition phenomena, *Prog. Energy Combust. Sci.* 63 (2017) 1-78.
- [19] U. Burke, K.P. Somers, P. O'Toole, C.M. Zinner, N. Marquet, G. Bourque, E.L. Petersen, W.K. Metcalfe, Z. Serinyel, H.J. Curran, An ignition delay and kinetic modeling study of methane, dimethyl ether, and their mixtures at high pressures, *Combust. Flame* 162 (2015) 315-330.

- [20] E.E. Dames, A.S. Rosen, B.W. Weber, C.W. Gao, C.-J. Sung, W.H. Green, A detailed combined experimental and theoretical study on dimethyl ether/propane blended oxidation, *Combust. Flame* 168 (2016) 310-330.
- [21] S. Chih-Jen, H.J. Curran, Using rapid compression machines for chemical kinetics studies, *Prog. Energy Combust. Sci.* 44 (2014) 1-18.
- [22] V. Gururajan, F.N. Eglolfopoulos, Direct sensitivity analysis for ignition delay times, *Combust. Flame* 209 (2019) 478-480.
- [23] W.K. Metcalfe, S.M. Burke, S.S. Ahmed, H.J. Curran, A hierarchical and comparative kinetic modeling study of C₁ – C₂ hydrocarbon and oxygenated fuels, *Int. J. Chem. Kinet.* 45 (2013) 638-675.
- [24] S.M. Burke, W. Metcalfe, O. Herbinet, F. Battin-Leclerc, F.M. Haas, J. Santner, F.L. Dryer, H.J. Curran, An experimental and modeling study of propene oxidation. Part 1: speciation measurements in jet-stirred and flow reactors, *Combust. Flame* 161 (2014) 2765-2784.
- [25] S.M. Burke, U. Burke, R. McDonagh, O. Mathieu, I. Osorio, C. Keesee, A. Morones, E.L. Petersen, W. Wang, T.A. DeVerter, M.A. Oehlschlaeger, B. Rhodes, R.K. Hanson, D.F. Davidson, B.W. Weber, C.-J. Sung, J. Santner, Y. Ju, F.M. Haas, F.L. Dryer, E.N. Volkov, E.J.K. Nilsson, A.A. Konnov, M. Alrefae, F. Khaled, A. Farooq, P. Dirrenberger, P.-A. Glaude, F. Battin-Leclerc, H.J. Curran, An experimental and modeling study of propene oxidation. Part 2: Ignition delay time and flame speed measurements, *Combust. Flame* 162 (2015) 296-314.
- [26] Y. Li, C.-W. Zhou, K.P. Somers, K. Zhang, H.J. Curran, The Oxidation of 2-Butene: a high-pressure ignition delay, kinetic modeling study and reactivity comparison with isobutene and 1-butene, *Proc. Combust. Inst.* 36 (2017) 403-411.
- [27] C.-W. Zhou, Y. Li, U. Burke, C. Banyon, K.P. Somers, S. Ding, S. Khan, J.W. Hargis, T. Sikes, O. Mathieu, E.L. Petersen, M. AlAbbad, A. Farooq, Y. Pan, Y. Zhang, Z. Huang, J. Lopez, Z. Loparo, S.S. Vasu, H.J. Curran, An experimental and chemical kinetic modeling study of 1,3-butadiene combustion: Ignition delay time and laminar flame speed measurements, *Combust. Flame* 197 (2018) 423-438.
- [28] H. Hashemi, J.G. Jacobsen, C.T. Rasmussen, J.M. Christensen, P. Glarborg, S. Gersen, M. van Essen, H.B. Levinsky, S.J. Klippenstein, High-pressure oxidation of ethane, *Combust. Flame* 182 (2017) 150-166.
- [29] G. Bagheri, E. Ranzi, M. Pelucchi, A. Parente, A. Frassoldati, T. Faravelli, Comprehensive kinetic study of combustion technologies for low environmental impact: MILD and OXY-fuel combustion of methane, *Combust. Flame* 212 (2020) 142-155.
- [30] Chemical-Kinetic Mechanisms for Combustion Applications. <http://combustion.ucsd.edu>.
- [31] G.P. Smith, D.M. Golden, M. Frenklach, N.W. Moriarty, B. Eiteneer, M. Goldenberg, C.T. Bowman, R.K. Hanson, S. Song, W.C. Gardiner, V.V. Lissianski, Z. Qin, http://www.me.berkeley.edu/gri_mech/.
- [32] G.P. Smith, Y. Tao, H. Wang, Foundational fuel chemistry model version 1.0 (FFCM-1), Stanford University, 2016.

- [33] A.W. Jasper, S.J. Klippenstein, L.B. Harding, Theoretical rate coefficients for the reaction of methyl radical with hydroperoxyl radical and for methylhydroperoxide decomposition, *Proc. Combust. Inst.* 32 (2009) 279-286.
- [34] R. Zhu, C. Lin, The $\dot{\text{C}}\text{H}_3+\dot{\text{H}}\text{O}_2$ reaction: first-principles prediction of its rate constant and product branching probabilities, *J. Phys. Chem. A* 105 (2001) 6243-6248.
- [35] S.M. Villano, L.K. Huynh, H.-H. Carstensen, A.M. Dean, High-pressure rate rules for alkyl+O₂ reactions. 1. the dissociation, concerted elimination, and isomerization channels of the alkyl peroxy radical, *J. Phys. Chem. A* 115 (2011) 13425-13442.
- [36] U. Burke, K.P. Somers, P. O'Toole, C.M. Zinner, N. Marquet, G. Bourque, E.L. Petersen, W.K. Metcalfe, Z. Serinyel, H.J. Curran, An ignition delay and kinetic modeling study of methane, dimethyl ether, and their mixtures at high pressures, *Combust. Flame* 162 (2015) 315-330.
- [37] I. R. Slagle, D. Gutman, J.W. Davies, M.J. Pilling, Study of the recombination reaction $\dot{\text{C}}\text{H}_3+\dot{\text{C}}\text{H}_3\rightarrow\text{C}_2\text{H}_6$ Part 1. experiment, *J. Phys. Chem.* 92 (1988) 2455-2462.
- [38] M. Sangwan, C. Yan, E.N. Chesnokov, L.N. Krasnoperov, Reaction $\dot{\text{C}}\text{H}_3+\dot{\text{C}}\text{H}_3\rightarrow\text{C}_2\text{H}_6$ studied over the 292–714 K temperature and 1–100 bar pressure ranges, *J. Phys. Chem. A* 119 (2015) 7847-7857.
- [39] K. Glänzer, M. Quack, J. Troe, High temperature uv absorption and recombination of methyl radicals in shock waves, *Symposium (International) on Combustion* 16 (1977) 949-960.
- [40] M.A. Blitz, N.J.B. Green, R.J. Shannon, M.J. Pilling, P.W. Seakins, C.M. Western, S.H. Robertson, Reanalysis of rate data for the reaction $\dot{\text{C}}\text{H}_3+\dot{\text{C}}\text{H}_3\rightarrow\text{C}_2\text{H}_6$ using revised cross sections and a linearized second-order master equation, *J. Phys. Chem. A* 119 (2015) 7668-7682.
- [41] B. Wang, H. Hou, L.M. Yoder, J.T. Muckerman, C. Fockenberg, Experimental and theoretical investigations on the methyl–methyl recombination reaction, *J. Phys. Chem. A* 107 (2003) 11414-11426.
- [42] S. J. Klippenstein, Y. Georgievskii, L.B. Harding, Predictive theory for the combination kinetics of two alkyl radicals, *Phys. Chem. Chem. Phys.* 8 (2006) 1133-1147.
- [43] P.D. Lightfoot, P. Roussel, F. Caralp, R. Lesclaux, Flash photolysis study of the $\text{CH}_3\dot{\text{O}}_2+\text{CH}_3\dot{\text{O}}_2$ and $\text{CH}_3\dot{\text{O}}_2+\dot{\text{H}}\text{O}_2$ reactions between 600 and 719 K: unimolecular decomposition of methylhydroperoxide, *J. Chem. Soc. Faraday Trans.* 87(19) (1991) 3213-3220.
- [44] M. Keiffer, A.J. Miscampbell, M.J. Pilling, A global technique for analysing multiple decay curves application to the $\dot{\text{C}}\text{H}_3+\text{O}_2$ system *J. Chem. Soc., Faraday Trans.* 2 (1988) 505-514.
- [45] Origin(Pro), Version 8.5. OriginLab Corporation, Northampton, MA, USA.

Chapter 5: An experimental and kinetic modelling study of the ignition delay characteristics of binary blends of ethane/propane and ethylene/propane in multiple shock tubes and rapid compression machines over a wide range of temperature, pressure, equivalence ratio, and dilution

Published in: Combustion and Flame, Volume 228, February 2021, 401-414.

DOI : <https://doi.org/10.1016/j.combustflame.2021.02.009>

Author Contributions

- 1) Sergio Martinez (National University of Ireland, Galway, Ireland)
Contribution: Performed calculations, chemical kinetic modelling, and manuscript preparation.
- 2) Mohammadreza Baigmohammadi (National University of Ireland, Galway, Ireland)
Contribution: High pressure shock tube experiments.
- 3) Vaibhav Patel (National University of Ireland, Galway, Ireland)
Contribution: RCM experiments.
- 4) Snehasish Panigrahy (National University of Ireland, Galway, Ireland)
Contribution: Chemical kinetic modelling.
- 5) Amrit B. Sahu (National University of Ireland, Galway, Ireland)
Contribution: Chemical kinetic modelling.
- 6) Shashank S. Nagaraja (National University of Ireland, Galway, Ireland)
Contribution: Low pressure shock tube experiments.
- 7) Ajoy Ramalingam (PCFC, RWTH Aachen, Germany)
Contribution: RCM experiments.
- 8) Ahmed Abd El-Sabor Mohamed (National University of Ireland, Galway, Ireland)
Contribution: RCM experiments.
- 9) Kieran P. Somers (National University of Ireland, Galway, Ireland)
Contribution: Chemical kinetic modelling.
- 10) Karl A. Heufer (PCFC, RWTH Aachen, Germany)
Contribution: Project management and manuscript review.

11) Andrzej Pekalski (Shell research limited, Shell Centre London)

Contribution: Project management as industrial sponsor and manuscript review.

12) Henry J. Curran (National University of Ireland, Galway, Ireland)

Contribution: Managed the project, made technical contributions and reviewed the project and manuscript throughout.

Abstract

In this work, the ignition delay time characteristics of C₂–C₃ binary blends of gaseous hydrocarbons including ethylene/propane and ethane/propane are studied over a wide range of temperatures (750–2000 K), pressures (1–135 bar), equivalence ratios ($\phi = 0.5–2.0$) and dilutions (75–90%). A matrix of experimental conditions is generated using the Taguchi (L9) approach to cover the range of conditions for the validation of a chemical kinetic model. The experimental ignition delay time data are recorded using low- and high-pressure shock tubes and two rapid compression machines (RCM) to include all the designed conditions. These novel experiments provide a direct validation of the chemical kinetic model, NUIGMech1.1, and its performance is characterized via statistical analysis, with the agreement between experiments and model being within ~ 26.4% over all of the conditions studied, which is comparable with a general absolute uncertainty of the applied facilities (~ 20%). Sensitivity and flux analyses allow for the key reactions controlling the ignition behavior of the blends to be identified. Subsequent analyses are performed to identify those reactions which are important for the pure fuel components and for the blended fuels, and synergistic/antagonistic blending effects are therefore identified over the wide range of conditions. The overall performance of NUIGMech1.1 and the correlations generated are in good agreement with the experimental data.

Keywords: Ethane, ethylene, propane, shock-tube, rapid compression machine, ignition delay time, detailed kinetic model

5.1 Introduction

According to the U.S. Energy Information Administration (EIA) report 2019 [1], it is projected that global energy consumption will increase by approximately 28% in 2050 compared to 2018 levels, with fossil fuels providing around 77% of the total energy demand. Liquid fuels, natural gas, and coal are the most important sources amongst all fossil fuels. Liquid fuels, such as gasoline, diesel, etc. are predicted to represent around 33% of energy consumption, with natural gas at close to 30%, coal near 18%, with the remaining 19% corresponding to nuclear, hydropower, and renewable sources [2].

The combustion of fossil fuels is the main sources of CO₂, SO_x, and NO_x emissions, among other pollutants. In this regard, natural gas is considered preferable to other fossil fuels including liquid fuels and coal as it is a cleaner energy source, having the highest hydrogen/carbon among them. Widely used in the domestic, transportation, and industrial sectors, liquefied natural gas (LNG) is

typically composed of methane (82 – 100%) but can contain substantial amounts of ethane, propane and butane, while liquified petroleum gas (LPG) includes mainly propane, and butane. To reduce emissions, it is necessary to improve the efficiency of the combustion systems for which a detailed understanding of the combustion chemistry is essential. The oxidation kinetics of small hydrocarbons play an important role as the base of any mechanism for alternative fuels. For these reasons, the combustion community is interested in enhancing our understanding of the chemistry controlling the oxidation of hydrocarbons to increase the efficiency of engines and to reduce the emission of pollutants such as soot, NO_x, UHCs (unburned hydrocarbons), and greenhouse gases in general. A hierarchical [3-6] (bottom-up) strategy has proven to be a good way to develop reliable chemical kinetic mechanisms and improve our understanding of the chemistry controlling pyrolysis and oxidation.

Combustion properties of fuels such as ignition delay time (IDT), speciation profiles, flame speed, among others become invaluable for the optimization of combustors. Relevant experiments and modelling studies for mono-fuels and some blends, such as ethylene, ethane, and propane, have been carried out with different methods and are available in the literature [7-14].

Dagaut et al. [15-17] studied species profiles consumed and produced during the oxidation ethylene, ethane, and propane in a jet-stirred reactor (JSR) using fuel mixtures diluted with nitrogen, at equivalence ratios (ϕ) of 0.1 – 4.0, at pressures ranging from 1 – 10 atm in the temperature range 800 – 1250 K. Their work showed the importance of small molecule sub-mechanisms including CO₂, CH₂O, CH₄, C₂H₂, C₂H₄, and C₃H₆ on the combustion of higher hydrocarbons.

Lowry et al. [18] measured laminar premixed flame speeds of pure methane, ethane, propane, and their binary blends with methane, at $\phi = 0.7 – 1.3$, in a constant-volume cylindrical vessel, in the pressure range 1 – 10 atm, at room temperature (298 K). They highlighted the need to extensively study the synergistic effect of blends in comparison to pure fuels.

Baigmohammadi et al. [5, 6] measured IDTs for pure ethylene, ethane, and propane, and binary alkane/alkene blends in a shock tube (ST) and a rapid compression machine (RCM) at $\phi = 0.5 – 2.0$, at pressures ranging from 20 – 40 atm in the temperature range of 800 – 2000 K. They showed that the synergistic effect on the reactivity of the mixture is important not only based on the fuel blends but in each variable considered during the combustion phenomena such as pressure, temperature, dilution, etc. These previous studies [5, 6, 15-17] also used chemical kinetic mechanisms to predict

the experimental data presented and identify the most relevant chemical reactions controlling the oxidation of these fuels.

Despite the large amount of data for pure ethylene, ethane, and propane fuels, there are comparatively fewer studies of their blends, Table 5-1.

Table 5-1. IDTs for C₂H₄, C₂H₆, C₃H₈, and binary blends from the literature.

Facility	Fuel	p_C / atm	T_C / K	Year	Reference
ST/RCM	C ₂ H ₄	1–40	773–2200	1999–2020	[1-6]
ST/RCM	C ₂ H ₆	1–40	830–1862	1971–2020	[6-10]
ST/RCM	C ₃ H ₈	1–40	689–2615	1977–2013	[11-16]
ST/RCM	C ₂ H ₄ /C ₂ H ₆	1–40	800–2000	2020	[17]

The current study aims to address the lack of data for mixtures by providing IDT data for binary C₂H₄/C₃H₈ and C₂H₆/C₃H₈ blends over a wide range of temperatures, pressures, equivalence ratios, and dilutions relevant to engine and gas turbine conditions. It also aims to validate a detailed chemical kinetic model using the novel experiments and literature data. We first provide a summary of the experimental condition and approaches taken for this study, followed by details of the modelling work. The results and discussion section encompasses all the comparisons of the model performance with the experimental data. Additionally, a comparison of the most important reactions for the pure fuels and their binary blends are presented to determine the kinetics controlling the reactivity of the blends.

5.2 Design of experiments and experimental approaches

All of the measured IDTs collected and presented in this study were obtained using two different shock tubes (ST) and two rapid compression machines (RCMs). For those experiments carried out at NUI Galway at pressures ranging from 1–40 bar and intermediate-to-high-temperatures (> 1000 K), low- (LPST) ($p_C = 1$ bar) and high-pressure ($p_C \geq 20$ bar) shock tubes (HPSTs) were applied. The IDT experiments corresponding to the relatively high-pressure ($20 \leq p_C \leq 40$ bar) and low-temperature (< 1000 K) regimes were taken using a twin-piston RCM. Some experiments at working pressures of 40 bar and greater were measured using a single-piston RCM at the Physico-Chemical Fundamentals of Combustion (PCFC)-RWTH [32, 33] Aachen University to enhance the fidelity of the experimental IDTs. Details of these facilities and their operating characteristics are available in the literature [6, 34, 35].

For the IDT experiments performed at NUIG, ethane, ethylene, and propane gases with a purity of 99.95% were supplied by Air liquid UK. BOC Ireland provided all other gases with purities of 99.99% for oxygen, nitrogen, argon, and 99.96% for helium. At the PCFC-RWTH Aachen University, the alkane/alkene gases were supplied by Westfalen AG with a 99.95% purity. All other gases were supplied by Westfalen AG and Praxair with purities of oxygen $\geq 99.995\%$, nitrogen $\geq 99.95\%$, and argon $\geq 99.996\%$.

To stochastically distribute the experimental IDTs, the experimental conditions for this study were generated using the Taguchi [36] approach by applying an L₉ matrix based on four parameters of propane concentration, pressure, equivalence ratio, and dilution and also three different levels for each parameter studied. This approach has already been described by Baigmohammadi et al. [5, 6].

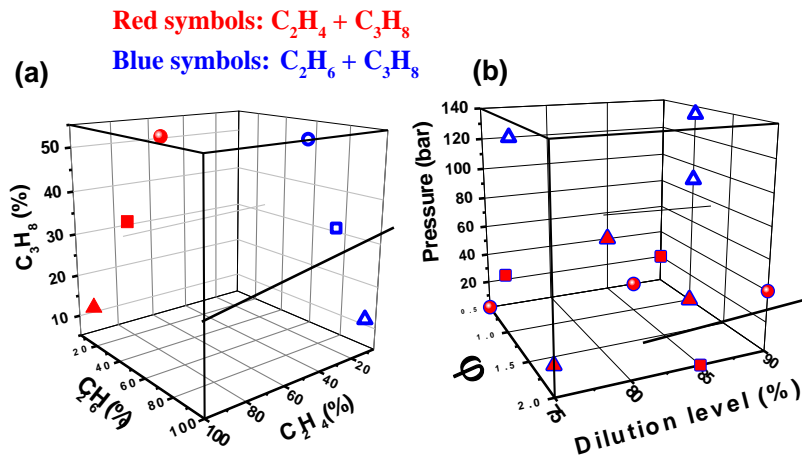


Figure 5-1. Experimental Taguchi [36] L₉ matrix of conditions. For 90%/10%, 70%/30%, and 50%/50% ratios (a) red: binary C₂H₄/C₃H₈ blends, blue: binary C₂H₆/C₃H₈ blends; and (b) pressure, equivalence ratio, and dilution parameters.

For the mixture conditions studied, the propane concentration in the fuel blends varies from 10–50%, at pressures ranging from 10–135 bar, for φ of 0.5–2.0 and at dilutions of 75–90% (75% N₂ + 0–15% Ar). However, the ratio between the diluents were changed at low-temperature regime (RCM) depending on the desired compressed gas temperature. A synopsis of the designed conditions is presented Fig. 5-1 in Table 5-1.

In the current study, most of the measured IDTs in the HPST and RCMs [10, 33, 37-42] are defined as the time between the end of compression and the maximum gradient in pressure ($\frac{dp}{dt}$) behind the

reflected shock. However, we define the ignition event as the maximum gradient in $CH^* \left(\frac{dCH^*}{dt} \right)$ behind the reflected shock in the LPST measured by a photomultiplier and also when the test mixture is highly diluted in the HPST.

Table 5-2. C₂H₄/C₃H₈ and C₂H₆/C₃H₈ mixture compositions in % mole volume in the current study. Where keywords NUIG refers to ST/RCM facilities at C³-NUIGalway, and PCFC refers to RCM facility at PCFC-RWTH Aachen University, respectively.

	No.	% C ₂ H ₆	% C ₂ H ₄	% C ₃ H ₈	% O ₂	Dilution	ϕ	p_C / bar	Facility
C ₂ H ₄ /C ₃ H ₈ 50%/50%	1	0.000	1.40	1.400	22.20	75% N ₂	0.5	1	NUIG
	2	0.000	1.50	1.500	12.00	75% N ₂ +10% Ar	1.0	20	NUIG
	3	0.000	1.70	1.700	6.60	75% N ₂ +15% Ar	2.0	40	NUIG/ PCFC
C ₂ H ₄ /C ₃ H ₈ 70%/30%	4	0.000	3.75	1.610	9.64	75% N ₂ +10% Ar	2.0	1	NUIG
	5	0.000	0.85	0.360	8.790	75% N ₂ +15% Ar	0.5	20	NUIG
	6	0.000	3.80	1.600	19.60	75% N ₂	1.0	40	NUIG
C ₂ H ₄ /C ₃ H ₈ 90%/10%	7	0.000	2.10	0.200	7.70	75% N ₂ +15% Ar	1.0	1	NUIG
	8	0.000	8.60	1.000	15.40	75% N ₂	2.0	20	NUIG
	9	0.000	1.80	0.200	13.00	75% N ₂ +10% Ar	0.5	40	NUIG/ PCFC
C ₂ H ₆ /C ₃ H ₈ 50%/50%	10	1.300	0.00	1.300	22.40	75% N ₂	0.5	1	NUIG
	11	1.430	0.00	1.430	12.14	75% N ₂ +10% Ar	1.0	20	NUIG
	12	1.600	0.00	1.600	6.80	75% N ₂ +15% Ar	2.0	40	NUIG/ PCFC
C ₂ H ₆ /C ₃ H ₈ 70%/30%	13	3.530	0.00	1.510	9.96	75% N ₂ +10% Ar	2.0	1	NUIG
	14	0.790	0.00	0.340	8.87	75% N ₂ +15% Ar	0.5	20	NUIG
	15	3.535	0.00	1.515	19.95	75% N ₂	1.0	40	NUIG
C ₂ H ₆ /C ₃ H ₈ 90%/10%	16	1.940	0.00	0.220	7.84	75% N ₂ +15% Ar	1.0	1	NUIG
	17	8.000	0.00	0.900	16.10	75% N ₂	2.0	20	NUIG
	18	1.600	0.00	0.200	13.20	75% N ₂ +10% Ar	0.5	40	NUIG/ PCFC
	19	1.860	0.00	0.210	7.53	45.2% N ₂ +45.2% Ar	1.0	90	PCFC
	20	2.520	0.00	0.280	20.40	76.8% N ₂	0.5	120	PCFC
	21	1.860	0.00	0.210	7.53	65.4% N ₂ +25% Ar	1.0	135	PCFC

The corresponding uncertainties involved in the measured IDTs are discussed by Baigmohammadi et al. [5, 6]. Based on the analysis, the uncertainties in compressed mixture temperatures ($\sigma_{T_{c,5}}$) and measured IDTs change for every individual experimental point depending on the initial temperature, pressure, and/or mixture composition. In this regard, the average uncertainties of the compressed temperatures and the measured IDTs in NUIG-L/HPSTs are estimated to be approximately $\pm 10/20$ K and $\pm 25\%$, respectively. However, the compressed temperature uncertainty and the measured IDT variation in the NUIG and PCFC RCMs are evaluated to be about $\pm 5 - 15$ K and $\pm 20\%$ over the entire range of conditions.

5.3 Computational modelling

In the current study, NUIGMech1.1 is used to simulate the experimental targets. This mechanism comprises 2746 species and 11270 reactions, which is developed based on series of recent experimental [4-6, 43-47] and theoretical studies [48-50]. These works are outcome of continuous evolution of the detailed NUIGMech1.1 model which is extensively validated in the prior studies for oxidation of C₁ – C₂ hydrocarbons [5, 6], natural gas mixtures [44], propane/propene blends [47], propyne [45], iso-butene [51], as well as auto-ignition and pyrolysis of C₂ – C₆ alkenes [4, 46]. The current work is a part of simultaneous development of the overall NUIGMech1.1 mechanism. For the purpose of comparison, AramcoMech3.0 [52] is also utilized to perform simulations against the IDT experimental data from this study. Modifications of the most important reactions explicit to ethane, ethylene and propane chemistry in NUIGMech1.1 haven't been mentioned in detail in the previous publications [5, 6, 43, 50], and thus are discussed in this study.

The experimental results were simulated using Python scripts based on the Cantera 2.4 [53] library and the CHEMKIN-Pro 18.2 [54] software, Cantera is suitable for automatization making data manipulation faster; however, Chemkin-Pro is faster for simulations involving large mechanisms and thus is more suitable for simulations when a full mechanism is required. As mentioned above, the definition of IDT is taken as the maximum gradient of pressure or radical concentration with respect to time for the ST simulations. In the RCM simulations, facility effects are included using the volume-time profiles derived from non-reactive experimental pressure-time traces in which O₂ is replaced by N₂ in the mixture [55, 56].

The global model uncertainties, ϵ_{MAD} and ϵ_{MAPE} , are calculated based on the differences between experimental data and mechanism simulated data using the Mean Absolute Deviations (MAD), and the Mean Absolute Percentage Error (MAPE), Eqns. 5-1 and 5-2 respectively. However, to analyze the data with an individual error, the Relative Percentage Error (RPE), ϵ_{RPE} , was used (Eqn. 5-3) to generate the histograms presented in this work. The mathematical expressions used are the following:

$$\epsilon_{MAD} = \frac{1}{n} \sum |IDT_{mod} - IDT_{exp}| \quad (5-1)$$

$$\epsilon_{MAPE} = \frac{1}{n} \sum \left(\left| \frac{IDT_{mod} - IDT_{exp}}{IDT_{exp}} \right| \right) * 100 \quad (5-2)$$

$$\epsilon_{RPE} = \left(\frac{IDT_{mod} - IDT_{exp}}{IDT_{exp}} \right) * 100 \quad (5-3)$$

where n is the total number of experimental measurements. Further details about the statistical analysis are provided as Supplementary material in Appendix C.

To identify the reactions controlling IDTs, brute-force sensitivity analyses were performed at the experimental conditions presented in this study. The sensitivity coefficient (S ; [57]) is defined as:

$$S = \frac{\ln(\tau_+/\tau_-)}{\ln(k_+/k_-)} = \frac{\ln(\tau_+/\tau_-)}{\ln(2.0/0.5)}$$

The sensitivity coefficient S calculated using the brute force method is based on the IDT (τ), with the pre-exponential factor in the Arrhenius equations for each reaction perturbed in the sensitivity analysis. The sensitivity coefficient can be negative or positive, where a negative value refers to a reaction promoting reactivity (decreasing IDT), while a positive value refers to a reaction inhibiting reactivity (increasing IDT). Furthermore, rate of production (ROP) analyses was carried out to track the consumption of the blends and the production of intermediate species.

A global correlation discussion based on constant volume (CV) IDT simulations using NUIGMech1.1 is presented in the “Regression analysis” section (Section 5.4.5), together with general equations sorted by various temperature and pressure conditions. The aim of these correlations is to provide an easy and quick way to determine the IDT behavior of the binary fuels. It does not require any kind of software pre-set up, and the coefficients of interest can be directly substituted in the equations provided in the respective section. A complete table of coefficient values and further details are provided in Appendix B.

5.4 Results and discussion

All of the experimental results for the ethane/propane (C_2H_6/C_3H_8) and ethylene/propane (C_2H_4/C_3H_8) blends are presented in Section 5.4.1 together with simulations using NUIGMech1.1 and AramcoMech3.0 [52]. Henceforth, in all figures, the open symbols represent experimental LPST and/or HPST data, and the solid symbols represent the experimental low-temperature RCM data. Sections 5.4.2 – 5.4.4 present results for the effects of blend composition, pressure, and equivalence ratio using NUIGMech1.1 and their corresponding correlations. Finally, Section 5.4.5 discusses the correlation performance.

5.4.1 Ethylene/propane and ethane/propane blends

Figures 5-2 and 5-3 present experimental data and model predictions of IDTs over the range of conditions studied for the binary C_2H_4/C_3H_8 and C_2H_6/C_3H_8 blends. Figures 5-2 and 5-3 show that NUIGMech1.1 is in better agreement than AramcoMech3.0 with the experimental data. Statistical analyses were conducted using the IDTs from the experiments, and those calculated using both NUIGMech1.1 and AramcoMech3.0. A total sample of 328 IDTs was used to determine the mean, standard deviation (σ), mean absolute deviation (MAD), relative percentage error (RPE), and mean absolute percentage error (MAPE). Figures CS10(a) and CS10(b), with “CS” notation referring to the Supplementary material in Appendix C, provide the RPE frequency distribution for NUIGMech1.1 and AramcoMech3.0 relative to the IDT experiments. It can be inferred that the differences between NUIGMech1.1 and AramcoMech3.0 are a consequence of the poor predictions of AramcoMech3.0 in the low-temperature regime for the C_2H_4/C_3H_8 blends. Furthermore, the absolute values of MAPE calculated over the entire dataset using NUIGMech1.1 were 26.4%, while that for AramcoMech3.0 is 31.9%, indicating the greater accuracy of NUIGMech1.1. As it can accurately predict the IDT data measured over a wide range of temperatures, pressures and equivalence ratios, CV simulations are performed using NUIGMech1.1 to understand the effects of these operating conditions on the IDTs of pure fuels and their binary blends.

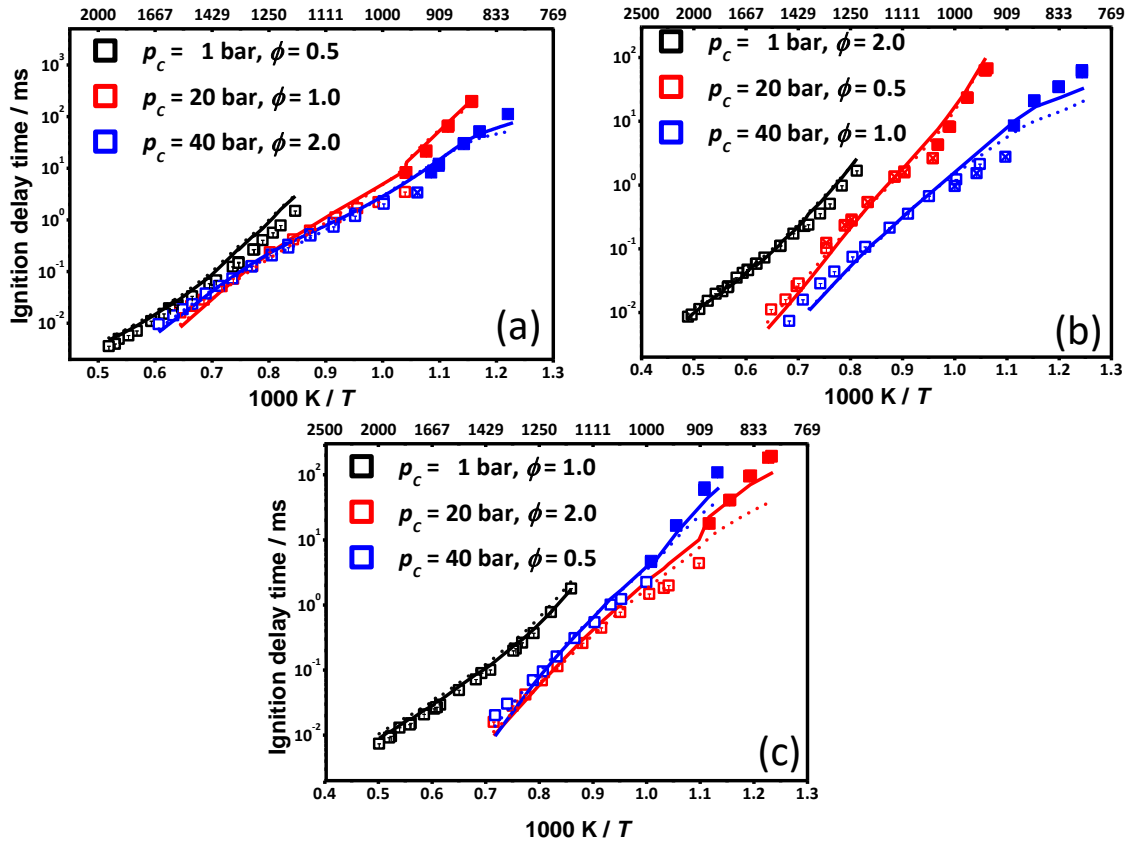


Figure 5-2. Comparisons of experimental ST (\square) and RCM (\blacksquare) data against model predictions using NUIGMech1.1 (solid lines) and AramcoMech3.0 (dashed lines) for; (a) a 50% C₂H₄/50% C₃H₈ blend at 75% N₂ (black symbols/lines), 75% N₂ + 10% Ar (red symbols/lines), and 75% N₂ + 15% Ar (blue symbols/lines); (b) a 70% C₂H₄/30% C₃H₈ blend at 75% N₂ + 10% Ar (black symbols/lines), 75% N₂ + 15% Ar (red symbols/lines), and 75% N₂ (blue symbols/lines); and (c) a 90% C₂H₄/10% C₃H₈ blend at 75% N₂ + 15% Ar (black symbols/lines), 75% N₂ (red symbols/lines), and 75% N₂ + 10% Ar (blue symbols/lines).

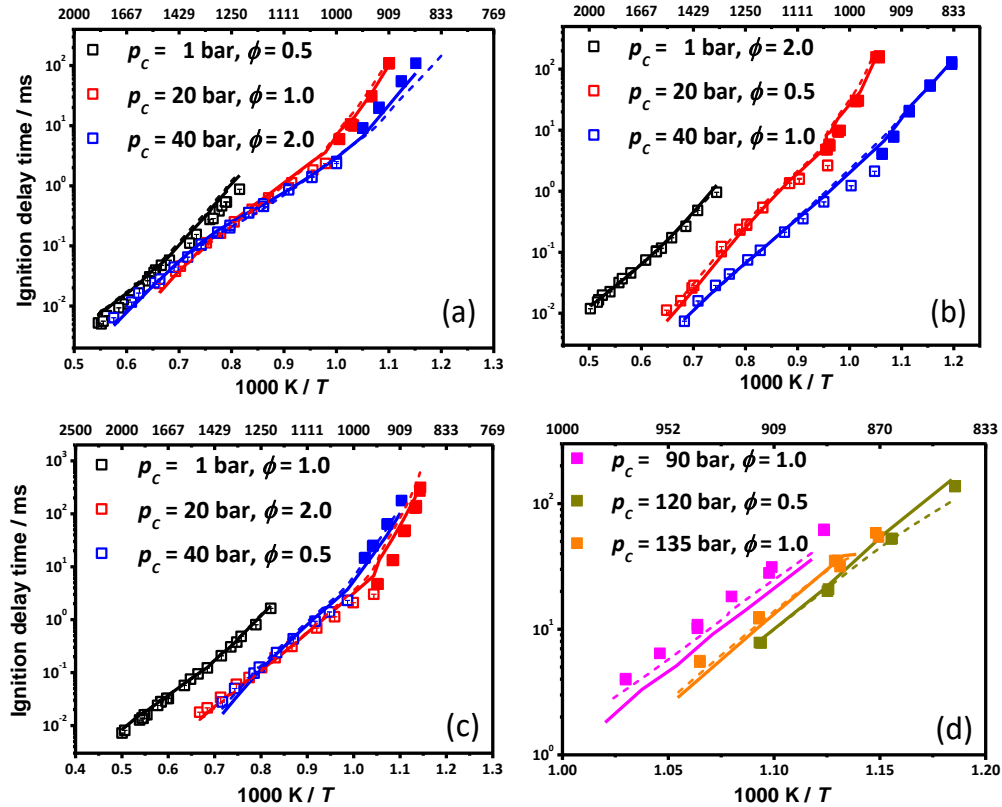


Figure 5-3. Comparisons of experimental ST (\square) and RCM (\blacksquare) data against model predictions using NUIGMech1.1 (solid lines) and AramcoMech3.0 (dashed lines), for; (a) a 50% C_2H_6 /50% C_3H_8 blend at 75% N_2 (black symbols/lines), 75% $N_2 + 10\%$ Ar (red symbols/lines), and 75% $N_2 + 15\%$ Ar (blue symbols/lines); (b) a 70% C_2H_6 /30% C_3H_8 blend at 75% $N_2 + 10\%$ Ar (black symbols/lines), 75% $N_2 + 15\%$ Ar (red symbols/lines), and 75% N_2 (blue symbols/lines); (c) a 90% C_2H_6 /10% C_3H_8 blend at 75% $N_2 + 15\%$ Ar (black symbols/lines), 75% N_2 (red symbols/lines), and 75% $N_2 + 10\%$ Ar (blue symbols/lines); and (d) a 90% C_2H_6 /10% C_3H_8 blend at 45.2% $N_2 + 45.2\%$ Ar (magenta symbols/lines), 76.8% N_2 (green symbols/lines), and 65.4% $N_2 + 25\%$ Ar (orange symbols/lines).

5.4.2 Synergistic/antagonistic effect of blends

First, the ignition behavior of pure fuels is analyzed to determine the important reactivity controlling reactions. In Fig. 5-4, the IDT predictions for C_2H_4 /air, C_2H_6 /air, and C_3H_8 /air mixtures at fuel-lean conditions, at $p_c = 40$ bar and T_c in the range 740 – 1660 K are shown. At lower temperatures ($T_c < 1050$ K), C_3H_8 is the fastest fuel to ignite, however, the trend reverses at higher temperatures, and propane is the slowest to react compared to both the C_2H_4 and C_2H_6 mixtures. The reactivity of C_2H_4 is observed to be higher than C_2H_6 at all temperatures studied here.

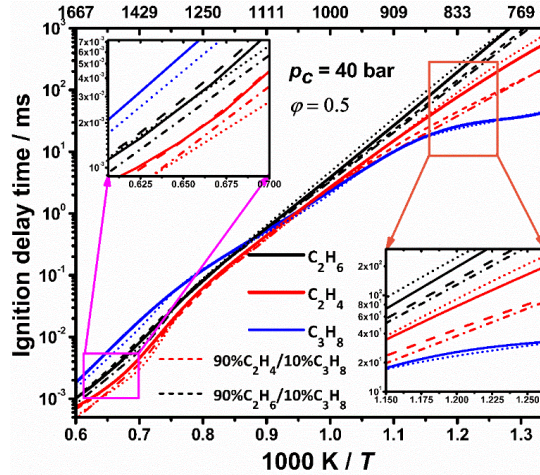


Figure 5-4. IDT predictions of pure fuels, 90% C₂H₄/10% C₃H₈ and 90% C₂H₆/10% C₃H₈ binary blend in air. The corresponding derived correlation predictions are marked as dotted lines for pure fuels and dotted-dashed for binary blends.

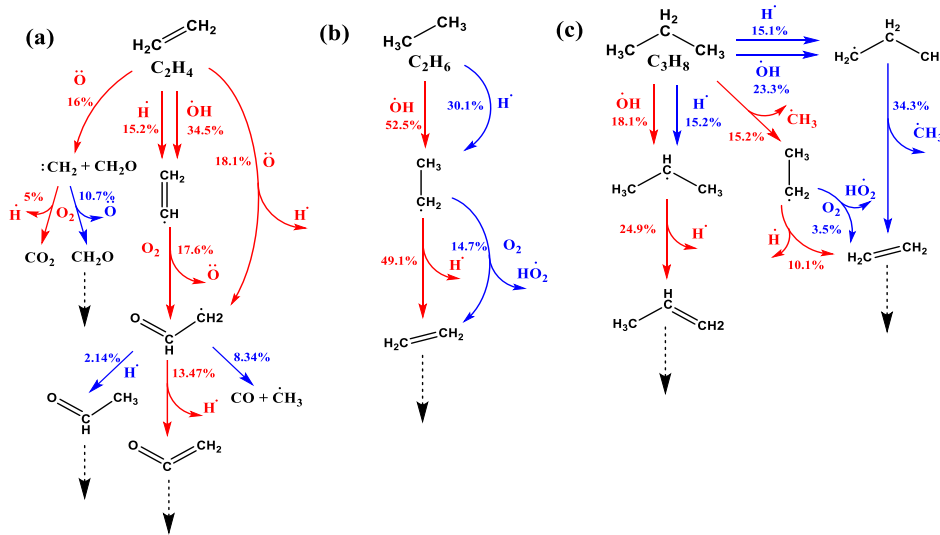


Figure 5-5. Flux analyses of pure (a) C₂H₄, (b) C₂H₆, and (c) C₃H₈ fuel ignition for $T_C = 1430$ K, $p = 40$ bar and $\phi = 0.5$, at the time of 15% fuel consumption.

To explore the controlling chemistry at high-temperature conditions, ROP analyses for C₂H₄/air, C₂H₆/air, and C₃H₈/air mixtures are illustrated in Fig. 5-5 at $T_C = 1430$ K and $p_C = 40$ bar. The ROP analyses are performed following an elemental carbon (C) balance. The percentage value above the arrow refers to the percentage of the fuel proceeding through that pathway. The reaction paths represent the promoting (red color) and inhibiting (blue color) channels of the corresponding fuels. At high temperatures, the reactivity of all fuels is governed by the dominating chain branching reaction $\dot{H} + O_2 \leftrightarrow \dot{O} + \dot{OH}$, which depends on the concentrations of \dot{H} atoms and O₂. In the case of

C_2H_4 /air ignition, at 1430 K, the fuel mainly undergoes H-atom abstraction by $\dot{O}H$ and \dot{H} producing vinyl (\dot{C}_2H_3) radicals. This radical reacts with O_2 to generate vinyloxy radical ($\dot{C}H_2CHO$) through the chain branching reaction $\dot{C}_2H_3 + O_2 \leftrightarrow \dot{C}H_2CHO + \ddot{O}$. Oxygen atoms further react with ethylene greatly promoting reactivity by generating \dot{H} atoms through two different channels, $C_2H_4 + \ddot{O} \leftrightarrow \dot{C}H_2CHO + \dot{H}$ (18.1%) and $C_2H_4 + \ddot{O} \leftrightarrow \dot{C}H_2 + CH_2O$ (16%) followed by $\dot{C}H_2 + O_2 \leftrightarrow CO_2 + \dot{H} + \dot{H}$. For the reaction of oxygen atoms with ethylene the total rate constant and the branching fractions through the various product channels ($\dot{C}H_3 + H\dot{C}O$, $\dot{C}H_2CHO + \dot{H}$, $\dot{C}H_2 + CH_2O$, $CH_2CO + H_2$) are taken from the calculations by Li et al. [58]. These are in good agreement available experimental data, as shown in Fig. 5-6(a). Figure 5-6(b) compares the rate constants for the individual pathways associated with the $C_2H_4 + \ddot{O}$ system. AramcoMech3.0 used the rate constants for $C_2H_4 + \ddot{O}$ producing $\dot{C}H_3 + H\dot{C}O$ and $\dot{C}H_2CHO + \dot{H}$ based on the Baulch et al. [59] recommendation. The pathway producing $\dot{C}H_2 + CH_2O$ was not included in AramcoMech3.0, and its inclusion in NUIGMech1.1 significantly increases the predicted reactivity. The effect on IDT predictions of updating the rate constant for $C_2H_4 + \ddot{O} \rightarrow$ products for C_2H_4 /air mixtures is shown in Fig. CS19 of appendix B. The $\dot{C}H_2CHO$ radical formed here further decomposes to produce ketene and \dot{H} atom, Fig. 5-5(a). The formation of substantial concentrations of \dot{H} atoms is responsible for the faster ignition of C_2H_4 /air mixtures at higher temperatures.

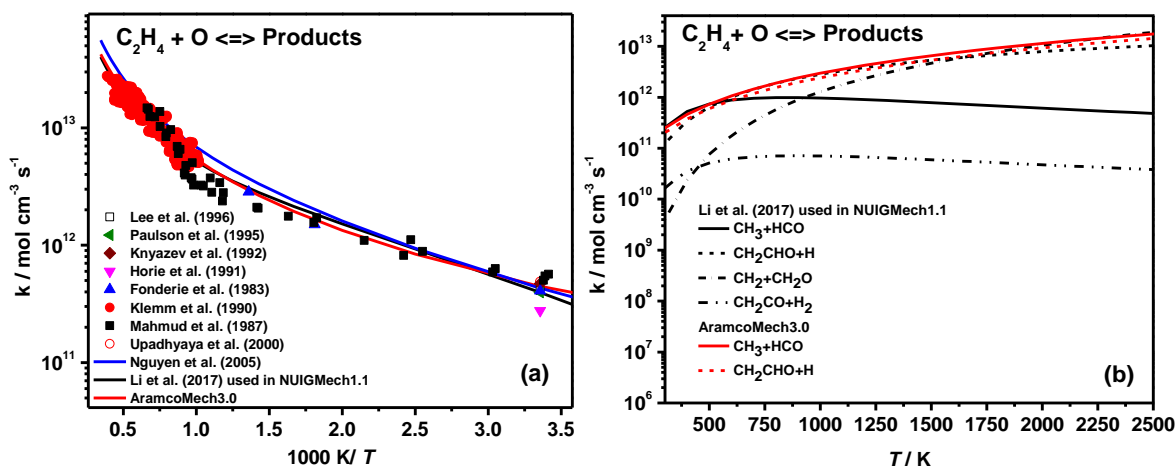


Figure 5-6. Comparisons for experimental and theoretical determinations for (a) the total reaction rate constant of $C_2H_4 + \ddot{O}$ [58, 60-68] and (b) product pathways for the reaction $C_2H_4 + \ddot{O}$.

Ethylene is an important intermediate in C_2H_6 oxidation. At 1430 K, C_2H_6 consumption is initiated by H-atom abstraction primarily by $\dot{O}H$ and \dot{H} forming ethyl (\dot{C}_2H_5) radicals. There has been a wide

variety of experimental investigations for these rate constants, as shown in Fig. CS13. NUIGMech1.1 has an updated rate constant for H-atom abstraction by $\dot{\text{O}}\text{H}$ based on the fit recommended by Krasnoperov and Michael [69]. For H-atom abstraction by $\dot{\text{H}}$, we have adopted the theoretical calculations from Sivaramakrishnan et al. [70]. $\dot{\text{C}}_2\text{H}_5$ radicals decompose promptly to C_2H_4 and $\dot{\text{H}}$ atoms, which undergo chain branching by reacting with O_2 via $\dot{\text{H}} + \text{O}_2 \leftrightarrow \ddot{\text{O}} + \dot{\text{O}}\text{H}$, promoting reactivity. However, at 1430 K, approximately 15% of $\dot{\text{C}}_2\text{H}_5$ radicals react with O_2 to form C_2H_4 via H-atom abstraction reaction that competes with $\dot{\text{C}}_2\text{H}_5$ radical decomposition. The subsequent reaction pathways associated with the C_2H_6 consumption flux are governed by the high-temperature chemistry of C_2H_4 , as discussed in the previous paragraph. At higher temperature conditions, $\dot{\text{C}}_2\text{H}_5 + \text{O}_2 \leftrightarrow \text{C}_2\text{H}_4 + \text{H}\dot{\text{O}}_2$, as well as the H-atom abstraction by $\dot{\text{H}}$ from the fuel which competes with the major chain branching reaction $\dot{\text{H}} + \text{O}_2 \leftrightarrow \ddot{\text{O}} + \dot{\text{O}}\text{H}$, are responsible for the lower reactivity of C_2H_6 compared to C_2H_4 .

Similar to ethane and ethylene, propane oxidation is mainly driven by H-atom abstraction by $\dot{\text{O}}\text{H}$ radicals and $\dot{\text{H}}$ atoms, generating primary ($\text{n}\dot{\text{C}}_3\text{H}_7$) and secondary propyl ($\text{i}\dot{\text{C}}_3\text{H}_7$) radicals. Due to the importance of H-atom abstraction by $\dot{\text{O}}\text{H}$ from propane, there have been a large number of measurements performed, Fig. CS14. The rate constant adopted in this work is the best fit from the more recent direct measurements by Sivaramakrishnan et al. [71], who investigated the branching fraction for the abstraction of the secondary C–H bond in the temperature range 927 – 1146 K, together with the measurement by Droege and Tully [72] over the temperature range 298 – 900 K (Fig. CS14). At 1430 K, approximately 15% of the C_3H_8 is consumed by unimolecular decomposition producing $\dot{\text{C}}_2\text{H}_5$ and methyl radicals ($\dot{\text{C}}\text{H}_3$), Fig. 5-5(c). Substantial concentrations of $\dot{\text{C}}\text{H}_3$ radicals are also formed from the β -scission of $\text{n}\dot{\text{C}}_3\text{H}_7$ radicals. Methyl radicals are consumed by reaction with $\text{H}\dot{\text{O}}_2$ to produce methoxy radicals through the chain branching reaction $\dot{\text{C}}\text{H}_3 + \text{H}\dot{\text{O}}_2 \leftrightarrow \dot{\text{C}}\text{H}_3\text{O} + \dot{\text{O}}\text{H}$, which promotes reactivity. The route through the chain-terminating reaction $\dot{\text{C}}\text{H}_3 + \text{H}\dot{\text{O}}_2 \leftrightarrow \text{CH}_4 + \text{O}_2$ inhibits reactivity. This competition between chain branching and termination significantly influences IDT predictions for C_3H_8 . The rate constants for these reactions are taken from the theoretical calculations of Jasper et al. [73] and Zhu and Lin [74] respectively. The rate constants and the branching ratio of the two $\dot{\text{C}}\text{H}_3 + \text{H}\dot{\text{O}}_2$ channels agree well with the most recent experimental measurements by Hong et al. [75] (Fig. CS15). The self-recombination of $\dot{\text{C}}\text{H}_3$ radicals producing C_2H_6 further contributes to a reduction in the reactivity of propane. The presence of high

concentrations of $\dot{\text{C}}\text{H}_3$ radicals ultimately decreases the reactivity of C_3H_8 compared to C_2H_6 at high-temperature conditions.

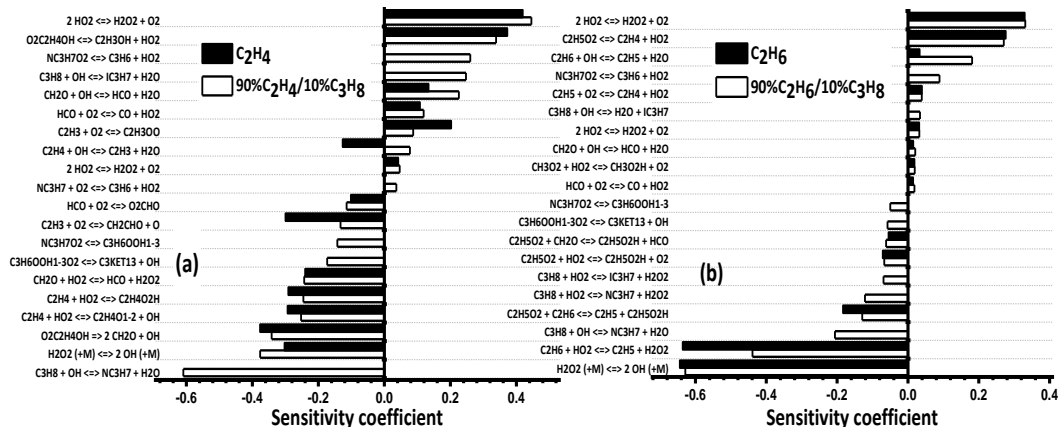


Figure 5-7. Sensitivity analyses to IDT at 790 K, 40 atm, and $\varphi = 0.5$, for; (a) C_2H_4 and 90% C_2H_4 /10% C_3H_8 , in air; and (b) C_2H_6 and 90% C_2H_6 /10% C_3H_8 in air.

The effects on IDTs of the addition of C_3H_8 to C_2H_4 /air and C_2H_6 /air mixtures are presented in Fig. 5-4. The reactivities of the mixtures increase significantly for the 90% C_2H_4 /10% C_3H_8 and 90% C_2H_6 /10% C_3H_8 binary blends at lower temperatures in the range 740 – 1000 K. The addition of only 10% C_3H_8 to the C_2H_4 /air and C_2H_6 /air mixtures shortens IDTs by a factor of 2.8 and 2.0 respectively, at 790 K. To interpret the influence of C_3H_8 addition on the ignition of the C_2H_4 /air and C_2H_6 /air mixtures, sensitivity analyses were performed at 790 K, Fig. 5-7. Moreover, Fig. 5-8 illustrates the flux analyses performed for these mixtures in the same condition. The black color represents the flux for the pure C_2H_4 /air or C_2H_6 /air mixtures, and the red color represents the flux for the C_3H_8 blended binary mixtures. The flux analysis presented in Fig. 5-8 shows that adding propane in the mixture does not alter the reaction pathways of ethylene and ethane chemistry and it also makes insignificant changes to their flux values.

At 790 K, for both pure C_2H_4 and 90% C_2H_4 /10% C_3H_8 blend, ethylene is primarily consumed by the addition of $\dot{\text{O}}\text{H}$ radical to the double bond forming hydroxyethyl radicals, which accounts for around 70% of the overall C_2H_4 consumption. These add to molecular oxygen producing hydroxyethyl-peroxy radicals ($\dot{\text{O}}_2\text{C}_2\text{H}_4\text{OH}$), which subsequently decompose, producing two formaldehyde molecules and an $\dot{\text{O}}\text{H}$ radical or form vinyl alcohol and HO_2 radicals, the former being the most favorable product channel promoting reactivity for the C_2H_4 /air mixture, Fig. 5-8(a). Besides

$\dot{\text{O}}\text{H}$ addition, HO_2 addition to ethylene producing oxirane ($\text{C}_2\text{H}_4\text{O}1-2$) and $\dot{\text{O}}\text{H}$ radical also has a large promoting effect on the reactivity of ethylene at low temperatures, especially for fuel-rich conditions.

The importance of the $\text{C}_2\text{H}_4 + \text{HO}_2 \leftrightarrow \text{C}_2\text{H}_4\text{O}1-2 + \dot{\text{O}}\text{H}$ and $\dot{\text{O}}_2\text{C}_2\text{H}_4\text{OH} \rightarrow \text{products}$ reaction systems on C_2H_4 oxidation is shown in Fig. 5-9(a), which also presents the performance of the current mechanism and AramcoMech3.0 as can be seen by red solid line and black dashed line, respectively for 90% $\text{C}_2\text{H}_6/10\%$ C_3H_8 mixtures at $p_C = 20$ atm, and $\varphi = 2.0$.

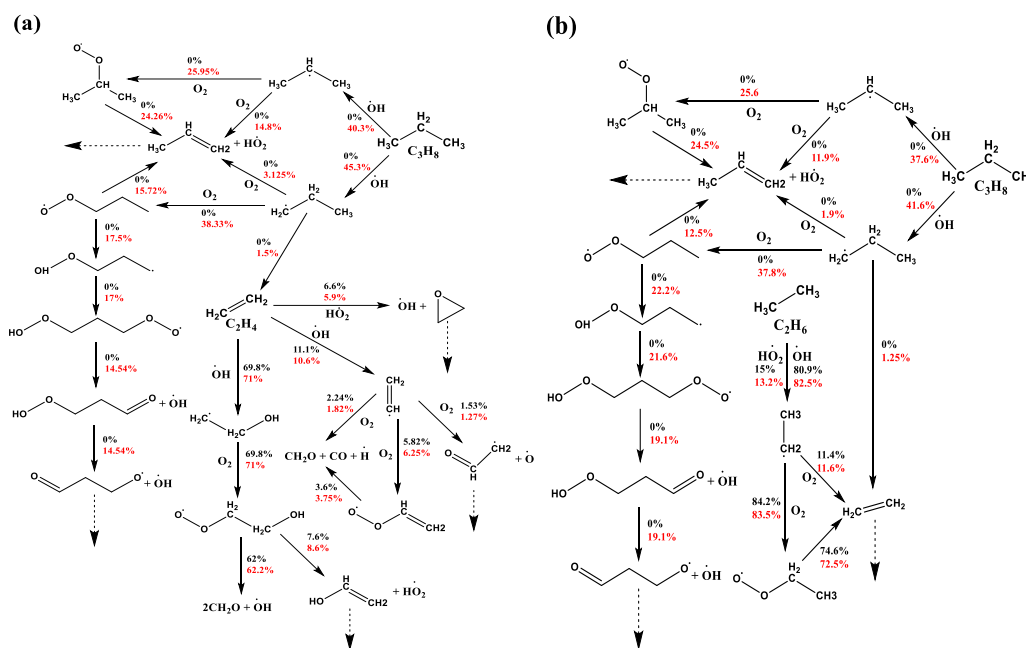


Figure 5-8. Flux analyses for; (a) pure C_2H_4 (black) and 90% $\text{C}_2\text{H}_4/10\%$ C_3H_8 (red); and (b) pure C_2H_6 (black) and 90% $\text{C}_2\text{H}_6/10\%$ C_3H_8 (red) mixtures ignition for 790 K and at 40 atm, and $\varphi = 0.5$.

AramcoMech3.0 severely underpredict the IDT, particularly in the low temperature region in the range of 800 – 900 K. AramcoMech3.0 implemented a reaction rate for $\text{C}_2\text{H}_4 + \text{HO}_2 \leftrightarrow \text{C}_2\text{H}_4\text{O}1-2 + \dot{\text{O}}\text{H}$ based on the recommendation by Zsély et al. [11]. Recently Zádor et al. [77] and Klippenstein et al. [76] studied the potential energy surfaces of the $\text{C}_2\text{H}_5\dot{\text{O}}_2$ system using high-level quantum chemistry calculations.

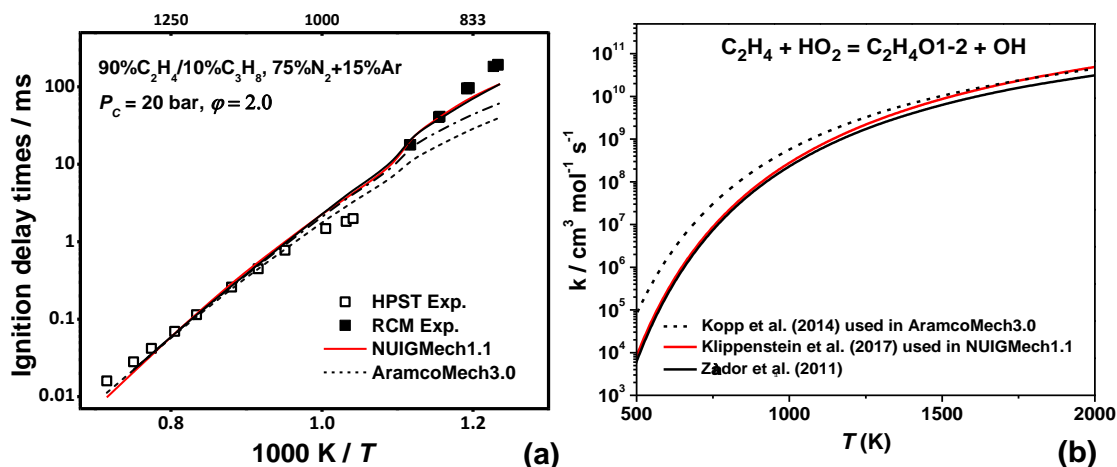


Figure 5-9. (a) Effect of changing the rate constant for $C_2H_4 + HO_2 \leftrightarrow C_2H_4O1-2 + OH$ and $\dot{O}_2C_2H_4OH \rightarrow$ products on IDT predictions for 90% C_2H_4 /10% C_3H_8 mixtures, — NUIGMech1.1, ----- AramcoMech3.0, -.-.- AramcoMech3.0 plus updated rate constant [76] for $C_2H_4 + HO_2 \leftrightarrow C_2H_4O1-2 + OH$, — AramcoMech3.0 plus updated rate constant for $C_2H_4 + HO_2 \leftrightarrow C_2H_4O1-2 + OH$ and $\dot{O}_2C_2H_4OH \rightarrow$ products [77]; and (b) Comparison of current rate constant [75] for $C_2H_4 + HO_2 \leftrightarrow C_2H_4O1-2 + OH$ against the study by Zsély et al. [11] and Zádor et al. [78].

NUIGMech1.1 has adopted the rate constant for $C_2H_4 + HO_2$ from Klippenstein et al. [76], which is approximately a factor of three lower than the rate constant recommended by Zsély et al [11] at 800 K, Fig. 5-9(b), and updating this rate constant in AramcoMech3.0 leads to a significant improvement in IDT predictions as depicted by the dashed-dotted line in Fig. 5-9(a). Another important reaction pathway controlling ethylene IDT is the consumption of $\dot{O}_2C_2H_4OH$ radicals through the Waddington [79] mechanism $\dot{O}_2C_2H_4OH \rightarrow 2CH_2O + OH$ and the HO_2 elimination channel producing C_2H_3OH which inhibits reactivity. In NUIGMech1.1 the rate constant for the dissociation of $\dot{O}_2C_2H_4OH$ radicals is adopted from Zádor et al. [78]. AramcoMech3.0 utilized an estimated rate constant for the Waddington pathway that is an order of magnitude higher than the rate determined by Zádor et al. [78], while surprisingly, the HO_2 elimination channel was not included in the mechanism. The last agreement represented by black solid line in Fig. 5-9(a) is attained by updating both $C_2H_4+HO_2$ and dissociations of $\dot{O}_2C_2H_4OH$ reactions in AramcoMech3.0 that leads to significant improvement in the agreement of the simulations compared to experimental measurements.

As seen in Fig. 5-8(a), \dot{OH} radicals can abstract a hydrogen atom from ethylene producing \dot{C}_2H_3 radicals. These add to O_2 generating vinyl-peroxy radicals, which subsequently dissociate to formaldehyde, CO, and \dot{H} atoms. Some \dot{C}_2H_3 radicals also produce $\dot{C}H_2CHO$ and \dot{O} atoms increasing the reactivity of ethylene ignition, as shown in Fig. 5-8(a). For the C_2H_6 /air mixture, the fuel is mainly

consumed by H-atom abstraction reaction by $\dot{\text{O}}\text{H}$ and $\text{H}\dot{\text{O}}_2$ radicals forming $\dot{\text{C}}_2\text{H}_5$ radicals. These react with O_2 to produce ethylperoxy ($\text{C}_2\text{H}_5\dot{\text{O}}_2$) radicals, which subsequently decompose to C_2H_4 and $\text{H}\dot{\text{O}}_2$ radicals. Figure 5-7(b) shows that the concerted elimination reaction $\text{C}_2\text{H}_5\dot{\text{O}}_2 \leftrightarrow \text{C}_2\text{H}_4 + \text{H}\dot{\text{O}}_2$ is important in inhibiting the autoignition of C_2H_6 .

Figures 5-7(a) and 5-7(b) show that C_3H_8 specific reactions become important when propane is added to the $\text{C}_2\text{H}_4/\text{air}$ and $\text{C}_2\text{H}_6/\text{air}$ mixtures. At 790 K, H-atom abstraction from C_3H_8 by $\dot{\text{O}}\text{H}$ producing $\text{n}\dot{\text{C}}_3\text{H}_7$ and H_2O is the most sensitive reaction promoting reactivity, while abstraction leading to $\text{i}\dot{\text{C}}_3\text{H}_7$ radicals inhibits reactivity. At 790 K, $\sim 14.8\%$ ($\text{C}_2\text{H}_4/\text{C}_3\text{H}_8$ blend) and $\sim 11.9\%$ ($\text{C}_2\text{H}_6/\text{C}_3\text{H}_8$ blend) of $\text{i}\dot{\text{C}}_3\text{H}_7$ radicals react with O_2 to form C_3H_6 and $\text{H}\dot{\text{O}}_2$ radicals, which reduces reactivity. However, $\sim 38.3\%$ ($\text{C}_2\text{H}_4/\text{C}_3\text{H}_8$ blend) and $\sim 37.8\%$ ($\text{C}_2\text{H}_6/\text{C}_3\text{H}_8$ blend) of $\text{n}\dot{\text{C}}_3\text{H}_7$ radicals add to O_2 forming n-propyl-peroxy ($\text{n}\dot{\text{C}}_3\text{H}_7\text{O}_2$) radicals which undergo isomerization generating hydroperoxyl-propyl ($\dot{\text{C}}_3\text{H}_6\text{OOH1-3}$) radicals. These then further add to O_2 producing hydroperoxyl-propyl peroxy radical ($\dot{\text{C}}_3\text{H}_6\text{OOH1-3O}_2$), which isomerizes to produce a carbonylhydroperoxide and an $\dot{\text{O}}\text{H}$ radical. The carbonylhydroperoxide further dissociates, producing a carbonyl-alkoxy radical and a second $\dot{\text{O}}\text{H}$ radical, which is a chain branching pathway, resulting in higher reactivity of the C_3H_8 blended mixtures compared to the pure $\text{C}_2\text{H}_4/\text{air}$ or $\text{C}_2\text{H}_6/\text{air}$ mixtures.

5.4.3 Effect of pressure on ignition

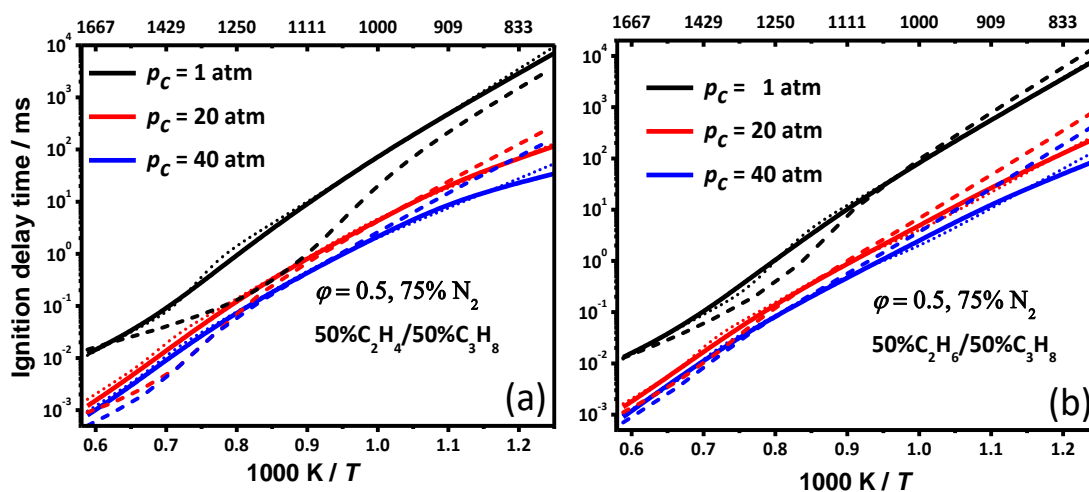


Figure 5-10. Effect of pressure for; (a) 50% $\text{C}_2\text{H}_4/50\%$ C_3H_8 (solid lines) binary blend and pure ethylene (dashed lines); and (b) 50% $\text{C}_2\text{H}_6/50\%$ C_3H_8 (solid lines) binary blend and pure ethane (dashed lines). The derived correlation predictions for binary blends are represented by dotted lines.

Figure 5-10 presents the influence of pressure on the IDTs for the 50% C₂H₄/50% C₃H₈ and 50% C₂H₆/50% C₃H₈ binary mixtures as well as for the pure C₂H₄ and C₂H₆ at $\phi = 0.5$ and 75% N₂ dilution. The model predicts that the reduction in reactivity due to the addition of C₃H₈ with C₂H₄ at 1 atm is more than its corresponding 20 atm and 40 atm cases at intermediate and higher temperature conditions. The self-recombination of methyl radicals is responsible for the lower reactivity of the propane blended mixtures as discussed in Section 5.4.2. In the case of the C₂H₄/C₃H₈ blend at 1250 K, as the pressure decreases to 1 atm the $\dot{C}H_3 + \dot{C}H_3 (+M) \leftrightarrow C_2H_6 (+M)$ reaction more strongly inhibits reactivity, accounting for 35% of the total flux through methyl radicals, while at 40 bar this reaction contributes only 12% to $\dot{C}H_3$ consumption. Furthermore, from Fig. 5-10 it is observed that the overall reactivity of the system increases with pressure due to the corresponding increase in the concentration of the reactants. At 800 K, upon increasing the pressure from 1 to 20 atm, there is an order of magnitude increase in reactivity observed for both the C₂H₄/C₃H₈ and C₂H₆/C₃H₈ mixtures. There is approximately a four-fold increase in reactivity by increasing the pressure from 20 to 40 atm. To determine the reactions controlling IDT predictions at these conditions, sensitivity analyses are presented in Fig. 5-11 and Fig. CS16 for the binary mixtures at $p_C = 1, 20,$ and 40 atm.

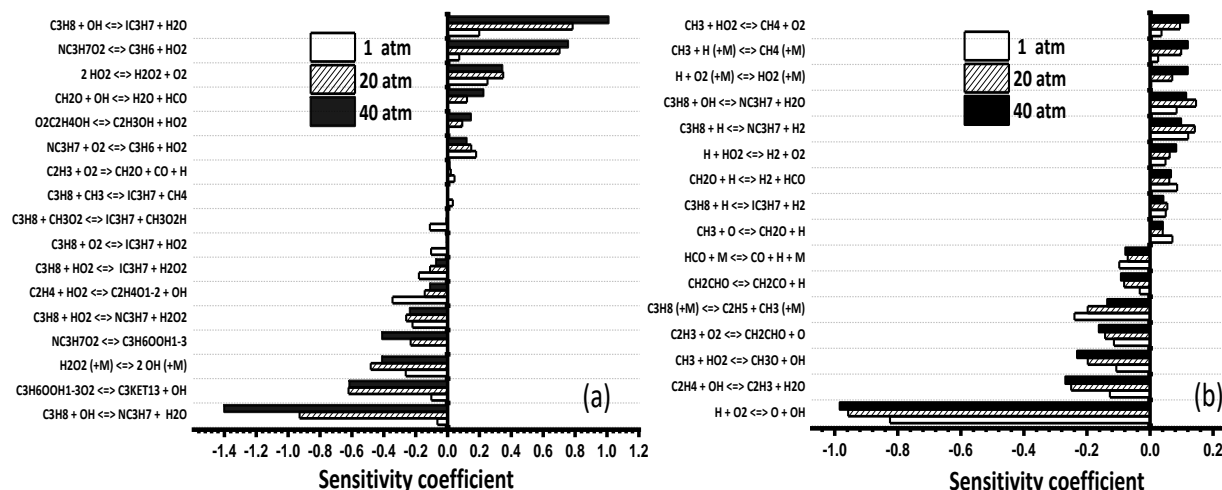


Figure 5-11. Sensitivity analyses to IDT predictions as function of pressure at $\phi = 0.5$, 50% C₂H₄/50% C₃H₈; (a) 800 K; and (b) 1600 K.

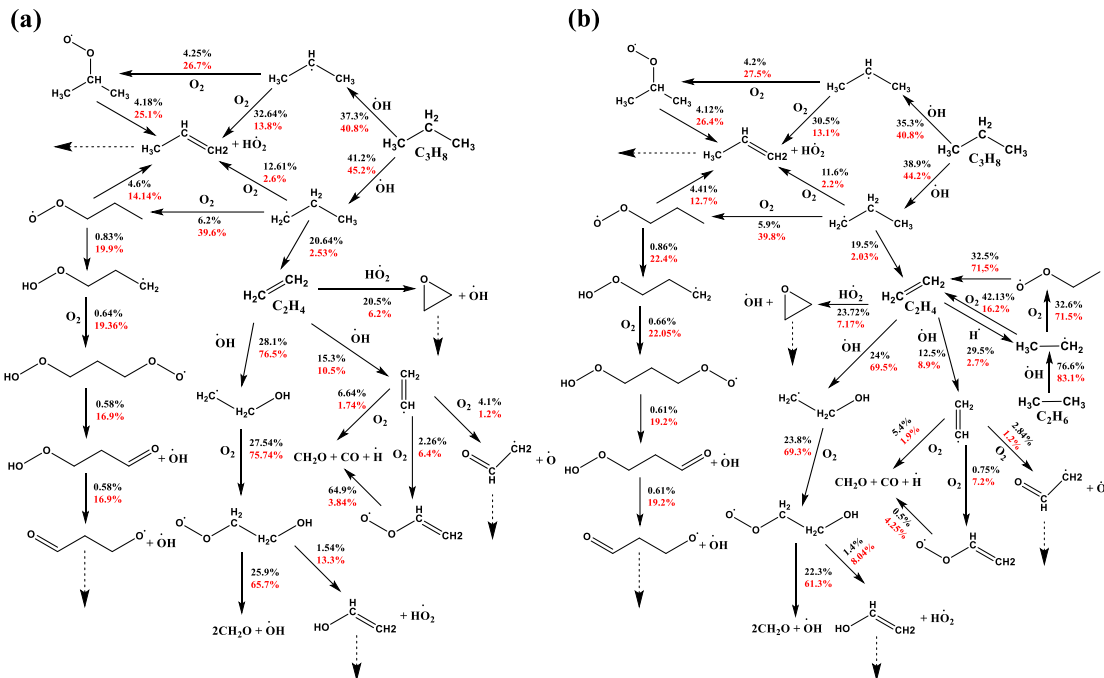


Figure 5-12. Flux analyses at 800 K, $\phi = 0.5$, $p = 1$ (black), and 40 atm (red), with 75% N_2 as diluent for; (a) 50% C_2H_4 /50% C_3H_8 ; and (b) 50% C_2H_6 /50% C_3H_8 .

Figure 5-11 shows that at low temperature (800 K) and high-pressure conditions (20 and 40 atm), the reactivity of the binary blends is mainly controlled by H-atom abstraction from C_3H_8 by $\dot{O}H$ radicals, with the formation of $n\dot{C}_3H_7$ radicals promoting reactivity and $i\dot{C}_3H_7$ radicals inhibiting reactivity. However, at 800 K and 1 atm, H-atom abstraction from C_3H_8 no longer influences IDT predictions, but rather the competition between the reactions generating and consuming hydrogen peroxide, via $H\dot{O}_2 + H\dot{O}_2 \leftrightarrow H_2O_2 + O_2$ and $H_2O_2 (+M) \leftrightarrow \dot{O}H + \dot{O}H (+M)$, respectively control the reactivity of the binary blends. The flux analyses presented in Fig. 5-12 show that, at 40 atm pressure, the percentage contribution of $n\dot{C}_3H_7$ radical β -scission forming C_2H_4 and $\dot{C}H_3$ reduces, while the importance of $n\dot{C}_3H_7$ radical addition to O_2 increases compared to the 1 atm case. Since the addition of $n\dot{C}_3H_7$ radicals to O_2 and the subsequent chain branching channels produces two reactive $\dot{O}H$ radicals and thus increases reactivity, the formation of $n\dot{C}_3H_7$ radicals, and other low-temperature reactions those are not favorable at low pressures become significant at higher pressures in controlling the overall reactivity of binary mixtures. At the higher temperature of 1600 K, the reactivity is only controlled by the chain branching reaction, $\dot{H} + O_2 \leftrightarrow \ddot{O} + \dot{O}H$ irrespective of pressure, as seen in Figs. 5-11(b) and CS16. The reactions that consume \dot{H} atoms such as, $C_3H_8 + \dot{H} \leftrightarrow n\dot{C}_3H_7 + H_2$, C_3H_8

$+ \dot{H} \leftrightarrow i\dot{C}_3H_7 + H_2$, $C_2H_6 + \dot{H} \leftrightarrow \dot{C}_2H_5 + H_2$, $CH_2O + \dot{H} \leftrightarrow H\dot{C}O + H_2$ and $\dot{H} + O_2 (+M) \leftrightarrow H\dot{O}_2 (+M)$ compete with $\dot{H} + O_2 \leftrightarrow \dot{O} + \dot{O}H$ and thus inhibit the reactivity of the binary mixtures (Fig. 11).

5.4.4 Effect of equivalence ratio on ignition

Figure 5-13 presents the effect of equivalence ratio on IDTs for the pure fuels, 50% $C_2H_4/50\%$ C_3H_8 and 50% $C_2H_6/50\%$ C_3H_8 binary mixtures at $p_C = 20$ atm, 75% N_2 , and at $\phi = 0.5, 1.0$, and 2.0. It is observed that at temperatures above 1250 K, the reactivities of both pure fuels and binary mixtures are fastest for the fuel-lean mixtures and slowest for the fuel-rich mixtures.

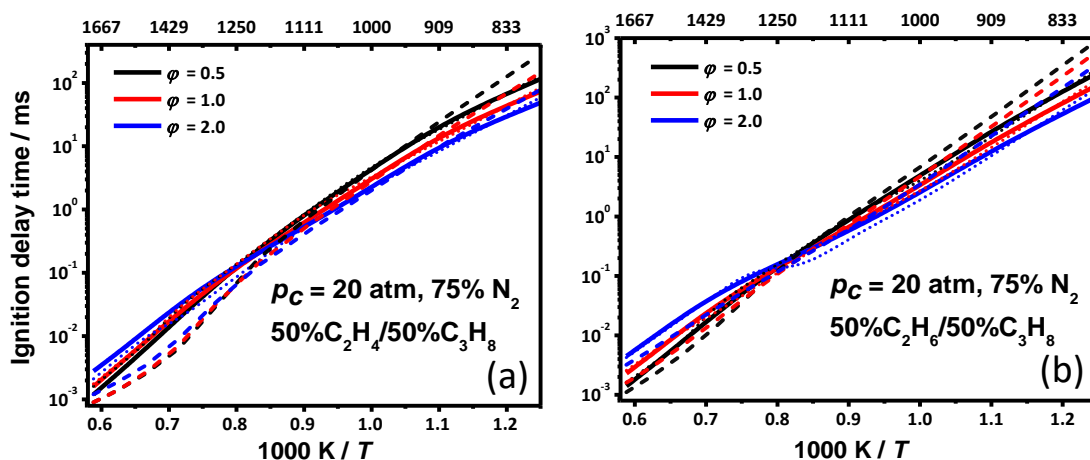


Figure 5-13. Effect of equivalence ratio in (a) 50% $C_2H_4/50\%$ C_3H_8 (solid lines) binary blend and pure ethylene (dashed lines); and (b) 50% $C_2H_6/50\%$ C_3H_8 (solid lines) binary blend and pure ethane (dashed lines). The derived correlation predictions for binary blends are represented by dotted lines.

However, at a temperature below 1250 K, fuel-rich mixtures are fastest to ignite, and the fuel-lean mixtures are slowest. To determine the governing chemistry under these conditions, sensitivity analyses were performed, the results of which are presented as a function of equivalence ratio in Figs. CS17 and CS18 at 800 K and 1600 K. At high temperatures (> 1250 K), IDTs are mainly controlled by the concentration of O_2 in the binary blends through the main chain branching reaction $\dot{H} + O_2 \leftrightarrow \dot{O} + \dot{O}H$, and its influence increases as the mixture become leaner. Thus, fuel-lean mixtures are fastest to ignite at high temperatures. However, at low temperatures (< 1250 K), the reactivity is mainly governed by the addition of the fuel derived alkyl radicals to O_2 and the following low-temperature chemistry leading to chain branching, which is limited by the fuel concentration through H-atom abstraction from propane by $\dot{O}H$ radicals. Thus, at a lower temperature, the dependence on the equivalence ratio is reversed, with fuel-rich mixtures being the most reactive.

5.4.5 Regression analysis

Global regression equations have been developed using NUIGMech1.1 with approximately 17280 CV simulations for each blend mixture spanning over five parameters: p_C (1–40 atm), T_C (800–2000 K), ϕ (0.2–2.0), dilution (75%–90%) and fuel ratio composition (50% C₂H₄ or C₂H₆/50% C₃H₈, and 70% C₂H₄ or C₂H₆/30% C₃H₈). The regression equations developed using the predictions are compared with the ST experimental data in Figs. CS20 and CS21 of the Appendix C. The expression (τ_{corr}) used is analogous to the Arrhenius rate expression and is defined as shown in Eq. 5-4 below:

$$\tau_{\text{corr}} = 10^A e^{\frac{B}{T_C}} [C_2H_4]^C [C_2H_6]^D [C_3H_8]^E [\text{oxidizer}]^F [\text{diluent}]^G \quad (5-4)$$

where A represents the pre-exponential factor coefficient, B represents the activation energy, and C – G represent concentrations of ethylene, ethane, propane, oxidizer, and dilution, respectively. A synopsis of the derived correlations for the binary fuels studied in the pressure range $20 \leq p_C \leq 40$ atm over three regimes of temperature is presented below. However, details of the coefficients of the derived correlations along with their corresponding χ^2 and R^2 for the C₂H₄/C₃H₈ and C₂H₆/C₃H₈ mixtures are presented in Table CS6 and CS7, respectively.

For $1500 \leq T_C \leq 2000$ K:

$$\tau_{\text{corr}} = 10^{-10.34} e^{\frac{21386.6}{T_C}} [C_2H_4]^{-0.502} [C_3H_8]^{0.463} [\text{oxidizer}]^{-1.080} [\text{diluent}]^{0.354} \quad (5-5)$$

$$\tau_{\text{corr}} = 10^{-9.402} e^{\frac{20465}{T_C}} [C_2H_6]^{0.113} [C_3H_8]^{0.413} [\text{oxidizer}]^{-1.344} [\text{diluent}]^{0.131} \quad (5-6)$$

For $1100 \leq T_C \leq 1500$ K:

$$\tau_{\text{corr}} = 10^{-9.89} e^{\frac{19220.37}{T_C}} [C_2H_4]^{-0.491} [C_3H_8]^{-0.056} [\text{oxidizer}]^{-0.447} [\text{diluent}]^{0.149} \quad (5-7)$$

$$\tau_{\text{corr}} = 10^{-9.79} e^{\frac{19065.65}{T_C}} [C_2H_6]^{-0.408} [C_3H_8]^{-0.169} [\text{oxidizer}]^{-0.330} [\text{diluent}]^{0.062} \quad (5-8)$$

For $800 \leq T_C \leq 1100$ K:

$$\tau_{\text{corr}} = 10^{-7.217} e^{\frac{14136.9}{T_C}} [C_2H_4]^{-0.44} [C_3H_8]^{-0.392} [\text{oxidizer}]^{-0.427} [\text{diluent}]^{-0.017} \quad (5-9)$$

$$\tau_{\text{corr}} = 10^{-9.52} e^{\frac{18630.7}{T_C}} [C_2H_6]^{-0.145} [C_3H_8]^{-0.555} [\text{oxidizer}]^{-0.186} [\text{diluent}]^{-0.145} \quad (5-10)$$

At high temperatures (1500–2000 K), the coefficient for ethylene is strongly negative, while those for ethane and propane are positive. This is because at high temperatures increasing the ethylene concentration increases the concentration of vinyl radicals, which react with O₂ ($\dot{C}_2H_3 + O_2 \leftrightarrow \dot{C}H_2CHO + \ddot{O}$) in a reaction which is chain branching. On the other hand, both ethane and propane

compete with O_2 for \dot{H} atoms, and if their concentrations increase, the rate of $\dot{H} + O_2 \leftrightarrow \ddot{O} + \dot{OH}$ will decrease, reducing reactivity. For ethane/propane mixtures, both coefficients are positive, but it is less positive for ethane than propane, as the oxidation of ethane leads to higher concentrations of ethylene. Thus, increasing the concentration of ethane relative to propane will increase reactivity and vice versa.

At low temperatures (800–1100 K), the coefficients associated with ethylene, ethane, and propane become negative, with ethane being less negative than propane. At low temperatures, propane promotes reactivity through the addition of propyl radicals to O_2 that proceeds to chain branching through the low-temperature reaction sequence that generates two highly active \dot{OH} radicals. Thus, for the ethane/propane mixtures, increasing the propane concentration will increase mixture reactivity. However, for ethylene/propane mixtures, the coefficient of ethylene is comparable to that of propane, as ethylene and propane exhibit similar reactivity in the temperature range between 900–1100 K, as seen in Fig. 5-4.

It is interesting to note that, at high temperatures (Eqns. 5-5 and 5-6), the magnitude of the oxidizer coefficients (–1.08 and –1.344 for C_2H_4/C_3H_8 and C_2H_6/C_3H_8 blends, respectively) are significantly larger, by a factor of two or more, than for the corresponding fuel coefficients, thus showing a higher sensitivity towards oxidizer concentrations at these conditions. As we approach the lower temperature regimes (Eqns. 5-9 and 5-10), the coefficients associated with each fuel become higher and are even larger than the corresponding oxidizer coefficients, thus representing the increasing importance of fuel-based kinetics. These characteristics observed in the correlations corroborate the underlying kinetics understanding discussed in Section 5.4 above and enable the correlations to capture the IDT trends effectively.

5.5 Conclusions

An experimental and kinetic modelling study of the IDT characteristics of C_2 – C_3 binary blends of C_2H_4/C_3H_8 and C_2H_6/C_3H_8 mixtures over a wide range of experimental conditions, pressures (1–135 atm), temperatures (~750–2000 K), equivalence ratios ($0.5 \leq \phi \leq 2.0$) and 75–90% of dilution percentage were presented. The performance of NUIGMech1.1 and its corresponding derived correlations have been evaluated against the experimental data collected. Results show that NUIGMech1.1 is in good agreement within ~26.4% of model uncertainty to the measured IDTs over the studied conditions, compared to ~35% for AramcoMech3.0. Moreover, the correlations can

predict the experimental IDTs appropriately under specific regimes, becoming a useful tool for predicting the behavior of C₂–C₃ binary blends at specific conditions.

Finally, the effects of blend composition, pressure and equivalence ratio on the IDTs were investigated for various mixtures containing C₂H₄, C₂H₆, and C₃H₈ as reactants. It was observed that for all mixtures, as the temperature and pressure increase, IDTs decrease. For the equivalence ratio, an expected crossover point was observed at $T_C \sim 1250$ K, wherein the controlling chemistry switches such that the trends invert their behavior. The reactivity of C₂H₄ was found to be higher than for C₂H₆ throughout the temperature range examined in this study. At higher temperatures, vinoxy radicals and oxygen atoms formed from vinyl radical's reaction with O₂, proceed via dissociation and bimolecular reactions with C₂H₄, to produce a substantial amount of \dot{H} atoms resulting in faster ignition of C₂H₄/air mixtures. The concerted elimination reaction between \dot{C}_2H_5 and O₂ is responsible for the reduction in ethane reactivity. It was observed that C₃H₈ blended fuels were the fastest to ignite at lower temperatures (< 1250 K), however, the trend is reversed at higher temperatures, and C₃H₈ exhibited the slowest reactivity compared to both C₂H₄ and C₂H₆ at $T > 1250$ K. In the case of C₃H₈, at low temperatures n-propyl radical formation, followed the classical low-temperature chain branching pathways via its addition to O₂ generate $\dot{O}H$ radicals promoting reactivity, while methyl radical recombination and its consumption by HO₂ leading to CH₄ and O₂ reduce reactivity at higher temperatures.

Acknowledgements

The authors would like to express their gratitude to Science Foundation Ireland (SFI) via their Research Centre Program through project numbers 15/IA/3177 and 16/SP/3829, KAY-ICHEC via the project ngche079c, and to Shell Research Ltd. The authors from PCFC RWTH Aachen University would like to recognize the funding support from the German Research Foundation (Deutsche Forschungsgemeinschaft, DFG) through the project number –322460823 (HE7599/2-1).

References

- [1] U.S.E.I. Administration, International Energy Outlook 2019 with projections to 2050, IEO2019, (2019).
- [2] S. Bilgen, Structure and environmental impact of global energy consumption, *Renew. Sust. Energ. Rev.* 38 (2014) 890-902.

- [3] W.K. Metcalfe, S.M. Burke, S.S. Ahmed, H.J. Curran, A hierarchical and comparative kinetic modeling study of $C_1 - C_2$ hydrocarbon and oxygenated fuels, *Int. J. Chem. Kinet.* 45 (2013) 638-675.
- [4] S.S. Nagaraja, J. Liang, S. Dong, S. Panigrahy, A. Sahu, G. Kukkadapu, S.W. Wagnon, W.J. Pitz, H.J. Curran, A hierarchical single-pulse shock tube pyrolysis study of $C_2 - C_6$ 1-alkenes, *Combust. Flame* 219 (2020) 456-466.
- [5] M. Baigmohammadi, V. Patel, S. Martinez, S. Panigrahy, A. Ramalingam, U. Burke, K.P. Somers, K.A. Heufer, A. Pekalski, H.J. Curran, A comprehensive experimental and simulation study of ignition delay time characteristics of single fuel $C_1 - C_2$ hydrocarbons over a wide range of temperatures, pressures, equivalence ratios, and dilutions, *Energy Fuels* 34(3) (2020) 3755-3771.
- [6] M. Baigmohammadi, V. Patel, S. Nagaraja, A. Ramalingam, S. Martinez, S. Panigrahy, A. A.E. Mohamed, K.P. Somers, U. Burke, K.A. Heufer, A. Pekalski, H.J. Curran, Comprehensive experimental and simulation study of the ignition delay time characteristics of binary blended methane, ethane, and ethylene over a wide range of temperature, pressure, equivalence ratio, and dilution, *Energy Fuels* 34(7) (2020) 8808-8823.
- [7] M.M. Kopp, N.S. Donato, E.L. Petersen, W.K. Metcalfe, S.M. Burke, H.J. Curran, Oxidation of ethylene-air mixtures at elevated pressures, part 1: Experimental results, *J. Propuls. Power* 30 (2014) 790-798.
- [8] M.M. Kopp, E.L. Petersen, W.K. Metcalfe, S.M. Burke, H.J. Curran, Oxidation of ethylene-air mixtures at elevated pressures, part 2: Chemical kinetics, *J. Propuls. Power* 30 (2014) 799-811.
- [9] C.J. Aul, W.K. Metcalfe, S.M. Burke, H.J. Curran, E.L. Petersen, Ignition and kinetic modeling of methane and ethane fuel blends with oxygen: A design of experiments approach, *Combust. Flame* 160 (2013) 1153-1167.
- [10] S.M. Gallagher, H.J. Curran, W.K. Metcalfe, D. Healy, J.M. Simmie, G. Bourque, A rapid compression machine study of the oxidation of propane in the negative temperature coefficient regime, *Combust. Flame* 153 (2008) 316-333.
- [11] I.G. Zsély, T. Nagy, J.M. Simmie, H.J. Curran, Reduction of a detailed kinetic model for the ignition of methane/propane mixtures at gas turbine conditions using simulation error minimization methods, *Combust. Flame* 158 (2011) 1469-1479.
- [12] A. Burcat, R.W. Crossley, K. Scheller, Shock tube investigation of ignition in ethane-oxygen-argon mixtures, *Combust. Flame* 18 (1972) 115-123.
- [13] H. Hashemi, J.G. Jacobsen, C.T. Rasmussen, J.M. Christensen, P. Glarborg, S. Gersen, M. van Essen, H.B. Levinsky, S.J. Klippenstein, High-pressure oxidation of ethane, *Combust. Flame* 182 (2017) 150-166.
- [14] S. Gersen, A.V. Mokhov, J.H. Darneveil, H.B. Levinsky, P. Glarborg, Ignition-promoting effect of NO_2 on methane, ethane and methane/ethane mixtures in a rapid compression machine, *Proc. Combust. Inst.* 33 (2011) 433-440.
- [15] P. Dagaut, J.-C. Boettner, M. Cathonnet, Ethylene pyrolysis and oxidation: A kinetic modeling study, *Int. J. Chem. Kinet.* 22 (1990) 641-664.

- [16] P. Dagaut, M. Cathonnet, J.-C. Boettner, F. Gaillard, Kinetic modeling of propane oxidation, *Combust. Sci. Technol.* 56 (1987) 23-63.
- [17] P. Dagaut, M. Cathonnet, J.-C. Boettner, Kinetics of ethane oxidation, *Int. J. Chem. Kinet.* 23 (1991) 437-455.
- [18] W Lowry, J de Vries, M Krejci, E Petersen, Z Serinyel, W Metcalfe, H Curran, G. Bourque, Laminar flame speed measurements and modeling of pure alkanes and alkane blends at elevated pressures, *ASME. J. Eng. Gas Turbines Power.* 133(9) (2011) 091501. <https://doi.org/10.1115/1.4002809>.
- [19] C.J. Brown, G.O. Thomas, Experimental studies of shock-induced ignition and transition to detonation in ethylene and propane mixtures, *Combust. Flame* 117(4) (1999) 861-870.
- [20] D. Davidson, W. Ren, R. Hanson, Experimental database for development of a HiFiRE JP-7 surrogate fuel mechanism, 50th AIAA Aerospace Sciences Meeting including the New Horizons Forum and Aerospace Exposition, (2012).
- [21] O.G. Penyazkov, K.L. Sevrouk, V. Tangirala, N. Joshi, High-pressure ethylene oxidation behind reflected shock waves, *Proc. Combust. Inst.* 32 (2009) 2421-2428.
- [22] S. Saxena, M.S.P. Kahandawala, S.S. Sidhu, A shock tube study of ignition delay in the combustion of ethylene, *Combust. Flame* 158 (2011) 1019-1031.
- [23] A. Burcat, K. Scheller, and A. Lifshitz, Shock-tube investigation of comparative ignition delay times for C₁ – C₅ alkanes, *Combust. Flame* 16 (1971) 29-33 (1971).
- [24] J. de Vries, J.M. Hall, S.L. Simmons, M.J.A. Rickard, D.M. Kalitan, E.L. Petersen, Ethane ignition and oxidation behind reflected shock waves, *Combust. Flame* 150 (2007) 137-150.
- [25] Y. Hidaka, K. Sato, H. Hoshikawa, T. Nishimori, R. Takahashi, H. Tanaka, K. Inami, N. Ito, Shock-tube and modeling study of ethane pyrolysis and oxidation, *Combust. Flame* 120 (2000) 245-264.
- [26] A.G. McLain, C.J. Jachimowski, Chemical kinetic modeling of propane oxidation behind shock waves, National Aeronautics and Space Administration, (1977).
- [27] P. Cadman, G.O. Thomas, P. Butler, The auto-ignition of propane at intermediate temperatures and high pressures, *Phys. Chem. Chem. Phys.* 2(23) (2000) 5411-5419.
- [28] Z. Qin, V.V. Lissianski, H. Yang, W.C. Gardiner, S.G. Davis, H. Wang, Combustion chemistry of propane: a case study of detailed reaction mechanism optimization, *Proc. Combust. Inst.* 28 (2000) 1663-1669.
- [29] K.G. Yeong, S.G. Su, Shock tube and modeling study of the ignition of propane, *Bull. Korean Chem. Soc* 22(3) (2001) 303-307.
- [30] J. Herzler, L. Jerig, P. Roth, Shock-tube study of the ignition of propane at intermediate temperatures and high pressures, *Combust. Sci. Technol.* 176 (2004) 1627-1637.
- [31] E. Hu, Z. Zhang, L. Pan, J. Zhang, Z. Huang, Experimental and modeling study on ignition delay times of dimethyl ether/propane/oxygen/argon mixtures at 20 bar, *Energy Fuels* 27 (2013) 4007-4013.

- [32] C. Lee, S. Vranckx, K.A. Heufer, S.V. Khomik, Y. Uygun, H. Olivier, On the chemical kinetics of ethanol oxidation: shock tube, rapid compression machine and detailed modeling study, *Z. für Phys. Chem.* 226(1) (2012) 1-28.
- [33] A. Ramalingam, K. Zhang, A. Dhongde, L. Virnich, H. Sankhla, H. Curran, A. Heufer, An RCM experimental and modeling study on CH₄ and CH₄/C₂H₆ oxidation at pressures up to 160 bar, *Fuel* 206 (2017) 325-333.
- [34] L. Brett, J. Macnamara, P. Musch, J.M. Simmie, Brief communication: simulation of methane autoignition in a rapid compression machine with creviced pistons, *Combust. Flame* 124 (2001) 326-329.
- [35] E.L. Petersen, M. Röhrig, D.F. Davidson, R.K. Hanson, C.T. Bowman, High-pressure methane oxidation behind reflected shock waves, *Symp. (Int.) Combust* 26 (1996) 799-806.
- [36] P.J. Ross, *Taguchi techniques for quality engineering*, New York, 1988.
- [37] S.M. Burke, U. Burke, R. Mc Donagh, O. Mathieu, I. Osorio, C. Keesee, A. Morones, E.L. Petersen, W. Wang, T.A. DeVerter, M.A. Oehlschlaeger, B. Rhodes, R.K. Hanson, D.F. Davidson, B.W. Weber, C.J. Sung, J. Santner, Y. Ju, F.M. Haas, F.L. Dryer, E.N. Volkov, E.J.K. Nilsson, A.A. Konnov, M. Alrefae, F. Khaled, A. Farooq, P. Dirrenberger, P.A. Glaude, F. Battin-Leclerc, H.J. Curran, An experimental and modeling study of propene oxidation. Part 2: Ignition delay time and flame speed measurements, *Combust. Flame* 162 (2015) 296-314.
- [38] S.M. Burke, W. Metcalfe, O. Herbinet, F. Battin-Leclerc, F.M. Haas, J. Santner, F.L. Dryer, H.J. Curran, An experimental and modeling study of propene oxidation. Part 1: speciation measurements in jet-stirred and flow reactors, *Combust. Flame* 161 (2014) 2765-2784.
- [39] U. Burke, K.P. Somers, P. O'Toole, C.M. Zinner, N. Marquet, G. Bourque, E.L. Petersen, W.K. Metcalfe, Z. Serinyel, H.J. Curran, An ignition delay and kinetic modeling study of methane, dimethyl ether, and their mixtures at high pressures, *Combust. Flame* 162 (2015) 315-330.
- [40] D. Healy, H.J. Curran, S. Dooley, J.M. Simmie, D.M. Kalitan, E.L. Petersen, G. Bourque, Methane/propane mixture oxidation at high pressures and at high, intermediate and low temperatures, *Combust. Flame* 155 (2008) 451-461.
- [41] D. Healy, H.J. Curran, J.M. Simmie, D.M. Kalitan, C.M. Zinner, A.B. Barrett, E.L. Petersen, G. Bourque, Methane/ethane/propane mixture oxidation at high pressures and at high, intermediate and low temperatures, *Combust. Flame* 155 (2008) 441-448.
- [42] D. Healy, D.M. Kalitan, C.J. Aul, E.L. Petersen, G. Bourque, H.J. Curran, Oxidation of C₁ – C₅ alkane quinary natural gas mixtures at high pressures, *Energy Fuels* 24 (2010) 1521-1528.
- [43] A. Mohamed, S. Panigrahy, A. Sahu, G. Bourque, H.J. Curran, An experimental and modeling study of the auto-ignition of natural gas blends containing C₁ – C₇ n-alkanes, *Proc. Combust. Inst.* 38 (2021) 365-373.
- [44] S. Nagaraja, J. Power, G. Kukkadapu, S. Dong, S.W. Wangon, W.J. Pitz, H.J. Curran, A single pulse shock tube study of pentene isomer pyrolysis, *Proc. Combust. Inst.* 38 (2021) 881-889.
- [45] S. Panigrahy, J. Liang, S. Nagaraja, Z. Zuo, G. Kim, T. MacDougall, S.S. Vasu, H.J. Curran, A comprehensive experimental and improved kinetic modeling study on the pyrolysis and oxidation of propyne, *Proc. Combust. Inst.* 38 (2021) 479-488.

- [46] S. Dong, K. Zhang, P.K. Senecal, G. Kukkadapu, S.W. Wagnon, S. Barrett, N. Lokachari, S. Panigrahy, W.J. Pitz, H.J. Curran, A comparative reactivity study of 1-alkene fuels from ethylene to 1-heptene, *Proc. Combust. Inst.* 38 (2021) 611-619.
- [47] A. Ramalingam, S. Panigrahy, Y. Fenard, H. Curran, K.A. Heufer, A chemical kinetic perspective on the low-temperature oxidation of propane/propene mixtures through experiments and kinetic analyses, *Combust. Flame* 223 (2021) 361-375.
- [48] Y. Sun, C.-W. Zhou, K.P. Somers, H.J. Curran, An ab initio/transition state theory study of the reactions of C₅H₉ species of relevance to 1,3-pentadiene, part I: potential energy surfaces, thermochemistry and high-pressure limiting rate constants, *J. Phys. Chem. A* 123 (2019) 9019-9052.
- [49] Y. Sun, C.-W. Zhou, K.P. Somers, H.J. Curran, An ab initio/transition state theory study of the reactions of C₅H₉ species of relevance to 1,3-pentadiene, part II: pressure dependent rate constants and implications for combustion modelling, *J. Phys. Chem. A* 124 (2020) 4605-4631.
- [50] J. Power, K.P. Somers, C.-W. Zhou, S. Peukert, H.J. Curran, A theoretical, experimental and modeling study of the reaction of hydrogen atoms with 1- and 2-Pentene, *J. Phys. Chem. A* 123 (2019) 8506-8526.
- [51] N. Lokachari, S. Panigrahy, G. Kukkadapu, G. Kim, S.S. Vasu, W.J. Pitz, H.J. Curran, The influence of iso-butene kinetics on the reactivity of di-isobutylene and iso-octane, *Combust. Flame* 222 (2020) 186-195.
- [52] C.W. Zhou, Y. Li, U. Burke, C. Banyon, K.P. Somers, S. Ding, S. Khan, J.W. Hargis, T. Sikes, O. Mathieu, E.L. Petersen, M. AlAbbad, A. Farooq, Y. Pan, Y. Zhang, Z. Huang, J. Lopez, Z. Loparo, S.S. Vasu, H.J. Curran, An experimental and chemical kinetic modeling study of 1,3-butadiene combustion: Ignition delay time and laminar flame speed measurements, *Combust. Flame* 197 (2018) 423-438.
- [53] D.G. Goodwin, R.L. Speth, H.K. Moffat, B.W. Weber, Cantera: An object-oriented software toolkit for chemical kinetics, thermodynamics, and transport processes. <https://www.cantera.org>, (2018). Version 2.4.0. doi:10.5281/zenodo.170284.
- [54] Reaction-Design, CHEMKIN-PRO 18.2, San Diego, (2013).
- [55] S. Chih-Jen, H.J. Curran, Using rapid compression machines for chemical kinetics studies, *Prog. Energy Combust. Sci.* 44 (2014) 1-18.
- [56] S. S. Goldsborough, S. Hochgreb, G. Vanhove, M. S. Wooldridge, H. J. Curran, S. Chih-Jen, Advances in rapid compression machine studies of low- and intermediate-temperature autoignition phenomena, *Prog. Energy Combust. Sci.* 63 (2017) 1-78.
- [57] V. Gururajan, F.N. Egolfopoulos, Direct sensitivity analysis for ignition delay times, *Combust. Flame* 209 (2019) 478-480.
- [58] X. Li, A.W. Jasper, J. Zádor, J.A. Miller, S.J. Klippenstein, Theoretical kinetics of $\ddot{O} + C_2H_4$, *Proc. Combust. Inst.* 36 (2017) 219-227.
- [59] D.L. Baulch, C.T. Bowman, C.J. Cobos, R.A. Cox, Th. Just, J.A. Kerr, M.J. Pilling, D. Stocker, J. Troe, W. Tsang, R.W. Walker, J. Warnatz, Evaluated kinetic data for combustion modeling: supplement II, *J. Phys. Chem. Vol.* 34 (2005).

- [60] H.P. Upadhyaya, A. Kumar, P.D. Naik, A.V. Sapre, Discharge flow reaction kinetic studies of $O(^3P)$ with chloroethylenes CH_2CCl_2 , $CHClCCl_2$, CCl_2CCl_2 , Chem. Phys. Lett. 321 (2000) 411-418.
- [61] S.Y. Lee, H.S. Yoo, W.K. Kang, K.H. Jung, Reaction of $O(^3P)$ atoms with $CF_2 = CXY$ (X, Y = H, F, Cl, Br). Discharge flow-chemiluminescence imaging technique, Chem. Phys. Lett. 257 (1996) 415-420.
- [62] S.E. Paulson, J.J. Orlando, G.S. Tyndall, J.G. Calvert, Rate coefficients for the reactions of $O(^3P)$ with selected biogenic hydrocarbons, Int. J. Chem. Kinet. Vol. 27 (1995) 997-1008.
- [63] V.D. Knyazev, V.S. Arutyunov, V.I. Vedeneev, The mechanism of $O(^3P)$ atom reaction with ethylene and other simple olefins, Int. J. Chem. Kinet. Vol. 24 (1992) 545-561.
- [64] O. Horie, R. Taege, B. Reimann, N.L. Arthur, P. Potzinger, Kinetics and mechanism of the reactions of $O(^3P)$ with SiH_4 , CH_3SiH_3 , $(CH_3)_2SiH_2$, and $(CH_3)_3SiH$, J. Phys. Chem. 95(11) (1991) 4393-4400.
- [65] V. Fonderie, D. Maes, J. Peeters, The kinetic coefficient of the $C_2H_4 + \dot{O}$ reaction over extended pressure and temperature ranges, Physico-Chemical Behaviour of Atmospheric Pollutants, Springer, Dordrecht (1984) 274-282.
- [66] R.B. Klemm, J.W. Sutherland, M.A. Wickramaaratchi, G. Yarwood, Flash photolysis-shock tube kinetic study of the reaction of atomic oxygen (3P) with ethylene: $1052\text{ K} \leq T \leq 2284\text{ K}$, J. Phys. Chem. 94(8) (1990) 3354-3357.
- [67] K. Mahmud, P. Marshall, A. Fontijn, A high-temperature photochemistry kinetics study of the reaction of oxygen (3P) atoms with ethylene from 290 to 1510 K, J. Phys. Chem. 91(6) (1987) 1568-1573.
- [68] T.L. Nguyen, L. Vereecken, X.J. Hou, M.T. Nguyen, J. Peeters, Potential energy surfaces, product distributions and thermal rate coefficients of the reaction of $O(^3P)$ with C_2H_4 (XAg): a comprehensive theoretical study, J. Phys. Chem. A 109(33) (2005) 7489-7499.
- [69] L.N. Krasnoperov, J.V. Michael, Shock tube studies using a novel multipass absorption Cell: Rate constant results for $\dot{O}H + H_2$ and $\dot{O}H + C_2H_6$, J. Phys. Chem. A 108 (2004) 5643-5648.
- [70] R. Sivaramakrishnan, J.V. Michael, B. Ruscic, High-temperature rate constants for $H/D + C_2H_6$ and C_3H_8 , Int. J. Chem. Kinet. 44(3) (2012) 194-205.
- [71] R. Sivaramakrishnan, C.F. Goldsmith, S. Peukert, J.V. Michael, Direct measurements of channel specific rate constants in $\dot{O}H + C_3H_8$ illuminates prompt dissociations of propyl radicals, Proc. Combust. Inst. 37 (2019) 231-238.
- [72] A.T. Droege, F.P. Tully, Hydrogen-atom abstraction from alkanes by hydroxyl. 3. Propane, J. Phys. Chem. 90 (1986) 1949-1954.
- [73] A.W. Jasper, S.J. Klippenstein, L.B. Harding, Theoretical rate coefficients for the reaction of methyl radical with hydroperoxyl radical and for methylhydroperoxide decomposition, Proc. Combust. Inst. 32 (2009) 279-286.
- [74] R. Zhu, C. Lin, The $\dot{C}H_3 + \dot{H}O_2$ reaction: First-principles prediction of its rate constant and product branching probabilities, J. Phys. Chem. A 105 (2001) 6243-6248.
- [75] Z. Hong, D.F. Davidson, K.-Y. Lam, R.K. Hanson, A shock tube study of the rate constants of $\dot{H}O_2$ and $\dot{C}H_3$ reactions, Combust. Flame 159 (2012) 3007.

- [76] S.J. Klippenstein, From Theoretical reaction dynamics to chemical modeling of combustion, *Proc. Combust. Inst.* 36 (2017) 77-111.
- [77] J. Zádor, R.X. Fernandes, Y. Georgievskii, G. Meloni, C.A. Taatjes, J.A. Miller, The reaction of hydroxyethyl radicals with O₂: a theoretical analysis and experimental product study, *Proc. Combust. Inst.* 32 (2009) 271-277.
- [78] J. Zador, S.J. Klippenstein, J.A. Miller, Pressure-dependent $\dot{O}H$ yields in alkene+HO₂ reactions: a theoretical study, *J. Phys. Chem. A* 115 (2011) 10218-10225.
- [79] M.S. Stark, D.J. Waddington, Oxidation of propene in the gas phase, *Int. J. Chem. Kinet.* 27(2) (1995) 123-151.

Chapter 6: Comprehensive experimental and simulation study of the ignition delay time characteristics of binary blended methane, ethane, and ethylene over a wide range of temperature, pressure, equivalence ratio, and dilution

Published in: Energy and Fuels, Volume 34, Issue 7, July 2020, Pages 8808–8823.
DOI : <https://doi.org/10.1021/acs.energyfuels.0c00960>

Author Contributions

- 1) Mohammadreza Baigmohammadi (National University of Ireland, Galway, Ireland)
Contribution: High pressure shock tube experiments and manuscript preparation.
- 2) Vaibhav Patel (National University of Ireland, Galway, Ireland)
Contribution: RCM experiments
- 3) Shashank S. Nagaraja (National University of Ireland, Galway, Ireland)
Contribution: Low pressure shock tube experiments.
- 4) Ajoy Ramalingam (PCFC, RWTH Aachen, Germany)
Contribution: RCM experiments.
- 5) Sergio Martinez (National University of Ireland, Galway, Ireland)
Contribution: Performed calculations, and chemical kinetic modelling.
- 6) Snehasish Panigrahy (National University of Ireland, Galway, Ireland)
Contribution: Chemical kinetic modelling.
- 7) Ahmed Abd El-Sabor Mohamed (National University of Ireland, Galway, Ireland)
Contribution: RCM experiments.
- 8) Kieran P. Somers (National University of Ireland, Galway, Ireland)
Contribution: Chemical kinetic modelling.
- 9) Ultan Burke (National University of Ireland, Galway, Ireland)
Contribution: Chemical kinetic modelling.
- 10) Karl A. Heufer (PCFC, RWTH Aachen, Germany)
Contribution: Project management and manuscript review.
- 11) Andrzej Pekalski (Shell research limited, Shell Centre London)
Contribution: Project management as industrial sponsor and manuscript review.

12) Henry J. Curran (National University of Ireland, Galway, Ireland)

Contribution: Managed the project, made technical contributions and reviewed the project and manuscript throughout.

Abstract

A comprehensive experimental and kinetic modelling study of the ignition delay time (IDT) characteristics of some binary blends of $C_1 - C_2$ gaseous hydrocarbons such as methane/ethylene, methane/ethane, and ethane/ethylene was performed over a wide range of composition (90/10, 70/30, 50/50), temperature ($\sim 800 - 2000$ K), pressure ($\sim 1 - 40$ bar), equivalence ratio ($\sim 0.5 - 2.0$), and dilution ($\sim 75 - 90\%$). An extensive literature review was conducted, and available data were extracted to create a comprehensive database for our simulations. Based on existing literature data, an experimental matrix was designed using the Taguchi approach (L_9) in order to identify and complete the experimental matrix required to generate a comprehensive experimental IDT set necessary for the validation of a chemical kinetic model. The required high- and low-temperature IDTs were collected using low-/high-pressure shock tubes and rapid compression machines, respectively. The predictions of NUIGMech1.0 are examined versus all of the available experimental data, including those taken in the current study using the IDT simulations and a correlation technique. Moreover, the individual effect of the studied parameters, including mixture composition, pressure, equivalence ratio, and dilution on IDT, is investigated over the studied temperature range. Correlations that were developed based on NUIGMech1.0 are presented for each specific blended fuel over the conditions studied. These correlations show an acceptable performance versus the experimental data.

6.1 Introduction

Explaining the pyrolysis and/or oxidation processes of heavy and complex hydrocarbon fuels depends on the development of high-fidelity chemical mechanisms. In this regard, understanding the pyrolysis and/or oxidation processes of small ($C_1 - C_2$) hydrocarbons are important because of their crucial role in kinetic behavior at the end-chain of the pyrolysis and/or oxidation processes of larger hydrocarbons. Therefore, developing a high-fidelity chemical mechanism that can precisely explain the pyrolysis and/or oxidation processes of small hydrocarbons is very desirable in terms of explaining conditions relevant to industrial burners, gas turbines, and internal combustion engines. Ignition delay time (IDT) is a criterion extensively used to validate chemical mechanisms, and it is often used for comparing various chemical mechanisms and developing new ones. To do so, a comprehensive IDT database is required as a prerequisite so that mechanisms can be tested and

validated. Therefore, an extensive literature review was performed, and available IDTs for binary fuel mixtures of methane/ethylene [1], methane/ethane [2-11], and ethane/ethylene were extracted and stored, as shown in Fig. 6-1. It can be seen that, although there is sufficient IDT data in the literature for methane/ethane (alkane–alkane) mixtures, there is no comprehensive data for alkane/alkene mixtures including methane/ethylene and ethane/ethylene over a wide range of pressures, temperatures, equivalence ratios, and dilutions (squares in Fig. 6-1). Therefore, new experimental tests were defined for targeted binary fuel mixtures (alkane/alkene) + O₂ + N₂ + Ar (spheres in Fig. 6-1) to encapsulate a wide range of temperature, pressure, equivalence ratio, alkane ratio, and dilution.

It is believed that conducting the required experiments over the compressed pressure range of ~1 – 40 bar and also the compressed temperature range of ~800 – 2000 K from fuel-lean to fuel-rich conditions, at different levels of dilution, and with different alkene concentrations may disclose data which could not be interpreted from the available literature. Thus, we aim to present a comprehensive chemical mechanism that can precisely reproduce the experimental IDTs of various binary fuel C₁ – C₂ mixtures over a wide range of operating conditions. In the present study, the Taguchi design of experiments (DOE) method was applied to optimize the number of required experiments.

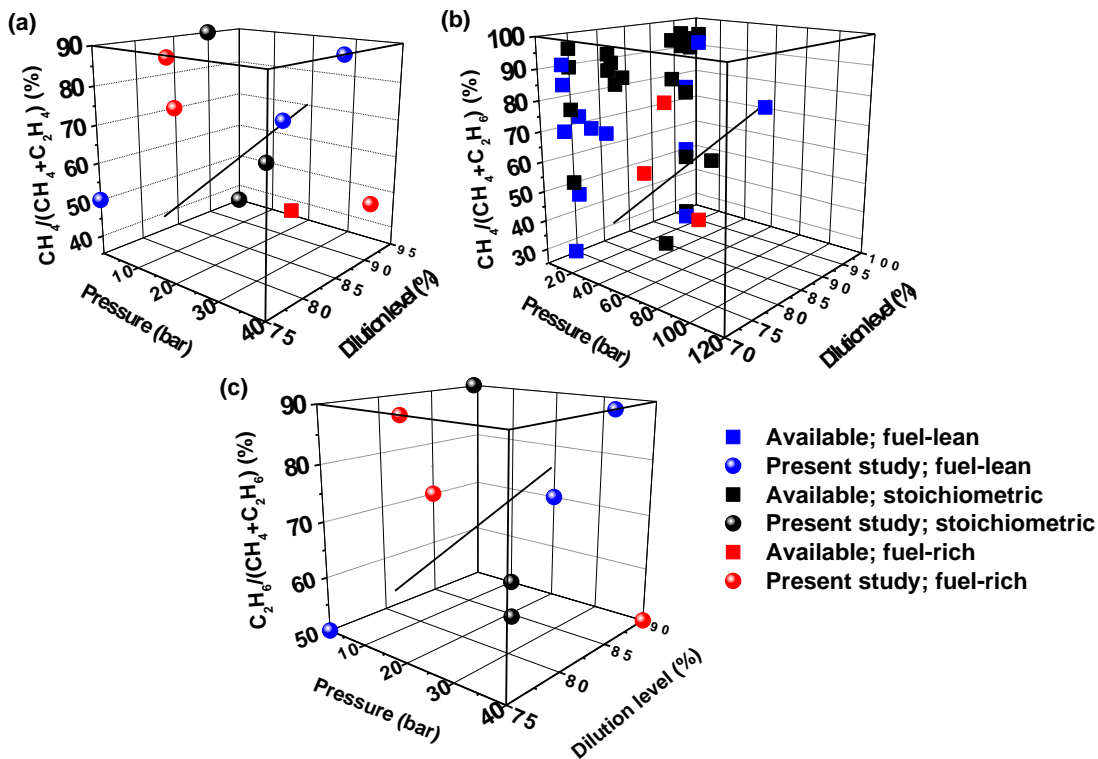


Figure 6-1. Extracted data from the studied literature (squares); new experimental tests defined in the current study (spheres); blue spheres/squares: fuel-lean mixtures; black spheres/squares: stoichiometric mixtures; red spheres/squares: fuel-rich mixtures.

6.2 Design of experiments and experimental approach

The experiments were designed using an L_9 Taguchi matrix [12] for four parameters of ethylene concentration, pressure, equivalence ratio, and dilution. This approach is analogous to previous work by Baigmohammadi et al. [13], and details can be found there. In this current study, alkanes (methane and ethane) are the abundant components, so that the presence of the alkene (ethylene) in a mixture is varied from 10 to 50%. Also, the concentrations of diluents (N_2 and Ar) are varied from 75 to 90% of the reactive mixtures. Three equivalence ratios, 0.5, 1.0, and 2.0, and three compressed mixture pressures (p_5 , p_C), namely, 1, 20, and 40 bar, were selected to cover the proposed cubes presented in Figs. 6-1(a) and (c). Besides, the temperature (T_5 , T_C) range was varied from ~ 800 – 2000 K based on the defined cases and the viability of the applied instruments in measuring IDTs with acceptable accuracy.

The IDTs of the defined mixtures and conditions presented in Table 6-1 were measured using low-/high-pressure shock tubes (L/HPST) and rapid compression machines (RCMs) all at NUI Galway in the low- and high-temperature regimes, respectively. However, some low-temperature IDTs (RCM; P8C3,4,8 in Table 6-1) were measured in collaboration with the Physico-Chemical Fundamentals of Combustion (PCFC) group of RWTH Aachen University to increase the fidelity of the database and to ensure that they are facility independent. The physical performance of the facilities are well known and have been extensively discussed previously [5, 10, 11, 14-19]. However, a summary of the facilities' characteristics and exemplary pressure traces are provided in Appendix C (Sections 2–6).

As seen in Fig. 6-1(b), sufficient available IDT data exists in the literature for methane/ethane mixtures precluding the need for more experiments. As presented in Table 6-1, a unique code has been assigned to each experiment. It should be noted that the presented data in this paper is a part of a larger project (3 of 12; phases (P): 5, 6, and 8) such that for better handling of the data, we have been using a common description for the applied mixtures and conditions throughout the papers. In this regard, "Px" refers to the fuel blends, which is "P5: methane/ethylene", "P6: methane/ethane", and "P8: ethane/ethylene", respectively. Also, the "C" notation refers to the studied conditions, which change from 1 to 9 in accordance with changes in fuel composition, pressure, equivalence ratio, and dilution.

6.2.1 Set-up and procedure

The current study is categorized into six different stages; 1: an extensive literature review; 2: database development; 3: simulating the available literature data using NUIGMech1.0; 4: defining new experimental tests using an L9 Taguchi matrix; 5: conducting the RCM and L/HPST experiments; 6: modelling the new experimental results with NUIGMech1.0. To make the study more concise, comprehensive Supplementary material files are provided in Appendix C. The Supplementary material includes non-reactive RCM traces, the original spreadsheets of the experimental tests, L/HPST oscilloscope traces, and the combined figures of reactive, non-reactive, and simulation pressure traces. Furthermore, all of the general information related to the applied gases (fuel/oxygen/argon/nitrogen), the applied facilities, and data acquisition systems to collect the IDTs are provided in Appendix C.

Table 6-1. Test conditions defined in the current study.

No	Code	Mixture composition (mole fraction)					ϕ	T (K)	p (bar)	Ref.
		CH ₄	C ₂ H ₄	C ₂ H ₆	O ₂	N ₂ +Ar				
1	P5C1	0.02083	0.02083	0	0.2083	0.75+0.0	0.5	1167–2024	1	
2	P5C2	0.02143	0.02143	0	0.1071	0.85	1.0	923–1546	20	
3	P5C3	0.0222	0.0222	0	0.0555	0.90	2.0	869–1745	40	<i>This study:</i> NUIG ST and RCM
4	P5C4	0.05303	0.02273	0	0.17424	0.75	1.0	845–1465	40	
5	P5C5	0.0488	0.0209	0	0.0802	0.75+0.10	2.0	1471–2022	1	
6	P5C6	0.0125	0.0054	0	0.082	0.90	0.5	995–1783	20	
7	P5C7	0.10976	0.0122	0	0.12805	0.75	2.0	947–1840	20	
8	P5C8	0.02596	0.00288	0	0.12115	0.85	0.5	921–1738	40	
9	P5C9	0.029	0.0032	0	0.0677	0.75+0.15	1.0	1570–2082	1	
10	P6C1	0.0015	0	0.0015	0.0017	0.0+0.98	0.5	1248–1571	1.46	
11	P6C2	0.0067	0	0.0067	0.0367	0.0+0.95	1.0	1190–1377	32.02	
12	P6C3	0.0316	0	0.0316	0.0868	0.0+0.85	2.0	1094–1366	15.44	Aul et al. [9]
13	P6C4	0.0091	0	0.0273	0.1136	0.0+0.85	1.0	1166–1266	31.42	
14	P6C5	0.0514	0	0.0171	0.0814	0.0+0.85	2.0	1143–1513	29.03	
15	P6C6	0.0228	0	0.0123	0.2015	0.7574+0.0	0.5	1091–1437	22.26	Petersen et al. [5]
16	P6C7	0.0419	0	0.0047	0.2003	0.7531+0.0	0.6	848–883	9.62	Beerer and McDonell [8]
17	P6C8	0.0801	0	0.0089	0.1913	0.7197+0.0	0.5	1155–1532	22.71	Petersen et al. [5]
		0.0766	0	0.0085	0.1830	0.7197+0.0	1.0	911–1221	40	Huang and Bushe [3]
18	P6C9	0.0012	0	0.0036	0.0152	0.3+0.432	1.0	909–1038	1.36	Gersen et al.[7]
19	P8C1	0	0.0167	0.0167	0.2167	0.0+0.98	1.0	1324–1700	1.36	Aul et al. [9]
20	P8C2	0	0.01765	0.01765	0.11471	0.75+0.0	0.5	1153–1862	1	<i>This study:</i> NUIG ST and RCM
21	P8C3	0	0.0190	0.0190	0.0619	0.85	1.0	901–1452	20	<i>This study:</i> NUIG (ST) & RWTH Aachen (RCM)
22	P8C4	0	0.01724	0.04023	0.19253	0.90	2.0	892–1540	40	<i>This study:</i> NUIG (ST)
							1.0	1106–1411	40	<i>This study:</i> RWTH Aachen (RCM)
							2.0	902–971	30	
23	P8C5	0	0.0168	0.0392	0.0939	0.75+0.10	2.0	1252–1870	1	<i>This study:</i> NUIG ST and RCM
24	P8C6	0	0.0039	0.0091	0.087	0.90	0.5	958–1503	20	
25	P8C7	0	0.0092	0.0826	0.1583	0.75	2.0	892–1520	20	
26	P8C8	0	0.0019	0.0171	0.1310	0.85	0.5	933–1446	40	<i>This study:</i> NUIG (ST) & RWTH Aachen (RCM)
27	P8C9	0	0.0022	0.0202	0.0775	0.75+0.15	1.0	1250–1930	1	<i>This study:</i>

6.2.2 Uncertainty analysis

To increase the fidelity of the results, a comprehensive uncertainty analysis was conducted using the data taken in both our L/HPST and RCM and is briefly discussed here. The uncertainty analysis was developed based on studies conducted by Petersen et al. [20] and Weber et al. [21]. In this regard, the average uncertainties in the compressed mixture temperatures (T_C or T_5) and measured IDTs in STs and RCM are summarized in Table 6-2. Details of this analysis are provided in Appendix C (Section 2).

Table 6-2. Average uncertainties for compressed mixture temperature (T_C or T_5) and measured IDTs.

Facility	$\sigma_{T_{c,5}}$ (K)	σ_{IDT} (%)
NUIG-L/HPST	$\pm 30/20$	± 25
NUIG-RCM	± 10	± 20
PCFC-RCM [10]	± 5	

According to the literature, [20,22,23][20, 22, 23] and also the conditions studied here, values of $\pm 30/20$ K (L/HPST), $\pm 5 - 15$ K (RCM), and $\pm 25\%$ (L/HPST) and 20% (RCM) are estimated as the average uncertainties for both the end of compression temperature (T_C) and the measured IDTs, respectively.

6.3 Computational modelling

Simulations were conducted using NUIGMech1.0 to simulate the experimental targets. This is a modified version of NUIGMech0.9 [13][13] for higher hydrocarbons up to C_7 and aromatics. In this regard, the experimental data were simulated using a Python script based on the CANTERA [24] library (ST simulations) and also CHEMKIN-Pro 18.2 [25] software (RCM simulations). As already comprehensively discussed in the literature [22, 23], although the simulations in the ST operating regimes are performed using the constant volume reactor model, the RCM simulations are performed using the effective volume approach by imposing a heat loss boundary condition on the calculations because of facility effects, including heat losses, during compression and in the post-compression zone of the reaction chamber [10, 14, 26].

6.4 Results and discussion

All experimental results related to the studied conditions in Table 6-1, whether taken from the literature or from the present study, are presented in the following figures in accordance to the applied fuels (methane/ethylene, methane/ethane, and ethane/ethylene) and the wide range of operating conditions examined.

6.4.1 General performance of the NUIG mechanism and the correlations versus experimental data
The performance of NUIGMech1.0 versus all experimental available IDT data is shown in Figs. 6-2 – 6-4. The symbols refer to the experimental data; however, the square symbols with a cross through them demonstrate experimental data affected by pre-ignition or facility effects. The solid black line refers to NUIGMech1.0 predictions.

Figures 6-2 – 6-4 show that NUIGMech1.0 predicts the methane/ethylene, methane/ethane, and ethane/ethylene binary fuel blend IDT measurements very well over the wide range of conditions studied (ϕ : 0.5 – 2.0, T : ~830 – 2100 K, p : 1 – 40 bar, 9 different compositions, and dilution: 75 – 90%). However, there is a deviation between the simulations and experimental data in Figs. 6-3(h) and 6-4(d). Figure 6-4(d) illustrates that the experimental data are affected by the facility's boundary conditions in the temperature range 900 – 1050 K at $p_C = 40$ bar. These data suffer from pre-ignition events that occur behind the reflected shock in the NUIG-HPST. This pre-ignition was observed even on cleaning the shock tube after each experiment. The same phenomenon occurred for the same mixture at 40 bar in the low-temperature regime in the PCFC-RCM. In both cases, pre-ignition appeared as a gradual increase in pressure before the main ignition, shortening the overall IDT. In the case of the RCM, some deposits have been observed on the reactor end wall, which may induce the pre-ignition. However, these deposits were only present for the 40 bar experiments so that they and related pre-ignitions were suppressed by reducing the compressed pressure to 30 bar. Similarly, it might be inferred that the experimental data presented in Fig. 6-3(h) (Fig. DS34) may suffer from a kind of pre-ignition (specifically in ref [9] because of the very short reported IDTs of < 3 ms) in the intermediate-to-low temperature regime in ref [7] and at 1000 – 1050 K in ref [9]. Comparing the conditions presented in Figs. 6-3(h) and 6-4(d), it is interesting to note that ethane is the common fuel component in the mixtures, and the common conditions are 40 bar and 75% dilution. Therefore, it may be concluded that this undesirable effect stems from the presence of ethane in the blends at 40 bar and at fuel/air conditions (~71 – 75% dilution). Although it is known that ethylene and ethane are

more reactive fuels compared to methane, the individual effect and portion of each studied parameter on the reactivity of the mixtures cannot be understood directly from Figs. 6-2 – 6-4 as too many parameters, for example, binary fuel combination, pressure, equivalence ratio, and dilution, are all changing at once. Thus, the individual and combined effects of the studied parameters on IDTs of the studied methane/ethylene and ethane/ethylene mixtures are considered below.

Furthermore, comprehensive comparisons of IDT, laminar burning velocities (LBVs), and speciation plots shown in Appendix D (Figs. DS26 – DS37 in Section 9) demonstrate that NUIGMech1.0 can not only accurately predict the experimental IDTs studied but also reasonably anticipate experimental LBVs and speciation data taken from the literature in comparison to the available chemical mechanisms (Table DS11).

6.4.2 Individual effect of the studied parameters on IDT

The general performance of NUIGMech1.0 and its fidelity in predicting the IDTs of the various C₁–C₂ binary fuel mixtures over the wide range of conditions studied has been demonstrated. In this section, the effects on IDTs of the studied parameters on the mixtures are discussed in detail, whereas the focus will be on the description of the individual parameters. To investigate the effect of each individual parameter on IDT, the P5C1 and P8C1 ($\phi = 0.5$, $p_C = 1$ bar, dilution = 75%) conditions are chosen as the base cases for each binary fuel combination (methane/ethylene and ethane/ethylene). For example, in studying the effect of equivalence ratio on ethylene IDT, we only perturb the equivalence ratio to 1.0 and 2.0 in the P5/8C1 cases, so that the other parameters remain unchanged. Namely, by perturbing the equivalence ratio from 1.0 to 2.0, the new cases are defined as ($\phi = 1.0$, $p_C = 1$ bar, dilution = 75%) and ($\phi = 2.0$, $p_C = 1$ bar, dilution = 75%), respectively. The same procedure is followed for the other parameters. Therefore, the effect of each parameter on IDT in the temperature range (800–2100 K) is calculated as follows:

$$IDT \text{ ratio} = \frac{IDT|_{\phi, p_C, dilution, PxCy}}{IDT|_{PxC1}} \quad (6-1)$$

where “x”, and “y” are “5, 8” and “2–9”, respectively. In the above equation, values larger than unity indicate a decrease in reactivity, whereas values smaller than unity show an increase in reactivity in comparison to the base cases. The individual effect of each parameter on methane/ethylene and ethane/ethylene IDTs are presented in Fig. 6-5. For better visualization, the y-axis in Fig. 6-5 is scaled in “log₂” so that 2⁻¹, 2⁰, and 2¹ refers to a decrease by a factor of 2, no change, and an increase by a

factor of 2 in the IDT ratio, respectively. It is seen that the individual effect of each parameter on IDT changes qualitatively and quantitatively over the temperature range studied. In this regard, the individual effect of the studied parameters such as the binary blend composition, pressure, equivalence ratio, and dilution on IDT predictions of methane/ethylene and ethane/ethylene mixtures are discussed in detail.

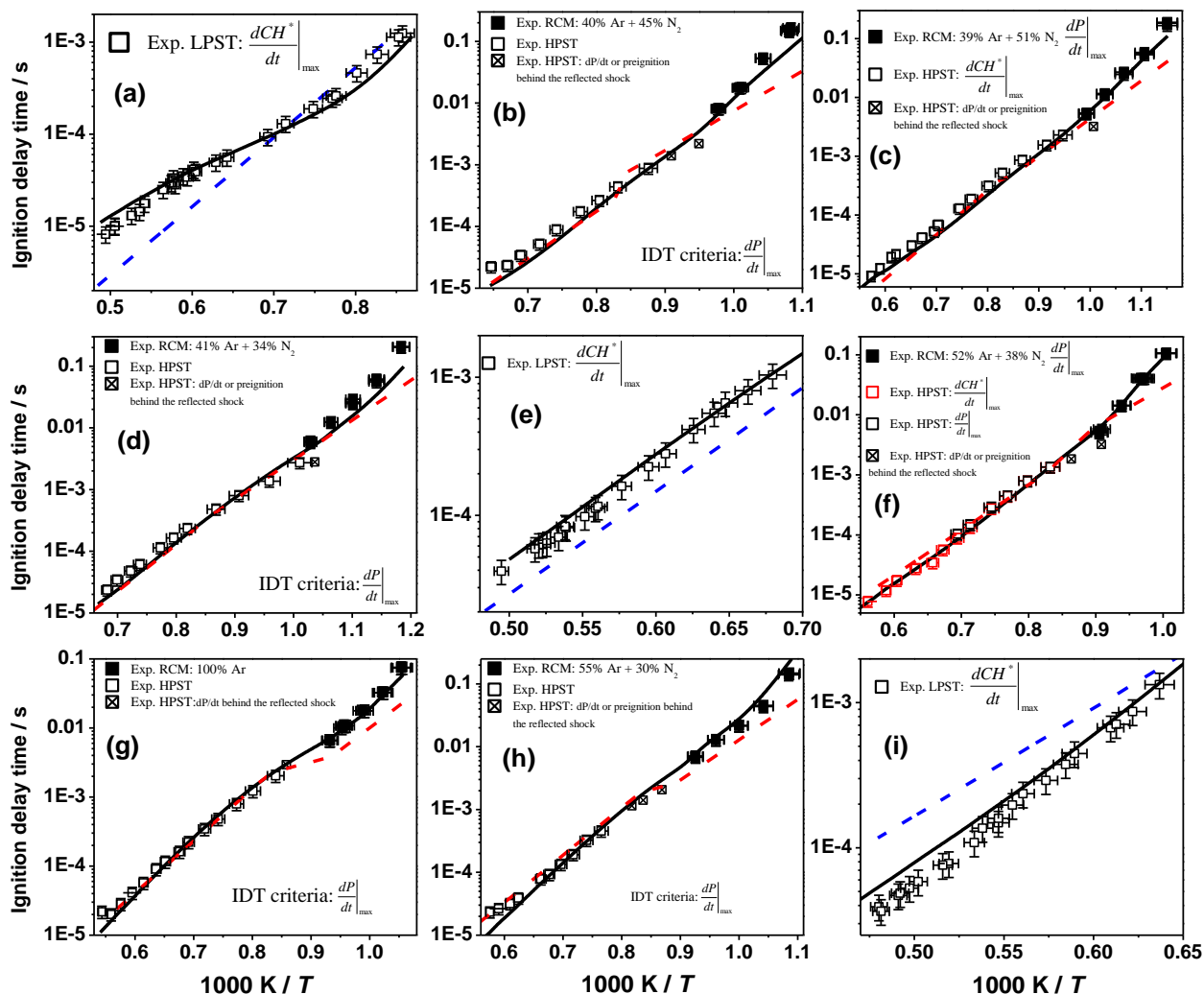


Figure 6-2. Experimental and simulation data of methane/ethylene's IDT values: (a) 2.08% CH₄, 2.08% C₂H₄, 20.83% O₂, ($\phi = 0.5$) in 75% N₂ at $p_c = 1$ bar, P5C1; (b) 2.143% CH₄, 2.143% C₂H₄, 10.71% O₂, ($\phi = 1.0$) in 75% N₂, 10% Ar, $p_c = 20$ bar, P5C2; (c) 2.22% CH₄, 2.22% C₂H₄, 5.55% O₂, ($\phi = 2.0$) in 75% N₂, 15% Ar, $p_c = 40$ bar, P5C3; (d) 5.303% CH₄, 2.273% C₂H₄, 17.424% O₂, ($\phi = 1.0$) in 75% N₂, $p_c = 40$ bar, P5C4; (e) 4.88% CH₄, 2.09% C₂H₄, 8.02% O₂, ($\phi = 2.0$) in 75% N₂, 10% Ar, $p_c = 1$ bar, P5C5; (f) 1.25% CH₄, 0.54% C₂H₄, 8.2% O₂ ($\phi = 0.5$) in 75% N₂, 15% Ar at $p_c = 20$ bar, P5C6; (g) 10.976% CH₄, 1.22% C₂H₄, 12.805% O₂, ($\phi = 2.0$) in 75% N₂, $p_c = 20$ bar, P5C7; (h) 2.596% CH₄, 0.288% C₂H₄, 12.115% O₂ ($\phi = 0.5$) in 75% N₂, 10% Ar at $p_c = 40$ bar, P5C8; (i) 2.9% CH₄, 0.32% C₂H₄, 6.77% O₂, ($\phi = 2.0$) in 75% N₂, 15% Ar, $p_c = 1$ bar, P5C9. (solid line: NUIGMech1.0, dashed-line: derived correlations (Section 6.4.3)).

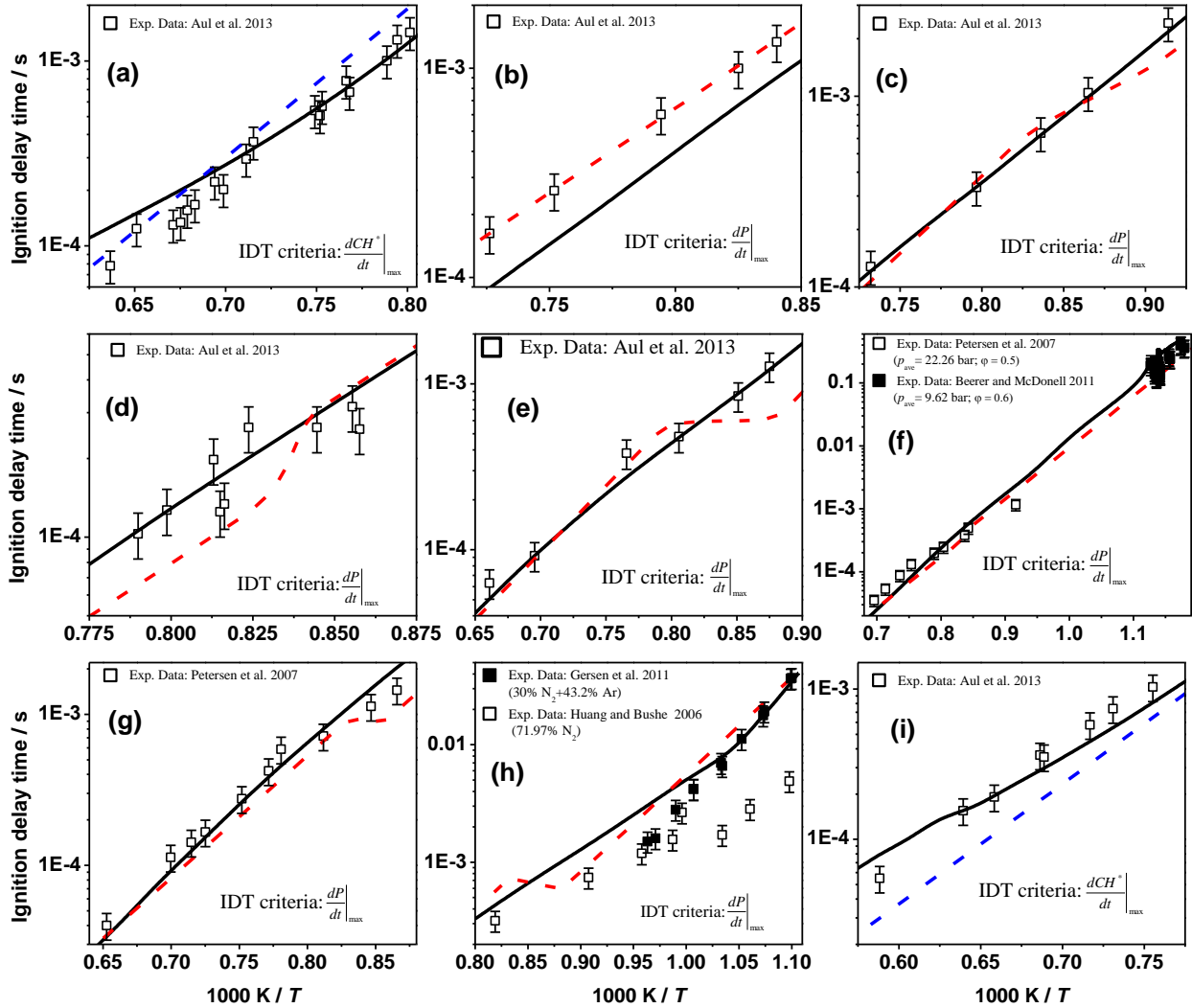


Figure 6-3. Available experimental and simulated data of methane/ethane's IDT values at: (a) 0.15% CH₄, 0.15% C₂H₆, 1.7% O₂, ($\varphi = 0.5$) in 98% Ar, $p_c = 1.46$ bar, P6C1; (b) 0.67% CH₄, 0.67% C₂H₆, 3.67% O₂, ($\varphi = 1.0$) in 95% Ar, $p_c = 32.02$ bar, P6C2; (c) 3.16% CH₄, 3.16% C₂H₆, 8.68% O₂, ($\varphi = 2.0$) in 85% Ar, $p_c = 15.44$ bar, P6C3; (d) 0.91% CH₄, 2.73% C₂H₆, 11.36% O₂, ($\varphi = 1.0$) and 85% Ar, $p_c = 31.42$ bar, P6C4; (e) 5.14% CH₄, 1.71% C₂H₆, 8.14% O₂, ($\varphi = 2.0$) in 85% Ar, $p_c = 29.03$ bar, P6C5; (f) 2.28% CH₄, 1.23% C₂H₆, 20.15% O₂, ($\varphi = 0.5$ [5] and 0.6 [8]) in 75.74% N₂, $p_c = 22.26$ bar [5] and 9.62 bar [8], P5C6; (g) 4.19% CH₄, 0.47% C₂H₆, 20.03% O₂, ($\varphi = 0.5$) in 75.31% N₂, $p_c = 22.71$ bar, P5C7; (h) 8.01% [3]/7.66% [7] CH₄, 0.89% [3]/0.85% [7] C₂H₆, 19.13% [3]/18.3% [7] O₂, ($\varphi = 1.0$) in 71.97% N₂ [3]/30% N₂+43.2% Ar [7], $p_c = 40$ bar; P6C8; (i) 0.12% CH₄, 0.36% C₂H₆, 1.52% O₂, ($\varphi = 1.0$) and 98% Ar, $p_c = 1.36$ bar, P6C9. (solid line: NUIGMech1.0, dashed line: derived correlations (Section 6.4.3)).

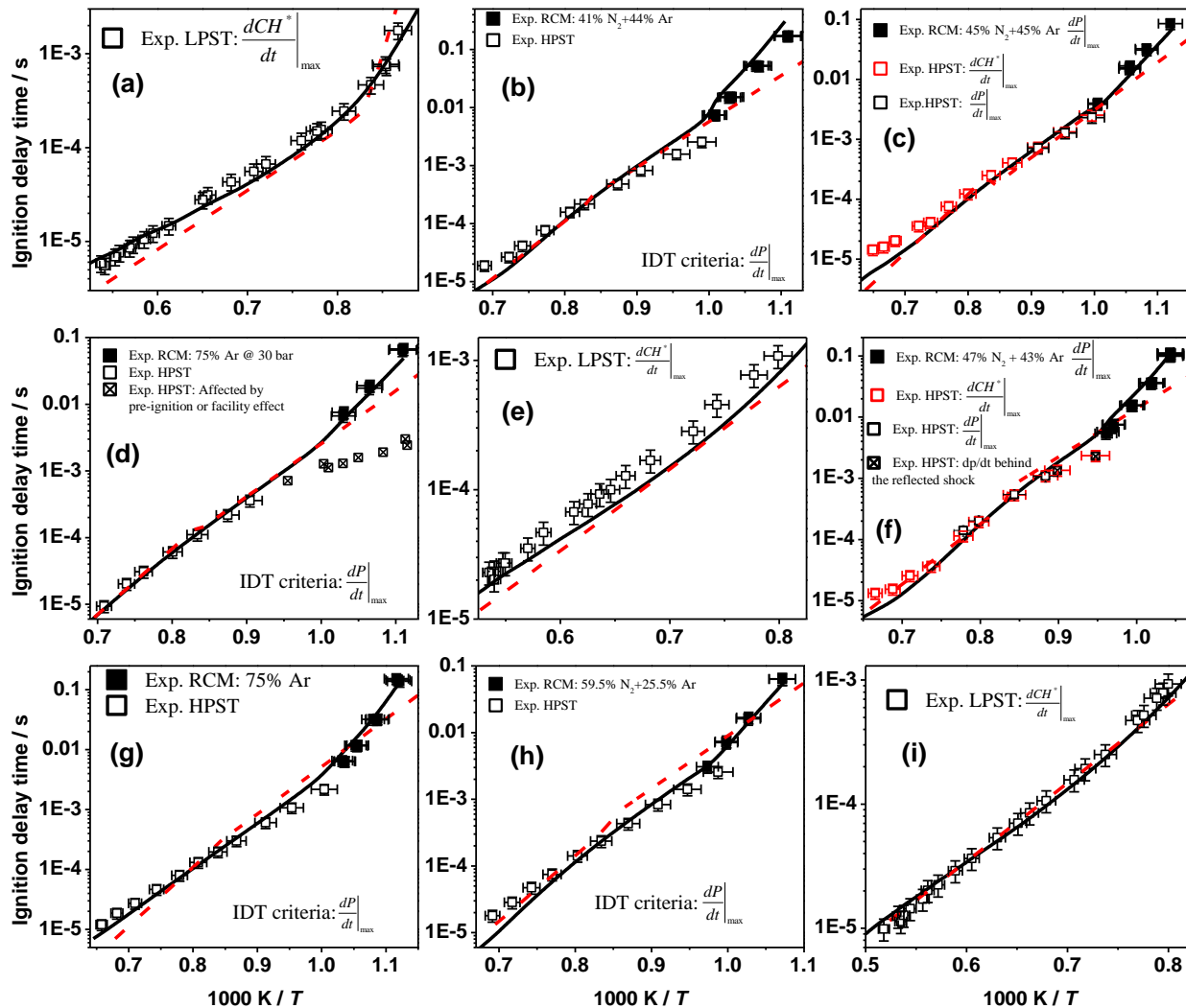


Figure 6-4. Experimental and simulation data for ethane/ethylene oxidation at: (a) 1.67% C₂H₆, 1.67% C₂H₄, 21.67% O₂ ($\phi = 0.5$), 75% N₂, $p_c = 1$ bar, P8C1; (b) 1.765% C₂H₆, 1.765% C₂H₄, 11.471% O₂ ($\phi = 1.0$), 75% N₂, 10% Ar, $p_c = 20$ bar, P8C2; (c) 1.9% C₂H₆, 1.9% C₂H₄, 6.19% O₂ ($\phi = 2.0$), 75% N₂, 15% Ar, $p_c = 40$ bar, P8C3; (d) 4.023% C₂H₆, 1.724% C₂H₄, 19.253% O₂ ($\phi = 1.0$), 75% N₂, $p_c = 40$ bar, P8C4; (e) 3.92% C₂H₆, 1.68% C₂H₄, 9.39% O₂ ($\phi = 2.0$), 75% N₂, 10% Ar, $p_c = 1$ bar, P8C5; (f) 0.91% C₂H₆, 0.39% C₂H₄, 8.7% O₂ ($\phi = 0.5$), 75% N₂, 15% Ar, $p_c = 20$ bar, P8C6; (g) 8.26% C₂H₆, 0.92% C₂H₄, 15.83% O₂ ($\phi = 2.0$), 75% N₂, $p_c = 20$ bar, P8C7; (h) 1.71% C₂H₆, 0.19% C₂H₄, 13.10% O₂ ($\phi = 0.5$), 75% N₂, 10% Ar, $p_c = 40$ bar, P8C8; (i) 2.02% C₂H₆, 0.22% C₂H₄, 7.75% O₂ ($\phi = 1.0$), 75% N₂, 15% Ar, $p_c = 1$ bar, P8C9. (solid line: NUIGMech1.0, dashed line: derived correlations (Section 6.4.3)).

6.4.2.1.1 Effect of binary blend compositions

As seen in Fig. 6-5(a), decreasing the ethylene concentration in the methane and the ethane blends have a significant semi-Gaussian distribution on decreasing reactivity, especially in the intermediate temperature regime (~ 1200 K). Specifically, decreasing the ethylene concentration in the methane/ethylene blend progressively from 50 to 30% and finally to 10% suppresses the average

mixture reactivity by approximately 120 and 990%, respectively, whereas decreasing the ethylene concentration in the ethane/ethylene blend only suppresses the reactivity by approximately 11 and 22%, respectively. This clearly shows that methane is much more sensitive to ethylene blending than ethane. Moreover, Fig. 6-5(a) shows that although the reduction in ethylene concentration has a less negative effect on the reactivity of the methane/ethylene mixtures at high (≥ 1670 K) and low temperatures (≤ 900 K), the effect of ethylene concentration on the reactivity of the ethane/ethylene mixture is minor over the entire temperature range. In this way, one can see in Fig. 6-5(a) that decreasing ethylene concentration has no significant effect on the reactivity of ethane/ethylene mixtures at temperatures higher than 1670 K ($1000/T = 0.6$). To understand this more fully, sensitivity analyses to IDT, including both brute-force and direct sensitivity analyses [27] (Fig. 6-6) followed by flux analyses (not shown here for brevity) were conducted at 1200 K (0.833), where the effect of ethylene addition is most prominent. In the brute-force and the direct sensitivity analyses, the sensitivity coefficient (S) is calculated as:

$$S = \frac{\ln\left(\frac{\tau^+}{\tau^-}\right)}{\ln\left(\frac{z}{0.5}\right)} \quad (6-2)$$

As shown above, the rate constant for each reaction is increased/decreased by a factor of two, and IDTs are calculated as τ^+ (increased) and τ^- (decreased), respectively. A positive sensitivity coefficient indicates inhibition of reactivity, whereas a negative coefficient indicates a promotion in reactivity. Figure 6-6 indicates that adding ethylene to methane makes the chemistry more complex in terms of the number of important reactions involved (sensitivity coefficient ≥ 0.1) in IDT in comparison to addition to ethane.

Figure 6-6 shows that increasing methane concentration in the methane/ethylene blend promotes the chain-termination reactions: $\dot{\text{C}}\text{H}_3 + \dot{\text{C}}\text{H}_3 (+\text{M}) \leftrightarrow \text{C}_2\text{H}_6 (+\text{M})$ and $\dot{\text{C}}\text{H}_3 + \text{H}\dot{\text{O}}_2 \leftrightarrow \text{CH}_4 + \text{O}_2$. Simultaneously, increasing the methane concentration promotes the reactions $\text{CH}_4 + \dot{\text{O}}\text{H} \leftrightarrow \dot{\text{C}}\text{H}_3 + \text{H}_2\text{O}$, $\text{CH}_4 + \dot{\text{O}} \leftrightarrow \dot{\text{C}}\text{H}_3 + \dot{\text{O}}\text{H}$, $\dot{\text{C}}\text{H}_3 + \text{H}\dot{\text{O}}_2 \leftrightarrow \text{CH}_3\dot{\text{O}} + \dot{\text{O}}\text{H}$, $\dot{\text{C}}\text{H}_3 + \text{O}_2 \leftrightarrow \text{CH}_2\dot{\text{O}} + \dot{\text{O}}\text{H}$ in competition with the reactions: $\text{C}_2\text{H}_4 + \dot{\text{O}}\text{H} \leftrightarrow \dot{\text{C}}_2\text{H}_3 + \text{H}_2\text{O}$, $\text{C}_2\text{H}_4 + \dot{\text{O}} \leftrightarrow \dot{\text{C}}\text{H}_2\text{CHO} + \dot{\text{H}}$, $\dot{\text{C}}_2\text{H}_3 + \text{O}_2 \leftrightarrow \dot{\text{C}}\text{H}_2\text{CHO} + \dot{\text{O}}$, which all dramatically suppress the blends reactivity at 1200 K. Thus, increasing the ethylene concentration in the fuel blend promotes reactivity by inhibiting methyl radical ($\dot{\text{C}}\text{H}_3$) reactions but instead promotes reactions of vinyl radicals, which are more reactive than methyl radicals. As seen in Fig. 6-6, increasing the ethane concentration (50%→90%) in the ethane/ethylene blend at 1200 K

has no significant effect on the ten most prominent reactions, so that this increment promotes $\dot{H} + O_2 (+M) \leftrightarrow H\dot{O}_2 (+M)$, $\dot{H} + H\dot{O}_2 \leftrightarrow \dot{O}H + \dot{O}H$, and $\dot{C}H_3 + H\dot{O}_2 \leftrightarrow CH_3\dot{O} + \dot{O}H$ against the suppression of the important reaction $\dot{C}_2H_3 + O_2 \leftrightarrow \dot{C}H_2CHO + \ddot{O}$. Thus, the decrease in reactivity of the ethane/ethylene fuel blend with increasing ethane concentration (Fig. 6-5(a)), mainly stems from competition among the chain propagating reactions $\dot{C}_2H_5 + O_2 \leftrightarrow C_2H_4 + H\dot{O}_2$ and $C_2H_4 + \dot{H} (+M) \leftrightarrow \dot{C}_2H_5 (+M)$ and the chain branching reaction $\dot{C}_2H_3 + O_2 \leftrightarrow \dot{C}H_2CHO + \ddot{O}$ by scavenging \dot{C}_2H_5 radicals and O_2 molecules from the radical pool.

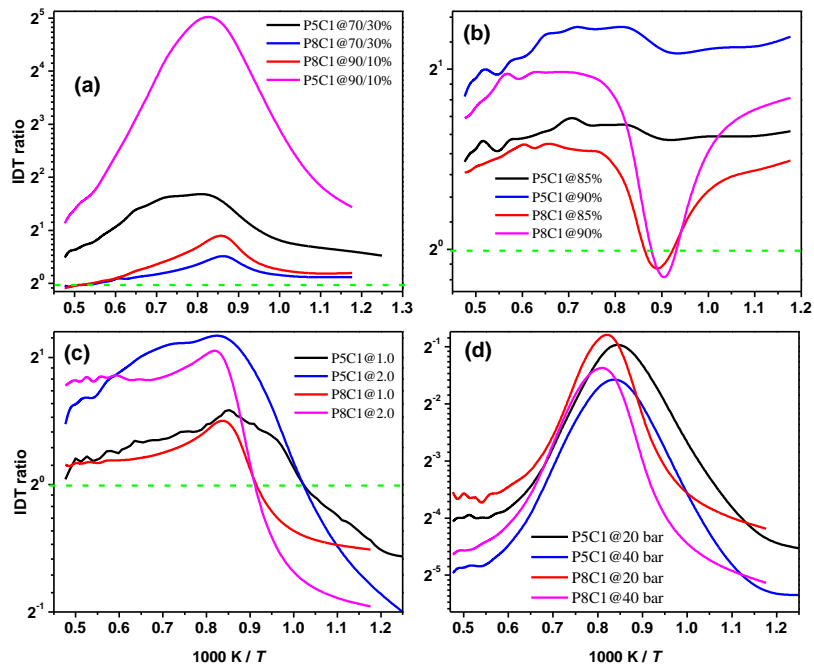


Figure 6-5. Individual effects of the studied parameters on methane/ethylene and ethane/ethylene IDTs: (a) effect of blending composition; (b) effect of dilution level; (c) effect of equivalence ratio; and (d) effect of pressure.

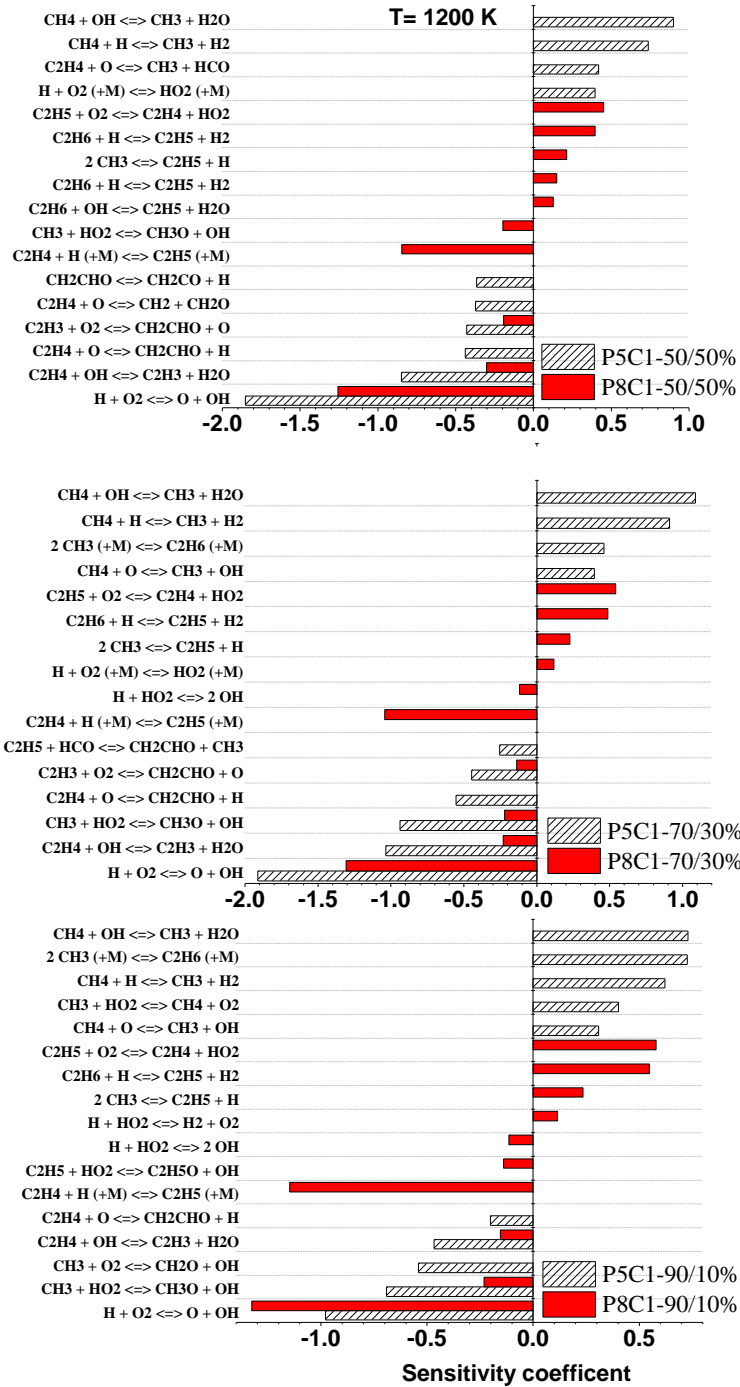


Figure 6-6. Sensitivity analysis of IDT corresponding to the temperature of 1200 K (0.833) in Fig. 6-5(a).

6.4.2.1.2 Effect of dilution

The effect on the reactivity of increasing dilution on the methane/ethylene and ethane/ethylene mixtures is demonstrated in Fig. 6-5(b). It is seen that increasing dilution from 75 to 85% and then 90% in the methane/ethylene mixtures decreases reactivity by approximately 55 and 115%,

respectively. However, this effect on the ethane/ethylene mixture is not monotonic. Surprisingly, it is seen in Fig. 6-5(b) that increasing the dilution level in the ethane/ethylene mixture not only suppresses the negative effect of dilution on reactivity within the temperature range of 1000 – 1250 K but also enhances reactivity by ~10% at 1100 K (0.909). In this regard, three new experimental datasets within the target temperature range (1000 – 1200 K) at 1 bar, 50% C₂H₆ + 50% C₂H₄, $\phi = 0.5$, and dilution levels (Ar) of 75, 85, and 90% conditions were performed. However, some of the measured IDTs (> 4 – 5 ms) are located at the upper working limit of NUIG-LPST. As mentioned, although some of the IDTs are relatively long for available LPST in C³-NUIG, most of them have been taken under tailoring conditions with almost plateau pressure profiles behind the reflected shock ($dp/dt \approx 0$) during the induction time before ignition. However, those data with significant dp/dt behind the reflected shock had already been removed from the graph for increasing the reliability of the data demonstrated in Fig. 6-7. As seen in Fig. 6-7, although NUIGMech1.0 can somewhat capture the behaviour and the IDT trends by increasing the dilution level from 75 to 90%, it fails to reproduce the experimental IDTs beyond the dilution level of 75%, so that the predictions of NUIGMech1.0 are consistently shorter than the experimental measurements over the temperature range studied. By comparing the effect of dilution on the reactivities of the methane/ethylene and ethane/ethylene blends shown in Fig. 6-8, it is inferred that this behaviour stems from the effect of dilution (third body) and the competition between $\dot{C}_2H_4 + \dot{H} (+M) \leftrightarrow \dot{C}_2H_5 (+M)$ and $\dot{C}_2H_5 + O_2 \leftrightarrow C_2H_4 + \dot{H}O_2$ in consuming \dot{C}_2H_5 radicals. On the one hand, increasing the dilution level intensifies the reverse reaction of $\dot{C}_2H_4 + \dot{H} (+M) \leftrightarrow \dot{C}_2H_5 (+M)$ which produces more reactive \dot{H} atoms. On the other hand, increasing the dilution level decreases the oxygen concentration in the radical pool, which suppresses the reaction $\dot{C}_2H_5 + O_2 \leftrightarrow C_2H_4 + \dot{H}O_2$. Also, Fig. 6-8 shows that increasing the dilution level inhibits the reaction of $H_2O_2 (+M) \leftrightarrow \dot{O}H + \dot{O}H (+M)$ and simultaneously promotes $\dot{C}H_3 + \dot{H}O_2 \leftrightarrow CH_3\dot{O} + \dot{O}H$, $\dot{H} + O_2 (+M) \leftrightarrow \dot{H}O_2 (+M)$, and $\dot{H} + \dot{H}O_2 \leftrightarrow \dot{O}H + \dot{O}H$. Apart from the intermediate temperature regime, it is seen in Fig. 6-5(b) that the effect on the reactivity of increasing the dilution level is much less pronounced in the ethane/ethylene mixtures compared to the methane/ethylene mixtures.

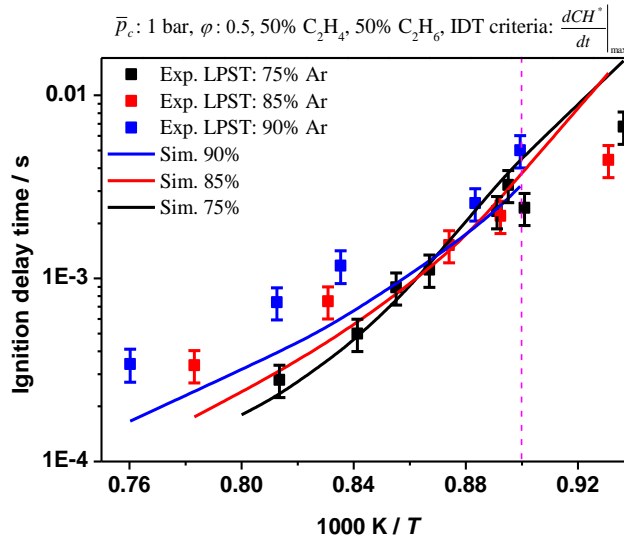


Figure 6-7. Experimental and simulation data for ethane/ethylene oxidation concerning Fig. 6-5(b). The magenta dashed line refers to the turning point temperature (0.909) in Fig. 6-5(b).

6.4.2.1.3 Effect of equivalence ratio

The effect of increasing the equivalence ratio from 0.5 to 1.0 and 2.0 on the reactivity of the methane/ethylene and ethane/ethylene mixtures is depicted in Fig. 6-5(c). Increasing the equivalence ratio has a complex effect on the reactivity of the mixtures over the temperatures studied. Increasing the equivalence ratio has a drastic effect on decreasing the mixtures' reactivity in the temperature range 800 – 1200 K, which is followed by a mild effect in increasing mixture reactivity at temperatures ≥ 1200 K. It is seen in Fig. 6-5(c) that although the reactivity of ethane/ethylene blends is less sensitive to an increasing equivalence ratio with temperature compared to methane/ethylene mixtures, it shows a higher sensitivity in the temperature range 1050 – 1200 K. The maximum gradient in decreasing the reactivity of the ethane/ethylene mixtures $\left(\left. \frac{\partial IDT \text{ ratio}}{\partial T} \right|_{max} \right)$ is about 0.73 and 1.36 %/K (at 1100 K) at equivalence ratios of 1.0 and 2.0, respectively, in the temperature range 800–1200 K, whereas the values for the methane/ethylene mixtures are about 0.4 and 0.82 % K⁻¹ (at 1000 K) at equivalence ratios of 1.0 and 2.0, respectively.

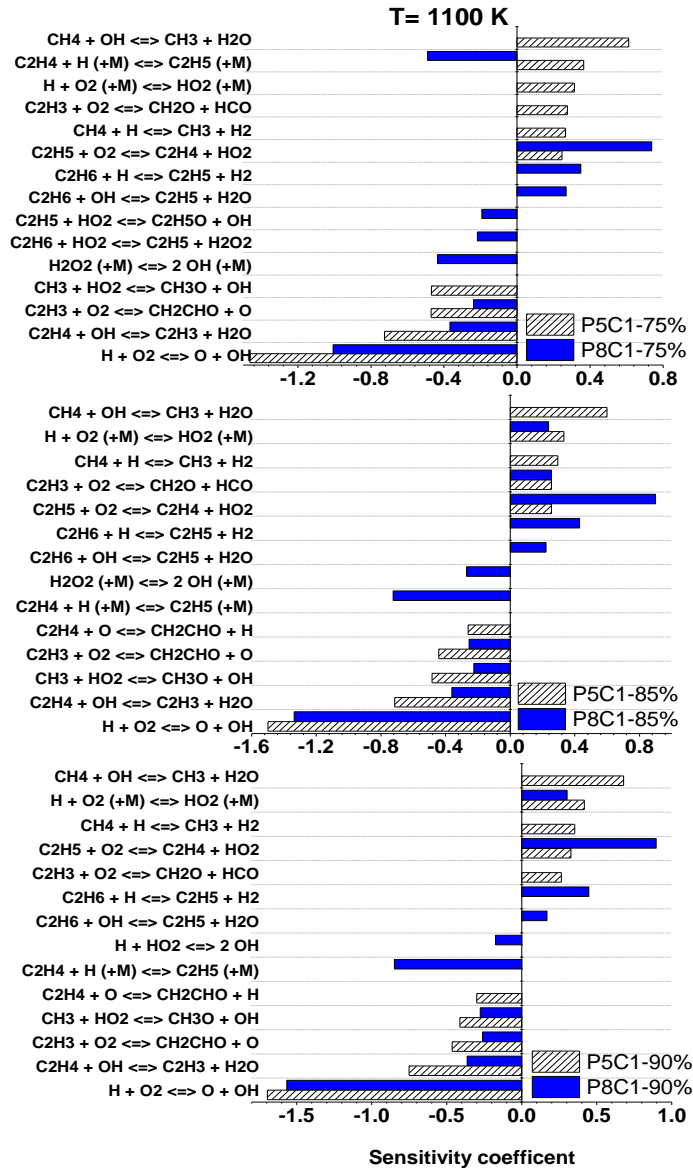


Figure 6-8. Sensitivity analysis of IDT corresponding to the temperature 1100 K (0.91) in Fig. 6-5(b).

The reactivity of the fuel-rich mixtures is much more affected by changes in temperature, especially in the 800 – 1200 K temperature range. In this regard, Figs. 6-9 and DS40 show that increasing the equivalence ratio in the methane/ethylene blends at 1200 K intensifies H-atom abstraction from CH₄ and C₂H₄ by \dot{H} atoms instead of $\dot{O}H$ radicals. This effect makes the system less reactive (Fig. DS41). However, increasing the equivalence ratio promotes the chain branching reaction of $\dot{C}_2H_3 + O_2 \leftrightarrow \dot{C}H_2CHO + \dot{O}$ compared to the more reactive chain branching reaction $C_2H_4 + \dot{O} \leftrightarrow \dot{C}H_2CHO + \dot{H}$, so that as seen in Fig. DS41 this promotion reduces the blend reactivity. Also, Fig. 6-9 shows that

increasing the equivalence ratio to 2.0 promotes the reverse reaction of $C_3H_6 + \dot{H} \leftrightarrow C_2H_4 + \dot{C}H_3$ in competition with $C_2H_4 + \ddot{O} \leftrightarrow \ddot{C}H + CH_2O$ and $\dot{C}H_2CHO \leftrightarrow CH_2CO + \dot{H}$.

Similar to the methane/ethylene blend, it is shown in Figs. 6-9 and DS42 that increasing the equivalence ratio of the ethane/ethylene blend from 0.5 to 2.0 at 1200 K changes the H-atom abstraction pattern from $\dot{O}H$ radicals to \dot{H} atoms so that this shift makes the blend less reactive at 1200 K. In fact, decreasing oxygen concentration by increasing the equivalence ratio and also competition between C_2H_6 and C_2H_4 in consuming \dot{H} atoms and $\dot{O}H$ radicals and producing \dot{C}_2H_5 and \dot{C}_2H_4 radicals affect blend reactivity because of the higher reactivity of vinyl radicals compared to ethyl radicals in the blends studied.

6.4.2.1.4 Effect of pressure

The effect of pressure on the reactivity of the methane/ethylene and ethane/ethylene blends is demonstrated in Fig. 6-5(d). One can see that increasing pressure increases the reactivity of all mixtures. In this regard, it can be seen in Fig. 6-5(d) that increasing the pressure from 1 to 40 bar has a Gaussian distribution effect on reactivity with temperature in that it decreases reactivity in the temperature range 1050–1550 K, whereas its effect on the reactivity is almost constant at $T \geq 1540$ K and $T \leq 1050$ K for the ethane/ethylene blends and at $T \leq 920$ K for the methane/ethylene blends. Moreover, Fig. 6-5(d) shows that although the positive effect of increasing pressure for the methane/ethylene blends at $T \geq 1200$ K is higher than for the ethane/ethylene mixtures, this trend is reversed at $T \leq 1200$ K. At 1200 K, the minimum effect of the Gaussian distribution on increasing the reactivity of the methane/ethylene mixtures is about 48% at 20 bar and 66% at 40 bar, whereas the values for the ethane/ethylene mixtures at 20 and 40 bar are 42 and 62%, respectively.

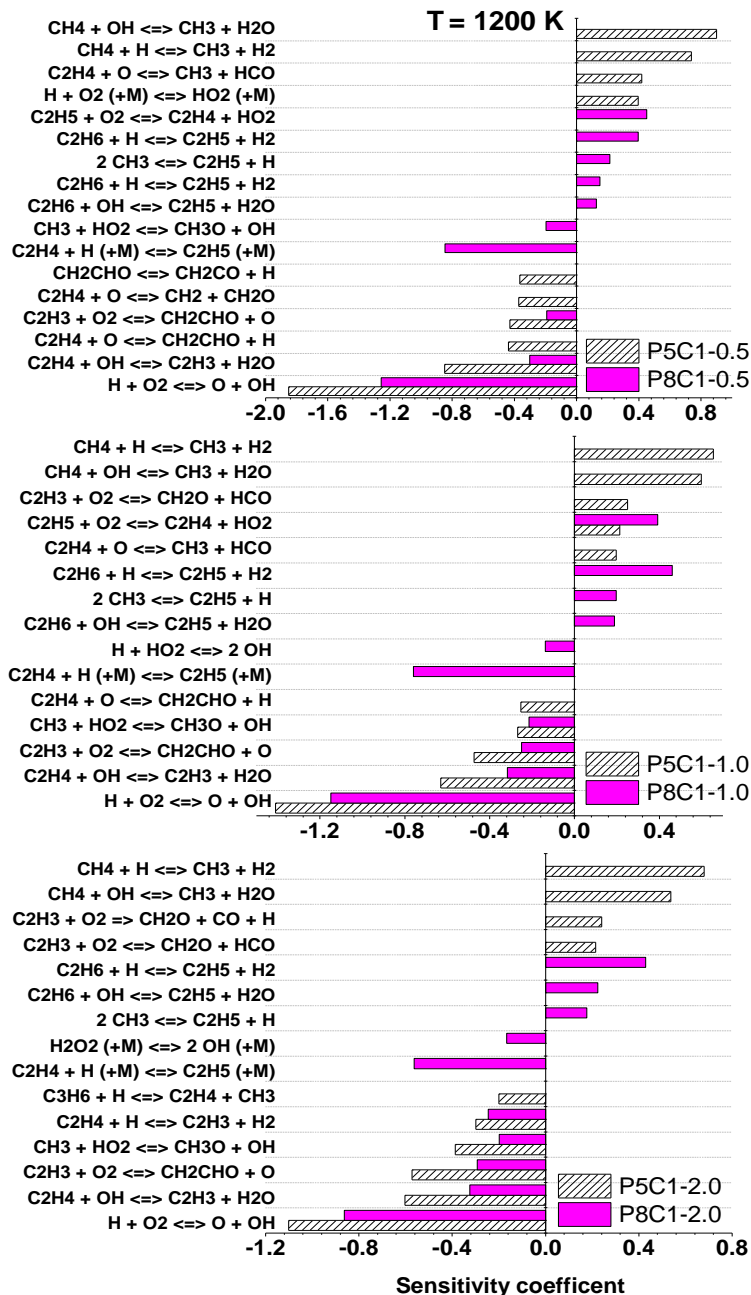
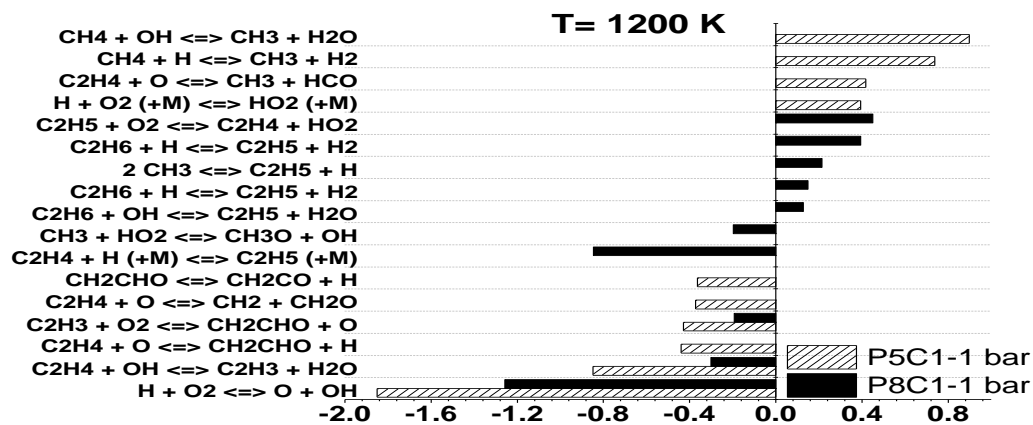


Figure 6-9. Sensitivity analysis of IDT corresponding to the temperature 1200 K (0.833) in Fig. 6-5(c).

In addition, Fig. 6-5(d) shows that although the effect of pressure on the reactivity of the methane/ethylene mixtures is more sensitive to temperature in comparison to the ethane/ethylene mixtures, this effect shows a very high sensitivity to temperature for the ethane/ethylene mixtures in the temperature range 1050–1500 K. Increasing the temperature of the ethane/ethylene mixture from 1050 to 1220 K decreases the reactivity by approximately 48%, whereas further increasing the temperature to 1500 K retrieves the mixture’s reactivity. Furthermore, it is demonstrated in Fig. 6-

5(d) that the reactivity of ethane/ethylene mixtures is more sensitive to pressure rise compared to the methane/ethylene mixtures. However, they show almost the same sensitivity and dependency at high-temperatures (≥ 1666 K) and low-temperatures (≤ 900 K). Fig. 6-5(d) also shows that for both the methane/ethylene and ethane/ethylene mixtures, increasing pressure has the most prominent effect on reactivity in the temperature range 1100–1330 K.

Sensitivity and flux analyses (Figs. 6-10, DS43 and DS44) reveal that increasing the pressure of the methane/ethylene and ethane/ethylene blends from 1 to 40 bar at 1200 K, intensifies H-atom abstraction from CH_4 , C_2H_6 , and C_2H_4 by $\dot{\text{O}}\text{H}$ and $\text{H}\dot{\text{O}}_2$ radicals and simultaneously inhibits abstraction by $\dot{\text{H}}$ atoms. These may stem from the promotions in importance of the reactions $\dot{\text{H}} + \text{O}_2 (+\text{M}) \leftrightarrow \text{H}\dot{\text{O}}_2 (+\text{M})$ and $\text{H}_2\text{O}_2 (+\text{M}) \leftrightarrow \dot{\text{O}}\text{H} + \dot{\text{O}}\text{H} (+\text{M})$ with increasing pressure. One can see in Figs. 6-10 and DS44 that these effects are more pronounced in the ethane/ethylene blend, and thus, the blend shows a higher sensitivity to the effects at 1200 K. As seen in Fig. 6-10, increasing the pressure at 1200 K suppresses the $\text{C}_2\text{H}_4 + \ddot{\text{O}} \leftrightarrow \dot{\text{C}}\text{H} + \text{CH}_2\text{O}/\dot{\text{C}}\text{H}_3 + \text{H}\dot{\text{C}}\text{O}$ reactions and in particular the important chain branching reaction $\text{C}_2\text{H}_4 + \ddot{\text{O}} \leftrightarrow \dot{\text{C}}\text{H}_2\text{CHO} + \dot{\text{H}}$. Moreover, Figs. 6-10 and DS44 demonstrate that increasing the pressure of the ethane/ethylene blend at 1200 K suppresses the reverse chain branching reaction $\dot{\text{C}}_2\text{H}_4 + \dot{\text{H}} (+\text{M}) \leftrightarrow \dot{\text{C}}_2\text{H}_5 (+\text{M})$ and simultaneously promotes the chain propagating reactions $\text{C}_2\text{H}_6 + \text{H}\dot{\text{O}}_2 \leftrightarrow \dot{\text{C}}_2\text{H}_5 + \text{H}_2\text{O}_2$ and $\text{C}_2\text{H}_4 + \text{H}\dot{\text{O}}_2 \leftrightarrow \dot{\text{C}}_2\text{H}_3 + \text{H}_2\text{O}_2$. All of these effects make the methane/ethylene and the ethane/ethylene blends less reactive compared to the base cases (P5C1 and P8C1).



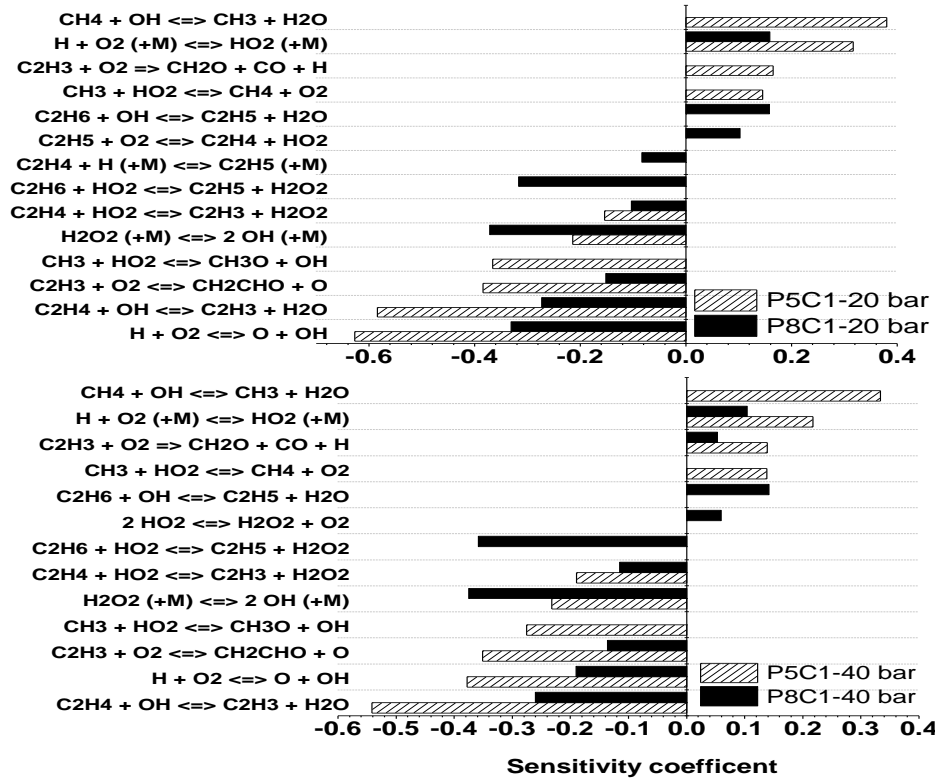


Figure 6-10. Sensitivity analysis of IDT corresponding to the temperature 1200 K (0.833) in Fig. 6-5(d).

6.4.3 Correlations and their performances

Having reliable global expressions that can properly explain the reactivity of different mixtures under different physico-chemical conditions is demanding. Global correlations can significantly decrease the computational time of real-time/scale combustion systems and computational fluid dynamics simulations. Hence, in this section, several correlations are derived based on the constant volume simulations of NUIGMech1.0 [13], which we have shown can reasonably predict IDTs for methane/ethylene, methane/ethane, and ethane/ethylene mixtures over a wide range of binary blended fuel conditions. The applied procedure for deriving the correlations has already been discussed by the authors [13]. The validity ranges of the correlations are $1 \leq p \leq 50$ atm, $800 \leq T \leq 2000$ K, $0.25 \leq \varphi \leq 3.0$, $75\% \leq \text{dilution} \leq 95\%$, and Fuel₁/Fuel₂: 30/70, 50/50, and 70/30% which stems from the targets of the current study. Thus, the following simple correlation style is used to mathematically explain the relationship for the conditions studied:

$$\tau_{\text{idt,corr}} = 10^A \exp\left(\frac{B}{T}\right) [\text{Fuel}_1]^C [\text{Fuel}_2]^D [\text{Oxygen}]^E [\text{Diluent}]^F \quad (6-3)$$

where the concentrations (mol m^{-3}) of fuels, oxygen, and diluent are calculated based on the ideal gas law in accordance with the partial pressure of each species in the mixture at a specific temperature. Tables 6-3–6-8 show that the correlations are evaluated by sub-dividing the numerically studied conditions into two regimes: (a) low, intermediate, and high temperatures and (b) high and low pressures, corresponding to the different chemistry controlling ignition over these conditions. However, based on our correlation procedure (constant-volume adiabatic simulations), the derived correlations for the low-temperature regime are not able to capture the experimental IDTs where non-ideal effects (mostly heat loss effects) are prominent. Therefore, the performance of the correlations is evaluated only in the intermediate-to-high temperature regime. In this regard, Origin 8.5 software [28][28] is used to derive the correlation parameters included in Eqn. 6-3. The coefficients of the extracted correlations for methane/ethylene, methane/ethane, and ethane/ethylene, including standard errors and validity ranges over the studied conditions, are presented in Tables 6-3–6-8.

The performance of the derived correlations versus the available experimental IDT data in the literature (methane/ethane) and the newly taken data of the present study (methane/ethylene and ethane/ethylene) is already shown in Figs. 6-2–6-4. In these figures, the red dashed lines refer to the derived correlations. However, the red dashed line is replaced by a blue line if one parameter (e.g., pressure or dilution) is outside the range of correlation. It is seen in Fig. 6-2 that the correlation formula can duplicate the experimental IDT data trend of the methane/ethylene mixtures over a wide range of conditions. The correlation coefficients for the methane/ethylene mixtures are presented in Table 6-3. As seen in Figs. 6-2(a), (e), and (i), correlating the simulation results using the format presented in Eqn. 6-3 is inaccurate with significant uncertainties because of the highly nonlinear behavior of the methane/ethylene mixtures at pressures in the range 1–15 atm. As already shown in the sensitivity analysis plots, the high nonlinearity of IDTs within 1–15 bar range almost stems from high sensitivity of the IDTs to $\dot{H} + \text{O}_2 (+M) \leftrightarrow \text{HO}_2 (+M)$ and $\dot{H} + \text{O}_2 \leftrightarrow \ddot{\text{O}} + \dot{\text{O}}\text{H}$, which change significantly with pressure over the range investigated. In this regard, the average ($\bar{\delta}_{corr-exp}$) and standard ($\bar{\sigma}_{corr-exp}$) deviation of the methane/ethylene correlations from the experimental data (only shock-tube data) over the studied temperature range is presented in Table 6-6.

Here, it should be noted that highly nonlinear behavior of the oxidation chemistry of the studied binary blended fuels over certain ranges of the studied conditions may cause that the simple form of the correlation presented in Eqn. 6-3 fails to accurately predict experimental IDTs, especially in the

range 1 – 20 atm. In fact, high sensitivity of IDT to some non-linear dependency of vital reactions and also changing the vital reactions over certain ranges of fuel concentration, temperature, and pressure make the chemically predicted IDTs more scattered in terms of the defined parameters in Eqn. 6-3, so that the derived regressions would be less accurate depending on the scattering level of the calculated IDTs by the parent high fidelity chemical mechanism. Such deviations could be somehow understood by looking at R^2 , χ^2 , and importantly high standard errors of the derived coefficients for the parameters in Eqn. 6-3. Therefore, as seen in the relevant table for methane + ethylene blends, it was not possible to derive a proper simple shape correlation for IDTs in the pressure range of 1 – 15 atm. To compensate for this issue, the authors tried to divide the correlation zones into several regions in accordance with temperature, pressure, and equivalence ratios and bundle the same pose regions into one category to get more accurate correlations. Moreover, as mentioned above, in some regions related to low temperatures in which the experimental IDTs were measured using RCM, again, some discrepancies between the correlation and the model predictions could be seen. These discrepancies stem from the fact that the correlations are derived based on constant volume adiabatic calculations, while the experiments suffer from nonidealities such as heat loss, which substantially can affect the measured IDTs. However, these nonidealities can be robustly treated in the RCM simulations of the parent chemical model by imposing volume history profiles. Thus, the red dashed lines for IDTs above 10 ms often show under prediction, which can be explained by the heat loss effect that occurs in the RCM experiments, which are not taken into account in the correlations. Furthermore, the IDT criterion is another parameter that may affect the performance of the correlations versus the parent chemical mechanism. The correlations have been derived based on IDTs calculated by the maximum gradient in pressure history, while some experimental IDTs and their respective simulation data (especially < 10 bar) were determined using different definitions such as the maximum gradient in CH^* or OH^* history.

Figure 6-3 shows that the simple derived correlations which are reported in Table 6-4 for the methane/ethane mixtures can reasonably reproduce the experimental IDTs and their trends, even for those outside of the range of the correlation (Fig. 6-3(a), (i); dilution level > 95%). Thus, the average and standard deviation of the methane/ethane correlations from the experimental data (only shock tube data) over the temperature range studied are provided in Table 6-7. It is seen that the average deviation between the correlations and the experimental data over the studied conditions in the high-temperature regime is approximately 35%.

The performance of the derived correlations in predicting the IDTs of the ethane/ethylene mixtures is shown in Fig. 6-4. The coefficients of the correlations are presented in Table 6-5 at both low and high temperatures. By comparing the experimental data and the correlations in Fig. 6-4, it is apparent that the derived correlations can acceptably predict the measured IDTs with an accuracy comparable to NUIGMech1.0. In this regard, it is observed in Table 6-8 that the average deviation between the correlations and the experimental data over the studied conditions in the high-temperature regime is approximately 40%.

Furthermore, by increasing the compressed pressure to 20 and 40 bar, it is seen in Figs. 6-2 – 6-4 that all of the correlations can acceptably predict experimental IDTs even in the intermediate-to-low temperature regime. This stems from the fact that the high-pressure chemistry does not significantly change within the 15 – 50 bar (3.33 times) window in deriving the correlations, while this effect is dramatically sensitive to changes in pressure in the range 1 – 15 bar (15 times). This fact is somehow demonstrated in Fig. 6-11. Although the correlations were derived over 1 – 50 atm, according to the pressure effect discussed above, the correlation could satisfactorily predict the experimental IDTs (within $\pm 40\%$) over 125 bar, low temperature, and relatively short IDT regimes, where the heat loss effect would be minor in RCM facilities. This finding could be interesting in terms of mimicking gas engine operating pressure, which is almost above 40 bar. Furthermore, it is interesting to note that the performance of the simple correlations in reproducing the experimental IDTs is better than NUIGMech1.0 at some conditions (e.g., high-temperature regime > 1400 K) such as in Figs. 6-2(h), 6-3(b), 6-4(f), (h).

Table 6-3. Evaluated coefficients for correlation of the simulated IDTs for methane + ethylene mixtures.

$0.25 \leq \phi \leq 2.0$ $75 \leq \text{Dilution} \leq 95\%$	$20 \leq p_{5,c} \leq 50 \text{ /atm}$	
	$800 \leq T_{5,c} < 1200 \text{ /K}$	$1200 \leq T_{5,c} \leq 2000 \text{ /K}$
A	-8.335 ± 0.021	-9.901 ± 0.0236
B	15676.25 ± 36.39	18356.2 ± 63.216
C [methane]	-0.214 ± 0.0018	1.047 ± 0.0053
D [ethylene]	-0.598 ± 0.0019	-1.1196 ± 0.0054
E	-0.1362 ± 0.0023	-1.2955 ± 0.0046
F	0.0746 ± 0.004	0.684 ± 0.0069
R²	0.991	0.976
χ^2	2.54E-04	3.05E-10

Table 6-4. Evaluated coefficients for correlation of the simulated IDTs for methane + ethane mixtures.

$0.25 \leq \phi \leq 2.0$ $75 \leq \text{Dilution} \leq 95\%$	$20 \leq p_{5,c} \leq 50 \text{ /atm}$	$1 \leq p_{5,c} \leq 15 \text{ /atm}$	$15 < p_{5,c} \leq 50 \text{ /atm}$
	$800 \leq T_{5,c} < 1200 \text{ /K}$	$1200 \leq T_{5,c} < 2000 \text{ /K}$	
A	-9.783 ± 0.0151	-9.101 ± 0.033	-9.949 ± 0.0264
B	19718.499 ± 26.840	19258.657 ± 97.04	19458.945 ± 72.877
C [methane]	$-0.1653 \pm 9.26E-04$	1.439 ± 0.008	0.7469 ± 0.0042
D [ethane]	-0.4759 ± 0.001	-0.2413 ± 0.009	-0.717 ± 0.0045

E	-0.067 ± 0.0012	-2.111 ± 0.0107	-1.129 ± 0.0044
F	-0.1378 ± 0.002	0.3386 ± 0.0054	0.4771 ± 0.007
R²	0.998	0.974	0.973
χ^2	3.74E-04	4.32E-09	2.34E-10

Table 6-5. Evaluated coefficients for correlation of the simulated IDTs for ethane + ethylene mixtures.

0.25 ≤ φ ≤ 2.0 75 ≤ Dilution ≤ 95%	20 ≤ p_{5,c} ≤ 50 /atm	1 ≤ p_{5,c} ≤ 15 /atm	15 < p_{5,c} ≤ 50 /atm
	800 ≤ T_{5,c} < 1200 /K	1200 ≤ T_{5,c} < 2000 /K	
A	-9.827 ± 0.0261	-8.6581 ± 0.0209	-12.118 ± 0.0298
B	19125.037 ± 46.261	15455.624 ± 62.281	23088.771 ± 86.772
C [ethylene]	-0.466 ± 0.0017	-0.0348 ± 0.004	-0.2374 ± 0.0027
D [ethane]	-0.2555 ± 0.0018	0.4395 ± 0.0044	0.0316 ± 0.0029
E	-0.0496 ± 0.0021	-1.2105 ± 0.0057	-0.4924 ± 0.0034
F	-0.08497 ± 0.0037	0.2072 ± 0.0045	0.41 ± 0.0056
R²	0.992	0.977	0.976
χ^2	5.19E-04	1.12E-10	1.19E-11

Table 6-6. Performance of the methane/ethylene correlations versus the experimental data shown in Fig. 6-2.

Experimental data set	$\bar{\delta}_{corr-exp}$ (%)	$\bar{\sigma}_{corr-exp}$ (%)
P5C1	47.5	22.1
P5C2	28.3	7.5
P5C3	29.0	15.0
P5C4	33.8	22.8
P5C5	38.4	5.9
P5C6	26.0	17.0
P5C7	9.9	9.6
P5C8	19.8	9.1
P5C9	131.0	56.4

Table 6-7. Performance of the methane/ethane correlations versus the experimental data shown in Fig. 6-3.

Experimental data set	$\bar{\delta}_{corr-exp}$ (%)	$\bar{\sigma}_{corr-exp}$ (%)
P6C1	34.1	15.5
P6C2	2.1	0.8
P6C3	18.5	7.1
P6C4	49.1	47.2
P6C5	40.8	36.3
P6C6	30.7	10.1
P6C7	68.1	8.3
P6C8	24.5	26.0
P6C9	45.3	3.8

Table 6-8. Performance of the ethane/ethylene correlations versus the experimental data shown in Fig. 6-4.

Experimental data set	$\bar{\delta}_{corr-exp}$ (%)	$\bar{\sigma}_{corr-exp}$ (%)
P8C1	39.5	11.8
P8C2	28.8	3.4
P8C3	80.6	92.9
P8C4	36.5	37.3
P8C5	36.8	4.0
P8C6	24.9	33.9
P8C7	24.7	11.9

P8C8	74.6	92.5
P8C9	9.9	11.8

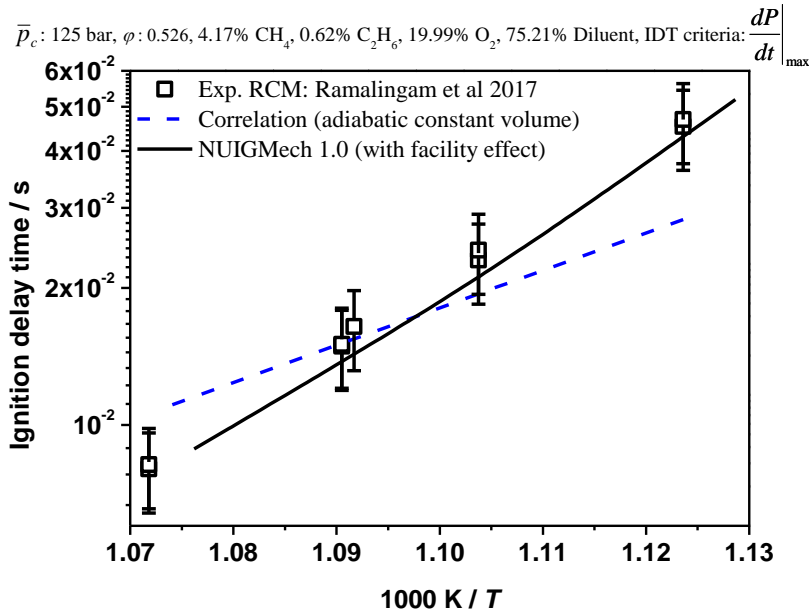


Figure 6-11. Performance of the derived correlation under an over-pressure (> 50 bar) condition [11].

6.5 Conclusions

To create a comprehensive IDT database, a detail experimental and simulation study of the IDT characteristics of binary blended C₁ – C₂ alkane/alkene fuels including methane/ethylene, methane/ethane, and ethane/ethylene combinations over a wide range of temperature, pressure, equivalence ratio, binary combination, and dilution was performed. An extensive literature review was conducted, and available data, especially for methane/ethane blends, were extracted to be used in the simulations. The experimental tests were designed using the Taguchi matrix (L₉). Nine data sets including 160 data points for methane + ethylene (p_c : 1, 20 and 40 bar; ϕ : 0.5, 1.0, and 2.0; dilution: 75, 85, and 90%) and nine data sets including 140 data points for ethane + ethylene (p_c : 1, 20, and 40 bar; ϕ : 0.5, 1.0, and 2.0; dilution: 75, 85, and 90%) were recorded using L/HPST and RCM facilities at C³-NUIG and PCFC-RWTH Aachen University. The experimental data presented here provides a new insight into the oxidation of alkane/alkene blended fuel mixtures. These findings are technologically important in terms of safety and the design of new low-emission and size-efficient combustion systems.

The individual effects of the studied parameters (alkane/alkene ratio, dilution, equivalence ratio, and dilution) on the IDTs have been considered in detail. The results showed that most parameters do not have a monotonic effect on mixture's reactivity over the entire temperature range (800–2100 K), in that the mixture reactivity in certain temperature ranges can be very sensitive to the studied parameters, while this sensitivity can be low over other temperature ranges. Interestingly, it was shown that increasing the alkane concentration in the alkane + alkene blends at 1 bar, ϕ : 0.5 and dilution of 75% has a Gaussian distribution with temperature around 1200 K. However, increasing the pressure or dilution percent has a minimum effect on the blends reactivity at 1200 and 1100 K, respectively.

Furthermore, the performances of NUIGMech1.0, in addition to several derived correlations for the blended fuels, were evaluated using all of the available and measured experimental IDT data. The results showed that NUIGMech1.0 could acceptably predict the measured IDTs. Moreover, the results showed that the derived correlations based on NUIGMech1.0 for the studied blended fuel mixtures could satisfactorily reproduce the experimental IDT data within the studied range. This can be a very versatile rule-of-thumb tool to use in predicting the IDT characteristics of the fuel blends studied.

Acknowledgements

The authors would like to express their gratitude to Shell Research Ltd. and Science Foundation Ireland (SFI) for funding via project numbers 15/IA/3177 and 16/SP/3829. The authors from PCFC, RWTH Aachen University, would like to recognize the funding support from the German Research Foundation (Deutsche Forschungsgemeinschaft, DFG) through the project number – 322460823 (HE7599/2-1).

References

- [1] J. Shao, D.F. Davidson, R.K. Hanson, A shock tube study of ignition delay times in diluted methane, ethylene, propene and their blends at elevated pressures, *Fuel* 225 (2018) 370-380.
- [2] C.J. Aul, W.K. Metcalfe, S.M. Burke, H.J. Curran, E.L. Petersen, Ignition and kinetic modeling of methane and ethane fuel blends with oxygen: A design of experiments approach, *Combust. Flame* 160 (2013) 1153-1167.
- [3] D.J. Beerer, V.G. McDonell, An experimental and kinetic study of alkane autoignition at high pressures and intermediate temperatures, *Proc. Combust. Inst.* 33 (2011) 301-307.

- [4] J. de Vries, E.L. Petersen, Autoignition of methane-based fuel blends under gas turbine conditions, *Proc. Combust. Inst.* 31 (2007) 3163-3171.
- [5] S.M. Burke, W.K. Metcalfe, O. Herbinet, F. Battin-Leclerc, F.M. Haas, J. Santner, F.L. Dryer, H.J. Curran, An experimental and modeling study of propene oxidation. part 1: speciation measurements in jet-stirred and flow reactors, *Combust. Flame* 161 (2014) 2765-2784.
- [6] N. Lamoureux, C.-E. Paillard, Natural gas ignition delay times behind reflected shock waves: application to modelling and safety, *Shock Waves* 13 (2003) 57-68.
- [7] J. Huang, W.K. Bushe, Experimental and kinetic study of autoignition in methane/ethane/air and methane/propane/air mixtures under engine-relevant conditions, *Combust. Flame* 144 (2006) 74-88.
- [8] E.L. Petersen, J.M. Hall, S.D. Smith, J. de Vries, A.R. Amadio, M.W. Crofton, Ignition of lean methane-based fuel blends at gas turbine pressures, *J. Eng. Gas Turbines Power* 129 (2007) 937-944.
- [9] S. Gersen, A.V. Mokhov, J.H. Darmeveil, H.B. Levinsky, P. Glarborg, Ignition-promoting effect of NO₂ on methane, ethane and methane/ethane mixtures in a rapid compression machine, *Proc. Combust. Inst.* 33 (2011) 433-440.
- [10] A. Ramalingam, K. Zhang, A. Dhongde, L. Virnich, H. Sankhla, H.J. Curran, A. Heufer, An RCM experimental and modeling study on CH₄ and CH₄/C₂H₆ oxidation at pressures up to 160 bar, *Fuel* 206 (2017) 325-333.
- [11] J. Herzler, C. Naumann, Shock-tube study of the ignition of methane/ethane/hydrogen mixtures with hydrogen contents from 0% to 100% at different pressures, *Proc. Combust. Inst.* 32 (2009) 213-220.
- [12] P.J. Ross, *Taguchi Techniques for Quality Engineering*, McGraw-Hill, NY., (1988).
- [13] M. Baigmohammadi, V. Patel, S. Martinez, S. Panigrahy, A. Ramalingam, U. Burke, K.P. Somers, K.A. Heufer, A. Pekalski, H.J. Curran, A comprehensive experimental and simulation study of ignition delay time characteristics of single fuel C₁ – C₂ hydrocarbons over a wide range of temperatures, pressures, equivalence ratios, and dilutions, *Energy, Fuels* 34 (2020) 3755-3771.
- [14] U. Burke, K.P. Somers, P. O'Toole, C.M. Zinner, N. Marquet, G. Bourque, E.L. Petersen, W.K. Metcalfe, Z. Serinyel, H.J. Curran, An ignition delay and kinetic modeling study of methane, dimethyl ether, and their mixtures at high pressures, *Combust. Flame* 162 (2015) 315-330.
- [15] N. Donohoe, K.A. Heufer, C.J. Aul, E.L. Petersen, G. Bourque, R. Gordon, H.J. Curran, Influence of steam dilution on the ignition of hydrogen, syngas and natural gas blends at elevated pressures, *Combust. Flame* 162 (2015) 1126–1135.
- [16] S.M. Gallagher, H.J. Curran, W.K. Metcalfe, D. Healy, J.M. Simmie, G. Bourque, A rapid compression machine study of the oxidation of propane in the negative temperature coefficient regime, *Combust. Flame* 153 (2008) 316–333.
- [17] D. Healy, H.J. Curran, S. Dooley, J.M. Simmie, D. Kalitan, E.L. Petersen, G. Bourque, Methane/propane mixture oxidation at high pressures and at high, intermediate and low temperatures, *Combust. Flame* 155 (2008) 451–461.
- [18] D. Healy, H.J. Curran, J.M. Simmie, D. Kalitan, C.M. Zinner, A.B. Barrett, E.L. Petersen, G. Bourque, ethane/ethane/propane mixture oxidation at high pressures and at high, intermediate and low temperatures, *Combust. Flame* 155 (2008) 441–448.

- [19] D. Healy, D.M. Kalitan, C.J. Aul, E.L. Petersen, G. Bourque, H.J. Curran, Oxidation of C₁ – C₅ alkane quinary natural gas mixtures at high pressures, *Energy Fuels* 24 (2010) 1521-1528.
- [20] E.L. Petersen, M.J.A. Rickard, M.W. Crofton, E.D. Abbey, M.J. Traum, D.M. Kalitan, A facility for gas- and condensed-phase measurements behind shock waves, *Meas. Sci. Technol.* 16 (2005) 1716-1729.
- [21] B.W. Weber, C.-J. Sung, M.W. Renfro, On the uncertainty of temperature estimation in a rapid compression machine, *Combust. Flame* 162 (2015) 2518-2528.
- [22] S.S. Goldsborough, S. Hochgreb, G. Vanhove, M.S. Wooldridge, H.J. Curran, C.-J. Sung, Advances in rapid compression machine studies of low- and intermediate-temperature autoignition phenomena, *Prog. Energy Combust. Sci.* 63 (2017) 1-78.
- [23] C.-J. Sung, H.J. Curran, Using rapid compression machines for chemical kinetics studies, *Prog. Energy Combust. Sci.* 44 (2014) 1-18.
- [24] D.G. Goodwin, R.L. Speth, H.K. Moffat, B.W. Weber, Cantera: An object-oriented software toolkit for chemical kinetics, thermodynamics, and transport processes. <https://www.cantera.org>, (2018). Version 2.4.0. doi:10.5281/zenodo.170284.
- [25] Reaction Design, CHEMKIN-Pro 18.2: San Diego, (2013).
- [26] E.E. Dames, A.S. Rosen, B.W. Weber, C.W. Gao, C.-J. Sung, W.H. Green, A detailed combined experimental and theoretical study on dimethyl ether/propane blended oxidation, *Combust. Flame* 168 (2016) 310-330.
- [27] V. Gururajan, F.N. Egolfopoulos, Direct sensitivity analysis for ignition delay times, *Combust. Flame* 209 (2019) 478-480.
- [28] Origin (Pro), version 8.5; OriginLab Corporation: Northampton, MA, USA, 2010.

Chapter 7: A comprehensive experimental and simulation study of ignition delay time characteristics of single fuel C₁ – C₂ hydrocarbons over a wide range of temperatures, pressures, equivalence ratios, and dilutions

Published in: Energy and Fuels, Volume 34, Issue 3, February 2020, Pages 3755–3771.
DOI : <https://doi.org/10.1021/acs.energyfuels.9b04139>

Author Contributions

- 1) Mohammadreza Baigmohammadi (National University of Ireland, Galway, Ireland)
Contribution: High pressure shock tube experiments and manuscript preparation.
- 2) Vaibhav Patel (National University of Ireland, Galway, Ireland)
Contribution: RCM experiments
- 3) Sergio Martinez (National University of Ireland, Galway, Ireland)
Contribution: Performed calculations, and chemical kinetic modelling.
- 4) Snehasish Panigrahy (National University of Ireland, Galway, Ireland)
Contribution: Chemical kinetic modelling.
- 5) Ajoy Ramalingam (PCFC, RWTH Aachen, Germany)
Contribution: RCM experiments.
- 6) Ultan Burke (National University of Ireland, Galway, Ireland)
Contribution: Chemical kinetic modelling.
- 7) Kieran P. Somers (National University of Ireland, Galway, Ireland)
Contribution: Chemical kinetic modelling.
- 8) Karl A. Heufer (PCFC, RWTH Aachen, Germany)
Contribution: Project management and manuscript review.
- 9) Andrzej Pekalski (Shell research limited, Shell Centre London)
Contribution: Project management as industrial sponsor and manuscript review.
- 10) Henry J. Curran (National University of Ireland, Galway, Ireland)
Contribution: Managed the project, made technical contributions and reviewed the project and manuscript throughout.

Abstract

A comprehensive experimental and modelling study of the ignition delay time (IDT) characteristics of some single prominent $C_1 - C_2$ hydrocarbons including methane, ethane, and ethylene have been performed over a wide range of temperatures ($\sim 800 - 2000$ K), pressures ($\sim 1 - 80$ bar), equivalence ratios ($\sim 0.5 - 2.0$), and dilutions ($\sim 75 - 90\%$). An extensive literature review was conducted, and available data were extracted to create a comprehensive database used in our simulations. Based on existing literature data, an experimental matrix was designed using the Taguchi approach (L_9) in order to identify and complete the experimental matrix required to generate a comprehensive validation set necessary for validation of a chemical kinetic model. The required IDTs were recorded using a high-pressure shock tube for shorter IDTs and a rapid compression machine for longer times, which encompass high- and low-temperature ranges, respectively. The predictions of a C^3 -NUIG mechanism have been compared with all of the available experimental data including those from the current study using the IDT simulations and the correlation technique. Moreover, individual and total effects of the studied parameters including pressure, equivalence ratio, and dilution on IDT have been studied over a wide temperature range. Moreover, correlations which were developed based on the NUIG mechanism are presented for each specific fuel over the conditions studied. These correlations show acceptable performance versus the experimental Taguchi matrix data.

7.1 Introduction

Developing high-fidelity chemical mechanisms based on a hierarchy or core-to-shell system is an efficient approach in developing large reliable chemical kinetic mechanisms, which can precisely describe the pyrolysis and/or oxidation processes of progressively larger hydrocarbons. This strategy can help researchers better understand these processes by recognising critical reactions and consumption pathways. In this way, the prominent reactions which control pyrolysis and oxidation processes can be recognised for relatively simple fuels (e.g., hydrogen-syngas, methane, ethane, etc.) up to very complex ones (e.g., gasoline, diesel). Ignition delay time (IDT) is one of the parameters which is extensively used to validate chemical mechanisms. Therefore, in this study, IDT is employed as the main criterion for evaluating the performance of C^3 -NUIG mechanism versus experimental data. This required the development of a comprehensive IDT database, which is used as target data in our simulations.

To develop this database an extensive literature review was performed, and available IDT data for single component methane [1-37], ethane [1, 11, 15, 18, 26, 32, 33, 35, 38-41] and ethylene [5, 42-49], mixtures were extracted and stored (Fig. 7-1). One can observe that although there is sufficient IDT data in the literature for methane mixtures, the available information at high temperatures (> 1000 K) for ethane and at low temperatures (< 1000 K) for ethane and ethylene is very limited (black solid spheres in Fig. 7-1). Therefore, in the present study new complementary experimental tests were defined for single fuel alkane/alkene+O₂+N₂+Ar mixtures (red solid spheres in Fig. 7-1) to encapsulate a wide range of temperatures, pressures, equivalence ratios, and dilutions. According to the available literature IDTs for C₁ – C₂ alkane–alkene mixtures, the IDT characteristics of most of these experimental points have not yet been reported. Moreover, as shown in Appendix E (Fig. ES1), although AramcoMech 3.0 [18] is a high-fidelity chemical kinetic model for larger hydrocarbons ($> C_2$), it could not properly predict some new IDTs taken in the study due to the fact that all available chemical models (some of them presented in Table ES1) have been developed based on available experimental data. Thus, adding new experimental IDT data to a developed database, especially under extreme conditions such as those for highly diluted fuel-lean mixtures at low temperatures (800 – 1000 K), permits the evaluation of the performance of available mechanisms at these more extreme conditions.

In the current study, the diluent (N₂ and Ar) concentrations are varied from 75% to 90% of the reactive mixtures. Also, three equivalence ratios of 0.5, 1.0, and 2.0 and four compressed mixture pressures (p_5 or p_C) of 1, 20, 40, and 80 bar (only for ethane in the low-temperature regime) have been chosen to encapsulate the proposed cubic matrix depicted in Fig. 7-1. In this regard, six data sets including 70 data points for ethylene ($p_C = 20$ and 40 bar; $\phi = 0.5, 1.0, \text{ and } 2.0$; dilution = 75, 85, and 90%) and eight data sets including 85 data points for ethane ($p_C = 20, 40, \text{ and } 80$ bar; $\phi = 0.5, 1.0, \text{ and } 2.0$; dilution = 75, 85, and 90%) were recorded in the present study. To efficiently cover a wide range of effective parameters (e.g., pressure, equivalence ratio, percentage dilution, and fuel composition), the experiments have been designed using the Taguchi method [1, 51]. Moreover, the temperature (T_5 or T_C) range was varied from ~ 800 – 2000 K based on the defined cases. Conducting the required experiments over the initial range of pressures, temperatures, equivalence ratios, and dilutions reported here provided data in the range which is not available in the literature. Furthermore, we present a chemical mechanism which can predict most of the experimental IDT data of various single fuel C₁ – C₂ mixtures over a wide range of operating conditions. Moreover, the selected

conditions over this wide range of working conditions mimics the physical conditions in many combustion-based systems including gas turbines and internal combustion engines. In this regard, the highly diluted cases could specifically resemble situations related to internal combustion engines with excessive exhaust gas recirculation or combustion chambers that work under the “mild” combustion regime [52].

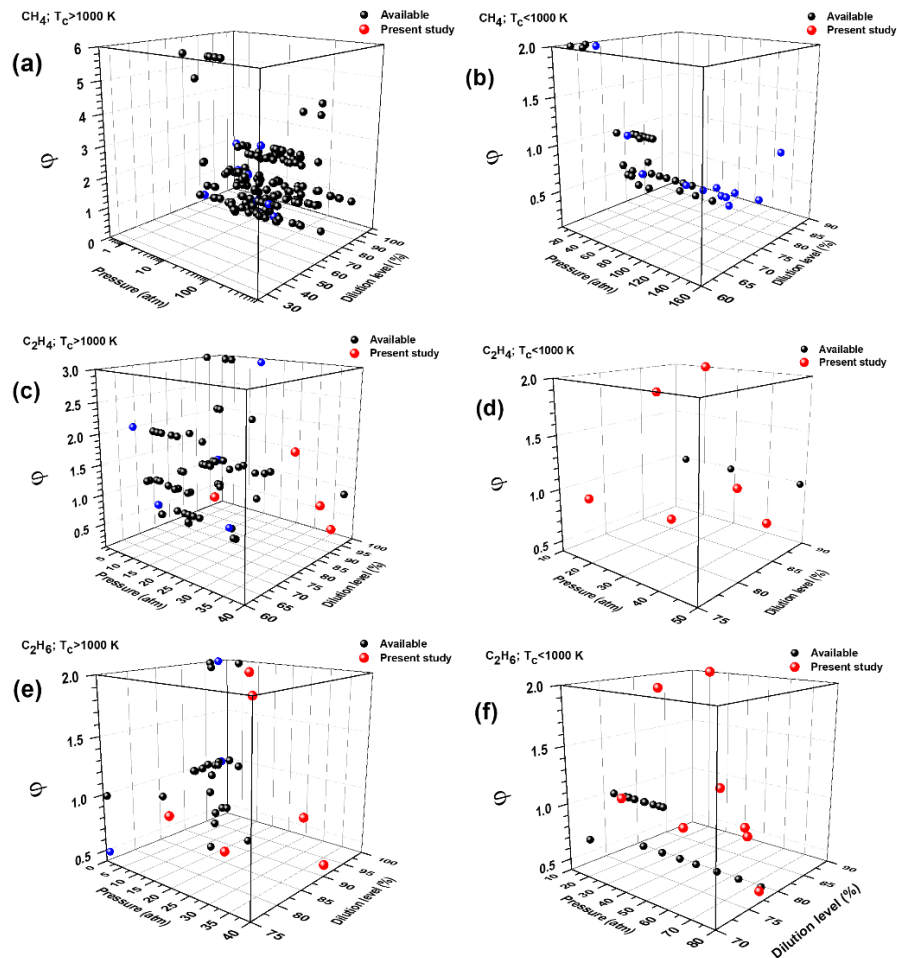


Figure 7-1. Extracted data from the studied literature (black spheres); the literature data used in the study (Table 7-1) (blue spheres); and new experimental tests defined in the current study (red spheres); T_c : the compressed gas mixture temperature.

7.2 Design of experiments and experimental approaches

Most experiments were conducted at NUI Galway using a high-pressure shock tube (HPST) and rapid compression machine (RCM). The data at 80 bar were recorded by the Physico-Chemical Fundamentals of Combustion (PCFC) group using the RCM facility at RWTH Aachen University. Both of these facilities were described previously [2, 11, 13, 18, 34, 53-55].

The experimental tests have been designed using an L₉ Taguchi matrix [19] for three variables of compressed pressures of 1, 20, and 40 bar, equivalence ratios of 0.5, 1.0 and 2.0, and dilutions of 75%, 85%, and 90%, respectively. Further details are provided in Section 2 of Appendix D. The details of the experimental tests considered here are listed in Table 7-1.

It was determined, (Fig. 7-1 and Table 7-1), that all of the defined experiments for methane have already been investigated, so there was no need for us to add experimental data to the database. However, those data marked by blue spheres in Fig. 7-1 have been applied in the study (except those under very high pressure, > 100 bar, and in the low temperature, < 1000 K, regime shown in Fig. ES80), as mentioned in Table 7-1. Furthermore, we have named all of the defined experimental datasets using a unique coding system to better reference our database. In this regard, “P” refers to the applied fuels in the study which are “1: methane”, “2: ethylene”, and “3: ethane”, respectively. However, “C” notation refers to the studied conditions which are changed from 1 to 9 in accordance to the change in pressure, equivalence ratio, and dilution.

Table 7-1. Test conditions defined in the current study.

No	Code	Mixture composition (mole fraction)					ϕ	T (K)	p (bar)	ref
		CH ₄	C ₂ H ₄	C ₂ H ₆	O ₂	N ₂ +Ar				
1	P1C1	0.05	0	0	0.2	0.0+0.75	0.5	1540–1820	0.849	Aul et al.[7]
2	P1C2	0.0951	0	0	0.1901	0.0+0.7148	1.0	1175–1480	24.318	Burke et al.[20]
3	P1C3	0.2	0	0	0.133	0.0+0.667	3.0	1335–1540	40.53	Petersen et al.[21]
4	P1C4	0.05	0	0	0.2	0.75+0.0	0.5	1250–1540	24.3	Burke et al.[20]
5	P1C5	0.0951	0	0	0.1891	0.7157+0.0	1.0	1000–1110	43.23	Burke et al.[20]
6	P1C6	0.01	0	0	0.01	0.0+0.98	2.0	1308–1348	0.85	Mathieu et al.[22]
7	P1C7	0.0499	0	0	0.1996	0.7505+0.0	0.5	1800–2160	44.53	Burke et al.[20]
8	P1C8	0.0067	0	0	0.0133	0.0+0.98	1.0	1238–1425	0.93	Mathieu et al.[22]
9	P1C9	0.174	0	0	0.174	0.0+0.652	2.0	1780–2160	24.32	Burke et al.[20]
10	P2C1	0	0.0338	0	0.2030	0.0+0.7632	0.5	1350–1565	1.0254	Gillespie[23]
11	P2C2	0	0.0625	0	0.1875	0.75	1.0	860–980	20	NUIG
12	P2C3	0	0.1	0	0.15	0.75	2.0	1065–1380	40	NUIG
13	P2C4	0	0.0338	0	0.2030	0.0+0.7632	0.5	770–1315	23.24	Kopp et al.[24]
14	P2C5	0	0.0214	0	0.1286	0.48+0.37	1.0	905–991	20	NUIG
15	P2C6	0	0.0375	0	0.1125	0.85	2.0	835–1335	40	NUIG
16	P2C7	0	0.1229	0	0.1843	0.6929+0.0	0.5	1125–1265	1.1	Kopp et al.[24]
17	P2C8	0	0.0143	0	0.0857	0.9	1.0	875–1515	40	NUIG
18	P2C9	0	0.005	0	0.015	0.0+0.98	3.0	1280–1820	1.159	Mathieu et al.[22]
19	P3C1	0	0.035	0	0.035	0.0+0.93	2.0	1040–1600	18.75	Saxena et al.[5]
20	P3C2	0	0.04	0	0.06	0.45+0.45	0.5	895–980	20	NUIG
21	P3C3	0	0	0.0313	0.2188	0.0+0.75	1.0	1190–1405	1.29	Aul et al.[7]
22	P3C4	0	0	0.056	0.194	0.75	2.0	890–1390	20	NUIG
23	P3C5	0	0	0.0909	0.1590	0.75	0.5	820–1350	40	NUIG
24	P3C6	0	0	0.0188	0.1313	0.85	1.0	930–1390	20	NUIG
25	P3C7	0	0	0.0333	0.1167	0.85	2.0	900–1390	40	NUIG
26	P3C8	0	0	0.001	0.0175	0.0+0.9725	0.5	1290–1820	1.0	de Vries et al.[25]
		0	0	0.0125	0.0875	0.9	1.0	900–1565	40	NUIG
		0	0	0.005	0.0175	0.0+0.9775	2.0	1233–1805	1.15	de Vries et al.[25]

27	P3C9	0	0	0.0364	0.0636	0.9	2.0	922–1695	20	NUIG
28	P3C10	0	0	0.0291	0.2039	0.3835+0.3835	0.5	864–962	80	RWTH Aachen ¹
29	P3C11	0	0	0.0566	0.1981	0.7453+0.0	1.0	848–927	80	RWTH Aachen

7.2.1 Setup and procedure

The current study has been divided into six distinct stages: 1, extensive literature review; 2, database development; 3, simulating the available literature data using available kinetic mechanisms; 4, defining new experimental tests using an L_9 Taguchi matrix; 5, performing the RCM and HPST experiments; and 6, simulating the new experimental data with the available mechanisms. It should be noted that although some low to moderate temperature range experimental IDT data for the fuels studied from RCMs are available in the literature, most cannot be simulated as the appropriate files necessary to simulate facility effects are not available. Therefore, we have repeated a limited number of previously reported literature experiments (e.g., see Fig. 7-1(f); $p_c = 20$ and 80 bar, $\phi = 0.5$ and 1.0, and dilution = 75%, respectively) to account for this gap in validation data. Comprehensive files are provided in the Supporting Information, including non-reactive traces, the original spreadsheets of experimental tests, HPST and RCM oscilloscope traces, and the combined plots of reactive, non-reactive, and modelling pressure traces. Moreover, all of the general information concerning the gases used in preparing the mixtures studied, with the applied facility and data acquisition system information to collect the IDT data, are provided in Appendix D.

7.2.2 Uncertainty analysis

A comprehensive uncertainty analysis of the data taken in both our HPST and RCM is provided in Appendix D with the outcomes briefly discussed here. These analyses try to explain the effect of specific parameters including pressure, temperature, and equivalence ratio on observed IDT measurements. The uncertainty analysis presented here was developed based on studies conducted by Petersen et al. [56] and Weber et al. [57]. The uncertainty of each experimental point changes in varying the temperature, pressure, and mixture composition, and is not identical for each experimental test. The average uncertainties in the compressed mixture temperatures (T_C or T_5) and measured IDTs are summarized in Table 7-2.

¹ Experimental data is measured at PCFC of RWTH Aachen University

Table 7-2. Average uncertainties for compressed mixture temperature (T_C or T_5) and measured IDTs.

Facility	$\sigma_{T_{C,5}}$ (K)	σ_{IDT} (%)
NUIG-HPST	± 20	± 25
NUIG-RCM	± 13	± 25

The analysis presented in the section is consistent with that presented by Mittal and Sung [58]. The uncertainty in the compressed temperature for the PCFC-RCM is estimated to be ± 5 K with an observed variation of less than 20% for the IDTs [34]. According to the literature [56, 59, 60], and also the conditions studied here, values of ± 20 K (HPST), $\pm 5 - 20$ K (RCM), and $\pm 25\%$ have been reported as the average uncertainties for both the compressed gas temperature (T_C) and the measured IDT, respectively, over the entire range of cases studied here.

7.3 Computational modelling

In the current study, an under-development comprehensive chemical mechanism NUIGMech0.9 was used to simulate the experimental targets. All of the experimental results have been simulated using a Python script based on the CANTERA [61] library (ST/RCM simulations) and also CHEMKIN-Pro 18.2 [62] software (RCM simulations). All simulations in both ST and RCM operating regimes are performed using the constant volume reactor model. However, the adiabatic constant volume reactor model for RCM simulations is modified by imposing a heat loss boundary condition on the calculations due to significant heat losses in the post-compression zone of the reaction chamber [2, 34, 63]. It is also assumed that the walls of the HPST and RCM are inert, so that the effect of surface reactions (heterogeneous reactions) [64] on measured IDTs is ignored in the simulations.

7.4 Results and discussion

In this section, all experimental results, whether taken from the literature or from the present study, are collected in the following plots in accordance to the applied fuels (methane, ethylene, and ethane) and the wide range of examined operating conditions. All experimental points are simulated using the chemical mechanism mentioned in Section 7.6.3 .

7.4.1 General performance of NUIG mechanism and the correlations versus experimental data

The performance of NUIGMech0.9 versus available IDT experimental data in the literature and the newly taken data in the present study for various methane, ethylene, and ethane mixtures are shown in Figs. 7-2–7-4. In all plots the symbols refer to the experimental data, and the black solid line refers to NUIGMech0.9 predictions. Also, the red dashed lines refer to the derived correlations which will be discussed later in section 7.6.4.3 . However, the red dashed line is altered to a blue line if one parameter (e.g., pressure or dilution) is out of the range of correlation, and it is changed to a blue dotted line if there are two parameters (e.g., pressure and dilution) out of the correlation range.

7.4.1.1 Methane

It is seen in Fig. 7-2 that NUIGMech0.9 predicts methane IDTs well. As seen in Fig. 7-2, the IDT data for methane at 1 bar is very sensitive to oxygen concentration over the temperature range studied, so that decreasing the oxygen mole fraction from 20% in Fig. 7-2(a) to 1% in Fig. 7-2(f) increases the IDT by over a factor of five due to the dominance of the main chain–branching reaction $\dot{H} + O_2 \leftrightarrow \ddot{O} + \dot{O}H$ in this temperature range ($T_C > 1540$ K). Also, Fig. 7-2 shows that, at lower temperatures ($T_C < 1000$ K), IDTs for methane oxidation reduce with increasing equivalence ratio and fuel concentration. This shows that, at lower temperatures, the concentration of fuel radical reactions governs reactivity. NUIGMech0.9 shows consistent agreement over the conditions examined at 24 bar (Fig. 7-2).

Moreover, Fig. 7-2 shows that decreasing the oxygen concentration in the mixtures increases the IDTs. These trends are reproduced well by NUIGMech0.9. Further evaluations (Fig. ES80) show that NUIGMech0.9 is not only able to predicts methane’s IDTs at low–to–moderate pressures and temperatures, but it can also reproduce methane’s IDTs at very high–pressure and low–temperature conditions [34, 36].

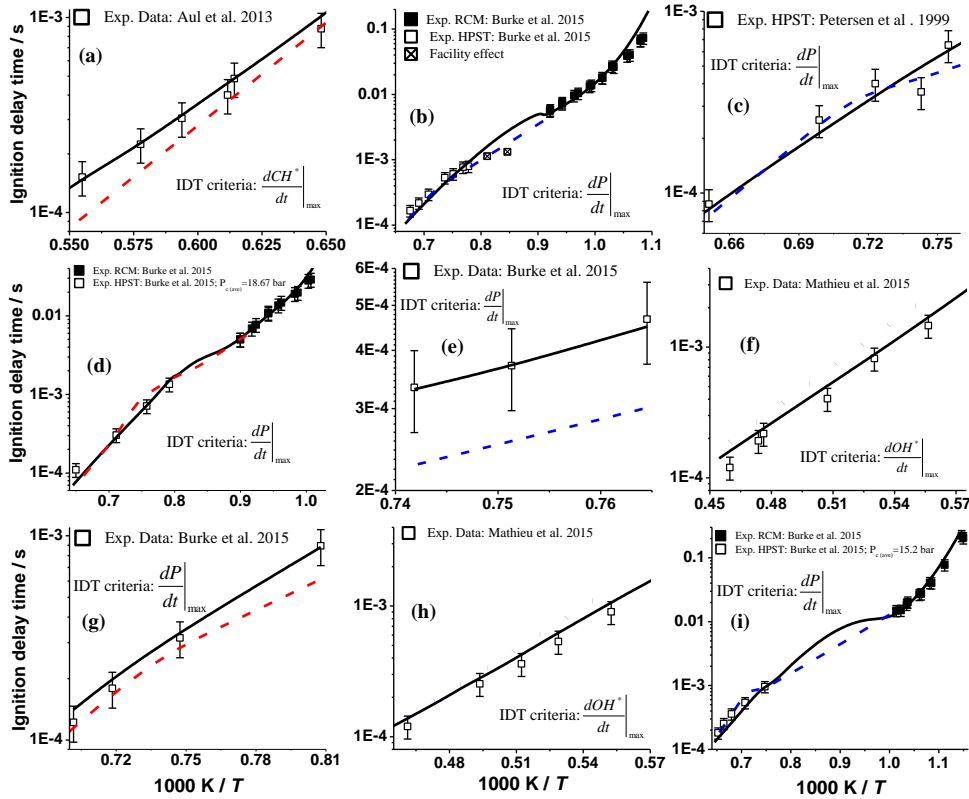


Figure 7-2. Available experimental and simulation data of methane’s IDT values for average compressed reactive mixture pressure (p_c): (a) $\phi = 0.5$, 75% Ar, 0.85 bar, P1C1; (b) $\phi = 1.0$, 71.48% Ar, 24.32 bar, P1C2; (c) $\phi = 2.0$, 66.7% Ar, 40.53 bar, P1C3; (d) $\phi = 0.5$, 75% N₂, 24.3 bar, P1C4; (e) $\phi = 1.0$, 71.57% N₂, 43.23 bar, P1C5; (f) $\phi = 2.0$, 98% Ar, 0.85 bar, P1C6; (g) $\phi = 0.5$, 75.05% N₂, 44.53 bar, P1C7; (h) $\phi = 1.0$, 98% Ar, 0.93 bar, P1C8; (i) $\phi = 2.0$, 65.2% Ar, 24.32 bar, P1C9.

7.4.1.2 Ethylene

The IDT characteristics for ethylene oxidation are shown in Fig. 7-3 over a wide range of pressures, temperatures, equivalence ratios, and dilutions together with simulations from NUIGMech0.9. Ethylene plays a significant role in the oxidation of heavy hydrocarbons [46], and its chemistry changes dramatically with varying conditions of pressure and fuel/O₂/diluent composition. Fig. 7-3 shows that the IDTs for ethylene mixtures are significantly shorter than those for methane at the same operating conditions. Similar to methane at 1 bar, reducing the oxygen concentration in the mixture increases IDTs. This trend is well captured by NUIGMech0.9. By increasing the compressed pressure to 20 bar, it is seen in Fig. 7-3(b), (d), (i) that NUIGMech0.9 best reproduces the experimental IDT results, particularly at low temperatures ($T_c < 1000$ K). By further increasing the compressed pressure to 40 bar (Figs. 7-3(c), (e), (g)), the IDTs significantly decrease in comparison to those at 20 bar.

NUIGMech0.9 captures the trends observed in the experimental IDTs, so that it shows a good performance over all the studied conditions, particularly at low temperatures.

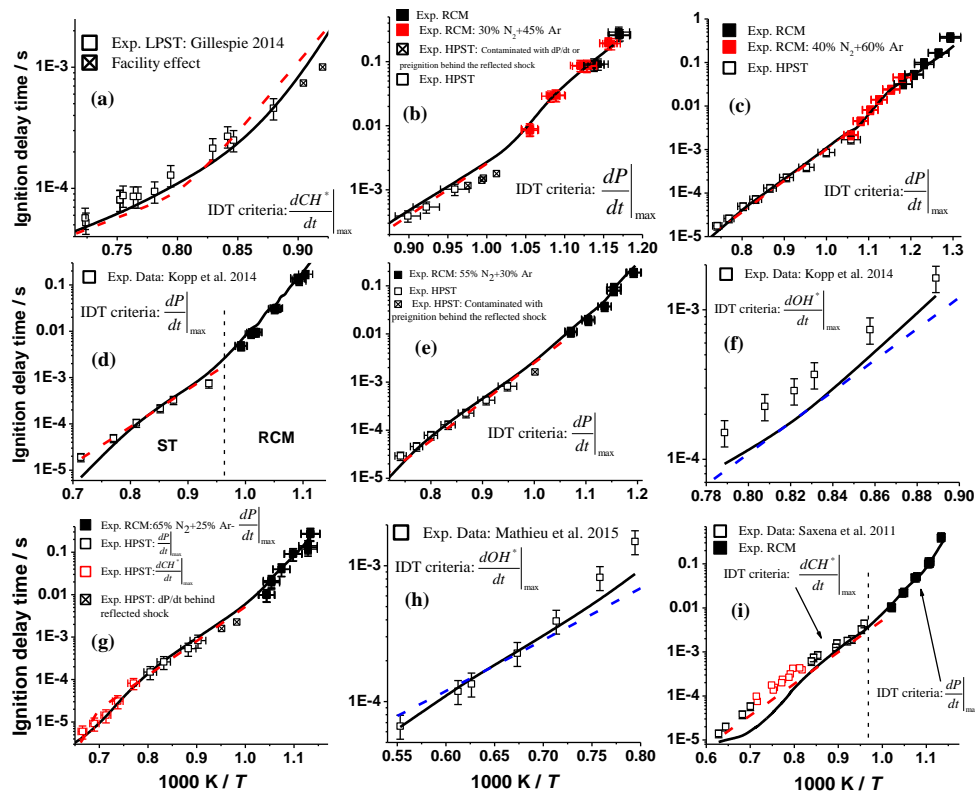


Figure 7-3. Available experimental and simulated data of ethylene’s IDT values at (a) $\phi = 0.5$, 76.32% N₂, 1.025 bar, P2C1; (b) $\phi = 1.0$, 75.0% N₂, 20 bar, P2C2; (c) $\phi = 2.0$, 75% N₂, 40 bar, P2C3; (d) (ST) $\phi = 0.5$, 76.32% N₂, 23.24 bar, (RCM) $\phi = 0.5$, 37% Ar + 48% N₂, 20 bar, P2C4; (e) $\phi = 1.0$, 10% Ar + 75% N₂, 40 bar, P2C5; (f) $\phi = 2.0$, 69.29% N₂, 1.1 bar, P2C6; (g) $\phi = 0.5$, 15% Ar + 75% N₂, 40 bar, P2C7; (h) $\phi = 1.0$, 98% Ar, 1.16 bar; P2C8; (i) (ST) $\phi = 3.0$, 93% Ar, 18.75 bar, (RCM) $\phi = 2.0$, 45% Ar + 45% N₂, 20 bar, P2C9.

7.4.1.3 Ethane

Understanding fully the combustion chemistry of ethane is very important, as it can be a significant component of natural gas. Thus, the ignition characteristics of various ethane mixtures were also studied over a wide range of pressures, temperatures, equivalence ratios, and dilutions. The performances of NUIGMech0.9 versus the experimental IDT data are summarized in Fig. 7-4. Fig. 7-4(a), (f), (h) shows that, for the same oxygen concentration, the IDTs for ethane mixtures lie between those for methane and ethylene. As seen again, NUIGMech0.9 can reasonably predict the experimental results at 1 bar.

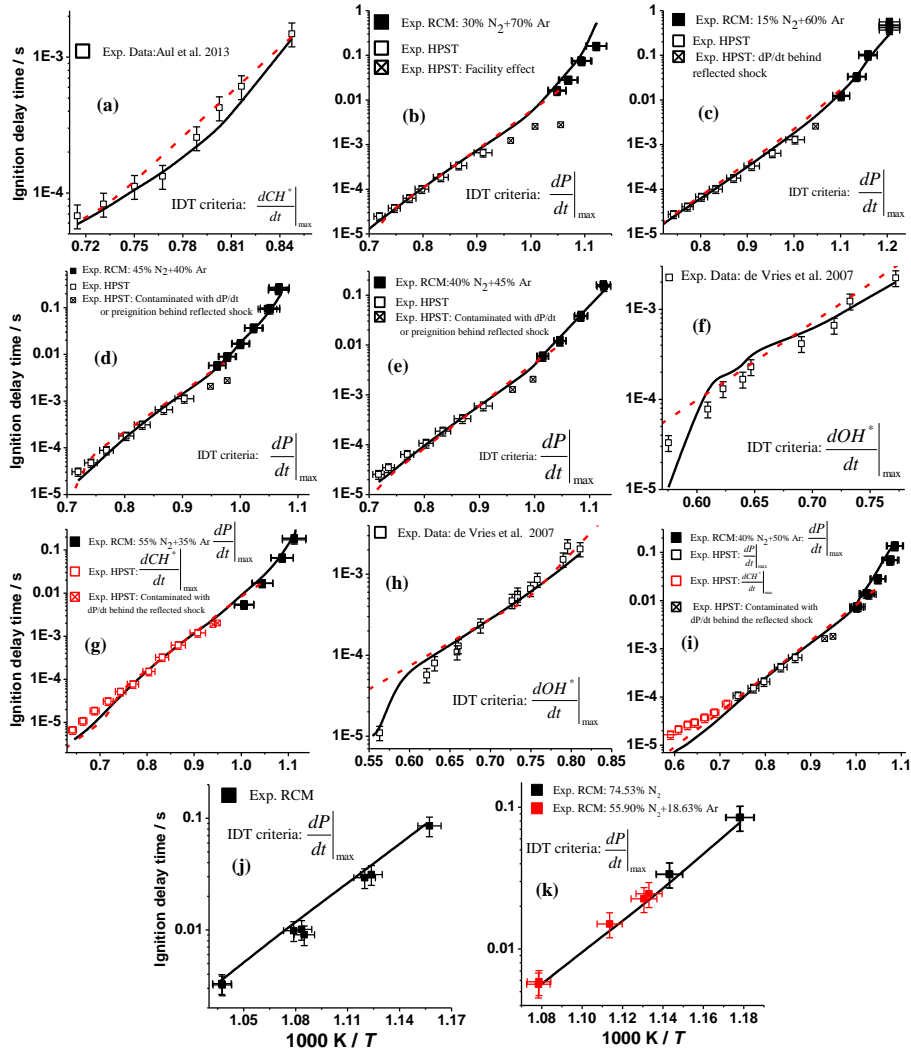


Figure 7-4. Available experimental and constant volume simulation data for ethane oxidation at (a) $\phi = 0.5$, 75% Ar, 1.31 bar, P3C1; (b) $\phi = 1.0$, 75% N₂, 20 bar, P3C2; (c) $\phi = 2.0$, 75% N₂, 40 bar, P3C3; (d) $\phi = 0.5$, 75% N₂, 10% Ar, 20 bar, P3C4; (e) $\phi = 1.0$, 75% N₂, 10% Ar, 40 bar, P3C5; (f) $\phi = 2.0$, 97.25% Ar, 0.98 bar, P3C6; (g) $\phi = 0.5$, 75% N₂, 15% Ar, 40 bar, P3C7; (h) $\phi = 1.0$, 97.75% Ar, 1.17 bar, P3C8; (i) $\phi = 2.0$, 75% N₂, 15% Ar, 20 bar, P3C9; (j) $\phi = 0.5$, 38.35% Ar, 38.35% N₂, 80 bar, P3C10; (k) $\phi = 1.0$, 80 bar, P3C11.

By increasing the compressed mixture pressure to 20 bar in Fig. 7-4(b), (d), (i) we see that the experimental IDTs decrease at high temperatures (> 1000 K). Moreover, there is no sensible effect on IDT with changes in equivalence ratio due to the simultaneous variations in oxygen and diluent concentrations. However, there is a positive dependence of fuel concentration and a negative dependence of the diluent on measured IDTs at temperatures below 1000 K. The individual and combined effects of these parameters on the IDTs will be discussed in detail later in the following sections. Fig. 7-4(b), (d), (i) also shows that NUIGMech0.9 can reproduce the experimental IDTs.

Furthermore, as shown in Fig. 7-4(c), (e), (g) elevating the pressure for ethane oxidation to 40 bar decreases the measured IDTs compared to those at 20 bar. In the low temperature regime (< 1000 K) in Fig. 7-4(c), (e), (g) it is observed that increasing the compressed pressure in tandem with fuel concentration and simultaneously reducing the diluent concentration has a significant effect in decreasing the measured IDTs. It can be inferred from Fig. 7-4(c), (e), (g) that increasing the fuel concentration, by increasing the equivalence ratio, in tandem with decreasing the diluent concentration significantly affects the measured IDTs over the entire range of the conditions studied. Figure 7-4(c), (e), (g) also demonstrates that NUIGMech0.9 is able to reasonably predict the experimental IDTs for the conditions studied.

Moreover, increasing the compressed pressure to 80 bar at low temperatures (RCM data) leads to a significant decrease in measured IDTs, compared to those at 20 and 40 bar (Figs. 7-4(j), (k)). Figure 7-4(k) also shows that, in the low temperature regime, increasing the equivalence ratio to $\phi = 1.0$ leads to a decrease in measured IDTs, compared to the measurements at $\phi = 0.5$, Fig. 7-4(j). It is shown that NUIGMech0.9 can acceptably reproduce the IDTs.

7.4.1.4 Performance of NUIGMech0.9 for predicting laminar burning velocity and chemical speciation

Although evaluating the performance of NUIGMech0.9 in predicting laminar burning velocity (LBV) and chemical speciation measurements is not the main target of the current study, some information in this regard is presented in Appendix E (Figs. ES81 – ES86). As seen in Figs. 7-2 – 7-4 and ES81 – 86, NUIGMech0.9 can reasonably predict all IDTs, LBVs, and chemical speciations, while AramcoMech 3.0 fails to predict IDTs of ethylene mixtures at low-temperature regime as well as NUIGMech0.9 (Fig. ES1). This difference almost stems from high fidelity and optimised low-temperature chemistry of NUIGMech0.9, especially those reactions which control IDT predictions. Moreover, when comparing the performance of AramcoMech 3.0 with NUIGMech0.9 on LBVs (Figs. ES84 and ES85), it can be observed that NUIGMech0.9 slightly over predicts LBVs of ethylene and ethane.

7.4.2 Individual and combined effects of the studied parameters on IDT

The general performance of NUIGMech0.9 and its fidelity for predicting the IDTs of various $C_1 - C_2$ single fuel mixtures over a wide range of the studied conditions has been demonstrated. According to the nature of the applied Taguchi approach in designing the experiments, which makes it possible

to populate the experimental points over a wide range of conditions which have never been studied before and simultaneously reduce the required tests, it is not possible to experimentally consider the effect of each individual parameter (pressure, equivalence ratio, and dilution) on the IDT characteristics of the studied fuels due to multiple parameters changing from case to case. Therefore, these effects can be considered using NUIGMech0.9, showing its fidelity for reproducing the stochastically distributed experimental IDTs in Section 7.7.4.1 . Thus, the individual and combined effects of temperature, pressure, equivalence ratio and dilution on the IDTs of the studied mixtures are considered in detail with a focus on the experimental data taken in the current study and NUIGMech0.9 performance (Fig. 7-5). In considering the effect of each individual parameter on IDTs, several constant volume adiabatic simulations have been performed using NUIGMech0.9 over the conditions studied. In this regard, the P2C2 and P3C2 ($\phi = 1.0$, $p_C = 20$ bar, dilution = 75%) mixture conditions are chosen as the base cases. For instance, if we want to study the effect of equivalence ratio on the measured IDTs for ethylene, we only perturb the equivalence ratio to 0.5 and 2.0 in the P2C2 case, so that the other parameters remain constant. The same procedure is followed for the other parameters. Therefore, the effect of each parameter on the IDTs over the studied temperature range (750 – 1700 K) is calculated as follows:

$$IDT \text{ ratio} = \frac{IDT|_{\phi, p_C, dilution, PxCy}}{IDT|_{PxC2}} \quad (7-1)$$

Where x is 2 and 3 and y is 3 – 11, respectively. Thus, when the IDT ratio is unity, it means that there is no change in IDT value corresponding to the perturbed parameter(s).

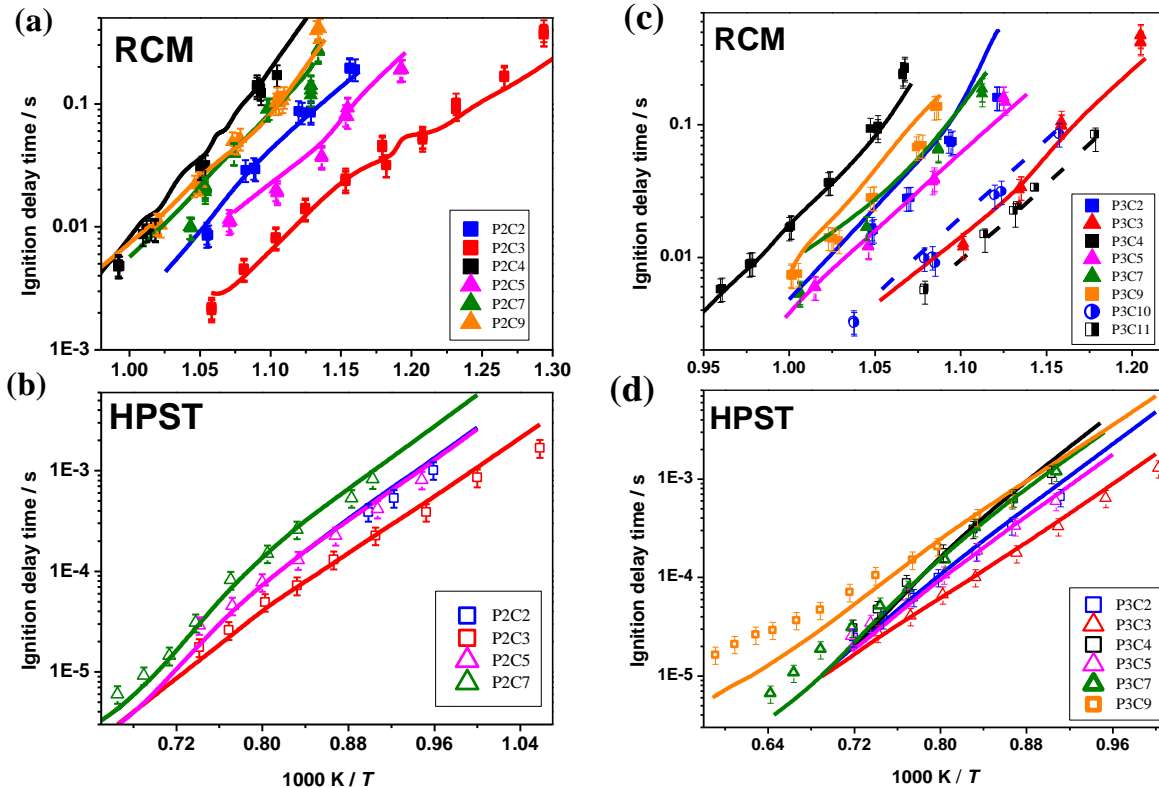


Figure 7-5. Experimental and simulation (NUIGMech0.9) IDT data. (a, b) Ethylene: (P2C2) $\phi = 1.0$, 75% N₂, 20 bar; (P2C3) $\phi = 2.0$, 75% N₂, 40 bar; (P2C4) $\phi = 0.5$, 37% Ar + 48% N₂, 20 bar; (P2C5) $\phi = 1.0$, 10% Ar + 75% N₂, 40 bar; (P2C7) $\phi = 0.5$, 15% Ar + 75% N₂, 40 bar; (P2C9) $\phi = 2.0$, 45% Ar + 45% N₂, 20 bar. (c, d) Ethane: (P3C2) $\phi = 1.0$, 75% N₂, 20 bar; (P3C3) $\phi = 2.0$, 75% N₂, 40 bar; (P3C4) $\phi = 0.5$, 75% N₂ + 10% Ar, 20 bar; (P3C5) $\phi = 1.0$, 75% N₂ + 10% Ar, 40 bar; (P3C7) $\phi = 0.5$, 75% N₂ + 15% Ar, 40 bar; (P3C9) $\phi = 2.0$, 75% N₂ + 15% Ar, 20 bar; (P3C10) $\phi = 0.5$, 38.35% Ar + 38.35% N₂, 80 bar; (P3C11) $\phi = 1.0$, 80 bar.

7.4.2.1 Ethylene

The individual and combined effects of the studied parameters on ethylene's IDTs are shown in Figs. 7-6 and ES87. In fact, these effects on IDTs in Fig. ES87 are enlarged and more pronounced in Fig. 7-6 in accordance to Eqn. 7-1. It is observed that the effect of each parameter on the IDTs changes quantitatively (Fig. ES87) and qualitatively (Fig. 7-6) over the temperature range, so that some parameters control the pattern of the IDTs, while others control the quantity of IDTs with temperature.

7.4.2.1.1 Effect of pressure

It can be seen in Fig. 7-6(a), (c), (d) that increasing the pressure from 20 to 40 bar has a non-monotonic effect on the reactivity with temperature. On the one hand, increasing the temperature from 750 K to 1350 K leads to a decrease in the effect of pressure on reactivity, so that this effect is negligible at 1380 K. On the other hand, this trend is reversed at temperatures higher than 1380 K, so

that increasing pressure leads to an increasing reactivity with associated shorter IDTs. According to the sensitivity and flux analyses demonstrated in Figs. ES89 and ES90, respectively, the ascending–descending effect of pressure on the IDT in the determined zone in Fig. 7-6(a) stems from a competition between promoting and suppressing the prominent reactions shown in Fig. ES89. As seen in Fig. ES90, increasing the pressure significantly intensifies the net flux of the vital reactions in comparison to the baseline case, so that increasing the pressure by a factor of two elevates the net fluxes on average by a factor of 3.5. As seen, by increasing the temperature from 1177 K to 1370 K, although there is a reduction in the number of critical promoting reactions, $C_2H_4 + \dot{H} \leftrightarrow \dot{C}_2H_5 (+M)$, $\dot{C}_2H_3 + O_2 \leftrightarrow CH_2O + H\dot{C}O$, and $C_2H_4 + \dot{O} \leftrightarrow \dot{C}H_3 + H\dot{C}O$ are dominant. The inhibiting reactions can sensibly decrease the mixture reactivity. One can see that, by increasing the temperature beyond 1370 K, $\dot{H} + O_2 (+M) \leftrightarrow H\dot{O}_2 (+M)$ is the most vital inhibiting reaction which can govern IDT in competition with the three main promoting reactions.

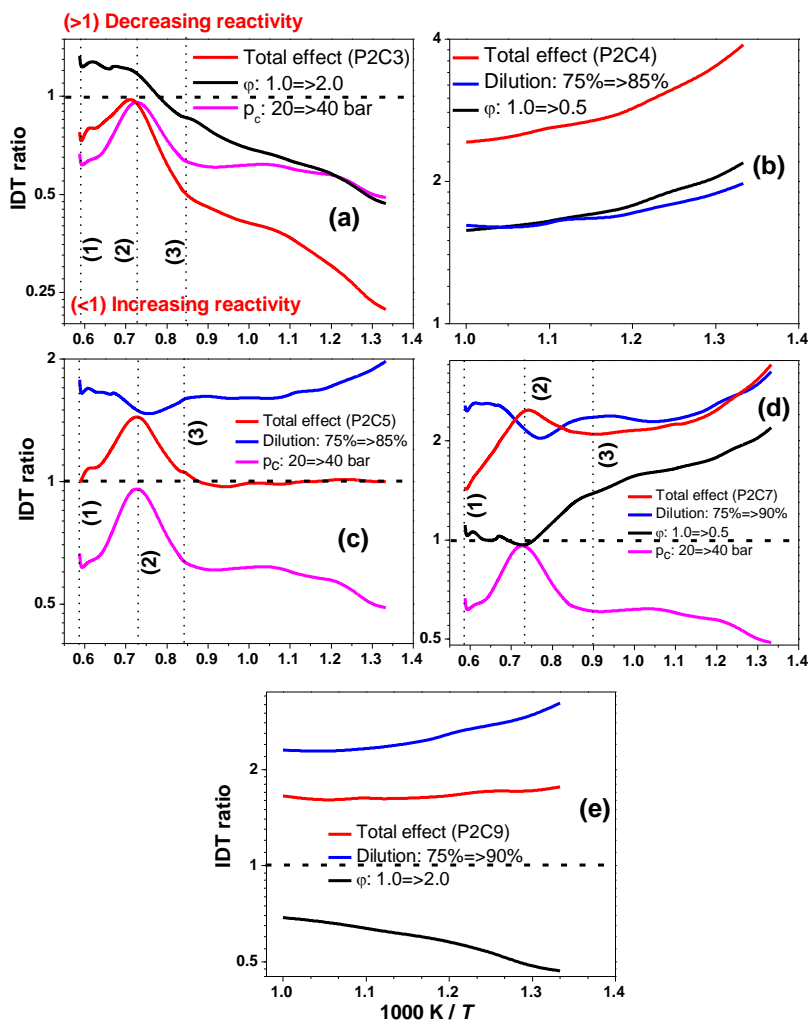


Figure 7-6. Constant volume adiabatic simulations of individual and combined effects of pressure, equivalence ratio, and dilution on variations of IDTs for ethylene (Eqn. 7-1) (y-axis is in \log_2 scale); dashed line (1): 1700 K, dashed line (2): 1370 K, and dashed line (3): 1177 K (1112 K at Fig. 7-6(d)).

7.4.2.1.2 Effect of equivalence ratio

Figures 7-6(a), (b), (d), (e) show that increasing the equivalence ratio to 2.0 has a monotonic effect on increasing the IDT with increasing temperatures from 750 K to 1700 K, while decreasing the equivalence ratio to 0.5 has a mixed effect on the reactivity. As seen in Fig. 7-6(d), although decreasing the equivalence ratio to 0.5 makes the reactivity very sensitive to gradients in temperature in the range 750–1350 K, its effect is minor at temperatures higher than 1350 K.

From the flux analyses, increasing the equivalence ratio suppresses the vital chain branching reaction $\dot{H} + O_2 \leftrightarrow \dot{O} + \dot{OH}$ by about 23% at 1700 K, while there is no significant change in the fluxes of the other important reactions shown in Fig. ES91 in comparison to the baseline case. However, as shown in Fig. ES92, increasing the equivalence ratio promotes the reaction $\dot{C}_2H_3 + \dot{H} \leftrightarrow C_2H_2 + H_2$

at 1700 K which inhibits reactivity. Interestingly, Fig. ES92 shows that increasing or decreasing the equivalence ratio from the stoichiometric condition intensifies the chain propagation reaction of $C_2H_4 + \ddot{O} \leftrightarrow \dot{C}H_2 + CH_2O$ instead of the chain branching reaction of $C_2H_4 + \ddot{O} \leftrightarrow \dot{C}H_2CHO + \dot{H}$ at 1700 K. All of these effects reduce the reactivity of the fuel-rich ethylene mixture at 1700 K in Fig. 7-6(a).

By reducing the temperature to 1370 K, Fig. 7-6(a), it is seen in Fig. ES91 that increasing the equivalence ratio intensifies the net fluxes of reactivity promoting reactions: $C_2H_4 + \dot{H} \leftrightarrow \dot{C}_2H_3 + H_2$, $C_2H_4 + H\dot{O}_2 \leftrightarrow \dot{C}_2H_3 + H_2O_2$, $\dot{C}_2H_3 + O_2 \leftrightarrow \dot{C}H_2CHO + \ddot{O}$. However, increasing the equivalence ratio at 1370 K promotes $\dot{C}_2H_3 + O_2 \rightarrow CH_2O + \ddot{C}O + \dot{H}$ instead of $C_2H_4 + \ddot{O} \leftrightarrow \dot{C}H_3 + H\dot{C}O$ and, simultaneously, intensifies the net fluxes of some important reactivity inhibiting reactions of $C_2H_4 + \dot{H} (+M) \leftrightarrow \dot{C}_2H_5 (+M)$ and $\dot{C}_2H_3 + O_2 \leftrightarrow CH_2O + H\dot{C}O$. An accumulative effect of these changes makes ethylene slightly more reactive in comparison to 1700 K. The sensitivity and flux analyses at $\varphi: 2.0$ and 1177 K (Fig. 7-6(a) show that increasing the equivalence ratio promotes the $\dot{C}_2H_3 + O_2 \leftrightarrow C_2H_3O\ddot{O}$ reaction instead of $\dot{H} + O_2 (+M) \leftrightarrow H\dot{O}_2 (+M)$ and significantly intensifies the net fluxes of some important reactivity promoting reactions of $\dot{C}_2H_3 + O_2 \leftrightarrow \dot{C}H_2CHO + \ddot{O}$, $\dot{H} + O_2 \leftrightarrow \dot{O} + \dot{O}H$, $C_2H_4 + H\dot{O}_2 \leftrightarrow C_2H_4O_{1-2} + \dot{O}H$, and $C_2H_4 + H\dot{O}_2 \leftrightarrow \dot{C}_2H_3 + H_2O_2$ at this temperature. However, this increase in equivalence ratio also promotes the net fluxes of some inhibiting reactions, including $\dot{C}_2H_3 + O_2 \rightarrow CH_2O + \ddot{C}O + \dot{H}$, $C_2H_4 + \dot{H} (+M) \leftrightarrow \dot{C}_2H_5 (+M)$, $\dot{C}_2H_3 + O_2 \leftrightarrow CH_2O + H\dot{C}O$, and $\dot{C}_2H_3 + O_2 \leftrightarrow C_2H_3O\ddot{O}$.

Furthermore, decreasing the equivalence ratio to 0.5 at 1112 K promotes the reaction $\dot{H} + O_2 (+M) \leftrightarrow H\dot{O}_2 (+M)$ over $C_2H_4 + \dot{H} (+M) \leftrightarrow \dot{C}_2H_5 (+M)$ and significantly reduces the net fluxes of all of the important reactions, especially the two most promoting reactions $\dot{C}_2H_3 + O_2 \leftrightarrow \dot{C}H_2CHO + \ddot{O}$ and $\dot{H} + O_2 \leftrightarrow \dot{O} + \dot{O}H$. These effects reduce the mixture reactivity. By increasing the temperature to 1370 K, the net fluxes of all of the important reactions, whether promoting or inhibiting, are increased by a factor of 2.5 which increases mixture reactivity. Unlike the fuel-rich condition, decreasing the equivalence ratio at 1370 K promotes the reaction $C_2H_4 + \ddot{O} \leftrightarrow \dot{C}H_2CHO + \dot{H}$ and simultaneously suppresses the reaction $C_2H_4 + \dot{H} \leftrightarrow \dot{C}_2H_3 + H_2$ due to the abundance of oxygen in the mixture. Although all of the fluxes are still lower than those for the baseline condition, the mixture reactivity is balanced by a simultaneous increase in the net fluxes of both reactivity promoting and suppressing reactions, specifically $\dot{H} + O_2 \leftrightarrow \dot{O} + \dot{O}H$ and $\dot{H} + O_2 (+M) \leftrightarrow H\dot{O}_2 (+M)$, so that there is no change in reactivity of the mixture in comparison to the baseline case. As seen in Fig. 7-6(d), further increasing the temperature to 1700 K at the fuel-lean condition has no effect on reactivity in

comparison to the baseline case. Fig. ES92 shows that decreasing the equivalence ratio at this temperature promotes the reaction $C_2H_4 + \ddot{O} \leftrightarrow \dot{C}H_2 + CH_2O$ and suppresses $\dot{C}H_2CHO \leftrightarrow \dot{C}H_3 + \ddot{C}O$ in comparison to the base condition. It is seen in Fig. ES91 that increasing the temperature to 1700 K for the fuel-lean condition intensifies the net fluxes of all of the important reactions by a factor of 1.6 in comparison to 1370 K, so that the normalized net fluxes of some vital reactions such as $\dot{H} + O_2 \leftrightarrow \dot{O} + \dot{O}H$, $\dot{H} + O_2 (+M) \leftrightarrow H\dot{O}_2 (+M)$, $H\dot{C}O + O_2 \rightarrow \ddot{C}O + H\dot{O}_2$ are close to unity, which means that there is no appreciable effect on reactivity of the mixture at the temperature.

7.4.2.1.3 Effect of dilution

As expected, increasing dilution results in a decrease in reactivity. However, this effect is not monotonic with temperature. Figure 7-6(c), (d) shows that increasing the dilution to 85% and 90% increases the IDTs by approximately 63% and 141%, respectively. This sensitivity is very significant at temperatures below 1000 K. In this regard, it can be seen in Fig. ES93 that increasing the dilution level significantly suppresses the net fluxes of all the important reactions listed in Fig. ES94, so that increasing the dilution level from 75% to 85% and from 85% to 90% decreases the net fluxes by a factor of two on average, respectively. However, as shown in Fig. ES94, its effect on the patterns of the 10 most prominent reactions is limited to a few reactions. Fig. ES94 shows that increasing the dilution level to 85% promotes the $H\dot{C}O (+M) \rightarrow \ddot{C}O + \dot{H} (+M)$ reaction at 1370 K, and simultaneously suppresses only $C_2H_4 + \ddot{O} \leftrightarrow \dot{C}H_3 + H\dot{C}O$ at 1370 K. However, increasing the dilution level to 90% in Fig. ES94 promotes $\dot{C}_2H_3 + O_2 \leftrightarrow C_2H_3O\dot{O}$ reaction at 1112 K and suppresses $\dot{H} + O_2 (+M) \leftrightarrow H\dot{O}_2 (+M)$ (at 1112 K), $C_2H_4 + \ddot{O} \leftrightarrow \dot{C}H_3 + H\dot{C}O$, and $\dot{C}_2H_3 + O_2 \leftrightarrow CH_2O + H\dot{C}O$ (at 1370 K).

7.4.2.1.4 Combined effects

Figure 7-6 shows that there is a turning point on the temperature axis where the qualitative effect of each parameter on the reactivity of the ethylene mixtures changes. This turning temperature lies between 1330–1350 K. As seen in Fig. 7-6(a), the combined effect of increasing both the equivalence ratio and the pressure follows the pressure pattern, particularly at temperatures higher than 1250 K, while it seems that the combined effect almost follows the equivalence ratio pattern at temperatures below 1250 K. Moreover, as demonstrated in Figs. 7-6(a), (b) if the individual effects of parameters on the reactivity behave in the same way, their combined effect is synergetic in increasing or

decreasing the reactivity of the new condition (e.g., P2C2→P2C3 and P2C2→P2C4 in Fig. 7-6). Similar to Fig. 7-6(a), one can see in Fig. 7-6(c) that the total effect of increasing both the pressure and the dilution follows the pattern for pressure over the temperature range studied. As discussed in sub-section 7.4.2.1.3, increasing the dilution level almost affects (reduces) the net fluxes of the important reactions, so that its effect on the pattern of the top ten most important reactions is minor. As seen in Fig. 7-7 and Figs. ES95 and ES96, it is understood that the normalized net fluxes at each temperature stem from the following rough correlation:

$$NnF_i(P2Cx) \approx NnF_{i,D} \times NnF_{i,P} \times NnF_{i,\varphi} \quad (7-2)$$

where, NnF_i , D , p , and φ refer to the normalized net flux of each specific (i -th) reaction, dilution effect, pressure effect, and equivalence ratio effect, respectively. According to the above formulation and also the above discussion about the effect of dilution, one can conclude that the reactivity pattern of P2C5 (Fig. ES96) case over the studied temperature range in Fig. 7-6(c) stems from the effect of pressure on the reactivity/chemistry pattern of the studied mixture which is suppressed by a factor of 0.39, 0.31, and 0.23 at 1700 K, 1370 K, and 1177 K, respectively.

As seen in Fig. ES97, the combined effect of pressure, dilution, and equivalence ratio brings chain propagating reaction of $\dot{C}H_3 + H\dot{O}_2 \leftrightarrow CH_3\dot{O} + \dot{O}H$ into the top ten most important reactions at 1370 K, which is not among the first 10 important reactions in the sensitivity analysis of each individual effect. Although Fig. 7-6(d) shows that the increasing pressure almost promotes reactivity over the studied temperature range, it is seen that the reactivity pattern of P2C7 in comparison to the P2C2 condition follows a specific pattern which comes from a combination between the decreasing equivalence ratio (1→0.5) and the increasing dilution (75%→90%) patterns over the temperature range 750 – 1325 K due to the synergy of these effects on decreasing the reactivity of P2C7. This behaviour implies that the deficient fuel concentration and the abundant third-body effects are controlling the reactivity of the P2C7 mixture in comparison to the P2C2 base condition in the temperature range 750 – 1325 K. However, one can see in Fig. 7-6(d) that this trend seems to be surpassed by the effect of increasing pressure on increasing reactivity in the temperature range 1325 – 1700 K, so that the P2C7 pattern within temperature range of 1325 – 1700 K follows the pressure pattern.

Furthermore, Fig. 7-6(e) shows how the promoting effect of the equivalence ratio on the reactivity is balanced by the inhibiting effect of dilution in the low-temperature regime, so that the reactivity of combined case (P2C9) is almost constant over low-temperature regime.

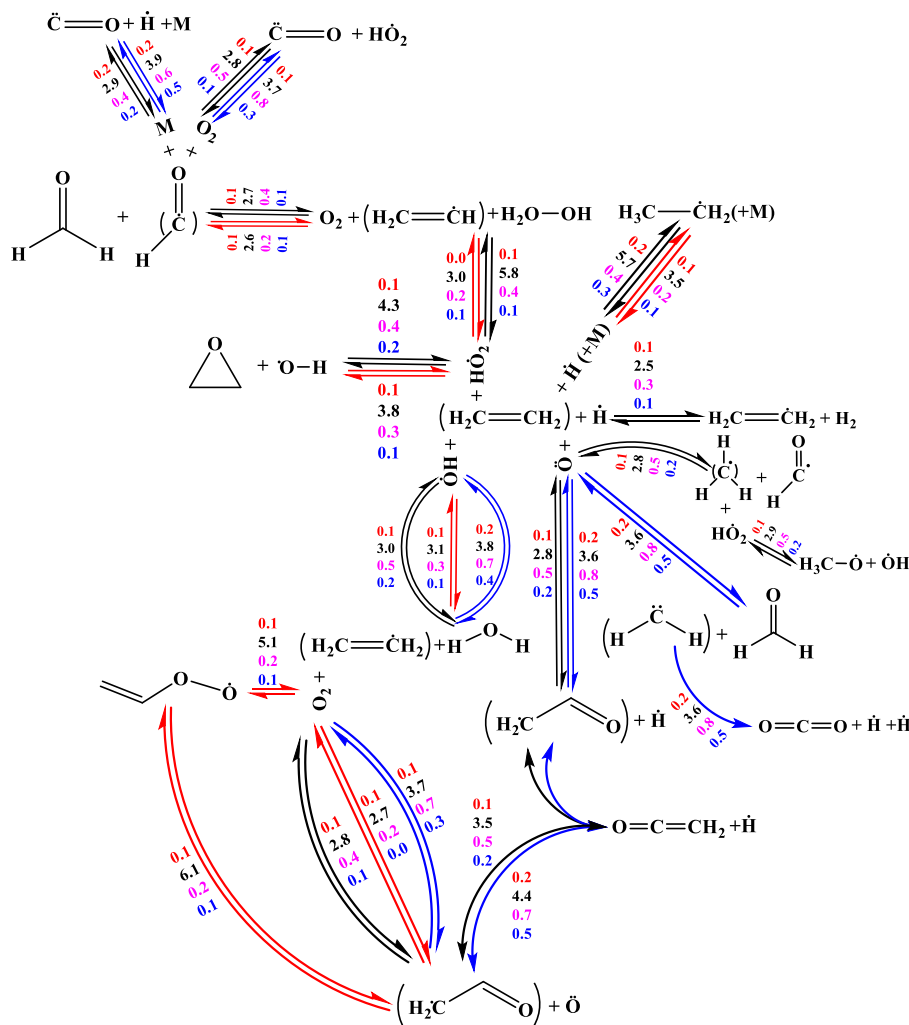


Figure 7-7. Normalized flux analysis (based on the flux analysis of P2C2 base case when 20% of ethylene is consumed) of some important reactions corresponding to Fig. 7-6(d). Blue lines: case (1), $T_C = 1700$ K. Black lines: case (2), $T_C = 1370$ K. Red lines: case (3), $T_C = 1112$ K. Red numbers: effect of dilution. Black numbers: effect of pressure. Magenta numbers: effect of equivalence ratio. Blue numbers: combined effects.

7.4.2.2 Ethane

The individual and combined effects of the studied parameters on the ethane's simulated IDTs are shown in Fig. 7-8 and ES88. Similar to the ethylene case, the effect of each parameter on the IDTs is changing quantitatively and qualitatively over the temperature range and certain parameters control the mixture reactivity in terms of pattern and quantity.

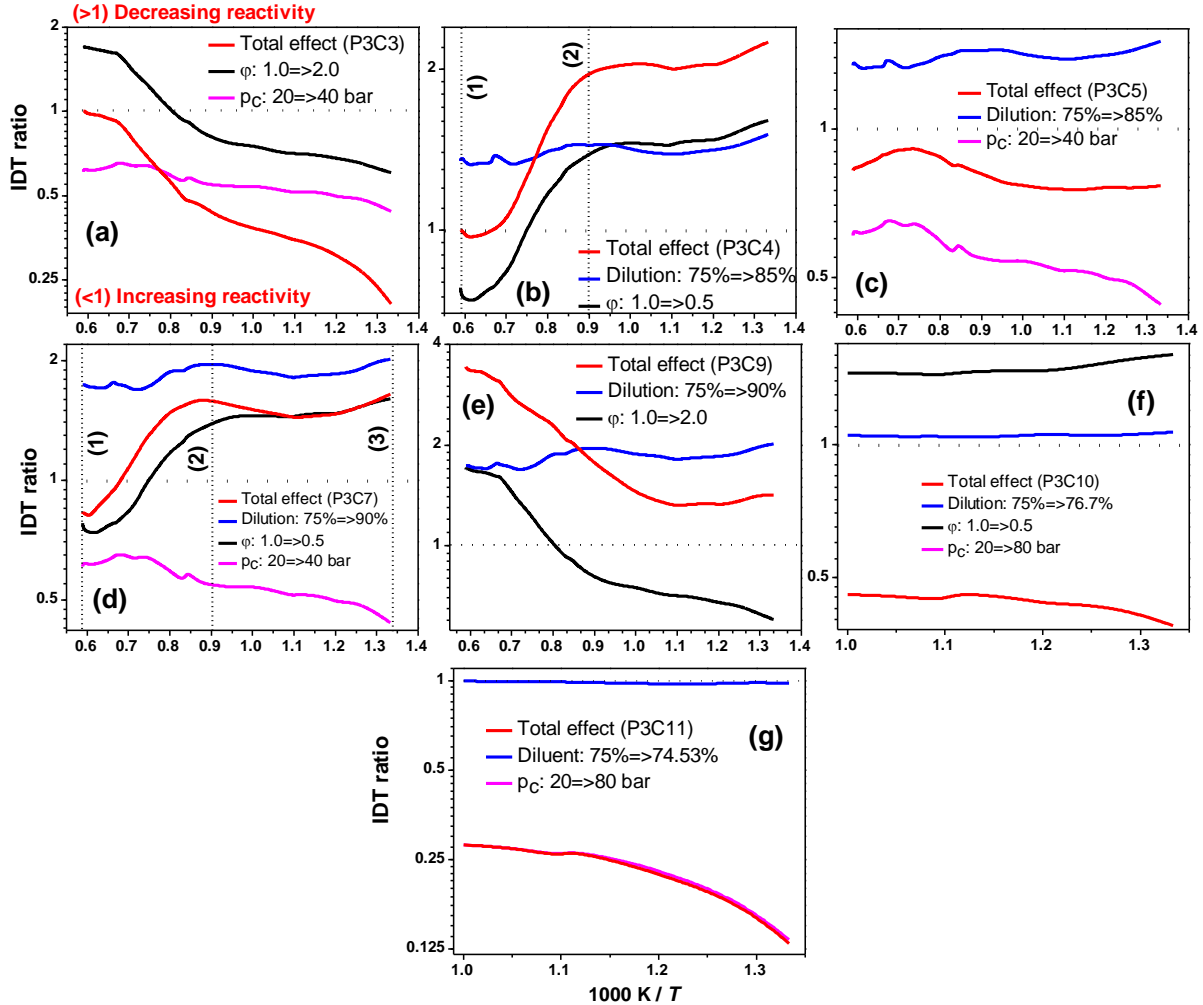


Figure 7-8. Constant volume adiabatic simulation of individual and combined effects of pressure, equivalence ratio, and dilution on variations IDTs for ethane (Eqn. 7-1) (y-axis is in log₂ scale). Dashed line (1): 1700 K. Dashed line (2): 1112 K. Dashed line (3): 750 K.

7.4.2.2.1 Effect of pressure

As seen in Fig. 7-8, unlike the ethylene case, pressure has almost a monotonic effect on the IDTs, so that its effect significantly promotes the reactivity over the temperature range. However, a kind of decreasing effect can be seen over the temperature range (Fig. 7-8(a), (c), (d)) so that the promoting effect of the pressure rise on the reactivity of ethane's mixtures is slightly suppressed by increasing the temperature. Although it is not obvious from the sensitivity analysis (Fig. ES99) to understand which reactions are responsible for suppressing the pressure effect on the reactivity by increasing the temperature in Fig. 7-8, Fig. ES100 shows that the normalized net fluxes of reactions corresponding to the pressure effect are significantly decreased by increasing the temperature from 750 K (~ 8.7) to

1112 K (~ 4), while there are no significant changes in the fluxes beyond 1112 K (at 1700 K: ~ 3.3). In general, increasing the compressed pressure to 40 bar (Fig. 7-8(a), (c), (d)) and 80 bar (Fig. 7-8(f), (g)) over the low-temperature regime (<1000 K) make the average IDTs shorter about 50% and 77%, respectively. However, this effect for the 40 bar case over >1000 K is about 36%.

7.4.2.2.2 Effect of equivalence ratio

Similar to the ethylene case, Fig. 7-8(a), (b), (d), (e), (f) shows that increasing the equivalence ratio to 2.0 has a monotonic (power curve instead of almost linear curve for the ethylene case) increasing effect on the IDT by increasing the temperature from 750 K to 1700 K, while decreasing the equivalence ratio to 0.5 has a mixed effect on the reactivity. As seen in Fig. 7-8(b), although decreasing the equivalence ratio to 0.5 makes the reactivity very sensitive to the gradient in temperature over the temperature range 1050–1480 K, its effect is constant over temperatures beyond the range. Here, it should be noticed that the sensitivity of ethane to increasing equivalence ratio ($\phi:1.0 \rightarrow 2.0$) over the temperature range (~120%) is higher than the ethylene's sensitivity (~84%), while this behavior is reversed for decreasing equivalence ratio ($\phi:1.0 \rightarrow 0.5$). In the temperature range of 1350–1700 K, decreasing the equivalence ratio has a promoting effect on the reactivity, while this effect on the reactivity of ethylene in the same temperature range is minor. Also, the effect of decreasing the equivalence ratio on the reactivity over the low-temperature regime (<1000 K) is not significantly changed by temperature, while this change in the reactivity is obvious over the temperature range for ethylene (Fig. 7-6(d)). One can see in Fig. ES101 that the effect of decreasing the equivalence ratio from the stoichiometric condition at P3C2 to 0.5 on increasing the reactivity over 1112–1700 K may stem from suppression of the inhibiting reactivity reactions of $C_3H_8 (+M) \leftrightarrow \dot{C}_2H_5 + \dot{C}H_3 (+M)$ (backward reaction) and $C_2H_6 + \dot{H} \leftrightarrow \dot{C}_2H_5 + H_2$ and intensification of the promoting reactivity reaction of $\dot{C}H_3 + \dot{C}H_3 (+M) \leftrightarrow C_2H_6 (+M)$ (backward reaction). However, by looking at Fig. ES102, it is inferred that increasing effect of the reduced equivalence ratio on the reactivity with increasing temperature is pronounced by intensifying the normalized net flux of all reactions, specifically $\dot{H} + O_2 \leftrightarrow \ddot{O} + \dot{O}H$ and $C_2H_4 + \dot{H} (+M) \leftrightarrow \dot{C}_2H_5 (+M)$ (backward reaction), which have determining role in increasing the reactivity of ethane's mixtures (Figs. ES101 and ES103) within the temperature window of 1112–1700 K (Figs. 7-8(b), (d)).

7.4.2.2.3 Effect of dilution

Figure 7-8(b) – (g) shows that increasing the dilution to 85% and 90% can increase the IDT to about 37% and 80%, respectively. This shows that the reactivity of ethane's mixtures are very sensitive to dilution. However, this sensitivity is lower than that for ethylene's mixtures. Although Fig. 7-8(b) shows that the effect of increasing the dilution level to 85% on decreasing the reactivity is almost constant over the temperature range, it is demonstrated in Fig. 7-8(d) that this effect is not constant for 90% case. As seen in Figs. ES104 and ES105, increasing the dilution level from 85% to 90% decreases the normalized net fluxes of the prominent reactions by a factor of two. The direct effect of such a change in the normalized net fluxes can be easily seen in Fig. ES105 where the reactivity is decreased by a factor of two due to 5% increase in the dilution level. Therefore, the accumulative effects of change in the prominent promoting or inhibiting reactions and the normalized net fluxes of these reactions cause such a sensible oscillating effect of 90% dilution level on the reactivity of ethane's mixture over the studied temperature range.

7.4.2.2.4 Combined effects

Figure 7-8(a) shows that, unlike the ethylene case ($P2C2 \rightarrow P2C3$), the combined effect of increasing both the equivalence ratio and the pressure ($P3C2 \rightarrow P3C3$) on the reactivity almost follows the equivalence ratio pattern. This effect stems from the negligible gradient of the pressure effect on the IDT over the temperature range (~ -0.021 %/K) in comparison to the equivalence ratio effect (~ -0.111 %/K). However, according Eqn. 7-2, it seems that its quantity is mostly affected by the pressure effect in the temperature range of 1300 – 1700 K. Similar to the ethylene cases, the synergetic influence of the same effects on the final reactivity of the ethane's mixture is demonstrated in Fig. 7-8(a), (b) over the temperature range of 750 – 1250 K (e.g., $P3C2 \rightarrow P3C3$ and $P3C2 \rightarrow P3C4$). As seen in Fig. 7-9, the normalized net fluxes of the $P3C4$ case are increased by a factor of ~ 2.75 by increasing the temperature from 1112 K to 1700 K. This increase in the net fluxes alongside with promoting $\dot{H} + O_2 \leftrightarrow \dot{O} + \dot{O}H$ and $C_2H_4 + \dot{H} (+M) \leftrightarrow \dot{C}_2H_5 (+M)$ (backward reaction) reactions which come from the equivalence ratio effect cancel out the divers effects of increasing dilution and decreasing equivalence ratio on the reactivity, so that their combined effects makes $P3C4$ neutral in comparison to $P3C2$ case in the temperature range of 1430 – 1700 K. Similar to Fig. 7-8(a), one can see in Fig. 7-8(c) that the total effect of increasing both pressure and dilution on the reactivity not only follows the pressure pattern but also its quantitative effect is almost skewed toward the pressure

effect over the studied temperature range. As mentioned above, this effect comes from the fact that both the pressure and the dilution effects on the reactivity are not very sensitive to a change in the temperature, so according to Eqn. 7-2 their combined effect on the reactivity and also prominent reactions involved in the reactivity of the P3C5 case make the P3C5 case more reactive (~20%) than the P3C2 baseline case by intensifying the normalized net fluxes of important reactions in the P3C5 case by a factor of 2.5 ($\overline{NnF}_i(P3C5) = \overline{NnF}_{i,D85\%} \times \overline{NnF}_{i,P40bar} = 0.47 \times 5.3 = 2.5$). The combined effects of the three individual parameters on the IDTs of the final case (P3C7) are shown in Fig. 7-8(d). Although, the pressure has an obvious effect on the reactivity of the P3C7 case because of suppressing the synergetic effect of the dilution and equivalence ratio over the temperature range of 750 – 1320 K, it is seen that the total effects of the parameters (P3C7) almost follows the equivalence ratio pattern over temperature. As seen in Figs. ES99 – ES105, although the combination of the pressure (20→40 bar), equivalence ratio (1.0→0.5), and dilution (75%→90%) effects yields new reactions into the first 10 important reactions of IDT of P3C7 case, promoting or suppressing of some of the reactions come from the effect of the specific parameter (such as pressure, equivalence ratio, and dilution) on the IDT of P3C7. For instance, by comparing the prominent reactions of P3C7 and 90% dilution cases at 1700 K in Figs. ES106 and ES107, one can see that $C_2H_6 + \dot{C}H_3 \leftrightarrow \dot{C}_2H_5 + CH_4$, $H\dot{C}O (+M) \leftrightarrow \ddot{C}O + \dot{H} (+M)$, $H_2 + \dot{O}H \leftrightarrow \dot{H} + H_2O$, and $\dot{C}H_3 + \dot{H} (+M) \leftrightarrow CH_4 (+M)$ reactions stem from the dilution effect on the reactivity of the P3C7 condition. Furthermore, Fig. 7-8(e) shows that although the equivalence ratio pattern almost controls the reactivity of P3C9 over the temperature range, its quantitative effect is skewed toward the dilution effect for the temperatures higher than 1170 K because of approaching the equivalence ratio effect toward the neutrality line (IDT ratio = 1). Also, the synergetic effect of the equivalence ratio and dilution substantially decreases the reactivity of P3C9 over the temperature range of 1450 – 1700 K. Finally, Figs. 7-8(f), (g) show how the promoting effect of pressure rise (20→80 bar) on the reactivity controls the ethane mixture reactivity over the low-temperature regime, so that the inhibiting effect of the decreasing equivalence ratio on the reactivity of P3C10 (Fig. 7-8(f)) is almost suppressed by the prominent effect of pressure on reactivity.

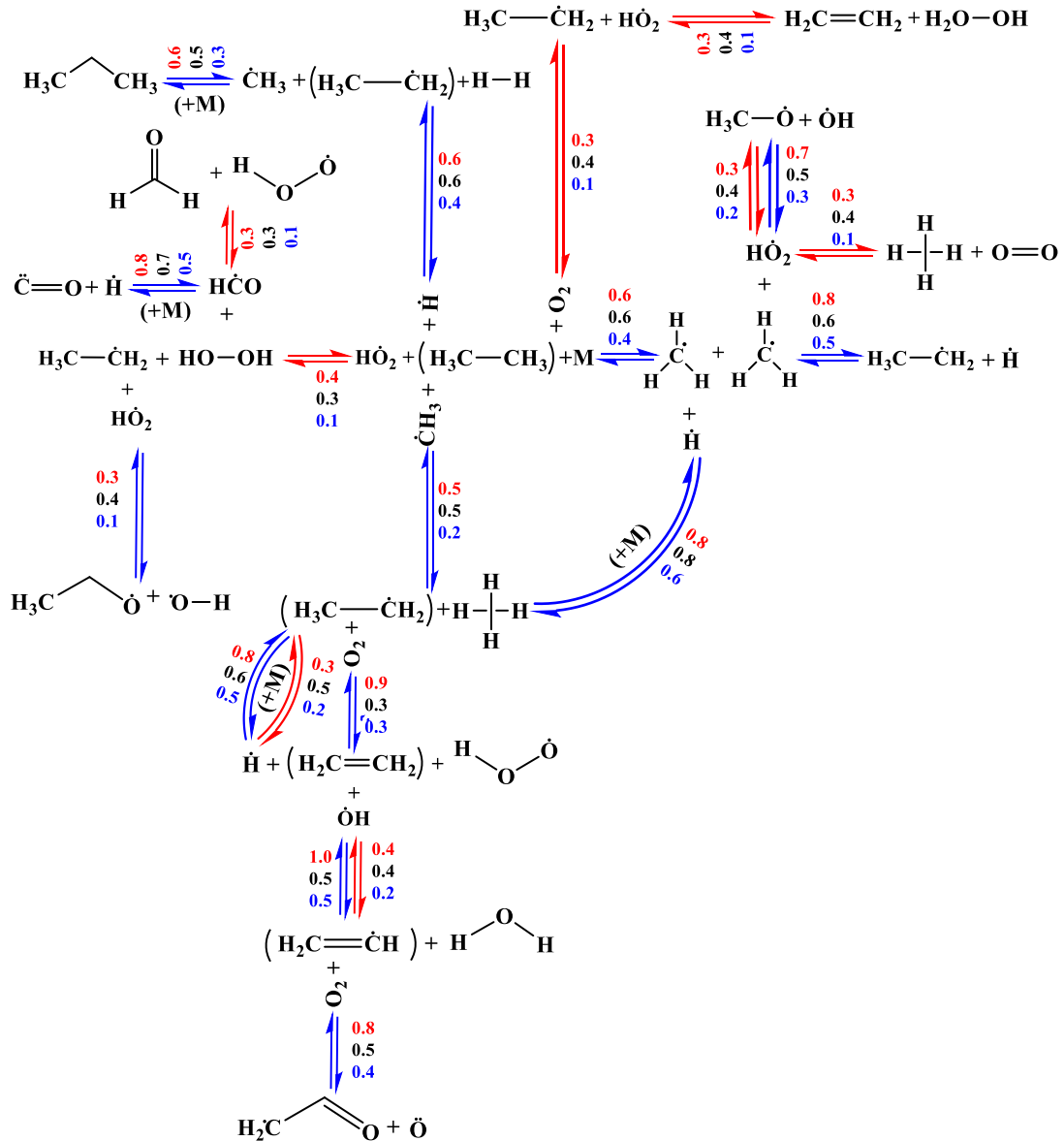


Figure 7-9. Normalized flux analysis (based on the flux analysis of P3C2 base case when 20% of ethane (fuel) is consumed) of some important reactions shown in Figs. ES99 – ES102 corresponding to Fig. 7-8(b). Blue line: case (1), $T_C = 1700$ K. Red line: case (2), $T_C = 1112$ K. Red numbers: effect of equivalence ratio. Black number: effect of dilution. Blue number: combined effects (P3C4).

7.4.3 Correlations and their performances

In engineering applications and specifically computational fluid dynamics (CFD) of reactive flows, having reliable global equations which could properly explain IDT characteristics of a reactive mixture would be in demand. This will enormously decrease computation times in real-time combustion controlling systems and real-scale CFD simulations. Therefore, in this section, we attempt to explain the IDT characteristics of the studied fuels using simple correlations over the wide

range of studied conditions. As shown in the previous sections, NUIGMech0.9 could acceptably reproduce the IDTs of various methane, ethane, and ethylene mixtures. Thus, this mechanism is used to derive some correlations as abstracted versions of the mechanism for the conditions shown in Fig. 7-10. In this regard, several correlations are derived which can reasonably predict the IDTs of methane, ethane, and ethylene mixtures over a wide range of temperatures, pressures, equivalence ratios, and dilutions. As shown in Fig. 7-10, to derive the relevant correlations to describe the IDT characteristics of the fuels studied over the conditions studied (Fig. 7-10(a)), a comprehensive constant-volume adiabatic modelling study using NUIGMech0.9 is performed to completely encapsulate the designed cube (Fig. 7-10(b); $1 \leq p \leq 50$ atm, $1000 \leq T \leq 2000$ K, $0.25 \leq \varphi \leq 3.0$, $75\% \leq \text{dilution} \leq 95\%$). In fact, this cube and its corresponding ranges stem from the targets of the current study as discussed in Sections 7.0 and 7.7.2. In this regard, there is a strategy that if the derived correlations from the IDT modelling can predict the experimental results randomly distributed in the cube using the L₉ Taguchi output, they can then acceptably reproduce all imaginable IDTs inside the cube. Therefore, the following formula is applied to correlate the relationship between the numerically studied conditions:

$$\tau_{\text{idt,corr}} = 10^A \exp\left(\frac{B}{T}\right) [\text{Fuel}]^C [\text{Oxygen}]^D [\text{Diluent}]^E \quad (7-3)$$

where the concentrations of fuel, oxygen, and diluent are calculated based on the ideal gas law in accordance to the partial pressure of each species in the mixture under specific temperature with units of mol m⁻³. As seen in Tables ES26–ES36 of the Appendix E, the correlations are evaluated by subdividing the numerically studied conditions into three zones: (a) low-, intermediate- and high-temperatures; (b) fuel-lean, stoichiometric, and fuel-rich; and (c) high and low pressure, corresponding to the different chemical pathways controlling ignition over these conditions. However, based on our correlation procedure (constant volume adiabatic simulations), the derived correlations for the low temperature regime are not able to capture the experimental IDTs where non-ideal effects (e.g., heat loss effect on measured IDTs) are prominent. Therefore, the performance of the correlations is compared to the experimental data only in the intermediate-to-high temperature regime. Moreover, Origin 8.5 software [26] is used to evaluate the correlation parameters of “A” to “E” mentioned in Eqn. 7-3. The results of the correlation for methane, ethane, and ethylene including standard errors and validity ranges over the studied conditions are presented in Tables ES26–ES36 of the Supporting Information file and in the following discussion.

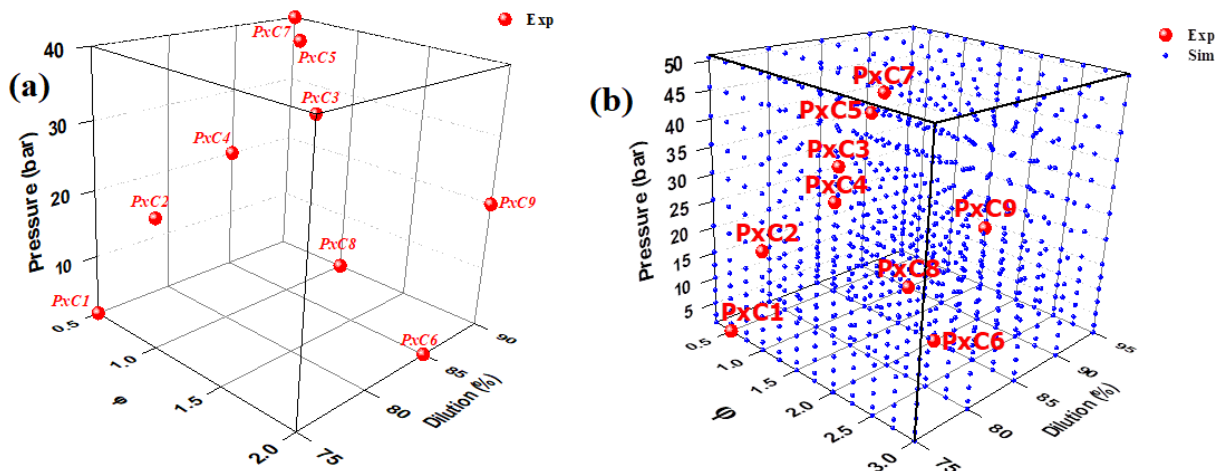


Figure 7-10. (a) Populated experimental points using the Taguchi approach, “Exp” refers to targeted experimental conditions derived from the L9 Taguchi matrix (“x” is 1 – 3). (b) Populated simulation points inside the studied cube. “Sim” refers to simulations performed over the designed cube using the NUIGMech0.9 mechanism for deriving the correlations in accordance to the applied fuels.

The performance of the derived correlations versus available IDT experimental data in the literature and the newly taken data in the present study for various methane, ethylene, and ethane mixtures is shown in Figs. 7-2 – 7-4.

It is seen in Fig. 7-2 that the correlation formula fitted to the IDT characteristics of methane can duplicate the experimental data trend. However, according to Fig. 7-10(b), all of the experimental cases presented in Fig. 7-2(b), (c), (e), (f), (h), (i) are outside of the range of methane’s correlations ($p \geq 1$ atm, $75\% \leq \text{dilution} \leq 95\%$). In this regard, the maximum deviations of the correlations from the experimental data over the studied temperature ranges in Fig. 7-2(a), (f), (h) is 44%, 69%, and 49%, respectively. Note that the fitted correlations to methane’s IDTs in Fig. 7-2(b), (d), (i) can reasonably capture all of the experimental data, so that the maximum deviations of the correlations from the experimental data over the studied conditions in Fig. 7-3(b), (d), (i) are 21%, 41%, and 36%, respectively. Also, all demonstrated trends in Fig. 7-2(c), (e), (g) are reproduced well by the correlations. This shows that the correlations can not only reproduce the IDT characteristics of various methane mixtures inside the defined parameter space but also predict IDTs at conditions located roughly $\pm 10\%$ outside this range. In this regard, the maximum deviations of the correlations from the experimental data in Fig. 7-2(c), (e), (g) are changing in the order of 27%, 36%, and 32%, respectively.

The performances of the derived correlations for predicting the IDT characteristics of ethylene oxidation are shown in Fig. 7-3. The details of the fitted correlations are presented in Tables ES31 –

ES33 of Appendix E for the low temperature, fuel-lean, and fuel-rich regimes, respectively. By comparing the experimental data and the correlations in Fig. 7-3(a), (f), (h), it is observed that the maximum deviations between the correlation and the experimental data is 39%, 45%, and 57%, respectively.

By increasing the compressed pressure to 20 bar, it is seen in Fig. 7-3(b), (d), (i) that the correlations all predict well the measured IDTs at high temperatures. It is interesting to note that the performance of the correlations in predicting the experimental data at some conditions presented in Fig. 7-3(d), (i) is better than NUIGMech0.9, which was the base mechanism used to derive the correlations. Thus, the correlations can better reproduce the chemical behavior of a specific reactive mixture as a function pressure, temperature, equivalence ratio, and dilution. In this regard, the maximum deviations of the correlations from the experimental data in Fig. 7-3(b), (d), (i) are 40%, 47%, and 58%, respectively. By further increasing the compressed pressure to 40 bar (Fig. 7-3(c), (e), (g)), it is seen that the performance of the correlations at high temperatures (≥ 1000 K) is acceptable, with the performance being similar to that of NUIGMech0.9. The maximum deviations of the correlations from the experimental data in Fig. 7-3(c), (e), (g) are 23%, 30%, and 48%, respectively.

The performances of the derived correlations versus the experimental IDT data of the ethane mixtures are summarized in Fig. 7-4. Moreover, the details of the fitted correlations to the comprehensive set of IDT data are provided in Tables ES34 – ES36 of Appendix E for the low temperature, fuel-lean, and fuel-rich conditions, as discussed in Section 7.6.3 . Similar to the acceptable performance of the presented correlations for various mixtures of methane and ethylene, Fig. 7-4 illustrates that the correlations can satisfactorily reproduce most of the experimental data. In this way, the maximum deviation of the correlations from the experimental data in Fig. 7-4(a), (f), (h) is changing from 42.2% to 83.2%. By increasing the compressed mixture pressure to 20 bar in Fig. 7-4(b), (d), (i) we see that the correlations describing ethane oxidation can also predict the IDTs of the various mixtures presented in these plots. In this regard, the maximum deviations between the correlations and the experimental IDTs in Fig. 7-4(b), (d), (i) are 47%, 52%, and 52%, respectively. Furthermore, Fig. 7-4(c), (e), (g) demonstrates that the derived correlations can reasonably predict the experimental IDTs for the conditions studied. Moreover, by considering Fig. 7-4(c), (e), (g) one can see that the maximum deviation of the correlations from the experimental data are 76%, 48%, and 58%, respectively.

7.5 Conclusions

A comprehensive experimental and modelling study of the IDT characteristics of $C_1 - C_2$ single fuel hydrocarbons over a wide range of temperatures ($\sim 800 - 2000$ K), pressures ($\sim 1 - 80$ bar), equivalence ratios ($\sim 0.5 - 2.0$), and dilutions ($\sim 75 - 90\%$) was conducted. An extensive literature review was conducted, and available data were extracted to create the comprehensive database used in our simulations. Based on existing literature data, an experimental matrix was designed using the Taguchi approach (L_9) in order to identify and complete the experimental matrix required to generate a comprehensive validation set necessary for validation of a chemical kinetic model. In this regard, six data sets including 70 data points for ethylene (p_c : 20 and 40 bar; ϕ : 0.5, 1.0, and 2.0; dilution: 75, 85, and 90%) and eight data sets including 85 data points for ethane (p_c : 20, 40, and 80 bar; ϕ : 0.5, 1.0, and 2.0; dilution: 75, 85, and 90%) were recorded using a high-pressure shock tube and rapid compression machine for short and longer induction times, which encompass high- and low-temperature ranges, respectively.

The performance of the NUIGMech0.9 in addition to several derived correlations for the studied fuels have been evaluated against all the available and measured experimental IDTs. The results showed that although NUIGMech0.9 could acceptably predict the measured IDTs over the wide range of studied conditions, some modifications and improvements are still required to get a high-fidelity chemical mechanism. Moreover, the results showed that the derived correlations based on NUIGMech0.9 for the studied fuels could satisfactorily anticipate the experimental IDT data within the studied range. This could be a very versatile rule-of-thumb tool to anticipate the IDT characteristics of the studied fuels over the studied conditions.

Finally, the individual and combined effects of the studied parameters on the IDTs were investigated in detail. The results showed that most parameters did not have a monotonic effect on the mixture reactivity over the entire temperature range ($750 - 1700$ K), so that the reactivity of the mixtures at certain temperature ranges was very sensitive to the studied parameters, while this sensitivity was low over other temperature ranges. Furthermore, it was shown that if the individual effects of parameters on the reactivity behave in the same way, their combined effect has a synergistic influence (by a power close to unity for each parameter in Eqn. 7-2) on the reactivity at the new condition.

Acknowledgements

The authors would like to express their gratitude to Shell Research Ltd and Science Foundation Ireland (SFI) via their Research Centre Program through project number 16/SP/3829. The authors from PCFC, RWTH Aachen University would like to recognize the funding support from the German Research Foundation (Deutsche Forschungsgemeinschaft, DFG) through the Project Number 322460823 (HE7599/2-1).

References

- [1] C.J. Aul, W.K. Metcalfe, S.M. Burke, H.J. Curran, E.L. Petersen, Ignition and kinetic modeling of methane and ethane fuel blends with oxygen: a design of experiments approach, *Combust. Flame* 160 (2013) 1153-1167.
- [2] U. Burke, K.P. Somers, P. O'Toole, C.M. Zinner, N. Marquet, G. Bourque, E.L. Petersen, W.K. Metcalfe, Z. Serinyel, H.J. Curran, An ignition delay and kinetic modeling study of methane, dimethyl ether, and their mixtures at high pressures, *Combust. Flame* 162 (2015) 315-330.
- [3] E.L. Petersen, D.F. Davidson, R.K. Hanson, Ignition delay times of ram accelerator CH₄/O₂/diluent mixtures, *J. Propul. Power* 15 (1999) 82-91.
- [4] H. El Merhubi, A. Kéromnès, G. Catalano, B. Lefort, L. Le Moyne, A high pressure experimental and numerical study of methane ignition, *Fuel* 177 (2016) 164-172.
- [5] O. Mathieu, J. Goulier, F. Gourmel, M.S. Mannan, N. Chaumeix, E.L. Petersen, Experimental study of the effect of CF₃I addition on the ignition delay time and laminar flame speed of methane, ethylene, and propane, *Proc. Combust. Inst* 35 (2015) 2731-2739.
- [6] D.J. Seery, C.T. Bowman, An experimental and analytical study of methane oxidation behind shock waves, *Combust. Flame* 14 (1970) 37-48.
- [7] C.S. Eubank, M.J. Rabinowitz, W.C. Gardiner Jr., R.E. Zellner, Shock-initiated ignition of natural gas-air mixtures, *Proc. Combust. Inst* 13 (1981) 1767-1773.
- [8] C.J. Jachimowski, Kinetics of oxygen atom formation during the oxidation of methane behind shock wave, *Combust. Flame* 23 (1974) 233-248.
- [9] A. Lifshitz, K. Scheller, A. Burcat, G.B. Skinner, Shock-tube investigation of ignition in methane-oxygen-argon mixtures, *Combust. Flame* 16 (1971) 311-321.
- [10] L.J. Spadaccini, M.B. Colket, Ignition delay characteristics of methane fuels, *Prog. Energy Combust. Sci.* 20 (1994) 431-460.
- [11] D. Healy, H.J. Curran, J.M. Simmie, D.M. Kalitan, C.M. Zinner, A.B. Barrett, E.L. Petersen, G. Bourque, Methane/ethane/propane mixture oxidation at high pressures and at high, intermediate and low temperatures, *Combust. Flame* 155 (2008) 441-448.
- [12] E.L. Petersen, D.M. Kalitan, S. Simmons, G. Bourque, H.J. Curran, J.M. Simmie, Methane/propane oxidation at high pressures: Experimental and detailed chemical kinetic modeling, *Proc. Combust. Inst.* 31 (2007) 447-454.
- [13] D. Healy, H.J. Curran, S. Dooley, J.M. Simmie, D.M. Kalitan, E.L. Petersen, G. Bourque, Methane/propane mixture oxidation at high pressures and at high, intermediate and low temperatures, *Combust. Flame* 155 (2008) 451-461.
- [14] K.A. Heufer, H. Olivier, Determination of ignition delay times of different hydrocarbons in a new high pressure shock tube, *Shock Waves* 20 (2010) 307-316.
- [15] D.J. Beerer, V.G. McDonell, An experimental and kinetic study of alkane autoignition at high

pressures and intermediate temperatures, *Proc. Combust. Inst.* 33 (2011) 301-307.

[16] M.A. Boumehdi, S.A. Stepanyan, P. Desgroux, G. Vanhove, S.M. Starikovskaia, Ignition of methane- and n-butane-containing mixtures at high pressures by pulsed nanosecond discharge, *Combust. Flame* 162 (2015) 1336-1349.

[17] O. Mathieu, J.M. Pemelton, G. Bourque, E.L. Petersen, Shock-induced ignition of methane sensitized by NO₂ and N₂O, *Combust. Flame* 162 (2015) 3053-3070.

[18] N. Donohoe, K.A. Heufer, C.J. Aul, E.L. Petersen, G. Bourque, R. Gordon, H.J. Curran, Influence of steam dilution on the ignition of hydrogen, syngas and natural gas blends at elevated pressures, *Combust. Flame* 162 (2015) 1126-1135.

[19] F.Q. Deng, F.Y. Yang, P. Zhang, Y.S. Pan, Y.J. Zhang, Z.H. Huang, Ignition delay time and chemical kinetic study of methane and nitrous oxide mixtures at high temperatures, *Energy Fuel* 30 (2016) 1415-1427.

[20] B. Koroglu, O.M. Pryor, J. Lopez, L. Nash, S.S. Vasu, Shock tube ignition delay times and methane time-histories measurements during excess CO₂ diluted oxy-methane combustion, *Combust. Flame* 164 (2016) 152-163.

[21] F.Q. Deng, F.Y. Yang, P. Zhang, Y.S. Pan, J. Bugler, H.J. Curran, Y.J. Zhang, Z.H. Huang, Towards a kinetic understanding of the NO_x promoting-effect on ignition of coalbed methane: a case study of methane/nitrogen dioxide mixtures, *Fuel* 181 (2016) 188-198.

[22] E.L. Petersen, M. Röhrig, D.F. Davidson, R.K. Hanson, C.T. Bowman, High-pressure methane oxidation behind reflected shock waves, *Symp. (Int.) Combust.*, 26 (1996) 799-806.

[23] E.L. Petersen, D.F. Davidson, R.K. Hanson, Kinetics modeling of shock-induced ignition in low-dilution CH₄/O₂ mixtures at high pressures and intermediate temperatures, *Combust. Flame* 117 (1999) 272-290.

[24] J. Huang, P.G. Hill, W.K. Bushe, S.R. Munshi, Shock-tube study of methane ignition under engine-relevant conditions: experiments and modeling, *Combust. Flame* 136 (2004) 25-42.

[25] V.P. Zhukov, V.A. Sechenov, A.Y. Starikovskii, Spontaneous ignition of methane-air mixtures in a wide range of pressures, *Combust. Explo. Shock Wave* 39 (2003) 487-495.

[26] J. Huang, W.K. Bushe, Experimental and kinetic study of auto-ignition in methane/ethane/air and methane/propane/air mixtures under engine-relevant conditions, *Combust. Flame* 144 (2006) 74-88.

[27] S. Gersen, H. Darneveil, H.B. Levinsky, The effects of CO addition on the auto-ignition of H₂, CH₄ and CH₄/H₂ fuels at high pressure in an RCM, *Combust. Flame* 159 (2012) 3472-3475.

[28] S. Gersen, N.B. Anikin, A.V. Mokhov, H.B. Levinsky, Ignition properties of methane/hydrogen mixtures in a rapid compression machine, *Int. J. Hydrogen Energ.* 33 (2008) 1957-1964.

[29] C. Strozzi, A. Mura, J. Sotton, M. Bellenoue, Experimental analysis of propagation regimes during the auto-ignition of a fully premixed methane-air mixture in the presence of temperature inhomogeneities, *Combust. Flame* 159 (2012) 3323-3341.

[30] C.L. Tang, L.J. Wei, J.X. Zhang, X.J. Man, Z.H. Huang, Shock tube measurements and kinetic investigation on the ignition delay times of methane/dimethyl ether mixtures, *Energy Fuel* 26 (2012) 6720-6728.

[31] Y.J. Zhang, Z.H. Huang, L.J. Wei, J.X. Zhang, C.K. Law, Experimental and modeling study on ignition delays of lean mixtures of methane, hydrogen, oxygen, and argon at elevated pressures, *Combust. Flame* 159 (2012) 918-931.

[32] E.L. Petersen, J.M. Hall, S.D. Smith, J. de Vries, A.R. Amadio, M.W. Crofton, Ignition of lean methane-based fuel blends at gas turbine pressures, *J. Eng. Gas Turbines Power* 129 (2007) 937-944.

[33] J. de Vries, E.L. Petersen, Autoignition of methane-based fuel blends under gas turbine

conditions, *Proc. Combust. Inst.* 31 (2007) 3163-3171.

[34] A. Ramalingam, K.W. Zhang, A. Dhongde, L. Virnich, H. Sankhla, H. Curran, A. Heufer, An RCM experimental and modeling study on CH₄ and CH₄/C₂H₆ oxidation at pressures up to 160 bar, *Fuel* 206 (2017) 325-333.

[35] S. Gersen, A.V. Mokhov, J.H. Darneveil, H.B. Levinsky, P. Glarborg, Ignition-promoting effect of NO₂ on methane, ethane and methane/ethane mixtures in a rapid compression machine, *Proc. Combust. Inst.* 33 (2011) 433-440.

[36] R.F. Pachler, A.K. Ramalingam, K.A. Heufer, F. Winter, Reduction and validation of a chemical kinetic mechanism including necessity analysis and investigation of CH₄/C₃H₈ oxidation at pressures up to 120 bar using a rapid compression machine, *Fuel* 172 (2016) 139-145.

[37] J.W. Hargis, E.L. Petersen, Methane ignition in a shock tube with high levels of CO₂ dilution: consideration of the reflected-shock bifurcation, *Energy Fuel* 29 (2015) 7712-7726.

[38] A. Burcat, K. Scheller, A. Lifshitz, Shock-tube investigation of comparative ignition delay times for C₁–C₅ Alkanes, *Combust. Flame* 16 (1971) 29-33.

[39] J. de Vries, J.M. Hall, S.L. Simmons, M.J.A. Rickard, D.M. Kalitan, E.L. Petersen, Ethane ignition and oxidation behind reflected shock waves, *Combust. Flame* 150 (2007) 137–150.

[40] Y. Hidaka, K. Sato, H. Hoshikawa, T. Nishimori, R. Takahashi, H. Tanaka, K. Inami, N. Ito, Shock-tube and modeling study of ethane pyrolysis and oxidation, *Combust. Flame* 120 (2000) 245-264.

[41] H. Hashemi, J.G. Jacobsen, C.T. Rasmussen, J.M. Christensen, P. Glarborg, S. Gersen, M. van Essen, H.B. Levinsky, S.J. Klippenstein, High-pressure oxidation of ethane, *Combust. Flame* 182 (2017) 150-166.

[42] C.J. Brown, G.O. Thomas, Experimental studies of shock-induced ignition and transition to detonation in ethylene and propane mixtures, *Combust. Flame* 117 (1999) 861-870.

[43] D.F. Davidson, W. Ren, R.K. Hanson, Experimental database for development of a HiFiRE JP-7 surrogate fuel mechanism, 50th AIAA Aerospace Sciences Meeting including the New Horizons Forum and Aerospace Exposition, AIAA, Tennessee, (2012).

[44] F.R. Gillespie, An Experimental and modelling study of the combustion of oxygenated hydrocarbons, School of Chemistry, National University of Ireland, Galway, National University of Ireland, Galway, (2014).

[45] D.C. Horning, A study of the high-temperature autoignition and thermal decomposition of hydrocarbons, Stanford University, Stanford University, (2001).

[46] M.M. Kopp, N.S. Donato, E.L. Petersen, W.K. Metcalfe, S.M. Burke, H.J. Curran, Ignition and oxidation of ethylene-air mixtures at elevated pressures, part 1: experimental results, *J Propul Power* 30 (2014) 790–798.

[47] O.G. Penyazkov, K.L. Sevrouk, V. Tangirala, N. Joshi, High-pressure ethylene oxidation behind reflected shock waves, *Proc. Combust. Inst.* 32 (2009) 2421-2428.

[48] S. Saxena, M.S.P. Kahandawala, S.S. Sidhu, A shock tube study of ignition delay in the combustion of ethylene, *Combust. Flame* 158 (2011) 1019-1031.

[49] K. Kumar, G. Mittal, C.J. Sung, C.K. Law, An experimental investigation of ethylene/O₂/diluent mixtures: laminar flame speeds with preheat and ignition delays at high pressures, *Combust. Flame* 153 (2008) 343-354.

[50] C.-W. Zhou, Y. Li, U. Burke, C. Banyon, K.P. Somers, S.T. Ding, S. Khan, J.W. Hargis, T. Sikes, O. Mathieu, E.L. Petersen, M. AlAbbad, A. Farooq, Y.S. Pan, Y.J. Zhang, Z.H. Huang, J. Lopez, Z. Loparo, S.S. Vasu, H.J. Curran, An experimental and chemical kinetic modeling study of 1,3-butadiene combustion: Ignition delay time and laminar flame speed measurements, *Combust. Flame*

197 (2018) 423-438.

[51] P.J. Ross, Taguchi Techniques for Quality Engineering, McGraw-Hill, New York, (1988).

[52] G. Bagheri, E. Ranzi, M. Pelucchi, A. Parente, A. Frassoldati, T. Faravelli, Comprehensive kinetic study of combustion technologies for low environmental impact: MILD and OXY-fuel combustion of methane, *Combust. Flame* 212 (2020) 142-155.

[53] S.M. Burke, W. Metcalfe, O. Herbinet, F. Battin-Leclerc, F.M. Haas, J. Santner, F.L. Dryer, H.J. Curran, An experimental and modeling study of propene oxidation. part 1: speciation measurements in jet-stirred and flow reactors, *Combust. Flame* 161 (2014) 2765-2784.

[54] S.M. Gallagher, H.J. Curran, W.K. Metcalfe, D. Healy, J.M. Simmie, G. Bourque, A rapid compression machine study of the oxidation of propane in the negative temperature coefficient regime, *Combust. Flame* 153 (2008) 316-333.

[55] D. Healy, D.M. Kalitan, C.J. Aul, E.L. Petersen, G. Bourque, H.J. Curran, Oxidation of C₁ – C₅ alkane quinary natural gas mixtures at high pressures, *Energy Fuels* 24 (2010) 1521–1528.

[56] E.L. Petersen, M.J.A. Rickard, M.W. Crofton, E.D. Abbey, M.J. Traum, D.M. Kalitan, A facility for gas- and condensed-phase measurements behind shock waves, *Meas. Sci. Technol.* 16 (2005) 1716-1729.

[57] B.W. Weber, C.-J. Sung, M.W. Renfro, On the uncertainty of temperature estimation in a rapid compression machine, *Combust. Flame* 162 (2015) 2518-2528.

[58] G. Mittal, C.-J. Sung, Autoignition of toluene and benzene at elevated pressures in a rapid compression machine, *Combust. Flame* 150 (2007) 355-368.

[59] S.S. Goldsborough, S. Hochgreb, G. Vanhove, M.S. Wooldridge, H.J. Curran, C.-J. Sung, Advances in rapid compression machine studies of low- and intermediate-temperature autoignition phenomena, *Prog. Energy Combust. Sci.* 63 (2017) 1-78.

[60] C.-J. Sung, H.J. Curran, Using rapid compression machines for chemical kinetics studies, *Prog. Energy Combust. Sci.* 44 (2014) 1-18.

[61] D.G. Goodwin, R.L. Speth, H.K. Moffat, B.W. Weber, Cantera: An object-oriented software toolkit for chemical kinetics, thermodynamics, and transport processes. <https://www.cantera.org>, (2018). doi:10.5281/zenodo.170284.

[62] Reaction-Design, CHEMKIN-PRO 18.2, San Diego, (2013).

[63] E.E. Dames, A.S. Rosen, B.W. Weber, C.W. Gao, C.-J. Sung, W.H. Green, A detailed combined experimental and theoretical study on dimethyl ether/propane blended oxidation, *Combust. Flame* 168 (2016) 310-330.

[64] S. Wan, Y. Fan, K. Maruta, Y. Suzuki, Wall chemical effect of metal surfaces on DME/air cool flame in a micro flow reactor, *Proc. Combust. Inst.* 37 (2019) 5655-5662.

[65] Origin(Pro), "Version 8.5". OriginLab Corporation, Northampton, MA, USA.

Chapter 8: Performance of NUIGMech models

In this thesis, four different versions of NUIGMech have been presented: NUIGMech0.9, NUIGMech1.0, NUIGMech1.1, and NUIGMech1.2. These models are detailed mechanisms that include not only natural gas components (NG) but also contain higher molecular weight species. The models were developed and validated using the ignition delay times (IDTs) parameter, specifically for $C_1 - C_3$ targets. The corresponding validation range for temperature (T), pressure (p), equivalence ratio (ϕ), and blend compositions can be found in Chapters 4-7 of the experimental sections. This chapter presents an analysis of the performance of these models by comparing them to an extensive database available at the Combustion Chemistry Centre (C^3). This database was not necessarily used for the development of these models, some data might be used but not the entire database. The computational chemistry tools included in this thesis and found in Appendix A were used for this analysis. The primary combustion property used to evaluate the performance of these mechanisms is the IDT. For this statistical analysis, more than ten times the original number of IDTs used during the development of these models was used. To give an idea of the magnitude, consider that the previous study presented in Chapter 5 used a total of 328 IDTs for the statistical analyses of NUIGMech1.1 against AramcoMech3.0. For the current analysis, approximately 7817 IDTs were used.

8.1 Statistical analyses of mechanism performance

The overall performance of the different versions of NUIGMech models was evaluated using statistical analysis based on three key parameters: the Mean Absolute Deviation (MAD), the Mean Absolute Percentage Error (MAPE), and the Relative Percentage Error (RPE). The MAD demonstrates how far each data point is from the mean, with a small MAD ($0 \leq MAD \leq 1$) indicating that the data is more clustered and predictable, while a large MAD indicates that the data is spread far out from the mean. The MAPE, also known as the Mean Absolute Percentage Deviation (MAPD), is a commonly used measure of prediction accuracy, expressed as a percentage. It works well when there are no extreme data points or zeros. The RPE, or Relative Percentage Deviation (RPD), compares the difference between two measurements by normalizing the difference by dividing it by the experimental measurement, which is the mean. In a perfectly symmetrical distribution, the mean and median are the same.

The process of determining the global uncertainties, ϵ_{MAD} and ϵ_{MAPE} , of the models involve using mathematical equations such as MAD, MAPE, and RPE and the experimental and simulated IDTs. These equations are used to calculate the differences between experimental data and simulated data for each mechanism and each point in the data sets. Specially, the RPE technique which is used to analyse the individual errors in the data and present them in format of histograms with $2 \times \sigma$, with σ as the standard deviations. This method has been previously applied in Chapter 5, Section 5.3 (Eqns. 5-1, 5-2, and 5-3), of this thesis to generate a numerical analysis based on histograms. The mathematical expressions used in this process are provided here for clarity,

$$\epsilon_{\text{MAD}} = \frac{1}{n} \sum |IDT_{\text{mod}} - IDT_{\text{exp}}| \quad (8-1)$$

$$\epsilon_{\text{MAPE}} = \frac{1}{n} \sum \left(\left| \frac{IDT_{\text{mod}} - IDT_{\text{exp}}}{IDT_{\text{exp}}} \right| \right) * 100 \quad (8-2)$$

$$\epsilon_{\text{RPE}} = \left(\frac{IDT_{\text{mod}} - IDT_{\text{exp}}}{IDT_{\text{exp}}} \right) * 100 \quad (8-3)$$

where n is the total number of experimental IDTs.

On the other hand, to calculate any statistics we need both the experimental IDTs and the simulated IDTs for the four models. Figure 8-1 show the comparison of experimental data with model predictions for IDTs across various conditions. The data of 24 species was simulated using 4 models, resulting in 674 sets of data (553 ST and 121 RCM), totalling ~ 7817 IDT points. The species simulated are the next listed; H₂, CH₄, CH₄/H₂, CH₃OH, CH₃OCH₃, CH₃COCH₃, CH₃CHO, C₂H₂, C₂H₄, C₂H₅OH, C₂H₆, C₃H₄-a, C₃H₄-p, C₃H₆, C₃H₈, CH₄/C₂H₄, CH₄/C₂H₆, CH₄/C₃H₈, CH₄/CH₃OCH₃, C₂H₄/C₂H₆, C₂H₄/C₃H₈, C₂H₆/C₃H₈, CH₄/C₂H₄/C₂H₆, and CH₄/C₂H₄/C₂H₆/C₃H₈ blends.

The individual comparison graphs can be found in Appendix F of the chemical kinetic report. The report was generated using the LaTeX-python code in Appendix A of the thesis. The models are differentiated by line style, with the best performer **—**NUIGMech1.2 shown as a solid red line, followed by **—**NUIGMech1.1 with a solid black line, **- - - - -**NUIGMech0.9 in dashed lines, and **.....**NUIGMech1.0 by dotted lines with the relative worst performance. It is worth noticing that the whole NUIGMech family exhibits an acceptable accuracy in their predictions, but the statistical analysis was performed to determine the best overall performer based on a numerical analysis.

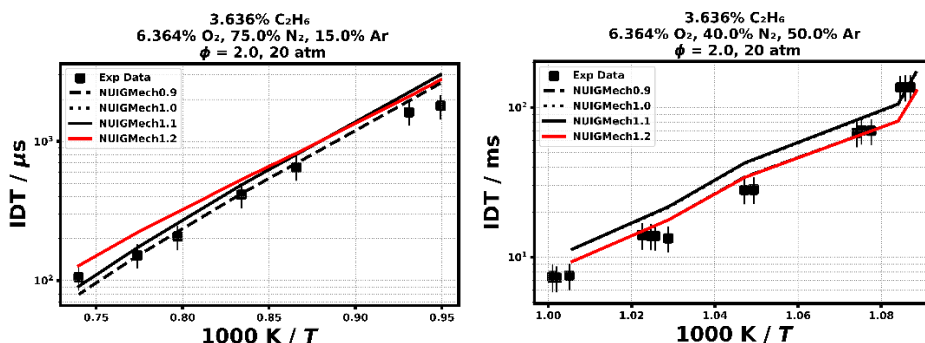


Figure 8-1. Graphical example of the experimental data (■), against model predictions (— NUIGMech0.9, NUIGMech1.0, ----- NUIGMech1.1, ——— NUIGMech1.2). The left plot covers the high-temperature range (ST), and the right one the low-temperature range (RCM). Appendix F includes the chemical kinetic report based on the total of samples used in these analyses, and it can be consulted there.

Once the total of the IDTs has been gathered, the next step is to compare the simulated IDT against the experimental IDT and to proceed to calculate the corresponding MAD, MAPE, and RPE using Eqns. 8-1, 8-2, and 8-3, respectively. As mentioned early, the total number of IDTs was initially 7817. However, when the final calculations were performed the outlier points were not included. This filtering of the outliers leaves a total of 5102 IDTs to present in the histograms. Histograms are a powerful tool for visualizing the distribution of data and can provide valuable insights into the properties of a dataset, or comparison of datasets, like in our case. Moreover, to have a histogram with $2 \times \sigma$ refers to a graphical representation of the datasets, where the data is divided into a set of bins, and the height of each bin represents the frequency of data points in that bin.

The $2 \times \sigma$ is a measure of the uncertainty in the data. It means that approximately 95% of the data falls within the two standard deviations of the mean. In a histogram, this is represented by showing the mean and the two standard deviation lines or presenting the corresponding values, indicating the region within which 95% of the data lies. In the case of this work, histograms have these lines represented by dotted black vertical lines which comprise the 95% of the data. As mentioned earlier, data were filtered by a criterion of $-100\% \leq \text{RPE} \leq 100\%$, any value falling beyond this limit was considered an outlier point. In statistics, outlier points are data points that fall significantly outside the overall pattern of the rest of the data. They are considered outliers because they differ significantly ($\geq 100\%$) from the other values in the dataset. Outlier points can have a significant impact on statistical analysis, as they can skew the results if not properly handled. There are various methods for identifying outlier points, such as using statistical tests, visual inspection of the data, and using specialized software. The method used to identify outliers depends on the data

and the purpose of the analysis. It is important not to include these points in a histogram because they can skew the results, leading to incorrect conclusions about the data distribution. Moreover, outliers can cause a disproportionate impact on the histogram's appearance, making it difficult to see the actual distribution of the data. Therefore, excluding outliers from a histogram can provide a clearer and more accurate representation of the data distribution.

8.1.1 Results and discussion

Figure 8-2 shows the four histograms corresponding to the four models. It provides the RPE frequency distribution for NUIGMech0.9, NUIGMech1.0, NUIGMech1.1, and NUIGMech1.2 relative to the experimental IDTs. A total of 5102 IDTs for high-temperature range were used to calculate the mean (μ), median (\tilde{x}), standard deviation (σ), MAD, MAPE, and RPE. Table 8-1 presents summarise the value of n , μ , \tilde{x} , σ , MAD, and MAPE for the four models here analysed. In this analysis, we are considering the four histograms involving the four mechanisms and comparing their main parameters. NUIGMech0.9 has a μ of 8.92 and an \tilde{x} of 8.34, indicating that the data is slightly positively skewed. The σ of 38.68 is relatively large, indicating that there is a lot of variation in the data. The MAD of 11.82 and the MAPE of 32.16% further support the idea that there is a lot of variation in the data and that (a) NUIGMech0.9 predicts the difference between the experimental and mathematical modelled data with moderate error.

NUIGMech1.0 has a μ of 11.67 and an \tilde{x} of 10.33, indicating that the data is positively skewed. The σ of 38.64 is similar to NUIGMech0.9, indicating that there is also a lot of variation in the data for NUIGMech1.0. The MAD of 12.06 and the MAPE of 32.44% further support that NUIGMech1.0 predicts the difference with moderate error. NUIGMech1.1 has a μ of 9.43 and an \tilde{x} of 8.55, indicating that the data is slightly positively skewed. The σ of 36.99 is slightly lower than for NUIGMech0.9 and NUIGMech1.0, suggesting that there is slightly less variation in the data for NUIGMech1.1. The MAD of 11.40 and the MAPE of 30.72% support this conclusion and suggest that NUIGMech1.1 predicts the difference with less error compared to NUIGMech0.9 and NUIGMech1.0.

Finally, NUIGMech1.2 has a μ of 6.67 and an \tilde{x} of 4.5, indicating that the data is negatively skewed. The σ of 35.3 is similar to NUIGMech0.9 and NUIGMech1.0, indicating that there is still a lot of variation in the data for NUIGMech1.2. The MAD of 10.53 and the MAPE of 28.45% support this conclusion and suggest that NUIGMech1.2 predicts the difference with the least amount of error compared to the other histograms. Overall, the histograms show a lot of variation in the data, with

NUIGMech1.1 having slightly less variation compared to NUIGMech0.9 and NUIGMech1.0. The skewness of the data ranges from negative to slightly positive, with NUIGMech1.2 having the most negative skewness. Based on the MAPE values, NUIGMech1.2 is the best in predicting the difference between the experimental data and mathematical modelled data with the least amount of error, with a MAPE of 28.45%. NUIGMech1.1 is the second best with a MAPE of 30.72%, followed by NUIGMech0.9 with a MAPE of 32.16% and NUIGMech1.0 with the highest MAPE of 32.44%. A lower MAPE value indicates that the model predicts the actual value more closely, so in this case, NUIGMech1.2 is the best at predicting the difference between the experimental data and mathematical modelled data.

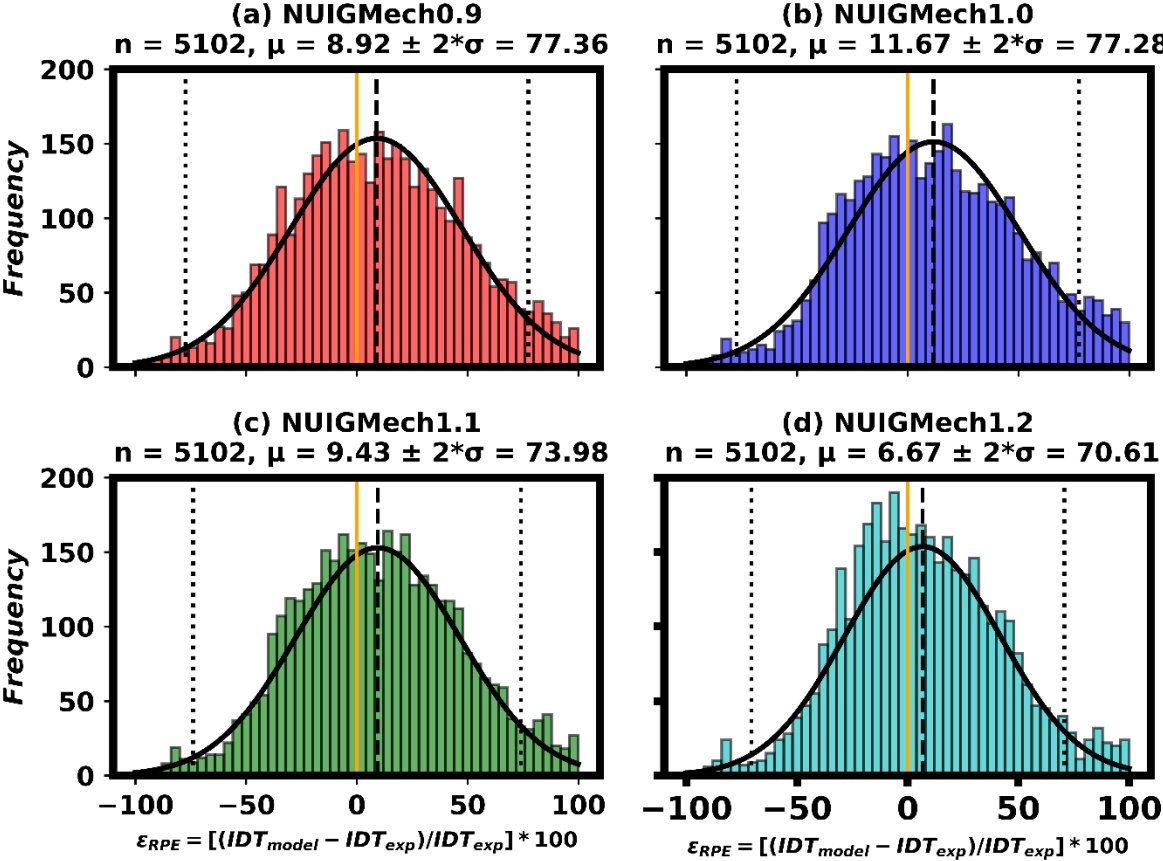


Figure 8-2. Histograms for high temperature presenting the total sample size taken (n), mean of the sample (μ), and the standard deviation (2σ) for each mechanism. The occurrence of each specific % error is plotted as a function of individual relative percentage errors (RPE) for (a) NUIGMech0.9, (b) NUIGMech1.0, (c) NUIGMech1.1, and (d) NUIGMech1.2, respectively.

Table 8-1. Overall statistical analyses parameters for the different mechanism versions of NUIGMech in the current study for high temperature, $\sim 1000 \leq T \leq \sim 2000$.

Data source	n	μ	\bar{x}	σ	MAD	MAPE
NUIGMech0.9 vs experiment	5120	8.92	8.34	38.68	11.82	32.16%
NUIGMech1.0 vs experiment	5120	11.67	10.33	38.64	12.06	32.44%
NUIGMech1.1 vs experiment	5120	9.43	8.55	36.99	11.40	30.72%
NUIGMech1.2 vs experiment	5120	6.67	4.50	35.3	10.53	28.45%

In this case, NUIGMech1.2 the final version of NUIGMech is the most likely to predict better targets from $C_0 - C_3$ and its blends for a wide range of conditions. However, that does not mean that for specific individual cases or conditions, assuming the outlier points, other previous versions of the model can predict relatively better than this one.

The story changes slightly when we analyse the low-temperature range. A total of 121 sets of IDTs (RCM) were analysed using the same principle, and the same equations and only replacing the IDTs with the area under the curve formed by these data points. For the IDTs corresponding to low temperature, we do not consider the shift in temperature or compressed temperature (T_C) variable. Thus, from a problem of two variables (T_C , IDT) we reduced it to a problem with only one variable (IDT) assuming simulations and experiment has no shift in T_C . Now, that means that from each set of experimental IDTs, we will gather only one value, the area of that data, both experimental data and simulated one.

Two main methods were used to calculate the area under the curve in this analysis. One of the methods applied to the IDTs for low-temperature range (RCM data) was the “numpy.trapz” module which integrate along the given axis using the composite trapezoidal rule. If x is provided, the integration happens in sequence along its elements – they are not sorted. Integrate y (x) along each 1d slice on the given axis, compute $\int y(x)dx$. When x is specified, this integrates along the parametric curve, computing $\int_t^0 y(t)dt = \int_t^0 y(t) \frac{dx}{dt} \Big|_{x=x(t)} dt$. The second method is the

“scipy.integrate.simpson” which integrates $y(x)$ using samples along the given axis and the composite Simpson’s rule. If x is None, spacing of dx is assumed to be the unit, $dx=1$. If there are an even number of samples, N , then there are an odd number of intervals ($N-1$), but Simpson’s rule requires an even number of intervals. The parameter ‘even’ controls how this is handled. At the end we do the average of both results. After this, we can compare one experimental value ($IDT_{AreaExp}$) against its simulated one ($IDT_{AreaMod}$) obtained in the same way. Based on these methods and our statistical analyses adapting Eqns. 8-1, 8-2, and 8-3, we can calculate the mean (μ), median (\tilde{x}), standard deviation (σ), MAD, MAPE, and RPE. All these parameters for low temperature are comprise in Table 8-2.

Figure 8-3 shows the four histograms for low temperature corresponding to the four models. It provides the RPE frequency distribution for NUIGMech0.9, NUIGMech1.0, NUIGMech1.1, and NUIGMech1.2 relative to the experimental IDTs. NUIGMech0.9 has a μ of -72.62 , an \tilde{x} of -78.34 , a standard deviation of 24.11 , a MAD equal to 69.31 , and a MAPE equal to 74.53% . These values indicate that the data in NUIGMech0.9 is distributed with an average difference of -72.62 between the simulated and experimental scatter data, with a relatively high degree of variability as indicated by the standard deviation of 24.11 . The \tilde{x} value of -78.34 is close to the mean value, which suggests that the data is symmetrically distributed. The MAD value of 69.31 and MAPE value of 74.53% suggest that the simulation has a relatively low degree of accuracy.

NUIGMech1.0 has a μ of -68.89 , an \tilde{x} of -74.68 , a standard deviation of 26.45 , a MAD equal to 56.27 , and a MAPE equal to 70.37% . These values suggest that the data in NUIGMech1.0 is distributed with a mean difference of -68.89 between the simulated and experimental scatter data, with a slightly higher degree of variability than NUIGMech0.9, as indicated by the standard deviation of 26.45 . The \tilde{x} value of -74.68 is close to the mean value, which suggests that the data is symmetrically distributed. The MAD value of 56.27 and MAPE value of 70.37% suggest that the simulation has a slightly higher degree of accuracy compared to NUIGMech0.9.

NUIGMech1.1 has a μ of -68.27 , an \tilde{x} of -74.00 , a standard deviation of 26.58 , a MAD equal to 62.30 , and a MAPE equal to 70.37% . These values suggest that the data in NUIGMech1.1 is distributed with a mean difference of -68.27 between the simulated and experimental scatter data, with a slightly higher degree of variability than NUIGMech1.0, as indicated by the standard deviation of 26.58 . The \tilde{x} value of -74.00 is close to the mean value, which suggests that the data is symmetrically distributed. The MAD value of 62.30 and MAPE value of 70.37% suggest that the

simulation has a slightly higher degree of accuracy compared to NUIGMech0.9, but not as high as NUIGMech1.0.

NUIGMech1.2 has a μ of -71.44 , an \tilde{x} of -77.15 , a standard deviation of 23.09 , a MAD equal to 77.66 , and a MAPE equal to 73.97% . These values suggest that the data in NUIGMech1.2 is distributed with a mean difference of -71.44 between the simulated and experimental scatter data, with a slightly lower degree of variability than NUIGMech0.9, as indicated by the standard deviation of 23.09 . The \tilde{x} value of -77.15 is close to the mean value, which suggests that the data is symmetrically distributed. The MAD value of 77.66 and MAPE value of 73.97% suggest that the simulation has a relatively low degree of accuracy compared to NUIGMech1.0 and NUIGMech1.1. For instance, if the main concern is to understand the spread of the data, the standard deviation would be a useful metric. In this case, NUIGMech1.2 with a standard deviation of 23.09 would have a tighter distribution compared to NUIGMech1.0 and NUIGMech1.1 with standard deviations of 26.45 and 26.58 respectively. On the other hand, if the goal is to understand the average deviation of the data from the true value, the Mean Absolute Percentage Error (MAPE) could be used. Based on the MAPE values, NUIGMech1.0 with a value of 70.37% has a lower average deviation compared to the other histograms.

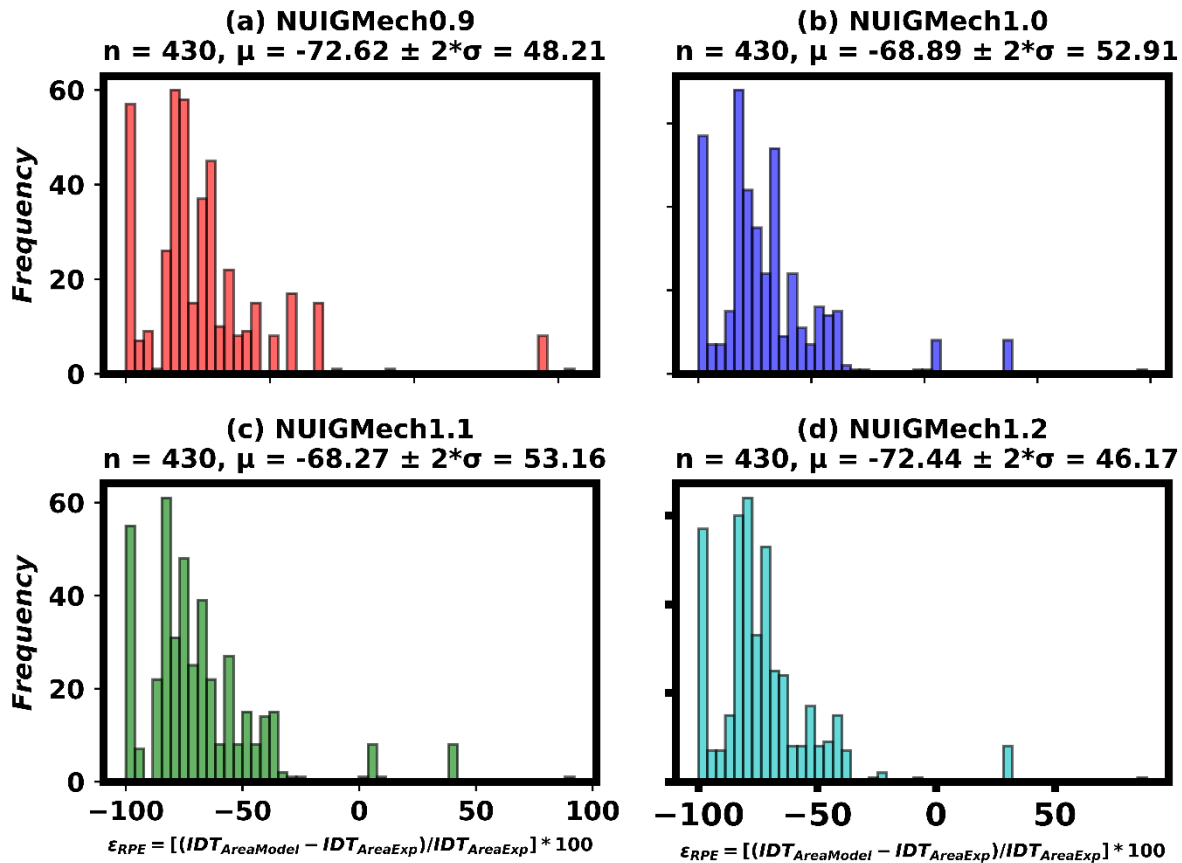


Figure 8-3. Histograms for low temperature presenting the total sample size taken (n), mean of the sample (μ), and the standard deviation ($2 \times \sigma$) for each mechanism. The occurrence of each specific % error is plotted as a function of individual relative percentage errors (RPE) for (a) NUIGMech0.9, (b) NIGMech1.0, (c) NUIGMech1.1, and (d) NUIGMech1.2.

Table 8-2. Overall statistical analyses parameters for the different mechanism versions of NUIGMech in the current study for low temperature, $\sim 700 \leq T \leq \sim 1000$.

Data source	n	μ	\tilde{x}	σ	MAD	MAPE
NUIGMech0.9 vs experiment	430	-72.62	-78.34	24.11	69.31	74.53%
NUIGMech1.0 vs experiment	430	-68.89	-74.68	26.45	56.27	70.90%
NUIGMech1.1 vs experiment	430	-68.27	-74.00	26.58	62.30	70.37%
NUIGMech1.2 vs experiment	430	-72.44	-77.15	23.09	77.66	73.97%

8.2 Chemistry updates in NUIGMech core mechanisms

In general, the four mechanism versions of the model NUIGMech keep the main core mechanism. However, the small differences between these versions make the mechanism improve in the predictions, especially for the low-temperature range of the small hydrocarbons ($C_0 - C_3$). It is worth noticing that every version of the NUIGMech model was already discussed in Chapters 4-7, for more details refer to those chapters. For example, NUIGMech0.9 was presented in Chapter 7, while NUIGMech1.0 was first discussed in Chapter 6. The next level in the development of this model was discussed in Chapter 5 with the NUIGMech1.1 version. This version was widely validated and tested against the whole C^3 database available in UG and the literature. The targets used for the validation can be consulted on the C^3 website in the section for “Mechanism Downloads”, in the subsection “Mechanism Validation”. The chemical kinetic report available ranges from $C_0 - C_7$ hydrocarbon species. Finally, the NUIGMech 1.2 was discussed in Chapter 4, and like the 0.9, and 1.0 versions, it was validated only against a smaller number of targets compared to NUIGMech1.1’s validation. Regardless of this, NUIGMech1.2 seems to be more accurate than other versions. Also, it is good to mention that all the important reactions for the whole range of conditions that NUIGMech versions cover are wide and very extensive, here we mention, list and discussed only those reactions that are important and have had changes, updates, refits, or any other modification in its rate constants.

Tables 8-3 - 8-6 show the rate constant for the most important reactions which were updated or changed for the different NUIGMech versions, respectively. Table 8-3 shows all reactions upgraded, new, or refitted corresponding to the C_0 chemistry. Table 8-4 is presented those reactions corresponding to C_1 chemistry. Followed by Table 8-5 which exhibits the reactions corresponding to C_2 chemistry. Finally, Table 8-6 presents all the most important reactions for the C_3 chemistry than have suffered any changes or updates in between NUIGMech versions.

These Tables were made for comparing the different model versions. Considering (a) as NUIGMech0.9, (b) for NUIGMech1.0, (c) for NUIGMech1.1, and (d) as NUIGMech1.2. Tables are formed by six columns whose headers are self-explanatory. The first column includes the reaction name, e.g., $\dot{C}H_3 + \dot{C}H_3 (+M) \leftrightarrow C_2H_6 (+M)$. If the word “Dup” appears before the name it means is a duplicate reaction, thus, this reaction might appear more than once with different values for the different parameters in columns 2 – 4. Column five is a space to place the reference to the author of that rate constant. The (a – d) letters mean that the reaction was included in that version of the mechanism. A new reaction will appear in column six with the word “New”, and a refitted one as

“New Fit” if the exponential coefficient was reduced, e.g., by 30%, it will appear in the legend “A×0.7”, etc.

The first few reactions that were changed/updated/refitted were those controlling the C₀ chemistry, and consequently, the chemistry of the fuels studied in this thesis at low/high temperatures. Reactions for the formation of hydroperoxide (H₂O₂) such as $\dot{\text{H}}\dot{\text{O}}_2 + \dot{\text{H}}\dot{\text{O}}_2 \leftrightarrow \text{H}_2\text{O}_2 + \text{O}_2$, studied by Klippenstein et al [1] were taken in a new fit in NUIGMech0.9 and then put it back to the original values from NUIGMech1.0 to NUIGMech1.2. Klippenstein et al [1] provided a better understanding of the kinetics of this reaction and highlighted the importance of this reaction, particularly at temperatures above about 1000 K. They employed a combination of high-level electronic structure theory (ANL0), a sophisticated transition state theory, and the master equation analyses to predict the thermal kinetics. This reaction is important because it helps to control the levels of hydroxyl ($\dot{\text{H}}\dot{\text{O}}_2$) radicals in atmosphere, which play a crucial role in the atmospheric chemistry and air quality. $\dot{\text{H}}\dot{\text{O}}_2$ radicals are highly reactive species that are involved in the destruction of atmospheric pollutants such as ozone (O₃) and volatile organic compounds (VOCs), to mention a few.

Moreover, another important reaction for hydrogen chemistry, but studied at relatively high temperatures is the recombination reaction $\dot{\text{H}} + \text{O}_2 (+\text{M}) \leftrightarrow \dot{\text{H}}\dot{\text{O}}_2 (+\text{M})$ which was studied by laser flash photolysis in a high-pressure flow cell, over the temperature range 300 – 900 K, the pressure range 1.5 – 950 bar and in the bath gases M = He and N₂ and published by Fernandes et al [2] in 2008. Both rate constants are shown in Table 8-3, with (a–d) symbols referring to the different versions of NUIGMech applying the corresponding changes. Another reaction having a big effect on speciation targets, $\dot{\text{H}}\dot{\text{O}}_2 + \dot{\text{H}} \leftrightarrow \text{O}_2 + \text{H}_2$, was studied by Mueller et al [3] in 1999 using a flow reactor with temperatures ranging from $750 \text{ K} \leq T \leq 1100 \text{ K}$, and pressures of 0.4 – 14.0 atm. Another reaction involved in the hydrogen chemistry studied by Tsang et al [4] is $\text{H}_2\text{O}_2 + \dot{\text{H}} \leftrightarrow \dot{\text{H}}\dot{\text{O}}_2 + \text{H}_2$. Another falloff reaction included in all versions of NUIGMech is the $\dot{\text{H}} + \dot{\text{O}}\text{H} (+\text{M}) \leftrightarrow \text{H}_2\text{O} (+\text{M})$ by Sellevåg et al [5] using high-level quantum chemistry methods. Furthermore, a class of important reactions added to all versions of NIGMech were those ones corresponding to the $\dot{\text{O}}\text{H}\text{V}$ deactivation to $\dot{\text{O}}\text{H}$, such as $\dot{\text{H}} + \ddot{\text{O}} (+\text{M}) \leftrightarrow \dot{\text{O}}\text{H}\text{V} (+\text{M})$, $\dot{\text{O}}\text{H}\text{V} + \text{N}_2 \leftrightarrow \dot{\text{O}}\text{H} + \text{N}_2$, $\dot{\text{O}}\text{H}\text{V} + \ddot{\text{O}} \leftrightarrow \dot{\text{O}}\text{H} + \ddot{\text{O}}$, $\dot{\text{O}}\text{H}\text{V} + \text{Ar} \leftrightarrow \dot{\text{O}}\text{H} + \text{Ar}$, $\dot{\text{O}}\text{H}\text{V} + \dot{\text{O}}\text{H} \leftrightarrow \dot{\text{O}}\text{H} + \dot{\text{O}}\text{H}$, $\dot{\text{O}}\text{H}\text{V} \leftrightarrow \dot{\text{O}}\text{H}$, and $\dot{\text{O}}\text{H}\text{V} + \dot{\text{H}} \leftrightarrow \dot{\text{O}}\text{H} + \dot{\text{H}}$, reported by Hall and Petersen [6] using shock-tube experiments that were conducted in mixtures of H₂/O₂/Ar, CH₄/O₂/Ar, and CH₄/H₂/O₂/Ar with high levels of argon dilution (>98%).

Table 8-3. Rate constants from the C₀ chemistry for the development of (a) NUIGMech0.9, (b) NUIGMech1.0, (c) NUIGMech1.1, and (d) NUIGMech1.2 that have had an upgrade, any change, a refit or simply were aggregated as new reactions. Rate constants are presented in the form of $k = A T^n \exp(-Ea/RT)$ with units of first and second-order reactions are s⁻¹ and cm³ mol⁻¹ s⁻¹, and cal mol⁻¹ for activation energy.

Reactions	A	n	Ea	Ref	Comments
(a) $\dot{\text{H}}\text{O}_2 + \dot{\text{H}}\text{O}_2 \leftrightarrow \text{H}_2\text{O}_2 + \text{O}_2$	1.930×10^{-02}	4.120	-4960.00	[1]	New Fit
Dup (a) $\dot{\text{H}}\text{O}_2 + \dot{\text{H}}\text{O}_2 \leftrightarrow \text{H}_2\text{O}_2 + \text{O}_2$	$6.410 \times 10^{+17}$	-1.540	8540.00	[1]	New Fit
(b-d) $\dot{\text{H}}\text{O}_2 + \dot{\text{H}}\text{O}_2 \leftrightarrow \text{H}_2\text{O}_2 + \text{O}_2$	$1.214 \times 10^{+10}$	0.422	-1480.52	[1]	Original
Dup (b-d) $\dot{\text{H}}\text{O}_2 + \dot{\text{H}}\text{O}_2 \leftrightarrow \text{H}_2\text{O}_2 + \text{O}_2$	$1.688 \times 10^{+16}$	-0.681	12931.66	[1]	Original
(a-d) $\dot{\text{H}} + \text{O}_2 (+\text{M}) \leftrightarrow \dot{\text{H}}\text{O}_2 (+\text{M})$	Falloff, see model			[2]	A×0.7
(a) $\dot{\text{H}}\text{O}_2 + \dot{\text{H}} \leftrightarrow \text{H}_2 + \text{O}_2$	$3.060 \times 10^{+06}$	2.090	-1451.00	[3]	New Fit
(b-d) $\dot{\text{H}}\text{O}_2 + \dot{\text{H}} \leftrightarrow \text{H}_2 + \text{O}_2$	$2.800 \times 10^{+06}$	2.090	-1451.00	[3]	A×0.9
(a-d) $\text{H}_2\text{O}_2 + \dot{\text{H}} \leftrightarrow \dot{\text{H}}\text{O}_2 + \text{H}_2$	$5.020 \times 10^{+06}$	2.070	4300.00	[4]	New
(a-d) $\dot{\text{H}} + \dot{\text{O}}\text{H} (+\text{M}) \leftrightarrow \text{H}_2\text{O} (+\text{M})$	Falloff, see model			[5]	New
(a-d) $\dot{\text{H}} + \dot{\text{O}} (+\text{M}) \leftrightarrow \dot{\text{O}}\text{H}\text{V} (+\text{M})$	$4.430 \times 10^{+14}$	0.000	10000.00	[6]	New
(a-d) $\dot{\text{O}}\text{H}\text{V} + \text{N}_2 \leftrightarrow \dot{\text{O}}\text{H} + \text{N}_2$	$2.100 \times 10^{+12}$	0.500	-482.00	[6]	New
(a-d) $\dot{\text{O}}\text{H}\text{V} + \dot{\text{O}} \leftrightarrow \dot{\text{O}}\text{H} + \dot{\text{O}}$	$1.500 \times 10^{+12}$	0.500	0.00	[6]	New
(a-d) $\dot{\text{O}}\text{H}\text{V} + \text{Ar} \leftrightarrow \dot{\text{O}}\text{H} + \text{Ar}$	$2.170 \times 10^{+10}$	0.500	2060.00	[6]	New
(a-d) $\dot{\text{O}}\text{H}\text{V} + \dot{\text{O}}\text{H} \leftrightarrow \dot{\text{O}}\text{H} + \dot{\text{O}}\text{H}$	$1.500 \times 10^{+12}$	0.500	0.00	[6]	New
(a-d) $\dot{\text{O}}\text{H}\text{V} \leftrightarrow \dot{\text{O}}\text{H}$	$1.400 \times 10^{+06}$	0.000	0.00	[6]	New
(a-d) $\dot{\text{O}}\text{H}\text{V} + \dot{\text{H}} \leftrightarrow \dot{\text{O}}\text{H} + \dot{\text{H}}$	$1.500 \times 10^{+12}$	0.500	0.00	[6]	New

Additionally, to those changes in the mechanisms for C₀, Table 8-4 presents those updates done to the mechanisms corresponding to C₁ chemistry. The inhibiting and promoting, termination and chain reactions for C₁, such as the bimolecular reaction $\dot{\text{C}}\text{H}_3 + \dot{\text{H}}\text{O}_2 \leftrightarrow \text{CH}_4 + \text{O}_2$ and $\dot{\text{C}}\text{H}_3 + \dot{\text{H}}\text{O}_2 \leftrightarrow \text{CH}_3\dot{\text{O}} + \dot{\text{O}}\text{H}$, were calculated using direct variable reaction coordinate transition state theory (VRC-TST), coupled with high level multireference electronic structure calculations, and use to compute capture rates for the $\dot{\text{C}}\text{H}_3 + \dot{\text{H}}\text{O}_2$ reaction in this study by Jasper et al. [7]. Followed by a pair of falloff reactions included as a new fit of the original rates, $\text{CH}_2\text{O}_2 (+\text{M}) \leftrightarrow \text{CO} + \text{H}_2\text{O} (+\text{M})$ and $\text{CH}_2\text{O}_2 (+\text{M}) \leftrightarrow \text{CO}_2 + \text{H}_2 (+\text{M})$, published by Chang et al [8] in 2007, they studied computationally by the high-level G2M(CC1) method and microcanonical RRKM the kinetics and mechanisms for the unimolecular decomposition reactions of formic acid and oxalic acid.

An important addition to the NUIGMech versions was the methoxy and methyldioxy classes with new fits reported by Lightfoot et al. [9], this includes the next reactions; $\text{CH}_3\dot{\text{O}}_2 + \dot{\text{C}}\text{H}_3 \leftrightarrow \text{CH}_3\dot{\text{O}}$

+ $\text{CH}_3\dot{\text{O}}$, $\text{CH}_3\dot{\text{O}}_2 + \text{CH}_3\dot{\text{O}}_2 \leftrightarrow \text{CH}_3\dot{\text{O}} + \text{CH}_3\dot{\text{O}} + \text{O}_2$, and $\text{CH}_3\dot{\text{O}}_2 + \text{CH}_3\dot{\text{O}}_2 \rightarrow \text{CH}_2\text{O} + \text{CH}_3\text{OH} + \text{O}_2$, they studied for temperatures between 600 and 719 K and at atmospheric pressure, using the flash photolysis/UV absorption method. Together with the inclusion of the $\text{CH}_3\dot{\text{O}}_2$ dissociation reaction ($\text{CH}_3\dot{\text{O}}_2 \leftrightarrow \text{CH}_2\text{O} + \dot{\text{O}}\text{H}$) by Villano et al. [10] that used electronic structure calculations performed at the CBS-QB3 level of theory in NUIGMech1.2. The methyl +methyl radical self-recombination reaction important for methane blends in both low/high temperatures was first updated using Wang et al. [11] using time-resolved time-of-flight mass spectrometry from NUIGMech0.9 – NUIGMech1.1. Nonetheless, an excellent improvement in IDT prediction is achieved by updating the $\dot{\text{C}}\text{H}_3 + \dot{\text{C}}\text{H}_3 (+\text{M}) \leftrightarrow \text{C}_2\text{H}_6 (+\text{M})$ rate constants with Blitz et al [12] which used a master equation (ME) that utilized inverse Laplace transformation to link the microcanonical rate constants for dissociation, updated in NUIGMech1.2. Another addition improving the predictions and extends the chemistry involved in C_1 , is the thermal decomposition of alkyl hydroperoxides ($\text{R}'\text{OOH}$) through the reaction $\text{CH}_4 + \dot{\text{O}}_2\text{CHO} \leftrightarrow \dot{\text{C}}\text{H}_3 + \text{HO}_2\text{CHO}$, reported by Carstensen et al. [13] it was first included in NUIGMech0.9 and stay unchanged until NUIGMech1.2.

Moreover, new fits for the methyldiyne ($\ddot{\text{C}}\text{H}$) class addition for NUIGMech0.9 – NUIGMech1.2 from Hall et al [6] rates that used shock-tube experiments, $\ddot{\text{C}}\text{H} + \text{O}_2 \leftrightarrow \text{CO} + \dot{\text{O}}\text{H}\text{V}$, $\ddot{\text{C}}\text{H} + \text{O}_2 \leftrightarrow \text{HCO} + \ddot{\text{O}}$, $\ddot{\text{C}}\text{H} + \text{O}_2 \rightarrow \dot{\text{H}} + \text{CO} + \ddot{\text{O}}$, and $\ddot{\text{C}}\text{H} + \text{O}_2 \leftrightarrow \dot{\text{H}} + \text{CO}_2$, these reactions are an important update because $\ddot{\text{C}}\text{H}$ serves as a building block for more complex organic compounds and participates in numerous chemical reactions. Also, $\ddot{\text{C}}\text{H}$ is a key species in astrochemistry and the study of star formation, as it has been detected in various astronomical environments, including molecular clouds and star-forming regions. Analogous to $\ddot{\text{C}}\text{H}$ class, a set of reactions were included for methylene ($\ddot{\text{C}}\text{H}_2$) class reactions, reported by Klippenstein [14] and calculated using high-level theory, $\ddot{\text{C}}\text{H}_2 + \text{O}_2 \leftrightarrow \text{CH}_2\text{O} + \ddot{\text{O}}$ using original values from NUIGMech0.9 – NUIGMech1.1, and then increased by 1.5 times for NUIGMech1.2. Similarly, for $\ddot{\text{C}}\text{H}_2 + \text{O}_2 \rightarrow \text{CO}_2 + \dot{\text{H}} + \dot{\text{H}}$ the original values were used in NUIGMech0.9 – NUIGMech1.1, and then updated to $\text{A} \times 2.0$ times for NUIGMech1.2. Also, methylene units can be linked to form polymers, which make a wide range of materials, including plastics, synthetic fibres, and rubber. Methylene is also involved in several critical biological processes, such as the synthesis of cholesterol and other lipids, and the metabolism of amino acids.

Table 8-4. Rate constants from the C₁ chemistry for the development of (a) NUIGMech0.9, (b) NUIGMech1.0, (c) NUIGMech1.1, and (d) NUIGMech1.2 that have had an upgrade, any change, a refit or simply were aggregated as new reactions. Rate constants are presented in the form of $k = A T^n \exp(-Ea/RT)$ with units of first and second-order reactions are s⁻¹ and cm³ mol⁻¹ s⁻¹, and cal mol⁻¹ for activation energy.

Reactions	A	n	Ea	Ref	Comments
(a) $\dot{\text{C}}\text{H}_3 + \text{H}\dot{\text{O}}_2 \leftrightarrow \text{CH}_4 + \text{O}_2$	$1.200 \times 10^{+05}$	2.227	-3021.36	[7]	New Fit
(b-d) $\dot{\text{C}}\text{H}_3 + \text{H}\dot{\text{O}}_2 \leftrightarrow \text{CH}_4 + \text{O}_2$	$1.819 \times 10^{+03}$	2.830	-3730.00	[7]	New Fit
(a-d) $\dot{\text{C}}\text{H}_3 + \text{H}\dot{\text{O}}_2 \leftrightarrow \text{CH}_3\dot{\text{O}} + \dot{\text{O}}\text{H}$	$1.000 \times 10^{+12}$	0.269	-687.50	[7]	New Fit
(a-d) $\text{HOCHO} (+\text{M}) \leftrightarrow \text{CO} + \text{H}_2\text{O} (+\text{M})$	Falloff, see model			[8]	New Fit
(a-d) $\text{HOCHO} (+\text{M}) \leftrightarrow \text{CO}_2 + \text{H}_2$	Falloff, see model			[8]	New Fit
(a) $\text{CH}_3\dot{\text{O}}_2 + \dot{\text{C}}\text{H}_3 \leftrightarrow \text{CH}_3\dot{\text{O}} + \text{CH}_3\dot{\text{O}}$	$5.080 \times 10^{+12}$	0.000	-1411.00	[9]	New Fit
(b-d) $\text{CH}_3\dot{\text{O}}_2 + \dot{\text{C}}\text{H}_3 \leftrightarrow \text{CH}_3\dot{\text{O}} + \text{CH}_3\dot{\text{O}}$	$5.849 \times 10^{+11}$	0.353	-1460.00	[9]	New Fit
(b) $\text{CH}_3\dot{\text{O}}_2 + \text{CH}_3\dot{\text{O}}_2 \leftrightarrow \text{CH}_3\dot{\text{O}} + \text{CH}_3\dot{\text{O}} + \text{O}_2$	$1.400 \times 10^{+16}$	-1.610	1860.00	[9]	New Fit
(b) $\text{CH}_3\dot{\text{O}}_2 + \text{CH}_3\dot{\text{O}}_2 \rightarrow \text{CH}_2\text{O} + \text{CH}_3\text{OH} + \text{O}_2$	$3.110 \times 10^{+14}$	-1.610	-1051.00	[9]	New Fit
(d) $\text{CH}_3\dot{\text{O}}_2 \leftrightarrow \text{CH}_2\text{O} + \dot{\text{O}}\text{H}$	$8.250 \times 10^{+02}$	0.850	39000.00	[10]	New Fit
(a-c) $\dot{\text{C}}\text{H}_3 + \dot{\text{C}}\text{H}_3 (+\text{M}) \leftrightarrow \text{C}_2\text{H}_6 (+\text{M})$	Falloff, see model			[11]	New Fit
(d) $\dot{\text{C}}\text{H}_3 + \dot{\text{C}}\text{H}_3 (+\text{M}) \leftrightarrow \text{C}_2\text{H}_6 (+\text{M})$	Falloff, see model			[12]	New Fit
(a-d) $\text{CH}_4 + \dot{\text{O}}_2\text{CHO} \leftrightarrow \dot{\text{C}}\text{H}_3 + \text{HO}_2\text{CHO}$	$3.220 \times 10^{+03}$	3.1300	15200.00	[13]	New Fit
(a-d) $\dot{\text{C}}\text{H} + \text{O}_2 \leftrightarrow \text{CO} + \dot{\text{O}}\text{H}\text{V}$	$3.240 \times 10^{+14}$	-0.4000	4150.00	[6]	New Fit
(a-d) $\dot{\text{C}}\text{H} + \text{O}_2 \leftrightarrow \text{HCO} + \dot{\text{O}}$	$3.240 \times 10^{+14}$	-0.4000	4150.00	[6]	New Fit
(a-d) $\dot{\text{C}}\text{H} + \text{O}_2 \rightarrow \dot{\text{H}} + \text{CO} + \dot{\text{O}}$	$4.860 \times 10^{+14}$	-0.4000	4150.00	[6]	A×1.5
(a-d) $\dot{\text{C}}\text{H} + \text{O}_2 \leftrightarrow \dot{\text{H}} + \text{CO}_2$	$4.860 \times 10^{+14}$	-0.4000	4150.00	[6]	A×1.5
(a-c) $\ddot{\text{C}}\text{H}_2 + \text{O}_2 \leftrightarrow \text{CH}_2\text{O} + \dot{\text{O}}$	$1.300 \times 10^{+14}$	2.4202	1604.00	[14]	New Fit
(d) $\ddot{\text{C}}\text{H}_2 + \text{O}_2 \leftrightarrow \text{CH}_2\text{O} + \dot{\text{O}}$	$1.950 \times 10^{+05}$	2.4202	1604.00	[14]	A×1.5
(a-c) $\ddot{\text{C}}\text{H}_2 + \text{O}_2 \rightarrow \text{CO}_2 + \dot{\text{H}} + \dot{\text{H}}$	$1.050 \times 10^{+09}$	0.9929	-269.00	[14]	New Fit
(d) $\ddot{\text{C}}\text{H}_2 + \text{O}_2 \rightarrow \text{CO}_2 + \dot{\text{H}} + \dot{\text{H}}$	$2.100 \times 10^{+09}$	0.9929	-269.00	[14]	A×2

Furthermore, promoting and inhibiting reactions for C₂ blends corresponding to those directly influencing ethylene chemistry such as $\dot{\text{C}}_2\text{H}_3 + \dot{\text{H}} \leftrightarrow \text{C}_2\text{H}_4$, and $\text{C}_2\text{H}_4 (+\text{M}) \leftrightarrow \text{H}_2 + \text{H}_2\text{C}\dot{\text{C}} (+\text{M})$, were updated in all versions of NUIGMech to improve predictions, these rates were reported by Klippenstein et al [15], and Gimenez-Lopez et al [16], respectively. Also, the reaction for hydrogen abstraction by H-atom from C₂H₄, $\text{C}_2\text{H}_4 + \dot{\text{H}} \leftrightarrow \dot{\text{C}}_2\text{H}_3 + \text{H}_2$, reported by Somers [17] was used in NUIGMech0.9–NIGMech1.1 but updated using Power et al [18] rate calculated with high-level theory in NUIGMech1.2, improving in this way the quality of the chemistry in the mechanism. Similarly, the rate for the reaction of the radical addition or n-propyl radical dissociation, $\text{C}_2\text{H}_4 + \dot{\text{C}}\text{H}_3$

$\leftrightarrow n\dot{C}_3H_7$, was applied first using Miller et al [19] rate in NUIGMech0.9–NUIGMech1.1, which was updated with the rate reported by Power et al [18], both studies reported rates calculated with a high level of theory, however, Power et al [18] rate are from 2021 with the latest approaches to guarantee accuracy in the calculations.

On the other hand, reactions with hydroperoxyl ($H\dot{O}_2$) radicals producing hydroperoxide (H_2O_2) and vinyl radicals, such as $C_2H_4 + H\dot{O}_2 \leftrightarrow \dot{C}_2H_3 + H_2O_2$, and the O-atom reaction with ethylene, $C_2H_4 + \ddot{O} \leftrightarrow \ddot{C}H_2 + CH_2O$, producing formaldehyde which is a key intermediate at relatively low/high temperatures was adopted from Li et al [20] that studied this reaction at elevated temperatures employing empirical treatments of intersystem crossing (ISC), they predicted the kinetics of $C_2H_4 + \ddot{O}$ using an ab initio transition state theory based master equation (AITSTME) approach that includes an a priori description of ISC. Additionally, the pressure dependant Arrhenius reactions that produce oxirane molecules and $\dot{O}H$ radicals, $C_2H_4 + H\dot{O}_2 \leftrightarrow C_2H_4O_{1-2} + \dot{O}H$, reported by Klippenstein [21] was updated from NUIG0.9 and keep it unchanged until NUIGMech1.2 version. Followed by the falloff rate for $C_2H_4 + \dot{H} (+M) \leftrightarrow \dot{C}_2H_5 (+M)$ constant reported by Power et al [18] and updated for the low/high-pressure limits (LP/HPL) using $A \times 0.7$ factor in NUIGMech0.9 – NUIGMech1.1 and further reducing the formation of ethyl radical in NUIGMech1.2 while this rate was put back to the original values for LP/HPL.

Moreover, those reactions for C_2 blends corresponding influencing directly ethane chemistry, like, $C_2H_5\dot{O}_2 \leftrightarrow C_2H_4 + H\dot{O}_2$, first was updated in NUIGMech0.9, but after changing the HPL by a factor of $HPL \times 1.3$ in NUIGMech1.0 – NUIGMech1.2, this reported by Klippenstein [21] in 2017. Another reaction producing $R'\dot{O}$ and $\dot{O}H$ radicals, $\dot{C}_2H_5 + H\dot{O}_2 \leftrightarrow C_2H_5\dot{O} + \dot{O}H$. Additionally, the hydrogen abstraction from ethane by $H\dot{O}_2$, $C_2H_6 + H\dot{O}_2 \leftrightarrow \dot{C}_2H_5 + H_2O_2$, producing ethyl radicals and hydroperoxide molecules published by Aguilera-Iparraguirre et al [22], first used with original values for the rate in NUIGMech0.9, then updated by a factor of $A \times 0.8$ to reduce the production. However, in the final version of NUIGMech, it was needed to increase this production of radicals by a factor of $A \times 1.25$. Finally, the reactions for $R'O\dot{O} \rightarrow R'OOH$ with ethane reported by Carstensen et al [30] in 2007 studied the associated activation energies followed an Evans–Polanyi relationship while a common A-factor could be used to describe the kinetics, $C_2H_6 + \dot{O}_2CHO \leftrightarrow \dot{C}_2H_5 + HO_2CHO$, $C_2H_6 + CH_3\dot{O}_2 \leftrightarrow \dot{C}_2H_5 + CH_3O_2H$, and $C_2H_6 + C_2H_5\dot{O}_2 \leftrightarrow \dot{C}_2H_5 + C_2H_5O_2H$, were included in NUIGMech0.9 and kept unchanged until NUGMech1.2.

Table 8-5. Rate constants from the C₂ chemistry for the development of (a) NUIGMech0.9, (b) NUIGMech1.0, (c) NUIGMech1.1, and (d) NUIGMech1.2 that have had an upgrade, any change, a refit or simply were aggregated as new reactions. Rate constants are presented in the form of $k = A T^n \exp(-E_a/RT)$ with units of first and second-order reactions are s⁻¹ and cm³ mol⁻¹ s⁻¹, and cal mol⁻¹ for activation energy.

Reactions	A	n	E _a	Ref	Comments
(a-d) $\dot{C}_2H_3 + \dot{H} \leftrightarrow C_2H_4$	pdep, see model			[15]	A×0.7
(a-d) $C_2H_4 (+M) \leftrightarrow H_2 + H_2C\dot{C} (+M)$	Falloff, see model			[16]	A/2
(a-c) $C_2H_4 + \dot{H} \leftrightarrow \dot{C}_2H_3 + H_2$	$6.189 \times 10^{+06}$	2.310	12829.90	[17]	New Fit
(d) $C_2H_4 + \dot{H} \leftrightarrow \dot{C}_2H_3 + H_2$	$4.790 \times 10^{+05}$	2.550	12400.00	[18]	New Fit
(a-c) $C_2H_4 + \dot{C}H_3 \leftrightarrow n\dot{C}_3H_7$	pdep, see model			[19]	New Fit
(d) $C_2H_4 + \dot{C}H_3 \leftrightarrow n\dot{C}_3H_7$	pdep, see model			[18]	New Fit
(a-d) $C_2H_4 + \dot{H}O_2 \leftrightarrow \dot{C}_2H_3 + H_2O_2$	$1.914 \times 10^{+03}$	3.059	20798.60	[7]	A×1.2
(a-d) $C_2H_4 + \ddot{O} \leftrightarrow \ddot{C}H_2 + CH_2O$	$5.775 \times 10^{+06}$	1.991	2859.75	[20]	A×1.3
(a-d) $C_2H_4 + \dot{H}O_2 \leftrightarrow C_2H_4O1-2 + \dot{O}H$	pdep, see model			[21]	A×1.2
(a-c) $C_2H_4 + \dot{H} (+M) \leftrightarrow \dot{C}_2H_5 (+M)$	Falloff, see model			[18]	HP/LP×0.7
(d) $C_2H_4 + \dot{H} (+M) \leftrightarrow \dot{C}_2H_5 (+M)$	Falloff, see model			[18]	New Fit
(a) $C_2H_5\dot{O}_2 \leftrightarrow C_2H_4 + \dot{H}O_2$	pdep, see model			[21]	New Fit
(b-d) $C_2H_5\dot{O}_2 \leftrightarrow C_2H_4 + \dot{H}O_2$	pdep, see model			[21]	HPL×1.3
(a-d) $\dot{C}_2H_5 + \dot{H}O_2 \leftrightarrow C_2H_5\dot{O} + \dot{O}H$	$1.000 \times 10^{+12}$	0.269	-688.00	[7]	A×1.1
(a) $C_2H_6 + \dot{H}O_2 \leftrightarrow \dot{C}_2H_5 + H_2O_2$	$3.460 \times 10^{+01}$	3.590	15600.00	[22]	New Fit
(b-c) $C_2H_6 + \dot{H}O_2 \leftrightarrow \dot{C}_2H_5 + H_2O_2$	$2.770 \times 10^{+01}$	3.590	15600.00	[22]	A×0.8
(d) $C_2H_6 + \dot{H}O_2 \leftrightarrow \dot{C}_2H_5 + H_2O_2$	$3.460 \times 10^{+01}$	3.590	15600.00	[22]	A×1.25
(a-d) $C_2H_6 + O_2CHO \leftrightarrow \dot{C}_2H_5 + HO_2CHO$	$4.230 \times 10^{+03}$	2.960	10500.00	[13]	New Fit
(a-d) $C_2H_6 + CH_3\dot{O}_2 \leftrightarrow \dot{C}_2H_5 + CH_3O_2H$	$4.040 \times 10^{+01}$	3.550	16900.00	[13]	New Fit
(a-d) $C_2H_6 + C_2H_5\dot{O}_2 \leftrightarrow \dot{C}_2H_5 + C_2H_5O_2H$	$5.880 \times 10^{+01}$	3.490	17100.00	[13]	New Fit

Finally, from Table 8-5, some important promoting reactions for propane chemistry such as H-atom abstraction by $\dot{O}H$ were added since NUIGMech0.9 and keep it until the last version NUIGMech1.2 unchanged, for low temperatures, $C_3H_8 + \dot{O}H \leftrightarrow n\dot{C}_3H_7 + H_2O$, and the inhibiting reaction $C_3H_8 + \dot{O}H \leftrightarrow i\dot{C}_3H_7 + H_2O$ reported by Badra et al [23] in 2014 were determined experimentally by monitoring the reaction of $\dot{O}H$ with two normal and six deuterated alkanes. Moreover, falloff reactions such as $C_3H_8 (+M) \leftrightarrow \dot{C}_2H_5 + \dot{C}H_3 (+M)$ published by Sivaramakrishnan et al [24] using both shock tube experiments and ab initio transition state theory-based master equation calculations, and the reverse reaction $n\dot{C}_3H_7 + \dot{H} (+M) \leftrightarrow C_3H_8 (+M)$ by Tsang et al [25], are important because they help us to understand the limiting reaction rates and the transition state of

chemical reactions. These reactions were added in NUIGMech0.9 and stayed unchanged until NUIGMech1.2. Also, the addition of the reactions corresponding to H-atom abstraction by $\dot{\text{H}}$, such as $n\dot{\text{C}}_3\text{H}_7 + \dot{\text{H}} \leftrightarrow \text{C}_3\text{H}_6 + \text{H}_2$ and $i\dot{\text{C}}_3\text{H}_7 + \dot{\text{H}} \leftrightarrow \text{C}_3\text{H}_6 + \text{H}_2$ published by Tsang et al [25] was implemented.

Moreover, a pair of important reactions with hydroperoxyl (HO_2) radicals are the next, $\text{C}_3\text{H}_8 + \text{HO}_2 \leftrightarrow n\dot{\text{C}}_3\text{H}_7 + \text{H}_2\text{O}_2$ and $\text{C}_3\text{H}_8 + \text{HO}_2 \leftrightarrow i\dot{\text{C}}_3\text{H}_7 + \text{H}_2\text{O}_2$ studied by Aguilera-Iparraguirre et al [26] using explicitly correlated coupled-cluster theory with singles and doubles (CCSD-R12) in a large 19s14p8d6f4g3h basis (9s6p4d3f for $\dot{\text{H}}$) to approach the basis-set limit at the coupled-cluster singles–doubles level, were included also. Another important change is the inclusion of pressure-dependent Arrhenius reactions which are important because they help us to understand the effect of pressure on the rate and mechanism of chemical reactions. The addition of the RO_2 reaction, $n\text{C}_3\text{H}_7\dot{\text{O}}_2 \leftrightarrow \text{HO}_2 + \text{C}_3\text{H}_6$, was reported by Goldsmith et al [27] using high-level ab initio calculations. Additionally, to improve the quality of the chemistry involved in the detailed mechanism, NUIGMech1.2, the reactions of alkene +methyl, and alkene + H-atom in the propane chemistry, were included. These reactions $n\dot{\text{C}}_3\text{H}_7 \leftrightarrow \text{C}_2\text{H}_4 + \dot{\text{C}}\text{H}_3$, and $i\dot{\text{C}}_3\text{H}_7 \leftrightarrow \text{C}_2\text{H}_4 + \dot{\text{C}}\text{H}_3$ along with $\text{C}_3\text{H}_6 + \dot{\text{H}} \leftrightarrow n\dot{\text{C}}_3\text{H}_7$, and $\text{C}_3\text{H}_6 + \dot{\text{H}} \leftrightarrow i\dot{\text{C}}_3\text{H}_7$, reported by Power et al [18] were calculated with high-level theory ab initio and replace those reported by Miller et al [19] and used from NUIGMech0.9 to NUIGMech1.1. These changes help to improve the chemistry involved in the propane blends; however, it has a setback effect in propene blends, especially in pure propane and propene. This needs to be addressed in future versions of chemical kinetic models with further development.

Table 8-6. Rate constants from the C_3 chemistry for the development of (a) NUIGMech0.9, (b) NUIGMech1.0, (c) NUIGMech1.1, and (d) NUIGMech1.2 that have had an upgrade, any change, a refit or simply were aggregated as new reactions. Rate constants are presented in the form of $k = A T^n \exp(-Ea/RT)$ with units of first and second-order reactions are s^{-1} and $\text{cm}^3 \text{mol}^{-1} \text{s}^{-1}$, and cal mol^{-1} for activation energy.

Reactions	A	n	Ea	Ref	Comments
(a–d) $\text{C}_3\text{H}_8 + \dot{\text{O}}\text{H} \leftrightarrow n\dot{\text{C}}_3\text{H}_7 + \text{H}_2\text{O}$	$6.865 \times 10^{+06}$	2.000	677.31	[23]	New Fit
(a–d) $\text{C}_3\text{H}_8 + \dot{\text{O}}\text{H} \leftrightarrow i\dot{\text{C}}_3\text{H}_7 + \text{H}_2\text{O}$	$3.738 \times 10^{+05}$	2.305	–561.32	[23]	New Fit
(a–d) $\text{C}_3\text{H}_8 (+\text{M}) \leftrightarrow \dot{\text{C}}_2\text{H}_5 + \dot{\text{C}}\text{H}_3 (+\text{M})$	Falloff, see model			[24]	New Fit
(a–d) $n\dot{\text{C}}_3\text{H}_7 + \dot{\text{H}} (+\text{M}) \leftrightarrow \text{C}_3\text{H}_8 (+\text{M})$	Falloff, see model			[25]	New Fit
(a–d) $n\dot{\text{C}}_3\text{H}_7 + \dot{\text{H}} \leftrightarrow \text{C}_3\text{H}_6 + \text{H}_2$	$1.810 \times 10^{+12}$	0.000	0.00	[25]	New Fit
(a–d) $i\dot{\text{C}}_3\text{H}_7 + \dot{\text{H}} \leftrightarrow \text{C}_3\text{H}_6 + \text{H}_2$	$3.610 \times 10^{+12}$	0.000	0.00	[25]	New Fit
(a–d) $\text{C}_3\text{H}_8 + \text{HO}_2 \leftrightarrow n\dot{\text{C}}_3\text{H}_7 + \text{H}_2\text{O}_2$	$2.080 \times 10^{+01}$	3.590	15600.00	[26]	New Fit
(a–d) $\text{C}_3\text{H}_8 + \text{HO}_2 \leftrightarrow i\dot{\text{C}}_3\text{H}_7 + \text{H}_2\text{O}_2$	$6.320 \times 10^{+01}$	3.370	13720.00	[26]	A×0.6

(a–d) $n\text{C}_3\text{H}_7\dot{\text{O}}_2 \leftrightarrow \text{H}\dot{\text{O}}_2 + \text{C}_3\text{H}_6$	pdep, see model	[27]	New Fit
(a–c) $n\dot{\text{C}}_3\text{H}_7 \leftrightarrow \text{C}_2\text{H}_4 + \dot{\text{C}}\text{H}_3$	pdep, see model	[19]	New Fit
(d) $n\dot{\text{C}}_3\text{H}_7 \leftrightarrow \text{C}_2\text{H}_4 + \dot{\text{C}}\text{H}_3$	pdep, see model	[18]	New Fit
(a–c) $i\dot{\text{C}}_3\text{H}_7 \leftrightarrow \text{C}_2\text{H}_4 + \dot{\text{C}}\text{H}_3$	pdep, see model	[19]	New Fit
(d) $i\dot{\text{C}}_3\text{H}_7 \leftrightarrow \text{C}_2\text{H}_4 + \dot{\text{C}}\text{H}_3$	pdep, see model	[18]	New Fit
(a–c) $\text{C}_3\text{H}_6 + \dot{\text{H}} \leftrightarrow n\dot{\text{C}}_3\text{H}_7$	pdep, see model	[19]	New Fit
(d) $\text{C}_3\text{H}_6 + \dot{\text{H}} \leftrightarrow n\dot{\text{C}}_3\text{H}_7$	pdep, see model	[18]	New Fit
(a–c) $\text{C}_3\text{H}_6 + \dot{\text{H}} \leftrightarrow i\dot{\text{C}}_3\text{H}_7$	pdep, see model	[19]	New Fit
(d) $\text{C}_3\text{H}_6 + \dot{\text{H}} \leftrightarrow i\dot{\text{C}}_3\text{H}_7$	pdep, see model	[18]	New Fit

References

- [1] S.J. Klippenstein, R. Sivaramakrishnan, U. Burke, K.P. Somers, H.J. Curran, L. Cai, H. Pitsch, M. Pelucchi, T. Faravelli, P. Glarborg, $\text{H}\dot{\text{O}}_2 + \text{H}\dot{\text{O}}_2$: High level theory and the role of singlet channels, *Combustion and Flame*, 243(2022), 111975.
- [2] R.X. Fernandes, K. Luther, J. Troe and V.G. Ushakov, Experimental and modelling study of the recombination reaction $\dot{\text{H}} + \text{O}_2(+\text{M}) \rightarrow \text{H}\dot{\text{O}}_2(+\text{M})$ between 300 and 900 K, 1.5 and 950 bar, and in the bath gases $\text{M} = \text{He}, \text{Ar}, \text{and } \text{N}_2$, *Phys. Chem. Chem. Phys.* 10(2008), 4313-4321.
- [3] M.A. Mueller, R.A. Yetter, and F.L. Dryer, Flow reactor studies and kinetic modeling of the $\text{H}_2/\text{O}_2/\text{NOX}$ and $\text{CO}/\text{H}_2\text{O}/\text{O}_2/\text{NOX}$ reactions, *Int. J. Chem. Kinet.*, 31(1999), 705-724.
- [4] W. Tsang, R.F. Hampson, Chemical kinetic data base for combustion chemistry. part I. methane and related compounds, *J. Phys. Chem. Ref. Data* 15(1986), 1087–1279.
- [5] S.R. Sellevåg, Y. Georgievskii, and J.A. Miller; The Temperature and pressure dependence of the reactions $\dot{\text{H}} + \text{O}_2(+\text{M}) \rightarrow \text{H}\dot{\text{O}}_2(+\text{M})$ and $\dot{\text{H}} + \dot{\text{O}}\text{H}(+\text{M}) \rightarrow \text{H}_2\text{O}(+\text{M})$, *J. Phys. Chem. A* 112(2008), 5085-5095.
- [6] J.M. Hall, E.L. Petersen, An optimized kinetics model for $\dot{\text{O}}\text{H}$ chemiluminescence at high temperatures and atmospheric pressures, *Int. J. Chem. Kinet.*, 38(2006), 714-724.
- [7] A.W. Jasper, S.J. Klippenstein, L.B. Harding, Theoretical rate coefficients for the reaction of methyl radical with hydroperoxyl radical and for methylhydroperoxide decomposition, *Proc Combust Inst.*, 32 (2009) 279-286.
- [8] J.-G. Chang, H.-T. Chen, S. Xu, and M.C. Lin, Computational study on the kinetics and mechanisms for the unimolecular decomposition of formic and oxalic acids, *J. Phys. Chem. A* 111(2007), 29, 6789-6797.
- [9] P.D. Lightfoot, P. Roussel, F. Caralp, and R. Lesclaux, Flash photolysis study of the $\text{CH}_3\dot{\text{O}}_2 + \text{CH}_3\dot{\text{O}}_2$ and $\text{CH}_3\dot{\text{O}}_2 + \text{H}\dot{\text{O}}_2$ reactions between 600 and 719 K: unimolecular decomposition of methylhydroperoxide, *J. Chem. Soc. Faraday Trans.* (1991), 87(19), 3213--3220.
- [10] S.M. Villano, L.K. Huynh, H.-H. Carstensen, and A.M. Dean, High-pressure rate rules for alkyl+ O_2 reactions. 1. the dissociation, concerted elimination, and isomerization channels of the alkyl peroxy radical, *J. Phys. Chem. A* 115(2011), 46, 13425–13442.
- [11] C.-H. Wang, S.V. Panteleev, A.E. Masunov, T.C. Allison, S. Chang, C. Lim, Y. Jin, and S.S. Vasu, Molecular dynamics of combustion reactions in supercritical carbon dioxide. part 5: computational study of ethane dissociation and recombination reactions $\text{C}_2\text{H}_6 \rightleftharpoons \dot{\text{C}}\text{H}_3 + \dot{\text{C}}\text{H}_3$, *The Journal of Physical Chemistry A* (2019) 123 (22), 4776-4784.
- [12] M.A. Blitz, N.J.B. Green, R.J. Shannon, M.J. Pilling, P.W. Seakins, C.M. Western, S.H. Robertson, Reanalysis of rate data for the reaction $\dot{\text{C}}\text{H}_3 + \dot{\text{C}}\text{H}_3 \rightarrow \text{C}_2\text{H}_6$ using revised cross sections and a linearized second-order master equation, *J. Phys. Chem. A* 119(2015), 28, 7668-7682.
- [13] H.-H. Carstensen, A.M. Dean, O. Deutschmann, Rate constants for the H-abstraction from alkanes ($\text{R}-\text{H}$) by $\text{R}'\text{O}_2$ radicals: a systematic study on the impact of R and R', *Proc. Combust. Inst.* 31(2007) 149-157.
- [14] Private communication with S. J. Klippenstein.

- [15] S.J. Klippenstein and L.B. Harding, A theoretical study of the kinetics of $\dot{C}_2H_3 + \dot{H}$, *Phys. Chem. Chem. Phys.* 1(1999), 989-997.
- [16] J. Gimenez-Lopez, C.T. Rasmussen, H. Hashemi, M.U. Alzueta, Y. Gao, P. Marshall, P. Glarborg, Experimental and kinetic modeling study of C_2H_2 oxidation at high pressure. *Int. J. of Chem. Kin.*, (2016), 48(11), 724-738.
- [17] Private communication with K.P. Somers.
- [18] J. Power, K.P. Somers, S.S. Nagaraja, H.J. Curran, A hierarchical study of the reactions of hydrogen atoms to alkenes: a theoretical study of the reactions of hydrogen atoms with C_2-C_4 alkenes, *J. Phys. Chem. A* (2021), 125(23), 5124-5145.
- [19] J.A. Miller, S.J. Klippenstein, Dissociation of propyl radicals and other reactions on a \dot{C}_3H_7 potential, *J. Phys. Chem. A* 117(2013) 2718-2727.
- [20] X. Li, A.W. Jasper, J. Zádor, J.A. Miller, and S.J. Klippenstein, Theoretical kinetics of $\ddot{O} + C_2H_4$, *Proc. Combust. Inst.* volume 36(2017), 219-227.
- [21] S.J. Klippenstein, From theoretical reaction dynamics to chemical modeling of combustion, *Proc. Combust. Inst.* volume 36(2017), 77-111.
- [22] J. Aguilera-Iparraguirre, H.J. Curran, W. Klopper, and J.M. Simmie, Accurate benchmark calculation of the reaction barrier height for hydrogen abstraction by the hydroperoxyl radical from methane, implications for C_nH_{2n+2} where $n=2 \rightarrow 4$, *J Phys. Chem. A* (2008) 112(30): 7047-7054.
- [23] J. Badra, E.F. Nasir, and A. Farooq, Site-specific rate constant measurements for primary and secondary H- and D-abstraction by $\dot{O}H$ radicals: propane and n-butane, *J. Phys. Chem. A* (2014), 118, 26, 4652-4660.
- [24] R. Sivaramakrishnan, M.-C. Su, J.V. Michael, S.J. Klippenstein, L.B. Harding, and B. Ruscic, Shock tube and theoretical studies on the thermal decomposition of propane: evidence for a roaming radical channel, *J. Phys. Chem. A* (2011), 115, 15, 3366-3379.
- [25] W. Tsang, Chemical kinetic data base for combustion chemistry. part 3: propane, *J. Phys. Chem. Ref. Data* 17(1988), 887-951.
- [26] J. Aguilera-Iparraguirre, Accurate benchmark calculation of the reaction barrier height for hydrogen abstraction by the hydroperoxyl radical from methane, implications for C_nH_{2n+2} where $n=2 \rightarrow 4$, *J Phys. Chem. A* (2008) 112(30): 7047-7054.
- [27] C.F. Goldsmith, W.H. Green, and S.J. Klippenstein, Role of $O_2 + QOOH$ in low-temperature ignition of propane. 1. temperature and pressure dependent rate coefficients, *J. Phys. Chem. A* (2012), 116, 13, 3325-3346.

Chapter 9: Conclusions and future work

9.1 General conclusions

The main objective of this thesis was to develop a computational toolkit to produce reliable thermodynamic properties using the group additivity method (GAV) for use in chemical kinetic models. Moreover, this a computational toolkit is used to efficiently to perform chemical kinetic modeling of pyrolytic and oxidative systems for application to combustors. To do this, extrapolation techniques, key thermodynamic and kinetic concepts, and programming skills were employed. The output of this work is a collection of codes developed in a python script language. These codes are integral to the chemical kinetic computational toolkit currently employed at the Combustion Chemistry Centre in Galway.

This toolkit was used for the investigation of $C_1 - C_3$ single (CH_4 , C_2H_4 , C_2H_6 , C_3H_8), binary (CH_4/C_2H_4 , CH_4/C_2H_6 , C_2H_4/C_2H_6 , C_2H_4/C_3H_8 , C_2H_6/C_3H_8), ternary ($CH_4/C_2H_4/C_2H_6$), and quaternary ($CH_4/C_2H_4/C_2H_6/ C_3H_8$) fuel blends characteristics using specific definitions of IDT. Moreover, a total of four different versions of NUIGMech were validated: NUIGMech0.9, NUIGMech1.0, NUIGMech1.1, and NUIGMech1.2. These mechanisms, and the corresponding derived correlations, can accurately predict the experimental data associated with the C^3 database which includes data taken at Galway and published in the literature.

The general conclusions of the research study can be summarized as follows:

- The development of software in python language called THERM23 which can be executed using either Windows or Linux operating systems. This software can be used to calculate, re-calculate, and plot the thermodynamic properties of gas phase fuels. It uses Benson's group additivity method to estimate these properties using Wilhoit extrapolation functions and produce thermodynamic data over a temperature range of 300–5000 K. Moreover, it determines and provides NASA polynomials in a suitable format, and it can plot the results in individual or comparison plots. These thermodynamic properties generated by the code are essential for the development of chemical kinetic models.
- A detailed kinetic modeling study of the IDT characteristics of $C_1 - C_3$ novel ternary and quaternary blends of $CH_4/C_2H_4/C_2H_6$ and $CH_4/C_2H_4/C_2H_6/C_3H_8$ was performed over a wide range of experimental conditions, temperature ($\sim 750 - 2000$ K), pressure (1 – 135 bar), equivalence ratio

($0.5 \leq \phi \leq 2.0$), and dilution ($\sim 75 - 90\%$). A total of 36 new IDT datasets including ST, and RCM with 289 and 223 data points, respectively. As result, NUIGMech1.2 and its corresponding correlations can predict the IDT characteristics of the blends studied with high fidelity over the wide range of conditions presented. In fact, the main difference between the ternary and quaternary blends is the addition of propane to the latter. Thus, it is found that at high temperatures ($T > 1100$ K), the ternary blends are more reactive compared to the quaternary blends, this is in part because the chemistry of the blends is mainly driven by methyl radical chemistry, $\dot{\text{C}}\text{H}_3 + \text{H}\dot{\text{O}}_2 \leftrightarrow \text{CH}_4 + \text{O}_2$, and $\dot{\text{C}}\text{H}_3 + \dot{\text{C}}\text{H}_3 (+\text{M}) \leftrightarrow \text{C}_2\text{H}_6 (+\text{M})$. However, from the C_3H_8 component of the quaternary blend, the n-propyl radical channels ($\text{n}\dot{\text{C}}_3\text{H}_7$) produce a considerable amount of methyl radicals which inhibits the reactivity of this blend at temperatures above 1100 K. Conversely, at lower temperatures ($T < 1100$ K), the quaternary blend promotes reactivity compared to the ternary blends, this is due to the extra source of $\dot{\text{O}}\text{H}$ radicals generated by the addition of n-propyl ($\text{n}\dot{\text{C}}_3\text{H}_7$) radicals to O_2 reacting to chain branching reactions at these temperatures.

- A kinetic modeling study of the IDT characteristics of $\text{C}_2 - \text{C}_3$ binary blends of $\text{C}_2\text{H}_4/\text{C}_3\text{H}_8$ and $\text{C}_2\text{H}_6/\text{C}_3\text{H}_8$ mixtures over a wide range of experimental conditions, pressures (1–135 atm), temperatures ($\sim 750 - 2000$ K), equivalence ratios ($0.5 \leq \phi \leq 2.0$) and 75–90% of dilution percentage are presented in Chapter 4. In this regard, 18 ST data sets including 264 data points, and 12 RCM data sets including 138 data points, for ethylene/propane and ethene/propane binary blends. The performance of NUIGMech1.1 and its corresponding derived correlations were evaluated and in good agreement with the experimental data collected. The individual components were investigated to understand the binary blend behaviour. Indeed, it was found that at high temperatures, C_2H_4 was the most reactive while for low temperatures was C_3H_8 . At high temperatures, the responsible to produce a substantial amount of $\dot{\text{H}}$ atoms resulting in faster ignition of C_2H_4 is the vinoxy radicals and oxygen atoms formed from the reaction of vinyl radical ($\dot{\text{C}}_2\text{H}_3 + \text{O}_2$). Additionally, at low temperatures n-propyl ($\text{n}\dot{\text{C}}_3\text{H}_7$) radical formation, followed the classical low temperature chain branching pathways via its addition to O_2 generate $\dot{\text{O}}\text{H}$ radicals promoting the reactivity of C_3H_8 and its mixtures in the temperature range 600–1100 K.
- A modeling study of the IDT characteristics of binary blended $\text{C}_1 - \text{C}_2$ alkane/alkene fuels including methane/ethylene, methane/ethane, and ethane/ethylene over a wide range of composition (90/10, 70/30, 50/50%), temperatures ($\sim 800 - 2000$ K), pressure ($\sim 1 - 40$ bar),

equivalence ratio (~ 0.5 – 2.0), binary combination, and dilution (~ 75 – 90%) was performed and is presented in Chapter 5. A total of 17 ST data sets including 206 data points, and 7 RCM data sets including 97 data points were used to validate the NUIGMech1.0 model. Furthermore, the results show that NUIGMech1.0 and the corresponding derived correlations, can reliably predict the measured IDTs over a wide range of the mentioned conditions.

- A modelling study of the IDT characteristics of C_1 – C_2 single fuel hydrocarbons over a wide range of temperatures (~ 800 – 2000 K), pressures (~ 1 – 80 bar), equivalence ratios (~ 0.5 – 2.0), and dilutions (~ 75 – 90%) was conducted and is presented in Chapter 6. A total of 28 ST data sets including 212 data points, and 17 RCM data sets including 262 data points for methane, ethylene, and ethane were used for the model validation. The results showed that NUIGMech0.9 and the corresponding derived correlations, could acceptably predict the measured IDTs over a wide range of studied conditions.

9.2 Future work and recommendations

The objective of this thesis is outlined in the development of a chemical kinetic computational toolkit for the estimation of thermodynamic properties of fuels by manual/automated execution of a collection of python scripts. Nevertheless, further development of this tool, improvements in these codes, and employing faster interfaces is recommended. A slow but steady transition to Linux with the sub-routines and codes, in general, is required.

Potential future studies are listed as follows:

- (1) THERM23 in Chapter 2, with a paper in preparation, already has multiple features accessible to a user. However, it is strongly recommended to include an InChI reader in this code. This feature will allow any user, novice or advanced, to calculate the thermodynamic properties of any fuel species by providing only its InChI identifier. This would mean that a user could generate a list of thermochemistry parameters almost instantly by providing a list of InChIs in an appropriate format.
- (2) The C^3 database is a large collection of, not only experimental data measured in Galway, but also from collaborators and the general literature. It is recommended that this database be constantly updated, which is not an easy task. For this reason, a systematic review of every item in the database needs to be done.

(3) Lastly, the author would like to recommend the creation of proper manuals for the instruction of new group members that have not been trained in computational topics. A slow but constant transition from Windows to Linux Operative System is a must. The C³ group already has access to the clusters; it is required that people be trained in order to gain the maximum advantage of this privilege.

Appendix A

(Supplementary material for Chapter 2)

1. Figures codes

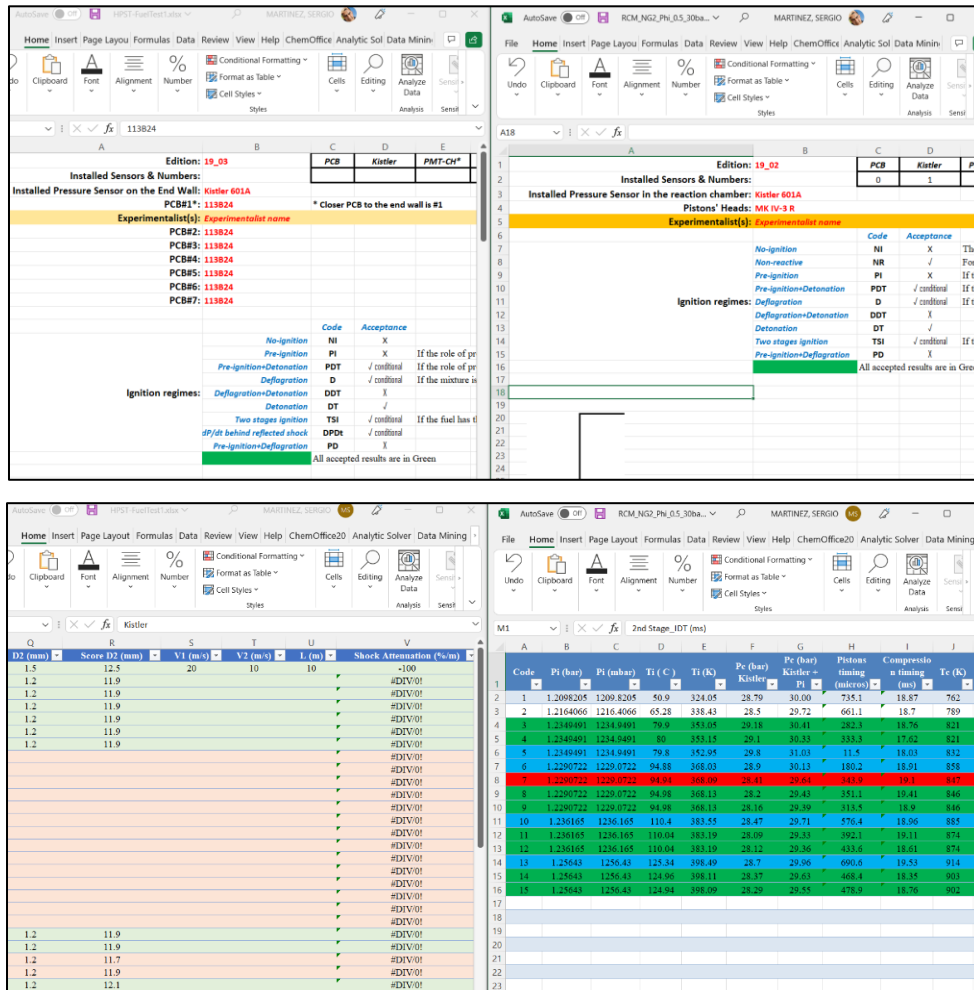


Figure A1. Excel files with experimental data from HPST and RCM (C³) were gathered by the experimentalist performing the experiments. Top: sheet corresponding to general information regarding the experimental conditions. Bottom: every experiment performed is registered in this sheet, fail or not.

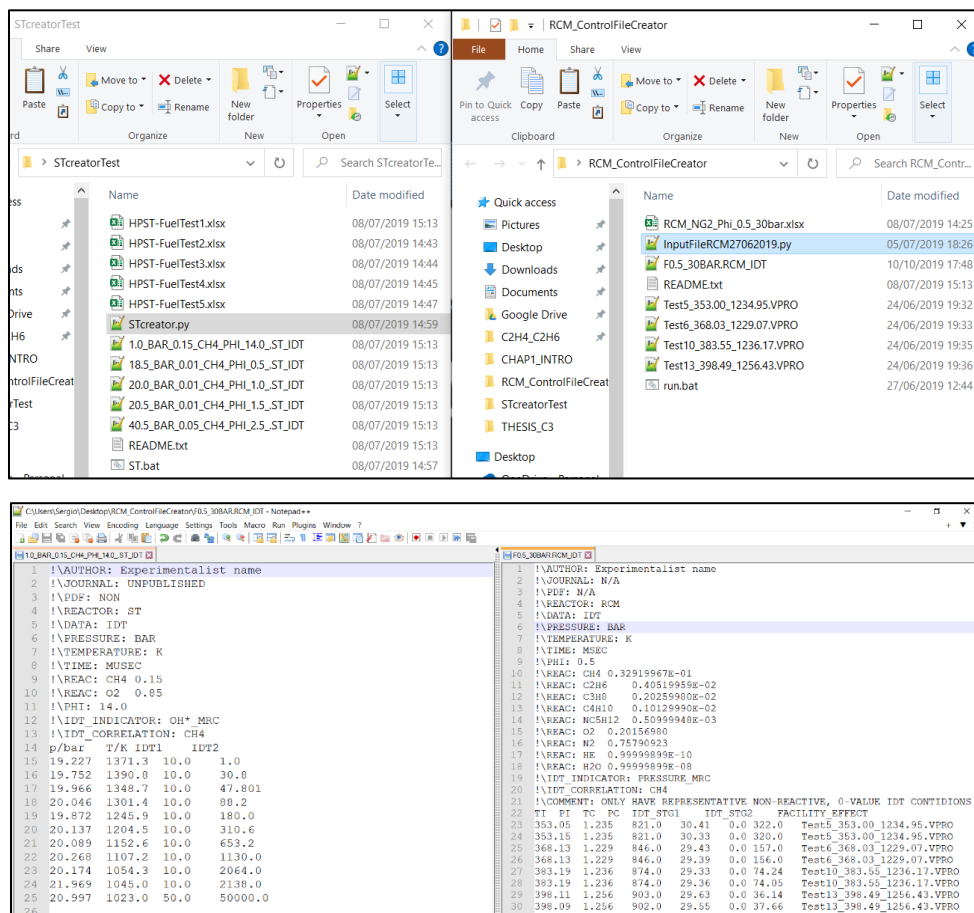


Figure A2. Input files generated by the python code to add to the C³ database for HPST and RCM. Top: the content of the folders “STcreatorTest” and “RCMcreatorTest” with the Excel files from experiments, STcreator.py and InputFileRCM27062019.py, the input files generated with extension ST_IDT and RCM_IDT, and the bat file to execute the code in windows. Bottom: the content of the input files for HPST and RCM which includes from general information from the experimentalist, journal, and type of reactor, until the data corresponding to the experiments performed.

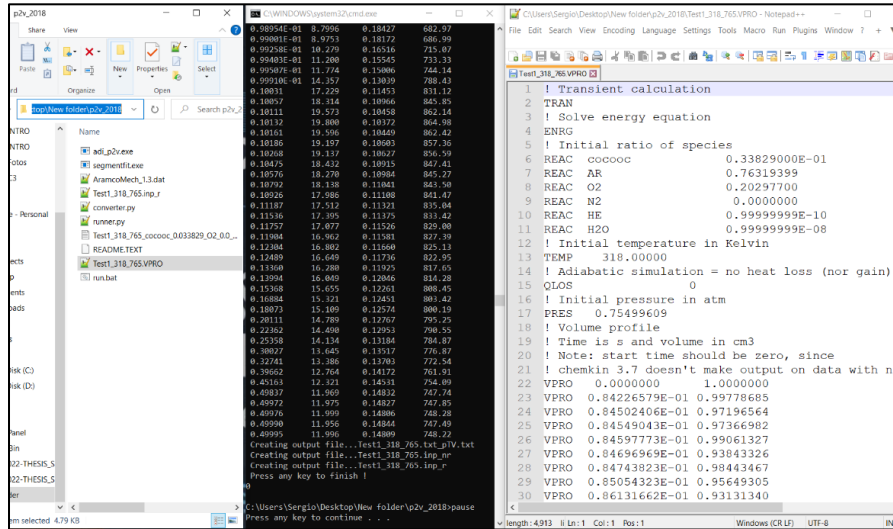


Figure A3. Content of p2v folder, code in execution, and format of the VPRO file. This VPRO file is the volume-time profile, based on the pressure history, which is used as the facility effects for the RCM simulations.

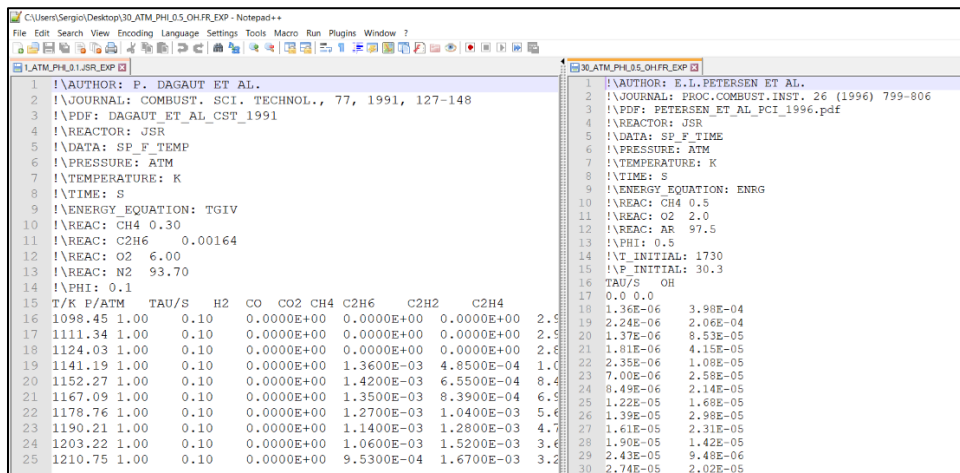


Figure A4. Input file format for JSR and FR reactors.

```

1 !\AUTHOR: William Lowry, Jaap de Vries, Michael Krejci and Eric Petersen, Zeynep Serinyel, Wayne Metcalfe, and Henry Curran, Gilles
2 !\JOURNAL: Proceedings of ASME Turbo Expo 2010: Power for Land, Sea and Air GT2010
3 !\PDF: NA
4 !\REACTOR: CVB
5 !\DATA: LBV
6 !\PRESSURE: ATM
7 !\TEMPERATURE: K
8 !\LBV: CM/S
9 !\COLLECTED BY: KPS
10 !\DATE: 06/02/2019
11 !\SOURCE: Uitan Excel Sheet
12 !\LBV: CM/S
13 !\INTM: H H2 O OH HO2 H2O CH2O HCO CH3
14 PRESSURE      TEMPERATURE      PHI          LBV          CH4          O2          N2
15 1.000          298.000          0.700        14.850       1.000        2.857       10.7
16 1.000          298.000          0.800        22.630       1.000        2.500       9.40
17 1.000          298.000          0.900        29.170       1.000        2.222       8.36
18 1.000          298.000          1.000        33.830       1.000        2.000       7.52
19 1.000          298.000          1.050        34.850       1.000        1.905       7.16
20 1.000          298.000          1.100        35.120       1.000        1.818       6.84
21 1.000          298.000          1.150        34.750       1.000        1.739       6.54
22 1.000          298.000          1.200        32.640       1.000        1.667       6.27
23 1.000          298.000          1.300        24.180       1.000        1.538       5.78

```

Figure A5. Input file format for LBV. Content includes author information, reactor information, and experimental conditions.

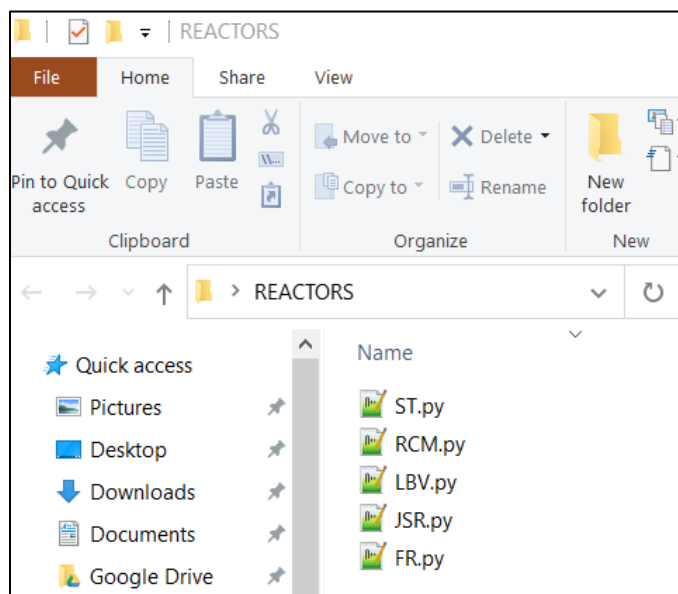


Figure A6. Content of the folder REACTORS. Corresponding to the python codes ST.py, RCM.py, LBV.py, JSR.py, and FR.py.

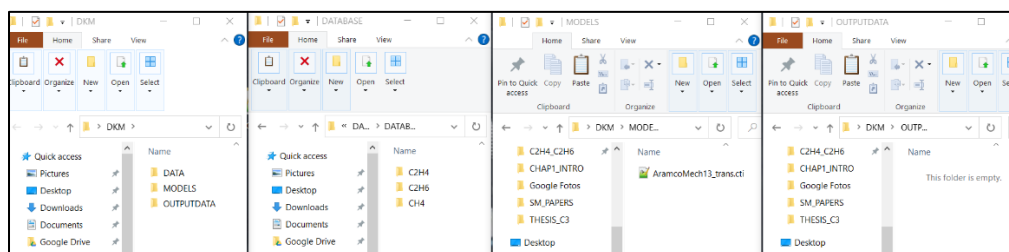


Figure A7. Content of the DKM directory. Followed by the content of the folder DATA which is the example database. Next, the content of the folder MODELS with the mechanism AramcoMech1.3. Finally, the OUTPUTDATA directory which is empty because we have not generated any data yet.

```

PS C:\> python .\DirTools.py ST
Running Sdp...
ICHECH version1.0
S.W. C:\NUGALway, IE
0b1111100100
01001010_01001101_01010011_01010000
0b11111010101

> Working path given:
C:\VDM\DATA
> Directories: 74
> Files: 301
> ST Files: 88
> RCM Files: 29
> LBV Files: 4
> JSR Files: 15
> FR Files: 26
> Total Reac Files: 162
Others formats : 139
Total Files scanned: 301

PS C:\> python .\DirTools.py RCM
Running Sdp...
ICHECH version1.0
S.W. C:\NUGALway, IE
0b1111100100
01001010_01001101_01010011_01010000
0b11111010101

> Working path given:
C:\VDM\DATA
> Directories: 74
> Files: 301
> ST Files: 88
> RCM Files: 29
> LBV Files: 4
> JSR Files: 15
> FR Files: 26
> Total Reac Files: 162
Others formats : 139
Total Files scanned: 301

PS C:\> python .\DirTools.py LBV
Running Sdp...
ICHECH version1.0
S.W. C:\NUGALway, IE
0b1111100100
01001010_01001101_01010011_01010000
0b11111010101

> Working path given:
C:\VDM\DATA
> Directories: 74
> Files: 301
> ST Files: 88
> RCM Files: 29
> LBV Files: 4
> JSR Files: 15
> FR Files: 26
> Total Reac Files: 162
Others formats : 139
Total Files scanned: 301

PS C:\> python .\DirTools.py JSR
Running Sdp...
ICHECH version1.0
S.W. C:\NUGALway, IE
0b1111100100
01001010_01001101_01010011_01010000
0b11111010101

> Working path given:
C:\VDM\DATA
> Directories: 74
> Files: 301
> ST Files: 88
> RCM Files: 29
> LBV Files: 4
> JSR Files: 15
> FR Files: 26
> Total Reac Files: 162
Others formats : 139
Total Files scanned: 301

PS C:\> python .\DirTools.py FR
Running Sdp...
ICHECH version1.0
S.W. C:\NUGALway, IE
0b1111100100
01001010_01001101_01010011_01010000
0b11111010101

> Working path given:
C:\VDM\DATA
> Directories: 74
> Files: 301
> ST Files: 88
> RCM Files: 29
> LBV Files: 4
> JSR Files: 15
> FR Files: 26
> Total Reac Files: 162
Others formats : 139
Total Files scanned: 301
  
```

Figure A8. Command line to execute one by one the different reactor codes, ST, RCM, LBV, JSR, and FR. In this case, the blue window is the PowerShell from Windows, but it can be used as the CMD terminal too. With a simple instruction as `>python DirTools.py ST` the code will generate the corresponding executables for running the simulations. In the command line, ST can be replaced for any of the other reactor name options.

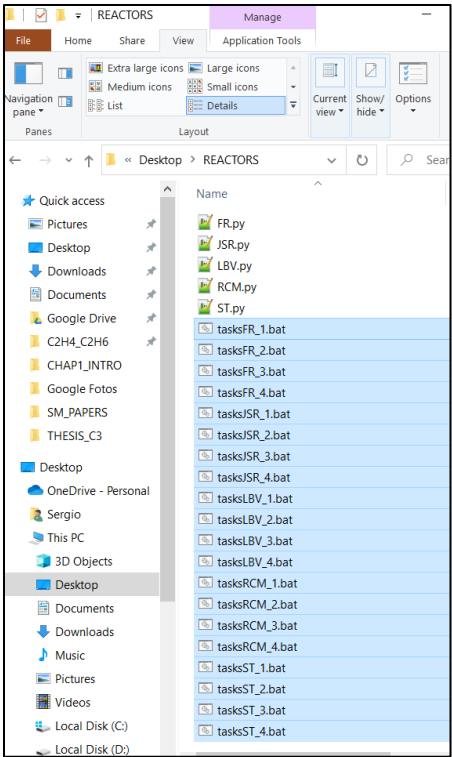


Figure A9. Collection of bat files to run the simulations for ST, RCM, LBV, JSR, and FR.

```

C:\Users\Sergio\Desktop\REACTORS\tasksST_4.bat - Notepad++
File Edit Search View Encoding Language Settings Tools Macro Run Plugins Window ?
tasksST_4.bat
1 python ST.py C:\DKM\DATA\DATABASE\C2H4\ST\BAIGMOHAMMADI\20_ATM_0.0625_C2H4_PHI_1.0.ST_IDT
2 python ST.py C:\DKM\DATA\DATABASE\C2H4\ST\GILLESPIE\1_ATM_0.3_C2H4_PHI_0.3.ST_IDT
3 python ST.py C:\DKM\DATA\DATABASE\C2H4\ST\KOPP\10_ATM_C2H4_IN_AIR_PHI_0.3.ST_IDT
4 python ST.py C:\DKM\DATA\DATABASE\C2H4\ST\KOPP\1_ATM_12.285_C2H4_IN_AIR_PHI_2.0.ST_IDT
5 python ST.py C:\DKM\DATA\DATABASE\C2H4\ST\KOPP\1_ATM_C2H4_IN_AIR_PHI_2.0.ST_IDT
6 python ST.py C:\DKM\DATA\DATABASE\C2H4\ST\SAXENA\10_ATM_0.5_C2H4_PHI_1.0.ST_IDT
7 python ST.py C:\DKM\DATA\DATABASE\C2H4\ST\SAXENA\18_ATM_0.5_C2H4_PHI_1.0.ST_IDT
8 python ST.py C:\DKM\DATA\DATABASE\C2H4\ST\SAXENA\2_ATM_1.75_C2H4_PHI_1.0.ST_IDT
9 python ST.py C:\DKM\DATA\DATABASE\C2H6\ST\BAIGMOHAMMADI\20_ATM_0.01875_C2H6_PHI_0.5.ST_IDT
10 python ST.py C:\DKM\DATA\DATABASE\C2H6\ST\BAIGMOHAMMADI\40_ATM_0.0125_C2H6_PHI_0.5_CH.ST_IDT
11 python ST.py C:\DKM\DATA\DATABASE\C2H6\ST\BURCAT\2_ATM_2_C2H6_PHI_1.0.ST_IDT
12 python ST.py C:\DKM\DATA\DATABASE\C2H6\ST\BURCAT\7_ATM_2_C2H6_PHI_1.0.ST_IDT
13 python ST.py C:\DKM\DATA\DATABASE\CH4\ST\BURKE\10_ATM_4.99_CH4_N2_PHI_0.5.ST_IDT
14 python ST.py C:\DKM\DATA\DATABASE\CH4\ST\BURKE\20_ATM_4.99_CH4_N2_PHI_0.5.ST_IDT
15 python ST.py C:\DKM\DATA\DATABASE\CH4\ST\BURKE\2_ATM_9.51_CH4_N2_PHI_1.0.ST_IDT
16 python ST.py C:\DKM\DATA\DATABASE\CH4\ST\BURKE\8_ATM_17.35_CH4_N2_PHI_2.0.ST_IDT
17 python ST.py C:\DKM\DATA\DATABASE\CH4\ST\PETERSEN\100_ATM_3.8_CH4_PHI_0.4.ST_IDT
18 python ST.py C:\DKM\DATA\DATABASE\CH4\ST\PETERSEN\130_ATM_27.3_CH4_PHI_3.0.ST_IDT
19 python ST.py C:\DKM\DATA\DATABASE\CH4\ST\PETERSEN\180_ATM_27.3_CH4_N2_PHI_3.0.ST_IDT
20 python ST.py C:\DKM\DATA\DATABASE\CH4\ST\PETERSEN\40_ATM_20_CH4_PHI_3.0.ST_IDT
21 python ST.py C:\DKM\DATA\DATABASE\CH4\ST\PETERSEN\55_ATM_50_CH4_HE_PHI_6.0.ST_IDT
22 python ST.py C:\DKM\DATA\DATABASE\CH4\ST\PETERSEN\85_ATM_20_CH4_N2_PHI_3.0.ST_IDT
23

```

Figure A10. Content of the *tasksST4.bat* file. Every line is an input file that will be simulated, each input file has a collection of experimental points to be simulated also.

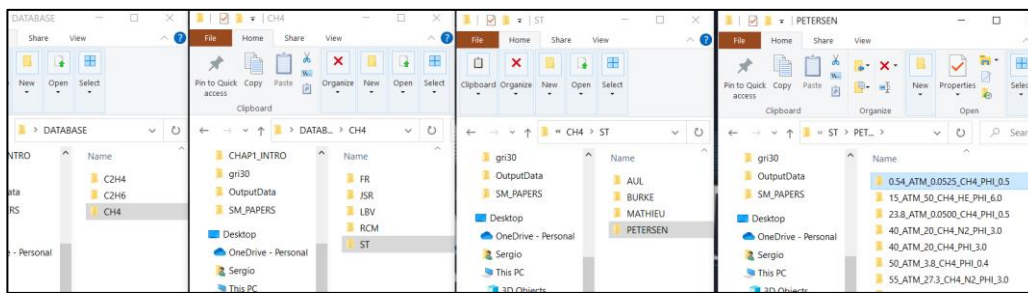


Figure A11. Top to bottom different levels of the “*OUTPUTDATA*” database folders.

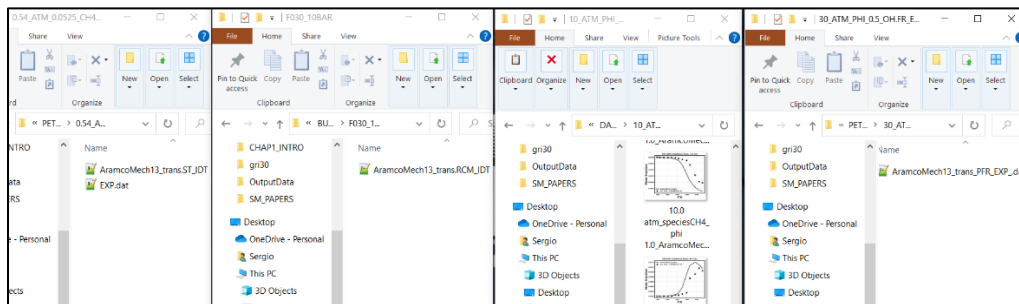


Figure A12. Different type of output file depending on the type of simulation, ST, RCM, JSR, and FR.

ST	RCM
1 14/atm T1/K 1.7791510293644564e-07	1 T1 /K P1 /mbar Tc /K Pc /bar 1000/T (1/K) Max(dp/dt) /s Max(dT/dt) /K
2 945.36 3.5351107997939324e-07	2 340.0 352.95 1080.133 10.13 0.925912 0.1895745 0.1895745
3 959.56 3.5351107997939324e-07	3 350.0 352.95 1109.001 10.12 0.901647 0.0930329 0.0930329
4 980.91 1.06230631519275e-06	4 360.0 352.95 1138.202 10.13 0.878579 0.0413906 0.0413906
5 1002.31 3.263892795737850e-06	5 370.0 352.95 1167.609 10.13 0.856392 0.0179916 0.0179916
6 1021.4 8.46723259359002e-06	
7 1040.55 2.08048640269226e-05	
8 1057.36 4.62373799799253e-05	
9 1076.45 0.000121842712519344	

Figure A13. Format of the output file from the simulated data for ST in the left, and RCM in the right.

JSR	FR
1 Temperature_K H2 CO CO2	1 time Ta Temperature OH
2 945.36 1.7791510293644564e-07 7.30329539734114e-07 1.11755761337241	2 1.3599999999999999e-09 0.0100000136 1729.999749936457 2.680
3 959.56 3.5351107997939324e-07 1.4640850740021825e-06 3.15642402039043	3 2.7199999999999997e-09 0.0100000272 1729.99949973021 1.06
4 980.91 1.06230631519275e-06 4.275976304666279e-06 1.583082525919313	4 4.0799999999999999e-09 0.0100000408 1729.999249502457 2.38
5 1002.31 3.263892795737850e-06 1.2242013854393905e-05 7.939985437655974	5 5.4399999999999999e-09 0.01000005440000001 1729.999899190036 4.22
6 1021.4 8.46723259359002e-06 2.92323827242859e-05 3.15926570902523	6 6.8e-09 0.0100000069 1729.999748930362 6.56
7 1040.55 2.08048640269226e-05 6.639582091672803e-05 1.240106237018324	7 8.11e-09 0.01000000816 1729.9998498343605 9.39
8 1057.36 4.62373799799253e-05 0.0001395675030658102 4.55956412706369	8 9.52e-09 0.01000000952 1729.9998247814312 1.27
9 1076.45 0.000121842712519344 0.0003702092932393425 2.67911715835699	9 1.088e-08 0.01000001088 1729.9997997217806 1.65
10 1098.45 0.0002600452802802e-06 0.000914869188678039 0.000161380042939	10 1.224e-08 0.01000001224 1729.999746556659 2.07
11 1115.49 0.000314676295711339 0.001267836402891599 0.000388172619356	11 1.3600000000000001e-08 0.0100000136 1729.9997495933186 2.55
12 1142.42 0.0002930428691662914 0.0014091347726108482 0.00086876325167	12 1.496e-08 0.01000001496 1729.9997245049876 3.06
13 1163.38 0.000251938156269456 0.0012967094977746037 0.001339783931443	13 1.632e-08 0.010000016320000001 1729.9996994208846 3.63
14 1180.75 0.0002244682915188165 0.0011548003097835197 0.001521149419544	14 1.768e-08 0.01000001768 1729.999743312474 4.23
15	15 1.904e-08 0.01000001904 1729.99849262898 4.88

Figure A14. Format of the output file from the simulated data for JSR in the left, and FR in the right.

The terminal window shows the following commands and output:

```

> RUNNING SENSITIVITY ANALYSIS MULTIPROCESSING
> Update: 30/05/2019, S.H & C3-team NUIGalway, IE
> Running with mechanism:
> D:\V6_02_2022-FOLDERSandFILES\tester\Parallel\Mechanisms\gri30.cti
Running: Ethane_P3C9_06082019 -----> ST with # 7 workers
> T1 = 1100.0 K, P1 = 19.8 atm
Ignition Delay is: 13.6192 ms
Start Brute Force
> Running with 7 processors
> T1 = 1050.0 K, P1 = 19.8 atm
Ignition Delay is: 49.8430 ms
Start Brute Force
> Running with 7 processors
> T1 = 1000.0 K, P1 = 19.8 atm
Ignition Delay is: 208.6214 ms
Start Brute Force
> Running with 7 processors

```

ST	RCM
1 C2H3 + H <=> C2H2 + H2 72 5.605189120068863e-07	1 Begin of log file.
2 CH2OH + H <=> CH3 + OH 60 3.606624688628889e-07	2
3 CH + H <=> C + H2 46 5.53703102095975e-07	3 > Simulation took 5.99 minutes
4 AR + H + O2 <=> AR + HO2 36 0.000589479501370639	4 > With # 325 reactions
5 2 O + M <=> O2 + M 0 2.2372529682761243e-07	5 > With mechanism : gri30
6 C2H4 + O <=> CH3 + HCO 24 -0.001417823642842085	6 > Date of simulation : 2022-09-20
7 HCO + O <=> CO + OH 12 5.07126014969175e-07	7
8 CH2OH + H <=> CH2(S) + H2O 61 3.581569199253861e-07	8 > System info :
9 H + O + M <=> OH + M 1 5.28074384395739e-07	9 > machine : AMD64
10 H + O2 <=> O + OH 37 -0.033286974960059786	10 > version : 10.0.19041
11 CH2 + H (+M) <=> CH3 (+M) 49 2.8287138682935997e-07	11 > platform : Windows-10-10.0.19041-SP0
12 C2H5 + O <=> CH2O + CH3 25 3.442295036790064e-06	12 > uname : uname_result(system='Windows', node='
13 C2H4 + H (+M) <=> C2H5 (+M) 73 -0.014930121225430195	13 > system : Windows
14 HCO + O <=> CO2 + H 13 2.893741699079397e-07	14 > # processors : 7
15 CH3O + H (+M) <=> CH3OH (+M) 62 6.014591055014041e-07	15
16 H2 + O <=> H + OH 2 4.419680545413119e-07	16 End of log file.
17 CH2(S) + H <=> CH + H2 50 2.3579149084258902e-07	17
18 C2H8 + H <=> C2H3 + H2 74 -0.001045973301360566	18
19 C2H6 + O <=> C2H5 + OH 26 0.0019899704600338325	
20 H + M <=> H2 + M 38 1.7268126522647773e-07	

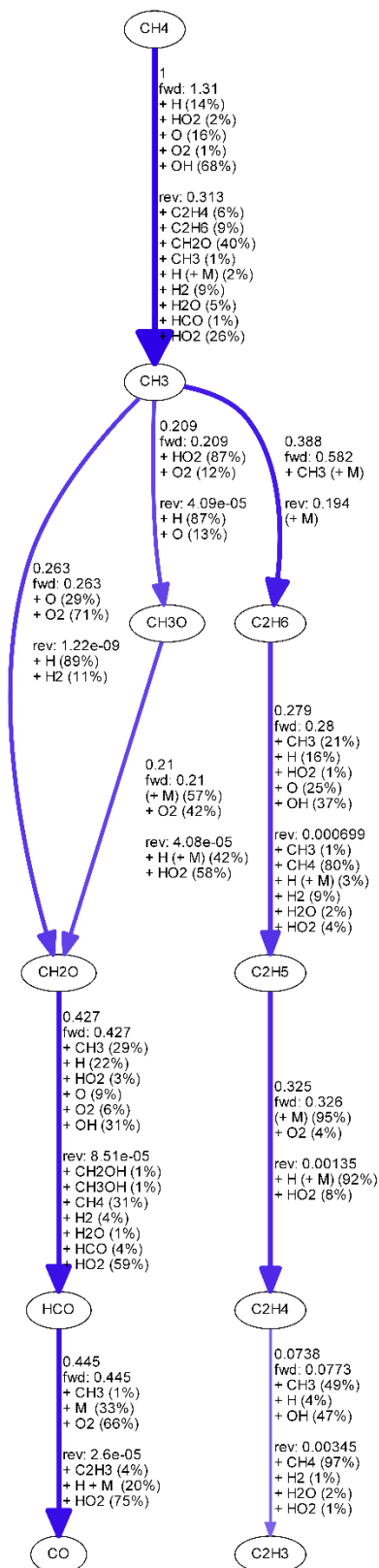
Figure A15. SA brute force example using gri3.0 mechanism. From top to down, and from left to right: content of the SA brute force folder, content of the “mechanism name” folder for this case gri30 folder, terminal black screen showing the code execution. Format of the txt, log.txt, and csv files which contain the reaction names, the brute force value, and a report about the system where user ran the code.

The image shows a Windows desktop environment with three main windows:

- File Explorer:** Displays the 'OutputData' folder containing subfolders like 'ZZZ_CASE_Qc3_H8', 'ZZZ_CASE_TyCH_8', and '80ATMCASES_Flu_xAnalysis_PHL_0_AramcoMech1_3.trans_1500.0K'.
- Notepad++:** Contains a Cantera input file with the following content:


```

1 # RP (Rxn Paths) Cantera Python Code
2 # Input a list means write down the Temp,
3 # Initial Temperature /K (could be a list)
4 TEMP 1500.0
5 TEMP 800.0
6 # Initial Pressure /atm (could be a list)
7 PRESS 1.0
8 PRESS 1.0
9
10 # Mole Fraction of Mixture Composition
11 REAC CH4 0.04
12 REAC N2 0.75
13 REAC O2 0.21
14 # Equivalence ratio of mixture tested (EqRatio)
15 EqRatio 1.0
16
17 # Fuel to consume (one Fuel to consume by FUELN CH4
18 FUELN CH4
19 FUELN CH4
20
21 # Percentage of consumption (%) Ex. 20%
22 PER 0.2
23 PER 0.2
24
25 # Delta time (1E-6, 1.0) /seconds Ex. 1e-6
26 DELTA 1.0E-6
27 DELTA 1.0E-6
28
29 # Element to follow during reactions Ex. ELEMENT C
30 ELEMENT C
      
```
- Terminal:** Shows the execution of the Cantera simulation. It reports the mechanism used, gas properties at 1500 K and 1.0132e+05 Pa, and a table of thermodynamic data for CH4, O2, N2, and CH. The simulation concludes with fuel consumption criteria and file paths for graphviz output.



Scale = 0.24
 Reaction path diagram following C

Figure A16. Reaction path (RP) analyses. From left to right; Content of the “*RP_cantera*” folder, format of the initial conditions to run the RP, RP code running, and below, output file showing the possible reaction paths for the specific case.

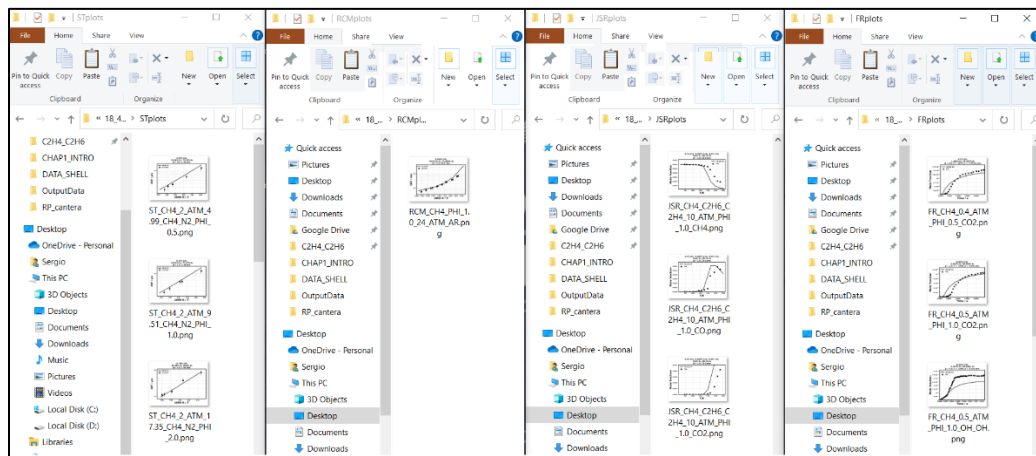


Figure A17. From left to right; ST plots, RCM plots, JSR plots, and FR plots. All these plots were generated by a plotter code using the simulated results.

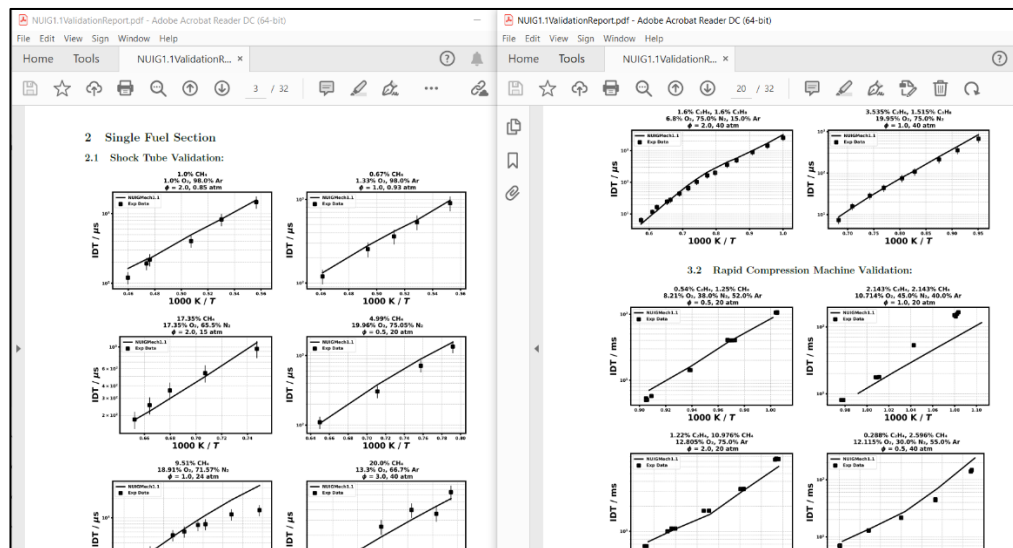


Figure A18. LaTeX report converted in PDF format that shows the ignition delay time (IDT) for ST on the left, and RCM on the right.

2. Python code for STcreator.py

```
# -*- coding: utf-8 -*-
```

```
"""
```

```
Created on Sun Dec 16 13:29:46 2018
```

```
@author: Sergio
```

```
"""
```

```

#=====
import os
import glob
import pandas as pd
#=====

path = os.getcwd();

#####
# EXTRACTION DATA FROM RCM Excel sheets
#####

ExcelName = glob.glob(path+"\\*.xlsx")
if len(ExcelName) == 0:
    print("\t> No excel file found!\n\t> Impossible to create STinputfile\n\t> *.ST_IDT")
else:
    for r in ExcelName:
        ExcelPhi = pd.read_excel(r,sheet_name="Mixture")

        AuthorKeyword = "Experimentalist(s):"
        ExcelAuthor = pd.read_excel(r,sheet_name="Read_Me")
        AUTHOR_INDEX = list(ExcelAuthor).index("Edition:")
        AUTH_EXP = (ExcelAuthor.iloc[3,1])

        ExcelFile = pd.read_excel(r,sheet_name="Exp_Data")

        COL_INDEX = list(ExcelFile).index("Status")
        COMMENTS_INDEX = list(ExcelFile).index("Comments")
        IDT1st_INDEX = list(ExcelFile).index("1st Stage_IDT (us)")
        IDT2nd_INDEX = list(ExcelFile).index("2nd Stage_IDT (us)")
        IDTCRI_INDEX = list(ExcelFile).index("IDT Criteria")
        TI_INDEX = list(ExcelFile).index("T5 (K)")
        PI_INDEX = list(ExcelFile).index("P5 (bar)")

        IDT2 = []; IDT1 = []; TII = []; PII=[];
        TC = []; PC =[]; CRITERIA = [];
        for u in range(len(ExcelFile)):
            IDT1_EXP = (ExcelFile.iloc[u,IDT1st_INDEX])
            IDT2_EXP = (ExcelFile.iloc[u,IDT2nd_INDEX])
            IDT_CRITERIA = (ExcelFile.iloc[u,IDTCRI_INDEX])
            TI_EXP = (ExcelFile.iloc[u,TI_INDEX])
            PI_EXP = (ExcelFile.iloc[u,PI_INDEX])

            if ExcelFile.iloc[u,COL_INDEX] == 'Accepted':
                IDT1.append(float(IDT1_EXP));
                IDT2.append(float(IDT2_EXP));
                if "Kistler" in IDT_CRITERIA:
                    CRITERIA.append("pressure")
                elif "PMT-CH*" in IDT_CRITERIA:
                    CRITERIA.append("ch*")
                elif "PDA-CH*" in IDT_CRITERIA:
                    CRITERIA.append("ch*")
                elif "PMT-OH*" in IDT_CRITERIA:
                    CRITERIA.append("oh*")
                elif "PDA-OH*" in IDT_CRITERIA:

```

```

        CRITERIA.append("oh*")
    else:
        CRITERIA.append(str(IDT_CRITERIA))
    TII.append(float(TI_EXP));
    PII.append(float(PI_EXP))

#-----
# BUILDING THE OUTPUTFILE FORMAT
#-----
specie = []; concen = []; together = [];
ExcelMix = pd.read_excel(r,sheet_name="Mixture")
Phi_INDEX = list(ExcelMix).index("Phi")
PHI = ExcelMix.iloc[0,Phi_INDEX];
P_INDEX = list(ExcelMix).index("P / bar")
P = ExcelMix.iloc[0,P_INDEX];
NameIndex = list(ExcelMix).index("Name")
ConcIndex = list(ExcelMix).index("[C]")

for y in range(len(ExcelMix)):
    IdtExp = (ExcelMix.iloc[y,NameIndex])
    ValExp = (ExcelMix.iloc[y,ConcIndex])
    if "nan" in str(IdtExp) and "nan" in str(ValExp):
        pass
    else:
        specie.append(IdtExp)
        concen.append(ValExp)
        together.append(str(IdtExp)+' '+str(ValExp))

if round(concen[0]) == 0:
    f =
open(path+"\\"+str(P)+"_BAR"+'_'+str(round(concen[0],3))+'+'+str(specie[0])+'_'+PHI+'_'+str(PHI)+'_'+ ".ST_IDT", "w")
else:
    f =
open(path+"\\"+str(P)+"_BAR"+'_'+str(round(concen[0]))+'_'+str(specie[0])+'_'+PHI+'_'+str(PHI)+'_'+ ".ST_IDT", "w")
    f.write("\AUTHOR: "+str(AUTH_EXP)+"\n")
    f.write("\JOURNAL: UNPUBLISHED\n")
    f.write("\PDF: NON\n")
    f.write("\REACTOR: ST\n")
    f.write("\DATA: IDT\n")
    f.write("\PRESSURE: BAR\n")
    f.write("\TEMPERATURE: K\n")
    f.write("\TIME: MUSEC\n")
    for m in range(len(specie)):
        f.write("\REAC:\t'+str(specie[m])+' \t'+str(concen[m])+' \n')

    f.write("\PHI: "+str(PHI)+"\n")
    f.write("\IDT_INDICATOR: "+str(CRITERIA[0]).upper()+"_MRC\n")
    f.write("\IDT_CORRELATION: "+str(specie[0])+"\n")
    if (IDT1[0]) == 0:
        Props = ['p/bar','T/K','IDT']
        f.write('\t'.join(Props)+'\n')
        for n in range(len(PII)):
            f.write(str(PII[n])+' \t'+str(TII[n])+' \t'+str(IDT2[n])+' \n')
    else:
        Props = ['p/bar','T/K','IDT1','IDT2']

```

```

        f.write('\t'.join(Props)+'\n')
        for n in range(len(PII)):
            f.write(str(PII[n])+'\t'+str(TII[n])+'\t'+str(IDT1[n])+'\t'+str(IDT2[n])+'\n')
f.close()
print("\t> File name:")
print("\t. "+str(F)+str(PHI)+"_"+str((P))+"BAR.ST_IDT")
#=====
# END OF SCRIPT
#=====

```

3. Python code for RCMcreator.py

```

# -*- coding: utf-8 -*-
"""
Created on Sun Dec 16 13:29:46 2018
@author: Sergio
"""
#=====
import os
import sys
import glob
import numpy as np
import pandas as pd
import cantera as ct
#=====

path = os.getcwd();
form = '\\*.VPRO'
#-----
# FOLDERS WITH VPRO FILES
#-----

VFNames = []; Ti = []; Pi = [];
FOLDER = glob.glob(path+form);
if len(FOLDER) == 0:
    New = glob.glob(path+'\\*.inp_r');
    for v in range(len(New)):
        newname = New[v].replace('.inp_r', '.VPRO');
        output = os.rename(New[v], newname)
    vpros = glob.glob(path+'\\*.VPRO')
    if len(vpros) == 0:
        for v in range(len(New)):
            newname = New[v].replace('.INP_r', '.VPRO');
            output = os.rename(New[v], newname)

```

```

vpros = glob.glob(path+'\\*.VPRO')
if len(vpros) == 0:
    for v in range(len(New)):
        newname = New[v].replace('.INP_R', '.VPRO');
        output = os.rename(New[v], newname)
vpros = glob.glob(path+'\\*.VPRO')
if len(vpros) == 0:
    for v in range(len(New)):
        newname = New[v].replace('.inp_R', '.VPRO');
        output = os.rename(New[v], newname)
else:
    pass

form = '\\*.VPRO';
FOLDER = glob.glob(path+form);
FileReac = pd.read_csv(FOLDER[0],names=['col']);
Foldername = (FOLDER[0].split('\\'))[-2]
REACS = ((FileReac[FileReac.col.str.contains("REAC")==True]).col.str.split());

#####
# EXTRACTION DATA FROM RCM Excel sheets
#####
ExcelName = glob.glob(path+'\\*.xlsx')
ExcelPhi = pd.read_excel(ExcelName[0],sheet_name="Mixture")

AuthorKeyword = "Experimentalist(s):"
ExcelAuthor = pd.read_excel(ExcelName[0],sheet_name="Read_Me")
AUTHOR_INDEX = list(ExcelAuthor).index("Edition:")
AUTH_EXP = (ExcelAuthor.iloc[3,1])

ExcelFile = pd.read_excel(ExcelName[0],sheet_name="Exp_Data")

COL_INDEX = list(ExcelFile).index("Status")
COMMENTS_INDEX = list(ExcelFile).index("Comments")
IDT2nd_INDEX = list(ExcelFile).index("2nd Stage_IDT (ms)")
IDT1st_INDEX = list(ExcelFile).index("1st Stage_IDT (ms)")
IDTCRI_INDEX = list(ExcelFile).index("IDT Criteria")
TEMP_INDEX = list(ExcelFile).index("Tc (K)")
PRESS_INDEX = list(ExcelFile).index("Pc (bar) Kistler + Pi")
TI_INDEX = list(ExcelFile).index("Ti (K)")
PI_INDEX = list(ExcelFile).index("Pi (bar)")

IDT2 = [];IDT1 = []; TII = []; PII=[];
TC = []; PC = []; CRITERIA = [];
for u in range(len(ExcelFile)):
    IDT2_EXP = (ExcelFile.iloc[u,IDT2nd_INDEX])
    IDT1_EXP = (ExcelFile.iloc[u,IDT1st_INDEX])
    IDT_CRITERIA = (ExcelFile.iloc[u,IDTCRI_INDEX])
    TEMP_EXP = (ExcelFile.iloc[u,TEMP_INDEX])
    PRESS_EXP = (ExcelFile.iloc[u,PRESS_INDEX])
    TI_EXP = (ExcelFile.iloc[u,TI_INDEX])
    PI_EXP = (ExcelFile.iloc[u,PI_INDEX])

    if ExcelFile.iloc[u,COL_INDEX] == 'Accepted':
        TC.append(float(TEMP_EXP));

```

```

        PC.append(float(PRESS_EXP))
        IDT2.append(float(IDT2_EXP));
        IDT1.append(float(IDT1_EXP));
        CRITERIA.append(str(IDT_CRITERIA))
    #if ExcelFile.iloc[u,COMMENTS_INDEX] == 'NR':
        TII.append(float(TI_EXP));
        PII.append(float(PI_EXP))

#=====
# EXTRACTION DATA FROM RCM VPRO FILES
#=====
print("\t> Using the next volume profile files (VPRO): \n\t")
for i in range(len(FOLDER)):
    VproFileNames = (FOLDER[i].split("\\"))[-1]; print("\t. "+VproFileNames)
    VFNames.append(VproFileNames);
    FileRCM = pd.read_csv(FOLDER[i],names=['col']);
    TI = ((FileRCM[FileRCM.col.str.contains("TEMP")==True]).col.str.split());
    TI = float(TI.iloc[0][1])
    Ti.append(TI);# print(TI)
    PI = ((FileRCM[FileRCM.col.str.contains("PRES")==True]).col.str.split());
    PI = (float(PI.iloc[0][1]))
    Pi.append(PI);# print(PI)
print("\n")

#-----
# BUILDING THE OUTPUTFILE FORMAT
#-----
#print("\t> Using the next volume profile files (VPRO): \n\t"+str(len(VFNames)))
#ry:
#     FoldNamecrack = (Foldername.split('_'))[0]
#     PHI = (FoldNamecrack.split('F'))[-1] ; Phis = float(PHI)/100
#except:
PHI = ExcelPhi.iloc[4,3]; print(PHI)
Phis = str(PHI).split(" ")[2]
#print(Phis)
f = open(path+"\F"+str(Phis)+"_"+str(int(PC[0]))+"BAR.RCM_IDT", "w")
f.write("!\\AUTHOR: "+str(AUTH_EXP)+"\n")
f.write("!\\JOURNAL: N/A\n")
f.write("!\\PDF: N/A\n")
f.write("!\\REACTOR: RCM\n")
f.write("!\\DATA: IDT\n")
f.write("!\\PRESSURE: BAR\n")
f.write("!\\TEMPERATURE: K\n")
f.write("!\\TIME: MSEC\n")
f.write("!\\PHI: "+str(Phis)+"\n")
for m in range(len(REACS)):
    f.write("!\\REAC:\t'+str((REACS.iloc[m][1]+''+REACS.iloc[m][2]))+"\n")
f.write("!\\IDT_INDICATOR: "+str(CRITERIA[0]).upper()+"_MRC\n")
f.write("!\\IDT_CORRELATION: "+str(REACS.iloc[0][1])+"\n")
f.write("!\\COMMENT: ONLY HAVE REPRESENTATIVE NON-REACTIVE, 0-VALUE IDT CONTIDIONS WILL NOT BE PLOTTED\n")
Props = ['TI','PI','TC','PC','IDT_STG1','IDT_STG2','FACILITY_EFFECT']
f.write('\t'.join(Props)+"\n")

```



```

Tc = []; Pc = []; STG1 = []; STG2 = [];
for k in range(len(TC)):
    Tc.append(round(TC[k],2))
    Pc.append(round(PC[k],2))
    STG1.append(IDT1[k])
    STG2.append(IDT2[k])
#print(len(TC))
for p in range(len(TC)):
    cwd = os.getcwd()
    vpro = glob.glob(cwd+"\\*" +str(int((TII[p])))+"*.VPRO"); print(PII[p])
    if len(vpro) > 0:
        vpro = str(vpro).split("\\")[-1]; print(vpro)
        vpro = vpro.split("")[0]; print(vpro)

    f.write((str(round(TII[p],3))+'\t'+str(round(PII[p],3))+'\t'+str(Tc[p])+'\t'+str(Pc[p])+'\t'+str(STG1[p])+'\t'+str(S
TG2[p])+'\t'+str(vpro)+'\n")
    else:
        vpro = glob.glob(cwd+"\\*" +str(int((PII[p])))+"*.VPRO"); print(PII[p])
        vpro = str(vpro).split("\\")[-1]; print(vpro)
        vpro = vpro.split("")[0]; print(vpro)

    f.write((str(round(TII[p],3))+'\t'+str(round(PII[p],3))+'\t'+str(Tc[p])+'\t'+str(Pc[p])+'\t'+str(STG1[p])+'\t'+str(S
TG2[p])+'\t'+str(vpro)+'\n")

f.close()
print("t> File name:")
print("t. "+str('F'+str(Phis)+"_"+str(int(PC[0]))+"BAR.RCM_IDT"))
#=====
# END OF SCRIPT
#=====

```

4. Python code for p2v_converter.py

4.1.python runner.py

```

# -*- coding: utf-8 -*-
#"""
#Created on 2018
#@author: Sergio
#"""
#++++++
# IMPORT MODULES
#++++++
import os
from scipy import optimize
import numpy as np
import pandas as pd

```

```

import cantera as ct
import subprocess as sp
import glob
import matplotlib.pyplot as plt
np.set_printoptions(precision=5)
ct.suppress_thermo_warnings(); ReadPath = os.getcwd()
#+++++
# CONVERTING PRESSURE TRACE TO VOLUME TRACE
#+++++
def P2V(path):
# path= os.getcwd()+"\\VPRO\\";
names= glob.glob(path+"\\*.txt");
for m in range(len(names)):
    Mod=names[m].rsplit("\\", 1)
    FileName = str(Mod[-1])
    s= Mod[1]; sm=s.rsplit('.csv.txt',1); s1=sm[0];
    ss = s1.split("_"); Pi=ss[2]; Pinitial = float(Pi)/1000;
    ProgramName = "segmentfit.exe"
    FileName = names[m]; NUMBER = "00100";
    segment = sp.Popen([ProgramName, FileName,str(NUMBER)])
    wait = sp.Popen.wait(segment)
    print(wait)
    FitFile = FileName+"_"+str(NUMBER)+"_fit.txt"
    os.remove(FileName+"_00100_fit0x.txt")
    os.remove(FileName+"_00100_fit0.txt")
    os.remove(FileName+"_00100_fitd.txt")
    os.remove(FileName+"_00100_fitx.txt")
    os.remove(FileName+"_error.txt")
    file = pd.read_table(FitFile,names=['col'], skipinitialspace=True)
    df = pd.DataFrame(file.col.str.split(' ',1).tolist(),columns = ['time','press'])
    df["press"] = df.press.apply(lambda x: ( float(x)))
    D = Pinitial - df["press"][0]
    df["press"] = df.press.apply(lambda x: ((float(x) + D)*0.986923))
    df.to_csv(FitFile,index=False,header=False,sep="\t")
    print(df["press"])
if __name__ == "__main__":
    path = os.getcwd()
    P2V(path);
#####

```

4.2.python converter.py

```

# -*- coding: utf-8 -*-
#"""
#Created on 2018
#@author: Sergio
#"""
#+++++
# IMPORT MODULES
#+++++
import os

```

```

import glob
import shutil
import numpy as np
import pandas as pd
import cantera as ct
import subprocess as sp
from shutil import copyfile
from scipy import optimize
import matplotlib.pyplot as plt

#+++++
#+++++
# CONVERTING PRESSURE TRACE TO VOLUME TRACE +
#+++++
def P2V(path,mech):
# path= os.getcwd()+"\\VPRO\\";
ct.suppress_thermo_warnings();
names= glob.glob(path+"\\*.txt_00100_fit.txt");
for m in range(len(names)):
    Mod=names[m].rsplit("\\", 1);
    FileName = str(Mod[-1]);
    s= Mod[1]; sm=s.rsplit('.',1); s1=sm[0];
    ss = s1.split("_"); NameTest = ss[0]; Ti = ss[1];Pi=ss[2];
    PC = ss[-1] ; Pinitial = float(Pi)* 0.000986923;
    size = len(ss)
    number = int((size - 4)/2)
#+++++
##### MAKING NONREACTIVE AND REACTIVE LISTS AND FILLING THEM
#+++++
    specie = []; x = []; ALL = []; REAC = []; NREAC = []; pNREAC = [];
    for n in range(number):
        specie.append(ss[int(2*n+3)])
        x.append(ss[int(2*n+4)])
    INDEX_N2 = specie.index("N2");
    xN2 = x[INDEX_N2];
    xOX = x[-1];
    for i in range(number):
        ALL.append(str(specie[i]) + " " + (x[i]))
    INDEX_OX = ALL.index("O2 0.0")
    NREAC = ALL.copy()
    NREAC.remove(NREAC[INDEX_OX])
    NREAC.remove(NREAC[-1])
    NEW_N2 = "N2" + " " + str(float(xN2) - float(xOX))
    pNREAC = ALL.copy()
    pNREAC.remove(NREAC[INDEX_OX])
    pNREAC.remove("O2 0.0")
    REAC = pNREAC.copy()
#+++++
##### DOING SOME MATHS FOR THE REACTIVE MOLE FRACTIONS
#+++++
#+++++
# WRITTING THE INPUT FILE TO FEED adip2v.exe
#+++++
    Input = NameTest+"_"+Ti+"_"+Pi+".inp"
    PressFile = NameTest+"_"+Ti+"_"+Pi+".txt"

```

```

Output = NameTest+"_"+Ti+"_"+Pi
copyfile(FileName,PressFile)
output_file = open(Input, 'w')
output_file.write("!Input file for adip2v.exe\n")
output_file.write("!End time for the simulation\n")
output_file.write("TIME 1\n")
output_file.write("!Time-step for printing to diagnostic ouput file\n")
output_file.write("DELTA 1e-4\n")
output_file.write("!Initial Temperature K\n")
output_file.write("TEMP"+" "+Ti+"\n")
output_file.write("!Non Reactive Mixture\n")
for p in range(len(NREAC)):
    output_file.write("NREAC" + " " + str(NREAC[p])+"\n")
output_file.write("!Reactive Mixture\n")
for s in range(len(REAC)):
    output_file.write("REAC" + " " + str(REAC[s])+"\n")
output_file.write("REAC" + " " + str(NEW_N2)+"\n")
output_file.write("!Added to prevent convergence issues in CKPro 15101\n")
output_file.write("REAC HE 1e-10\n")
output_file.write("!Added to prevent convergence issues in CKPro 15101\n")
output_file.write("REAC H2O 1e-8\n")
output_file.close()
#####
ProgramName = "adi_p2v.exe"
RawFile = Input
segment = sp.Popen([ProgramName,RawFile,str(mech),PressFile])
wait = sp.Popen.wait(segment)
print(wait)
os.remove(Output+".INP_pTV.txt")
os.remove(Output+".INP_"+str(mecha)+"_gamma.txt")
os.remove(PressFile)
os.remove(FileName)
os.remove(Input)
os.remove(Input+"_NR")
shutil.copy(path+"\\"+Output+'.inp_r',path+"\\"+Output+'.VPRO')
# os.rename(Input+"_R",NameTest+"_"+Ti+"_"+Pi+'.VPRO')
#####
if __name__ == "__main__":
    path_traces = os.getcwd()
    path_mechs = os.getcwd()
    mech = (glob.glob(path_mechs+"\\"*.dat"));
    for i in mech:
        mecha = i.split("\\")[1];
        P2V(path_traces,mecha);
#####

```

5. Python code for Shock Tube (ST)

```

#####
# Shock tube python-cantera code
# S.M. C3-NUIG, IE. 12-12-2019

```

```

# Merry Christmas to everyone!
# S1E9S8M1J1M9S9P4, "La verdad os hara libres!"
#=====
# ++++++
# Import Modules
# ++++++
import os
import sys
import glob
import math
import time
import datetime
import warnings
import numpy as np
import pandas as pd
import cantera as ct
import matplotlib.pyplot as plt
#-----
#+++++
# READING THE INPUT FILE TO GET FUEL NAME(S), TYPE OF REACTOR, Ti, Pi,...
#+++++
""" EXAMPLE OF THE FORMAT FOR SIMULATION FILES:
    !\AUTHOR: U. BURKE ET AL.
    !\JOURNAL: COMBUST. FLAME, 162, 2015, 315-330
    !\PDF: BURKE_CNF_CH4_DME_2015
    !\REACTOR: ST
    !\DATA: IDT
    !\PRESSURE: ATM
    !\TEMPERATURE: K
    !\TIME: MUSEC
    !\REAC:CH3OCH3      1.7270E-02
    !\REAC:O2          2.0150E-01
    !\REAC:N2          7.8130E-01
    !\PHI: 0.3
    !\IDT_INDICATOR: PRESSURE_MRC
    !\IDT_CORRELATION: CH3OCH3
    P/ATM T/K      IDT
    12.70  1124.00  1458.00
    12.70  1160.00  985.00
    12.20  1161.00  981.00
    12.00  1204.00  636.00
    11.90  1262.00  377.00
    11.90  1266.00  359.00
    11.40  1317.00  165.00
    11.00  1358.00  124.00
    10.40  1423.00  46.00
"""""
#+++++
# FOR THE SHOCKTUBE ++++++
#+++++
def InputFileReaderST(FileNamePath,OutputPath):
    FILENAME = FileNamePath.split("\\"); #print(FileNamePath)
    INPUTFILENAME = FILENAME[-1];
    InputDir = FileNamePath.split(str(INPUTFILENAME))[0]

```

```

FileST = pd.read_csv(FileNamePath, names=['col'], sep='%s',
encoding='cp1252', engine='python', comment='#');
FolderName = FILENAME[3:-1]; #print(FolderName)
InputFileNames = (INPUTFILENAME.split(".ST_IDT"))[0];
FolderDir = "\\".join(FolderName) + "\\ " + InputFileNames; #print(FolderDir)
# ++++++
# FILTERING DATA BY SPECIFIC NAMES, FROM HERE WE WILL GET THE FUEL,OXIDIZERS,
# CONCENTRATIONS, INITIAL TEMPERATURES AND INITIAL PRESSURES, ETC... MAKING
# DICTIONARIES TO STORAGE THE DATA READ IT.
# ++++++
NamesDict = {}
ReactorsDict = {}
UnitsDict = {}
try:
    REACS = (FileST[FileST.col.str.contains("REAC:")]).col.str.split(':')
except:
    FileST = pd.read_fwf(FileNamePath, names=['col']);
    REACS = (FileST[FileST.col.str.contains("REAC:")]).col.str.split(':')
#print(REACS)
REACTANTS = []
for i in range(len(REACS)):
    REAC1 = REACS.iloc[i][1]
    REAC1 = ";".join(REAC1.split())
    REACTANTS.append(REAC1)
REACTANTS = str(";".join(REACTANTS))
#print(REACTANTS)
AUTHOR = ((FileST[FileST.col.str.contains("AUTHOR:")]
).iloc[0].str.split(':')[0][1])
JOURNAL = ((FileST[FileST.col.str.contains("JOURNAL:")]
).iloc[0].str.split(':')[0][1])
PDF = ((FileST[FileST.col.str.contains("PDF:")]
).iloc[0].str.split(':')[0][1])
REACTOR = ((FileST[FileST.col.str.contains("REACTOR:")]
).iloc[0].str.split(':')[0][1])
DATA = ((FileST[FileST.col.str.contains("DATA:")]
).iloc[0].str.split(':')[0][1])
PRESSURE = ((FileST[FileST.col.str.contains("PRESSURE:")]
).iloc[0].str.split(':')[0][1])
PRESSURE = str(PRESSURE)
PHI = ((FileST[FileST.col.str.contains("PHI:")]
).iloc[0].str.split(':')[0][1])
IDT_INDICATOR = ((FileST[FileST.col.str.contains("IDT_INDICATOR:")]
).iloc[0].str.split(':')[0][1])
IDT_CORRELATION = ((FileST[FileST.col.str.contains("IDT_CORRELATION:")]
).iloc[0].str.split(':')[0][1])
TEMPERATURE = ((FileST[FileST.col.str.contains(
"TEMPERATURE:")]
).iloc[0].str.split(':')[0][1])
TIME = ((FileST[FileST.col.str.contains("TIME:")]
).iloc[0].str.split(':')[0][1])
DroppingStuff = FileST[FileST.col.str.contains("!") == False]
DroppingStuff2 = DroppingStuff[DroppingStuff.col.str.contains("IDT") == False]
dataST = pd.DataFrame(DroppingStuff2.col.str.split().tolist())
NamesDict["AUTHOR"] = AUTHOR
NamesDict["JOURNAL"] = JOURNAL
NamesDict["PDF"] = PDF

```

```

NamesDict["InpFileName"] = INPUTFILENAME
NamesDict["FolderDir"] = FolderDir
ReactorsDict["REACTOR"] = REACTOR
ReactorsDict["IDT_CORRELATION"] = IDT_CORRELATION
ReactorsDict["DATA"] = DATA
ReactorsDict["REACTANTS"] = REACTANTS
ReactorsDict["PHI"] = PHI
ReactorsDict["IDT_INDICATOR"] = IDT_INDICATOR
UnitsDict["PRESSURE"] = PRESSURE
UnitsDict["TEMPERATURE"] = TEMPERATURE
UnitsDict["TIME"] = TIME
return (dataST, NamesDict, ReactorsDict, UnitsDict)
#=====

def idt_calc(var_dep, var_indep):
# ++++++
# This definition calculates the derivative as: d(var_dep)/d(var_indep),
# gets the maximum value and give you the var_indep value corresponding to
# the index calculated. Ex. given idtRCM(p,t) will give you the time which
# of max(dp/dt) happens.
# ++++++
idt = np.diff(var_dep) / np.diff(var_indep)
#idt = derivative(var_dep)/derivative(var_indep)
idt = np.append(idt, 0)
ArgMax = np.argmax(idt)
idt = var_indep[ArgMax]
# ++++++
# return(s)
# ++++++
return (idt,ArgMax)
# ++++++

def DerivativeAveragedThermProp(TIME, TEMPERATURE):
# ++++++
# Takes derivative(s) and calculate Ignition Delay Time(s).
# ++++++
tau_dTdt, ArgMax = idt_calc(TEMPERATURE, TIME)
# ++++++
idt = tau_dTdt
# ++++++
return (idt,ArgMax)
# ++++++
#=====

def STCanteraSimulator(
    time_stop,
    dataST,
    MechFile,
    OUTPUT_PATH,
    ReactorsDict,
    UnitsDict,
    NamesDict,
    traces,
    average):
start = time.time(); warnings.simplefilter(action='ignore', category=FutureWarning);

```

```

ct.suppress_thermo_warnings(); now = datetime.datetime.now(); NOW = str(now)[:10];
gas = ct.Solution(MechFile)
MechFile2 = MechFile.split("\\")[-1]
Mech3 = MechFile2.split(".cti")[0];
simname = NamesDict["InpFileName"]
T_list = list(dataST.iloc[:,1])
SUMS= np.array(dataST.iloc[:,0], dtype=np.float32)
SUMAS =math.fsum(SUMS)
lista = SUMAS/(len(dataST));
p = [];
for i in range(len(dataST)):
    p.append(lista)
if "yes" in str(average):
    P_list = p
elif "no" in str(average):
    P_list = dataST.iloc[:, 0];
IDT_STG2 = dataST.iloc[:, 2];
size_data = len(dataST)
print("-"*90)
TIMEPLOT = UnitsDict["TIME"];
if "MSEC" in TIMEPLOT :
    TIMEPLOT = 0;
elif "MUSEC" in TIMEPLOT :
    TIMEPLOT = 1;
elif "SEC" in TIMEPLOT :
    TIMEPLOT = 2;
print("\t>Running ST Reactor...\n\t>With mechanism: {0}
    >With input file: {1}".format(MechFile2,simname))
print("\t>The next data columns are: \n')
print("\t>% 10s % 10s % 10s' %(IDT (s)',Temperature[K]',Pressure[atm]'))
print("-"*65)
IDT = []
IDTus = []
TI = []
PI = []
Tinv=[]
fname = (OUTPUT_PATH + (NamesDict["FolderDir"]) + "\\(+M)ech3+'.ST_IDT');
OutputPath = OUTPUT_PATH + (NamesDict["FolderDir"]);
if not os.path.isdir(OutputPath):
    os.makedirs(OutputPath)
exp_name = OutputPath+ "\\EXP.dat";
deltat = 5E-3 # 0.0005 * 1000 = 0.5
time_stop2 = 0.001*time_stop
for i in range(size_data):
    if UnitsDict["PRESSURE"].strip() == "ATM":
        press = float(P_list[i])
        reactorPressure = (press)* ct.one_atm
        reactorTemperature = (float(T_list[i])) # Kelvin
        gas.TPX = (reactorTemperature, reactorPressure ,
            ReactorsDict["REACTANTS"])
    elif UnitsDict["PRESSURE"].strip() == "BAR":
        press = float(P_list[i])
        reactorPressure = (press)* 1E5
        reactorTemperature = (float(T_list[i])) # Kelvin
        gas.TPX = (reactorTemperature, reactorPressure ,

```



```

        ReactorsDict["REACTANTS"])
    #print(gas.TPX)
else:
    print("PRESSURE UNITS ARE NOT ATM/BAR...STOPPING PROGRAM");
    sys.exit(1)
#
#print(gas.TPX)
#
r = ct.IdealGasReactor(gas)
sim = ct.ReactorNet([r]);
#print("\t reactorTemperature:", reactorTemperature) # > 500 and reactorTemperature < 700:
# deltat
steps = 1000 #time_stop2/deltat
counter = 0
t = 0.0;
t1 = np.zeros(int(steps));
s = np.zeros(int(steps)); ppp = np.zeros(int(steps));
specie2follow = ((ReactorsDict["IDT_INDICATOR"].split("_"))[0]).strip()
YLabel = str(specie2follow)
specie1 = "OHV"; specie11 = "OH*"; specie12 = "OH";
specie2 = "CHV"; specie21 = "CH*"; specie22 = "CH";
#print("\t deltat:", deltat)
#print("\t steps:", steps)
while counter < (int(steps)):
    #t += deltat
    tete = sim.step() #advance(t);
    ppp[counter] = r.thermo.P;
    #print(counter)
    #print(sim.time)
    t1[counter] = tete #sim.time
    if specie2follow == "PRESSURE":
        s[counter] = r.thermo.P
    elif specie2follow == "TEMPERATURE":
        s[counter] = r.T
    else:
        if specie2follow == str(specie1):
            try:
                s[counter] = r.thermo[specie2follow].X[0]
            except:
                try:
                    s[counter] = r.thermo[str(specie11)].X[0]
                except:
                    s[counter] = r.thermo[str(specie12)].X[0]
        elif specie2follow == str(specie2):
            try:
                s[counter] = r.thermo[specie2follow].X[0]
            except:
                try:
                    s[counter] = r.thermo[str(specie21)].X[0]
                except:
                    s[counter] = r.thermo[str(specie22)].X[0]
        elif specie2follow == str(specie11):
            try:
                s[counter] = r.thermo[specie11].X[0]
            except:

```

```

    try:
        s[counter] = r.thermo[str(specie1)].X[0]
    except:
        s[counter] = r.thermo[str(specie12)].X[0]
elif specie2follow == str(specie21):
    try:
        s[counter] = r.thermo[specie21].X[0]
    except:
        try:
            s[counter] = r.thermo[str(specie2)].X[0]
        except:
            s[counter] = r.thermo[str(specie22)].X[0]
else:
    s[counter] = r.thermo[specie2follow].X[0]
counter += 1

idt,ArgMax = DerivativeAveragedThermProp(t1,s)
# re-run finished!
if idt < 0.001:
    deltat = 1E-7
    time_stop2 = 0.01*time_stop
elif idt > 0.0001 and idt < 0.001:
    deltat = 1E-6
    time_stop2 = 0.1*time_stop
elif idt > 0.001 and idt < 0.1:
    deltat = 1E-5
    time_stop2 = 1.0*time_stop
elif idt > 0.1 and idt < 100:
    deltat = 1E-3
    time_stop2 = 100*time_stop
elif idt >= 100:
    deltat = 1E-2
    time_stop2 = 1000*time_stop
IDT.append(round(idt,8))
IDTus.append(round(idt*1e6,4))
TL.append(round(reactorTemperature, 2))
Tinv.append(round(1000/reactorTemperature,5))
PI.append(round(press, 2))
print("\t>% 10.8f % 10.1f % 10.2f" %(idt,reactorTemperature,press))
df1 = pd.DataFrame({"Pi/"+(UnitsDict["PRESSURE"].strip()).lower():PI,
                    "Ti/"+(UnitsDict["TEMPERATURE"].strip()):TI,
                    'IDT/s':IDT,"1000/T":Tinv, 'IDT/us':IDTus})
print("-"*65);
SimTime = time.time() - start
if SimTime <= 60:
    df2 = pd.DataFrame({"REAC":ReactorsDict['REACTANTS'],
                       "PHI": ReactorsDict['PHI'],
                       "IDT_INDICATOR":ReactorsDict['IDT_INDICATOR'],
                       "ORIGIN_FILE_NAME":simname,
                       "deltat /s":deltat,
                       "SimTime /s":round(SimTime,2), "DATE":NOW},index=[0])
elif SimTime > 60:
    df2 = pd.DataFrame({"REAC":ReactorsDict['REACTANTS'],
                       "PHI": ReactorsDict['PHI'],
                       "IDT_INDICATOR":ReactorsDict['IDT_INDICATOR'],

```

```

        "ORIGIN_FILE_NAME":simname,
        "deltat /s":deltat,
        "SimTime /min":round((float(SimTime)/60),2), "DATE":NOW},index=[0])
elif SimTime > 3600:
    df2 = pd.DataFrame({"REAC":ReactorsDict['REACTANTS'],
        "PHI": ReactorsDict['PHI'],
        "IDT_INDICATOR":ReactorsDict['IDT_INDICATOR'],
        "ORIGIN_FILE_NAME":simname,
        "deltat /s":deltat,
        "SimTime /hr":round((float(SimTime)/3600),2), "DATE":NOW},index=[0])
df = df1.join(df2,lsuffix='_df1', rsuffix='_df2')
TC_XP = []; EXP_STG2 = [];
Tlist = dataST.iloc[:,1]
for m in range(len(T_list)):
    TC_XP.append(round(1000/float(Tlist[m]),6))
    EXP_STG2.append(float(IDT_STG2[m]))
if TIMEPLOT == 0:
    df4 = pd.DataFrame({'1000/T(1/K)':TC_XP,"ExpIDT/ms":IDT_STG2})
elif TIMEPLOT == 1:
    df4 = pd.DataFrame({'1000/T(1/K)':TC_XP,"ExpIDT/us":IDT_STG2})
elif TIMEPLOT == 2:
    df4 = pd.DataFrame({'1000/T(1/K)':TC_XP,"ExpIDT/s":IDT_STG2})
if not os.path.isfile(exp_name+".exp"):
    df4.to_csv(exp_name,index=False,sep="\t")
print(">It took {0:0.1f} seconds".format(SimTime))
output_file = df.to_csv(fname, index=False, sep="\t")
return ( fname)
#-----
#-----
if __name__ == "__main__":
    mech_list = [];
    path = "C:\\DKM\\MODELS\\"#os.getcwd();
    fname = glob.glob(path+'/*.cti');
    #print("\t>Running with mechanism: \n\t',mechanism);
    #Mechanism = "/DKM/MODELS/19_48_C7.cti"
    for m in fname:
        print("\t>Running with mechanism: \n\t',m);
        Input = sys.argv[1] #"InputFileNameWithFullPath"
        (dataST, NamesDict, ReactorsDict, UnitsDict) = InputFileReaderST(Input,m);
        #print(dataST, NamesDict, ReactorsDict, UnitsDict)
        STCanteraSimulator(1.0, dataST, m, "C:\\DKM\\OUTPUTDATA\\", ReactorsDict, UnitsDict, NamesDict, "no",
"no")
#-----
# Eppur si muove! - Galileo Galilei (1564-1642)
#-----

```

6. Python code for Rapid Compression Machine (RCM)

```

"""=====
Created on 2018: May-August.

```

@author: version 1.0. S.M.
 C3-Combustion Chemistry Centre
 National University of Ireland, Galway
<http://c3.nuigalway.ie/>

```

===== """
# -----
# ++++++
# IMPORT MODULES
# ++++++

import os
import sys
import time
import numpy as np
import cantera as ct
import pandas as pd
import glob
# from Definitions.InputFileReader import KindOfFiles
# from Definitions.Definitions import DefinitionStandar
# from scipy.signal import find_peaks

# ++++++

#+++++
class DefinitionStandar(object):
    """A SIMPLE CLASS THAT INCLUDE ALL DEFINITIONS FOR USE DURING THE RCM SIMULATION"""
#-----
    def SOME_STUFF(line_size,inp_file_format1,inp_file_format2):
        my_path= os.getcwd()
        dash = '=' *line_size
        print(dash)
        print('{:^20s}'.format('C3: Combustion Chemistry Centre, NUIGalway. http://c3.nuigalway.ie/'))
        print('{:^20s}'.format('Python script to simulate a Rapid Compression Machine (RCM)) using cantera module'))
        print(dash)
        print('Running Python version: '+ sys.version);
        #print('Running Cantera version: '+ ct.__version__);
        print(dash)
        print("")

```

=====

THIS SCRIPT IS USING A VARIABLE VOLUME PROFILE FILE TO PERFORM A RAPID COMPRESSION MACHINE (RCM) SIMULATION IN PYTHON LANGUAGE WITH CANTERA, PANDAS AND NUMPY MODULES USED TO PRE- AND POST-PROCESSING OF DATA. YOU SHOULD PLACE YOUR VOLUME PROFILE FILE(S) IN A FOLDER CALLED 'FILES', THE CODE AUTOMATICALLY WILL READ THIS FOLDER AND START WORKING WITH THE FILE NAME(S).

=====

=====

THE NAME OF YOUR FILE(S) SHOULD BE AS FOLLOW:

-

NAME_INITIALTEMPERATURE_INITIALPRESSURE_FUELNAME_XFUEL_OX1NAME_XOX1_OX2NAME_XOX2_OX3NAME_XOX3_COMMENT.txt

- EXAMPLE: Test1_353_800_C2H6_0.055556_N2_0.225_AR_0.525_O2_0.194444_CKinpr.txt

Please be aware that the program is reading the underscores to separate names and values.
 If you need to add more fuels, just add them after the first one in similar format.

=====

AT THE END OF THE SIMULATION(S) YOU WILL GET A FILE WITH '.CSV' EXTENSION, IN WHICH YOU WILL FIND ALL DATA NEEDED TO PLOT YOUR RESULTS IN YOU PREFERRED SOFTWARE.

THE FORMAT OF THE OUTPUT FILE IS (BY COLUMNS):

- Ti[K](initial temperature),Pi[mbar](initial pressure), Tc[K](compressed temperature),
 - Pc[bar](compressed pressure),Pc[atm],1000/Tc[K], idt[ms](Ignition Delay Time).
-

```

    ")
    print(dash)
#   otherpath= my_path+'/IDT/'
#   if not os.path.isdir(otherpath):
#       os.makedirs(otherpath)
    print('\n{:<20s}'.format('List of files (.xml/.cti) in your folder/subfolders: \n'));
    lstDir = os.walk(my_path)
    for root, dirs, files in lstDir:
        for File in files:
            if File.endswith(inp_file_format1):
                print(File)
            if File.endswith(inp_file_format2):
                print(File)
    return dash, File
#-----
def idt_RCM(var_dep,var_indep):
    """This definition calculates the derivative as: d(var_dep)/ d(var_indep)
    gets the maximum value and give you the var_indep value corresponding to
    the index calculated. Ex. given idtRCM(p,t) will give you the time which
    of max(dp/dt) happens """
    idt = np.diff(var_dep)/np.diff(var_indep)
    idt = np.append(idt,0)
    idt = var_indep[np.argmax(idt)]
    return idt
#-----
def Min_Vol(var_dep,var_indep):
    """This definition is for get Tc and Pc from the Non-Reactive simulation"""
    idt = np.diff(var_dep)/np.diff(var_indep)
    idt = np.append(idt,0)
    idt = var_indep[np.argmin(idt)]
    return (idt)
#-----
def Min_Vol2(var_dep,var_indep):
    """This definition is for get Tc and Pc from the Non-Reactive simulation"""
    idt = np.diff(var_dep)/np.diff(var_indep)
    idt = np.append(idt,0)
    idt = np.argmin(idt)
    return (idt)
#-----
def Properties_RCM(var_dep,prop):
    """This definition is for get Tc and Pc from the Non-Reactive simulation"""
    prp = prop[np.argmin(var_dep)]
    return (prp)

```

```

#-----#
class variable_volume_velocity(object):
    """ Pistons velocity taken from volume profile file given and filtered
    using pandas and numpy modules.
    'vel' is
    """ # THIS IS USING THE CLASS: cantera.Func1. Pandas(IPython,numpy).
    def __init__(self,df):
        self.vpro_time = pd.to_numeric(df.iloc[:,0])
        self.vpro_volume = pd.to_numeric(df.iloc[:,1])
        self.vel = np.append((self.vpro_volume.diff()/(self.vpro_time.diff()),0)
    def __call__(self, t):
        if t == self.vpro_time.iloc[0]:
            return 0
        elif t < self.vpro_time.iloc[-1]:
            idx = np.where(self.vpro_time == (self.vpro_time[self.vpro_time >= t].iloc[0]))[0][0]
            return self.vel[idx]
        else:
            return 0
#-----#
def Convert(folder_name,format_file):
    my_path= os.getcwd()+folder_name;
    fname= glob.glob(my_path+'*.*'); size=len(fname);
    VOL_LIST=[];
    for i in range(size):
        mod=fname[i].rsplit("\\", 1); #print(fname,mod)
        s= mod[1]; sm=s.rsplit('.',1); s1=sm[0]; #s=s1+'*.*';
        chemkin_file = pd.read_table(my_path+s,names=['col'])
        df = pd.DataFrame(chemkin_file.col.str.split('VPRO',1).tolist(),columns = ['flips','row'])
        VOL=pd.DataFrame((df['row'].dropna()).reset_index(drop=True).str.strip());
        file_output=VOL.to_csv(my_path+s1+format_file,index=False,header=None)
        VOL_LIST.append(s1+format_file)
    return file_output , VOL_LIST
#++++++
def DERIVATIVES_AVERAGED_THERMPROP(TIME,TEMPERATURE, PRESSURE, VOLUME,OH,CH):
    tau_EOC =DefinitionStandar.Properties_RCM(VOLUME,TIME)
    Tc = DefinitionStandar.Properties_RCM(VOLUME,TEMPERATURE)
    Pc = DefinitionStandar.Properties_RCM(VOLUME,PRESSURE)
    tau_dTdt = DefinitionStandar.idt_RCM(TEMPERATURE,TIME);
    tau_dpdt = DefinitionStandar.idt_RCM(PRESSURE,TIME);
    tauOH=DefinitionStandar.idt_RCM(OH,TIME);
    tauCH=DefinitionStandar.idt_RCM(CH,TIME);
    # tauOHv=DefinitionStandar.idt_RCM(OHv,TIME);
    # tauCHv=DefinitionStandar.idt_RCM(CHv,TIME);
    if tau_dpdt <= tau_EOC:
        idt_dpdt = 0.0
    else:
        idt_dpdt = tau_dpdt-tau_EOC
    if tau_dTdt <= tau_EOC:
        idt_dTdt = 0.0
    else:
        idt_dTdt = tau_dTdt-tau_EOC
    if tauOH <= tau_EOC:
        idt_OH = 0.0
    else:

```

```

    idt_OH    = tauOH - tau_EOC
if tauCH <= tau_EOC:
    idt_CH = 0.0
else:
    idt_CH    = tauCH - tau_EOC
# if tauOHv <= tau_EOC:
#   idt_OHv = 0.0
# else:
#   idt_OHv    = tauOHv - tau_EOC
# if tauCHv <= tau_EOC:
#   idt_CHv = 0.0
# else:
#   idt_CHv    = tauCHv - tau_EOC
return (Tc,Pc,tau_EOC,idt_dpdt,idt_dTdt,idt_OH,idt_CH)
#+++++
def FileFormat(names,path):
for m in range(len(names)):
    filename, file_extension = os.path.splitext(names[0])
    print('=*20);
    Ti=[];Pi=[];fuelname=[];whole_X=[]; volname=[]; TMP=[];
if file_extension == '.inp_r':
    print('Reactive file format');
    for i in range(len(names)):
        dataRCM,WHOLE_X,TI,PI,FuelName = KindOfFiles.InputFileReaderINP_R(names[i]);
        tmp_file = path+'\\'+FuelName+'_'+str(TI)+'_'+str(PI)+'.tmp'
        dataRCM.to_csv(tmp_file,index=False)
        mod = filename.rsplit('\\',1);
        s = FuelName+'_'+str(round(TI))+"K"+'_'+str(round(PI/1e5,2))+ "bar" #mod[-1];
        fuelname.append(FuelName);
        Ti.append(TI); Pi.append(PI);TMP.append(tmp_file)
        whole_X.append(WHOLE_X); volname.append(s);
    elif file_extension == '.INP_R':
    print('Non-Reactive file format');
    for i in range(len(names)):
        dataRCM,WHOLE_X,TI,PI,FuelName = KindOfFiles.InputFileReaderINP_R(names[i]);
        tmp_file = path+'\\'+FuelName+'_'+str(TI)+'_'+str(PI)+'.tmp'
        dataRCM.to_csv(tmp_file,index=False)
        mod = filename.rsplit('\\',1);
        s = FuelName+'_'+str(round(TI))+"K"+'_'+str(round(PI/1e5,2))+ "bar" #mod[-1];
        fuelname.append(FuelName);
        Ti.append(TI); Pi.append(PI);TMP.append(tmp_file)
        whole_X.append(WHOLE_X); volname.append(s);
    elif file_extension == '.INP_r':
    print('Non-Reactive file format');
    for i in range(len(names)):
        dataRCM,WHOLE_X,TI,PI,FuelName = KindOfFiles.InputFileReaderINP_R(names[i]);
        tmp_file = path+'\\'+FuelName+'_'+str(TI)+'_'+str(PI)+'.tmp'
        dataRCM.to_csv(tmp_file,index=False)
        mod = filename.rsplit('\\',1);
        s = FuelName+'_'+str(round(TI))+"K"+'_'+str(round(PI/1e5,2))+ "bar" #mod[-1];
        fuelname.append(FuelName);
        Ti.append(TI); Pi.append(PI);TMP.append(tmp_file)
        whole_X.append(WHOLE_X); volname.append(s);
    elif file_extension == '.VPRO':
    print('Non-Reactive file format');

```

```

for i in range(len(names)):
    dataRCM,WHOLE_X,TI,PI,FuelName = KindOfFiles.InputFileReaderINP_R(names[i]);
    tmp_file = path+'\\'+FuelName+'_'+str(TI)+'_'+str(PI)+'.tmp'
    dataRCM.to_csv(tmp_file,index=False)
    mod = filename.rsplit('\\',1);
    s = FuelName+'_'+str(round(TI)+"K"+"_'+str(round(PI/1e5,2))+ "bar" #mod[-1];
    fuelname.append(FuelName);
    Ti.append(TI); Pi.append(PI);TMP.append(tmp_file)
    whole_X.append(WHOLE_X); volname.append(s);
elif file_extension == '.inp_nr':
    print('Non-Reactive file format');
elif file_extension == '.txt':
    print('Pressure trace file format')
return (Ti,Pi,fuelname,whole_X,volname,TMP)
#+++++
# =====
# Input reader:.....
# =====
# +++++
# READING THE INPUT FILE TO GET FUEL NAME(S), TYPE OF REACTOR, Ti, Pi,... +++++
# +++++
""" EXAMPLE OF THE FORMAT FOR SIMULATION FILES:
! Transient calculation
TRAN
! Solve energy equation
ENRG
! Initial ratio of species
REAC C2H6      5.6600555E-2
REAC O2       1.9811194E-1
REAC N2       7.4528730E-1
REAC Ar       0.0000000E+0
REAC HE       1.0000098E-7
REAC H2O      1.0000098E-7
! Initial temperature in Kelvin
TEMP  3.4786813E+2
! Adiabatic simulation = no heat loss (nor gain)
QLOS      0
! Initial pressure in atm
PRES  2.2343943E+0
! Volume profile
! Time is s and volume in cm3
! Note: start time should be zero, since
! chemkin 3.7 doesn't make output on data with negative times (error)
VPRO  0.0000000E+0 1.0000000E+0
VPRO  4.9832000E-2 1.0000000E+0
VPRO  5.0687790E-2 9.6844077E-1
VPRO  5.1548004E-2 9.3527765E-1
VPRO  5.2407742E-2 8.9814888E-1
VPRO  5.3267956E-2 8.4651408E-1
VPRO  5.4127693E-2 7.9312742E-1
"""
# +++++
# FOR THE RAPID COMPRESSION MACHINE +++++
# +++++
class KindOfFiles(object):

```



```

"""THIS CLASS IDENTIFY WHAT KIND OF FORMAT THE INPUT FILE HAS AND RUN THE RCM
SIMULATOR WITH THE INITIAL PARAMETERS GOT FROM THE FORMAT OR NAME"""
def downsample(s, n, phase=0):
    """Decrease sampling rate by integer factor n with included offset phase.
    """
    return s[phase::n]
#+++++
def InputFileReaderINP_R(FileNamePath):
    try:
        FileRCM = pd.read_csv(FileNamePath,names=['col'],sep="%s", encoding='cp1252', engine="python",
comment=#);
        REACS = ((FileRCM[FileRCM.col.str.contains
("REAC")==True]).col.str.split());
        REACTANTS = [];
        for i in range(len(REACS)):
            REAC1=REACS.iloc[i][-2];
            REAC2=REACS.iloc[i][-1];
            REAC = REAC1+' '+REAC2
            REACTANTS.append(REAC);
        WHOLE_X = ','.join(REACTANTS);
        WHOLE_X = str(WHOLE_X);
        FuelName = str((REACTANTS[0].split(':')[0])
        TI = ((FileRCM[FileRCM.col.str.contains
("TEMP")==True]).col.str.split());
        TI = float(TI.iloc[0][1])
        PI = ((FileRCM[FileRCM.col.str.contains
("PRES")==True]).col.str.split());
        PI = (float(PI.iloc[0][1]))*ct.one_atm
        DroppingStuff = (pd.DataFrame(FileRCM.col.str.split
('VPRO',1).tolist(),
columns = ['flips','row']))
        dataRCM = (pd.DataFrame((DroppingStuff['row']
.dropna()).reset_index(drop=True).str.strip()));
        dataRCM = (pd.DataFrame(dataRCM.row.str.split(' ',1).tolist(),columns = ['time(s)','volume(cm3)']));
#+++++
    except:
        dataRCM = (pd.DataFrame(dataRCM.row.str.split(' ',1).tolist(),columns = ["col"]));
        dataRCM = (pd.DataFrame(dataRCM.col.str.split
('\t',1).tolist(),
columns = ['time(s)','volume(cm3)']))
        compression_Time = (KindOfFiles.downsample(dataRCM['time(s)'],int(30))).reset_index(drop=True)
        compression_Volume = (KindOfFiles.downsample(dataRCM['volume(cm3)'],int(30))).reset_index(drop=True)
        dataRCM = pd.DataFrame({'time(s)':compression_Time,"volume(cm3)":compression_Volume})
    return (dataRCM,WHOLE_X,TI,PI,FuelName)

# =====

ct.suppress_thermo_warnings();
dash= '*90; half= '*90; gato= '*90;
OUTPUT_PATH= "C:\\DKM\\OUTPUTDATA\\"
# =====
# RAPID COMPRESSION MACHINE PYTHON CLASS
# =====
class RCM_SIMULATION(object):
    'A SIMPLE CLASS TO RUN THE RCM SIMULATION USING THE PREVIOUS CLASS DEFINED'

```

```

#+++++++
def RUN(mech,Input):
    start = time.time();
    inp2 = Input.rsplit('\',1);
    inp3 = inp2[0]; InpName = inp2[1]
    FILENAME = Input.split('\')
    FolderName = FILENAME[3:-1]
    FolderDir = "\'".join(FolderName)
    try:
        os.remove(inp3+"\'*.tmp')
    except:
        pass
    if not os.path.isdir(OUTPUT_PATH+'\'+FolderDir):
        os.makedirs(OUTPUT_PATH+'\'+FolderDir)
    names = glob.glob(inp3+"\'*.*VPRO');
    Ti,Pi,fuelname,whole_X,volname,TMP = (DefinitionStandar.FileFormat(names,inp3));
    TCOMP=[]; TCOMP_INVERSE=[]; PCOMP_BAR=[];
    T_INITIAL=[]; IDT2 = []; IDT1 = []; TC = [];
    INVERSE = []; PC = [];P_INITIAL=[]; IDT2=[]; IDT3=[];
    IDT4 = [];
    for i in range(len(names)):
        file_name= TMP[i];
        df = pd.read_csv(file_name);
        vpro_time = pd.to_numeric(df.iloc[:,0]);
        vpro_vol = pd.to_numeric(df.iloc[:,1]);
        mech2=mech.rsplit('\',1);
        mech3=mech2[-1].split(".cti")[0];
        sim_name= OUTPUT_PATH+'\'+FolderDir+'\'+mech3+'.RCM_IDT'
        #sim_nametr = OUTPUT_PATH+str(volname[i])+'_'+mech3+'_'+str(i)
        gas=ct.Solution(mech)
        gas.TPX=Ti[i], Pi[i], whole_X[i]
        print('Fuel and mole fractions:\t\n',whole_X[i]);
        print(); print(gas());print(gato)
        print("""RUNNING NOW:\nTi[K]={:<10.2f}\nPi[mbar]={:<10.2f}
\nVprofile NAME={:<10s}\n...""")
        .format(Ti[i],Pi[i]/1E2,volname[i])
        print();
        r = ct.IdealGasReactor(gas)
        env = ct.Reservoir(ct.Solution('air.xml'))
        w = ct.Wall(r,env);
        Tini = float(gas.T); Pini=float(gas.P/1E2)
        w.set_velocity(DefinitionStandar.variable_volume_velocity(df))
        sim = ct.ReactorNet([r]);
        end_time = 1.2*float(vpro_time.iloc[-1]);
        Deltat = float(vpro_time.iloc[1]/100)
        TIMES=[];TEMPERATURES=[];PRESSURES=[];V=[];#OH=[];CH=[];
        t=0; os.remove(TMP[i]);
        # ++++++
        #sim.rtol = 1.0e-15
        #sim.atol = 1.0e-15
        #sim.ftol = 1.0e-13
        while t <(end_time):
            t+= Deltat
            sim.advance(t)
            TIMES.append(sim.time)

```

```

TEMPERATURES.append(gas.T)
PRESSURES.append(gas.P/1E5)
V.append(r.volume)
# ++++++
# os.remove(TMP[i]);
# ++++++
# THERMODYNAMIC PROPERTIES
# ++++++
EocArg = np.argmin(V); EocArgEmpiric = np.argmin(vpro_vol);
EocTime = TIMES[EocArg]; EocEmpTime = TIMES[EocArgEmpiric];
dpdt = np.append(np.diff(PRESSURES)/np.diff(TIMES),0);
dTdt = np.append(np.diff(TEMPERATURES)/np.diff(TIMES),0);
MaxP = np.argmax(PRESSURES); MaxT = np.argmax(TEMPERATURES);
# ++++++
# CALCULATING IGNITION DELAY TIMES
# ++++++
eoc = EocTime
IdtDpdt = TIMES[np.argmax(dpdt)] - eoc;
IdtDTdt = TIMES[np.argmax(dTdt)] - eoc;
IdtMaxP = TIMES[MaxP] - eoc;
IdtMaxT = TIMES[MaxT] - eoc;
Tc = round(TEMPERATURES[EocArg],3); Pc = round(PRESSURES[EocArg],2);
Invers = round(1000/float(Tc),6);
print("\t>% 10s % 20s % 20s % 20s"%(
    Tc /K,'Pc /bar','1000/T /K','EOC'))
print("\t>% 10.8f % 20.8f % 20.8f % 20.8f"%(
    Tc,Pc,Invers,eoc))
#print(half);
print("\t>% 10s % 20s % 20s % 20s"%(
    IdtDpdt,IdtDTdt,IdtMaxP,IdtMaxT))
print("\t>% 10.8f % 20.8f % 20.8f % 20.8f"%(
    IdtDpdt,IdtDTdt,IdtMaxP,IdtMaxT))
print(half);
T_INITIAL.append(round(Tini,2)); P_INITIAL.append(round(Pini,2));
TC.append(Tc); PC.append(Pc); INVERSE.append(Invers);
IDT1.append(round(IdtDpdt,7));
IDT2.append(round(IdtDTdt,7));
IDT3.append(round(IdtMaxP,7));
IDT4.append(round(IdtMaxT,7));
df=pd.DataFrame({'Ti /K':T_INITIAL, 'Pi /mbar':P_INITIAL,
    'Tc /K':TC,'Pc /bar':PC,
    '1000/T(1/K)':INVERSE,
    'Max(dp/dt) /s':IDT1,
    'Max(dT/dt) /s':IDT2,
    'Max(Press) /s':IDT3,
    'Max(Temp) /s':IDT4
    })
dftr=pd.DataFrame({'time /ms':TIMES, 'P /bar':PRESSURES,
    'T /K':TEMPERATURES,"Vol":V
    })
#dftr.to_csv(sim_nametr+".traces",index=False,sep="\t")
df.to_csv(sim_name,index=False,sep="\t")
end=time.time(); print("It's Done!");
print("It took {0:0.1f} seconds".format(end - start)); print(dash);

```

```

# -----
# -----
if __name__ == "__main__":
    "\t>JUST RUNNING THE CODE"
    DefinitionStandar.SOME_STUFF(60,'cti','xml');
    print(half);
    mech_list = [];
    path = "C:\\DKM\\MODELS\\" #os.getcwd()
    fname = glob.glob(path+"\\*.cti");
    # ++++++
    for i,mechanism in enumerate(fname):
        print("\t>Running with mechanism: \n',mechanism);
        print(half,\n');
        Input = sys.argv[1]#"InputFileNameWithFullPath"
        print(half,\n');
        RCM_SIMULATION.RUN(mechanism,Input);
    # ++++++

```

7. Python code for Laminar Burning Velocity (LBV)

```

# #####
# # S.M. C3-NUIG, IE. 12-12-2019 #
# # S1E9S8M1J1M9S9P4, "La verdad os hara libres!" #
# #####
import os
import sys
import glob
import cantera as ct
import numpy as np
from matplotlib import pyplot as plt
import re
import scipy
import scipy.optimize
import pandas as pd
import time
import datetime
# #####
#
# #####

def InputFileReaderLBV(FileNamePath,OutputPath):
    FILENAME = FileNamePath.split("\\")
    INPUTFILENAME = FILENAME[-1];
    FileLBV= pd.read_csv(FileNamePath, names=['col'],sep='%s',engine='python');
    FolderName = FILENAME[3:-1];
    InputFileNames = (INPUTFILENAME.split(".PFP_EXP"))[0];
    FolderDir = "\\".join(FolderName) + "\\\" + InputFileNames
    if not os.path.isdir(OutputPath + FolderDir):
        os.makedirs(OutputPath + FolderDir)

```

```

FinalPath = str(OutputPath + FolderDir)
# ++++++
# FILTERING DATA BY SPECIFIC NAMES, FROM HERE WE WILL GET THE FUEL,OXIDIZERS,
# CONCENTRATIONS, INITIAL TEMPERATURES AND INITIAL PRESSURES, ETC... MAKING
# DICTIONARIES TO STORAGE THE DATA READ IT.
# ++++++
NamesDict = {}
ReactorsDict = {}
UnitsDict = {}
print("\t>',FileNamePath)
AUTHOR = ((FileLBV[FileLBV.col.str.contains("AUTHOR:")]
).iloc[0].str.split(':')[0][1]
JOURNAL = ((FileLBV[FileLBV.col.str.contains("JOURNAL:")]
).iloc[0].str.split(':')[0][1]
PDF = ((FileLBV[FileLBV.col.str.contains("PDF:")]
).iloc[0].str.split(':')[0][1]
REACTOR = ((FileLBV[FileLBV.col.str.contains("REACTOR:")]
).iloc[0].str.split(':')[0][1]
DATA = ((FileLBV[FileLBV.col.str.contains("DATA:")]
).iloc[0].str.split(':')[0][1]
PRESSURE = ((FileLBV[FileLBV.col.str.contains("PRESSURE:")]
).iloc[0].str.split(':')[0][1]
#PRESSURE = str(PRESSURE)
#COLLECT = ((FileLBV[FileLBV.col.str.contains("COLLECTED_BY:")]
#).iloc[0].str.split(':')[0][1]
#DATE = ((FileLBV[FileLBV.col.str.contains("DATE:")]
#).iloc[0].str.split(':')[0][1]
#SOURCE = ((FileLBV[FileLBV.col.str.contains("SOURCE:")]
#).iloc[0].str.split(':')[0][1]
#INTM = ((FileLBV[FileLBV.col.str.contains("INTM:")]
#).iloc[0].str.split(':')[0][1]
TEMPERATURE = ((FileLBV[FileLBV.col.str.contains("TEMPERATURE:")]
).iloc[0].str.split(':')[0][1]
DroppingStuff = FileLBV[FileLBV.col.str.contains("!") == False]
TimeScale = ((FileLBV[FileLBV.col.str.contains("LBV:")]
).iloc[0].str.split(':')[0][1]
dataLBV = pd.DataFrame((DroppingStuff.col.str.split()).tolist())
NamesDict["AUTHOR"] = AUTHOR
NamesDict["JOURNAL"] = JOURNAL
NamesDict["PDF"] = PDF
#NamesDict["COLLECT"] = COLLECT
#NamesDict["DATE"] = DATE
#NamesDict["SOURCE"] = SOURCE
NamesDict["InpFileName"] = INPUTFILENAME
NamesDict["FolderDir"] = FolderDir
ReactorsDict["REACTOR"] = REACTOR
ReactorsDict["DATA"] = DATA
#ReactorsDict["INTM"] = INTM
UnitsDict["PRESSURE"] = PRESSURE
UnitsDict["TEMPERATURE"] = TEMPERATURE
UnitsDict["TIMESCALE"] = TimeScale
return (NamesDict, ReactorsDict, UnitsDict,dataLBV,FinalPath)
# #####

OUTPUT_PATH= "C:\\DKM\\OUTPUTDATA\\"
dash= '*90; half= '*90; gato = '#*90;

```

```

#####
def LBVCanteraSimulator(MechFile, Input):
    start = time.time()
    (NamesDict, ReactorsDict, UnitsDict, TP, FinalPath) = InputFileReaderLBV(Input,OUTPUT_PATH)
    filename = str(NamesDict["InpFileName"])
    ct.suppress_thermo_warnings(); now = datetime.datetime.now();
    NOW = str(now)[:10]; #INTM = ((ReactorsDict["INTM"]).split(' '));
    #print(TP)
    #INTM2 = [];
    #for p in range(len(INTM)):
    #    if INTM[p] == " ":
    #        continue
    #    else:
    #        INTM2.append(INTM[p])
    if not os.path.isdir(FinalPath + "\\SENS\\"):
        os.makedirs(FinalPath + "\\SENS\\");
    #assert os.path.exists(cantera_file_path)
    gas = ct.Solution(MechFile); #print(INTM);#print(INTM2);
    mech2 = MechFile.rsplit("\\",1)[-1];
    mech3 = mech2.split(".cti")[0];
    Ti = []; Pi = []; PHI = []; LVB = []; SPEED = [];
    ERROR = []; FITTED = [];
    print("\t>With {0} Mechanism\n ".format(mech2 )); print("="*60)
    CHMols = []; O2Mols = []; DilMols = []; ProdMols = [];
    for i in (TP.iloc[0,:]):
        if "CO2" in i or "H2O" in i:
            ProdMols.append(i)
        elif "N2" in i or "AR" in i or "HE" in i:
            DilMols.append(i)
        elif "O2" in i:
            O2Mols.append(i)
        elif "C" in i:
            CHMols.append(i)
        elif "H2" in i:
            CHMols.append(i)
    if len(CHMols) == 1:
        fuel = "mono"
    elif len(CHMols) == 2:
        fuel = "binary"
    elif len(CHMols) == 6:
        fuel = "puto"
    else:
        print("More than two and puto fuels")
        sys.exit(1)
    print(len(CHMols),CHMols)
    NumCols = len(TP.columns); #print(NumCols)
    LabelCols = TP.iloc[0,:]; #print(LabelCols[6])
    for f in range(len(TP)-1):
        if fuel == "mono":
            fuels = CHMols[0]+' '+str(TP.iloc[(f+1),4])
            oxidizer = O2Mols[0]+' '+str(TP.iloc[(f+1),5])
            dilution = DilMols[0]+' '+str(TP.iloc[(f+1),6])
        elif fuel == "binary":
            fuels = CHMols[0]+' '+str(TP.iloc[(f+1),4])+' '+CHMols[1]+' '+str(TP.iloc[(f+1),5])
            oxidizer = O2Mols[0]+' '+str(TP.iloc[(f+1),6])

```

```

    dilution = DilMols[0]+' '+str(TP.iloc[(f+1),7])
elif fuel == "puto":
    fuels =
CHMols[0]+' '+str(TP.iloc[(f+1),4])+" "+CHMols[1]+' '+str(TP.iloc[(f+1),5])+" "+CHMols[2]+' '+str(TP.iloc[(f+1),6])
+" "+CHMols[3]+' '+str(TP.iloc[(f+1),7])+" "+CHMols[4]+' '+str(TP.iloc[(f+1),8])+" "+CHMols[5]+' '+str(TP.iloc[(f+
1),9])
    oxidizer = O2Mols[0]+' '+str(TP.iloc[(f+1),6])
    dilution = DilMols[0]+' '+str(TP.iloc[(f+1),7])

resto = oxidizer+' '+dilution
ExpResult = str(TP.iloc[(f+1),3]); LVB.append(ExpResult)
phi = float(TP.iloc[(f+1),2]); PHL.append(str(phi))
temperature = float(TP.iloc[(f+1),1]); Ti.append(str(temperature))
pressure = float(TP.iloc[(f+1),0]); Pi.append(str(pressure))
print("T = {} K".format(temperature))
print("P = {} atm".format(pressure))
gas.set_equivalence_ratio(phi, fuels, resto)
gas.mole_fraction_dict()
gas.TP = (temperature,pressure*ct.one_atm)
gas()
print(gas())
#+++++
#
#+++++
def extrapolate_uncertainty(grids, speeds,f):
    """
    Given a list of grid sizes and a corresponding list of flame speeds,
    extrapolate and estimate the uncertainty in the final flame speed.
    Also makes a plot.
    """
    grids = list(grids)
    speeds = list(speeds)
    #+++++
    #
    #+++++

def speed_from_grid_size(grid_size, true_speed, error):
    """
    Given a grid size (or an array or list of grid sizes)
    return a prediction (or array of predictions)
    of the computed flame speed, based on
    the parameters `true_speed` and `error`
    """
    return true_speed + error * np.array(grid_size)**-1.

popt, pcov = scipy.optimize.curve_fit(speed_from_grid_size, grids[-4:], speeds[-4:])
perr = np.sqrt(np.diag(pcov))
true_speed = pop[0]
percent_error_in_true_speed = 100.0*perr[0] / pop[0]
print("Fitted true_speed is {:.4f} ± {:.4f} cm/s
({:.1f}%)".format(pop[0]*100,perr[0]*100,percent_error_in_true_speed))
Fitted_speed =
str(round(pop[0]*100,3)+' ± '+str(round(perr[0]*100,3))+ '('+str(round(percent_error_in_true_speed,3))+')')
#print "convergence rate wrt grid size is {:.1f} ± {:.1f}".format(pop[2], perr[2])
estimated_percent_error = 100. * (speed_from_grid_size(grids[-1], *pop) - true_speed) / true_speed

```

```

print("Estimated error in final calculation {:.1f}%".format(estimated_percent_error))
total_error_estimate = abs(percent_error_in_true_speed) + abs(estimated_percent_error)
print("Estimated total error {:.1f}%".format(total_error_estimate))
#++++++
# Plotting
#++++++
###plt.semilogx(grids,speeds,'o-')
###plt.ylim(min(speeds[-5:]+[true_speed-perr[0]]*.95, max(speeds[-5:]+[true_speed+perr[0]]*1.05)
###plt.plot(grids[-4:], speeds[-4:], 'or')
###extrapolated_grids = grids + [grids[-1] * i for i in range(2,8)]
###plt.plot(extrapolated_grids,speed_from_grid_size(extrapolated_grids,*popt),':r')
###plt.xlim(*plt.xlim())
###plt.hlines(true_speed, *plt.xlim(), colors='u'r', linestyle='u'dashed')
###plt.hlines(true_speed+perr[0], *plt.xlim(), colors='u'r', linestyle='u'dashed', alpha=0.3)
###plt.hlines(true_speed-perr[0], *plt.xlim(), colors='u'r', linestyle='u'dashed', alpha=0.3)
###plt.fill_between(plt.xlim(), true_speed-perr[0],true_speed+perr[0], facecolor='red', alpha=0.1 )
###plt.text(grids[-1],speeds[-1], "{:.1f}%".format(estimated_percent_error))
###above = popt[1]/abs(popt[1]) # will be +1 if approach from above or -1 if approach from below
###plt.annotate("",
###    xy=(grids[-1], true_speed),
###    xycoords='data',
###    xytext=(grids[-1], speed_from_grid_size(grids[-1], *popt)),
###    textcoords='data',
###    arrowprops=dict(arrowstyle='|-|',
###        connectionstyle='arc3',
###        color='black', shrinkA=0, shrinkB=0),
###    )
###plt.annotate("{:.2f}%".format(abs(estimated_percent_error)),
###    xy=(grids[-1], speed_from_grid_size(grids[-1], *popt)),
###    xycoords='data',
###    xytext=(10,20*above),
###    textcoords='offset points',
###    arrowprops=dict(arrowstyle='->',
###        connectionstyle='arc3')
###    )
###plt.annotate("",
###    xy=(grids[-1]*4, true_speed-(above*perr[0])),
###    xycoords='data',
###    xytext=(grids[-1]*4, true_speed),
###    textcoords='data',
###    arrowprops=dict(arrowstyle='|-|',
###        connectionstyle='arc3',
###        color='black', shrinkA=0, shrinkB=0),
###    )
###plt.annotate("{:.2f}%".format(abs(percent_error_in_true_speed)),
###    xy=(grids[-1]*4, true_speed-(above*perr[0])),
###    xycoords='data',
###    xytext=(10,-20*above),
###    textcoords='offset points',
###    arrowprops=dict(arrowstyle='->',
###        connectionstyle='arc3')
###    )
###plt.ylabel("Flame speed (m/s)")
###plt.xlabel("Grid size")
###plt.savefig(FinalPath+'\\IMAGES\\'+filename+'_PHI_'+str(phi)+

```



```

###      '_'+str(mech3)+'_'+str(f)+'_extrapolate.png',dpi=800)
###plt.close()
return (true_speed, total_error_estimate,Fitted_speed)

#++++++
#
#++++++
def make_callback(flame):
    speeds = []
    grids = []
    #+++++
    #
    #+++++
    def callback(_):
        speed = flame.u[0]
        grid = len(flame.grid)
        speeds.append(speed)
        grids.append(grid)
        print("Iteration {}".format(len(grids)))
        print("Current flame speed is is {:.4f} cm/s".format(speed*100.))
        if len(grids) < 5:
            #+++++
            # Returnning data
            #+++++
            return 1.0 #
        try:
            extrapolate_uncertainty(grids, speeds,f)
        except Exception as e:
            print("Couldn't estimate uncertainty", e.message)
            #+++++
            # Returnning data
            #+++++
            return 1.0 # continue anyway
        #+++++
        # Returnning data
        #+++++
        return 1.0
        #+++++
        # Returnning data
        #+++++
    return callback, speeds, grids
# flame.set_steady_callback(make_callback()[0])
# Domain width in metres
width = 0.015
# Create the flame object
flame = ct.FreeFlame(gas, width=width)
# Define tolerances for the solver
# (these are used throughout the notebook)
#refine_criteria = {'ratio':3, 'slope': 0.1, 'curve': 0.1} # around 145 grid size, Error from 0.4 - 6% ## refine_criteria
= {'ratio':2, 'slope': 0.01, 'curve': 0.01} # around 1000 grid size, Error from 0.0 - 0.6%
refine_criteria = {'ratio':2, 'slope': 0.01, 'curve': 0.01}
flame.set_refine_criteria(**refine_criteria)
#flame.set_max_grid_points(flame.domains[flame.domain_index('flame')], 1e4)
try:
    flame.set_max_grid_points(flame.domains[flame.domain_index('flame')], 1e4)

```

```

except:
    flame.set_max_grid_points(flame.domains[flame.domain_index('flame')], 1e6)
    callback, speeds, grids = make_callback(flame)
    flame.set_steady_callback(callback)
    # Define logging level
    loglevel = 1
    flame.solve(loglevel=loglevel, auto=True)
    final_true_speed, percentage_uncertainty, Fitted_speed = extrapolate_uncertainty(grids, speeds, f)
    print("Final grid was size {}".format(grids[-1]))
    print("Final speed was {:.4f} cm/s".format(100*speeds[-1]))
    print("Estimated uncertainty is {:.1f}%".format(percentage_uncertainty))
    print("i.e. {:.3f} +/- {:.3f} cm/s".format(100*speeds[-1],
        percentage_uncertainty*speeds[-1]))
    for i in range(4, len(grids)):
        print("At step {}".format(i))
        print("Grid was size {}".format(grids[i]))
        print("Speed was {:.4f} cm/s".format(100*speeds[i]))
        true_speed, percentage_uncertainty, Fitted_speed = extrapolate_uncertainty(grids[:i], speeds[:i], f)
        print("Estimated uncertainty was {:.1f}%".format(percentage_uncertainty))
        print("i.e. {:.3f} +/- {:.3f} cm/s".format(100*speeds[i],
            percentage_uncertainty*speeds[i]))
        print("or {:.3f} -- {:.3f} cm/s".format((100-percentage_uncertainty)*speeds[i],
            (100+percentage_uncertainty)*speeds[i]))
        print("(For reference, the 'final' extrapolated speed was {:.3f} cm/s".format(100*final_true_speed))
        print("=*80)
    SPEED.append(round(100*final_true_speed, 3))
    ERROR.append(round(percentage_uncertainty, 3))
    FITTED.append(Fitted_speed)
    ## Solve with multi-component transport properties
    flame.transport_model = 'Multi'
    flame.soret_enabled = True
    flame.solve(loglevel) # don't use 'auto' on subsequent solves
    ##print('multicomponent flamespeed = {0} m/s'.format(flame.u[0]))
    #####+++++
    ##### Plotting sensitivity analyses
    #####+++++
    if "sens" in sys.argv:
        #+++++
        # Starting sensitivity analysis of the reactions
        #+++++
        #ListOfEqRats = [0.5, 1.0, 2.0]
        sens1 = flame.get_flame_speed_reaction_sensitivities()
        # print the reaction number followed by the associated sensitivity
        #print()
        #print('Rxn # k/S*dS/dk Reaction Equation')
        #print('-----')
        #for m in range(gas.n_reactions):
        # #print(m)
        # print('{: 5d} {:.10.3e} {}'.format(m, sens1[m], gas.reaction_equation(m)))
        # use argsort to obtain an array of the *indices* of the values of the sens1 array sorted by absolute value
        newOrder = np.argsort(np.abs(sens1))
        # argsort ranks from small to large, but we want large to small, so we flip this around
        newOrder = newOrder[::-1]
        # make some storage variables so that we can plot the results later in a bar graph
        IndexSpecies = np.zeros(len(newOrder))

```

```

newOrder2 = np.zeros(len(newOrder))
sens2     = np.zeros(len(newOrder))
reactionList = []
# using the same method above, print the sensitivities but call the new indices that we defined
print()
print('Rxn #   k/S*dS/dk   Reaction Equation')
print('-----')
for ii in range(gas.n_reactions):
    print('{: 5d}   {: 10.3e}   {}'.format(newOrder[ii], sens1[newOrder[ii]], gas.reaction_equation(newOrder[ii])))
    # assign new variables values for plot use
    IndexSpecies[ii] = newOrder[ii]
    newOrder2[ii] = ii
    sens2[ii] = sens1[newOrder[ii]]
    reactionList.append(gas.reaction_equation(newOrder[ii]))
# generate horizontal bar graph
numTopReactions = 11; # how many of the top reactions do we want to look at?
#+++++
# Plotting
#+++++
plt.rcParams()
fig, ax = plt.subplots()
# plot results
ax.barh(newOrder2[0:numTopReactions-1], sens2[0:numTopReactions-1], align='center', color='black',
ecolor='black')
# make sure that every single tick on the y-axis is marked
ax.set_yticks(np.arange(len(reactionList[0:numTopReactions-1])))
# label these y-ticks with the reaction in question
ax.set_yticklabels(reactionList[0:numTopReactions-1])
# invert the y-axis so that the most sensitive reaction is at the top instead of the bottom
ax.invert_yaxis()
fig.tight_layout()
plt.show();
plt.savefig( str(FinalPath) + '\\SENS\\'+ str(filename) + '_PHI_' + str(phi) + '_FlameSENS.png', dpi=800);
plt.close()
IndexSpeciations = [int(x) for x in IndexSpecies[0:numTopReactions-1]]
dfXs = pd.DataFrame({"RxnIndex":IndexSpeciations, "RxnName":reactionList[0:numTopReactions-1],
"RxnSens":sens2[0:numTopReactions-1]})
dfXs2 = pd.DataFrame({"RxnIndex":IndexSpeciations, "RxnName":reactionList[0:numTopReactions-1],
"RxnSens":sorted(sens2[0:numTopReactions-1])})
dfXs.to_csv(str(FinalPath) + '\\SENS\\'+ str(filename) + '_PHI_' + str(phi) + '_FlameSENS.dat', sep="\t", index =
False)
dfXs2.to_csv(str(FinalPath) + '\\SENS\\'+ str(filename) + '_PHI_' + str(phi) + '_FlameSENS_sorted.dat', sep="\t",
index = False)
else:
    pass
#+++++
# Saving the DataFrame data in a *.dat format file
#+++++
SimTime = time.time() - start
if SimTime <= 60:
    df2 = pd.DataFrame({"File_Name":filename, "SimTime /s":round(SimTime,2), "DATE":NOW}, index=[0])
elif SimTime > 60:
    df2 = pd.DataFrame({"File_Name":filename, "SimTime
/min":round((float(SimTime)/60),2), "DATE":NOW}, index=[0])
elif SimTime > 3600:

```

```

df2 = pd.DataFrame({"File_Name":filename,"SimTime
/hr":round((float(SimTime)/3600),2),"DATE":NOW},index=[0])
df1 = pd.DataFrame({"Tinitial /K":Ti,"Pinitial /atm":Pi,"Eq.Ratio":PHI,"Exp.Result cm/s":LVB,"Sim.Result
cm/s":SPEED,"% Error":ERROR,"FittedTrueSpeed cm/s and (%) Error":FITTED})
df = df1.join(df2,lsuffix='_df1',rsuffix='_df2')
ResultsJVB = df.to_csv(FinalPath+"\'+mech3+'_LBV_EXP_.dat',index=False, sep='\t')
#+++++
# Returning data
#+++++
return (ResultsJVB)
#+++++
# -----
# -----
if __name__ == "__main__":
    "\t>JUST RUNNING THE CODE"
    print(half);
    mech_list = [];
    path = "C:\\DKM\\MODELS\\" #os.getcwd()
    fname = glob.glob(path+"\\*.cti");
    # +++++
    for i,mechanism in enumerate(fname):
        Input = sys.argv[1]#"InputFileNameWithFullPath"
        print("\t> Running LBV reactor for Flame speed calculation");
        print("\t> Running with mechanism: \n\t',mechanism);
        print("\t> Case: \n\t",Input)
        print(half,'\n');
        LBVCanteraSimulator(mechanism,Input);
    # +++++

```

8. Python code for Flow Reactor (FR)

```

#####
# Created on 2018
# @author: version 1.0. S.M.
# C3-Combustion Chemistry Centre
# National University of Ireland, Galway
# http://c3.nuigalway.ie/
#####
import os
import glob
import cantera as ct
import numpy as np
import re
import scipy
import scipy.optimize
import pandas as pd
import time
import datetime
import sys

```

```

import time

# ++++++
def InputFileReaderPFR(FileNamePath,OutputPath):
    FILENAME = FileNamePath.split("\\")
    INPUTFILENAME = FILENAME[-1];
    FilePFR= pd.read_csv(FileNamePath, names=['col'],sep='%s',engine='python');
    FolderName = FILENAME[3:-1];
    InputFileNames = (INPUTFILENAME.split(".PFR_EXP"))[0];
    FolderDir = "\\".join(FolderName) + "\\ " + InputFileNames
    if not os.path.isdir(OutputPath + FolderDir):
        os.makedirs(OutputPath + FolderDir)
    FinalPath = str(OutputPath + FolderDir)
    # ++++++
    # FILTERING DATA BY SPECIFIC NAMES, FROM HERE WE WILL GET THE FUEL,OXIDIZERS,
    # CONCENTRATIONS, INITIAL TEMPERATURES AND INITIAL PRESSURES, ETC... MAKING
    # DICTIONARIES TO STORAGE THE DATA READ IT.
    # ++++++
    NamesDict = {}
    ReactorsDict = {}
    UnitsDict = {}
    print("\t>',FileNamePath)
    try:
        REACS = (FilePFR[FilePFR.col.str.contains("REAC:")] ).col.str.split(':')
    except:
        FilePFR = pd.read_fwf(FileNamePath,names=['col']);
        REACS = (FilePFR[FilePFR.col.str.contains("REAC:")] ).col.str.split(':')
    REACTANTS = []
    for i in range(len(REACS)):
        REAC1 = REACS.iloc[i][1]
        REAC1 = ":".join(REAC1.split())
        REACTANTS.append(REAC1)
    REACTANTS = str(",".join(REACTANTS))
    AUTHOR = ((FilePFR[FilePFR.col.str.contains("AUTHOR:")]
        ).iloc[0].str.split(':')[0][1]
    JOURNAL = ((FilePFR[FilePFR.col.str.contains("JOURNAL:")]
        ).iloc[0].str.split(':')[0][1]
    PDF = ((FilePFR[FilePFR.col.str.contains("PDF:")]
        ).iloc[0].str.split(':')[0][1]
    REACTOR = ((FilePFR[FilePFR.col.str.contains("REACTOR:")]
        ).iloc[0].str.split(':')[0][1]
    DATA = ((FilePFR[FilePFR.col.str.contains("DATA:")]
        ).iloc[0].str.split(':')[0][1]
    PRESSURE = ((FilePFR[FilePFR.col.str.contains("PRESSURE:")]
        ).iloc[0].str.split(':')[0][1]
    #PRESSURE = str(PRESSURE)
    TIME = ((FilePFR[FilePFR.col.str.contains("TIME:")]
        ).iloc[0].str.split(':')[0][1]
    ENERGY_EQUATION = ((FilePFR[FilePFR.col.str.contains("ENERGY_EQUATION:")]
        ).iloc[0].str.split(':')[0][1]
    #T_INITIAL = ((FilePFR[FilePFR.col.str.contains("T_INITIAL:")]
    # ).iloc[0].str.split(':')[0][1]
    #P_INITIAL = ((FilePFR[FilePFR.col.str.contains("P_INITIAL:")]
    # ).iloc[0].str.split(':')[0][1]
    #

```

```

try:
    T_INITIAL = ((FilePFR[FilePFR.col.str.contains("T_INITIAL:")]
                 ).iloc[0].str.split(':')[0][1])
    P_INITIAL = ((FilePFR[FilePFR.col.str.contains("P_INITIAL:")]
                 ).iloc[0].str.split(':')[0][1])
    ReactorsDict["T_INITIAL"] = T_INITIAL
    ReactorsDict["P_INITIAL"] = P_INITIAL
except:
    ReactorsDict["T_INITIAL"] = 0
    ReactorsDict["P_INITIAL"] = 0
#
PHI = ((FilePFR[FilePFR.col.str.contains("PHI:")]
       ).iloc[0].str.split(':')[0][1])
TEMPERATURE = ((FilePFR[FilePFR.col.str.contains(
    "TEMPERATURE:")]
               ).iloc[0].str.split(':')[0][1])
DroppingStuff = FilePFR[FilePFR.col.str.contains("!") == False]
ITMM = DroppingStuff[DroppingStuff.col.str.contains("TAU") == True]
ITM = pd.DataFrame((ITMM.col.str.split()).tolist())
dataPFR = pd.DataFrame((DroppingStuff.col.str.split()).tolist())
NamesDict["AUTHOR"] = AUTHOR
NamesDict["JOURNAL"] = JOURNAL
NamesDict["PDF"] = PDF
NamesDict["ENERGY_EQUATION"] = ENERGY_EQUATION
NamesDict["InpFileName"] = INPUTFILENAME
NamesDict["FolderDir"] = FolderDir
NamesDict["ITM"] = ITM
ReactorsDict["REACTANTS"] = REACTANTS
ReactorsDict["REACTOR"] = REACTOR
ReactorsDict["DATA"] = DATA
ReactorsDict["PHI"] = PHI
ReactorsDict["P_INITIAL"] = P_INITIAL
ReactorsDict["T_INITIAL"] = T_INITIAL
UnitsDict["PRESSURE"] = PRESSURE
UnitsDict["TEMPERATURE"] = TEMPERATURE
UnitsDict["TIME"] = TIME
return (NamesDict, ReactorsDict, UnitsDict, dataPFR, FinalPath, ITM)
# ++++++
def PFRCanteraSimulator(NamesDict, ReactorsDict, UnitsDict, dataPFR, FinalPath, ITM, MechFile):
    start = time.time()
    TP = dataPFR
    filename = str(NamesDict["InpFileName"])
    NumCols = len(TP.columns); print("\t> Number of species of interest: {0}".format(NumCols))

    LabelCols = TP.iloc[0,:]; INTER = [];
    for u in range(NumCols-1):
        INTER.append(str(ITM[u+1][0]))

    print("\t> List of species of interest:\n\t> {0}".format(INTER))
    ct.suppress_thermo_warnings(); now = datetime.datetime.now();
    NOW = str(now)[:10]; dash= '-'*100; half= '-'*100; gato= '#'*100;
    #simname = input('Please give a name for this job: ') or 'a';
    #print(simname)
    #####
    # Input Parameters

```

```

#####
T_0 = float(ReactorsDict["T_INITIAL"])
# inlet temperature [K]
pressure = float(ReactorsDict["P_INITIAL"])*ct.one_atm # constant pressure [Pa]
# .....
if T_0 == 0.0:
    Temps = TP[0]
    Ti = list(map(float, Temps.tolist()))
    Temps = Ti
    ResTime0 = TP[2]
    ResTimei = [list(map(float, ResTime0))[-1]]
    resTime = ResTimei
    press = TP[1]
    Po = press
    Pi = [list(map(float, Po))[0]]
    pressures = Pi
    print(T_0, pressure)
else:
    # .....
    print(T_0, pressure)
    # .....
    composition_0 = ReactorsDict["REACTANTS"]
    phi = float(ReactorsDict["PHI"])
    length = 8.0*5.0 # *approximate* PFR length [m]
    u_0 = 8.0 # inflow velocity [m/s]
    #area = 0.00812 # cross-sectional area [m**2]
    area = 1.e-4 # cross-sectional area [m**2]
    # Resolution:
    #The PFR will be simulated by 'n_steps' time steps or by a chain
    # of 'n_steps' stirred reactors.
    n_steps = 10000
    #####
    #####
    # Method 1: Lagrangian Particle Simulation
    #####
    # A Lagrangian particle is considered which travels through the PFR. Its
    # state change is computed by upwind time stepping. The PFR result is produced
    # by transforming the temporal resolution into spatial locations.
    # The spatial discretization is therefore not provided a priori but is instead
    # a result of the transformation.
    # import the gas model and set the initial conditions
    gas1 = ct.Solution(MechFile)
    mech2 = MechFile.rsplit("\\",1)[-1];
    mech3 = mech2.split(".cti")[0];
    print("\t>With {0} Mechanism\n ".format(mech2 )); print("=*60)
    gas1.TPX = T_0, pressure, composition_0
    mass_flow_rate1 = u_0 * gas1.density * area
    # create a new reactor
    r1 = ct.IdealGasConstPressureReactor(gas1)
    # create a reactor network for performing time integration
    sim1 = ct.ReactorNet([r1])
    # approximate a time step to achieve a similar resolution as in the next method
    t_total = 3100/T_0
    if float(TP.iloc[1,0]) == 0:
        dt = float(TP.iloc[2,0])*0.001

```

```

else:
    dt = float(TP.iloc[1,0])*0.001 #t_total / n_steps
    # define time, space, and other information vectors
    #t1 = (np.arange(n_steps) + 1)* dt

    n1 = 0
    t = 0.0
    #for n1, t_i in enumerate(t1):
    end_time = 20000 #int(((2*float(TP.iloc[-1,0])))/dt);
    t1 = np.zeros(end_time)
    z1 = np.zeros(end_time)
    u1 = np.zeros(end_time)
    states1 = ct.SolutionArray(r1.thermo)
    Tem=[];
    print("\t> This is your deltatime: {:.10f}".format(dt))
    print("\t> Simulation is going to finish when: {0} passed\n".format(end_time))
    print("-"*90)
    print("\t> Next file...")
    print("-"*90)
    while n1 < (end_time): # and r.T < T_equi - 0.1:
        t += dt
        # perform time integration
        sim1.advance(t)
        t1[n1] = sim1.time
        # compute velocity and transform into space
        u1[n1] = mass_flow_rate1 / area / r1.thermo.density
        z1[n1] = z1[n1 - 1] + u1[n1] * dt
        states1.append(r1.thermo.state)
        Tem.append(r1.T)
        n1 += 1
    for m in range(NumCols-1):

        if NumCols == 2:
            label1 = TP.iloc[0,1]

            df2 = pd.DataFrame({str(label1):states1.X[:, gas1.species_index(str(label1))]); #sp1.append(df2)
        elif NumCols == 3:
            label1 = TP.iloc[0,1]
            label2 = TP.iloc[0,2]

            df2 = pd.DataFrame({str(label1):states1.X[:, gas1.species_index(str(label1))],str(label2):states1.X[:,
gas1.species_index(str(label2))]); #sp1.append(df2)
        elif NumCols == 4:
            label1 = TP.iloc[0,1]
            label2 = TP.iloc[0,2]
            label3 = TP.iloc[0,3]

            df2 = pd.DataFrame({str(label1):states1.X[:, gas1.species_index(str(label1))],str(label2):states1.X[:,
gas1.species_index(str(label2))],str(label3):states1.X[:, gas1.species_index(str(label3))]); #sp1.append(df2)
        elif NumCols == 5:
            label1 = TP.iloc[0,1]
            label2 = TP.iloc[0,2]
            label3 = TP.iloc[0,3]
            label4 = TP.iloc[0,4]

```



```

df2 = pd.DataFrame({str(label1):states1.X[:, gas1.species_index(str(label1))],str(label2):states1.X[:,
gas1.species_index(str(label2))],str(label3):states1.X[:, gas1.species_index(str(label3))],str(label4):states1.X[:,
gas1.species_index(str(label4))]); #sp1.append(df2)

```

```

elif NumCols == 6:

```

```

    label1 = TP.iloc[0,1]
    label2 = TP.iloc[0,2]
    label3 = TP.iloc[0,3]
    label4 = TP.iloc[0,4]
    label5 = TP.iloc[0,5]

```

```

df2 = pd.DataFrame({str(label1):states1.X[:, gas1.species_index(str(label1))],str(label2):states1.X[:,
gas1.species_index(str(label2))],str(label3):states1.X[:, gas1.species_index(str(label3))],str(label4):states1.X[:,
gas1.species_index(str(label4))],str(label5):states1.X[:, gas1.species_index(str(label5))]); #sp1.append(df2)

```

```

elif NumCols == 7:

```

```

    label1 = TP.iloc[0,1]
    label2 = TP.iloc[0,2]
    label3 = TP.iloc[0,3]
    label4 = TP.iloc[0,4]
    label5 = TP.iloc[0,5]
    label6 = TP.iloc[0,6]

```

```

df2 = pd.DataFrame({str(label1):states1.X[:, gas1.species_index(str(label1))],str(label2):states1.X[:,
gas1.species_index(str(label2))],str(label3):states1.X[:, gas1.species_index(str(label3))],str(label4):states1.X[:,
gas1.species_index(str(label4))],str(label5):states1.X[:, gas1.species_index(str(label5))],str(label6):states1.X[:,
gas1.species_index(str(label6))]); #sp1.append(df2)

```

```

elif NumCols == 8:

```

```

    label1 = TP.iloc[0,1]
    label2 = TP.iloc[0,2]
    label3 = TP.iloc[0,3]
    label4 = TP.iloc[0,4]
    label5 = TP.iloc[0,5]
    label6 = TP.iloc[0,6]
    label7 = TP.iloc[0,7]

```

```

df2 = pd.DataFrame({str(label1):states1.X[:, gas1.species_index(str(label1))],str(label2):states1.X[:,
gas1.species_index(str(label2))],str(label3):states1.X[:, gas1.species_index(str(label3))],str(label4):states1.X[:,
gas1.species_index(str(label4))],str(label5):states1.X[:, gas1.species_index(str(label5))],str(label6):states1.X[:,
gas1.species_index(str(label6))],str(label7):states1.X[:, gas1.species_index(str(label7))]); #sp1.append(df2)

```

```

elif NumCols == 9:

```

```

    label1 = TP.iloc[0,1]
    label2 = TP.iloc[0,2]
    label3 = TP.iloc[0,3]
    label4 = TP.iloc[0,4]
    label5 = TP.iloc[0,5]
    label6 = TP.iloc[0,6]
    label7 = TP.iloc[0,7]
    label8 = TP.iloc[0,8]

```

```

df2 = pd.DataFrame({str(label1):states1.X[:, gas1.species_index(str(label1))],str(label2):states1.X[:,
gas1.species_index(str(label2))],str(label3):states1.X[:, gas1.species_index(str(label3))],str(label4):states1.X[:,
gas1.species_index(str(label4))],str(label5):states1.X[:, gas1.species_index(str(label5))],str(label6):states1.X[:,
gas1.species_index(str(label6))],str(label7):states1.X[:, gas1.species_index(str(label7))],str(label8):states1.X[:,
gas1.species_index(str(label8))]); #sp1.append(df2)

```

```

elif NumCols == 10:

```

```

    label1 = TP.iloc[0,1]

```

```

label2 = TP.iloc[0,2]
label3 = TP.iloc[0,3]
label4 = TP.iloc[0,4]
label5 = TP.iloc[0,5]
label6 = TP.iloc[0,6]
label7 = TP.iloc[0,7]
label8 = TP.iloc[0,8]
label9 = TP.iloc[0,9]

df2 = pd.DataFrame({str(label1):states1.X[:, gas1.species_index(str(label1))],str(label2):states1.X[:,
gas1.species_index(str(label2))],str(label3):states1.X[:, gas1.species_index(str(label3))],str(label4):states1.X[:,
gas1.species_index(str(label4))],str(label5):states1.X[:, gas1.species_index(str(label5))],str(label6):states1.X[:,
gas1.species_index(str(label6))],str(label7):states1.X[:, gas1.species_index(str(label7))],str(label8):states1.X[:,
gas1.species_index(str(label8))],str(label9):states1.X[:, gas1.species_index(str(label9))]); #sp1.append(df2)
SimTime = time.time() - start
simname = NamesDict["InpFileName"]
df1 = pd.DataFrame({'time':t1,'Ts':t1+0.01,'temperature':states1.T})
df3 = pd.DataFrame({"REAC":ReactorsDict["REACTANTS"],
                    "PHI": ReactorsDict["PHI"],
                    "ORIGIN_FILE_NAME":simname,
                    "deltat /s":round(dt,7),
                    "SimTime /s":round((float(SimTime)),2), "DATE":NOW},index=[0])
df = df1.join(df2,lsuffix='_df1', rsuffix='_df2')
dff = df.join(df3,lsuffix='_df', rsuffix='_df3')
ds = dff.to_csv(FinalPath+"\\"+mech3+'_PFR_EXP_.dat',index=False, sep="\t");
# PLOTTING:
#for w in range(len(observables)):
# plt.rcParams["font.weight"] = "bold"
# plt.tick_params(axis='both', direction='out', length=4, width=2, labelsz=10)
# plt.rcParams["axes.labelweight"] = "bold"
# plt.rcParams["axes.linewidth"] = "3"
# #plt.scatter(ExpTempos[0],DFn[observables[w]], marker="s", label=str(observables[w].translate(subscript)),
lw=4,color='black')
# plt.plot(ExpTempos[0],b[observables[w]], label=str(observables[w].translate(subscript)))
# #
# #
# #
# #plt.savefig(c + "\\" + NamesDict["InpFileName"] + "_" + observables[w] + '.png',dpi=800,
bbox_inches="tight")
# Y = pd.to_numeric(DFn[observables[w]])
# YY = (Y).sort_values(ascending=False)
# plt.scatter(ExpTempos[0],YY, marker="s", label=str(observables[w].translate(subscript)), lw=4,color='black')
# plt.legend()
# plt.show()
# plt.close()

return (ds)

#-----
#=====
if __name__ == "__main__":
mech_list = [];
path = "C:\\DKM\\MODELS\\"#os.getcwd();
fname = glob.glob(path+'/*.cti');
#print("\t>Running with mechanism: \n\t',mechanism);

```

```

#Mechanism = "/DKM/MODELS/19_48_C7.cti"
for m in fname:
    print("\t>Running with mechanism: \n\t',m);
    Input = sys.argv[1] #"InputFileNameWithFullPath"
    (NamesDict, ReactorsDict, UnitsDict,dataPFR,FinalPath,ITM) = InputFileReaderPFR(Input,
"C:\\DKM\\OUTPUTDATA\\");
    PFRCanteraSimulator(NamesDict, ReactorsDict, UnitsDict,dataPFR,FinalPath,ITM, m)
#=====
# Eppur si muove! - Galileo Galilei (1564-1642)
#=====

```

9. Python code for Jet Stirred Reactor (JSR)

```

#####
# Created on 2019
# @author: version 1.0. S.M.
# C3-Combustion Chemistry Centre
# National University of Ireland, Galway
# http://c3.nuigalway.ie/
#####
import os
import numpy as np
import pandas as pd
import os
import sys
import time
import matplotlib.pyplot as plt
import cantera as ct
import glob
import math
import datetime
import warnings
subscript = str.maketrans("0123456789", "0123456789")

#from InputFileReader import InputFileReaderJSR as R
#####
#PLOTTER FOR JSR ONLY
#++++++
def plotSpecies(results,species,conditions,pressures,phi,FinalPath,Title,author,DFn,ExpTempos,filenames):
    temps=[]
    for i in results:
        if i.solution['temperature'].values[0] not in temps:
            temps.append(i.solution['temperature'].values[0])
    filename=[]
    for i in results:
        if i.mechanism not in filename:
            filename.append(i.mechanism)
    res=[]
    for i in results:
        if i.residence_time not in res:
            res.append(i.residence_time)
    pre=[]
    for i in results:
        if i.final_pressure not in pre:

```

```

pre.append(i.final_pressure)

length=len(conditions)
length2=len(res)
#length3=len(pre)
sortedresults=[results[i::length] for i in range(length)]
for j in np.arange(len(sortedresults)):
    sortedresults[j]=[sortedresults[j][i::length2] for i in range(length2)]
for j in np.arange(len(sortedresults)):
    for f in np.arange(len(sortedresults[j])):
        sortedresults[j][f]=[sortedresults[j][f][i::len(filename)] for i in range(len(filename))]
#return sortedresults
species2save = {}
counter = 0
for w in range(2):
    plt.rcParams["font.weight"] = "bold"
    plt.tick_params(axis='both', direction='out', length=4, width=2, labelsz=10)
    plt.rcParams["axes.labelweight"] = "bold"
    plt.rcParams["axes.linewidth"] = "3"
    for j in np.arange(len(sortedresults)):
        for f in np.arange(len(sortedresults[j])):
            for poop in np.arange(len(species)):
                for mech in filenames:
                    #spec=[]
                    for c in np.arange(len(filename)):
                        for p in np.arange(len(phi)):
                            specieslist=[];
                            for d in np.arange(len(temps)):
                                #print(j,f,poop,c,d)
                                specieslist.append((sortedresults[j][f][c][d].solution[species[poop]].values[0]))
                                #title = Title + " : " + author
                                #plt.title(title, fontsize=10, weight= 'bold')
                                #try:
                                Y = pd.to_numeric(DFn[species[poop]])
                                #YY = (Y).sort_values(ascending=False)
                                #print(DFn.iloc[:,0])
                                #print(ExpTempos[0])
                                plt.scatter(temps,Y, marker='s', label="Exp. data: "+author, lw=4,color='black')
                                #except:
                                # print("\t Not experimental data to plot was found, skipping...")
                                MECHA = (mech.rsplit("\\",1)[-1]).split(".cti")[0]
                                plt.plot(temps,specieslist, color="k", label=str(MECHA), lw=3)
                                plt.title(str(species[poop]).translate(subscript) + ' with residence time: ' + str(res[f])+ ' sec', fontsize=14,
weight= 'bold')
                                #df=pd.DataFrame({'Temperature_K':temps, species[poop]+'_molefraction':specieslist})
                                species2save[str(species[poop])] = specieslist
                                #counter += 1
                                #df.to_csv(FinalPath+'\\'+str(pressures[0])+
atm+'+_species'+species[poop]+'_phi'+str(phi[p])+'_'+FileNamePlotter+'.txt',sep='t',index=False)
                                FileNamePlotter = (((str(filename[c]).split("\\")[-1]).split(".cti"))[0]
                                plt.xlabel('$T / K$', fontsize=20, weight= 'bold');
                                plt.ylabel('Mole fraction', fontsize=20, weight= 'bold')
                                plt.legend(fontsize="medium",frameon=True)
                                plt.grid(b=True, which='major', color='grey', linestyle=':'); plt.grid(b=True, which='minor', color='grey',
linestyle=':')

```

```

plt.savefig(FinalPath+'\\'+str(pressures[0])+
atm+'+_species'+species[poop]+'_phi'+str(phi[p])+'+_'+FileNamePlotter+'.png',dpi=800, bbox_inches="tight")
    OutDir = (FinalPath)+'\\'+str(pressures[0])+
atm+'+_species'+species[poop]+'_phi'+str(phi[p])+'+_'+FileNamePlotter+'.png',dpi=800, bbox_inches="tight")
    #plt.savefig(FinalPath+'\\'+str(pressures[0])+
atm+'+_species'+_phi'+str(phi[p])+'+_'+FileNamePlotter+'.png',dpi=800)
    plt.close() #print(temps, specieslist)
df = pd.DataFrame({'Temperature_K':temps})
Names = list(species2save.keys())
Values = list(species2save.values())
#df2 = pd.DataFrame()
for g in range(len(species2save)):
    df2 = pd.DataFrame({Names[g]:Values[g]})
    df = pd.concat([df,df2], axis=1)
#print(df)
#print(df2)
#print(df3)
df.to_csv(FinalPath+'\\'+str(pressures[0])+
atm+'+_species'+_phi'+str(phi[p])+'+_'+FileNamePlotter+'.txt',sep='\t',index=False)
    #df.to_csv(FinalPath+'\\'+str(pressures[0])+
atm+'+_species'+species[poop]+'_phi'+str(phi[p])+'+_'+FileNamePlotter+'.txt',sep='\t',index=False)
    #print(species2save)
    #print(len(species2save))
    return sortedresults, df, OutDir
#+++++

```

```

def plotsens(sortedresults,observables,conditions,filename,temps,top10,FinalPath,Title,author):
    if not os.path.isdir(FinalPath + '\\SA\\'):
        os.makedirs(FinalPath + '\\SA\\');
    linetypes=['k-', 'b-', 'r-', 'g-', 'c-', 'm-', 'y-', 'k-', 'b-', 'r-', 'g-', 'c-', 'm-', 'y-', 'k-', 'b-', 'r-', 'g-', 'c-', 'm-', 'y-',
    'k:', 'b:', 'r:', 'g:', 'c:', 'm:', 'y:']
    count=0
    for j in np.arange(len(sortedresults)):
        for f in np.arange(len(sortedresults[j])):
            for o in np.arange(len(observables)):
                title = Title + " : " + author
                plt.title(title, fontsize=10, weight= 'bold')
                plt.rcParams["font.weight"] = "bold"
                plt.tick_params(axis= 'both', direction='out', length=4, width=2, labelsz=10)
                plt.rcParams["axes.labelweight"] = "bold"
                plt.rcParams["axes.linewidth"] = "3"
                fig=plt.figure()
                ax=plt.subplot(111)
                ax.set_xlabel('Temperature (K)')
                ax.set_ylabel(r'Sensitivity coefficient,  $\frac{\partial \ln S_u}{\partial \ln k}$ ')
                plt.title('Top '+str(top10)+' sensitivities for observable '+observables[o])
                for c in np.arange(len(filename)):
                    sens=[]
                    sens=pd.DataFrame(sortedresults[j][f][c][0].Index[1],columns=['rxn'])
                    for d in np.arange(len(temps)):
                        #print(j,f,c,d,o)
                        sens=pd.concat([sens,
pd.DataFrame(sortedresults[j][f][c][d].k_sens[0],columns=[temps[d]]*len(observables)).iloc[:,o], axis=1)
                        maxes=sens.loc[:, sens.columns != 'rxn'].max(axis=1)

```

```

maxes=maxes.nlargest(top10)
max_index=np.array(maxes.index)

for i in max_index:
    plt.plot(temps,sens.iloc[i][1:],linetypes[count],label=sens['rxn'][i]+'
'+os.path.splitext(filename[c])[0].split("\\")[-1])
    count=count+1
    box = ax.get_position()
    ax.legend(loc='center left', bbox_to_anchor=(1, 0.5),
             fancybox=False, shadow=False, ncol=1)

plt.savefig(FinalPath+'\\'+sensitivities_conditions+str(j)+'_resTime'+str(f)+'_'+observables[o]+' .png',dpi=800,bbox_inches='tight')
# ++++++

```

class model_data:

```

def
__init__(self,simtype,kinetic_sens=np.array(),physical_sens=np.array(),Solution=pd.DataFrame(),Index=[],pIndex=
[]):
    self.k_sens=kinetic_sens
    self.p_sens=physical_sens
    self.solution=Solution
    self.Index=Index
    self.pIndex=pIndex
    self.sensitivities = self.all_sensitivities()
    self.overall_index = self.sens_index()
    self.simtype=simtype

```

Primarily for use with JSR data, the addition operator is overloaded to combine two datasets/simulations into one array.

Only use this for addition of data along first axis of sensitivities

```

def __add__(self, data):
    if self.simtype==data.simtype and (self.solution.columns==data.solution.columns).all()==True:
        #If statement above checks to ensure that the two datasets come from the same type of experiment.
        if self.k_sens.any()==True and data.k_sens.any()==True:
            temp=self.k_sens.T
            temp2=data.k_sens.T
            temp=np.dstack((temp,temp2))
            self.k_sens=temp.T

        if self.p_sens.any()==True and data.p_sens.any()==True:
            temp=self.p_sens.T
            temp2=data.p_sens.T
            temp=np.dstack((temp,temp2))
            self.p_sens=temp.T

        if self.sensitivities.any()==True and data.sensitivities.any()==True:
            temp=self.sensitivities.T
            temp2=data.sensitivities.T
            temp=np.dstack((temp,temp2))
            self.sensitivities=temp.T

        if self.k_sens.any()==True and data.k_sens.any()==True:

```

```

    self.Index[0]=self.Index[0]+data.Index[0]
if self.p_sens.any()==True and data.p_sens.any()==True:
    self.pIndex[0]=self.pIndex[0]+data.pIndex[0]
if self.sensitivities.any()==True and data.sensitivities.any()==True:
    self.overall_index=self.sens_index()

temp=self.solution
temp2=data.solution
temp = temp.append(temp2,ignore_index=True)

self.solution=temp

return self

else:
    raise Exception('Simulation types must be equal in order to add model data objects together. Simulation must
also use same mechanism.')

#The following functions take slices of sensitivity arrays eliminating one axis to create a 2d array according to
observable,position,
# or reaction. There is a version for kinetic, physical, and all sensitivities. Current version for position sensitivities
checks
# if there is a sensitivity at that location, and if not it will interpolate. This portion may be re-written later. Validity
of
#interpolated sensitivities may be questionable
def species_slice_ksens(self,species_name):
    if self.k_sens.any()==True:
        position = self.Index[2].index(species_name)
        return self.k_sens[:,:,position]
    else:
        print('No kinetic sensitivities provided by simulation')
def reaction_slice_ksens(self,reaction):
    if self.k_sens.any()==True:
        position = self.Index[1].index(reaction)
        return self.k_sens[:,position,:]
    else:
        print('No kinetic sensitivities provided by simulation')
def x_slice_ksens(self,location):
    if self.k_sens.any()==True:
        for j in np.arange(len(self.Index[0])):
            if self.Index[0][j]==location:
                return self.k_sens[j,::]
            elif j<(len(self.Index[0])-1):
                if self.Index[0][j]<location and self.Index[0][j+1]>location:
                    result = (self.k_sens[j+1,::]-self.k_sens[j,::])*np.divide((location-self.Index[0][j]),(self.Index[0][j+1]-
self.Index[0][j]))+self.k_sens[j,::]
                    print('Returning an interpolated result')
                    return result
            else:
                print('Invalid grid location: check position and submit a location in range of flame solution')
    else:
        print('No kinetic sensitivities provided by simulation')
def species_slice_psens(self,species_name):

```

```

if self.p_sens.any()==True:
    position = self.pIndex[2].index(species_name)
    return self.p_sens[:,:,position]
else:
    print('No physical sensitivities provided by simulation')
def parameter_slice_psens(self,parameter):
    if self.p_sens.any()==True:
        position = self.pIndex[1].index(parameter)
        return self.p_sens[:,position,:]
    else:
        print('No physical sensitivities provided by simulation')
def x_slice_psens(self,location):
    if self.p_sens.any()==True:
        for j in np.arange(len(self.pIndex[0])):
            if self.pIndex[0][j]==location:
                return self.p_sens[j,::]
            elif j<(len(self.pIndex[0])-1):
                if self.pIndex[0][j]<location and self.pIndex[0][j+1]>location:
                    result = (self.p_sens[j+1,::]-self.p_sens[j,::])*np.divide((location-
self.pIndex[0][j]),(self.pIndex[0][j+1]-self.pIndex[0][j]))+self.p_sens[j,::]
                    print('Returning an interpolated result')
                return result
            else:
                print('Invalid grid location: check position and submit a location in range of flame solution')
    else:
        print('No physical sensitivities provided by simulation')

def species_slice_sens(self,species_name):
    if self.sensitivities.any()==True:
        position = self.overall_index[2].index(species_name)
        return self.sensitivities[:,:,position]
    else:
        print('No sensitivities provided by simulation')
def parameter_slice_sens(self,parameter):
    if self.sensitivities.any()==True:
        position = self.overall_index[1].index(parameter)
        return self.sensitivities[:,position,:]
    else:
        print('No sensitivities provided by simulation')
def x_slice_sens(self,location):
    if self.sensitivities.any()==True:
        for j in np.arange(len(self.overall_index[0])):
            if self.overall_index[0][j]==location:
                return self.sensitivities[j,::]
            elif j<(len(self.overall_index[0])-1):
                if self.overall_index[0][j]<location and self.overall_index[0][j+1]>location:
                    result = (self.sensitivities[j+1,::]-self.sensitivities[j,::])*np.divide((location-
self.overall_index[0][j]),(self.overall_index[0][j+1]-self.overall_index[0][j]))+self.sensitivities[j,::]
                    print('Returning an interpolated result')
                return result
            else:
                print('Invalid grid location: check position and submit a location in range of flame solution')
    else:
        print('No sensitivities provided by simulation')

```



```

def species_slice_MFExp(self,species_name):
    if self.expMolFracData.any() == True:
        if (int(np.shape(self.expMolFracData)[0])) > 1:
            position = self.MFExpIndex[1].index(species_name)
            return self.expMolFracData[:,position]
        else:
            if species_name in self.MFExpIndex[1]:
                return self.expMolFracData
            else:
                print('Species is not in the index')
    else:
        print('No Mole Fraction Data Provided')

def species_slice_MF_differences(self,species_name):
    if self.st_mf_differences.any() == True:
        if (int(np.shape(self.st_mf_differences)[0])) > 1:
            position = self.MFExpIndex[1].index(species_name)
            return self.st_mf_differences[:,position]
        else:
            if species_name in self.MFExpIndex[1]:
                return self.st_mf_differences
            else:
                print('That species is not in the index')
    else:
        print('No Mole Fraction Data Provided')

def wavelength_slice_AExp(self,wavelength):
    if self.expAbsorbanceData.any() == True:
        if (int(np.shape(self.expAbsorbanceData)[0])) > 1:
            position = self.AExpIndex[1].index(wavelength)
            return self.expAbsorbanceData[:,position]
        else:
            if wavelength in self.AExpIndex[1]:
                return self.expAbsorbanceData
            else:
                print('That wavelength is not in the index')
    else:
        print('No Absorption Data Provided')

def wavelength_slice_A_differences(self,wavelength):
    if self.st_abs_differences.any() == True :
        if (int(np.shape(self.st_abs_differences)[0])) > 1:
            position = self.AExpIndex[1].index(wavelength)
            return self.expAbsorbanceData[:,position]
        else:
            if wavelength in self.AExpIndex[1]:
                return self.expAbsorbanceData
            else:
                print('That wavelength is not in the index')
    else:
        print('No Absorption Data Provided')

def Absorb_sens_slice(self,wavelength):

```

```

if bool(self. absorbance_sens) == True:
    return self. absorbance_sens[wavelength]
else:
    print('No Absorption Data Provided')
def Absorb_sens_A_slice(self,wavelength):
    if bool(self. absorb_a_sens) == True:
        return self. absorb_a_sens[wavelength]

def Absorb_sens_n_slice(self,wavelength):
    if bool(self. absorb_n_sens) == True:
        return self. absorb_n_sens[wavelength]

def Absorb_sens_Ea_slice(self,wavelength):
    if bool(self. absorb_Ea_sens) == True:
        return self. absorb_Ea_sens[wavelength]

def reaction_slice_Absorb_sens(self,reaction,wavelength):
    if bool(self. absorbance_sens) == True:
        position = self.Index[1].index(reaction)
        return self. absorbance_sens[wavelength][:,position]
    else:
        print('No AbsorptionData Provided')

def species_slice_CExp(self,species_name):
    if self.expConcentrationData.any() == True:
        if (int(np.shape(self.expConcentrationData)[0])) > 1:
            position = self.CExpInex[1].index(species_name)
            return self.expConcentrationData[:,position]
        else:
            if species_name in self.CExpInex[1]:
                return self.expConcentrationData
            else:
                print('That species is not in the index')
    else:
        print('No Concentration Data Provided')

def species_slice_C_differences(self,species_name):
    if self.st_conc_differences.any() == True:
        if (int(np.shape(self.st_conc_differences)[0])) > 1:
            position = self.CExpInex[1].index(species_name)
            return self.st_conc_differences[:,position]
        else:
            if species_name in self.CExpInex[1]:
                return self.st_conc_differences
            else:
                print('That species is not in the index')
    else:
        print('No Concentration Data Provided')
def species_slice_ksens_mappedA(self,species_name):
    if self.a_sens.any() == True:
        position = self.Index[2].index(species_name)
        return self.a_sens[:, :, position]
    else:
        print('No kinetic sensitivities provided by simulation')

```

```

def reaction_slice_ksens_mappedA(self, reaction):
    if self.a_sens.any() == True:
        position = self.Index[1].index(reaction)
        return self.a_sens[:, position, :]
    else:
        print('No kinetic sensitivities provided by simulation')
def species_slice_ksens_mappedn(self, species_name):
    if self.n_sens.any() == True:
        position = self.Index[2].index(species_name)
        return self.n_sens[:, :, position]
    else:
        print('No kinetic sensitivities provided by simulation')

def reaction_slice_ksens_mappedn(self, reaction):
    if self.n_sens.any() == True:
        position = self.Index[1].index(reaction)
        return self.n_sens[:, position, :]
    else:
        print('No kinetic sensitivities provided by simulation')
def species_slice_ksens_mappedEa(self, species_name):
    if self.e_sens.any() == True:
        position = self.Index[2].index(species_name)
        return self.e_sens[:, :, position]
    else:
        print('No kinetic sensitivities provided by simulation')

def reaction_slice_ksens_mappedEa(self, reaction):
    if self.a_sens.any() == True:
        position = self.Index[1].index(reaction)
        return self.a_sens[:, position, :]
    else:
        print('No kinetic sensitivities provided by simulation')

```

#The following function exists to return an array of the profile of a sensitivity in one parameter with respect to an observable as

```

#as a function of the independent variable (location, time, temperature)
def sensitivity_profile(self, observable, parameter):
    position = self.overall_index[2].index(observable)
    position_param = self.overall_index[1].index(parameter)
    sens = self.sensitivities[:, position_param, position]
    independentVar = np.asarray(self.overall_index[0])
    sens = np.flatten(sens)
    return np.vstack((independentVar, sens))

```

#all_sensitivities returns an array which is a concatenation of physical and kinetic sensitivities available in the model

```

def all_sensitivities(self):
    if self.p_sens.any() == False and self.k_sens.any() != False:
        return self.k_sens
    if self.p_sens.any() != False and self.k_sens.any() == False:
        return self.p_sens
    if self.p_sens.any() != False and self.k_sens.any() != False:
        return np.hstack((self.p_sens, self.k_sens))
    else:
        return np.array(())

```

```

def reaction_slice_Asens(self, reaction):
    if self.a_sens.any() == True:
        position = self.Index[1].index(reaction)
        return self.a_sens[:, position, :]
    else:
        print('No A sensitivities provided by simulation')

def reaction_slice_nsens(self, reaction):
    if self.n_sens.any() == True:
        position = self.Index[1].index(reaction)
        return self.n_sens[:, position, :]
    else:
        print('No n sensitivities provided by simulation')
def reaction_slice_Esens(self, reaction):
    if self.e_sens.any() == True:
        position = self.Index[1].index(reaction)
        return self.e_sens[:, position, :]
    else:
        print('No Ea sensitivities provided by simulation')
#sens_index returns the concatenation of the indices for the kinetic and physical sensitivities in the model. physical
#parameters are placed on same axis as reaction rate constants, but before the first reaction constant (eg.
T, P, k1, k2, ...)
def sens_index(self):
    if self.p_sens.any() == False and self.k_sens.any() != False:
        return self.Index
    if self.p_sens.any() != False and self.k_sens.any() == False:
        return self.pIndex
    if self.p_sens.any() != False and self.k_sens.any() != False:
        return [self.Index[0], self.pIndex[1] + self.Index[1], self.Index[2]]
    else:
        return self.Index
def assign_flamespeed_sens(self, fsens, equations):
    self.flamespeed_sens = pd.DataFrame(data=[], index=equations)
    self.flamespeed_sens['Su'] = fsens
def plot_flamespeed_sens(self, phi, model):
    threshold = 0.02

    self.firstColumn = self.flamespeed_sens.columns[0]

    # For plotting, collect only those steps that are above the threshold
    # Otherwise, the y-axis gets crowded and illegible
    self.sensitivitiesSubset = self.flamespeed_sens[self.flamespeed_sens[self.firstColumn].abs() > threshold]
    #print(sensitivitiesSubset)
    self.indicesMeetingThreshold =
self.sensitivitiesSubset[self.firstColumn].abs().sort_values(ascending=False).index
    self.sensitivitiesSubset.loc[self.indicesMeetingThreshold].plot.barh(title="Sensitivities for "+model+" at
phi="+str(phi),
                                legend=None)
    plt.gca().invert_yaxis()

    plt.rcParams.update({'axes.labelsize': 20})
    plt.xlabel(r'Sensitivity: $\frac{\partial \ln \{ S_{u} \}}{\partial \ln \{ k \}}$');

```

```

# Uncomment the following to save the plot. A higher than usual resolution (dpi) helps
plt.savefig('sensitivityPlot', dpi=600)
def add_mechanism(self,mech):
    self.mechanism=mech
def add_yaml(self,yaml):
    self.yaml_input=yaml
def assign_phi(self,phi):
    self.phi=phi
def add_fuel(self,fuel):
    self.fuel=fuel
def add_exp_shocktube_MolFrac(self,molFracData= np.array()),differences= np.array(), index=[]):
    self.expMolFracData=molFracData
    self.st_mf_differences=differences
    self.MFExpIndex= index
def add_exp_shocktube_absorbance(self,absorbanceData = np.array()),differences = np.array(),absorbanceProfiles
= {},absorbanceSens = {}, index = [],absorbancePSens =[]):
    self.expAbsorbanceData=absorbanceData
    self.st_abs_differences=differences
    self.absorbance_profiles=absorbanceProfiles
    self.absorbance_sens = absorbanceSens
    self.AExpIndex = index
    self.absorbance_p_sens = absorbancePSens
def add_exp_shocktube_concentrations(self,concData = np.array()),differences = np.array(),index = []):
    self.expConcentrationData=concData
    self.st_conc_differences=differences
    self.CExpIndex = index
def add_S_Matrix(self, SMatrix = np.array()):
    self.S_matrix = SMatrix
def add_Y_Matrix(self, YMatrix = np.array()):
    self.Y_matrix = YMatrix
def assign_ksens_mappings(self, asens = np.array(),nsens= np.array(),easens= np.array()):
    self.a_sens=asens
    self.n_sens=nsens
    self.e_sens=easens
def absorbance_sens_mappings(self,asens = {}, nsens = {}, easens = {}):
    self.absorb_a_sens = asens
    self.absorb_n_sens = nsens
    self.absorb_Ea_sens = easens
def add_parameter_arrays(self,molecularParameterArray = [],molecularParameterArrayCombinedReaction = [],
fullArray = np.array()):
    self.molecular_parameter_sens = molecularParameterArray
    self.molecular_parameter_sens_combined_reaction = molecularParameterArrayCombinedReaction
    self.full_array_parameter_sens = fullArray
def write_model_to_file(self,filename):
    items=self.__dict__.keys()
    #print(dir(self))
    with open(filename,'w') as f:
        for j in items:
            f.write(j+'\n')
            if j=='simtype':
                f.write(getattr(self,j)+'\n')
            elif j=='Index' and self.Index!=[]:
                for k in np.arange(len(self.Index)):
                    if k==0:
                        f.write(' z_T_t\n')

```

```

    elif k==1:
        f.write(' reactions\n')
    elif k==2:
        f.write(' observables\n')
    for val in self.Index[k]:
        f.write(str(val)+'\n')
elif j=='overall_index' and self.overall_index!=[]:
    for k in np.arange(len(self.overall_index)):
        if k==0:
            f.write(' z_T_t\n')
        elif k==1:
            f.write(' reactions and physical_params\n')
        elif k==2:
            f.write(' observables\n')
        for val in self.Index[k]:
            f.write(str(val)+'\n')
elif j=='final_pressure':
    f.write(str(getattr(self,j)+'\n')
elif j=='pIndex' and self.pIndex!=[]:
    for k in np.arange(len(self.pIndex)):
        if k==0:
            f.write(' z_T_t\n')
        elif k==1:
            f.write(' physical_params\n')
        elif k==2:
            f.write(' observables\n')
        for val in self.Index[k]:
            f.write(str(val)+'\n')
elif j=='mechanism':
    f.write(self.mechanism+'\n')
elif j=='yaml_input':
    f.write(self.yaml_input+'\n')
elif j=='phi':
    f.write(str(self.phi)+'\n')
elif j=='fuel':
    f.write(self.fuel+'\n')
elif j=='solver_time':
    f.write(str(self.solver_time)+'\n')
    #f.writelines(getattr(self,j)+'\n')
def add_interpolated_temps_for_physical_sens(self,listOfTemperatureArrays = []):
    self.temps_for_physical_sens = listOfTemperatureArrays
def add_interpolated_pressure_for_physical_sens(self,listOfPressureArrays = []):
    self.pressure_for_physical_sens = listOfPressureArrays
def add_interpolated_concentration_for_physical_sens(self,listOfConcentrationDataFrames = []):
    self.concentration_for_physical_sens = listOfConcentrationDataFrames
def add_psens_array(self,fullArray = np.array()):
    self.full_pSens_array = fullArray
def
add_target_values(self,initialTemperature,initialPressure,initialMoleFractions,initialKvalues=[],initialMolecularProperti
es=[]):
    self.initial_temp = initialTemperature
    self.initial_pressure = initialPressure
    self.initial_MF = initialMoleFractions
    self.target_rate_constants = initialKvalues
    self.target_molecular_props = initialMolecularProperties

```

```

def add_final_pressure(self,pressure):
    self.final_pressure=pressure
def add_solver_time(self,solvertime):
    self.solver_time=solvertime
def add_residence_time(self,res):
    self.residence_time=res
def add_temperature_sensitivity(self,sens):
    self.temp_sens=np.array(sens)
def add_forward_rates(self,rates):
    self.forward_rates=rates
def add_reverse_rates(self,rates):
    self.reverse_rates=rates
def add_net_rates_of_progress(self,rates):
    self.net_rates_of_progress=rates
def tags(self,tags):
    self.tags=tags
#This function is for pre-mixed burner flame
# *****

def InputFileReaderJSR(FileNamePath,OutputPath):
    FILENAME = FileNamePath.split("\\")
    INPUTFILENAME = FILENAME[-1];
    FileJSR= pd.read_csv(FileNamePath, names=['col'],sep='%s',engine='python');
    FolderName = FILENAME[3:-1];
    InputFileNames = (INPUTFILENAME.split(".JSR_EXP"))[0];
    FolderDir = "\\".join(FolderName) + "\\" + InputFileNames
    if not os.path.isdir(OutputPath + FolderDir):
        os.makedirs(OutputPath + FolderDir)
    FinalPath = str(OutputPath + FolderDir)
    # ++++++
    # FILTERING DATA BY SPECIFIC NAMES, FROM HERE WE WILL GET THE FUEL,OXIDIZERS,
    # CONCENTRATIONS, INITIAL TEMPERATURES AND INITIAL PRESSURES, ETC... MAKING
    # DICTIONARIES TO STORAGE THE DATA READ IT.
    # ++++++
    NamesDict = {}
    ReactorsDict = {}
    UnitsDict = {}
    print("\t>',FileNamePath)
    try:
        REACS = (FileJSR[FileJSR.col.str.contains("REAC:"))].col.str.split(':')
    except:
        FileJSR = pd.read_fwf(FileNamePath,names=['col']);
        REACS = (FileJSR[FileJSR.col.str.contains("REAC:"))].col.str.split(':')
    REACTANTS = []
    for i in range(len(REACS)):
        REAC1 = REACS.iloc[i][1]
        REAC1 = ":".join(REAC1.split())
        REACTANTS.append(REAC1)
    REACTANTS = str(",".join(REACTANTS))
    AUTHOR = ((FileJSR[FileJSR.col.str.contains("AUTHOR:")]
        ).iloc[0].str.split(':')[0])[1]
    JOURNAL = str(FileJSR.iloc[1,:])#((FileJSR[FileJSR.col.str.contains("JOURNAL:")]
    #         ).iloc[0].str.split(':')[0])[1]
    PDF = ((FileJSR[FileJSR.col.str.contains("PDF:")]

```

```

        ).iloc[0].str.split(':')[0][1]
REACTOR = ((FileJSR[FileJSR.col.str.contains("REACTOR:")]
        ).iloc[0].str.split(':')[0][1]
DATA = ((FileJSR[FileJSR.col.str.contains("DATA:")]
        ).iloc[0].str.split(':')[0][1]
PRESSURE = ((FileJSR[FileJSR.col.str.contains("PRESSURE:")]
        ).iloc[0].str.split(':')[0][1]
PRESSURE = str(PRESSURE)
PHI = ((FileJSR[FileJSR.col.str.contains("PHI:")]
        ).iloc[0].str.split(':')[0][1]
E_EQUATION = ((FileJSR[FileJSR.col.str.contains("ENERGY_EQUATION:")]
        ).iloc[0].str.split(':')[0][1]
try:
    T_INITIAL = ((FileJSR[FileJSR.col.str.contains("T_INITIAL:")]
        ).iloc[0].str.split(':')[0][1]
    P_INITIAL = ((FileJSR[FileJSR.col.str.contains("P_INITIAL:")]
        ).iloc[0].str.split(':')[0][1]
    ReactorsDict["T_INITIAL"] = T_INITIAL
    ReactorsDict["P_INITIAL"] = P_INITIAL
except:
    ReactorsDict["T_INITIAL"] = 0
    ReactorsDict["P_INITIAL"] = 0
TEMPERATURE = ((FileJSR[FileJSR.col.str.contains(
    "TEMPERATURE:"))].iloc[0].str.split(':')[0][1]
TIME = ((FileJSR[FileJSR.col.str.contains("TIME:")]
        ).iloc[0].str.split(':')[0][1]
DSpeciesJSR = FileJSR[FileJSR.col.str.contains("!") == False]
DSJSR = DSpeciesJSR[DSpeciesJSR.col.str.contains("TAU") == True]
DataEspeciesJSR = pd.DataFrame((DSJSR.col.str.split()).tolist())
DroppingStuff = FileJSR[FileJSR.col.str.contains("!") == False]
DroppingStuff2 = DroppingStuff[DroppingStuff.col.str.contains("TAU") == False]
dataJSR = pd.DataFrame((DroppingStuff2.col.str.split()).tolist())
NamesDict["AUTHOR"] = AUTHOR
NamesDict["JOURNAL"] = JOURNAL
NamesDict["PDF"] = PDF
NamesDict["InpFileName"] = INPUTFILENAME
NamesDict["FolderDir"] = FolderDir
ReactorsDict["REACTOR"] = REACTOR
ReactorsDict["DATA"] = DATA
ReactorsDict["REACTANTS"] = REACTANTS
ReactorsDict["PHI"] = PHI
ReactorsDict["ENERGY_EQUATION"] = E_EQUATION
UnitsDict["PRESSURE"] = PRESSURE
UnitsDict["TEMPERATURE"] = TEMPERATURE
UnitsDict["TIME"] = TIME
return (NamesDict, ReactorsDict, UnitsDict,DataEspeciesJSR,dataJSR,FinalPath)
# ++++++
#This function is for pre-mixed burner flame
def
burner_flame(gas,grid,mdot,data=pd.DataFrame(columns=['z','T']),kinetic_sens=0,physical_sens=0,observables=[],phy
sical_params=['T','P'],energycon=False,soret=True):
    #when energycon is off treat flame as burner stabilized, with known T-profile
    simtype = 'burner flame'
    baseConditions=gas.TPX

```



```

tol_ss = [1.0e-5, 1.0e-13] # [rtol atol] for steady-state problem
tol_ts = [1.0e-4, 1.0e-10] # [rtol atol] for time stepping
loglevel = 1 # amount of diagnostic output (0 to 5)

f = ct.BurnerFlame(gas, width=grid)
f.burner.mdot = mdot

f.set_initial_guess()
# read temperature vs. position data from a file.
# The file is assumed to have one z, T pair per line, separated by a comma.
if data.empty==False and energycon==False:
    zloc=data['z']
    tvalues=data['T']
    zloc /= max(zloc)

    #print(tvalues)

    f.flame.set_fixed_temp_profile(zloc, tvalues) #sets a fixed temperature profile for the flame simulation. May
    come from a measurement. Requires no energy conservation
    elif data.empty==False and energycon!='off':
        raise Exception('User has supplied fixed temperature dataset but energy conservation is not off. Remove dataset
        or turn energy conservation off')

f.flame.set_steady_tolerances(default=tol_ss) #Set steady tolerances
f.flame.set_transient_tolerances(default=tol_ts) #Set transient tolerances
f.show_solution()

f.energy_enabled = energycon #This must be set to false for a burner stabilized flame with known T-profile

f.transport_model = 'Multi' #Sets to multicomponent transport for simulation. Needs to be set this way to use Soret
effect
f.set_max_jac_age(10, 10) #Age limits on Jacobian-leave as is for best results
f.solve(loglevel, refine_grid=False) #Solve for initial estimate without grid refinement

f.soret_enabled = soret #Enable Soret effect. Remember transport must be set to multi. Mix causes failure

f.set_refine_criteria(ratio=2.0, slope=0.05, curve=0.5) #Establishes refinement criteria for grid

#print('mixture-averaged flamespeed = ', f.u[0])

f.transport_model = 'Multi' #This block solves problem again with grid refinement on
f.solve(loglevel, refine_grid=True)
f.show_solution()
print('multicomponent flamespeed = ', f.u[0])

#solution = f
##Begin section to calculate sensitivities
dk = 0.010
solution = f.X
if kinetic_sens==1 and bool(observables):

```

```

#Calculate kinetic sensitivities
sensIndex = [f.grid.tolist(),gas.reaction_equations(),observables]

S = np.zeros((len(f.grid),gas.n_reactions,len(observables)))
#print(solution.X[solution.flame.component_index(observables[0])-4,len(f.grid)-1])
#a=solution.X[solution.flame.component_index(observables[0])-4,len(f.grid)-1]
for m in range(gas.n_reactions):
    gas.set_multiplier(1.0)
    gas.set_multiplier(1+dk,m)
    f.solve(loglevel=1,refine_grid=False)
    for i in np.arange(len(observables)):
        for k in np.arange(len(f.grid)):
            S[k,m,i]=f.X[f.flame.component_index(observables[i])-4,k]-
solution[f.flame.component_index(observables[i])-4,k]
            #print(solution.X[solution.flame.component_index(observables[i])-4,k])
            #print(f.X[f.flame.component_index(observables[i])-4,k])
            S[k,m,i]=np.divide(S[k,m,i],solution[f.flame.component_index(observables[i])-4,k])
            S[k,m,i]=np.divide(S[k,m,i],dk)

if physical_sens==1 and bool(observables):
    #Calculate physical sensitivities
    gas.set_multiplier(1.0)

    psensIndex = [f.grid.tolist(),physical_params,observables]
    pS = np.zeros((len(f.grid),len(physical_params),len(observables)))
    for m in range(len(physical_params)):
        gas.TPX=baseConditions
        if physical_params[m]=='T':
            gas.TPX=baseConditions[0]+dk,baseConditions[1],baseConditions[2]
        elif physical_params[m]=='P':
            gas.TPX=baseConditions[0],baseConditions[1]+dk,baseConditions[2]
        f.solve(loglevel=1,refine_grid=False)
        for i in np.arange(len(observables)):
            for k in np.arange(len(f.grid)):
                pS[k,m,i] =np.log10(solution[f.flame.component_index(observables[i])-4,k])-
np.log10(f.X[f.flame.component_index(observables[i])-4,k])
                pS[k,m,i] = np.divide(pS[k,m,i],np.log10(dk))

    elif kinetic_sens==1 and bool(observables)==False:
        raise Exception('Please supply a list of observables in order to run kinetic sensitivity analysis')
    elif physical_sens==1 and bool(observables)==False:
        raise Exception('Please supply a list of observables in order to run physical sensitivity analysis')
    gas.set_multiplier(1.0)
    gas.TP = baseConditions[0],baseConditions[1]
    f.solve(loglevel=1,refine_grid=False)
    solution=pd.DataFrame(columns=f.flame.component_names)
    #for i in f.flame.component_names:
        #solution[i]=f.solution(i)
    for i in np.arange(len(f.flame.component_names)):

```

```

    if i<=3:
        solution[f.flame.component_names[i]]=f.solution(i)
    else:
        solution[f.flame.component_names[i]]=f.X[i-4,:]

if kinetic_sens==1 and bool(observables) and physical_sens!=1:
    results = model_data(simtype,kinetic_sens=S,Solution=solution,Index=sensIndex)
    return results
elif physical_sens==1 and bool(observables) and kinetic_sens!=1:
    results = model_data(simtype,Solution=solution,pIndex=psensIndex,physical_sens=pS)
    return results
elif kinetic_sens==1 and physical_sens==1 and bool(observables):
    results =
model_data(simtype,Solution=solution,pIndex=psensIndex,Index=sensIndex,physical_sens=pS,kinetic_sens=S)
    return results
elif kinetic_sens!=1 and physical_sens!=1:
    Index = [f.grid.tolist()]
    results = model_data(simtype,Solution=solution,Index=Index)
    return results
else:
    print('Something went wrong with the parameters given. Kinetic and physical sens may be set to either 0 or 1,
and require a list of observables')

def
JSR_steadystate(gas,resTime,volume,kinetic_sens=0,physical_sens=0,observables=[],physical_params=['T','P'],energycon=
'off',pressureValveCoefficient=0.01,maxsimulationTime=1000):
    # Inlet gas conditions are passed into function in the "gas" object, which is a cantera object
    # Reactor parameters passed into function as resTime and volume. Residence time and volume of JSR
    #kinetic sens and physical sens are optional parameters which are set to zero by default. Set them to 1 to
    #calculate sensitivity based on kinetic or physical parameters. If these are set to 1 you must pass
    #an array of all observables to calculate sensitivities for

    simtype='jsr'
    reactorPressure=gas.P
    # This is the "conductance" of the pressure valve and will determine its efficiency in
    # holding the reactor pressure to the desired conditions. It is an optional parameter
    pressureValveCoefficient=pressureValveCoefficient

    # This parameter will allow you to decide if the valve's conductance is acceptable. If there
    # is a pressure rise in the reactor beyond this tolerance, you will get a warning
    maxPressureRiseAllowed = 0.001

    # Simulation termination criterion
    #maxSimulationTime = maxsimulationTime # seconds. An optional parameter
    fuelAirMixtureTank = ct.Reservoir(gas)
    exhaust = ct.Reservoir(gas)

    stirredReactor = ct.IdealGasReactor(gas, energy=energycon, volume=volume)

    massFlowController =
ct.MassFlowController(upstream=fuelAirMixtureTank,downstream=stirredReactor,midot=stirredReactor.mass/resTime)

    pressureRegulator = ct.Valve(upstream=stirredReactor,downstream=exhaust,K=pressureValveCoefficient)

```

```

reactorNetwork = ct.ReactorNet([stirredReactor])

#This block adds kinetic sensitivity parameters for all reactions if desired.
if kinetic_sens==1 and bool(observables):
    for i in range(gas.n_reactions):
        stirredReactor.add_sensitivity_reaction(i)

if kinetic_sens==1 and bool(observables)==False:
    print('Please supply a non-empty list of observables for sensitivity analysis or set kinetic_sens=0')

#if physical_sens==1 and bool(observables):
#    print('Placeholder')
if physical_sens==1 and bool(observables)==False:
    print('Please supply a non-empty list of observables for sensitivity analysis or set physical_sens=0')

# now compile a list of all variables for which we will store data
columnNames = [stirredReactor.component_name(item) for item in range(stirredReactor.n_vars)]
columnNames = ['pressure'] + columnNames

# use the above list to create a DataFrame
timeHistory = pd.DataFrame(columns=columnNames)

# Start the stopwatch
tic = time.time()

#Names=[]
#for l in np.arange(stirredReactor.n_vars):
#    #Names.append(stirredReactor.component_name(l))
#global b

#Names = [stirredReactor.component_name(item) for item in range(stirredReactor.n_vars)]
#state = np.hstack([stirredReactor.mass,
#                   stirredReactor.volume, stirredReactor.T, stirredReactor.thermo.X])
#print(state)
#b=pd.DataFrame(data=state).transpose()
#b.columns=Names

#Establish a matrix to hold sensitivities for kinetic parameters, along with tolerances
if kinetic_sens==1 and bool(observables):
    #senscolumnNames = ['Reaction']+observables
    senscolumnNames = observables
    #sensArray = pd.DataFrame(columns=senscolumnNames)
    sensArray = np.zeros((gas.n_reactions,len(observables)))
    reactorNetwork.rtol_sensitivity = 1.0e-6
    reactorNetwork.atol_sensitivity = 1.0e-6

dk=0.01

if physical_sens==1 and bool(observables):
    #psenscolumnNames = ['Parameter'] + observables
    #psensArray = pd.DataFrame(columns=senscolumnNames)
    pIndex=[[gas.T],physical_params,observables]
    psensArray = np.zeros((len(observables),len(physical_params)))

```

```

tempSol=[]
conditions=gas.TPX
for i in np.arange(len(physical_params)):
    if physical_params[i]=='T':
        gas.TPX=conditions[0]+dk,conditions[1],conditions[2]
    if physical_params[i]=='P':
        gas.TPX=conditions[0],conditions[1]+dk,conditions[2]

tempMixTank=ct.Reservoir(gas)
tempExhaust = ct.Reservoir(gas)
tempReactor=ct.IdealGasReactor(gas,energy=energycon,volume=volume)

tempMassFlowCt=ct.MassFlowController(upstream=tempMixTank,downstream=tempReactor,mdot=tempReactor.mass/resTime)
tempPresReg=ct.Valve(upstream=tempReactor,downstream=tempExhaust,K=pressureValveCoefficient)
tempNetwork=ct.ReactorNet([tempReactor])
tempNetwork.advance_to_steady_state()
tempSol.append(tempReactor.get_state())
gas.TPX=conditions

reactorNetwork.advance_to_steady_state()
final_pressure=stirredReactor.thermo.P
global b
b=reactorNetwork.sensitivities()
if kinetic_sens==1 and bool(observables):
    for k in np.arange(len(observables)):
        for j in np.arange(gas.n_reactions):
            try:
                sensTempArray[j,k]=reactorNetwork.sensitivity(observables[k],j)
            except:
                sensTempArray[j,k]=-1

#sensArray['Reaction']=gas.reaction_equations()
#sensArray[observables]=sensTempArray.T
#temp = sensArray.as_matrix()
kIndex = [[gas.T],gas.reaction_equations(),senscolumnNames]

if physical_sens==1 and bool(observables):
    for k in np.arange(len(observables)):
        for j in np.arange(len(['T','P'])):
            psensTempArray[j,k]=np.log10(stirredReactor.get_state()[stirredReactor.component_index(observables[k])])-
np.log10(tempSol[j][stirredReactor.component_index(observables[k])])
            psensTempArray[j,k]=np.divide(psensTempArray[j,k],np.log10(dk))

#state = np.hstack([stirredReactor.thermo.P, stirredReactor.mass,
                    #stirredReactor.volume, stirredReactor.T, stirredReactor.thermo.X])

# Stop the stopwatch
toc = time.time()

print('Simulation Took {:.2f}s to compute'.format(toc-tic))
columnNames = []
#Store solution to a solution array

```

```

# for l in np.arange(stirredReactor.n_vars):
#     #columnNames.append(stirredReactor.component_name(l))
columnNames=[stirredReactor.component_name(item) for item in range(stirredReactor.n_vars)]
#state=stirredReactor.get_state()
state=np.hstack([stirredReactor.mass,
                 stirredReactor.volume, stirredReactor.T, stirredReactor.thermo.X])
data=pd.DataFrame(state).transpose()
data.columns=columnNames

# We now check to see if the pressure rise during the simulation, a.k.a the pressure valve
# was okay
pressureDifferential = timeHistory['pressure'].max()-timeHistory['pressure'].min()
if(abs(pressureDifferential/reactorPressure) > maxPressureRiseAllowed):
    print("WARNING: Non-trivial pressure rise in the reactor. Adjust K value in valve")

if kinetic_sens==1 and bool(observables) and physical_sens!=1:

modelData=model_data(simtype,kinetic_sens=np.expand_dims(senstempArray,axis=0),Solution=data,Index=kIndex)
    modelData.add_final_pressure(final_pressure)
    return modelData
if physical_sens==1 and bool(observables) and kinetic_sens!=1:

modelData=model_data(simtype,physical_sens=np.expand_dims(psenstempArray,axis=0),Solution=data,pIndex=pIndex)
x)
    modelData.add_final_pressure(final_pressure)
    return modelData
if physical_sens==1 and bool(observables) and kinetic_sens==1:

modelData=model_data(simtype,physical_sens=np.expand_dims(psenstempArray,axis=0),kinetic_sens=np.expand_dims(senstempArray,axis=0),Solution=data,Index=kIndex,pIndex=pIndex)
    modelData.add_final_pressure(final_pressure)
    return modelData
else:
    modelData=model_data(simtype,Solution=data)
    modelData.add_final_pressure(final_pressure)
    return modelData

def
multiTemp(cti,gas,Temps,f,kinetic_sens=0,physical_sens=0,observables=[],physical_params=['T','P'],energycon='off',pressureValveCoefficient=0.01,maxsimulationTime=1000):
    gas.TPX=Temps[0],f['pressure']*ct.one_atm,f['conditions']

model=JSR_steadystate(gas,f['residenceTime'],f['reactorVolume'],kinetic_sens=kinetic_sens,physical_sens=physical_sens,observables=observables,physical_params=physical_params,energycon=energycon,pressureValveCoefficient=pressureValveCoefficient)
    for i in np.arange(len(Temps)):
        if i!=0:
            try:

                gas.TPX = Temps[i],f['pressure']*ct.one_atm,f['conditions']

```

```

        solutionObject =
JSR_steadystate(gas,f['residenceTime'],f['reactorVolume'],kinetic_sens=kinetic_sens,physical_sens=physical_sens,obse
rvables=observables,physical_params=physical_params,energycon=energycon,presureValveCoefficient=presureValv
eCoefficient)

```

```

        model=solutionObject+model
    except:
        print('Simulation at '+str(Temps[i])+ ' K failed.')
    pass
    return model

```

def

```

JSR_steadystate2(gas,resTime,volume,kinetic_sens=0,physical_sens=0,observables=[],physical_params=['T','P'],energ
ycon='off',pressureValveCoefficient=0.01,maxsimulationTime=1000,initial_conditions_gas=0,tempsens=0):

```

```

    # Inlet gas conditions are passed into function in the "gas" object, which is a cantera object
    # Reactor parameters passed into function as resTime and volume. Residence time and volume of JSR
    #kinetic sens and physical sens are optional parameters which are set to zero by default. Set them to 1 to
    #calculate sensitivity based on kinetic or physical parameters. If these are set to 1 you must pass
    #an array of all observables to calculate sensitivities for

```

```

    simtype='jsr'
    reactorPressure=gas.P
    # This is the "conductance" of the pressure valve and will determine its efficiency in
    # holding the reactor pressure to the desired conditions. It is an optional parameter
    pressureValveCoefficient=pressureValveCoefficient

```

```

    # This parameter will allow you to decide if the valve's conductance is acceptable. If there
    # is a pressure rise in the reactor beyond this tolerance, you will get a warning
    maxPressureRiseAllowed = 0.001

```

```

    # Simulation termination criterion
    #maxSimulationTime = maxsimulationTime # seconds. An optional parameter
    fuelAirMixtureTank = ct.Reservoir(gas)
    exhaust = ct.Reservoir(gas)
    if initial_conditions_gas==0:
        stirredReactor = ct.IdealGasReactor(gas, energy=energycon, volume=volume)
        mdot=stirredReactor.mass/resTime
    else:
        stirredReactor = ct.IdealGasReactor(initial_conditions_gas,energy=energycon,volume=volume)
        dummyReactor = ct.IdealGasReactor(gas,energy=energycon,volume=volume)
        mdot=dummyReactor.mass/resTime

```

```

    massFlowController =
ct.MassFlowController(upstream=fuelAirMixtureTank,downstream=stirredReactor,mdot=mdot)

```

```

    pressureRegulator = ct.Valve(upstream=stirredReactor,downstream=exhaust,K=pressureValveCoefficient)

```

```

    reactorNetwork = ct.ReactorNet([stirredReactor])

```

```

    #This block adds kinetic sensitivity parameters for all reactions if desired.

```

```

    if kinetic_sens==1 and bool(observables):
        for i in range(gas.n_reactions):
            stirredReactor.add_sensitivity_reaction(i)

```

```

if kinetic_sens==1 and bool(observables)==False:
    print('Please supply a non-empty list of observables for sensitivity analysis or set kinetic_sens=0')

#if physical_sens==1 and bool(observables):
    #print('Placeholder')
if physical_sens==1 and bool(observables)==False:
    print('Please supply a non-empty list of observables for sensitivity analysis or set physical_sens=0')

# now compile a list of all variables for which we will store data
columnNames = [stirredReactor.component_name(item) for item in range(stirredReactor.n_vars)]
columnNames = ['pressure'] + columnNames

# use the above list to create a DataFrame
timeHistory = pd.DataFrame(columns=columnNames)

# Start the stopwatch
tic = time.time()

#print('Simulation Took {:.2f}s to compute'.format(toc-tic))

#Names=[]
#for l in np.arange(stirredReactor.n_vars):
    #Names.append(stirredReactor.component_name(l))
#global b

#Names = [stirredReactor.component_name(item) for item in range(stirredReactor.n_vars)]
#state = np.hstack([stirredReactor.mass,
    #stirredReactor.volume, stirredReactor.T, stirredReactor.thermo.X])
#print(state)
#b=pd.DataFrame(data=state).transpose()
#b.columns=Names

#Establish a matrix to hold sensitivities for kinetic parameters, along with tolerances
if kinetic_sens==1 and bool(observables):
    #senscolumnNames = ['Reaction']+observables
    senscolumnNames = observables
    #sensArray = pd.DataFrame(columns=senscolumnNames)
    senstempArray = np.zeros((gas.n_reactions,len(observables)))
    reactorNetwork.rtol_sensitivity = 1.0e-12
    reactorNetwork.atol_sensitivity = 1.0e-12

dk=0.01

if physical_sens==1 and bool(observables):

    #psenscolumnNames = ['Parameter'] + observables
    #psensArray = pd.DataFrame(columns=senscolumnNames)
    pIndex=[[gas.T],physical_params,observables]
    psenstempArray = np.zeros((len(observables),len(physical_params)))
    tempSol=[]
    conditions=gas.TPX
    for i in np.arange(len(physical_params)):
        if physical_params[i]=='T':

```



```

    gas.TPX=conditions[0]+dk,conditions[1],conditions[2]
if physical_params[i]=='P':
    gas.TPX=conditions[0],conditions[1]+dk,conditions[2]

tempMixTank=ct.Reservoir(gas)
tempExhaust = ct.Reservoir(gas)
tempReactor=ct.IdealGasReactor(gas,energy=energycon,volume=volume)

tempMassFlowCt=ct.MassFlowController(upstream=tempMixTank,downstream=tempReactor,mdot=tempReactor.mass/resTime)
tempPresReg=ct.Valve(upstream=tempReactor,downstream=tempExhaust,K=pressureValveCoefficient)
tempNetwork=ct.ReactorNet([tempReactor])
tempNetwork.advance_to_steady_state()
tempSol.append(tempReactor.get_state())
gas.TPX=conditions
#reactorNetwork.rtol=1e-9
#resid=reactorNetwork.advance_to_steady_state(return_residuals=True)
#print(resid)
t = 0
while t < maxsimulationTime:
    t = reactorNetwork.step()
toc = time.time()
print("t> Reactor Network rtol:\n\t> {0}".format(reactorNetwork.rtol))
final_pressure=stirredReactor.thermo.P
global b
b=reactorNetwork.sensitivities()
if kinetic_sens==1 and bool(observables):
    for k in np.arange(len(observables)):
        for j in np.arange(gas.n_reactions):
            try:
                sensTempArray[j,k]=reactorNetwork.sensitivity(observables[k],j)
            except:
                sensTempArray[j,k]=-1

#sensArray['Reaction']=gas.reaction_equations()
#sensArray[observables]=sensTempArray.T
#temp = sensArray.as_matrix()
kIndex = [[gas.T],gas.reaction_equations(),senscolumnNames]

if physical_sens==1 and bool(observables):
    for k in np.arange(len(observables)):
        for j in np.arange(len(['T','P'])):
            psenTempArray[j,k]=np.log10(stirredReactor.get_state()[stirredReactor.component_index(observables[k])]-
np.log10(tempSol[j][stirredReactor.component_index(observables[k])])
            psenTempArray[j,k]=np.divide(psenTempArray[j,k],np.log10(dk))

#state = np.hstack([stirredReactor.thermo.P, stirredReactor.mass,
                    #stirredReactor.volume, stirredReactor.T, stirredReactor.thermo.X])

# Stop the stopwatch
toc = time.time()
print("t> Simulation at T={ }K took {:3.2f}s to compute".format(gas.T, toc-tic))

```

```

columnNames = []
#Store solution to a solution array
#for l in np.arange(stirredReactor.n_vars):
    #columnNames.append(stirredReactor.component_name(l))
columnNames=[stirredReactor.component_name(item) for item in range(stirredReactor.n_vars)]
#state=stirredReactor.get_state()
state=np.hstack([stirredReactor.mass,
                stirredReactor.volume, stirredReactor.T, stirredReactor.thermo.X])
data=pd.DataFrame(state).transpose()
data.columns=columnNames

# We now check to see if the pressure rise during the simulation, a.k.a the pressure valve
# was okay
pressureDifferential = timeHistory['pressure'].max()-timeHistory['pressure'].min()
if(abs(pressureDifferential/reactorPressure) > maxPressureRiseAllowed):
    print("WARNING: Non-trivial pressure rise in the reactor. Adjust K value in valve")

if kinetic_sens==1 and bool(observables) and physical_sens!=1:

modelData=model_data(simtype,kinetic_sens=np.expand_dims(senstempArray,axis=0),Solution=data,Index=kIndex)
    modelData.add_final_pressure(final_pressure)
    modelData.add_solver_time(toc-tic)
    return modelData
if physical_sens==1 and bool(observables) and kinetic_sens!=1:

modelData=model_data(simtype,physical_sens=np.expand_dims(psenstempArray,axis=0),Solution=data,pIndex=pIndex)
x)
    modelData.add_final_pressure(final_pressure)
    modelData.add_solver_time(toc-tic)
    return modelData
if physical_sens==1 and bool(observables) and kinetic_sens==1:

modelData=model_data(simtype,physical_sens=np.expand_dims(psenstempArray,axis=0),kinetic_sens=np.expand_dims(senstempArray,axis=0),Solution=data,Index=kIndex,pIndex=pIndex)
    modelData.add_final_pressure(final_pressure)
    modelData.add_solver_time(toc-tic)
    return modelData
else:
    modelData=model_data(simtype,Solution=data)
    modelData.add_final_pressure(final_pressure)
    modelData.add_solver_time(toc-tic)
    return modelData

def
multiTemp2(cti,gas,Temps,f,kinetic_sens=0,physical_sens=0,observables=[],physical_params=['T','P'],energycon='off',
pressureValveCoefficient=0.01,maxsimulationTime=1000,initial_condition_gas=0,tempsens=0):
    gas.TPX=Temps[0],f['pressure']*ct.one_atm,f['conditions']

model=JSR_steadystate2(gas,f['residenceTime'],f['reactorVolume'],kinetic_sens=kinetic_sens,physical_sens=physical_sens,observables=observables,physical_params=physical_params,energycon=energycon,pressureValveCoefficient=pressureValveCoefficient,initial_conditions_gas=initial_condition_gas,tempsens=tempsens)

```

```

for i in np.arange(len(Temps)):
    if i!=0:
        try:
            gas.TPX = Temps[i],f['pressure']*ct.one_atm,f['conditions']
            solutionObject =
JSR_steadystate2(gas,f['residenceTime'],f['reactorVolume'],kinetic_sens=kinetic_sens,physical_sens=physical_sens,observables=observables,physical_params=physical_params,energycon=energycon,pressureValveCoefficient=pressureValveCoefficient,initial_condition_gas=initial_condition_gas,tempsens=tempsens)

            model=solutionObject+model
        except:
            print('Simulation at '+str(Temps[i])+ ' K failed.')
            pass
    return model

#+++++
# end of the definition of model_data
#+++++
#####
# definition for SOLVER class:::
#+++++

def JSR(filenamees,Temps,pressures,resTime,conditions,sens,volume,observables):
    expConditions=[]
    for T in Temps:
        for filename in filenamees:
            for P in pressures:
                for r in resTime:
                    for X in conditions:
                        expConditions.append([T,P,filename,r,X])
    tempresults=[]
    results=[]
    for i in expConditions:
        gas=ct.Solution(i[2])
        f={'residenceTime':i[3],'reactorVolume':volume,'pressure':i[1],'conditions':i[4]}

results.append(multiTemp2(i[2],gas,[i[0]],f,kinetic_sens=0,physical_sens=0,observables=observables,physical_params=[T,P],
    energycon='off',pressureValveCoefficient=0.01,maxsimulationTime=10000))
    results[-1].add_mechanism(i[2])
    #results[-1].add_fuel(fuel)
    #results[-1].assign_phi(phi)
    results[-1].add_residence_time(i[3])
    print("\t> Final pressure:\n\t> {0} atm".format(round((results[-1].final_pressure)/101325,2)))
    return (results)

#+++++
# End of the definition for SOLVER
#+++++

#Change inputs here
def JSRCanteraSimulator(NamesDict, ReactorsDict, UnitsDict, DataSpeciesJSR, TP, FinalPath, MechFile, sa):

    ct.suppress_thermo_warnings()
    Mech = [MechFile]
    start = time.time();

```

```

#print("NamesDict: ", NamesDict)
#print("ReactorsDict: ", ReactorsDict)
#print("UnitsDict: ", UnitsDict)
#print("DataEspeciesJSR: ", DataEspeciesJSR)
#print("TP: ", TP)
#print("FinalPath: ", FinalPath)
#print("MechFile: ", MechFile)
#print("sa: ", sa)
TINI = float(ReactorsDict["T_INITIAL"]);
PINI = float(ReactorsDict["P_INITIAL"]);
#print(TINI,PINI)
if TINI == 0.0:
    Temps = TP[0]
    Ti = list(map(float, Temps.tolist()))
    Temps = Ti
    ResTime0 = TP[2]
    ResTimei = [list(map(float, ResTime0))[-1]]
    resTime = ResTimei
elif TINI >= 1.0:
    Temps = [ReactorsDict["T_INITIAL"]];
    Temps = list(map(float, Temps)); print(Temps)
    ResTime0 = TP[0]
    ResTimei = list(map(float, ResTime0))
    resTime = ResTimei; print(ResTimei)
# except:
# print("No valid Initial Temperature in Input File...")
# sys.exit(1)

if PINI == 0.0:
    press = TP[1]
    Po = press
    Pi = [list(map(float, Po))[0]]
    pressures = Pi
elif PINI >= 1.0:
    press = [ReactorsDict["P_INITIAL"]]
    pressures = list(map(float, press)); print(pressures)

# except:
# print("No valid Initial Pressure in Input File...")
# sys.exit(1)
print(" ", "***43")
print("\\t> Running case:\\n")
print("\\t- List of temperatures:")
print("\\t ", *Temps, " / K")
print("\\t- Initial pressure:")
print("\\t ", round(pressures[0],2), " / atm")
print("\\t- Residence time:")
print("\\t ", round(ResTimei[0],2), " / s")
print(" ", "***43")

for m in range(len(ResTimei)):
    if ResTimei[m] == 0:
        ResTimei[m] = 0.00001
    else:

```

```

    pass
Species = list(DataEspeciesJSR)#.split('\t')
SP = len(Species); #print(SP)
#print(Species)
Prods = [];
for k in range(SP):
#print(DataEspeciesJSR.iloc[0,k])
    if str(DataEspeciesJSR.iloc[0,k]) == 'T/K':
        pass
    elif str(DataEspeciesJSR.iloc[0,k]) == 'P/ATM':
        pass
    elif str(DataEspeciesJSR.iloc[0,k]) == 'TAU/S':
        pass

    else:
        Prods.append(str(DataEspeciesJSR.iloc[0,k]))

#cwd = os.getcwd()
filenames = Mech

phi=[ReactorsDict["PHI"]]
conditions={ReactorsDict["REACTANTS"]}

speciesToPlot= Prods
observables=Prods
volume=1e-6
sens=sa #Edit to 1 to run sensitivities
#####
#####

resultsJSR = JSR(filenames,Temps,pressures,resTime,conditions,sens,volume,observables)
#(resJSR) = Solutions(resultsJSR,
#    speciesToPlot,
#    conditions,
#    pressures,
#    phi,
#    FinalPath)
#if sens==1:
#print("FinalPath: ", FinalPath)
#print("Data: ")
#print(observables)
#print(TP[3:-1])
DFn = pd.DataFrame()
ExpTempos = []
for u in range(len(observables)):
    dfx = pd.DataFrame({observables[u]:TP[u+3]})
    DFn = pd.concat([DFn,dfx], axis=1)
ExpTempos.append(TP[0])
#print(ExpTempos)
#print(ExpTempos[0])
a, b, c =
plotSpecies(resultsJSR,speciesToPlot,conditions,pressures,phi,FinalPath,NamesDict["InpFileName"],NamesDict["AUT
HOR"],DFn,ExpTempos,filenames)

```

```

#else:
# pass
#if sens==1:
#plotsens(a,observables,conditions,filenames,Temps,4,FinalPath)
#
SimTime = time.time() - start
#resultsJSR.
#print(b[observables[0]])
# PLOTTING:
#for w in range(len(observables)):
# plt.rcParams["font.weight"] = "bold"
# plt.tick_params(axis='both', direction='out', length=4, width=2, labelsz=10)
# plt.rcParams["axes.labelweight"] = "bold"
# plt.rcParams["axes.linewidth"] = "3"
# #plt.scatter(ExpTempos[0],DFn[observables[w]], marker="s", label=str(observables[w].translate(subscript)),
lw=4,color='black')
# plt.plot(ExpTempos[0],b[observables[w]], label=str(observables[w].translate(subscript)))
# #
# #
# #
# #plt.savefig(c + "\\\" + NamesDict["InpFileName"] + "_" + observables[w] + '.png',dpi=800,
bbox_inches="tight" )
# Y = pd.to_numeric(DFn[observables[w]])
# YY = (Y).sort_values(ascending=False)
# plt.scatter(ExpTempos[0],YY, marker="s", label=str(observables[w].translate(subscript)), lw=4,color='black')
# plt.legend()
# plt.show()
# plt.close()
#print(b)
print(">It took {0:0.1f} seconds".format(SimTime))
return (resultsJSR)

#+++++
#
#+++++

#-----
#=====
if __name__ == "__main__":
mech_list = [];
path = "C:\\DKM\\MODELS\\"#os.getcwd();
fname = glob.glob(path+'/*.cti');
#print("\t>Running with mechanism: \n\t',mechanism);
#Mechanism = "/DKM/MODELS/19_48_C7.cti"
for m in fname:
print("\t>Running with mechanism: \n\t',m);
Input = sys.argv[1] #"InputFileNameWithFullPath"
(NamesDict, ReactorsDict, UnitsDict,DataEspeciesJSR,dataJSR,FinalPath) = InputFileReaderJSR(Input,
"C:\\DKM\\OUTPUTDATA\\");
JSRCanteraSimulator(NamesDict, ReactorsDict, UnitsDict, DataEspeciesJSR, dataJSR, FinalPath, m, 1)
#=====
=====
# Eppure si muove! - Galileo Galilei (1564-1642)
#=====
=====

```

10. Python code for SA bruteforce

```
#!/usr/bin/env python
# -*- coding: utf-8 -*-
#"""
#Created on Tue Jan 15 11:06:39 2019
#@C3 group- NUIGalway
#@author: sergio
#"""
#+++++
# IMPORTING MODULES - LET'S ROCK!
#+++++
import os
import numpy as np
import cantera as ct
import pandas as pd
import glob
from InputReader import KindOfFiles
import itertools
import multiprocessing
from Definitions.Definitions import DefinitionStandar
import csv
from time import time
import datetime
import platform

gases = {}

def idtST(mech, T, P, X, factor):

    ct.suppress_thermo_warnings();
    mech, T, P, X, factor
    gas = ct.Solution(mech)
    gas.TPX = T, P, X
    gas.set_multiplier(1.0)
    for i in range(gas.n_reactions):
        gas.set_multiplier(factor[i],i)

    r = ct.IdealGasReactor(gas)
    sim = ct.ReactorNet([r])

    time = []
    temp = []
    pres = []
    states = ct.SolutionArray(gas, extra=['t'])
    print("\t>Ti = {0} K, Pi= {1} atm".format(T,round(P*9.86923e-6,3)))
    while sim.time < 1.0 and r.T < (400+T):
        sim.step()
        time.append(sim.time)
```

```

    temp.append(r.T)
    pres.append(r.thermo.P)
    states.append(r.thermo.state, t=sim.time)
time = np.array(time)
temp = np.array(temp)
pres = np.array(pres)
diff_temp = np.diff(temp)/np.diff(time)
dpdt = np.diff(pres)/np.diff(time)
ign_temp = np.argmax( diff_temp )
ign_pres = np.argmax( dpdt )
ign = time[ign_pres]
if ign == 0:
    ign = time[ign_temp]
return (ign, T, P, X)

```

def idtST2(mech, T, P, X, factor):

```

ct.suppress_thermo_warnings();
mech, T, P, X, factor
gas = ct.Solution(mech)
gas.TPX = T, P, X
gas.set_multiplier(1.0)
for i in range(gas.n_reactions):
    gas.set_multiplier(factor[i],i)

```

```

r = ct.IdealGasReactor(gas)
sim = ct.ReactorNet([r])

```

```

time = []
temp = []
pres = []
states = ct.SolutionArray(gas, extra=['t'])
#print("\t>Ti = {0} K, Pi= {1} atm".format(T,P))
while sim.time < 1.0 and r.T < (400+T):
    sim.step()
    time.append(sim.time)
    temp.append(r.T)
    pres.append(r.thermo.P)
    states.append(r.thermo.state, t=sim.time)
time = np.array(time)
temp = np.array(temp)
pres = np.array(pres)
diff_temp = np.diff(temp)/np.diff(time)
dpdt = np.diff(pres)/np.diff(time)
ign_temp = np.argmax( diff_temp )
ign_pres = np.argmax( dpdt )
ign = time[ign_pres]
if ign == 0:
    ign = time[ign_temp]
return (ign)

```

def ign_RCM(mech, factor):


```

ct.suppress_thermo_warnings()

gato = '#' * 90

DefinitionStandar.SOME_STUFF(90, 'cti', 'xml')
path = os.getcwd() + '\\FILES\\'
names = glob.glob(path + '*inp_r')
Ti, Pi, fuelname, whole_X, volname, TMP = (DefinitionStandar.
      FileFormat(names, path))

# ++++++++++++++++++++++++++++++++++++++++++++++++++++++++++++++++++++++
#for i in range(len(names)):
file_name = TMP[0]
df = pd.read_csv(file_name)
vpro_time = pd.to_numeric(df.iloc[:, 0])
gas = ct.Solution(mech)
gas.set_multiplier(1.0)
for i in range(gas.n_reactions):
    gas.set_multiplier(factor[i],i)
gas.TPX = Ti[0], Pi[0], whole_X[0]
print('Fuel and mole fractions:\t\n', whole_X[0])
print(gato)
print(gas())
print(gato)
print("""RUNNING NOW:\nTi[K]={:<10.2f}\nPi[mbar]={:<10.2f}
      \nVprofile NAME={:<10s}\n...""")
      .format(Ti[0], Pi[0] / 1E2, volname[0])
print(gato)
r = ct.IdealGasReactor(gas)
env = ct.Reservoir(ct.Solution('air.xml'))
w = ct.Wall(r, env)
w.set_velocity(DefinitionStandar.variable_volume_velocity(df))
sim = ct.ReactorNet([r])
end_time = float(vpro_time.iloc[-1] * 10)
Deltat = float(vpro_time.iloc[1] / 100)
# ++++++++++++++++++++++++++++++++++++++++++++++++++++++++++++++++++++++
TIMES = []
TEMPERATURES = []
PRESSURES = []
V = []
t = 0
while t < (end_time):
    t += Deltat
    sim.advance(t)
    TIMES.append(sim.time)
    TEMPERATURES.append(gas.T)
    PRESSURES.append(gas.P / 1E5)
    V.append(r.volume)
EocArg = np.argmin(V)
EocTime = TIMES[EocArg]
dpdt = np.append(np.diff(PRESSURES) / np.diff(TIMES), 0)
dTdt = np.append(np.diff(TEMPERATURES) / np.diff(TIMES), 0)
eoc = EocTime
IdtDpdt = TIMES[np.argmax(dpdt)] - eoc
if IdtDpdt < 0:
    IdtDpdt = 0.0

```

```

IdtDTdt = TIMES[np.argmax(dTdt)] - eoc
if IdtDTdt < 0:
    IdtDTdt = 0.0
gas.set_multiplier(1.0)
return (IdtDpdt, Ti[0], Pi[0], whole_X[0])

def ign_RCM2(mech, T, P, X, factor):

    ct.suppress_thermo_warnings()

    # ++++++
    for i in range(len(names)):
        CWD = os.getcwd()
        TMP = glob.glob(CWD+"\\FILES\\*.tmp")
        file_name = TMP[0]
        df = pd.read_csv(file_name)
        vpro_time = pd.to_numeric(df.iloc[:, 0])
        gas = ct.Solution(mech)
        gas.set_multiplier(1.0)
        for i in range(gas.n_reactions):
            gas.set_multiplier(factor[i], i)
        gas.TPX = T, P, X
        print('Fuel and mole fractions:\t\n', X)
        print(gas())
        #print("""RUNNING NOW:\nTi[K]={:<10.2f}\nPi[mbar]={:<10.2f}\n...""")
        #         .format(T, P/1E2))

    r = ct.IdealGasReactor(gas)
    env = ct.Reservoir(ct.Solution('air.xml'))
    w = ct.Wall(r, env)
    w.set_velocity(DefinitionStandar.variable_volume_velocity(df))
    sim = ct.ReactorNet([r])
    end_time = float(vpro_time.iloc[-1] * 10)
    Deltat = float(vpro_time.iloc[1] / 100)
    # ++++++
    TIMES = []
    TEMPERATURES = []
    PRESSURES = []
    V = []
    t = 0
    while t < (end_time):
        t += Deltat
        sim.advance(t)
        TIMES.append(sim.time)
        TEMPERATURES.append(gas.T)
        PRESSURES.append(gas.P / 1E5)
        V.append(r.volume)
    EocArg = np.argmin(V)
    EocTime = TIMES[EocArg]
    dpdt = np.append(np.diff(PRESSURES) / np.diff(TIMES), 0)
    dTdt = np.append(np.diff(TEMPERATURES) / np.diff(TIMES), 0)
    eoc = EocTime
    IdtDpdt = TIMES[np.argmax(dpdt)] - eoc
    if IdtDpdt < 0:
        IdtDpdt = 0.0

```

```

IdtDTdt = TIMES[np.argmax(dTdt)] - eoc
if IdtDTdt < 0:
    IdtDTdt = 0.0
gas.set_multiplier(1.0)
return (IdtDpdt)

```

```

def BF(args):
    mech, k, dk, factor, T, P, X, ign0, FileInputName, FacilityName = args
    gas = ct.Solution(mech)
    gas.TPX = T, P, X;

```

```

    reactions = []; m = gas.n_reactions;
    ds = pd.DataFrame(data=[], index=gas.reaction_equations(range(m)))
    ds["index"] = ""
    ds["bruteforce"] = ""
    all_reactions = ct.Reaction.listFromFile(mech)
    for R in all_reactions:
        reactions.append(R)
    factor[k] = 1+dk
    if "ST" in FacilityName:
        ign = idtST2(mech,T,P,X,factor)
    elif "RCM" in FacilityName:
        ign = ign_RCM2(mech, T, P, X, factor)
    factor[k] = 1.0
    ds["bruteforce"][k] = (ign-ign0)/(ign0*dk)
    ds["index"][k] = k

```

```

    SIDTs=open(str(FileInputName)+".txt","a")
    SIDTs.writelines(str(reactions[k]))
    SIDTs.writelines(' ')
    SIDTs.writelines(str(ds["index"][k]))
    SIDTs.writelines(' ')
    SIDTs.writelines(str(ds["bruteforce"][k])+"\n")
    SIDTs.close()

```

```

def init_process(mech):
    """
    This function is called once for each process in the Pool. We use it to
    initialize any Cantera objects we need to use.
    """
    ct.suppress_thermo_warnings();
    gases[mech] = ct.Solution(mech)

```

```

def parallel(mech, predicate, nProcs, nTemps,dk,factor,T,P,X,ign0,FileInputName,FacilityName):
    """
    Call the function ``predicate`` on ``nProcs`` processors for ``nTemps``
    different temperatures.
    """
    ct.suppress_thermo_warnings();

    pool = multiprocessing.Pool(processes=nProcs,
                               initializer=init_process,
                               initargs=(mech,))

```

```

reactionslist = range(nTemps);
y = pool.map(predicate,
             zip(itertools.repeat(mech),
                 reactionslist,
                 itertools.repeat(dk),
                 itertools.repeat(factor),
                 itertools.repeat(T),
                 itertools.repeat(P),
                 itertools.repeat(X),
                 itertools.repeat(ign0),
                 itertools.repeat(FileInputName),
                 itertools.repeat(FacilityName)))
#pool.close()
#pool.join()
#pool.terminate()
return (y)

def SENS(mechanism):
#+++++
# RCM DEFINITION: IDT CALCULATION
#+++++
#+++++
# RUNNING THE WHOLE SENSITIVITY ANALYSIS
#+++++
# Global storage for Cantera Solution objects
#

def SecondRound(m,gas, factor, dk, reactions, nProcs,T,P,X,mechanism,ds,FileInputName,FacilityName):
    if "ST" in FacilityName:
        ign0, TT, PP, XX = idtST(mechanism,T,P,X,factor)
    elif "RCM" in FacilityName:
        ign0, TT, PP, XX = ign_RCM(mechanism, factor)
    print("Ignition Delay is: {:.4f} ms".format(ign0*1000))
    factor = np.ones( ( gas.n_reactions, 1 ) )
    print("Start Brute Force")
    print("\t> Running with {0} processors ".format(nProcs))
    ds = parallel(mechanism, BF, nProcs, m, dk,factor,TT,PP,XX,ign0,FileInputName,FacilityName)
    return (ds)

# +++++
# CODE TO RUN: ALL SYSTEM'S FEATURES
# +++++
ct.suppress_thermo_warnings();
gas = ct.Solution(mechanism)
all_reactions = ct.Reaction.listFromFile(mechanism)
reactions = []
for R in all_reactions:
    reactions.append(R)
InputFileName = (os.getcwd()+"\\Input.inp");
(WHOLE_XF,WHOLE_XO,Ti,Pi,DK,onedict) = (KindOfFiles.InputFileReader(InputFileName))
for mm in range(len(Ti)):
    temp = Ti[mm]

```

```

pres = Pi[mm]
fuel = str(WHOLE_XF)
oxidizer = str(WHOLE_XO)
simtype = 'SV'
mecha1 = str(mechanism).split("\\")[-1]
mecha2 = str(mecha1).split(".cti")[0]
Path = os.getcwd()
Output = Path + "\\ " + str(mecha2)
if not os.path.isdir(Output):
    os.makedirs(Output)
FacilityName = str(onedict["FACILITY"])+ "_Ti_" + str(temp) + "_pi_" + str(pres)
FileInputName = Output + "\\ " + FacilityName + "_" + str(onedict["NAMEFILE"]) + "_" + str(mecha2)

dk = DK[mm]
X = fuel+' '+oxidizer
P = pres*ct.one_atm
T = temp
gas.TPX = T, P, X
gas.equilibrate(simtype)
ds = pd.DataFrame(data=[], index=gas.reaction_equations(range(10)))
m = gas.n_reactions
cpus = int(multiprocessing.cpu_count())
if "auto" in onedict["WORKERS"]:
    nProcs = cpus
elif "semi" in onedict["WORKERS"]:
    nProcs = cpus-1
else:
    nProcs = int(onedict["WORKERS"])
pd.options.display.float_format = '{:,.2e}'.format
ds["index"] = ""
ds["bruteforce"] = ""
factor = np.ones( gas.n_reactions )

SecondRound(m,gas,factor,dk,reactions,nProcs,T,P,X,mechanism,ds,FileInputName,FacilityName)
converter =
pd.read_csv(str(FileInputName)+".txt",sep="\t",names=["reactions","index","bruteforce","bruteforcetabs"])
df = pd.DataFrame(data=converter)
df.to_csv(str(FileInputName)+".csv",index=False)
return (str(FileInputName),m,nProcs)
#+++++++
if __name__ == "__main__":
    print("=*90,\n");
    print("\\t> RUNNING SENSITIVITY ANALYSIS MULTIPROCESSING\\n\\t> Update: 30/05/2019. S.M.& C3-team
    NUIGalway,IE")
    print("=*90,\n");

mech_list = [];
fname = glob.glob(os.getcwd()+"\\Mechanisms\\*.");
for i,mechanism in enumerate(fname):
    t1 = time()
    print("=*90);
    print("\\t> Running with mechanism: \\n\\t>',mechanism);
    print("=*90,\n");
    outname,numreacs,nProcs = SENS(mechanism)
    t2 = time()

```

```

clock = t2-t1
today = datetime.date.today()
mecha1 = str(mechanism).split("\\")[-1]
mecha2 = str(mecha1).split(".cti")[0]
machina = platform.machine()
version = platform.version()
uname = platform.uname()
system = platform.system()
procs = nProcs
platformA = platform.platform()
if clock <= 60:
    reloj = round(clock,2)
    print("\\t> Simulation took:{0:0.2f} seconds".format(reloj))
    print("Printing log.txt file...")
    SIDTs=open(outname+".log.txt","a")
    SIDTs.writelines("Begin of log file.\\n")
    SIDTs.writelines("-----\\n")
    SIDTs.writelines("> Simulation took:{0:0.2f} seconds\\n".format(reloj))
    SIDTs.writelines("> With # {0} reactions\\n".format(str(numreacs)))
    SIDTs.writelines("> With mechanism : {0}\\n".format(str(mecha2)))
    SIDTs.writelines("> Date of simulation : {0}\\n".format(str(today)))
    SIDTs.writelines("-----\\n")
    SIDTs.writelines("> System info : \\n")
    SIDTs.writelines("> machine : {0}\\n".format(str(machina)))
    SIDTs.writelines("> version : {0}\\n".format(str(version)))
    SIDTs.writelines("> platform : {0}\\n".format(str(platformA)))
    SIDTs.writelines("> uname : {0}\\n".format(str(uname)))
    SIDTs.writelines("> system : {0}\\n".format(str(system)))
    SIDTs.writelines("> # processors : {0}\\n".format(str(procs)))
    SIDTs.writelines("-----\\n")
    SIDTs.writelines("End of log file\\n")
    SIDTs.writelines("-----\\n")
    SIDTs.close()
elif clock > 60:
    reloj = round((float(clock)/60),2)
    print("\\t> Simulation took:{0:0.2f} minutes".format(reloj))
    print("Printing log.txt file...")
    SIDTs=open(outname+".log.txt","a")
    SIDTs.writelines("Begin of log file.\\n")
    SIDTs.writelines("-----\\n")
    SIDTs.writelines("> Simulation took:{0:0.2f} minutes\\n".format(reloj))
    SIDTs.writelines("> With # {0} reactions\\n".format(str(numreacs)))
    SIDTs.writelines("> With mechanism : {0}\\n".format(str(mecha2)))
    SIDTs.writelines("> Date of simulation : {0}\\n".format(str(today)))
    SIDTs.writelines("-----\\n")
    SIDTs.writelines("> System info : \\n")
    SIDTs.writelines("> machine : {0}\\n".format(str(machina)))
    SIDTs.writelines("> version : {0}\\n".format(str(version)))
    SIDTs.writelines("> platform : {0}\\n".format(str(platformA)))
    SIDTs.writelines("> uname : {0}\\n".format(str(uname)))
    SIDTs.writelines("> system : {0}\\n".format(str(system)))
    SIDTs.writelines("> # processors : {0}\\n".format(str(procs)))
    SIDTs.writelines("-----\\n")
    SIDTs.writelines("End of log file\\n")
    SIDTs.writelines("-----\\n")

```

```

        SIDTs.close()
    print("All done!.")
#+++++
# le fini...
#+++++

```

11. Python code for RP (fluxes)

```

#!/usr/bin/env python
# -*- coding: utf-8 -*-
#"""
#Created on Tue Jan 15 11:06:39 2019
#@C3 group- NUIGalway
#@author: sergio
#"""
#####
# MODULES TO IMPORT -----
#####
import os
import sys
import time
import glob
import numpy as np
import cantera as ct
from InputReader import KindOfFiles
import matplotlib.pyplot as plt
#####
# READING MECHANISMS FOLDER -----
#####
ct.suppress_thermo_warnings();
def ROP(mechanism):
    mechanism2 = mechanism.split("\\")[-1];
    mechanism3 = mechanism2.split(".cti")[0]
    gas = ct.Solution(mechanism)
    InputFileName = (os.getcwd()+"\Input.inp");
    WHOLE_X,Ti,Pi,Elements,Percent,onedict = (
        KindOfFiles.InputFileReader(InputFileName))
    for r in range(len(Elements)):
        ELE = Elements[r]
        print("\t>Doing Reaction Path Diagram for: ",ELE)
        for m in range(len(Ti)):
            gas.TPX = Ti[m], Pi[m]*ct.one_atm, str(WHOLE_X)
            r = ct.IdealGasReactor(gas)
            sim = ct.ReactorNet([r])
            t = 0.0
            Specie = str(onedict["FUEL"])
            percentage = Percent[m]
            perper = percentage*100
            FuelConsumsion = float((r.thermo[Specie].X[0])*percentage)
            StopFuelConsumsion =float((r.thermo[Specie].X[0]) - FuelConsumsion);
            Fuel = r.thermo[Specie].X[0];

```

```

print("\t>Fuel X initial: ",Fuel," ", "100% ");
print("\t>Fuel consumption percentage criteria: ",
      percentage*100,"%")
print("\t>Which means, simulation will stop when Fuel X is: ",
      StopFuelConsumsion , "reached")
TIMES=[]; TEMP=[];PRESS=[];XFUEL=[];
while r.thermo[Specie].X[0] > StopFuelConsumsion:
    t += float(onedict["DELTA"])
    sim.advance(t)
    TIMES.append(sim.time)
    TEMP.append(r.T)
    PRESS.append(r.thermo.P/1E5)
    XFUEL.append(r.thermo["O2"].X[0])
#+++++
# IF YOU WANT TO PRINT ON SCREEN THE TERMODINAMIC PROPERTIES USE THE NEXT LINE
# print(sim.time, " ",gas.T, " ",r.thermo['C2H4'].X[0], " ",r.thermo['CH4'].X[0])
#+++++
    element = str(ELE)
    diagram = ct.ReactionPathDiagram(gas, element)
    diagram.title =Reaction path diagram following {0}'.format(element)
    diagram.scale=-1
    diagram.threshold = float(onedict["THRES"])
    diagram.label_threshold = float(onedict["LABEL"])
    diagram.show_details = True
    outputdata = os.getcwd()+"\\OutputData_ROP\\"
    dot_file = outputdata+str(mechanism3)+"_"+str(Ti[m])+ "K_"+str(
        onedict["FUEL"])+ "_ "+element+"_"+str(perper)+ "%_path.dot"
    img_file = outputdata+str(mechanism3)+"_"+str(Ti[m])+ "K_"+str(
        onedict["FUEL"])+ "_ "+element+"_"+str(perper)+ "%_path.png"
    img_path = os.path.join(os.getcwd(), img_file)
    diagram.write_dot(dot_file)
# print(diagram.get_data())
print("="*90, "\n");
print("\t>Wrote graphviz input file to '{0}'".format(
    os.path.join(os.getcwd(), dot_file)))
os.system('dot {0} -Tpng -o{1} -Gdpi=200'.format(
    dot_file, img_file))
print("\t>Wrote graphviz output file to '{0}'".format(
    img_path))
print("="*90, "\n");
dTdt = np.append(np.diff(TEMP)/np.diff(TIMES),0)
idt = TIMES[np.argmax(dTdt)]
print("IDT = ",idt); print("Time = ",TIMES[-1])
plt.plot(TIMES,XFUEL)
#plt.show()
#+++++
if __name__ == "__main__":
    print("="*90, "\n");
    print("\t>RUNNING RATE OF PRODUCTION (ROP) CODE")
    print("="*90, "\n");
    mech_list = [];
    fname = glob.glob(os.getcwd()+"\\mechanisms\\*.");
    for i,mechanism in enumerate(fname):
        print("="*90);
        print("\t>Running with mechanism: \n\t>',mechanism);

```



```
print("="*90, "\n");
ROP(mechanism)
```

12. Python code for Plots and LaTeX-PDF generator

12.1. Plotters

12.1.1. Plotter ST

```
#!/usr/bin/env python
# -*- coding: utf-8 -*-
"""
Created on Wed Dec 5 17:23:58 2018
@C3 group- NUIGalway
@author: sergio
"""
import os
import sys
import glob
import numpy as np
import pandas as pd
import matplotlib.pyplot as plt
from matplotlib import rc, rcParams
from matplotlib import colors as mcolors
from cycler import cycler
# -----

def plotter():
    counter = 0
    dicfiles = {}; FILES = [];
    dicdirs = {}; filesDirs = [];
    for root, dirs, files in os.walk(".", topdown=False):
        for name in dirs:
            filesDirs.append(os.path.join(root, name))
            dicdirs[counter] = os.path.join(root, name)
            counter += 1
    for root, dirs, files in os.walk(".", topdown=False):
        for k in filesDirs:
            File2track = k.rsplit("\\", 1)[-1]
            for name in files:
                if "NUIGMech1.1_C4_gas" in str(name):
                    pass
                elif "NUIGMech1.2_C4_V3_SM" in str(name):
                    pass
                elif File2track+".ST_IDT" == str(name):
```

```

        FILES.append(os.path.join(root, name))
        dicfiles[counter] = os.path.join(root, name)
        counter += 1
    else:
        pass
print("\t> # of mechanism to plot: ",str(len(sys.argv)-1))

if (len(sys.argv)) == 2:
    Mechas = [sys.argv[1]]
elif (len(sys.argv)) == 3:
    Mechas = [sys.argv[1],sys.argv[2]]
elif (len(sys.argv)) == 4:
    Mechas = [sys.argv[1],sys.argv[2],sys.argv[3]]
elif (len(sys.argv)) == 5:
    Mechas = [sys.argv[1],sys.argv[2],sys.argv[3],sys.argv[4]]
elif (len(sys.argv)) == 6:
    Mechas = [sys.argv[1],sys.argv[2],sys.argv[3],sys.argv[4],sys.argv[5]]
elif (len(sys.argv)) == 7:
    print("\t> Error, plotter is only allowed to work with")
    print("\t> 3 mechanism names")
    print("\t> Au revoir!")
    sys.exit(1)
else:
    print("\t> Error, plotter needs an argument...")
    print("\t> e.g. >python PloterRCM.py AramcoMech1.3")
    print("\t> No extension cti/xml is required at the end of mechanism name")
    sys.exit(1)

#-----
print("\t> Mechanisms to plot", str(Mechas))
path = os.getcwd()
subscript = str.maketrans("0123456789", "0123456789")
# reading experiments:
#print(FILES)

for r in range(2):
    for i in FILES:
        readexp = pd.read_csv(i,names=['col'],sep="%s",engine="python");
        DroppingStuff = readexp[readexp.col.str.contains("!") == False]
        DroppingStuff2 = DroppingStuff[DroppingStuff.col.str.contains("T/K") == False]
        dataST = pd.DataFrame(DroppingStuff2.col.str.split().tolist())
        ##### author and journal
        AUTHOR = ((readexp[readexp.col.str.contains("AUTHOR:")] ).iloc[0].str.split(':')[0][1]
        JOURNAL = ((readexp[readexp.col.str.contains("JOURNAL:")] ).iloc[0].str.split(':')[0][1]
        PDF = ((readexp[readexp.col.str.contains("PDF:")] ).iloc[0].str.split(':')[0][1]
        REACS = (readexp[readexp.col.str.contains("REAC:")] ).col.str.split(':')
        #-----
        REACTANTS = []
        OxDil = []
        DILS = []
        FuelNamesList = []
        #-----
        SUMAVAL = []; #print(TimeScale);
        for m in range(len(REACS)):
            REAC1 = REACS.iloc[m][1];

```

```

SUMAVAL.append(float(REAC1.split()[-1]))
SumaRValues = sum(SUMAVAL); #print(SumaRValues)
# -----
if SumaRValues < 2:
    for u in range(len(REACS)):
        if "C" in REACS.iloc[u][1]:
            REAC1 = (REACS.iloc[u][1]); namb = round(float(REAC1.split()[-1])*100,3);
FuelNamesList.append(REAC1.split()[0]);
            REAC11 = str(namb)+"% "+str(REAC1.split()[-0]).translate(subscript) #":".join(REAC1.split())
            REACTANTS.append(REAC11)
        if "O2" in REACS.iloc[u][1]:
            REAC1 = REACS.iloc[u][1]; namb = round(float(REAC1.split()[-1])*100,3);
            REAC1 = str(namb)+"% "+str(REAC1.split()[-0]).translate(subscript) #":".join(REAC1.split())
            OxDil.append(REAC1)
        if "N2" in REACS.iloc[u][1]:
            REAC1 = REACS.iloc[u][1]; namb = round(float(REAC1.split()[-1])*100,3);
            if namb > 0:
                REAC1 = str(namb)+"% "+str(REAC1.split()[-0]).translate(subscript) #":".join(REAC1.split())
                DILS.append(REAC1)
            else:
                pass
        if "Ar" in REACS.iloc[u][1]:
            REAC1 = REACS.iloc[u][1]; namb = round(float(REAC1.split()[-1])*100,3);
            if namb > 0:
                REAC1 = str(namb)+"% Ar" #":".join(REAC1.split())
                DILS.append(REAC1)
            else:
                pass
        if "AR" in REACS.iloc[u][1]:
            REAC1 = REACS.iloc[u][1]; namb = round(float(REAC1.split()[-1])*100,3);
            if namb > 0:
                REAC1 = str(namb)+"% Ar" #":".join(REAC1.split())
                DILS.append(REAC1)
        if "CO2" in REACS.iloc[u][1]:
            REAC1 = REACS.iloc[u][1]; namb = round(float(REAC1.split()[-1])*100,3);
            if namb > 0:
                REAC1 = str(namb)+"% Ar" #":".join(REAC1.split())
                DILS.append(REAC1)
            else:
                pass
# -----
if SumaRValues >= 2:
    for u in range(len(REACS)):
        if "C" in REACS.iloc[u][1]:
            REAC1 = (REACS.iloc[u][1]); namb = round(float(REAC1.split()[-1]),3);
FuelNamesList.append(REAC1.split()[0]);
            REAC11 = str(namb)+"% "+str(REAC1.split()[-0]).translate(subscript) #":".join(REAC1.split())
            REACTANTS.append(REAC11)
        if "O2" in REACS.iloc[u][1]:
            REAC1 = REACS.iloc[u][1]; namb = round(float(REAC1.split()[-1]),3);
            REAC1 = str(namb)+"% "+str(REAC1.split()[-0]).translate(subscript) #":".join(REAC1.split())
            OxDil.append(REAC1)
        if "N2" in REACS.iloc[u][1]:
            REAC1 = REACS.iloc[u][1]; namb = round(float(REAC1.split()[-1]),3);
            if namb > 0:

```

```

    REAC1 = str(namb)+"% "+str(REAC1.split()[-0]).translate(subscript) #":".join(REAC1.split())
    DILS.append(REAC1)
else:
    pass
if "Ar" in REACS.iloc[u][1]:
    REAC1 = REACS.iloc[u][1]; namb = round(float(REAC1.split()[-1]),3);
    if namb > 0:
        REAC1 = str(namb)+"% Ar" #":".join(REAC1.split())
        DILS.append(REAC1)
    else:
        pass
if "AR" in REACS.iloc[u][1]:
    REAC1 = REACS.iloc[u][1]; namb = round(float(REAC1.split()[-1]),3);
    if namb > 0:
        REAC1 = str(namb)+"% Ar" #":".join(REAC1.split())
        DILS.append(REAC1)
if "CO2" in REACS.iloc[u][1]:
    REAC1 = REACS.iloc[u][1]; namb = round(float(REAC1.split()[-1]),3);
    if namb > 0:
        REAC1 = str(namb)+"% Ar" #":".join(REAC1.split())
        DILS.append(REAC1)
    else:
        pass
# -----
REACTANTS = str(", ".join(REACTANTS)); OxDil = str(", ".join(OxDil))
DILS = str(", ".join(DILS));
#####
# .....
# .....
print("\t> Plotting directory/file/case: ",i)
temp = pd.to_numeric(dataST.iloc[:,1]);
idt = pd.to_numeric(dataST.iloc[:,2]);
tempplot = 1000/temp;
idtplot = (idt); Yerr = [(0.2*x) for x in idt]
# Activate latex text rendering
plt.rcParams["font.weight"] = "bold"
plt.tick_params(axis='both', direction='out', length=4, width=3, labelsz=10)
plt.rcParams["axes.labelweight"] = "bold"
plt.rcParams["axes.linewidth"] = "3"
plt.rc('axes', prop_cycle=(cycler('color', ['k','r', 'b','g','m'])))
legend_properties = {'weight':'bold'}
plt.yscale("log")
plt.scatter(tempplot,idtplot, marker="s", label='Exp Data', lw=4,color='black')
plt.errorbar(tempplot,idtplot, yerr=Yerr, label=None, fmt='none', ecolor="k" )
# Reading Simulations:
for j in Mechas:
    FoldName = ((i.rsplit('.ST_IDT',1))[0]); FNam = ((i.split("\")[4]); print(FoldName)
    specs = "\\+str(FoldName);
    FILESS = glob.glob(FoldName+"\\'+j+'.ST_IDT');
    plt.yscale("log")
    for m in range(len(FILESS)):
        legend_properties = {'weight':'bold'}
        readmod = pd.read_table(FILESS[m]);
        mech = (((FILESS[m].split("\")[1]).split('.ST_IDT'))[0];
        tempMod2 = readmod[1000/T] #(readmod.iloc[:,3]);

```

```

tempMod2 = [x for x in tempMod2]; tempMod2 = sorted(tempMod2,reverse=True)
idtTMod2 = readmod['IDT/s'] #(readmod.iloc[:,4]); #readmod['IDT/s',reverse=True);
idtTMod2 = [(x) for x in idtTMod2]
idtTMod2 = sorted((idtTMod2),reverse=True)
try:
    idtMod2 = readmod['IDT/us'] #(readmod.iloc[:,2]); #readmod['IDT/s',reverse=True);
    idtMod2 = [(x) for x in idtMod2]
    idtMod2 = sorted((idtMod2),reverse=True)
except:
    idtMod2 = readmod['IDT/ms']
    idtMod2 = [(x)*1000 for x in idtMod2]
    idtMod2 = sorted((idtMod2),reverse=True)
tempMod = []; idtMod = [];
for m in range(len(idtMod2)):
    if idtMod2[m] > 0:
        idtMod.append(idtMod2[m])
        tempMod.append(tempMod2[m])
    elif idtMod2[m] == 0 and idtTMod2[m] > 0:
        idtMod.append(idtTMod2[m])
        tempMod.append(tempMod2[m])
    elif idtMod2[m] < 0:
        idtMod.append(idtTMod2[m])
        tempMod.append(tempMod2[m])
    elif idtMod2[m] < 0 and idtTMod2[m] < 0:
        idtMod.append(0.0)
        tempMod.append(tempMod2[m])

CASE = REACTANTS
initconds = FoldName.split("\\")[1];
PHIs = initconds.split("_")[-1];
PRESss = (initconds.split("_")[0]);
title = str(CASE)+"\n "+str(OxDil)+" , "+str(DILS)+"\n $phi$ = "+str(PHIs)+" , "+str(PRESss)+" atm";
plt.yscale("log");
if str(mech) == str(Mechas[0]):
    print("Yes, {0} mechanism found!".format(str(mech)))
    mecham = mech
    if mecham == "N13_C4_gas":
        mecham = "NUIGMech1.3"
    elif mecham == "NUIGMech1.2_C4":
        mecham = "NUIGMech1.2"
    elif mecham == "AM3.0":
        mecham = "AramcoMech3.0"
    else:
        pass
    print(mecham)
    mech = mecham
    plt.plot(tempMod, idtMod, linestyle='-', color="k", label=str(mecham), lw=3)
elif str(mech) == str(Mechas[1]):
    mecham = mech
    if mecham == "N13_C4_gas":
        mecham = "NUIGMech1.3"
    elif mecham == "NUIGMech1.2_C4":
        mecham = "NUIGMech1.2"
    elif mecham == "AM3.0":
        mecham = "AramcoMech3.0"

```

```

else:
    pass
print(mecham)
mech = mecham
plt.plot(tempMod, idtMod, linestyle='-', color="r", label=str(mech), lw=3)
else:
    mecham = mech
    if mecham == "N13_C4_gas":
        mecham = "NUIGMech1.3"
    elif mecham == "NUIGMech1.2_C4":
        mecham = "NUIGMech1.2"
    elif mecham == "AM3.0":
        mecham = "AramcoMech3.0"
    else:
        pass
print(mecham)
mech = mecham
plt.plot(tempMod, idtMod, linestyle='--', label=str(mech), lw=3)
plt.title(title, fontsize=14, weight='bold')
plt.xlabel('1000 K /  $\{T\}$ ', fontsize=20, weight='bold');
plt.ylabel('IDT /  $\{\mu\}$ ', fontsize=20, weight='bold')
plt.legend(frameon=True)
plt.grid(b=True, which='major', color='grey', linestyle=':'); plt.grid(b=True, which='minor', color='grey',
linestyle=':')
#if "BAIGMOHOMMADI" in AUTHOR:
#    plt.annotate(str(AUTHOR)+" - NUIG", (0.5,0.3), (0, -50),bbox=dict(facecolor='white', alpha=0.8),
xycoords='axes fraction', textcoords='offset points', va='top')
#elif "RAMALINGAM" in AUTHOR:
#    plt.annotate(str(AUTHOR)+" - AACHEN", (0.5,0.3), (0, -50),bbox=dict(facecolor='white', alpha=0.8),
xycoords='axes fraction', textcoords='offset points', va='top')
#else:
#    plt.annotate(str(AUTHOR), (0.5,0.3), (0, -50),bbox=dict(facecolor='white', alpha=0.8), xycoords='axes fraction',
textcoords='offset points', va='top')
directory = FoldName.rsplit("\\",1)[0]; FoldNamee = FoldName.rsplit("\\",1)[-1]
plt.tight_layout()
plt.savefig( directory+"\\"+FNam+'_'+FoldNamee+'.png',dpi=500)
plt.savefig( directory+"\\"+FNam+'_'+FoldNamee+'.png',dpi=500)
plt.close()
# -----

#def FileTexGen():
###k = (FILES[0])
###FNam = ((k.split("\\"))[-5]);
###EachFile = (path+str(k)).rsplit("\\",1)[0]
###EachSplitted = ((path+str(k)).rsplit("\\",1)[-1]).split(".RCM_IDT")[0]
###kiss = (EachFile+"/{"+FNam+"_"+EachSplitted+"}.png"); newPath = kiss.replace(os.sep, '/')

MONOS = ["CH4", "C2H4", "C2H6", "C3H8"]
BINARIES = ["CH4_C2H4", "CH4_C2H6", "C2H4_C2H6", "C2H4_C3H8", "C2H6_C3H8"]
TERNARIES = ["CH4_C2H4_C2H6"]
QUATERNARIES = ["CH4_C2H4_C2H6_C3H8"]

# *****
# MONOS
# *****

```

```

f = open("ST_data.LateX.out", "w")
for k in FILES:
    FNam      = ((k.split("\\"))[-4]); #print(FNam)
    if str(FNam) == MONOS[0]:
        print("yes")
        EachFile  = (path+str(k)).rsplit("\\",1)[0]
        EachSplitted = ((path+str(k)).rsplit("\\",1)[-1]).split(".ST_IDT")[0]
        kiss = (EachFile+"/{"+FNam+"_"+EachSplitted+"}.png"); newPath = kiss.replace(os.sep, '/')
        f.write("\includegraphics[scale=0.5]{"+str(newPath)+"}\n")
f.close()
f = open("ST_data.LateX.out", "a")
for k in FILES:
    FNam      = ((k.split("\\"))[-4]); #print(FNam)
    if str(FNam) == MONOS[1]:
        EachFile  = (path+str(k)).rsplit("\\",1)[0]
        EachSplitted = ((path+str(k)).rsplit("\\",1)[-1]).split(".ST_IDT")[0]
        kiss = (EachFile+"/{"+FNam+"_"+EachSplitted+"}.png"); newPath = kiss.replace(os.sep, '/')
        f.write("\includegraphics[scale=0.5]{"+str(newPath)+"}\n")
f.close()
f = open("ST_data.LateX.out", "a")
for k in FILES:
    FNam      = ((k.split("\\"))[-4]); #print(FNam)
    if str(FNam) == MONOS[2]:
        EachFile  = (path+str(k)).rsplit("\\",1)[0]
        EachSplitted = ((path+str(k)).rsplit("\\",1)[-1]).split(".ST_IDT")[0]
        kiss = (EachFile+"/{"+FNam+"_"+EachSplitted+"}.png"); newPath = kiss.replace(os.sep, '/')
        f.write("\includegraphics[scale=0.5]{"+str(newPath)+"}\n")
f.close()
f = open("ST_data.LateX.out", "a")
for k in FILES:
    FNam      = ((k.split("\\"))[-4]); #print(FNam)
    if str(FNam) == MONOS[3]:
        EachFile  = (path+str(k)).rsplit("\\",1)[0]
        EachSplitted = ((path+str(k)).rsplit("\\",1)[-1]).split(".ST_IDT")[0]
        kiss = (EachFile+"/{"+FNam+"_"+EachSplitted+"}.png"); newPath = kiss.replace(os.sep, '/')
        f.write("\includegraphics[scale=0.5]{"+str(newPath)+"}\n")
f.close()
# -----
# *****
# BINARIES
# *****
f = open("ST_data.LateX.out", "a")
for k in FILES:
    FNam      = ((k.split("\\"))[-4]); #print(FNam)
    if str(FNam) == BINARIES[0]:
        print("yes")
        EachFile  = (path+str(k)).rsplit("\\",1)[0]
        EachSplitted = ((path+str(k)).rsplit("\\",1)[-1]).split(".ST_IDT")[0]
        kiss = (EachFile+"/{"+FNam+"_"+EachSplitted+"}.png"); newPath = kiss.replace(os.sep, '/')
        f.write("\includegraphics[scale=0.5]{"+str(newPath)+"}\n")
f.close()
f = open("ST_data.LateX.out", "a")
for k in FILES:
    FNam      = ((k.split("\\"))[-4]); #print(FNam)
    if str(FNam) == BINARIES[1]:

```

```

EachFile = (path+str(k)).rsplit("\\",1)[0]
EachSplitted = ((path+str(k)).rsplit("\\",1)[-1]).split(".ST_IDT")[0]
kiss = (EachFile+"/"+FNam+"_"+EachSplitted+".png"); newPath = kiss.replace(os.sep, '/')
f.write("\includegraphics[scale=0.5]{"+str(newPath)+"}\n")
f.close()
f = open("ST_data.LateX.out", "a")
for k in FILES:
    FNam = ((k.split("\\"))[-4]); #print(FNam)
    if str(FNam) == BINARIES[2]:
        EachFile = (path+str(k)).rsplit("\\",1)[0]
        EachSplitted = ((path+str(k)).rsplit("\\",1)[-1]).split(".ST_IDT")[0]
        kiss = (EachFile+"/"+FNam+"_"+EachSplitted+".png"); newPath = kiss.replace(os.sep, '/')
        f.write("\includegraphics[scale=0.5]{"+str(newPath)+"}\n")
f.close()
f = open("ST_data.LateX.out", "a")
for k in FILES:
    FNam = ((k.split("\\"))[-4]); #print(FNam)
    if str(FNam) == BINARIES[3]:
        EachFile = (path+str(k)).rsplit("\\",1)[0]
        EachSplitted = ((path+str(k)).rsplit("\\",1)[-1]).split(".ST_IDT")[0]
        kiss = (EachFile+"/"+FNam+"_"+EachSplitted+".png"); newPath = kiss.replace(os.sep, '/')
        f.write("\includegraphics[scale=0.5]{"+str(newPath)+"}\n")
f.close()
f = open("ST_data.LateX.out", "a")
for k in FILES:
    FNam = ((k.split("\\"))[-4]); #print(FNam)
    if str(FNam) == BINARIES[4]:
        EachFile = (path+str(k)).rsplit("\\",1)[0]
        EachSplitted = ((path+str(k)).rsplit("\\",1)[-1]).split(".ST_IDT")[0]
        kiss = (EachFile+"/"+FNam+"_"+EachSplitted+".png"); newPath = kiss.replace(os.sep, '/')
        f.write("\includegraphics[scale=0.5]{"+str(newPath)+"}\n")
f.close()
# -----
# *****
# TERNARIES
# *****
f = open("ST_data.LateX.out", "a")
for k in FILES:
    FNam = ((k.split("\\"))[-4]); #print(FNam)
    if str(FNam) == TERNARIES[0]:
        print("yes")
        EachFile = (path+str(k)).rsplit("\\",1)[0]
        EachSplitted = ((path+str(k)).rsplit("\\",1)[-1]).split(".ST_IDT")[0]
        kiss = (EachFile+"/"+FNam+"_"+EachSplitted+".png"); newPath = kiss.replace(os.sep, '/')
        f.write("\includegraphics[scale=0.5]{"+str(newPath)+"}\n")
f.close()
# -----
# *****
# QUATERNARIES
# *****
f = open("ST_data.LateX.out", "a")
for k in FILES:
    FNam = ((k.split("\\"))[-4]); #print(FNam)
    if str(FNam) == QUATERNARIES[0]:
        print("yes")

```



```

EachFile = (path+str(k)).rsplit("\\",1)[0]
EachSplitted = ((path+str(k)).rsplit("\\",1)[-1]).split(".ST_IDT")[0]
kiss = (EachFile+"/{"+FNam+"_"+EachSplitted+"}.png"); newPath = kiss.replace(os.sep, '/')
f.write("\includegraphics[scale=0.5]{"+str(newPath)+"}\n")
f.close()

```

12.1.2. Plotter RCM

```

#!/usr/bin/env python
# -*- coding: utf-8 -*-
"""
Created on Wed Dec 5 17:23:58 2018
@C3 group- NUIGalway
@author: sergio
"""
import os
import sys
import glob
import numpy as np
import pandas as pd
import matplotlib.pyplot as plt
from matplotlib import rc,rcParams
from matplotlib import colors as mcolors
from cycler import cycler
# -----

counter = 0
dicfiles = {}; FILES = [];
dicdirs = {}; filesDirs = [];
for root, dirs, files in os.walk(".", topdown=False):
    for name in dirs:
        filesDirs.append(os.path.join(root, name))
        dicdirs[counter] = os.path.join(root, name)
        counter += 1
for root, dirs, files in os.walk(".", topdown=False):
    for k in filesDirs:
        File2track = k.rsplit("\\",1)[-1]; #print(File2track)
        for name in files:
            #print(os.path.join(root, name))
            if "NUIGMech1.1" in str(name):
                pass
            elif "21_08_C4" in str(name):
                pass
            elif "21_08_C4_ahmed" in str(name):
                pass
            elif File2track+".RCM_IDT" == str(name):
                #if File2track+".png" == str(name):
                    FILES.append(os.path.join(root, name))
                    dicfiles[counter] = os.path.join(root, name)
                    counter += 1

```

```

#print(os.path.join(root, name))
#print(dirs)
#print("LOL")
#print("FILES:")
#print(FILEs)
#print("DIRS:")
#print(filesDirs)

#Mechas = ["20_11_C4", "20_11_C4_100atmRate"]

#print(len(sys.argv))
print("\t> # of mechanism to plot: ", str(len(sys.argv)-1))

if (len(sys.argv)) == 2:
    Mechas = [sys.argv[1]]
elif (len(sys.argv)) == 3:
    Mechas = [sys.argv[1], sys.argv[2]]
elif (len(sys.argv)) == 4:
    Mechas = [sys.argv[1], sys.argv[2], sys.argv[3]]
elif (len(sys.argv)) == 5:
    Mechas = [sys.argv[1], sys.argv[2], sys.argv[3], sys.argv[4]]
elif (len(sys.argv)) == 6:
    Mechas = [sys.argv[1], sys.argv[2], sys.argv[3], sys.argv[4], sys.argv[5]]
elif (len(sys.argv)) == 7:
    print("\t> Error, plotter is only allowed to work with")
    print("\t> 3 mechanism names")
    print("\t> Au revoir!")
    sys.exit(1)
else:
    print("\t> Error, plotter needs an argument...")
    print("\t> e.g. >python PloterRCM.py AramcoMech1.3")
    print("\t> No extension cti/xml is required at the end of mechanism name")
    sys.exit(1)

#-----
print("\t> Mechanisms to plot", str(Mechas))
path = os.getcwd()
# EXPERIMENTS
#FILES = glob.glob(path+"\\EXP.dat");
#for p in range(2):
# READING EXPERIMENTAL INPUT FILE
subscript = str.maketrans("0123456789", "0123456789")

for i in FILES:
    readexp = pd.read_csv(i, names=['col'], sep="%s", engine="python");
    DroppingStuff = readexp[readexp.col.str.contains("!") == False]
    DroppingStuff2 = DroppingStuff[DroppingStuff.col.str.contains("TC") == False]
    dataRCM = pd.DataFrame(DroppingStuff2.col.str.split().tolist())
    ##### author and journal
    AUTHOR = ((readexp[readexp.col.str.contains("AUTHOR:")] ).iloc[0].str.split(':')[0][1])
    JOURNAL = ((readexp[readexp.col.str.contains("JOURNAL:")] ).iloc[0].str.split(':')[0][1])
    PDF = ((readexp[readexp.col.str.contains("PDF:")] ).iloc[0].str.split(':')[0][1])
    REACS = (readexp[readexp.col.str.contains("REAC:")] ).col.str.split(':')
# -----

```

```

REACTANTS = []
OxDil = []
DILS = []
FuelNamesList = []
# -----
SUMAVAL = []; #print(TimeScale);
for m in range(len(REACS)):
    REAC1 = REACS.iloc[m][1];
    SUMAVAL.append(float(REAC1.split()[-1]))
SumaRValues = sum(SUMAVAL); #print(SumaRValues)
# -----
if SumaRValues < 2:
    for u in range(len(REACS)):
        if "C" in REACS.iloc[u][1]:
            REAC1 = (REACS.iloc[u][1]); namb = round(float(REAC1.split()[-1])*100,3);
FuelNamesList.append(REAC1.split()[0]);
            REAC11 = str(namb)+"% "+str(REAC1.split()[-0]).translate(subscript) #":".join(REAC1.split())
            REACTANTS.append(REAC11)
        if "O2" in REACS.iloc[u][1]:
            REAC1 = REACS.iloc[u][1]; namb = round(float(REAC1.split()[-1])*100,3);
            REAC1 = str(namb)+"% "+str(REAC1.split()[-0]).translate(subscript) #":".join(REAC1.split())
            OxDil.append(REAC1)
        if "N2" in REACS.iloc[u][1]:
            REAC1 = REACS.iloc[u][1]; namb = round(float(REAC1.split()[-1])*100,3);
            if namb > 0:
                REAC1 = str(namb)+"% "+str(REAC1.split()[-0]).translate(subscript) #":".join(REAC1.split())
                DILS.append(REAC1)
            else:
                pass
        if "Ar" in REACS.iloc[u][1]:
            REAC1 = REACS.iloc[u][1]; namb = round(float(REAC1.split()[-1])*100,3);
            if namb > 0:
                REAC1 = str(namb)+"% Ar" #":".join(REAC1.split())
                DILS.append(REAC1)
            else:
                pass
        if "AR" in REACS.iloc[u][1]:
            REAC1 = REACS.iloc[u][1]; namb = round(float(REAC1.split()[-1])*100,3);
            if namb > 0:
                REAC1 = str(namb)+"% Ar" #":".join(REAC1.split())
                DILS.append(REAC1)
        if "CO2" in REACS.iloc[u][1]:
            REAC1 = REACS.iloc[u][1]; namb = round(float(REAC1.split()[-1])*100,3);
            if namb > 0:
                REAC1 = str(namb)+"% Ar" #":".join(REAC1.split())
                DILS.append(REAC1)
            else:
                pass
# -----
if SumaRValues >= 2:
    for u in range(len(REACS)):
        if "C" in REACS.iloc[u][1]:
            REAC1 = (REACS.iloc[u][1]); namb = round(float(REAC1.split()[-1]),3);
FuelNamesList.append(REAC1.split()[0]);
            REAC11 = str(namb)+"% "+str(REAC1.split()[-0]).translate(subscript) #":".join(REAC1.split())

```

```

    REACTANTS.append(REAC11)
if "O2" in REACS.iloc[u][1]:
    REAC1 = REACS.iloc[u][1]; namb = round(float(REAC1.split()[-1]),3);
    REAC1 = str(namb)+"% "+str(REAC1.split()[-0]).translate(subscript) #":".join(REAC1.split())
    OxDil.append(REAC1)
if "N2" in REACS.iloc[u][1]:
    REAC1 = REACS.iloc[u][1]; namb = round(float(REAC1.split()[-1]),3);
    if namb > 0:
        REAC1 = str(namb)+"% "+str(REAC1.split()[-0]).translate(subscript) #":".join(REAC1.split())
        DILS.append(REAC1)
    else:
        pass
if "Ar" in REACS.iloc[u][1]:
    REAC1 = REACS.iloc[u][1]; namb = round(float(REAC1.split()[-1]),3);
    if namb > 0:
        REAC1 = str(namb)+"% Ar" #":".join(REAC1.split())
        DILS.append(REAC1)
    else:
        pass
if "AR" in REACS.iloc[u][1]:
    REAC1 = REACS.iloc[u][1]; namb = round(float(REAC1.split()[-1]),3);
    if namb > 0:
        REAC1 = str(namb)+"% Ar" #":".join(REAC1.split())
        DILS.append(REAC1)
if "CO2" in REACS.iloc[u][1]:
    REAC1 = REACS.iloc[u][1]; namb = round(float(REAC1.split()[-1]),3);
    if namb > 0:
        REAC1 = str(namb)+"% Ar" #":".join(REAC1.split())
        DILS.append(REAC1)
    else:
        pass
# -----
REACTANTS = str(", ".join(REACTANTS)); OxDil = str(", ".join(OxDil))
DILS = str(", ".join(DILS));
#####
#for u in range(len(REACS)):
# if "N2" in REACS[u]:
#     print(str(REACS[u]))
####
print("t> Plotting directory/file/case: ",i)
temp = pd.to_numeric(dataRCM.iloc[:,2]);
idt = pd.to_numeric(dataRCM.iloc[:,5]);
tempplot = 1000/temp;
idtplot = (idt); Yerr = [(0.2*x) for x in idt]
# activate latex text rendering
plt.rcParams["font.weight"] = "bold"
plt.tick_params(axis='both', direction='out', length=4, width=3, labelsize=10)
plt.rcParams["axes.labelweight"] = "bold"
plt.rcParams["axes.linewidth"] = "3"
plt.rc('axes', prop_cycle=(cyclor('color', ['k','r', 'b','g','m'])))
legend_properties = {'weight':'bold'}
plt.yscale("log")
plt.scatter(tempplot,idtplot, marker="s", label='Exp Data', lw=4,color='black')
plt.errorbar(tempplot,idtplot, yerr=Yerr, label=None, fmt='none', ecolor="k" )
# SIMULATIONS

```

```

for j in Mechas:
    FoldName = ((i.rsplit("\",1))[0]); FNam = ((i.split("\")[0]); #print(FoldName)
    specs = '\'+str(FoldName);
    FILESS = glob.glob(FoldName+'\\'+j+'.RCM_IDT');
    #print(FILESS)
    plt.yscale("log")
    for m in range(len(FILESS)):
        legend_properties = {'weight':'bold'}
        readmod = pd.read_table(FILESS[m]);
        mech = (((FILESS[m].split("\")[0]).split('.RCM_IDT'))[0];
        tempMod2 = (readmod.iloc[:,4]);
        tempMod2 = [x for x in tempMod2]; tempMod2 = sorted(tempMod2,reverse=True)
        idtTMod2 = (readmod.iloc[:,6]); #readmod['IDT/s',reverse=True);
        idtTMod2 = [1000*(x) for x in idtTMod2]
        idtTMod2 = sorted((idtTMod2),reverse=True)
        idtMod2 = (readmod.iloc[:,5]); #readmod['IDT/s',reverse=True);
        if readmod.iloc[0,5] > 1:
            idtMod2 = [(x) for x in idtMod2]
        else:
            idtMod2 = [1000*(x) for x in idtMod2]
        idtMod2 = sorted((idtMod2),reverse=True)
        #FUEL = readmod.iloc[0,9]; FUEL1st = (str(FUEL).split(":")[0]
        #print(tempMod2,idtMod2);
        tempMod = []; idtMod = [];
        for m in range(len(idtMod2)):
            if idtMod2[m] > 0:
                idtMod.append(idtMod2[m])
                tempMod.append(tempMod2[m])
            elif idtMod2[m] == 0 and idtTMod2[m] > 0:
                idtMod.append(idtTMod2[m])
                tempMod.append(tempMod2[m])
            elif idtMod2[m] < 0:
                idtMod.append(idtTMod2[m])
                tempMod.append(tempMod2[m])
            elif idtMod2[m] < 0 and idtTMod2[m] < 0:
                idtMod.append(0.0)
                tempMod.append(tempMod2[m])

CASE = REACTANTS # i.split("\")[1];
initconds = FoldName.split("\")[0]; PHIs = initconds.split("_")[0];
PRESss = (initconds.split("_")[1]).rsplit("ATM",1)[0]; PRESs = (PRESss)
if PHIs == "F050":
    title = str(CASE)+"\n "+str(OxDil)+" ", "+str(DILS)+"\n $phi$ = 0.5, "+str(PRESs)+" atm";
elif PHIs == "F100":
    title = str(CASE)+"\n "+str(OxDil)+" ", "+str(DILS)+"\n $phi$ = 1.0, "+str(PRESs)+" atm";
elif PHIs == "F200":
    title = str(CASE)+"\n "+str(OxDil)+" ", "+str(DILS)+"\n $phi$ = 2.0, "+str(PRESs)+" atm";
else:
    title = str(CASE)+"\n "+str(OxDil)+" ", "+str(DILS)+"\n "+str(PHIs)+" ", "+str(PRESs)+" atm";
plt.yscale("log");
if str(mech) == str(Mechas[0]):
    print("Yes, {0} mechanism found!".format(mech)); mecham = mech;
    mecham = mech
    if mecham == "N13_C4_gas":
        mecham = "NUIGMech1.3"

```

```

elif mecham == "NUIGMech1.2_C4":
    mecham = "NUIGMech1.2"
elif mecham == "AM3.0":
    mecham = "AramcoMech3.0"
else:
    pass
print(mecham)
mech = mecham
plt.plot(tempMod, idtMod, linestyle='-', color="k", label=str(mech), lw=3)
elif str(mech) == str(Mechas[1]):
    print("Yes, NUIGMech1.1 mechanism found!");
    mecham = mech
    if mecham == "N13_C4_gas":
        mecham = "NUIGMech1.3"
    elif mecham == "NUIGMech1.2_C4":
        mecham = "NUIGMech1.2"
    elif mecham == "AM3.0":
        mecham = "AramcoMech3.0"
    else:
        pass
    print(mecham)
    mech = mecham
    plt.plot(tempMod, idtMod, linestyle='-',color="r", label=str(mech), lw=3)
else:
    mecham = mech
    if mecham == "N13_C4_gas":
        mecham = "NUIGMech1.3"
    elif mecham == "NUIGMech1.2_C4":
        mecham = "NUIGMech1.2"
    elif mecham == "AM3.0":
        mecham = "AramcoMech3.0"
    else:
        pass
    print(mecham)
    mech = mecham
    plt.plot(tempMod, idtMod, linestyle='--',label=str(mech), lw=3)
plt.title(title, fontsize=14, weight= 'bold')
plt.xlabel('1000 K /  $\{T\}$ ', fontsize=20, weight= 'bold');
plt.ylabel('IDT / ms', fontsize=20, weight= 'bold')
#plt.ylim( bottom = 0.5*min(idtplot),top=2*max(idtplot)) #bottom
plt.legend(frameon=True)#frameon=False); #plt.tight_layout()
plt.grid(b=True, which='major', color='grey', linestyle=':'); plt.grid(b=True, which='minor', color='grey',
linestyle=':')
#if "BAIGMOHOMMADI" in AUTHOR:
#    plt.annotate(str(AUTHOR)+" - NUIG", (0.5,0.3), (0, -50),bbox=dict(facecolor='white', alpha=0.8),
xycoords='axes fraction', textcoords='offset points', va='top'.)
#elif "RAMALINGAM" in AUTHOR:
#    plt.annotate(str(AUTHOR)+" - AACHEN", (0.5,0.3), (0, -50),bbox=dict(facecolor='white', alpha=0.8),
xycoords='axes fraction', textcoords='offset points', va='top')
#else:
#    plt.annotate(str(AUTHOR), (0.5,0.3), (0, -50),bbox=dict(facecolor='white', alpha=0.8), xycoords='axes fraction',
textcoords='offset points', va='top')
#plt.annotate(str(AUTHOR), (0.5,0.3), (0, -50), xycoords='axes fraction', textcoords='offset points', va='top')
#plt.annotate(str(PDF), (0.6,0.4), (0, -50), xycoords='axes fraction', textcoords='offset points', va='top')

```

```

    #plt.text(0.98*MaxX, MaxY, 'Solid line: '+str(mecham),horizontalalignment='left',verticalalignment='top',
fontsize=14)
    directory = FoldName.rsplit("\\",1)[0]; FoldNamee = FoldName.rsplit("\\",1)[-1]
    plt.tight_layout()
    plt.savefig( directory+"\\"+FNam+'_'+FoldNamee+'.png',dpi=500)
    plt.close()
    #plt.show()
#

path = os.getcwd()

# Get List of all images
FILES = glob.glob(path + "\\*\\RCM\\*\\.png', recursive=True)
# ---
# Block for monofuels:
# ---
###f = open("RCM_data.LateX.out", "w")
####print((FILES))
###for k in FILES:
###    FNam      = (k.split("\\")[-4]); #print(FNam+"\n")
###    FORCE      = (k.rsplit("\\",1)[0]); #print(FORCE+"\n")
###    EachSplitted = ((k.split("\\")[-1]).split(".png")[0]); #print(EachSplitted+"\n")
###    #print(k)
###    kiss = (FORCE+"/{"+EachSplitted+"}.png"); newPath = kiss.replace(os.sep, '/')
###    f.write("\\includegraphics[scale=0.5]{"+str(newPath)+"}\\n")
###f.close()

MONOS      = ["CH4", "C2H4", "C2H6", "C3H8"]
BINARIES   = ["CH4_C2H4", "CH4_C2H6", "C2H4_C2H6", "C2H4_C3H8", "C2H6_C3H8"]
TERNARIES  = ["CH4_C2H4_C2H6"]
QUATERNARIES = ["CH4_C2H4_C2H6_C3H8"]

#print(FILES[0])
# *****
# MONOS
# *****
f = open("RCM_data.LateX.out", "w")
for k in FILES:
    FNam      = ((k.split("\\")[-4]); #print(FNam)
    if str(FNam) == MONOS[0]:
        FORCE      = (k.rsplit("\\",1)[0]); #print(FORCE+"\n")
        EachSplitted = ((k.split("\\")[-1]).split(".png")[0]); #print(EachSplitted+"\n")
        kiss = (FORCE+"/{"+EachSplitted+"}.png"); newPath = kiss.replace(os.sep, '/')
        f.write("\\includegraphics[scale=0.5]{"+str(newPath)+"}\\n")
f.close()
f = open("RCM_data.LateX.out", "a")
for k in FILES:
    FNam      = ((k.split("\\")[-4]); #print(FNam)
    if str(FNam) == MONOS[1]:
        FORCE      = (k.rsplit("\\",1)[0]); #print(FORCE+"\n")
        EachSplitted = ((k.split("\\")[-1]).split(".png")[0]); #print(EachSplitted+"\n")
        kiss = (FORCE+"/{"+EachSplitted+"}.png"); newPath = kiss.replace(os.sep, '/')
        f.write("\\includegraphics[scale=0.5]{"+str(newPath)+"}\\n")
f.close()
f = open("RCM_data.LateX.out", "a")

```

```

for k in FILES:
    FNam      = ((k.split("\\"))[-4]); #print(FNAm)
    if str(FNAm) == MONOS[2]:
        FORCE      = (k.rsplit("\\,1")[0]); #print(FORCE+"\n")
        EachSplitted = ((k.split("\\"))[-1]).split(".png")[0]; #print(EachSplitted+"\n")
        kiss = (FORCE+/" "+EachSplitted+".png"); newPath = kiss.replace(os.sep, '/')
        f.write("\includegraphics[scale=0.5]{ "+str(newPath)+" }\n")
f.close()
f = open("RCM_data.LateX.out", "a")
for k in FILES:
    FNam      = ((k.split("\\"))[-4]); #print(FNAm)
    if str(FNAm) == MONOS[3]:
        FORCE      = (k.rsplit("\\,1")[0]); #print(FORCE+"\n")
        EachSplitted = ((k.split("\\"))[-1]).split(".png")[0]; #print(EachSplitted+"\n")
        kiss = (FORCE+/" "+EachSplitted+".png"); newPath = kiss.replace(os.sep, '/')
        f.write("\includegraphics[scale=0.5]{ "+str(newPath)+" }\n")
f.close()
# -----
# *****
# BINARIES
# *****
f = open("RCM_data.LateX.out", "a")
for k in FILES:
    FNam      = ((k.split("\\"))[-4]); #print(FNAm)
    if str(FNAm) == BINARIES[0]:
        FORCE      = (k.rsplit("\\,1")[0]); #print(FORCE+"\n")
        EachSplitted = ((k.split("\\"))[-1]).split(".png")[0]; #print(EachSplitted+"\n")
        kiss = (FORCE+/" "+EachSplitted+".png"); newPath = kiss.replace(os.sep, '/')
        f.write("\includegraphics[scale=0.5]{ "+str(newPath)+" }\n")
f.close()
f = open("RCM_data.LateX.out", "a")
for k in FILES:
    FNam      = ((k.split("\\"))[-4]); #print(FNAm)
    if str(FNAm) == BINARIES[1]:
        FORCE      = (k.rsplit("\\,1")[0]); #print(FORCE+"\n")
        EachSplitted = ((k.split("\\"))[-1]).split(".png")[0]; #print(EachSplitted+"\n")
        kiss = (FORCE+/" "+EachSplitted+".png"); newPath = kiss.replace(os.sep, '/')
        f.write("\includegraphics[scale=0.5]{ "+str(newPath)+" }\n")
f.close()
f = open("RCM_data.LateX.out", "a")
for k in FILES:
    FNam      = ((k.split("\\"))[-4]); #print(FNAm)
    if str(FNAm) == BINARIES[2]:
        FORCE      = (k.rsplit("\\,1")[0]); #print(FORCE+"\n")
        EachSplitted = ((k.split("\\"))[-1]).split(".png")[0]; #print(EachSplitted+"\n")
        kiss = (FORCE+/" "+EachSplitted+".png"); newPath = kiss.replace(os.sep, '/')
        f.write("\includegraphics[scale=0.5]{ "+str(newPath)+" }\n")
f.close()
f = open("RCM_data.LateX.out", "a")
for k in FILES:
    FNam      = ((k.split("\\"))[-4]); #print(FNAm)
    if str(FNAm) == BINARIES[3]:
        FORCE      = (k.rsplit("\\,1")[0]); #print(FORCE+"\n")
        EachSplitted = ((k.split("\\"))[-1]).split(".png")[0]; #print(EachSplitted+"\n")
        kiss = (FORCE+/" "+EachSplitted+".png"); newPath = kiss.replace(os.sep, '/')

```



```

        f.write("\includegraphics[scale=0.5]{"+str(newPath)+"}\n")
f.close()
f = open("RCM_data.LateX.out", "a")
for k in FILES:
    FNam      = ((k.split("\")[0]); #print(FNam)
    if str(FNam) == BINARIES[4]:
        FORCE   = (k.rsplit("\",1)[0]); #print(FORCE+"\n")
        EachSplitted = ((k.split("\")[0]).split(".png")[0]); #print(EachSplitted+"\n")
        kiss = (FORCE+"/{"+EachSplitted+"}.png"); newPath = kiss.replace(os.sep, '/')
        f.write("\includegraphics[scale=0.5]{"+str(newPath)+"}\n")
f.close()
# -----
# *****
# TERNARIES
# *****
f = open("RCM_data.LateX.out", "a")
for k in FILES:
    FNam      = ((k.split("\")[0]); #print(FNam)
    if str(FNam) == TERNARIES[0]:
        FORCE   = (k.rsplit("\",1)[0]); #print(FORCE+"\n")
        EachSplitted = ((k.split("\")[0]).split(".png")[0]); #print(EachSplitted+"\n")
        kiss = (FORCE+"/{"+EachSplitted+"}.png"); newPath = kiss.replace(os.sep, '/')
        f.write("\includegraphics[scale=0.5]{"+str(newPath)+"}\n")
f.close()
# -----
# *****
# QUATERNARIES
# *****
f = open("RCM_data.LateX.out", "a")
for k in FILES:
    FNam      = ((k.split("\")[0]); #print(FNam)
    if str(FNam) == QUATERNARIES[0]:
        FORCE   = (k.rsplit("\",1)[0]); #print(FORCE+"\n")
        EachSplitted = ((k.split("\")[0]).split(".png")[0]); #print(EachSplitted+"\n")
        kiss = (FORCE+"/{"+EachSplitted+"}.png"); newPath = kiss.replace(os.sep, '/')
        f.write("\includegraphics[scale=0.5]{"+str(newPath)+"}\n")
f.close()

```

12.1.3. Plotter FR

```

#!/usr/bin/env python
# -*- coding: utf-8 -*-
"""

```

```

Created on Wed Dec 5 17:23:58 2018
@C3 group- NUIGalway
@author: sergio
"""

```

```

import os
import sys
import glob

```

```

import numpy as np
import pandas as pd
import matplotlib.pyplot as plt
from matplotlib import rc,rcParams
from matplotlib import colors as mcolors
from cycler import cycler
# -----
import statistics
from matplotlib.ticker import ScalarFormatter
# -----
def FileFinder(Expspath, ext):
    FILEFINDER = []
    # traverse whole directory
    for root, dirs, files in os.walk(Expspath):
        # select file name
        for file in files:
            # check the extension of files
            if file.endswith(ext):
                # print whole path of files
                FILEFINDER.append(os.path.join(root, file))
            else:
                pass
    return FILEFINDER
# -----
# -----
counter = 0
dicfiles = {}; FILES = [];
dicdirs = {}; filesDirs = [];
for root, dirs, files in os.walk(".", topdown=False):
    for name in files:
        if ".JSR_EXP" in str(name):
            FILES.append(os.path.join(root, name))
            dicfiles[counter] = os.path.join(root, name)
            counter += 1
# -----
print("\t> # of mechanism to plot: ",str(len(sys.argv)-1))

if (len(sys.argv)) == 2:
    Mechas = [sys.argv[1]]
elif (len(sys.argv)) == 3:
    Mechas = [sys.argv[1],sys.argv[2]]
elif (len(sys.argv)) == 4:
    Mechas = [sys.argv[1],sys.argv[2],sys.argv[3]]
elif (len(sys.argv)) == 5:
    Mechas = [sys.argv[1],sys.argv[2],sys.argv[3],sys.argv[4]]
elif (len(sys.argv)) == 6:
    Mechas = [sys.argv[1],sys.argv[2],sys.argv[3],sys.argv[4],sys.argv[5]]
elif (len(sys.argv)) == 7:
    print("\t> Error, plotter is only allowed to work with")
    print("\t> 3 mechanism names")
    print("\t> Au revoir!")
    sys.exit(1)
else:
    print("\t> Error, plotter needs an argument...")
    print("\t> e.g. >python PloterRCM.py AramcoMech1.3")

```

```

    print("\t> No extension cti/xml is required at the end of mechanism name")
    sys.exit(1)
# -----
print("\t> Mechanisms to plot", str(Mechas))
# -----
path = os.getcwd()
subscript = str.maketrans("0123456789", "0123456789")
# Block of reading experiments:

# If you wanna work with only one file, edit next line with the whole path of that file, and uncomment it (remove the
dash symbol #)
#FILES =
["C:\\DKM\\DATA\\DATA_SHELL_EXP\\CH4\\SPECIES_TIME\\NATIVE\\I_ATM_PYR_0.1.JSR_EXP"]

# If you wanna work with only one folder, edit next line with the whole path of that directory, and uncomment it
(remove the dash symbol #)
#FILES = glob.glob("C:\\DKM\\DATA\\DATA_SHELL_EXP\\CH4\\SPECIES_TIME\\NATIVE\\*.JSR_EXP")
#FILES = glob.glob("C:\\DKM\\DATA\\DATA_SHELL_EXP\\CH4\\JSR\\NATIVE\\*.JSR_EXP")

#print(FILES)

for i in FILES:
    FileJSR = pd.read_csv(i,names=['col'],sep="%s",engine="python");
    DSpeciesJSR = FileJSR[FileJSR.col.str.contains("!") == False]
    DSJSR = DSpeciesJSR[DSpeciesJSR.col.str.contains("TAU") == True]
    DataEspeciesJSR = pd.DataFrame((DSJSR.col.str.split()).tolist())
    DroppingStuff = FileJSR[FileJSR.col.str.contains("!") == False]
    DroppingStuff2 = DroppingStuff[DroppingStuff.col.str.contains("TAU") == False]
    dataJSR = pd.DataFrame((DroppingStuff2.col.str.split()).tolist())
    # *****
    Species = list(DataEspeciesJSR#.split('\t'))
    SP = len(Species);
    Prods = [];
    for k in range(SP):
        #print(DataEspeciesJSR.iloc[0,k])
        if str(DataEspeciesJSR.iloc[0,k]) == 'T/K':
            pass
        elif str(DataEspeciesJSR.iloc[0,k]) == 'P/ATM':
            pass
        elif str(DataEspeciesJSR.iloc[0,k]) == 'TAU/S':
            pass
        else:
            Prods.append(str(DataEspeciesJSR.iloc[0,k]))
    speciesToPlot = Prods
    #print(Species, SP, Prods, speciesToPlot, observables)

# *****
#### author and journal
AUTHOR = ((FileJSR[FileJSR.col.str.contains("AUTHOR:")] ).iloc[0].str.split(':')[0])[1]
JOURNAL = ((FileJSR[FileJSR.col.str.contains("JOURNAL:")] ).iloc[0].str.split(':')[0])[1]
PDF = ((FileJSR[FileJSR.col.str.contains("PDF:")] ).iloc[0].str.split(':')[0])[1]
PHI = ((FileJSR[FileJSR.col.str.contains("PHI:")] ).iloc[0].str.split(':')[0])[1]
REACS = (FileJSR[FileJSR.col.str.contains("REAC:")] ).col.str.split(':')
REACTANTS = []; OxDil = []; DILS = []; FuelNamesList = [];

```

```

print("\t Species: {0}".format(speciesToPlot))
SUMAVAL = [];
for m in range(len(REACS)):
    REAC1 = REACS.iloc[m][1];
    SUMAVAL.append(float(REAC1.split()[-1]))
SumaRValues = sum(SUMAVAL); #print(SumaRValues)
#*****
if SumaRValues < 2:
    for u in range(len(REACS)):
        if "C" in REACS.iloc[u][1]:
            REAC1 = (REACS.iloc[u][1]); namb = round(float(REAC1.split()[-1])*100,3);
FuelNamesList.append(REAC1.split()[0]);
            REAC11 = str(namb)+"% "+str(REAC1.split()[-0]).translate(subscript) #":".join(REAC1.split())
            REACTANTS.append(REAC11)
        if "O2" in REACS.iloc[u][1]:
            REAC1 = REACS.iloc[u][1]; namb = round(float(REAC1.split()[-1])*100,3);
            REAC1 = str(namb)+"% "+str(REAC1.split()[-0]).translate(subscript) #":".join(REAC1.split())
            OxDil.append(REAC1)
        if "N2" in REACS.iloc[u][1]:
            REAC1 = REACS.iloc[u][1]; namb = round(float(REAC1.split()[-1])*100,3);
            if namb > 0:
                REAC1 = str(namb)+"% "+str(REAC1.split()[-0]).translate(subscript) #":".join(REAC1.split())
                DILS.append(REAC1)
            else:
                pass
        if "Ar" in REACS.iloc[u][1]:
            REAC1 = REACS.iloc[u][1]; namb = round(float(REAC1.split()[-1])*100,3);
            if namb > 0:
                REAC1 = str(namb)+"% Ar" #":".join(REAC1.split())
                DILS.append(REAC1)
            else:
                pass
        if "AR" in REACS.iloc[u][1]:
            REAC1 = REACS.iloc[u][1]; namb = round(float(REAC1.split()[-1])*100,3);
            if namb > 0:
                REAC1 = str(namb)+"% Ar" #":".join(REAC1.split())
                DILS.append(REAC1)
        if "CO2" in REACS.iloc[u][1]:
            REAC1 = REACS.iloc[u][1]; namb = round(float(REAC1.split()[-1])*100,3);
            if namb > 0:
                REAC1 = str(namb)+"% Ar" #":".join(REAC1.split())
                DILS.append(REAC1)
            else:
                pass
#*****
if SumaRValues >= 2:
    for u in range(len(REACS)):
        if "C" in REACS.iloc[u][1]:
            REAC1 = (REACS.iloc[u][1]); namb = round(float(REAC1.split()[-1]),3);
FuelNamesList.append(REAC1.split()[0]);
            REAC11 = str(namb)+"% "+str(REAC1.split()[-0]).translate(subscript) #":".join(REAC1.split())
            REACTANTS.append(REAC11)
        if "O2" in REACS.iloc[u][1]:
            REAC1 = REACS.iloc[u][1]; namb = round(float(REAC1.split()[-1]),3);
            REAC1 = str(namb)+"% "+str(REAC1.split()[-0]).translate(subscript) #":".join(REAC1.split())

```

```

OxDil.append(REAC1)
if "N2" in REACS.iloc[u][1]:
    REAC1 = REACS.iloc[u][1]; namb = round(float(REAC1.split()[-1]),3);
    if namb > 0:
        REAC1 = str(namb)+"% "+str(REAC1.split()[-0]).translate(subscript) #":".join(REAC1.split())
        DILS.append(REAC1)
    else:
        pass
if "Ar" in REACS.iloc[u][1]:
    REAC1 = REACS.iloc[u][1]; namb = round(float(REAC1.split()[-1]),3);
    if namb > 0:
        REAC1 = str(namb)+"% Ar" #":".join(REAC1.split())
        DILS.append(REAC1)
    else:
        pass
if "AR" in REACS.iloc[u][1]:
    REAC1 = REACS.iloc[u][1]; namb = round(float(REAC1.split()[-1]),3);
    if namb > 0:
        REAC1 = str(namb)+"% Ar" #":".join(REAC1.split())
        DILS.append(REAC1)
if "CO2" in REACS.iloc[u][1]:
    REAC1 = REACS.iloc[u][1]; namb = round(float(REAC1.split()[-1]),3);
    if namb > 0:
        REAC1 = str(namb)+"% Ar" #":".join(REAC1.split())
        DILS.append(REAC1)
    else:
        pass
*****
REACTANTS = str(", ".join(REACTANTS)); OxDil = str(", ".join(OxDil))
DILS = str(", ".join(DILS)); FNam = str("_".join(FuelNamesList))
# .....
#print(REACTANTS, OxDil, DILS, FNam)
print("\\t> Plotting directory/file/case: ",i); #print(REACTANTS)
temp = pd.to_numeric(dataJSR.iloc[:,0]);
tempplot = pd.to_numeric(temp)
PCC = (dataSR.iloc[:,1]); CompressedPressureAverage = [];
for v in range(len(PCC)):
    CompressedPressureAverage.append(float(PCC.loc[v]))
PC = round(statistics.mean(CompressedPressureAverage),2)
for u in range(len(speciesToPlot)):
    # Activate latex text rendering
    Specie2plot1 = pd.to_numeric(dataJSR.iloc[:,u+3]); #print(tempplot,Specie2plot);
    plt.rcParams["font.weight"] = "bold"
    plt.tick_params(axis='both', direction='out', length=4, width=3, labelsz=10)
    plt.rcParams["axes.labelweight"] = "bold"
    plt.rcParams["axes.linewidth"] = 3
    plt.rc('axes', prop_cycle=(cycler('color', ['k','r','b','g','m'])))
    legend_properties = {'weight':'bold'}
    plt.scatter(tempplot,Specie2plot1, marker="s", label=str(Prods[u].translate(subscript)), lw=4,color='black')
    FoldName = ((i.rsplit("\\",1))[0]); #print(FoldName); print(Mechas)
    FoldNamee = ((i.rsplit("\\",1))[-1]); FoldNamee = FoldNamee.split(".JSR_EXP")[0]
    LineStyles = ['-', '--', '-.', ':'];
    # Reading Simulations:
for j in Mechas:
    specs = "\\'+str(FoldName);

```

```

FILESS = glob.glob(FoldName+"\\"+j+"\\"*+"\str(FoldNamee)+".SP_OUT");
if len(FILESS) > 0:
    readmod = pd.read_csv(FILESS[0],names=['col'],sep="%s",engine="python");
    DroppingStuff = readmod[readmod.col.str.contains("!") == False]
    dataJSRMod = pd.DataFrame(DroppingStuff.col.str.split().tolist())
    dataJSRMod = (dataJSRMod.rename(columns=dataJSRMod.iloc[0])).drop(dataJSRMod.index[0]) ;
#dataST.columns = dataST.iloc[0]
    legend_properties = {'weight':'bold'}
    dataJSRMod = dataJSRMod.reset_index(drop=True)
    tempMod = pd.to_numeric(dataJSRMod["T/K"]); #print(tempMod)
    Specie2plot2 = pd.to_numeric((dataJSRMod.iloc[:,u+5]));#print(Specie2plot2)
#
    SpecieExpAverageValue = [];
for w in range(len(Specie2plot1)):
        SpecieExpAverageValue.append(float(Specie2plot1.loc[w]))
    SEAAV = statistics.mean(SpecieExpAverageValue)
#
CASE = REACTANTS
# *****
if len(REACTANTS) == 0:
    title = str(OxDil)+"\n "+str(DILS)+"\n $\phi$ $ = "+str(PHL.strip() )+", "+str(PC)+" atm";
if len(OxDil) == 0:
    title = str(CASE)+"\n "+str(DILS)+"\n $\phi$ $ = "+str(PHL.strip() )+", "+str(PC)+" atm";
if len(DILS) == 0:
    title = str(CASE)+"\n "+str(OxDil)+"\n $\phi$ $ = "+str(PHL.strip() )+", "+str(PC)+" atm";
if len(REACTANTS) > 0 and len(OxDil) > 0 and len(DILS) > 0:
    title = str(CASE)+"\n "+str(OxDil)+"\n "+str(DILS)+"\n $\phi$ $ = "+str(PHL.strip() )+", "+str(PC)+" atm";
# *****
q = Mechas.index(j); #print(q); print(Mechas); print(j)
if q ==0:
    plt.plot(tempMod, Specie2plot2, linestyle= LineStyles[q], color="k", label=str(j), lw=3)
elif q ==1:
    plt.plot(tempMod, Specie2plot2, linestyle= LineStyles[q], color="k", label=str(j), lw=3)
elif q ==2:
    plt.plot(tempMod, Specie2plot2, linestyle= LineStyles[q], color="k", label=str(j), lw=3)
elif q ==3:
    plt.plot(tempMod, Specie2plot2, linestyle= LineStyles[q], color="k", label=str(j), lw=3)
plt.tick_params(axis = "y", which = "both", bottom = False, left = False)

plt.title(title, fontsize=14, weight= 'bold')
plt.xlabel('$\it{T} / K$', fontsize=20, weight= 'bold');
plt.ylabel('Mole fraction', fontsize=20, weight= 'bold')
plt.legend(fontsize="large",frameon=True)
plt.grid(b=True, which='major', color='grey', linestyle=':'); plt.grid(b=True, which='minor', color='grey',
linestyle=:)
if SEAAV > 0:
    MAX = 1.2*max(Specie2plot1);
    MIN = 0.1*min(Specie2plot1);
    plt.ylim(bottom=MIN,top=MAX)
elif SEAAV <= 0:
    MAX = 1.2*max(Specie2plot2);
    MIN = 0.1*min(Specie2plot2);
    plt.ylim(bottom=MIN,top=MAX)
plt.tight_layout();
elif len(FILESS) == 0:

```

```

    pass
    directory = FoldName
    if not os.path.isdir(directory+"\\j+\"\\JSRplots\\"):
        os.makedirs(directory+"\\j+\"\\JSRplots\\")
    plt.savefig( directory+"\\j+\"\\JSRplots\\"+"\\JSR_"+FNam+'_'+FoldNameee+'_'+str(Prods[u])+'.png',dpi=500)
    #plt.savefig( directory+"\\j+\"\\JSRplots\\"+"\\j+\"\\JSR_"+FNam+'_'+FoldNameee+'_'+str(Prods[u])+'.png',dpi=500)
    plt.close()
# -----
# ""

```

12.1.4. Plotter JSR

```

#!/usr/bin/env python
# -*- coding: utf-8 -*-
"""
Created on Wed Dec 5 17:23:58 2018
@C3 group- NUIGalway
@author: sergio
"""
import os
import sys
import glob
import numpy as np
import pandas as pd
import matplotlib.pyplot as plt
from matplotlib import rc,rcParams
from matplotlib import colors as mcolors
from cycler import cycler
# -----
import statistics
from matplotlib.ticker import ScalarFormatter
# -----
def FileFinder(Expspath, ext):
    FILEFINDER = []
    # traverse whole directory
    for root, dirs, files in os.walk(Expspath):
        # select file name
        for file in files:
            # check the extension of files
            if file.endswith(ext):
                # print whole path of files
                FILEFINDER.append(os.path.join(root, file))
            else:
                pass
    return FILEFINDER
# -----
# -----
counter = 0
dicfiles = {}; FILES = [];
dicdirs = {}; filesDirs = [];
for root, dirs, files in os.walk(".", topdown=False):

```

```

for name in files:
    if ".JSR_EXP" in str(name):
        FILES.append(os.path.join(root, name))
        dicfiles[counter] = os.path.join(root, name)
        counter += 1

# -----
print("\t> # of mechanism to plot: ",str(len(sys.argv)-1))

if (len(sys.argv)) == 2:
    Mechas = [sys.argv[1]]
elif (len(sys.argv)) == 3:
    Mechas = [sys.argv[1],sys.argv[2]]
elif (len(sys.argv)) == 4:
    Mechas = [sys.argv[1],sys.argv[2],sys.argv[3]]
elif (len(sys.argv)) == 5:
    Mechas = [sys.argv[1],sys.argv[2],sys.argv[3],sys.argv[4]]
elif (len(sys.argv)) == 6:
    Mechas = [sys.argv[1],sys.argv[2],sys.argv[3],sys.argv[4],sys.argv[5]]
elif (len(sys.argv)) == 7:
    print("\t> Error, plotter is only allowed to work with")
    print("\t> 3 mechanism names")
    print("\t> Au revoir!")
    sys.exit(1)
else:
    print("\t> Error, plotter needs an argument...")
    print("\t> e.g. >python PloterRCM.py AramcoMech1.3")
    print("\t> No extension cti/xml is required at the end of mechanism name")
    sys.exit(1)

# -----
print("\t> Mechanisms to plot", str(Mechas))
# -----
path = os.getcwd()
subscript = str.maketrans("0123456789", "0123456789")
# Block of reading experiments:

# If you wanna work with only one file, edit next line with the whole path of that file, and uncomment it (remove the
dash symbol #)
#FILES =
["C:\\DKM\\DATA\\DATA_SHELL_EXP\\CH4\\SPECIES_TIME\\NATIVE\\1_ATM_PYR_0.1.JSR_EXP"]

# If you wanna work with only one folder, edit next line with the whole path of that directory, and uncomment it
(remove the dash symbol #)
#FILES = glob.glob("C:\\DKM\\DATA\\DATA_SHELL_EXP\\CH4\\SPECIES_TIME\\NATIVE\\*.JSR_EXP")
#FILES = glob.glob("C:\\DKM\\DATA\\DATA_SHELL_EXP\\CH4\\JSR\\NATIVE\\*.JSR_EXP")

#print(FILES)

for i in FILES:
    FileJSR = pd.read_csv(i,names=['col'],sep="%s",engine="python");
    DSpeciesJSR = FileJSR[FileJSR.col.str.contains("!") == False]
    DSJSR = DSpeciesJSR[DSpeciesJSR.col.str.contains("TAU") == True]
    DataEspeciesJSR = pd.DataFrame((DSJSR.col.str.split()).tolist())
    DroppingStuff = FileJSR[FileJSR.col.str.contains("!") == False]
    DroppingStuff2 = DroppingStuff[DroppingStuff.col.str.contains("TAU") == False]
    dataJSR = pd.DataFrame((DroppingStuff2.col.str.split()).tolist())

```



```

# *****
Species = list(DataEspeciesJSR#.split('\t')
SP = len(Species);
Prods = [];
for k in range(SP):
#print(DataEspeciesJSR.iloc[0,k])
if str(DataEspeciesJSR.iloc[0,k]) == 'T/K':
pass
elif str(DataEspeciesJSR.iloc[0,k]) == 'P/ATM':
pass
elif str(DataEspeciesJSR.iloc[0,k]) == 'TAU/S':
pass
else:
Prods.append(str(DataEspeciesJSR.iloc[0,k]))
speciesToPlot = Prods
#print(Species, SP, Prods, speciesToPlot, observables)

# *****
#### author and journal
AUTHOR = ((FileJSR[FileJSR.col.str.contains("AUTHOR:")] ).iloc[0].str.split(':')[0][1]
JOURNAL = ((FileJSR[FileJSR.col.str.contains("JOURNAL:")] ).iloc[0].str.split(':')[0][1]
PDF = ((FileJSR[FileJSR.col.str.contains("PDF:")] ).iloc[0].str.split(':')[0][1]
PHI = ((FileJSR[FileJSR.col.str.contains("PHI:")] ).iloc[0].str.split(':')[0][1]
REACS = (FileJSR[FileJSR.col.str.contains("REAC:")] ).col.str.split(':')
REACTANTS = []; OxDil = []; DILS = []; FuelNamesList = [];
print("\t Species: {0}".format(speciesToPlot))
SUMAVAL = [];
for m in range(len(REACS)):
REAC1 = REACS.iloc[m][1];
SUMAVAL.append(float(REAC1.split()[-1]))
SumaRValues = sum(SUMAVAL); #print(SumaRValues)
#*****
if SumaRValues < 2:
for u in range(len(REACS)):
if "C" in REACS.iloc[u][1]:
REAC1 = (REACS.iloc[u][1]); namb = round(float(REAC1.split()[-1])*100,3);
FuelNamesList.append(REAC1.split()[0]);
REAC11 = str(namb)+"% "+str(REAC1.split()[-0]).translate(subscript) #":".join(REAC1.split())
REACTANTS.append(REAC11)
if "O2" in REACS.iloc[u][1]:
REAC1 = REACS.iloc[u][1]; namb = round(float(REAC1.split()[-1])*100,3);
REAC1 = str(namb)+"% "+str(REAC1.split()[-0]).translate(subscript) #":".join(REAC1.split())
OxDil.append(REAC1)
if "N2" in REACS.iloc[u][1]:
REAC1 = REACS.iloc[u][1]; namb = round(float(REAC1.split()[-1])*100,3);
if namb > 0:
REAC1 = str(namb)+"% "+str(REAC1.split()[-0]).translate(subscript) #":".join(REAC1.split())
DILS.append(REAC1)
else:
pass
if "Ar" in REACS.iloc[u][1]:
REAC1 = REACS.iloc[u][1]; namb = round(float(REAC1.split()[-1])*100,3);
if namb > 0:
REAC1 = str(namb)+"% Ar" #":".join(REAC1.split())

```

```

        DILS.append(REAC1)
    else:
        pass
    if "AR" in REACS.iloc[u][1]:
        REAC1 = REACS.iloc[u][1]; namb = round(float(REAC1.split()[-1])*100,3);
        if namb > 0:
            REAC1 = str(namb)+"% Ar" #:".join(REAC1.split())
            DILS.append(REAC1)
    if "CO2" in REACS.iloc[u][1]:
        REAC1 = REACS.iloc[u][1]; namb = round(float(REAC1.split()[-1])*100,3);
        if namb > 0:
            REAC1 = str(namb)+"% Ar" #:".join(REAC1.split())
            DILS.append(REAC1)
    else:
        pass
    *****
    if SumaRValues >= 2:
        for u in range(len(REACS)):
            if "C" in REACS.iloc[u][1]:
                REAC1 = (REACS.iloc[u][1]); namb = round(float(REAC1.split()[-1]),3);
                FuelNamesList.append(REAC1.split()[0]);
                REAC11 = str(namb)+"% "+str(REAC1.split()[-0]).translate(subscript) #:".join(REAC1.split())
                REACTANTS.append(REAC11)
            if "O2" in REACS.iloc[u][1]:
                REAC1 = REACS.iloc[u][1]; namb = round(float(REAC1.split()[-1]),3);
                REAC1 = str(namb)+"% "+str(REAC1.split()[-0]).translate(subscript) #:".join(REAC1.split())
                OxDil.append(REAC1)
            if "N2" in REACS.iloc[u][1]:
                REAC1 = REACS.iloc[u][1]; namb = round(float(REAC1.split()[-1]),3);
                if namb > 0:
                    REAC1 = str(namb)+"% "+str(REAC1.split()[-0]).translate(subscript) #:".join(REAC1.split())
                    DILS.append(REAC1)
            else:
                pass
            if "Ar" in REACS.iloc[u][1]:
                REAC1 = REACS.iloc[u][1]; namb = round(float(REAC1.split()[-1]),3);
                if namb > 0:
                    REAC1 = str(namb)+"% Ar" #:".join(REAC1.split())
                    DILS.append(REAC1)
            else:
                pass
            if "AR" in REACS.iloc[u][1]:
                REAC1 = REACS.iloc[u][1]; namb = round(float(REAC1.split()[-1]),3);
                if namb > 0:
                    REAC1 = str(namb)+"% Ar" #:".join(REAC1.split())
                    DILS.append(REAC1)
            if "CO2" in REACS.iloc[u][1]:
                REAC1 = REACS.iloc[u][1]; namb = round(float(REAC1.split()[-1]),3);
                if namb > 0:
                    REAC1 = str(namb)+"% Ar" #:".join(REAC1.split())
                    DILS.append(REAC1)
            else:
                pass
    *****
    REACTANTS = str(", ".join(REACTANTS)); OxDil = str(", ".join(OxDil))

```

```

DILS   = str(", ").join(DILS); FNam = str("_").join(FuelNamesList)
# .....
#print(REACTANTS, OxDi1, DILS, FNam)
print("< Plotting directory/file/case: ",i); #print(REACTANTS)
temp   = pd.to_numeric(dataJSR.iloc[:,0]);
tempplot = pd.to_numeric(temp)
PCC    = (dataJSR.iloc[:,1]); CompressedPressureAverage = [];
for v in range(len(PCC)):
    CompressedPressureAverage.append(float(PCC.loc[v]))
PC = round(statistics.mean(CompressedPressureAverage),2)
for u in range(len(speciesToPlot)):
    # Activate latex text rendering
    Specie2plot1 = pd.to_numeric(dataJSR.iloc[:,u+3]); #print(tempplot,Specie2plot);
    plt.rcParams["font.weight"] = "bold"
    plt.tick_params(axis='both', direction='out', length=4, width=3, labelsz=10)
    plt.rcParams["axes.labelweight"] = "bold"
    plt.rcParams["axes.linewidth"] = "3"
    plt.rc('axes', prop_cycle=(cycler('color', ['k','r', 'b','g','m'])))
    legend_properties = {'weight':'bold'}
    plt.scatter(tempplot,Specie2plot1, marker="s", label=str(Prods[u].translate(subscript)), lw=4,color='black')
    FoldName = ((i.rsplit("\\",1))[0]); #print(FoldName); print(Mechas)
    FoldNamee = ((i.rsplit("\\",1))[-1]); FoldNameee = FoldNameee.split(".JSR_EXP")[0]
    LineStyles = ['-','--','-.-',':'];
    # Reading Simulations:
    for j in Mechas:
        specs = "\\ "+str(FoldName);
        FILESS = glob.glob(FoldName+"\\ "+j+"\\*"+str(FoldNameee)+".SP_OUT");
        if len(FILESS) > 0:
            readmod = pd.read_csv(FILESS[0],names=['col'],sep="%s",engine="python");
            DroppingStuff = readmod[readmod.col.str.contains("!") == False]
            dataJSRMod = pd.DataFrame(DroppingStuff.col.str.split().tolist())
            dataJSRMod = (dataJSRMod.rename(columns=dataJSRMod.iloc[0])).drop(dataJSRMod.index[0] );
#dataST.columns = dataST.iloc[0]
            legend_properties = {'weight':'bold'}
            dataJSRMod = dataJSRMod.reset_index(drop=True)
            tempMod = pd.to_numeric(dataJSRMod["T/K"]); #print(tempMod)
            Specie2plot2 = pd.to_numeric((dataJSRMod.iloc[:,u+5]));#print(Specie2plot)
#
            SpecieExpAverageValue = [];
            for w in range(len(Specie2plot1)):
                SpecieExpAverageValue.append(float(Specie2plot1.loc[w]))
            SEAAV = statistics.mean(SpecieExpAverageValue)
#
            CASE = REACTANTS
            # *****
            if len(REACTANTS) == 0:
                title = str(OxDi1)+" "+str(DILS)+"\\n$\\phi$ = "+str(PHL.strip() )+", "+str(PC)+" atm";
            if len(OxDi1) == 0:
                title = str(CASE)+"\\n "+str(DILS)+"\\n$\\phi$ = "+str(PHL.strip() )+", "+str(PC)+" atm";
            if len(DILS) == 0:
                title = str(CASE)+"\\n "+str(OxDi1)+"\\n$\\phi$ = "+str(PHL.strip() )+", "+str(PC)+" atm";
            if len(REACTANTS) > 0 and len(OxDi1) > 0 and len(DILS) > 0:
                title = str(CASE)+"\\n "+str(OxDi1)+" "+str(DILS)+"\\n$\\phi$ = "+str(PHL.strip() )+", "+str(PC)+" atm";
            # *****
            q = Mechas.index(j); #print(q); print(Mechas); print(j)

```

```

if q ==0:
    plt.plot(tempMod, Specie2plot2, linestyle= LineStyles[q], color="k", label=str(j), lw=3)
elif q ==1:
    plt.plot(tempMod, Specie2plot2, linestyle= LineStyles[q], color="k", label=str(j), lw=3)
elif q ==2:
    plt.plot(tempMod, Specie2plot2, linestyle= LineStyles[q], color="k", label=str(j), lw=3)
elif q ==3:
    plt.plot(tempMod, Specie2plot2, linestyle= LineStyles[q], color="k", label=str(j), lw=3)
plt.tick_params(axis = "y", which = "both", bottom = False, left = False)

plt.title(title, fontsize=14, weight= 'bold')
plt.xlabel("${it{T}} / K$", fontsize=20, weight= 'bold');
plt.ylabel('Mole fraction', fontsize=20, weight= 'bold')
plt.legend(fontsize="large",frameon=True)
plt.grid(b=True, which='major', color='grey', linestyle=':'); plt.grid(b=True, which='minor', color='grey',
linestyle=':')
if SEAAV > 0:
    MAX   = 1.2*max(Specie2plot1);
    MIN   = 0.1*min(Specie2plot1);
    plt.ylim(bottom=MIN,top=MAX)
elif SEAAV <= 0:
    MAX   = 1.2*max(Specie2plot2);
    MIN   = 0.1*min(Specie2plot2);
    plt.ylim(bottom=MIN,top=MAX)
plt.tight_layout();
elif len(FILESS) == 0:
    pass
directory = FoldName
if not os.path.isdir(directory+"\\"+j+"\\JSRplots\\"):
    os.makedirs(directory+"\\"+j+"\\JSRplots\\")
plt.savefig( directory+"\\"+j+"\\JSRplots\\"+"\\JSR_"+FNam+'_'+FoldNamee+'_'+str(Prods[u])+'.png',dpi=500)
#plt.savefig( directory+"\\"+j+"\\JSRplots\\"+"\\"+FNam+'_'+FoldNamee+'_'+str(Prods[u])+'.png',dpi=500)
plt.close()

# -----
# ""

```

12.2. LaTeX to pdf generator

```

#!/usr/bin/env python
# -*- coding: utf-8 -*-
"""

```

```

Created on Wed Dec 5 17:23:58 2018
@C3 group- NUIGalway
@author: sergio
"""

```

```

import subprocess
import time
import os

```

```

import sys
import glob
import shutil
import subprocess
import numpy as np
import pandas as pd
import matplotlib.pyplot as plt
from matplotlib import rc,rcParams
from matplotlib import colors as mcolors
from cycler import cycler
import time
timestr = time.strftime("%d_%m_%Y")
print(timestr)
# -----
#from STplotter.py import
# -----

CWD    = os.getcwd();

MONOS    = ["CH4","C2H4","C2H6","C3H8"]
BINARIES = ["CH4_C2H4","CH4_C2H6","C2H4_C2H6","C2H4_C3H8","C2H6_C3H8"]
TERNARIES = ["CH4_C2H4_C2H6"]
QUATERNARIES = ["CH4_C2H4_C2H6_C3H8"]

STreader = pd.read_csv(CWD+"\\ST_data.LateX.out");
RCMreader = pd.read_csv(CWD+"\\RCM_data.LateX.out");

FileNameInit = "LatexOutputFile_"+timestr+".tex"
f = open(FileNameInit, "w")

f.write("%++++++++++++++++++++++++++++++++++++++++++++++++++++++++\n")
f.write("\\documentclass{article}                \n")
f.write("%++++++++++++++++++++++++++++++++++++++++++++++++++++++++\n")
f.write("% REQUESTED PACKAGES                \n")
f.write("%++++++++++++++++++++++++++++++++++++++++++++++++++++++++\n")
f.write("\\usepackage{fullpage} % USER REQUESTED PACKAGE \n")
f.write("\\usepackage{amssymb} % USER REQUESTED PACKAGE \n")
f.write("\\usepackage{amsmath} % USER REQUESTED PACKAGE \n")
f.write("\\usepackage{rotating} % USER REQUESTED PACKAGE \n")
f.write("\\usepackage{ctable} % USER REQUESTED PACKAGE \n")
f.write("\\usepackage{longtable} % USER REQUESTED PACKAGE \n")
f.write("\\usepackage{lscap} % USER REQUESTED PACKAGE \n")
f.write("\\usepackage{graphicx} % USER REQUESTED PACKAGE \n")
f.write("\\usepackage{color} % USER REQUESTED PACKAGE \n")
f.write("\\usepackage{subfig} % USER REQUESTED PACKAGE \n")
f.write("\\usepackage{caption} % USER REQUESTED PACKAGE \n")
f.write("\\usepackage{hyperref} % USER REQUESTED PACKAGE \n")
f.write("\\usepackage{makeidx} % USER REQUESTED PACKAGE \n")
f.write("%++++++++++++++++++++++++++++++++++++++++++++++++++++++++\n")
f.write("\\makeindex\n")
f.write("%++++++++++++++++++++++++++++++++++++++++++++++++++++++++\n")
f.write("% TITLE INFORMATION                \n")
f.write("%++++++++++++++++++++++++++++++++++++++++++++++++++++++++\n")
f.write("\\title{\\textbf{\\break \\Huge Combustion Chemistry Centre} \n")
f.write("\\break \\textbf{\\LARGE National University of Ireland Galway}}\n")

```

```

f.write("\\")
f.write("\\textbf{NUIGMech1.2\_C4 \\ VS \\ NUIGMech1.3\_C4 \\ Mechanism \\ validation}\\n")
f.write("\\break \\textit{Chemical Kinetics Report:\\n")
f.write("\\ Single C1, C2, and C3\\n")
f.write("\\ Binary, Ternary and Quaternary blends\\n")
f.write("\\ of gaseous hydrocarbons}\\n")
f.write("\\date{\\today}\\n")
f.write("\\author{Sergio Martinez}\\n")
f.write("%++++++\\n")
f.write("\\begin{document}\\n")
f.write("\\maketitle\\n")
f.write("\\tableofcontents{ }\\n")
#f.write("\\listoffigures\\n")
f.write("\\clearpage\\n")

f.write("%++++++\\n")
f.write("% Introduction\\n")
f.write("%++++++\\n")
#f.write("\\section{Introduction}\\n")
#f.write("\\subsection{How to cite NUIGMech1.1:}\\n")
#f.write("\\paragraph{NUIGMech1.1 - October 2nd 2020 \\ Important notice: NUIGMech1.0 Published first in citation
no 1 below. Please cite all papers below when referencing it.}\\n")
#f.write("\\paragraph{1. M. Baigmohammadi, V. Patel, S. Nagaraja, A. Ramalingam, S. Martinez, S. Panigrahy, A.
Mohamed, K.P. Somers, U. Burke, K.A. Heufer, A. Pekalski, H.J. Curran, Comprehensive experimental and simulation
study of the ignition delay time characteristics of binary blended methane, ethane, and ethylene over a wide range of
temperature, pressure, equivalence ratio, and dilution, Energy Fuels 34 (2020) 8808-8823.\\n")
#f.write("\\ 2. S.S. Nagaraja, J. Liang, S. Dong, S. Panigrahy, A.B. Sahu, G. Kukkadapu, W.J. Pitz, H.J. Curran, A
hierarchical single-pulse shock tube pyrolysis study of C2-C6 1-alkenes, Combustion and Flame 219 (2020) 456-466.
\\n")
#f.write("\\ 3. N. Lokachari, S. Panigrahy, G. Kukkadapu, G. Kim, T. MacDougall, S. Vasu, W.J. Pitz, H.J. Curran,
The influence of isobutene kinetics on the reactivity of di-isobutylene and iso-octane, Combustion and Flame 222
(2020) 186-195.
\\n")
#f.write("\\ 4. S. Panigrahy, J. Liang, S.S. Nagaraja, Z. Zuo, G. Kim, T. MacDougall, S.S. Vasu, H.J. Curran, A
comprehensive experimental and improved kinetic modeling study on the pyrolysis and oxidation of propyne,
Proceedings of the Combustion Institute 38 (2021) accepted.
\\n")
#f.write("\\ 5. A. Abd El-Sabor Mohamed, S. Panigrahy, A.B. Sahu, G. Bourque, H.J. Curran, An experimental and
modeling study of the auto-ignition of natural gas blends containing C1-C7 n-alkanes, Proceedings of the Combustion
Institute 38 (2021) accepted.
\\n")
#f.write("\\ 6. S.S. Nagaraja, J. Power, G. Kukkadapu, S. Dong, S.W. Wagnon, W.J. Pitz, H.J. Curran, A single pulse
shock tube study of pentene isomer pyrolysis, Proceedings of the Combustion Institute 38 (2021) accepted.
\\n")
#f.write("\\ 7. S. Dong, K. Zhang, P.K. Senecal, G. Kukkadapu, S.W. Wagnon, S. Barrett, N. Lokachari, S. Panigrahy,
W.J. Pitz, H.J. Curran, A comparative reactivity study of 1-alkene fuels from ethylene to 1-heptene, Proceedings of the
Combustion Institute 38 (2021) accepted.
\\n")
#f.write("\\ 8. S. Dong, K. Zhang, E.M. Ninnemann, A. Najjar, G. Kukkadapu, J. Baker, F. Arafin, Z. Wang, W.J. Pitz,
S.S. Vasu, S.M. Sarathy, P.K. Senecal, H.J. Curran, A comprehensive experimental and kinetic modeling study of 1-
and 2-pentene, Combustion and Flame (2021)
accepted.
}}\\n")
#f.write("\\subsection{Main changes: from NUIGMech1.0 to NUIGMech1.1}\\n")
#f.write("\\paragraph{This is just an illustrative document to compare mechanism's performance.}\\n")

```

```

f.write("%+++++\n")
f.write("% Single Fuels Section:\n")
f.write("%+++++\n")
f.write("\section{Single Fuel Section}\n")
f.write("\subsection{Shock Tube Validation:}\n")
f.write("\begin{center}\n")
for k in range(len(STreader)):
    FNam = ((str(STreader.iloc[k,0]).split('/'))[-4]);
    if str(FNam) == MONOS[0]:
        f.write(str(STreader.iloc[k,0])+"\n")
    if str(FNam) == MONOS[1]:
        f.write(str(STreader.iloc[k,0])+"\n")
    if str(FNam) == MONOS[2]:
        f.write(str(STreader.iloc[k,0])+"\n")
    if str(FNam) == MONOS[3]:
        f.write(str(STreader.iloc[k,0])+"\n")
f.write("%+++++\n")
f.write("\subsection{Rapid Compression Machine Validation:}\n")
for k in range(len(RCMreader)):
    FNam = ((str(RCMreader.iloc[k,0]).split('/'))[-4]);
    if str(FNam) == MONOS[0]:
        f.write(str(RCMreader.iloc[k,0])+"\n")
    if str(FNam) == MONOS[1]:
        f.write(str(RCMreader.iloc[k,0])+"\n")
    if str(FNam) == MONOS[2]:
        f.write(str(RCMreader.iloc[k,0])+"\n")
    if str(FNam) == MONOS[3]:
        f.write(str(RCMreader.iloc[k,0])+"\n")
f.write("\end{center}\n")
f.write("\clearpage\n")

f.write("%+++++\n")
f.write("% Binary Blends Section:\n")
f.write("%+++++\n")
f.write("\section{Binary Blends Section}\n")
f.write("\subsection{Shock Tube Validation:}\n")
f.write("\begin{center}\n")
for k in range(len(STreader)):
    FNam = ((str(STreader.iloc[k,0]).split('/'))[-4]);
    if str(FNam) == BINARIES[0]:
        f.write(str(STreader.iloc[k,0])+"\n")
    if str(FNam) == BINARIES[1]:
        f.write(str(STreader.iloc[k,0])+"\n")
    if str(FNam) == BINARIES[2]:
        f.write(str(STreader.iloc[k,0])+"\n")
    if str(FNam) == BINARIES[3]:
        f.write(str(STreader.iloc[k,0])+"\n")
    if str(FNam) == BINARIES[4]:
        f.write(str(STreader.iloc[k,0])+"\n")
f.write("%+++++\n")
f.write("\subsection{Rapid Compression Machine Validation:}\n")
for k in range(len(RCMreader)):
    FNam = ((str(RCMreader.iloc[k,0]).split('/'))[-4]);
    if str(FNam) == BINARIES[0]:
        f.write(str(RCMreader.iloc[k,0])+"\n")

```

```

    if str(FNam) == BINARIES[1]:
        f.write(str(RCMreader.iloc[k,0])+"\n")
    if str(FNam) == BINARIES[2]:
        f.write(str(RCMreader.iloc[k,0])+"\n")
    if str(FNam) == BINARIES[3]:
        f.write(str(RCMreader.iloc[k,0])+"\n")
    if str(FNam) == BINARIES[4]:
        f.write(str(RCMreader.iloc[k,0])+"\n")
f.write("\end{center}\n")
f.write("\clearpage\n")

f.write("%+++++\n")
f.write("% Ternary Blends Section:\n")
f.write("%+++++\n")
f.write("\section{Ternary Blends Section}\n")
f.write("\subsection{Shock Tube Validation:}\n")
f.write("\begin{center}\n")
for k in range(len(STreader)):
    FNam = ((str(STreader.iloc[k,0]).split('/'))[-4]);
    if str(FNam) == TERNARIES[0]:
        f.write(str(STreader.iloc[k,0])+"\n")
f.write("%+++++\n")
f.write("\subsection{Rapid Compression Machine Validation:}\n")
for k in range(len(RCMreader)):
    FNam = ((str(RCMreader.iloc[k,0]).split('/'))[-4]);
    if str(FNam) == TERNARIES[0]:
        f.write(str(RCMreader.iloc[k,0])+"\n")
f.write("\end{center}\n")
f.write("\clearpage\n")

f.write("%+++++\n")
f.write("% Quaternary Blends Section:\n")
f.write("%+++++\n")
f.write("\section{Quaternary Blends Section}\n")
f.write("\subsection{Shock Tube Validation:}\n")
f.write("\begin{center}\n")
for k in range(len(STreader)):
    FNam = ((str(STreader.iloc[k,0]).split('/'))[-4]);
    if str(FNam) == QUATERNARIES[0]:
        f.write(str(STreader.iloc[k,0])+"\n")
f.write("%+++++\n")
f.write("\subsection{Rapid Compression Machine Validation:}\n")
for k in range(len(RCMreader)):
    FNam = ((str(RCMreader.iloc[k,0]).split('/'))[-4]);
    if str(FNam) == QUATERNARIES[0]:
        f.write(str(RCMreader.iloc[k,0])+"\n")
f.write("\end{center}\n")
f.write("\clearpage\n")

f.write("\printindex{\n")
f.write("\end{document}")
f.close()

```



```

for k in range(2):
    subprocess.call(["pdflatex",FileNameInit])
#
#time.sleep(5)
#
#pdfreader = "C:\\Program Files (x86)\\Adobe\\Acrobat Reader DC\\Reader\\AcroRd32.exe"
#pre, ext = os.path.splitext(FileNameInit)
#pdfoutput = pre + ".pdf"
#
#subprocess.call([pdfreader,pdfoutput])

```

13. Python main subroutine code for Unix-Slurm servers

```

#####
# " Eppur si muove, Sinead na Paor - S.M. (2020-3986) " #
# ++++++
# Import Modules
# ++++++

import sys
import os
import stat
import subprocess
from subprocess import call
from itertools import izip_longest
from DosTitles.DosTitles import PrintDosHeader

# ++++++
#print"Edited paths and ICHEC project by VPatel on 01/08/2021 "
#print"\n"
#print"/\\"*25
#print" All cleaned!           "
#print" Thanks for use this Code      "
#print" HOPE YOU ENJOY IT!           "
#print"                               "
#print" Guv + A*(guv) = [8*(pi)*G]/(Tuv)      "
#print" Hope all your problems stay beyond      "
#print" the boundary of the event horizon,      "
#print" so they won't affect you any more...    "
#print" Gral. Rel. Eq. Albert Einstein      "

```

```

#print"
#print" @JMSPSoft@ ^>.< ^ @SineadnaPoir Subroutine@ "
#print"      U      "
#print"      |____|      "
#print"      \___/      "
#print" S.M. 16/01/2020      "
#print"/\\ "*25
#####
## La mujer perfecta... #
## 15/01/2020 C3-JMSP #
## NUIGALWAY, IE #
## IT - 103 BUILDING #
#####
"""

```

example(s):

```

f = open("jobST.sh","w+")
f.write("#!/bin/sh\n")
f.write("#SBATCH -t 01:00:00\n")
f.write("#SBATCH -p DevQ\n")
f.write("#SBATCH -N 1\n")
f.write("#SBATCH -A ngche114c\n")
f.write("#SBATCH --job-name=ST\n")
f.write("\n")
f.write("cd $SLURM_SUBMIT_DIR\n")
f.write("\n")
f.write("module load taskfarm\n")
f.write("module load conda/2\n")
f.write("source activate val\n")
f.write("\n")
f.write("time taskfarm tasksST\n")
f.close()

```

```

f = open("jobRCM.sh","w+")
f.write("#!/bin/sh\n")
f.write("#SBATCH -t 05:00:00\n")
f.write("#SBATCH -p ProdQ\n")
f.write("#SBATCH -N 1\n")
f.write("#SBATCH -A ngche114c\n")
f.write("#SBATCH --job-name=RCM\n")
f.write("\n")
f.write("cd $SLURM_SUBMIT_DIR\n")
f.write("\n")
f.write("module load taskfarm\n")
f.write("module load conda/2\n")
f.write("source activate val\n")
f.write("\n")
f.write("time taskfarm tasksRCM\n")
f.close()

```

"""

```

# ++++++
# Reads in the bin control file that contains paths to databases/folders that
# are regularly used -- takes as input the name of the BinCon file
# ++++++

```

```

def ReadBinControlFile(file_path,inp_file_bin):
# ++++++
# Read in the BinCon file
# ++++++
PrintDosHeader("", "=", 90)
print(">Reading BinCon File:", file_path)
PrintDosHeader("", "=", 90)
dict = {
    "ExpsPath": "/ichec/work/ngche114c/vpatel/DKM/DATA/",
    "ModelsPath": "/ichec/work/ngche114c/vpatel/DKM/MODELS/",
    "OutputPath": "/ichec/work/ngche114c/vpatel/DKM/OUTPUTDATA/",
    "ExpDB": inp_file_bin,
    "ModelDB": inp_file_bin
}
# ++++++
# ++++++
# Open the file, read it in, and provide
# a dictionary containing keys that provide
# paths to certain bins
# ++++++
return(dict)

# ++++++
# ++++++
# Gets a list of subdirectories and files within the path provided
# ++++++

def GetDirFileLists(base_path):
# ++++++
# Walk the dir and return lists of files, dirs etc.
# ++++++
returnval = "Yes"
DirList = []
FileList = []
for root, dirs, files in os.walk(base_path, topdown=True):
    DirList.append(root)
    for f in files:
        FileList.append(os.path.join(root, f))
return(DirList, FileList)
# ++++++
# ++++++

CWD      = "/ichec/work/ngche114c/vpatel/DKM/DATA/"

if (len(sys.argv)) == 5:
    ListOfSpecies = str(sys.argv[2]).rsplit(',')
    ST = []
    RCM = []
    LBV = []
    JSR = []
    FR = []
    BIN = []
    DIRS = []; FILES = []; WPATH = []
    for k in ListOfSpecies:

```

```

        WPath = CWD+k; WPATH.append(WPath)
        Dirs,Files = GetDirFileLists(str(WPath))
        for j in range(len(Dirs)):
            DIRS.append(Dirs[j]);
        for j in range(len(Files)):
            FILES.append(Files[j])
# Reading all the data in directories/subdirs inside
counter = 1
for i in FILES:
    if i.endswith('.ST_IDT'):
        ST.append(i)
    elif i.endswith('.RCM_IDT'):
        RCM.append(i)
    elif i.endswith('.FPF_EXP'):
        LBV.append(i)
    elif i.endswith('.JSR_EXP'):
        JSR.append(i)
    elif i.endswith('.FR_EXP'):
        FR.append(i)
    else:
        BIN.append(i)
Dirs = DIRS; Files = FILES; WPath = WPATH

else:
    Dirs,Files = GetDirFileLists(CWD)
    ST = []
    RCM = []
    LBV = []
    JSR = []
    FR = []
    BIN = []
    counter = 1
    for i in Files:
        if i.endswith('.ST_IDT'):
            ST.append(i)
        elif i.endswith('.RCM_IDT'):
            RCM.append(i)
        elif i.endswith('.FPF_EXP'):
            LBV.append(i)
        elif i.endswith('.JSR_EXP'):
            JSR.append(i)
        elif i.endswith('.FR_EXP'):
            FR.append(i)
        else:
            BIN.append(i)
    WPath = [CWD]
print"-.*20
print"\tRunning SdP... "
print"\tICHEC version1.0"
print"\tS.M.-C3-NUIGalway, IE"
print"\t0b11111100100"
print"\t01001010,01001101,01010011,01010000"
print"\t0b11111010101"
print"-.*20
print"\n"

```

```

print"\t> Working path given:"
for b in WPath:
    print"\t"+str(b)
print"+"*60
print"\t> Directories: ",len(Dirs)
print"\t> Files: ",len(Files)
print"+"*60
print"+"*60
print"\t> ST files: ",len(ST)
print"\t> RCM files: ",len(RCM)
print"\t> LBV files: ",len(LBV)
print"\t> JSR files: ",len(JSR)
print"\t> FR files: ",len(FR)
print"\t> Total Reac files: ",len(ST)+len(RCM)+len(LBV)+len(JSR)+len(FR)
print"\t Others formats : ",len(BIN)
print"\t Total files scanned: ",len(ST)+len(RCM)+len(LBV)+len(JSR)+len(FR)+len(BIN)
print"+"*60
if (len(sys.argv) > 1):
    if str(sys.argv[1]) == "ST":
        # Generating all slurm files to run individual simulations
        # Making a control bash script file to run all the simulations in one go...

        f = open("jobST_"+str(sys.argv[3])+".sh","w+")
        #f = open("jobST.sh","w+")
        f.write("#!/bin/sh\n")
        f.write("#SBATCH -t 1:00:00\n")
        f.write("#SBATCH -p DevQ\n")
        f.write("#SBATCH -N 1\n")
        f.write("#SBATCH -A ngche114c\n")
        f.write("#SBATCH --job-name=ST\n")
        f.write("\n")
        f.write("cd $SLURM_SUBMIT_DIR\n")
        f.write("\n")
        f.write("module load taskfarm\n")
        f.write("module load conda/2\n")
        f.write("source activate val\n")
        f.write("\n")
        f.write("time taskfarm tasksST_"+str(sys.argv[3]))
        #f.write("time taskfarm tasksST\n")
        f.close()

        # Giving privileges to st.sh file, to execute from python
        # Making a control bash script file to run all the simulations in one go...

        f = open("tasksST_"+str(sys.argv[3]),"w+")
        #f = open("tasksST","w+")
        f.close()

    for i in ST:
        subprocess.call("./probST_"+str(sys.argv[3])+".sh "+i+" "+str(sys.argv[4]),shell=True)
        #subprocess.call("./probST.sh "+i+" "+str(sys.argv[4]),shell=True)
        ### Here add the calling to BASH to run all simulations prepared before

        f = open("callST.sh","w+")
        f.write("#!/bin/sh\n")

```

```

f.write("sbatch jobST_"+str(sys.argv[3])+".sh")
#f.write("sbatch jobST.sh")
f.close()
other = os.stat("callST.sh")
os.chmod("callST.sh",other.st_mode | stat.S_IEXEC)
subprocess.call("./callST.sh")
os.remove("callST.sh")
#####
# RCM
#####
elif str(sys.argv[1]) == "RCM":
    # Generating all slurm files to run individual simulations
    # Making a control bash script file to run all the simulations in one go... ProdQ/DevQ

    f = open("jobRCM_"+str(sys.argv[3])+".sh","w+")
    f.write("#!/bin/sh\n")
    f.write("#SBATCH -t 8:00:00\n")
    f.write("#SBATCH -p ProdQ\n")
    f.write("#SBATCH -N 1\n")
    f.write("#SBATCH -A ngche114c\n")
    f.write("#SBATCH --job-name=RCM\n")
    f.write("\n")
    f.write("cd $SLURM_SUBMIT_DIR\n")
    f.write("\n")
    f.write("module load taskfarm\n")
    f.write("module load conda/2\n")
    f.write("source activate val\n")
    f.write("\n")
    f.write("time taskfarm tasksRCM_"+str(sys.argv[3]))
    f.close()
    #print(str(sys.argv[3]))
    # Giving privileges to st.sh file, to execute from python
    # Making a control bash script file to run all the simulations in one go...
    f = open("tasksRCM_"+str(sys.argv[3]),"w+")
    f.close()

    ### Reading all the data in directories/subdirs inside "/ichec/work/ngche079c/sergito/DKM/DATA"

    for i in RCM:
        subprocess.call("./probRCM_"+str(sys.argv[3])+".sh "+i+" "+str(sys.argv[4]),shell=True)

    ### Here add the calling to BASH to run all simulations prepared before

    f = open("callRCM.sh","w+")
    f.write("#!/bin/sh\n")
    f.write("sbatch jobRCM_"+str(sys.argv[3])+".sh")
    f.close()
    other = os.stat("callRCM.sh")
    os.chmod("callRCM.sh",other.st_mode | stat.S_IEXEC)
    subprocess.call("./callRCM.sh")
    os.remove("callRCM.sh")
# ###
# LBV
# ###
elif str(sys.argv[1]) == "LBV":

```

```
# Generating all slurm files to run individual simulations
# Making a control bash script file to run all the simulations in one go... ProdQ/DevQ
```

```
f = open("jobLBV_"+str(sys.argv[3])+".sh","w+")
#f = open("jobLBV.sh","w+")
f.write("#!/bin/sh\n")
f.write("#SBATCH -t 72:00:00\n")
f.write("#SBATCH -p ProdQ\n")
f.write("#SBATCH -N 1\n")
f.write("#SBATCH -A ngche114c\n")
f.write("#SBATCH --job-name=LBV\n")
f.write("\n")
f.write("cd $SLURM_SUBMIT_DIR\n")
f.write("\n")
f.write("module load taskfarm\n")
f.write("module load conda/2\n")
f.write("source activate val\n")
f.write("\n")
f.write("time taskfarm tasksLBV_"+str(sys.argv[3]))
#f.write("time taskfarm tasksLBV\n")
f.close()
```

```
# Giving privileges to st.sh file, to execute from python
# Making a control bash script file to run all the simulations in one go...
```

```
f = open("tasksLBV_"+str(sys.argv[3]),"w+")
#f = open("tasksLBV","w+")
f.close()
```

```
### Reading all the data in directories/subdirs inside "/ichec/work/ngche101c/vpatel/DKM/DATA"
```

```
for i in LBV:
```

```
    subprocess.call("./probLBV_"+str(sys.argv[3])+".sh "+i+" "+str(sys.argv[4]), shell=True)
    #subprocess.call("./probLBV.sh "+i,shell=True)
```

```
### Here add the calling to BASH to run all simulations prepared before
```

```
f = open("callLBV.sh","w+")
f.write("#!/bin/sh\n")
f.write("sbatch jobLBV_"+str(sys.argv[3])+".sh")
#f.write("sbatch jobLBV.sh")
f.close()
other = os.stat("callLBV.sh")
os.chmod("callLBV.sh",other.st_mode | stat.S_IEXEC)
subprocess.call("./callLBV.sh")
os.remove("callLBV.sh")
```

```
#
#
#
```

```
else:
```

```
    print("#"*75)
    print("\tSERGITO WARNING!!! PAY ATENTION!!!")
    print("#"*75)
    print("\t> Nothing to do here...")
    print("\t> You need to specify the reactor")
```

```

print("\t> Ex. > python DirTools.py ST")
#print(
print("\t> You are welcome, now run it again :)")
print("-"*75)
else:
    print("#"*75)
    print("\t SERGITO WARNING!!! PAY ATENTION!!!")
    print("#"*75)
    print("\t> Nothing to do here...")
    print("\t> You need to specify the reactor")
    print("\t> Ex. > python DirTools.py ST")
#####
## ALL YOU NEED IS LOVE! & Science :) S.M. #
#####
#print"\n"
#print"/\\"*25
#print" All cleaned!           "
#print" Thanks for use this Code      "
#print" HOPE YOU ENJOY IT!           "
#print"                               "
#print" Guv + A*(guv) = [8*(pi)*G]/(Tuv)  "
#print" Hope all your problems stay beyond "
#print" the boundary of the event horizon, "
#print" so they won't affect you any more... "
#print" Gral. Rel. Eq. Albert Einstein 1915 "
#print"                               "
#print" @      @ ^>.< ^ @      @ "
#print"      U      "
#print"      |__|      "
#print"      \_      "
#print" S.M.J.P. 16/01/2020      "
#print"/\\"*25
#####
## 15/01/2020 C3      #
## NUIGALWAY, IE      #
## IT - 103 BUILDING  #
#####

```


Appendix B

(Supplementary material for Chapter 4)

1. Design of experiments

According to the complexity of classical approaches for designing experiments, the Taguchi method is a robust approach to design complex experimental research through reducing experimental tests. This methodology is prominent when many experiments need to be performed in accordance to increasing numbers of variables. Hence, to handle experimental studies with many experiments, the Taguchi approach can tackle the issue using a specific design of orthogonal arrays which permits a comprehensive experimental investigation by doing a minimal number of experimental tests. In this regard, the minimum number of experiments is determined as follows:

$$N_{\text{Taguchi}} = 1 + NF(L - 1) \quad (\text{B4})$$

where, N_{Taguchi} , NF , and L are the number of experiments, number of factors, and number of levels, respectively. According to the Taguchi approach, its performance is optimal when there are limited interactions between desired variables. Therefore, in the current research, it was supposed that the interactions between the various factors and variables are negligible. To use the Taguchi method, it is essential to define the controlling factors and levels. According to the factors and levels, several design of experiments (DOE) matrices are available. For instance, as seen, if there are three or four factors (e.g. fuel composition; A, dilution level; B, equivalence ratio; C, and pressure; D) and 3 levels for each parameter (e.g. three pressure levels, 1.0, 20.0, and 40.0 bar) an L_9 orthogonal array can be employed to design the required experiments. According to Equation (B4) and one can easily determine N_{Taguchi} based on the number of factors and levels, which is 9. Therefore, an L_9 DOE matrix is required to cover such test numbers.

Table BS1. Applied factors/variables and levels for designing the current experiments (Quaternary blended $C_1 - C_3$ fuels) using the Taguchi method.

Factor levels	Fuel composition (A)	Dilution (B)	ϕ (C)	p_C (bar) (D)
1	80% CH_4 + 5% C_2H_4 + 10% C_2H_6 + 5% C_3H_8	75%	0.5	1.0
2	70% CH_4 + 10% C_2H_4 + 10% C_2H_6 + 10% C_3H_8	85%	1.0	20.0
3	60% CH_4 + 15% C_2H_4 + 15% C_2H_6 + 10% C_3H_8	90%	2.0	40.0

A sample form of a L₉ Taguchi array applied in the study is shown in the following:

A	B	C	D	A	B	C	D
1	1	1	1	80/10/5/5	75	0.5	1.0
1	2	2	2	80/10/5/5	85	1.0	20.0
1	3	3	3	80/10/5/5	90	2.0	40.0
2	1	2	3	70/10/10/10	75	1.0	40.0
2	2	3	1	70/10/10/10	85	2.0	1.0
2	3	1	2	70/10/10/10	90	0.5	20.0
3	1	3	2	60/15/15/10	75	2.0	20.0
3	2	1	3	60/15/15/10	85	0.5	40.0
3	3	2	1	60/15/15/10	90	1.0	1.0

As mentioned before, the selection of a proper DOE Taguchi matrix is only based on the number of desired parameters (here, fuel composition, pressure, equivalence ratio, and dilution percent) and their variation levels (here, three levels have been chosen (e.g., 0.5, 1.0, and 2.0 for equivalence ratio). In accordance to the selected parameters and their respective levels, the proper Taguchi matrix will give the least number of experiments which are required to get accurate results using the best configuration of the experiments with the desired levels [1]. However, it should be noted that, according to the statistical mathematics fundamentals which the Taguchi matrices are based upon, unnecessarily increasing the selected parameters and their respective levels (for example: increasing the parameters from 4 to 5 and the levels from 3 to 4) will significantly increase the number of tests (from L₉ with 9 configurations to L₁₆ with 16 configurations) and consequently substantially increase the required time needed to complete the experimental test array. Therefore, regarding the available data in literature, it was decided to select main parameters of fuel composition, pressure, equivalence ratio, and dilution percent as study parameters with three levels to satisfy the requirements of the study.

2. Applied gases for making the mixtures

As mentioned in Section 2 of the manuscript, in the current study, the ignition delay time (IDT) characteristics of methane/ethylene/ethane (CH₄/C₂H₄/C₂H₆) and methane/ethylene/ethane/propane (CH₄/C₂H₄/C₂H₆/C₃H₈) were investigated individually over a wide range of temperature, pressure, ethylene concentration, equivalence ratio, and dilution. For those experiments performed at the combustion chemistry centre (C³) NUI Galway, the alkane/alkene fuels of 99.5% (Grade: 2.5) purity were supplied through high pressure bottles which were provided from Air liquide UK. The other applied gases such as oxygen, argon, nitrogen, and helium in the experiments have been provided by BOC Ireland at purities of O₂ (99.99%), N₂ (99.99%), Ar (99.99%), and He (99.96%). However, for those experiments performed at the Physico-Chemical Fundamentals of Combustion (PCFC) of RWTH Aachen University, the applied methane, ethane, propane, ethylene gases with purity of 99.95% (Grade: 3.5) were provided by Westfalen AG. Also, the other

applied gases such as oxygen, argon, and nitrogen, in the experiments have been provided by Westfalen AG and Praxair with purities of O₂ ($\geq 99.995\%$), N₂ ($\geq 99.95\%$), and Ar ($\geq 99.996\%$).

3. Low-pressure shock tube

As known, shock-tube is a robust facility for getting the IDT data under low and high pressures and high temperature (≥ 1000 K) regimes and IDTs ≤ 2 ms. Thus, the NUIG-LPST has been used to measure IDT data at 1 bar. The applied NUIG-LPST has been previously documented and explained in detail [2, 3]. Here, only general information of the facility is presented in Table BS2. In the current study, He was used as the primary driver gas unless there was a need to reduce the incident shock velocity through adding nitrogen to helium for the tailored conditions.

Table BS2. Specifications of the applied low-pressure shock tube.

Total length		6.33 m	
Section	Length (m)	Diameter (mm)	
Driver	0.53	520	
Driven	5.8	102.4	
Material	Stainless steel		
Controlling system	Sharp edges arrow		
Diaphragm's material	Polycarbonate/Polyester		
Diaphragm's thickness	105–120 μm (nominal)		

Further, as presented in

Table BS3, the incident shock velocity has been measured using five piezoelectric pressure transducers located on the driven section of the LPST and then the shock velocity at the end-wall was extrapolated through a fitted line to the collected shock velocities over these pressure transducers. All of the conditions such as the compressed gas temperature (T_5) and pressure (p_5) behind the reflected shock were calculated using the shock velocity at the end-wall using “Gaseq” software [4]. Also, the ignition delay times of the studied mixtures were measured using photomultiplier (PMT) systems equipped with CH* filter (CWL: 430 nm \pm 10 FWHM; Thorlabs) installed on the side wall of the shock tube's endcap due to very weak pressure signals. Also, it is demonstrated in Figure that the ignition delay time is defined as a maximum gradient in pressure ($\left. \frac{dP}{dt} \right|_{max}$) or CH* ($\left. \frac{dCH^*}{dt} \right|_{max}$) behind the reflected shock. Further, for increasing the accuracy of experiments and reducing scattered points, all the measured pressures behind the reflected shocks have been forced to be restricted to ± 0.05 bar of the target pressure of 1 bar. In this regard, all pressure versus time data including oscilloscope

files (software is accessible through <https://www.tiepie.com/en/oscilloscope-software>) and the experimentalist spreadsheets related to the current studied conditions in NUIG–LPST are provided as the Supplementary data files.

Table BS3. Number of installed PCB sensors on the driven section of LPST shock tube and their distances from the end–wall.

Sensors	Distance from the end wall (m)
PCB#1	0.03
PCB#2	0.237
PCB#3	0.366
PCB#4	0.495
PCB#5	1.89

4. High-pressure shock tube

The NUIG-HPST has been used for getting the IDT data for 20 and 40 bar operating conditions. As already mentioned, the applied NUIG-HPST has been previously documented and explained in details [5] and ,here, only general information of the facility is presented. In the current study, helium was used as the primary driver gas for doing the experiments unless there was a need to reduce the incident shock velocity through adding nitrogen to helium for the tailored conditions.

Table BS4. Specifications of the applied high–pressure shock tube.

Total length		9.1 m
Section	Length (m)	Diameter (mm)
Driver	3.0	63.5
Middle	0.04	63.5
Driven	5.7	63.5
Material	Stainless-steel (1.4571/316Ti and 1.4462/F51)	
Controlling system	Double-diaphragm type	
Diaphragm’s material	Aluminium (1050 H14)	
Diaphragm’s thickness	0.8~2 mm; according to target pressure	
Pre-scoring the diaphragms	0.2~1.1 mm; according to target pressure and the diaphragms’ thickness	

Further, as presented in Table , the incident shock velocity has been measured using six piezoelectric pressure transducers located on the driven section of the HPST and then the shock velocity at the end-wall was extrapolated through a fitted line to the collected shock velocities over these pressure transducers. All of the

conditions such as the compressed gas temperature (T_5) and pressure (p_5) behind the reflected shock were calculated using the shock velocity at the end-wall through “Gaseq” software [4]. Also, the ignition delay times of the studied normal mixtures (pressure–time profiles) with diluent concentration of $\leq 85\%$ were recorded using a Kistler 603B transducer mounted at the end-wall, while for the mixtures with 90% dilution, the ignition delay times were measured using photodiode array detector (PDA) or photomultiplier (PMT) systems equipped with CH* filter (CWL: 430 nm \pm 10 FWHM; Thorlabs) installed on the side wall of the shock tube’s endcap due to very weak signals of the Kistler pressure transducer. For increasing the accuracy of experiments and reducing scattered points, all of the measured pressures behind the reflected shocks have been forced to be restricted to ± 0.5 bar of the target pressures (20 and 40 bar). Moreover, all of the experimental results have been divided into two main categories of the acceptable and the affected by facility, so that the affected results have been marked using “☒” symbol. Thus, these data wouldn’t be reliable to be applied for evaluating the performance of a chemical mechanism. In this regard, all of the pressure versus time data including oscilloscope files (software is accessible through <https://www.tiepie.com/en/oscilloscope-software>) and the experimentalist spreadsheets related to the current studied conditions in NUIG–HPST are provided as the Supplementary data files.

Table BS5. Number of installed PCB sensors on the driven section of the shock–tube and their distances from the end-wall.

Sensors	Distance from the end wall (m)
PCB#1	0.01
PCB#2	0.15
PCB#3	0.29
PCB#4	0.57
PCB#5	0.85
PCB#6	1.165

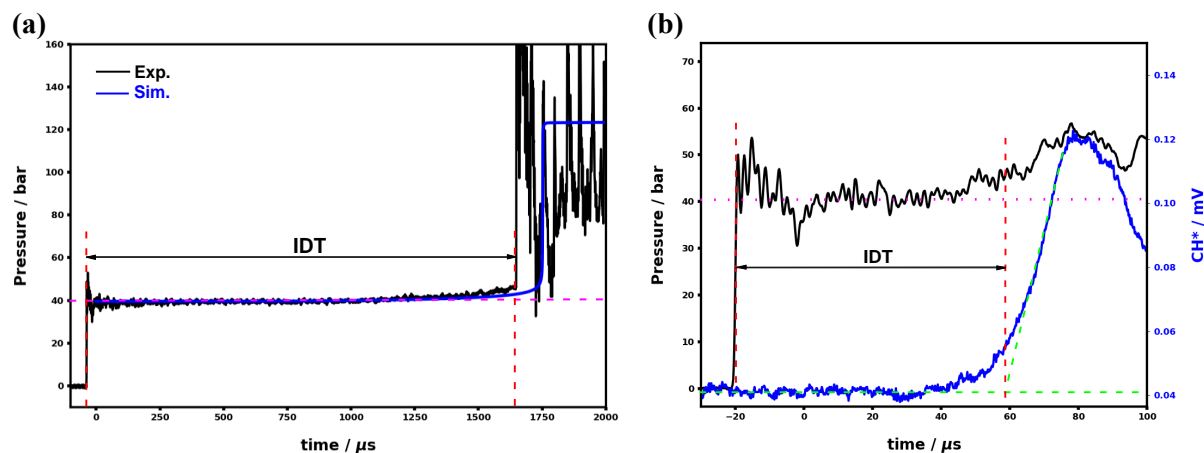


Figure BS1. Applied definition for measuring IDT in the NUIG–shock tubes: (a) using Kistler transducer’s pressure trace mounted on the end–wall; (b) using PMT/PDA–CH* trace mounted on the side wall of the end–cap.

5. Rapid compression machine

The rapid compression machine is a common facility to measure the IDT data under high pressure and low-to-intermediate temperature regimes (< 1000 K). In the current study, the experiments have been taken using NUIG- and PCFC-RCMs. According to the previous studies [6, 7], the experimental IDTs have been modelled using the adiabatic core assumption in which the non-adiabatic condition can be compensated by imposing the volume-time profiles of the same non-reactive mixtures to calculations. Thus, general information about each facility is presented in the following sub-sections.

5.1. NUIG-RCM

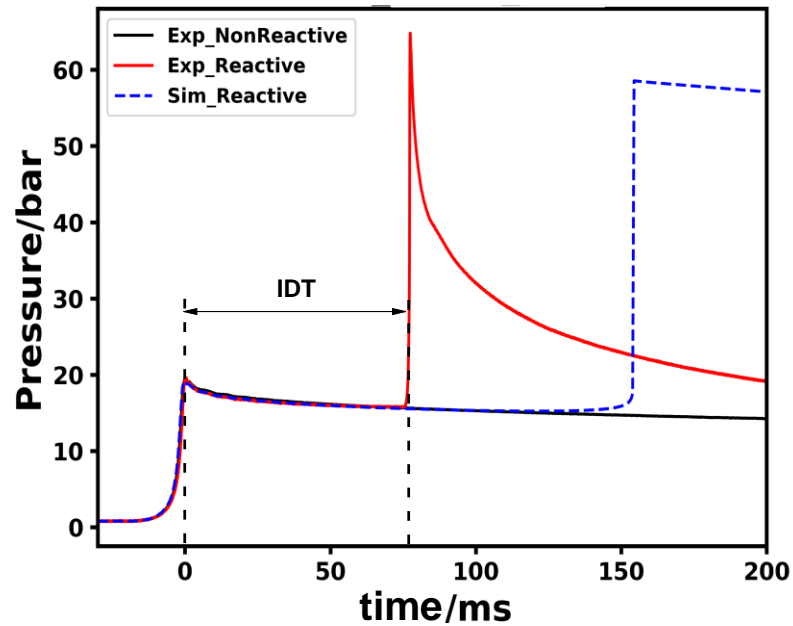
The general specifications of NUIG-RCM have been presented in Table . The details of the facility has been already documented and explained in details [5, 6, 8-11]. In this facility, the ignition delay time of the normal studied mixtures (diluent concentration = 75%) and the pressure–time histories of their relevant non–reactive mixtures were recorded using a Kistler 6045A transducer mounted on the reaction chamber. However, the ignition delay times of the mixtures with 85% and 90% dilution percent and the post-compression pressures of 20 and 40 bar, were reordered using both the Kistler and a photomultiplier (PMT) equipped with CH* filter (CWL: 430 nm \pm 10 FWHM; Thorlabs) due to vague signal of the Kistler pressure transducer under these conditions. Also, as shown in Figure , the ignition delay time is defined as a maximum gradient in pressure ($\left. \frac{dP}{dt} \right|_{max}$) or CH* ($\left. \frac{dCH^*}{dt} \right|_{max}$) after compressing the studied mixtures. Subsequently, the post compression temperatures (T_C) were calculated by assuming isentropic compression condition using Gaseq software [4]. Like the applied procedure in NUIG–HPST, all the measured post compression pressures (p_C) have been forced

to be restricted to ± 0.5 bar of the target pressures due to increasing the accuracy of experiments and also reducing the scattered points. Moreover, unlike the standard operating procedure in NUIG-HPST, all of the experimental results have been repeated at least three times and the repeatability of all of the reported IDTs was $\geq 90\%$. In this regard, all the pressure versus time profiles and the experimentalist spreadsheets related to the studied conditions in NUIG-RCM have been provided as the Supplementary files.

Table BS6. Specifications of NUIG-RCM.

Parameter	Value
Bore size of the reaction chamber (m)	0.03820
Volume of the reaction chamber (m ³)	3.3191×10^{-5}
Piston's velocity (U_p) (m/s)	9.34 ~ 12.94
Pistons' stroke length (m)	0.16817
Piston's type	Flat head with the crevice
Type	Twin-counter pistons

(a)



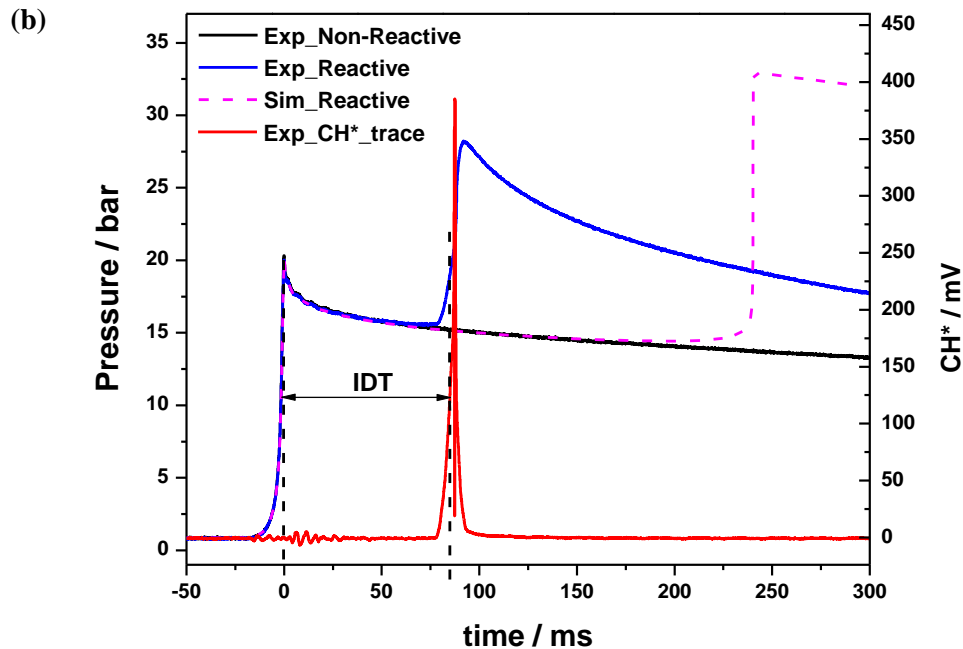


Figure BS2. Applied definition for measuring IDT in the NUIG-RCM: (a) using Kistler pressure trace; (b) using both pressure and PMT-CH* trace mounted on the side wall of the reaction chamber.

5.2. PCFC-RCM

The PCFC-RCM is a well-known facility which has been already introduced properly in literature. As presented in Table , this facility is constructed from a single-piston mechanism which is driven pneumatically and stopped hydraulically at the end of compression. Similar to the applied piston in NUIG-RCM, the crevice piston design has been applied in the PCFC-RCM. In the facility, the pressure–time profile during the compression and the post–compression processes and the initial temperature in the reaction chamber were monitored and controlled using a Kistler 6125C pressure transducer and type ‘T’ thermocouple, respectively. In this regard, the detail information about the construction, measurement procedure, and the applied sensors in the study have been already presented in [12]. As the same process explained in section 0, the compressed mixture’s temperature (T_c) was calculated using the isentropic compression formulation of Gaseq software [4]. According to the procedure explained by Ramalingam et al. [7], the reproducibility of evaluated IDTs and also the experimental uncertainty of the compressed mixture’s temperature for the measured conditions in the study were within 15% and ± 5 K, respectively. In this regard, the related experimental data to PCFC-RCM facility and the volume/time profiles are reported in the Supplementary files.

Table BS7. Specifications of PCFC-RCM.

Parameter	Value
Bore size of the reaction chamber (m)	0.05
Volume of the reaction chamber (m ³)	$5.06 \times 10^{-4} - 5.51 \times 10^{-4}$
Piston's velocity (U_p) (m/s)	16.67
Pistons' stroke length (m)	0.25
Piston's type	Flat head with the crevice
Type	Single piston

6. Data acquisition system

As shown in Table , in the current study, many sensors have been used in the four applied facilities at C³-NUIG and PCFC-RWTH Aachen University to measure the required parameters. In this regard, all of the installed sensors in the NUIG low and high-pressure shock tubes which had been used for measuring the incident shock velocities and the ignition delay times, were synchronized and connected to two TiePie Handyscope HS4 oscilloscopes [13]. Also, all of the generated signals from the installed sensors on NUIG-RCM including the Kistler pressure transducer, the position sensors, and the photomultiplier were synchronized and collected using a PicoScope 5443B [14].

Table BS8. Applied sensors and detectors for measuring during the current study (NUIG-HPST/RCM and PCFC-RCM).

Sensor	Company	Model	Accuracy	Resolution
Pressure sensor transducer	Kistler	603B	$\leq \pm 1.0\%$ FSO; linearity	NA
Pressure sensor transducer	Kistler	6045A	$\leq \pm 0.4\%$ /FSO; linearity	NA
Pressure sensor transducer	Kistler	6125C	$\leq \pm 0.4\%$ /FSO; linearity	NA
Piezoelectric pressure sensor	PCB	113B24	$\leq \pm 1.0\%$ FS; Non-linearity	± 0.035 KPa
Digital Absolut pressure transmitter	Kurt J Lesker	ACG & HCG	0.25% of FS	± 0.01 Torr
Digital Absolut pressure transmitter	Edwards	600 Barocel	0.15% of reading	± 0.01 of FS
Digital Absolut pressure transmitter	MKS	Baratron 121AA-0100D	0.5% of reading	± 0.01 Torr
Digital Absolut pressure transmitter	MKS	Baratron 121AA-01000D	0.5% of reading	± 0.1 Torr
Digital Absolut pressure transmitter	MKS	Baratron 121AA-05000B	0.5% of reading	± 0.5 Torr
Analog vacuum pressure gauge	Edwards	Pirani-PRE10K	NA	± 2 of reading scale
Thermocouples and Controller	Radionics	T-type	± 1.0 °C	± 0.1 °C
Photodetector	Thorlabs	PDA36A/PDA55	NA	NA
Photomultiplier	EMI Electronics	9924P	NA	NA

7. Uncertainty analysis

To gain a deep understanding about uncertainty of the experimental tests, following subsections have been presented. In fact, these subsections try to analytically explain the effect of some important factors including pressure, temperature, and equivalence ratio on the total uncertainty of the experimental results. It seems that the output of the section could provide a good clue for better analysing and evaluating the quality of the experimental data.

7.1. Equivalence ratio

In the following lines, it is tried to somehow evaluate probable uncertainties which may be included in equivalence ratios of the applied mixtures.

Making a mixture:

$$\text{Fuel: } F = P_F = \sum_{i=1}^n P_i \rightarrow \sigma_F = \sqrt{\sum_{i=1}^n \sigma_i^2} \quad (\text{B5})$$

Where, p_i and σ_i are absolute pressure of i -th component in the fuel mixture and uncertainty of each absolute pressure of i -th component in the fuel mixture, respectively. Because, in the current study, tertiary- and quaternary-fuels mixtures have been studied, thus: Fuel: $F = (p_{F1} \pm \sigma_{F1}) + (p_{F2} \pm \sigma_{F2}) + (p_{F3} \pm \sigma_{F3}) + (p_{F4} \pm \sigma_{F4})$ and Oxygen: $O = p_{O2} \pm \sigma_{O2}$.

$$\text{Equivalence ratio: } \varphi = \frac{\left(\frac{F}{O}\right)_{real}}{\left(\frac{F}{O}\right)_{stoi}} \rightarrow \left(\frac{O}{F}\right)_{stoi} = Cte \rightarrow \varphi = Cte \left(\frac{F_1+F_2+F_3+F_4}{O}\right)_{real} \rightarrow \sigma_\varphi = \left(\frac{\partial \varphi}{\partial F_1}\right) \sigma_{F_1} + \left(\frac{\partial \varphi}{\partial F_2}\right) \sigma_{F_2} + \left(\frac{\partial \varphi}{\partial F_3}\right) \sigma_{F_3} + \left(\frac{\partial \varphi}{\partial F_4}\right) \sigma_{F_4} + \left(\frac{\partial \varphi}{\partial O}\right) \sigma_O \quad (\text{B6})$$

$$\varphi = Cte \left(\frac{\sum_{i=1}^n p_{F_i}}{p_{O_2}}\right)_{real} \rightarrow \frac{\partial \varphi}{\partial p_{F_n}} = \frac{1}{O} \rightarrow \frac{\partial \varphi}{\partial p_{O_2}} = -\frac{\sum_{i=1}^n p_{F_i}}{(p_{O_2})^2}$$

$$\sigma_\varphi = \frac{\partial \varphi}{\partial p_{F_1}} \cdot \sigma_{p_{F_1}} + \frac{\partial \varphi}{\partial p_{F_2}} \cdot \sigma_{p_{F_2}} + \frac{\partial \varphi}{\partial p_{F_3}} \cdot \sigma_{p_{F_3}} + \dots + \frac{\partial \varphi}{\partial p_{F_n}} \cdot \sigma_{p_{F_n}} + \left(-\frac{\sum_{i=1}^n p_{F_i}}{(p_{O_2})^2}\right) \sigma_{p_{O_2}}$$

If we assume that there is no correlation between measurements of $\sigma_i \sigma_j = 0$

$$\sigma_\varphi^2 = \left(\frac{\partial \varphi}{\partial p_{F_1}} \cdot \sigma_{p_{F_1}}\right)^2 + \left(\frac{\partial \varphi}{\partial p_{F_2}} \cdot \sigma_{p_{F_2}}\right)^2 + \left(\frac{\partial \varphi}{\partial p_{F_3}} \cdot \sigma_{p_{F_3}}\right)^2 + \dots + \left(\frac{\partial \varphi}{\partial p_{F_n}} \cdot \sigma_{p_{F_n}}\right)^2 + \left(\left(-\frac{\sum_{i=1}^n p_{F_i}}{(p_{O_2})^2}\right) \sigma_{p_{O_2}}\right)^2$$

$$\sigma_\varphi = \sqrt{\left(\frac{1}{p_{O_2}} \cdot \sigma_{p_{F_1}}\right)^2 + \left(\frac{1}{p_{O_2}} \cdot \sigma_{p_{F_2}}\right)^2 + \left(\frac{1}{p_{O_2}} \cdot \sigma_{p_{F_3}}\right)^2 + \dots + \left(\frac{1}{p_{O_2}} \cdot \sigma_{p_{F_n}}\right)^2 + \left(\left(-\frac{\sum_{i=1}^n p_{F_i}}{(p_{O_2})^2}\right) \sigma_{p_{O_2}}\right)^2}$$

$$\sigma_\varphi = \sqrt{\left(\frac{\sum_{i=1}^n \sigma_{F_i}^2}{(p_{O_2})^2}\right) + \left(\left(-\frac{\sum_{i=1}^n p_{F_i}}{(p_{O_2})^2}\right) \sigma_{p_{O_2}}\right)^2} = \sqrt{\left(\frac{\sigma_{F_1}}{p_{O_2}}\right)^2 + \left(\frac{\sigma_{F_2}}{p_{O_2}}\right)^2 + \left(\frac{\sigma_{F_3}}{p_{O_2}}\right)^2 + \left(\frac{\sigma_{F_4}}{p_{O_2}}\right)^2 + \left(\left(-\frac{p_F}{p_{O_2}^2}\right) \sigma_{p_{O_2}}\right)^2} = \frac{cte}{(p_{O_2})^2} \sqrt{(p_{O_2})^2 \sigma_{F_1}^2 + (p_{O_2})^2 \sigma_{F_2}^2 + (p_{O_2})^2 \sigma_{F_3}^2 + (p_{O_2})^2 \sigma_{F_4}^2 + p_F^2 \sigma_{p_{O_2}}^2} \quad (B7)$$

Based on the above analysis, the average uncertainty of the equivalence ratios is $\overline{\sigma_\varphi} \approx \pm 5 \times 10^{-3}$.

7.2. Diluent concentration

For determining the uncertainty of diluent concentration in the studied mixtures the following formulations are presented:

$$[D] = \frac{p_i}{RT_i} \quad (B8)$$

$$\sigma_{[D]} = \frac{\partial [D]}{\partial p_i} \sigma_{p_i} \quad (B9)$$

$$\frac{\partial [D]}{\partial p_i} = \frac{1}{RT_i} \quad (B10)$$

Because, in the study, all mixtures have been prepared under 303 K, so the Equation (B9) would be as follows:

$$\frac{\partial [D]}{\partial p_i} = 3.96961 \times 10^{-4}$$

Therefore, the worst uncertainty in diluent concentration in the studied mixtures is related to cases with 90% diluent in a mixture with total pressure of 4000 Torr which yields $\sigma_{[D]} = \pm 1.05848 \frac{\text{mol}}{\text{m}^3} = \pm 1.05848 \times 10^{-5} \frac{\text{mol}}{10^5 \cdot \text{m}^3} \approx \pm 0.56\% [D]$.

For calculating the uncertainty in concentration of each species under the compressed conditions, the following formulations are presented:

$$[D] = \frac{p_{c,[D]}}{RT_c} \quad (B11)$$

$$\sigma_{[D]} = \sqrt{\left(\frac{\partial [D]}{\partial p_{c,[D]}} \sigma_{p_{c,[D]}}\right)^2 + \left(\frac{\partial [D]}{\partial T_c} \sigma_{T_c}\right)^2} \quad (B12)$$

$$\sigma_{[D]} = \sqrt{\left(\frac{1}{RT_c} \sigma_{p_{c,[D]}}\right)^2 + \left(-\frac{p_{c,[D]}}{RT_c^2} \sigma_{T_c}\right)^2} = \frac{1}{8.314 \times T_c^2} \sqrt{\left(T_c \sigma_{p_{c,[D]}}\right)^2 + \left(p_{c,[D]} \sigma_{T_c}\right)^2} \quad (B13)$$

7.3. IDTs in Shock tube

To determine the total uncertainty of the measured ignition delay times in NUIG-L/HPST, it is assumed:

$$p_5 = p(p_1, V_s, \varphi, T_1); T_5 = T(T_1, V_s, \varphi)$$

As shown by Petersen et al. [15], one could assume that:

$$T_5 = \frac{T_1[2(\gamma_1-1)M^2+(3-\gamma_1)][(3\gamma_1-1)M^2-2(\gamma_1-1)]}{(\gamma_1+1)^2M^2}; M = \frac{V_s}{\sqrt{\gamma_1RT_1}}; V_s = \frac{\Delta z}{\Delta t} \quad (\text{B14})$$

$$\sigma_{V_s} = \sqrt{\left(\frac{\partial V_s}{\partial(\Delta z)} \sigma_{\Delta z}\right)^2 + \left(\frac{\partial V_s}{\partial(\Delta t)} \sigma_{\Delta t}\right)^2} = \sqrt{\left(\frac{1}{\Delta t} \sigma_{\Delta z}\right)^2 + \left(-\frac{\Delta z}{(\Delta t)^2} \sigma_{\Delta t}\right)^2} \quad (\text{B15})$$

$$\sigma_{T_5} = \sigma_T = \frac{\partial T_c}{\partial M} \sigma_M = \left(T_1 \left[\left(\frac{4(3\gamma_1^2-4\gamma_1+1)}{(\gamma_1+1)^2}\right) M + \left(\frac{4(\gamma_1-1)(3-\gamma_1)}{(\gamma_1+1)^2}\right) M^{-3}\right]\right) \frac{\sigma_{V_s}}{\sqrt{\gamma_1RT_1}} \quad (\text{B16})$$

$$p_5 = \frac{p_1[2\gamma_1M^2-(\gamma_1-1)][(3\gamma_1-1)M^2-2(\gamma_1-1)]}{2(\gamma_1+1)+M^2(\gamma_1^2-1)}; \sigma_{p_5} = \sigma_p = \frac{\partial p_5}{\partial M} \sigma_M = \left(p_1 \left[\frac{12M^5\gamma^4-4M^5\gamma^3+48M^3\gamma^3+32M^3\gamma^2-12M^5\gamma^2+4M^5\gamma-16M^3\gamma-20M\gamma^3+4M\gamma^2+20M\gamma-4M\gamma^4}{(M^2\gamma^2-M^2+2\gamma+2)^2}\right]\right) \frac{\sigma_{V_s}}{\sqrt{\gamma_1RT_1}} \quad (\text{B17})$$

Here, it was supposed that the effect of changing in equivalence ratio on γ is negligible. Here, it is supposed that the maximum $\sigma_{\Delta t}$ which is related to TiePie Handyscope HS4 Oscilloscope is $\pm 1 \mu\text{s}$, and $\sigma_{\Delta z}$ is $\pm 0.001 \text{ m}$. Now, if it could be assumed that the ignition delay times (IDT) could be correlated as follows, then:

$$\tau_{IDT} \cong A \cdot \exp\left(\frac{B}{T}\right) p^m \varphi^n [D]^q \rightarrow \partial \tau = \frac{\partial \tau}{\partial T} \cdot \partial T + \frac{\partial \tau}{\partial p} \cdot \partial p + \frac{\partial \tau}{\partial \varphi} \cdot \partial \varphi + \frac{\partial \tau}{\partial [D]} \cdot \partial [D] \rightarrow (\sigma_{\tau})^2 = \left(\frac{\partial \tau}{\partial T} \cdot \partial T\right)^2 + \left(\frac{\partial \tau}{\partial p} \cdot \partial p\right)^2 + \left(\frac{\partial \tau}{\partial \varphi} \cdot \partial \varphi\right)^2 + \left(\frac{\partial \tau}{\partial [D]} \cdot \partial [D]\right)^2 + 2 \left(\frac{\partial \tau}{\partial T} \cdot \frac{\partial \tau}{\partial p} \cdot \partial T \partial p\right) + 2 \left(\frac{\partial \tau}{\partial T} \cdot \frac{\partial \tau}{\partial \varphi} \cdot \partial T \partial \varphi\right) + 2 \left(\frac{\partial \tau}{\partial T} \cdot \frac{\partial \tau}{\partial [D]} \cdot \partial T \partial [D]\right) + 2 \left(\frac{\partial \tau}{\partial p} \cdot \frac{\partial \tau}{\partial [D]} \cdot \partial p \partial [D]\right) + 2 \left(\frac{\partial \tau}{\partial \varphi} \cdot \frac{\partial \tau}{\partial [D]} \cdot \partial \varphi \partial [D]\right) \quad (\text{B18})$$

Now, one assumes that there is no correlation between measurements of (p , T , and φ), so the above equation would be followed by:

$$(\sigma_{\tau,i})^2 = \left(\frac{\partial \tau}{\partial T} \cdot \partial T\right)^2 + \left(\frac{\partial \tau}{\partial p} \cdot \partial p\right)^2 + \left(\frac{\partial \tau}{\partial \varphi} \cdot \partial \varphi\right)^2 + \left(\frac{\partial \tau}{\partial [D]} \cdot \partial [D]\right)^2 + 2 \left(\frac{\partial \tau}{\partial T} \cdot \frac{\partial \tau}{\partial p} \cdot \partial T \partial p\right) + 2 \left(\frac{\partial \tau}{\partial T} \cdot \frac{\partial \tau}{\partial \varphi} \cdot \partial T \partial \varphi\right) + 2 \left(\frac{\partial \tau}{\partial \varphi} \cdot \frac{\partial \tau}{\partial p} \cdot \partial \varphi \partial p\right) + 2 \left(\frac{\partial \tau}{\partial T} \cdot \frac{\partial \tau}{\partial [D]} \cdot \partial T \partial [D]\right) + 2 \left(\frac{\partial \tau}{\partial p} \cdot \frac{\partial \tau}{\partial [D]} \cdot \partial p \partial [D]\right) + 2 \left(\frac{\partial \tau}{\partial \varphi} \cdot \frac{\partial \tau}{\partial [D]} \cdot \partial \varphi \partial [D]\right) \quad (\text{B19})$$

One could re-write the above equation as follows:

$$(\sigma_{\tau,i})^2 = \left(\frac{\partial \tau}{\partial T} \cdot \sigma_T\right)^2 + \left(\frac{\partial \tau}{\partial p} \cdot \sigma_p\right)^2 + \left(\frac{\partial \tau}{\partial \varphi} \cdot \sigma_\varphi\right)^2 + \left(\frac{\partial \tau}{\partial [D]} \cdot \sigma_{[D]}\right)^2 + 2 \left(\frac{\partial \tau}{\partial T} \cdot \frac{\partial \tau}{\partial [D]} \cdot \sigma_T \sigma_{[D]}\right) + 2 \left(\frac{\partial \tau}{\partial p} \cdot \frac{\partial \tau}{\partial [D]} \cdot \sigma_p \sigma_{[D]}\right) \quad (\text{B20})$$

$$\frac{\partial \tau}{\partial T} = A \cdot \left(-\frac{B}{T^2} \cdot \exp\left(\frac{B}{T}\right) p^m \varphi^n [D]^q\right) \quad (\text{B21})$$

$$\frac{\partial \tau}{\partial p} = A \cdot \left(m \cdot \exp\left(\frac{B}{T}\right) p^{m-1} \varphi^n [D]^q\right) \quad (\text{B22})$$

$$\frac{\partial \tau}{\partial \varphi} = A \cdot \left(n \cdot \exp\left(\frac{B}{T}\right) p^m \varphi^{n-1} [D]^q\right) \quad (\text{B23})$$

$$\frac{\partial \tau}{\partial [D]} = A \cdot \left(q \cdot \exp\left(\frac{B}{T}\right) p^m \varphi^n [D]^{q-1} \right) \quad (\text{B24})$$

$$\begin{aligned} (\sigma_{\tau,i})^2 = & A^2 \cdot \left(\left(-\frac{B}{T^2} \cdot \exp\left(\frac{B}{T}\right) p^m \varphi^n [D]^q \right) \cdot \sigma_T \right)^2 + A^2 \cdot \left(\left(m \cdot \exp\left(\frac{B}{T}\right) p^{m-1} \varphi^n [D]^q \right) \cdot \sigma_p \right)^2 \\ & + A^2 \cdot \left(\left(n \cdot \exp\left(\frac{B}{T}\right) p^m \varphi^{n-1} [D]^q \right) \cdot \sigma_\varphi \right)^2 + A^2 \cdot \left(\left(q \cdot \exp\left(\frac{B}{T}\right) p^m \varphi^n [D]^{q-1} \right) \cdot \sigma_{[D]} \right)^2 \\ & - 2A^2 \left(\frac{Bq}{T^2} \cdot \exp\left(\frac{2B}{T}\right) p^{2m} \varphi^{2n} [D]^{2q-1} \right) \cdot \rho_{T[D]} \sigma_T \sigma_{[D]} \\ & + 2A^2 \left(qm \cdot \exp\left(\frac{2B}{T}\right) p^{2m-1} \varphi^{2n} [D]^{2q-1} \right) \cdot \rho_{p[D]} \sigma_p \sigma_{[D]} \end{aligned} \quad (\text{B25})$$

$$\sigma_{\tau,i} \cong A \cdot \sqrt{\left(\left(-\frac{B}{T^2} \cdot \exp\left(\frac{B}{T}\right) p^m \varphi^n [D]^q \right) \cdot \sigma_T \right)^2 + \left(\left(m \cdot \exp\left(\frac{B}{T}\right) p^{m-1} \varphi^n [D]^q \right) \cdot \sigma_p \right)^2 + \left(\left(n \cdot \exp\left(\frac{B}{T}\right) p^m \varphi^{n-1} [D]^q \right) \cdot \sigma_\varphi \right)^2 + \left(\left(q \cdot \exp\left(\frac{B}{T}\right) p^m \varphi^n [D]^{q-1} \right) \cdot \sigma_{[D]} \right)^2 - 2 \left(\frac{Bq}{T^2} \cdot \exp\left(\frac{2B}{T}\right) p^{2m} \varphi^{2n} [D]^{2q-1} \right) \cdot \rho_{T[D]} \sigma_T \sigma_{[D]} + 2 \left(qm \cdot \exp\left(\frac{2B}{T}\right) p^{2m-1} \varphi^{2n} [D]^{2q-1} \right) \cdot \rho_{p[D]} \sigma_p \sigma_{[D]} \right)} \quad (\text{B26})$$

$$\rho_{ij} \sigma_i \sigma_j = \sigma_{ij} = \sum_{ij} f(i,j) (x_i - \bar{x}_i) (x_j - \bar{x}_j) \quad (\text{B27})$$

The uncertainty of the measured ignition delay times in shock tube could be acceptably estimated using the above equations. As seen in the above expressions, the uncertainty is changing by changing in the compressed temperature and pressure, and equivalence ratio, so that it is not a constant parameter during experimental tests. Thus, it should be calculated specifically for each case. Therefore, regarding Eq. 23 and Table , specific uncertainty for each fuel according to its specific temperature, pressure, and equivalence ratio could be estimated.

Table BS9. Correlation variables of the studied experimental datasets for different fuels in shock tubes.

$$\tau_{IDT} = 10^A \cdot \exp\left(\frac{B}{T}\right) p^m \varphi^n [D]^q$$

Fuel	A	B	m	n	q	R ²	Adj R ²	
CH ₄ + C ₂ H ₆ + C ₂ H ₄	90% + 5% + 5%	-7.98	17034.52	-0.62	1.06	0.0	0.987	0.986
	75% + 12.5% + 12.5%	-17.54	-7294.52	-18.86	2.63	18.91	0.997	0.997
	60% + 20% + 20%	-7.98	15072.65	-0.63	-0.56	0.0	0.994	0.994
CH ₄ + C ₂ H ₆ + C ₂ H ₄ + C ₃ H ₈	80% + 10% + 5% + 5%	-8.47	16842.49	-0.43	0.33	0.0	0.967	0.965
	70% + 10% + 10% + 10%	-16.75	-3721.38	-17.0	1.86	16.79	0.983	0.981
	60% + 15% + 15% + 10%	-14.41	4718.75	-11.46	0.51	10.95	0.948	0.944

7.4. Rapid compression machine

As shown in the previous section, the uncertainty of each experimental point is changing by varying temperature, pressure, and mixture composition, so that it is not identical during IDT measurement experimental tests. Therefore, for doing the uncertainty analysis for the studied RCM regimes, the same procedure performed for shock-tube is followed and relevant correlations between parameters and IDTs have

been evaluated as shown in Table . As already mentioned by Weber et al [16], using Monte Carlo analysis or independent parameters methodology doesn't led to significant change in the calculated uncertainties. Therefore, like the performed uncertainty analysis for NUIG–HPST, it is supposed that there is no correlation between p_C , T_C and φ which can affect measured ignition delay time in the rapid compression machine. However, the correlation between [D] and p_C , T_C is considered according to Eq. B24. In this regard, the effect of temperature on the measured ignition delay time has been correlated through fitting an exponential equation to the experimental IDT data, and then the individual effect of pressure on the measured ignition delay time has been estimated using the applied approach by Weber et al [16]. Also, the effect of each individual parameter such as equivalence ratio (0.5–2.0) and dilution (75–90%) on the simulated ignition delay times has been correlated using fitted equations to the experimentally measured ignition delay times. Therefore, the following formulations could be proposed to estimate available uncertainties in the measured independent parameters and consequently the measured ignition delay times:

$$\frac{\partial T_C}{\partial p_C} = \frac{W\left(\frac{b}{a} \exp\left[\frac{bT_0}{a}\right] T_0 \left[\frac{p_C}{p_0}\right]^{\frac{1}{a}}\right)}{bp_C \left(W\left(\frac{b}{a} \exp\left[\frac{bT_0}{a}\right] T_0 \left[\frac{p_C}{p_0}\right]^{\frac{1}{a}}\right) + 1\right)} \quad (\text{B28})$$

where, W, T₀, and P₀ are Lambert's W function, initial temperature, and initial pressure in the reaction chamber, respectively. In Eq. 25, “a”, “b”, and $\frac{\partial T_C}{\partial p_C}$ were calculated using a Python code developed by Weber et al [16].

$$\frac{\partial \tau_{IDT}}{\partial p_C} = \frac{\partial \tau_{IDT}}{\partial T_C} \cdot \frac{\partial T_C}{\partial p_C} = \frac{\partial \tau_{IDT}}{\partial T_C} (\text{from Table}) \cdot \frac{W\left(\frac{b}{a} \exp\left[\frac{bT_0}{a}\right] T_0 \left[\frac{p_C}{p_0}\right]^{\frac{1}{a}}\right)}{bp_C \left(W\left(\frac{b}{a} \exp\left[\frac{bT_0}{a}\right] T_0 \left[\frac{p_C}{p_0}\right]^{\frac{1}{a}}\right) + 1\right)} \quad (\text{B29})$$

$$(\sigma_{\tau,i})^2 = \left(\frac{\partial \tau}{\partial T} \cdot \sigma_T\right)^2 + \left(\frac{\partial \tau}{\partial p} \cdot \sigma_p\right)^2 + \left(\frac{\partial \tau}{\partial \varphi} \cdot \sigma_\varphi\right)^2 + \left(\frac{\partial \tau}{\partial [D]} \cdot \sigma_{[D]}\right)^2 + 2 \left(\frac{\partial \tau}{\partial T} \cdot \frac{\partial \tau}{\partial [D]} \cdot \sigma_T \sigma_{[D]}\right) + 2 \left(\frac{\partial \tau}{\partial p} \cdot \frac{\partial \tau}{\partial [D]} \cdot \sigma_p \sigma_{[D]}\right) \quad (\text{B30})$$

$$\tau_{IDT} = f(T_C, p_C, \varphi, [D]) \rightarrow \sigma_{\tau_{IDT}} = \sqrt{\left(\frac{\partial \tau_{IDT}}{\partial T_C} \cdot \sigma_{T_C}\right)^2 + \left(\frac{\partial \tau_{IDT}}{\partial p_C} \cdot \sigma_{p_C}\right)^2 + \left(\frac{\partial \tau_{IDT}}{\partial \varphi} \cdot \sigma_\varphi\right)^2 + \left(\frac{\partial \tau_{IDT}}{\partial [D]} \cdot \sigma_{[D]}\right)^2 + 2 \left(\frac{\partial \tau_{IDT}}{\partial T_C} \cdot \frac{\partial \tau_{IDT}}{\partial [D]} \cdot \sigma_{T_C} \sigma_{[D]}\right) + 2 \left(\frac{\partial \tau_{IDT}}{\partial p_C} \cdot \frac{\partial \tau_{IDT}}{\partial [D]} \cdot \sigma_{p_C} \sigma_{[D]}\right)} \quad (\text{B31})$$

By substituting the correlations from Table and Eqs. 24 and 26 into Eq. 28, the uncertainty of the measured ignition delay times in RCM regime would be calculated based on a Python code developed by Weber et al [16].

Table BS10. Correlation variables of the studied experimental datasets for different fuels in RCMs.

$$\tau_{IDT} = 10^A \cdot \exp\left(\frac{B}{T}\right) p^m \varphi^n [D]^q$$

Fuel		A	B	m	n	q	R ²	Adj R ²
CH ₄ + C ₂ H ₆ + C ₂ H ₄	90% + 5% + 5%	-3.74	33073.12	8.04	2.14	-9.64	0.985	0.984

	75% + 12.5% + 12.5%	-4.13	38213.43	-2.32	-0.01	-4.44	0.997	0.997
	60% + 20% + 20%	-7.97	29985.69	-4.96	-3.36	0.0	0.994	0.994
	80% + 10% + 5% + 5%	-12.85	32829.04	-2.29	0.37	0.0	0.986	0.985
CH ₄ + C ₂ H ₆ + C ₂ H ₄ + C ₃ H ₈	70% + 10% + 10% + 10%	-27.05	11999.48	-	-2.23	18.23	0.997	0.996
	60% + 15% + 15% + 10%	-6.54	24779.49	-4.49	-2.34	0.0	0.989	0.988

8. Pressure profiles of the applied rapid compression machines (RCMs)

The reactive and non-reactive pressure profiles of the applied rapid compression machines including NUIG-RCM and PCFC-RCM for the studied cases alongside the simulation profiles are shown in the following figures. Here, it should be noted that all the simulations were performed using NUIGMech1.2 mechanism, otherwise, it is mentioned in the caption or legend of the figures.

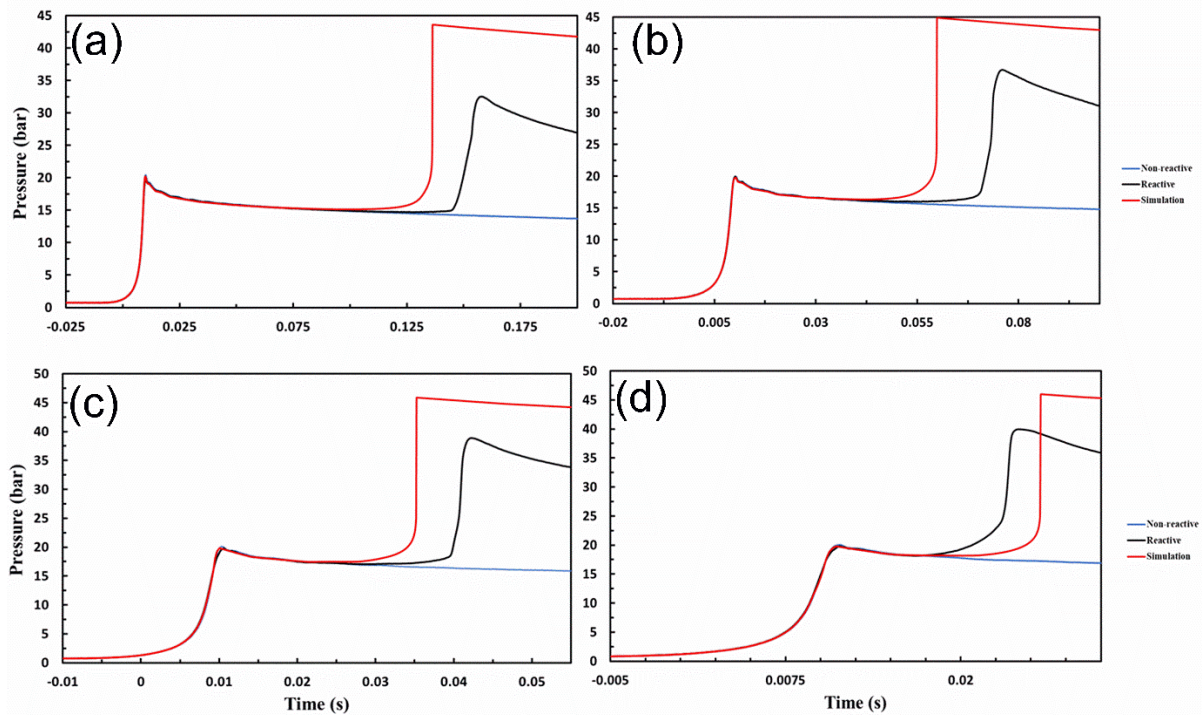


Figure BS3. Pressure history of tested reactive and non-reactive mixtures of 4.32% CH₄/0.24% C₂H₄/0.24% C₂H₆, 10.2% O₂, 10% Ar and 75% N₂ for $p_c = 20$ bar and $\phi = 1.0$ for initial temperature of (a) 338 K, (b) 353 K, (c) 368 K and (d) 383 K.

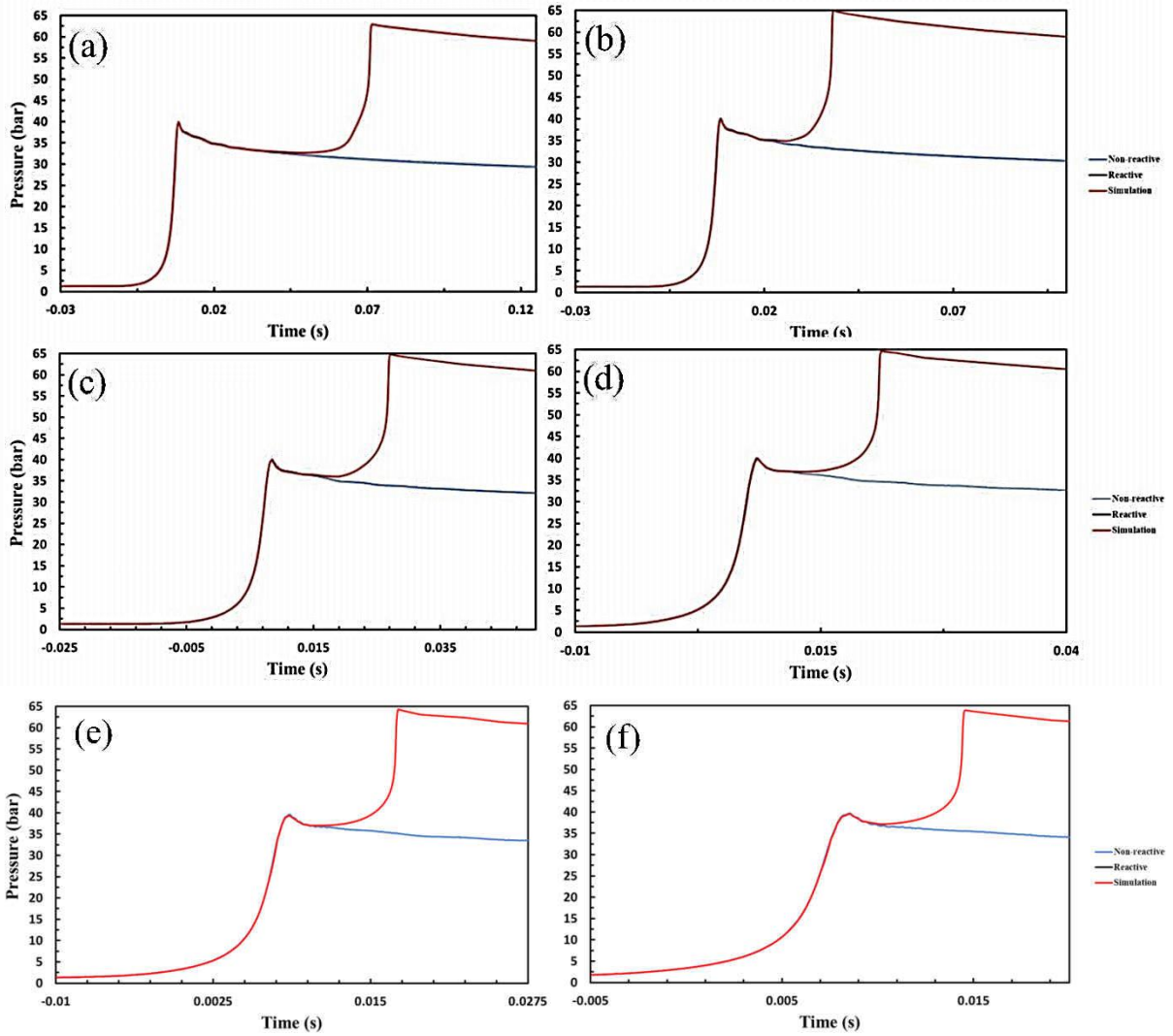


Figure BS4. Pressure history of tested reactive and non-reactive mixtures of 4.36% CH₄/0.24% C₂H₄/0.24% C₂H₆, 5.15% O₂, and 90% N₂ for $p_C = 40$ bar and $\varphi = 2.0$ for initial temperature of (a) 308 K, (b) 324 K, (c) 338 K, (d) 353 K, (e) 368 K, and (f) 383 K.

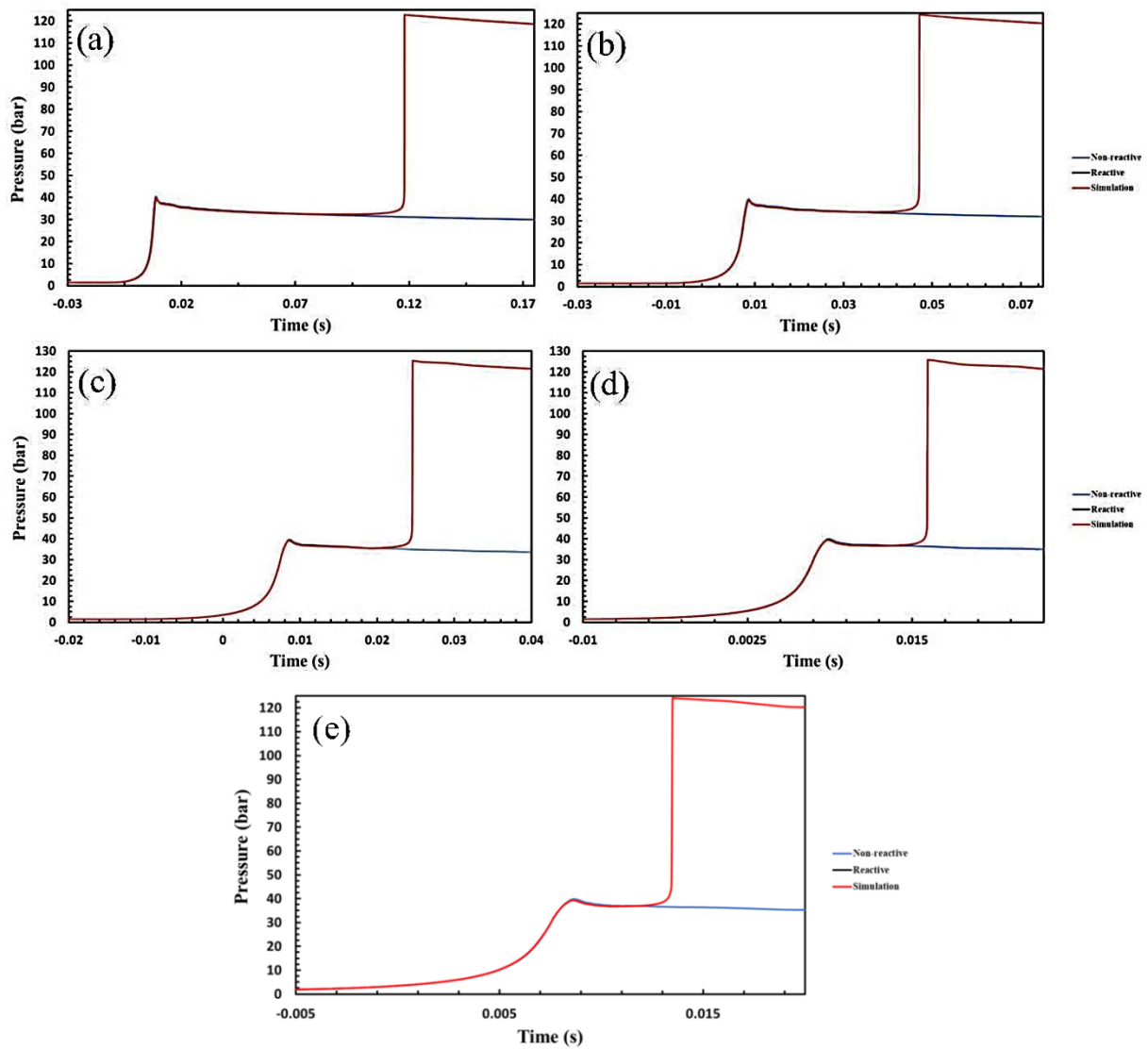


Figure BS5. Pressure history of tested reactive and non-reactive mixtures of 5.66% CH₄/0.94% C₂H₄/0.94% C₂H₆, 17.45% O₂, and 75% N₂ for $p_C = 40$ bar and $\phi = 1.0$ for initial temperature of (a) 323 K, (b) 338 K, (c) 353 K, (d) 353 K, and (e) 383 K.

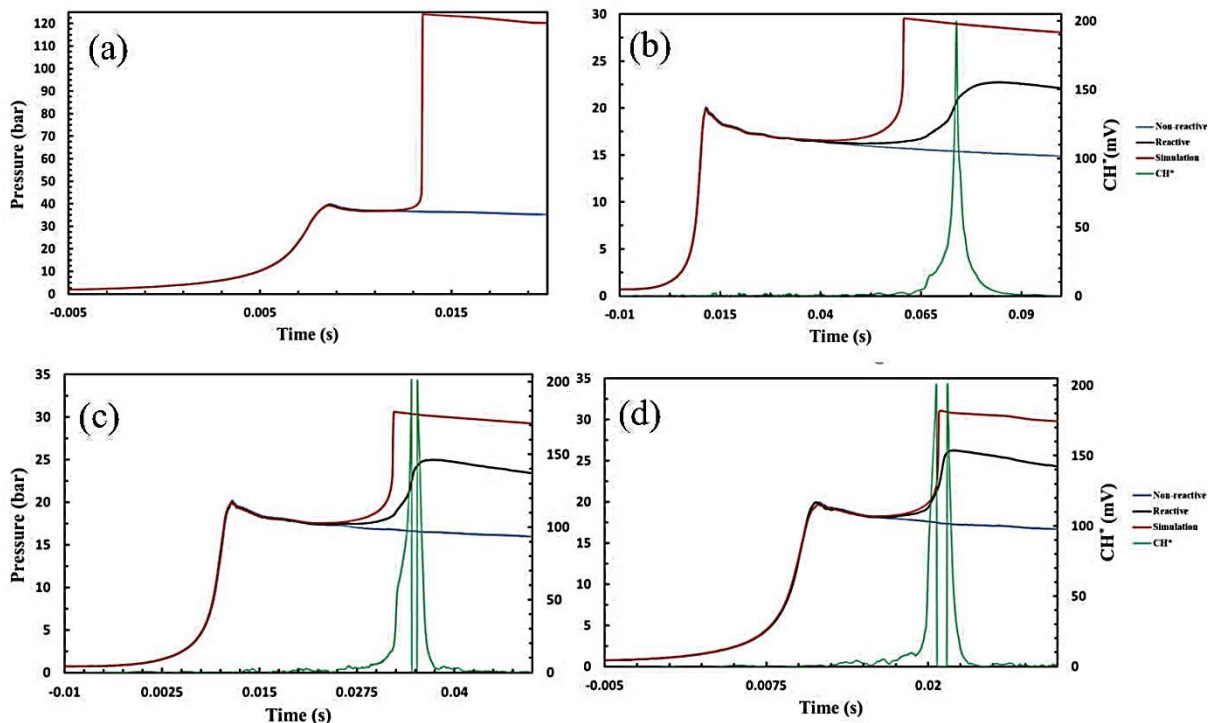


Figure BS6. Pressure history of tested reactive and non-reactive mixtures of 1.33% CH₄/0.22% C₂H₄/0.22% C₂H₆, 8.22% O₂, and 90% N₂ for $p_c = 20$ bar and $\phi = 0.5$ for initial temperature of (a) 343 K, (b) 353 K, (c) 368 K, and (d) 383 K.

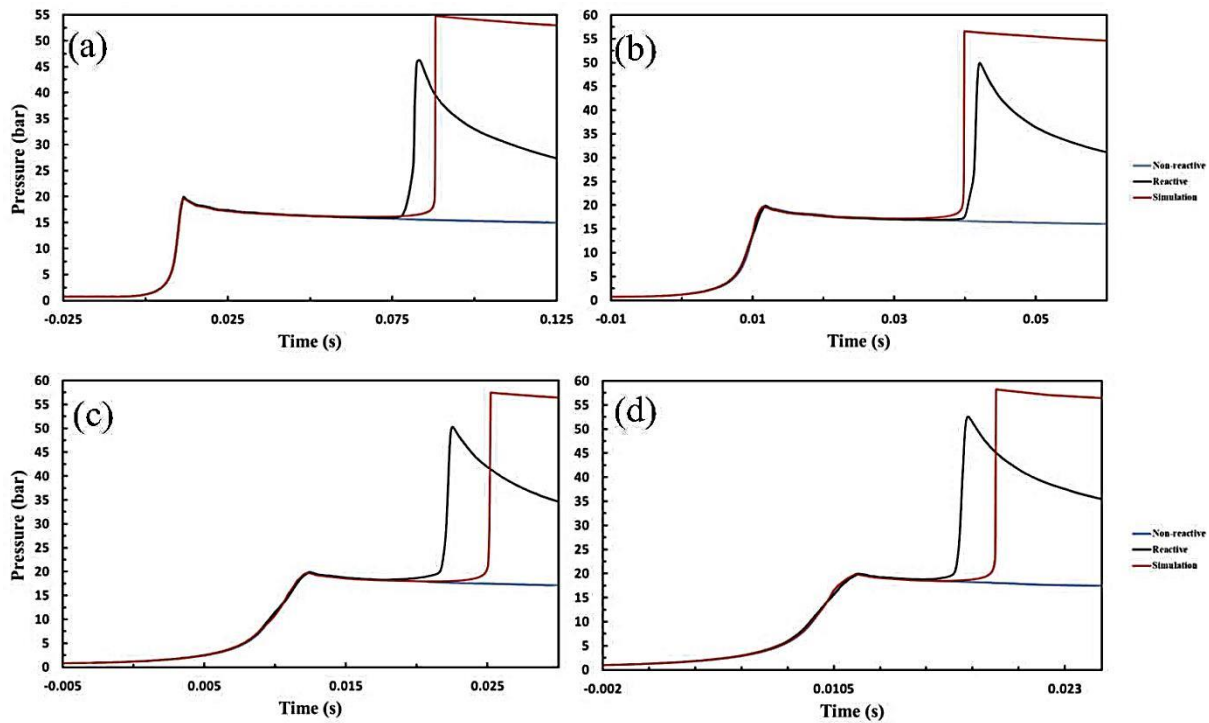


Figure BS7. Pressure history of tested reactive and non-reactive mixtures of 6.67% CH₄/2.22% C₂H₄/2.22% C₂H₆, 13.89% O₂, and 75% N₂ for $p_c = 20$ bar and $\phi = 2.0$ for initial temperature of (a) 338 K, (b) 353 K, (c) 368 K, and (d) 378 K.

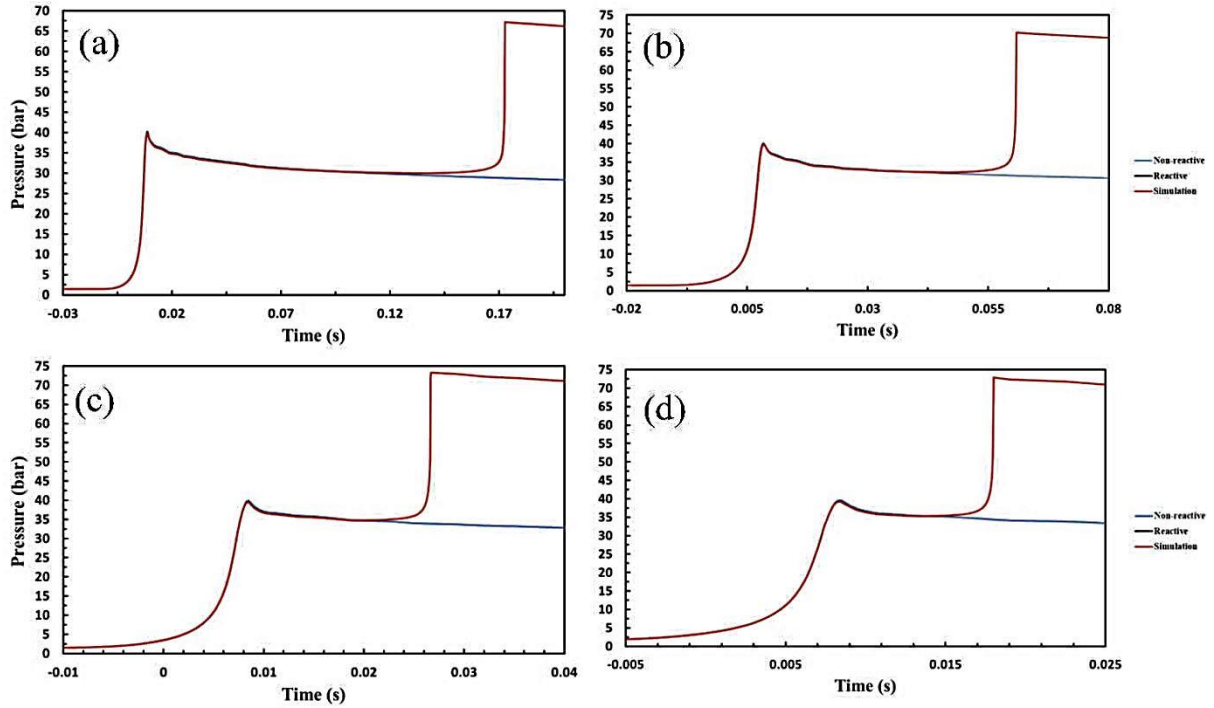
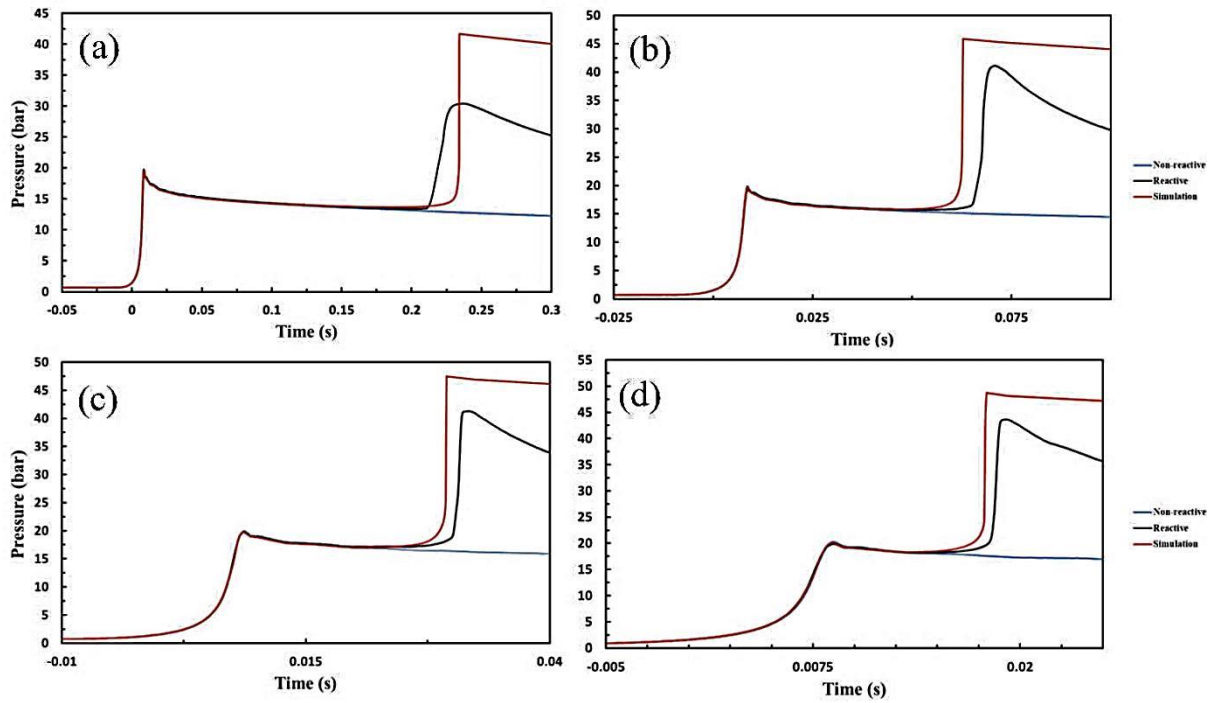


Figure BS8. Pressure history of tested reactive and non-reactive mixtures of 1.5% CH₄/0.5% C₂H₄/0.5% C₂H₆, 12.5% O₂, and 85% N₂ for $p_c = 40$ bar and $\phi = 0.5$ for initial temperature of (a) 338 K, (b) 353 K, (c) 368 K, and (d) 383 K.



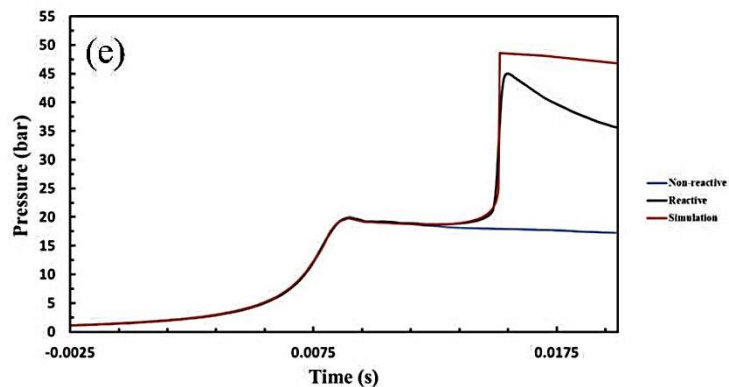


Figure BS9. Pressure history of tested reactive and non-reactive mixtures of 3.58% CH₄/0.22% C₂H₄/0.45% C₂H₆/0.22% C₃H₈, 10.5% O₂, 10% Ar and 75% N₂ for $p_C = 20$ bar and $\phi = 1.0$ for initial temperature of (a) 323 K, (b) 338 K, (c) 353 K, (d) 368 K, and (e) 378 K.

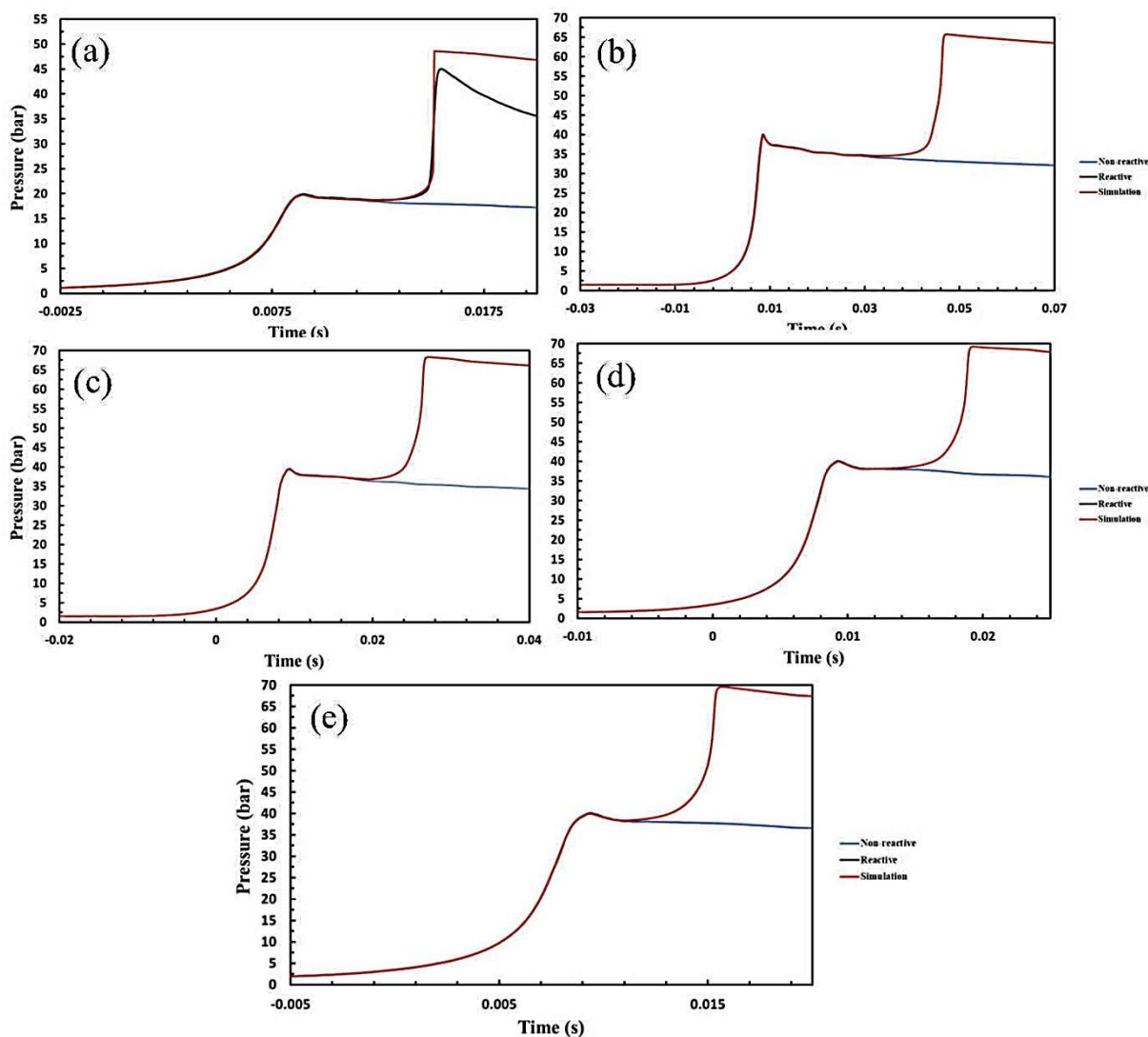


Figure BS10. Pressure history of tested reactive and non-reactive mixtures of 3.68% CH₄/0.23% C₂H₄/0.46% C₂H₆/0.23% C₃H₈, 5.4% O₂, and 90% N₂ for $p_C = 40$ bar and $\phi = 2.0$ for initial temperature of (a) 323 K, (b) 338 K, (c) 353 K, (d) 368 K, and (e) 383 K.

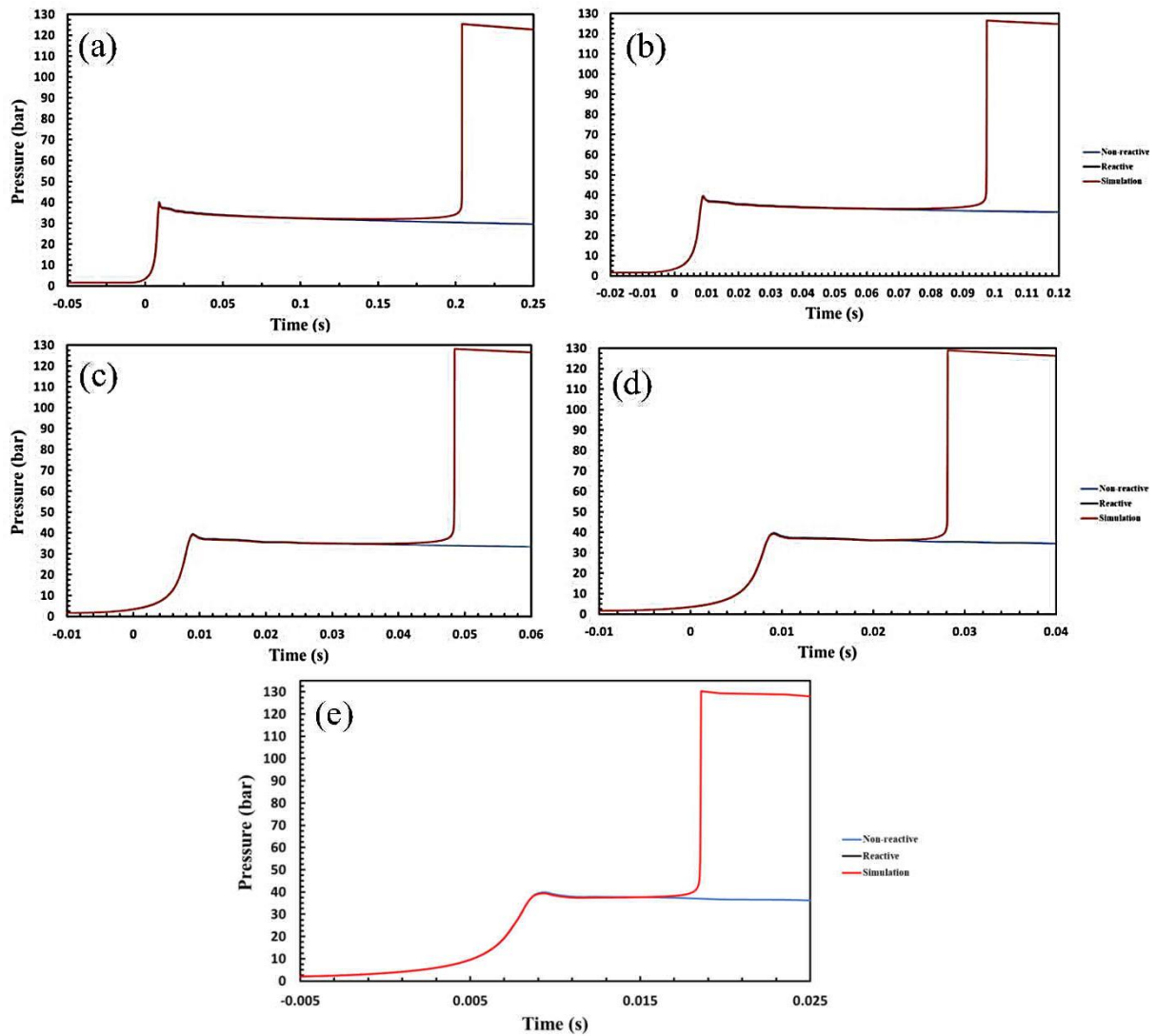


Figure BS11. Pressure history of tested reactive and non-reactive mixtures of 4.93% CH₄/0.7% C₂H₄/0.7% C₂H₆/0.7% C₃H₈, 17.96% O₂, and 75% N₂ for $p_C = 40$ bar and $\phi = 1.0$ for initial temperature of (a) 323 K, (b) 338 K, (c) 353 K, (d) 368 K, and (e) 383 K.

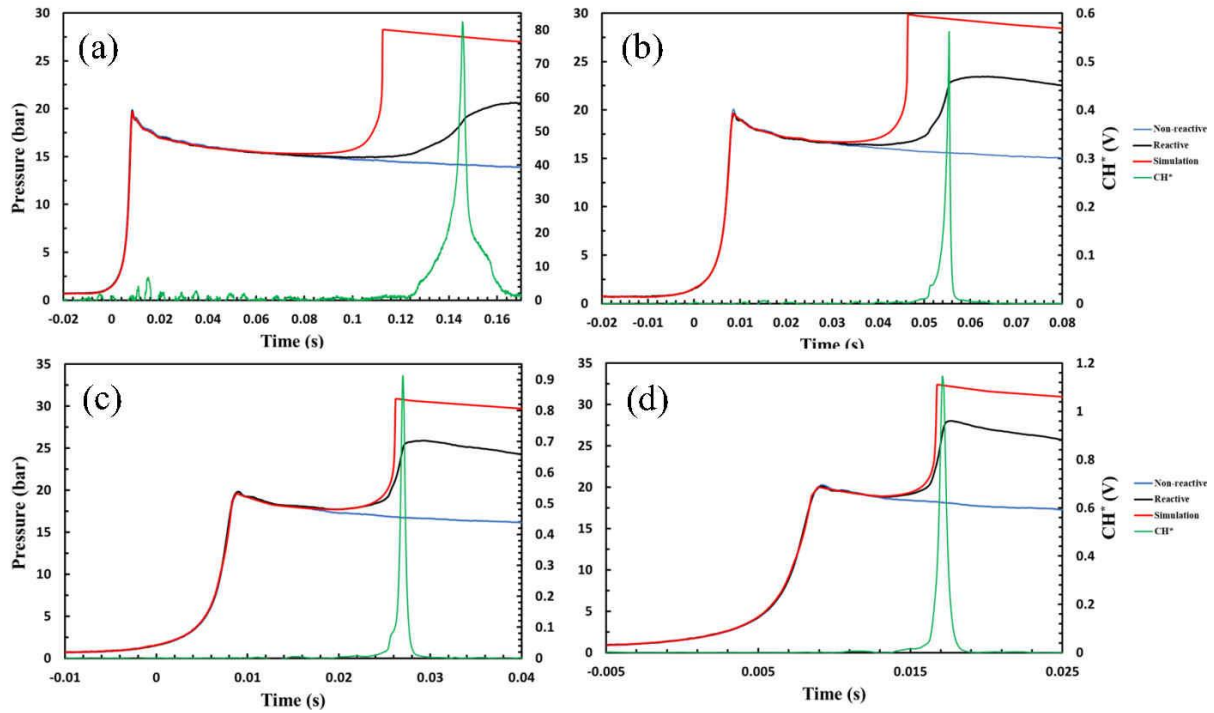


Figure BS12. Pressure history of tested reactive and non-reactive mixtures of 1.15% CH₄/0.16% C₂H₄/0.16% C₂H₆/0.16% C₃H₈, 8.36% O₂, and 90% N₂ for $p_c = 20$ bar and $\varphi = 0.5$ for initial temperature of (a) 338 K, (b) 353 K, (c) 368 K, and (d) 383 K.

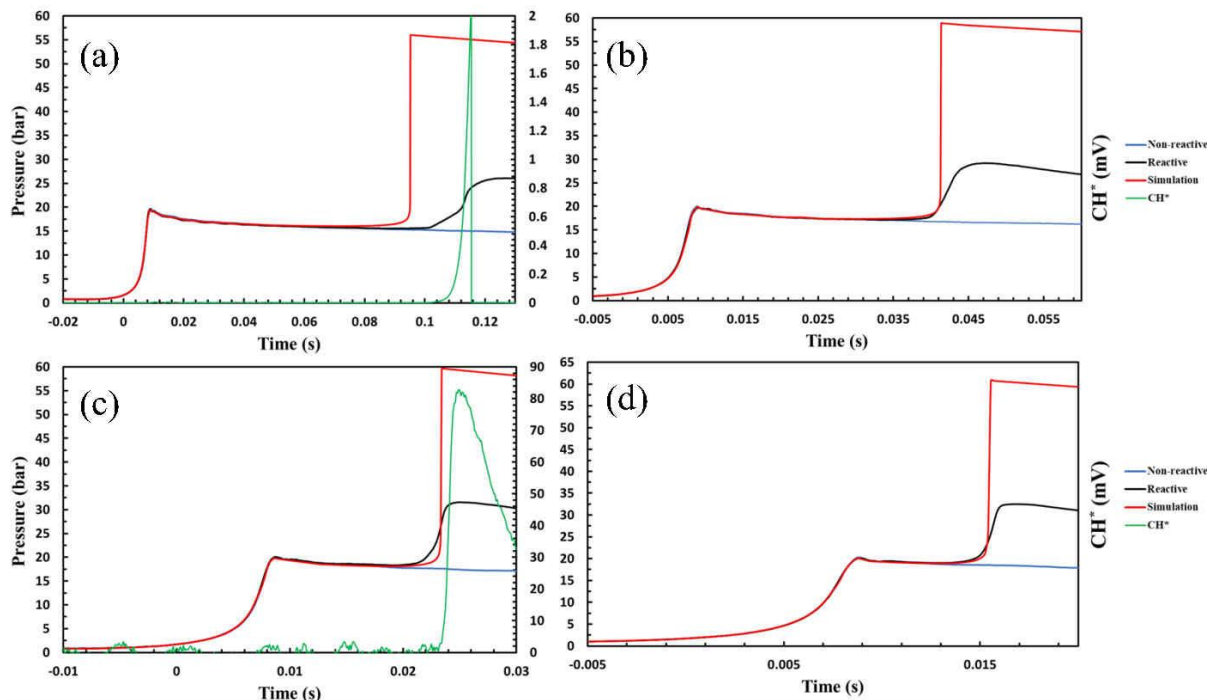


Figure BS13. Pressure history of tested reactive and non-reactive mixtures of 6.42% CH₄/1.6% C₂H₄/1.6% C₂H₆/1.07% C₃H₈, 14.3% O₂, and 75% N₂ for $p_c = 20$ bar and $\varphi = 2.0$ for initial temperature of (a) 338 K, (b) 353 K, (c) 368 K, and (d) 383 K.

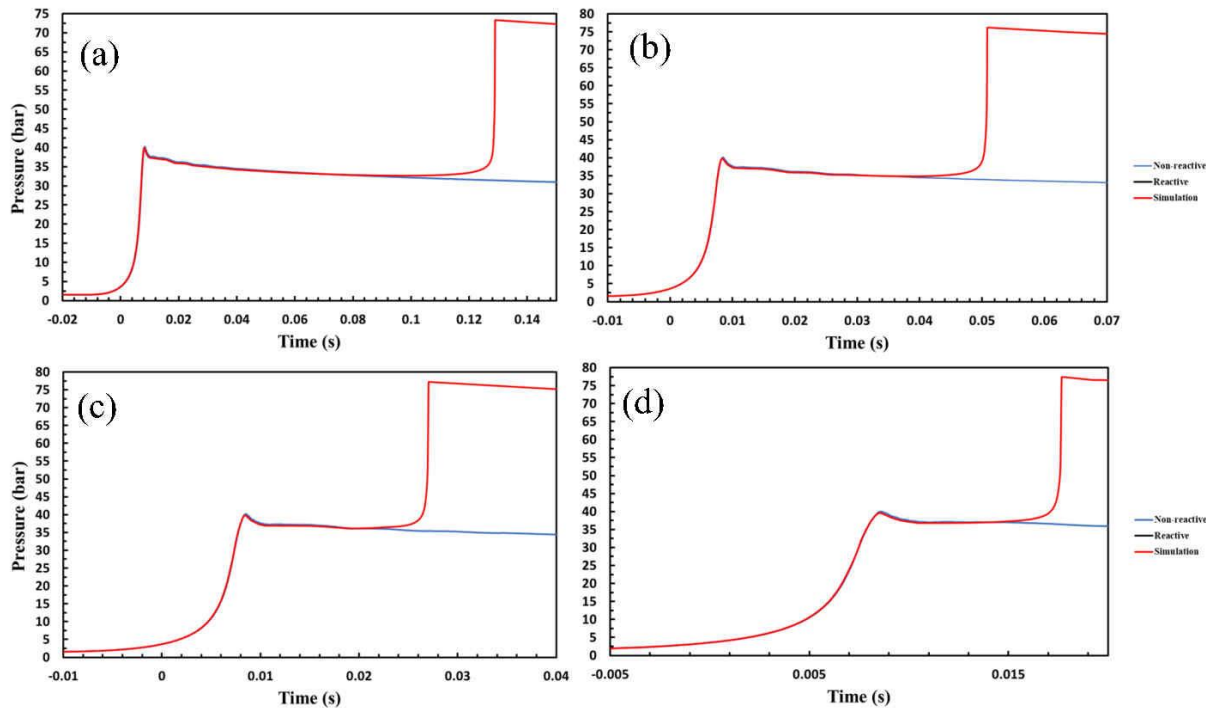


Figure BS14. Pressure history of tested reactive and non-reactive mixtures of 1.41% CH₄/0.35% C₂H₄/0.35% C₂H₆/0.24% C₃H₈, 12.64% O₂, and 85% N₂ for $p_C = 40$ bar and $\phi = 0.5$ for initial temperature of (a) 338 K, (b) 353 K, (c) 368 K, and (d) 383 K.

9. Performances of different chemical mechanisms

For doing the simulations and comparisons, the following mechanisms have been applied:

Table BS11. Applied chemical mechanisms.

No	Mechanism	Number of reactions	Number of species	Comments
1	NUIGMech1.2	11800	2913	
2	AramcoMech 3.0	3037	581	Released at 2018 [17]
3	AramcoMech 2.0	2716	493	Released at 2016 [18-24]
4	AramcoMech 1.3	1542	253	Released at 2013 [23]
5	DTU-C ₃	142	1308	Released at 2019 [25]
6	CRECK	1941	114	Released at 2020 [26]
7	UCSD	268	57	Released at 2016 [27]
8	GRI 3.0	325	53	Released at 2000 [28]
9	FFCM-1	291	38	C ₁ -C ₂ ; Low temperature reactions are not included; released at 2016 [29]

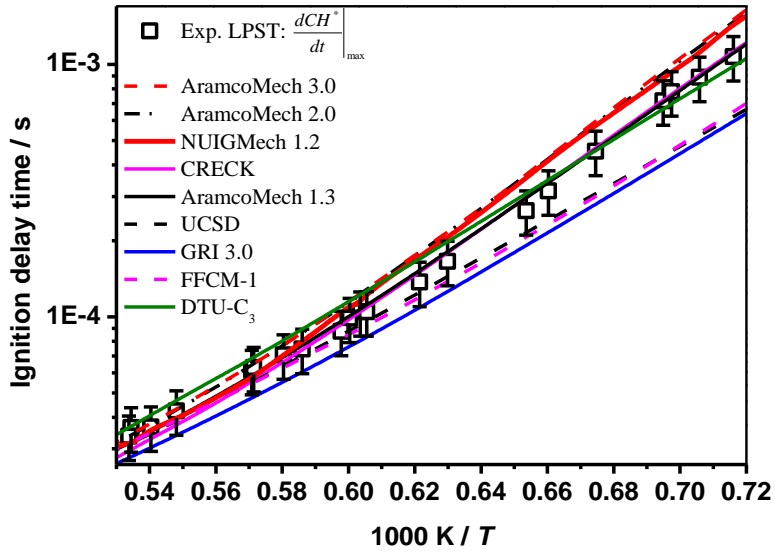


Figure BS15. Experimental and constant volume simulation data values of 4.29% CH₄/0.24% C₂H₄/0.24% C₂H₆, 20.24% O₂, and 75% N₂ at $p_C = 1$ bar and $\phi = 0.5$ for LPST.

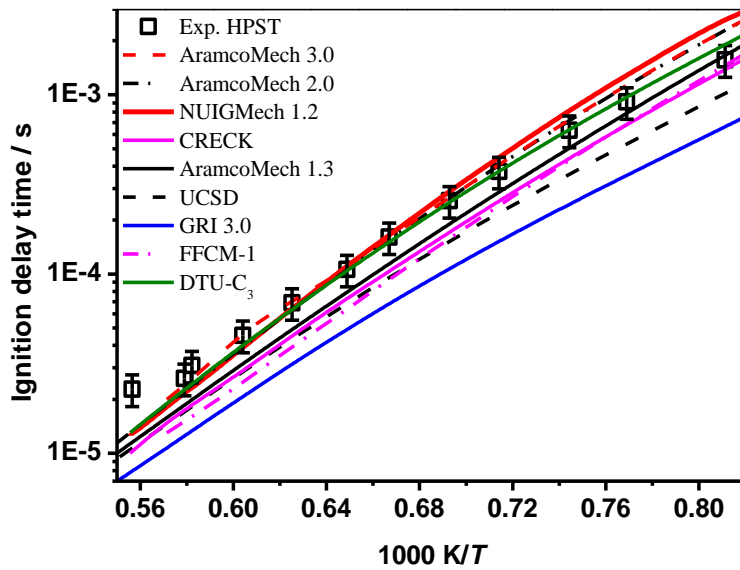


Figure BS16. Experimental and constant volume simulation data values of 4.32% CH₄/0.24% C₂H₄/0.24% C₂H₆, 10.2% O₂, 10% Ar and 75% N₂ at $p_C = 20$ bar and $\phi = 1.0$ for HPST.

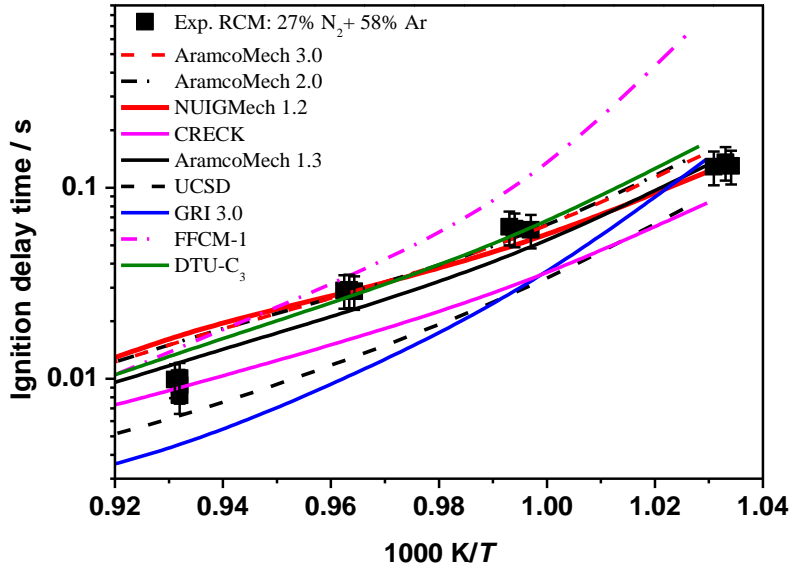


Figure BS17. Experimental and simulation data values of 4.32% CH₄/0.24% C₂H₄/0.24% C₂H₆, 10.2% O₂, 10% Ar and 75% N₂ at $p_C = 20$ bar and $\phi = 1.0$ for RCM.

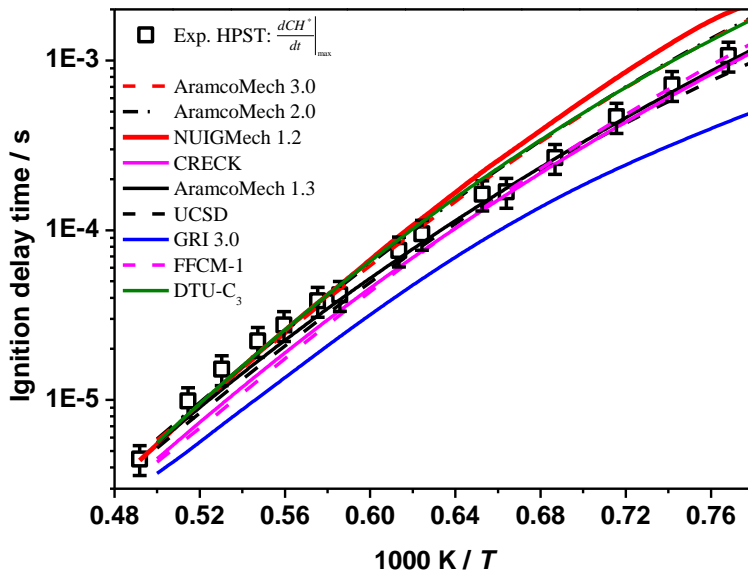


Figure BS18. Experimental and constant volume simulation data of 4.36% CH₄/0.24% C₂H₄/0.24% C₂H₆, 5.15% O₂, 15% Ar and 75% N₂ at $p_C = 40$ bar and $\phi = 2.0$ for HPST.

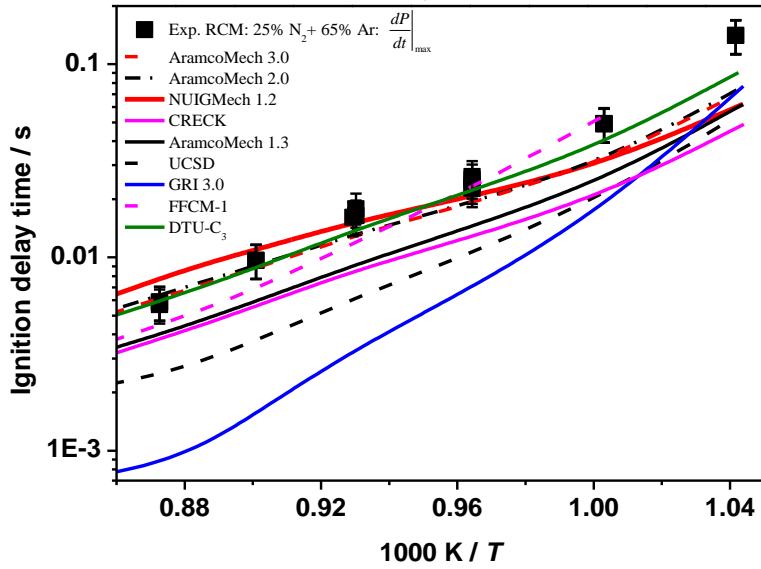


Figure BS19. Experimental and simulation data values of 4.36% CH₄/0.24% C₂H₄/0.24% C₂H₆, 5.15% O₂, 15% Ar and 75% N₂ at $p_C = 40$ bar and $\phi = 2.0$ for RCM.

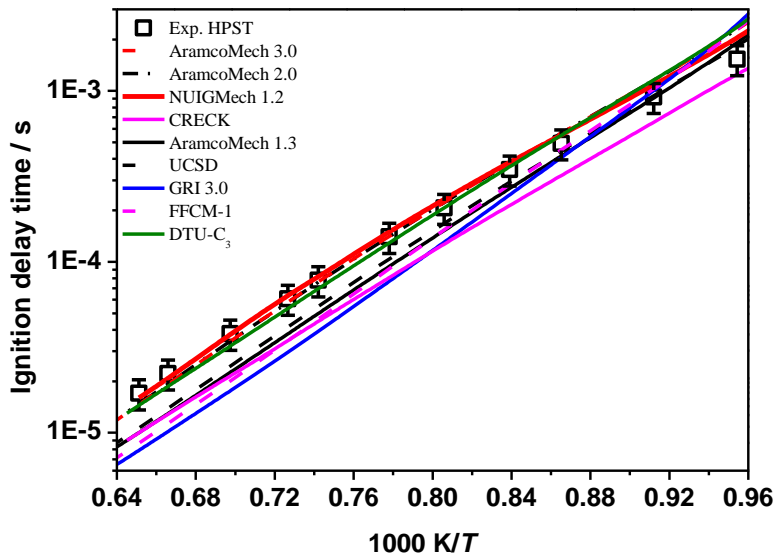


Figure BS20. Experimental and constant volume simulation data of 5.66% CH₄/0.94% C₂H₄/0.94% C₂H₆, 17.45% O₂ and 75% N₂ at $p_C = 40$ bar and $\phi = 1.0$ for HPST.

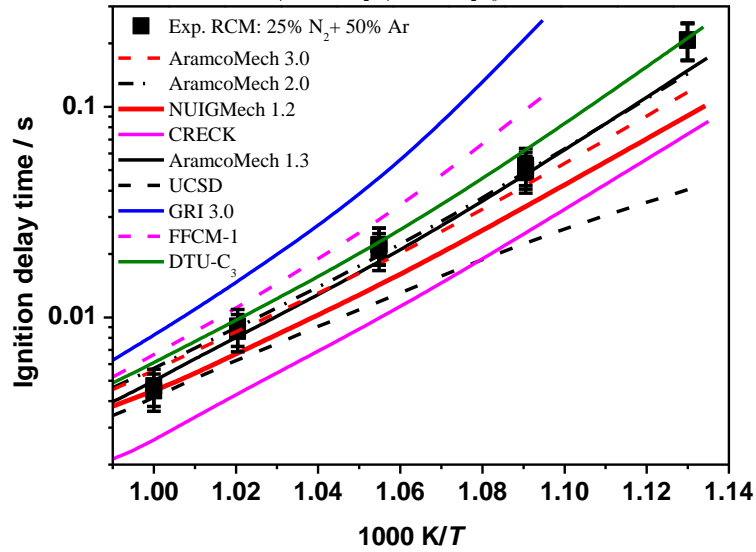


Figure BS21. Experimental and simulation data values of 5.66% CH₄/0.94% C₂H₄/0.94% C₂H₆, 17.45% O₂ and 75% N₂ at $p_C = 40$ bar and $\phi = 1.0$ for RCM.

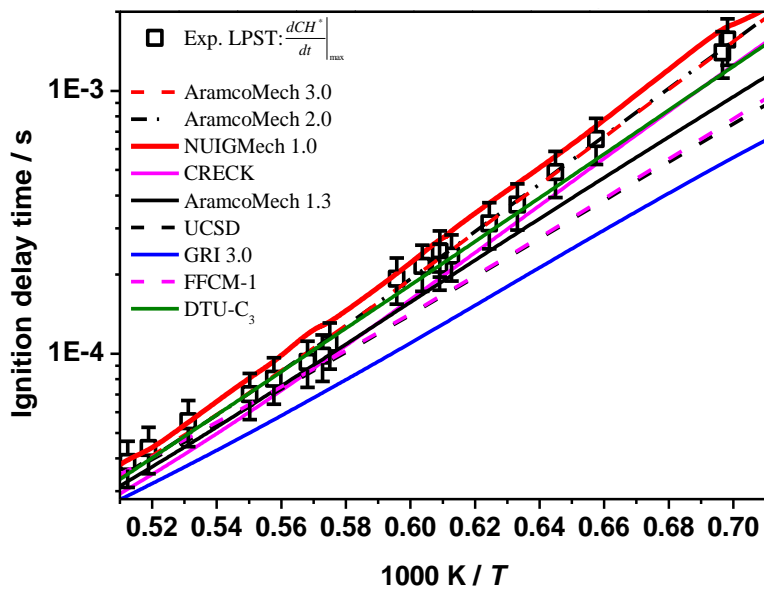


Figure BS22. Experimental and constant volume simulation data of 5.22% CH₄/0.87% C₂H₄/0.87% C₂H₆, 8.04% O₂, 10% Ar and 75% N₂ at $p_C = 1$ bar and $\phi = 2.0$ for LPST.

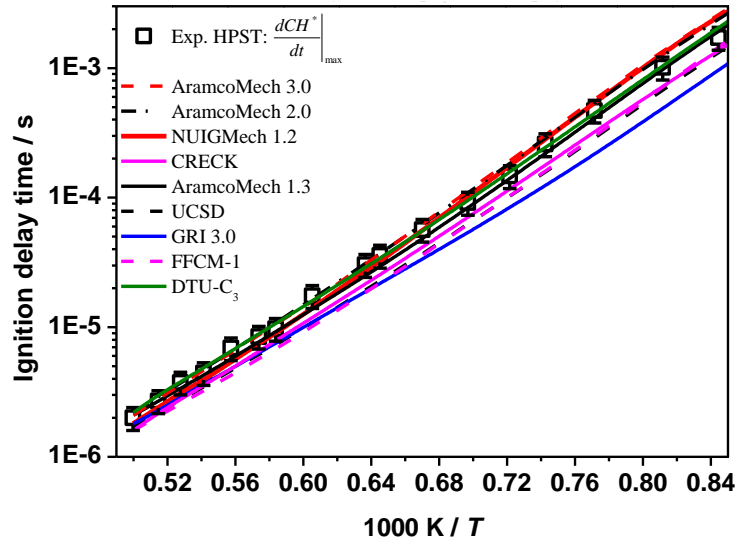


Figure BS23. Experimental and constant volume simulation data of 1.33% CH₄/0.22% C₂H₄/0.22% C₂H₆, 8.22% O₂, 15% Ar and 75% N₂ at $p_C = 20$ bar and $\phi = 0.5$ for HPST.

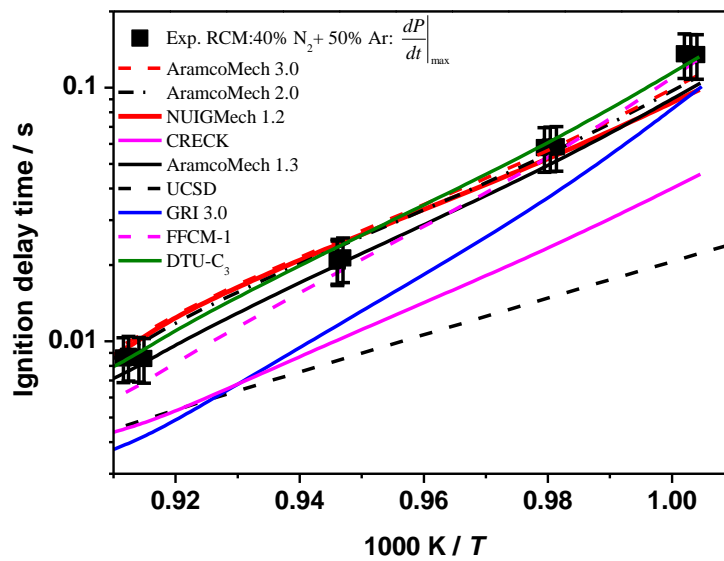


Figure BS24. Experimental and simulation data values of 1.33% CH₄/0.22% C₂H₄/0.22% C₂H₆, 8.22% O₂, 15% Ar and 75% N₂ at $p_C = 20$ bar and $\phi = 0.5$ for RCM.

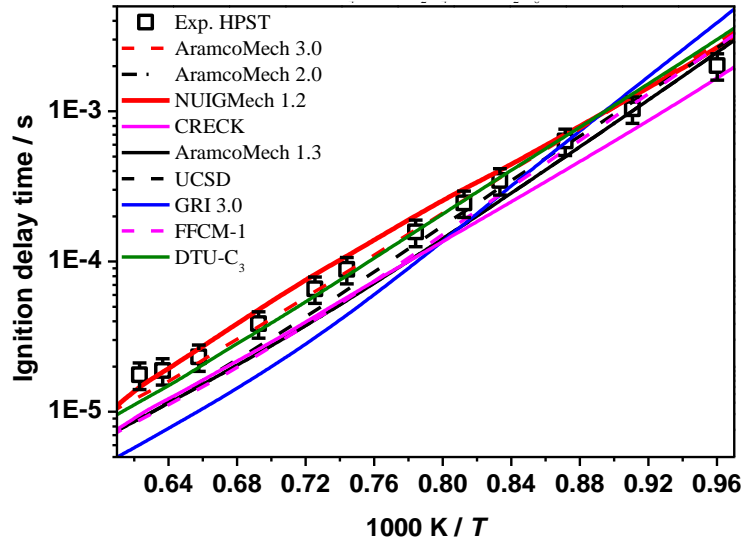


Figure BS25. Experimental and constant volume simulation data of 6.67% CH_4 /2.22% C_2H_4 /2.22% C_2H_6 , 13.89% O_2 , and 75% N_2 at $p_c = 20$ bar and $\varphi = 2.0$ for HPST.

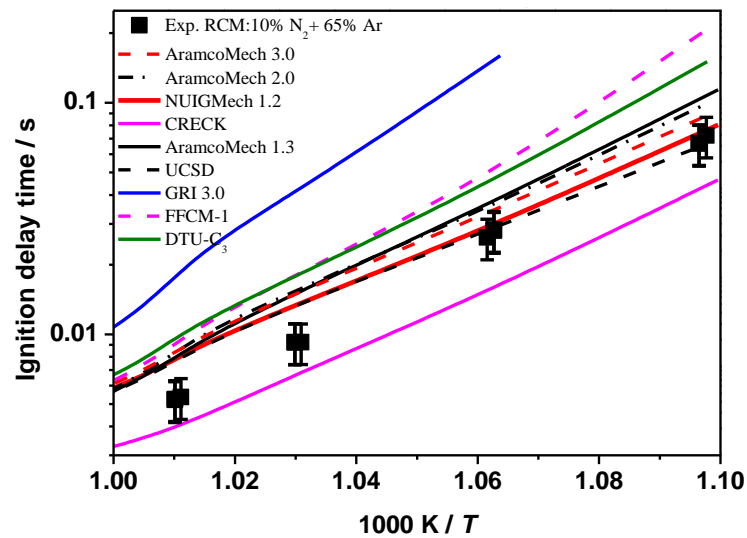


Figure BS26. Experimental and simulation data values of 6.67% CH_4 /2.22% C_2H_4 /2.22% C_2H_6 , 13.89% O_2 , 75% N_2 at $p_c = 20$ bar and $\varphi = 2.0$ for RCM.

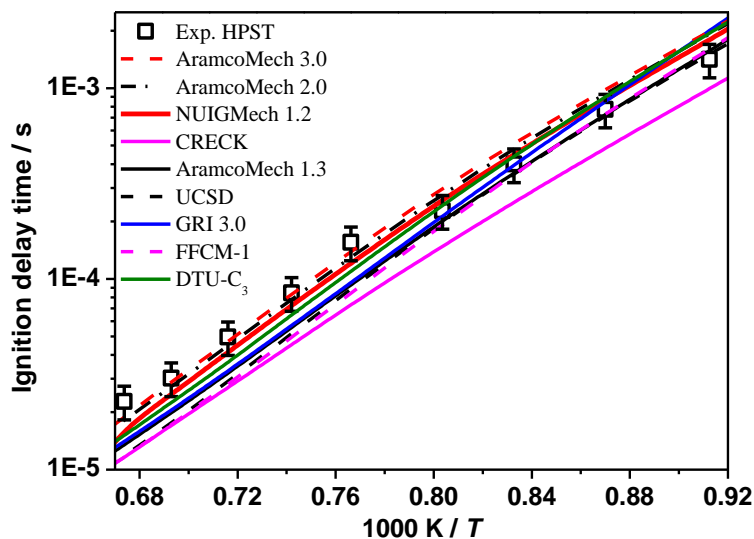


Figure BS27. Experimental and constant volume simulation data of 1.5% CH₄/0.5% C₂H₄/0.5% C₂H₆, 12.5% O₂, 10% Ar and 75% N₂ at $p_C = 40$ bar and $\varphi = 0.5$ for HPST.

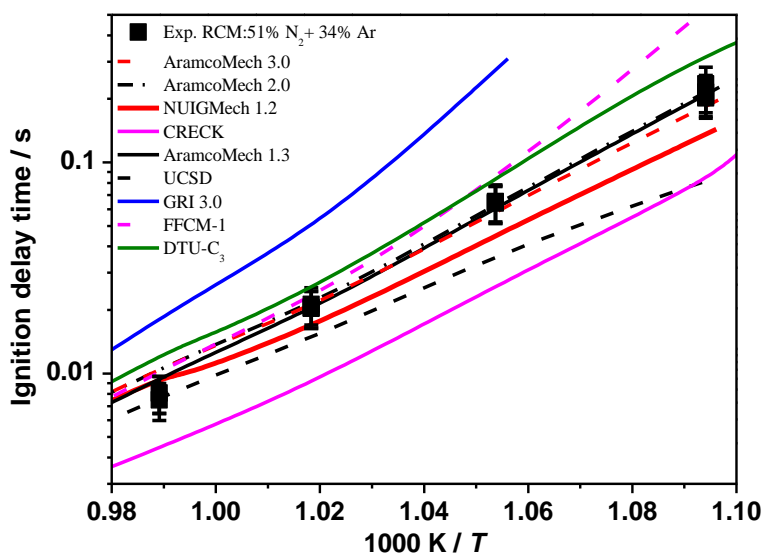


Figure BS28. Experimental and simulation data values of 1.5% CH₄/0.5% C₂H₄/0.5% C₂H₆, 12.5% O₂, 10% Ar and 75% N₂ at $p_C = 40$ bar and $\varphi = 0.5$ for RCM.

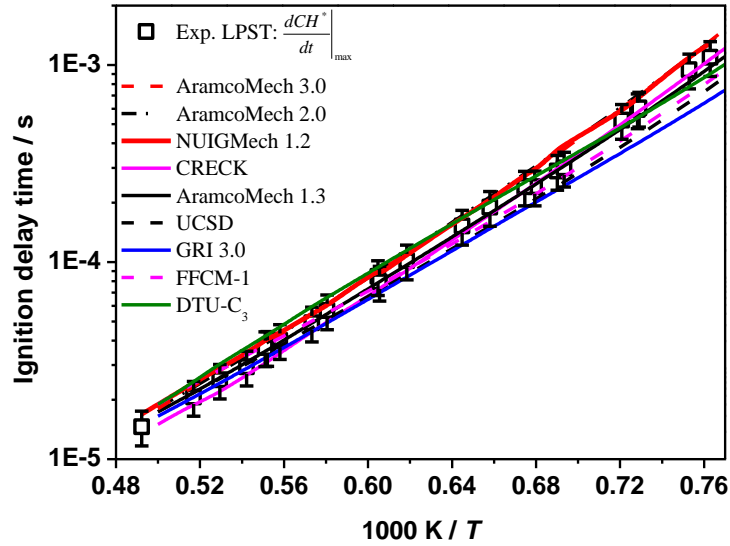


Figure BS29. Experimental and constant volume simulation data of 1.71% CH₄/0.57% C₂H₄/0.57% C₂H₆, 7.14% O₂, 15% Ar and 75% N₂ at $p_C = 1$ bar and $\phi = 1.0$ for LPST.

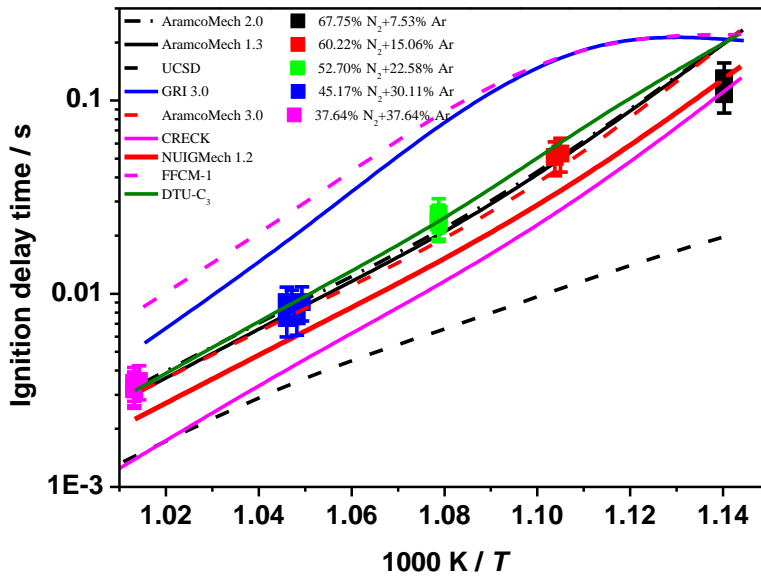


Figure BS30. Experimental and simulation data values of 4.24% CH₄/0.24% C₂H₄/0.24% C₂H₆, 20% O₂, at $p_C = 90$ bar and $\phi = 0.5$ for RCM.

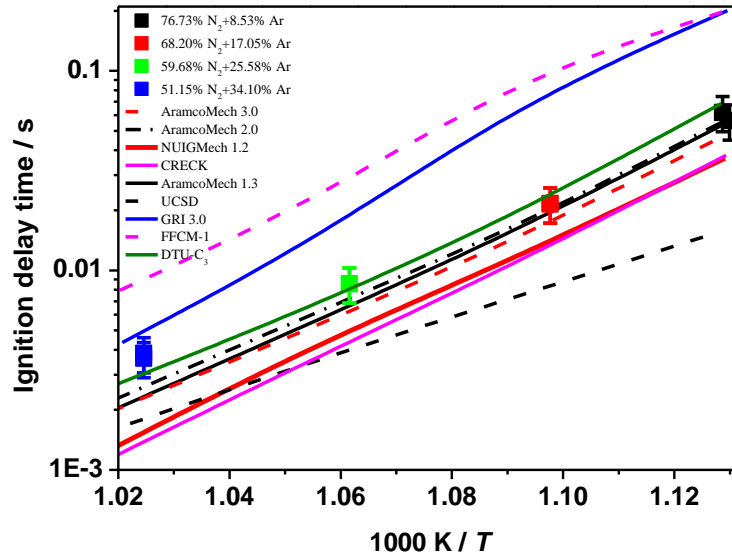


Figure BS31. Experimental and simulation data values of 4.24% CH_4 /0.24% C_2H_4 /0.24% C_2H_6 , 10% O_2 , at $p_C = 135$ bar and $\phi = 1.0$ for RCM.

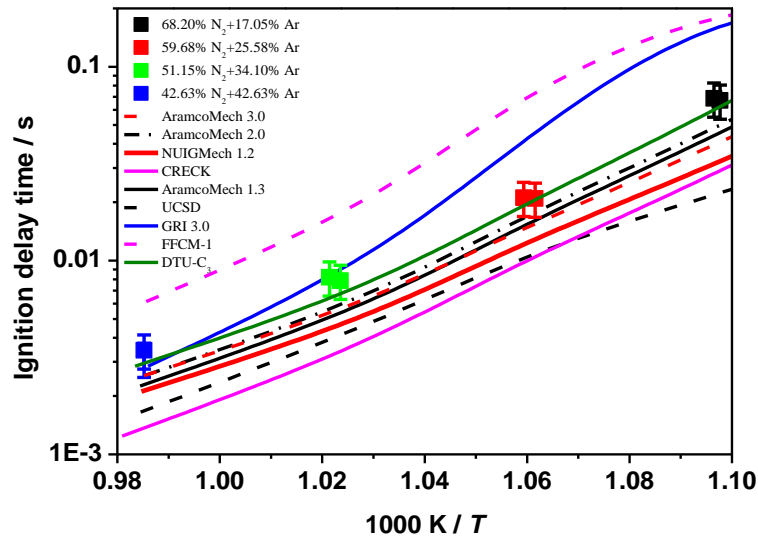


Figure BS32. Experimental and simulation data values of 4.24% CH_4 /0.24% C_2H_4 /0.24% C_2H_6 , 10% O_2 , at $p_C = 90$ bar and $\phi = 1.0$ for RCM.

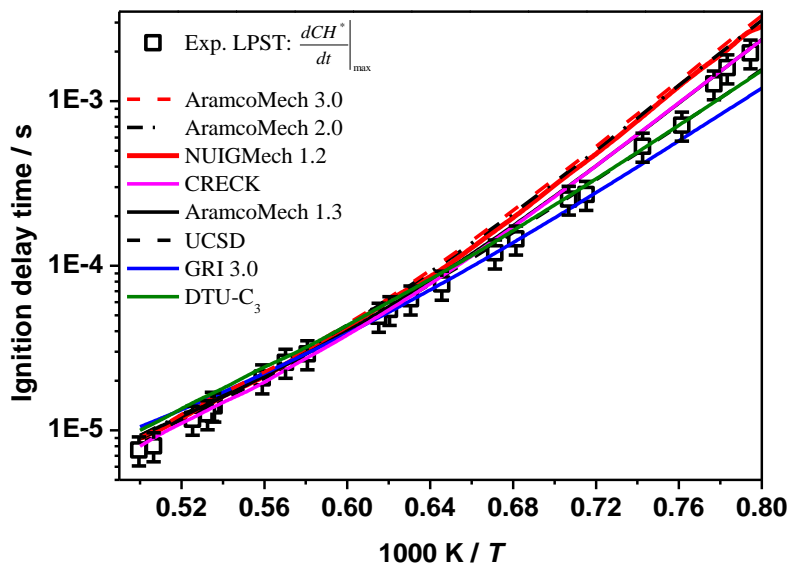


Figure BS33. Experimental and constant volume simulation data of 3.51% CH₄/0.22% C₂H₄/0.44% C₂H₆/0.22% C₃H₈, 20.61% O₂, and 75% N₂ at $p_C = 1$ bar and $\phi = 0.5$ for LPST.

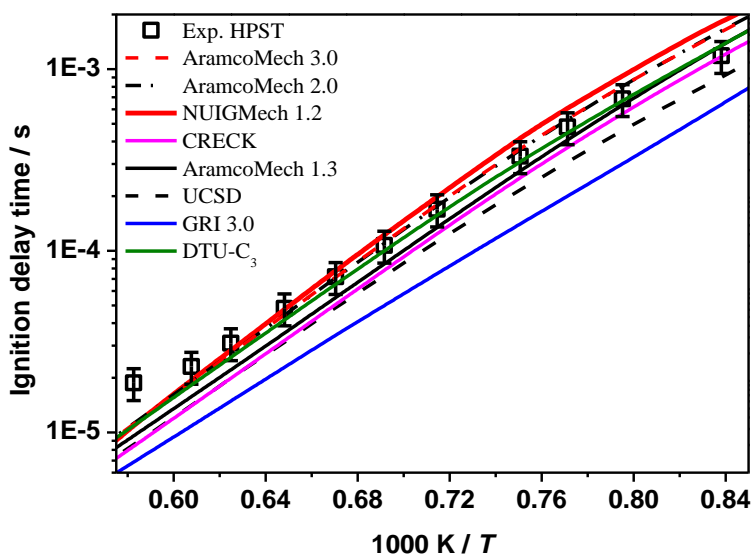


Figure BS34. Experimental and constant volume simulation data of 3.58% CH₄/0.22% C₂H₄/0.45% C₂H₆/0.22% C₃H₈, 10.5% O₂, 10% Ar and 75% N₂ at $p_C = 20$ bar and $\phi = 1.0$ for HPST.

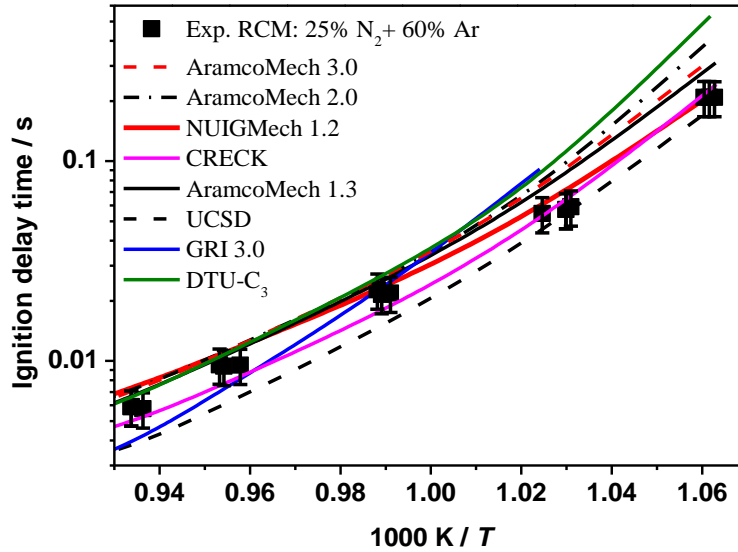


Figure BS35. Experimental and simulation data values of 3.58% CH₄/0.22% C₂H₄/0.45% C₂H₆/0.22% C₃H₈, 10.5% O₂, 10% Ar and 75% N₂ at $p_C = 20$ bar and $\phi = 1.0$ for RCM.

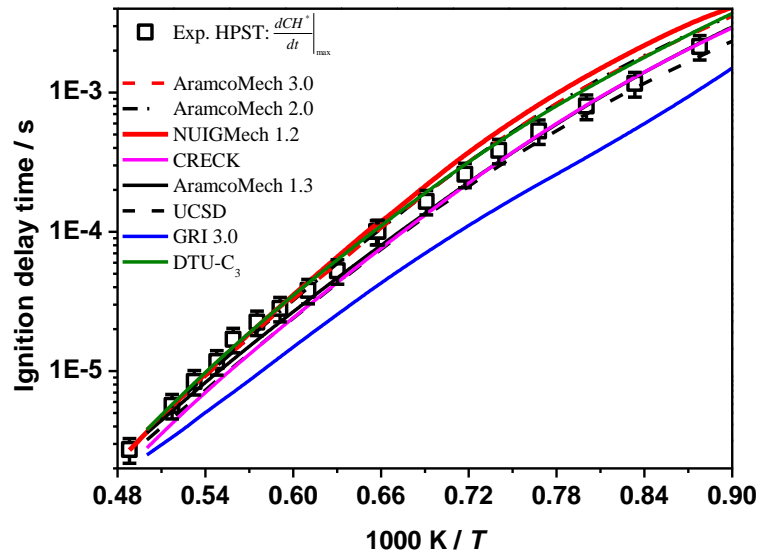


Figure BS36. Experimental and constant volume simulation data of 3.68% CH₄/0.23% C₂H₄/0.46% C₂H₆/0.23% C₃H₈, 5.4% O₂, 15% Ar and 75% N₂ at $p_C = 40$ bar and $\phi = 2.0$ for HPST.

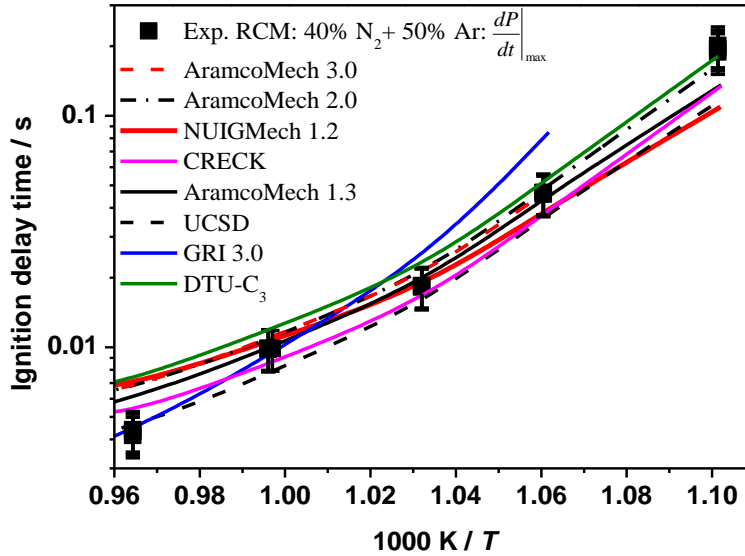


Figure BS37. Experimental and simulation data values of 3.68% CH₄/0.23% C₂H₄/0.46% C₂H₆/0.23% C₃H₈, 5.4% O₂, 15% Ar and 75% N₂ at $p_c = 40$ bar and $\phi = 2.0$ for RCM.

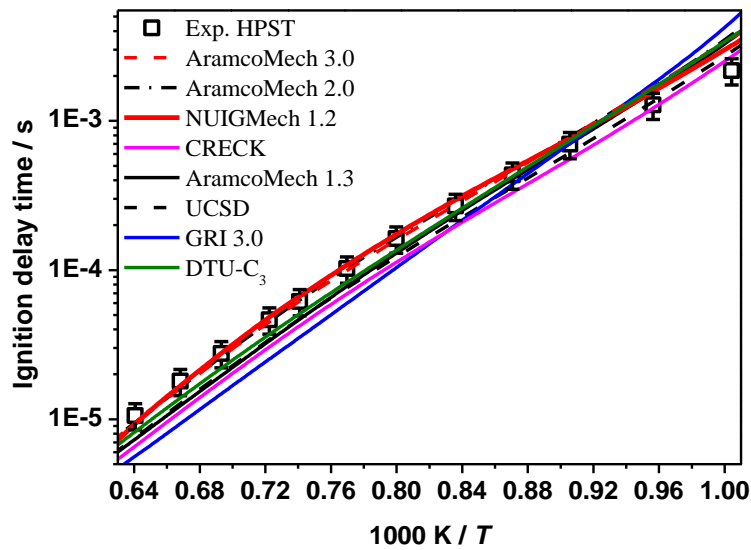


Figure BS38. Experimental and constant volume simulation data of 4.93% CH₄/0.7% C₂H₄/0.7% C₂H₆/0.7% C₃H₈, 17.96% O₂, and 75% N₂ at $p_c = 40$ bar and $\phi = 1.0$ for HPST.

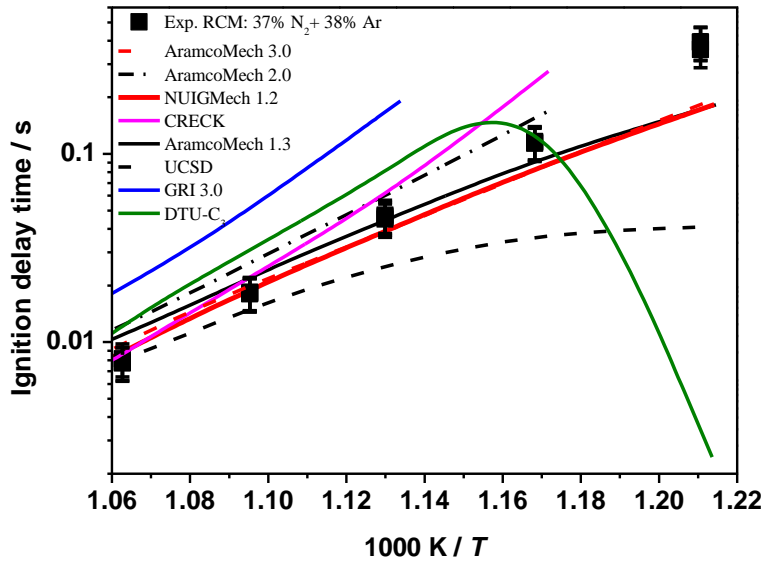


Figure BS39. Experimental and simulation data values of 4.93% CH₄/0.7% C₂H₄/0.7% C₂H₆/0.7% C₃H₈, 17.96% O₂, and 75% N₂ at $p_c = 40$ bar and $\varphi = 1.0$ for RCM.

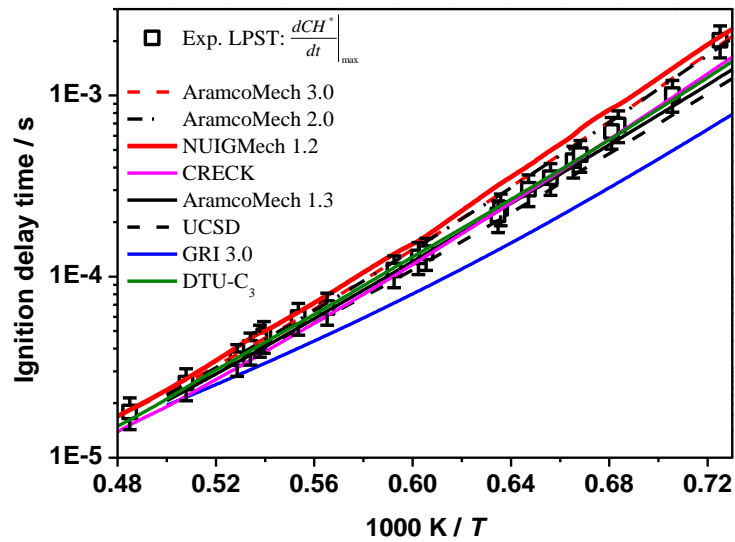


Figure BS40. Experimental and constant volume simulation data of 4.62% CH₄/0.66% C₂H₄/0.66% C₂H₆/0.66% C₃H₈, 8.41% O₂, 10% Ar and 75% N₂ at $p_c = 1$ bar and $\varphi = 2.0$ for LPST.

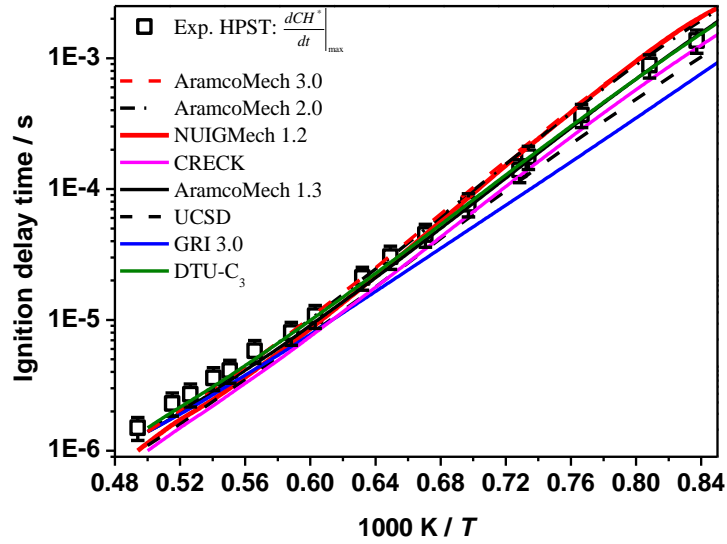


Figure BS41. Experimental and constant volume simulation data of 1.15% CH₄/0.16% C₂H₄/0.16% C₂H₆/0.16% C₃H₈, 8.36% O₂, 15% Ar and 75% N₂ at $p_C = 20$ bar and $\phi = 0.5$ for HPST.

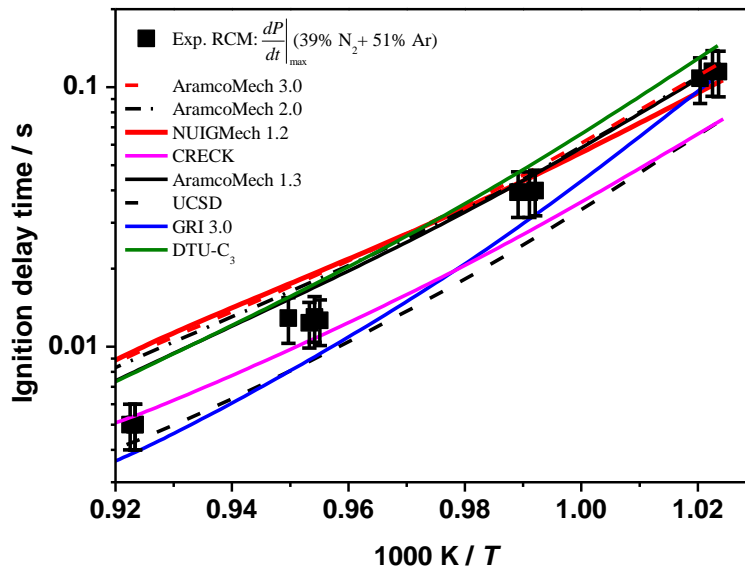


Figure BS42. Experimental and simulation data values of 1.15% CH₄/0.16% C₂H₄/0.16% C₂H₆/0.16% C₃H₈, 8.36% O₂, 15% Ar and 75% N₂ at $p_C = 20$ bar and $\phi = 0.5$ for RCM.

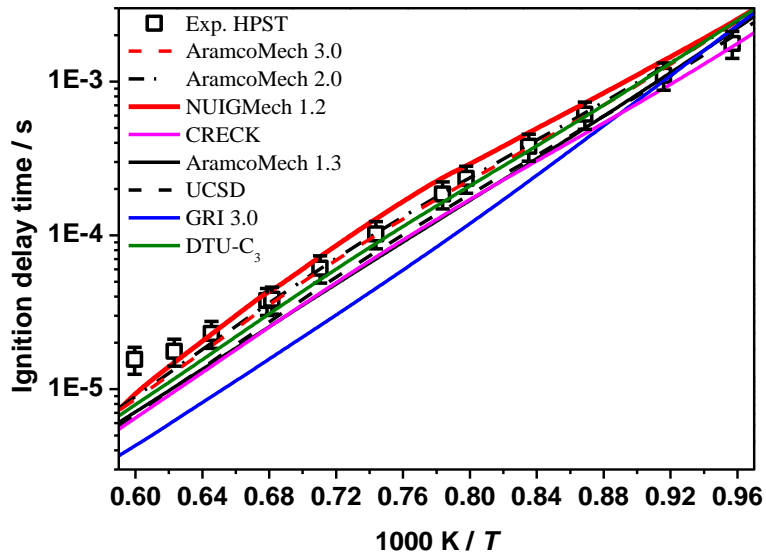


Figure BS43. Experimental and constant volume simulation data of 6.42% CH₄/1.6% C₂H₄/1.6% C₂H₆/1.07% C₃H₈, 14.3% O₂, and 75% N₂ at $p_C = 20$ bar and $\phi = 2.0$ for HPST.

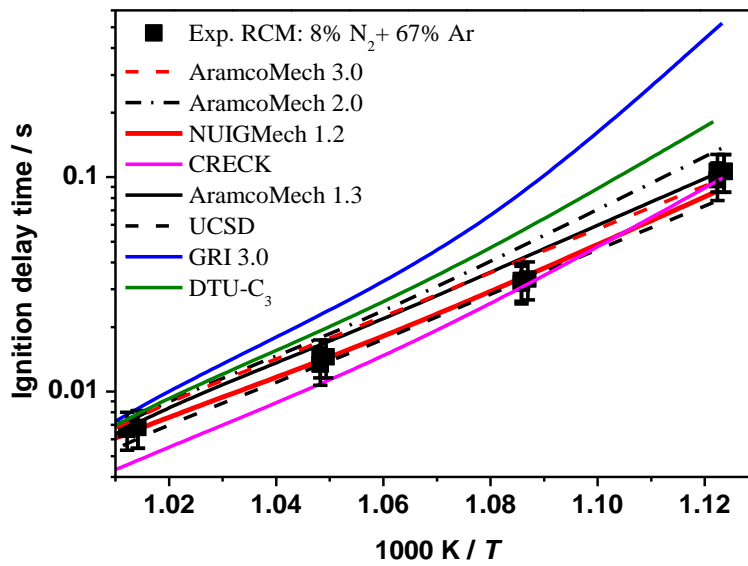


Figure BS44. Experimental and simulation data values of 6.42% CH₄/1.6% C₂H₄/1.6% C₂H₆/1.07% C₃H₈, 14.3% O₂, and 75% N₂ at $p_C = 20$ bar and $\phi = 2.0$ for RCM.

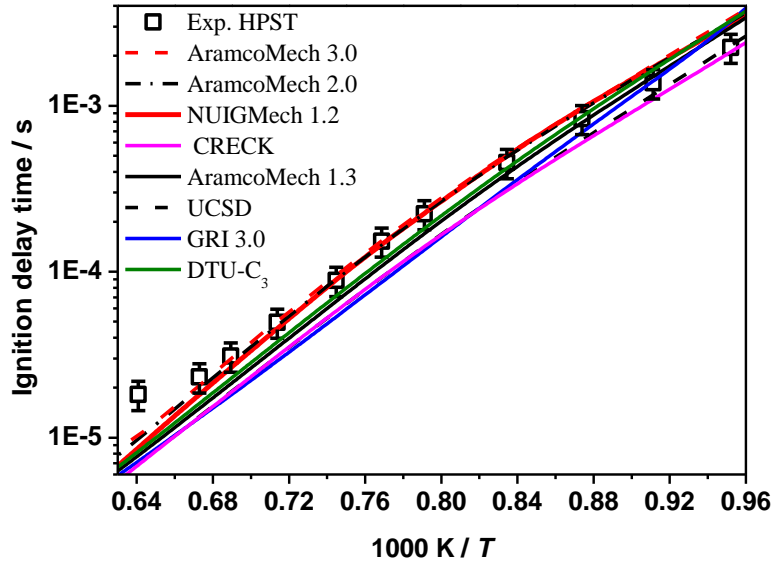


Figure BS45. Experimental and constant volume simulation data of 1.41% CH_4 /0.35% C_2H_4 /0.35% C_2H_6 /0.24% C_3H_8 , 12.64% O_2 , 10% Ar and 75% N_2 at $p_C = 40$ bar and $\varphi = 0.5$ for HPST.

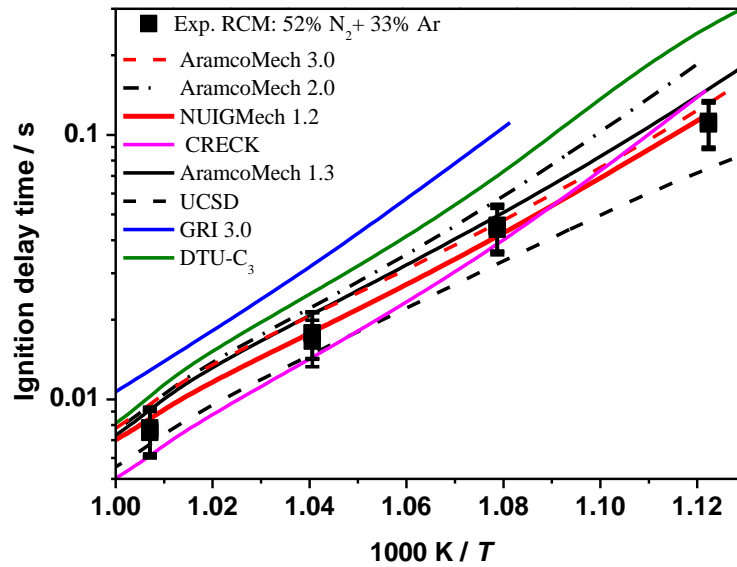


Figure BS46. Experimental and simulation data values of 1.41% CH_4 /0.35% C_2H_4 /0.35% C_2H_6 /0.24% C_3H_8 , 12.64% O_2 , 10% Ar and 75% N_2 at $p_C = 40$ bar and $\varphi = 0.5$ for RCM.

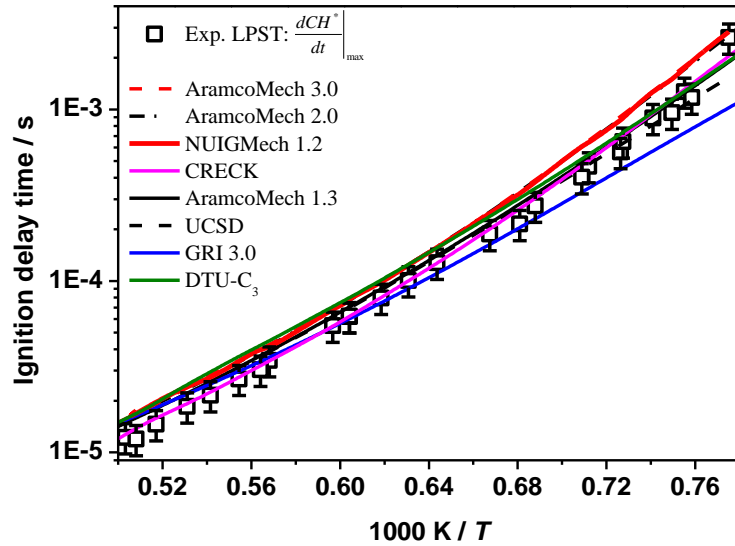


Figure BS47. Experimental and constant volume simulation data of 1.63% CH₄/0.41% C₂H₄/0.41% C₂H₆/0.27% C₃H₈, 7.28% O₂, 15% Ar and 75% N₂ at $p_C = 1$ bar and $\phi = 1.0$ for LPST.

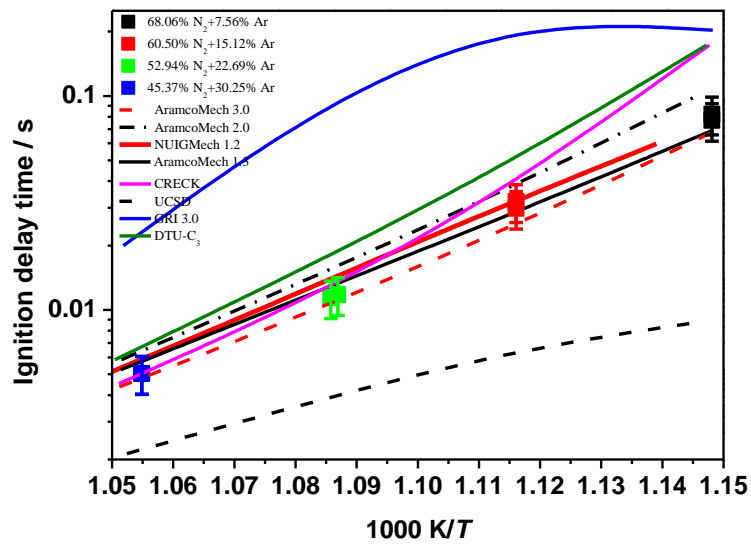


Figure BS48. Experimental and simulation data values of 3.42% CH₄/0.21% C₂H₄/0.43% C₂H₆/0.21% C₃H₈, 20.1% O₂, at $p_C = 90$ bar and $\phi = 0.5$ for RCM.

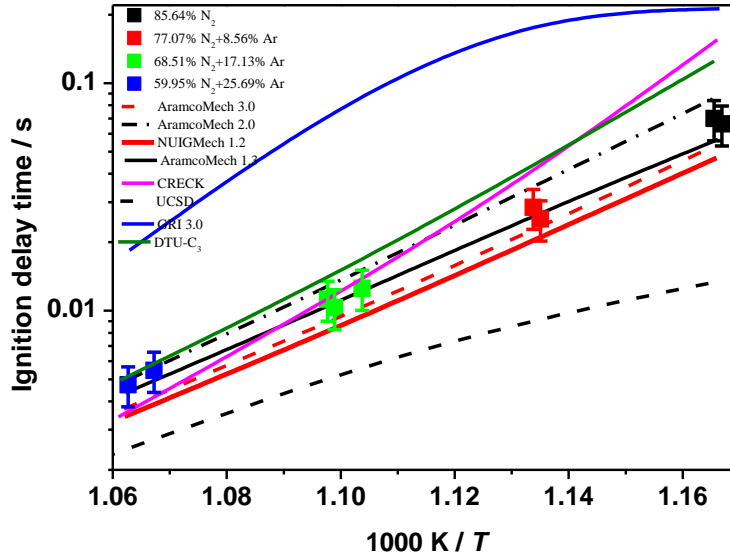


Figure BS49. Experimental and simulation data values of 3.43% CH₄/0.21% C₂H₄/0.43% C₂H₆/0.21% C₃H₈, 10.08% O₂, at $p_c = 135$ bar and $\phi = 1.0$ for RCM.

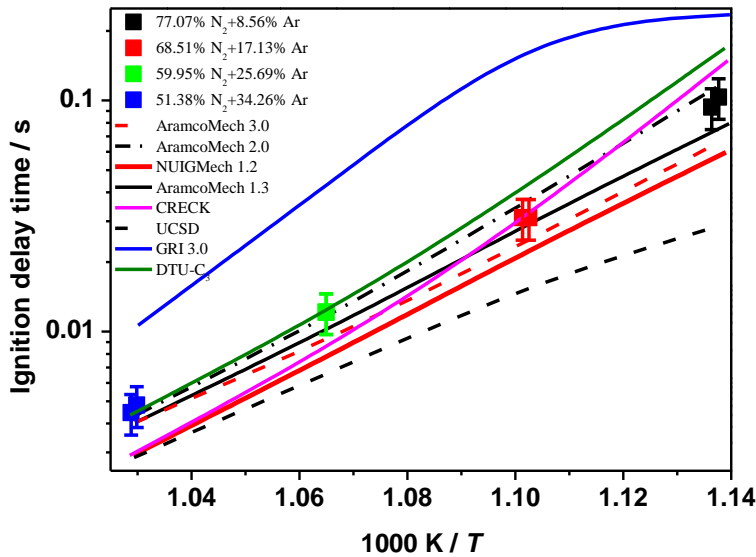


Figure BS50. Experimental and simulation data values of 3.43% CH₄/0.21% C₂H₄/0.43% C₂H₆/0.21% C₃H₈, 10.08% O₂, at $p_c = 90$ bar and $\phi = 1.0$ for RCM.

10. Correlation analyses

A simple form of the correlations applied in this study, follows those previously published by us, [30, 31] and is expressed in Eq. B3.

$$\tau_{\text{idt,corr}} = 10^A \exp\left(\frac{B}{T_C}\right) [\text{CH}_4]^C [\text{C}_2\text{H}_4]^D [\text{C}_2\text{H}_6]^E [\text{C}_3\text{H}_8]^F [\text{Oxygen}]^G [\text{Diluent}]^H \quad (\text{B32})$$

Hence, the performance of the derived correlations over the conditions studied is demonstrated in Figures B2 – B4(b), and 8 as dotted lines of the main document. As seen in Figure B2 for high-temperature range ($T \geq$

1100 K), the derived correlations based on Eq. B3 presented in Table BS12 can reasonably predict all the experimental IDTs with an absolute average error and standard deviation of 35% and 23%, respectively.

Table BS12. Evaluated coefficients for the high temperature correlations of the simulated IDTs for $\text{CH}_4/\text{C}_2\text{H}_4/\text{C}_2\text{H}_6$ (12–90% + 12–20% + 12–90%) mixtures.

$0.25 \leq \varphi \leq 2.0$ $75 \leq \text{dilution} \leq 90\%$	$1 \leq p_5 \leq 15 \text{ /atm}$ $1600 \leq T_5 \leq 2000 \text{ /K}$	$20 \leq p_5 \leq 40 \text{ /atm}$ $1300 \leq T_5 \leq 2000 \text{ /K}$
A	-10.18 ± 0.02	-10.94 ± 0.01
B	20432 ± 38	21208 ± 46
C [methane]	0.9778 ± 0.0027	1.004 ± 0.003
D [ethylene]	-0.0971 ± 0.0081	-0.0409 ± 0.0094
E [ethane]	-0.8513 ± 0.0091	-0.8882 ± 0.0107
F [propane]	0	0
G	-1.423 ± 0.003	-1.399 ± 0.003
H	0.4698 ± 0.0044	0.6658 ± 0.0041
R ²	0.992	0.985
χ^2	2.42E–10	3.48E–10
number of the simulated data points		18498
number of the simulated data sets		2313

As discussed above, according to the presence of significant facility effects (due to heat loss during compression plus induction times) involved in the experimental IDT data in the low temperature regime using the RCM, it is not reasonable to compare the adiabatic constant volume simulations (ACVSs) results with experimental IDTs longer than ~10 ms. As shown in Figure 2 for low-temperature range ($T \leq 1100 \text{ K}$), because NUIGMech1.2 can reliably predict the experimental IDTs by including facility effects, it can be hypothesised that if we could derive reasonable correlations based on the ACVSs using NUIGMech1.2 over the temperature range, these correlations would reliably predict the chemical response of IDTs at the conditions studied. Based on this hypothesis, Table S13 can acceptably follow the ACVSs generated using NUIGMech1.2 over the temperature range studied. Figure 2 in low-temperature range ($T \leq 1100 \text{ K}$) show that most of the correlations are completely compatible with the ACVSs or, at least, have slopes like the ACVSs (the $\exp\left(\frac{B}{T}\right)$ term in Eq.3 refers to the activation energy term in the Arrhenius equation). Hence, it could be maintained that the derived correlations (as proxies for NUIGMech1.2) are able to reasonably anticipate the response of IDTs to any change in the parameters involved in Eq.3 in their validity range. As presented in Table S13, the correlations can reasonably reproduce the experimental IDTs with an absolute average error and standard deviation of 52% and 18%, respectively.

Table BS13. Evaluated coefficients for the low temperature correlations of the simulated IDTs for $\text{CH}_4/\text{C}_2\text{H}_4/\text{C}_2\text{H}_6$ (12–90%/12–20%/12–90%) mixtures.

$$0.25 \leq \varphi \leq 2.0 \qquad 800 \leq T_c \leq 1000 \text{ /K}$$

$75 \leq \text{dilution} \leq 90\%$	$20 \leq p_c \leq 40 \text{ /atm}$	$80 \leq p_c \leq 140 \text{ /atm}$
A	-8.049 ± 0.0248	-9.314 ± 0.0525
B	16817 ± 45	17766 ± 85.27
C [methane]	-0.1383 ± 0.0025	-0.4868 ± 0.0045
D [ethylene]	-0.7222 ± 0.0038	-0.9303 ± 0.0058
E [ethane]	0.31 ± 0.0047	0.5047 ± 0.0071
F	0	0
G	-0.3978 ± 0.0033	-0.0125 ± 0.0066
H	-0.1625 ± 0.0042	0.0345 ± 0.0106
R ²	0.989	0.991
χ^2	4.47E-02	3.09E-05
number of the simulated data points		7542
number of the simulated data sets		943

Like Figure B2, it can be seen in Figure 3 that the derived correlations (Table S14) over the high-temperature range ($T \geq 1100$ K), can properly capture the experimental IDTs. However, the performance of the correlations in the temperature range 1000–1250 K is not as good as it is at higher temperatures in which the correlations were derived. This issue stems from the non-linear trend of IDTs measured over the wide range of temperature plotted in Figure 3. Accordingly, one can see in Table S14 that the absolute average error and standard deviation between the correlation predicted IDTs and the experimental ones in Figure 4 are acceptably within 25% and 16%, respectively.

Table BS14. Evaluated coefficients for the high temperature correlations of the simulated IDTs for $\text{CH}_4/\text{C}_2\text{H}_4/\text{C}_2\text{H}_6/\text{C}_3\text{H}_8$ (10–80%/5–15%/5–80%/5–10%) mixtures.

$0.25 \leq \varphi \leq 2.0$ $75 \leq \text{dilution} \leq 90\%$	$1 \leq p_5 \leq 20 \text{ / atm}$ $1200 \leq T_5 \leq 2000 \text{ / K}$	$20 \leq p_5 \leq 40 \text{ / atm}$ $1300 \leq T_5 \leq 2000 \text{ / K}$
A	-10.74 ± 0.02	-10.35 ± 0.02
B	22884 ± 50	21318 ± 43
C [methane]	1.240 ± 0.011	0.8343 ± 0.0082
D [ethylene]	-0.1457 ± 0.0114	-0.1656 ± 0.008
E [ethane]	-0.3401 ± 0.0130	-0.1857 ± 0.0102
F [propane]	-0.1500 ± 0.0127	-0.2225 ± 0.0083
G	-1.748 ± 0.003	-1.496 ± 0.003
H	0.3558 ± 0.003	0.4808 ± 0.0047
R ²	0.992	0.991
χ^2	2.93E-08	1.02E-11
number of the simulated data points		15360
number of the simulated data sets		1920

The performance of the derived correlations presented in Table S15 for the quaternary blended fuel studied in the low temperature regime (800–1000 K) is demonstrated in Figure B3. According to the analyses presented above for the performance of the correlation for the tertiary blended fuel at low temperatures, it is seen that like the previous case (Figure 2 for low-temperature range), most of the correlations are completely compatible with the ACVSSs, so that the correlations can reasonably predict the pattern of experimental IDTs

in terms of response to changes in the parameters involved in Eq. 3. Table S15 shows that the derived correlations for the quaternary blended fuel can predict experimental IDTs with an absolute average error and standard deviation of 50% and 23%, respectively, even though significant facility effects are involved in the experimental data.

Table BS15. Evaluated coefficients for correlation of the low temperature correlations IDTs for $\text{CH}_4/\text{C}_2\text{H}_4/\text{C}_2\text{H}_6/\text{C}_3\text{H}_8$ (10–80%/5–15%/5–80%/5–10%) mixtures.

	$800 \leq T_c \leq 1000 / \text{K}$	
	$0.25 \leq \Phi \leq 2.0$ $75 \leq \text{DILUTION} \leq 90\%$	$20 \leq p_c \leq 40 / \text{atm}$ $80 \leq p_c \leq 140 / \text{atm}$
A	-8.011 ± 0.021	-8.650 ± 0.033
B	15826 ± 34	15737 ± 50
C [METHANE]	-0.2569 ± 0.0032	-0.2376 ± 0.0045
D [ETHYLENE]	-0.5008 ± 0.0028	-0.4712 ± 0.0039
E [ETHANE]	0.1332 ± 0.0053	0.1760 ± 0.0078
F [PROPANE]	-0.1048 ± 0.0054	-0.3613 ± 0.0081
G	-0.2916 ± 0.0027	-0.1691 ± 0.0042
H	-0.0893 ± 0.0048	0.0639 ± 0.0079
R ²	0.991	0.984
X ²	1.53E-04	2.05E-5
NUMBER OF THE SIMULATED DATA POINTS		10559

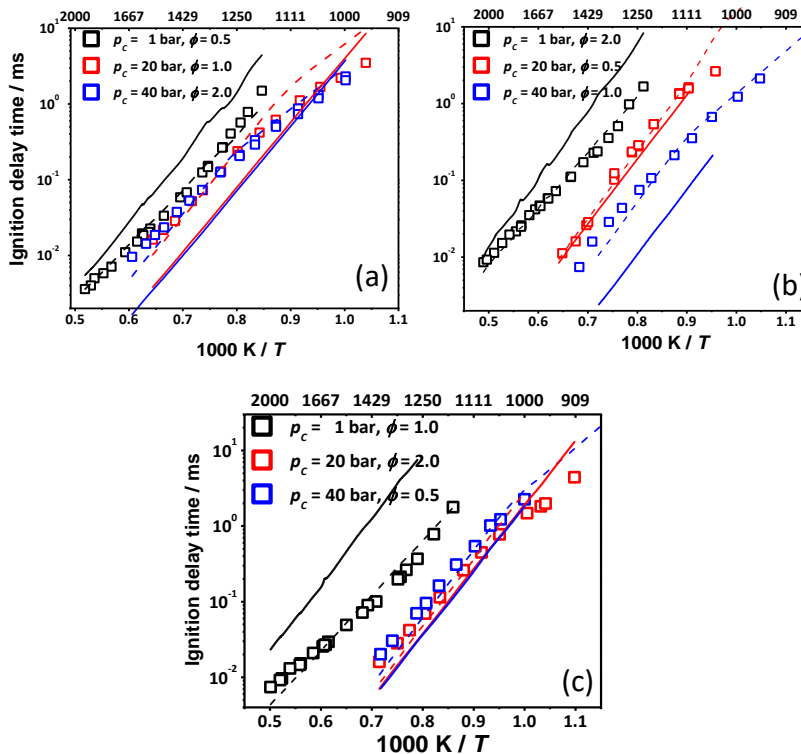


Figure BS51. Comparisons of quaternary correlations against the experimental IDTs of binary blends for C_2H_4/C_3H_8 [4]. Solid lines: quaternary correlation, dashed lines; binary correlation [4].

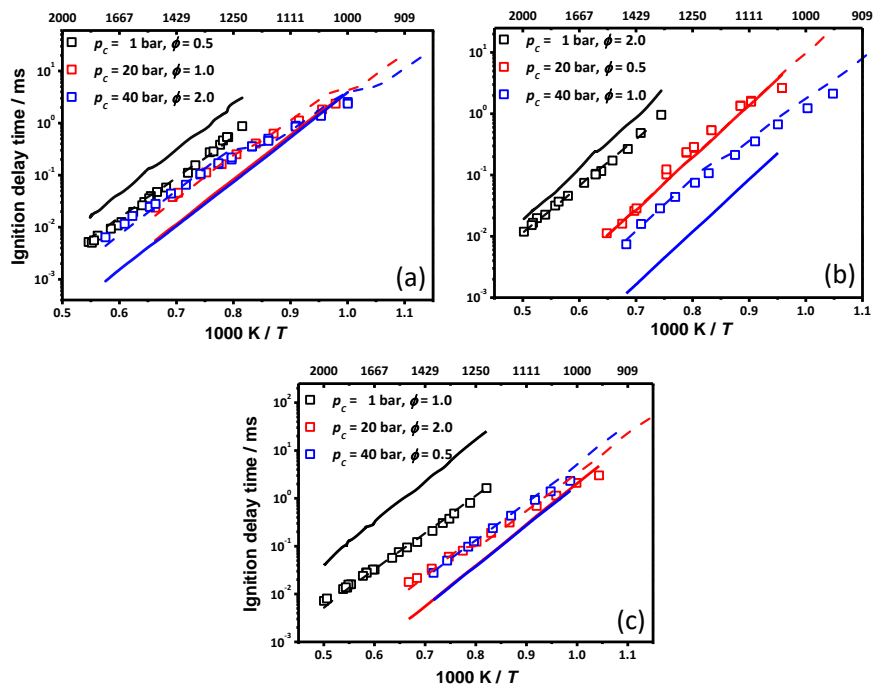


Figure BS52. Comparisons of quaternary correlations against the experimental IDTs of binary blends for C_2H_6/C_3H_8 [4]. Solid lines: quaternary correlation, dashed lines; binary correlation [4].

11. Rate constant graphs and sensitivity analyses

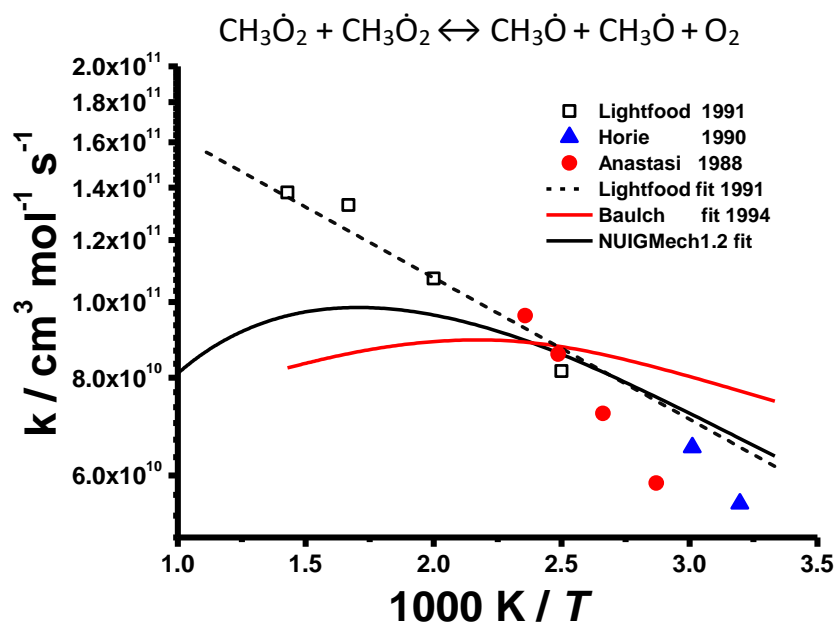


Figure BS53. Comparisons of the rate constants for $\text{CH}_3\dot{\text{O}}_2 + \text{CH}_3\dot{\text{O}}_2 \leftrightarrow \text{CH}_3\dot{\text{O}} + \text{CH}_3\dot{\text{O}} + \text{O}_2$, Lightfoot [32], Horie [33], Anastasi [34] and Baulch [35].

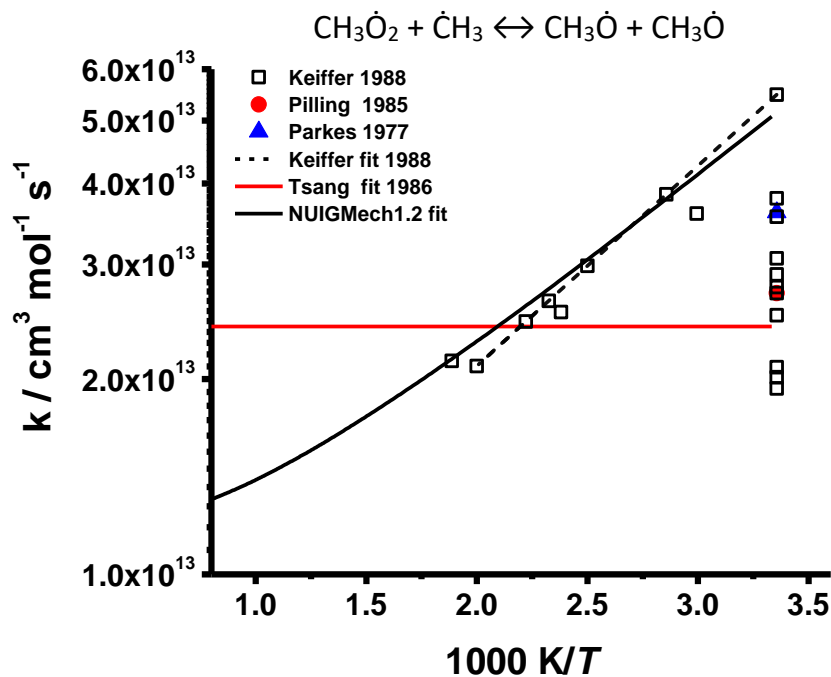


Figure BS54. Comparisons of the rate constants for $\text{CH}_3\dot{\text{O}}_2 + \dot{\text{C}}\text{H}_3 \leftrightarrow \text{CH}_3\dot{\text{O}} + \text{CH}_3\dot{\text{O}}$, Keiffer [36], Pilling [37], Parkes [38] and Tsang [39].

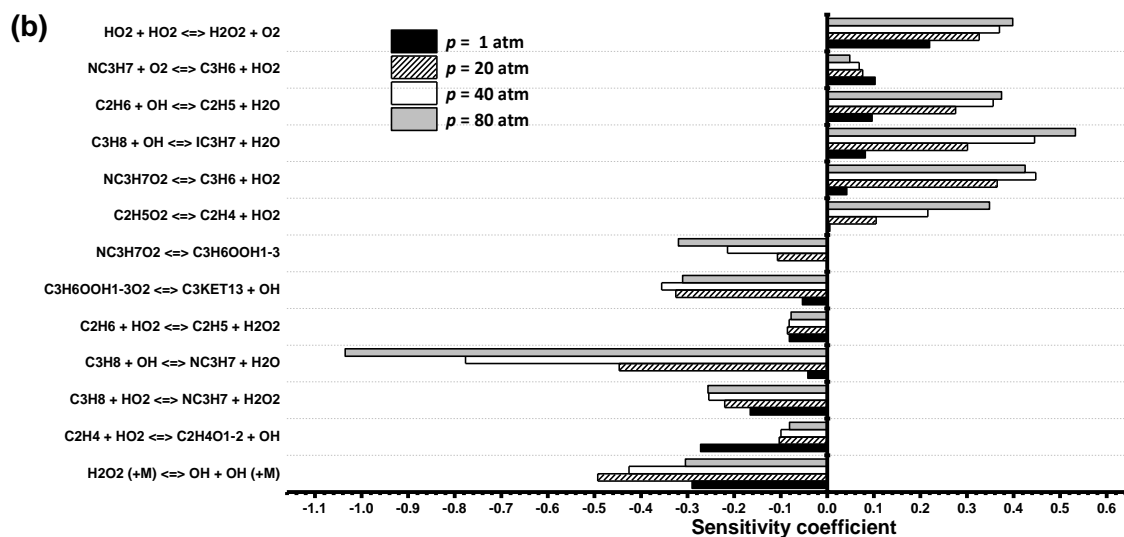
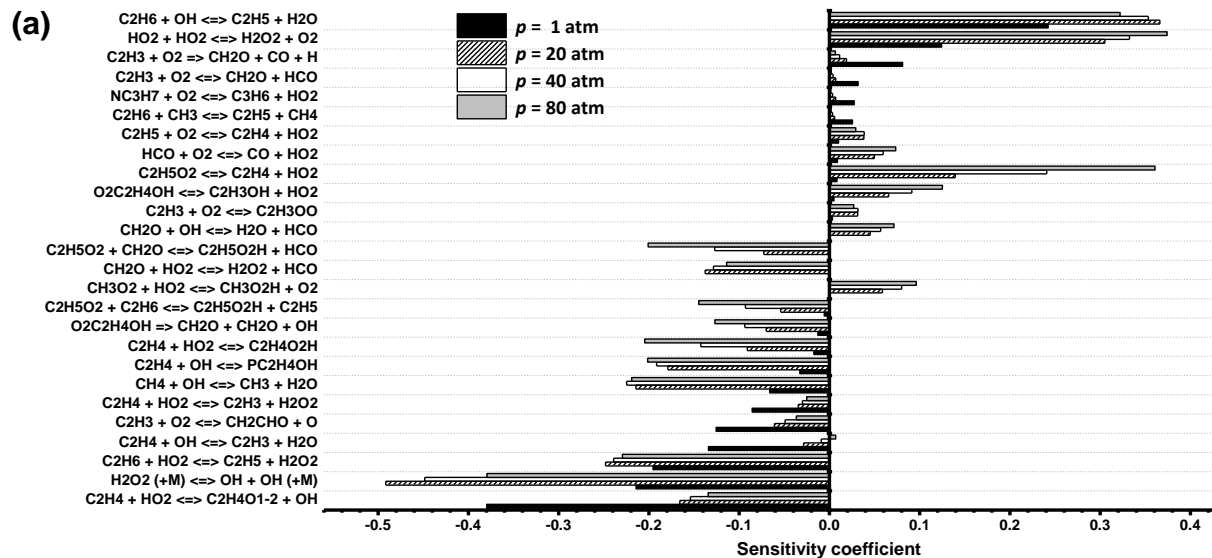


Figure BS55. Sensitivity analyses to IDT as function of pressure at $T_C = 800$ K, $\phi = 1.0$, for (a) 50% CH_4 /25% C_2H_4 /25% C_2H_6 , and (b) 50% CH_4 /16.66% C_2H_4 /16.66% C_2H_6 /16.66% C_3H_8 in air.

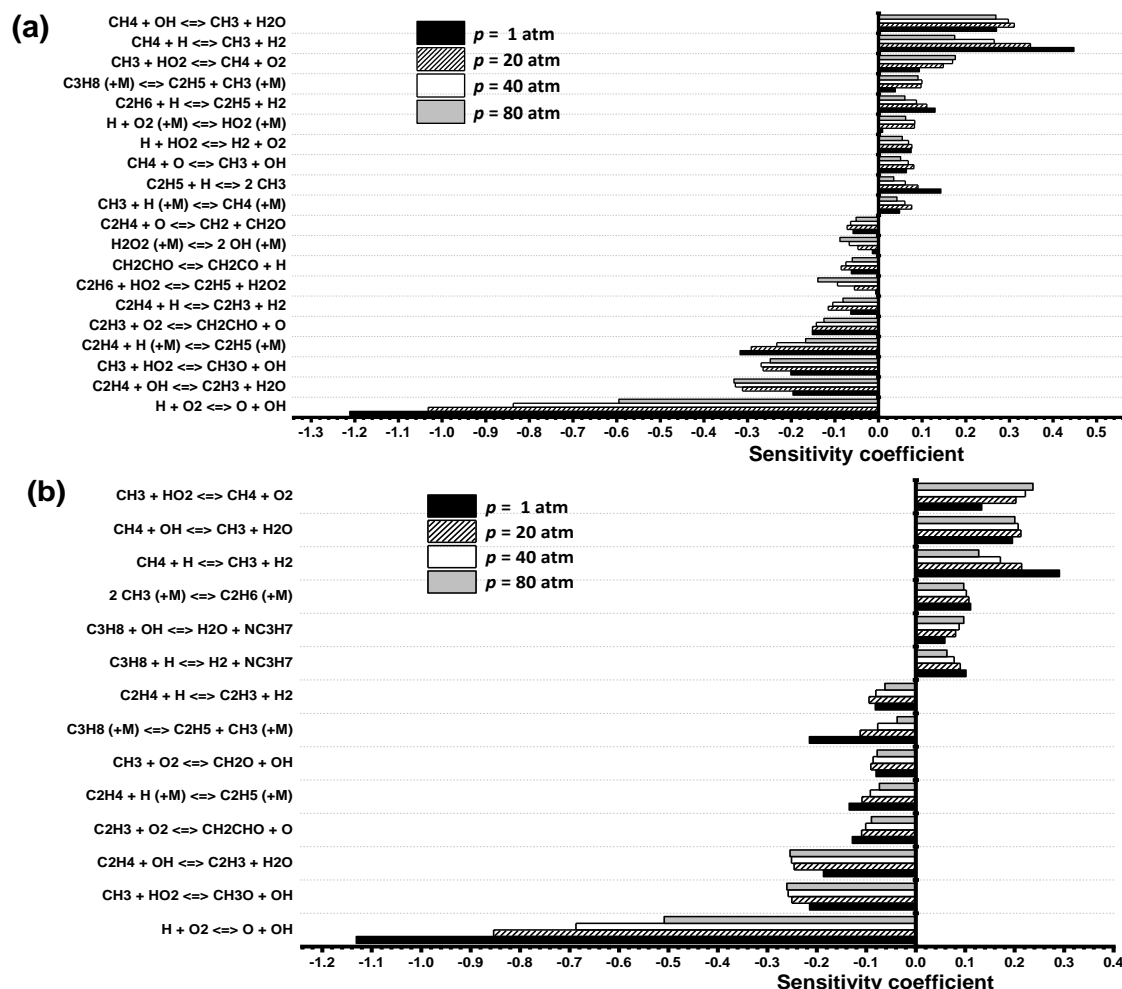


Figure BS56. Sensitivity analyses to IDT as function of pressure at $T_c = 1450$ K, $\phi = 1.0$, for (a) 50% CH_4 /25% C_2H_4 /25% C_2H_6 , and (b) 50% CH_4 /16.66% C_2H_4 /16.66% C_2H_6 /16.66% C_3H_8 in air.

12. References

- [1] C.J. Aul, W.K. Metcalfe, S.M. Burke, H.J. Curran, E.L. Petersen, Ignition and kinetic modeling of methane and ethane fuel blends with oxygen: A design of experiments approach, *Combust. Flame* 160 (2013) 1153-1167.
- [2] F.R. Gillespie, An experimental and modelling study of the combustion of oxygenated hydrocarbons, National University of Ireland, Galway, (2014), <http://hdl.handle.net/10379/4419>.
- [3] J Wurmel, M. McGuinness, J.M. Simmie, High-Temperature Oxidation of Ethylene Oxide in Shock Waves, *J. Chem. Soc., Faraday Trans. 92* (1996) 715-721.
- [4] C. Morley, Gaseq: a chemical equilibrium program for windows, (2004), <http://www.gaseq.co.uk>
- [5] H. Nakamura, D. Darcy, M. Mehl, C.J. Tobin, W.K. Metcalfe, W.J. Pitz, C.K. Westbrook, H.J. Curran, An experimental and modeling study of shock tube and rapid compression machine ignition of n-butylbenzene/air mixtures, *Combust. Flame* 161 (2014) 49-64.

- [6] U. Burke, K.P. Somers, P. O'Toole, C.M. Zinner, N. Marquet, G. Bourque, E.L. Petersen, W.K. Metcalfe, Z. Serinyel, H.J. Curran, An ignition delay and kinetic modeling study of methane, dimethyl ether, and their mixtures at high pressures, *Combust. Flame* 162 (2015) 315-330.
- [7] A. Ramalingam, K. Zhang, A. Dhongde, L. Virnich, H. Sankhla, H. Curran, A. Heufer, An RCM experimental and modeling study on CH₄ and CH₄/C₂H₆ oxidation at pressures up to 160 Bar, *Fuel* 206 (2017) 325-333.
- [8] D. Healy, H.J. Curran, S. Dooley, J.M. Simmie, D.M. Kalitan, E.L. Petersen, G. Bourque, Methane/propane mixture oxidation at high pressures and at high, intermediate and low temperatures, *Combust. Flame* 155 (2008) 451-461.
- [9] D. Healy, H.J. Curran, J.M. Simmie, D.M. Kalitan, C.M. Zinner, A.B. Barrett, E.L. Petersen, G. Bourque, Methane/ethane/propane mixture oxidation at high pressures and at high, intermediate and low temperatures, *Combust. Flame* 155 (2008) 441-448.
- [10] W.K. Metcalfe, S.M. Burke, S.S. Ahmed, H.J. Curran, A hierarchical and comparative kinetic modeling study of C₁ – C₂ hydrocarbon and oxygenated fuels, *Int. J. Chem. Kinet.* 45 (2013) 638-675.
- [11] S. Yousefian, N.J. Quinlan, R.F.D. Monaghan, Simulation of turbulent flow in a rapid compression machine: Large eddy simulation and computationally efficient alternatives for the design of ignition delay time experiments, *Fuel* 234 (2018) 30-47.
- [12] C. Hemken, U. Burke, K.Y. Lam, D.F. Davidson, R.K. Hanson, K.A. Heufer, K. Kohse-Hoinghaus, Toward a better understanding of 2-butanone oxidation: detailed species measurements and kinetic modeling, *Combust. Flame* 184 (2017) 195-207.
- [13] TiePie: Handyscope, <https://www.tiepie.com/en/oscilloscope-software>.
- [14] PicoScope, <https://www.picotech.com/downloads>.
- [15] E.L. Petersen, M.J.A. Rickard, M.W. Crofton, E.D. Abbey, M.J. Traum, D.M. Kalitan, A Facility for gas- and condensed-phase measurements behind shock waves, *Meas. Sci. Technol.* 16 (2005) 1716-1729.
- [16] B.W. Weber, C.-J. Sung, M.W. Renfro, On the uncertainty of temperature estimation in a rapid compression machine, *Combust. Flame* 162 (2015) 2518-2528.
- [17] C.-W. Zhou, Y. Li, U. Burke, C. Banyon, K.P. Somers, S.T. Ding, S. Khan, J.W. Hargis, T. Sikes, O. Mathieu, E.L. Petersen, M. AlAbbad, A. Farooq, Y.S. Pan, Y.J. Zhang, Z.H. Huang, J. Lopez, Z. Loparo, S.S. Vasu, H.J. Curran, An experimental and chemical kinetic modeling study of 1,3-butadiene combustion: Ignition delay time and laminar flame speed measurements, *Combust. Flame* 197 (2018) 423-438.
- [18] S.M. Burke, W. Metcalfe, O. Herbinet, F. Battin-Leclerc, F.M. Haas, J. Santner, F.L. Dryer, H.J. Curran, An experimental and modeling study of propene oxidation. Part 1: Speciation measurements in jet-stirred and flow reactors, *Combust. Flame* 161 (2014) 2765-2784.
- [19] Y. Li, C.-W. Zhou, K.P. Somers, K.W. Zhang, H.J. Curran, The oxidation of 2-butene: A high pressure ignition delay, kinetic modeling study and reactivity comparison with isobutene and 1-butene, *Proc Combust Inst* 36 (2017) 403-411.

- [20] C.-W. Zhou, Y. Li, E. O'Connor, K.P. Somers, S. Thion, C. Keesee, O. Mathieu, E.L. Petersen, T.A. DeVerter, M.A. Oehlschlaeger, G. Kukkadapu, C.J. Sung, M. Alrefae, F. Khaled, A. Farooq, P. Dirrenberger, P.A. Glaude, F. Battin-Leclerc, J. Santner, Y.G. Ju, T. Held, F.M. Haas, F.L. Dryer, H.J. Curran, A comprehensive experimental and modeling study of isobutene oxidation, *Combust Flame* 167 (2016) 353-379.
- [21] U. Burke, W.K. Metcalfe, S.M. Burke, K.A. Heufer, P. Dagaut, H.J. Curran, A detailed chemical kinetic modeling, ignition delay time and jet-stirred reactor study of methanol oxidation, *Combust Flame* 165 (2016) 125-136.
- [22] S.M. Burke, U. Burke, R. Mc Donagh, O. Mathieu, I. Osorio, C. Keesee, A. Morones, E.L. Petersen, W.J. Wang, T.A. DeVerter, M.A. Oehlschlaeger, B. Rhodes, R.K. Hanson, D.F. Davidson, B.W. Weber, C.J. Sung, J. Santner, Y.G. Ju, F.M. Haas, F.L. Dryer, E.N. Volkov, E.J.K. Nilsson, A.A. Konnov, M. Alrefae, F. Khaled, A. Farooq, P. Dirrenberger, P.A. Glaude, F. Battin-Leclerc, H.J. Curran, An experimental and modeling study of propene oxidation. Part 2: Ignition delay time and flame speed measurements, *Combust Flame* 162 (2015) 296-314.
- [23] W.K. Metcalfe, S.M. Burke, S.S. Ahmed, H.J. Curran, A hierarchical and comparative kinetic modeling study of C₁ – C₂ hydrocarbon and oxygenated fuels, *Int. J. Chem. Kinet.* 45 (2013) 638–675.
- [24] A. Keromnes, W.K. Metcalfe, K.A. Heufer, N. Donohoe, A.K. Das, C.J. Sung, J. Herzler, C. Naumann, P. Griebel, O. Mathieu, M.C. Krejci, E.L. Petersen, W.J. Pitz, H.J. Curran, An experimental and detailed chemical kinetic modeling study of hydrogen and syngas mixture oxidation at elevated pressures, *Combust Flame* 160 (2013) 995-1011.
- [25] H. Hashemi, J.M. Christensen, L.B. Harding, S.J. Klippenstein, P. Glarborg, High-pressure oxidation of propane, *Proc Combust Inst* 37 (2019) 461-468.
- [26] G. Bagheri, E. Ranzi, M. Pelucchi, A. Parente, A. Frassoldati, T. Faravelli, Comprehensive kinetic study of combustion technologies for low environmental impact: MILD and OXY-fuel combustion of methane, *Combust Flame* 212 (2020) 142-155.
- [27] Chemical-Kinetic Mechanisms for Combustion Applications. <http://combustion.ucsd.edu>.
- [28] G.P. Smith, D.M. Golden, M. Frenklach, N.W. Moriarty, B. Eiteneer, M. Goldenberg, C.T. Bowman, R.K. Hanson, S. Song, W.C. Gardiner, V.V. Lissianski, Z. Qin, http://www.me.berkeley.edu/gri_mech/
- [29] G.P. Smith, Y. Tao, H. Wang, Foundational fuel chemistry model version 1.0 (FFCM-1), Stanford University, (2016).
- [30] M. Baigmohammadi, V. Patel, S. Martinez, S. Panigrahy, A. Ramalingam, U. Burke, K.P. Somers, K.A. Heufer, A. Pekalski, H.J. Curran, A comprehensive experimental and simulation study of ignition delay time characteristics of single fuel C₁ – C₂ hydrocarbons over a wide range of temperatures, pressures, equivalence ratios, and dilutions, *Energ Fuel* 34 (2020) 3755-3771.
- [31] M. Baigmohammadi, V. Patel, S. Nagaraja, A.K. Ramalingam, S. Martinez, S. Panigrahy, A.A. El-Sabor Mohamed, K.P. Somers, U. Burke, K.A. Heufer, A. Pekalski, H.J. Curran, Comprehensive experimental and simulation study of the ignition delay time characteristics of binary blended

methane, ethane, and ethylene over a wide range of temperature, pressure, equivalence ratio, and dilution, *Energy Fuel* 34(7) (2020) 8808–8823.

[32] P. D. Lightfoot, P. Roussel, F. Caralp, R. Lesclaux, Flash photolysis study of the $\text{CH}_3\dot{\text{O}}_2 + \text{CH}_3\dot{\text{O}}_2$ and $\text{CH}_3\dot{\text{O}}_2 + \text{H}\dot{\text{O}}_2$, reactions between 600 and 719 K: unimolecular decomposition of methylhydroperoxide, *J. Chem. Soc. Faraday Trans.* 87(19) (1991) 3213-3220.

[33] O. Horie, J.N. Crowley, G.K. Moortgat, Methylperoxy self-reaction: products and branching ratio between 223 and 333 K, *J. Phys. Chem.* 94 (1990) 8198-8203.

[34] C. Anastasi, P.J. Couzens, D.J. Waddington, M.J. Brown, D.B. Smith, The self reactions of methylperoxy radicals in the gas phase, 10th Int. Symp. Gas Phase Kinet. Swansea, (1988) Abstracts.

[35] D.L. Baulch, C. Cobos, R.A. Cox, C. Esser, P. Frank, T. Just, & J. Warnatz, Evaluated kinetic data for combustion modelling, *J. Phys. Chem. Ref. Data.* 21(3) (1992) 411-734.

[36] M. Keiffer, A. J. Miscampbell, M.J. Pilling, A global technique for analysing multiple decay curves application to the $\dot{\text{C}}\text{H}_3 + \text{O}_2$ system *J. Chem. Soc., Faraday Trans.* 2 (1988) 505-514.

[37] M.J. Pilling, M.J.C. Smith, A laser flash photolysis study of the reaction $\dot{\text{C}}\text{H}_3 + \text{O}_2 \rightarrow \text{CH}_3\dot{\text{O}}_2$ at 298 K, *J. Phys. Chem.* 89 (1985) 4713-4720.

[38] D.A. Parkes, The oxidation of methyl radicals at room temperature, *Int. J. Chem. Kinet.* 9(3) (1977) 451-469.

[39] W. Tsang, R.F. Hampson, Chemical kinetic data base for combustion chemistry. Part I. Methane and related compounds, *Int. J. Chem. Kinet.* 15 (1986) 1087-1279.

Appendix C

(Supplementary material for Chapter 5)

1. Design of experiments

The method applied to design the matrix of experiments is a robust approach for experimental research with many parameters involved, and it has already been discussed by Baigmohammadi et al. [1, 2] for single and binary fuel blends. The variables and levels involved in designing the matrix of experiments for the current study are presented in Table S1 and Table S2, for C₂H₄/C₃H₈ and C₂H₆/C₃H₈ blends, respectively.

Table CS1. Variables and levels for designing of C₂H₄/C₃H₈ blend in the current experiments using the Taguchi [3] method.

<i>Variables</i>	<i>Fuel composition</i>	<i>Dilution</i>	<i>Equivalence ratio</i>	<i>Pressure (bar)</i>
<i>Levels</i>				
1	50% C ₂ H ₄ + 50% C ₃ H ₈	75%	0.5	1.0
2	70% C ₂ H ₄ + 30% C ₃ H ₈	85%	1.0	20.0
3	90% C ₂ H ₄ + 10% C ₃ H ₈	90%	2.0	40.0

Table CS2. Variables and levels for designing of C₂H₆/C₃H₈ blend in the current experiments using the Taguchi [3] method.

<i>Variable</i>	<i>Fuel composition</i>	<i>Dilution</i>	<i>Equivalence ratio</i>	<i>Pressure (bar)</i>
<i>Levels</i>				
1	50% C ₂ H ₆ + 50% C ₃ H ₈	75%	0.5	1.0
2	70% C ₂ H ₆ + 30% C ₃ H ₈	85%	1.0	20.0
3	90% C ₂ H ₆ + 10% C ₃ H ₈	90%	2.0	40.0

2. Facilities

All of the facilities used for the experiments performed in the current study, such as the low-pressure shock tube (LPST), high-pressure shock tube (HPST), and rapid compression machines (RCM), were described in detail by Baigmohammadi et al. [1, 2, 4-12] and thus here we present a summary description, especially for those facilities located at NUIG. The measured IDTs in the HPST and RCMs, as discussed in Section 2, “design of experiments”, are defined as the maximum gradient in pressure ($\frac{dP}{dt}$) behind the reflected shock, Figs. S1 and S3. However, for the LPST data and when the test mixture is highly diluted in the HPST, Fig. CS2, the IDT is defined as the maximum gradient in CH* ($\frac{dCH^*}{dt}$) behind the reflected shock.

2.1. Low-/High-pressure shock-tube

The ST is a facility that is most ideal to measure IDTs of ≤ 2 ms, for low- and high-pressure and high-temperature (≥ 1000 K) conditions. In this regard, for the current study, a LPST was used to record the IDT data at ~ 1 bar. Most of the experiments were carried out using helium as the primary driver gas, but some experiments were performed in which the incident shock velocity had to be reduced to reach the desired conditions, and so nitrogen was added to the helium driver gas to tailor the condition. The physical configuration of the five PCB sensors installed in the driven section is displayed in Table S3, including the distance from the endwall. The properties behind the reflected shock, such as the reflected-shock temperature (T_5) and pressure (p_5), were calculated using the Gaseq software [13]. Additionally, for the highly diluted cases which have weak pressure signals, IDTs were determined from light emission profiles using a photomultiplier with a Thorlabs CH* filter, within CWL:430 nm \pm 10 FWHM installed at the sidewall of the ST's endcap. Finally, to improve the accuracy of the experimental data collected, fluctuations allowed in pressure measurements were restricted to ± 0.05 bar of the target pressure of 1 bar.

Table CS3. Specifications of the applied LPST.

Total length	6.33 m	
Section	Length (m)	Diameter (mm)
Driver	0.53	520
Driven	5.8	102.4
Material	Stainless-steel	
Controlling system	Sharp edges arrow	
Diaphragm's material	Polycarbonate/Polyester	
Diaphragm's thickness	105–120 μ m (nominal)	
Sensor PCB#1	0.03 m	
Sensor PCB#2	0.237 m	
Sensor PCB#3	0.366 m	
Sensor PCB#4	0.495 m	
Sensor PCB#5	1.89 m	

The HPST was used to measure the IDTs for pressures ranging from 20 – 40 bar. Similar to the LPST, helium was used as the driver gas with a small number of tailored experiments performed in which nitrogen was added to helium for conditions where it was required to reduce the incident shock velocity. Six piezoelectric pressure transducers, located near the endwall of the driven section, were used to extrapolate and calculate the incident shock velocity at the endwall. As mentioned before for the LPST, the Gaseq software [13] was used to calculate the conditions behind the reflected shock wave by considering the mixture composition, incident shock pressure, temperature, and shock velocity. In mixtures with dilution concentrations of $\leq 85\%$, a Kistler 603B transducer mounted at the endwall was used to record the IDTs. For mixtures with dilution concentrations of $\geq 90\%$, IDTs were measured using a photodiode array detector system with a Thorlabs CH* filter, within CWL:430 nm \pm 10 FWHM installed on the sidewall of the ST's endcap.

Table CS4. Specifications of the applied high-pressure shock tube

Total length	9.1 m	
Section	Length (m)	Diameter (mm)
Driver	3.0	63.5
Middle	0.04	63.5
Driven	5.7	63.5
Material	Stainless-steel (1.4571/316Ti and 1.4462/F51)	
Controlling system	Double-diaphragm type	
Diaphragm's material	Aluminium (1050 H14)	
Diaphragm's thickness	0.8~2 mm; according to target pressure	
Pre-scoring the diaphragms	0.2~1.1 mm; according to target pressure and the diaphragms' thickness	
Sensor PCB#1	0.01 m	
Sensor PCB#2	0.15 m	
Sensor PCB#3	0.29 m	
Sensor PCB#4	0.57 m	
Sensor PCB#5	0.85 m	
Sensor PCB#6	1.165 m	

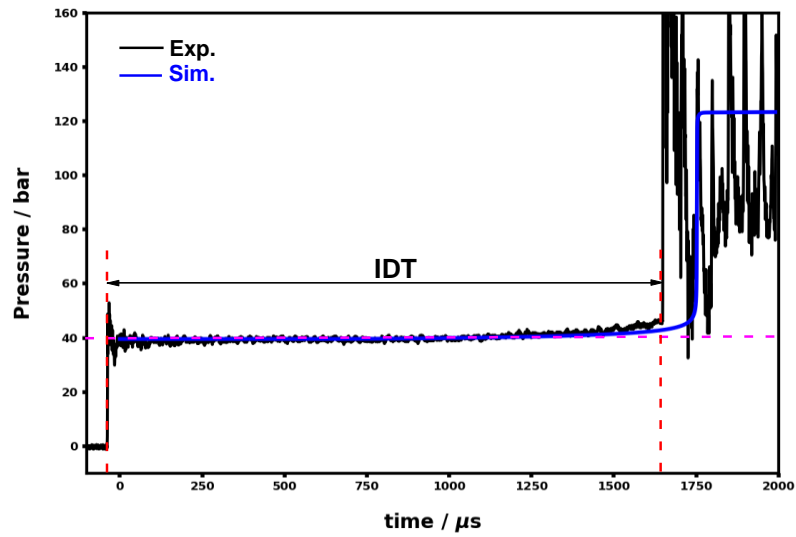


Figure CS1. IDT definition [1, 2] for the LPST and the HPST using the experimental pressure profile (solid black line) against the simulated profile (solid blue line).

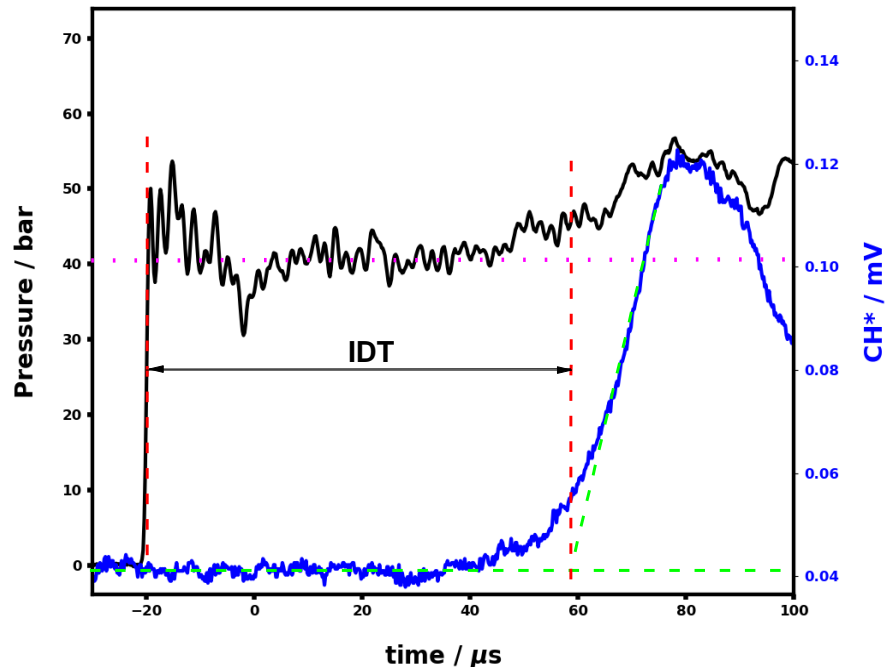


Figure CS2. Definition of IDT [1, 2] showing experimental pressure profile (solid black line) and experimental CH* history (solid blue line) for the LPST and the HPST.

2.2. NUIG/PCFC-RCM

The rapid compression machine (RCM) at NUIG is a facility designed to measure IDTs at high to moderate pressures ($\sim 10 - 40$ bar), and at low temperatures $600 \leq T \leq 1000$ K. The adiabatic core assumption was used to simulate the IDT measurements with the imposition of volume profiles based on the non-reactive pressure profiles to compensate for the non-adiabatic conditions. The general facility's specifications are presented in Table S5, along with the general parameters. For cases with dilution concentrations of 75% (close to fuel in air) the IDTs and the pressure-time profiles of the non-reactive mixtures were recorded using a Kistler 6045A transducer installed on the sidewall of the reaction chamber. However, for mixtures with dilution concentrations of approximately 85% and 90% and the post-compression pressures of 20 and 40 bar, a Kistler transducer and a photomultiplier with a Thorlabs CH* filter, within $\text{CWL}: 430 \text{ nm} \pm 10 \text{ FWHM}$ from Thorlabs, was used. Similar to the procedure used in the LPST and HPST experiments, the Gaseq software was used to calculate the post-compression temperature (T_c), assuming isentropic compression in the RCM. All post-compression pressures (p_c) were restricted to ± 0.5 bar of the target pressure to improve the measurement consistency.

Table CS5. Specifications of the NUIG–RCM.

Parameter	Value
Bore size of the reaction chamber (m)	0.03820
Volume of the reaction chamber (m ³)	3.3191x10 ⁻⁵
Piston's velocity (U_p) (m/s)	9.34 ~ 12.94
Piston's stroke length (m)	0.16817
Piston's type	Flat head with the crevice
Type	Twin-counter piston

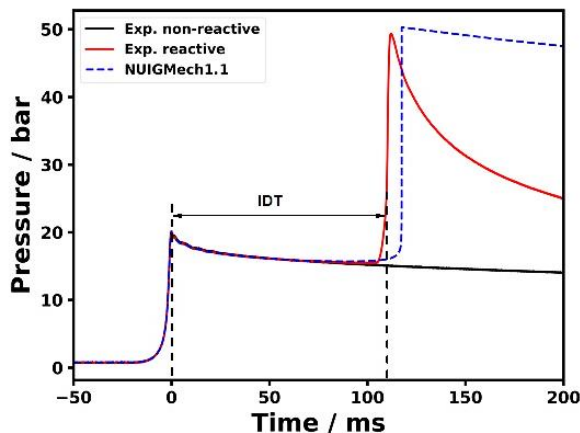


Figure CS3. IDT definition for NUIG–RCM showing pressure history profile of experimental non-reactive mixture (solid black line), experimental reactive mixture (solid red line), and mechanism simulated trace (blue dashed line).

Moreover, all of the experimental results have been divided into two categories, reliable or un-reliable. Some experiments exhibit pre-ignition, usually characterized by a noticeable pressure rise prior to the ignition event. When this occurs, we report the affected results using a symbol with an “x” through it, e.g, ☒. Thus, we also report all of these affected data in our Figures, together with the simulation using NUIGMech1.1. These affected data are not reliable in evaluating the performance of the chemical mechanism. In this regard, all pressure versus time data, including the oscilloscope [14] files and the experimentalist spreadsheets for the conditions studied in the LPST, HPST, and RCM are provided as zip files with this Supplemental material.

The relatively high-pressure experiments in the RCM were performed at PCFC-RWTH Aachen University. The description of the facility is provided in (Lee et al. doi: 0.1524/zpch.2012.0185), and the detailed explanation of the experimental procedure along with the uncertainty analysis is provided in (Ramalingam et al. doi: <https://doi.org/10.1016/j.fuel.2017.06.005>).

3. NUIG/PCFC–RCM pressure vs. time traces

In this section a collection of NUIG/PCFC–RCM pressure vs. time traces are presented to demonstrate the reliability of experiments and simulations performed for the current study. The traces are plotted using the experimental non-reactive versus reactive pressure/time history profile. Moreover, the simulated pressure/time profile using NUIGMech1.1 is included for comparison. Thus, the next graphs present low-temperature conditions for 20–40 bar, $\phi = 0.5–2.0$, dilution from 75–90% and different ratios for both of the blends, such as 50%/50%, 70%/30%, and 90%/10%.

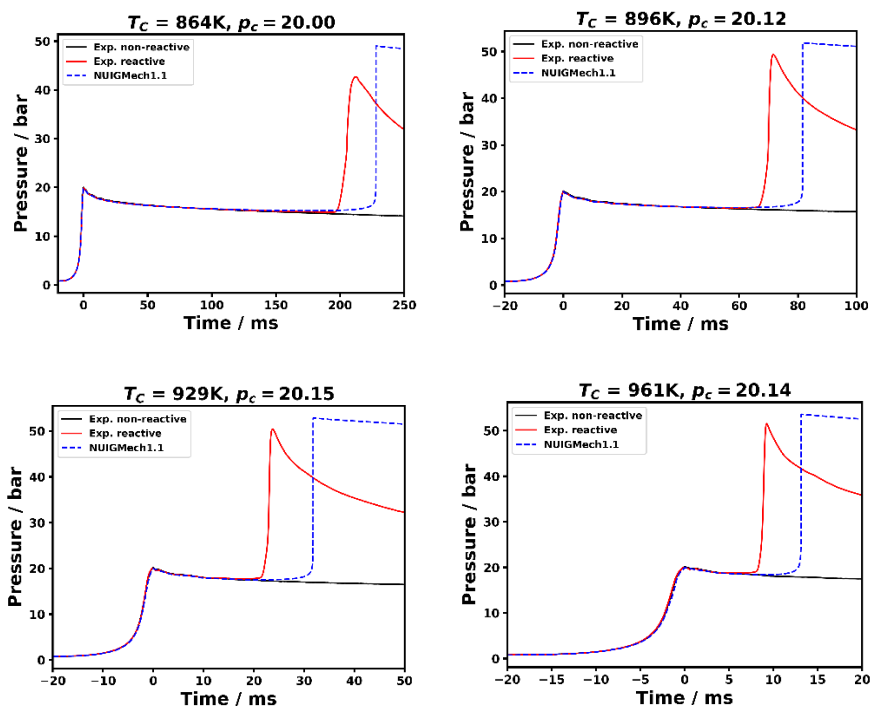


Figure CS4. NUIG–RCM experimental non-reactive (NR), reactive (R), and NUIGMech1.1 simulated pressure traces. For 50% C_2H_4 / 50% C_3H_8 blend with 75% N_2 +10% Ar, at 20 bar and $\phi = 1.0$.

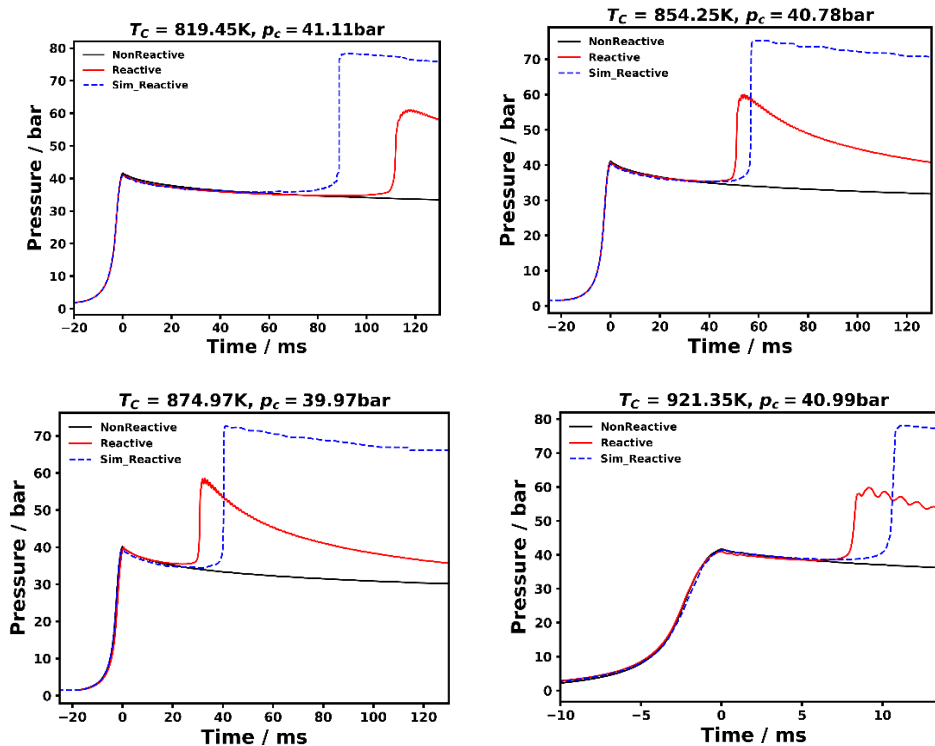


Figure CS5. PCFC-RCM experimental non-reactive (NR), reactive (R), and NUIGMech1.1 simulated pressure traces. For 50% C_2H_4 / 50% C_3H_8 blend with 75% N_2 +15% Ar, at 40 bar and $\phi = 2.0$.

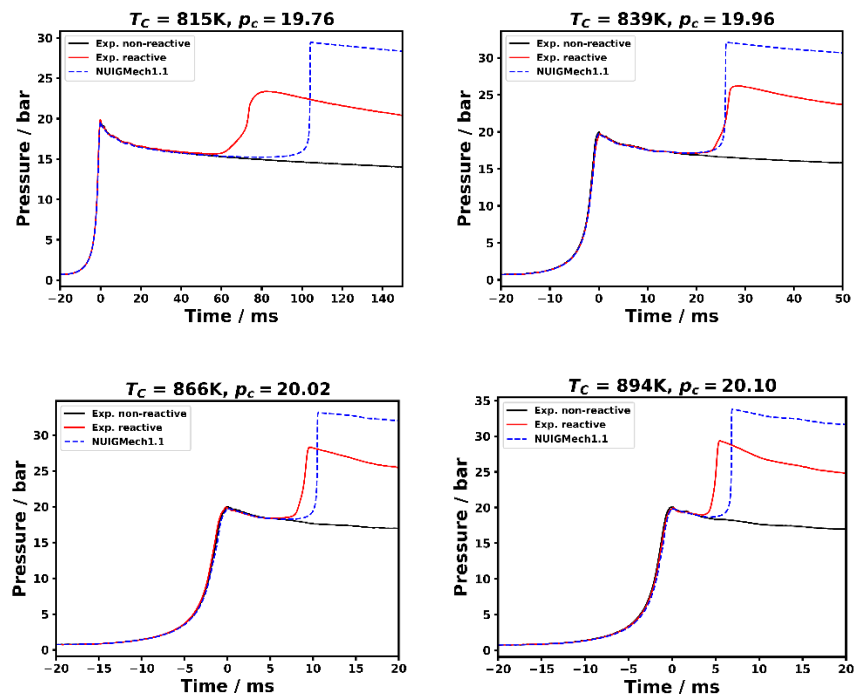


Figure CS6. NUIG-RCM experimental non-reactive (NR), reactive (R), and NUIGMech1.1 simulated pressure traces. For 70% C₂H₄/ 30% C₃H₈ blend with 75% N₂+15% Ar, at 20 bar and $\phi = 0.5$.

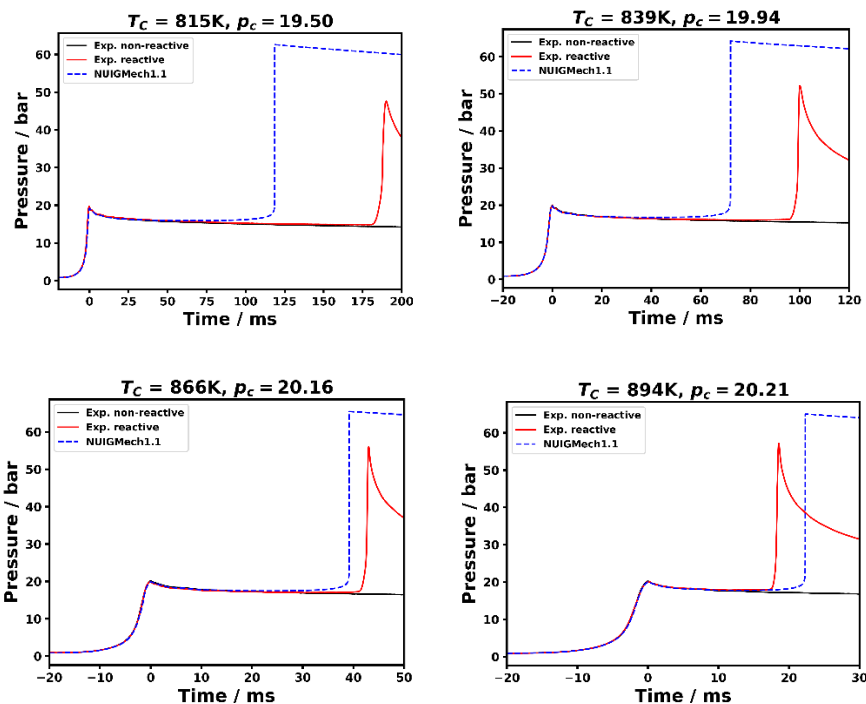


Figure CS7. NUIG-RCM experimental non-reactive (NR), reactive (R), and NUIGMech1.1 simulated pressure traces. For 90% C₂H₄/ 10% C₃H₈ blend with 75% N₂, at 20 bar and $\phi = 2.0$.

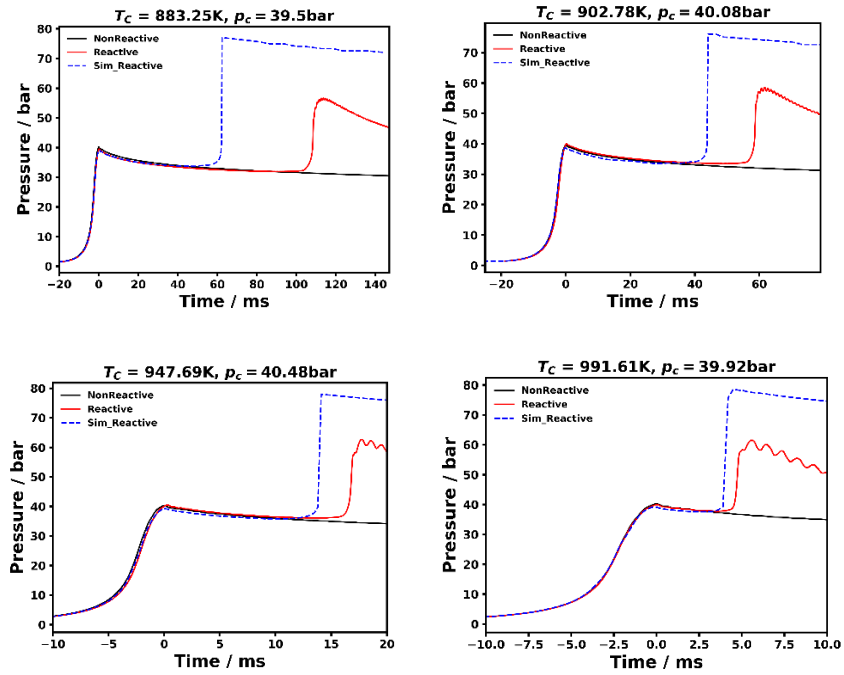


Figure CS8. PCFC-RCM experimental non-reactive (NR), reactive (R), and NUIGMech1.1 simulated pressure traces. For 90% C_2H_4 / 10% C_3H_8 blend with 75% N_2 + 10% Ar, at 40 bar and $\phi = 0.5$.

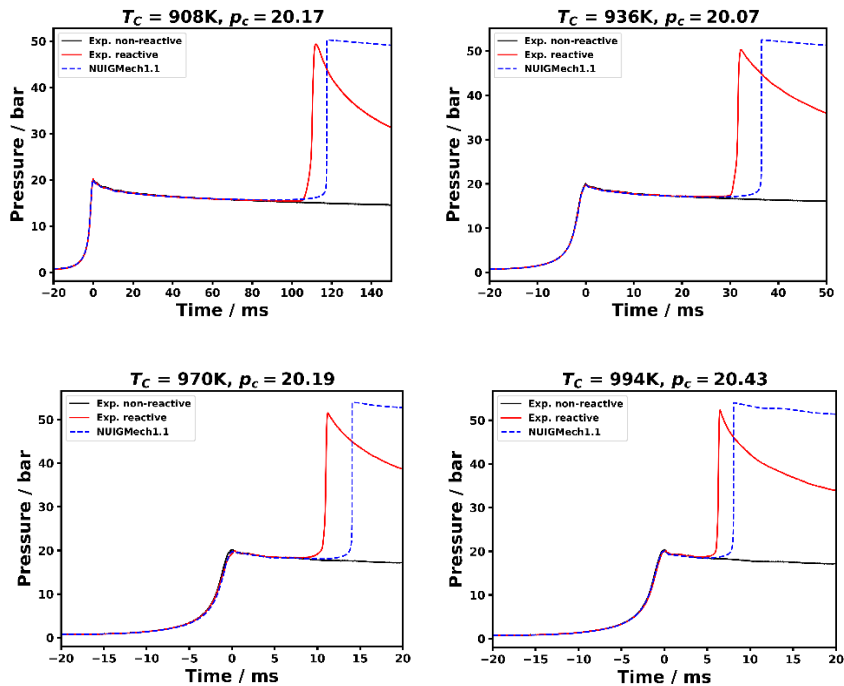


Figure CS9. NUIG-RCM experimental non-reactive (NR), reactive (R), and NUIGMech1.1 simulated pressure traces. For 50% C_2H_6 / 50% C_3H_8 blend with 75% N_2 + 10% Ar, at 20 bar and $\phi = 1.0$.

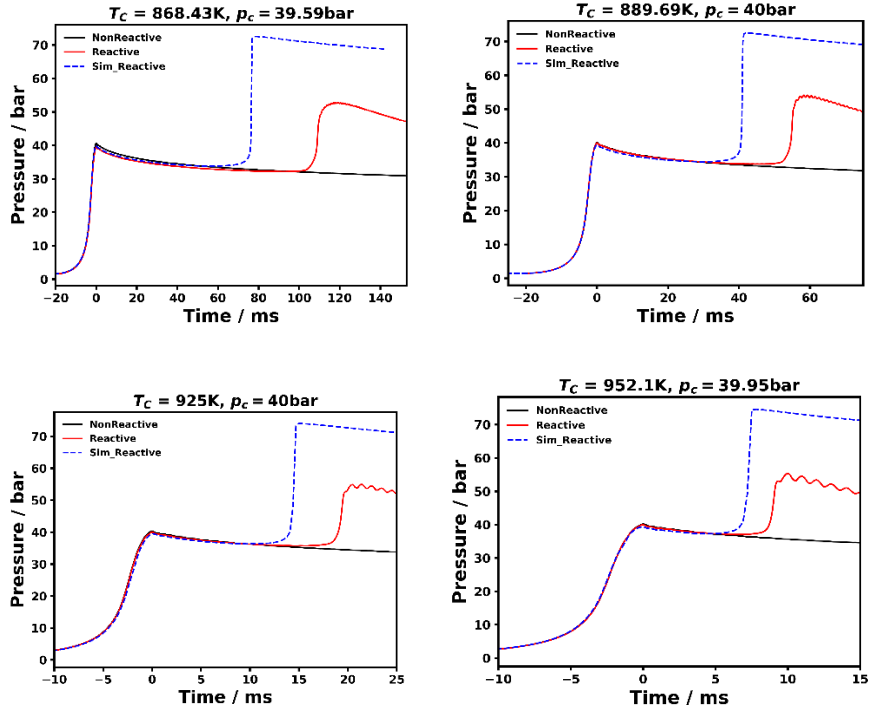


Figure CS10. PCFC–RCM experimental non-reactive (NR), reactive (R), and NUIGMech1.1 simulated pressure traces. For 50% C_2H_6 / 50% C_3H_8 blend with 75% N_2 +15% Ar, at 40 bar and $\varphi = 2.0$.

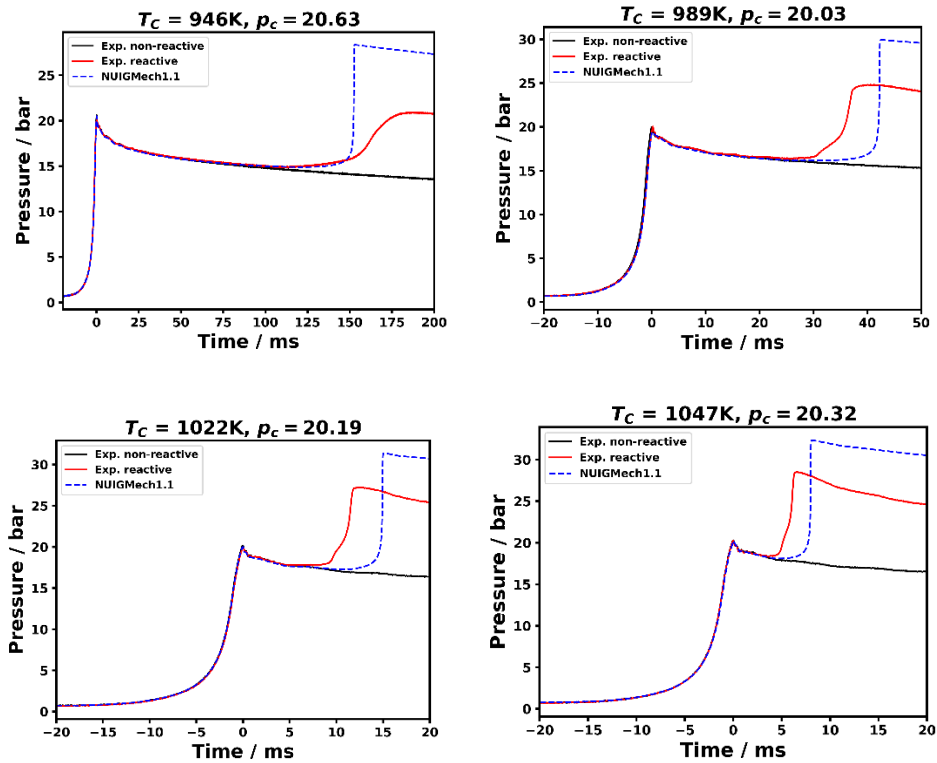


Figure CS11. NUIG-RCM experimental non-reactive (NR), reactive (R), and NUIGMech1.1 simulated pressure traces. For 70% C₂H₆/ 30% C₃H₈ blend with 75% N₂+15% Ar, at 20 bar and $\phi = 0.5$.

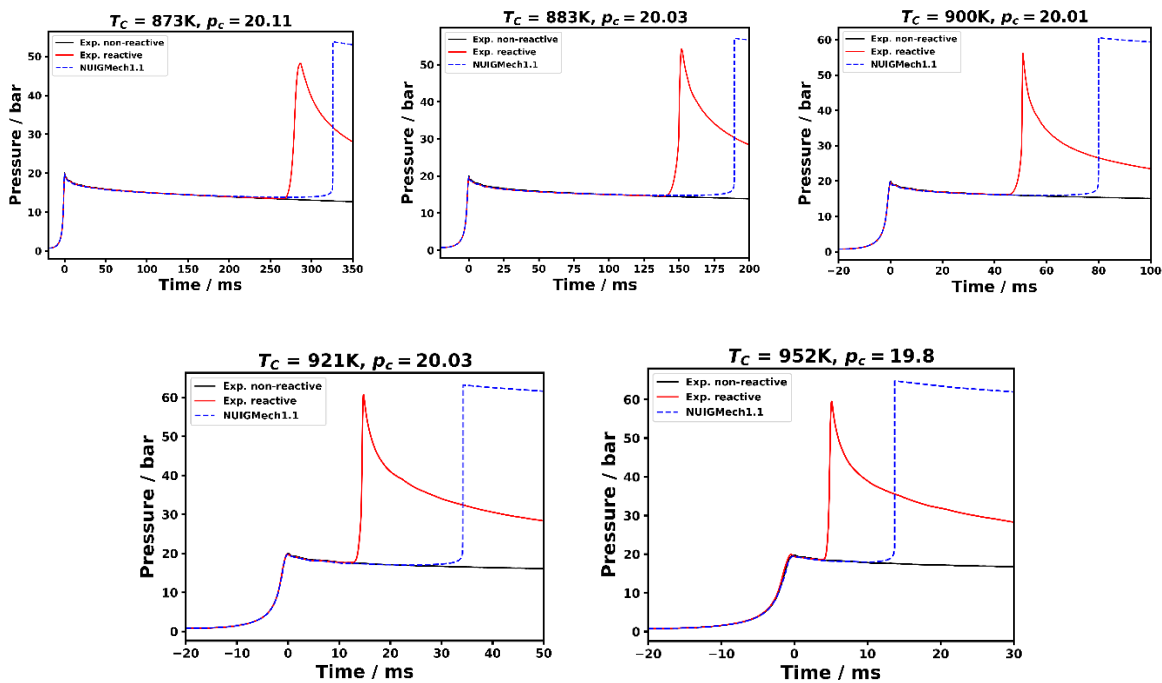


Figure CS12. NUIG-RCM experimental non-reactive (NR), reactive (R), and NUIGMech1.1 simulated pressure traces. For 90% C₂H₆/ 10% C₃H₈ blend with 75% N₂, at 20 bar and $\phi = 2.0$.

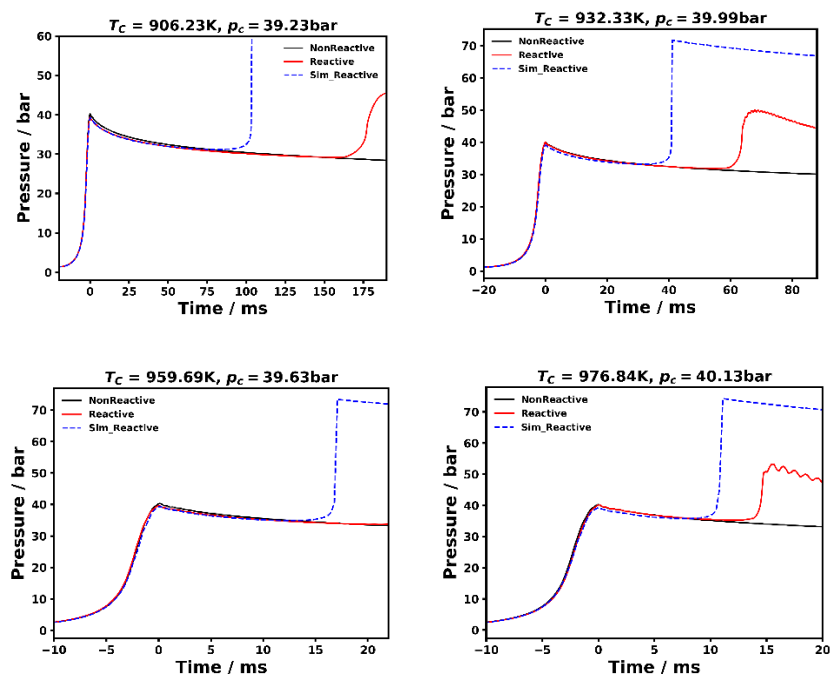


Figure CS13. PCFC–RCM experimental non-reactive (NR), reactive (R), and NUIGMech1.1 simulated pressure traces. For 90% C₂H₆/ 10% C₃H₈ blend with 75% N₂ +10% Ar, at 40 bar and $\phi = 0.5$.

4. Correlation parameters

As mentioned in Section 4.6 of the manuscript, global correlations were generated using an extensive sample of ~17280 IDTs calculated by Cantera using constant volume (CV) simulations and NUIGMech1.1. The expression used for correlating the IDTs is presented as Equation C1,

$$\tau_{\text{corr}} = 10^A e^{\frac{B}{T}} [C_2H_4]^C [C_2H_6]^D [C_3H_8]^E [\text{Oxidizer}]^F [\text{Dilution}]^G \quad (\text{C1})$$

where A, B, and C–G refer to the pre-exponential factor, the activation energy, and ethylene, ethane, propane, oxygen, and diluent concentrations, respectively. Table S6 and S7 present all of the coefficients, χ^2 , R², and the ranges wherein the correlations are valid.

Table CS6. Correlation coefficients for the C₂H₄/C₃H₈ blend.

Coefficients	1 ≤ p ≤ 20 atm		20 ≤ p ≤ 40 atm		
	800 ≤ T ≤ 1300 K	1300 ≤ T ≤ 2000 K	800 ≤ T ≤ 1100 K	1100 ≤ T ≤ 1500 K	1500 ≤ T ≤ 2000 K
A	-9.22 ±0.029	-8.93 ±0.021	-7.22 ±0.030	-9.89 ±0.04	-10.34±0.028
B	18501.31 ±52.86	17848.85 ±72.58	14136.92 ±48.38	19220.37 ±94.22	21386.61 ±77.49
C[ethylene]	-0.504 ±0.002	-0.077 ±0.004	-0.440 ±0.003	-0.491±0.003	-0.502 ±0.003
D[ethane]	0	0	0	0	0
E[propane]	-0.141 ±0.002	0.527 ±0.004	-0.392 ±0.002	-0.056 ±0.003	0.463 ±0.003
F	-0.221 ±0.003	-1.32 ±0.007	-0.427±0.005	-0.447 ±0.006	-1.08 ±0.005
G	-0.272±0.005	0.1824 ±0.006	-0.017 ±0.008	0.149 ±0.009	0.355 ±0.008
χ^2	0.013	6.01E-12	5.14E-05	2.38E-09	1.06E-11
R ²	0.994	0.982	0.986	0.987	0.985

5. Statistical analyses

As already mentioned in the results and discussion, Section 4 of the manuscript, all of the experimental IDTs, NUIGMech1.1, and AramcoMech3.0 predicted IDTs and correlated IDTs are reported in milliseconds (ms). For the experimental data presented in Figs. C2 and C3, a total of 328 IDTs were collected and simulated and were used to calculate the mean (μ), median, the standard deviation (σ), the mean absolute deviation (MAD), the mean square error (MSE), and the mean absolute percentage error (MAPE). Figs. CS10(a) and (b) provide the RPE frequency distribution for NUIGMech1.1 and AramcoMech3.0 relative to the IDT experiments. The most extreme points beyond ~150% RPE can be considered outliers due to the relatively low frequency and distance from the rest of the population sample. Both histograms are right-skewed distributions, and consequently, their mean is always bigger than the median of the data. The standard deviation (σ) of the NUIGMech1.1 histogram in Fig. S10(a) is ~35.4, while it is ~43.25 for AramcoMech3.0. This indicates that the values are more distributed around the mean for AramcoMech3.0 compared to NUIGMech1.1 predictions. Additionally, the MAD for the NUIGMech1.1 histogram was ~2.9, while it was ~5.0 using AramcoMech3.0, again highlighting that the discrepancies in predictions from measurements are more spread out for AramcoMech3.0 compared to those predicted using NUIGMech1.1.

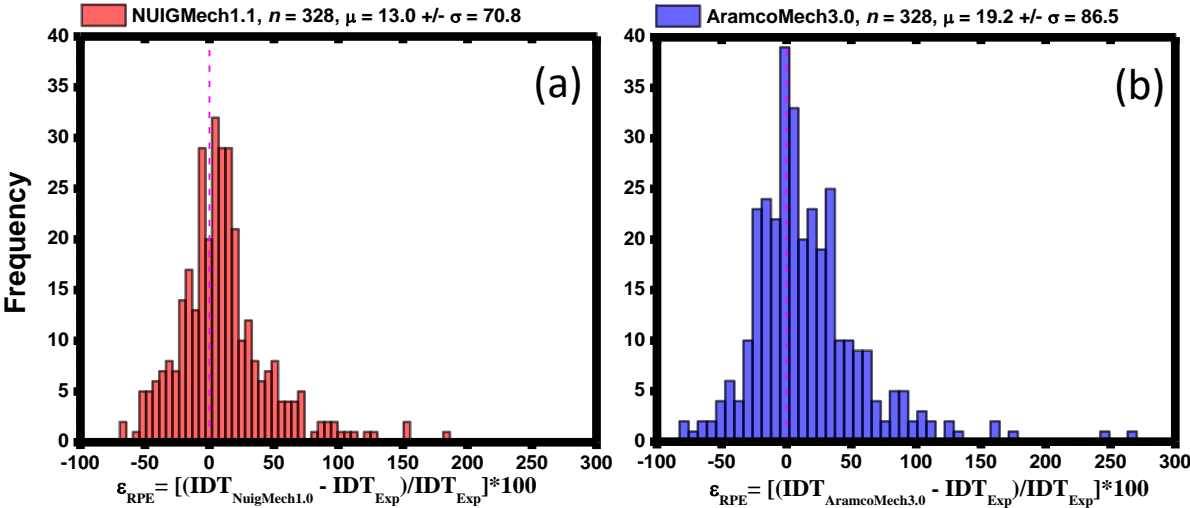


Figure CS10. Histograms presenting total sample size taken (n), mean of sample (μ), and the standard deviation (σ) for each mechanism. The occurrence of each specific % error is plotted as a function of individual relative percentage error (RPE) for (a) NUIGMech1.1, and (b) AramcoMech3.0 predictions against the corresponding experimental IDTs.

Thereafter, all of the correlated IDTs used in the graphs presented in Sections 4.2 – 4.5 were used to determine the MAD, MSE, MAPE, and σ , for the correlations using 263 IDTs. The blending effects presented

were correlated using 52 IDTs, and for the other effects such as pressure, equivalence ratio, and dilution, 78 IDTs were used. Table S8 presents the detailed values for the statistical analyses of the overall performance of NUIGMech1.1, AramcoMech3.0 and the correlations against the and the correlated individual effects compared to NUIGMech1.1.

Table CS8. Overall statistical analyses values for the different mechanisms and correlations presented in the current study.

	Data source	n	μ	median	σ	MAD	MSE	MAPE
Fig.S11 (a)	NUIGMech1.1 vs experiment	328	12.98	9.0	35.40	2.91	101.85	26.36%
Fig.S11 (b)	AramcoMech3.0 vs experiment	328	19.19	11.0	43.20	5.03	559.40	31.94%
Fig.S11 (c)	Correlation vs experiment	263	7.56	3.0	36.49	0.22	0.63	24.37%
Fig.S11 (d)	Correlation vs NUIGMech1.1	286	12.36	7.0	34.69	13627.71	2.1E+9	24.35%

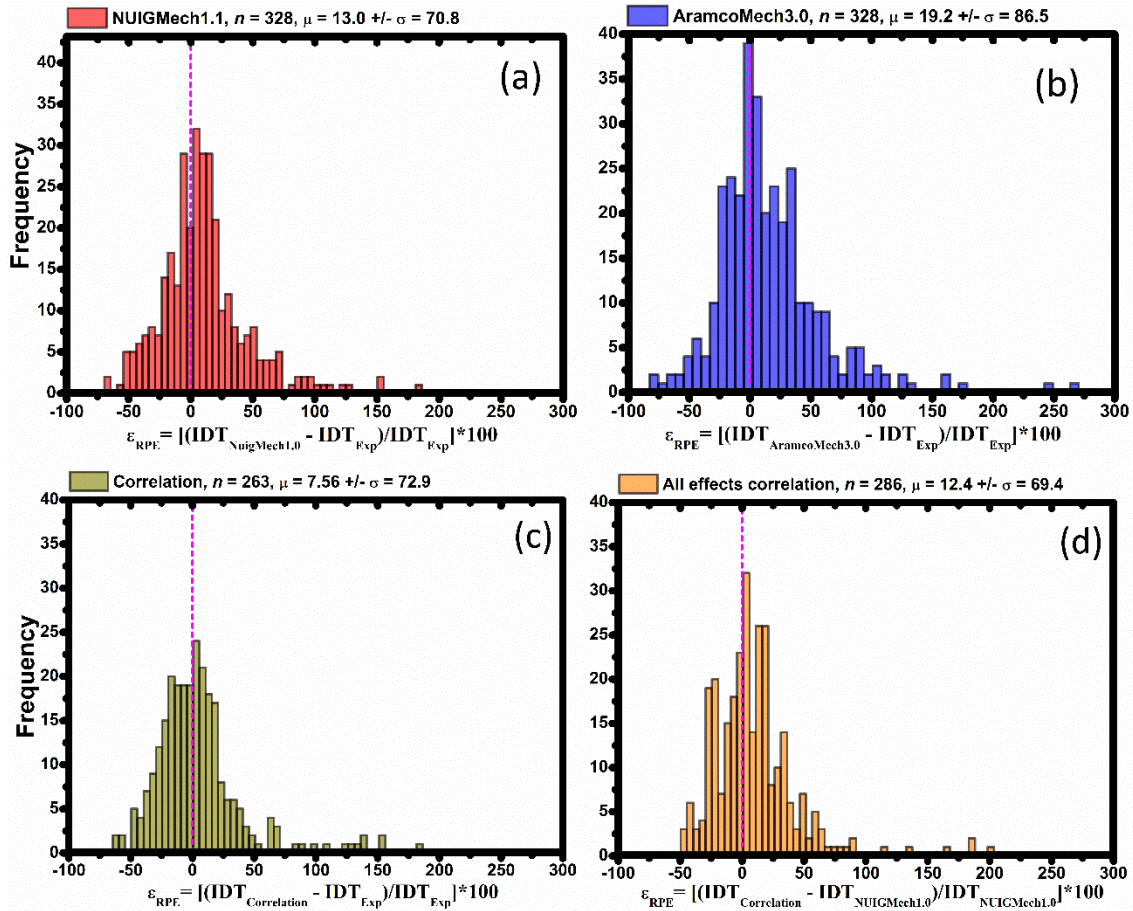


Figure CS11 Histograms presenting total sample size taken (n), mean of sample (μ) and the standard deviation (2σ) for each mechanism or correlation performance. On the y -axis, the occurrence of each specific % error against x -axis, that presents the individual relative percentage error (RPE). (a – c) All comparisons have been made versus the experimental data for (a) NUIGMech1.1 (red bars), (b) AramcoMech3.0 (blue bars), (c) the derived correlations (green bars), and (d) the performance of the derived correlations versus NUIGMech1.1 (orange bars).

Individual effects of the studied parameters such as blending in Section 4.2, pressure in Section 4.3, equivalence ratio in Section 4.4, and dilution in Section 4.5 graphs, the Table S9 shows that were correlated using 52 data points, and other effects such as pressure, equivalence ratio and dilution, used 78 data points, represented by n along with the detailed values for the statistical analyses done over all data sets.

Table CS9. Individual effects of the studied parameters on IDT, including statistical values for the derived correlations versus NUIGMech1.1.

	Data source	n	μ	median	σ	MAD	MSE	MAPE
Fig.S12 (a)	Blending effect correlation vs NUIGMech1.1	52	18.19	-1.0	58.61	5.644	640.525	35.401%
Fig.S12 (b)	Pressure effect correlation vs NUIGMech1.1	78	9.406	7.0	25.234	41.45	77954.098	20.399%
Fig.S12 (c)	ϕ effect correlation vs NUIGMech1.1	78	1.04	4.0	22.001	2.457	76.047	18.198%
Fig.S12 (d)	Dilution effect correlation vs NUIGMech1.1	78	22.68	19.0	27.114	2.299	50.2	27.085%

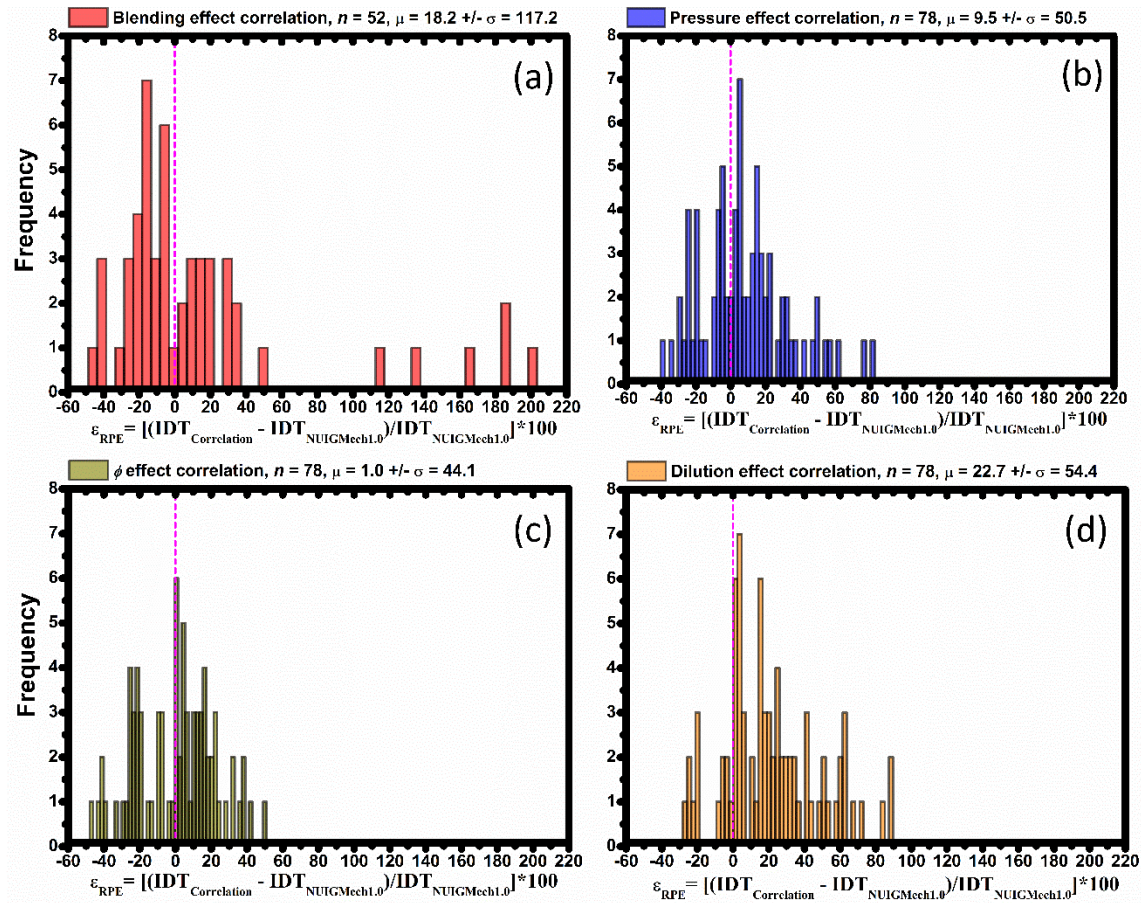


Figure CS12 Histograms presenting total sample size taken (n), mean of sample (μ) and the standard deviation (2σ) for the effect of each studied parameter. On the y-axis, the occurrence of each specific % error against x-axis, that presents the individual relative percentage error (RPE). For all cases, the correlated IDTs against NUIGMech1.1's IDTs have been used (a) for blending effect in red, (b) for pressure effect in blue, (c) for the equivalence ratio effect in green, and (d) for dilution effect in orange.

The blending effect correlated IDTs has already been discussed, and dedicated to the correlation performance, and Fig. CS12 presents a histogram to illustrate the influence of each effect along with the statistical parameters provided in Table BS9.

In Fig. C9 of Section 4.3 describing the effect of pressure on ignition, the derived correlations were included and represented as dotted lines for every pressure trend for each blend. For the binary blends, the coefficient values to calculate τ_{corr} were taken from Tables S6 and S7. In this regard, the correlation was compared using 78 correlated IDTs (τ_{corr}) compared to the simulated NUIGMech1.1 data, including a range of temperatures from 800–2000 K, at $\phi = 0.5$ in air and at pressures ranging from 1–40 atm. The correlated IDT behaves as expected for trends based on the effect of pressure, hence as we decrease the pressure from 40 to

20 atm, the τ_{corr} increased by ~50%, whereas going from 20 atm to 1 atm, the τ_{corr} increased dramatically to ~200%. The statistical comparison of τ_{corr} against IDT collected using NUIGMech1.1 leads to an overall performance of ~20.4% for the MAPE, a correlated MAD of 41.45 ms, and a standard deviation (σ) of ~25.2 ms that all details can be found in Table CS9.

As expected, such a behavior can be found in the correlated IDTs related to Figs. 12 and 13 of Sections 4.4 and 4.5, respectively. These correlations follow the simulated trends using NUIGMech1.1 for the effects of equivalence ratio and dilution. A total sample of 78 correlated IDTs compared to NUIGMech1.1's IDTs were used to calculate the statistical comparison of each effect, which leads to an overall performance of ~18.2% for the MAPE, a MAD of about 2.457 ms, and a standard deviation (σ) of ~22.0 ms for the equivalence ratio effect. The statistical comparison of τ_{corr} against IDT collected using NUIGMech1.1 for the dilution effect leads to an overall performance of ~27.0% of MAPE, a correlated MAD of about 2.3 ms, and a standard deviation (σ) of ~27.1 ms.

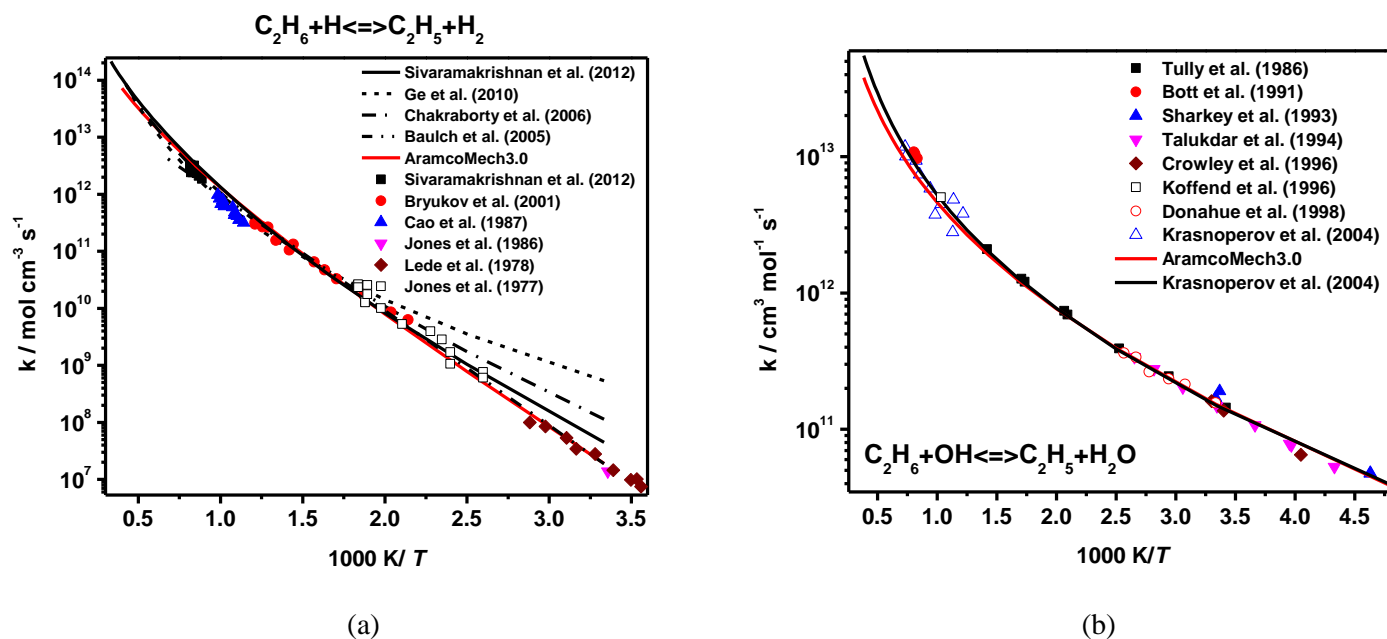
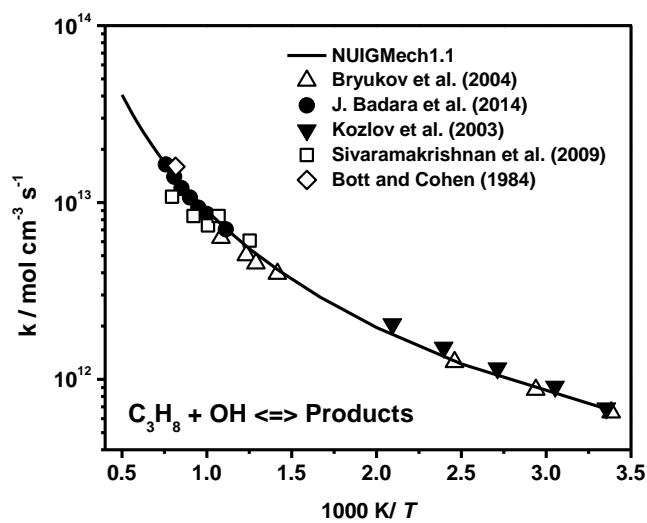
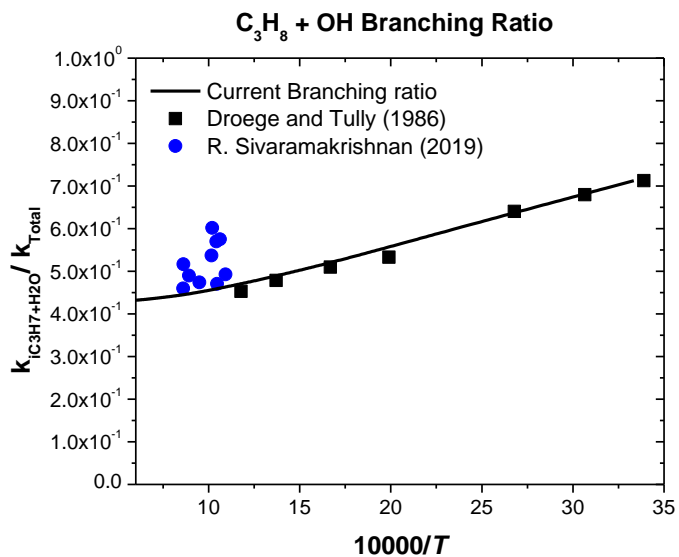


Figure CS13. Comparisons between experimental and theoretical data for the reaction rate constant of (a) $C_2H_6 + \dot{H}$ [15-23], (b) $C_2H_6 + \dot{OH}$ [32-39].

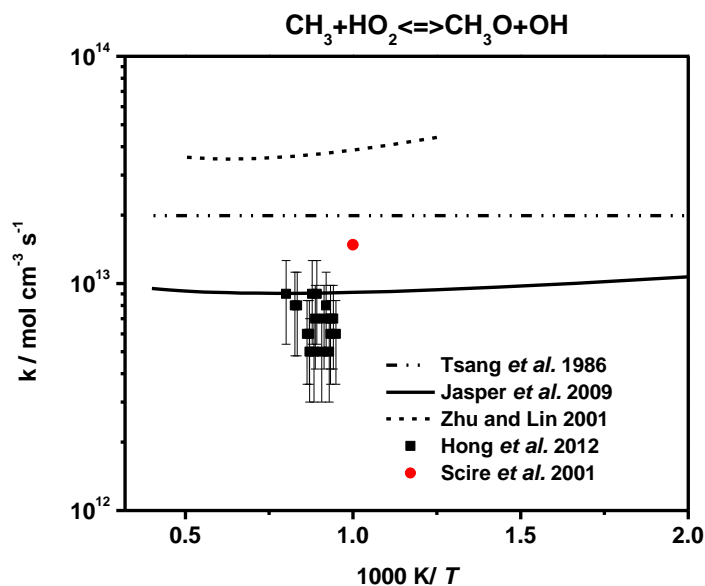
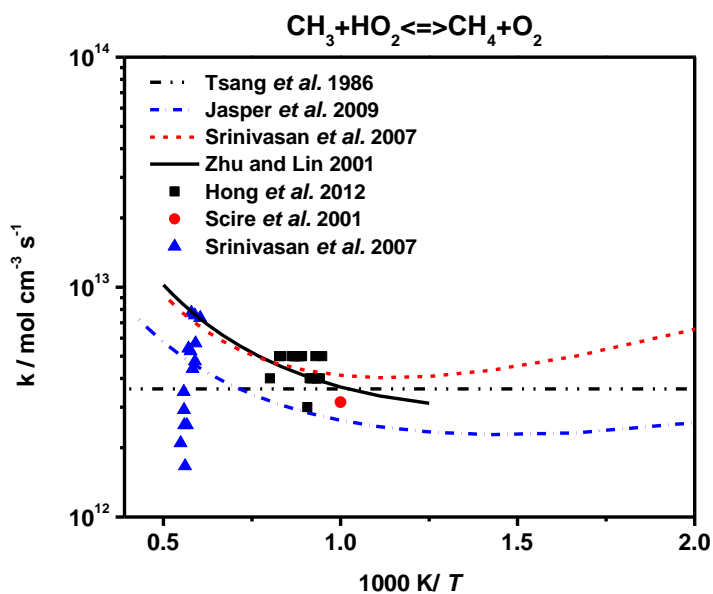


(a)



(b)

Figure CS14. Comparisons between experimental and theoretical data for (a) $\text{C}_3\text{H}_8 + \dot{\text{O}}\text{H}$ [40-44] rate and (b) branching product ratio for the reaction $\text{C}_3\text{H}_8 + \dot{\text{O}}\text{H}$ [24, 25]



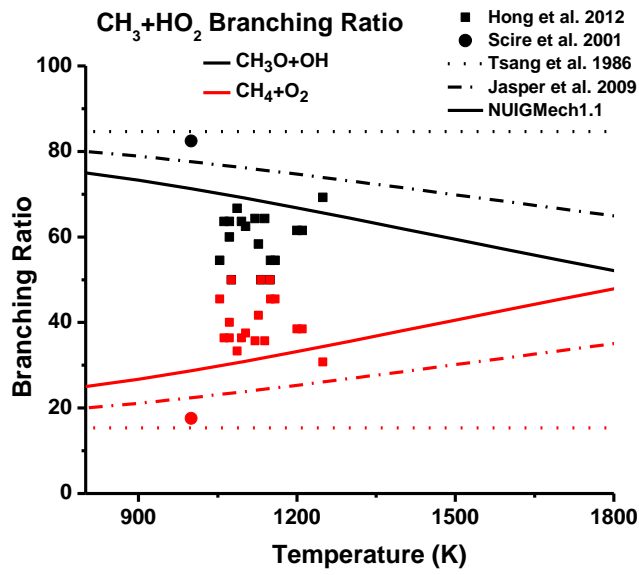


Figure CS15. Comparisons between experimental and theoretical data for the total reaction rate constant of CH₃+HO₂ system [26, 31] and the branching ratio of the two channels in CH₃+HO₂. The reverse rate constant for CH₄+O₂ = CH₃+HO₂ by Srinivasan et al. 2007 is obtained using the equilibrium constant based on NUIGMech1.1 thermodynamic property.

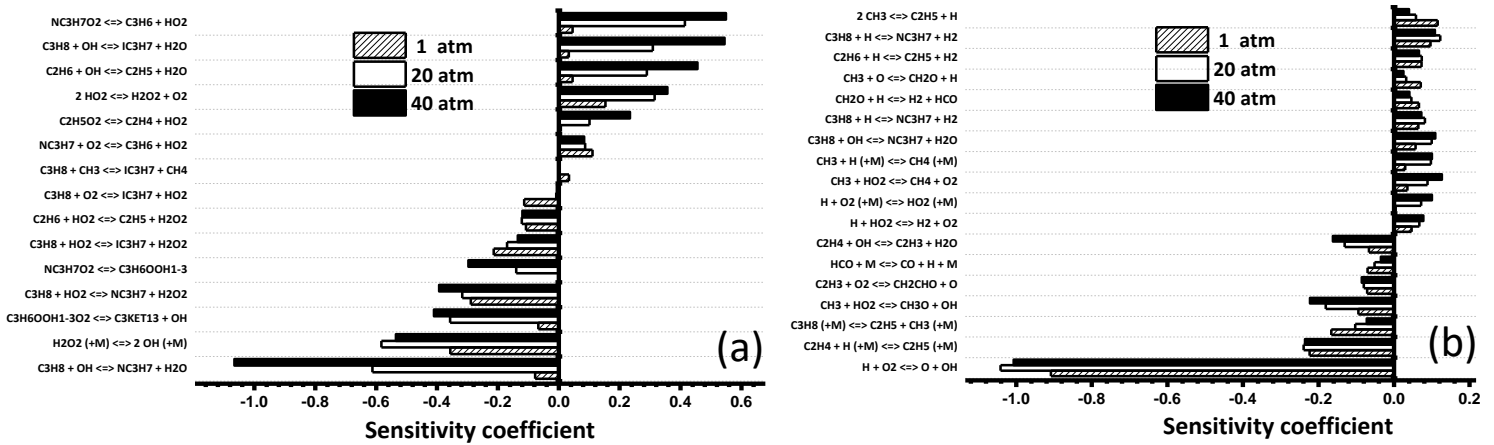


Figure CS16. Sensitivity analyses of IDT as a function of pressure at (a) 800K, and (b) 1600 K, $\phi = 0.5$, 50%/50% C₂H₆/C₃H₈ and 75% N₂ as diluent.

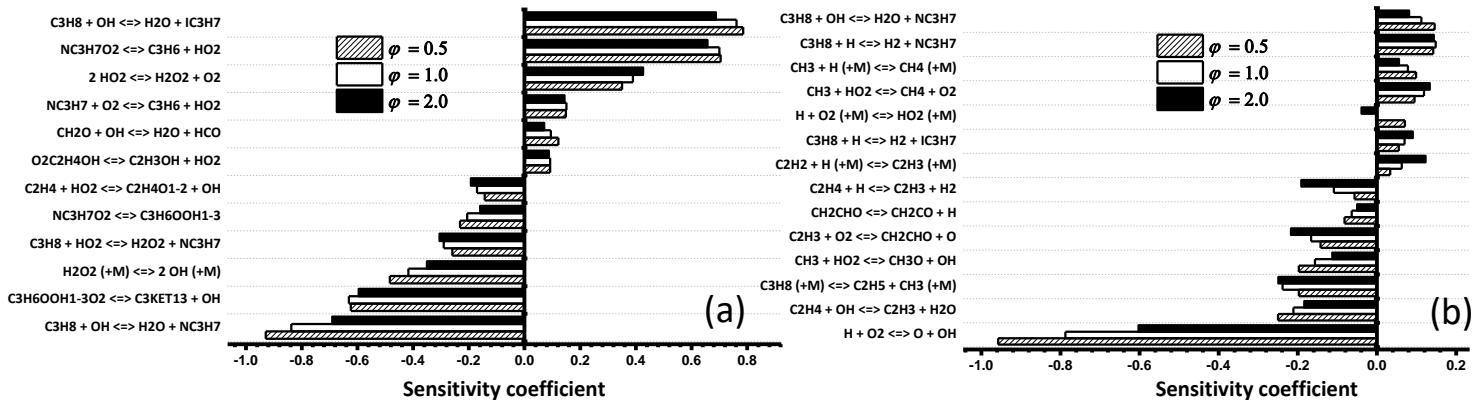


Figure CS17. Sensitivity analyses of IDT as function of equivalence ratio at (a) 800K, and (b) 1600 K, $p_c = 20$ atm, 50% $C_2H_4/50\% C_3H_8$ and 75% N_2 as diluent.

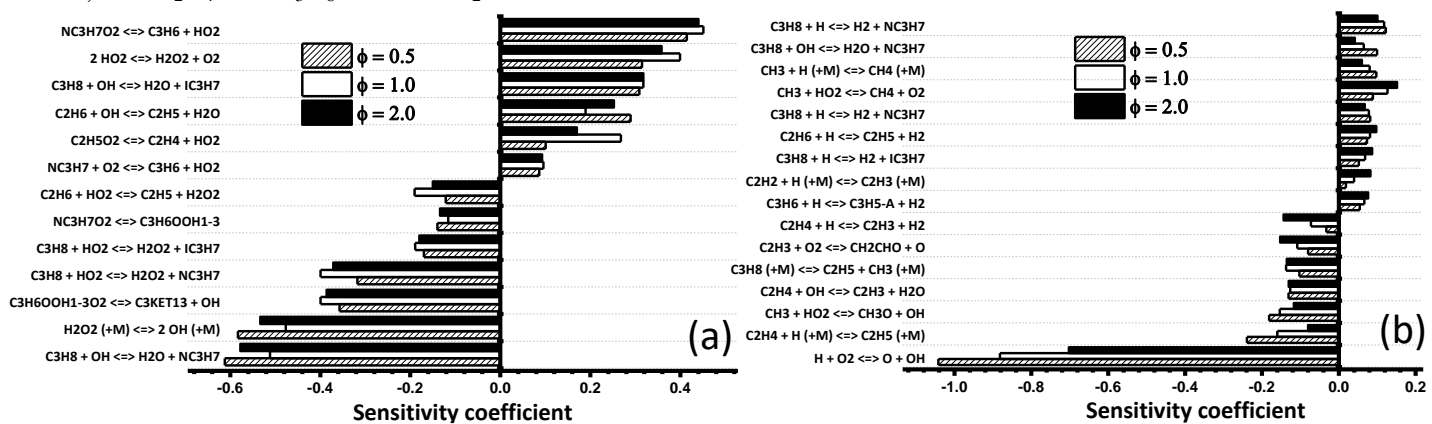


Figure BS18. Sensitivity analyses of IDT as a function of equivalence ratio for 50%/50% C_2H_6/C_3H_8 at 75% N_2 dilution at $p = 20$ atm and at (a) 800K and (b) 1600 K.

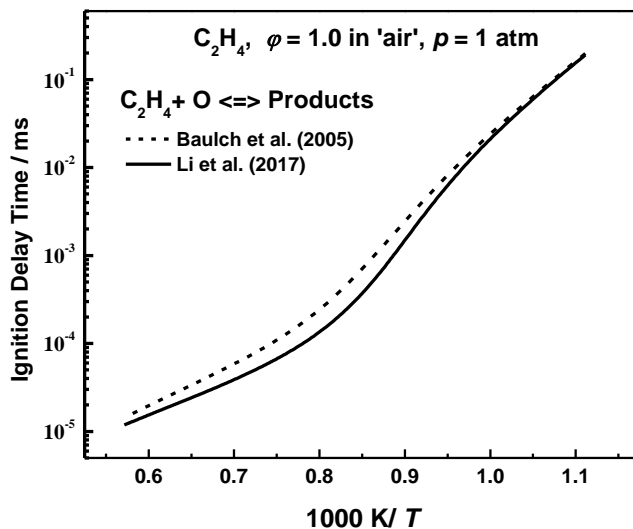


Figure CS19. Effect of updating the rate constant for $C_2H_4 + \ddot{O} \rightarrow$ products on IDT predictions for C_2H_4 /air mixtures.

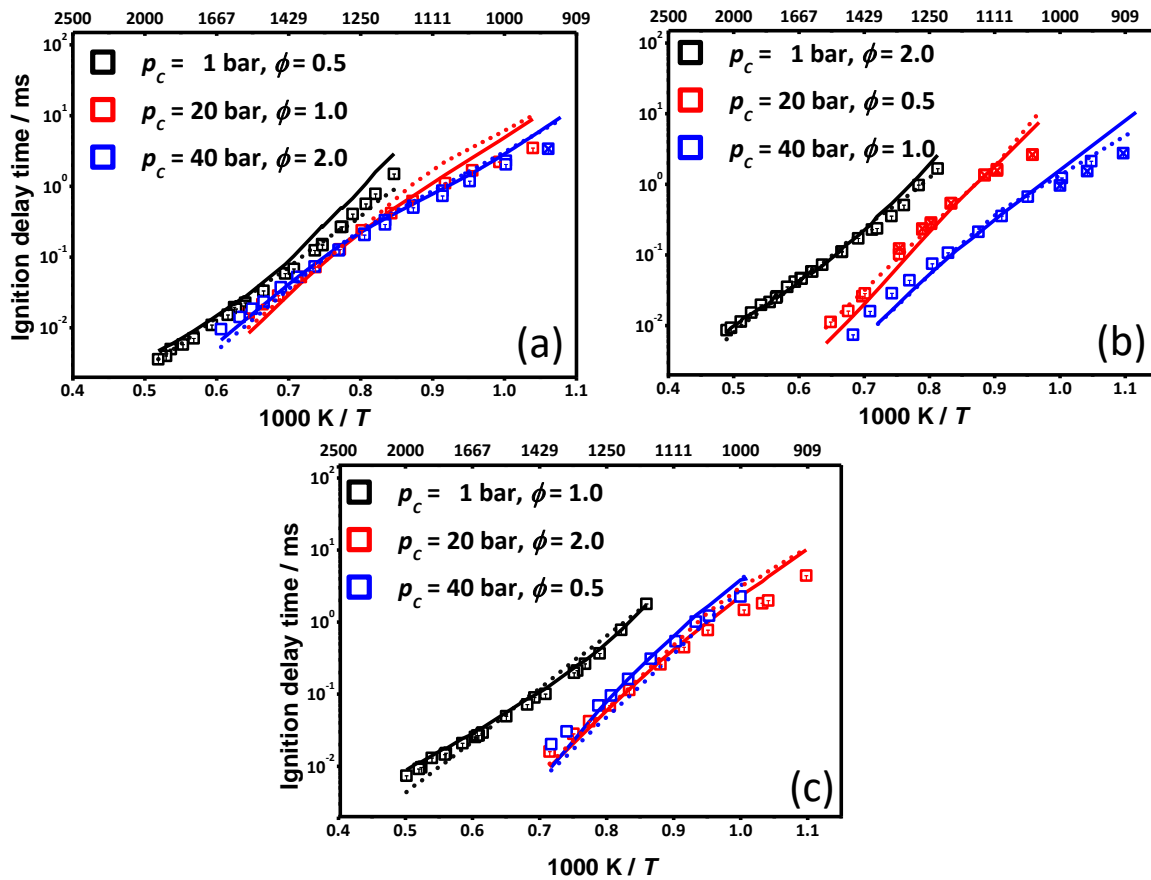


Figure CS20. Comparisons of experimental ST (\square) data against model predictions by NUIGMech1.1 (solid lines) and correlation (dotted lines) for (a) $50\% C_2H_4/50\% C_3H_8$ blend at $75\% N_2$ (black symbols/lines), $75\% N_2+10\% Ar$ (red symbols/lines), and $75\% N_2+15\% Ar$ (blue symbols/lines), (b) $70\% C_2H_4/30\% C_3H_8$ blend at $75\% N_2+10\% Ar$ (black symbols/lines), $75\% N_2+15\% Ar$ (red symbols/lines), and $75\% N_2$ (blue symbols/lines), and (c) $90\% C_2H_4/10\% C_3H_8$ blend at $75\% N_2+15\% Ar$ (black symbols/lines), $75\% N_2$ (red symbols/lines), and $75\% N_2+10\% Ar$ (blue symbols/lines).

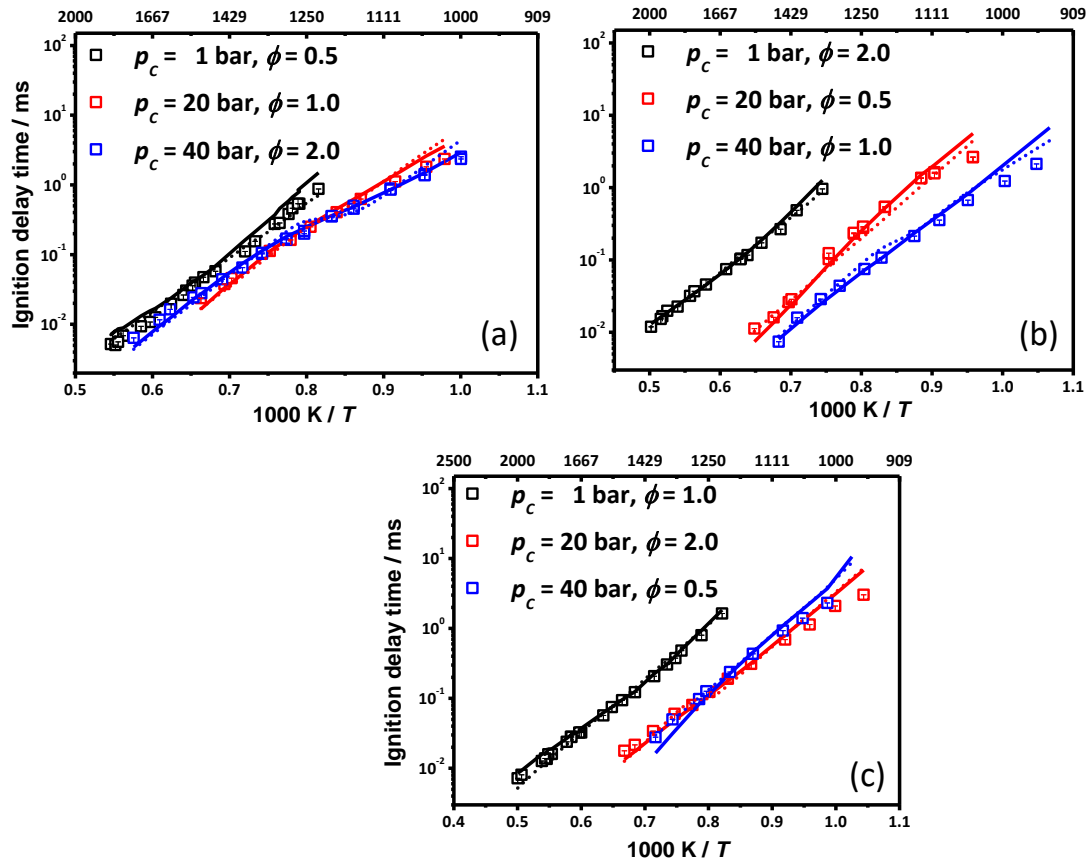


Figure CS21. Comparisons of experimental ST (\square) data, against model prediction by NUIGMech1.1 (solid lines) and correlation (dotted lines), for (a) 50% C₂H₆/50% C₃H₈ blend at 75% N₂ (black symbols/lines), 75% N₂+10% Ar (red symbols/lines), and 75% N₂+15% Ar (blue symbols/lines), (b) 70% C₂H₆/30% C₃H₈ blend at 75% N₂+10% Ar (black symbols/lines), 75% N₂+15% Ar (red symbols/lines), and 75% N₂ (blue symbols/lines), (c) 90% C₂H₆/10% C₃H₈ blend at 75% N₂+15% Ar (black symbols/lines), 75% N₂ (red symbols/lines), and 75% N₂+10% Ar (blue symbols/lines)

6. References

- [1] M. Baigmohammadi, V. Patel, S. Martinez, S. Panigrahy, A. Ramalingam, U. Burke, K.P. Somers, K.A. Heufer, A. Pekalski, H.J. Curran, A comprehensive experimental and simulation study of ignition delay time characteristics of single fuel C₁ – C₂ hydrocarbons over a wide range of temperatures, pressures, equivalence ratios, and dilutions, *Energy Fuels* 34(3) (2020) 3755-3771.
- [2] M. Baigmohammadi, V. Patel, S. Nagaraja, A. Ramalingam, S. Martinez, S. Panigrahy, A.A. El-Sabor Mohamed, K.P. Somers, U. Burke, K.A. Heufer, A. Pekalski, H.J. Curran, Comprehensive experimental and simulation study of the ignition delay time characteristics of binary blended methane, ethane, and ethylene over a wide range of temperature, pressure, equivalence ratio, and dilution, *Energy Fuels* 34(7) (2020) 8808-8823.
- [3] P.J. Ross, Taguchi techniques for quality engineering, New York, (1988).

- [4] F.R. Gillespie, An experimental and modelling study of the combustion of oxygenated hydrocarbons, National University of Ireland, Galway, (2014), <http://hdl.handle.net/10379/4419>.
- [5] J Wurmel, M. McGuinness, J.M. Simmie, High-temperature oxidation of ethylene oxide in shock waves, *J. Chem. Soc. Faraday* 92 (1996) 715-721.
- [6] S.S. Nagaraja, J. Liang, S. Dong, S. Panigrahy, A. Sahu, G. Kukkadapu, S.W. Wagnon, W.J. Pitz, H.J. Curran, A hierarchical single-pulse shock tube pyrolysis study of C₂–C₆ 1-alkenes, *Combust. Flame* 219 (2020) 456-466.
- [7] S.M. Gallagher, H.J. Curran, W.K. Metcalfe, D. Healy, J.M. Simmie, G. Bourque, A rapid compression machine study of the oxidation of propane in the negative temperature coefficient regime, *Combust. Flame* 153 (2008) 316-333.
- [8] S.M. Burke, U. Burke, R. Mc Donagh, O. Mathieu, I. Osorio, C. Keesee, A. Morones, E.L. Petersen, W. Wang, T.A. DeVerter, M.A. Oehlschlaeger, B. Rhodes, R.K. Hanson, D.F. Davidson, B.W. Weber, C.-J. Sung, J. Santner, Y. Ju, F.M. Haas, F.L. Dryer, E.N. Volkov, E.J.K. Nilsson, A.A. Konnov, M. Alrefae, F. Khaled, A. Farooq, P. Dirrenberger, P.-A. Glaude, F. Battin-Leclerc, H.J. Curran, An experimental and modeling study of propene oxidation. Part 2: Ignition delay time and flame speed measurements, *Combust. Flame* 162 (2015) 296-314.
- [9] S.M. Burke, W. Metcalfe, O. Herbinet, F. Battin-Leclerc, F.M. Haas, J. Santner, F.L. Dryer, H.J. Curran, An experimental and modeling study of propene oxidation. Part 1: Speciation measurements in jet-stirred and flow reactors, *Combust. Flame* 161 (2014) 2765-2784.
- [10] D. Healy, H.J. Curran, S. Dooley, J.M. Simmie, D.M. Kalitan, E.L. Petersen, G. Bourque, Methane/propane mixture oxidation at high pressures and at high, intermediate and low temperatures, *Combust. Flame* 155 (2008) 451-461.
- [11] D. Healy, H.J. Curran, J.M. Simmie, D.M. Kalitan, C.M. Zinner, A.B. Barrett, E.L. Petersen, G. Bourque, Methane/ethane/propane mixture oxidation at high pressures and at high, intermediate and low temperatures, *Combust. Flame* 155 (2008) 441-448.
- [12] D. Healy, D.M. Kalitan, C.J. Aul, E.L. Petersen, G. Bourque, H.J. Curran, Oxidation of C₁–C₅ alkane quinary natural gas mixtures at high pressures, *Energy & Fuels* 24 (2010) 1521-1528.
- [13] C. Morley, Gaseq: A chemical equilibrium program for windows, (2004), <http://www.gaseq.co.uk/>.
- [14] TiePie: Handyscope, <https://www.tiepie.com/en/oscilloscope-software>.
- [15] Y. Ge, M.S. Gordon, F. Battaglia, & R.O. Fox, Theoretical study of the pyrolysis of methyltrichlorosilane in the gas phase. 3. Reaction rate constant calculations., *J. Phys. Chem. A* 114(6) (2010) 2384-2392.
- [16] A. Chakraborty, Y. Zhao, H. Lin, D.G. Truhlar, Combined valence bond-molecular mechanics potential-energy surface and direct dynamics study of rate constants and kinetic isotope effects for the $\dot{H} + C_2H_6$ reaction, *J. Chem. Phys.* 124(4) (2006) 044315.
- [17] D.L. Baulch, C. Cobos, R.A. Cox, C. Esser, P. Frank, T. Just, & J. Warnatz, Evaluated kinetic data for combustion modelling, *J. Phys. Chem. Ref. Data* 21(3) (1992) 411-734.
- [18] M.G. Bryukov, I.R. Slagle, V.D. Knyazev, Kinetics of reactions of H atoms with ethane and chlorinated ethanes, *J. Phys. Chem. A* 105 (2001) 6900-6909.

- [19] J.R. Cao, M.H. Back, Kinetics of the reaction $\dot{H} + C_2H_6 \rightarrow H_2 + \dot{C}_2H_5$ in the temperature region of 1000 K, *Can. J. Chem.* 62(1) (1984) 86-91.
- [20] W.E. Jones, J.L. Ma, An electron spin resonance study of the reactions of hydrogen atoms with halocarbons, *Can. J. Chem.* 64(11) (1986) 2192-2195.
- [21] J. Lede, J. Villiermaux, Mesure de la constante de vitesse de réaction des atomes d'hydrogène sur l'éthane et le propane en réacteurs tubulaire et parfaitement agité ouverts, *Can. J. Chem.* 56(3) (1978) 392-401.
- [22] D. Jones, P.A. Morgan, J.H. Purnell, Mass spectrometric study of the reaction of hydrogen atoms with ethane, *J. Chem. Soc. Faraday Trans.* 73 (1977) 1311-1318.
- [23] R. Sivaramakrishnan, J.V. Michael, B. Ruscic, High-temperature rate constants for $H/D + C_2H_6$ and C_3H_8 , *Int. J. Chem. Kinet.* 44(3) (2012) 194-205.
- [24] A.T. Droege, F.P. Tully, Hydrogen-atom abstraction from alkanes by hydroxyl. 3. Propane, *J. Phys. Chem.* 90 (1986) 1949-1954.
- [25] R. Sivaramakrishnan, C.F. Goldsmith, S. Peukert, J.V. Michael, Direct measurements of channel specific rate constants in $\dot{O}H + C_3H_8$ illuminates prompt dissociations of propyl radicals, *Proc. Combust. Inst.* 37 (2019) 231-238.
- [26] A.W. Jasper, S.J. Klippenstein, L.B. Harding, Theoretical rate coefficients for the reaction of methyl radical with hydroperoxyl radical and for methylhydroperoxide decomposition, *Proc Combust Inst*, 32 (2009) 279-286.
- [27] R. Zhu, C. Lin, The $\dot{C}H_3 + \dot{H}O_2$ Reaction: First-principles prediction of its rate constant and product branching probabilities, *J Phys Chem A* 105 (2001) 6243-6248.
- [28] Z. Hong, D.F. Davidson, K.Y. Lam, R.K. Hanson, A shock tube study of the rate constants of HO_2 and CH_3 reactions, *Combust. Flame* 159 (2012) 3007-3013.
- [29] J. J. Scire Jr., R.A. Yetter, F.L. Dryer, Flow reactor studies of methyl radical oxidation reactions in methane-perturbed moist carbon monoxide oxidation at high pressure with model sensitivity analysis, *Int J Chem Kinet* 33 (2001) 75-100.
- [30] N.K. Srinivasan, J.V. Michael, L.B. Harding, S.J. Klippenstein, Experimental and theoretical rate constants for $CH_4 + O_2 \rightarrow \dot{C}H_3 + \dot{H}O_2$, *Combust Flame* 149 (2007) 104-111.
- [31] W. Tsang, R.F. Hampson, Chemical kinetic data base for combustion chemistry. Part I. Methane and related compounds, *Int J Chem Kinet* 15 (1986) 1087-1279.
- [32] F.P. Tully, A.T. Droege, M.L. Koszykowski, C.F. Melius, Hydrogen-atom abstraction from alkanes by OH. 2. Ethane, *J. Phys. Chem.* 90 (1986) 691-698.
- [33] J.F. Bott, N. Cohen, A shock tube study of the reaction of methyl radicals with hydroxyl radicals, *Int. J. Chem. Kinet.* 23 (1991) 1017-1033.
- [34] P. Sharkey, I.W. Smith, Kinetics of elementary reactions at low temperatures : Rate, *J. Chem. Soc., Faraday Trans.* 89 (1993) 631-638.
- [35] R.K. Talukdar, A. Mellouki, T. Gierczak, S. Barone, S.Y. Chiang, R. Ravishankara, Kinetics of the reactions of OH with alkanes, *Int. J. Chem. Kinet.* 26 (1994) 973-990.
- [36] J.N. Crowley, P. Campuzano-Jost, G.K. Moortgat, Temperature dependent rate constants for the gas-phase reaction between $\dot{O}H$ and CH_3OCl , *J. Phys. Chem.* 100 (1996) 3601-3606.

- [37] J.B. Koffend, N. Cohen, Shock tube study of $\dot{\text{O}}\text{H}$ reactions with linear hydrocarbons near 1100 K, *Int. J. Chem. Kinet.* 28 (1996) 79-87.
- [38] N.M. Donahue, J.G. Anderson, K.L. Demerjian, New rate constants for ten OH alkane reactions from 300 to 400 K: An assessment of accuracy, *J. Phys. Chem. A* 102 (1998) 3121-3126.
- [39] L.N. Krasnoperov, J.V. Michael, Shock tube studies using a novel multipass absorption Cell: Rate constant results for $\dot{\text{O}}\text{H} + \text{H}_2$ and $\dot{\text{O}}\text{H} + \text{C}_2\text{H}_6$, *J. Phys. Chem. A* 108 (2004) 5643-5648.
- [40] M.G. Bryukov, V.D. Knyazev, S.M. Lomnicki, C.A. McFerrin, B. Dellinger, Temperature-dependent kinetics of the gas-phase reactions of OH with Cl_2 , CH_4 , and C_3H_8 , *J. Phys. Chem. A* 108 (2004) 10464-10472.
- [41] J. Badra, E.F. Nasir, A. Farooq, Site-Specific Rate constant measurements for primary and secondary H- and D-abstraction by $\dot{\text{O}}\text{H}$ radicals: Propane and n-Butane, *J. Phys. Chem. A* 118 (2014) 4652-4660.
- [42] S.N. Kozlov, V.L. Orkin, R.E. Huie, M.J. Kurylo, OH reactivity and UV spectra of propane, n-propyl bromide, and isopropyl bromide, *J. Phys. Chem. A* 107 (2003) 1333-1338.
- [43] R. Sivaramakrishnan, C.F. Goldsmith, S. Peukert, J.V. Michael, Direct measurements of channel specific rate constants in $\dot{\text{O}}\text{H} + \text{C}_3\text{H}_8$ illuminates prompt dissociations of propyl radicals, *Proc. Combust. Inst.* 37 (2019) 231-238.
- [44] J.F. Bott, N. Cohen, A shock tube study of the reaction of the hydroxyl radical with propane, *Int. J. Chem. Kinet.* 16 (1984) 1557-1566.

Appendix D

(Supplementary material for Chapter 6)

1. Design of experiments

The applied approach for designing the experiments has been already discussed in details by Baigmohammadi et al [1]. As seen in Table DS1, there are four factors (e.g. fuel composition; A, dilution level; B, equivalence ratio; C, and pressure; D) and 3 levels for each parameter (e.g. three pressure levels, 1.0, 20.0, and 40.0 bar) L₉ orthogonal array could be still employed for designing the required experiments.

Table DS1. Applied factors/variables and levels for designing the current experiments using the Taguchi method.

<i>Factors</i> <i>Levels</i>	<i>Fuel composition (A)</i>	<i>Dilution (B)</i>	<i>Equivalence ratio (C)</i>	<i>Pressure (bar) (D)</i>
1	50% C ₂ H ₄ + 50% C ₂ H ₆	75%	0.5	1.0
2	30% C ₂ H ₄ + 70% C ₂ H ₆	85%	1.0	20.0
3	10% C ₂ H ₄ + 90% C ₂ H ₆	90%	2.0	40.0

2. Applied gases for making the mixtures

As mentioned in Section 7.2 of the manuscript, in the current study, the ignition delay time characteristics of methane + ethylene (CH₄ + C₂H₄), methane + ethane (CH₄ + C₂H₆), and ethane + ethylene (C₂H₆ + C₂H₄) have been investigated individually over a wide range of temperature, pressure, ethylene concentration, equivalence ratio, and dilution conditions. For those experiments performed at the combustion chemistry centre (C³) of National University of Ireland, the studied alkane/alkene fuels with purity of 99.5% (Grade: 2.5) have been supplied through high pressure bottles which were provided from Air liquide UK. The other applied gases such as oxygen, argon, nitrogen, and helium in the experiments have been provided by BOC Ireland with purities of O₂ (99.99%), N₂ (99.99%), Ar (99.99%), and He (99.96%). However, for those experiments performed at the Physico-Chemical Fundamentals of Combustion (PCFC) of RWTH Aachen University, the studied C₂H₄ + C₂H₆ with purity of 99.95% (Grade: 3.5) were provided by Westfalen AG. Also, the other applied gases such as oxygen, argon, and nitrogen, in the experiments have been provided by Westfalen AG and Praxair with purities of O₂ ((≥99.995%), N₂ ((≥99.95%), and Ar (≥99.996%).

3. Low–pressure shock tube

As known, shock-tube is a robust facility for getting the ignition delay time data under low and high pressures and high temperature (≥ 1000 K) regime and IDTs ≤ 2 ms. Thus, the NUIG–LPST has been used for getting the IDT data under 1 bar operating condition. The applied NUIG-LPST has been previously documented and explained in details [2,3]. Here, only general information of the facility is presented in Table DS2. In the current study, helium was used as the primary driver gas for doing the experiments unless there was a need to reduce the incident shock velocity through adding nitrogen to helium for the tailored cases.

Table DS2. Specifications of the applied low–pressure shock tube.

Total length	6.33 m	
Section	Length (m)	Diameter (mm)
Driver	0.53	520
Driven	5.8	102.4
Material	Stainless steel	
Controlling system	Sharp edges arrow	
Diaphragm’s material	Polycarbonate/Polyester	
Diaphragm’s thickness	105–120 μm (nominal)	

Further, as presented in Table DS3, the incident shock velocity has been measured using five piezoelectric pressure transducers located on the driven section of the LPST and then the shock velocity at the end-wall was extrapolated through a fitted line to the collected shock velocities over these pressure transducers. All conditions such as the compressed gas temperature (T_5) and pressure (p_5) behind the reflected shock were calculated using the shock velocity at the end-wall using “Gaseq” software [4]. Also, the ignition delay times of the studied mixtures were measured using photomultiplier (PMT) systems equipped with CH* filter (CWL: 430 nm \pm 10 FWHM; Thorlabs) installed on the side wall of the shock tube’s endcap due to very weak pressure signals. Also, it is demonstrated in Figure DS1 that the ignition delay time is defined as a maximum gradient in pressure ($\left. \frac{dP}{dt} \right|_{max}$) or CH* ($\left. \frac{dCH^*}{dt} \right|_{max}$) behind the reflected shock. Further, for increasing the accuracy of experiments and reducing the scattered points, all measured pressures behind the reflected shocks have been forced to be restricted to ± 0.05 bar of the target pressure of 1 bar. In this regard, all pressure versus time data including oscilloscope files (software is accessible through <https://www.tiepie.com/en/oscilloscope-software>) and the experimentalist spreadsheets related to the current studied conditions in NUIG–LPST are provided as Supplementary data files with the online version of the paper.

Table DS3. Number of installed PCB sensors on the driven section of LPST shock tube and their distances from the end-wall.

Sensors	Distance from the end wall (cm)
PCB#1	3.0
PCB#2	23.7
PCB#3	36.6
PCB#4	49.5
PCB#5	189.0

4. High-pressure shock-tube

The NUIG-HPST has been used for getting the IDT data for 20 and 40 bar operating conditions. As already mentioned, the applied NUIG-HPST has been previously documented and explained in details [5] and ,here, only general information of the facility is presented in Table DS4 **Error! Reference source not found.** In the current study, helium was used as the primary driver gas for doing the experiments unless there was a need to reduce the incident shock velocity through adding nitrogen to helium for the tailored cases.

Table DS4. Specifications of the applied high-pressure shock tube.

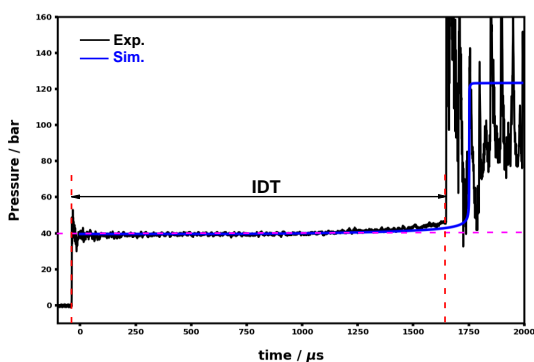
Total length	9.1 m	
Section	Length (m)	Diameter (mm)
Driver	3.0	63.5
Middle	0.04	63.5
Driven	5.7	63.5
Material	Stainless-steel (1.4571/316Ti and 1.4462/F51)	
Controlling system	Double-diaphragm type	
Diaphragm's material	Aluminium (1050 H14)	
Diaphragm's thickness	0.8~2 mm; according to target pressure	
Pre-scoring the diaphragms	0.2~1.1 mm; according to target pressure and the diaphragms' thickness	

Further, as presented in Table DS5, the incident shock velocity has been measured using six piezoelectric pressure transducers located on the driven section of the HPST and then the shock velocity at the end-wall was extrapolated through a fitted line to the collected shock velocities over these pressure transducers. All conditions such as the compressed gas temperature (T_5) and pressure (p_5) behind the reflected shock were calculated using the shock velocity at the end-wall through “Gaseq” software [4]. Also, the ignition delay times of the studied normal mixtures (pressure-time profiles) with diluent concentration of $\leq 85\%$ were recorded using a Kistler 603B transducer mounted on the end-wall, while for the mixtures with 90% dilution, the ignition delay times were measured using photodiode array detector (PDA) or photomultiplier (PMT) systems equipped with CH* filter (CWL: 430 nm \pm 10 FWHM; Thorlabs) installed on the side wall of the shock tube's endcap due to

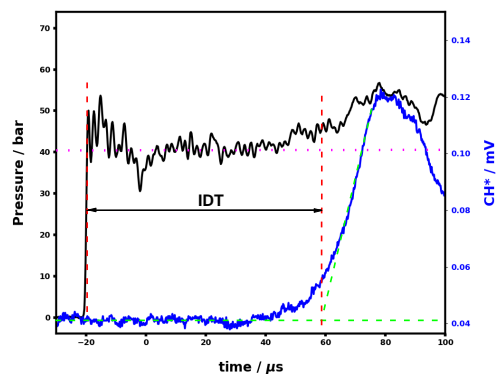
very weak signals of the Kistler pressure transducer. For increasing the accuracy of experiments and reducing the scattered points, all measured pressures behind the reflected shocks have been forced to be restricted to ± 0.5 bar of the target pressures (20 and 40 bar). Moreover, all of the experimental results have been divided into two main categories of the acceptable and the affected by facility, so that the affected results have been marked using “☒” symbol. Thus, these data wouldn’t be reliable to be applied for evaluating the performance of a chemical mechanism. In this regard, all of the pressure versus time data including oscilloscope files (software is accessible through <https://www.tiepie.com/en/oscilloscope-software>) and the experimentalist spreadsheets related to the current studied conditions in NUIG–HPST are provided as Supplementary data files with the online version of the paper.

Table DS5. Number of installed PCB sensors on the driven section of the shock-tube and their distances from the end-wall.

Sensors	Distance from the end wall (cm)
PCB#1	1.0
PCB#2	15.0
PCB#3	29.0
PCB#4	57.0
PCB#5	85.0
PCB#6	116.50



(a)



(b)

Figure DS1. Applied definition for measuring IDT in the NUIG-shock tube: (a) using Kistler pressure trace mounted on the end-wall of the endcap; (b) using PDA–CH* trace mounted on the side wall of the end-cap.

5. Rapid compression machine

The rapid compression machine is a common facility for getting the ignition delay time data under high pressure and low-to-moderate temperature regime (< 1000 K). In the current study, the

experiments have been taken using NUIG– and PCFC–RCMs. According to the previous studies [6,7], the experimental IDTs have been modelled using the adiabatic core assumption in which the non-adiabatic condition can be compensated by imposing the volume–time profiles of the same non–reactive mixtures to calculations. Thus, general information about each facility have been presented in the following subsections.

5.1. NUIG-RCM

The general specifications of NUIG–RCM have been presented in Table DS6. The details of the facility has been already documented and explained in details [5,6,8–11]. In this facility, the ignition delay time of the normal studied mixtures (diluent concentration = 75%) and the pressure-time histories of their relevant non-reactive mixtures were recorded using a Kistler 6045A transducer mounted on the reaction chamber. However, the ignition delay times of the mixtures with 85% and 90% dilution percent and the post–compression pressures of 20 and 40 bar, were reordered using both the Kistler and photomultiplier (PMT) equipped with CH* filter (CWL: 430 nm ± 10 FWHM; Thorlabs) due to vague signal of the Kistler pressure transducer under these conditions. Also, as shown in Figure DS2, the ignition delay time is defined as a maximum gradient in pressure ($\left. \frac{dP}{dt} \right|_{max}$) or CH* ($\left. \frac{dCH^*}{dt} \right|_{max}$) after compressing the studied mixtures. Subsequently, the post compression temperatures (T_C) were calculated by assuming isentropic compression condition using Gaseq software [4]. Similar to the applied procedure in NUIG–HPST, all measured post compression pressures (p_C) have been forced to be restricted to ±0.5 bar of the target pressures due to increasing the accuracy of experiments and also reducing the scattered points. Moreover, unlike the standard operating procedure in NUIG–HPST, all the experimental results have been repeated at least three times and the repeatability of all reported IDTs was ≥ 90%. In this regard, all pressure versus time data including pressure/volume profiles and the experimentalist spreadsheets related to the studied conditions in NUIG–RCM have been provided as the Supplementary files with the online version of the paper.

Table DS6. Specifications of NUIG–RCM.

Parameter	Value
Bore size of the reaction chamber (cm)	3.820
Volume of the reaction chamber (cm ³)	33.191

Piston's velocity (U_p) (cm/s)	934.0 ~ 1294.0
Pistons' stroke length (cm)	16.817
Piston's type	Flat head with the crevice
Type	Twin-counter pistons

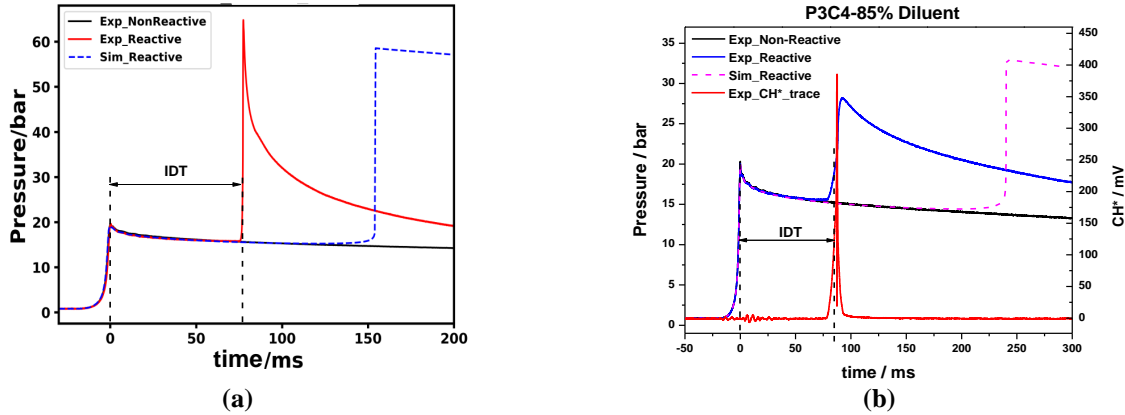


Figure DS2. Applied definition for measuring IDT in the NUIG-RCM: (a) using Kistler pressure trace; (b) using both pressure and PMT-CH* trace mounted on the side wall of the reaction chamber.

5.2.PCFC-RCM

The PCFC-RCM is a well-known facility which has been already introduced properly in literature. As presented in Table DS7, this facility is constructed from a single-piston mechanism which is driven pneumatically and stopped hydraulically at the end of compression. Similar to the applied piston in NUIG-RCM, the crevice piston design has been applied in the PCFC-RCM. In the facility, the pressure-time profile during the compression and the post-compression processes and the initial temperature in the reaction chamber were monitored and controlled using a Kistler 6125C pressure transducer and type 'T' thermocouple, respectively. In this regard, the detail information about the construction, measurement procedure, and the applied sensors in the study have been already presented in [12]. As the same process explained in section 7.2.1, the compressed mixture's temperature (T_5) was calculated using the isentropic compression formulation of Gaseq software [4]. According to the procedure explained by Ramalingam et al. [7], the reproducibility of evaluated IDTs and also the experimental uncertainty of the compressed mixture's temperature for the measured conditions in the study were within 15% and ± 5 K, respectively. In this regard, the related experimental data to PCFC-RCM facility and the volume-time profiles are reported in the Supplementary files.

Table DS7. Specifications of PCFC-RCM.

Parameter	Value
Bore size of the reaction chamber (cm)	5.0

Volume of the reaction chamber (cm ³)	506.0 – 551.0
Piston's velocity (U _p) (cm/s)	1667.0
Pistons' stroke length (cm)	25.0
Piston's type	Flat head with the crevice
Type	Single piston

6. Data acquisition system

As shown in Table DS8, in the current study, many sensors have been used in the four applied facilities at C³-NUIG and PCFC-RWTH Aachen University to measure the required parameters. In this regard, all installed sensors in NUIG-L/HPST which had been used for measuring the incident shock velocities and the ignition delay times, were synchronized and connected to two TiePie Handyscope HS4 oscilloscopes [13]. Also, all generated signals from the installed sensors on NUIG-RCM including the Kistler pressure transducer, the position sensors, and the photomultiplier were synchronized and collected using a PicoScope 5443B [14].

Table DS8. Applied sensors and detectors for measuring during the current study (NUIG-HPST/RCM and PCFC-RCM).

Sensor	Company	Model	Accuracy	Resolution
Pressure sensor transducer	Kistler	603B	≤±1.0 % FSO; linearity	NA
Pressure sensor transducer	Kistler	6045A	≤±0.4 % /FSO; linearity	NA
Pressure sensor transducer	Kistler	6125C	≤±0.4 % /FSO; linearity	NA
Piezoelectric pressure sensor	PCB	113B24	≤±1.0 % FS; Non-linearity	±0.035 KPa
Digital Absolut pressure transmitter	Kurt J Lesker	ACG & HCG	0.25% of FS	±0.01 Torr
Digital Absolut pressure transmitter	Edwards	600 Barocel	0.15% of reading	±0.01 of FS
Digital Absolut pressure transmitter	MKS	Baratron 121AA-0100D	0.5% of reading	±0.01 Torr
Digital Absolut pressure transmitter	MKS	Baratron 121AA-01000D	0.5% of reading	±0.1 Torr
Digital Absolut pressure transmitter	MKS	Baratron 121AA-05000B	0.5% of reading	±0.5 Torr
Analog vacuum pressure gauge	Edwards	Pirani-PRE10K	NA	±2 of reading scale
Thermocouples and Controller	Radionics	T-type	±1.0 °C	±0.1 °C
Photodetector	Thorlabs	PDA36A/PDA55	NA	NA
Photomultiplier	EMI Electronics	9924P	NA	NA

7. Uncertainty analysis

For getting a detailed understanding about the uncertainty of the experimental tests of the current study, the following subsections have been presented. In fact, these subsections try to analytically explain the effect of some important factors including pressure, temperature, and equivalence ratio on the total uncertainty of the experimental results. It seems that the output of the section could provide a good clue for better analysing and evaluating the quality of the experimental data.

7.1. Equivalence ratio

In the following lines, it is tried to somehow evaluate probable uncertainties which may be included in equivalence ratios of the applied mixtures of the current study.

Making a mixture:

$$\text{Fuel: } F = P_F = \sum_{i=1}^n P_i \rightarrow \sigma_F = \sqrt{\sum_{i=1}^n \sigma_i^2} \quad (\text{DS-1})$$

where, P_i and σ_i are absolute pressure of i -th component in the fuel mixture and uncertainty of each absolute pressure of i -th component in the fuel mixture, respectively. Because, in the current study, binary-fuel mixtures have been studied, thus:

$$\text{Fuel: } F = (p_{F1} \pm \sigma_{F1}) + (p_{F2} \pm \sigma_{F2}) \text{ and Oxygen: } O = p_{O2} \pm \sigma_{O2}.$$

$$\text{Equivalence ratio: } \varphi = \left(\frac{F}{O}\right)_{\text{real}} \rightarrow \left(\frac{O}{F}\right)_{\text{Stoi}} = \text{Cte} \rightarrow \varphi = \text{Cte} \left(\frac{F_1+F_2}{O}\right)_{\text{real}} \rightarrow \sigma_\varphi = \left(\frac{\partial\varphi}{\partial F_1}\right) \sigma_{F_1} + \left(\frac{\partial\varphi}{\partial F_2}\right) \sigma_{F_2} + \left(\frac{\partial\varphi}{\partial O}\right) \sigma_O \quad (\text{DS-2})$$

$$\varphi = \text{Cte} \left(\frac{\sum_{i=1}^n p_{F_i}}{p_{O_2}}\right)_{\text{real}} \rightarrow \frac{\partial\varphi}{\partial p_{F_n}} = \frac{1}{O} \rightarrow \frac{\partial\varphi}{\partial p_{O_2}} = -\frac{\sum_{i=1}^n p_{F_i}}{(p_{O_2})^2}$$

$$\sigma_\varphi = \frac{\partial\varphi}{\partial p_{F_1}} \cdot \sigma_{p_{F_1}} + \frac{\partial\varphi}{\partial p_{F_2}} \cdot \sigma_{p_{F_2}} + \frac{\partial\varphi}{\partial p_{F_3}} \cdot \sigma_{p_{F_3}} + \dots + \frac{\partial\varphi}{\partial p_{F_n}} \cdot \sigma_{p_{F_n}} + \left(-\frac{\sum_{i=1}^n p_{F_i}}{(p_{O_2})^2}\right) \sigma_{p_{O_2}}$$

If we assume that there is no correlation between measurements of $\sigma_i \sigma_j = 0$

$$\sigma_\varphi^2 = \left(\frac{\partial\varphi}{\partial p_{F_1}} \cdot \sigma_{p_{F_1}}\right)^2 + \left(\frac{\partial\varphi}{\partial p_{F_2}} \cdot \sigma_{p_{F_2}}\right)^2 + \left(\frac{\partial\varphi}{\partial p_{F_3}} \cdot \sigma_{p_{F_3}}\right)^2 + \dots + \left(\frac{\partial\varphi}{\partial p_{F_n}} \cdot \sigma_{p_{F_n}}\right)^2 + \left(\left(-\frac{\sum_{i=1}^n p_{F_i}}{(p_{O_2})^2}\right) \sigma_{p_{O_2}}\right)^2$$

$$\sigma_\varphi = \sqrt{\left(\frac{1}{p_{O_2}} \cdot \sigma_{p_{F_1}}\right)^2 + \left(\frac{1}{p_{O_2}} \cdot \sigma_{p_{F_2}}\right)^2 + \left(\frac{1}{p_{O_2}} \cdot \sigma_{p_{F_3}}\right)^2 + \dots + \left(\frac{1}{p_{O_2}} \cdot \sigma_{p_{F_n}}\right)^2 + \left(\left(-\frac{\sum_{i=1}^n p_{F_i}}{(p_{O_2})^2}\right) \sigma_{p_{O_2}}\right)^2}$$

$$\sigma_\varphi = \sqrt{\left(\frac{\sum_{i=1}^n \sigma_{F_i}^2}{(p_{O_2})^2}\right) + \left(\left(-\frac{\sum_{i=1}^n p_{F_i}}{(p_{O_2})^2}\right) \sigma_{p_{O_2}}\right)^2} = \sqrt{\left(\frac{\sigma_{F_1}}{p_{O_2}}\right)^2 + \left(\frac{\sigma_{F_2}}{p_{O_2}}\right)^2 + \left(\left(-\frac{p_F}{p_{O_2}}\right) \sigma_{p_{O_2}}\right)^2} = \frac{\text{Cte}}{(p_{O_2})^2} \sqrt{(p_{O_2})^2 \sigma_{F_1}^2 + (p_{O_2})^2 \sigma_{F_2}^2 + p_F^2 \sigma_{p_{O_2}}^2} \quad (\text{DS-3})$$

Based on the above analysis, the average uncertainty of the equivalence ratios is $\overline{\sigma_\varphi} = \pm 5 \times 10^{-3}$.

7.2. Diluent concentration

For determining the uncertainty of diluent concentration in the studied mixtures the following formulations are presented:

$$[D] = \frac{p_i}{RT_i} \quad (\text{DS-4})$$

$$\sigma_{[D]} = \frac{\partial[D]}{\partial p_i} \sigma_{p_i} \quad (\text{DS-5})$$

$$\frac{\partial[D]}{\partial p_i} = \frac{1}{RT_i} \quad (\text{DS-6})$$

Because, in the study, all mixtures have been prepared under 303 K, so the Eq. (6) would be as follows:

$$\frac{\partial[D]}{\partial P_i} = 3.96961 \times 10^{-4}$$

Therefore, the worst uncertainty in diluent concentration in the studied mixtures is related to cases with 90% diluent in a mixture with total pressure of 4000 Torr which yields $\sigma_{[D]} = \pm 1.05848 \frac{\text{mol}}{\text{m}^3} = \pm 1.05848 \times 10^{-5} \frac{\text{mol}}{10^5 \cdot \text{m}^3} \approx \pm 0.56\% [D]$

For calculating the uncertainty in concentration of each species under the compressed conditions, the following formulations are presented:

$$[D] = \frac{p_{c,[D]}}{RT_c} \quad (\text{DS-7})$$

$$\sigma_{[D]} = \sqrt{\left(\frac{\partial[D]}{\partial p_{c,[D]}} \sigma_{p_{c,[D]}}\right)^2 + \left(\frac{\partial[D]}{\partial T_c} \sigma_{T_c}\right)^2} \quad (\text{DS-8})$$

$$\sigma_{[D]} = \sqrt{\left(\frac{1}{RT_c} \sigma_{p_{c,[D]}}\right)^2 + \left(-\frac{p_{c,[D]}}{RT_c^2} \sigma_{T_c}\right)^2} = \frac{1}{8.314 \times T_c^2} \sqrt{(T_c \sigma_{p_{c,[D]}})^2 + (p_{c,[D]} \sigma_{T_c})^2} \quad (\text{DS-9})$$

7.3.IDTs in Shock tube

If the following equations, for determining total uncertainty of the measured ignition delay times in NUIG-L/HPST, it is assumed:

$$p_c = p(p_1, V_s, \varphi, T_1); T_c = T(T_1, V_s, \varphi)$$

As shown by Petersen et al. [15], one could assume that:

$$T_c = \frac{T_1[2(\gamma_1 - 1)M^2 + (3 - \gamma_1)](3\gamma_1 - 1)M^2 - 2(\gamma_1 - 1)}{(\gamma_1 + 1)^2 M^2}; M = \frac{V_s}{\sqrt{\gamma_1 RT_1}}; V_s = \frac{\Delta z}{\Delta t} \quad (\text{DS-10})$$

$$\sigma_{V_s} = \sqrt{\left(\frac{\partial V_s}{\partial(\Delta z)} \sigma_{\Delta z}\right)^2 + \left(\frac{\partial V_s}{\partial(\Delta t)} \sigma_{\Delta t}\right)^2} = \sqrt{\left(\frac{1}{\Delta t} \sigma_{\Delta z}\right)^2 + \left(-\frac{\Delta z}{(\Delta t)^2} \sigma_{\Delta t}\right)^2} \quad (\text{DS-11})$$

$$\sigma_{T_c} = \sigma_T = \frac{\partial T_c}{\partial M} \sigma_M = \left(T_1 \left[\left(\frac{4(3\gamma_1^2 - 4\gamma_1 + 1)}{(\gamma_1 + 1)^2}\right) M + \left(\frac{4(\gamma_1 - 1)(3 - \gamma_1)}{(\gamma_1 + 1)^2}\right) M^{-3} \right] \right) \frac{\sigma_{V_s}}{\sqrt{\gamma_1 RT_1}} \quad (\text{DS-12})$$

$$p_c = \frac{p_1[2\gamma_1 M^2 - (\gamma_1 - 1)](3\gamma_1 - 1)M^2 - 2(\gamma_1 - 1)}{2(\gamma_1 + 1) + M^2(\gamma_1^2 - 1)}; \sigma_{p_c} = \sigma_p = \frac{\partial p_c}{\partial M} \sigma_M \quad (\text{DS-13})$$

$$= \left(p_1 \left[\frac{12M^5\gamma^4 - 4M^5\gamma^3 + 48M^3\gamma^3 + 32M^3\gamma^2 - 12M^5\gamma^2 + 4M^5\gamma - 16M^3\gamma - 20M\gamma^3 + 4M\gamma^2 + 20M\gamma - 4M\gamma^4}{(M^2\gamma^2 - M^2 + 2\gamma + 2)^2} \right] \right) \frac{\sigma_{V_s}}{\sqrt{\gamma_1 RT_1}}$$

Here, it was supposed that the effect of changing in equivalence ratio on γ is negligible. Here, it is supposed that the maximum $\sigma_{\Delta t}$ which is related to TiePie Handyscope HS4 Oscilloscope is $\pm 1 \mu\text{s}$,

and, $\sigma_{\Delta z}$ is ± 0.001 m. Now, if it could be assumed the defined ignition delay time (IDT) could be correlated as follows, then:

$$\begin{aligned}
\tau_{IDT} &\cong A \cdot \exp\left(\frac{B}{T}\right) p^m \varphi^n [D]^q \rightarrow \partial\tau = \frac{\partial\tau}{\partial T} \cdot \partial T + \frac{\partial\tau}{\partial p} \cdot \partial p + \frac{\partial\tau}{\partial \varphi} \cdot \partial \varphi + \frac{\partial\tau}{\partial [D]} \cdot \partial [D] \rightarrow (\sigma_{\tau})^2 \\
&= \left(\frac{\partial\tau}{\partial T} \cdot \partial T\right)^2 + \left(\frac{\partial\tau}{\partial p} \cdot \partial p\right)^2 + \left(\frac{\partial\tau}{\partial \varphi} \cdot \partial \varphi\right)^2 + \left(\frac{\partial\tau}{\partial [D]} \cdot \partial [D]\right)^2 + 2 \left(\frac{\partial\tau}{\partial T} \cdot \frac{\partial\tau}{\partial p} \cdot \partial T \partial p\right) \\
&+ 2 \left(\frac{\partial\tau}{\partial T} \cdot \frac{\partial\tau}{\partial \varphi} \cdot \partial T \partial \varphi\right) + 2 \left(\frac{\partial\tau}{\partial \varphi} \cdot \frac{\partial\tau}{\partial p} \cdot \partial \varphi \partial p\right) + 2 \left(\frac{\partial\tau}{\partial T} \cdot \frac{\partial\tau}{\partial [D]} \cdot \partial T \partial [D]\right) \\
&+ 2 \left(\frac{\partial\tau}{\partial p} \cdot \frac{\partial\tau}{\partial [D]} \cdot \partial p \partial [D]\right) + 2 \left(\frac{\partial\tau}{\partial \varphi} \cdot \frac{\partial\tau}{\partial [D]} \cdot \partial \varphi \partial [D]\right)
\end{aligned} \tag{DS-14}$$

Now, one assumes that there is no correlation between measurements of (p , T , and φ), so the above equation would be followed by:

$$\begin{aligned}
(\sigma_{\tau,i})^2 &= \left(\frac{\partial\tau}{\partial T} \cdot \partial T\right)^2 + \left(\frac{\partial\tau}{\partial p} \cdot \partial p\right)^2 + \left(\frac{\partial\tau}{\partial \varphi} \cdot \partial \varphi\right)^2 + \left(\frac{\partial\tau}{\partial [D]} \cdot \partial [D]\right)^2 + 2 \left(\frac{\partial\tau}{\partial T} \cdot \frac{\partial\tau}{\partial p} \cdot \partial T \partial p\right) + 2 \left(\frac{\partial\tau}{\partial T} \cdot \frac{\partial\tau}{\partial \varphi} \cdot \partial T \partial \varphi\right) \\
&+ 2 \left(\frac{\partial\tau}{\partial \varphi} \cdot \frac{\partial\tau}{\partial p} \cdot \partial \varphi \partial p\right) + 2 \left(\frac{\partial\tau}{\partial T} \cdot \frac{\partial\tau}{\partial [D]} \cdot \partial T \partial [D]\right) + 2 \left(\frac{\partial\tau}{\partial p} \cdot \frac{\partial\tau}{\partial [D]} \cdot \partial p \partial [D]\right) \\
&+ 2 \left(\frac{\partial\tau}{\partial \varphi} \cdot \frac{\partial\tau}{\partial [D]} \cdot \partial \varphi \partial [D]\right)
\end{aligned} \tag{DS-15}$$

One could re-write the above equation as follows:

$$(\sigma_{\tau,i})^2 = \left(\frac{\partial\tau}{\partial T} \cdot \sigma_T\right)^2 + \left(\frac{\partial\tau}{\partial p} \cdot \sigma_p\right)^2 + \left(\frac{\partial\tau}{\partial \varphi} \cdot \sigma_\varphi\right)^2 + \left(\frac{\partial\tau}{\partial [D]} \cdot \sigma_{[D]}\right)^2 + 2 \left(\frac{\partial\tau}{\partial T} \cdot \frac{\partial\tau}{\partial [D]} \cdot \sigma_T \sigma_{[D]}\right) + 2 \left(\frac{\partial\tau}{\partial p} \cdot \frac{\partial\tau}{\partial [D]} \cdot \sigma_p \sigma_{[D]}\right) \tag{DS-16}$$

$$\frac{\partial\tau}{\partial T} = A \cdot \left(-\frac{B}{T^2} \cdot \exp\left(\frac{B}{T}\right) p^m \varphi^n [D]^q\right) \tag{DS-17}$$

$$\frac{\partial\tau}{\partial p} = A \cdot \left(m \cdot \exp\left(\frac{B}{T}\right) p^{m-1} \varphi^n [D]^q\right) \tag{DS-18}$$

$$\frac{\partial\tau}{\partial \varphi} = A \cdot \left(n \cdot \exp\left(\frac{B}{T}\right) p^m \varphi^{n-1} [D]^q\right) \tag{DS-19}$$

$$\frac{\partial\tau}{\partial [D]} = A \cdot \left(q \cdot \exp\left(\frac{B}{T}\right) p^m \varphi^n [D]^{q-1}\right) \tag{DS-20}$$

$$\begin{aligned}
(\sigma_{\tau,i})^2 &= A^2 \cdot \left(\left(-\frac{B}{T^2} \cdot \exp\left(\frac{B}{T}\right) p^m \varphi^n [D]^q\right) \cdot \sigma_T\right)^2 + A^2 \cdot \left(\left(m \cdot \exp\left(\frac{B}{T}\right) p^{m-1} \varphi^n [D]^q\right) \cdot \sigma_p\right)^2 \\
&+ A^2 \cdot \left(\left(n \cdot \exp\left(\frac{B}{T}\right) p^m \varphi^{n-1} [D]^q\right) \cdot \sigma_\varphi\right)^2 + A^2 \cdot \left(\left(q \cdot \exp\left(\frac{B}{T}\right) p^m \varphi^n [D]^{q-1}\right) \cdot \sigma_{[D]}\right)^2 \\
&- 2A^2 \left(\frac{Bq}{T^2} \cdot \exp\left(\frac{2B}{T}\right) p^{2m} \varphi^{2n} [D]^{2q-1}\right) \cdot \rho_{T[D]} \sigma_T \sigma_{[D]} + 2A^2 \left(qm \cdot \exp\left(\frac{2B}{T}\right) p^{2m-1} \varphi^{2n} [D]^{2q-1}\right) \\
&\cdot \rho_{p[D]} \sigma_p \sigma_{[D]}
\end{aligned} \tag{DS-21}$$

$$\sigma_{\tau,i} \cong A \cdot \sqrt{\left(\left(-\frac{B}{T^2} \cdot \exp\left(\frac{B}{T}\right) p^m \varphi^n [D]^q\right) \cdot \sigma_T\right)^2 + \left(\left(m \cdot \exp\left(\frac{B}{T}\right) p^{m-1} \varphi^n [D]^q\right) \cdot \sigma_p\right)^2 + \left(\left(n \cdot \exp\left(\frac{B}{T}\right) p^m \varphi^{n-1} [D]^q\right) \cdot \sigma_\varphi\right)^2 + \left(\left(q \cdot \exp\left(\frac{B}{T}\right) p^m \varphi^n [D]^{q-1}\right) \cdot \sigma_{[D]}\right)^2 - 2\left(\frac{Bq}{T^2} \cdot \exp\left(\frac{2B}{T}\right) p^{2m} \varphi^{2n} [D]^{2q-1}\right) \cdot \rho_{T[D]} \sigma_T \sigma_{[D]} + 2\left(qm \cdot \exp\left(\frac{2B}{T}\right) p^{2m-1} \varphi^{2n} [D]^{2q-1}\right) \cdot \rho_{p[D]} \sigma_p \sigma_{[D]}} \tag{DS-22}$$

$$\rho_{ij} \sigma_i \sigma_j = \sigma_{ij} = \sum_{ij} f(i, j) (x_i - \bar{x}_i) (x_j - \bar{x}_j) \tag{DS-23}$$

The uncertainty of the measured ignition delay time in shock tube could be acceptably estimated using the above equation. As seen in the above expression, the uncertainty parameter is changing by changing in the compressed temperature and pressure, and equivalence ratio, so that it is not a

constant parameter during the experimental tests. Thus, it should be calculated specifically for each case. Therefore, regarding Eq. (DS-22) and Table DS9, specific uncertainty for each fuel according to its specific temperature, pressure, and equivalence ratio could be estimated.

Table DS9. Correlation variables of the studied experimental datasets for different fuels in shock tubes.

$\tau_{IDT} = 10^A \cdot \exp\left(\frac{B}{T}\right) P^m \phi^n [D]^q$								
Fuel		A	B	m	n	q	R ²	Adj R ²
CH ₄ + C ₂ H ₄	50% + 50%	-8.189	14359.44	-0.268	0.293	0.0	0.993	0.993
	70% + 30%	-13.96	-552.43	-13.16	1.371	12.77	0.996	0.995
	90% + 10%	-15.02	-5834.91	-16.69	1.625	16.36	0.997	0.997
C ₂ H ₆ + C ₂ H ₄	50% + 50%	-12.14	7982.58	-7.49	-0.177	6.88	0.971	0.968
	70% + 30%	-20.50	-11369.34	-21.85	3.283	22.48	0.992	0.992
	90% + 10%	-15.27	1437.05	-12.64	0.770	12.48	0.999	0.999

7.4. Rapid compression machine

As shown in the previous section, the uncertainty of each experimental point is changing by varying temperature, pressure, and mixture composition, so that it is not identical during IDT measurement experimental tests. Therefore, for doing the uncertainty analysis for the studied RCM regimes, the same procedure performed for shock-tube is followed and relevant correlations between parameters and IDTs have been evaluated as shown in Table DS10. As already mentioned by Weber et al. [16], using Monte Carlo analysis or independent parameters methodology doesn't led to significant change in the calculated uncertainties. Therefore, like the performed uncertainty analysis for NUIG-HPST, it is supposed that there is no correlation between p_C , T_C and ϕ which can affect measured ignition delay time in the rapid compression machine. However, the correlation between $[D]$ and p_C , T_C is taken in to account according to Eq. (DS-23). In this regard, the effect of temperature on the measured ignition delay time has been correlated through fitting an exponential equation to the experimental IDT data, and then the individual effect of pressure on the measured ignition delay time has been estimated using the applied approach by Weber et al. [16]. Also, the effect of each individual parameter such as equivalence ratio (0.5-2.0) and dilution (75%-90%) on the simulated ignition delay times has been correlated using fitted equations to the experimentally measured ignition delay times. Therefore, the following formulations could be proposed to estimate available uncertainties in the measured independent parameters and consequently the measured ignition delay times:

$$\frac{\partial T_C}{\partial P_C} = \frac{W\left(\frac{b}{a} \exp\left[\frac{bT_0}{a}\right] T_0 \left[\frac{P_C}{P_0}\right]^{\frac{1}{a}}\right)}{bP_C \left(W\left(\frac{b}{a} \exp\left[\frac{bT_0}{a}\right] T_0 \left[\frac{P_C}{P_0}\right]^{\frac{1}{a}}\right) + 1\right)} \quad (\text{DS-24})$$

where, W , T_0 , and P_0 are Lambert's W function, initial temperature, and initial pressure in the reaction chamber, respectively. In Eq. (DS-24), “a”, “b”, and $\frac{\partial T_C}{\partial P_C}$ were calculated using a Python code developed by Weber et al. [16].

$$\frac{\partial \tau_{IDT}}{\partial P_C} = \frac{\partial \tau_{IDT}}{\partial T_C} \cdot \frac{\partial T_C}{\partial P_C} = \frac{\partial \tau_{IDT}}{\partial T_C} \text{ (from Table 10)} \cdot \frac{W\left(\frac{b}{a} \exp\left[\frac{bT_0}{a}\right] T_0 \left[\frac{P_C}{P_0}\right]^{\frac{1}{a}}\right)}{bP_C \left(W\left(\frac{b}{a} \exp\left[\frac{bT_0}{a}\right] T_0 \left[\frac{P_C}{P_0}\right]^{\frac{1}{a}}\right) + 1\right)} \quad (\text{DS-25})$$

$$(\sigma_{\tau,i})^2 = \left(\frac{\partial \tau}{\partial T} \cdot \sigma_T\right)^2 + \left(\frac{\partial \tau}{\partial p} \cdot \sigma_p\right)^2 + \left(\frac{\partial \tau}{\partial \varphi} \cdot \sigma_\varphi\right)^2 + \left(\frac{\partial \tau}{\partial [D]} \cdot \sigma_{[D]}\right)^2 + 2\left(\frac{\partial \tau}{\partial T} \cdot \frac{\partial \tau}{\partial [D]} \cdot \sigma_T \sigma_{[D]}\right) + 2\left(\frac{\partial \tau}{\partial p} \cdot \frac{\partial \tau}{\partial [D]} \cdot \sigma_p \sigma_{[D]}\right) \quad (\text{DS-26})$$

$$\tau_{IDT} = f(T_C, p_C, \varphi, [D]) \rightarrow \sigma_{\tau_{IDT}} = \sqrt{\left(\frac{\partial \tau_{IDT}}{\partial T_C} \cdot \sigma_{T_C}\right)^2 + \left(\frac{\partial \tau_{IDT}}{\partial p_C} \cdot \sigma_{p_C}\right)^2 + \left(\frac{\partial \tau_{IDT}}{\partial \varphi} \cdot \sigma_\varphi\right)^2 + \left(\frac{\partial \tau_{IDT}}{\partial [D]} \cdot \sigma_{[D]}\right)^2 + 2\left(\frac{\partial \tau_{IDT}}{\partial T_C} \cdot \frac{\partial \tau_{IDT}}{\partial [D]} \cdot \sigma_{T_C} \sigma_{[D]}\right) + 2\left(\frac{\partial \tau_{IDT}}{\partial p_C} \cdot \frac{\partial \tau_{IDT}}{\partial [D]} \cdot \sigma_{p_C} \sigma_{[D]}\right)} \quad (\text{DS-27})$$

By substituting correlations from Table DS10 and Eqs. (DS-23) and (DS-25) into Eq. (DS-27), the uncertainty of the measured ignition delay times in RCM regime would be calculated based on a Python code developed by Weber et al. [16].

Table DS10. Correlation variables of the studied experimental datasets for different fuels in RCMs.

$\tau_{IDT} = 10^A \cdot \exp\left(\frac{B}{T}\right) \varphi^n [D]^q$							
Fuel		A	B	n	q	R ²	Adj R ²
CH ₄ + C ₂ H ₄	50% + 50%	-33.82	16398.20	-14.03	10.79	0.995	0.994
	70% + 30%	-5.88	31697.98	-3.11	-4.22	0.996	0.996
	90% + 10%	204.42	126728.67	-63.23	-107.3	0.997	0.997
C ₂ H ₆ + C ₂ H ₄	50% + 50%	14.92	42743.02	15.25	-15.40	0.998	0.998
	70% + 30%	-118.99	-8476.95	-20.06	49.20	0.991	0.990
	90% + 10%	186.68	131240.51	-60.44	-101.1	0.975	0.971

8. Pressure profiles of the applied rapid compression machines (RCMs)

The reactive and non-reactive pressure profiles of the applied rapid compression machines including NUIG-RCM and PCFC-RCM for the studied cases alongside the simulation profiles are shown in

the following figures. Here, it should be noted that all the simulations were performed using NUIGMech1.0 mechanism, otherwise, it is mentioned in caption or legend of figures.

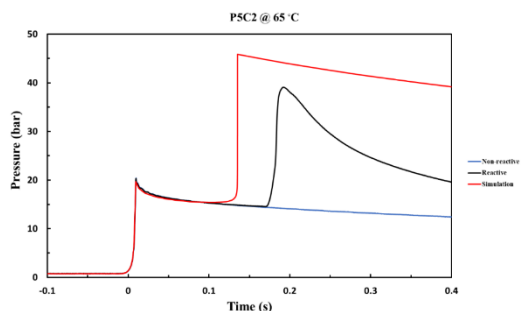


Figure DS3. Pressure history of tested reactive and non-reactive mixtures of P5C2 case alongside the simulation's profile for initial temperature of 338 K.

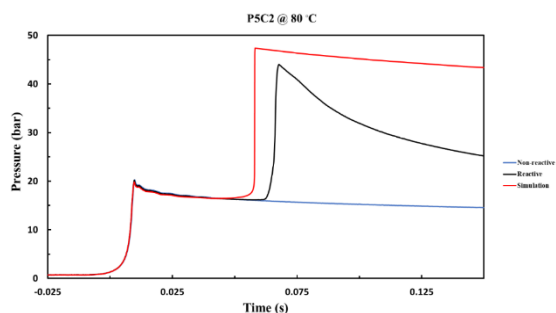


Figure DS4. Pressure history of tested reactive and non-reactive mixtures of P5C2 case alongside the simulation's profile for initial temperature of 353 K.

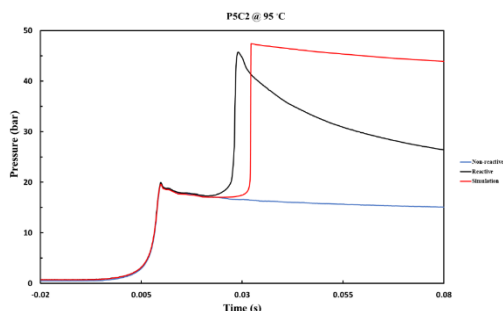


Figure DS5. Pressure history of tested reactive and non-reactive mixtures of P5C2 case alongside the simulation's profile for initial temperature of 368 K.

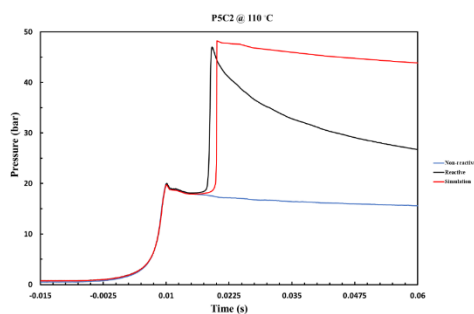


Figure DS6. Pressure history of tested reactive and non-reactive mixtures of P5C2 case alongside the simulation's profile for initial temperature of 383 K.

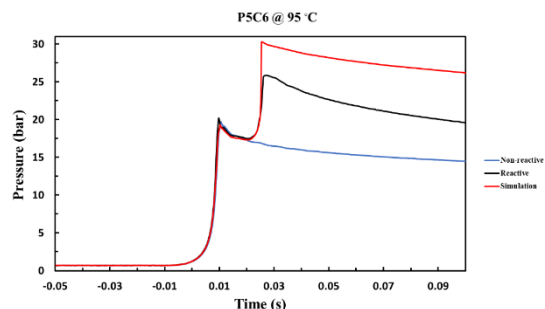


Figure DS7. Pressure history of tested reactive and non-reactive mixtures of P5C6 case alongside the simulation's profile for initial temperature of 368 K.

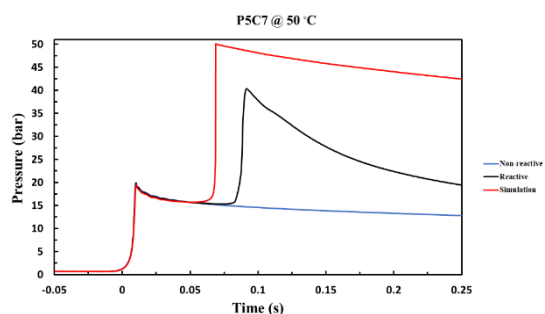


Figure DS8. Pressure history of tested reactive and non-reactive mixtures of P5C7 case alongside the simulation's profile for initial temperature of 323 K.

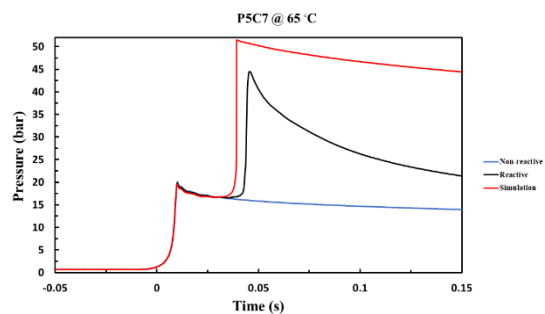


Figure DS9. Pressure history of tested reactive and non-reactive mixtures of P5C7 case alongside the simulation's profile for initial temperature of 338 K.

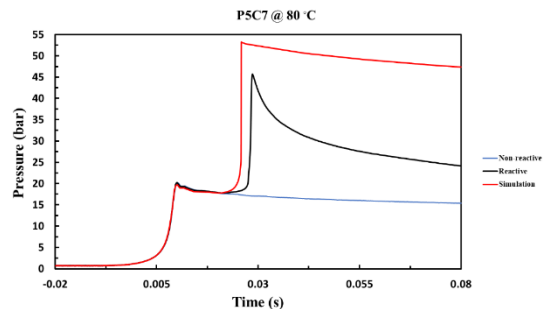


Figure DS10. Pressure history of tested reactive and non-reactive mixtures of P5C7 case alongside the simulation's profile for initial temperature of 353 K.

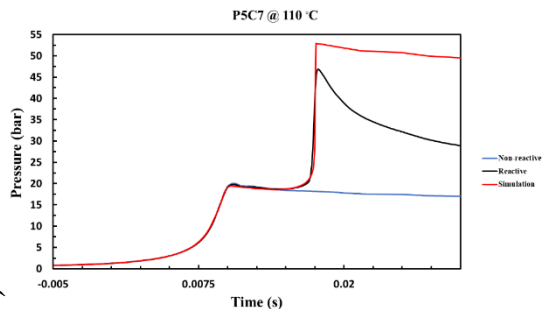


Figure DS11. Pressure history of tested reactive and non-reactive mixtures of P5C7 case alongside the simulation's profile for initial temperature of 383 K.

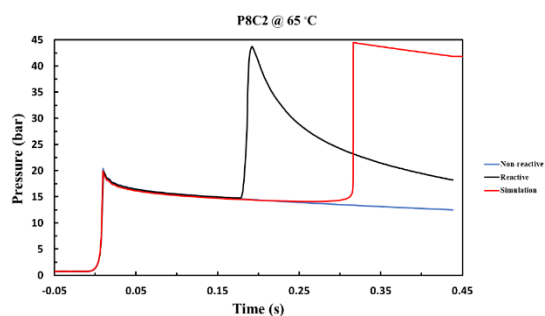


Figure DS12. Pressure history of tested reactive and non-reactive mixtures of P8C2 case alongside the simulation's profile for initial temperature of 338 K.

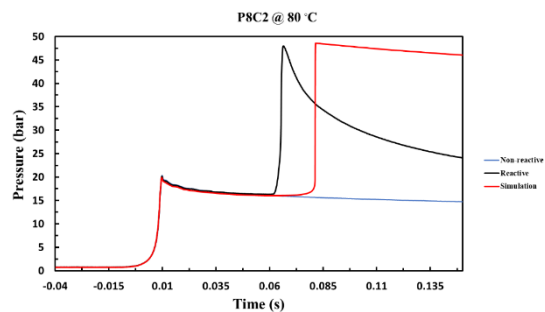


Figure DS13. Pressure history of tested reactive and non-reactive mixtures of P8C2 case alongside the simulation's profile for initial temperature of 353 K.

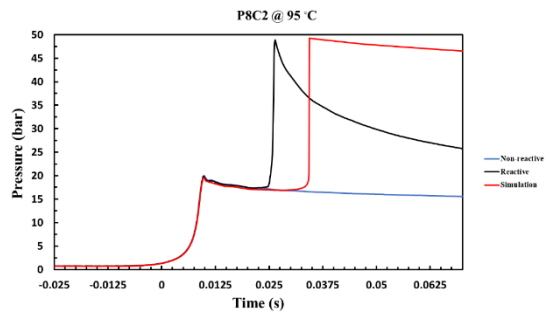


Figure DS14. Pressure history of tested reactive and non-reactive mixtures of P8C2 case alongside the simulation's profile for initial temperature of 368 K.

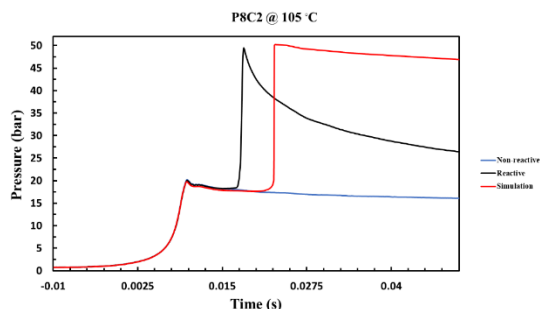


Figure DS15. Pressure history of tested reactive and non-reactive mixtures of P8C2 case alongside the simulation's profile for initial temperature of 378 K.

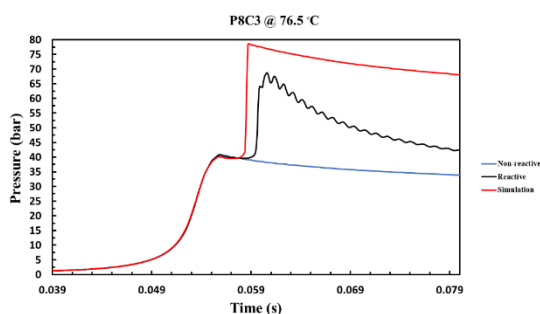


Figure DS16. Pressure history of tested reactive and non-reactive mixtures of P8C3 case alongside the simulation's profile for initial temperature of 349.5 K.

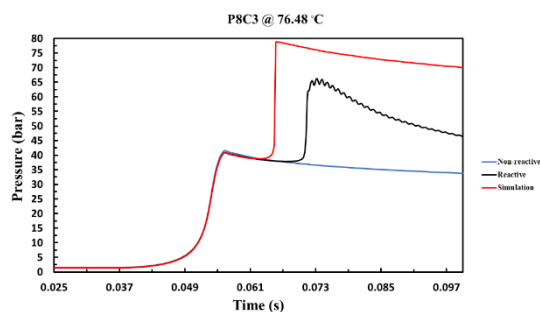


Figure DS17. Pressure history of tested reactive and non-reactive mixtures of P8C3 case alongside the simulation's profile for initial temperature of 349.6 K.

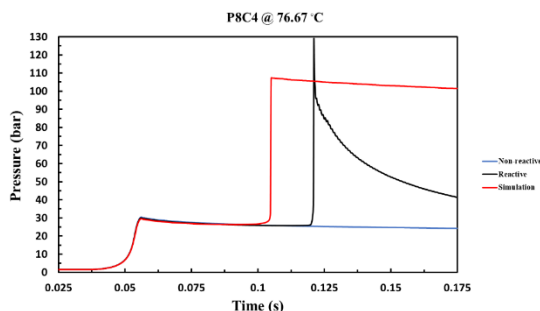


Figure DS18. Pressure history of tested reactive and non-reactive mixtures of P8C4 case alongside the simulation's profile for initial temperature of 349.8 K.

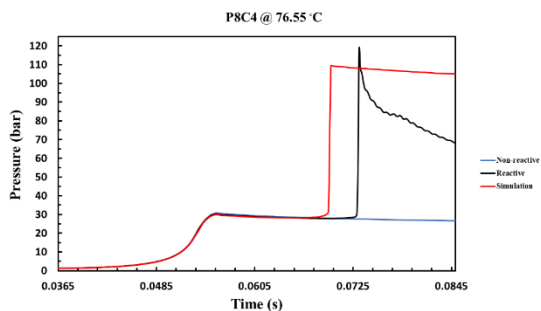


Figure DS19. Pressure history of tested reactive and non-reactive mixtures of P8C4 case alongside the simulation's profile for initial temperature of 349.7 K.

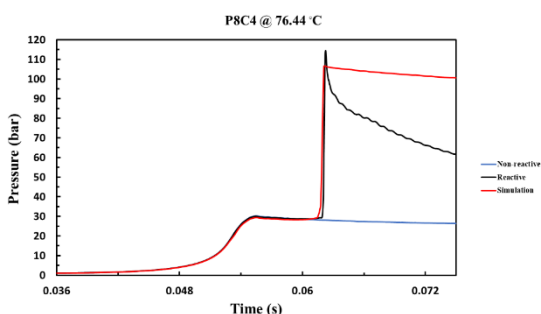


Figure DS20. Pressure history of tested reactive and non-reactive mixtures of P8C4 case alongside the simulation's profile for initial temperature of 349.6 K.

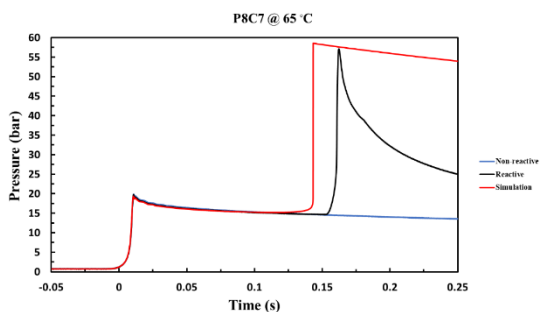


Figure DS21. Pressure history of tested reactive and non-reactive mixtures of P8C7 case alongside the simulation's profile for initial temperature of 338 K.

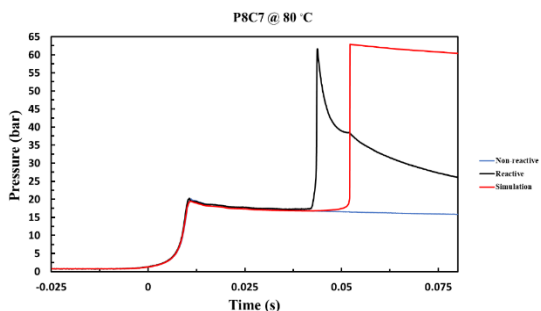


Figure DS22. Pressure history of tested reactive and non-reactive mixtures of P8C7 case alongside the simulation's profile for initial temperature of 353 K.

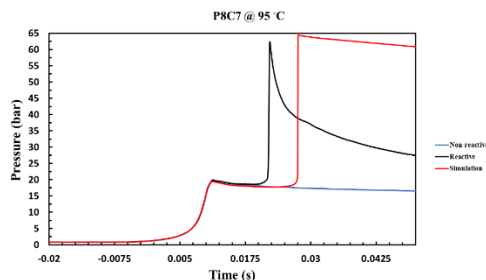


Figure DS23. Pressure history of tested reactive and non-reactive mixtures of P8C7 case alongside the simulation's profile for initial temperature of 368 K.

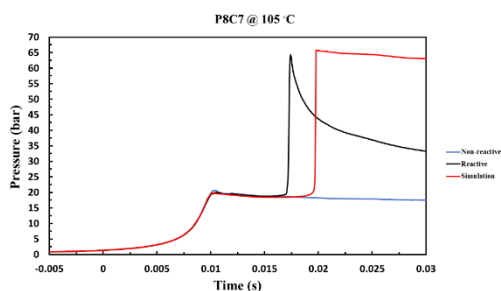


Figure DS24. Pressure history of tested reactive and non-reactive mixtures of P8C7 case alongside the simulation's profile for initial temperature of 378 K.

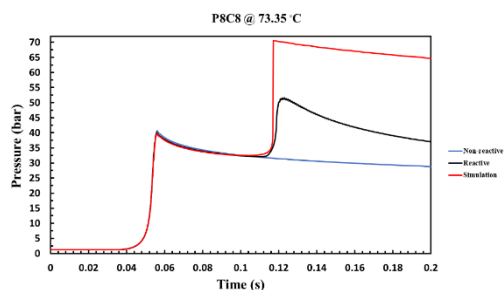


Figure DS25. Pressure history of tested reactive and non-reactive mixtures of P8C8 case alongside the simulation's profile for initial temperature of 346.5 K.

9. Comparing the performances of NUIGMech1.0 versus other available mechanisms

In this regard, the performances of chemical mechanisms presented in have been evaluated and compared over a wide range of conditions studied in the article.

Table DS11. Applied chemical mechanisms.

No	Mechanism	Number of reactions	Number of species	Comments
1	AramcoMech 3.0	3037	581	Released at 2018; [17]
2	AramcoMech 2.0	2716	493	Released at 2016; [10,18–23]

3	AramcoMech 1.3	1542	253	Released at 2013; [10]
4	DTU-C ₃	142	1308	Released at 2019; [24]
5	CRECK	1941	114	Released at 2020; [25]
6	UCSD	268	57	Released at 2016; [26]
7	GRI 3.0	325	53	Released at 2000; [27]
8	JetSurF 2.0	348	2163	Released at 2010; [28]
9	FFCM-1	291	38	C ₁ -C ₂ ; Low temperature reactions are not included; released at 2016; [29]

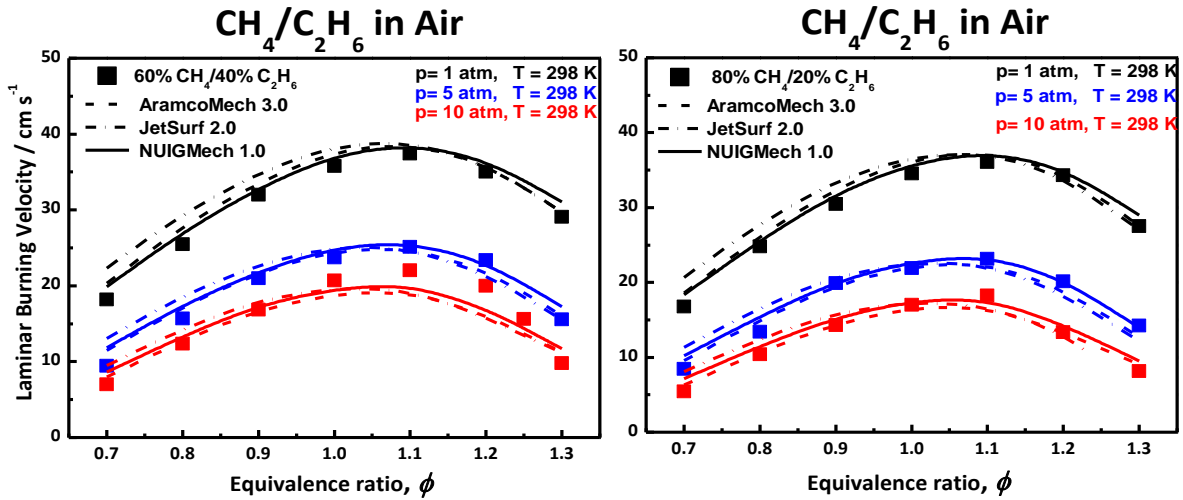


Figure DS26. Performance of NUIGMech1.0 for predicting LBVs in comparison to AramcoMech 3.0 and JetSurf II. [30].

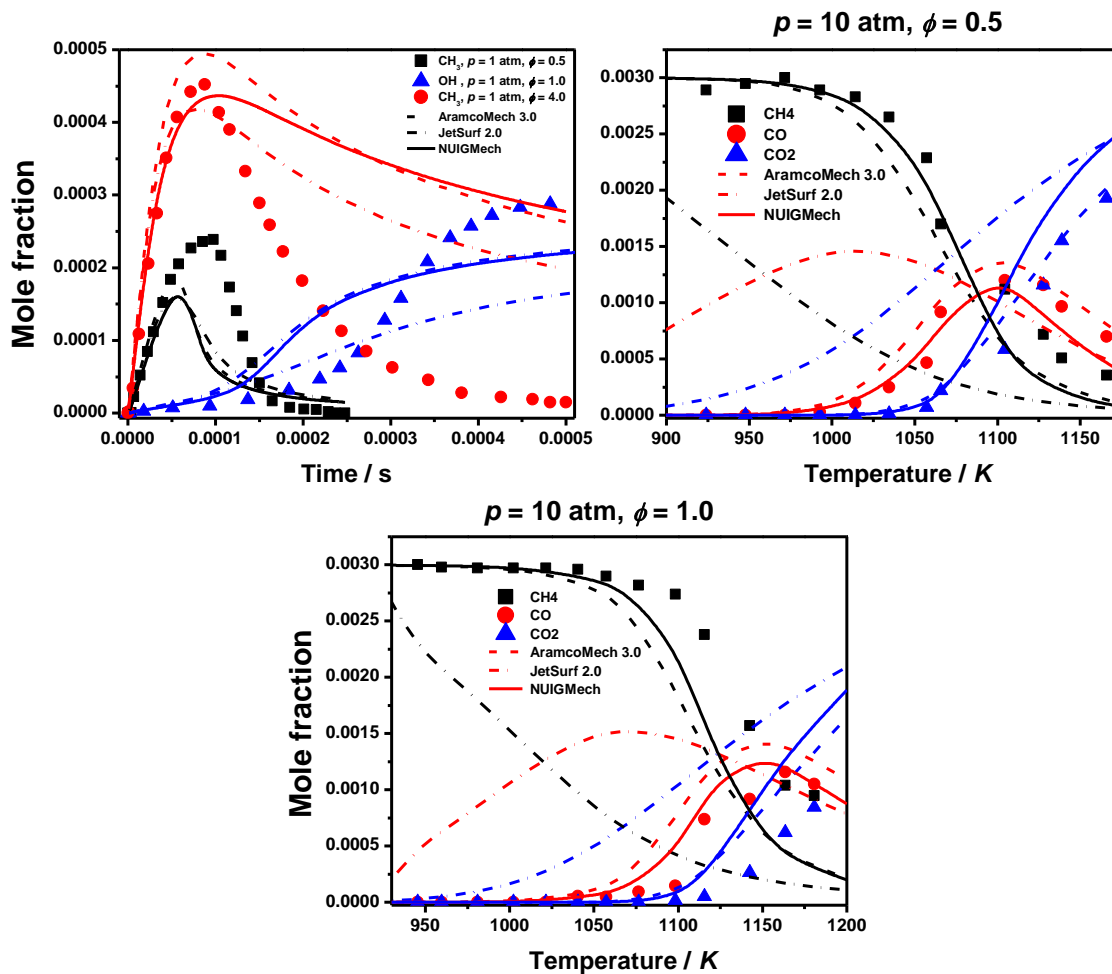


Figure DS27. Performance of NUIGMech1.0 for predicting methane's speciation in comparison to AramcoMech 3.0 and JetSurf II. [31,32].

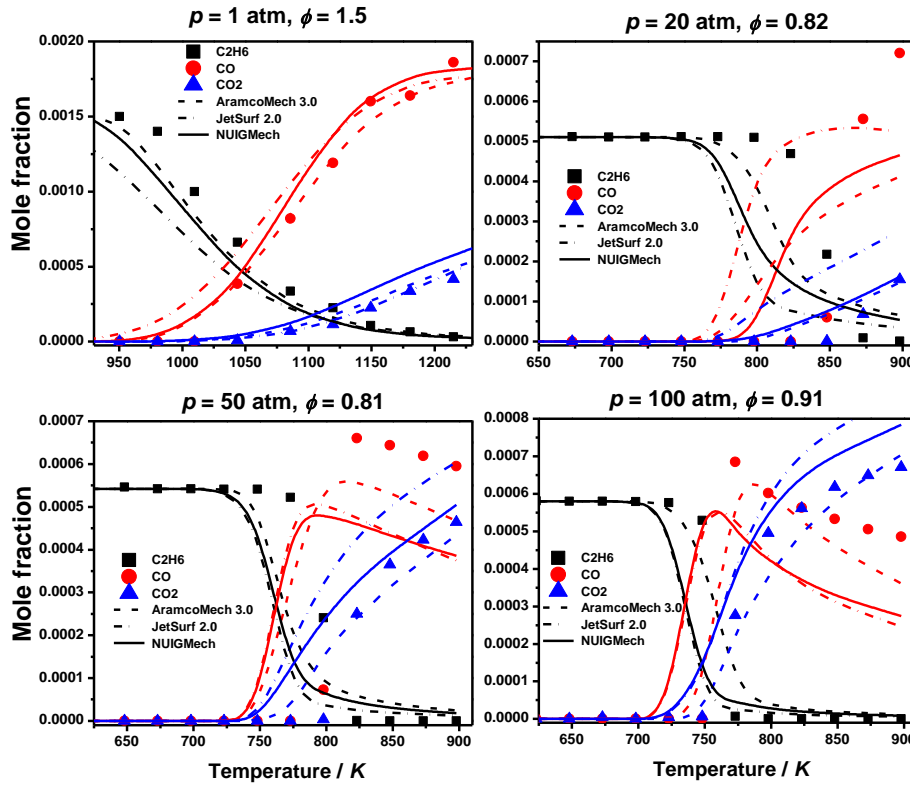


Figure DS28. Performance of NUIGMech1.0 for predicting ethane’s speciation in comparison to AramcoMech 3.0 and JetSurf II. [33,34].

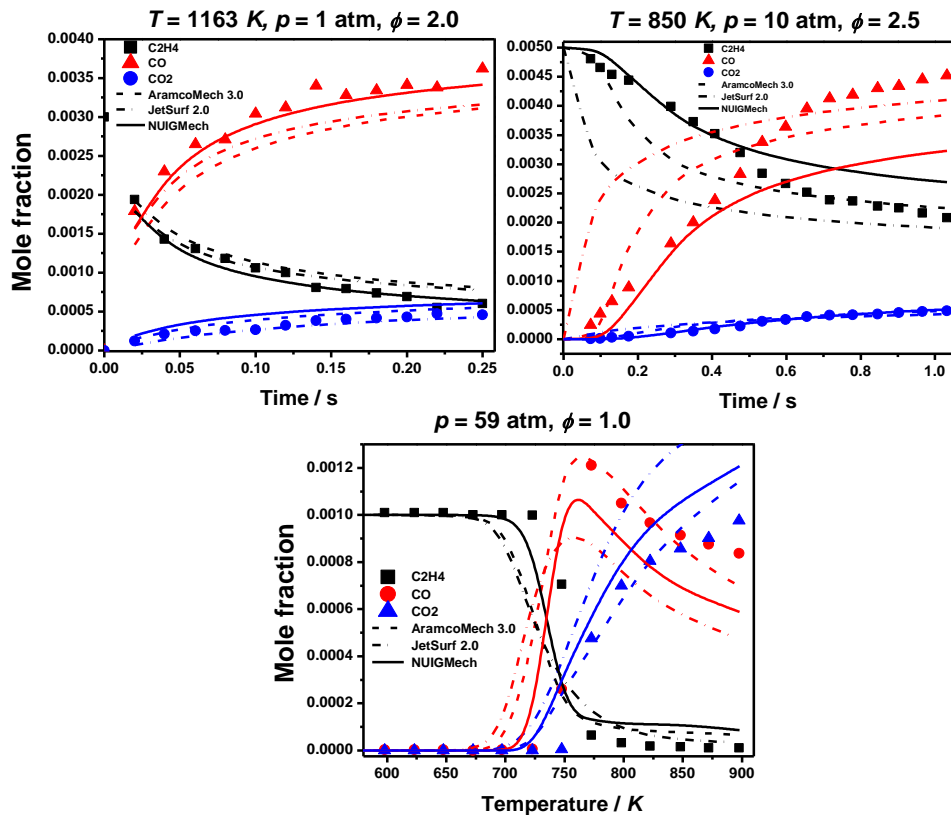
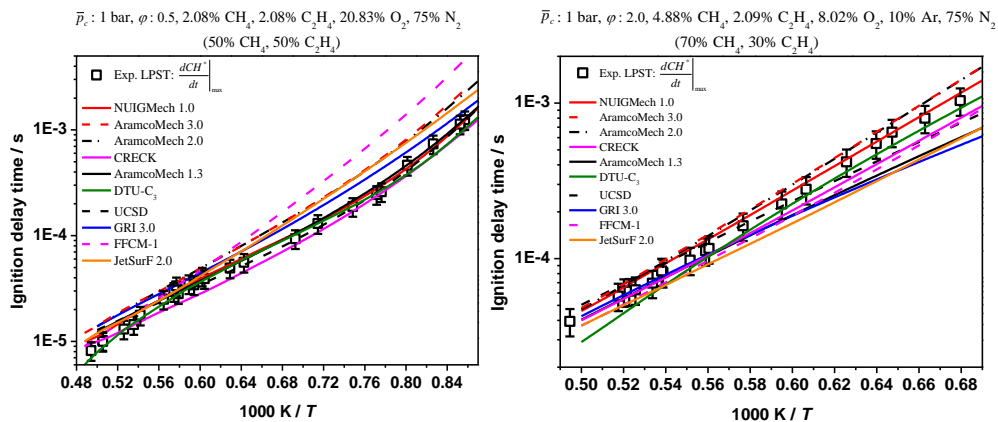


Figure DS29. Performance of NUIGMech1.0 for predicting ethylene's speciation in comparison to AramcoMech 3.0 and JetSurf II. [31,35,36].



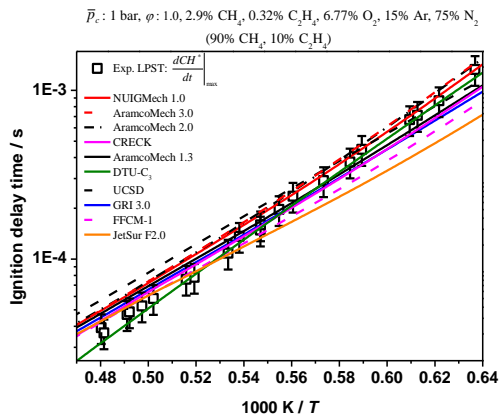
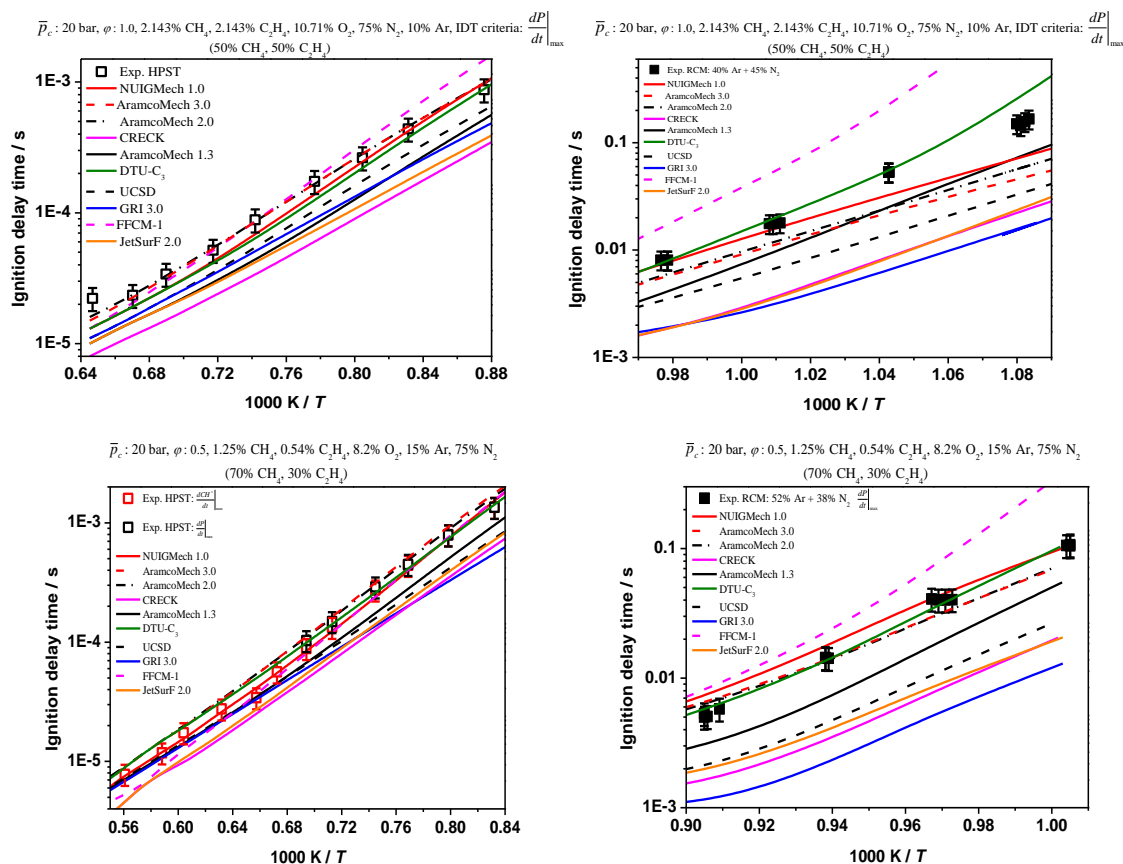


Figure DS30. Performance of NUIGMech1.0 for predicting methane + ethylene's IDTs at 1 bar in comparison to the other examined chemical mechanisms.



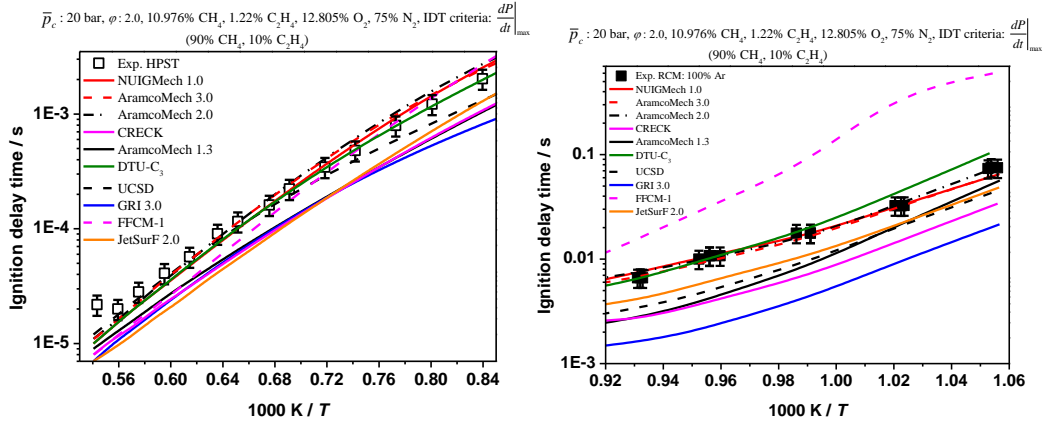
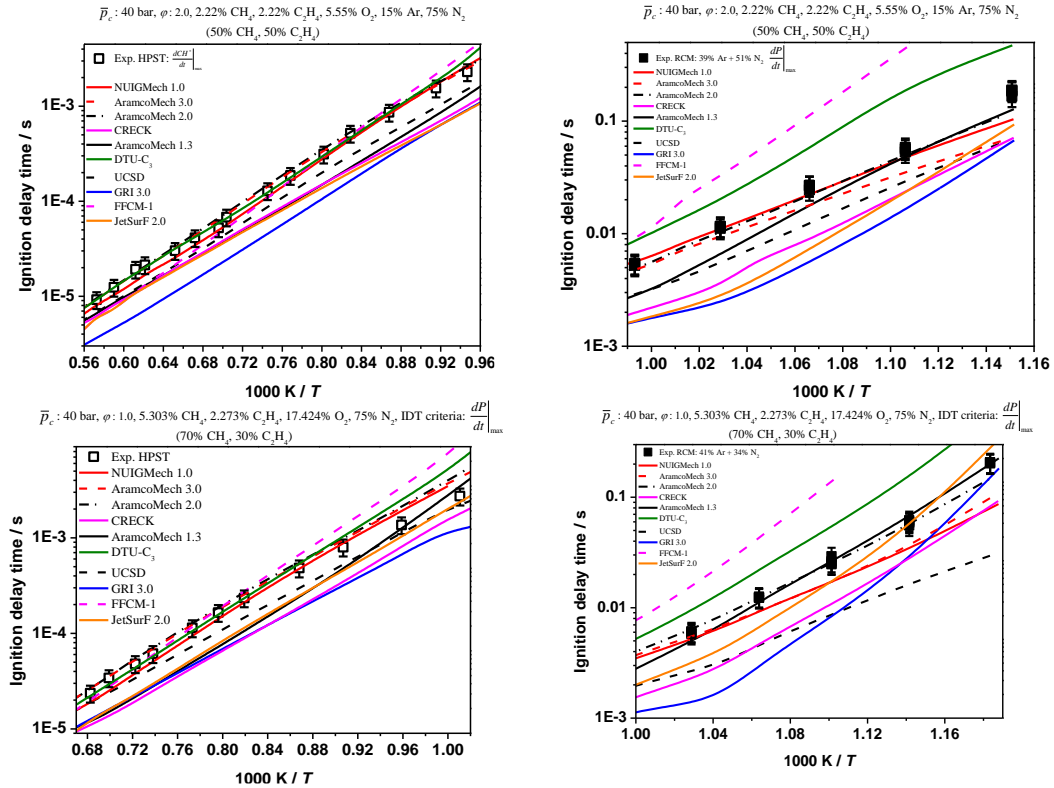


Figure DS31. Performance of NUIGMech1.0 for predicting methane + ethylene's IDTs at 20 bar in comparison to the other examined chemical mechanisms.



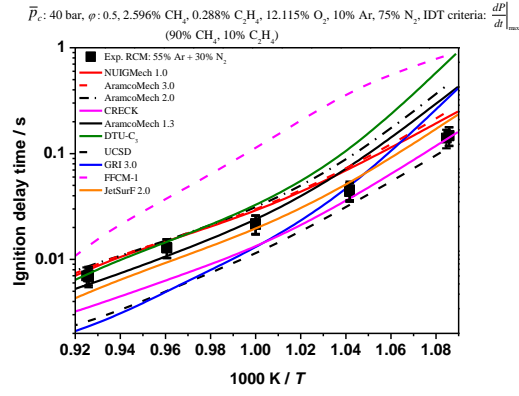
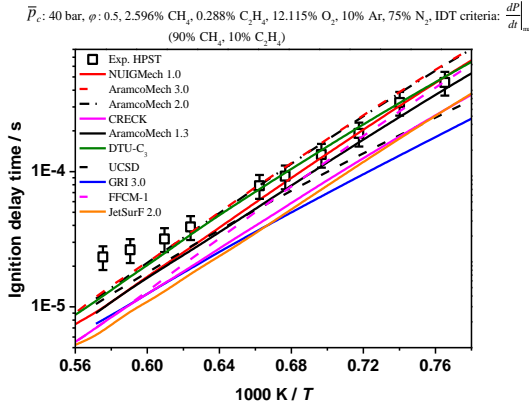
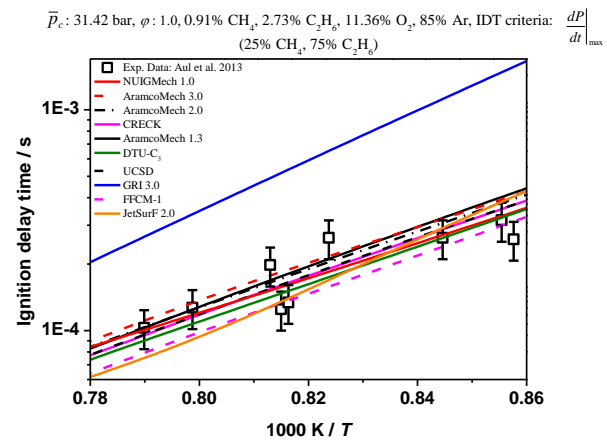
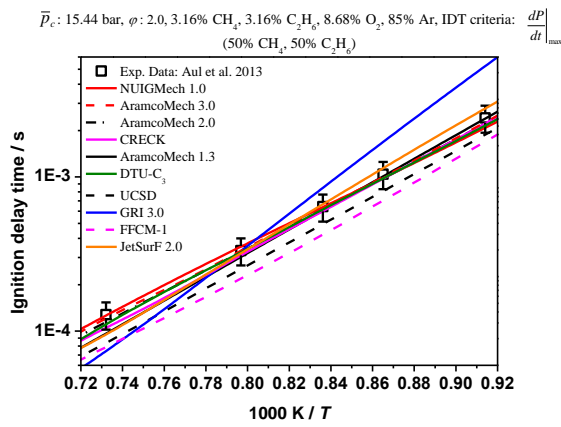
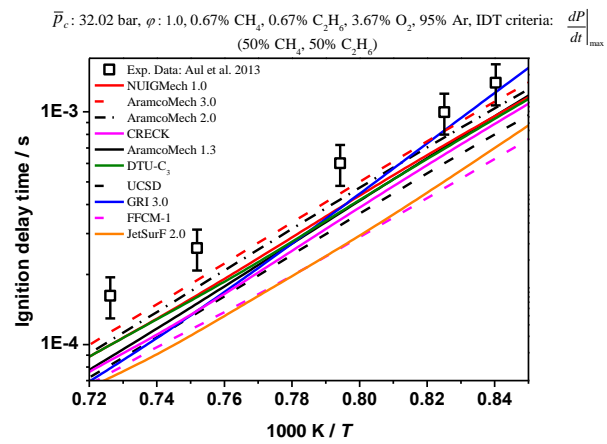
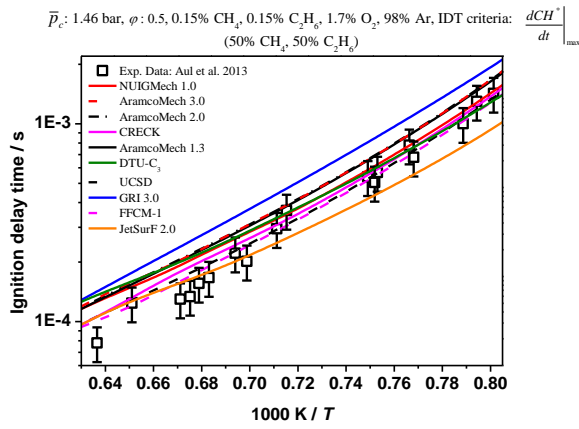


Figure DS32. Performance of NUIGMech1.0 for predicting methane + ethylene's IDTs at 40 bar in comparison to the other examined chemical mechanisms.



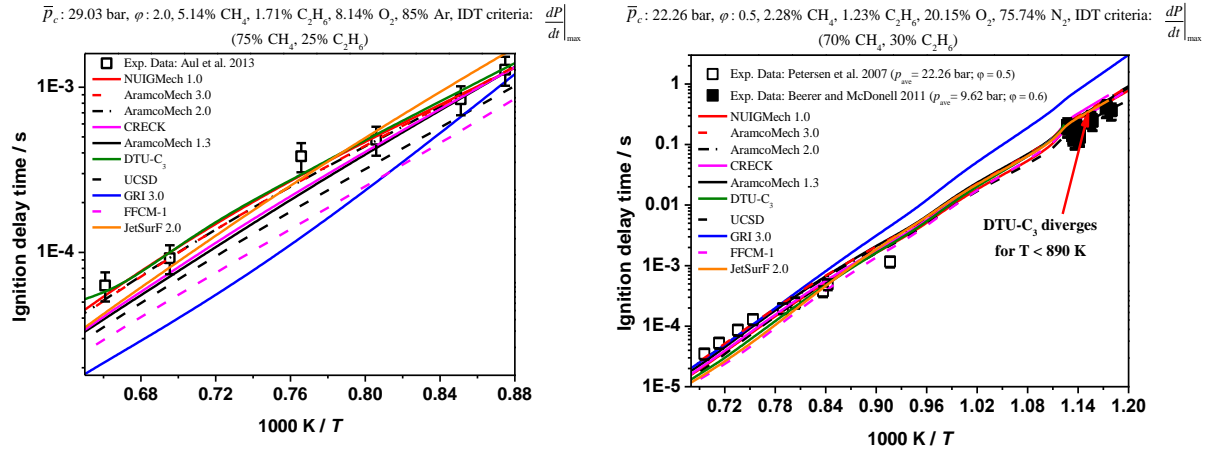


Figure DS33. Performance of NUIGMech1.0 for predicting methane + ethane's IDTs in comparison to the other examined chemical mechanisms.[37–39].

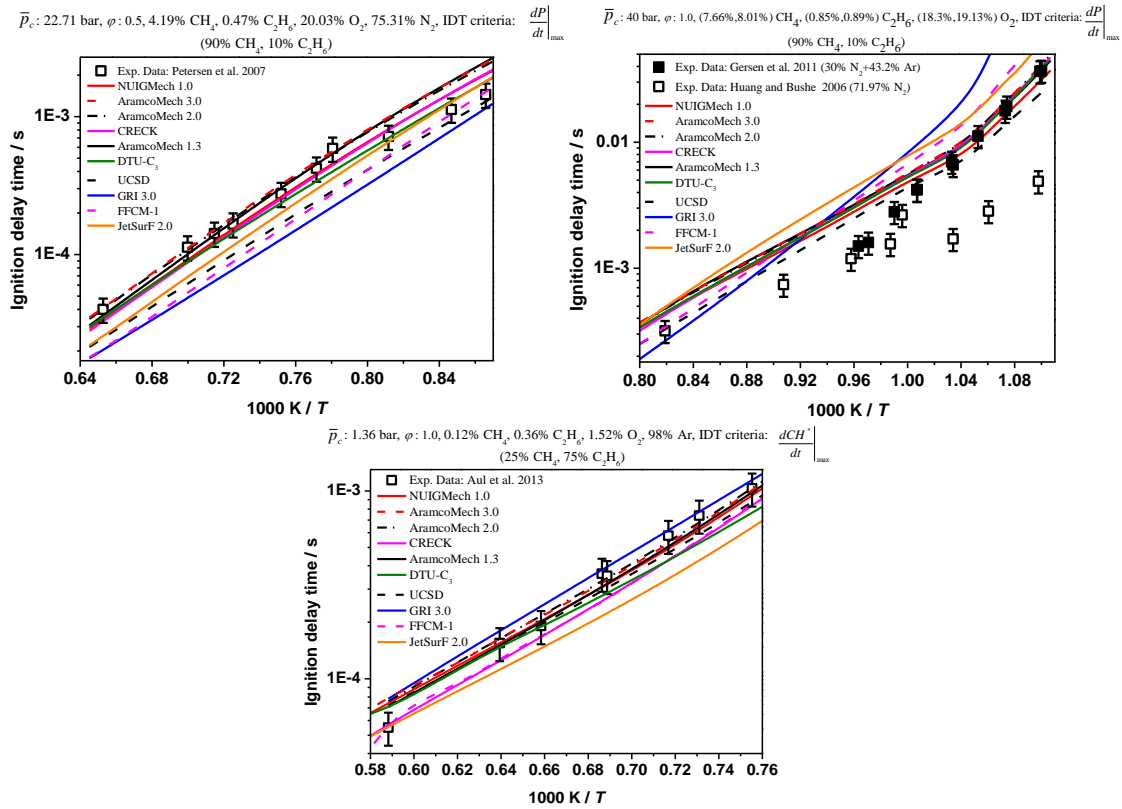


Figure DS34. Performance of NUIGMech1.0 for predicting methane + ethane's IDTs in comparison to the other examined chemical mechanisms. [37,39–41]

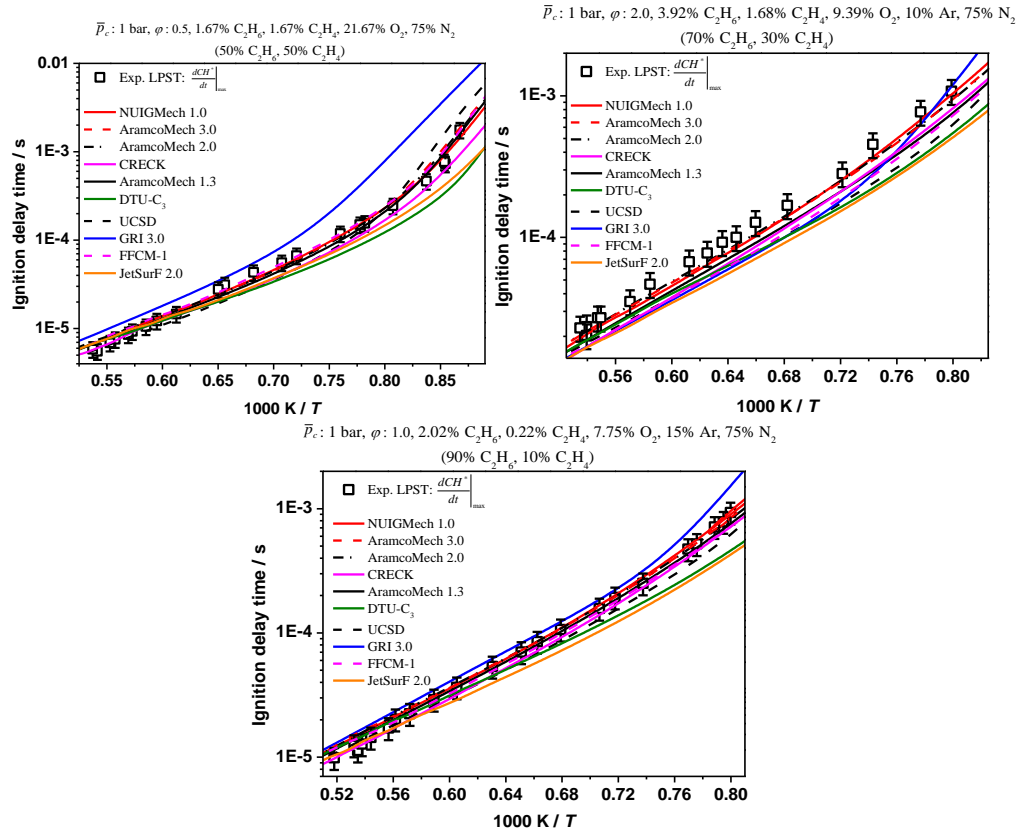
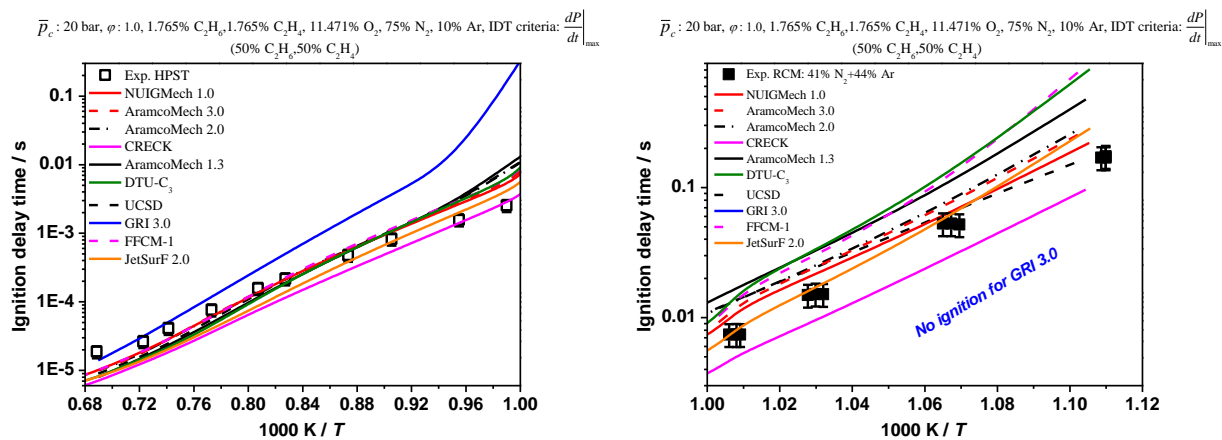


Figure DS35. Performance of NUIGMech1.0 for predicting ethane + ethylene's IDTs at 1 bar in comparison to the other examined chemical mechanisms.



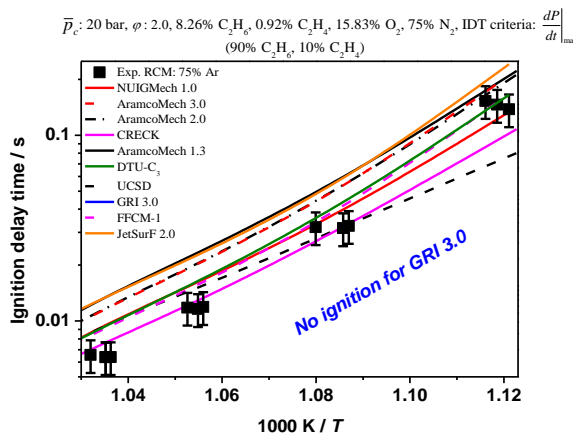
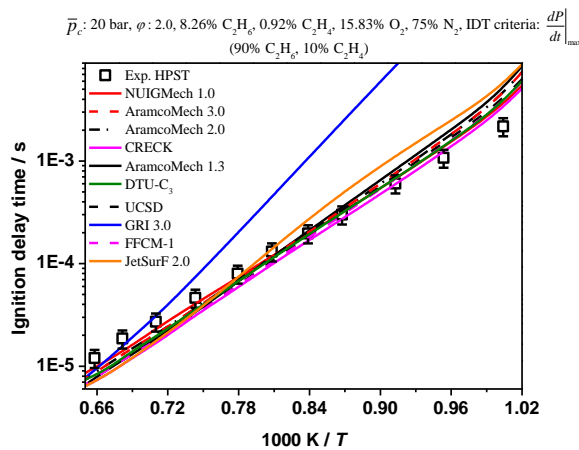
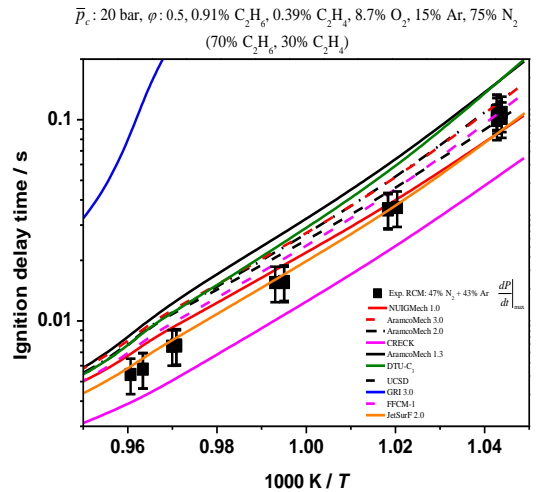
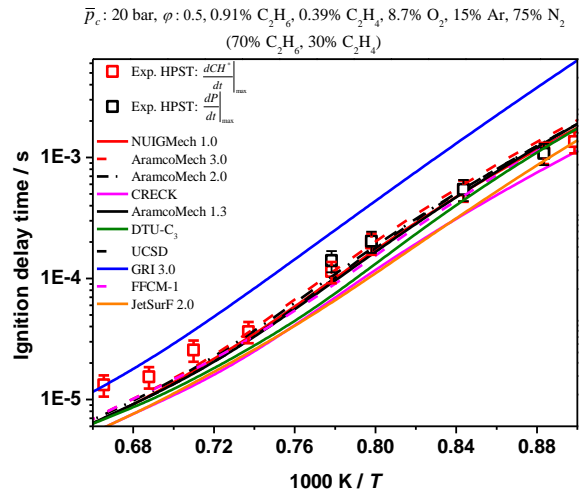
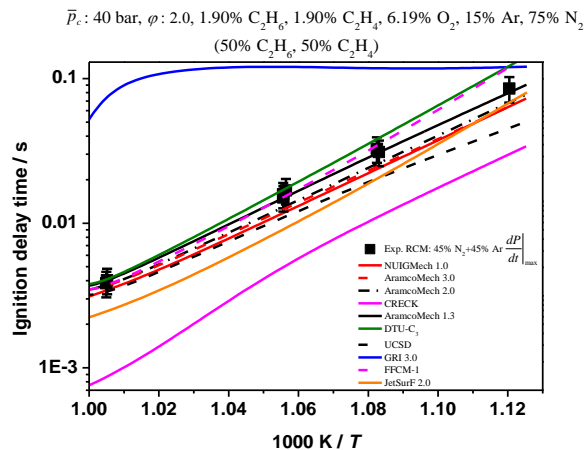
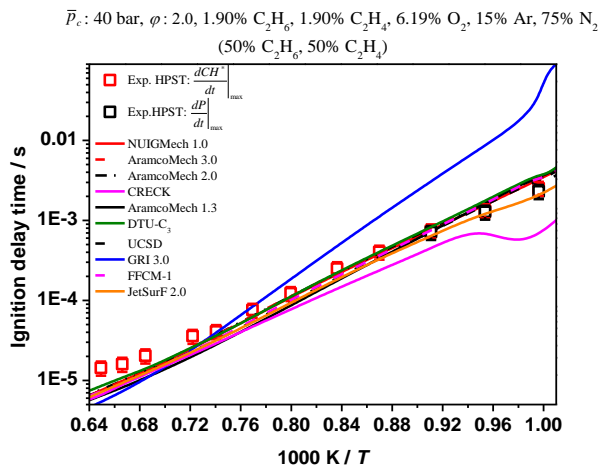


Figure DS36. Performance of NUIGMech1.0 for predicting ethane + ethylene's IDTs at 20 bar in comparison to the other examined chemical mechanisms.



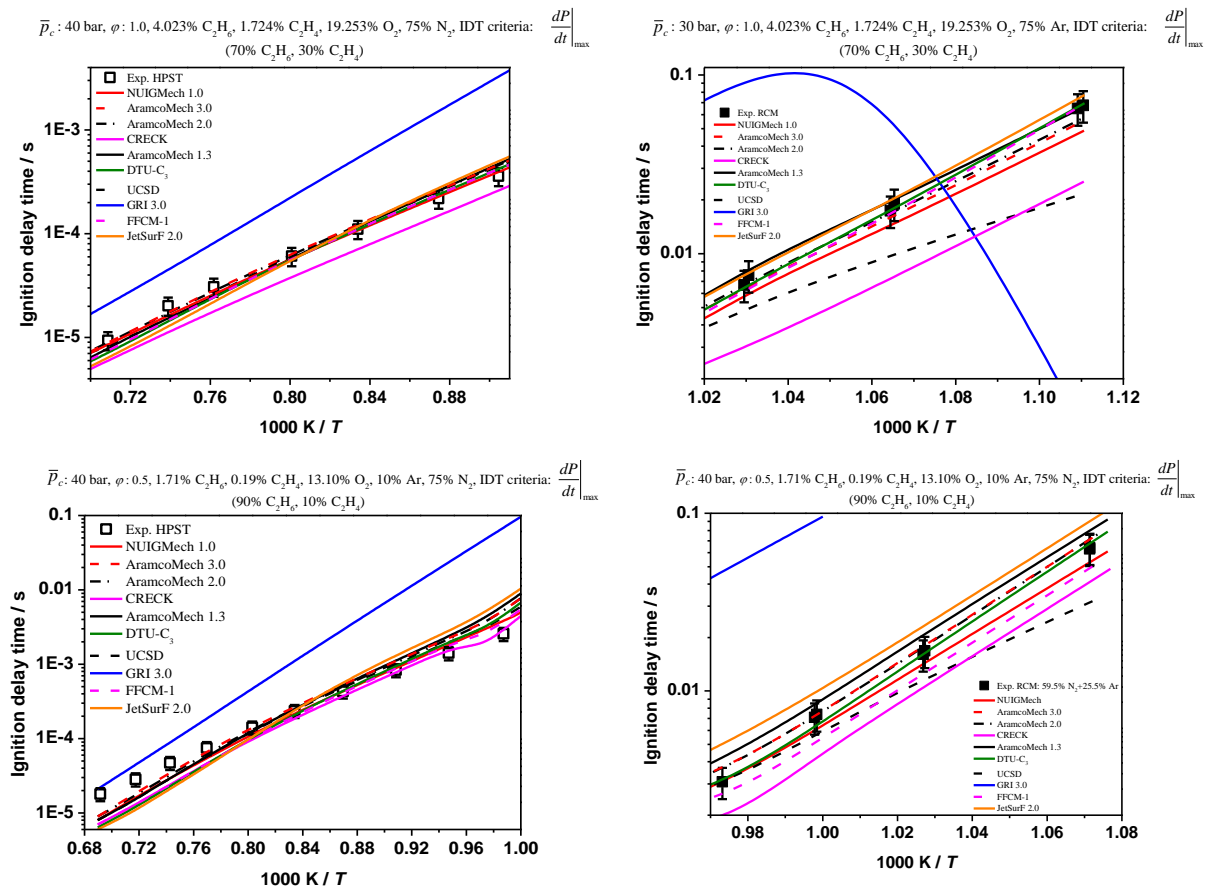


Figure DS37. Performance of NUIGMech1.0 for predicting ethane + ethylene's IDTs at 40 bar in comparison to the other examined chemical mechanisms.

10. Chemical kinetics development

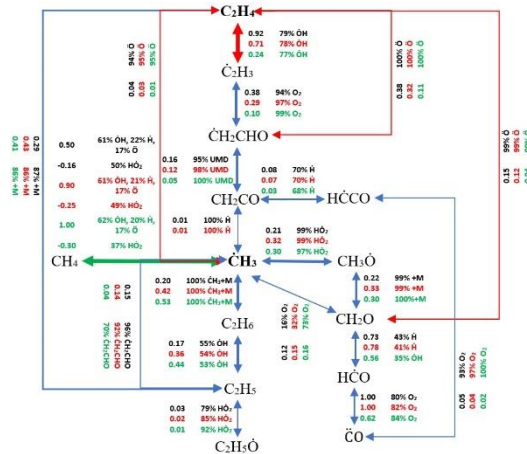


Figure DS38. Flux analysis of the ten prominent reactions at 1200 K in Figure 5(a) for the methane + ethylene blends at different methane/ethylene combinations; Black numbers: 50/50, Red numbers: 70/30, and Green numbers: 90/10.

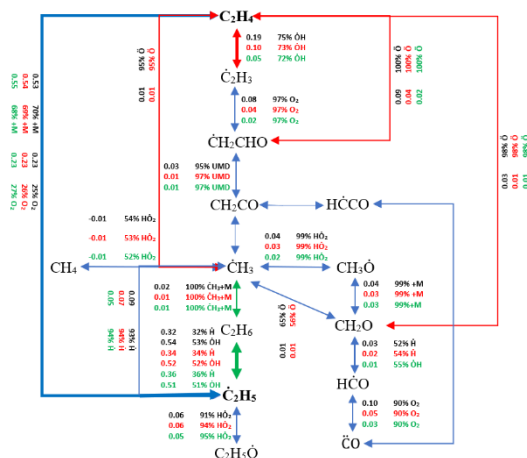


Figure DS39. Flux analysis of the ten prominent reactions at 1200 K in Figure 5(a) for the ethane + ethylene blends at different ethane/ethylene combinations; Black numbers: 50/50, Red numbers: 70/30, and Green numbers: 90/10.

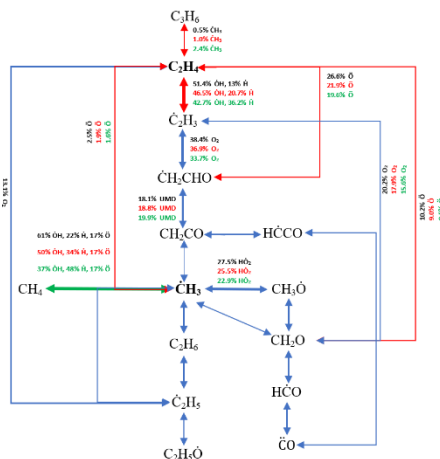


Figure DS40. Flux analysis of the ten prominent reactions at 1200 K in Figure 5(c) for the methane + ethylene blends at different equivalence ratios; Black numbers: 0.5, Red numbers: 1.0, and Green numbers: 2.0.

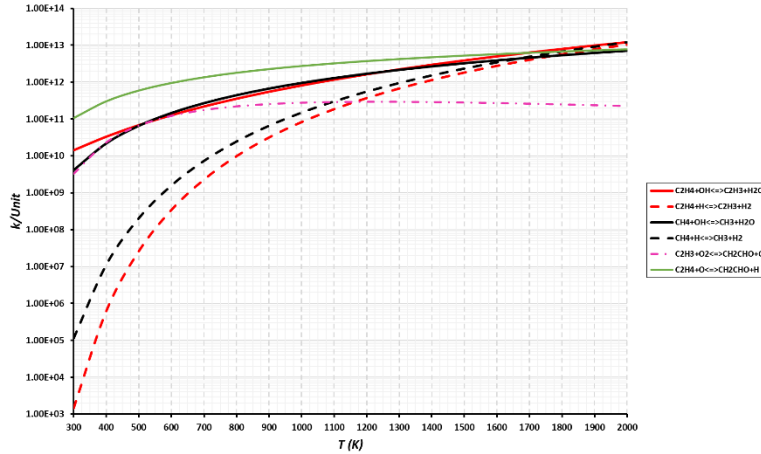


Figure DS41. Comparing the rates related to \dot{H} -abstraction reactions from fuel by \dot{H} atom or \dot{OH} radical and also two important reactions for production of vinyloxy radical.

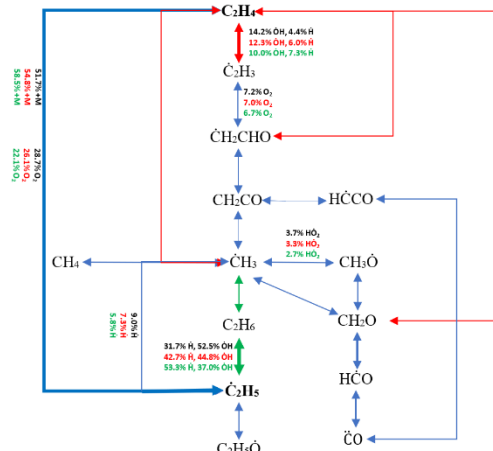


Figure DS42. Flux analysis of the ten prominent reactions at 1200 K in Figure 5(c) for the ethane + ethylene blends at different equivalence ratios; Black numbers: 0.5, Red numbers: 1.0, and Green numbers: 2.0.

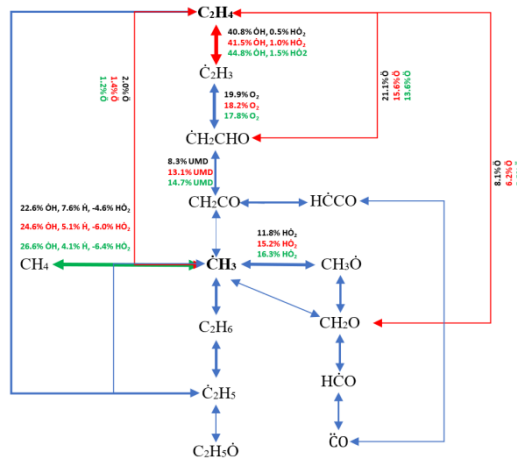


Figure DS43. Flux analysis of the ten prominent reactions at 1200 K in Figure 5(d) for the methane + ethylene blends at different pressures; Black numbers: 1 bar, Red numbers: 20 bar, and Green numbers: 40 bar.

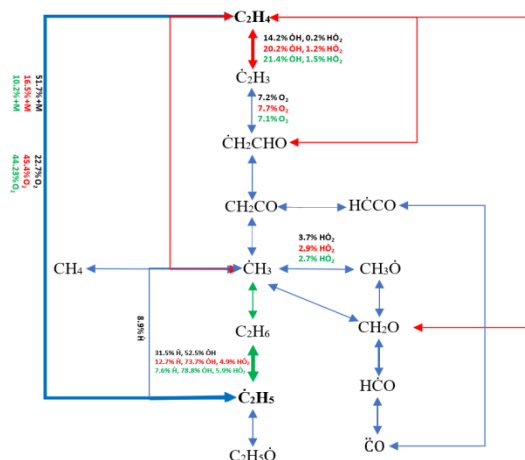


Figure DS44. Flux analysis of the ten prominent reactions at 1200 K in Figure 5(d) for the ethane + ethylene blends at different pressures; Black numbers: 1 bar, Red numbers: 20 bar, and Green numbers: 40 bar.

11. References

- [1] M. Baigmohammadi, V. Patel, S. Martinez, S. Panigrahy, A. Ramalingam, U. Burke, K.P. Somers, K.A. Heufer, A. Pekalski, H.J. Curran, A comprehensive experimental and simulation study of ignition delay time characteristics of single fuel $C_1 - C_2$ hydrocarbons over a wide range of temperatures, pressures, equivalence ratios, and dilutions, *Energy Fuels*. 34 (2020) 3755-3771.
- [2] F.R. Gillespie, An experimental and modelling study of the combustion of oxygenated hydrocarbons, National University of Ireland, Galway, (2014), <http://hdl.handle.net/10379/4419>.
- [3] J. Würmel, M. McGuinness, J.M. Simmie, High-temperature oxidation of ethylene oxide in shock waves, *J. Chem. Soc. Faraday Trans.* 92 (1996) 715-721.
- [4] C. Morley, Gaseq: A chemical equilibrium program for windows, (2004), <http://www.gaseq.co.uk>
- [5] H. Nakamura, D. Darcy, M. Mehl, C.J. Tobin, W.K. Metcalfe, W.J. Pitz, C.K. Westbrook, H.J. Curran, An experimental and modeling study of shock tube and rapid compression machine ignition of n-butylbenzene/air mixtures, *Combust. Flame*. 161 (2014) 49-64.
- [6] U. Burke, K.P. Somers, P. O'Toole, C.M. Zinner, N. Marquet, G. Bourque, E.L. Petersen, W.K. Metcalfe, Z. Serinyel, H.J. Curran, An ignition delay and kinetic modeling study of methane, dimethyl ether, and their mixtures at high pressures, *Combust. Flame*. 162 (2015) 315-330.
- [7] A. Ramalingam, K. Zhang, A. Dhongde, L. Virnich, H. Sankhla, H. Curran, A. Heufer, An RCM experimental and modeling study on CH_4 and CH_4/C_2H_6 oxidation at pressures up to 160 bar, *Fuel*. 206 (2017) 325-333.
- [8] D. Healy, H.J. Curran, S. Dooley, J.M. Simmie, D.M. Kalitan, D.K. Petersen, G. Bourque, Methane/propane mixture oxidation at high pressures and at high, intermediate and low temperatures, *Combust. Flame*. 155 (2008) 451-461.

- [9] D. Healy, H.J. Curran, J.M. Simmie, D.M. Kalitan, C.M. Zinner, A.B. Barrett, E.L. Petersen, G. Bourque, Methane/ethane/propane mixture oxidation at high pressures and at high, intermediate and low temperatures, *Combust. Flame*. 155 (2008) 441-448.
- [10] W.K. Metcalfe, S.M. Burke, S.S. Ahmed, H.J. Curran, A hierarchical and comparative kinetic modeling study of C₁ – C₂ hydrocarbon and oxygenated fuels, *Int. J. Chem. Kinet.* 45 (2013) 638-675.
- [11] S. Yousefian, N.J. Quinlan, R.F.D. Monaghan, Simulation of turbulent flow in a rapid compression machine: Large Eddy Simulation and computationally efficient alternatives for the design of ignition delay time experiments, *Fuel*. 234 (2018) 30-47.
- [12] C. Hemken, U. Burke, K.Y. Lam, D.F. Davidson, R.K. Hanson, K.A. Heufer, K. Kohse-Höinghaus, Toward a better understanding of 2-butanone oxidation: Detailed species measurements and kinetic modeling, *Combust. Flame*. 184 (2017) 195-207.
- [13] TiePie: Handyscope, <https://www.tiepie.com/en/oscilloscope-software>.
- [14] Picoscope: Oscilloscope, <https://www.picotech.com/downloads>.
- [15] E.L. Petersen, M.J.A. Rickard, M.W. Crofton, E.D. Abbey, M.J. Traum, D.M. Kalitan, A facility for gas- and condensed-phase measurements behind shock waves, *Meas. Sci. Technol.* 16 (2005) 1716-1729.
- [16] B.W. Weber, C.J. Sung, M.W. Renfro, On the uncertainty of temperature estimation in a rapid compression machine, *Combust. Flame* 162 (2015) 2518-2528.
- [17] C.-W. Zhou, Y. Li, U. Burke, C. Banyon, K.P. Somers, S. Ding, S. Khan, J.W. Hargis, T. Sikes, O. Mathieu, E.L. Petersen, M. AlAbbad, A. Farooq, Y. Pan, Y. Zhang, Z. Huang, J. Lopez, Z. Loparo, S.S. Vasu, H.J. Curran, An experimental and chemical kinetic modeling study of 1,3-butadiene combustion: Ignition delay time and laminar flame speed measurements, *Combust. Flame*. 197 (2018) 423-438.
- [18] S.M. Burke, W. Metcalfe, O. Herbinet, F. Battin-Leclerc, F.M. Haas, J. Santner, F.L. Dryer, H.J. Curran, An experimental and modeling study of propene oxidation. Part 1: Speciation measurements in jet-stirred and flow reactors, *Combust. Flame*. 161 (2014) 2765-2784.
- [19] A. Kéromnès, W.K. Metcalfe, K.A. Heufer, N. Donohoe, A.K. Das, C.-J. Sung, J. Herzler, C. Naumann, P. Griebel, O. Mathieu, M.C. Krejci, E.L. Petersen, W.J. Pitz, H.J. Curran, An experimental and detailed chemical kinetic modeling study of hydrogen and syngas mixture oxidation at elevated pressures, *Combust. Flame*. 160 (2013) 995-1011.
- [20] S.M. Burke, U. Burke, R. Mc Donagh, O. Mathieu, I. Osorio, C. Keesee, A. Morones, E.L. Petersen, W. Wang, T.A. DeVerter, M.A. Oehlschlaeger, B. Rhodes, R.K. Hanson, D.F. Davidson, B.W. Weber, C.J. Sung, J. Santner, Y. Ju, F.M. Haas, F.L. Dryer, E.N. Volkov, E.J.K. Nilsson, A.A. Konnov, M. Alrefae, F. Khaled, A. Farooq, P. Dirrenberger, P.A. Glaude, F. Battin-Leclerc, H.J. Curran, An experimental and modeling study of propene oxidation. Part 2: Ignition delay time and flame speed measurements, *Combust. Flame*. 162 (2015) 296-314.
- [21] U. Burke, W.K. Metcalfe, S.M. Burke, K.A. Heufer, P. Dagaut, H.J. Curran, A detailed chemical kinetic modeling, ignition delay time and jet-stirred reactor study of methanol oxidation, *Combust. Flame*. 165 (2016) 125-136.

- [22] C.-W. Zhou, Y. Li, E. O'Connor, K.P. Somers, S. Thion, C. Keesee, O. Mathieu, E.L. Petersen, T.A. DeVerter, M.A. Oehlschlaeger, G. Kukkadapu, C.-J. Sung, M. Alrefae, F. Khaled, A. Farooq, P. Dirrenberger, P.A. Glaude, F. Battin-Leclerc, J. Santner, Y. Ju, T. Held, F.M. Haas, F.L. Dryer, H.J. Curran, A comprehensive experimental and modeling study of isobutene oxidation, *Combust. Flame*. 167 (2016) 353-379.
- [23] Y. Li, C.-W. Zhou, K.P. Somers, K. Zhang, H.J. Curran, The oxidation of 2-butene: A high pressure ignition delay, kinetic modeling study and reactivity comparison with isobutene and 1-butene, *Proc. Combust. Inst.* 36 (2017) 403-411.
- [24] H. Hashemi, J.M. Christensen, L.B. Harding, S.J. Klippenstein, P. Glarborg, High-pressure oxidation of propane, *Proc. Combust. Inst.* 37 (2019) 461-468.
- [25] G. Bagheri, E. Ranzi, M. Pelucchi, A. Parente, A. Frassoldati, T. Faravelli, Comprehensive kinetic study of combustion technologies for low environmental impact: MILD and OXY-fuel combustion of methane, *Combust. Flame*. 212 (2020) 142-155.
- [26] Chemical-kinetic mechanisms for combustion applications, <https://web.eng.ucsd.edu/mae/groups/combustion/mechanism.html>.
- [27] G.P. Smith, D.M. Golden, M. Frenklach, N.W. Moriarty, B. Eiteneer, M. Goldenberg, C.T. Bowman, R.K. Hanson, S. Song, W.C. Gardiner, Jr., V.V. Lissianski, Z. Qin, http://www.me.berkeley.edu/gri_mech/.
- [28] H. Wang, E. Dames, B. Sirjean, D.A. Sheen, R. Tango, A. Violi, J.Y.W. Lai, F.N. Egolfopoulos, D.F. Davidson, R.K. Hanson, C.T. Bowman, C.K. Law, W. Tsang, N.P. Cernansky, D.L. Miller, R.P. Lindstedt, A high-temperature chemical kinetic model of n-alkane (up to n-dodecane), cyclohexane, and methyl-, ethyl-, n-propyl and n-butyl-cyclohexane oxidation at high temperatures, *JetSurF Version 2.0*, (2010).
- [29] G.P. Smith, Y. Tao, H. Wang, Foundational fuel chemistry model version 1.0 (FFCM-1), Stanford University, (2016).
- [30] W. Lowry, J. de Vries, M. Krejci, E. Petersen, Z. Serinyel, W. Metcalfe, H. Curran, G. Bourque, Laminar flame speed measurements and modeling of pure alkanes and alkane blends at elevated pressures, *J. Eng. Gas Turbines Power*. (2011), 133(9): 091501.
- [31] P. Dagaut, J.C. Boettner, M. Cathonnet, Methane oxidation: Experimental and kinetic modeling study, *Combust. Sci. Technol.* 77 (1991) 127-148.
- [32] E.J. Chang, Shock tube experiments for the development and validation of models of hydrocarbon combustion, Stanford University, (1995).
- [33] H. Hashemi, J.G. Jacobsen, C.T. Rasmussen, J.M. Christensen, P. Glarborg, S. Gersen, M. van Essen, H.B. Levinsky, S.J. Klippenstein, High-pressure oxidation of ethane, *Combust. Flame*. 182 (2017) 150-166.
- [34] P. Dagaut, M. Cathonnet, J. Boettner, Kinetics of ethane oxidation, *Int. J. Chem. Kinet.* 23 (1991) 437-455.
- [35] T. Carriere, P.R. Westmoreland, A. Kazakov, Y.S. Stein, F.L. Dryer, Modeling ethylene combustion from low to high pressure, *Proc. Combust. Inst.* 29 (2002) 1257-1266.

- [36] J.G. Lopez, C.L. Rasmussen, M.U. Alzueta, Y. Gao, P. Marshall, P. Glarborg, Experimental and kinetic modeling study of C₂H₄ oxidation at high pressure, *Proc. Combust. Inst.* 32 (2009) 367-375.
- [37] E.L. Petersen, J.M. Hall, S.D. Smith, J. de Vries, A.R. Amadio, M.W. Crofton, Ignition of lean methane-based fuel blends at gas turbine pressures, *J. Eng. Gas Turbines Power.* 129 (2007) 937-944.
- [38] D.J. Beerer, V.G. McDonell, An experimental and kinetic study of alkane autoignition at high pressures and intermediate temperatures, *Proc. Combust. Inst.* 33 (2011) 301-307.
- [39] C.J. Aul, W.K. Metcalfe, S.M. Burke, H.J. Curran, E.L. Petersen, Ignition and kinetic modeling of methane and ethane fuel blends with oxygen: A design of experiments approach, *Combust. Flame.* 160 (2013) 1153-1167.
- [40] S. Gersen, A. V Mokhov, J.H. Darmeveil, H.B. Levinsky, P. Glarborg, Ignition-promoting effect of NO₂ on methane, ethane and methane/ethane mixtures in a rapid compression machine, *Proc. Combust. Inst.* 33 (2011) 433-440.
- [41] J. Huang, W.K. Bushe, Experimental and kinetic study of autoignition in methane/ethane/air and methane/propane/air mixtures under engine-relevant conditions, *Combust. Flame.* 144 (2006) 74-88.

Appendix E

(Supplementary material for Chapter 7)

1. Motivation for taking new experimental data

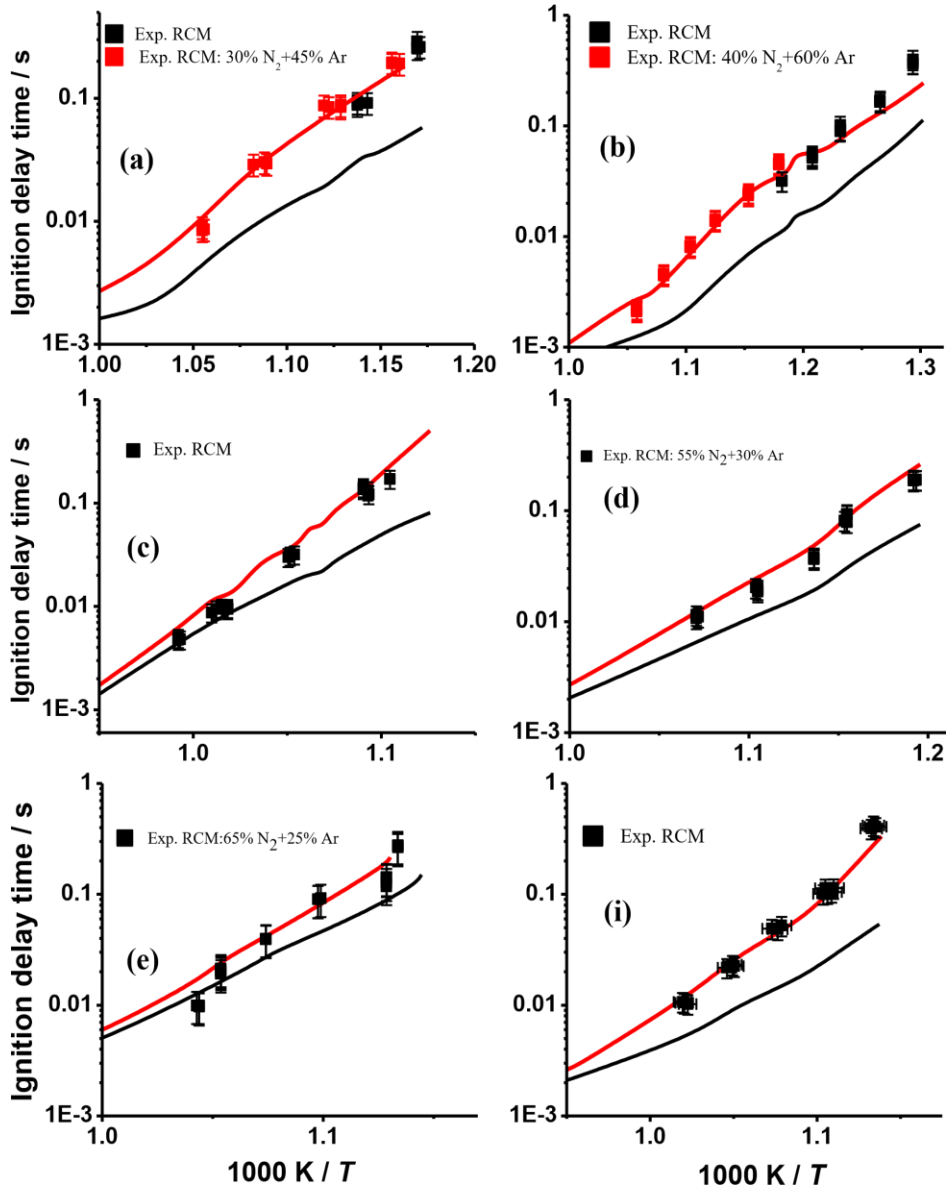


Figure ES1. Experimental and simulated data of ethylene's IDT values at: (a) 6.25% C_2H_4 , 18.75% O_2 , ($\phi = 1.0$) and 75.0% N_2 , $p_c^- = 20$ bar; (b) 10% C_2H_4 , 15% O_2 , ($\phi = 2.0$) and 75.0% N_2 , $p_c^- = 40$ bar; (c) 2.142% C_2H_4 , 12.857% O_2 , ($\phi = 0.5$) in 37% Ar + 48.0% N_2 , $p_c^- = 20$ bar; (d) 3.75% C_2H_4 , 11.25% O_2 , ($\phi = 1.0$) in 10% Ar + 75.0% N_2 , $p_c^- = 40$ bar; (e) 1.43% C_2H_4 , 8.57% O_2 , ($\phi = 0.5$) in 15% Ar + 75.0% N_2 , $p_c^- = 40$ bar; (f) 4% C_2H_4 , 6% O_2 , ($\phi = 2.0$) in 45% Ar + 45% N_2 , $p_c^- = 20$ bar; the red lines: NUIGMech0.9, the black line: AramcoMech 3.0.

2. Performance of the other kinetic models

Table ES1. Applied chemical mechanisms in the study.

No	Mechanism	Number of reactions	Number of species	Comments
1	AramcoMech 3.0 [1]	3037	581	Released at 2018
2	AramcoMech 2.0 [2-8]	2716	493	Released at 2016
3	AramcoMech 1.3 [7]	1542	253	Released at 2013
4	CRECK [9]	1941	114	Released at 2020
5	UCSD [10]	268	57	Released at 2016
6	GRI 3.0 [11]	325	53	Released at 2000
7	FFCM-1 (C1-C2) [12]	291	38	C ₁ -C ₂ ; Low temperature reactions are not included; released at 2016

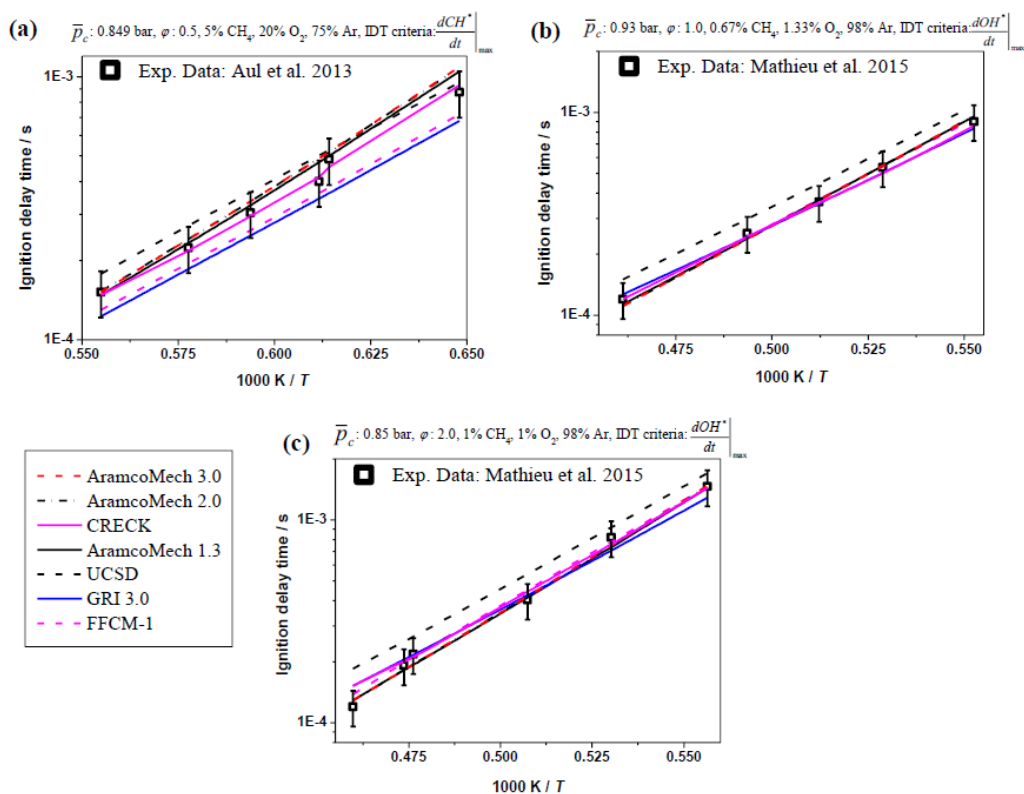


Figure ES2. Available experimental and simulation data of methane's IDT values for average compressed reactive mixture pressure (p_c): (a) P1C1; (b) P1C8; (c) P1C6. The CH* species is not included in CRECK, UCSD, and GRI 3.0 mechanisms, CH results are presented instead of CH*.

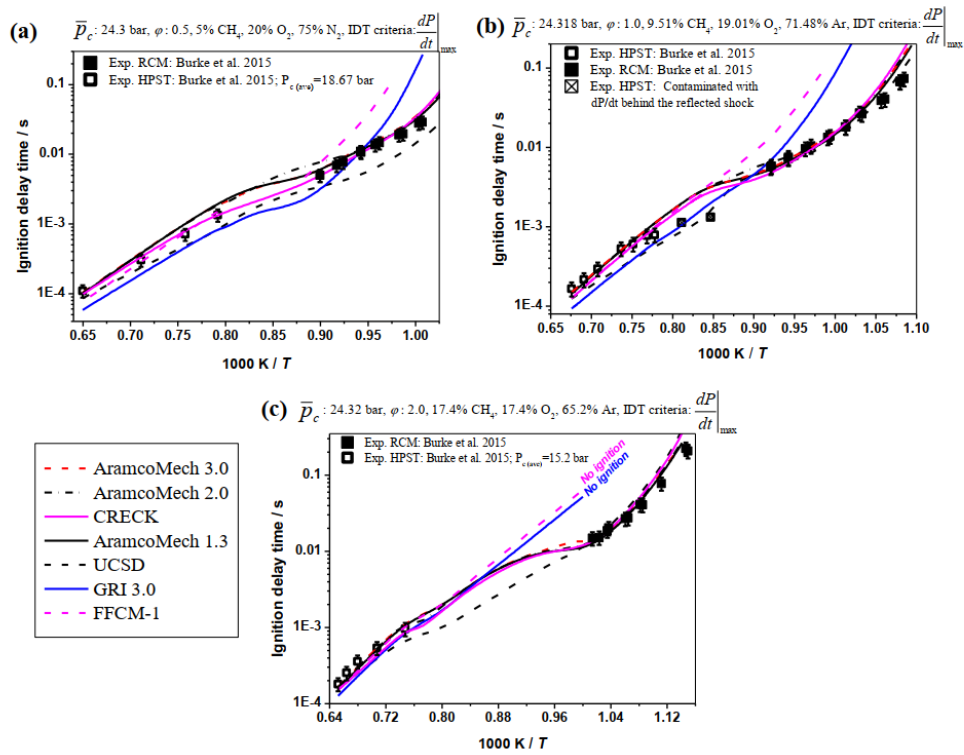


Figure ES3. Experimental and simulation data of methane's IDT values for average compressed reactive mixture pressure (p_c): (a) P1C4; (b) P1C2; (c) P1C9.

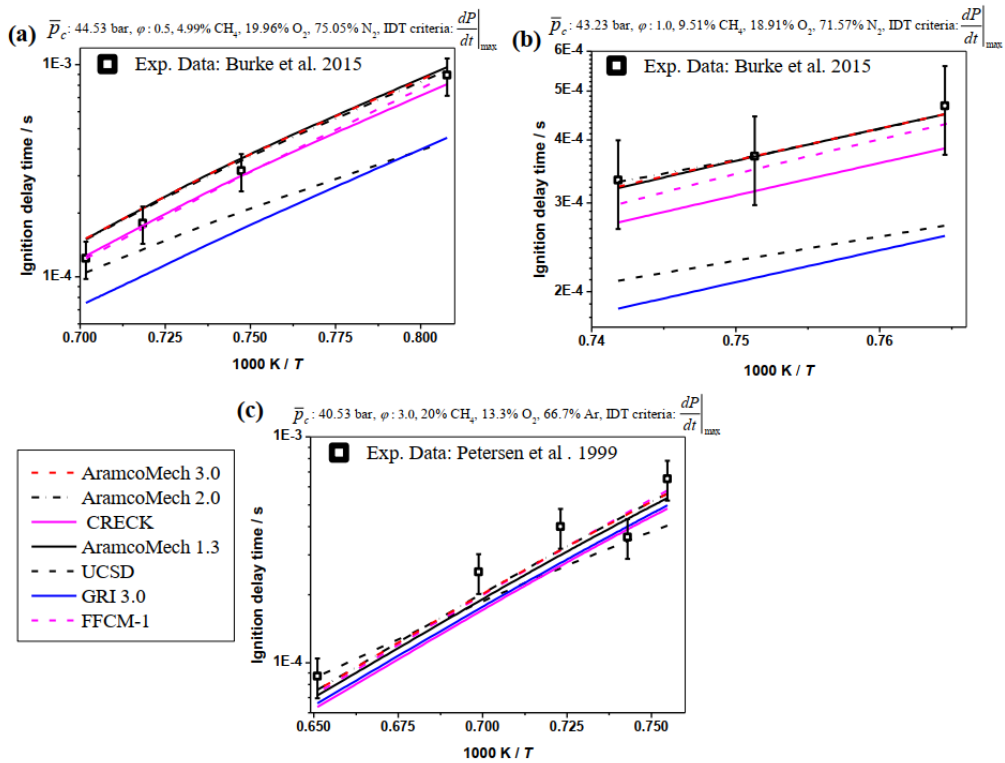


Figure ES4. Experimental and simulation data of methane's IDT values for average compressed reactive mixture pressure (\bar{p}_c): (a) P1C7; (b) P1C5; (c) P1C3.

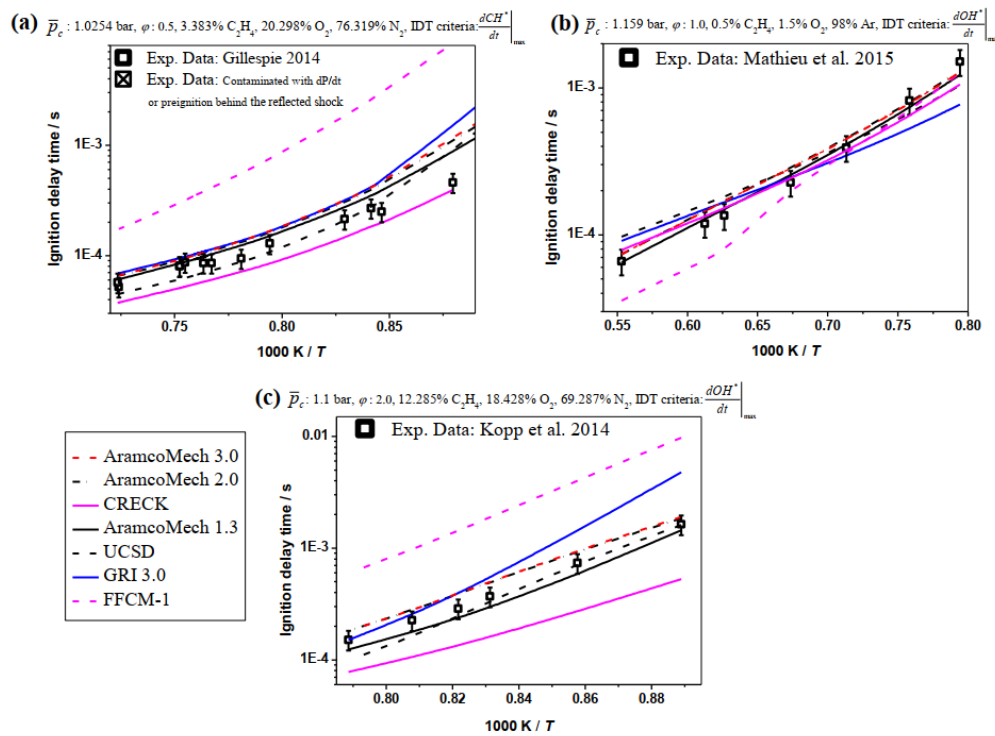


Figure S5. Available experimental and simulated data of ethylene's IDT values for average compressed reactive mixture pressure (p_c): (a) P2C1; (b) P2C8; (c) P2C6.

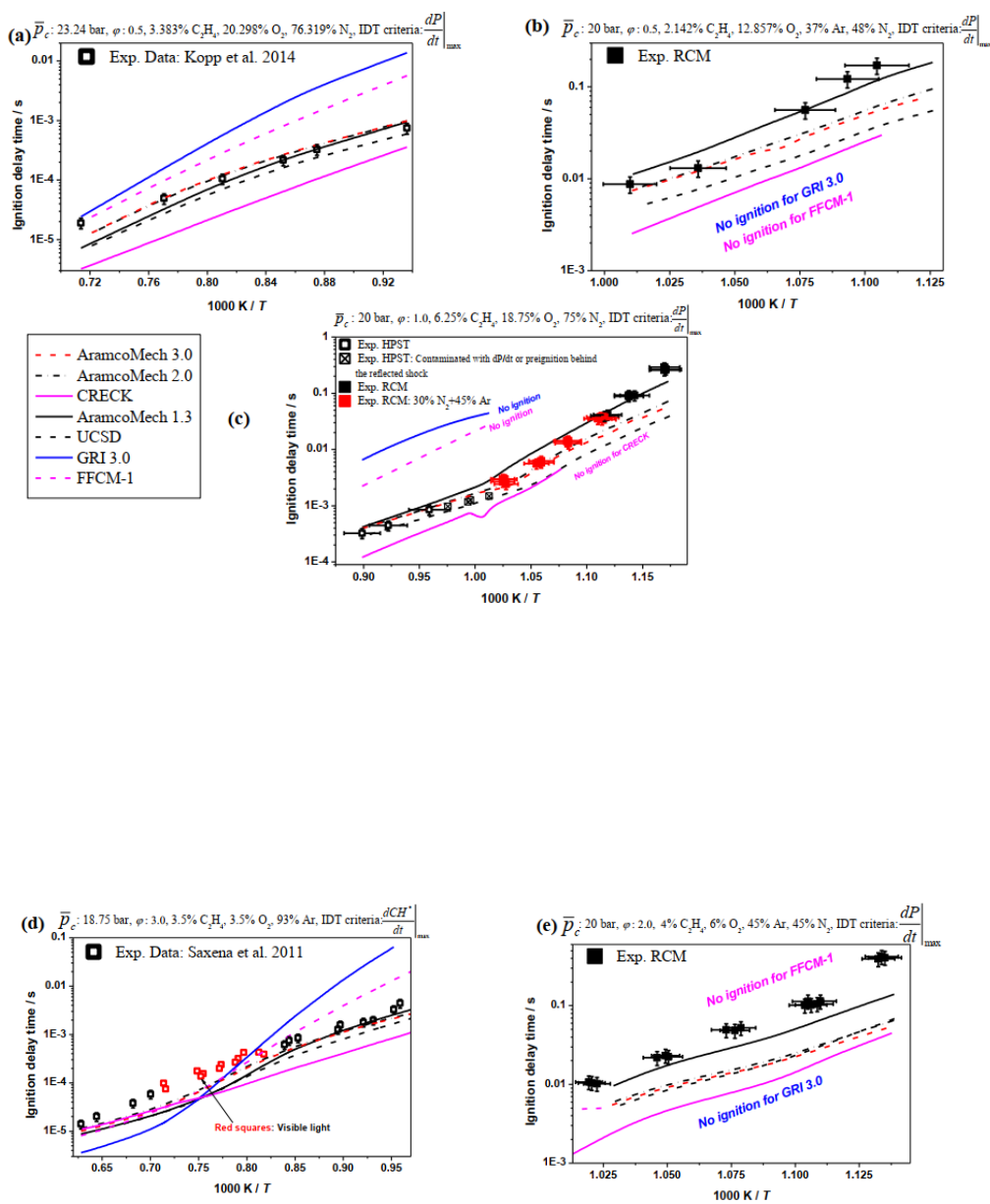


Figure ES6. Available experimental and simulated data of ethylene's IDT values for average compressed reactive mixture (p_c): (a) P2C4; (b) P2C4; (c) P2C2; (d) P2C9; (e) P2C9.

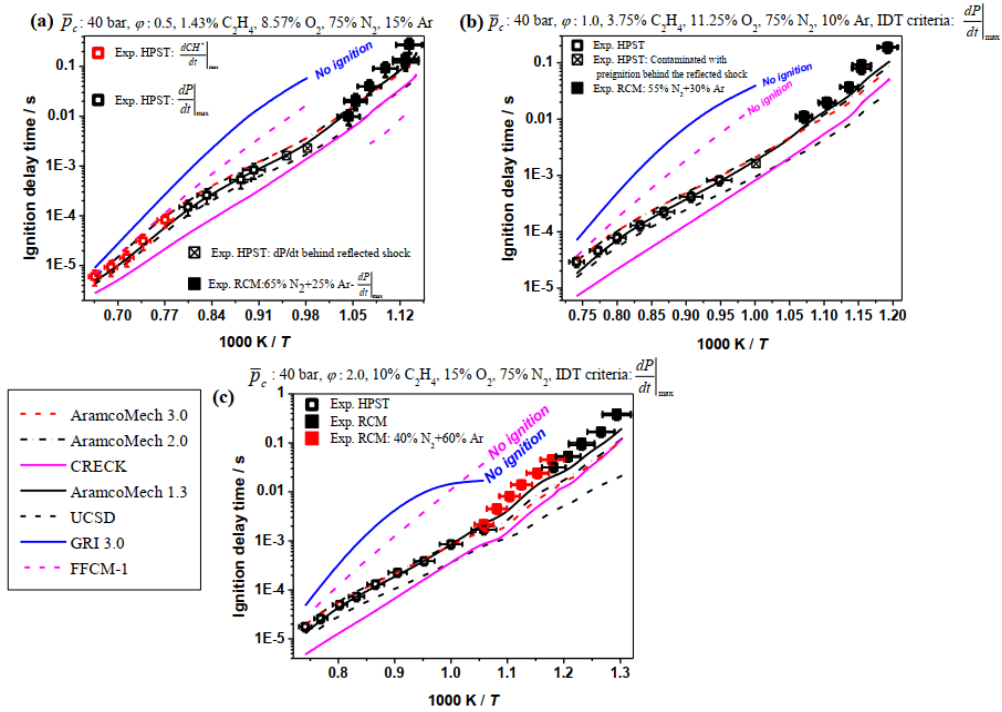


Figure ES7. Experimental and simulated data of ethylene's IDT values for average compressed reactive mixture pressure (p_c): (a) P2C7; (b) P2C5; (c) P2C3.

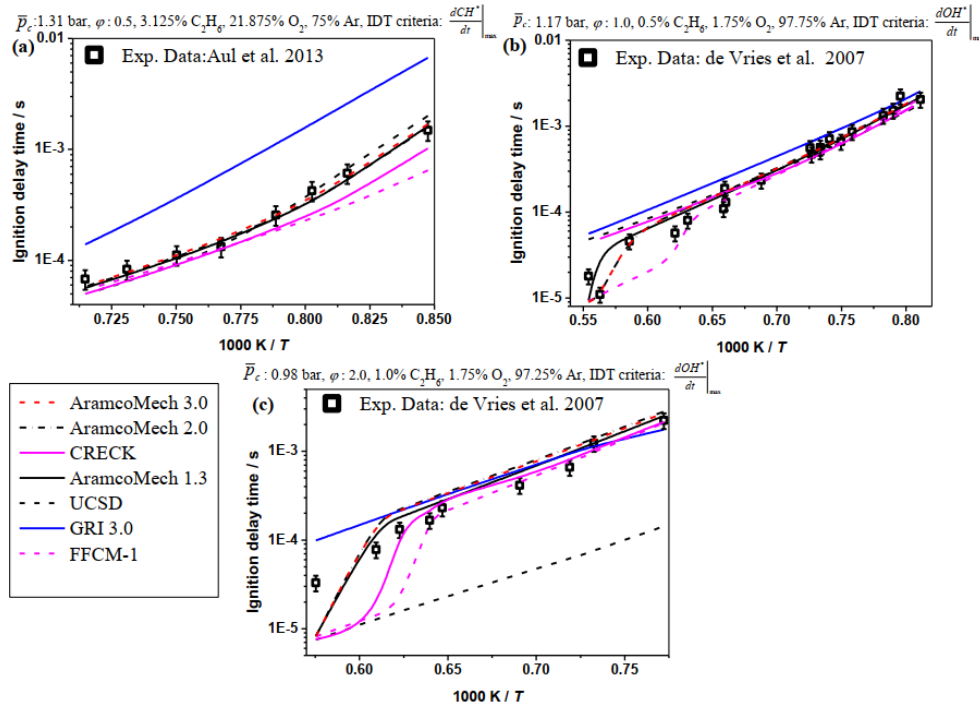


Figure ES8. Available experimental and constant volume simulation data of ethane's IDT values for average compressed reactive mixture pressure (p_c): (a) P3C1; (b) P3C8; (c) P3C6. Although, OH* species is not included in UCSD and GRI 3.0 mechanisms, OH results have been presented instead of OH*.

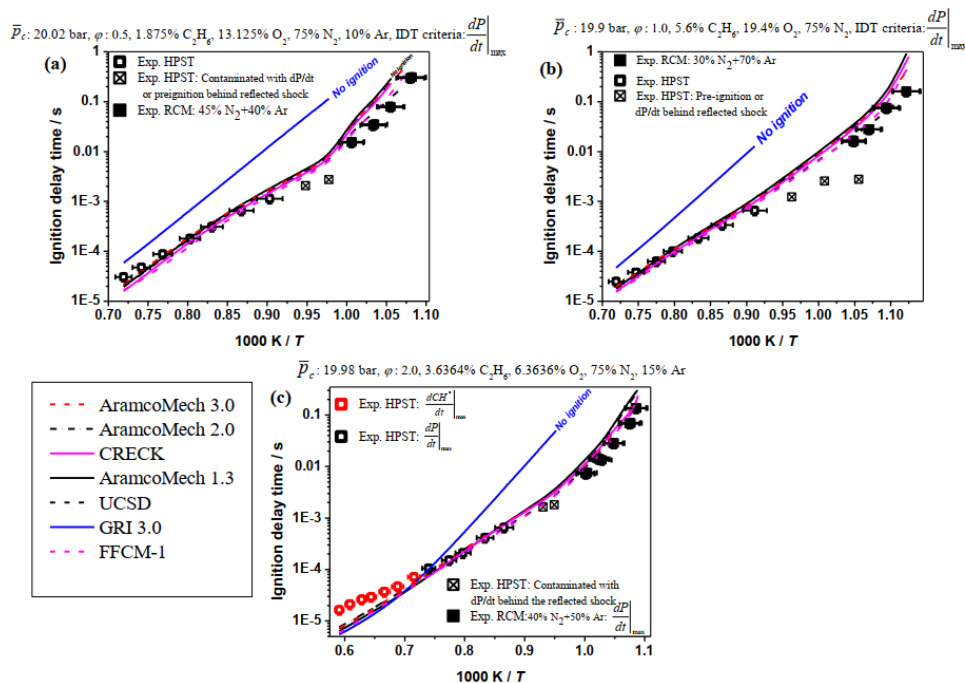


Figure ES9. Experimental and simulation data of ethane's IDT values for average compressed reactive mixture pressure (p_c): (a) P3C4; (b) P3C2; (c) P3C9.

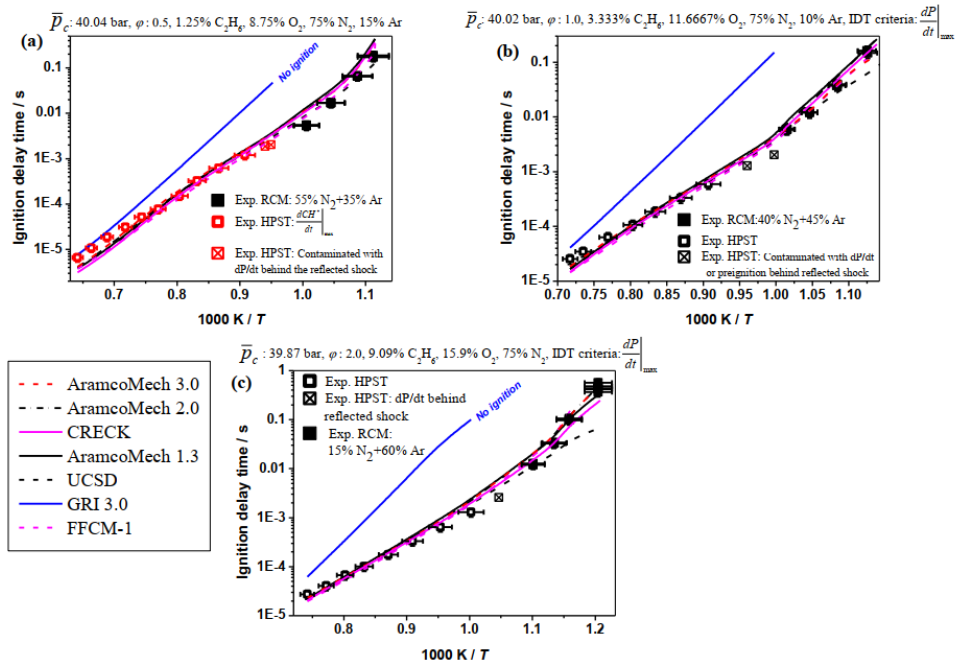


Figure ES10. Experimental and simulation data of ethane's IDT values for average compressed reactive mixture pressure (pc): (a) P3C7; (b) P3C5; (c) P3C3.

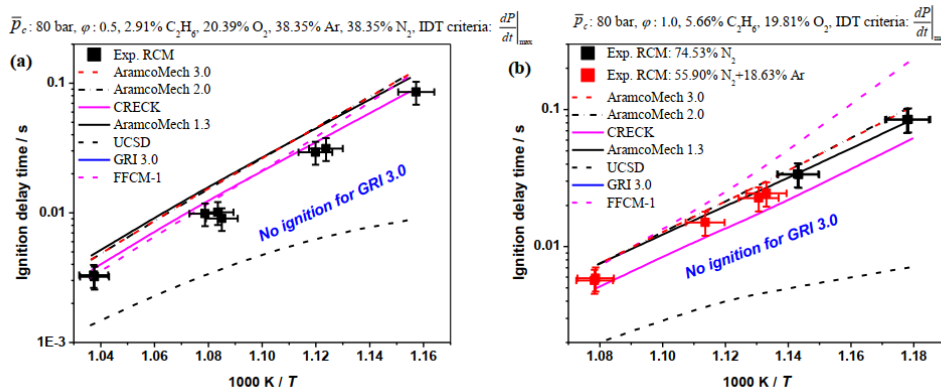


Figure ES11. Experimental and simulated data of ethane's IDT values for average compressed reactive mixture pressure (pc): (a) P3C10; (b) P3C11.

3. Design of experiments

According to complexity of classical approaches for designing experiments, the Taguchi method is a robust approach for designing complex experimental research through reducing the experimental tests. This methodology would be prominent when many experiments should be carried out in accordance to increasing numbers of variables. Hence, for handling experimental studies with many experiments (in the current study, 81 datasets), the Taguchi approach can tackle the issue using a specific design of orthogonal arrays which

allows to conduct a comprehensive investigation by doing minimized experimental tests. In this regard, the minimum number of experiments is determined as follows:

$$N_{\text{Taguchi}} = 1 + NF(L - 1) \quad (\text{E1})$$

Where, N_{Taguchi} , NF , and L are the number of experiments, number of factors, and number of levels, respectively. According to the Taguchi approach, its performance would be optimal when there are limited interactions between desired variables. Therefore, in the current research, it was supposed that the interactions between the various factors and variables are negligible. In order to use the Taguchi method, it is essential to define the controlling factors and levels. According to the factors and levels, several design of experiments (DOE) matrixes will be available. For instance, as seen in Table ES2, if there are three or four factors (e.g. fuel composition; A, dilution level; B, equivalence ratio; C, and pressure; D) and 3 levels for each parameter (e.g. three pressure levels, 1, 20, and 40 bar) L_9 orthogonal array could be employed for designing the required experiments. According to Equation E1 and Table ES2, one can easily determine N_{Taguchi} based on the number of factors and levels, which is 9. Therefore, it is required to use an L_9 DOE matrix to cover such test numbers. Here, it should be noted that although the first column in Table ES2 is identical in the current study, it will be changed to three levels in the upcoming studies of the authors for blended C_1 – C_3 fuels. Thus, it was preferred to use an identical style of the Taguchi matrix (L_9) for designing the whole sets of experiments which were required to complete the developed database.

Table ES2. Applied factors/variables and levels for designing the current experiments using the Taguchi method.

<i>Factors</i>	<i>Fuel composition (A)</i>	<i>Dilution (B)</i>	<i>Equivalence ratio (C)</i>	<i>Pressure (bar) (D)</i>
<i>1</i>	100% C ₂ H ₄	75%	0.5	1.0
<i>2</i>	100% C ₂ H ₄	85%	1.0	20.0
<i>3</i>	100% C ₂ H ₄	90%	2.0	40.0

A sample form of an L_9 Taguchi array is shown in the following:

A	B	C	D	A	B	C	D
1	1	1	1	100	75	0.5	1.0
1	2	2	2	100	85	1.0	20.0
1	3	3	3	100	90	2.0	40.0
2	1	2	3	100	75	1.0	40.0
2	2	3	1	100	85	2.0	1.0
2	3	1	2	100	90	0.5	20.0
3	1	3	2	100	75	2.0	20.0
3	2	1	3	100	85	0.5	40.0
3	3	2	1	100	90	1.0	1.0

As mentioned before, the selection of proper DOE Taguchi matrix is only based on the number of desired parameters (here, fuel composition, pressure, equivalence ratio, and dilution percent) and their variation levels (here, three levels have been chosen (e.g. 0.5, 1.0, and 2.0 for equivalence ratio). In accordance to the selected parameters and their respective levels, the proper Taguchi matrix will give the least number of experiments which are required to get accurate results using the best configuration of the experiments with the desired levels¹³. However, it should be noted that according to the statistical mathematics fundamentals which the Taguchi matrixes are derived based on, unnecessary increasing the selected parameters and their respective levels (for example: increasing the parameters from 4 to 5 and the levels from 3 to 4) will significantly increase the number of tests (from L₉ with 9 configurations to L₁₆ with 16 configurations) and consequently required time for completing the experimental tests. Therefore, regarding the available data in the literature, it was decided to select main parameters of fuel composition, pressure, equivalence ratio, and dilution percent as study parameters with three levels to satisfy the requirements of the study.

4. Applied gases for making the mixtures

As mentioned in the design of experiments' section of the paper, in the current study, the ignition delay time characteristics of ethane (C₂H₆) and ethylene (C₂H₄) have been investigated individually over a wide range of temperature, pressure, equivalence ratio, and dilution. For those experiments performed at the combustion chemistry centre (C³) of National University of Ireland, the studied alkane/alkene fuels with purity of 99.5% (Grade: 2.5) have been supplied through high pressure bottles which were provided from Air liquide UK. The other applied gases such as oxygen, argon, nitrogen, and helium in the experiments have been provided by BOC Ireland with purities of O₂ (99.99%), N₂ (99.99%), Ar (99.99%), and He (99.96%). However, for those experiments performed at the Physico– Chemical Fundamentals of Combustion (PCFC) of RWTH Aachen University, the studied C₂H₆ with purity of 99.95% (Grade: 3.5) was provided by Westfalen AG. Also, the other applied gases such as oxygen, argon, and nitrogen, in the experiments have been provided by Westfalen AG and Praxair with purities of O₂ ($\geq 99.995\%$), N₂ ($\geq 99.95\%$), and Ar ($\geq 99.996\%$).

5. High–pressure shock–tube

As known, shock–tube is a robust facility for getting the ignition delay time data under high pressure–high temperature (≥ 1000 K) regime and IDTs ≤ 2 ms. Thus, the NUIG–HPST has been used for getting the IDT data under these operating conditions. As already mentioned, the applied NUIG– HPST has been previously documented and explained in details¹⁴ and, here, only general information of the facility is presented in Table S3. In the current study, helium was used as the primary driver gas for doing the

experiments unless there was a need to reduce the incident shock velocity through adding nitrogen to helium for the tailored cases.

Table ES3. Specifications of the applied high–pressure shock tube.

Total length	9.1 m	
Section	Length (m)	Diameter (mm)
Driver	3.0	63.5
Middle	0.04	63.5
Driven	5.7	63.5
Material	Stainless–steel (1.4571/316Ti and 1.4462/F51)	
Controlling system	Double–diaphragm type	
Diaphragm’s material	Aluminium (1050 H14)	
Diaphragm’s thickness	0.8~2 mm; according to target pressure	
Pre-scoring the diaphragms	0.2~1.1 mm; according to target pressure and the diaphragms’ thickness	

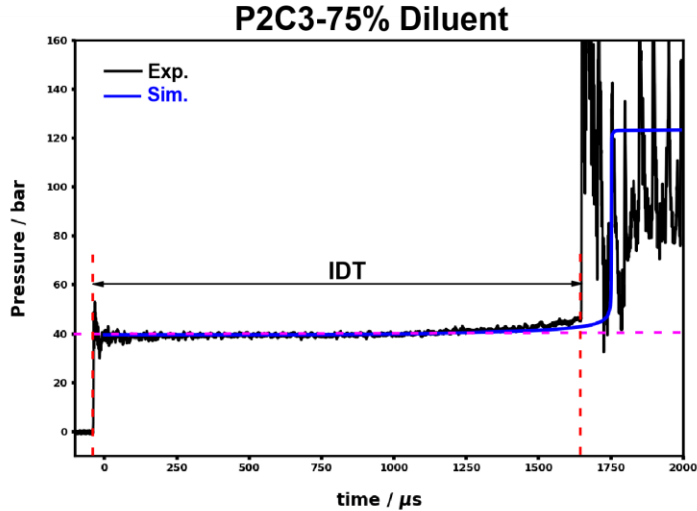
Further, as presented in Table S4, the incident shock velocity has been measured using six piezoelectric pressure transducers located on the driven section of the HPST and then the shock velocity at the end–wall was extrapolated through a fitted line to the collected shock velocities over these pressure transducers. All of conditions such as the compressed gas temperature (T_5) and pressure (p_5) behind the reflected shock were calculated using the shock velocity at the end–wall through “Gaseq” software¹⁵. Also, the ignition delay times of the studied normal mixtures (pressure–time profiles) with diluent concentration of $\leq 85\%$ were recorded using a Kistler 603B transducer mounted on the end– wall, while for the mixtures with 90% dilution, the ignition delay times were measured using photodiode array detector (PDA) or photomultiplier (PMT) systems equipped with CH* filter (CWL: 430 nm \pm 10 FWHM; Thorlabs) installed on the side wall of the shock tube’s endcap due to very weak signals of the Kistler pressure transducer. Also, it is demonstrated in Figure ES12 that the ignition delay time is defined as a maximum gradient in pressure ($\left. \frac{dp}{dt} \right|_{max}$) or CH* ($\left. \frac{dCH^*}{dt} \right|_{max}$) behind the reflected shock. Further, for increasing the accuracy of experiments and reducing the scattered points, all measured pressures behind the reflected shocks have been forced to be restricted to ± 0.5 bar of the target pressures (20 and 40 bar). Moreover, all

the experimental results have been divided into two main categories of the acceptable and the affected by facility, so that the affected results have been marked using “□” symbol. Thus, these data wouldn’t be reliable to be applied for evaluating the performance of a chemical mechanism. In this regard, all pressure versus time data including oscilloscope files (software is accessible through <https://www.tiepie.com/en/oscilloscope-software>) and the experimentalist spreadsheets related to the current studied conditions in NUIG–HPST are provided as supplementary files.

Table ES4. Number of installed PCB sensors on the driven section of the shock–tube and their distances from the end–wall

Sensors	Distance from the end wall (m)
PCB#1	0.01
PCB#2	0.15
PCB#3	0.29
PCB#4	0.57
PCB#5	0.85
PCB#6	1.165

(a)



(b)

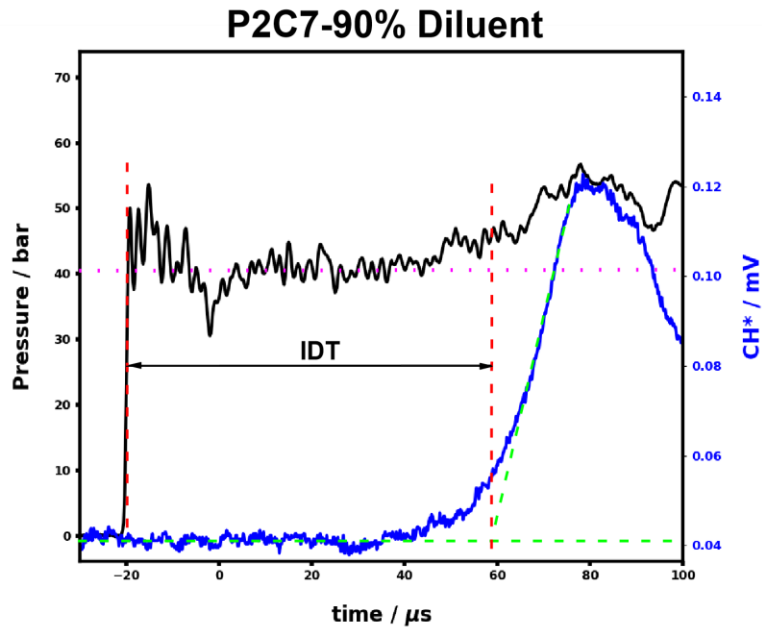


Figure ES12. Applied definition for measuring IDT in the NUIG-shock tube: (a) using Kistler pressure trace mounted on the end-wall of the endcap; (b) using PDA-CH* trace mounted on the side wall of the end-cap.

6. Rapid compression machine

The rapid compression machine is a common facility for getting the ignition delay time data under high pressure and low-to-moderate temperature regime (<1000 K). In the current study, the experiments related to the compressed mixture pressure $p_c \leq 40$ bar and $p_c > 40$ bar have been taken using NUIG-RCM and PCFC-RCM, respectively. According to the previous studies [16, 17], the experimental IDTs have been modelled using the adiabatic core assumption in which the non-adiabatic condition can be

compensated by imposing the volume–time profiles of the same non–reactive mixtures to calculations. Thus, general information about each facility have been presented in the following subsections.

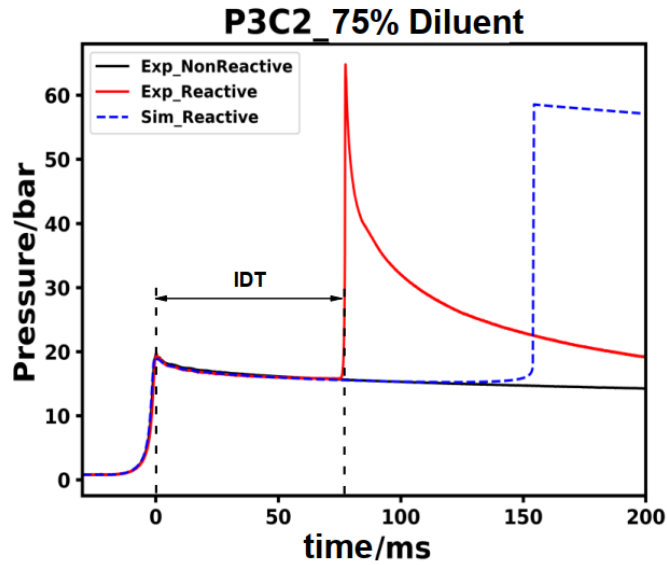
6.1. NUIG–RCM

The general specifications of NUIG–RCM have been presented in Table S5. The details of the facility has been already documented and explained in details by the authors [7, 14, 16, 18-20]. In this facility, the ignition delay time of the normal studied mixtures (diluent concentration = 75%) and the pressure– time histories of their relevant non–reactive mixtures were recorded using a Kistler 6045A/B transducer mounted on the reaction chamber. However, the ignition delay times of the mixtures with 85% and 90% dilution percent and the post–compression pressures of 20 and 40 bar, were reordered using both the Kistler and a photomultiplier (PMT) equipped with CH* filter (CWL: 430 nm ± 10 FWHM; Thorlabs) due to vague signal of the Kistler pressure transducer under these conditions. Also, as shown in Figure ES13, the ignition delay time is defined as a maximum gradient in pressure $\left(\frac{dp}{dt}\right)_{max}$ or CH* $\left(\frac{dCH^*}{dt}\right)_{max}$ after compressing the studied mixtures. Subsequently, the post compression temperatures (T_c) were calculated by assuming isentropic compression condition using Gaseq software ¹⁵. Similar to the applied procedure in NUIG–HPST, all of measured post compression pressures (p_c) have been forced to be restricted to ±0.5 bar of the target pressures due to increasing the accuracy of the experiments and also reducing scattered points. Moreover, unlike the standard operating procedure in NUIG–HPST, all of the experimental results have been repeated at least three times and the repeatability of all reported IDTs was ≥ 90%. In this regard, all pressure versus time data including pressure/volume profiles and the experimentalist spreadsheets related to the studied conditions in NUIG–RCM have been provided as supplementary files.

Table S5. Specifications of NUIG–RCM.

Parameter	Value
Bore size of the reaction chamber (m)	0.03820
Volume of the reaction chamber (m ³)	3.3191×10 ⁻⁵
Piston's velocity (U_p) (m/s)	9.34 ~ 12.94
Pistons' stroke length (m)	0.16817
Piston's type	Flat head with the crevice
Type	Twin–counter pistons

(a)



(b)

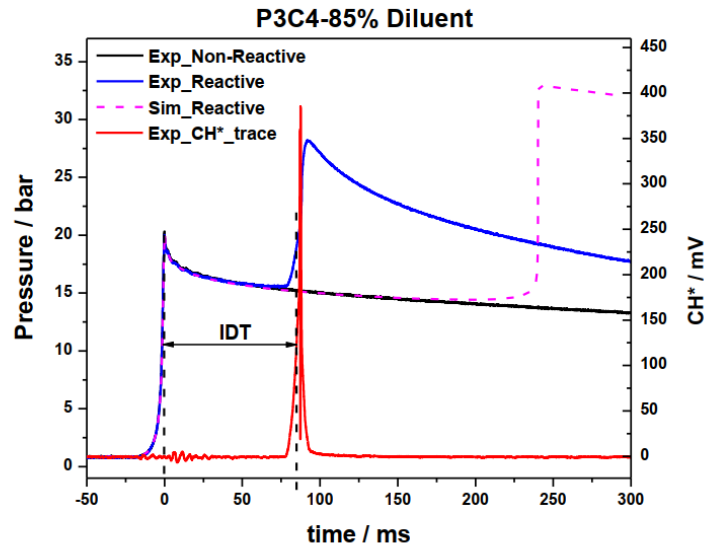


Figure ES13. Applied definition for measuring IDT in the NUIG-RCM: (a) using Kistler pressure trace; (b) using both pressure and PMT-CH* trace mounted on the side wall of the reaction chamber.

6.2. PCFC-RCM

The PCFC-RCM is a well-known facility which has been already introduced properly in literature. As mentioned above, all of the experimental tests related to the compressed pressures (p_c) of higher than 40 bar and within low-to-moderate temperature range, have been performed in RCM facility of the Physico-Chemical Fundamentals of Combustion (PCFC) of RWTH Aachen University. As presented in Table S5, this facility is constructed from a single-piston mechanism which is driven pneumatically and stopped

hydraulically at the end of compression. Similar to the applied piston in NUIG–RCM, the crevice piston design has been applied in the PCFC–RCM. In the facility, the pressure–time profile during the compression and post–compression processes and the initial temperature in the reaction chamber were monitored and controlled using a Kistler 6125C pressure transducer and type ‘T’ thermocouple, respectively. In this regard, the detail information about the construction, measurement procedure, and the applied sensors in the study have been already presented in ²¹. As the same process explained in section 6.1, the compressed mixture’s temperature (T_5) was calculated using the isentropic compression formulation of Gaseq software ¹⁵. According to the procedure explained by Ramalingam et al. ¹⁷, the reproducibility of evaluated IDTs and also the experimental uncertainty of the compressed mixture’s temperature for the measured conditions in the study were within 15% and ± 5 K, respectively. In this regard, the related experimental data to PCFC–RCM facility and the volume–time profiles are reported in supplementary files.

Table ES6. Specifications of PCFC–RCM.

Parameter	Value
Bore size of the reaction chamber (m)	0.05
Volume of the reaction chamber (m ³)	$5.06 \times 10^{-4} - 5.51 \times 10^{-4}$
Piston’s velocity (U_p) (m/s)	16.67
Pistons’ stroke length (m)	0.25
Piston’s type	Flat head with the crevice
Type	Single piston

7. Data acquisition system

As shown in Table ES7, in the current study, many sensors have been used in the three applied facilities at C³–NUIG and PCFC–RWTH Aachen University to measure the required parameters. In this regard, all installed sensors in NUIG–HPST which had been used for measuring the incident shock velocities and the ignition delay times, were synchronized and connected to two TiePie Handyscope HS4 oscilloscopes ²². Also, all generated signals from the installed sensors on NUIG–RCM including the Kistler pressure transducer, the position sensors, and the photomultiplier were synchronized and collected using a PicoScope 5443B ²³.

Table ES7. Applied sensors and detectors for measuring during the current study (NUIG–HPST/RCM and PCFC–RCM).

Sensor	Company	Model	Accuracy	Resolution
Pressure sensor transducer	Kistler	603B	$\leq \pm 1.0$ % FSO; linearity	NA

Pressure sensor transducer	Kistler	6045A	$\leq \pm 0.4\%$ /FSO; linearity	NA
Pressure sensor transducer	Kistler	6125C	$\leq \pm 0.4\%$ /FSO; linearity	NA
Piezoelectric pressure sensor	PCB	113B24	$\leq \pm 1.0\%$ FS; Non-linearity	± 0.035 KPa
Digital Absolut pressure transmitter	MKS	Baratron 121AA-0100D	0.5% of reading	± 0.01 Torr
Digital Absolut pressure transmitter	MKS	Baratron 121AA-0100D	0.5% of reading	± 0.1 Torr
Digital Absolut pressure transmitter	MKS	Baratron 121AA-05000B	0.5% of reading	± 0.5 Torr
Analog vacuum pressure gauge	Edwards	Pirani-PRE10K	NA	± 2 of reading scale
Thermocouples and Controller	Radionics	T-type	± 1.0 °C	± 0.1 °C
Photodetector	Thorlabs	PDA36A/PDA55	NA	NA
Photomultiplier	EMI Electronics	9924P	NA	NA

8. Uncertainty analysis

For getting a detailed understanding about the uncertainty of the experimental tests of the current study, the following subsections have been presented. In fact, these subsections try to analytically explain the effect of some important factors including pressure, temperature, and equivalence ratio on the total uncertainty of the experimental results. It seems that the output of the section could provide a good clue for better analysing and evaluating the quality of the experimental data.

8.1. Equivalence ratio

In the following lines, it is tried to somehow evaluate probable uncertainties which may be included in equivalence ratios of the applied mixtures of the current study.

Making a mixture:

$$\text{Fuel: } F = p_F = \sum_{i=1}^n p_i \rightarrow \sigma_F = \sqrt{\sum_{i=1}^n \sigma_i^2}$$

Where, p_i and σ_i are absolute pressure of i -th component in the fuel mixture and uncertainty of each absolute pressure of i -th component in the fuel mixture, respectively. Because, in the current study, only single fuel mixtures have been studied, thus: Fuel: $F = p_F \pm \sigma_F$ and Oxygen: $O = p_{O_2} \pm \sigma_{O_2}$.

$$\text{Equivalence ratio: } \varphi = \frac{\left(\frac{F}{O}\right)_{real}}{\left(\frac{F}{O}\right)_{Stoi}} \rightarrow \left(\frac{O}{F}\right)_{Stoi} = Cte \rightarrow \varphi = Cte \left(\frac{F}{O}\right)_{real} \rightarrow \sigma_\varphi = \left(\frac{\partial\varphi}{\partial F}\right) \sigma_F + \left(\frac{\partial\varphi}{\partial O}\right) \sigma_O \quad (3)$$

$$\frac{\partial\varphi}{\partial F} \cdot \sigma_F = \frac{\partial\varphi}{\partial p_1} \cdot \frac{\partial p_1}{\partial F} \cdot \sigma_1 + \frac{\partial\varphi}{\partial p_2} \cdot \frac{\partial p_2}{\partial F} \cdot \sigma_2 + \frac{\partial\varphi}{\partial p_3} \cdot \frac{\partial p_3}{\partial F} \cdot \sigma_3 + \dots + \frac{\partial\varphi}{\partial p_n} \cdot \frac{\partial p_n}{\partial F} \cdot \sigma_n \rightarrow \frac{\partial p_n}{\partial F} = 1 \rightarrow \frac{\partial\varphi}{\partial F} \cdot \sigma_F = \frac{\partial\varphi}{\partial p_1} \cdot \sigma_1 + \frac{\partial\varphi}{\partial p_2} \cdot \sigma_2 + \frac{\partial\varphi}{\partial p_3} \cdot \sigma_3 + \dots + \frac{\partial\varphi}{\partial p_n} \cdot \sigma_n \rightarrow \varphi = Cte \left(\frac{\sum_{i=1}^n p_i}{O}\right)_{real} \rightarrow \frac{\partial\varphi}{\partial p_n} = \frac{1}{O} \rightarrow \frac{\partial\varphi}{\partial O} = -\frac{\sum_{i=1}^n p_i}{O^2}$$

$$\sigma_\varphi = \frac{\partial\varphi}{\partial p_1} \cdot \sigma_1 + \frac{\partial\varphi}{\partial p_2} \cdot \sigma_2 + \frac{\partial\varphi}{\partial p_3} \cdot \sigma_3 + \dots + \frac{\partial\varphi}{\partial p_n} \cdot \sigma_n + \left(-\frac{\sum_{i=1}^n p_i}{O^2}\right) \sigma_O$$

If we assume that there is no correlation between measurements of $\sigma_i \sigma_j = 0$

$$\sigma_\varphi^2 = \left(\frac{\partial\varphi}{\partial p_1} \cdot \sigma_1\right)^2 + \left(\frac{\partial\varphi}{\partial p_2} \cdot \sigma_2\right)^2 + \left(\frac{\partial\varphi}{\partial p_3} \cdot \sigma_3\right)^2 + \dots + \left(\frac{\partial\varphi}{\partial p_n} \cdot \sigma_n\right)^2 + \left(\left(-\frac{\sum_{i=1}^n p_i}{O^2}\right) \sigma_O\right)^2$$

If we assume that there is no correlation between measurements of $\sigma_i \sigma_j = 0$

$$\sigma_\varphi^2 = \left(\frac{\partial\varphi}{\partial p_1} \cdot \sigma_1\right)^2 + \left(\frac{\partial\varphi}{\partial p_2} \cdot \sigma_2\right)^2 + \left(\frac{\partial\varphi}{\partial p_3} \cdot \sigma_3\right)^2 + \dots + \left(\frac{\partial\varphi}{\partial p_n} \cdot \sigma_n\right)^2 + \left(\left(-\frac{\sum_{i=1}^n p_i}{O^2}\right) \sigma_O\right)^2$$

$$\sigma_\varphi = \sqrt{\left(\frac{1}{p_{O_2}} \cdot \sigma_1\right)^2 + \left(\frac{1}{p_{O_2}} \cdot \sigma_2\right)^2 + \left(\frac{1}{p_{O_2}} \cdot \sigma_3\right)^2 + \dots + \left(\frac{1}{p_{O_2}} \cdot \sigma_n\right)^2 + \left(\left(-\frac{\sum_{i=1}^n p_i}{p_{O_2}^2}\right) \sigma_O\right)^2}$$

$$\sigma_\varphi = \sqrt{\left(\frac{\sum_{i=1}^n \sigma_i^2}{p_{O_2}^2}\right) + \left(\left(-\frac{p_F}{p_{O_2}^2}\right) \sigma_O\right)^2} = \sqrt{\left(\frac{\sigma_F}{p_{O_2}}\right)^2 + \left(\left(-\frac{p_F}{p_{O_2}^2}\right) \sigma_O\right)^2} = \frac{Cte}{p_{O_2}^2} \sqrt{p_{O_2}^2 \sigma_F^2 + p_F^2 \sigma_O^2}$$

Based on the above analysis, the uncertainties of all made mixtures in the current study are presented individually in Table ES8 as follows:

Table ES8. Uncertainty analysis of equivalence ratio for all made mixtures.

Code	Facility	O F Stoi	P _F (mbar)	±σ _f (mbar)	P _O (mbar)	±σ _O (mbar)	±σ _φ
P2C2	HPST	3	333.3	1.7	999.9	6.7	8.4211E-03
	RCM		125	0.6	375	2.5	8.2149E-03

P2C3	HPST	1.5	533.3	2.7	799.9	6.7	9.7879E-03
	RCM		200	1.0	300	2.5	9.7182E-03
P2C4	RCM	6	42.84	0.21	257.1	1.5	7.6185E-03
P2C5	HPST	3	200.0	1.0	599.9	4.0	8.3356E-03
	RCM		75	0.38	225	1.5	8.3735E-03
P2C7	HPST	6	76.26	0.38	457.0	2.7	7.7383E-03
	RCM		28.6	0.14	171.4	1.0	7.6247E-03
P2C9	RCM	1.5	80.00	0.40	120.0	1.0	9.7183E-03
P3C2	HPST	3.5	298.6	1.5	1034.6	6.7	8.2791E-03
	RCM		112	0.6	388	2.5	8.4658E-03
P3C3	HPST	1.75	484.8	2.4	848.0	6.7	9.3281E-03
	RCM		181.8	0.9	318.0	2.5	9.2948E-03
P3C4	HPST	7	99.99	0.50	699.9	4.0	7.5942E-03
	RCM		37.5	0.19	262.5	1.5	7.6370E-03
P3C5	HPST	3.5	177.7	0.9	622.2	4.0	8.1809E-03
	RCM		66.66	0.33	233.3	1.5	8.1149E-03
P3C7	HPST	7	66.66	0.33	466.6	2.7	7.6155E-03
	RCM		25	0.13	175	0.9	7.3136E-03
P3C9	HPST	1.75	193.9	1.0	339.4	2.7	9.4786E-03
	RCM		72.73	0.36	127.3	1.0	9.2832E-03

8.2. Diluent concentration

For determining the uncertainty of diluent concentration in the studied mixtures the following formulations are presented:

$$[D] = \frac{p_i}{RT_i} \quad (\text{E5})$$

$$\sigma_{[D]} = \frac{\partial [D]}{\partial p_i} \sigma_{p_i} \quad (\text{E6})$$

$$\frac{\partial [D]}{\partial p_i} = \frac{1}{RT_i} \quad (\text{E7})$$

Because, in the study, all mixtures have been prepared under 303 K, so the Equation E7 would be as follows:

$$\frac{\partial [D]}{\partial p_i} = 3.96961 \times 10^{-4}$$

Therefore, the worst uncertainty in diluent concentration in the studied mixtures is related to cases with 90% diluent in a mixture with total pressure of 4000 Torr which yields $\sigma_{[D]} = \pm 1.05848 \frac{\text{mol}}{\text{m}^3} = \pm 1.05848 \times 10^{-5} \frac{\text{mol}}{10^5 \text{m}^3} \approx \pm 0.56\% [D]$. For calculating the uncertainty in concentration of each species under the compressed conditions, the following formulations are presented:

$$[D] = \frac{p_{c,[D]}}{RT_c} \quad (\text{E8})$$

$$\sigma_{[D]} = \sqrt{\left(\frac{\partial [D]}{\partial p_{c,[D]}} \sigma_{p_{c,[D]}}\right)^2 + \left(\frac{\partial [D]}{\partial T_c} \sigma_{T_c}\right)^2} \quad (\text{E9})$$

$$\sigma_{[D]} = \sqrt{\left(\frac{1}{RT_c} \sigma_{p_{c,[D]}}\right)^2 + \left(-\frac{p_{c,[D]}}{RT_c^2} \sigma_{T_c}\right)^2} = \frac{1}{8.314 \times T_c^2} \sqrt{\left(T_c \sigma_{p_{c,[D]}}\right)^2 + \left(p_{c,[D]} \sigma_{T_c}\right)^2} \quad (\text{E10})$$

8.3. IDTs in Shock-tube

If the following equations, for determining total uncertainty of the measured ignition delay times in NUIG-HPST, it is assumed:

$$p_c = P(p_1, V_s, \varphi, T_1); T_c = T(T_1, V_s, \varphi)$$

As shown by Petersen et al. ²⁴, one could assume that:

$$T_c = \frac{T_1[2(\gamma_1-1)M^2+(3-\gamma_1)][(3\gamma_1-1)M^2-2(\gamma_1-1)]}{(\gamma_1+1)^2M^2}; M = \frac{V_s}{\sqrt{\gamma_1RT_1}}; V_s = \frac{\Delta z}{\Delta t} \quad (E11)$$

$$\sigma_{V_s} = \sqrt{\left(\frac{\partial V_s}{\partial(\Delta z)} \sigma_{\Delta z}\right)^2 + \left(\frac{\partial V_s}{\partial(\Delta t)} \sigma_{\Delta t}\right)^2} = \sqrt{\left(\frac{1}{\Delta t} \sigma_{\Delta z}\right)^2 + \left(-\frac{\Delta z}{(\Delta t)^2} \sigma_{\Delta t}\right)^2} \quad (E12)$$

$$\sigma_{T_c} = \sigma_T = \frac{\partial T_c}{\partial M} \sigma_M = \left(T_1 \left[\left(\frac{4(3\gamma_1^2-4\gamma_1+1)}{(\gamma_1+1)^2}\right) M + \left(\frac{4(\gamma_1-1)(3-\gamma_1)}{(\gamma_1+1)^2}\right) M^{-3}\right]\right) \frac{\sigma_{V_s}}{\sqrt{\gamma_1RT_1}} \quad (E13)$$

$$p_c = \frac{P_1[2\gamma_1M^2-(\gamma_1-1)][(3\gamma_1-1)M^2-2(\gamma_1-1)]}{2(\gamma_1+1)+M^2(\gamma_1^2-1)}; \sigma_{p_c} = \sigma_p = \frac{\partial p_c}{\partial M} \sigma_M = \left(p_1 \left[\frac{12M^5\gamma^4-4M^5\gamma^3+48M^3\gamma^3+32M^3\gamma^2-12M^5\gamma^2+4M^5\gamma-16M^3\gamma-20M\gamma^3+4M\gamma^2+20M\gamma-4M\gamma^4}{(M^2\gamma^2-M^2+2\gamma+2)^2}\right]\right) \frac{\sigma_{V_s}}{\sqrt{\gamma_1RT_1}} \quad (E14)$$

Here, it was supposed that the effect of changing in equivalence ratio on γ is negligible. Here, it is supposed that the maximum $\sigma_{\Delta t}$ which is related to TiePie Handyscope HS4 Oscilloscope is $\pm 1 \mu s$, and $\sigma_{\Delta z}$ is ± 0.001 m. Now, if it could be assumed the defined ignition delay time (IDT) could be correlated as follows, then:

$$\tau_{IDT} \cong A \cdot \exp\left(\frac{B}{T}\right) p^m \varphi^n [D]^q \rightarrow \partial \tau = \frac{\partial \tau}{\partial T} \cdot \partial T + \frac{\partial \tau}{\partial p} \cdot \partial p + \frac{\partial \tau}{\partial \varphi} \cdot \partial \varphi + \frac{\partial \tau}{\partial [D]} \cdot \partial [D] \rightarrow (\sigma_{\tau})^2 = \left(\frac{\partial \tau}{\partial T} \cdot \partial T\right)^2 + \left(\frac{\partial \tau}{\partial p} \cdot \partial p\right)^2 + \left(\frac{\partial \tau}{\partial \varphi} \cdot \partial \varphi\right)^2 + \left(\frac{\partial \tau}{\partial [D]} \cdot \partial [D]\right)^2 + 2\left(\frac{\partial \tau}{\partial T} \cdot \frac{\partial \tau}{\partial p} \cdot \partial T \partial p\right) + 2\left(\frac{\partial \tau}{\partial T} \cdot \frac{\partial \tau}{\partial \varphi} \cdot \partial T \partial \varphi\right) + 2\left(\frac{\partial \tau}{\partial \varphi} \cdot \frac{\partial \tau}{\partial p} \cdot \partial \varphi \partial p\right) + 2\left(\frac{\partial \tau}{\partial T} \cdot \frac{\partial \tau}{\partial [D]} \cdot \partial T \partial [D]\right) + 2\left(\frac{\partial \tau}{\partial p} \cdot \frac{\partial \tau}{\partial [D]} \cdot \partial p \partial [D]\right) + 2\left(\frac{\partial \tau}{\partial \varphi} \cdot \frac{\partial \tau}{\partial [D]} \cdot \partial \varphi \partial [D]\right) \quad (E15)$$

Now, one assumes that there is no correlation between measurements of (p , T , and φ), so the above equation would be followed by:

$$(\sigma_{\tau,i})^2 = \left(\frac{\partial \tau}{\partial T} \cdot \partial T\right)^2 + \left(\frac{\partial \tau}{\partial p} \cdot \partial p\right)^2 + \left(\frac{\partial \tau}{\partial \varphi} \cdot \partial \varphi\right)^2 + \left(\frac{\partial \tau}{\partial [D]} \cdot \partial [D]\right)^2 + 2\left(\frac{\partial \tau}{\partial T} \cdot \frac{\partial \tau}{\partial p} \cdot \partial T \partial p\right) + 2\left(\frac{\partial \tau}{\partial T} \cdot \frac{\partial \tau}{\partial \varphi} \cdot \partial T \partial \varphi\right) + 2\left(\frac{\partial \tau}{\partial \varphi} \cdot \frac{\partial \tau}{\partial p} \cdot \partial \varphi \partial p\right) + 2\left(\frac{\partial \tau}{\partial T} \cdot \frac{\partial \tau}{\partial [D]} \cdot \partial T \partial [D]\right) + 2\left(\frac{\partial \tau}{\partial p} \cdot \frac{\partial \tau}{\partial [D]} \cdot \partial p \partial [D]\right) + 2\left(\frac{\partial \tau}{\partial \varphi} \cdot \frac{\partial \tau}{\partial [D]} \cdot \partial \varphi \partial [D]\right) \quad (E16)$$

One could re-write the above equation as follows:

$$(\sigma_{\tau,i})^2 = \left(\frac{\partial \tau}{\partial T} \cdot \sigma_T\right)^2 + \left(\frac{\partial \tau}{\partial p} \cdot \sigma_p\right)^2 + \left(\frac{\partial \tau}{\partial \varphi} \cdot \sigma_\varphi\right)^2 + \left(\frac{\partial \tau}{\partial [D]} \cdot \sigma_{[D]}\right)^2 + 2 \left(\frac{\partial \tau}{\partial T} \cdot \frac{\partial \tau}{\partial [D]} \cdot \sigma_T \sigma_{[D]}\right) + 2 \left(\frac{\partial \tau}{\partial p} \cdot \frac{\partial \tau}{\partial [D]} \cdot \sigma_p \sigma_{[D]}\right) \quad (\text{E17})$$

$$\frac{\partial \tau}{\partial T} = A \cdot \left(-\frac{B}{T^2} \cdot \exp\left(\frac{B}{T}\right) p^m \varphi^n [D]^q\right) \quad (\text{E18})$$

$$\frac{\partial \tau}{\partial p} = A \cdot \left(m \cdot \exp\left(\frac{B}{T}\right) p^{m-1} \varphi^n [D]^q\right) \quad (\text{E19})$$

$$\frac{\partial \tau}{\partial \varphi} = A \cdot \left(n \cdot \exp\left(\frac{B}{T}\right) p^m \varphi^{n-1} [D]^q\right) \quad (\text{E20})$$

$$\frac{\partial \tau}{\partial [D]} = A \cdot \left(q \cdot \exp\left(\frac{B}{T}\right) p^m \varphi^n [D]^{q-1}\right) \quad (\text{E21})$$

$$\begin{aligned} (\sigma_{\tau,i})^2 &= A^2 \cdot \left(\left(-\frac{B}{T^2} \cdot \exp\left(\frac{B}{T}\right) p^m \varphi^n [D]^q\right) \cdot \sigma_T\right)^2 + A^2 \cdot \left(\left(m \cdot \exp\left(\frac{B}{T}\right) p^{m-1} \varphi^n [D]^q\right) \cdot \sigma_p\right)^2 + A^2 \cdot \left(\left(n \cdot \right.\right. \\ &\left.\left.\exp\left(\frac{B}{T}\right) p^m \varphi^{n-1} [D]^q\right) \cdot \sigma_\varphi\right)^2 + A^2 \cdot \left(\left(q \cdot \exp\left(\frac{B}{T}\right) p^m \varphi^n [D]^{q-1}\right) \cdot \sigma_{[D]}\right)^2 - 2A^2 \left(\frac{Bq}{T^2} \cdot \right. \\ &\left.\exp\left(\frac{2B}{T}\right) p^{2m} \varphi^{2n} [D]^{2q-1}\right) \cdot \rho_{T[D]} \sigma_T \sigma_{[D]} + 2A^2 \left(qm \cdot \exp\left(\frac{2B}{T}\right) p^{2m-1} \varphi^{2n} [D]^{2q-1}\right) \cdot \rho_{p[D]} \sigma_p \sigma_{[D]} \end{aligned} \quad (\text{E22})$$

$$\sigma_{\tau,i} \cong A \cdot \sqrt{\frac{\left(\left(-\frac{B}{T^2} \cdot \exp\left(\frac{B}{T}\right) p^m \varphi^n [D]^q\right) \cdot \sigma_T\right)^2 + \left(\left(m \cdot \exp\left(\frac{B}{T}\right) p^{m-1} \varphi^n [D]^q\right) \cdot \sigma_p\right)^2 + \left(\left(n \cdot \exp\left(\frac{B}{T}\right) p^m \varphi^{n-1} [D]^q\right) \cdot \sigma_\varphi\right)^2 + \left(\left(q \cdot \exp\left(\frac{B}{T}\right) p^m \varphi^n [D]^{q-1}\right) \cdot \sigma_{[D]}\right)^2 - 2\left(\frac{Bq}{T^2} \cdot \exp\left(\frac{2B}{T}\right) p^{2m} \varphi^{2n} [D]^{2q-1}\right) \cdot \rho_{T[D]} \sigma_T \sigma_{[D]} + 2\left(qm \cdot \exp\left(\frac{2B}{T}\right) p^{2m-1} \varphi^{2n} [D]^{2q-1}\right) \cdot \rho_{p[D]} \sigma_p \sigma_{[D]}}{\right.}} \quad (\text{E23})$$

$$\rho_{ij} \sigma_i \sigma_j = \sigma_{ij} = \sum_{ij} f(i,j) (x_i - \bar{x}_i) (x_j - \bar{x}_j) \quad (\text{E24})$$

The uncertainty of the measured ignition delay time in shock–tube could be acceptably estimated using the above equation. As seen in the above expression, the uncertainty parameter is changing by changing in the compressed temperature and pressure, equivalence ratio, and also diluent concentration, so that it is not a constant parameter during experimental tests. Thus, it should be calculated specifically for each case. Therefore, regarding Equation E23 and Table ES9, specific uncertainty for each data–point according to its specific temperature, pressure, equivalence ratio, and diluent concentration could be calculated as shown in Table ES10 to Table ES19.

Table ES9. Correlation variables of the studied experimental datasets for different fuels.

$$\tau_{IDT} = 10^A \cdot \exp\left(\frac{B}{T}\right) p^m \varphi^n [D]^q$$

Fuel	A	B	m	n	q	R ₂	Adj R ²
C ₂ H ₄	24.42832	4173.61647	-7.45375	0.04535	7.13584	0.9709	0.96927
C ₂ H ₆	13.35269	9724.30442	-5.42291	0.11308	4.81091	0.9085	0.90408

Table ES10. Estimated uncertainties for all measured IDTs of P2C2 dataset in shock-tube.

T_5 (K)	φ	$\pm\sigma_\varphi$	p_5 (bar)	$\pm\sigma_p$ (bar)	$\pm\sigma_T$ (K)	[D] $\frac{\text{mol}\cdot\text{m}^3}{10}$	$\frac{\pm\sigma_{[D]}}{10^5\cdot\text{m}^3}$ $\frac{\text{mol}}{10^5\cdot\text{m}^3}$	IDT (μs)	$\pm\sigma_{\text{IDT}}$ (μs)	$\pm\sigma_{\text{IDT}}$ (%)
1112.8	1.0	8.4E-03	20.75	0.3934	14.06	1.68E-3	3.83E-5	325	60.90	18.7
1084.3	1.0	8.4E-03	19.64	0.3736	13.49	1.63E-3	3.71E-5	447	81.71	18.3
1042.8	1.0	8.4E-03	19.71	0.3801	12.57	1.71E-3	3.88E-5	847.40	130.86	15.4

Table ES11. Estimated uncertainties for all measured IDTs of P2C3 dataset in shock tube.

T_5 (K)	φ	$\pm\sigma_\varphi$	p_5 (bar)	$\pm\sigma_p$ (bar)	$\pm\sigma_T$ (K)	[D] $\frac{\text{mol}\cdot\text{m}^3}{10}$	$\frac{\pm\sigma_{[D]}}{10^5\cdot\text{m}^3}$ $\frac{\text{mol}}{10^5\cdot\text{m}^3}$	IDT (μs)	$\pm\sigma_{\text{IDT}}$ (μs)	$\pm\sigma_{\text{IDT}}$ (%)
1245.9	2.0	9.8E-03	39.73	0.7673	17.87	2.88E-3	6.92E-5	49.6	16.69	33.6
1201.6	2.0	9.8E-03	40.12	0.7774	16.76	3.01E-3	7.19E-5	72.4	24.03	33.2
1154.4	2.0	9.8E-03	40.34	0.7831	15.58	3.15E-3	7.45E-5	130.6	36.68	28.1
1104.5	2.0	9.8E-03	40.38	0.7839	14.37	3.3E-3	7.71E-5	227.6	59.44	26.1
1050	2.0	9.8E-03	40.01	0.7872	13.33	3.44E-3	8.05E-5	389.2	105.14	27
1000.2	2.0	9.8E-03	40.04	0.8308	12.88	3.61E-3	8.82E-5	855.8	188.33	22
945.2	0.2	9.8E-03	39.55	0.7727	10.96	3.77E-3	8.58E-5	1686	338.42	20.1

Table ES12. Estimated uncertainties for all measured IDTs of P2C5 dataset in shock-tube.

T_5 (K)	φ	$\pm\sigma_\varphi$	p_5 (bar)	$\pm\sigma_p$ (bar)	$\pm\sigma_T$ (K)	$[D] \frac{\text{mol}\cdot\text{m}^3}{10}$	$\frac{\pm\sigma_{[D]}}{\text{mol}} \frac{\text{mol}}{10^5\cdot\text{m}^3}$	IDT (μs)	$\pm\sigma_{\text{IDT}}$ (μs)	$\pm\sigma_{\text{IDT}}$ (%)
1152.1	1.0	8.3E-03	40.16	0.7848	14.35	3.56E-3	8.26E-5	225.8	87.18	38.6
1102.4	1.0	8.3E-03	40.20	0.7811	13.30	3.73E-3	8.53E-5	418.6	141.16	33.7
1054.6	1.0	8.3E-03	40.39	0.7859	12.35	3.91E-3	8.89E-5	816.2	226.50	27.8

Table ES13. Estimated uncertainties for all measured IDTs of P2C7 dataset in shock-tube.

T_5 (K)	φ	$\pm\sigma_\varphi$	p_5 (bar)	$\pm\sigma_p$ (bar)	$\pm\sigma_T$ (K)	$[D] \frac{\text{mol}\cdot\text{m}^3}{10}$	$\frac{\pm\sigma_{[D]}}{\text{mol}} \frac{\text{mol}}{10^5\cdot\text{m}^3}$	IDT (μs)	$\pm\sigma_{\text{IDT}}$ (μs)	$\pm\sigma_{\text{IDT}}$ (%)
1201.5	0.5	7.74E-03	40.10	0.8022	15.24	3.61E-3	8.56E-5	260	84.99	32.7
1132.7	0.5	7.74E-03	38.81	0.8194	14.58	3.71E-3	9.17E-5	535	171.29	32.0
1107.9	0.5	7.74E-03	40.95	0.8534	14.01	4E-3	9.75E-5	827.68	210.51	25.4

Table ES14. Estimated uncertainties for all measured IDTs of P3C2 dataset in shock-tube.

T_5 (K)	φ	$\pm\sigma_\varphi$	p_5 (bar)	$\pm\sigma_p$ (bar)	$\pm\sigma_T$ (K)	$[D] \frac{\text{mol}\cdot\text{m}^3}{10}$	$\frac{\pm\sigma_{[D]}}{\text{mol}} \frac{\text{mol}}{10^5\cdot\text{m}^3}$	IDT (μs)	$\pm\sigma_{\text{IDT}}$ (μs)	$\pm\sigma_{\text{IDT}}$ (%)
1390.4	1.0	8.28E-03	19.73	0.3843	21.07	1.28E-3	3.16E-5	24.8	5.49	22.1
1339	1.0	8.28E-03	19.67	0.382	19.69	1.33E-3	3.23E-5	37.8	8.72	23.1
1290.6	1.0	8.28E-03	19.71	0.3671	17.89	1.38E-3	3.20E-5	63	13.08	20.8
1253.4	1.0	8.28E-03	20.11	0.3914	17.54	1.45E-3	3.47E-5	100.4	19.28	19.2
1200.4	1.0	8.28E-03	20.02	0.3899	16.28	1.50E-3	3.57E-5	184.8	32.90	17.8
1154.5	1.0	8.28E-03	20.17	0.396	15.12	1.58E-3	3.72E-5	337	55.94	16.6
1097.2	1.0	8.28E-03	19.89	0.392	13.89	1.64E-3	3.83E-5	657.4	112.54	17.1

Table ES15. Estimated uncertainties for all measured IDTs of P3C3 dataset in shock-tube.

T_5 (K)	φ	$\pm\sigma_\varphi$	p_5 (bar)	$\pm\sigma_p$ (bar)	$\pm\sigma_T$ (K)	$[D] \frac{\text{mol} \cdot \text{m}^3}{10}$	$\frac{\pm\sigma_{[D]}}{\text{mol}} \frac{\text{mol}}{10^5 \cdot \text{m}^3}$	IDT (μs)	$\pm\sigma_{\text{IDT}}$ (μs)	$\pm\sigma_{\text{IDT}}$ (%)
1348.2	2.0	9.3E-03	39.89	0.767	21.05	2.67E-3	6.61E-5	27.4	5.88	21.5
1295.4	2.0	9.3E-03	39.70	0.7644	19.66	2.76E-3	6.78E-5	40.6	9.51	23.4
1247.0	2.0	9.3E-03	39.80	0.7630	18.19	2.88E-3	6.94E-5	67.2	15.33	22.8
1201.2	2.0	9.3E-03	40.09	0.7711	17.16	3.01E-3	7.21E-5	100.6	24.68	24.5
1148.5	2.0	9.3E-03	39.88	0.7732	15.77	3.13E-3	7.44E-5	177	44.54	25.2
1099.7	2.0	9.3E-03	39.98	0.7715	14.57	3.28E-3	7.68E-5	330.4	80.08	24.2
1048.7	2.0	9.3E-03	39.89	0.7746	13.38	3.43E-3	7.97E-5	640.2	155.30	24.6
997.5	2.0	9.3E-03	39.77	0.7678	12.17	3.6E-3	8.21E-5	1290	319.95	24.8

Table ES16. Estimated uncertainties for all measured IDTs of P3C4 dataset in shock-tube.

T_5 (K)	φ	$\pm\sigma_\varphi$	p_5 (bar)	$\pm\sigma_p$ (bar)	$\pm\sigma_T$ (K)	$[D] \frac{\text{mol} \cdot \text{m}^3}{10}$	$\frac{\pm\sigma_{[D]}}{\text{mol}} \frac{\text{mol}}{10^5 \cdot \text{m}^3}$	IDT (μs)	$\pm\sigma_{\text{IDT}}$ (μs)	$\pm\sigma_{\text{IDT}}$ (%)
1390.1	0.5	7.6E-03	19.75	0.3843	19.24	1.45E-3	3.47E-5	30.8	8.86	28.8
1348.7	0.5	7.6E-03	19.97	0.3952	18.33	1.51E-3	3.63E-5	47.8	12.78	26.7
1301.4	0.5	7.6E-03	20.05	0.3884	17.26	1.58E-3	3.70E-5	88.2	19.94	22.6
1245.9	0.5	7.6E-03	19.87	0.3834	16.04	1.63E-3	3.78E-5	180	33.90	18.8
1204.5	0.5	7.6E-03	20.14	0.3933	15.19	1.71E-3	3.97E-5	310.6	52.41	16.9
1152.6	0.5	7.6E-03	20.09	0.3904	14.08	1.78E-3	4.09E-5	653.2	92.54	14.2
1107.2	0.5	7.6E-03	20.27	0.3957	13.18	1.87E-3	4.28E-5	1130	158.84	14.1

Table ES17. Estimated uncertainties for all measured IDTs of P3C5 dataset in shock-tube.

T_5 (K)	φ	$\pm\sigma_\varphi$	p_5 (bar)	$\pm\sigma_p$ (bar)	$\pm\sigma_T$ (K)	$[D] \frac{\text{mol}\cdot\text{m}^3}{10}$	$\frac{\pm\sigma_{[D]}}{\text{mol}} \frac{\text{mol}}{10^5 \cdot \text{m}^3}$	IDT (μs)	$\pm\sigma_{\text{IDT}}$ (μs)	$\pm\sigma_{\text{IDT}}$ (%)
1394.6	1.0	8.2E-03	39.70	0.7711	19.86	2.91E-3	7.01E-5	25.4	6.13	24.1
1360.3	1.0	8.2E-03	40.60	0.7919	19.05	3.05E-3	7.33E-5	34.6	8.15	23.6
1300.1	1.0	8.2E-03	40.01	0.7762	17.63	3.15E-3	7.45E-5	63.6	14.29	22.5
1244.8	1.0	8.2E-03	39.67	0.771	16.42	3.26E-3	7.65E-5	107	24.68	23.1
1199.2	1.0	8.2E-03	39.95	0.775	15.36	3.41E-3	7.92E-5	186.4	39.66	21.3
1150.4	1.0	8.2E-03	40.05	0.7779	14.32	3.56E-3	8.21E-5	333	68.09	20.5
1102.4	1.0	8.2E-03	40.19	0.7796	13.33	3.73E-3	8.52E-5	596	120.86	20.3

Table ES18. Estimated uncertainties for all measured IDTs of P3C7 dataset in shock-tube.

T_5 (K)	φ	$\pm\sigma_\varphi$	p_5 (bar)	$\pm\sigma_p$ (bar)	$\pm\sigma_T$ (K)	$[D] \frac{\text{mol}\cdot\text{m}^3}{10}$	$\frac{\pm\sigma_{[D]}}{\text{mol}} \frac{\text{mol}}{10^5 \cdot \text{m}^3}$	IDT (μs)	$\pm\sigma_{\text{IDT}}$ (μs)	$\pm\sigma_{\text{IDT}}$ (%)
1558	0.5	7.6E-03	40.41	0.8625	24.56	2.81E-3	7.45E-5	6.64	2.27	34.2
1506.9	0.5	7.6E-03	40.34	0.8503	23.25	2.9E-3	7.57E-5	10.80	3.28	30.4
1452.3	0.5	7.6E-03	40.12	0.8438	21.91	2.99E-3	7.74E-5	18.69	4.99	26.7
1393.7	0.5	7.6E-03	39.67	0.8382	20.49	3.08E-3	7.93E-5	30.98	8.14	26.3
1344.6	0.5	7.6E-03	39.71	0.8369	19.33	3.20E-3	8.16E-5	51.7	12.56	24.3
1298.6	0.5	7.6E-03	39.92	0.8405	18.21	3.33E-3	8.42E-5	77.31	19.11	24.7
1243.8	0.5	7.6E-03	39.62	0.8416	17.06	3.45E-3	8.72E-5	151.84	33.15	21.8
1202	0.5	7.6E-03	40.14	0.8452	16.09	3.61E-3	9.02E-5	324.29	50.29	15.5
1154.3	0.5	7.6E-03	40.31	0.8484	15.01	3.78E-3	9.35E-5	622.14	85.79	13.8
1101.6	0.5	7.6E-03	40.13	0.8464	13.93	3.94E-3	9.70E-5	1189	161.54	13.6

Table ES19. Estimated uncertainties for all measured IDTs of P3C9 dataset in shock-tube.

T_5 (K)	ϕ	$\pm\sigma_\phi$	p_5 (bar)	$\pm\sigma_p$ (bar)	$\pm\sigma_T$ (K)	$[D] \frac{\text{mol}\cdot\text{m}^3}{10}$	$\frac{\pm\sigma_{[D]}}{10^5 \cdot \text{mol}}$	IDT (μs)	$\pm\sigma_{\text{IDT}}$ (μs)	$\pm\sigma_{\text{IDT}}$ (%)
1692.6	2.0	9.5E-03	19.84	0.4075	29.81	1.27E-3	3.43E-5	16.46	1.7	10.3
1643.4	2.0	9.5E-03	19.85	0.4154	28.27	1.31E-3	3.54E-5	21.12	2.34	11.1
1591.6	2.0	9.5E-03	19.81	0.4234	26.76	1.35E-3	3.66E-5	26.25	3.36	12.8
1552.7	2.0	9.5E-03	20.06	0.4194	25.66	1.4E-3	3.73E-5	29.29	4.30	14.7
1501.0	2.0	9.5E-03	20.03	0.4228	24.26	1.44E-3	3.84E-5	36.80	6.21	16.9
1453.4	2.0	9.5E-03	20.09	0.4242	22.94	1.5E-3	3.94E-5	46.97	9.19	19.6
1397.7	2.0	9.5E-03	19.94	0.4187	21.48	1.54E-3	4.02E-5	71.24	14.19	19.9
1351.7	2.0	9.5E-03	20.05	0.4169	20.34	1.61E-3	4.12E-5	105.6	21.50	20.4
1292.2	2.0	9.5E-03	19.76	0.4143	18.86	1.66E-3	4.22E-5	151.67	37.76	24.9
1254.6	2.0	9.5E-03	20.15	0.4212	17.93	1.74E-3	4.40E-5	207.49	53.42	25.7
1199.1	2.0	9.5E-03	19.97	0.4212	16.58	1.8E-3	4.55E-5	413.04	95.19	23.0
1155.1	2.0	9.5E-03	20.19	0.4179	15.31	1.89E-3	4.65E-5	650.03	152.33	23.4

8.4. Rapid compression machine

As shown in the previous section, the uncertainty of each experimental point is changing by varying temperature, pressure, and mixture composition, so that it is not identical during IDT measurement experimental tests. Therefore, for doing the uncertainty analysis for the studied RCM regimes, P2C7 dataset has been chosen as one of the worst cases with high uncertainty. As already mentioned by Weber et al ²⁵, using Monte Carlo analysis or independent parameters methodology doesn't led to significant change in the calculated uncertainties. Therefore, like the performed uncertainty analysis for NUIG-HPST, it is supposed that there is no correlation between parameters which can affect measured ignition delay time in the rapid compression machine. In this regard, the average temperature of dataset in RCM regime is calculated as representative of the studied temperature range, and then the uncertainty analysis has been done for the test point. The average temperature for P2C7 dataset is 918.4 K. Here, it should be noted that according to the Taguchi DOE method, it is not possible to consider the effect of individual parameters such as pressure, equivalence ratio, and dilution percent on the measured ignition delay time,

so that the physical and chemical conditions of each dataset is completely different and it is not comparable with another one in terms of the effect of individual parameter on the measured ignition delay times. Thus, for covering the lack of information in this part, adiabatic constant volume IDT simulations have been done at the average temperature over the studied range of equivalence ratio and dilution percent, individually, using AramcoMech 3.0 chemical mechanism due to its better compatibility with the experimental results of P2C7 dataset. As shown in Figure S14, the effect of temperature on the measured ignition delay time has been correlated through fitting an exponential equation to the experimental IDT data, and then the individual effect of pressure on the measured ignition delay time has been estimated using the applied approach by Weber et al ²⁵. Also, the effect of each individual parameter such as equivalence ratio (0.5–2.0) and dilution (75%–90%) on the simulated ignition delay times has been correlated using fitted power equations (Figure S15 and Figure S16) to the simulated ignition delay times. Therefore, the following formulations could be proposed to estimate available uncertainties in the measured independent parameters and consequently the measured ignition delay times:

$$\tau_{IDT}(T_c) = 6 \times 10^{13} \exp(-0.038T_c) \rightarrow \frac{\partial \tau_{IDT}}{\partial T_c} = -2.28 \times 10^{12} \exp(-0.038T_c) \quad (E25)$$

$$\tau_{IDT}(\varphi) = 0.0119x^{-0.68} \rightarrow \frac{\partial \tau_{IDT}}{\partial \varphi} = -8.092 \times 10^{-3} x^{-1.68} \quad (E26)$$

$$\tau_{IDT}([D]) = 1 \times 10^9 x^{4.6821} \rightarrow \frac{\partial \tau_{IDT}}{\partial [D]} = 4.6821 \times 10^9 x^{3.6821} \quad (E27)$$

$$\frac{\partial T_c}{\partial p_c} = \frac{W\left(\frac{b}{a} \exp\left[\frac{bT_0}{a}\right] T_0 \left[\frac{p_c}{p_0}\right]^{\frac{1}{a}}\right)}{b p_c \left(W\left(\frac{b}{a} \exp\left[\frac{bT_0}{a}\right] T_0 \left[\frac{p_c}{p_0}\right]^{\frac{1}{a}}\right) + 1\right)} \quad (E28)$$

Where, W, T_0 , and p_0 are Lambert's W function, initial temperature, and initial pressure in the reaction chamber, respectively. In Equation E28, “a”, “b”, and $\frac{\partial T_c}{\partial p_c}$ were calculated using a Python code

$$\frac{\partial \tau_{IDT}}{\partial p_c} = \frac{\partial \tau_{IDT}}{\partial T_c} \cdot \frac{\partial T_c}{\partial p_c} = (-2.28 \times 10^{12} \exp(-0.038T_c)) \cdot \frac{W\left(\frac{b}{a} \exp\left[\frac{bT_0}{a}\right] T_0 \left[\frac{p_c}{p_0}\right]^{\frac{1}{a}}\right)}{b p_c \left(W\left(\frac{b}{a} \exp\left[\frac{bT_0}{a}\right] T_0 \left[\frac{p_c}{p_0}\right]^{\frac{1}{a}}\right) + 1\right)} \quad (E29)$$

$$\tau_{IDT} = f(T_c, p_c, \varphi, [D]) \rightarrow \sigma_{\tau_{IDT}} = \sqrt{\left(\frac{\partial \tau_{IDT}}{\partial T_c} \cdot \sigma_{T_c}\right)^2 + \left(\frac{\partial \tau_{IDT}}{\partial p_c} \cdot \sigma_{p_c}\right)^2 + \left(\frac{\partial \tau_{IDT}}{\partial \varphi} \cdot \sigma_{\varphi}\right)^2 + \left(\frac{\partial \tau_{IDT}}{\partial [D]} \cdot \sigma_{[D]}\right)^2} \quad (E30)$$

By substituting Equatons E25-29 into Equation E30 and using

average values for $\bar{\sigma}_{T_c} \approx \sigma_{\bar{T}_c}$ and $\frac{\partial \bar{T}_c}{\partial p_c} \approx \frac{\partial T_c}{\partial p_c} \Big|_{\bar{T}_c}$,

the average uncertainty ($\bar{\sigma}_{IDT}$) of the measured ignition delay times in RCM regime for P2C7 dataset (as one of the studied cases with high uncertainty) at $\bar{T}_c = 918.4 \text{ K}$ would be calculated based on a Python code developed by Weber et al ²⁵ as follows:

$$\bar{\sigma}_{T_c} = 3.55 \text{ K}$$

$$\bar{\sigma}_{IDT} = \sqrt{(-5.652628405 \times 10^{-3})^2 + (-2.572172296 \times 10^{-4})^2 + (-2.193803353 \times 10^{-4})^2 + (3.354450762 \times 10^{-4})^2} = \sqrt{3.217901972 \times 10^{-5}} = \pm 5.673 \text{ ms} \approx \pm 11\%$$

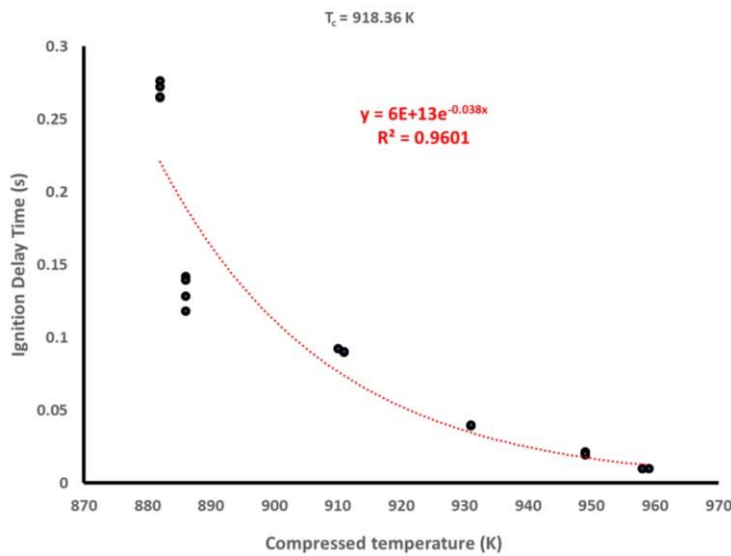


Figure ES14. Correlating ignition delay time versus compressed temperature data using an exponential expression.

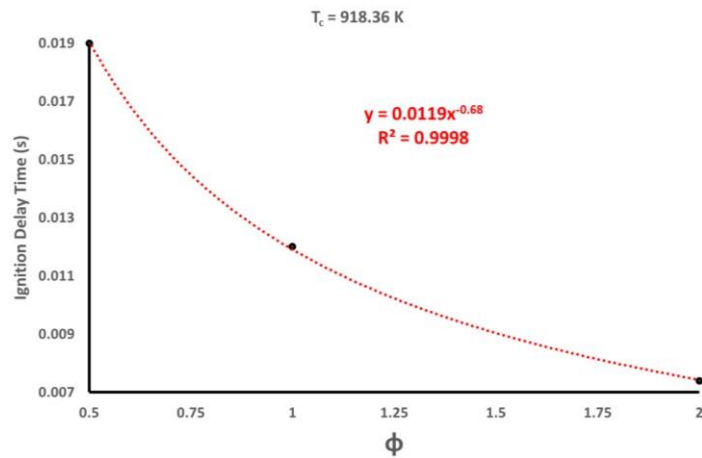


Figure ES15. Correlating ignition delay time versus equivalence ratio at $\bar{T}_c = 918.36 \text{ K}$ using a power expression.

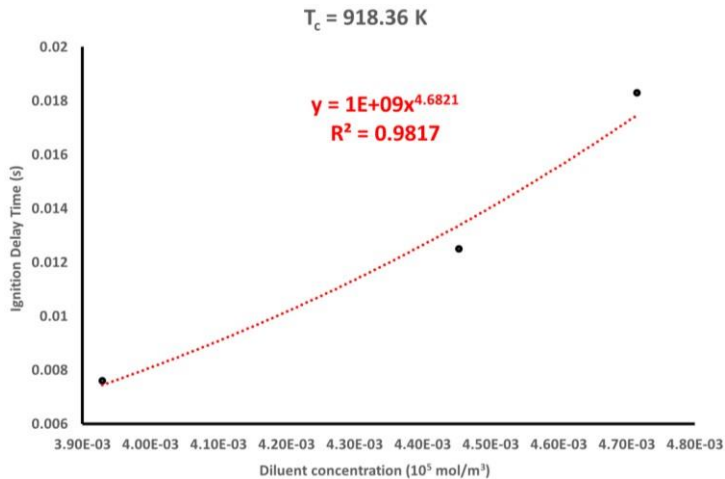


Figure ES16. Correlating ignition delay time versus diluent concentration at $T_c = 918.36 \text{ K}$ using a power expression.

9. NUIG Rapid Compression Machine Traces

In this section, the pressure histories of all tested reactive and non-reactive mixtures in NUIG-RCM alongside with their corresponding simulation's profile have been demonstrated in Figure S17 to Figure S79. All the simulations (sim_Reactive) have been carried out using AramcoMech 3.0 chemical mechanism, otherwise, it is mentioned in the caption or legend of each profile. Also, for covering the studied temperature range, the reaction chamber of NUIG-RCM has been heated-up from 30~110 °C for a specific test mixture. Otherwise, the diluent contents of the test mixtures have been changed (adding argon instead of nitrogen as a diluent to the test mixture) to achieve higher compressed temperatures.

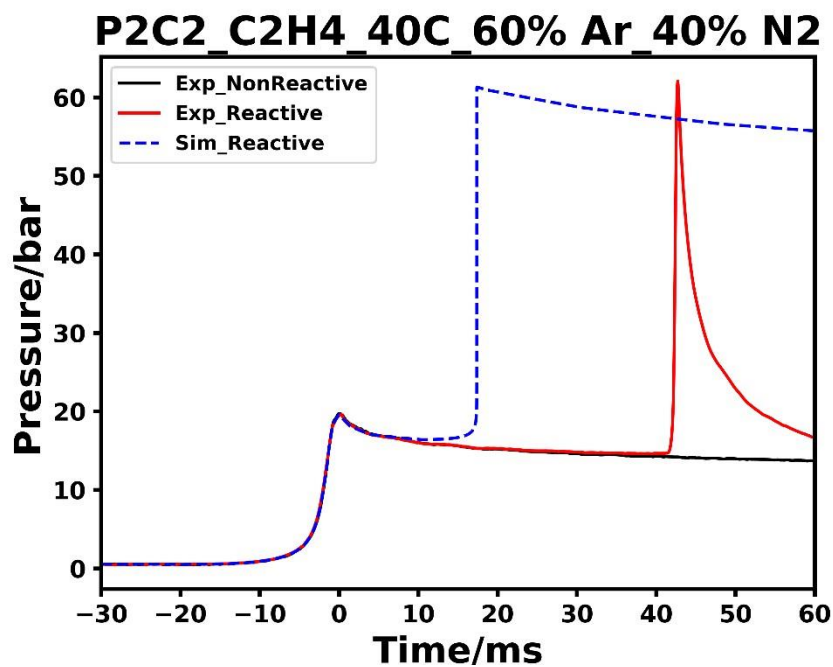


Figure ES17. Pressure history of tested reactive and non-reactive mixtures of P2C2 case alongside the simulation's profile for initial temperature of 313 K.

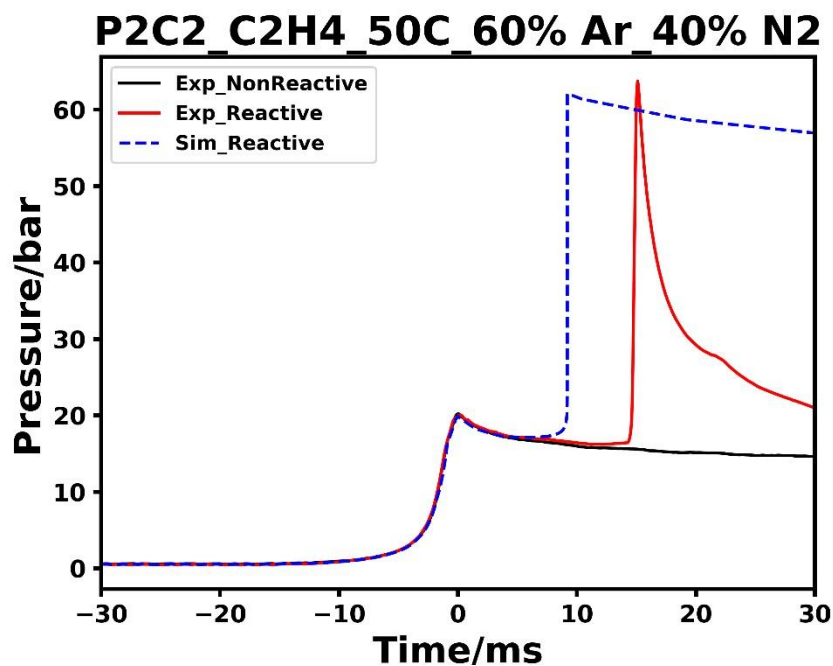


Figure ES18. Pressure history of tested reactive and non-reactive mixtures of P2C2 case alongside the simulation's profile for initial temperature of 323 K.

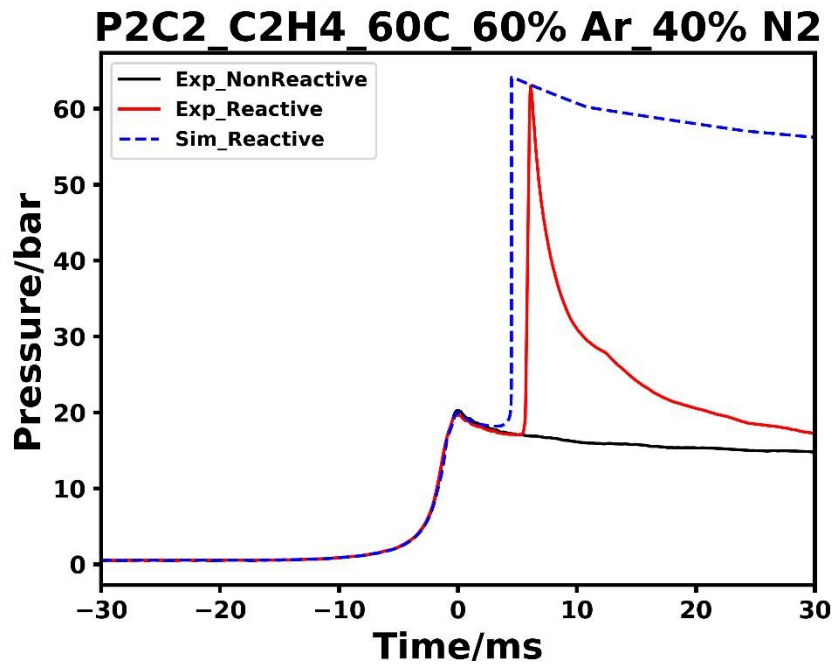


Figure ES19. Pressure history of tested reactive and non-reactive mixtures of P2C2 case alongside the simulation's profile for initial temperature of 333 K.

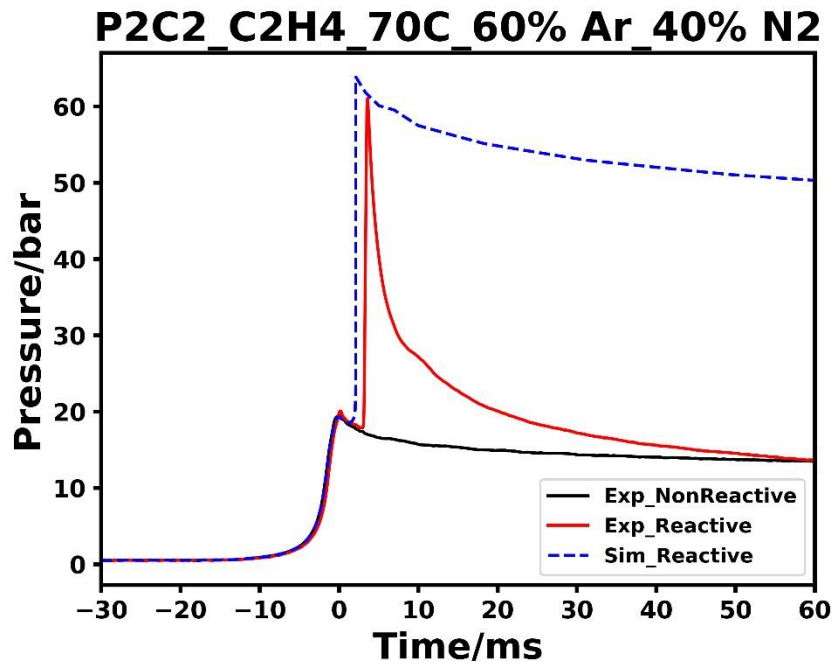


Figure ES20. Pressure history of tested reactive and non-reactive mixtures of P2C2 case alongside the simulation's profile for initial temperature of 343 K.

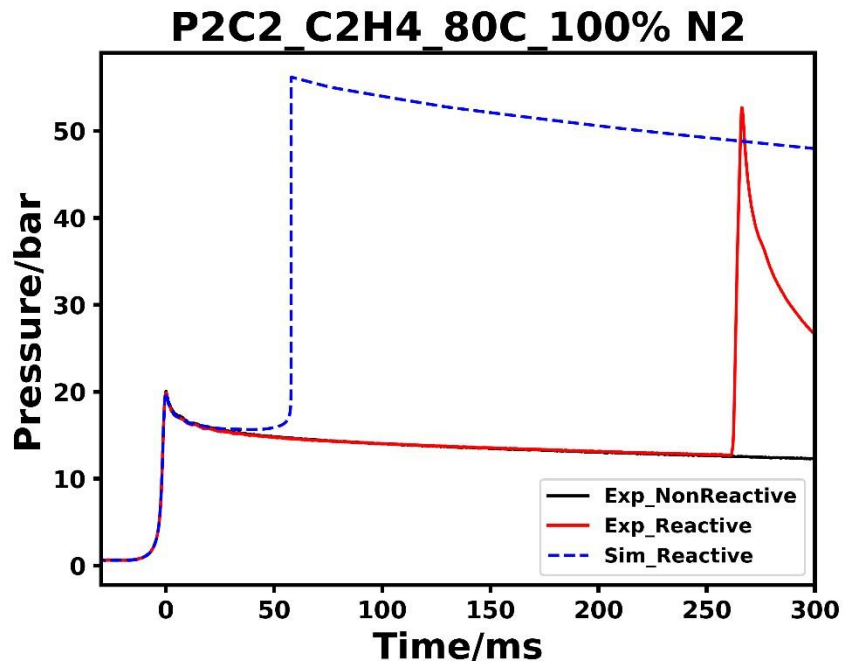


Figure ES21. Pressure history of tested reactive and non-reactive mixtures of P2C2 case alongside the simulation's profile for initial temperature of 353 K.

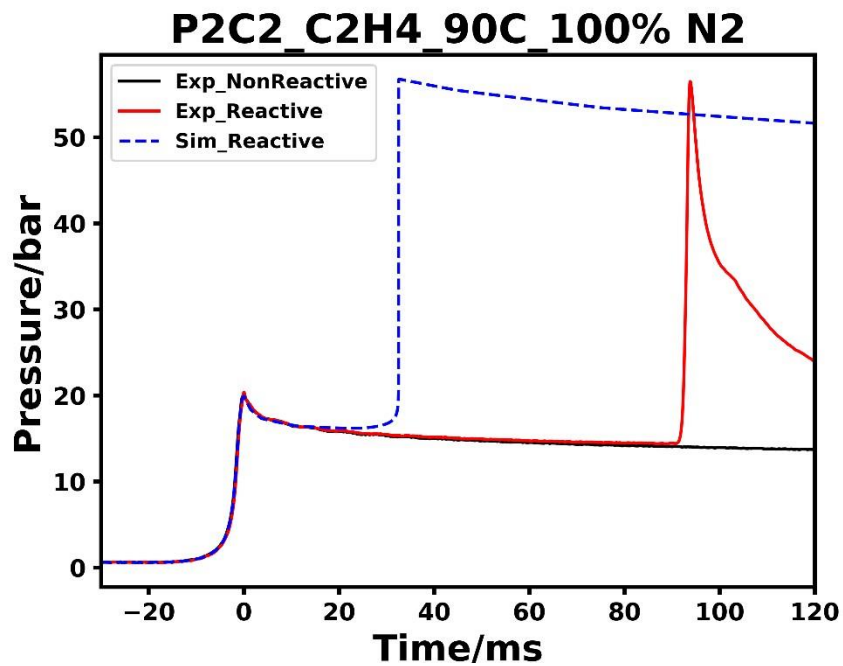


Figure ES22. Pressure history of tested reactive and non-reactive mixtures of P2C2 case alongside the simulation's profile for initial temperature of 363 K.

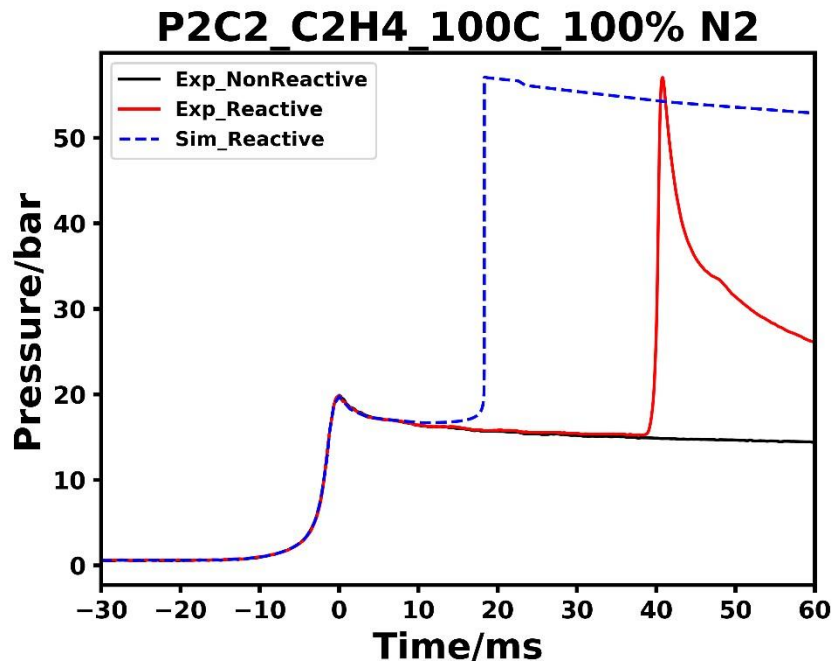


Figure ES23. Pressure history of tested reactive and non-reactive mixtures of P2C2 case alongside the simulation's profile for initial temperature of 383 K.

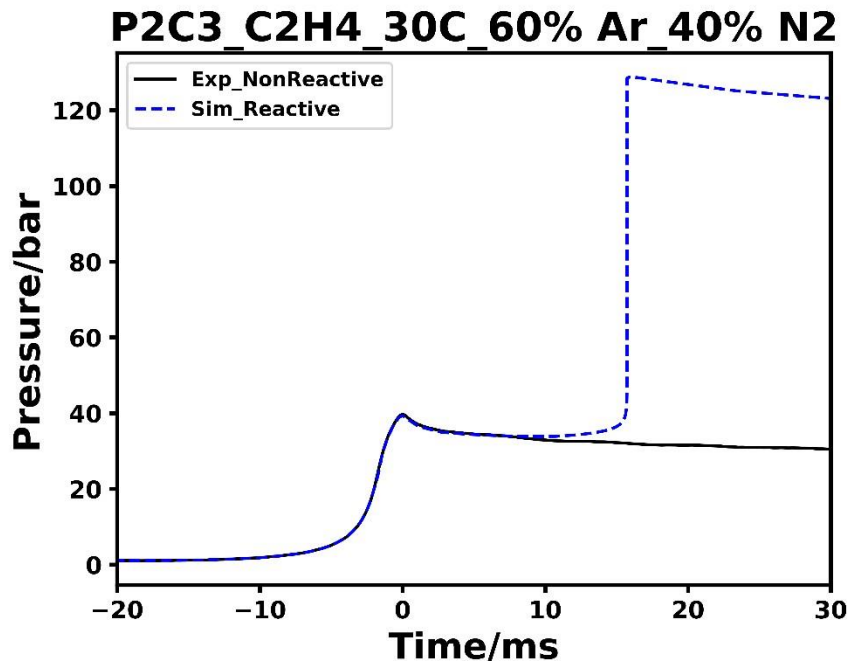


Figure ES24. Pressure history of tested reactive and non-reactive mixtures of P2C3 case alongside the simulation's profile for initial temperature of 303 K.

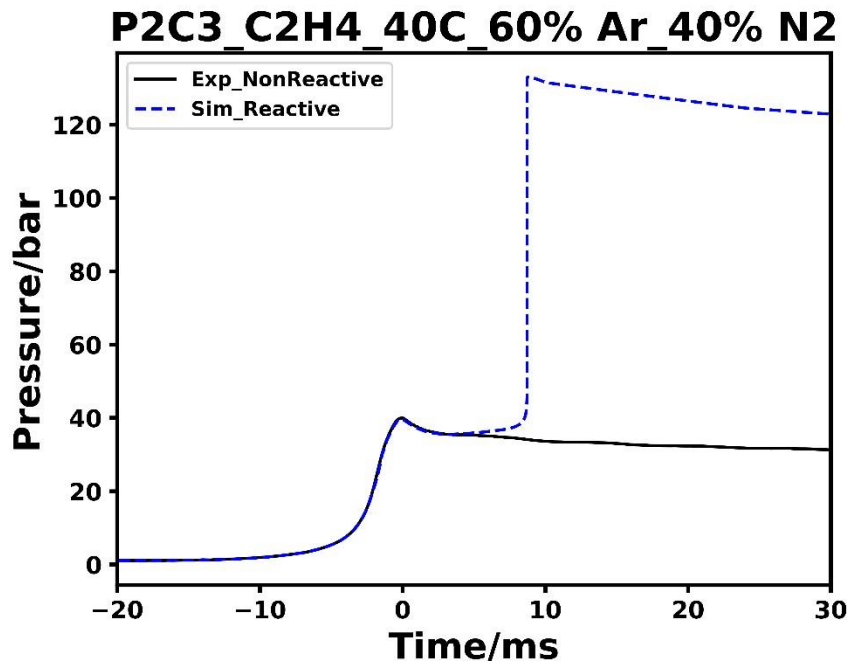


Figure ES25. Pressure history of tested reactive and non-reactive mixtures of P2C3 case alongside the simulation's profile for initial temperature of 313 K.

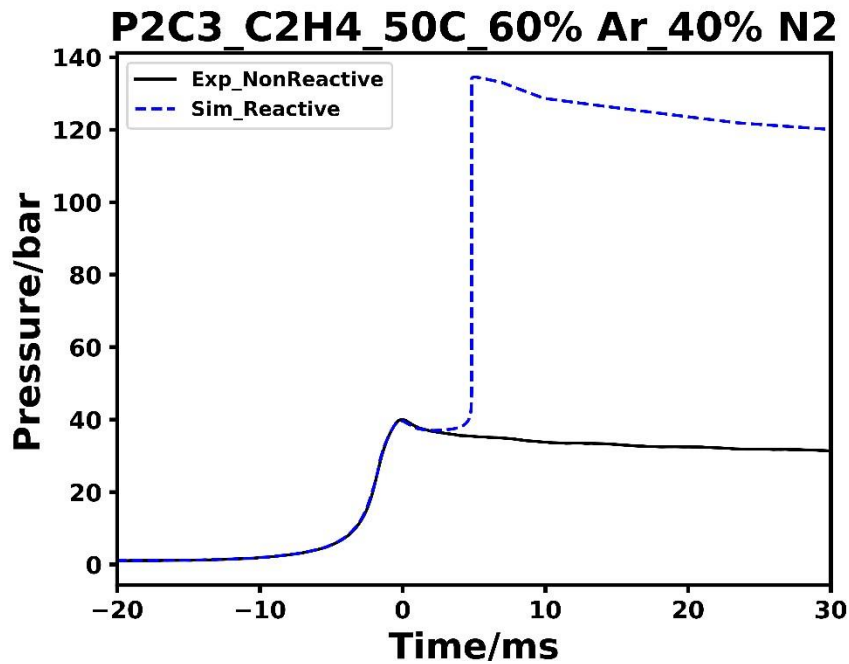


Figure ES26. Pressure history of tested reactive and non-reactive mixtures of P2C3 case alongside the simulation's profile for initial temperature of 323 K.

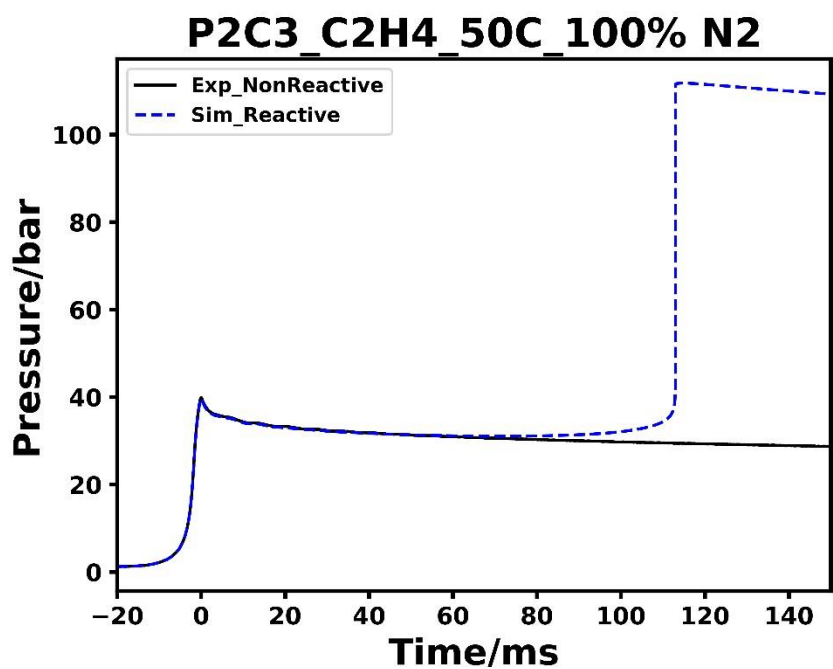


Figure ES27. Pressure history of tested reactive and non-reactive mixtures of P2C3 case alongside the simulation's profile for initial temperature of 323 K.

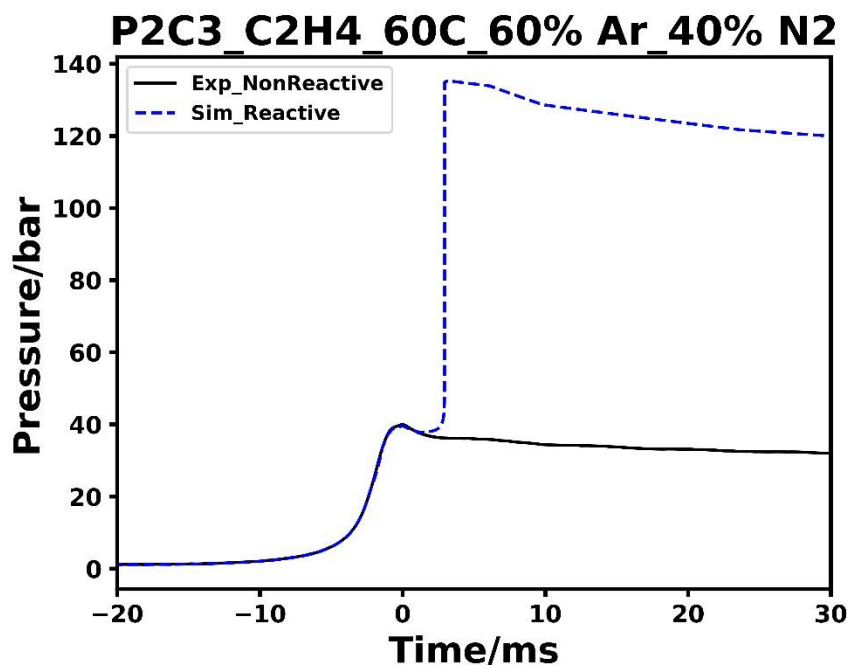


Figure ES28. Pressure history of tested reactive and non-reactive mixtures of P2C2 case alongside the simulation's profile for initial temperature of 333 K.

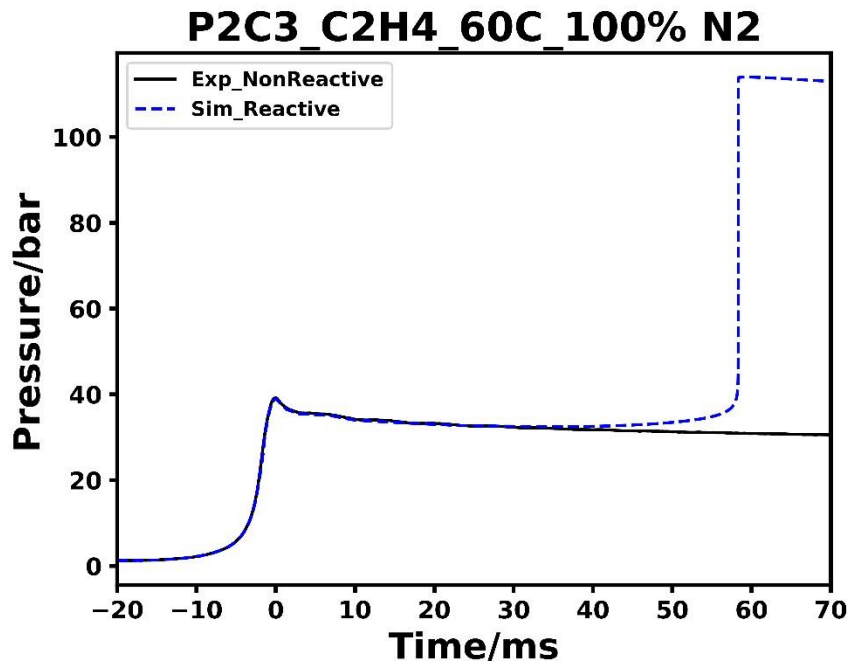


Figure ES29. Pressure history of tested reactive and non-reactive mixtures of P2C3 case alongside the simulation's profile for initial temperature of 333 K (100% N₂).

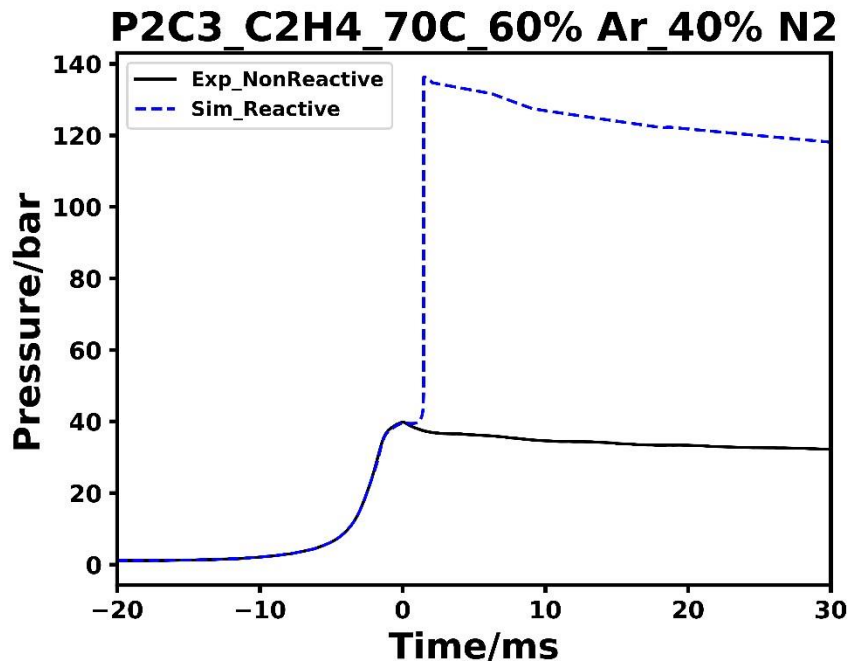


Figure ES30. Pressure history of tested reactive and non-reactive mixtures of P2C3 case alongside the simulation's profile for initial temperature of 343 K.

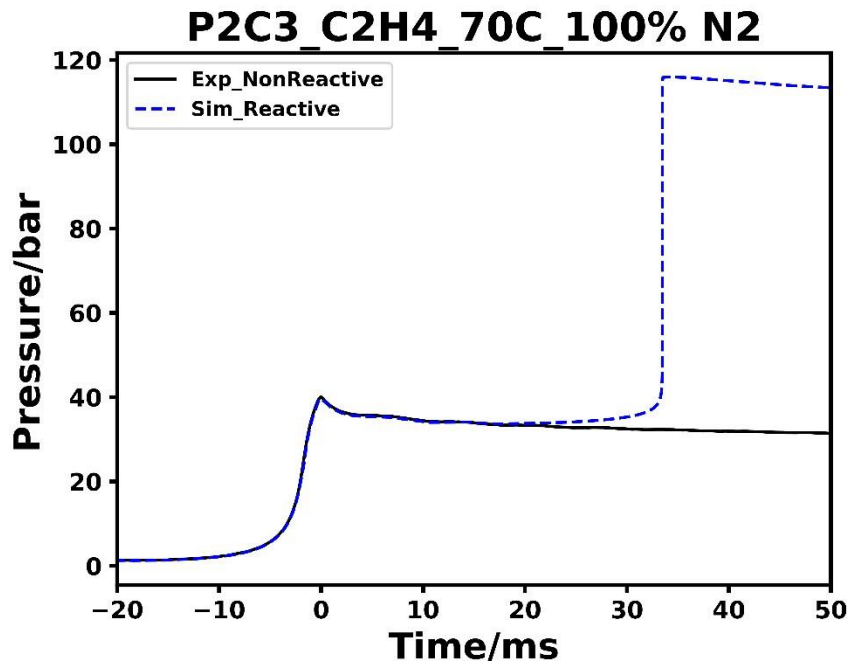


Figure ES31. Pressure history of tested reactive and non-reactive mixtures of P2C3 case alongside the simulation's profile for initial temperature of 343 K.

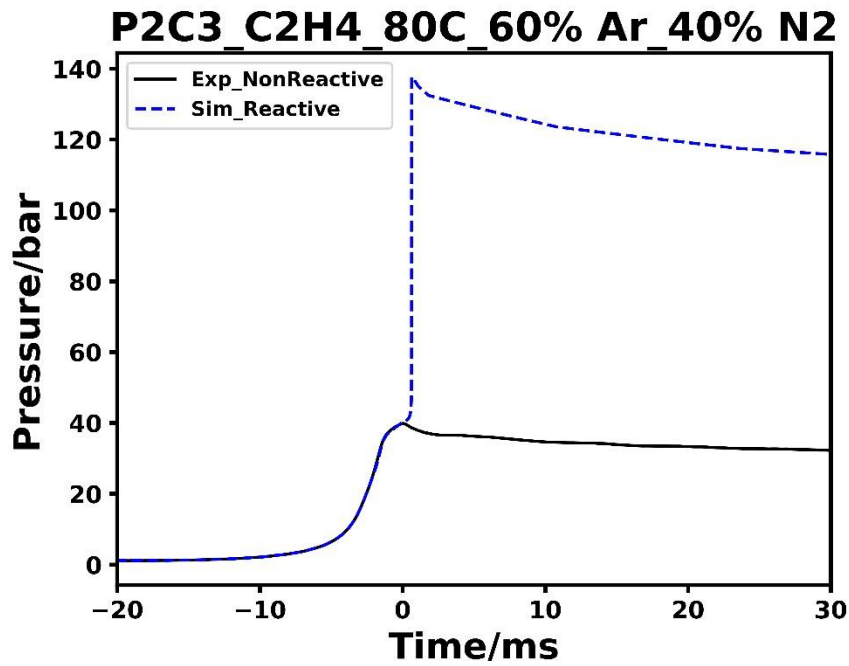


Figure ES32. Pressure history of tested reactive and non-reactive mixtures of P2C3 case alongside the simulation's profile for initial temperature of 353 K.

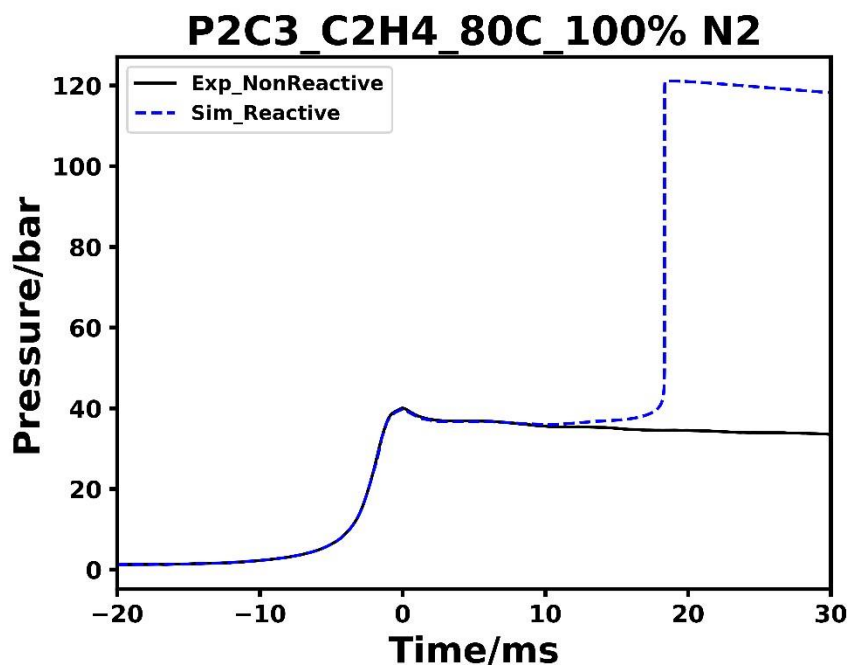


Figure ES33. Pressure history of tested reactive and non-reactive mixtures of P2C3 case alongside the simulation's profile for initial temperature of 353 K (100% N₂).

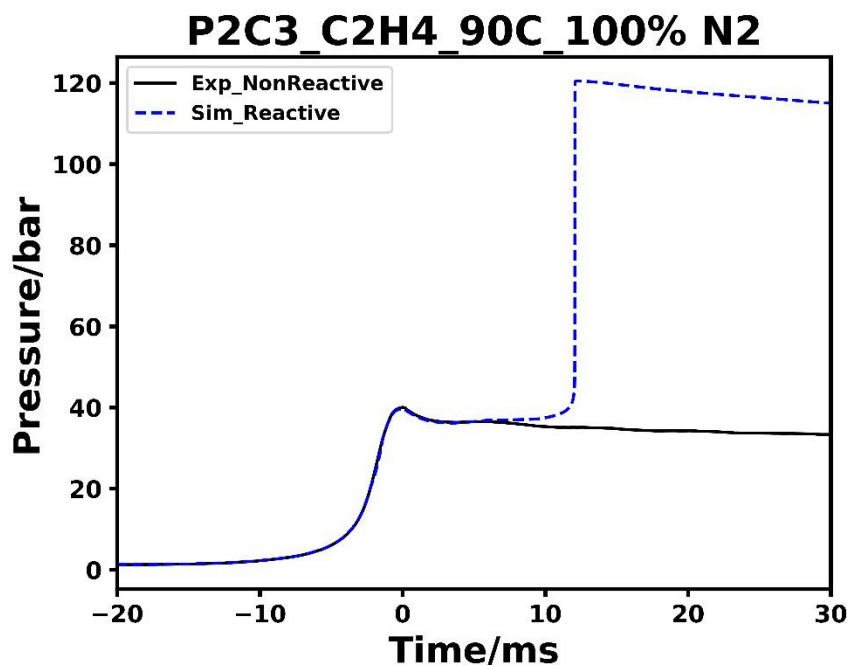


Figure ES34. Pressure history of tested reactive and non-reactive mixtures of P2C3 case alongside the simulation's profile for initial temperature of 363 K.

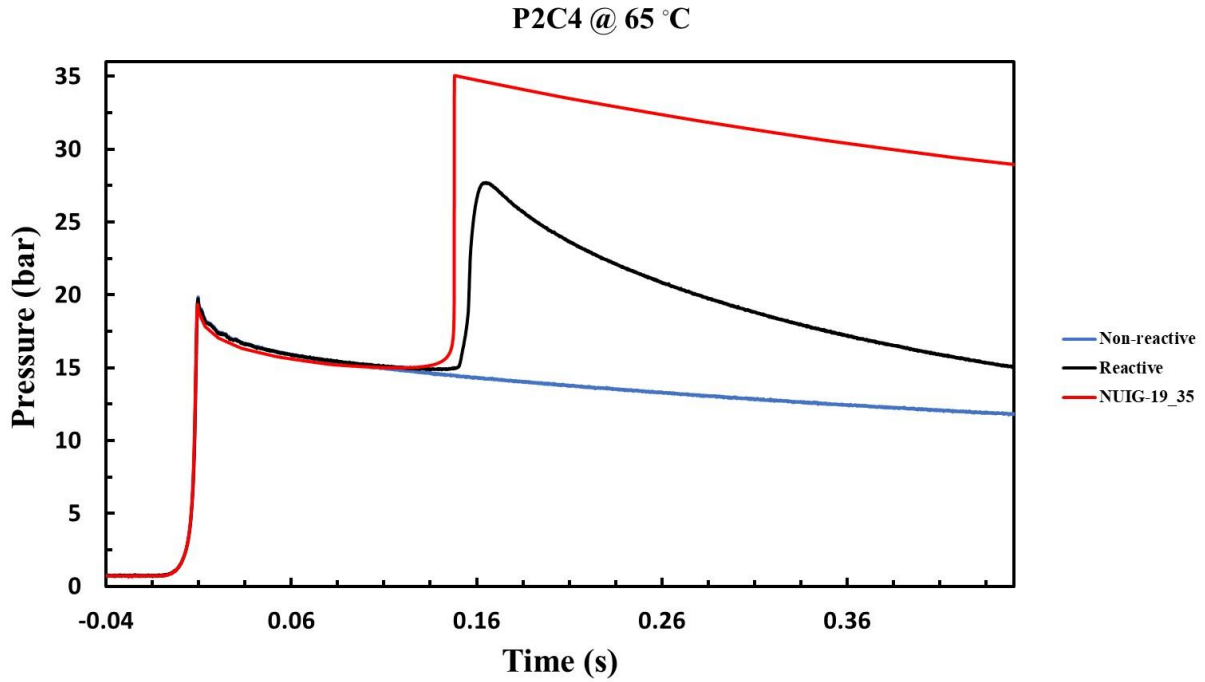


Figure ES35. Pressure history of tested reactive and non-reactive mixtures of P2C4 case alongside the simulation's profile for initial temperature of 338 K.

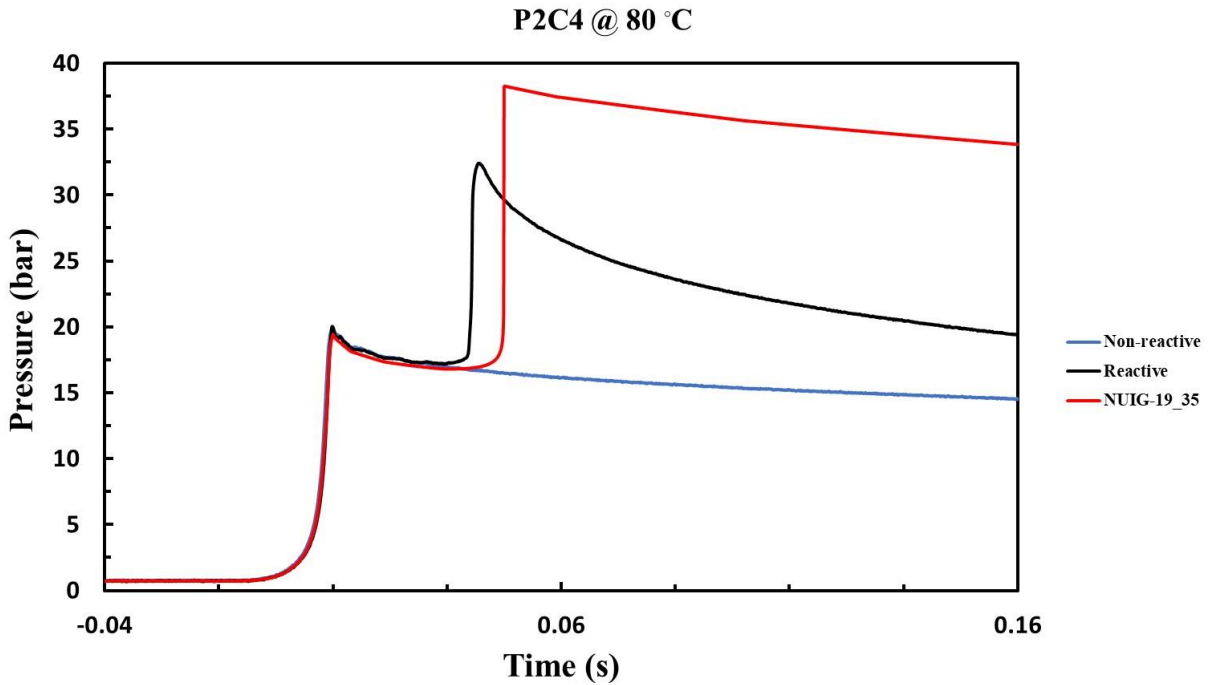


Figure ES36. Pressure history of tested reactive and non-reactive mixtures of P2C4 case alongside the simulation's profile for initial temperature of 353 K.

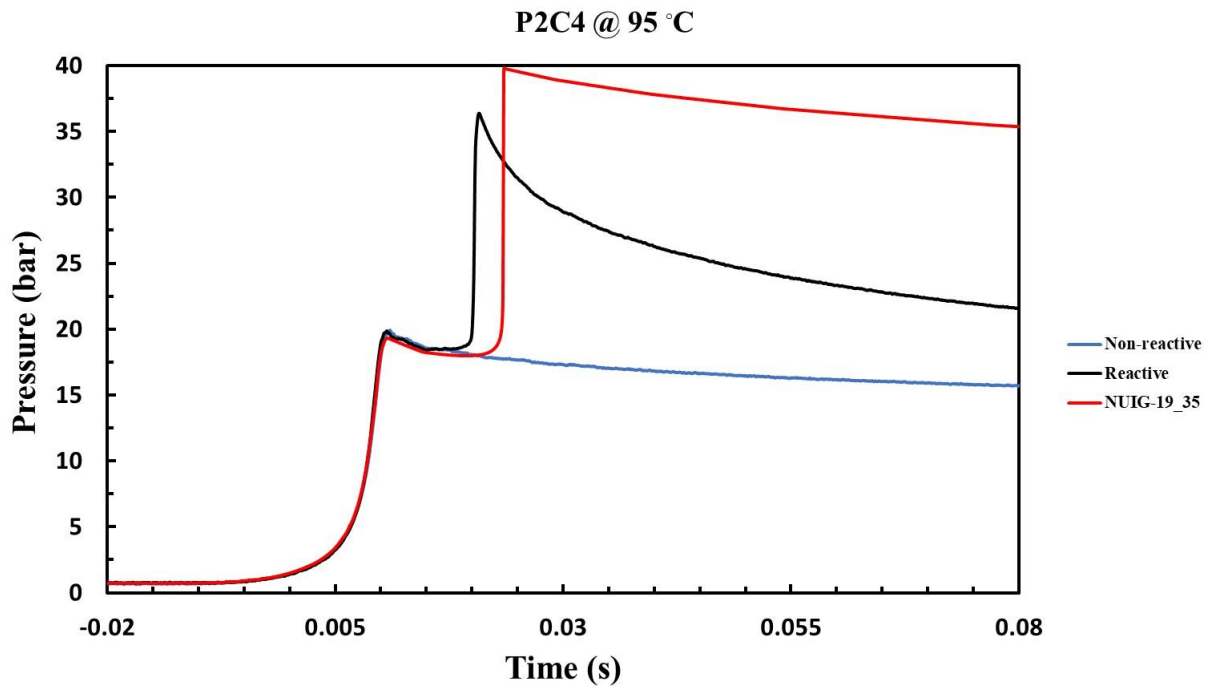


Figure ES37. Pressure history of tested reactive and non-reactive mixtures of P2C4 case alongside the simulation's profile for initial temperature of 368 K.

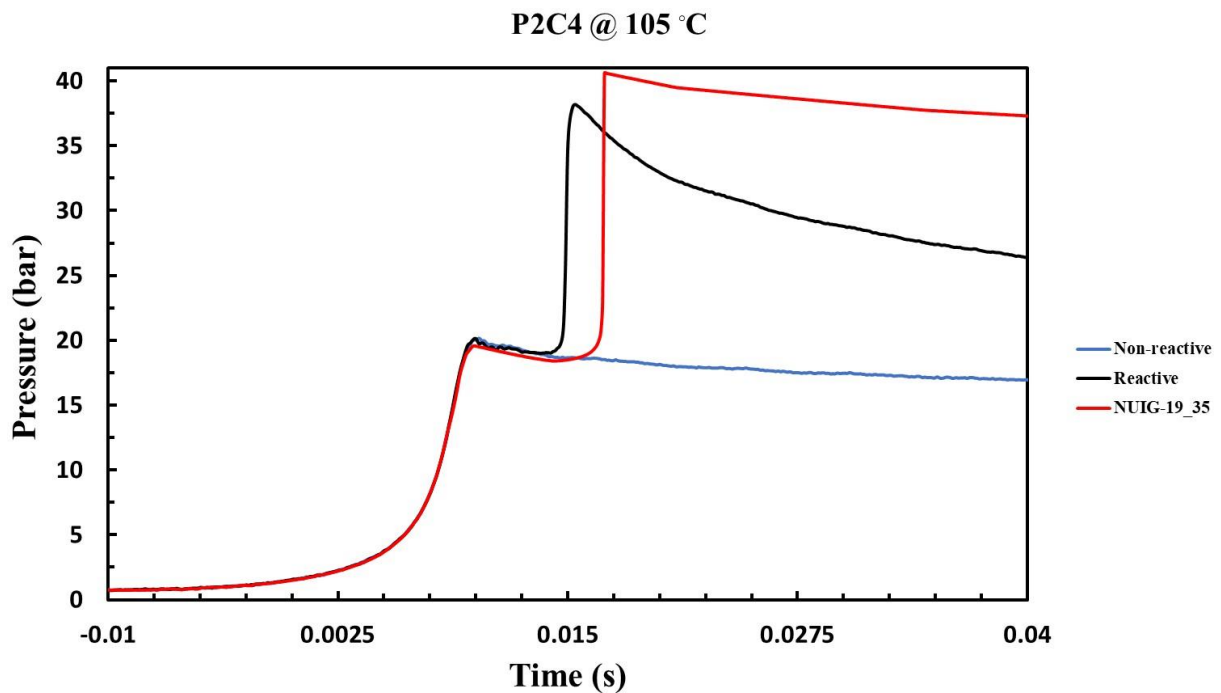


Figure ES38. Pressure history of tested reactive and non-reactive mixtures of P2C4 case alongside the simulation's profile for initial temperature of 378 K.

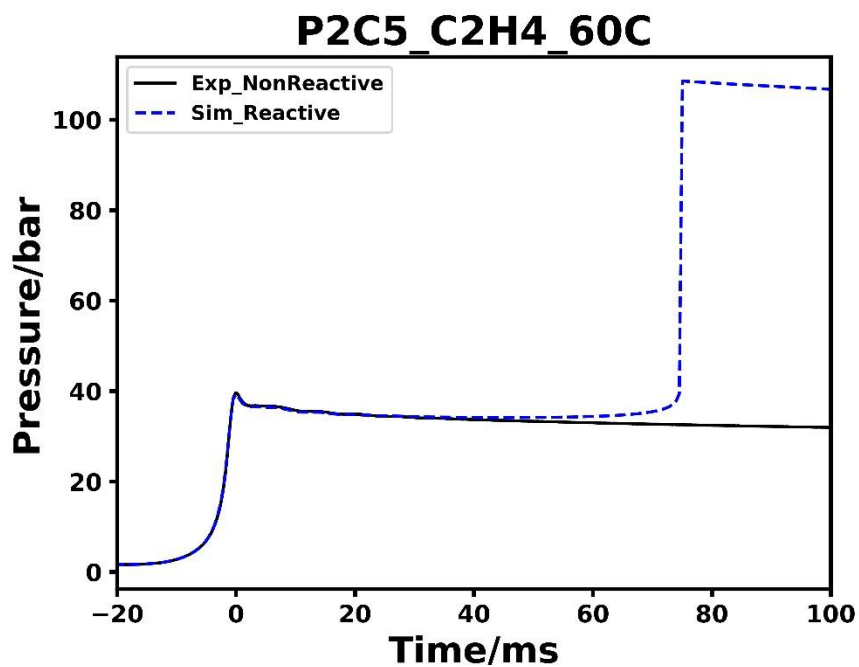


Figure ES39. Pressure history of tested reactive and non-reactive mixtures of P2C5 case alongside the simulation's profile for initial temperature of 333 K.

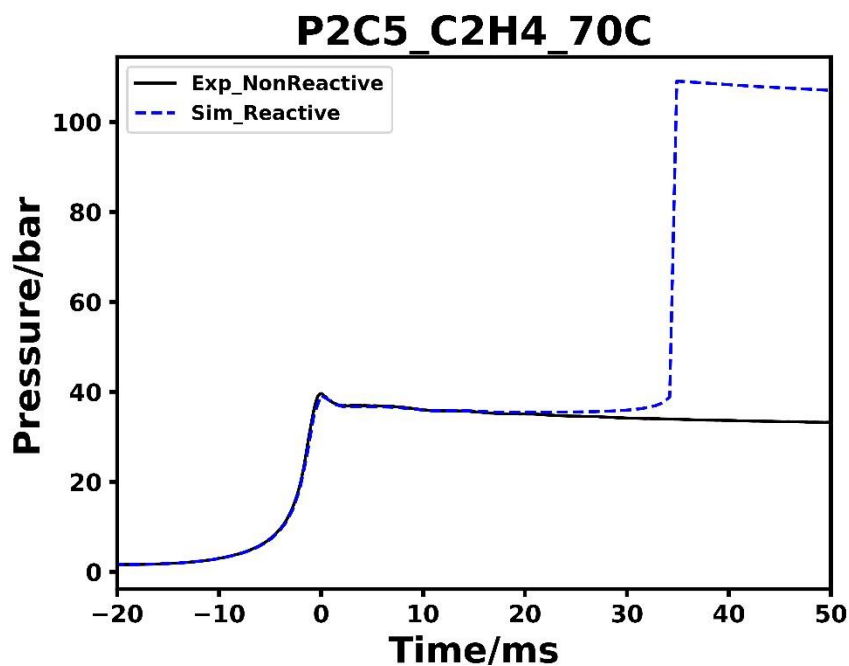


Figure ES40. Pressure history of tested reactive and non-reactive mixtures of P2C5 case alongside the simulation's profile for initial temperature of 343 K.

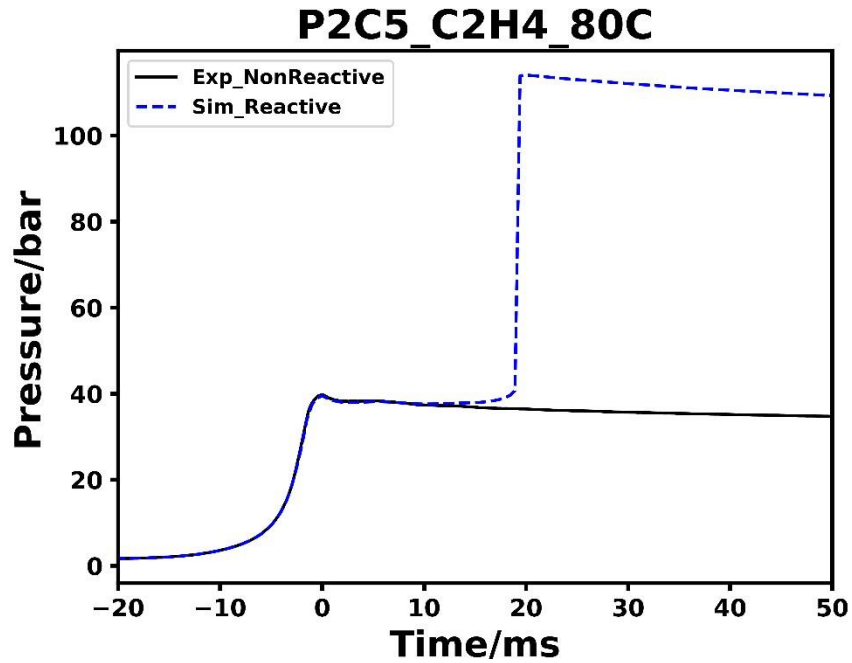


Figure ES41. Pressure history of tested reactive and non-reactive mixtures of P2C5 case alongside the simulation's profile for initial temperature of 353 K.

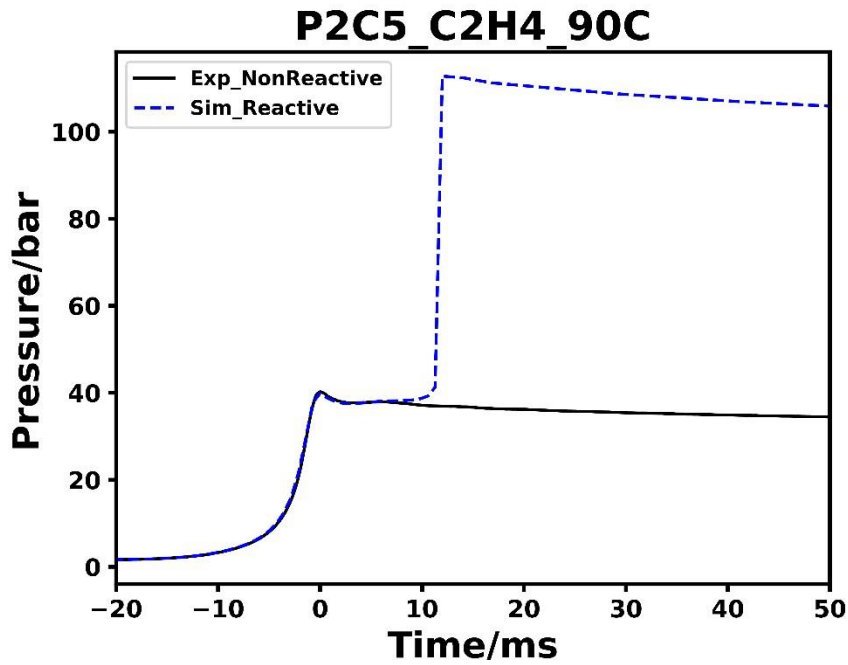


Figure ES42. Pressure history of tested reactive and non-reactive mixtures of P2C5 case alongside the simulation's profile for initial temperature of 363 K.

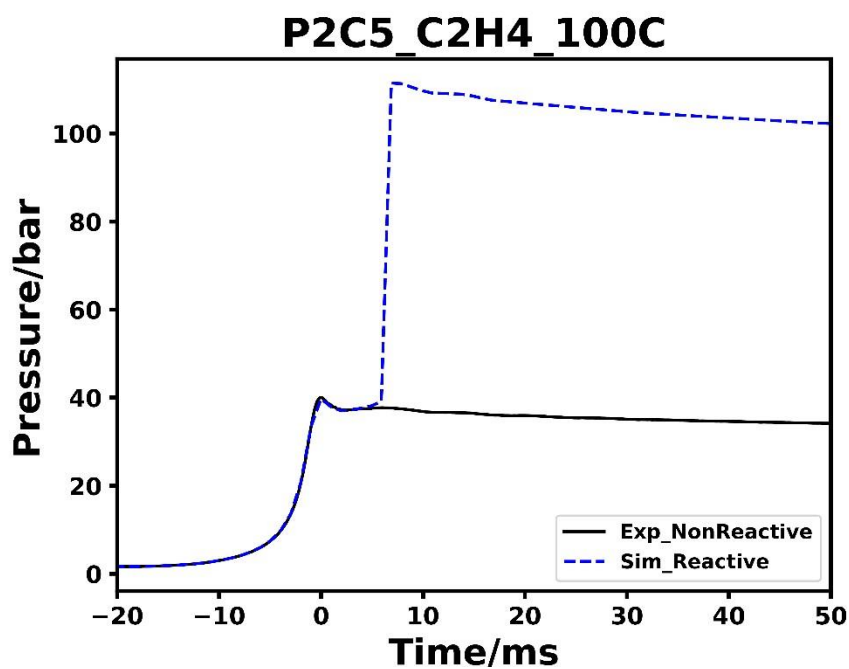


Figure ES43. Pressure history of tested reactive and non-reactive mixtures of P2C5 case alongside the simulation's profile for initial temperature of 373 K.

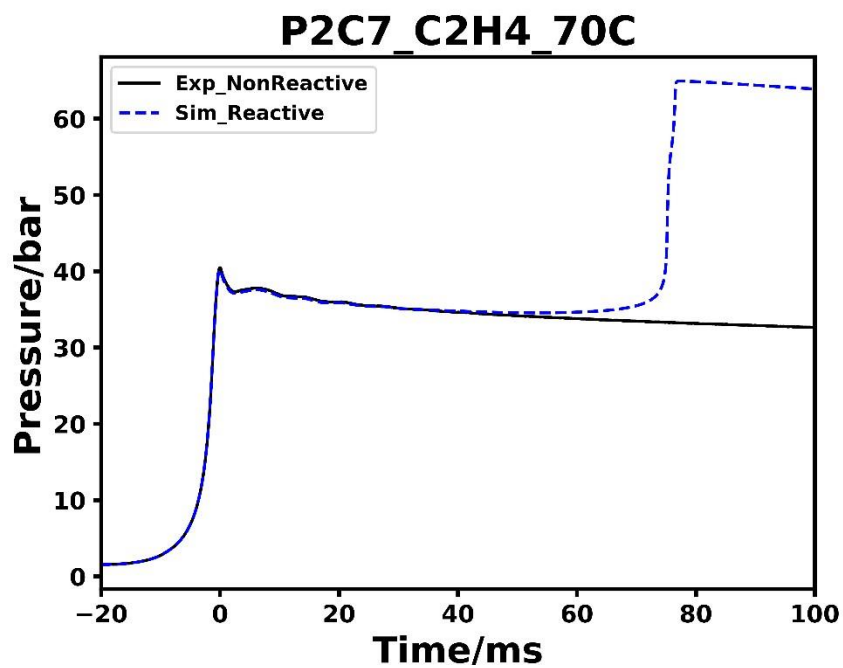


Figure ES44. Pressure history of tested reactive and non-reactive mixtures of P2C7 case alongside the simulation's profile for initial temperature of 343 K.

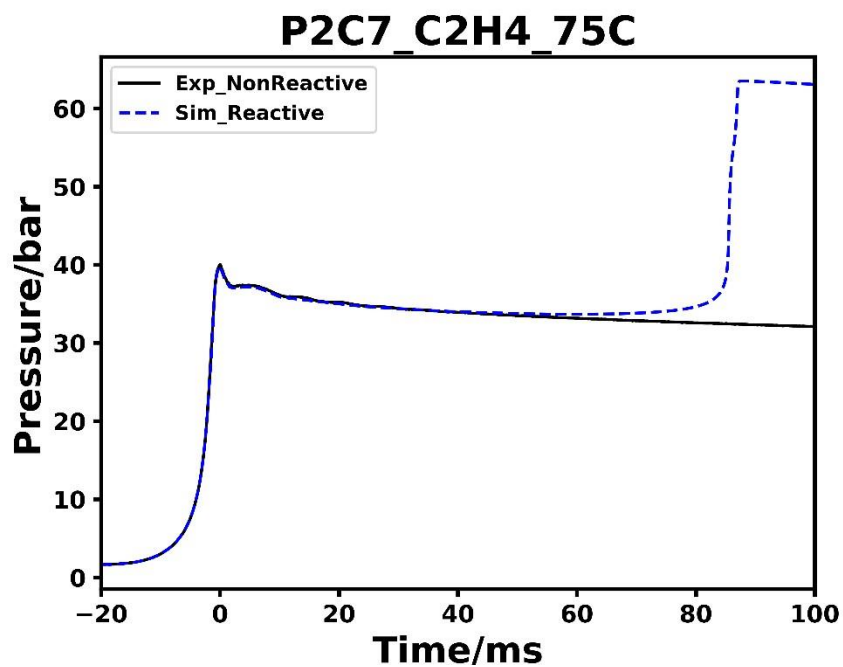


Figure ES45. Pressure history of tested reactive and non-reactive mixtures of P2C7 case alongside the simulation's profile for initial temperature of 348 K.

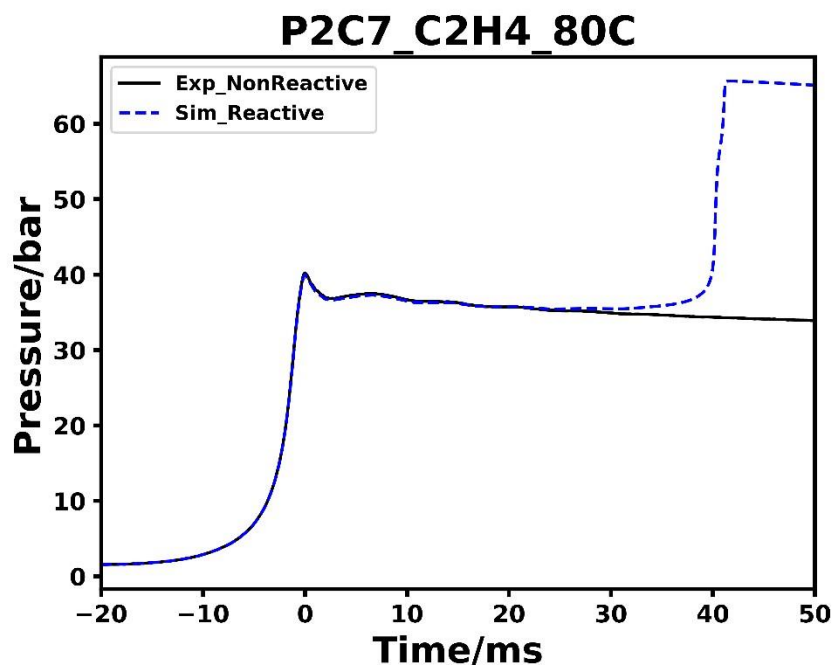


Figure ES46. Pressure history of tested reactive and non-reactive mixtures of P2C7 case alongside the simulation's profile for initial temperature of 353 K.

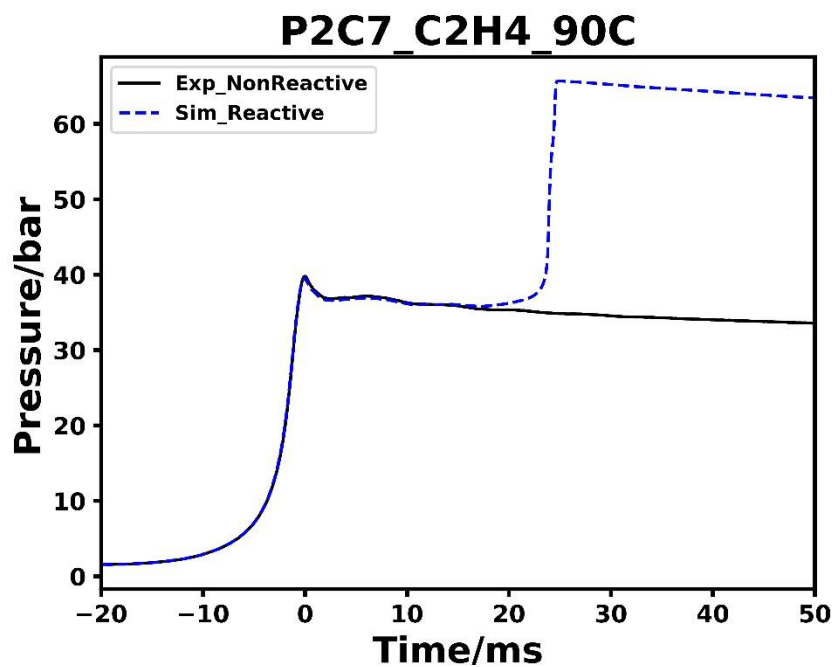


Figure ES47. Pressure history of tested reactive and non-reactive mixtures of P2C7 case alongside the simulation's profile for initial temperature of 363 K.

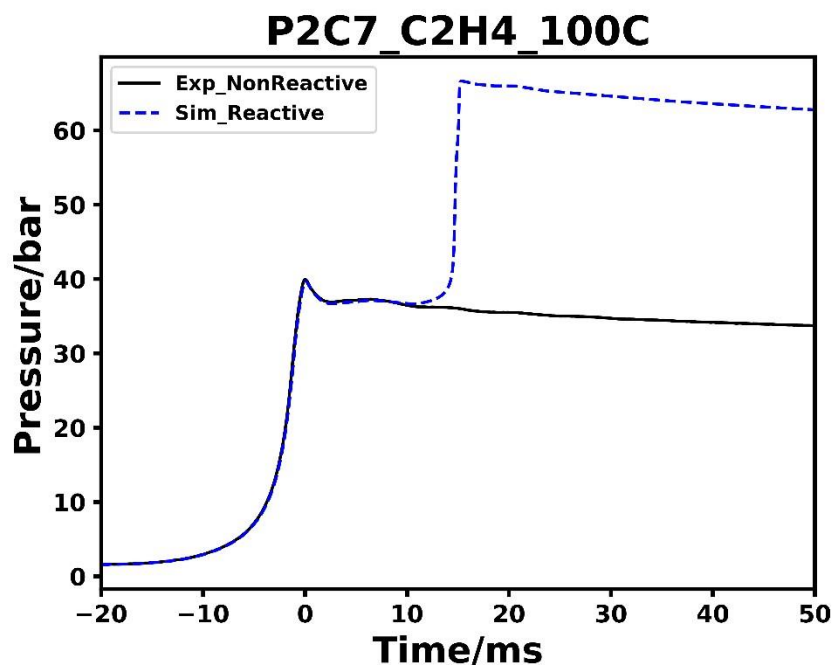


Figure ES48. Pressure history of tested reactive and non-reactive mixtures of P2C7 case alongside the simulation's profile for initial temperature of 373 K.

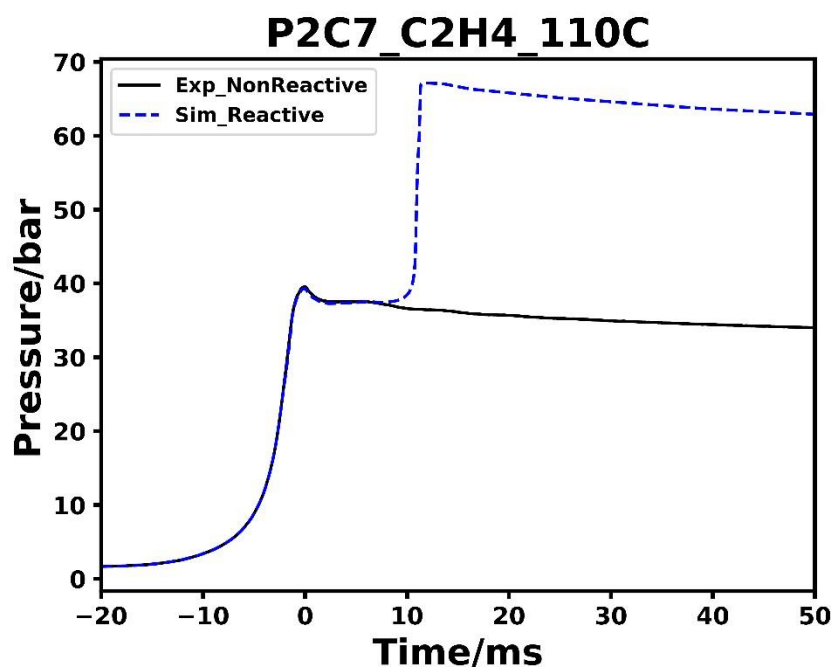


Figure ES49. Pressure history of tested reactive and non-reactive mixtures of P2C7 case alongside the simulation's profile for initial temperature of 383 K.

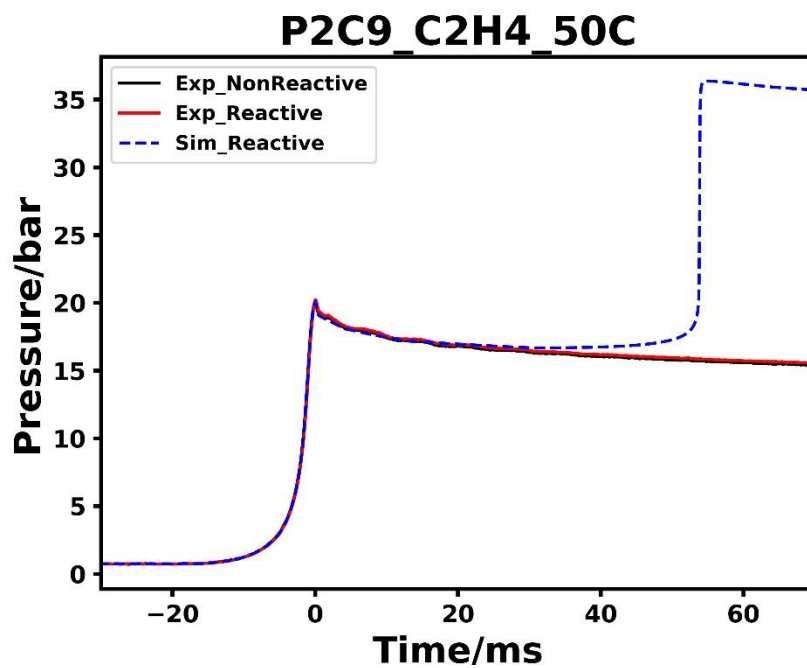


Figure ES50. Pressure history of tested reactive and non-reactive mixtures of P2C9 case alongside the simulation's profile for initial temperature of 323 K.

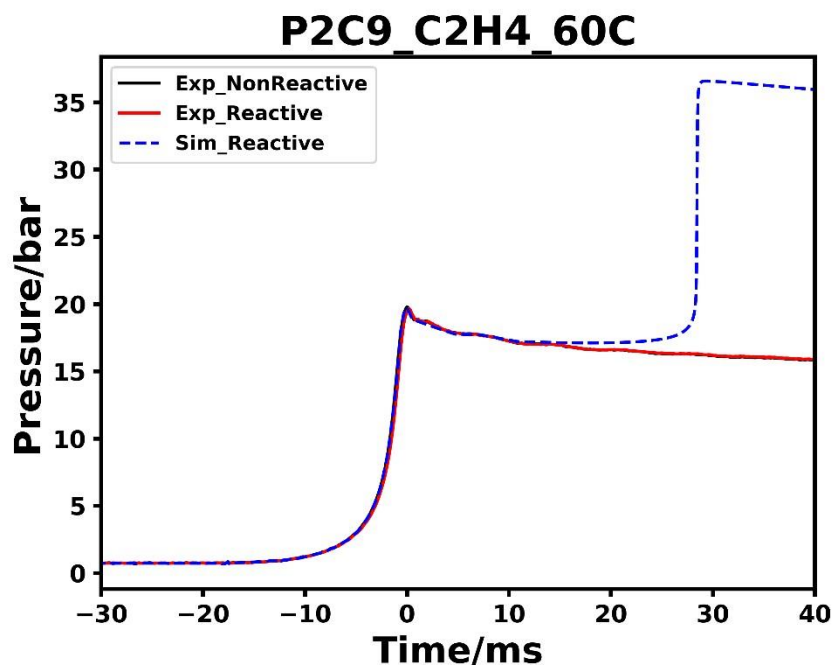


Figure ES51. Pressure history of tested reactive and non-reactive mixtures of P2C9 case alongside the simulation's profile for initial temperature of 333 K.

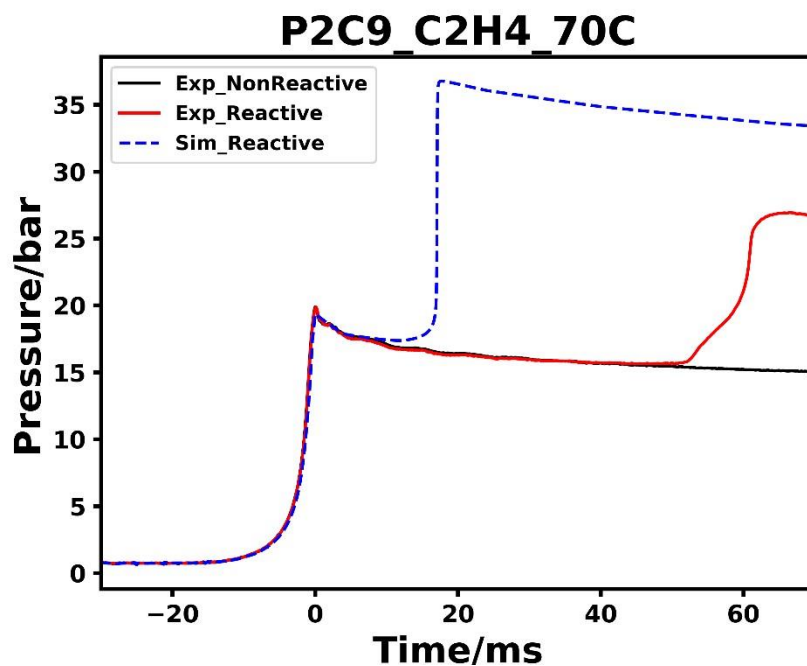


Figure ES52. Pressure history of tested reactive and non-reactive mixtures of P2C9 case alongside the simulation's profile for initial temperature of 343 K.

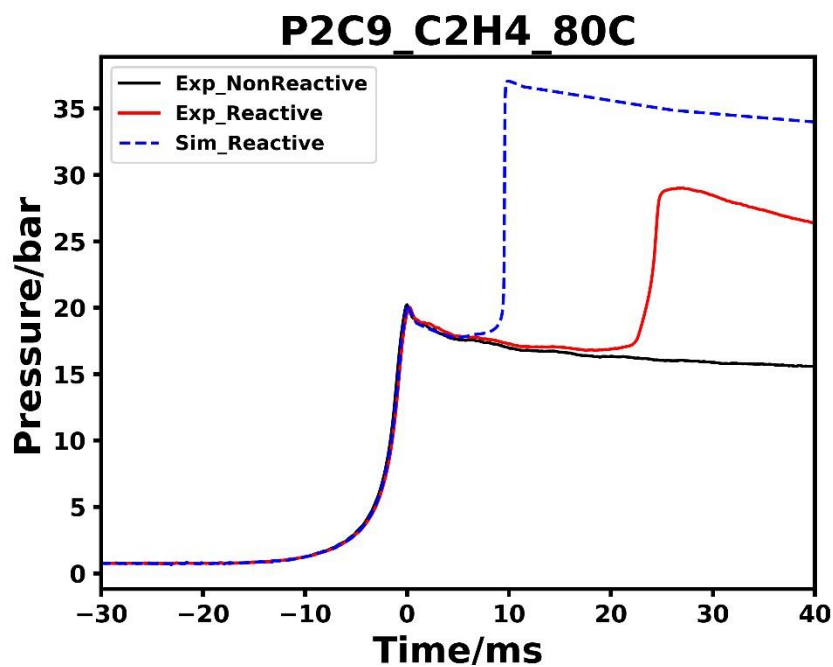


Figure ES53. Pressure history of tested reactive and non-reactive mixtures of P2C9 case alongside the simulation's profile for initial temperature of 353 K.

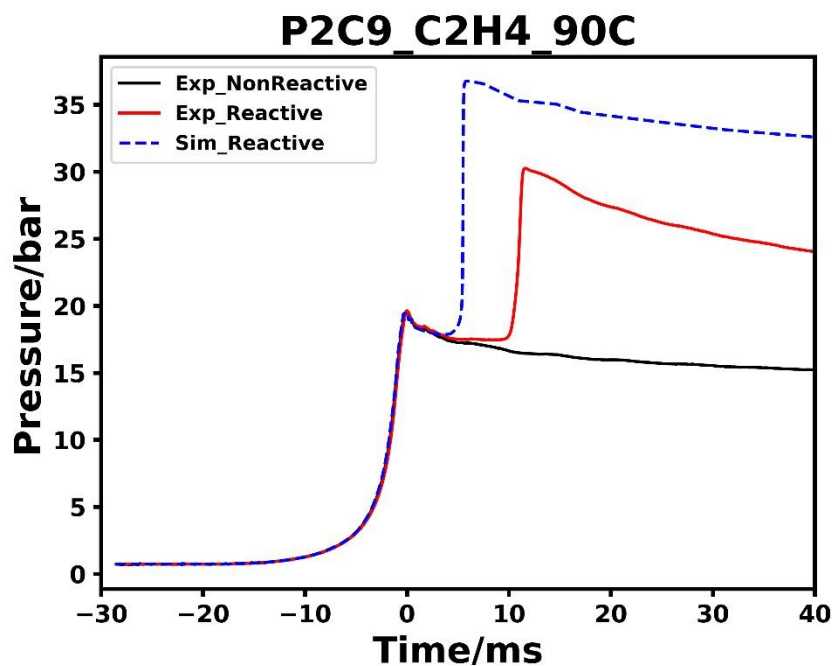


Figure ES54. Pressure history of tested reactive and non-reactive mixtures of P2C9 case alongside the simulation's profile for initial temperature of 363 K.

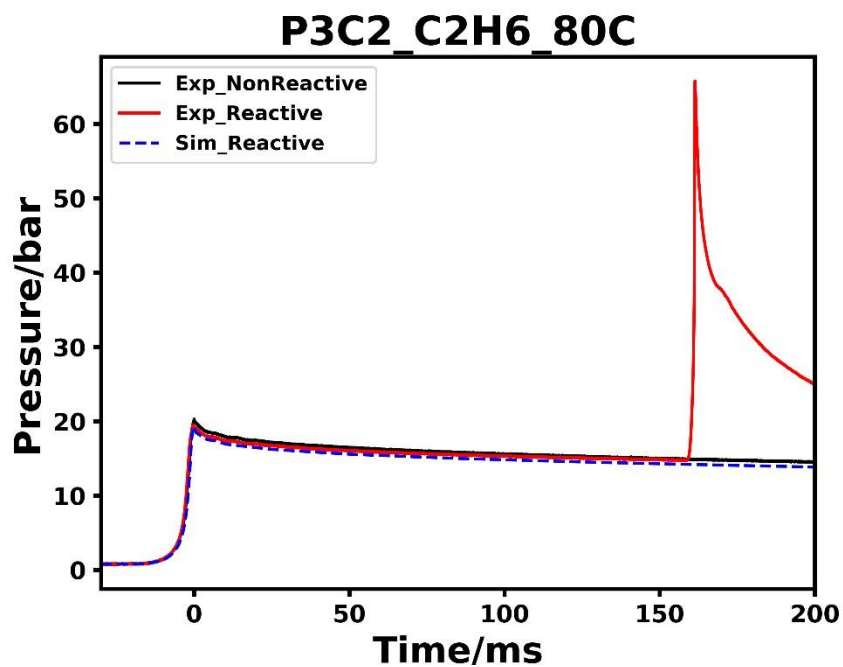


Figure ES55. Pressure history of tested reactive and non-reactive mixtures of P3C2 case alongside the simulation's profile for initial temperature of 353 K.

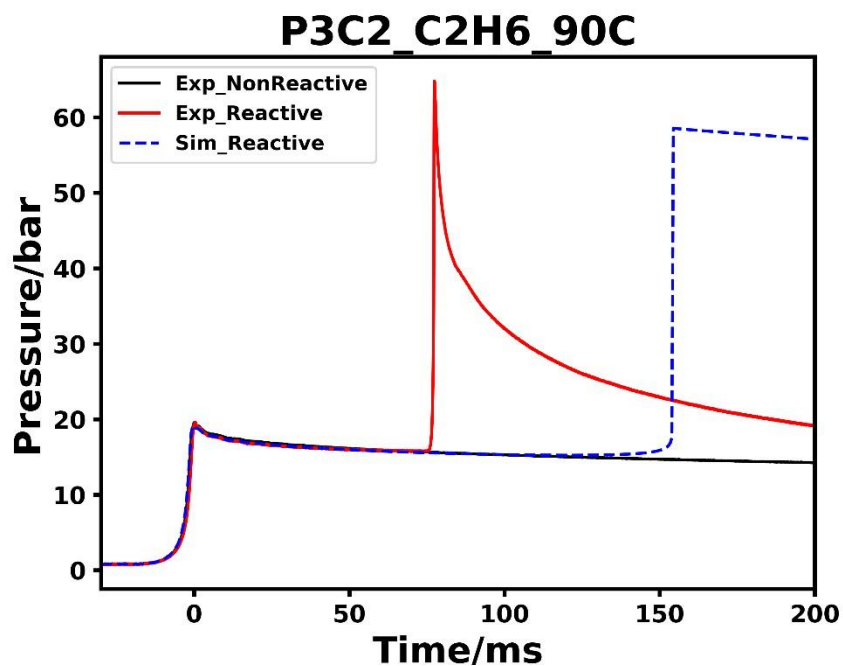


Figure ES56. Pressure history of tested reactive and non-reactive mixtures of P3C2 case alongside the simulation's profile for initial temperature of 363 K.

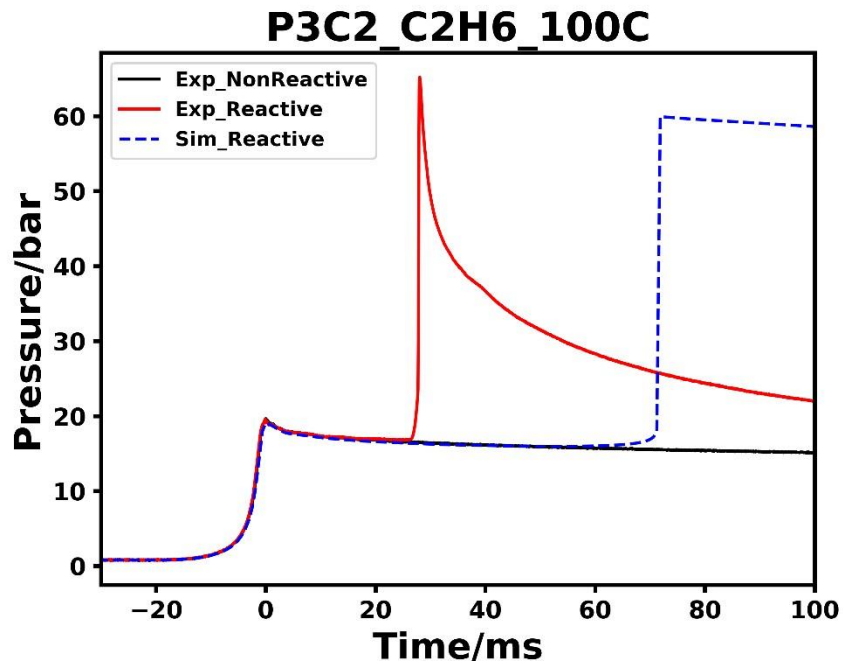


Figure ES57. Pressure history of tested reactive and non-reactive mixtures of P3C2 case alongside the simulation's profile for initial temperature of 373 K.

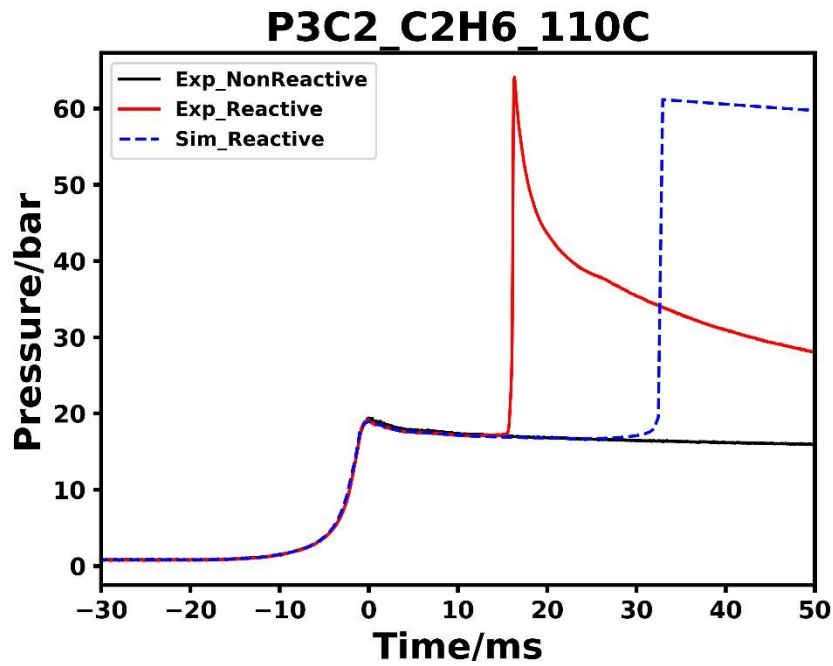


Figure ES58. Pressure history of tested reactive and non-reactive mixtures of P3C2 case alongside the simulation's profile for initial temperature of 383 K.

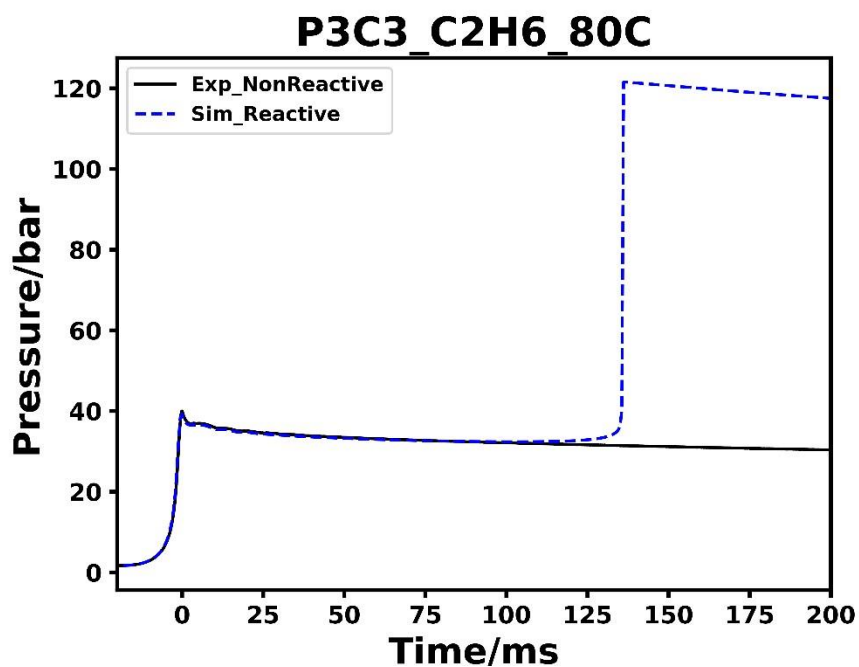


Figure ES59. Pressure history of tested reactive and non-reactive mixtures of P3C3 case alongside the simulation's profile for initial temperature of 353 K.

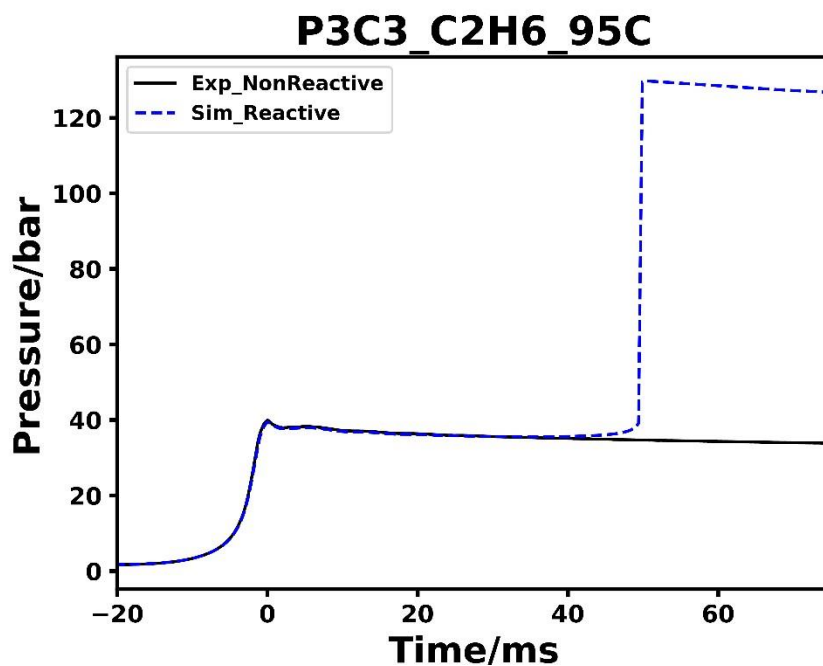


Figure ES60. Pressure history of tested reactive and non-reactive mixtures of P3C3 case alongside the simulation's profile for initial temperature of 368 K.

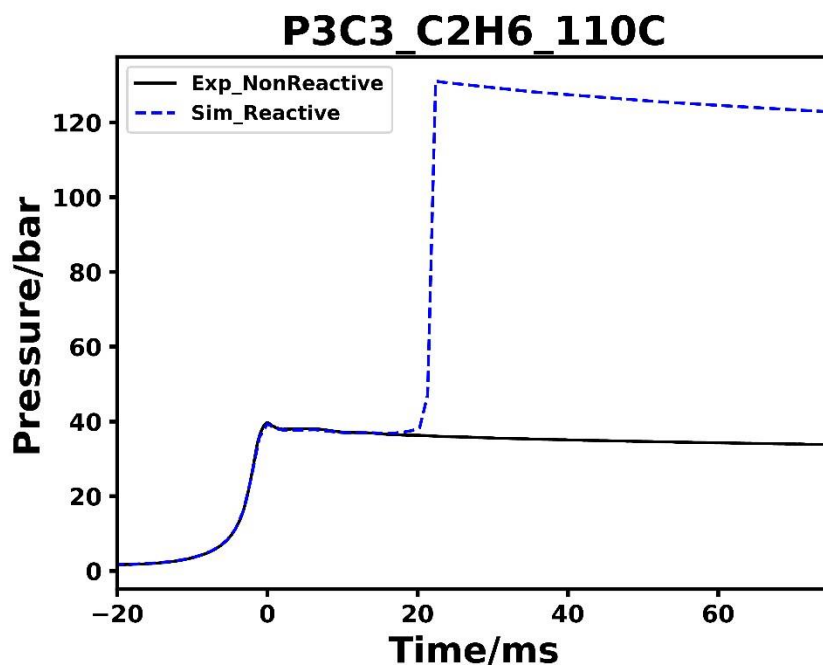


Figure ES61. Pressure history of tested reactive and non-reactive mixtures of P3C3 case alongside the simulation's profile for initial temperature of 383 K.

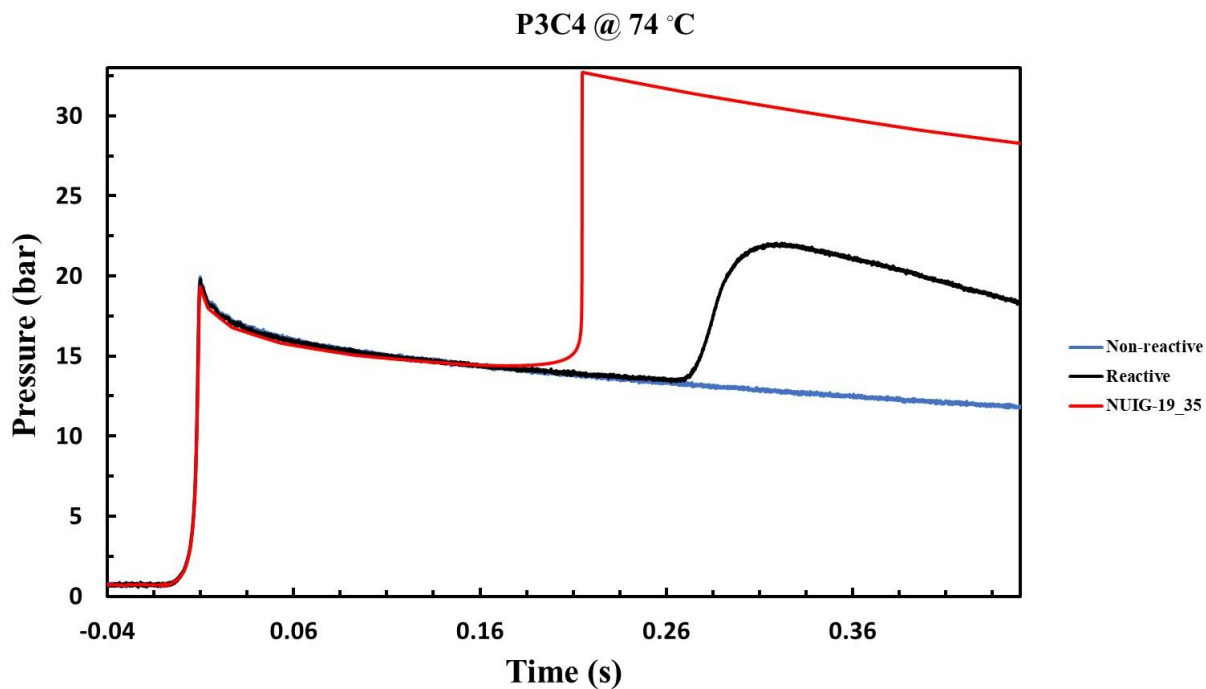


Figure ES62. Pressure history of tested reactive and non-reactive mixtures of P3C4 case alongside the simulation's profile for initial temperature of 347 K.

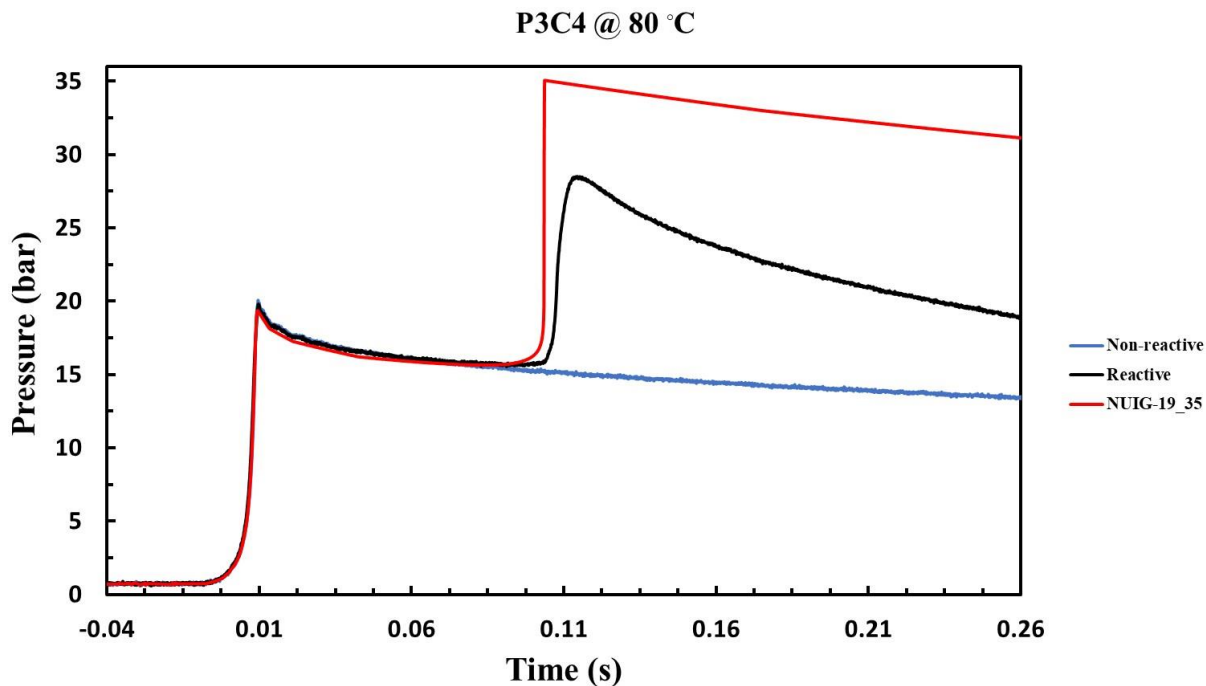


Figure ES63. Pressure history of tested reactive and non-reactive mixtures of P3C4 case alongside the simulation's profile for initial temperature of 353 K.

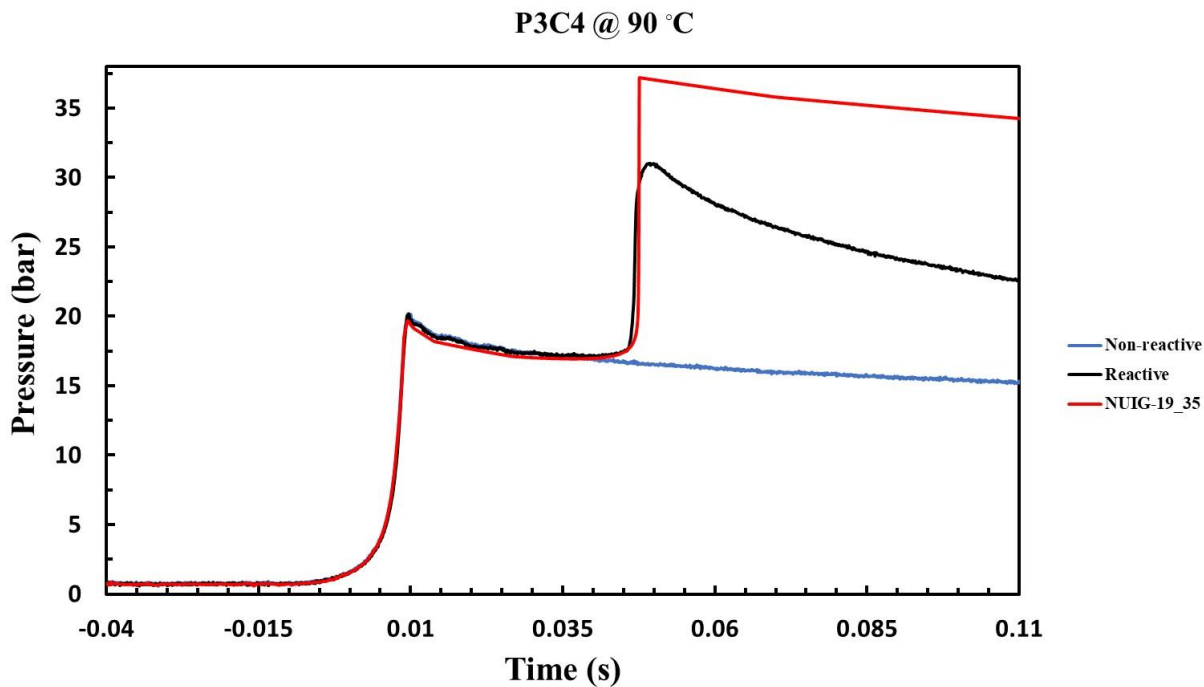


Figure ES64. Pressure history of tested reactive and non-reactive mixtures of P3C4 case alongside the simulation's profile for initial temperature of 363 K.

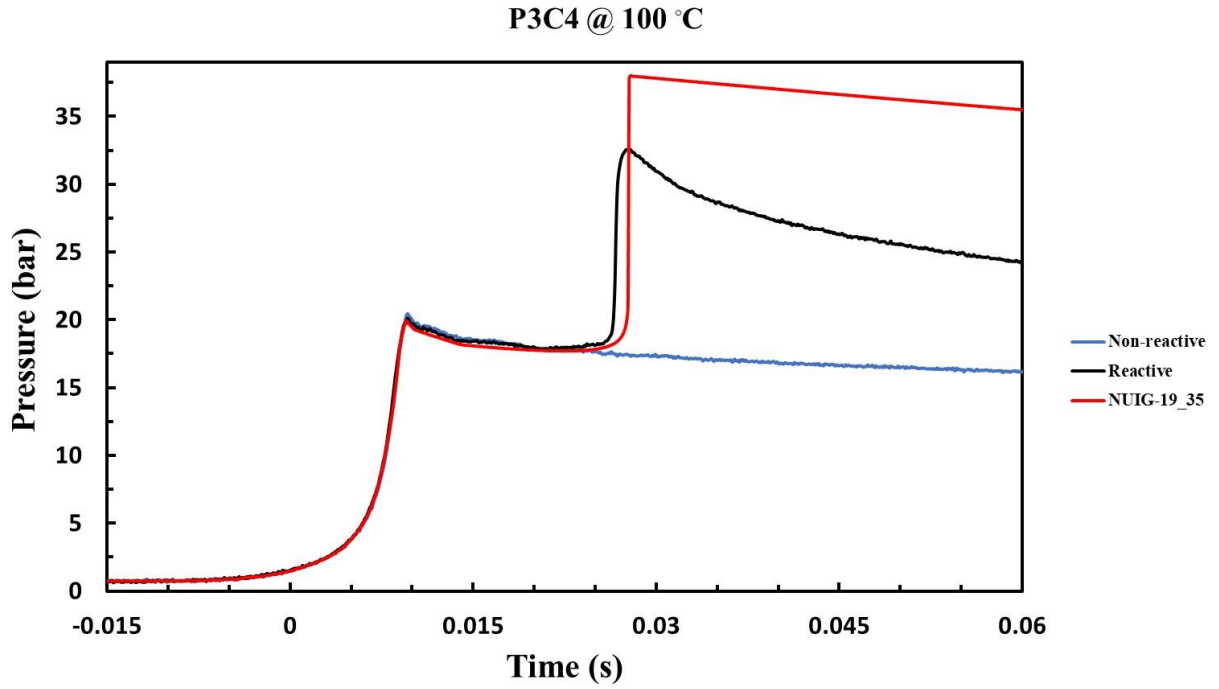


Figure ES65. Pressure history of tested reactive and non-reactive mixtures of P3C4 case alongside the simulation's profile for initial temperature of 373 K.

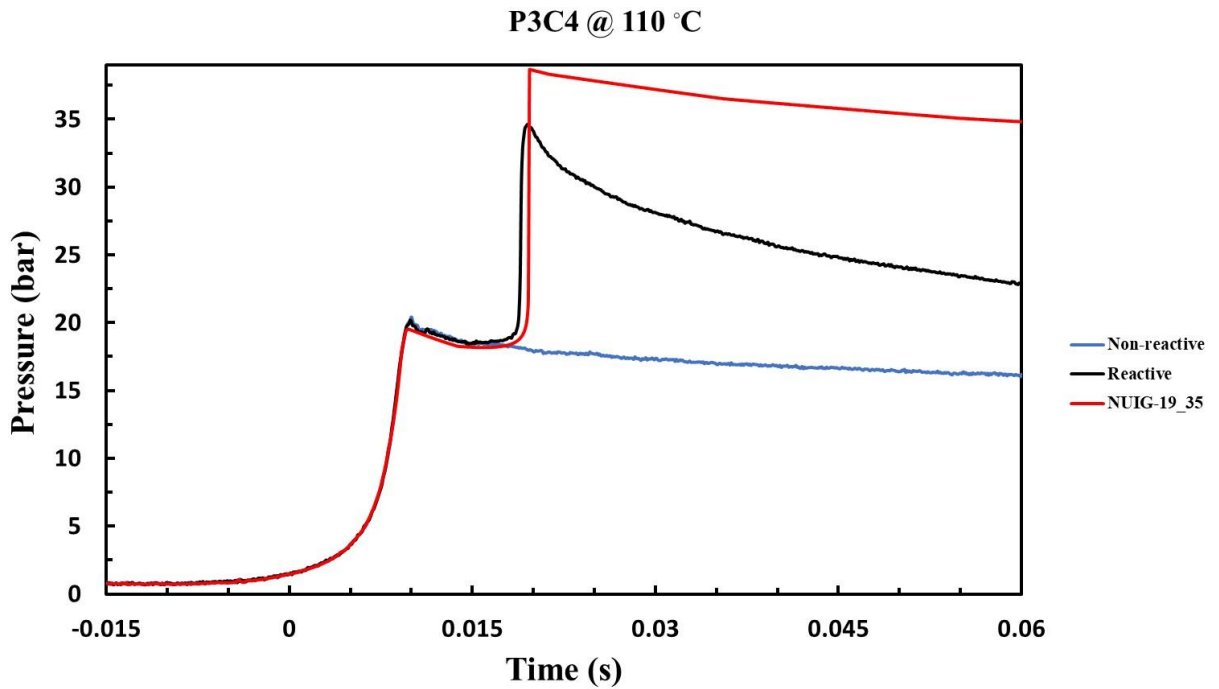


Figure ES66. Pressure history of tested reactive and non-reactive mixtures of P3C4 case alongside the simulation's profile for initial temperature of 383 K.

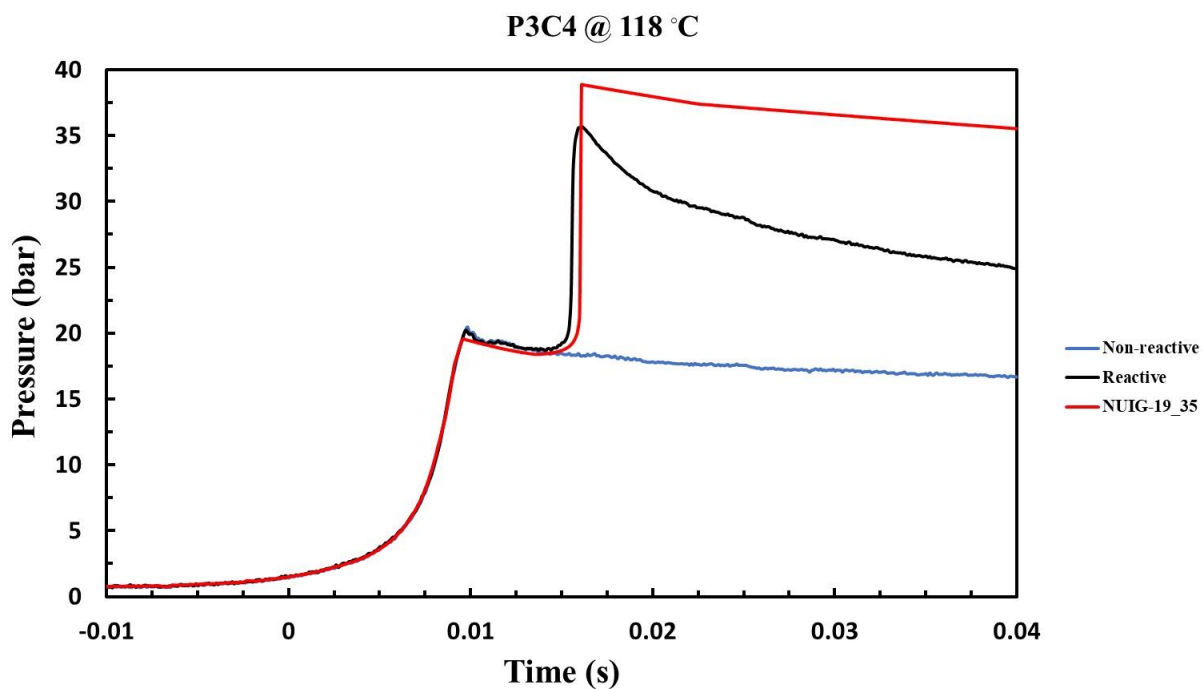


Figure ES67. Pressure history of tested reactive and non-reactive mixtures of P3C4 case alongside the simulation's profile for initial temperature of 391 K.

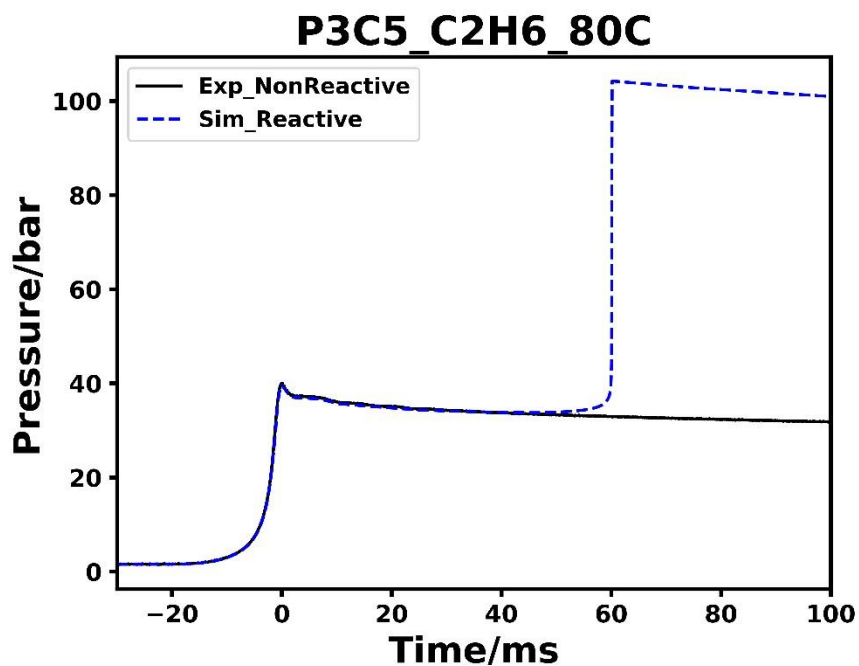


Figure ES68. Pressure history of tested reactive and non-reactive mixtures of P3C5 case alongside the simulation's profile for initial temperature of 353 K.

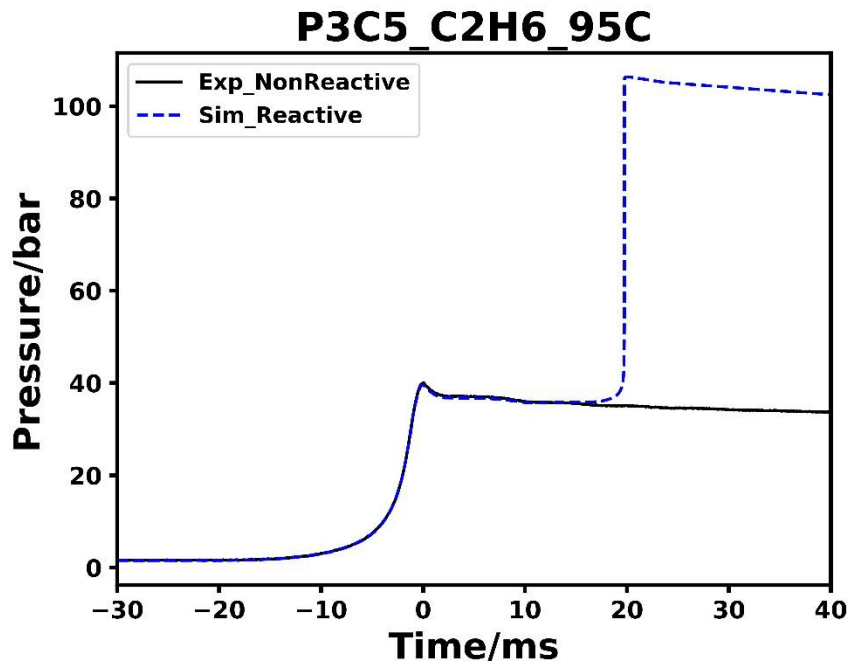


Figure ES69. Pressure history of tested reactive and non-reactive mixtures of P3C5 case alongside the simulation's profile for initial temperature of 368 K.

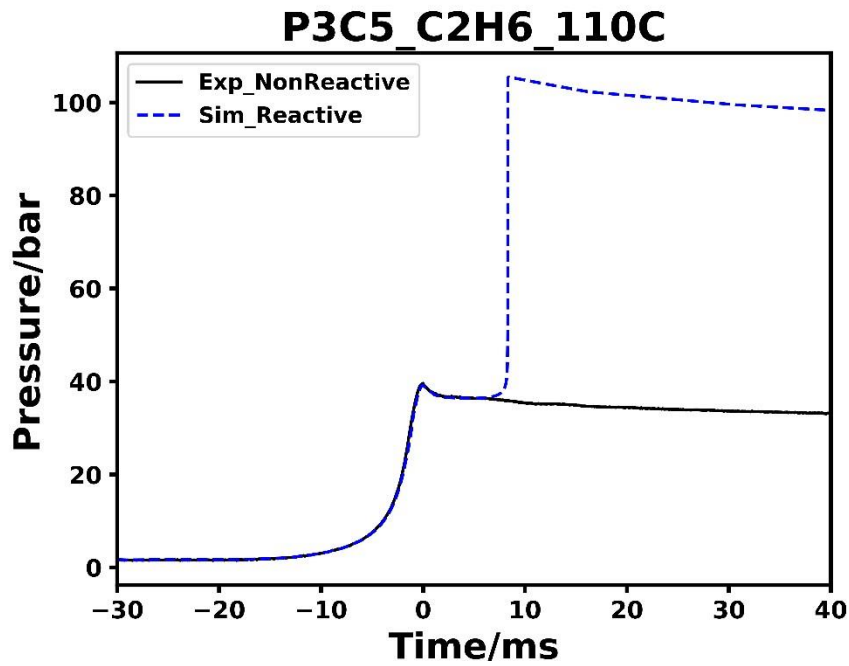


Figure ES70. Pressure history of tested reactive and non-reactive mixtures of P3C5 case alongside the simulation's profile for initial temperature of 383 K.

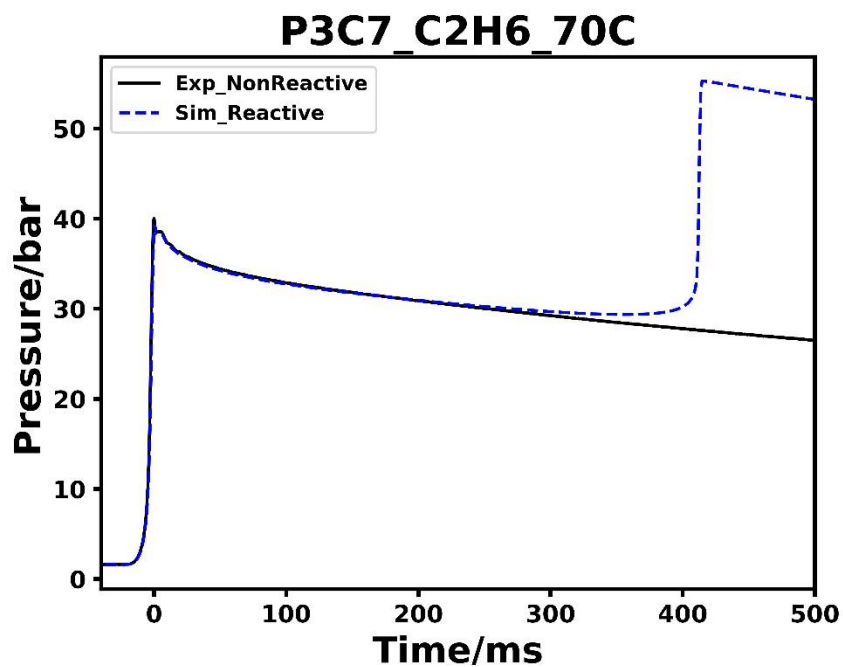


Figure ES71. Pressure history of tested reactive and non-reactive mixtures of P3C7 case alongside the simulation's profile for initial temperature of 343 K.

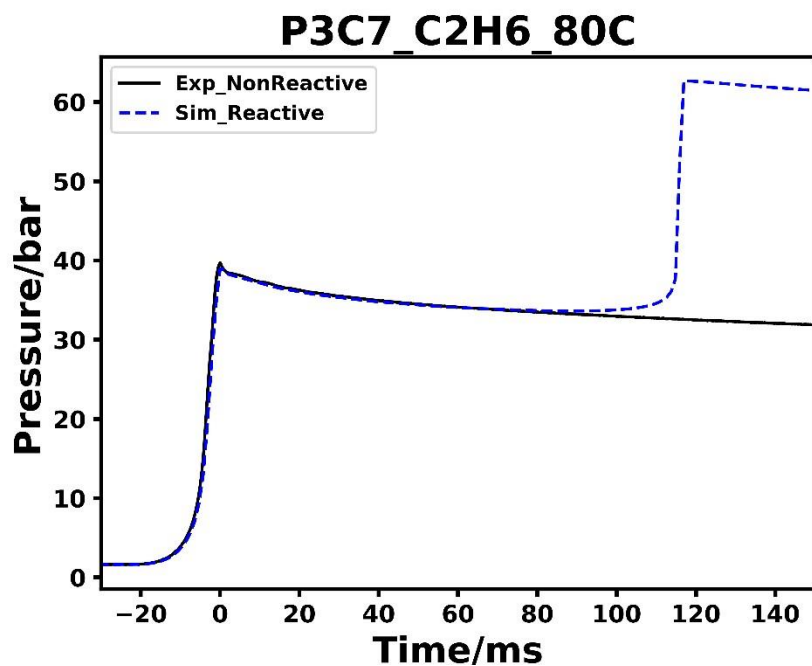


Figure ES72. Pressure history of tested reactive and non-reactive mixtures of P3C4 case alongside the simulation's profile for initial temperature of 353 K.

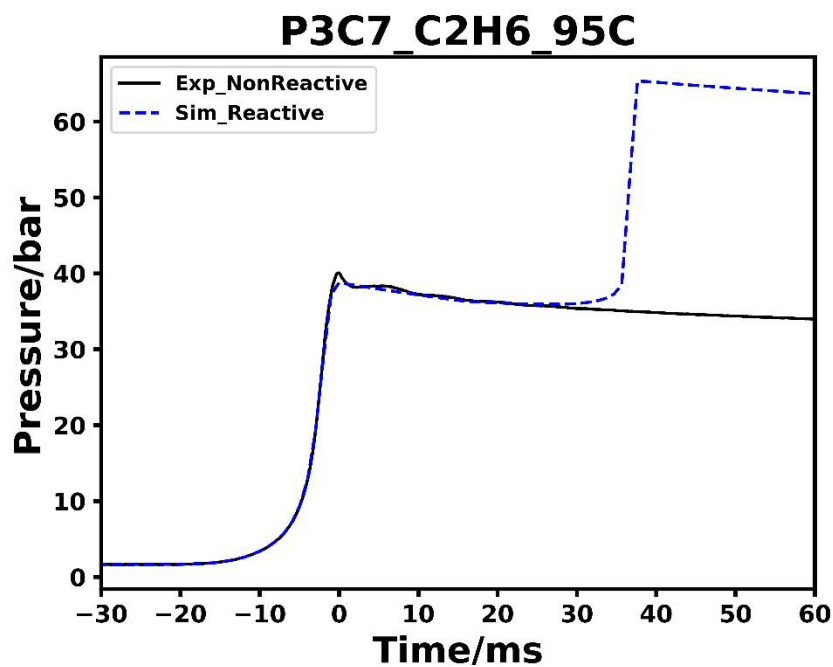


Figure ES73. Pressure history of tested reactive and non-reactive mixtures of P3C7 case alongside the simulation's profile for initial temperature of 368 K.

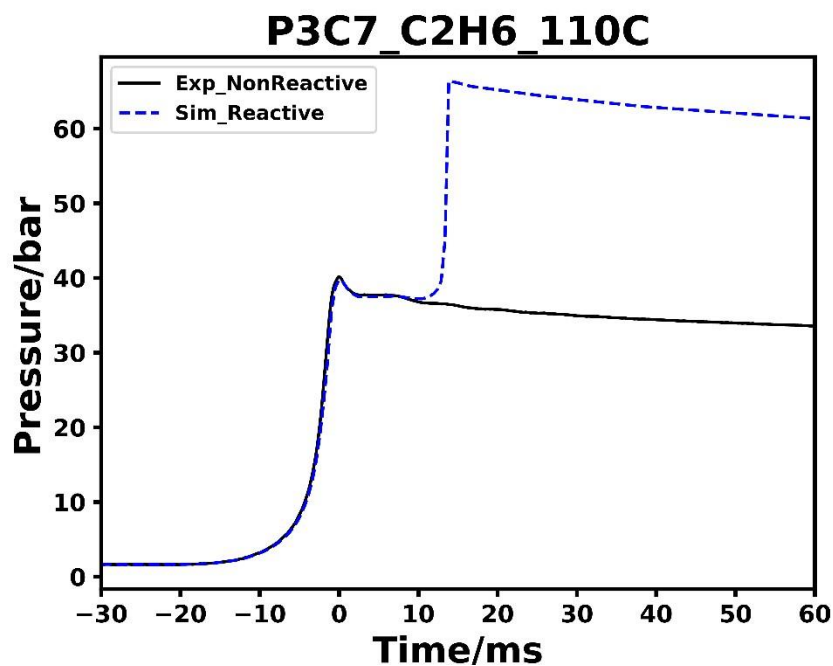


Figure ES74. Pressure history of tested reactive and non-reactive mixtures of P3C7 case alongside the simulation's profile for initial temperature of 383 K.

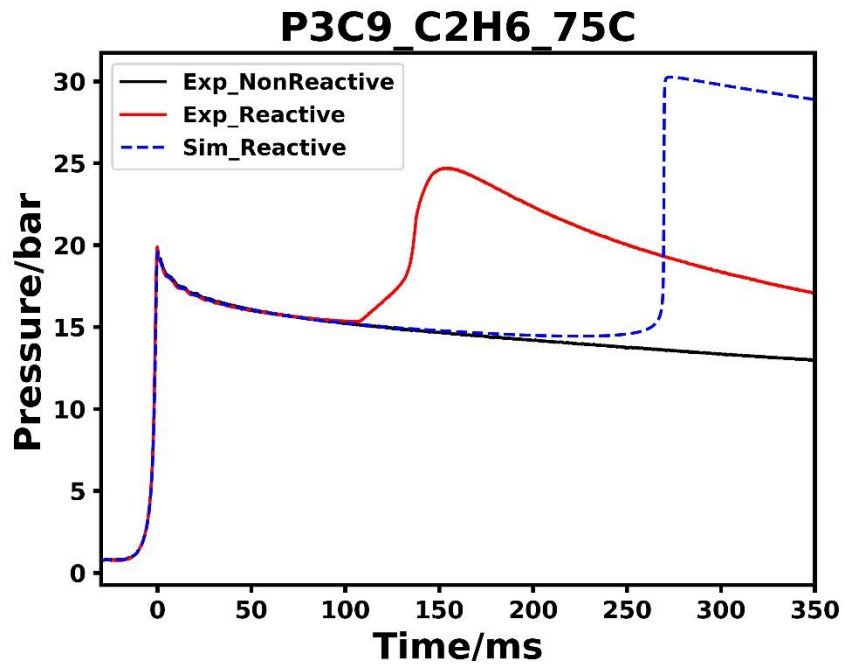


Figure ES75. Pressure history of tested reactive and non-reactive mixtures of P3C9 case alongside the simulation's profile for initial temperature of 348 K.

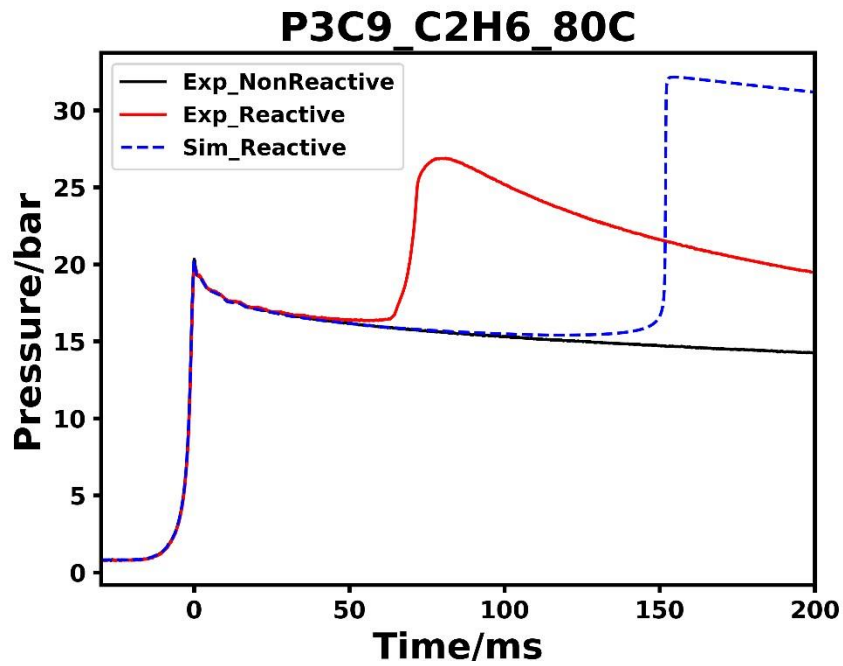


Figure ES76. Pressure history of tested reactive and non-reactive mixtures of P3C9 case alongside the simulation's profile for initial temperature of 353 K.

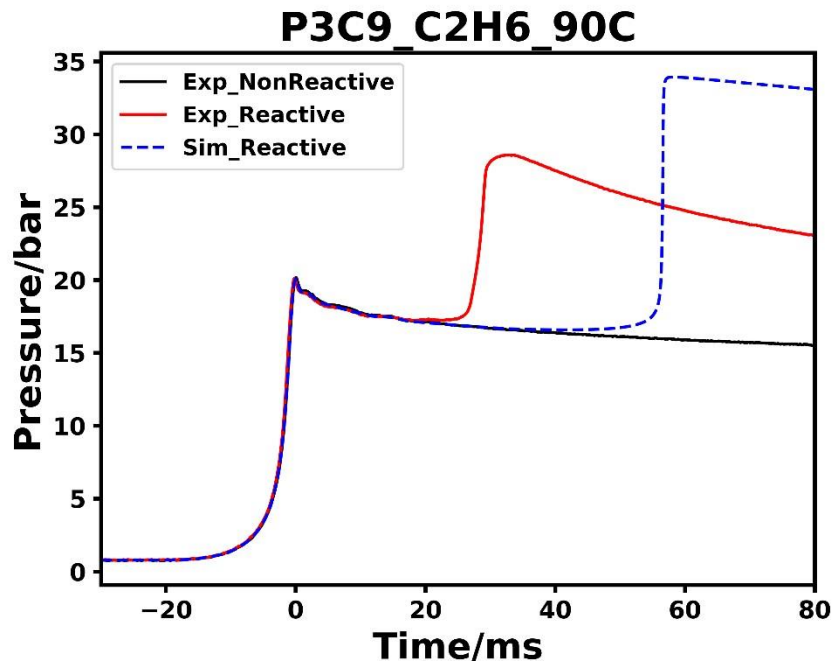


Figure ES77. Pressure history of tested reactive and non-reactive mixtures of P3C9 case alongside the simulation's profile for initial temperature of 363 K.

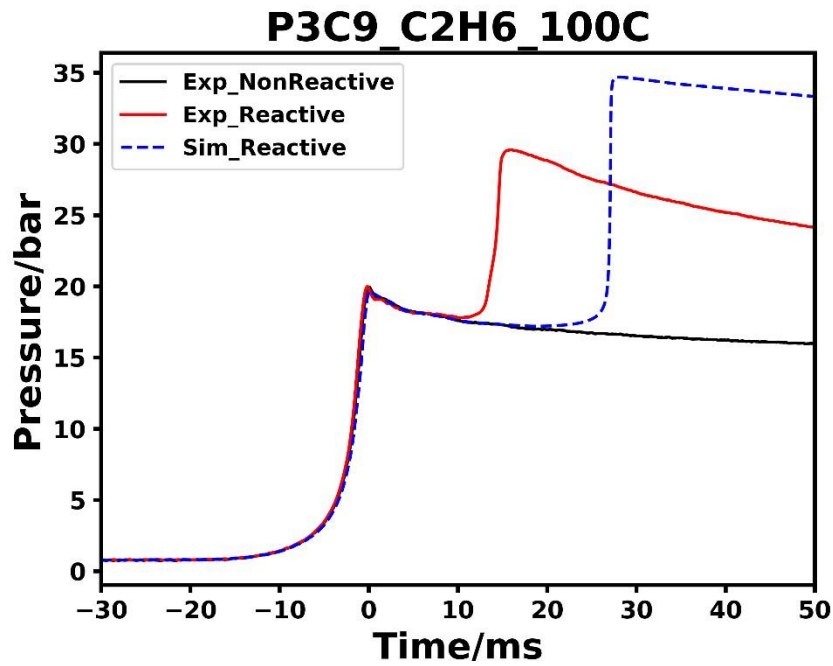


Figure ES78. Pressure history of tested reactive and non-reactive mixtures of P3C9 case alongside the simulation's profile for initial temperature of 373 K.

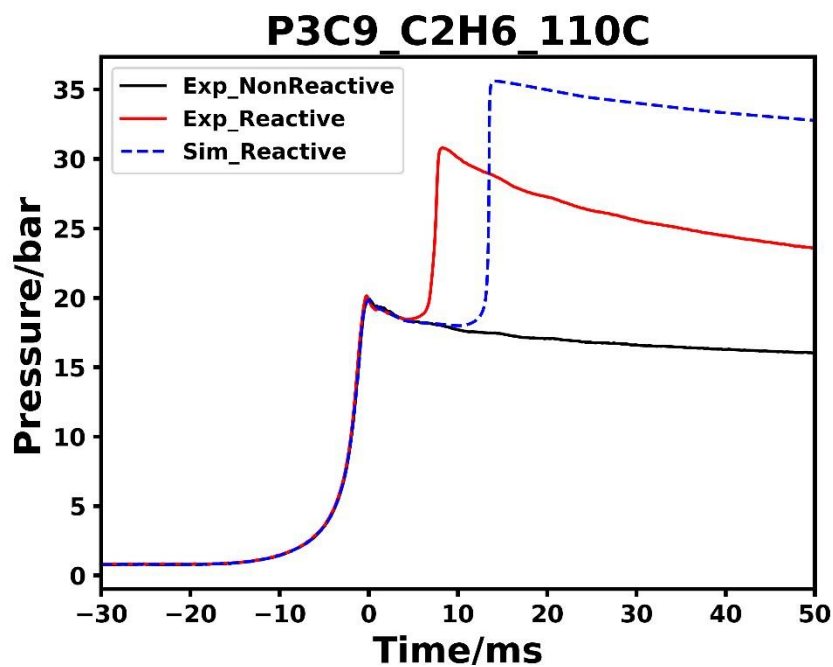


Figure ES79. Pressure history of tested reactive and non-reactive mixtures of P3C9 case alongside the simulation's profile for initial temperature of 383 K.

10. Performance of NUIGMech0.9 under high pressure–low temperature regime

The performance of NUIGMech0.9 under high-pressure and low-temperature regime is shown in Figure S80. As seen, this chemical mechanism reproduces the experimental IDTs of various methane mixtures under the studied conditions very well.

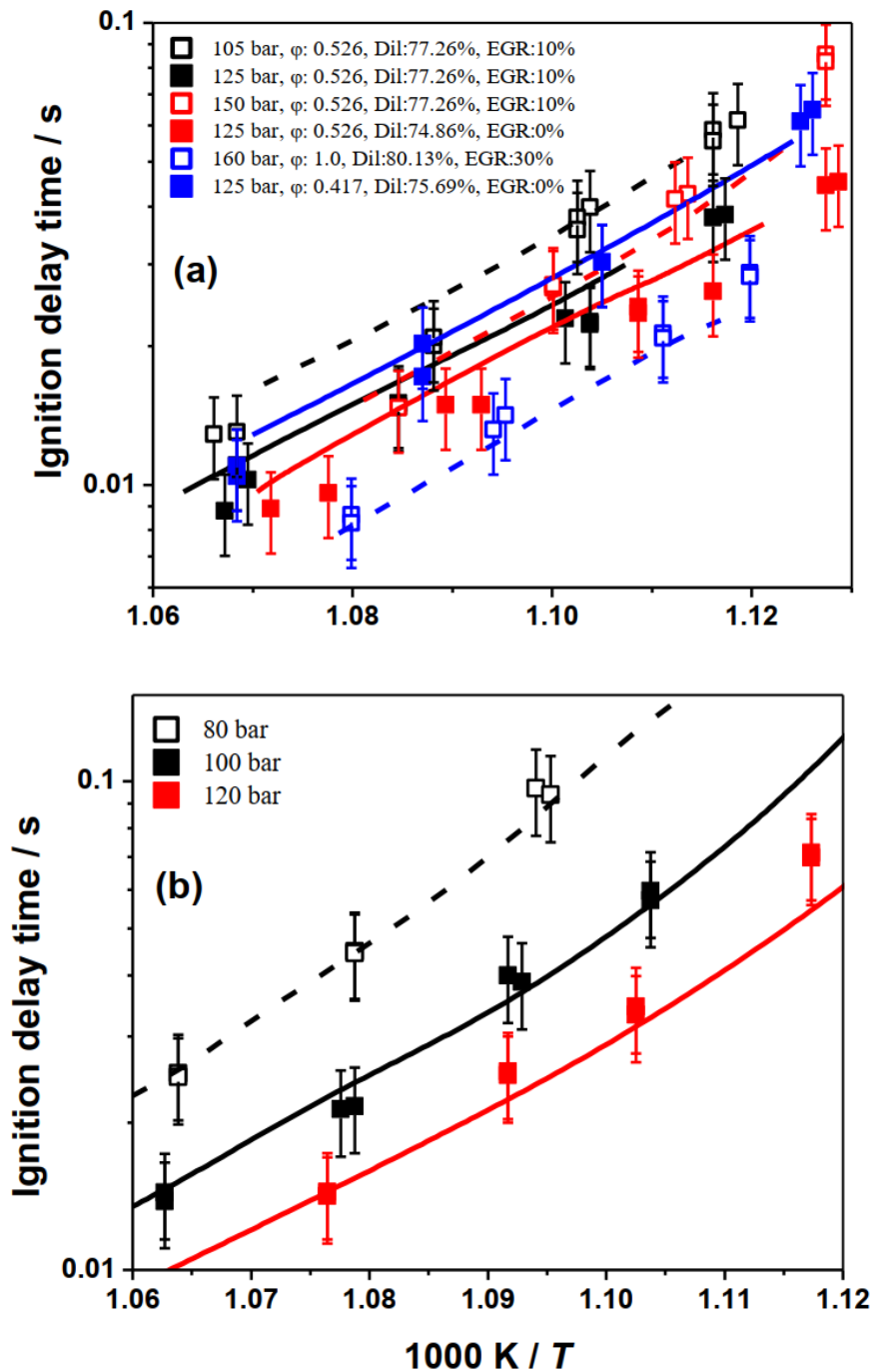


Figure ES80. Performance of NUIGMech0.9 under high–pressure and low–temperature regime for methane mixtures: Experimental and simulation data are shown by the same colour symbols and lines, respectively. Dashed lines correspond to the simulation data of the opened symbols; (a) Experimental data from ¹⁷, (b) Experimental data from ²⁶; methane + air mixture with $\phi = 0.526$.

11.Complementary analyses

11.1. Ignition delay time

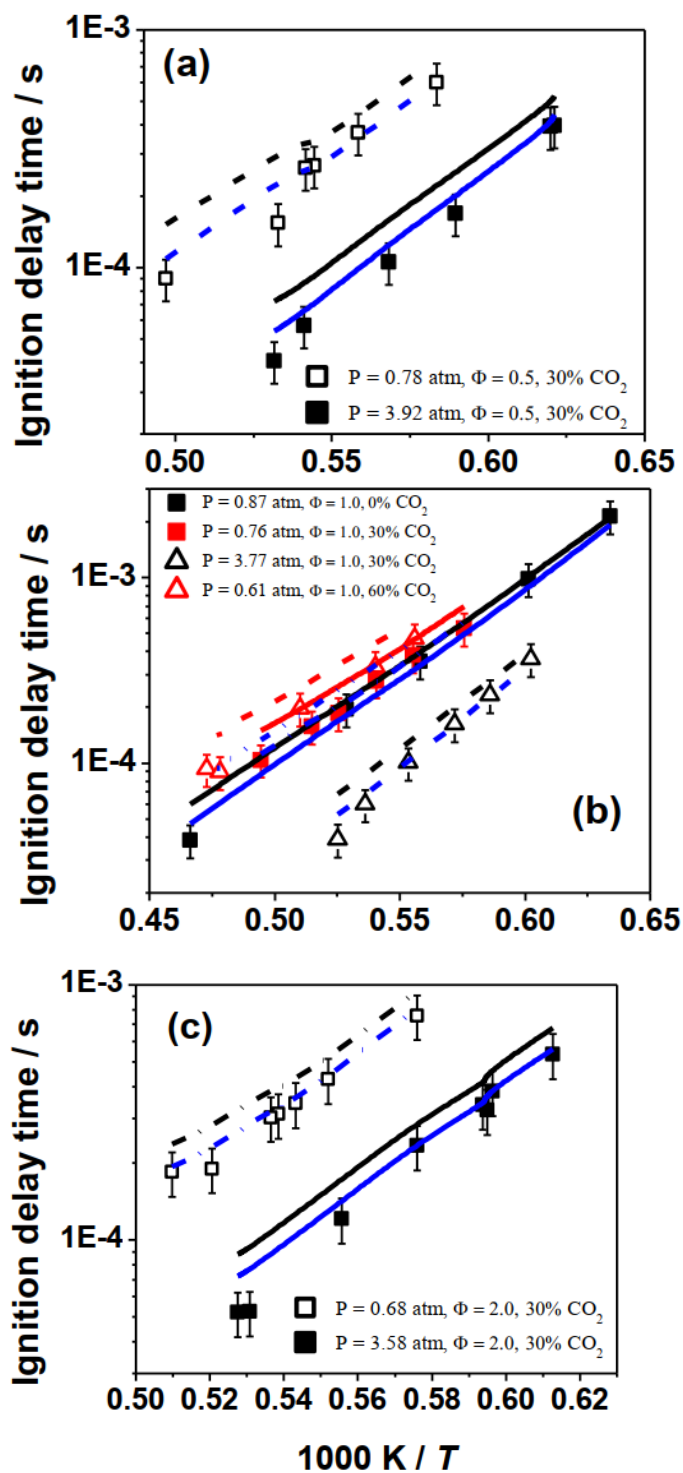
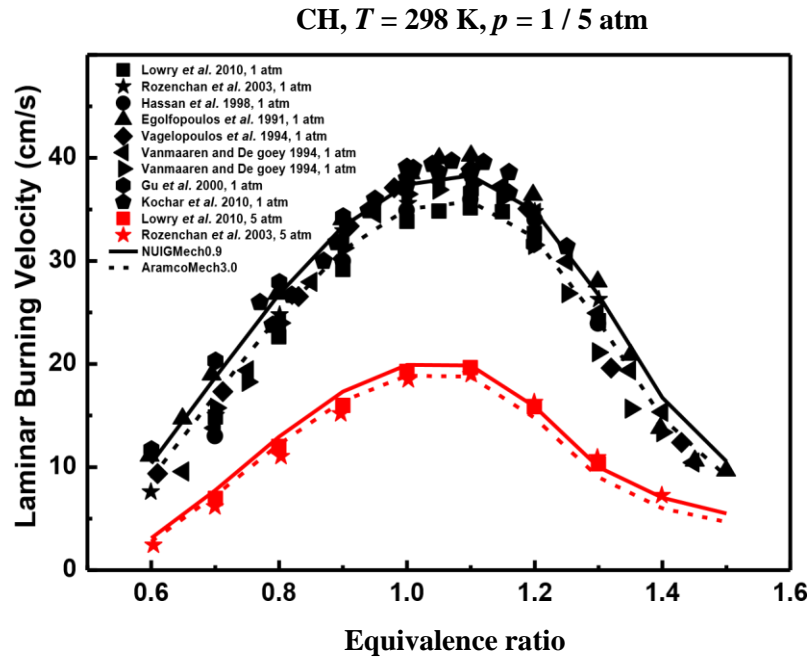


Figure ES81. Performance of NUIGMech0.9 under low-pressure and high-temperature regime for methane mixtures: Experimental and simulation data are shown by the same colour symbols and lines, respectively. Dashed lines correspond to the simulation data of the opened symbols; Blue lines correspond to the simulation data of CRECK chemical mechanism⁹; Experimental data from ²⁷.

11.2. Laminar burning velocity



50 4

Figure ES82. Performance of NUIGMech0.9 for predicting laminar burning velocity of methane + air mixtures under low– (the black symbols and lines) to elevated– (the red symbols and lines) pressures.²⁸⁻³⁵

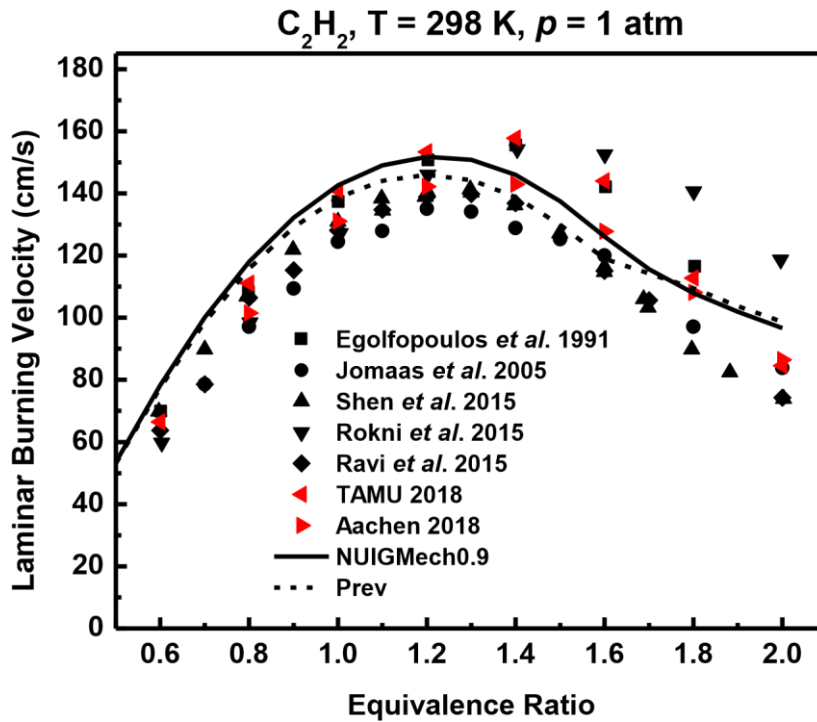


Figure ES83. Performance of NUIGMech0.9 for predicting laminar burning velocity of acetylene + air mixtures.^{28, 36-40}

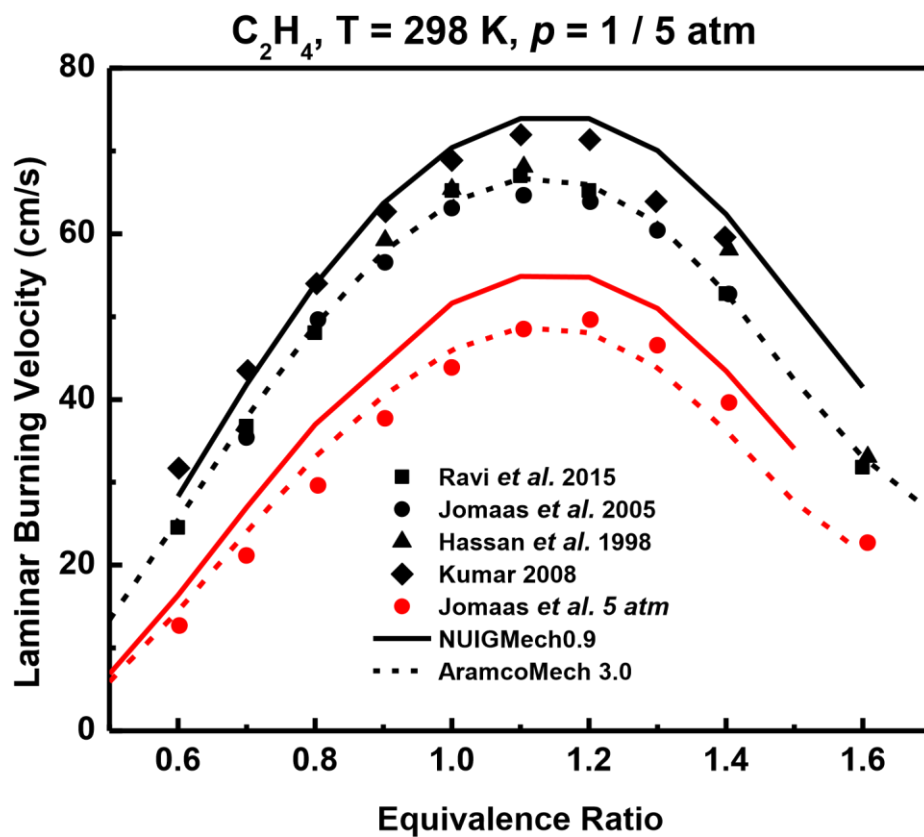


Figure ES84. Performance of NUIGMech0.9 for predicting laminar burning velocity of ethylene + air mixtures under low– (the black symbols and lines) to elevated– (the red symbols and lines) pressures.^{36, 39, 41, 42}

CH , $T = 298\text{ K}$, $p = 1 / 5\text{ atm}$

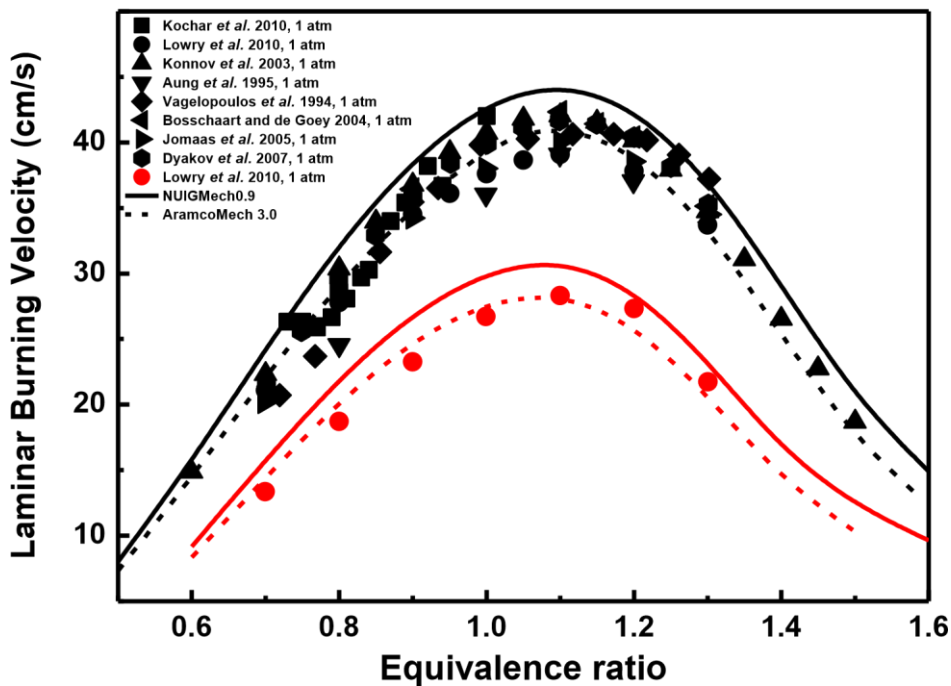
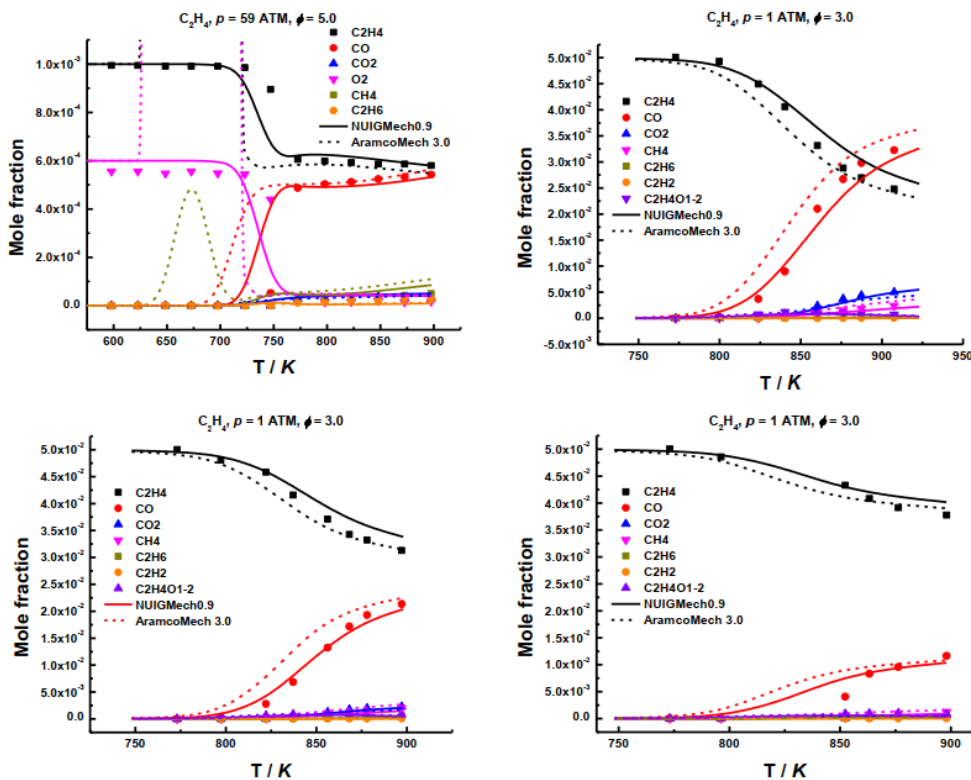


Figure ES85. Performance of NUIGMech0.9 for predicting laminar burning velocity of ethane + air mixtures under low- (the black symbols and lines) to elevated- (the red symbols and lines) pressures.^{29, 32, 35, 36, 43-46}

11.3. Speciation (JSR): Ethylene



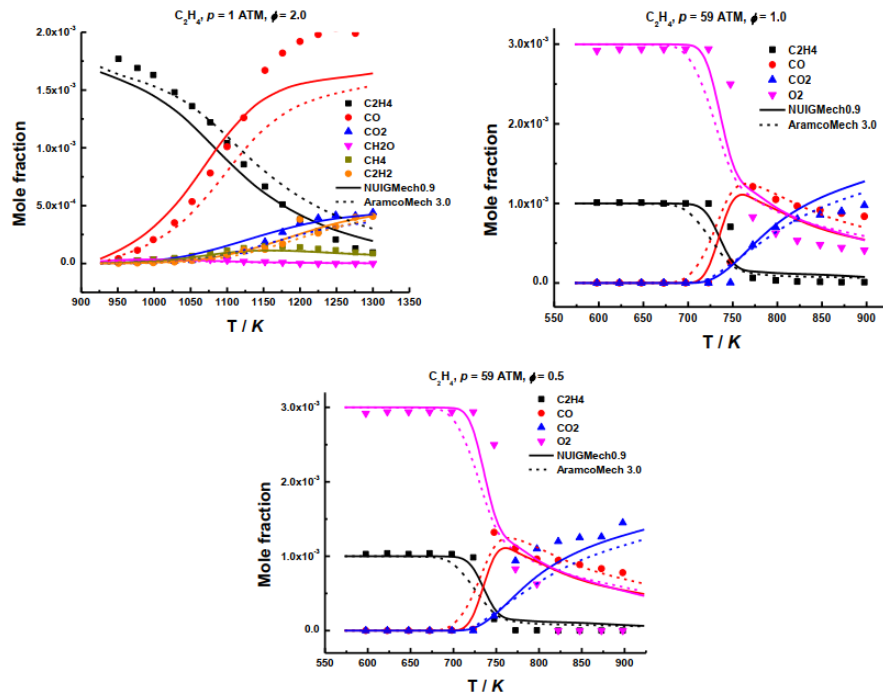


Figure ES86. Performance of NUIGMech0.9 for predicting mole fraction distribution of various species over temperature for ethylene + air mixtures at different pressures and equivalence ratios.⁴⁷⁻⁴⁹

11.4. Individual and combined effects of the studied parameters on IDTs

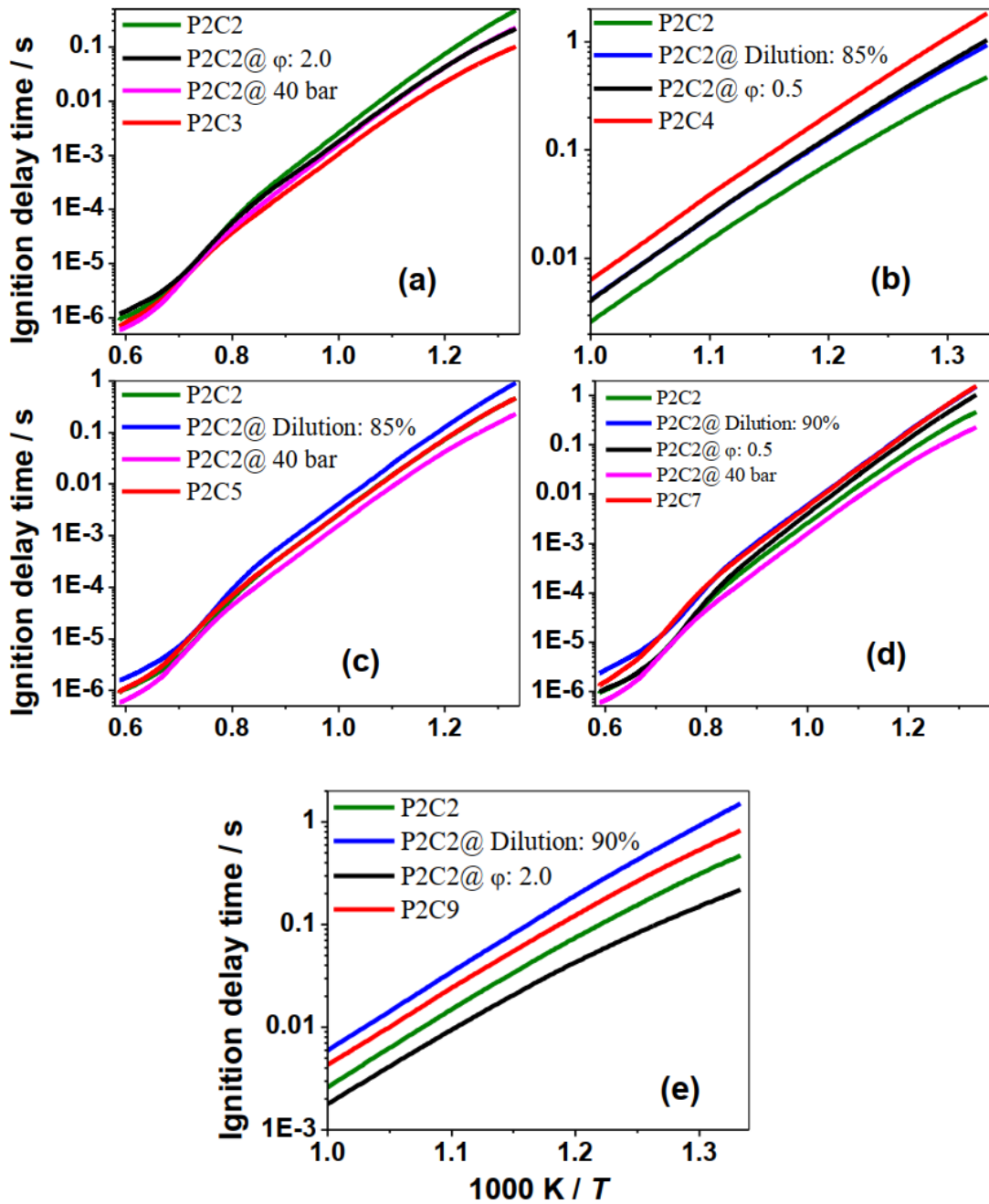


Figure ES87. Individual and combined effects of pressure, equivalence ratio and dilution on ethylene's IDTs. (For better interpretation of the colours, the reader is referred to the web version of this article)

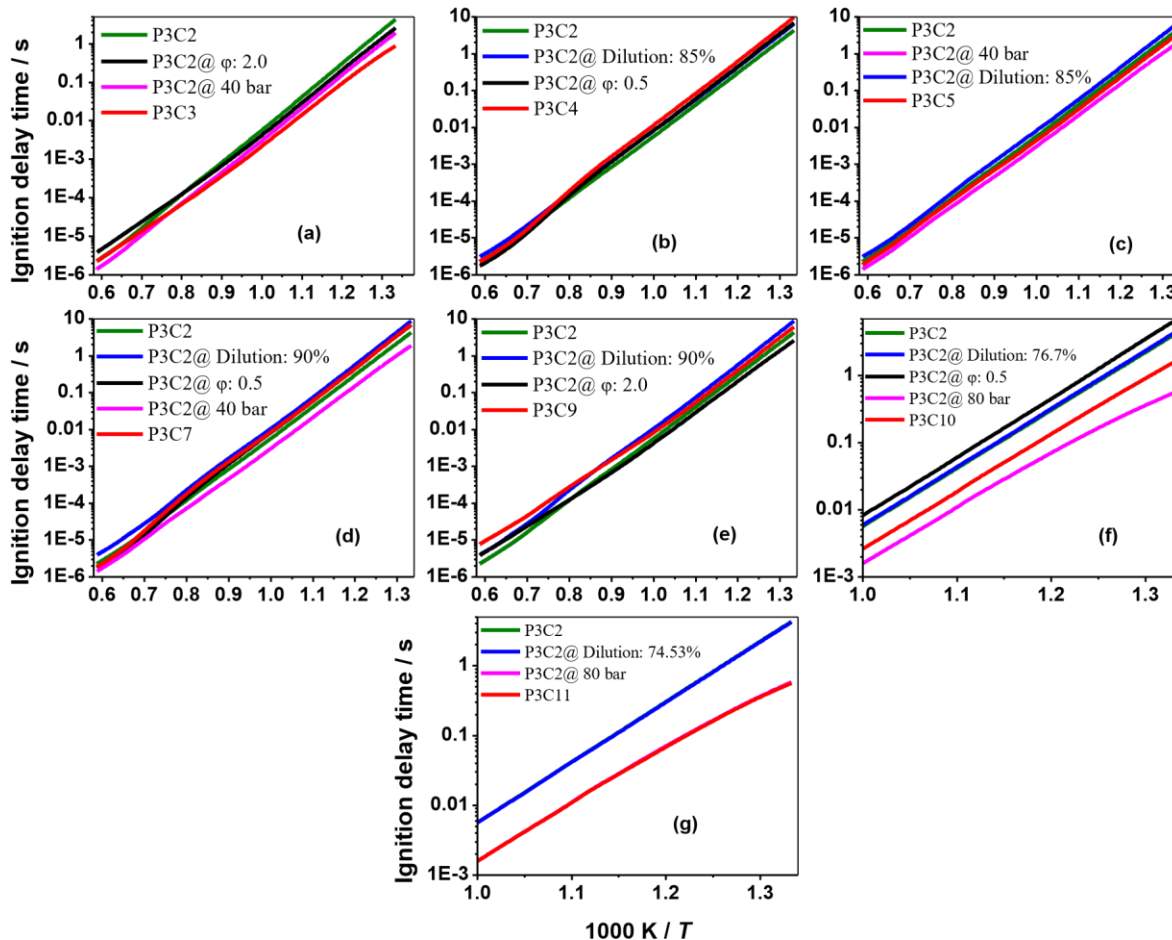


Figure S88. Individual and combined effects of pressure, equivalence ratio and dilution on ethane's IDTs. (For better interpretation of the colours, the reader is referred to the web version of this article)

11.5. Chemical kinetics development analyses

To gain a better understanding of the effect of the studied parameters on IDT, brute-force sensitivity analyses of IDT followed by flux analyses are performed for the important reactions in the individual zones (lines 1–3) identified in Figures 6 and 8. The sensitivity coefficient (S) of the brute-force sensitivity analysis is calculated as:

$$S = \frac{\ln(\tau_+/ \tau_-)}{\ln(k_+/ k_-)} = \frac{\ln(\tau_+/ \tau_-)}{\ln(2.0/0.5)}$$

As shown above, the rate constant for each reaction is increased/decreased by a factor of two and the related IDTs are calculated as τ^+ and τ^- , respectively. Also, the net flux values shown in the following figures are normalized with net fluxes of the corresponding reactions in the base condition (P2C2 for ethylene and P3C2 for ethane). Therefore, if there is no change in the net flux of a specific reaction, the

normalized value is unity, otherwise it may be higher or lower than unity in accordance with any change in the net flux rates.

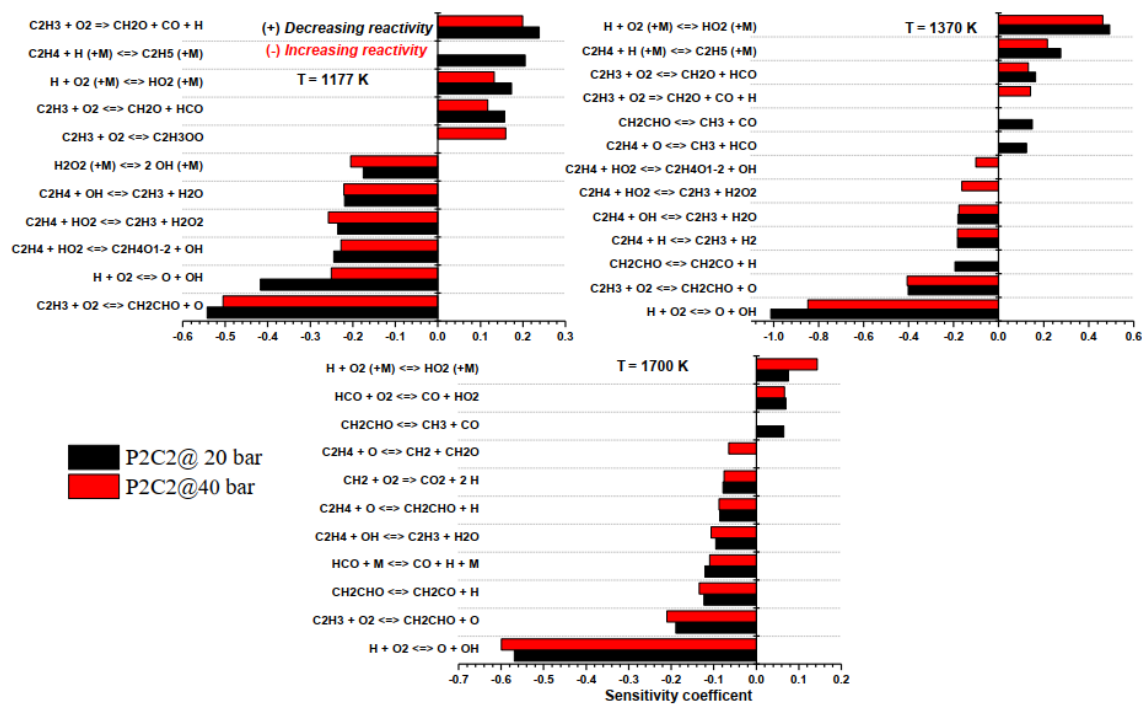


Figure ES89. Effect of pressure on the ten most prominent reactions and their fluxes, brute force sensitivity analysis of IDT corresponding to lines (1–3) in Figures 6(a, d); P2C2: $\phi = 1.0$, 75.0% N₂. (For better interpretation of the colours, the reader is referred to the web version of this article)

Table ES20. Effect of pressure rise on the ten most prominent reactions of ethylene at different temperatures.

Temperature (K)	Promoted reactions	Suppressed reactions
1177	$\dot{C}_2H_3 + O_2 = C_2H_3\dot{O}_2$	$C_2H_4 + \dot{H} (+M) = \dot{C}_2H_5 (+M)$
1370	$C_2H_4 + H\dot{O}_2 = \dot{C}_2H_3 + H_2O_2$	$\dot{C}H_2CHO = CH_2CO + \dot{H}$
	$C_2H_4 + H\dot{O}_2 = C_2H_4O1-2 + \dot{O}H$	$C_2H_4 + \ddot{O} = \dot{C}H_3 + H\dot{C}O$
	$\dot{C}_2H_3 + O_2 = CH_2O + CO + \dot{H}$	$\dot{C}H_2CHO = \dot{C}H_3 + CO$
1700	$C_2H_4 + \ddot{O} = \cdot\dot{C}H_2 + CH_2O$	$\dot{C}H_2CHO = \dot{C}H_3 + CO$

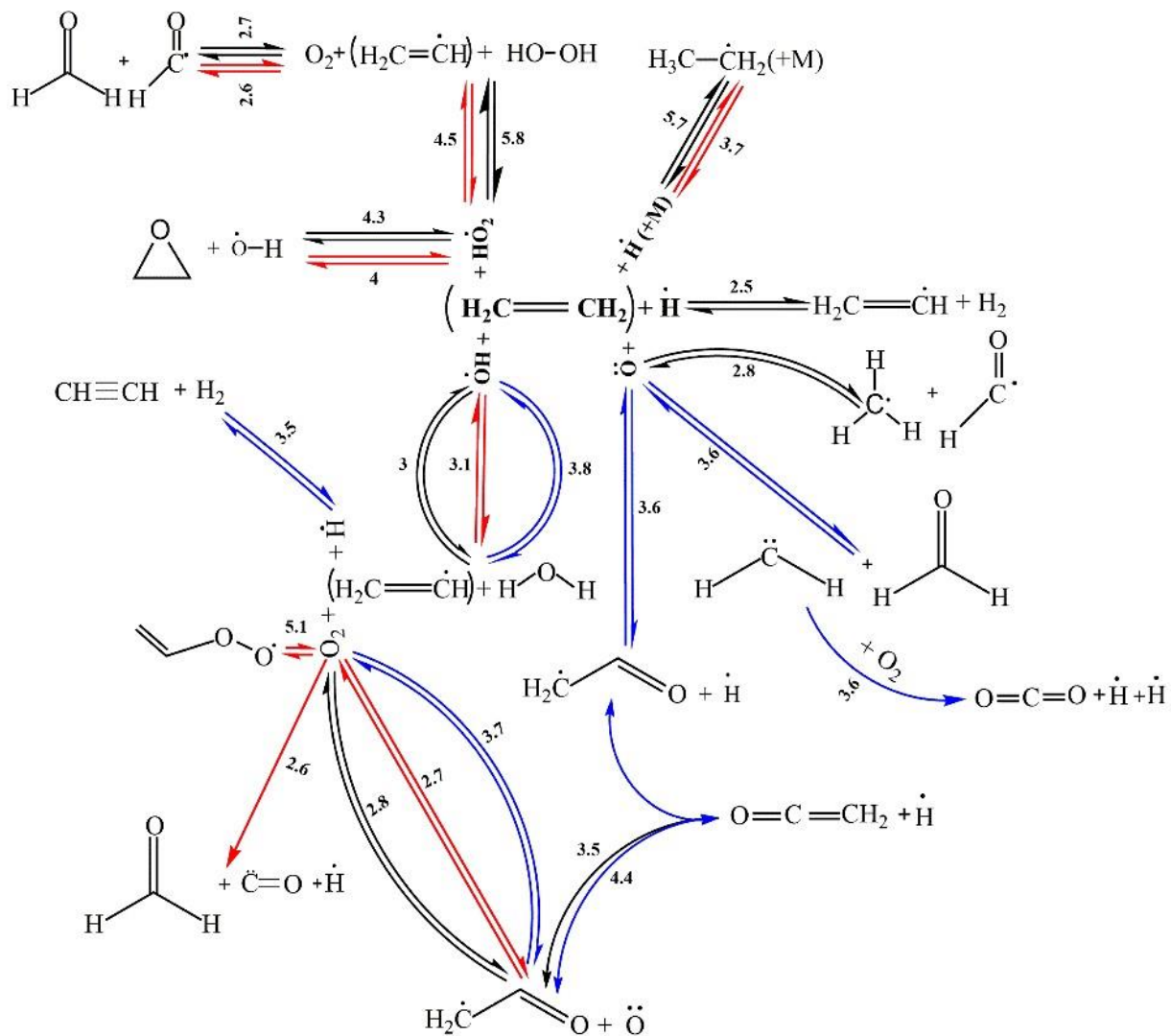


Figure ES90. Effect of pressure on the normalized flux analysis of the ten most prominent reactions corresponding to lines (1–3) in Figures 6(a,d); P2C2: $\phi = 1.0$, 75.0% N_2 (based on the flux analysis of P2C2 base case when 20% of ethylene (fuel) is consumed); the blue line: case (1), $T = 1700$ K, the black line: case (2), $T = 1370$ K, the red line: case (3), $T = 1177$ K (1112 K in Figure 6d). (For better interpretation of the colours, the reader is referred to the web version of this article)

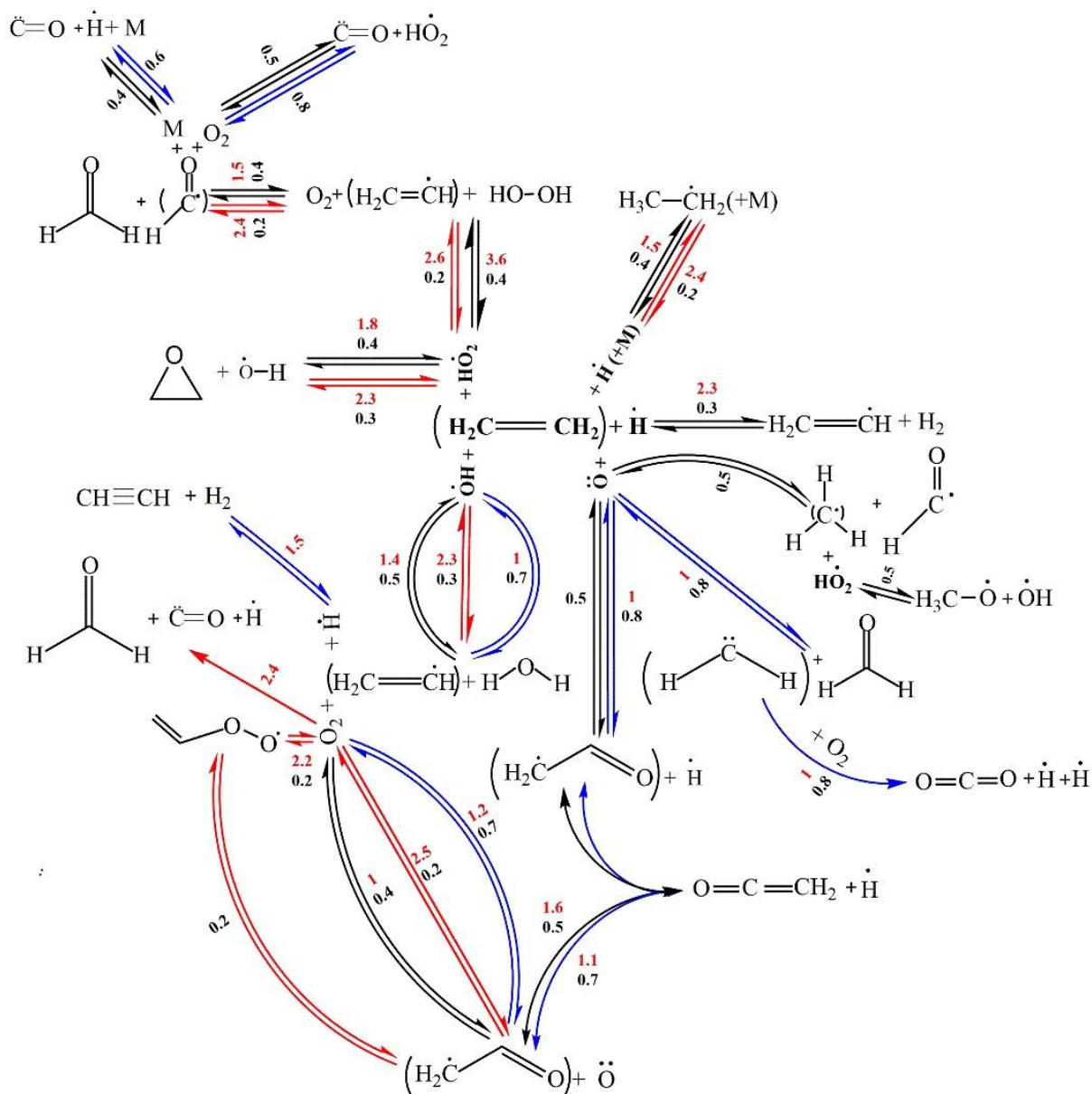


Figure ES91. Effect of changing in equivalence ratio on the normalized flux analysis of the ten most prominent reactions corresponding to lines (1–3) in Figures 6(a,d); P2C2: $\phi = 1.0$, 75.0% N_2 , 20 bar, (based on the flux analysis of P2C2 base case when 20% of ethylene (fuel) is consumed); the blue line: case (1), $T = 1700$ K, the black line: case (2), $T = 1370$ K, the red line: case (3), $T = 1177$ K ($\phi = 2.0$) and 1112 K ($\phi = 0.5$); the red number: $\phi = 2.0$, the black number: $\phi = 0.5$. (For better interpretation of the colours, the reader is referred to the web version of this article)

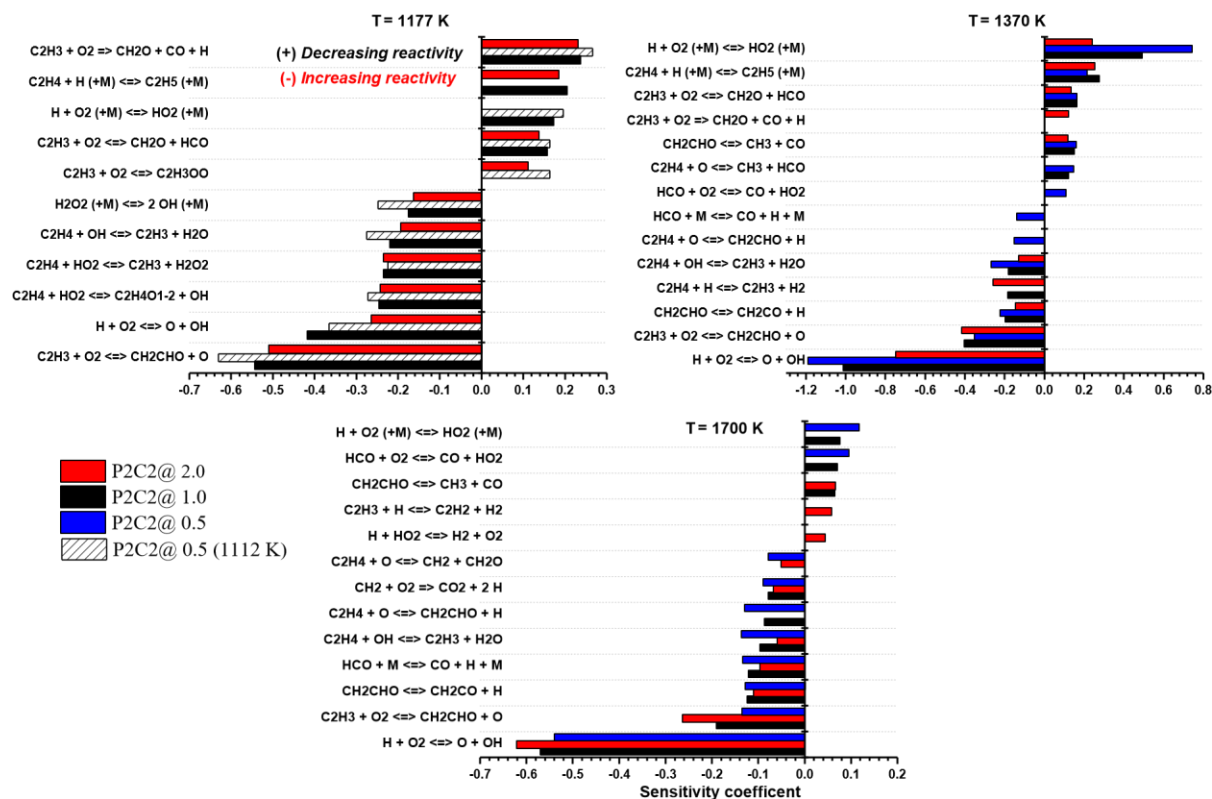


Figure ES92. Effect of changing in equivalence ratio on the ten most prominent reactions, brute force sensitivity analysis of IDT corresponding to lines (1–3) in Figures 6(a,d); P2C2: $\phi = 1.0$, 75.0% N₂, 20 bar (For better interpretation of the colours, the reader is referred to the web version of this article)

Table ES21. Effect of increasing equivalence ratio on the ten most prominent reactions of ethylene at different temperatures in comparison to P2C2 case.

Temperature (K)	Promoted reactions	Suppressed reactions
1177	$\dot{C}_2H_3 + O_2 = C_2H_3\dot{O}_2$	$\dot{H} + O_2 (+M) = H\dot{O}_2 (+M)$
1370	$\dot{C}_2H_3 + O_2 = CH_2O + CO + \dot{H}$	$C_2H_4 + \ddot{O} = \dot{C}H_3 + H\dot{C}O$
1700	$C_2H_4 + \ddot{O} = \cdot\dot{C}H_2 + CH_2O$	$\dot{H} + O_2 (+M) = H\dot{O}_2 (+M)$
	$\dot{H} + H\dot{O}_2 = H_2 + O_2$	$C_2H_4 + \ddot{O} = \dot{C}H_2CHO + \dot{H}$
	$\dot{C}_2H_3 + \dot{H} = C_2H_2 + H_2$	$H\dot{C}O + O_2 = CO + H\dot{O}_2$

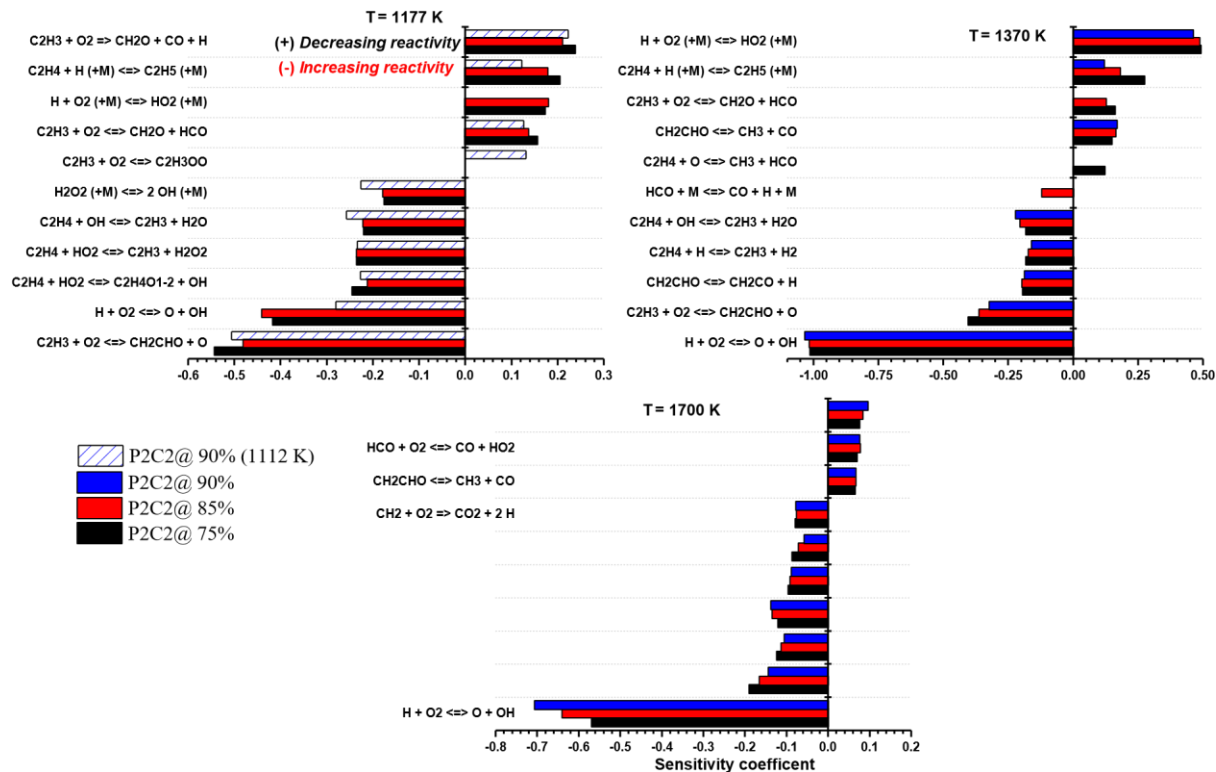


Figure ES94. Effect of changing in dilution level on the ten most prominent reactions, brute force sensitivity analysis of IDT corresponding to lines (1–3) in Figures 6(c,d); P2C2: $\phi = 1.0$, 75.0% N₂, 20 bar For better interpretation of the colours, the reader is referred to the web version of this article)

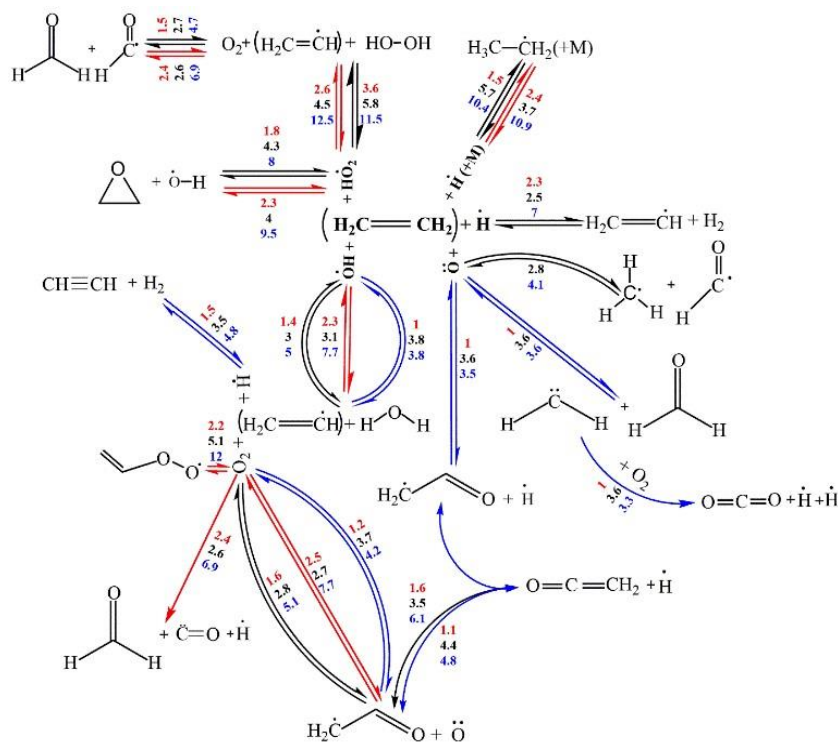


Figure ES95. Normalized flux analysis (based on the flux analysis of P2C2 base case when 20% of ethylene (fuel) is consumed) of some important reactions corresponding to Figure 6a; the blue line: case (1), $T = 1700$ K, the black line: case (2), $T = 1370$ K, the red line: case (3), $T = 1177$ K; the red number: effect of equivalence ratio, the black number: effect of pressure, and the blue number: combined effects. (For better interpretation of the colours, the reader is referred to the web version of this article)

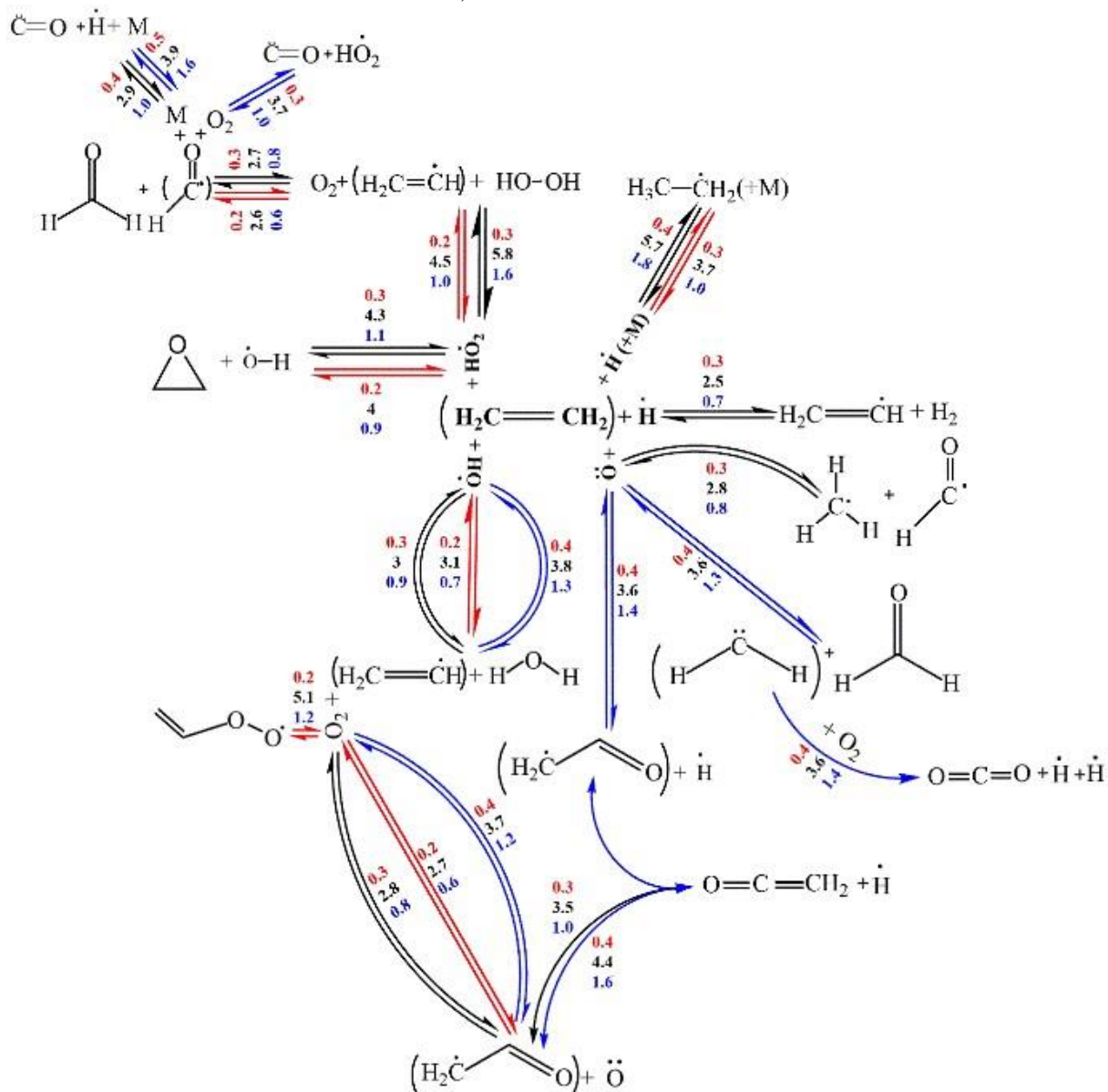


Figure ES96. Normalized flux analysis (based on the flux analysis of P2C2 base case when 20% of ethylene (fuel) is consumed) of some important reactions corresponding to Figure 6c; the blue line: case (1), $T = 1700$ K, the black line: case (2), $T = 1370$ K, the red line: case (3), $T = 1112$ K; the red number: effect of dilution, the black number: effect of pressure, and the blue number: combined effects. (For better interpretation of the colours, the reader is referred to the web version of this article)

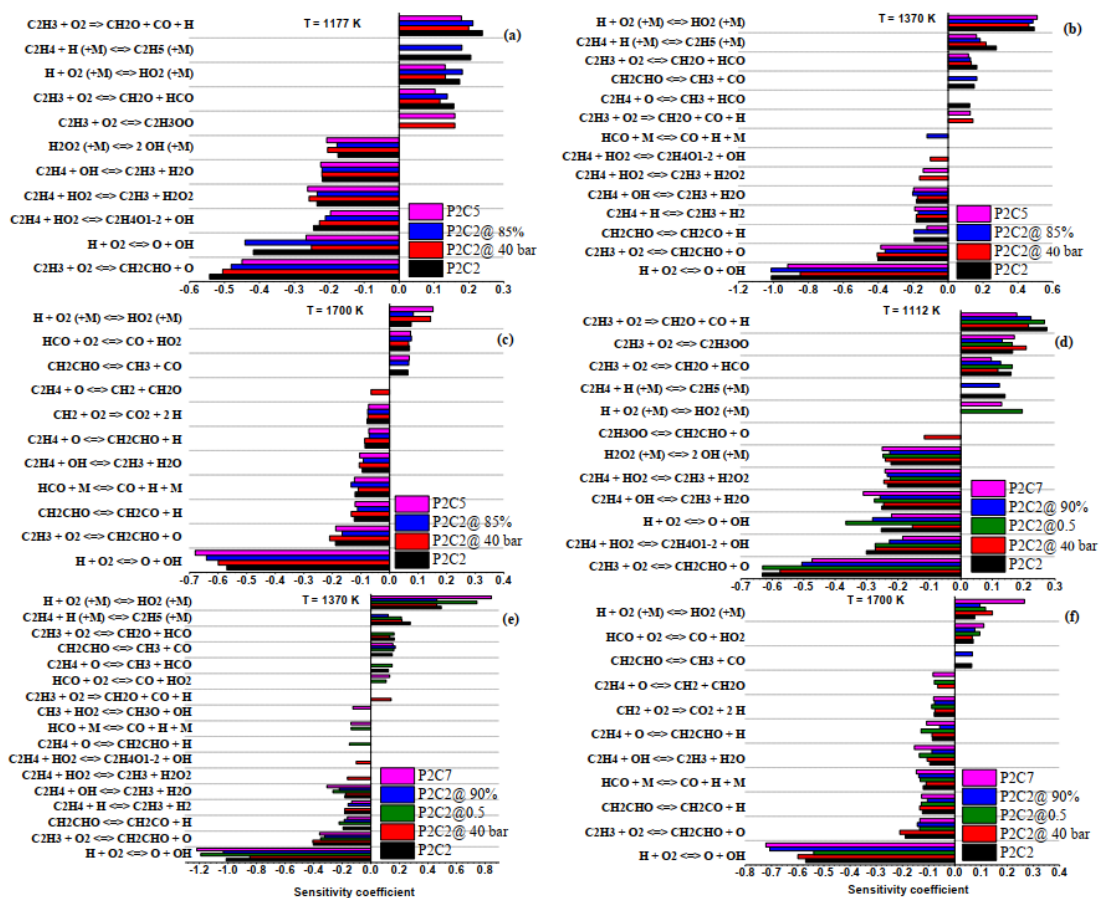


Figure ES97. Brute force sensitivity analysis of IDT corresponding to lines (1–3) in Figure 6c: (a) $T = 1177$ K; (b) $T = 1370$ K; (c) $T = 1700$ K; and figure 7(d): (d) $T = 1112$ K; (e) $T = 1370$ K; (f) $T = 1700$ K.

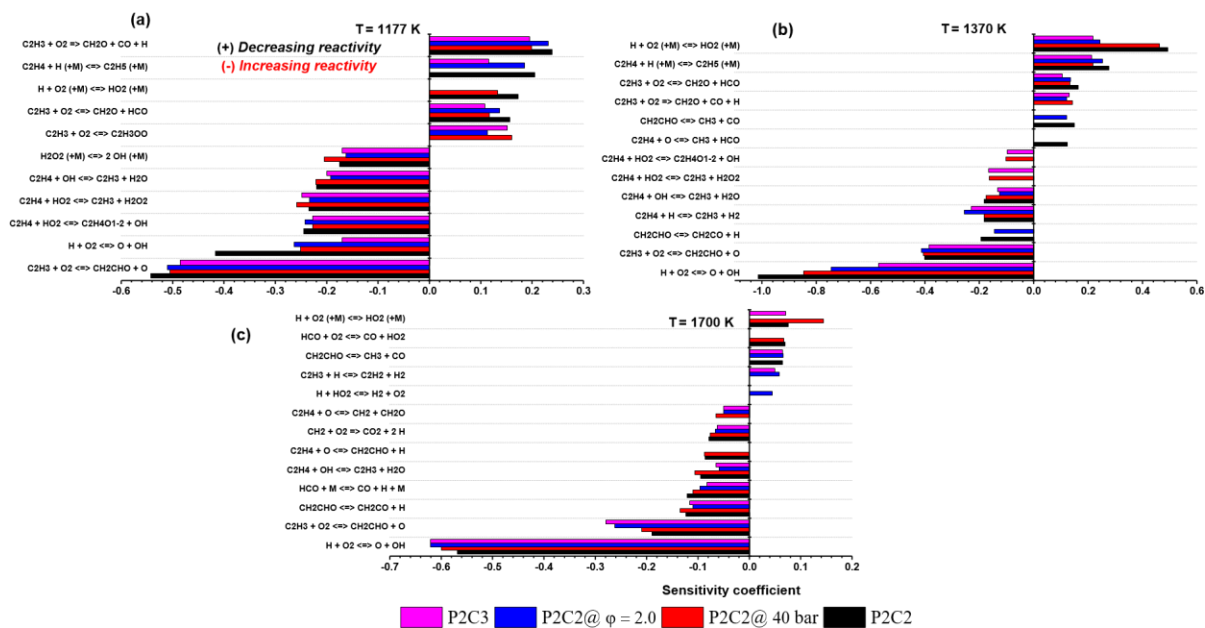


Figure ES98. Brute force sensitivity analysis of IDT corresponding to lines (1–3) in Figure 6a: (a) $T = 1177$ K; (b) $T = 1370$ K; (c) $T = 1700$ K.

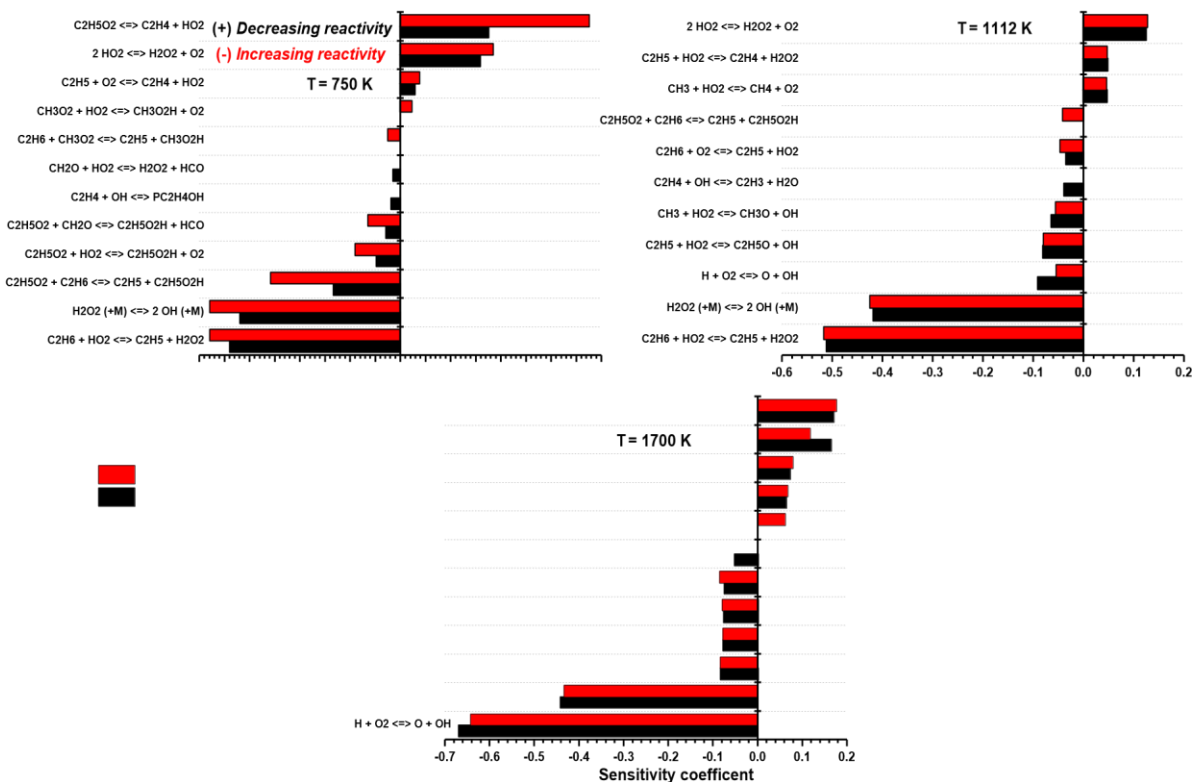


Figure ES99. Effect of pressure on the ten most prominent reactions, brute force sensitivity analysis of IDT corresponding to lines (1–3) in Figure 8d; P3C2: $\phi = 1.0$, 75% N₂, 20 bar. (For better interpretation of the colours, the reader is referred to the web version of this article)

Table ES22. Effect of increasing pressure on the ten most prominent reactions of ethane at different temperatures in comparison to P3C2 case.

Temperature (K)	Promoted reactions	Suppressed reactions
750	$C_2H_6 + H\dot{O}_2 = \dot{C}_2H_5 + CH_3O_2H$	$C_2H_4 + \dot{O}H = p\dot{C}_2H_4OH$
	$CH_3\dot{O}_2 + H\dot{O}_2 = CH_3O_2H + O_2$	$CH_2O + H\dot{O}_2 = H_2O_2 + H\dot{C}O$
1112	$C_2H_5\dot{O}_2 + C_2H_6 = \dot{C}_2H_5 + C_2H_5O_2H$	$C_2H_4 + \dot{O}H = \dot{C}_2H_3 + H_2O$
1700	$\dot{C}_2H_5 + \dot{H} (+M) = C_2H_6 (+M)$	$\dot{C}_2H_5 + O_2 = C_2H_4 + H\dot{O}_2$

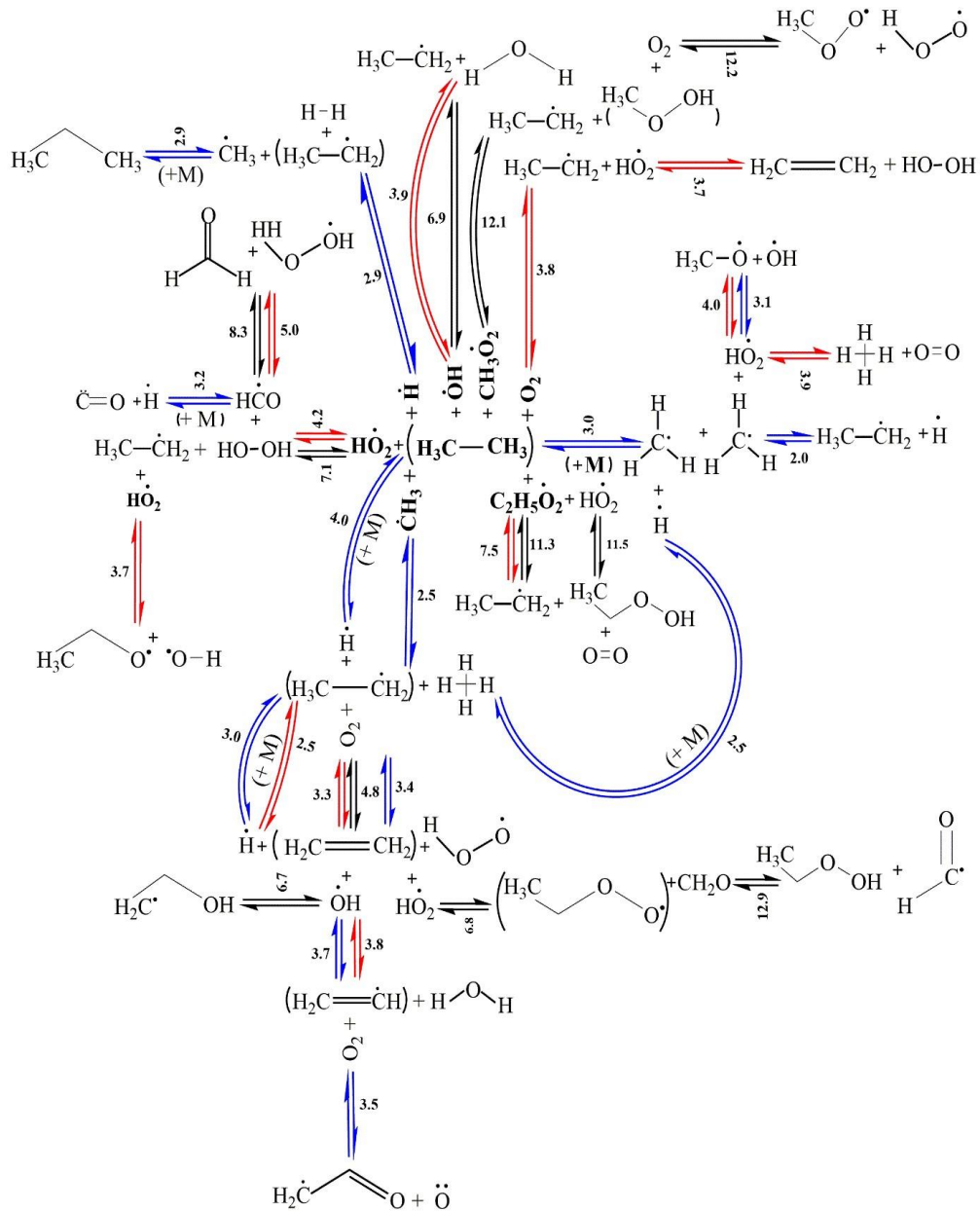


Figure ES100. Effect of pressure on the normalized flux analysis of ten most prominent reactions of ethane corresponding to lines (1–3) in Figure 8d; P3C2: $\varphi = 1.0$, 75% N_2 , 20 bar, (based on the flux analysis of P3C2 base case when 20% of ethane (fuel) is consumed); the blue line: case (1), $T = 1700 \text{ K}$, the red line: case (2), $T = 1112 \text{ K}$, the black line: case (3), $T = 750 \text{ K}$. (For better interpretation of the colours, the reader is referred to the web version of this article)

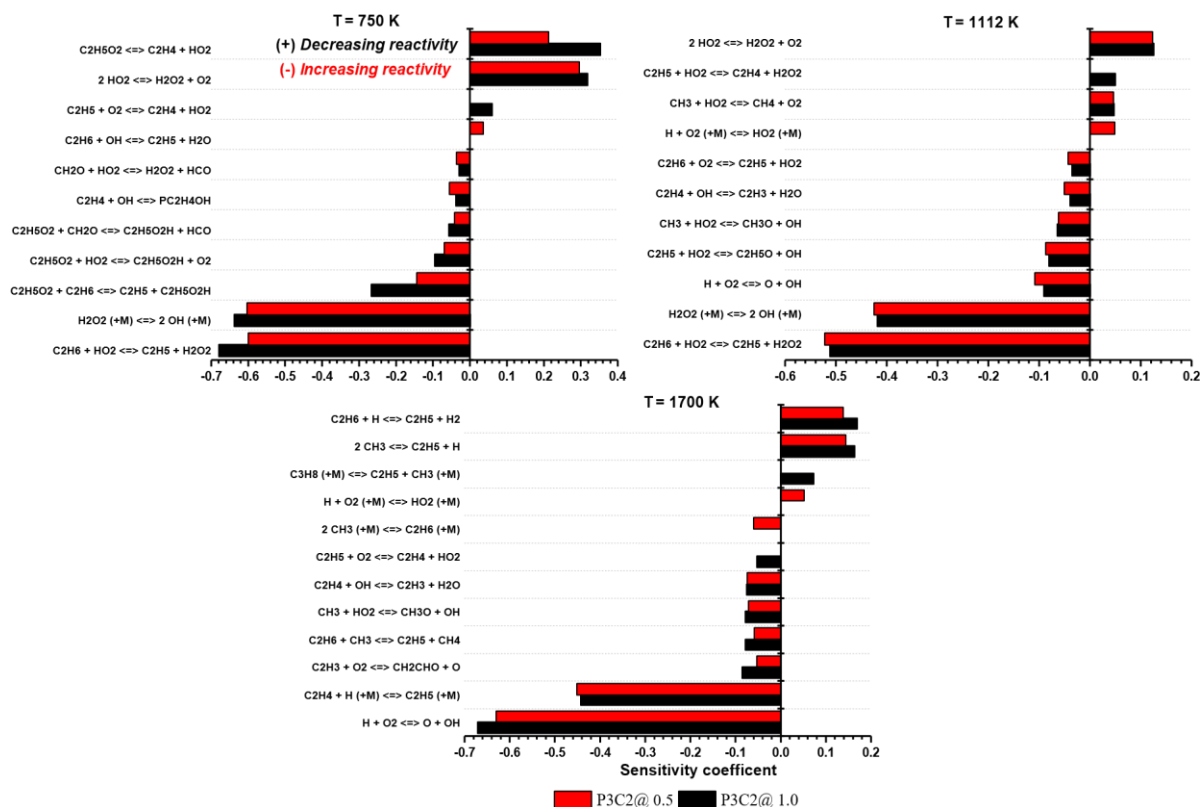


Figure ES101. Effect of equivalence ratio on the ten most prominent reactions, brute force sensitivity analysis of IDT corresponding to lines (1–3) in Figures 8(b, d); P3C2: $\phi = 1.0$, 75% N_2 , 20 bar. (For better interpretation of the colours, the reader is referred to the web version of this article)

Table ES23. Effect of decreasing equivalence ratio on the ten most prominent reactions of ethane at different temperatures in comparison to P3C2 case.

Temperature (K)	Promoted reactions	Suppressed reactions
750	$C_2H_6 + \dot{O}H = \dot{C}_2H_5 + H_2O$	$\dot{C}_2H_5 + O_2 = C_2H_4 + \dot{H}O_2$
1112	$\dot{H} + O_2 (+M) = \dot{H}O_2 (+M)$	$\dot{C}_2H_5 + \dot{H}O_2 = C_2H_4 + H_2O_2$
1700	$\dot{C}H_3 + \dot{C}H_3 (+M) = C_2H_6 (+M)$	$C_3H_8 (+M) = \dot{C}_2H_5 + \dot{C}H_3 (+M)$
		$C_2H_6 + \dot{H} = \dot{C}_2H_5 + H_2$
	$\dot{H} + O_2 (+M) = \dot{H}O_2 (+M)$	$\dot{C}_2H_5 + O_2 = C_2H_4 + \dot{H}O_2$

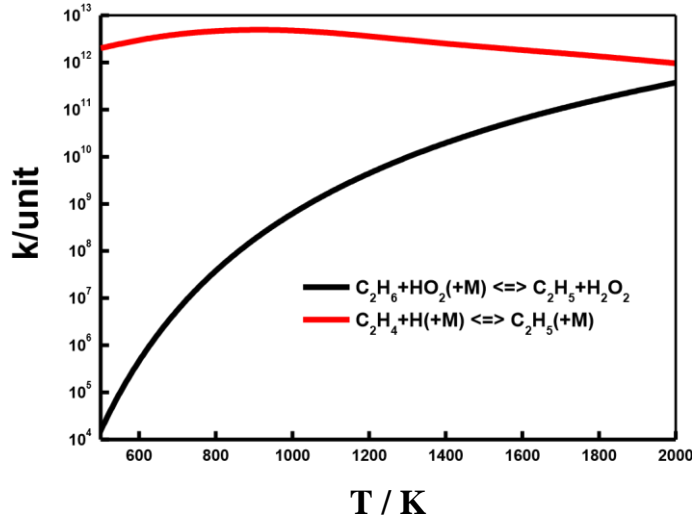


Figure ES103. A comparison between two important reactions involved in the effect of equivalence ratio on ethane oxidation.

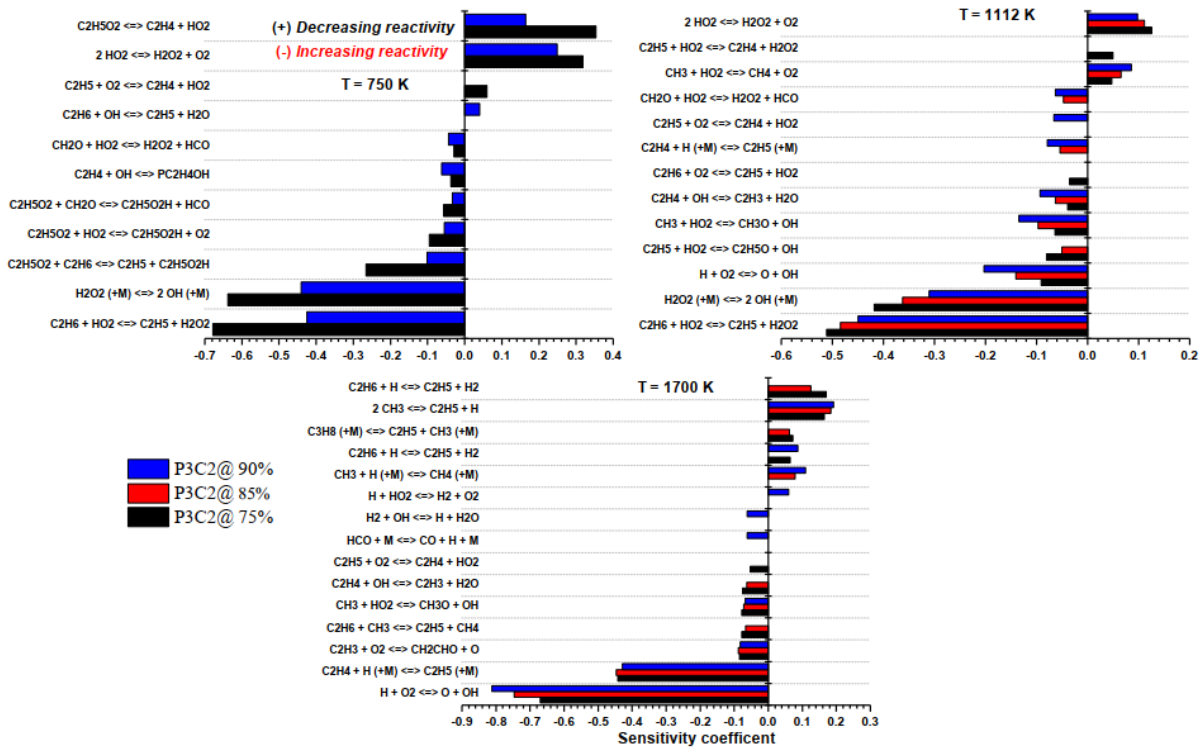


Figure ES104. Effect of dilution level on the ten most prominent reactions and their fluxes, brute force sensitivity analysis of IDT corresponding to lines (1–3) nFigures8(b, d); P3C2: $\phi = 1.0, 75\% \text{ N}_2, 20 \text{ bar}$ (For better interpretation of the colours, the reader is referred to the web version of this article)

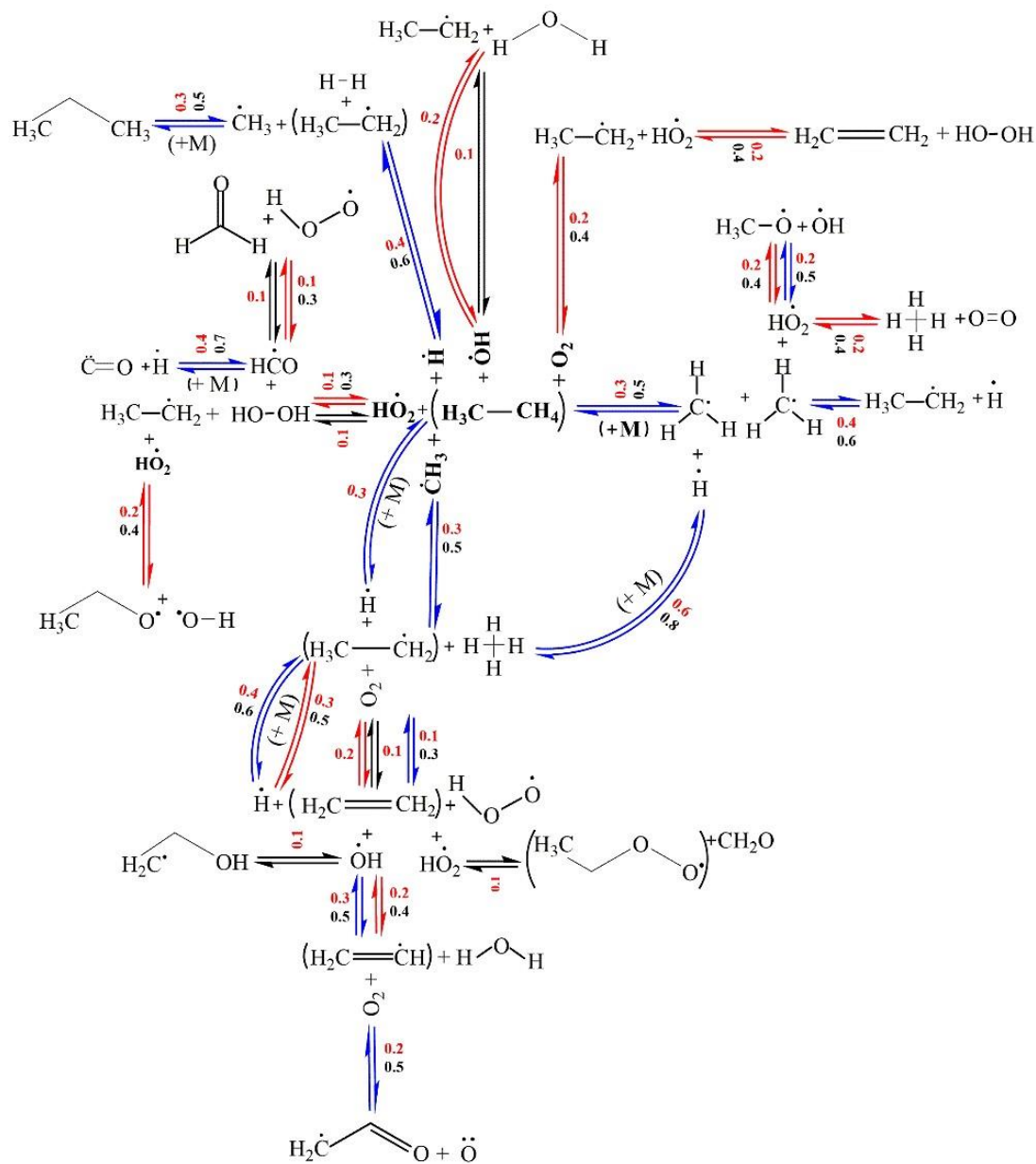


Figure S105. Effect of dilution level on the normalized flux analysis of the ten most prominent reactions corresponding to lines (1–3) in Figures 8(b,d); P3C2: $\phi = 1.0$, 75% N₂, 20 bar (based on the flux analysis of P3C2 base case when 20% of ethane (fuel) is consumed); the blue line: case (1), $T = 1700$ K, the red line: case (2), $T = 1112$ K, the black line: case (3), $T = 750$ K; the red number: 90% and the black number: 85% (For better interpretation of the colours, the reader is referred to the web version of this article)

Table ES24. Effect of increasing dilution (75% → 85%, Figure 8b) on the ten most prominent reactions of ethane at different temperatures in comparison to P3C2 case.

Temperature (K)	Promoted reactions	Suppressed reactions
1112	$C_2H_4 + \dot{H} (+M) = \dot{C}_2H_5 (+M)$	$C_2H_6 + O_2 = \dot{C}_2H_5 + \dot{H}O_2$
	$CH_2O + \dot{H}O_2 = H_2O_2 + \dot{H}CO$	$\dot{C}_2H_5 + \dot{H}O_2 = C_2H_4 + H_2O_2$
1700	$\dot{C}H_3 + \dot{H} (+M) = CH_4 (+M)$	$\dot{C}_2H_5 + O_2 = C_2H_4 + \dot{H}O_2$

Table ES25. Effect of increasing dilution (75% → 90% Figure 8d) on the ten most prominent reactions of ethane at different temperatures in comparison to P3C2 case.

Temperature (K)	Promoted reactions	Suppressed reactions
750	$C_2H_6 + \dot{O}H = \dot{C}_2H_5 + H_2O$	$\dot{C}_2H_5 + O_2 = C_2H_4 + \dot{H}O_2$
1112	$C_2H_4 + \dot{H} (+M) = \dot{C}_2H_5 (+M)$	$C_2H_6 + O_2 = \dot{C}_2H_5 + \dot{H}O_2$
	$CH_2O + \dot{H}O_2 = H_2O_2 + \dot{H}CO$	$\dot{C}_2H_5 + \dot{H}O_2 = C_2H_4 + H_2O_2$
	$\dot{C}_2H_5 + O_2 = C_2H_4 + \dot{H}O_2$	$\dot{C}_2H_5 + \dot{H}O_2 = C_2H_5\dot{O} + \dot{O}H$
1700	$\dot{C}H_3 + \dot{H} (+M) = CH_4 (+M)$	$C_2H_6 + \dot{H} = \dot{C}_2H_5 + H_2$
	$\dot{H}CO (+M) = CO + \dot{H} (+M)$	$C_3H_8 (+M) = \dot{C}_2H_5 + \dot{C}H_3 (+M)$
	$H_2 + \dot{O}H = \dot{H} + H_2O$	$C_2H_4 + \dot{O}H = \dot{C}_2H_3 + H_2O_2$
	$\dot{H} + \dot{H}O_2 = H_2 + O_2$	$C_2H_6 + \dot{C}H_3 = \dot{C}_2H_5 + CH_4$
		$\dot{C}_2H_5 + O_2 = C_2H_4 + \dot{H}O_2$

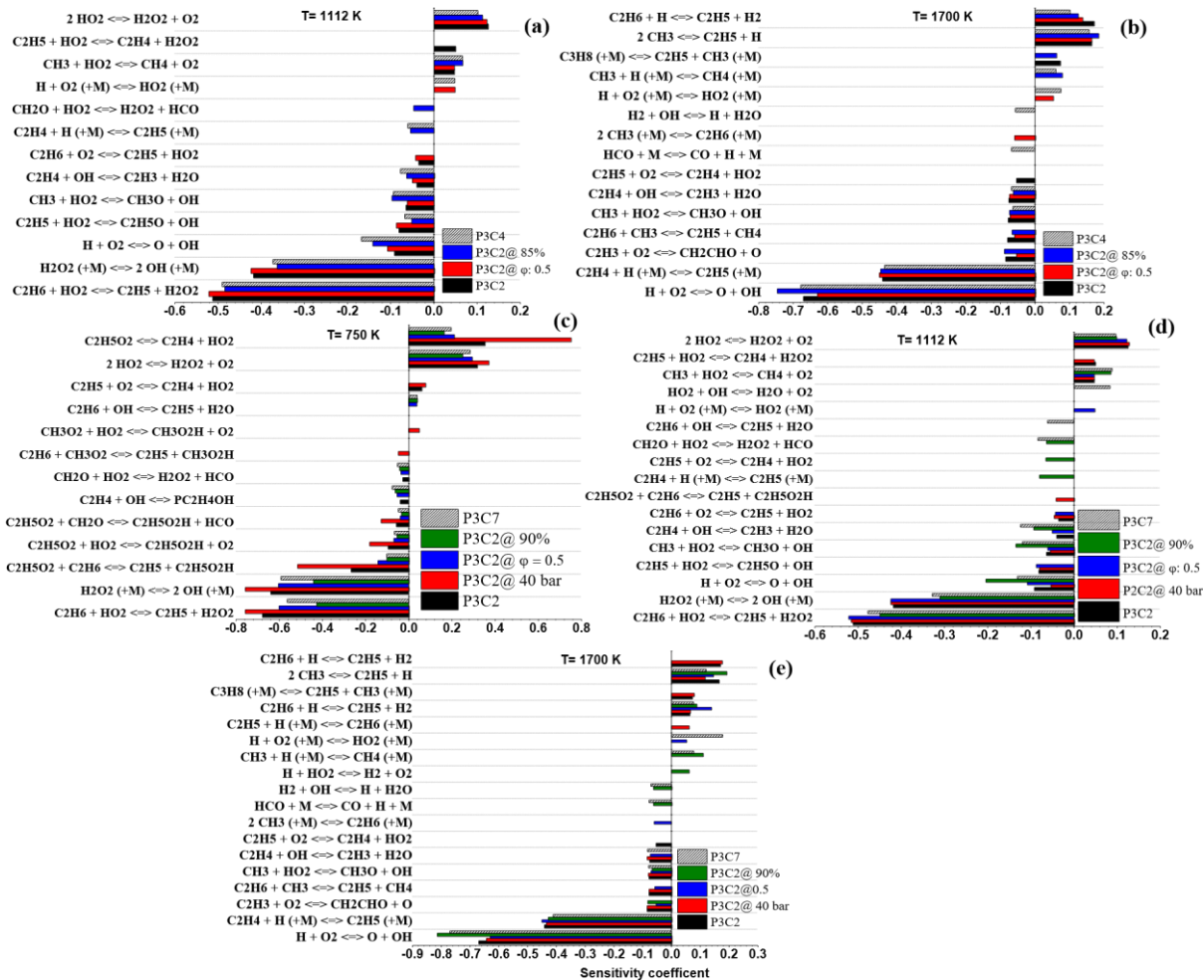


Figure ES106. Brute force sensitivity analysis of IDT corresponding to lines (1–3) in Figures 8(b,d).

12. Correlations

In this section, all the correlations and their relevant parameters derived individually for methane, ethylene, and ethane mixtures over a wide range of pressure, temperature, equivalence ratio, and dilution (based on the C³-NUIG comprehensive mechanism) have been presented in Table S26 to Table S36, respectively.

Table ES26. Evaluated coefficients for correlation of the simulated IDTs for low-temperature methane mixtures.

$0.25 \leq \varphi \leq 3.0$ $75 \leq$ <i>Dilution</i> $\leq 95\%$	$20 \leq p_{5,c} \leq 50$ /atm
	$800 \leq T_{5,c} \leq 1000$ /K
A	-6.671 ± 0.0439
B	14971.6 ± 73.50
C	-0.6812 ± 0.0031
D	-0.2510 ± 0.00455
E	-0.0784 ± 0.00934
R ²	0.98418
χ^2	0.00422

Table ES27. Evaluated coefficients for correlation of the simulated IDTs for fuel-lean, low pressure methane mixtures.

$0.25 \leq \varphi \leq 1.0$ $75 \leq$ <i>Dilution</i> $\leq 95\%$	$1 \leq p_{5,c} < 2$ /atm	
	$1000 \leq T_{5,c} < 1400$ /K	$1400 \leq T_{5,c} \leq 2000$ /K
A	-7.213 ± 0.033	-10.238 ± 0.007
B	17393.913 ± 63.785	26290.948 ± 20.224
C	0.2636 ± 0.0053	0.4025 ± 0.0013
D	-1.664 ± 0.007	-1.341 ± 0.002
E	0.3001 ± 0.007	0.2033 ± 0.0024
R ²	0.9940	0.9992
χ^2	5.7×10^{-04}	3.83×10^{-09}

Table ES28. Evaluated coefficients for correlation of the simulated IDTs for fuel-lean methane mixtures.

$0.25 \leq \varphi \leq 1.0$ $75 \leq$ <i>Dilution</i> $\leq 95\%$	$2 \leq p_{5,c} < 18$ /atm		$18 \leq p_{5,c} \leq 50$ /atm	
	$1000 \leq T_{5,c} < 1400$ /K	$1400 \leq T_{5,c} \leq 2000$ /K	$1000 \leq T_{5,c} < 1400$ /K	$1400 \leq T_{5,c} \leq 2000$ /K
A	-7.509 ± 0.0269	-10.064 ± 0.0181	-6.151 ± 0.0388	-9.872 ± 0.0141
B	18340.12 ± 61.24	25519.76 ± 61.30	14203.23 ± 72.16	24515.61 ± 43.09
C	0.4181 ± 0.0043	0.3268 ± 0.00301	-0.3979 ± 0.00546	0.2702 ± 0.00216
D	-1.704 ± 0.0052	-1.2890 ± 0.00357	-1.275 ± 0.0086	-1.439 ± 0.0026
E	0.2342 ± 0.0056	0.2143 ± 0.00299	0.3804 ± 0.01321	0.3329 ± 0.00381
R ²	0.99625	0.997	0.98213	0.99713
χ^2	0.0015	2.81549×10^{-09}	1.40601×10^{-05}	5.00059×10^{-11}

Table ES29. Evaluated coefficients for correlation of the simulated IDTs for fuel-rich, low-pressure methane mixtures.

$1.0 < \varphi \leq 3.0$ $75 \leq \text{Dilution} \leq 95\%$	$1 \leq p_{5,c} < 2 \text{ /atm}$	
	$1000 \leq T_{5,c} < 1400 \text{ /K}$	$1400 \leq T_{5,c} \leq 2000 \text{ /K}$
A	-6.653 ± 0.035	-11.011 ± 0.007
B	15797.165 ± 63.8	27930.373 ± 19.066
C	0.189 ± 0.0063	0.2931 ± 0.0019
D	-1.650 ± 0.007	-1.386 ± 0.002
E	0.3795 ± 0.0083	0.3908 ± 0.0018
R²	0.9821	0.9993
χ^2	0.01015	2.09×10^{-08}

Table ES30. Evaluated coefficients for correlation of the simulated IDTs for fuel-rich methane mixtures.

$1 < \varphi \leq 3.0$ $75 \leq \text{Dilution} \leq 95\%$	$2 \leq p_{5,c} < 18 \text{ /atm}$		$18 \leq p_{5,c} \leq 50 \text{ /atm}$	
	$1000 \leq T_{5,c} < 1400 \text{ /K}$	$1400 \leq T_{5,c} \leq 2000 \text{ /K}$	$1000 \leq T_{5,c} < 1400 \text{ /K}$	$1400 \leq T_{5,c} \leq 2000 \text{ /K}$
A	-7.802 ± 0.0199	-10.865 ± 0.0144	-4.738 ± 0.0376	-10.271 ± 0.0080
B	18448.14 ± 44.92	27588.99 ± 48.57	12466.82 ± 60.25	25468.16 ± 24.41
C	0.3263 ± 0.00452	0.2843 ± 0.00332	-0.0697 ± 0.0102	0.2424 ± 0.0019
D	-1.830 ± 0.0046	-1.350 ± 0.0034	-1.873 ± 0.0103	-1.554 ± 0.0019
E	0.3785 ± 0.00477	0.3619 ± 0.00228	0.2624 ± 0.01547	0.4447 ± 0.00218
R²	0.99742	0.99808	0.97586	0.99899
χ^2	0.00858	1.12508×10^{-08}	5.62546×10^{-05}	1.34144×10^{-10}

Table ES31. Evaluated coefficients for correlation of the simulated IDTs for low-temperature ethylene mixtures.

$0.25 \leq \varphi \leq 3.0$ $75 \leq \text{Dilution} \leq 95\%$	$1 \leq p_{5,c} \leq 50 \text{ /atm}$
	$800 \leq T_{5,c} < 1000 \text{ /K}$
A	-10.492 ± 0.0263
B	19936.06 ± 48.24
C	-0.8030 ± 0.00149
D	-0.0624 ± 0.00209
E	0.0331 ± 0.00221
R²	0.99639
χ^2	0.00269

Table ES32. Evaluated coefficients for correlation of the simulated IDTs for fuel–lean ethylene mixtures.

$0.25 \leq \varphi \leq 1.0$ $75 \leq \text{Dilution} \leq 95\%$	$1 \leq p_{5,c} < 18 \text{ /atm}$		$18 \leq p_{5,c} \leq 50 \text{ /atm}$	
	$1000 \leq T_{5,c} < 1250 \text{ /K}$	$1250 \leq T_{5,c} \leq 2000 \text{ /K}$	$1000 \leq T_{5,c} < 1500 \text{ /K}$	$1500 \leq T_{5,c} \leq 2000 \text{ /K}$
A	-13.637 ± 0.1978	-7.422 ± 0.0072	-10.321 ± 0.0125	-9.219 ± 0.0181
B	26956.76 ± 460.66	10029.53 ± 24.17	19335.80 ± 26.90	13917.03 ± 49.31
C	-0.0857 ± 0.01535	-0.2327 ± 0.00228	-0.7194 ± 0.00142	-0.2288 ± 0.00356
D	-0.6622 ± 0.01892	-0.6570 ± 0.00296	-0.1085 ± 0.00179	-0.5751 ± 0.00454
E	0.3652 ± 0.01448	-0.0288 ± 0.00285	0.1582 ± 0.00265	0.2716 ± 0.00674
R²	0.91273	0.9969	0.99884	0.98511
χ^2	2.97089×10^{-06}	6.58757×10^{-13}	4.85452×10^{-09}	3.40205×10^{-14}

Table ES33. Evaluated coefficients for correlation of the simulated IDTs for fuel–rich ethylene mixtures.

$1 < \varphi \leq 3.0$ $75 \leq \text{Dilution} \leq 95\%$	$1 \leq p_{5,c} < 18 \text{ /atm}$		$18 \leq p_{5,c} \leq 50 \text{ /atm}$	
	$1000 \leq T_{5,c} < 1400 \text{ /K}$	$1400 \leq T_{5,c} \leq 2000 \text{ /K}$	$1000 \leq T_{5,c} < 1650 \text{ /K}$	$1650 \leq T_{5,c} \leq 2000 \text{ /K}$
A	-12.533 ± 0.0614	-7.312 ± 0.0259	-9.405 ± 0.0124	-8.773 ± 0.0385
B	24802.68 ± 142.85	9861.48 ± 86.08	17493.71 ± 26.22	13588.02 ± 103.89
C	-0.3634 ± 0.0072	0.1626 ± 0.01446	-0.7408 ± 0.00199	-0.1212 ± 0.01156
D	-0.4497 ± 0.00734	-1.2163 ± 0.01433	-0.1708 ± 0.0021	-0.6130 ± 0.01146

Table ES34. Evaluated coefficients for correlation of the simulated IDTs for low–temperature ethane mixtures.

$0.25 \leq \varphi \leq 3.0$ $75 \leq \text{Dilution} \leq 95\%$	$1 \leq p_{5,c} \leq 50 \text{ /atm}$
	$800 \leq T_{5,c} < 1000 \text{ /K}$
A	-10.236 ± 0.0083
B	21737.98 ± 15.20
C	$-0.5890 \pm 3.68\text{E-}4$
D	$-0.0285 \pm 5.16\text{E-}4$
E	$-0.3357 \pm 6.29\text{E-}4$
R²	0.99976
χ^2	0.00408

Table ES35. Evaluated coefficients for correlation of the simulated IDTs of fuel–lean ethane mixtures.

$0.25 \leq \varphi \leq 1.0$ $75 \leq \text{Dilution} \leq 95\%$	$1 \leq p_{5,c} < 18 \text{ /atm}$		$18 \leq p_{5,c} \leq 50 \text{ /atm}$	
	$1000 \leq T_{5,c} < 1400 \text{ /K}$	$1400 \leq T_{5,c} \leq 2000 \text{ /K}$	$1000 \leq T_{5,c} < 1400 \text{ /K}$	$1400 \leq T_{5,c} \leq 2000 \text{ /K}$
A	-12.164 ± 0.0544	-8.233 ± 0.0129	-10.137 ± 0.0101	-10.219 ± 0.0237
B	26047.966 ± 194.156	15179.79 ± 38.132	20728.66 ± 21.89	19070.91 ± 69.52
C	-0.13576 ± 0.00777	0.38121 ± 0.00355	-0.6633 ± 0.00107	0.1545 ± 0.00475
D	-0.43406 ± 0.00959	-0.97271 ± 0.0042	-0.0524 ± 0.00133	-0.6044 ± 0.00537
E	-0.12038 ± 0.00772	-0.14879 ± 0.00293	-0.1253 ± 0.00198	0.0826 ± 0.00705
R²	0.96685	0.99179	0.99937	0.98886
χ^2	1.05×10^{-05}	3.35×10^{-12}	7.21×10^{-09}	6.15×10^{-14}

Table ES36. Evaluated coefficients for correlation of the simulated IDTs of fuel–rich ethane mixtures.

$1 < \varphi \leq 3.0$ $75 \leq \text{Dilution} \leq 95\%$	$1 \leq p_{5,c} < 18 \text{ /atm}$		$18 \leq p_{5,c} \leq 50 \text{ /atm}$	
	$1000 \leq T_{5,c} < 1400 \text{ /K}$	$1400 \leq T_{5,c} \leq 2000 \text{ /K}$	$1000 \leq T_{5,c} < 1400 \text{ /K}$	$1400 \leq T_{5,c} \leq 2000 \text{ /K}$
A	-9.967 ± 0.0265	-8.850 ± 0.0122	-9.966 ± 0.0265	-8.850 ± 0.0122
B	21153.95 ± 60.81	18155.50 ± 26.05	21153.95 ± 60.81	18155.50 ± 26.05
C	-0.2480 ± 0.00672	-0.5261 ± 0.00326	-0.2480 ± 0.00672	-0.5261 ± 0.00326
D	-0.4038 ± 0.00643	-0.2583 ± 0.00318	-0.4038 ± 0.00643	-0.2583 ± 0.00318
E	-0.24603 ± 0.00352	-0.1361 ± 0.00284	-0.2460 ± 0.00352	-0.1361 ± 0.00284
R²	0.99511	0.99776	0.99511	0.99776
χ^2	8.31×10^{-07}	3.20×10^{-09}	8.31×10^{-07}	3.20×10^{-09}

13. References

- [1] C.-W. Zhou, Y. Li, U. Burke, C. Banyon, K.P. Somers, S. Ding, S. Khan, J.W. Hargis, T. Sikes, O. Mathieu, E.L. Petersen, M. AlAbbad, A. Farooq, Y. Pan, Y. Zhang, Z. Huang, J. Lopez, Z. Loparo, S.S. Vasu, H.J. Curran, An experimental and chemical kinetic modeling study of 1,3-butadiene combustion: Ignition delay time and laminar flame speed measurements, *Combust. Flame* 197 (2018) 423-438.
- [2] S.M. Burke, W. Metcalfe, O. Herbinet, F. Battin-Leclerc, F.M. Haas, J. Santner, F.L. Dryer, H.J. Curran, An experimental and modeling study of propene oxidation. Part 1: Speciation measurements in jet-stirred and flow reactors, *Combust. Flame* 161 (2014) 2765-2784.
- [3] Y. Li, C.-W. Zhou, K.P. Somers, K. Zhang, H.J. Curran, The oxidation of 2-butene: A high pressure ignition delay, kinetic modeling study and reactivity comparison with isobutene and 1-butene, *Prog. Energy Combust. Sci* 36 (2017) 403-411.
- [4] C.-W. Zhou, Y. Li, E. O'Connor, K.P. Somers, S. Thion, C. Keesee, O. Mathieu, E.L. Petersen, T.A. DeVerter, M.A. Oehlschlaeger, G. Kukkadapu, C.-J. Sung, M. Alrefae, F. Khaled, A. Farooq, P. Dirrenberger, P.-A. Glaude, F. Battin-Leclerc, J. Santner, Y. Ju, T. Held, F.M. Haas, F.L. Dryer, H.J. Curran, A comprehensive experimental and modeling study of isobutene oxidation, *Combust. Flame* 167 (2016) 353-379.

- [5] U. Burke, W.K. Metcalfe, S.M. Burke, K.A. Heufer, P. Dagaut, H.J. Curran, A detailed chemical kinetic modeling, ignition delay time and jet-stirred reactor study of methanol oxidation, *Combust. Flame* 165 (2016) 125-136.
- [6] S.M. Burke, U. Burke, R. Mc Donagh, O. Mathieu, I. Osorio, C. Keesee, A. Morones, E.L. Petersen, W. Wang, T.A. DeVerter, M.A. Oehlschlaeger, B. Rhodes, R.K. Hanson, D.F. Davidson, B.W. Weber, C.-J. Sung, J. Santner, Y. Ju, F.M. Haas, F.L. Dryer, E.N. Volkov, E.J.K. Nilsson, A.A. Konnov, M. Alrefae, F. Khaled, A. Farooq, P. Dirrenberger, P.-A. Glaude, F. Battin-Leclerc, H.J. Curran, An experimental and modeling study of propene oxidation. Part 2: Ignition delay time and flame speed measurements, *Combust. Flame* 162 (2015) 296-314.
- [7] W.K. Metcalfe, S.M. Burke, S.S. Ahmed, H.J. Curran, A hierarchical and comparative kinetic modeling study of C₁ – C₂ hydrocarbon and oxygenated fuels, *Int. J. Chem. Kinet.* 45 (2013) 638-675.
- [8] A. Keromnes, W.K. Metcalfe, K.A. Heufer, N. Donohoe, A.K. Das, C.J. Sung, J. Herzler, C. Naumann, P. Griebel, O. Mathieu, M.C. Krejci, E.L. Petersen, W.J. Pitz, H.J. Curran, An experimental and detailed chemical kinetic modeling study of hydrogen and syngas mixture oxidation at elevated pressures, *Combust. Flame* 160 (2013) 995-1011.
- [9] G. Bagheri, E. Ranzi, M. Pelucchi, A. Parente, A. Frassoldati, T. Faravelli, Comprehensive kinetic study of combustion technologies for low environmental impact: MILD and OXY-fuel combustion of methane, *Combust. Flame.* 212 (2020) 142-155.
- [10]. Chemical-kinetic mechanisms for combustion applications. <http://combustion.ucsd.edu>
- [11] G.P. Smith, D.M. Golden, M. Frenklach, N.W. Moriarty, B. Eiteneer, M. Goldenberg, C.T. Bowman, R.K. Hanson, S. Song, W.C. Gardiner, Jr., V.V. Lissianski, Z. Qin, http://www.me.berkeley.edu/gri_mech/.
- [12]. G.P. Smith, Y. Tao, H. Wang, Foundational fuel chemistry model version 1.0 (FFCM-1), Stanford University, (2016).
- [13] C.J. Aul, W.K. Metcalfe, S.M. Burke, H.J. Curran, E.L. Petersen, Ignition and kinetic modeling of methane and ethane fuel blends with oxygen: A design of experiments approach, *Combust. Flame.* 160 (2013) 1153-1167.
- [14] H. Nakamura, D. Darcy, M. Mehl, C.J. Tobin, W.K. Metcalfe, W.J. Pitz, C.K. Westbrook, H.J. Curran, An experimental and modeling study of shock tube and rapid compression machine ignition of n-butylbenzene/air mixtures, *Combust. Flame* 161 (2014) 49-64.
- [15] C. Morley, Gaseq: A chemical equilibrium program for windows, 2004, <http://www.gaseq.co.uk>
- [16] U. Burke, K.P. Somers, P. O'Toole, C.M. Zinner, N. Marquet, G. Bourque, E.L. Petersen, W.K. Metcalfe, Z. Serinyel, H.J. Curran, An ignition delay and kinetic modeling study of methane, dimethyl ether, and their mixtures at high pressures, *Combust. Flame.* 162 (2015) 315-330.
- [17] A. Ramalingam, K. Zhang, A. Dhongde, L. Virnich, H. Sankhla, H. Curran, A. Heufer, An RCM experimental and modeling study on CH₄ and CH₄/C₂H₆ oxidation at pressures up to 160 bar, *Fuel.* 206 (2017) 325-333.

- [18] D. Healy, H.J. Curran, S. Dooley, J.M. Simmie, D.M. Kalitan, D.K. Petersen, G. Bourque, Methane/propane mixture oxidation at high pressures and at high, intermediate and low temperatures, *Combust. Flame*. 155 (2008) 451-461.
- [19] D. Healy, H.J. Curran, J.M. Simmie, D.M. Kalitan, C.M. Zinner, A.B. Barrett, E.L. Petersen, G. Bourque, Methane/ethane/propane mixture oxidation at high pressures and at high, intermediate and low temperatures, *Combust. Flame*. 155 (2008) 441-448.
- [20] S. Yousefian, N.J. Quinlan, R.F.D. Monaghan, Simulation of turbulent flow in a rapid compression machine: Large Eddy Simulation and computationally efficient alternatives for the design of ignition delay time experiments, *Fuel*. 234 (2018) 30-47.
- [21] C. Hemken, U. Burke, K.Y. Lam, D.F. Davidson, R.K. Hanson, K.A. Heufer, K. Kohse-Höinghaus, Toward a better understanding of 2-butanone oxidation: Detailed species measurements and kinetic modeling, *Combust. Flame*. 184 (2017) 195-207.
- [22]. TiePie <https://www.tiepie.com/en/oscilloscope-software>.
- [23]. PicoScope <https://www.picotech.com/downloads>.
- [24]. E.L. Petersen, M.J.A. Rickard, M.W. Crofton, E.D. Abbey, M.J. Traum, D.M. Kalitan, A facility for gas- and condensed-phase measurements behind shock waves, *Meas. Sci. Technol.* 16 (2005) 1716-1729.
- [25] B.W. Weber, C.-J. Sung, M.W. Renfro, On the uncertainty of temperature estimation in a rapid compression machine, *Combust. Flame* 162 (2015) 2518-2528.
- [26] R.F. Pachler, A.K. Ramalingam, K.A. Heufer, F. Winter, Reduction and validation of a chemical kinetic mechanism including necessity analysis and investigation of CH₄/C₃H₈ oxidation at pressures up to 120 bar using a rapid compression machine, *Fuel* 172 (2016) 139-145.
- [27] B. Koroglu, O.M. Pryor, J. Lopez, L. Nash, S.S. Vasu, Shock tube ignition delay times and methane time-histories measurements during excess CO₂ diluted oxy-methane combustion, *Combust. Flame* 164 (2016) 152-163.
- [28] F.N. Egolfopoulos, D.L. Zhu, C.K. Law, Experimental and numerical determination of laminar flame speeds: Mixtures of C₂-hydrocarbons with oxygen and nitrogen, *Symp. (Int.) Combust.* 23 (1991) 471-478.
- [29] W. Lowry, J. de Vries, M. Krejci, E. Petersen, Z. Serinyel, W. Metcalfe, H. Curran, G. Bourque, Laminar flame speed measurements and modeling of pure alkanes and alkane blends at elevated pressures, *J. Eng. Gas Turbines Power.* (2011), 133(9), 091501.
- [30] G. Rozenchan, D.L. Zhu, C.K. Law, S.D. Tse, Outward propagation, burning velocities, and chemical effects of methane flames up to 60 ATM, *Prog. Energy Combust. Sci* 29 (2002) 1461-1470.
- [31] M.I. Hassan, K.T. Aung, G.M. Faeth, Measured and predicted properties of laminar premixed methane/air flames at various pressures, *Combust. Flame* 115 (1998) 539-550.
- [32] C.M. Vagelopoulos, F.N. Egolfopoulos, C.K. Law, Further considerations on the determination of laminar flame speeds with the counterflow twin-flame technique, *Symp. (Int.) Combust.* 25 (1994) 1341-1347.
- [33] A. Van Maaren, L.P.H. De Goey, Stretch and The adiabatic burning velocity of methane- and propane-air flames, *Combust. Sci. Technol.* 102 (1994) 309-314.

- [34] X.J. Gu, M.Z. Haq, M. Lawes, R. Woolley, Laminar burning velocity and markstein lengths of methane–air mixtures, *Combust. Flame* 121 (2000) 41-58.
- [35] Y. Kochar, S. Vaden, T. Lieuwen, J. Seitzman, Laminar flame speed of hydrocarbon fuels with preheat and low oxygen content, In 48th AIAA Aerospace Sciences Meeting Including the New Horizons Forum and Aerospace Exposition, AIAA: Orlando, Florida, (2010).
- [36] G. Jomaas, X.L. Zheng, D.L. Zhu, C.K. Law, Experimental determination of counterflow ignition temperatures and laminar flame speeds of C₂–C₃ hydrocarbons at atmospheric and elevated pressures, *Prog. Energy Combust. Sci* 30 (2005) 193-200.
- [37] X. Shen, X. Yang, J. Santner, J. Sun, Y. Ju, Experimental and kinetic studies of acetylene flames at elevated pressures, *Prog. Energy Combust. Sci* 35 (2015) 721-728.
- [38] E. Rokni, A. Moghaddas, O. Askari, H. Metghalchi, Measurement of Laminar Burning Speeds and Investigation of Flame Stability of Acetylene (C₂H₂)/Air Mixtures, *J. Energy Resour. Technol.* 137 (2014).
- [39] S. Ravi, T.G. Sikes, A. Morones, C.L. Keesee, E.L. Petersen, Comparative study on the laminar flame speed enhancement of methane with ethane and ethylene addition, *Prog. Energy Combust. Sci* 35 (2015) 679-686.
- [40] N. Lokachari, U. Burke, A. Ramalingam, M. Turner, R. Hesse, K.P. Somers, J. Beeckmann, K.A. Heufer, E.L. Petersen, H.J. Curran, New experimental insights into acetylene oxidation through novel ignition delay times, laminar burning velocities and chemical kinetic modelling, *Prog. Energy Combust. Sci* 37 (2019) 583-591.
- [41] M. I. Hassan, K. T. Aung, O. C. Kwon, G. M. Faeth, Properties of laminar premixed hydrocarbon/air flames at various pressures. *J. Propul. Power* 14(4) (1998) 479-488.
- [42] K. Kumar, G. Mittal, C.-J. Sung, C.K. Law, An experimental investigation of ethylene/O₂/diluent mixtures: Laminar flame speeds with preheat and ignition delays at high pressures, *Combust. Flame* 153 (2008) 343-354.
- [43] A.A. Konnov, I.V. Dyakov, J. De Ruyck, Measurement of adiabatic burning velocity in ethane–oxygen–nitrogen and in ethane–oxygen–argon mixtures, *Exp. Therm Fluid Sci.* 27 (2003) 379-384.
- [44] K.T. Aung, L.K. Tseng, M.A. Ismail, G.M. Faeth, Response to comment by S.C. Taylor and D.B. Smith on “laminar burning velocities and markstein numbers of hydrocarbon/air flames”, *Combust. Flame* 102 (1995) 526-530.
- [45] K.J. Bosschaart, L.P.H. de Goey, The laminar burning velocity of flames propagating in mixtures of hydrocarbons and air measured with the heat flux method, *Combust. Flame* 136 (2004) 261-269.
- [46] A.A. Konnov, I.V. Dyakov, J. De Ruyck, Probe sampling measurements and modeling of nitric oxide formation in methane-air flames, *Combust. Sci. Technol.* 169 (2001) 127-153.
- [47] T.L. Cong, E. Bedjanian, P. Dagaut, Oxidation of Ethylene and Propene in the Presence of CO₂ and H₂O: Experimental and detailed kinetic modeling study, *Combust. Sci. Technol.* 182 (2010) 333-349.
- [48] S. Jallais, L. Bonneau, M. Auzanneau, V. Naudet, S. Bockel-Macal, An experimental and kinetic study of ethene oxidation at a high equivalence ratio, *Ind. Eng. Chem. Res.* 41 (2002) 5659-5667.

[49] J.G. Lopez, C.L. Rasmussen, M.U. Alzueta, Y. Gao, P. Marshall, P. Glarborg, Experimental and kinetic modeling study of C₂H₄ oxidation at high pressure, Proc. Combust. Inst. 32 (2009) 367-375.

Appendix F

(Supplementary material for Chapter 8)

1. Chemical kinetic report: Exp data vs NUIGMechs



OLLSCOIL NA GAILLIMHE
UNIVERSITY OF GALWAY

University of Galway
Combustion Chemistry Centre (C³)

NUIGMech0.9, NUIGMech1.0,
NUIGMech1.1, and NUIGMech1.2

Mechanism Validation

Chemical Kinetics Report of C₁ – C₃ of Gaseous Hydrocarbons

Sergio Enrique Sanchez Martinez

February 1, 2023

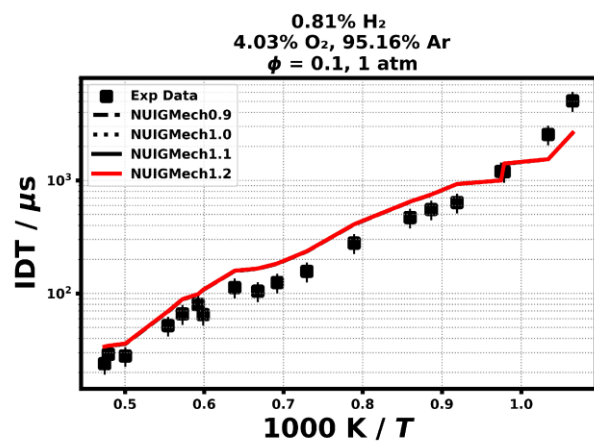
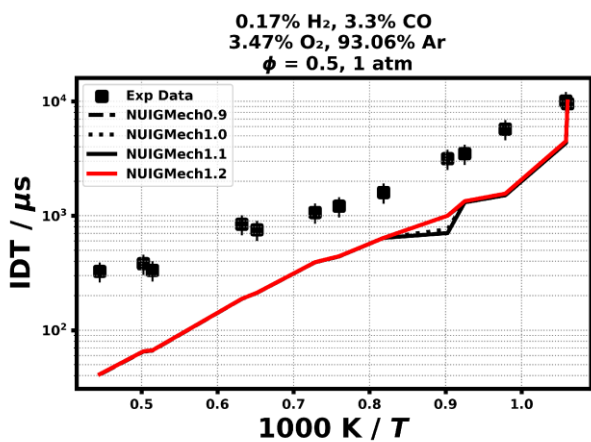
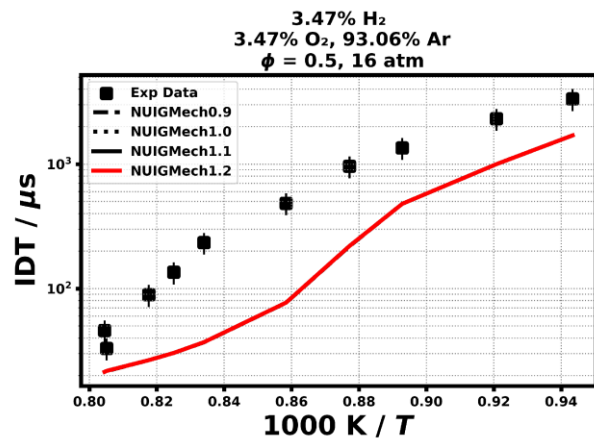
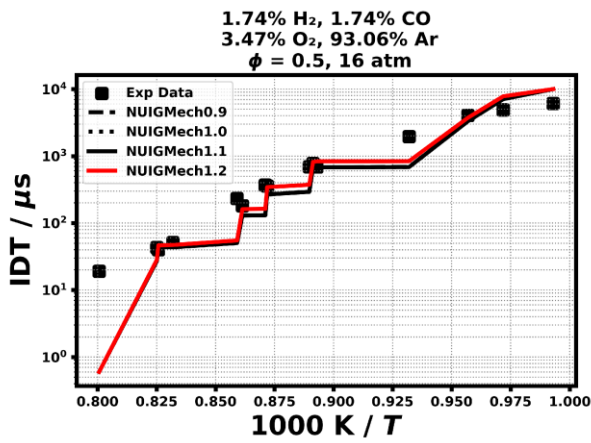
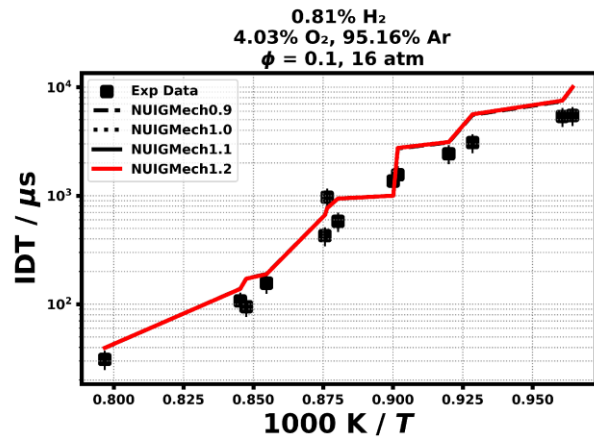
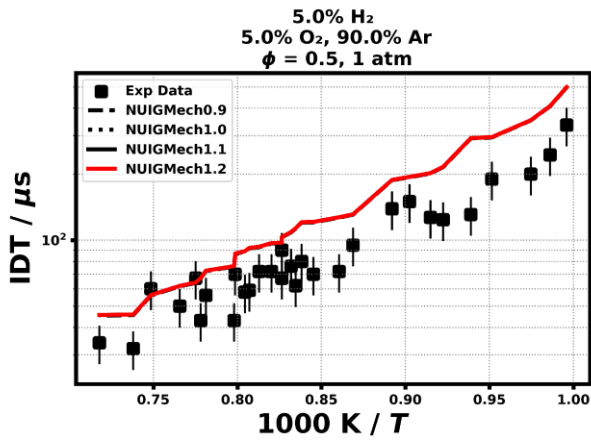
Range of experimental conditions used for mechanism validation.

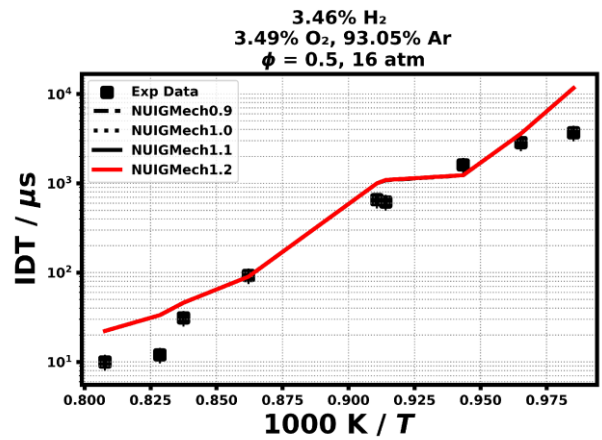
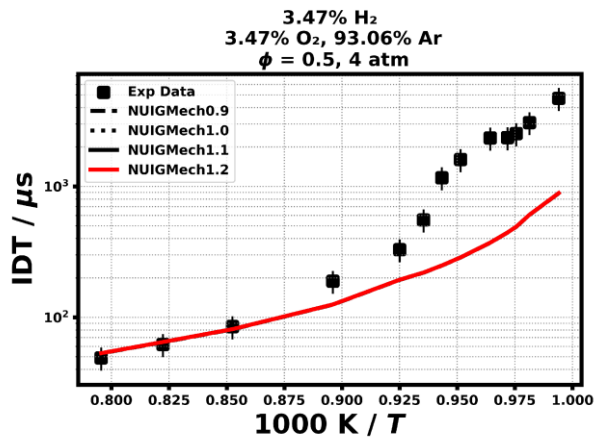
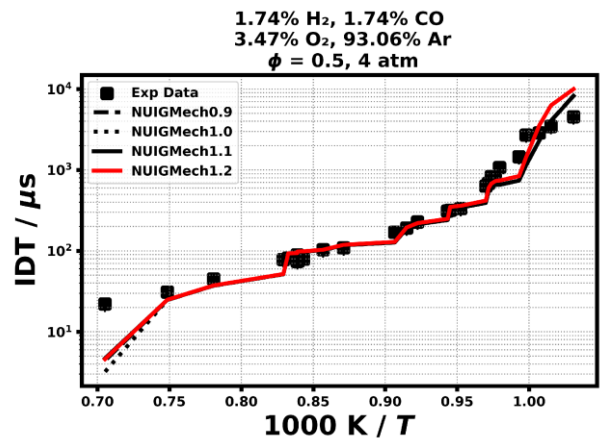
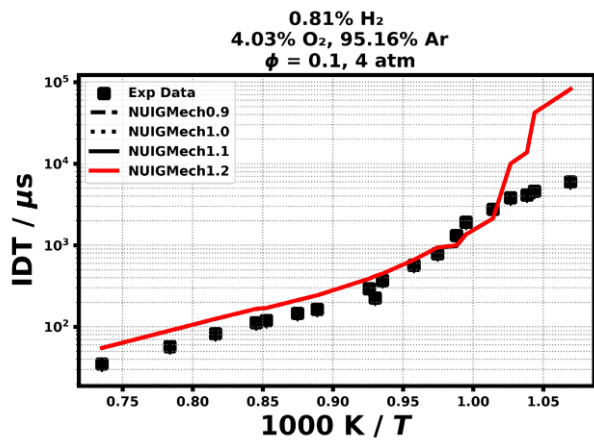
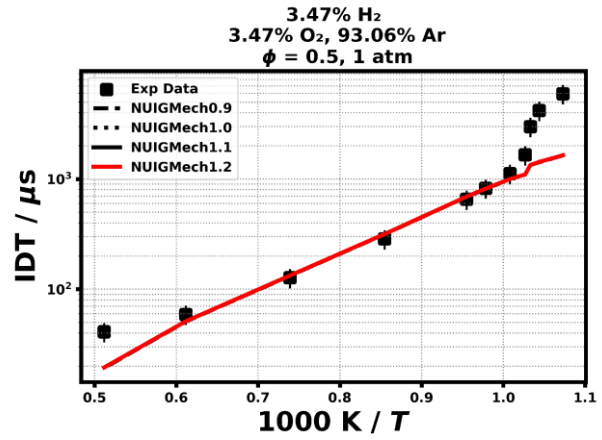
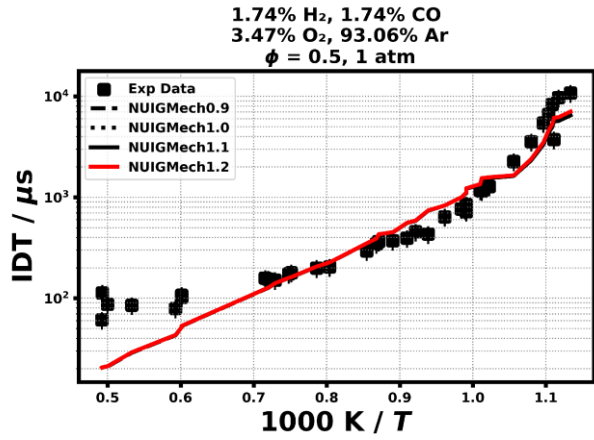
Species	ST	RCM		ST	RCM
H₂	□ 952.0 – 1818 K 1.62 – 270.5 atm 0.1 – 1.0	× — — —	CH₃CHO	□ 1250 – 1562.5 K 3 atm 0.5 – 1.5	× — — —
CH₃OH	□ 909.0 – 2180.0 K 0.99 – 51.71 atm 0.38 – 6.0	□ 817.0 – 980.0 K 9.27 – 40.64 atm 0.5 – 2.0	CH₄/C₂H₄	□ 989.5 – 2081.9 K 0.89 – 41.04 atm 0.5 – 2.0	□ 845.0 – 1105.0 K 19.71 – 40.44 atm 0.5 – 2.0
CH₄	□ 1041.0 – 2538.0 K 0.54 – 260.0 atm 0.1 – 6.0	□ 869.9 – 1178.19 K 10.0 – 24.0 atm 0.3 – 2.0	CH₄/C₂H₆	□ 911.0 – 1700.0 K 1.28 – 39.0 atm 0.5 – 2.0	□ 909.23 – 966.66 K 39.65 – 40.36 atm 1.0 – 1.0
C₂H₂	□ 808.6 – 2319.0 K 0.77 – 31.3 atm 0.06 – 2.0	□ 711.25 – 953.14 K 9.04 – 30.37 atm 0.5 – 2.0	C₂H₄/C₂H₆	□ 996.0 – 1930.4 K 0.9 – 40.57 atm 0.5 – 2.0	□ 892.0 – 1041.0 K 19.66 – 41.14 atm 0.5 – 2.0
C₂H₄	□ 945.2 – 2226.3 K 0.94 – 40.98 atm 0.3 – 3.0	□ 773.0 – 990.33 K 19.6 – 41.4 atm 0.5 – 2.0	C₂H₄/C₃H₈	□ 910.9 – 2044.5 K 0.87 – 40.14 atm 0.5 – 2.0	□ 804.0 – 1034.0 K 19.5 – 41.22 atm 0.5 – 2.0
C₂H₅OH	□ 778.1 – 1669.8 K 1.8 – 91.5 atm 0.25 – 2.0	□ 0.0 – 983.12 K 0.0 – 50.6 atm 0.3 – 2.0	C₂H₆/C₃H₈	□ 958.3 – 1998.7 K 0.91 – 41.06 atm 0.5 – 2.0	□ 836.0 – 1048.0 K 19.47 – 137 atm 0.5 – 2.0
C₂H₆	□ 947.3 – 1862.0 K 0.57 – 40.56 atm 0.1 – 2.0	□ 830.0 – 999.0 K 19.28 – 81.8 atm 0.5 – 2.0	CH₄/H₂	□ 1111.0 – 1666.0 K 20.0 atm 0.5	× — — —
CH₃OCH₃	□ 666.0 – 1880.9 K 1.01 – 40.35 atm 0.5 – 2.0	□ 645.0 – 1105.0 K 9.71 – 22.26 atm 4.0	CH₄/C₂H₄/ C₂H₆	□ 1052.0 – 1818.0 K 1.0 – 40.0 atm 0.5 – 2.0	□ 877.6 – 1052 K 20.0 – 135.0 atm 0.5 – 2.0
CH₃COCH₃	□ 666.0 – 1880.9 K 1.01 – 40.35 atm 0.5 – 2.0	× — — —	CH₄/C₂H₄/ C₂H₆/C₃H₈	□ 1000 – 2000 K 1– 40 atm 0.5 – 2.0	□ 819.0 – 1086.0 K 20.0 – 135.0 atm 0.5 – 2.0
C₃H₆	□ 999.0 – 1820.0 K 0.95 – 47.0 atm 0.5 – 2.0	□ 0.0 – 1241.0 K 0.0 – 41.62 atm 0.5 – 2.0	C₃H₈	□ 847.5 – 2615.0 K 0.82 – 41.34 atm 0.125 – 2.0	□ 714.0 – 909.0 K 30.0 – 50.0 atm 1.0
C₃H₈	□ 847.5 – 2615.0 K 0.82 – 41.34 atm 0.125 – 2.0	□ 714.0 – 909.0 K 30.0 – 50.0 atm 1.0	C₃H₄-A	□ 1175.0 – 1896.0 K 1.81 – 5.29 atm 0.5 – 2.0	× — — —
C₃H₄-P	□ 1131.0 – 2037.0 K 1.8 – 5.26 atm 0.5 – 2.0	× — — —			

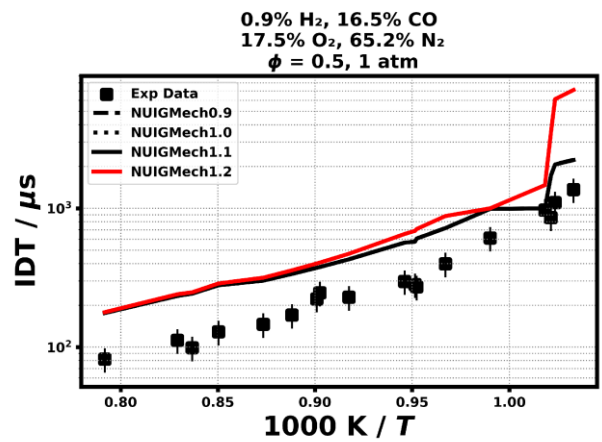
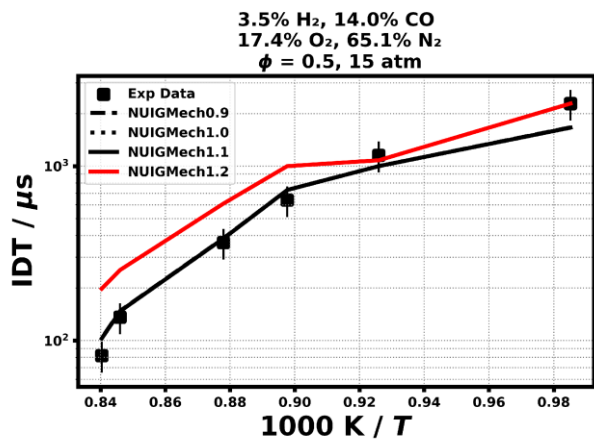
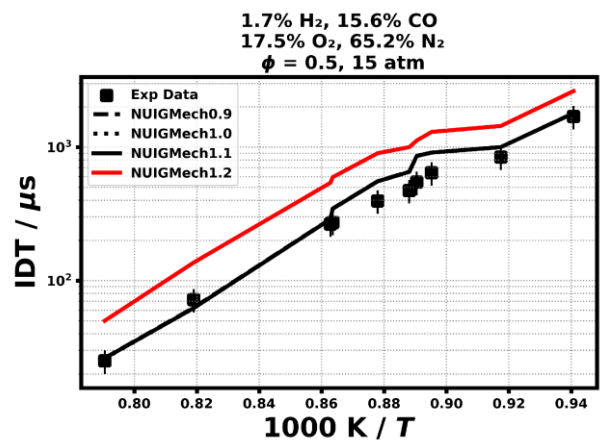
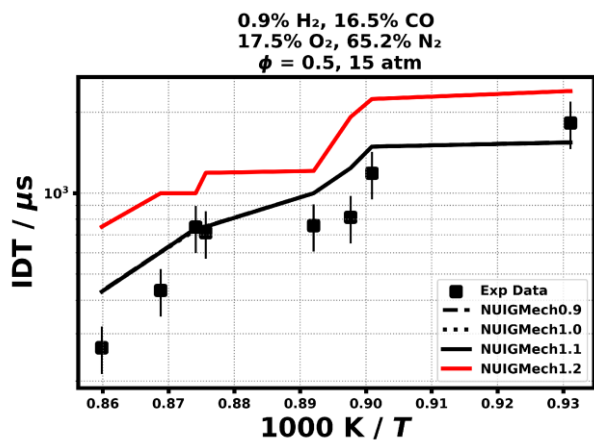
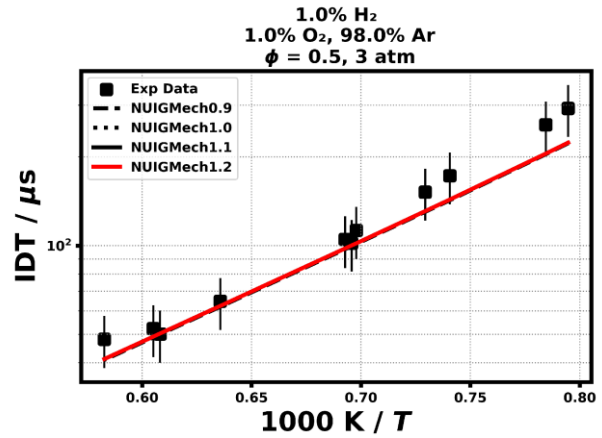
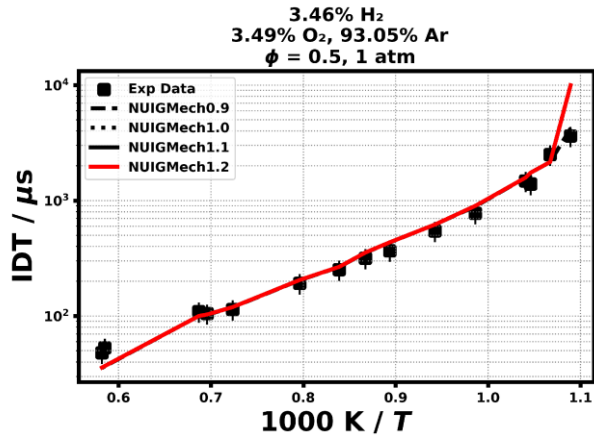
1 IDTs by Fuel Section

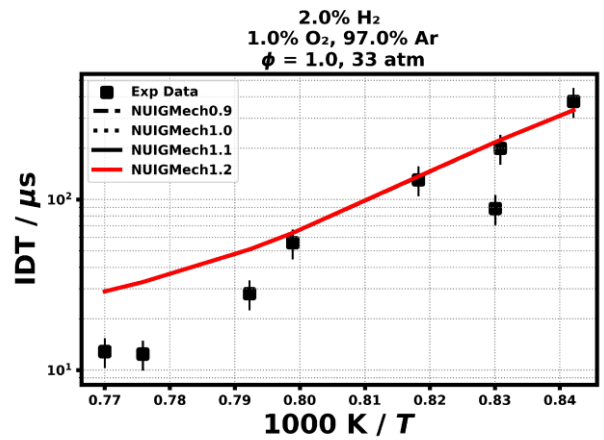
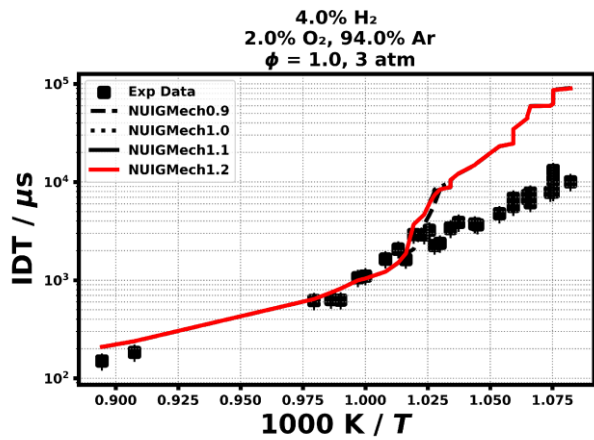
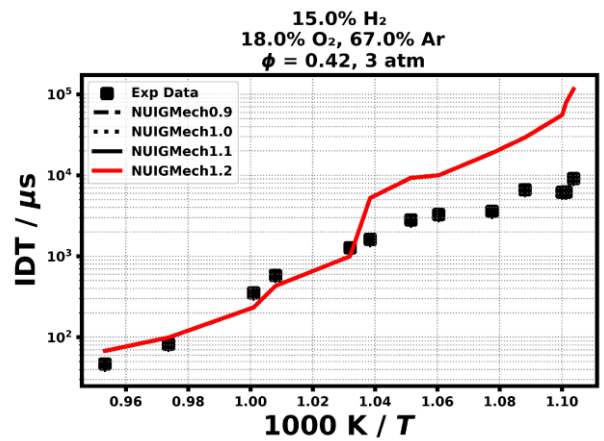
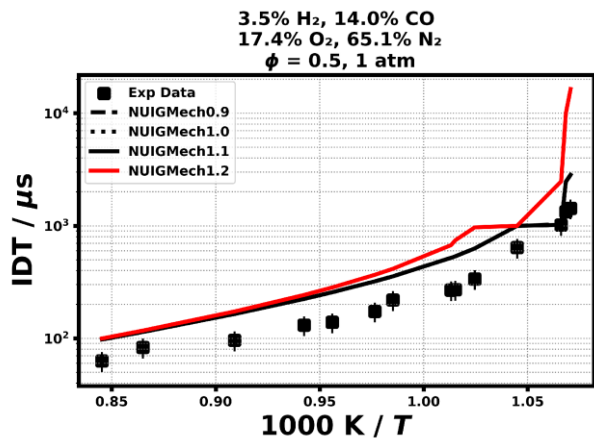
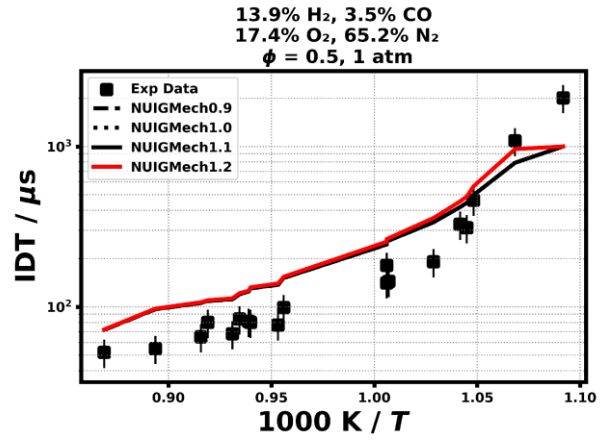
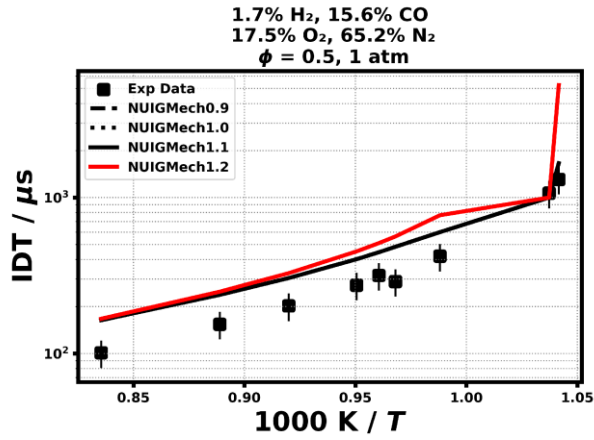
1.1 Shock Tube

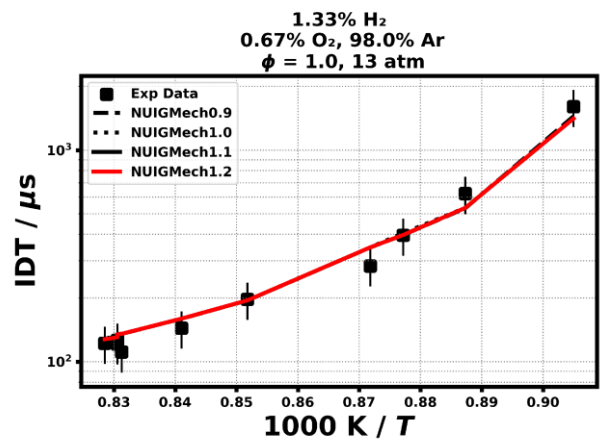
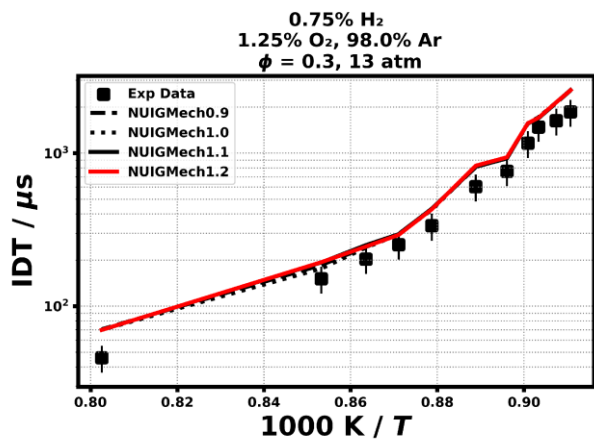
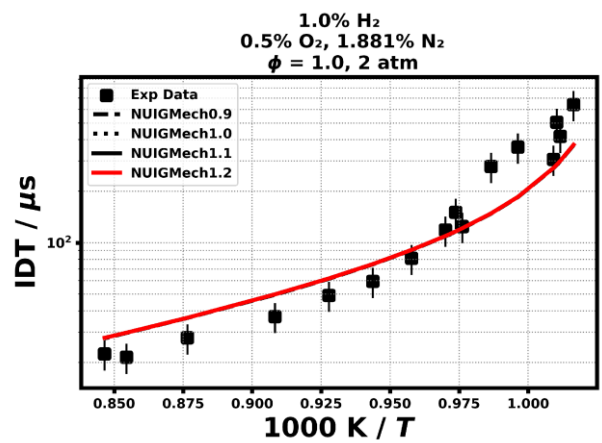
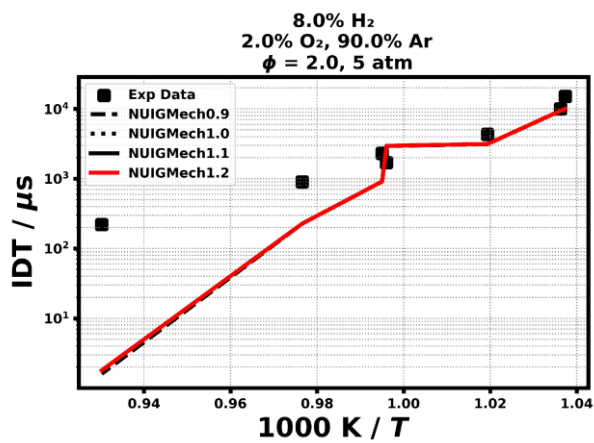
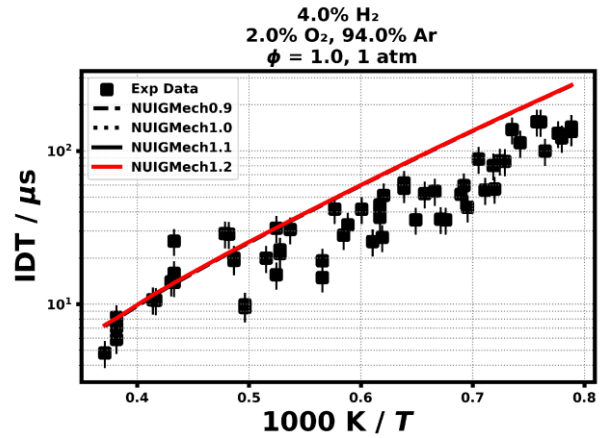
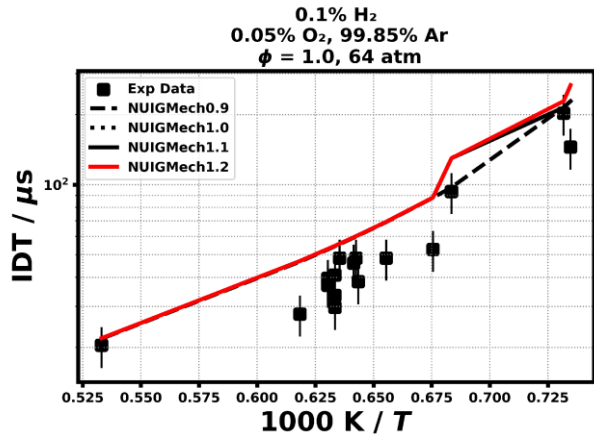
1.1.1 H₂

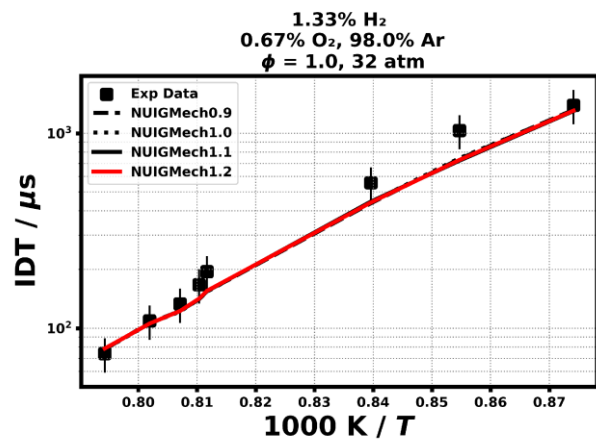
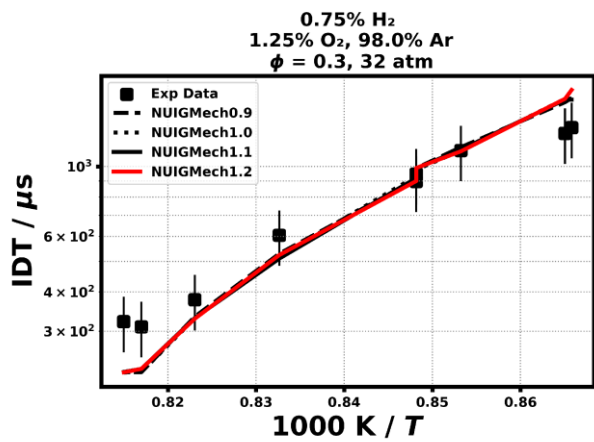
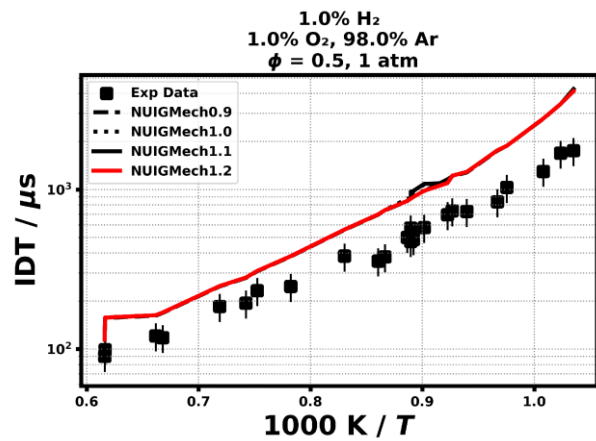
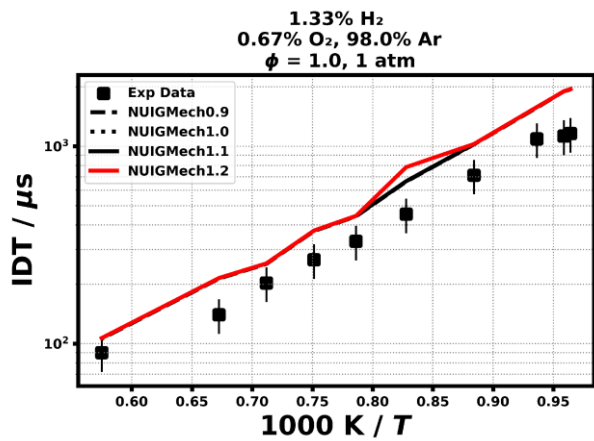
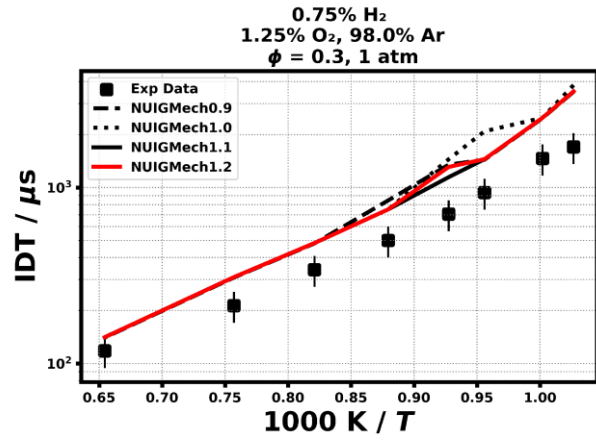
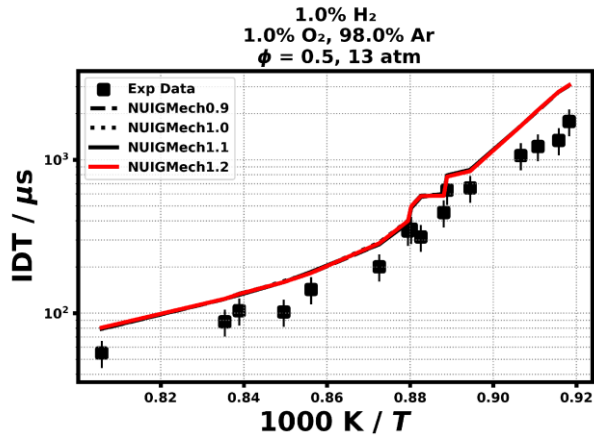


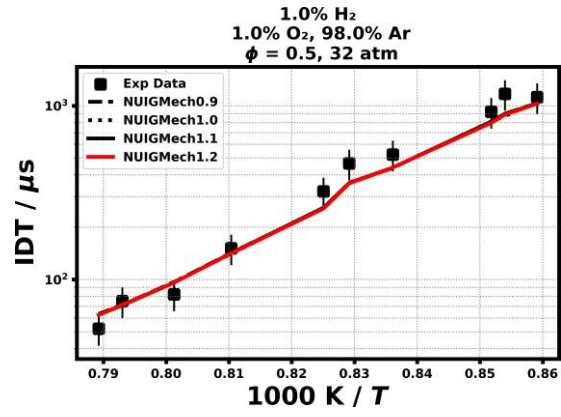




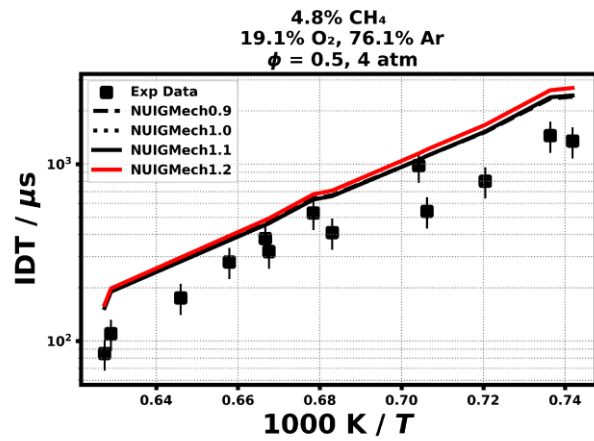
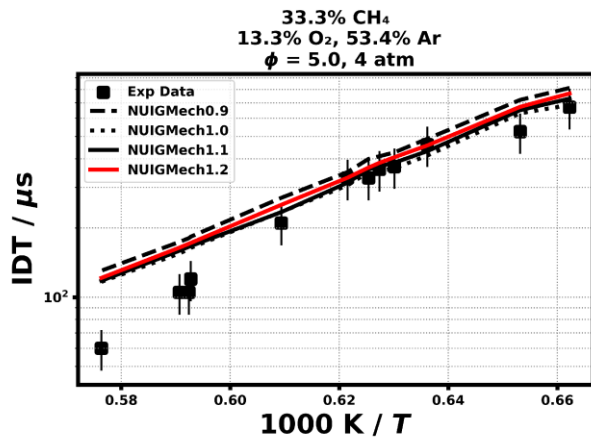
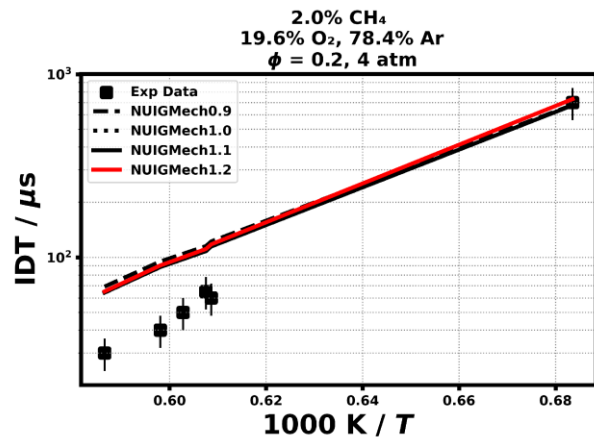
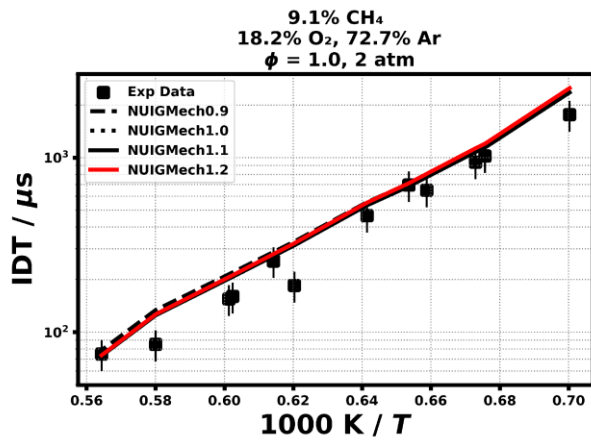
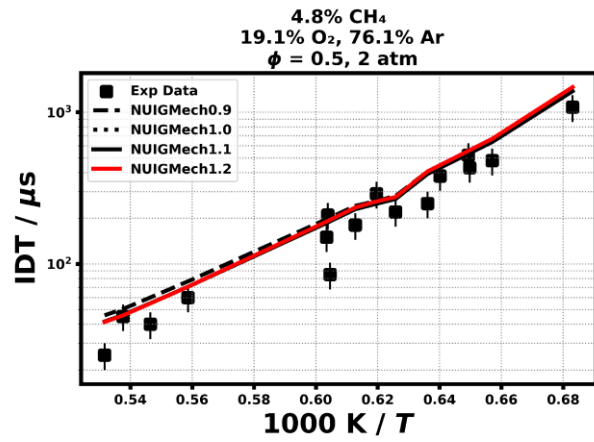
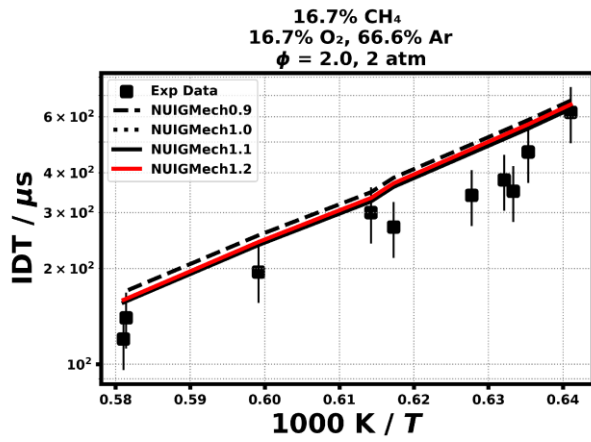


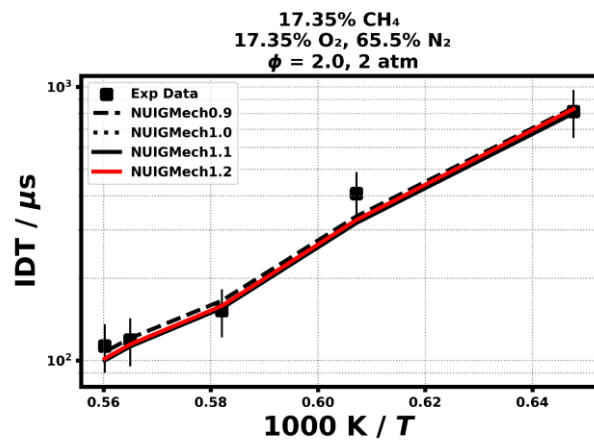
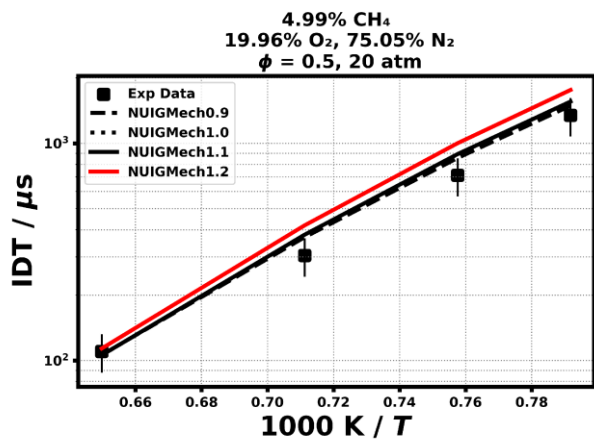
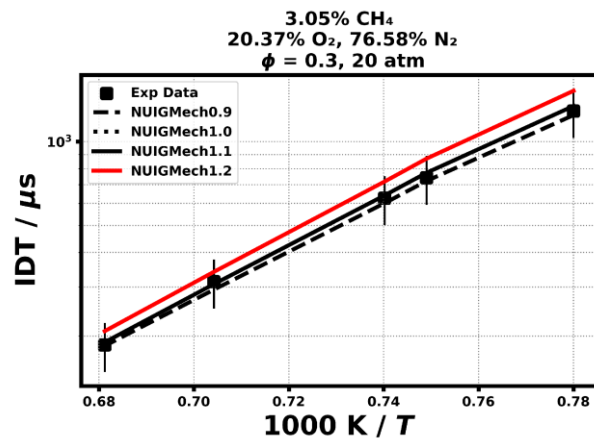
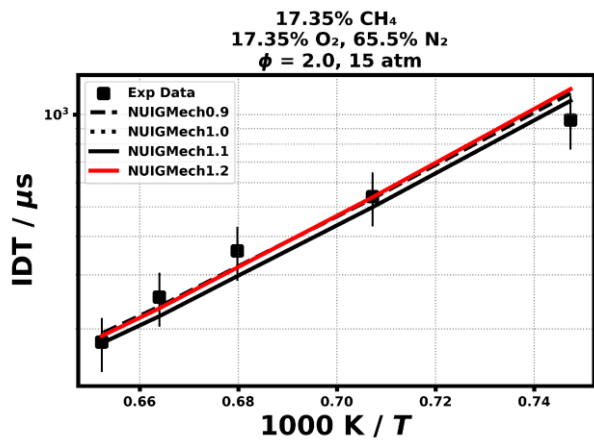
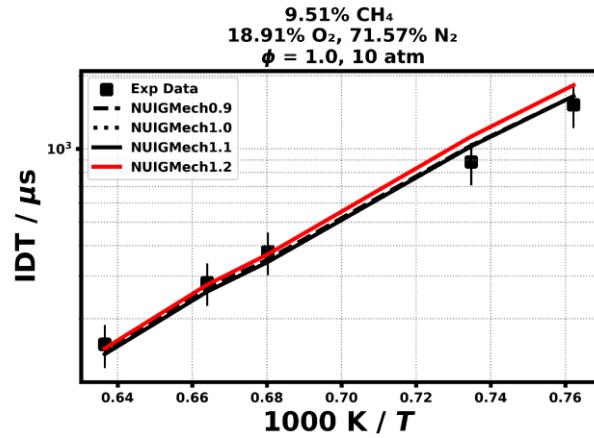
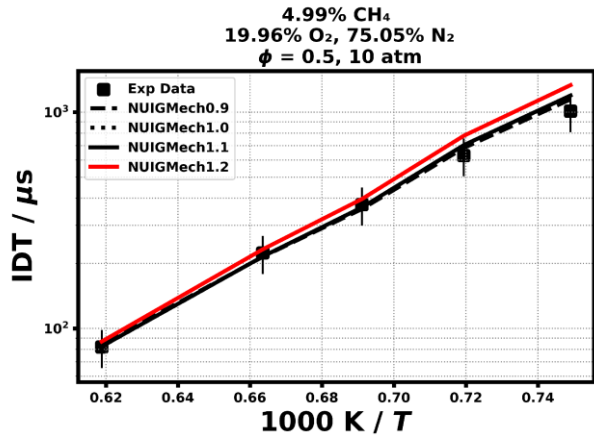


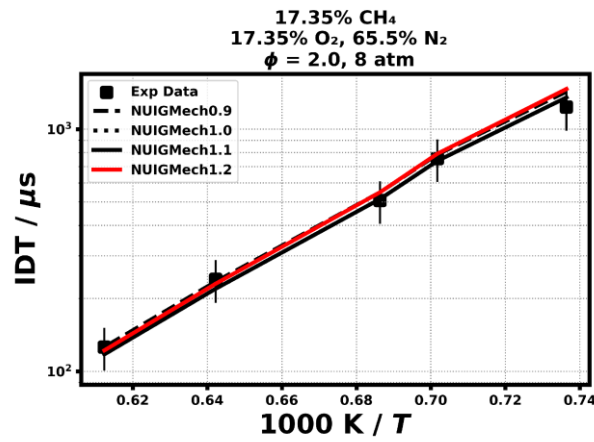
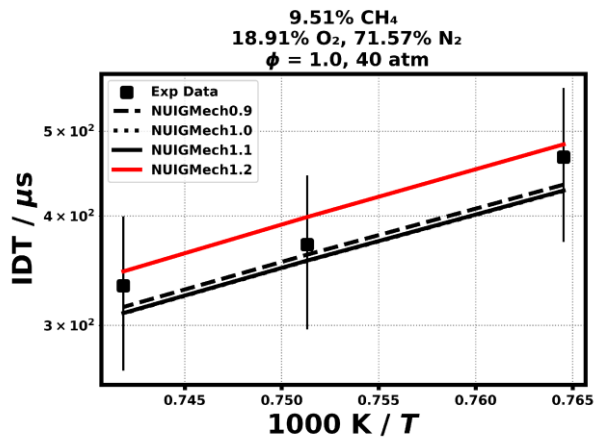
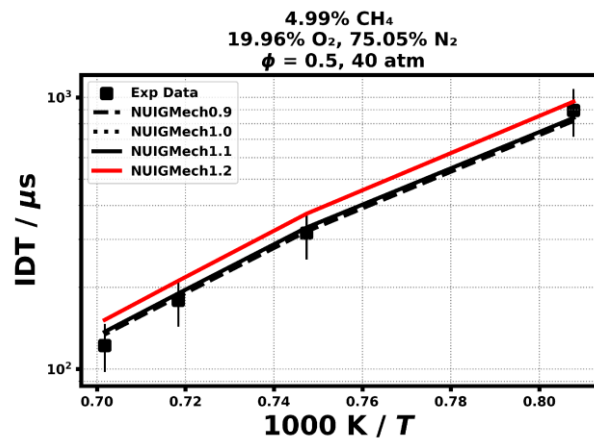
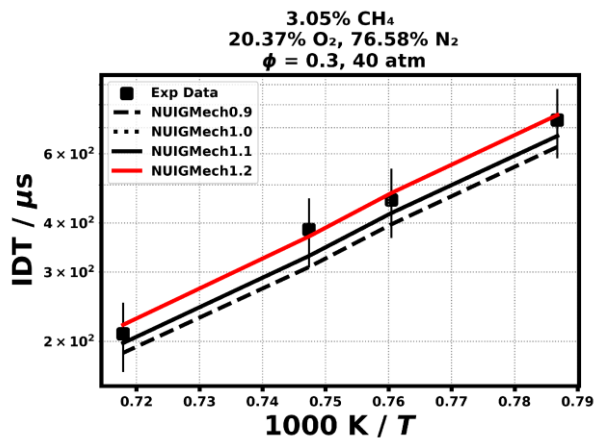
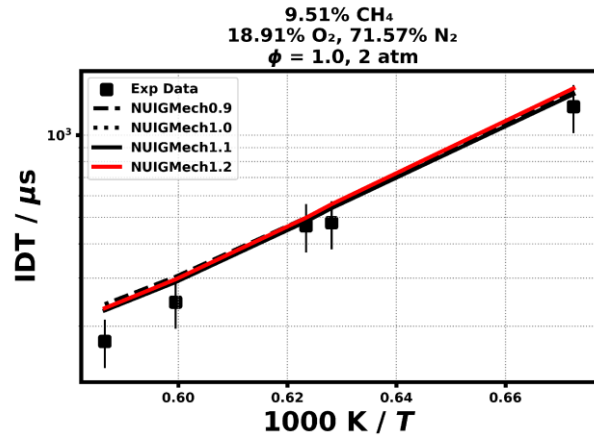
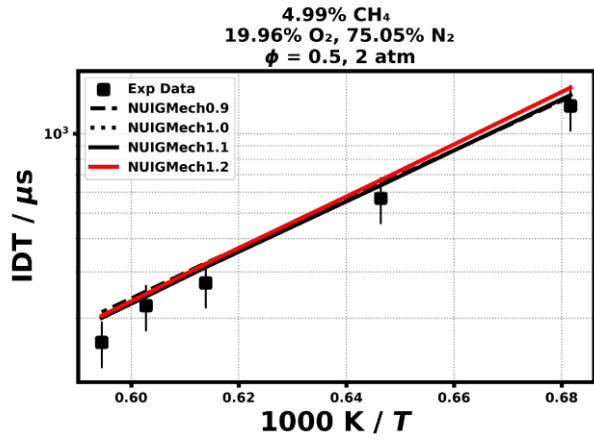


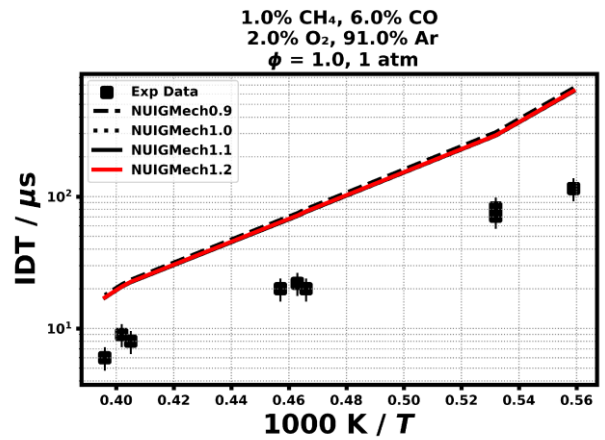
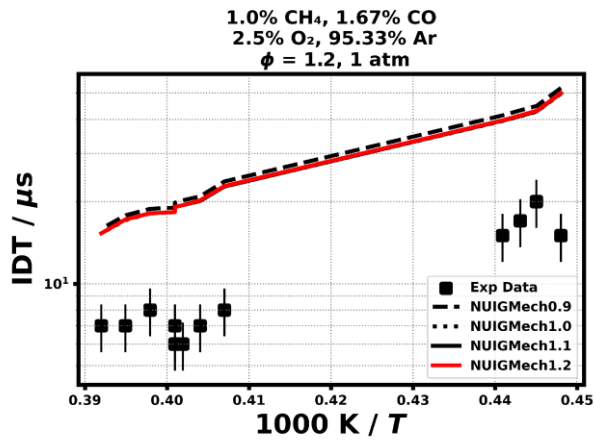
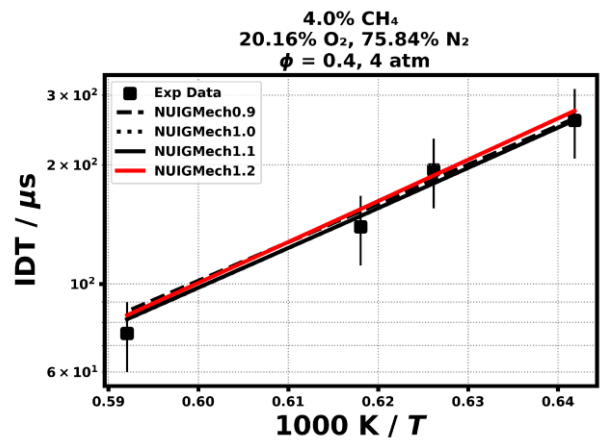
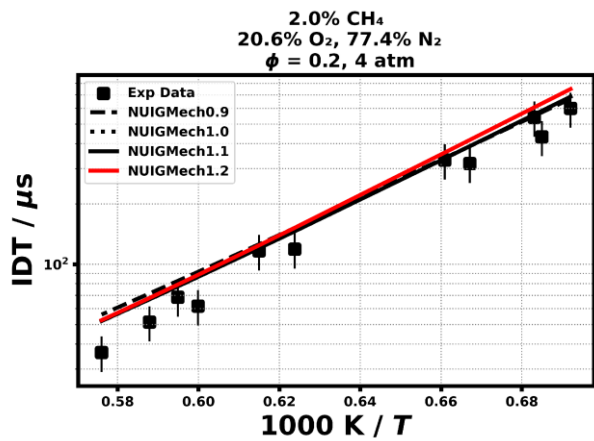
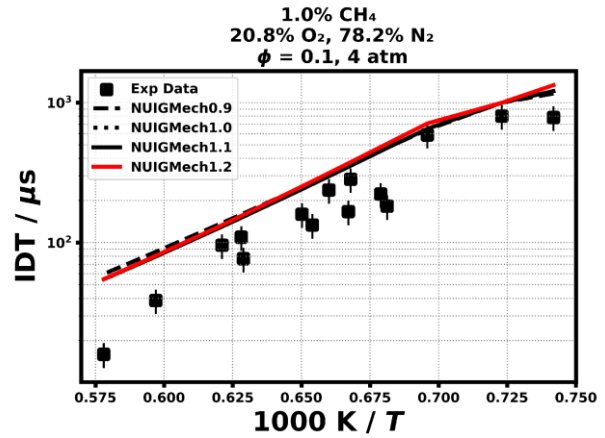
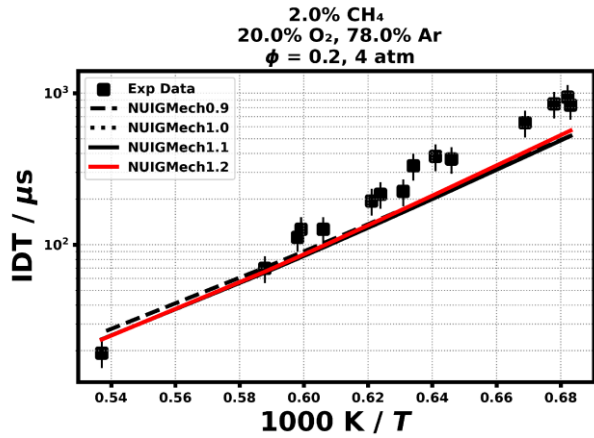


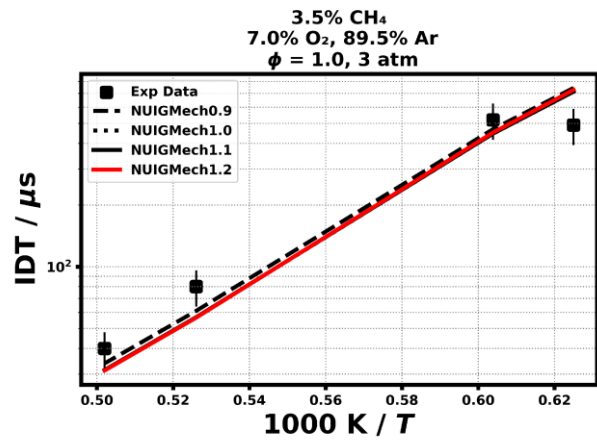
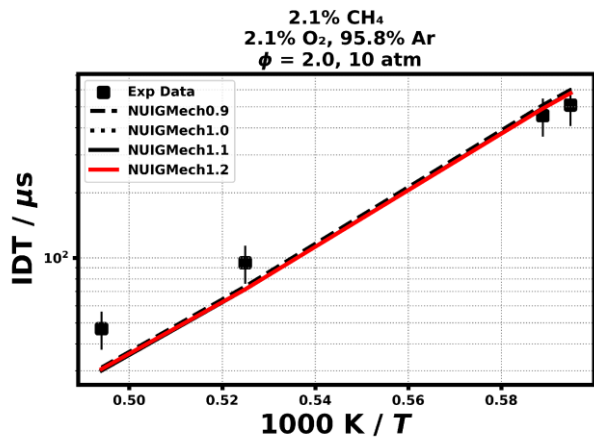
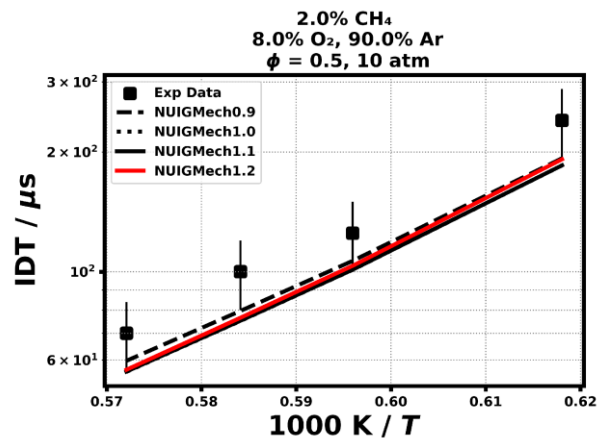
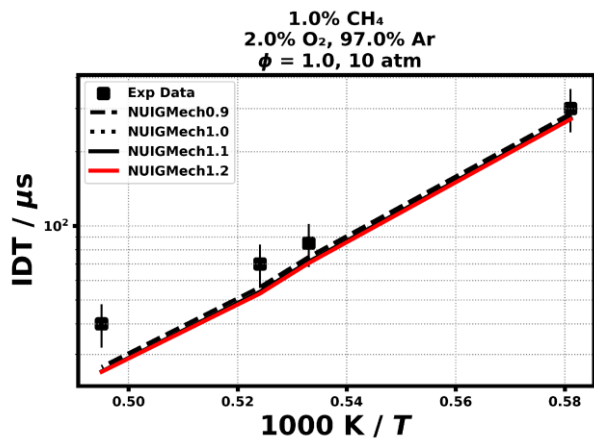
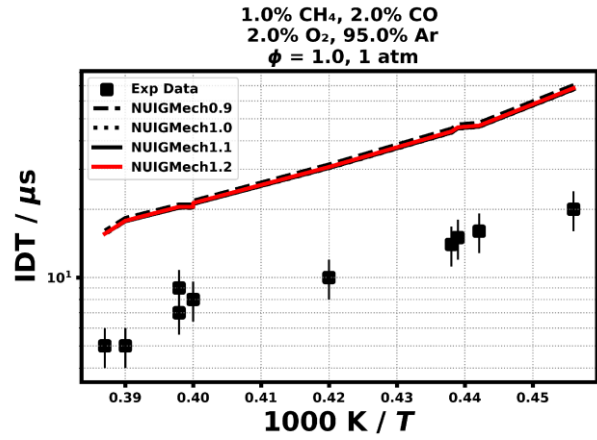
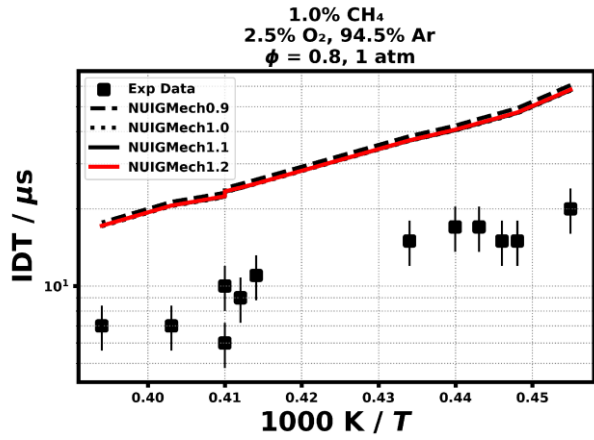
1.1.2 CH₄

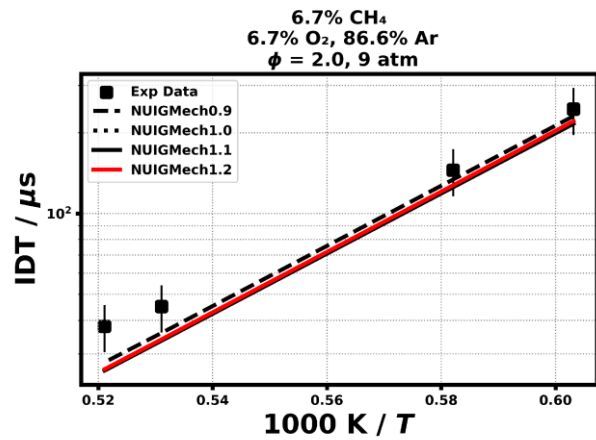
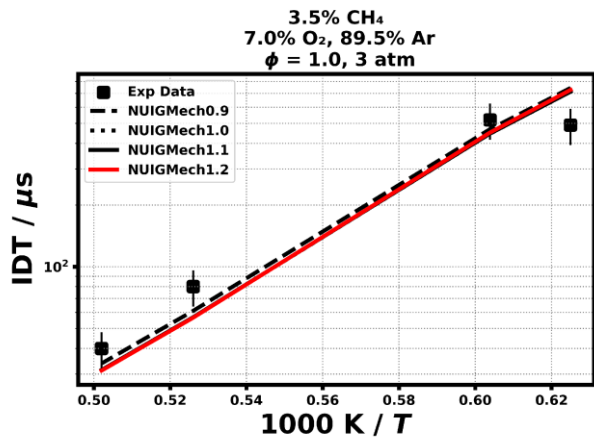
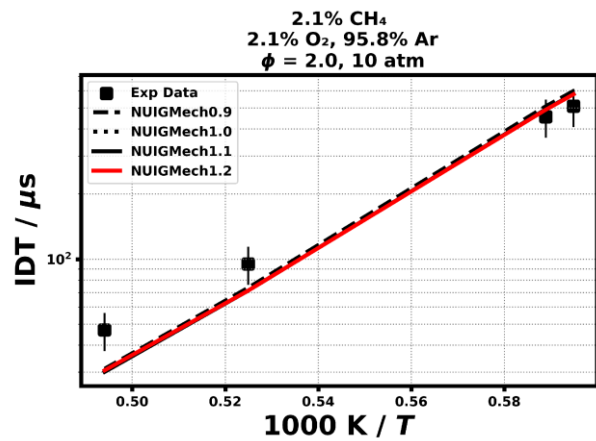
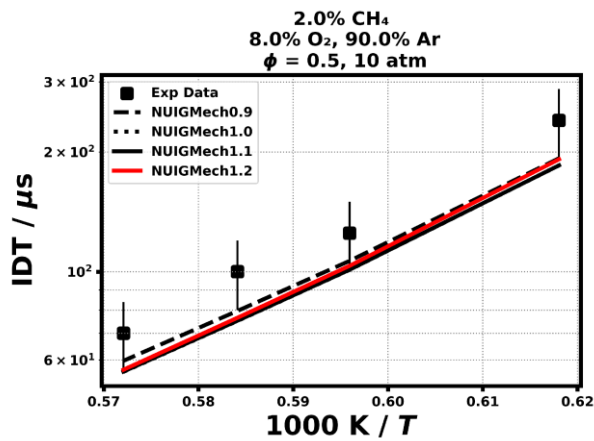
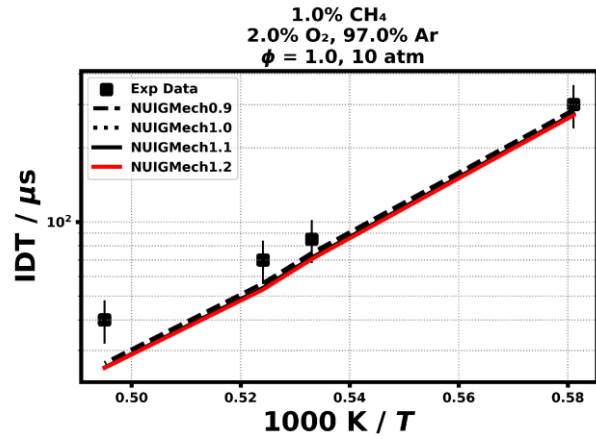
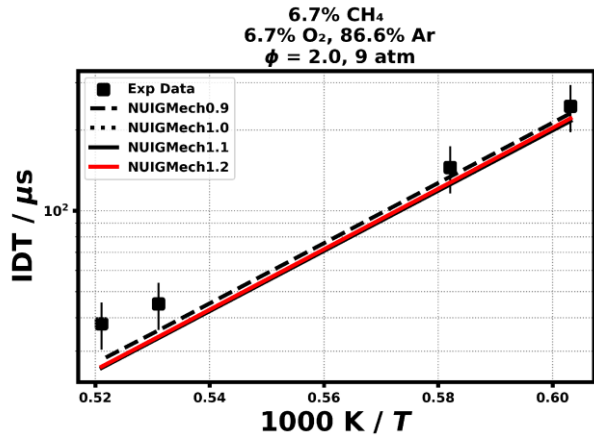


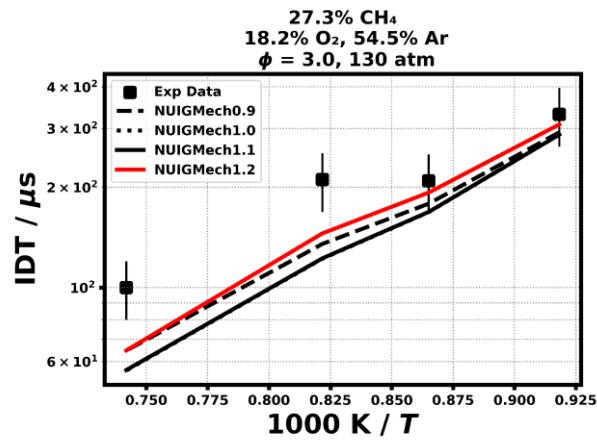
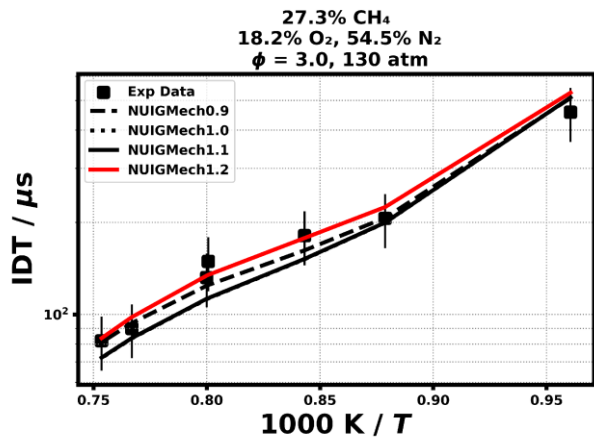
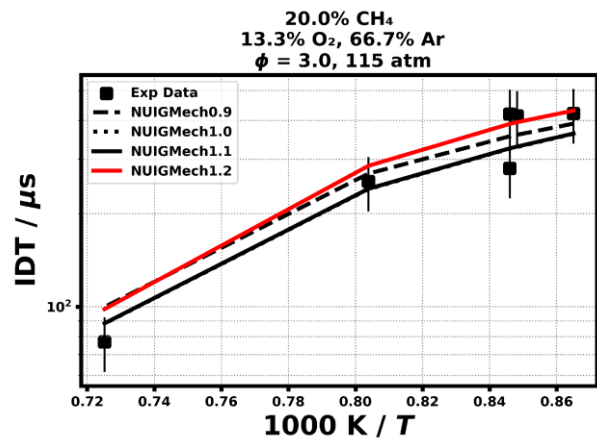
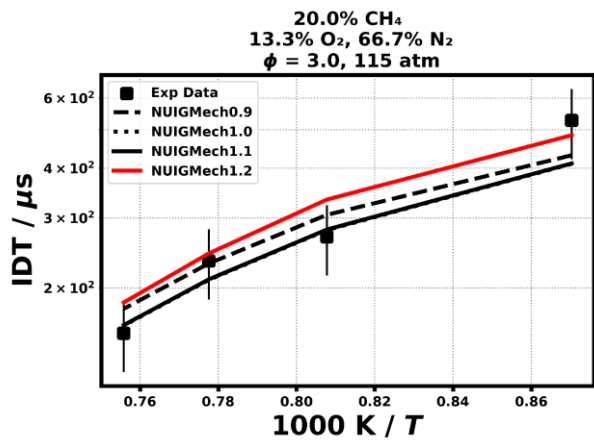
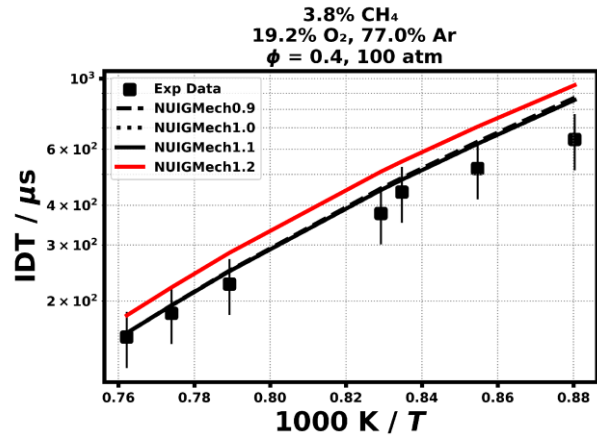
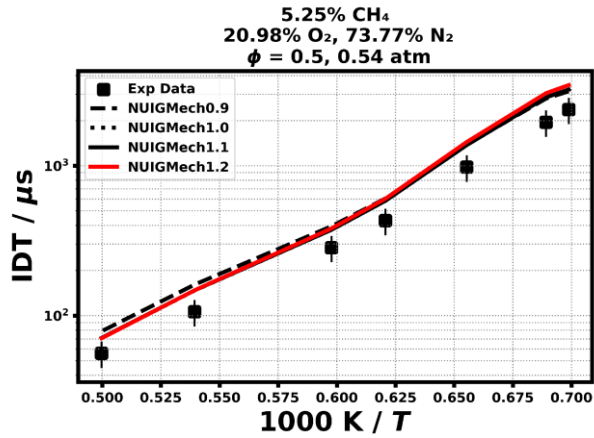


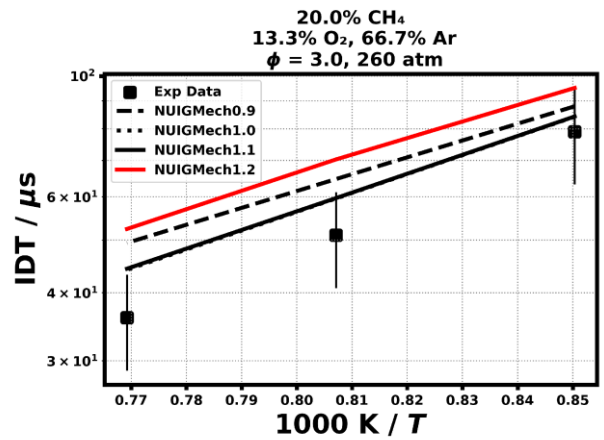
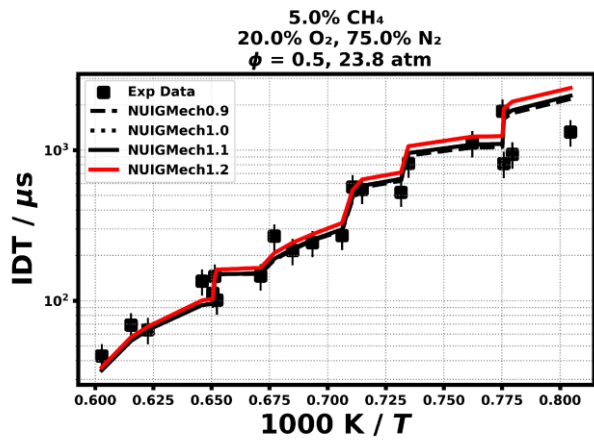
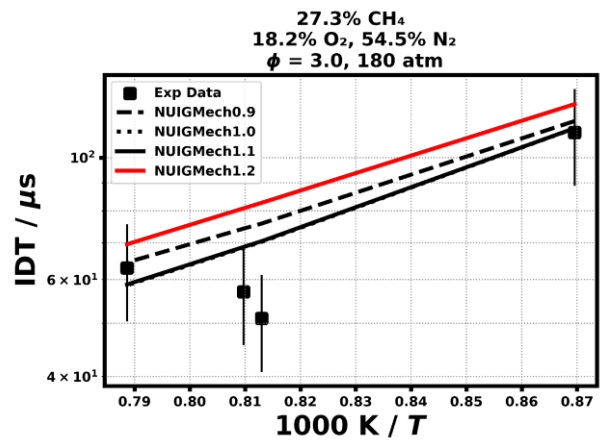
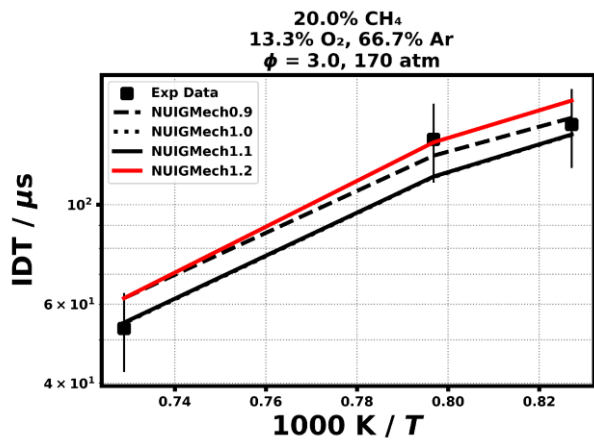
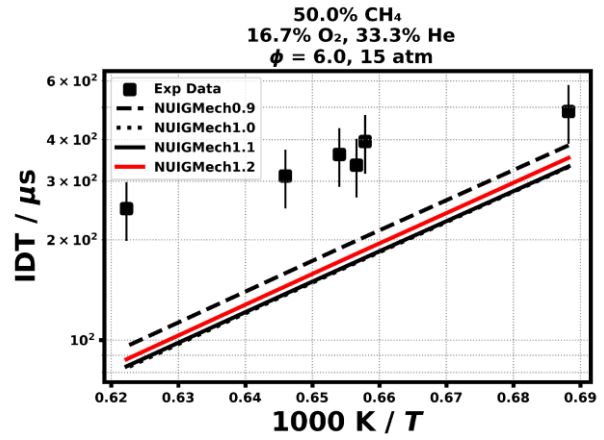
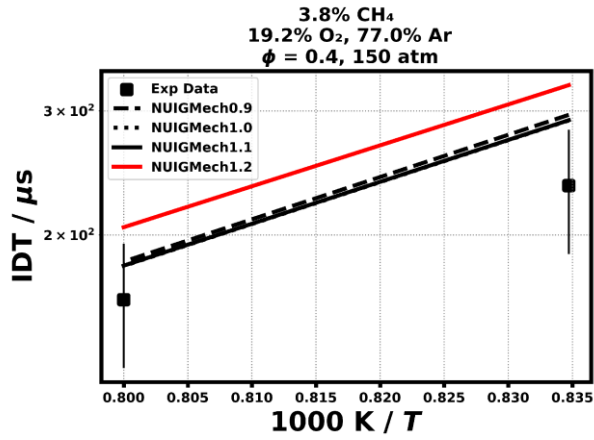


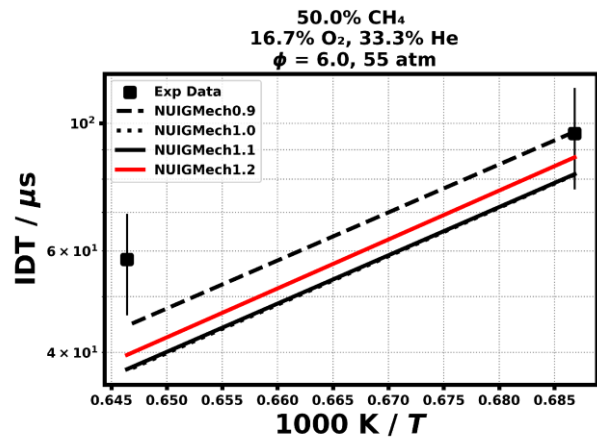
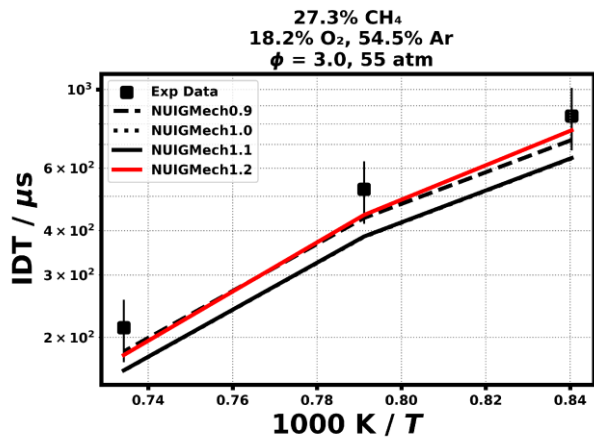
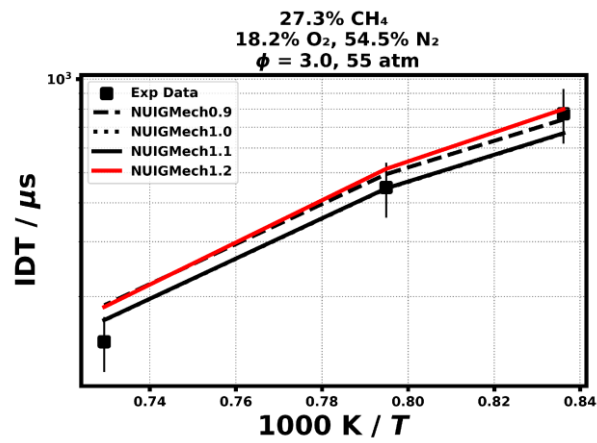
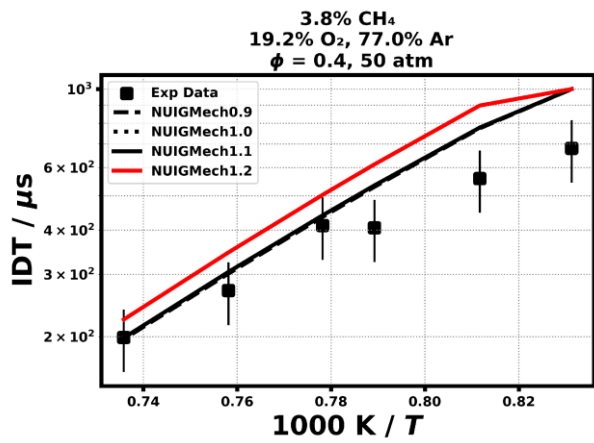
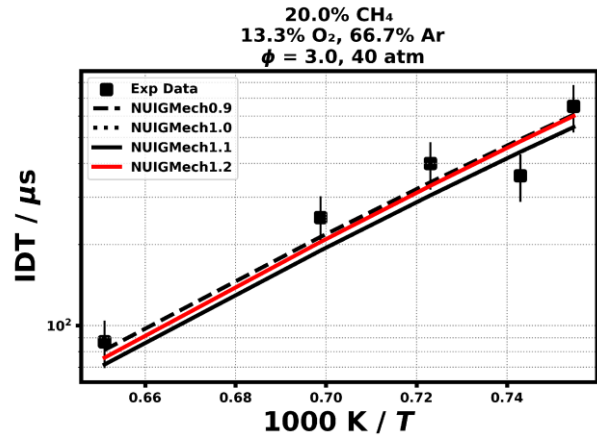
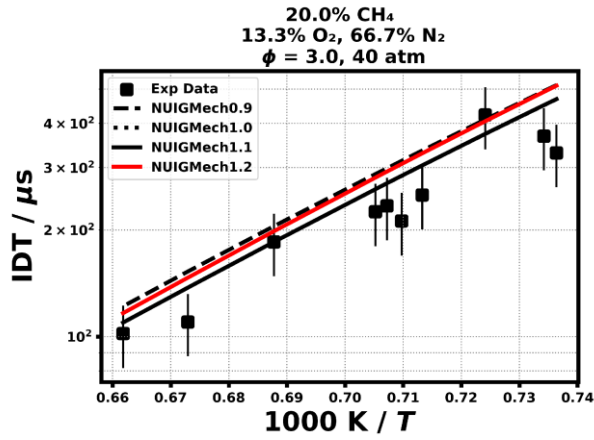


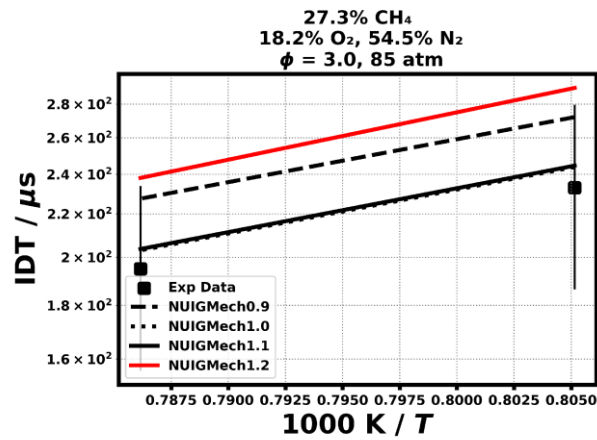
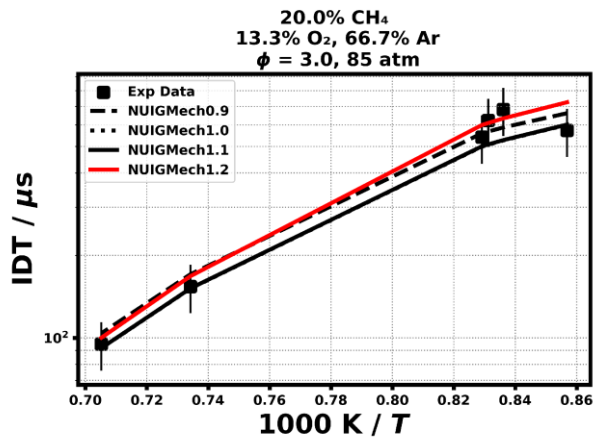
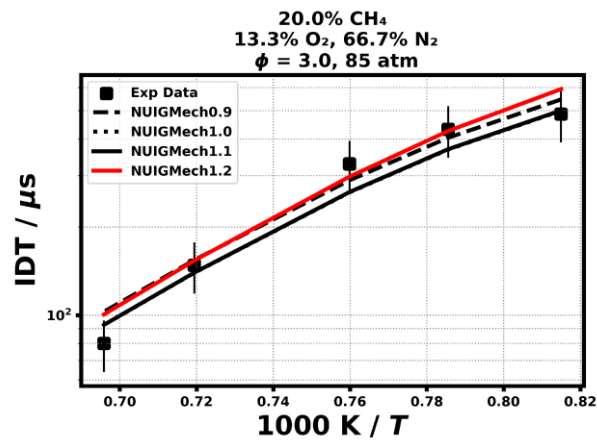
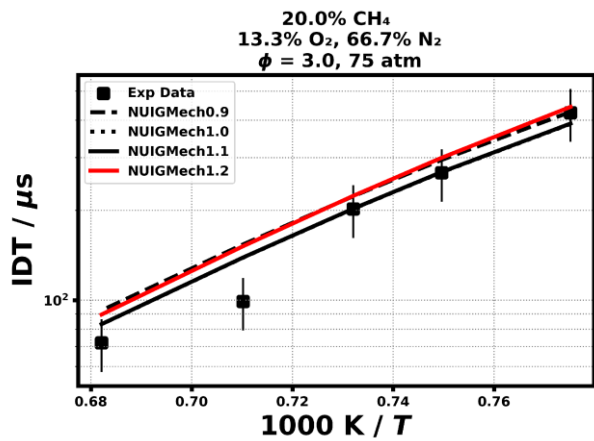
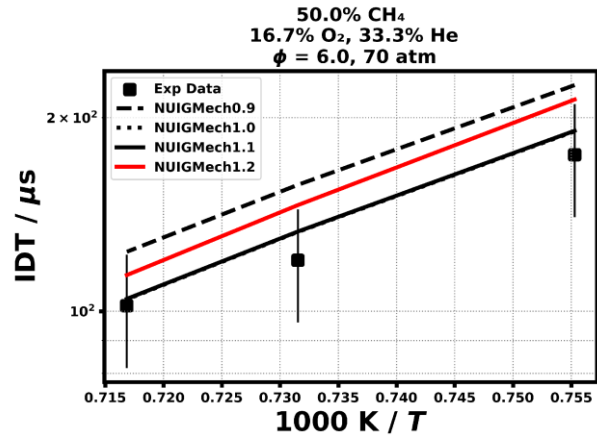
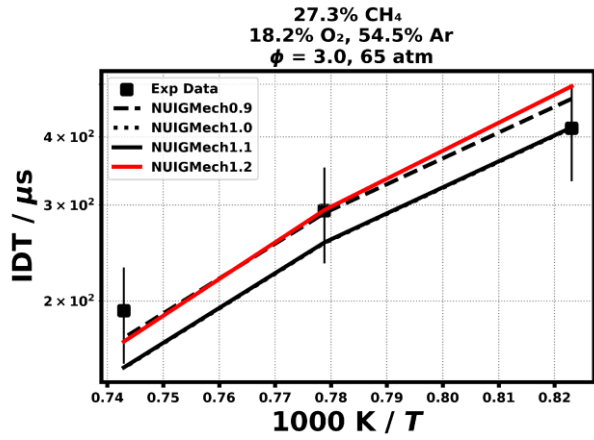


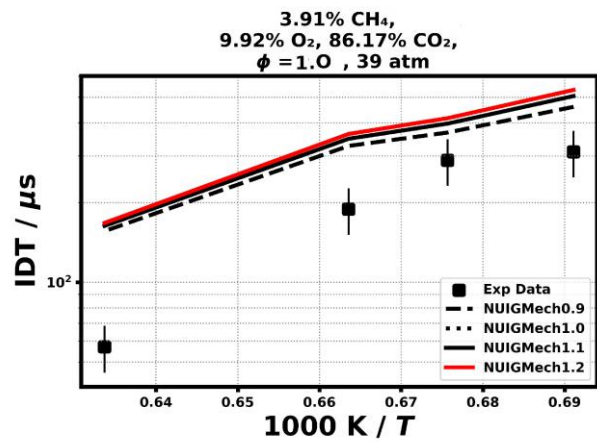
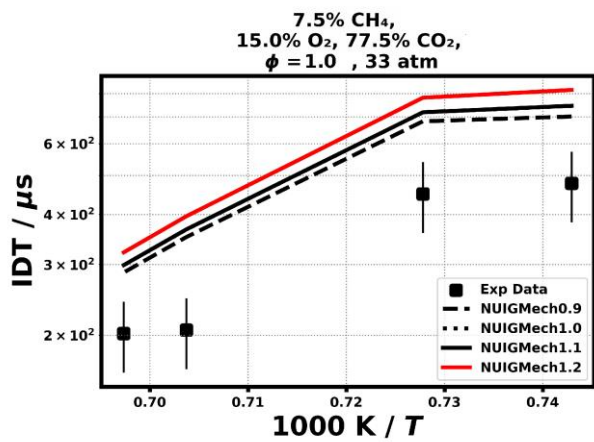
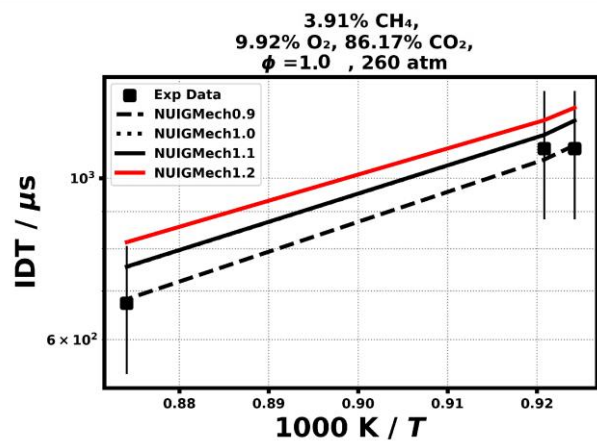
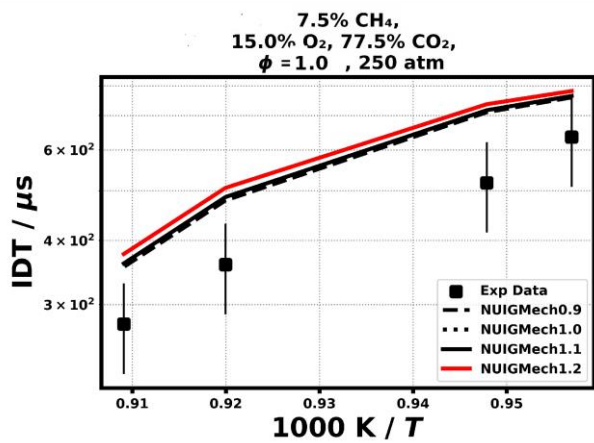
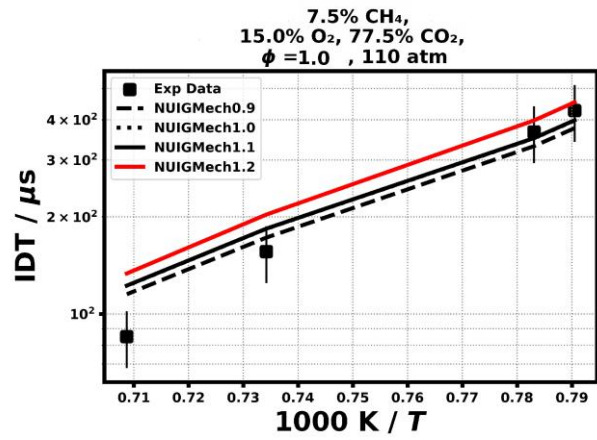
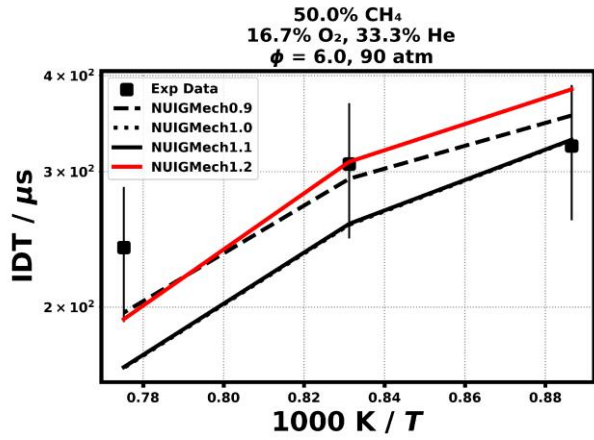


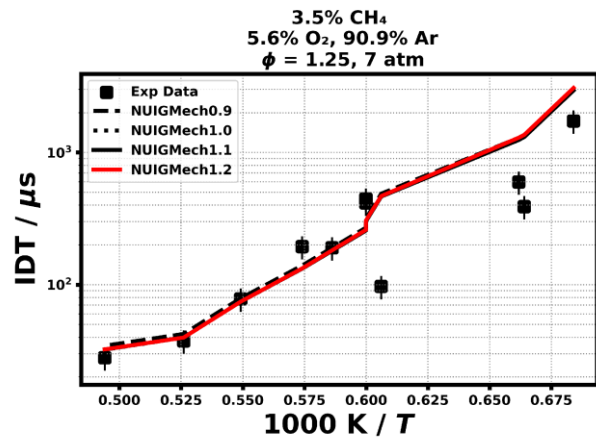
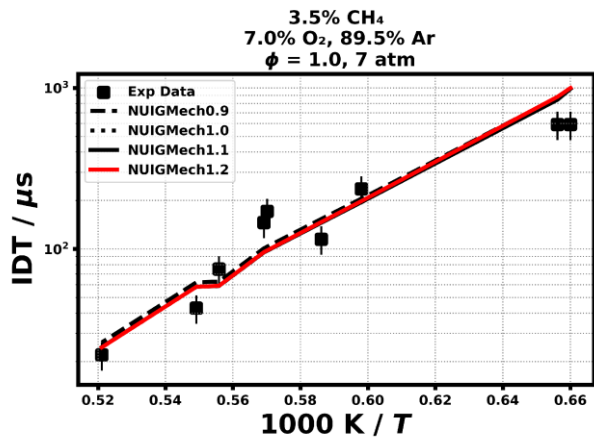
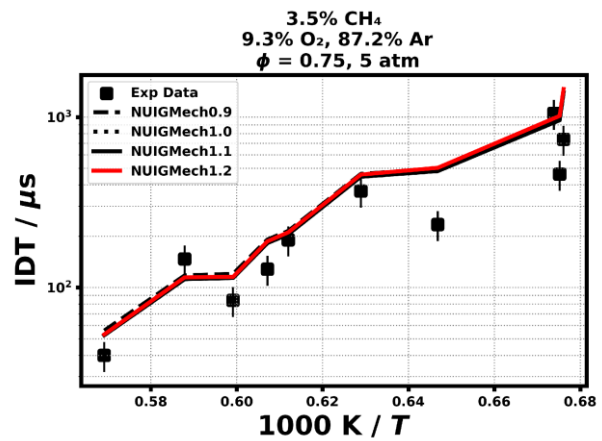
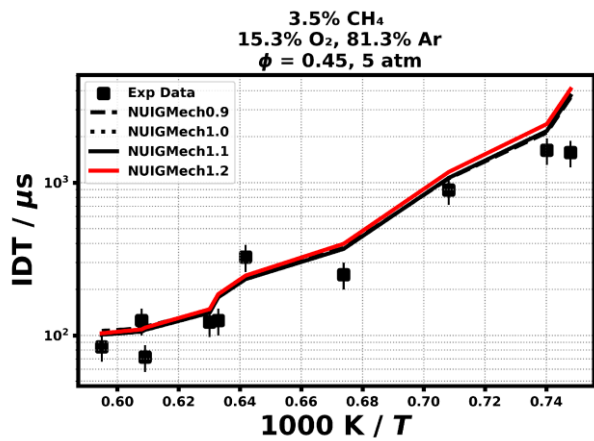
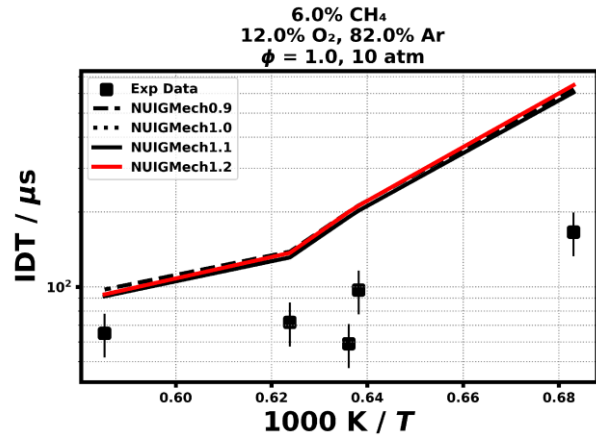
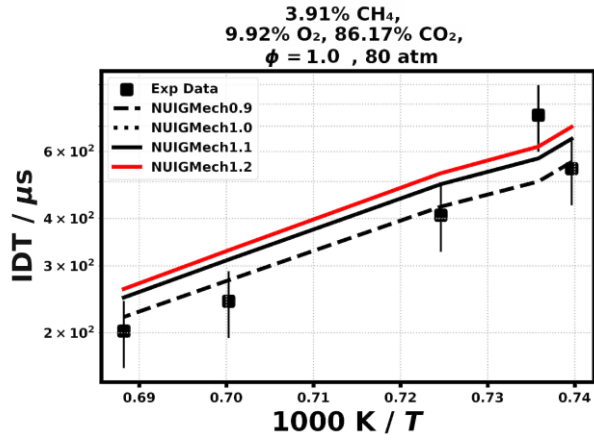




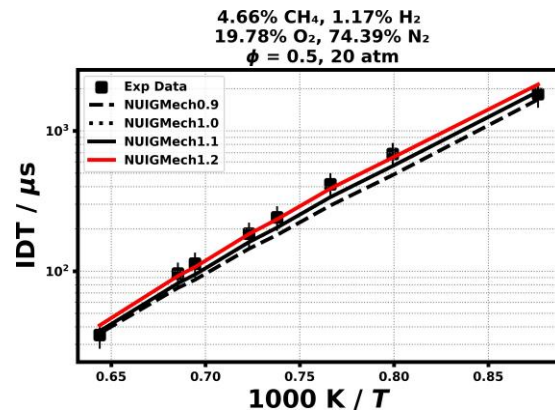
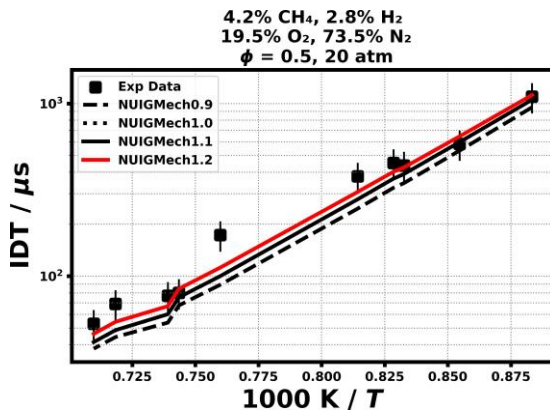




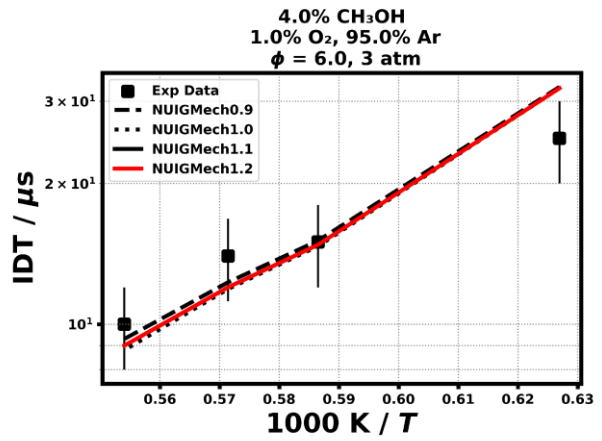
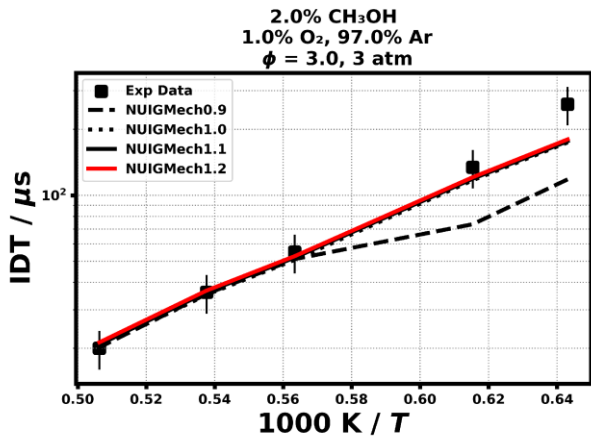
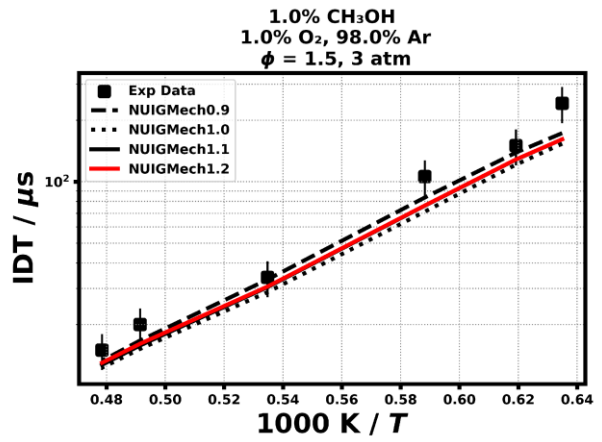
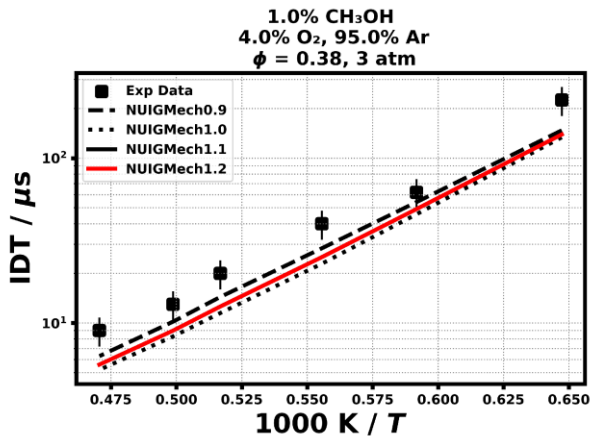
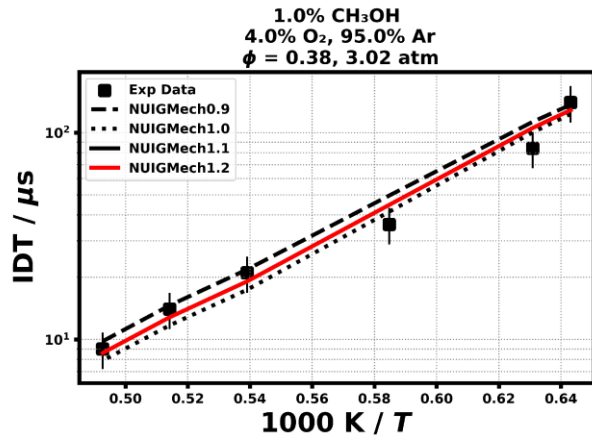
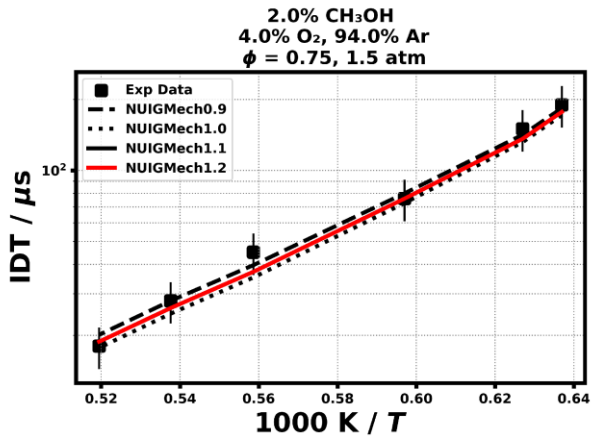


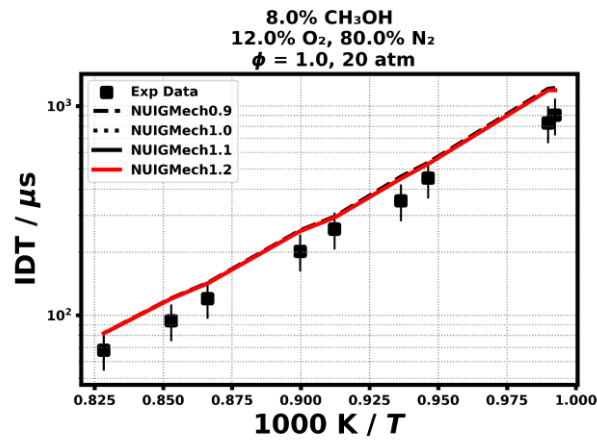
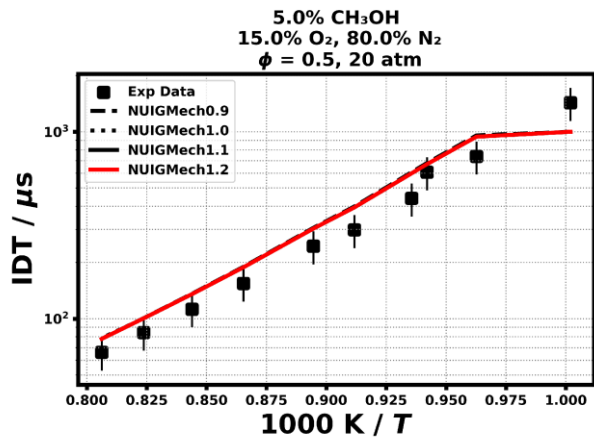
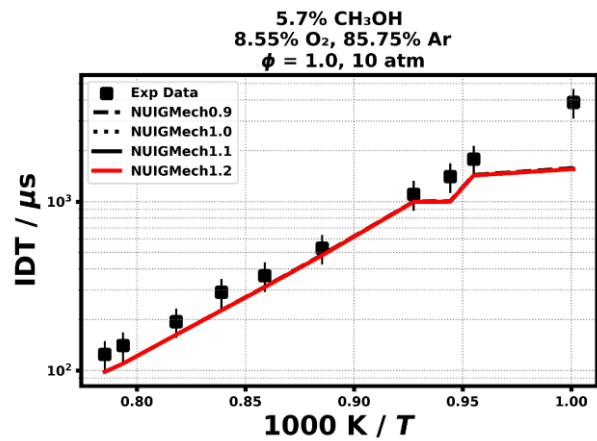
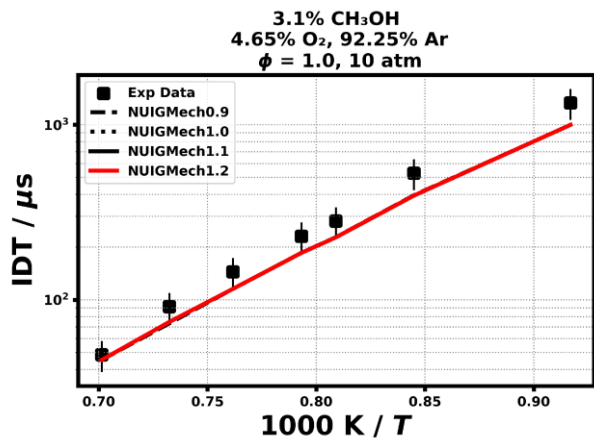
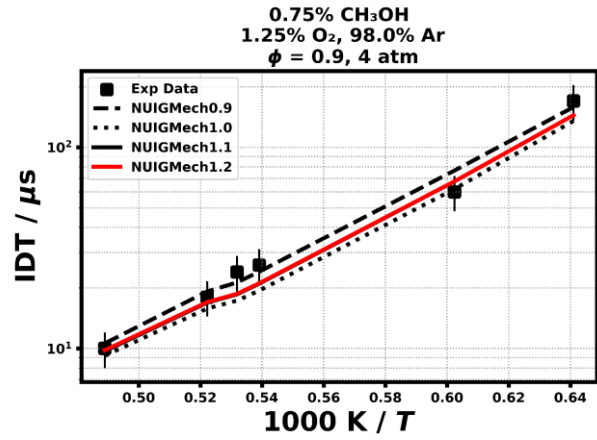
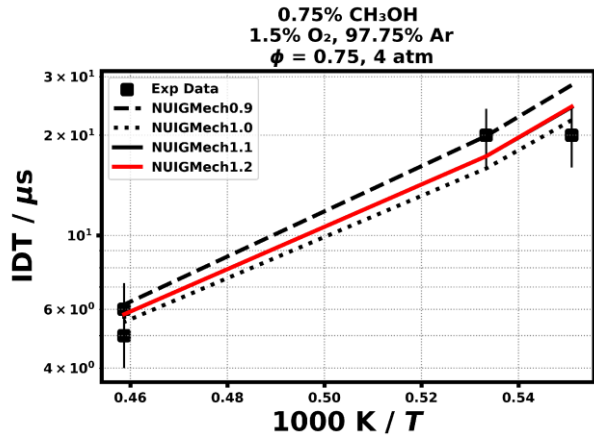


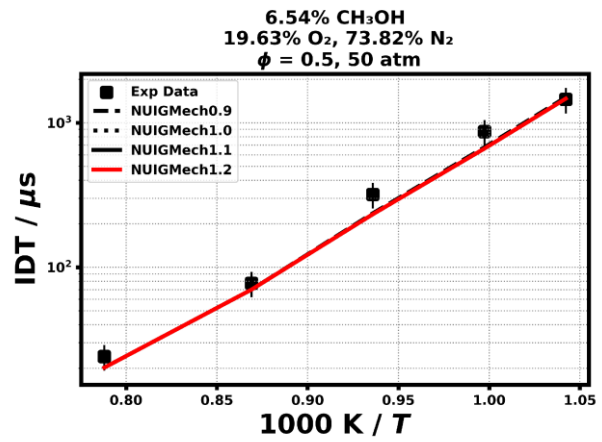
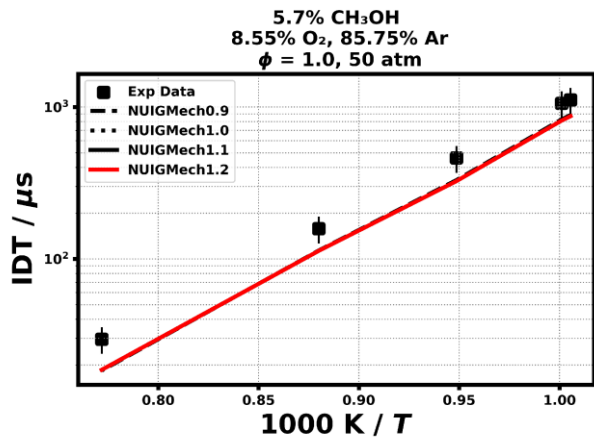
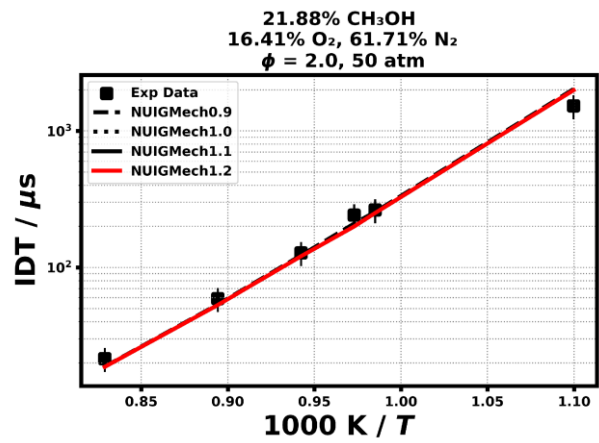
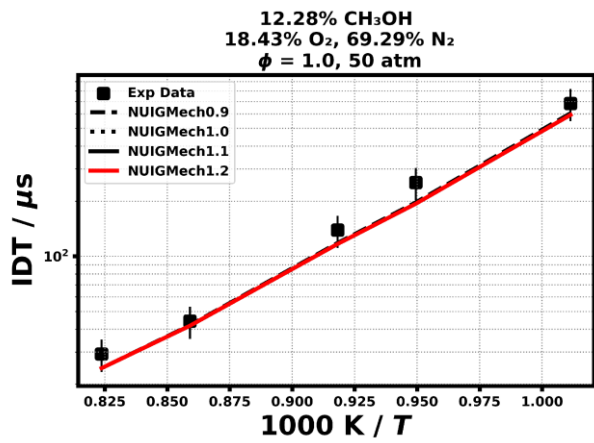
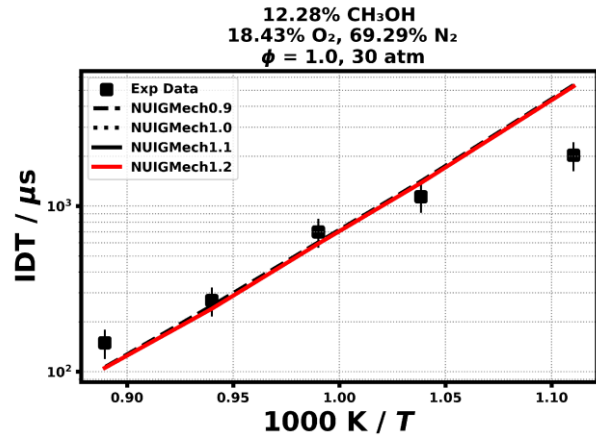
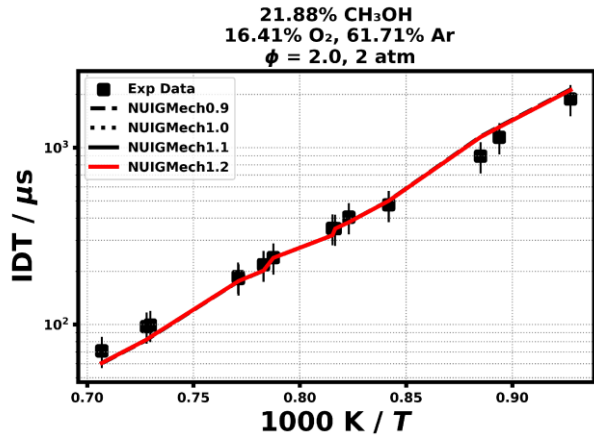
1.1.3 CH₄/H₂

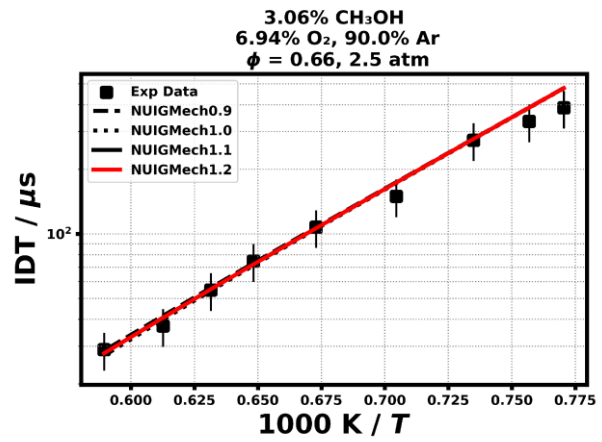
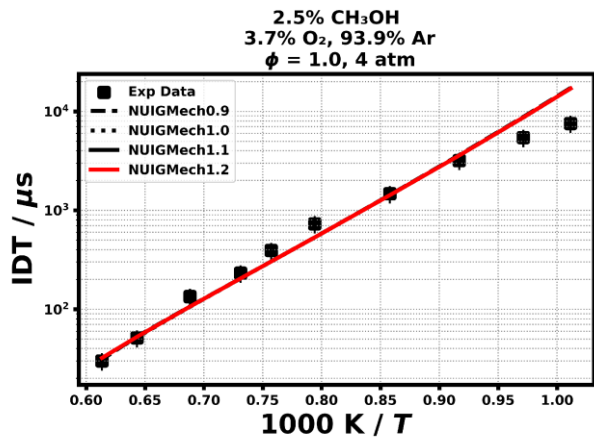
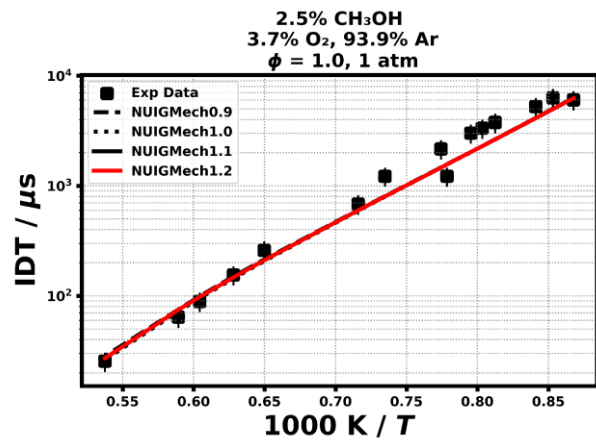
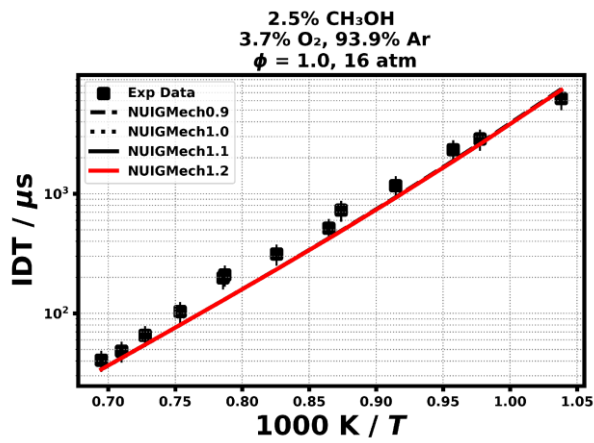
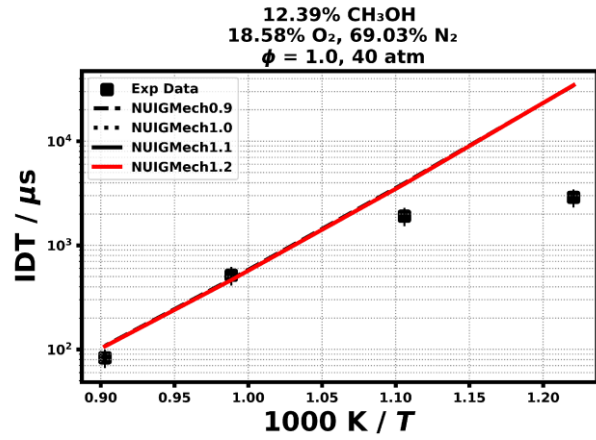
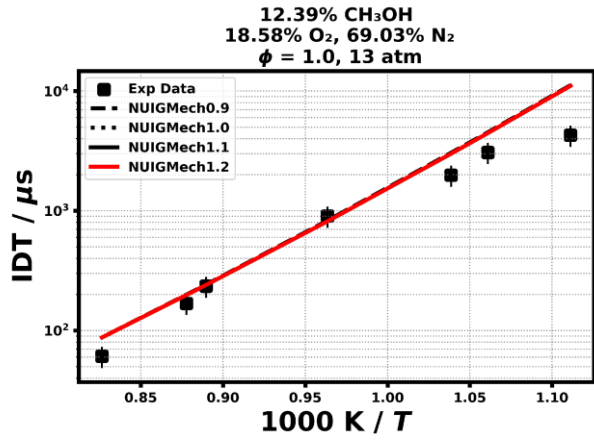


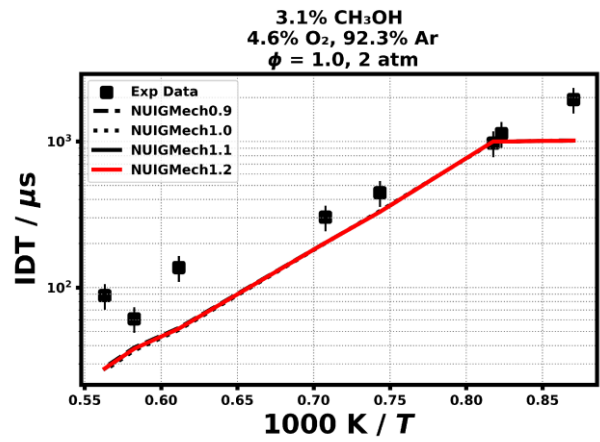
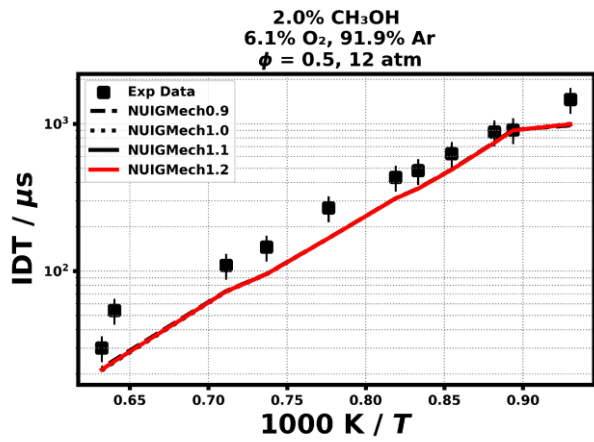
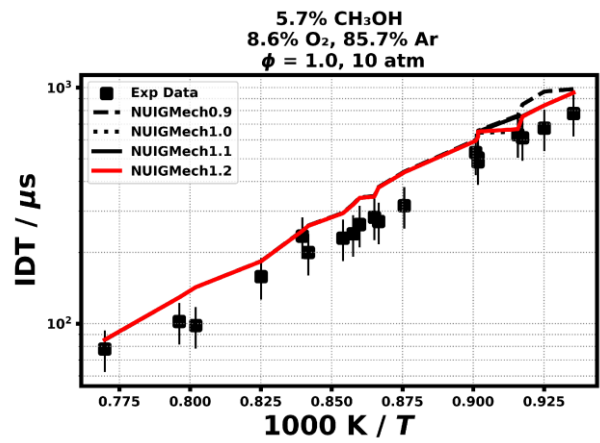
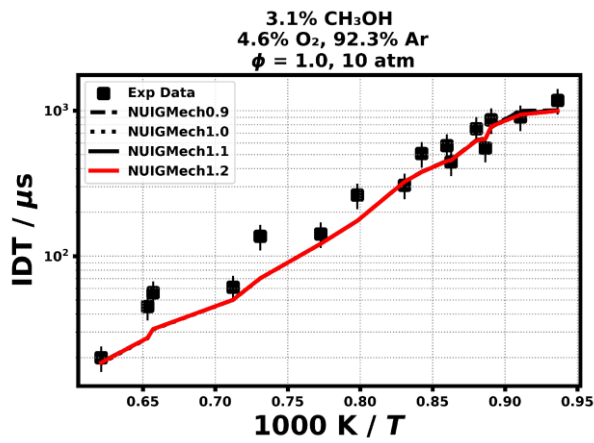
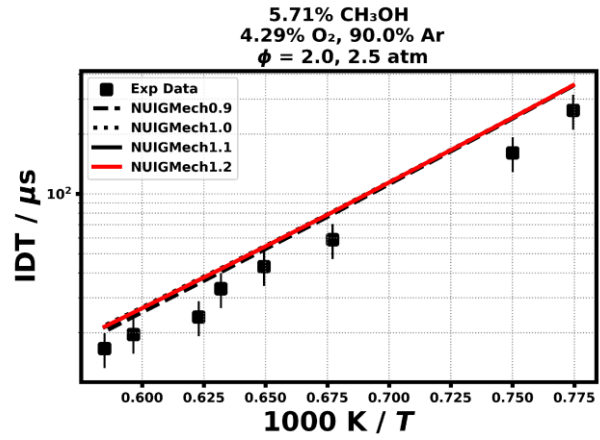
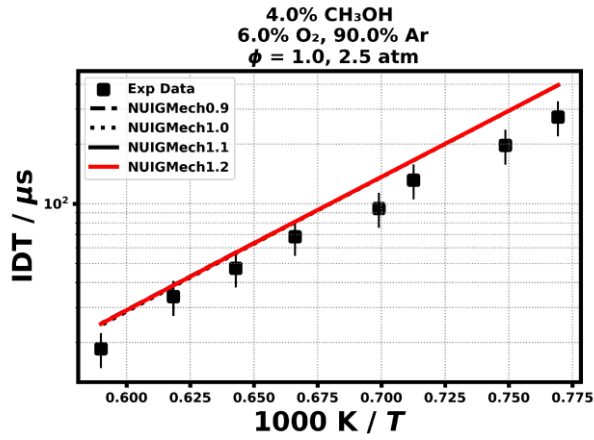
1.1.4 CH₃OH

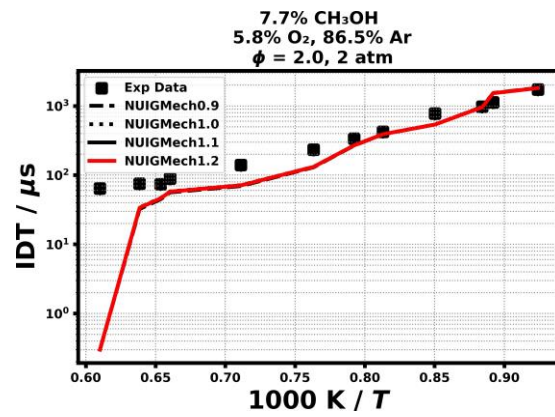
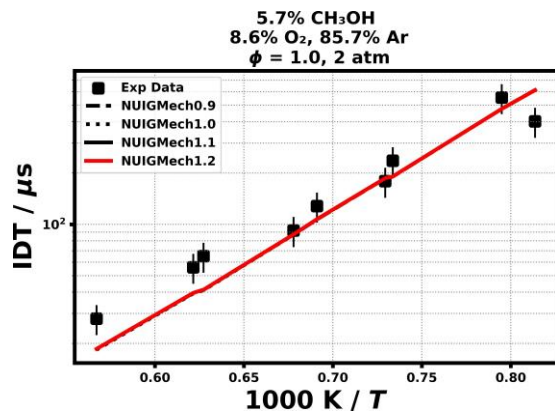




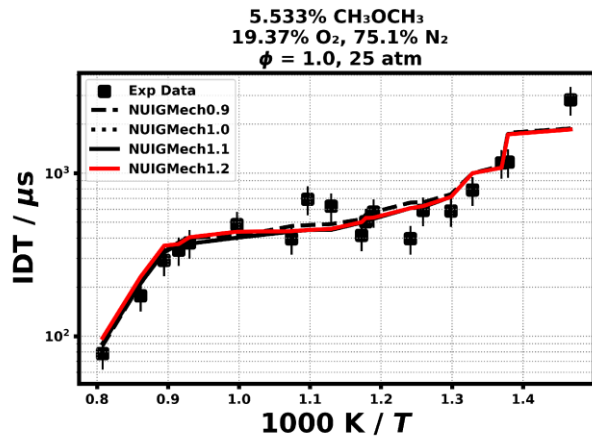
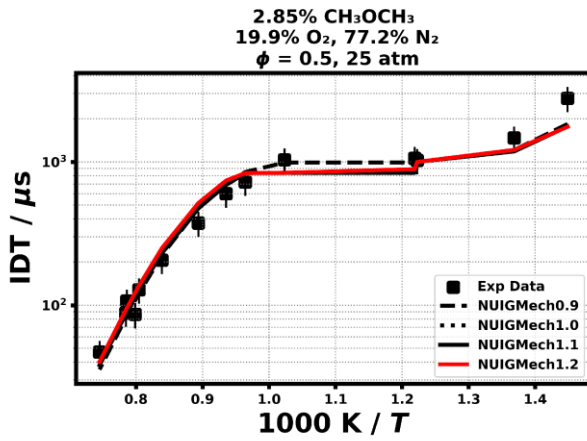
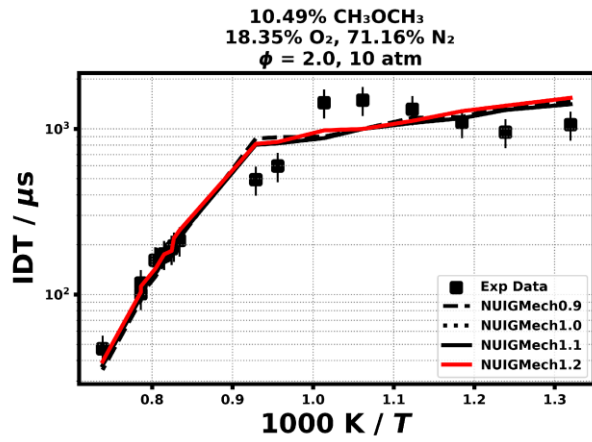
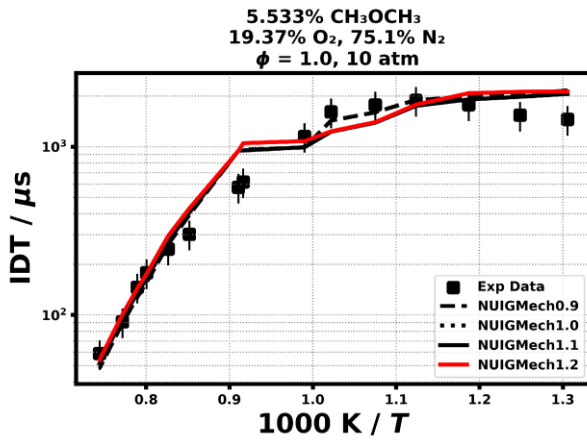
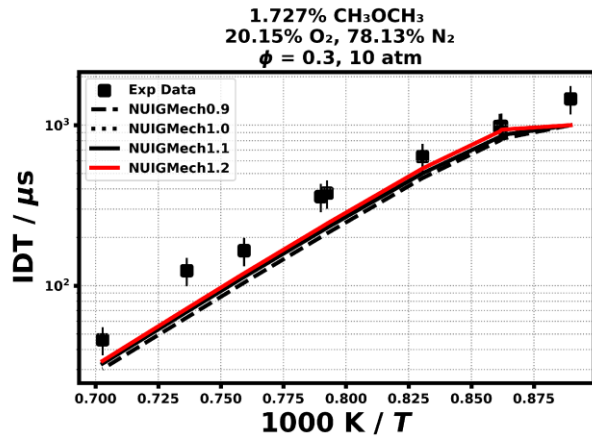
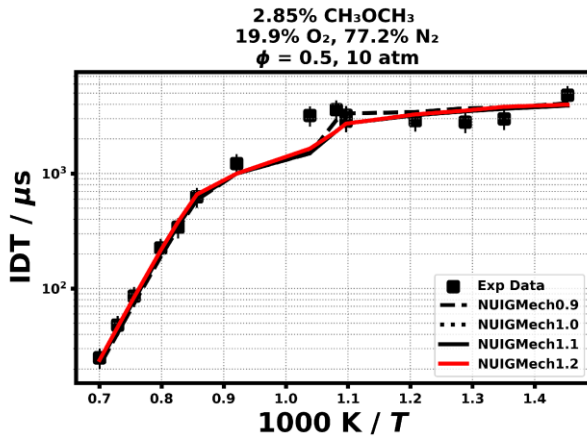


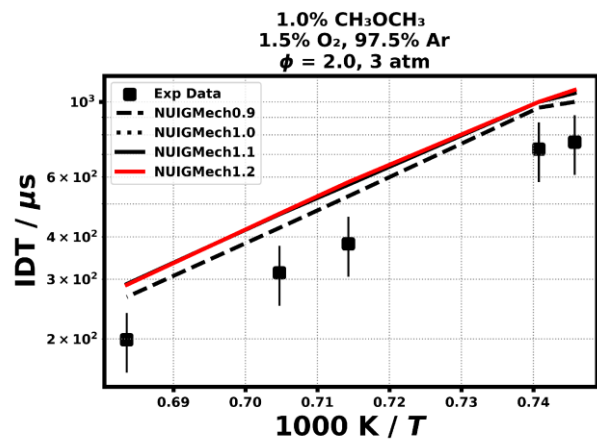
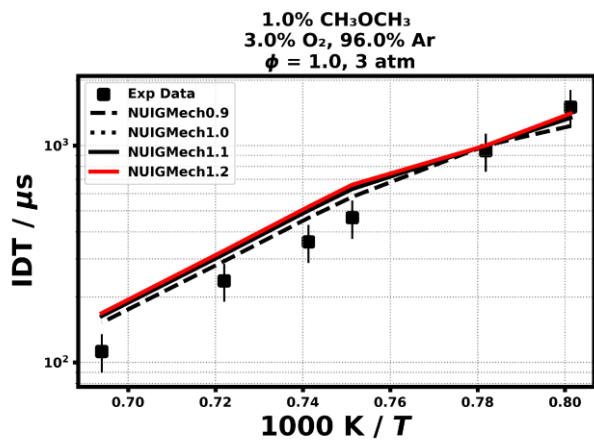
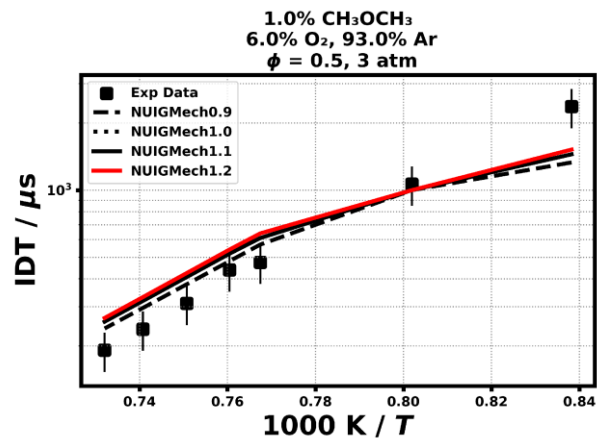
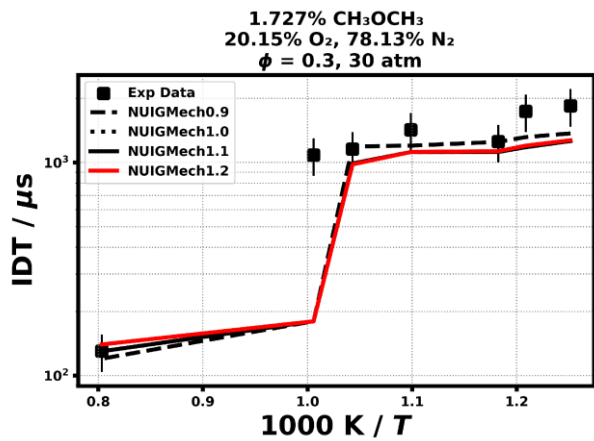
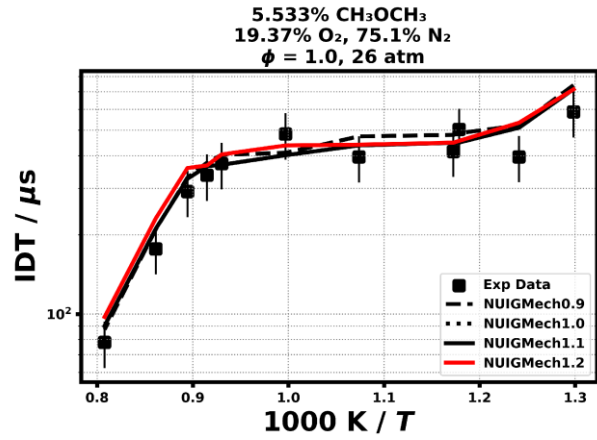
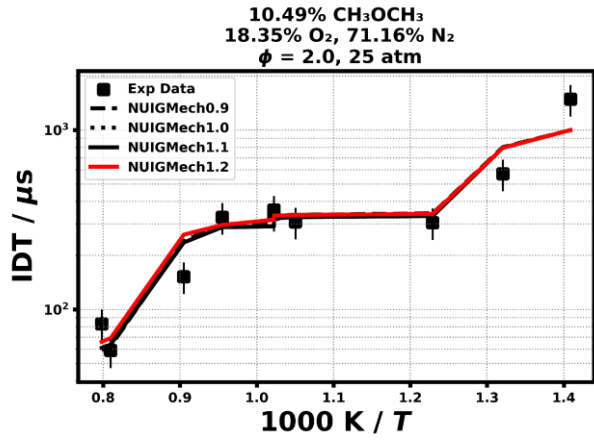


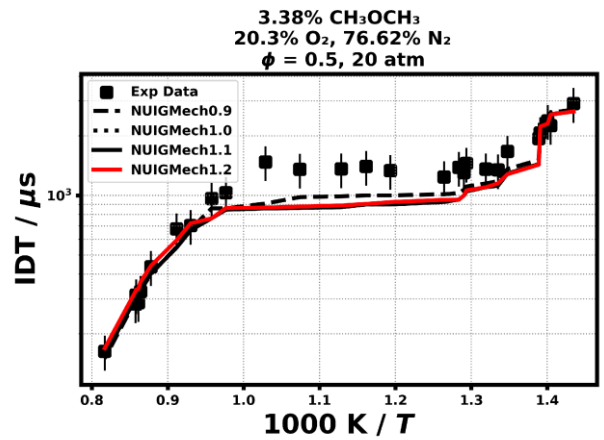
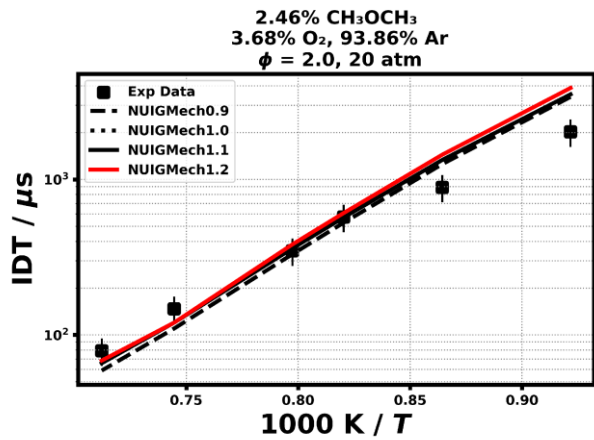
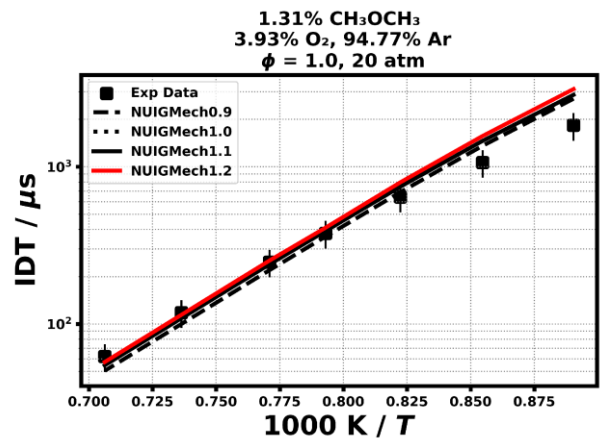
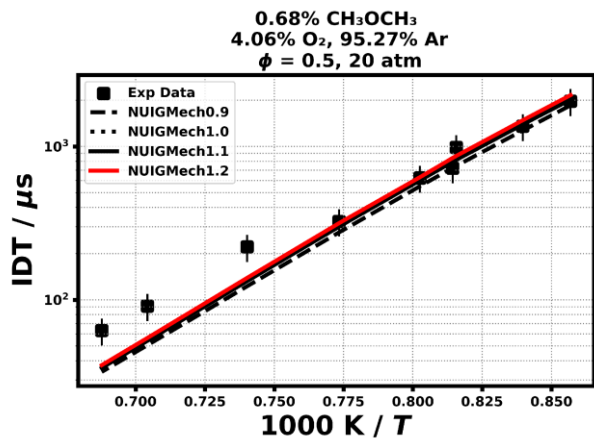
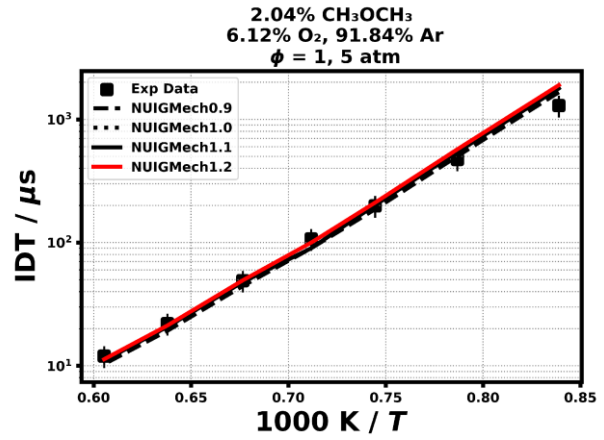
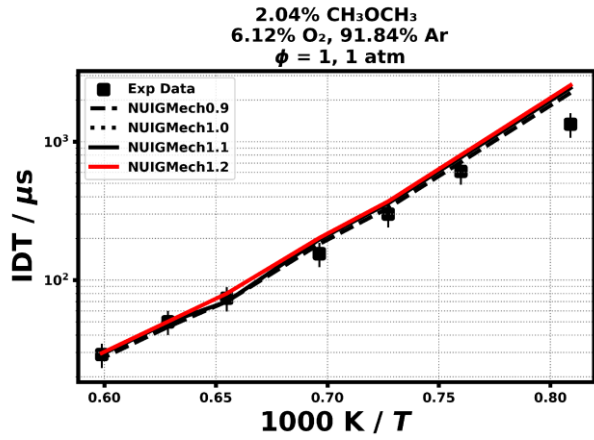


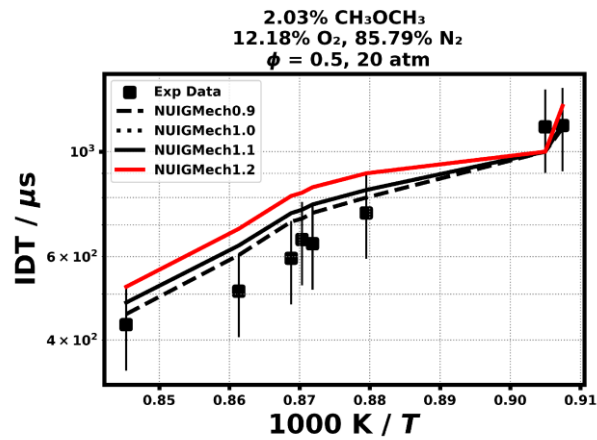
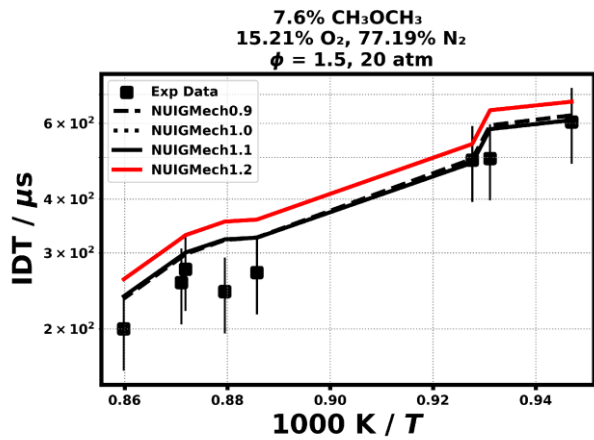
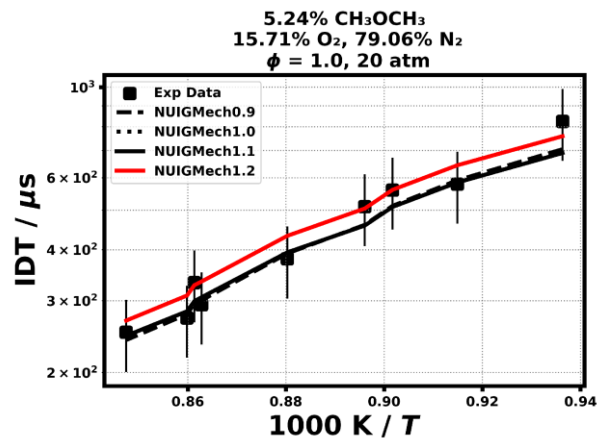
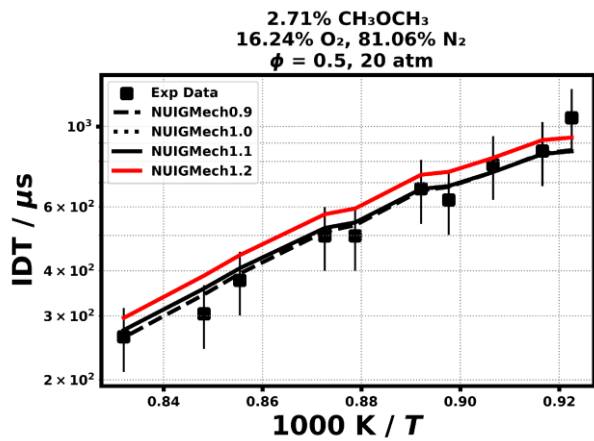
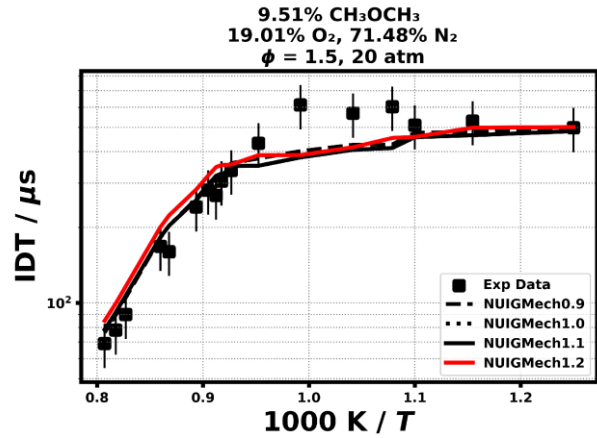
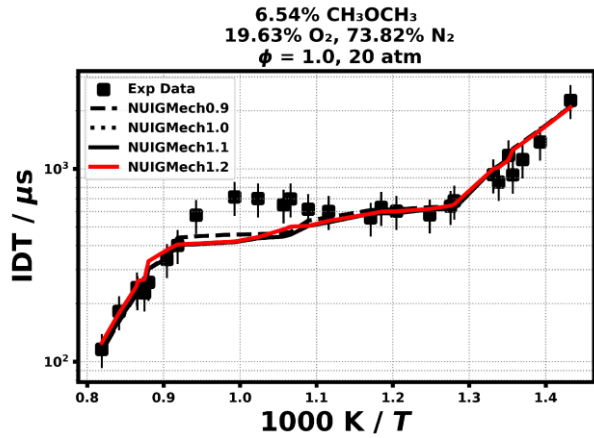


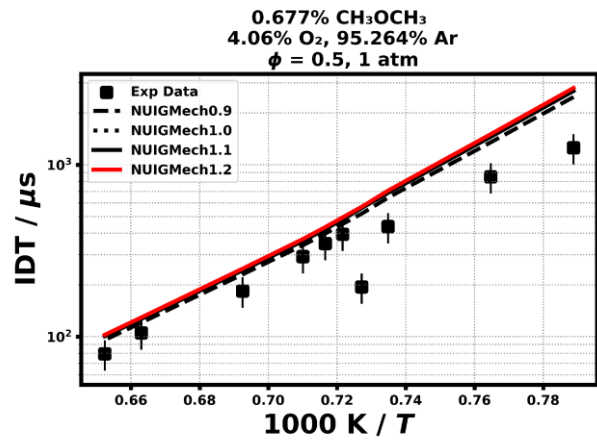
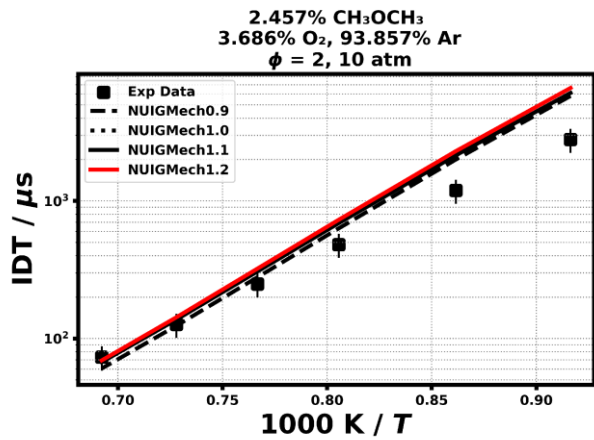
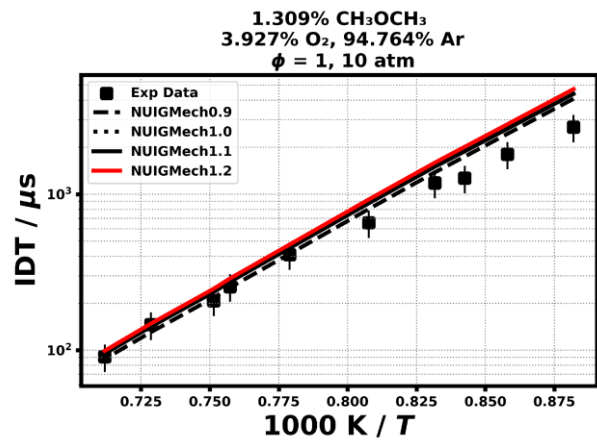
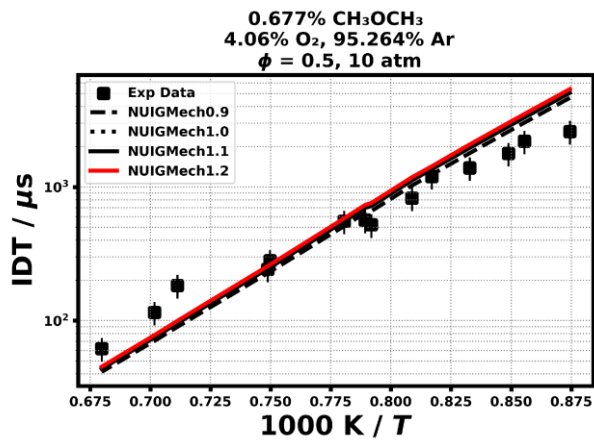
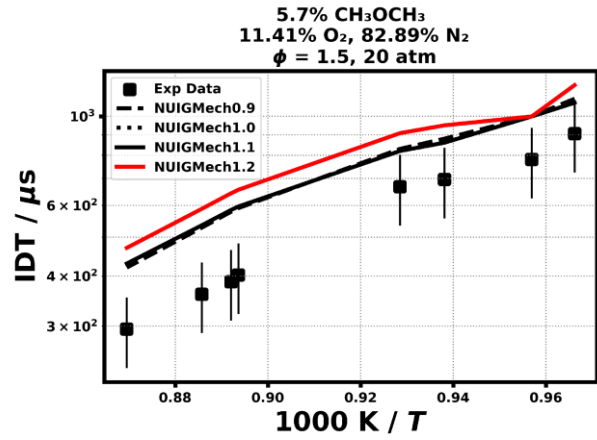
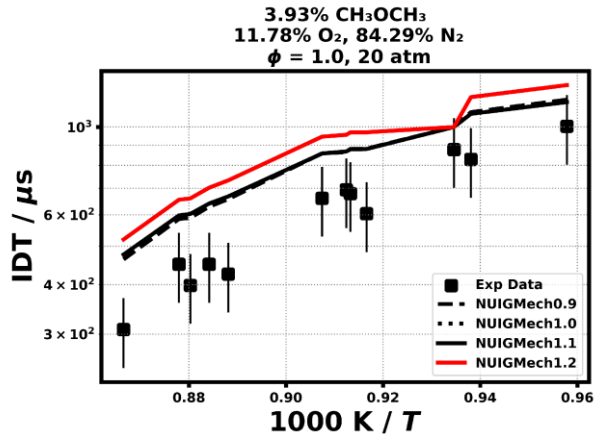
1.1.5 CH₃OCH₃

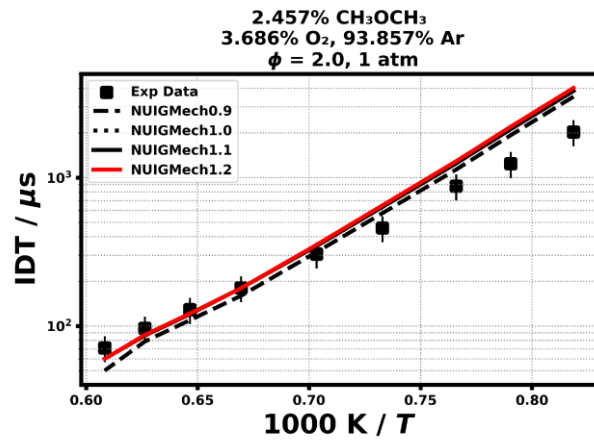
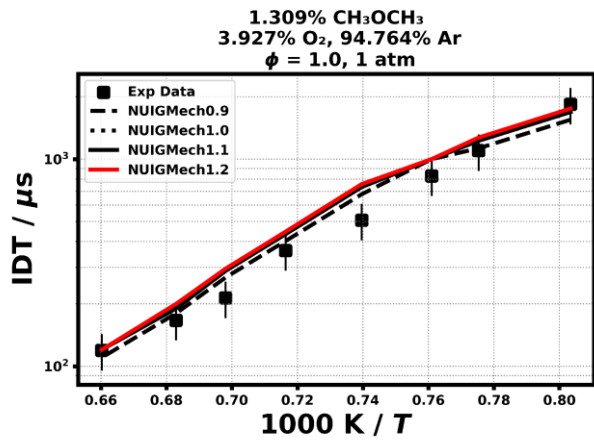
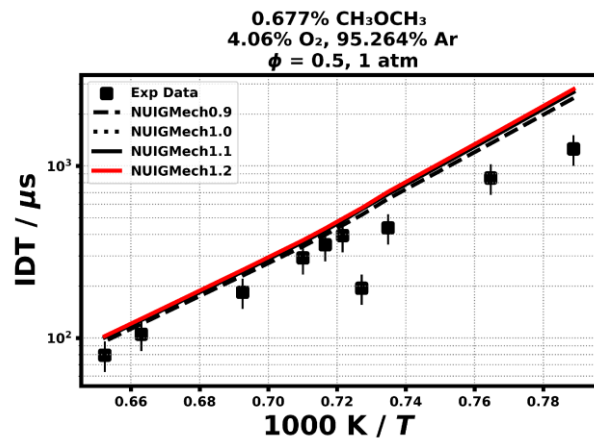
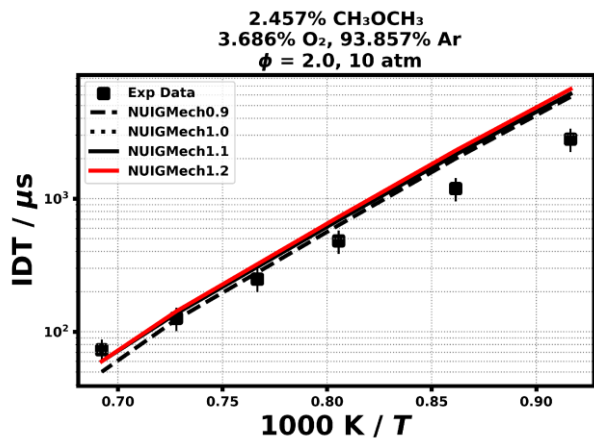
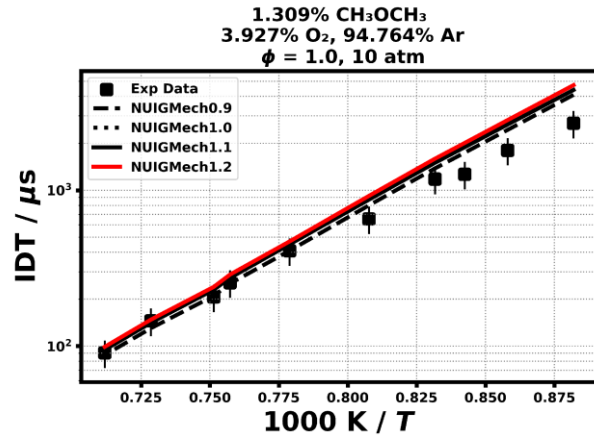
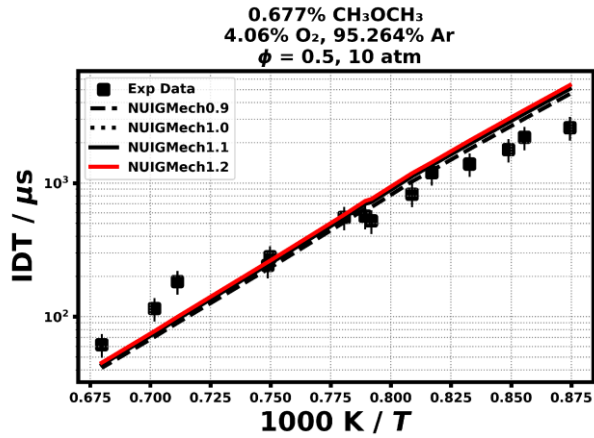


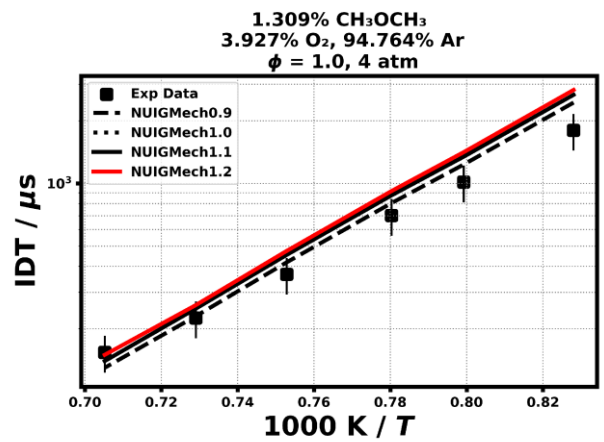
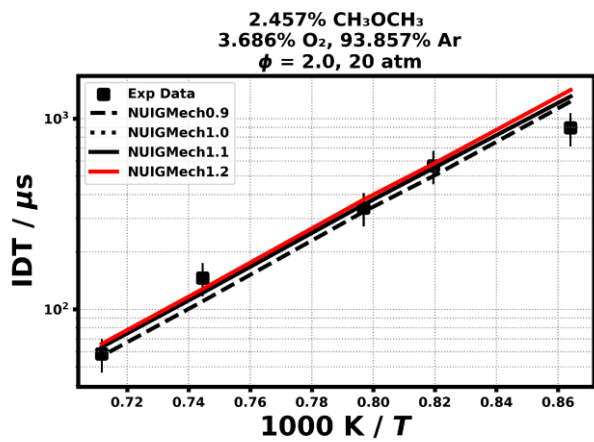
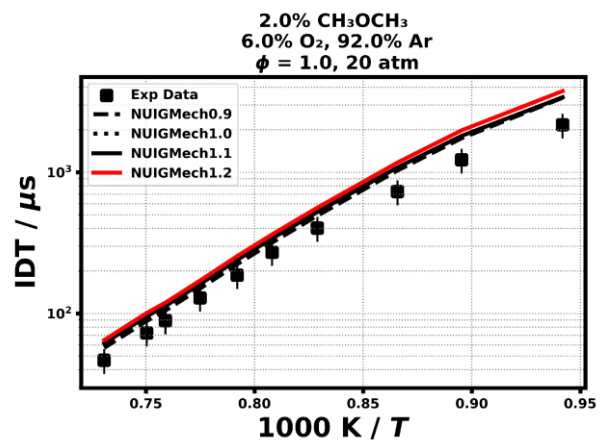
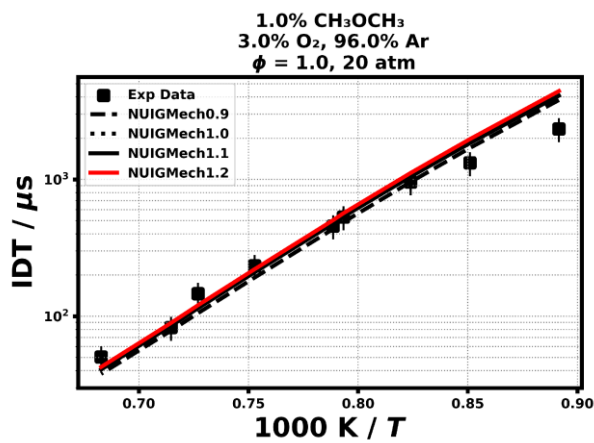
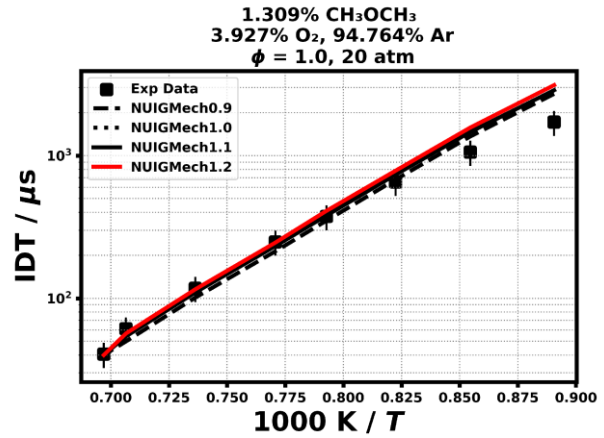
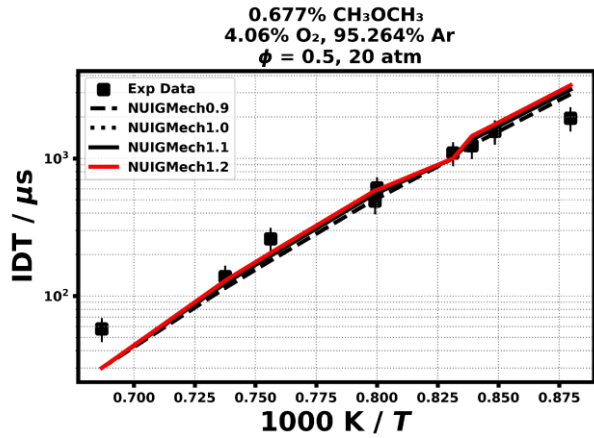


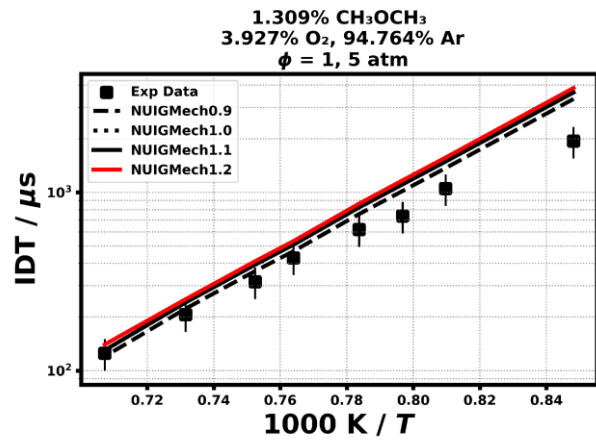
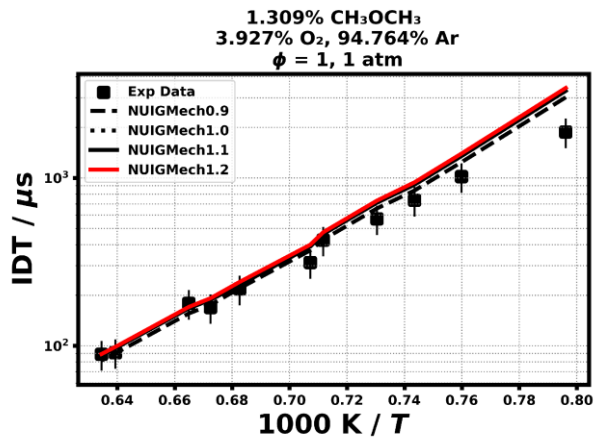
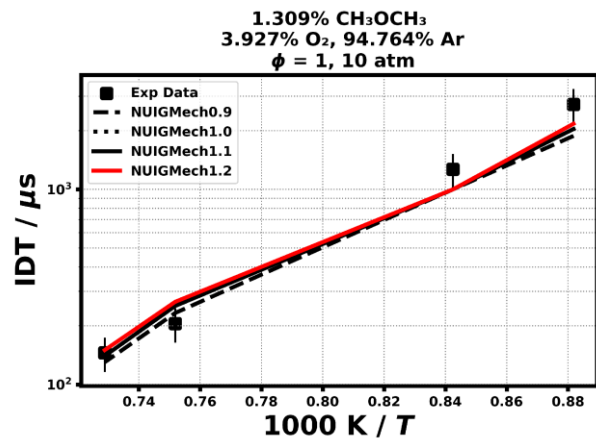
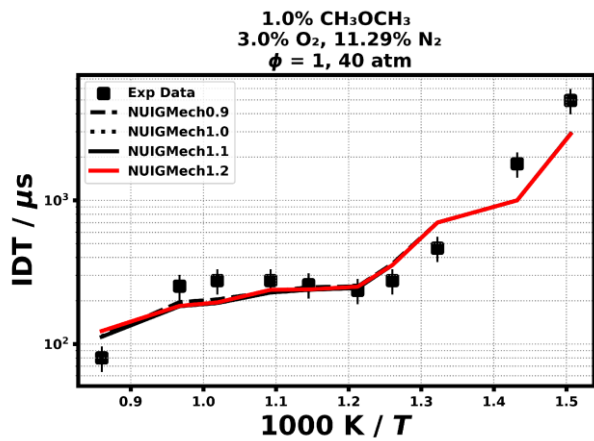
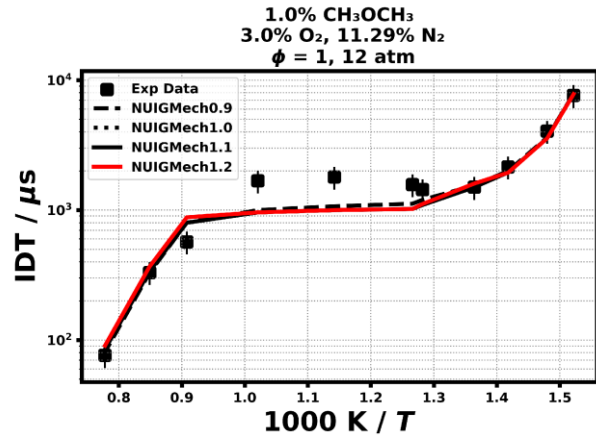
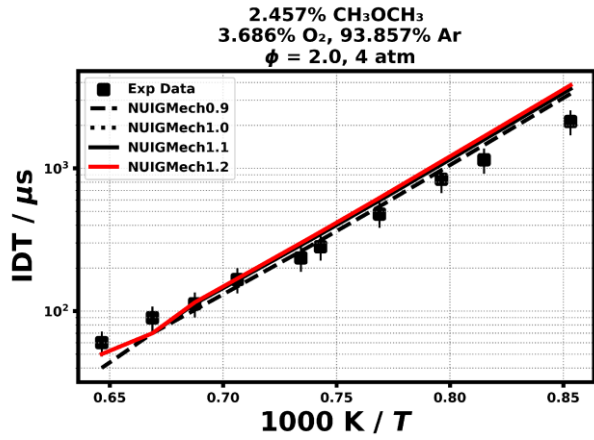




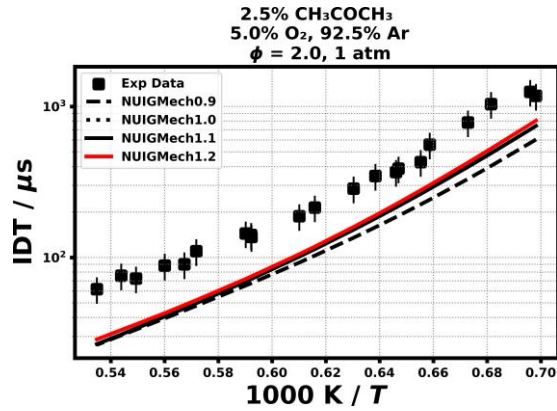
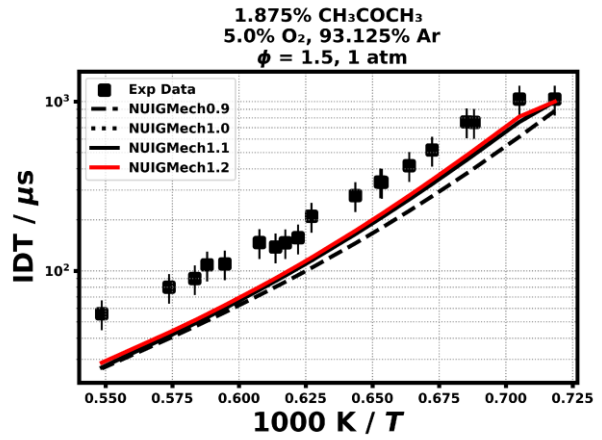
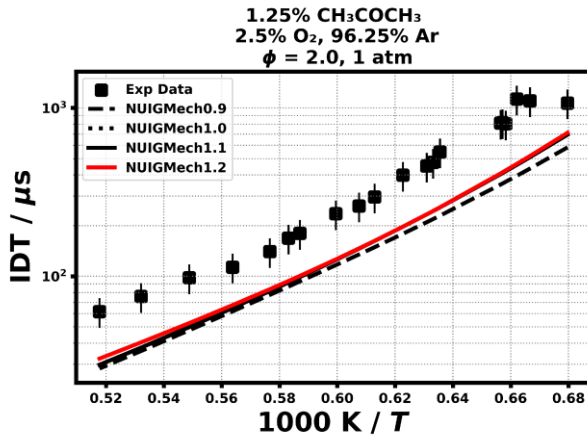
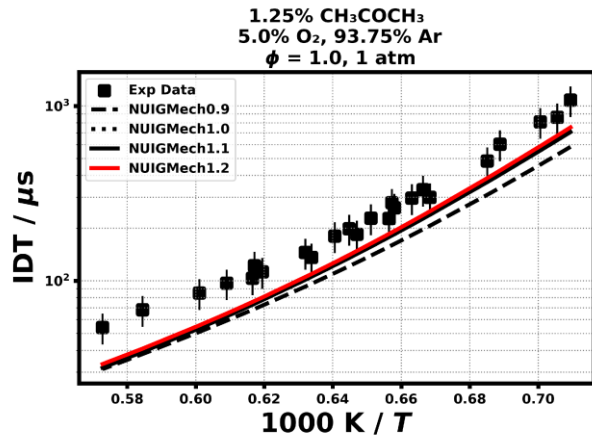
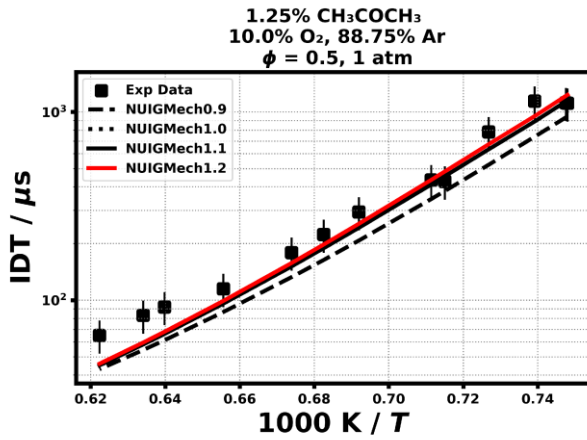




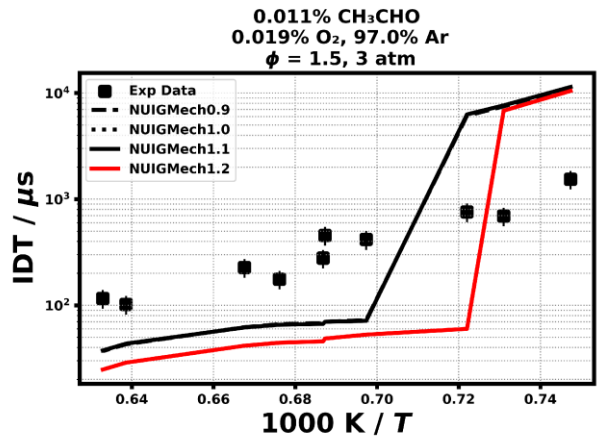
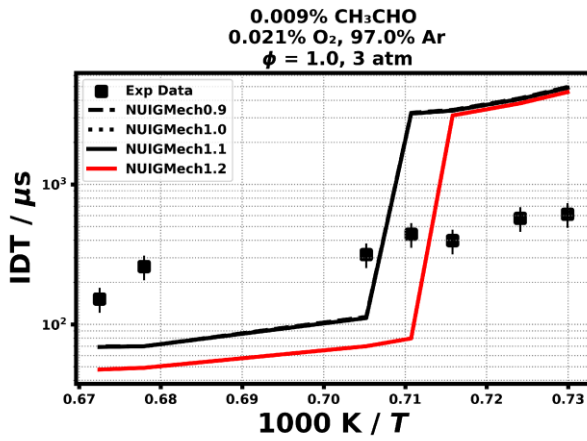
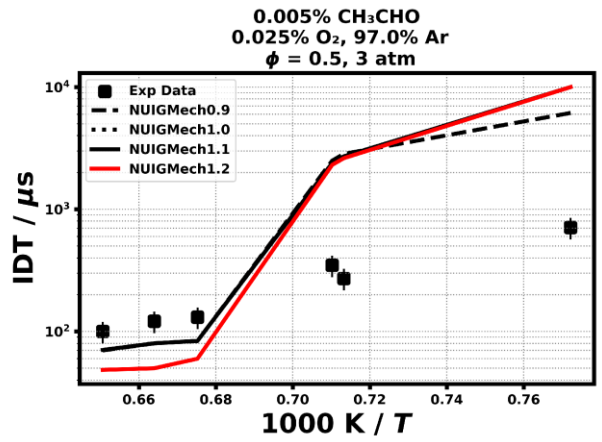
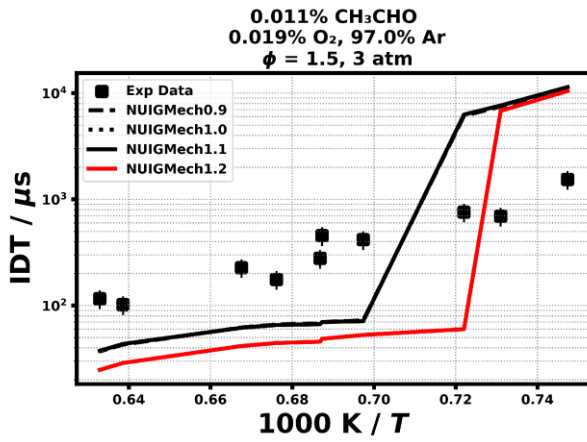
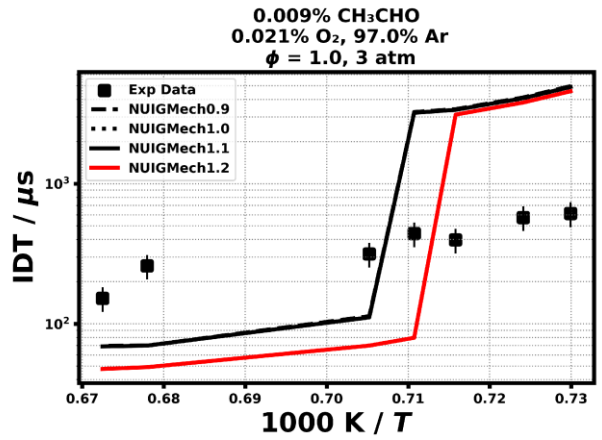
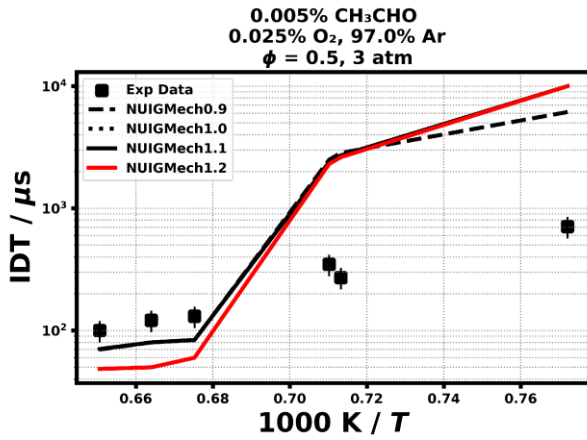




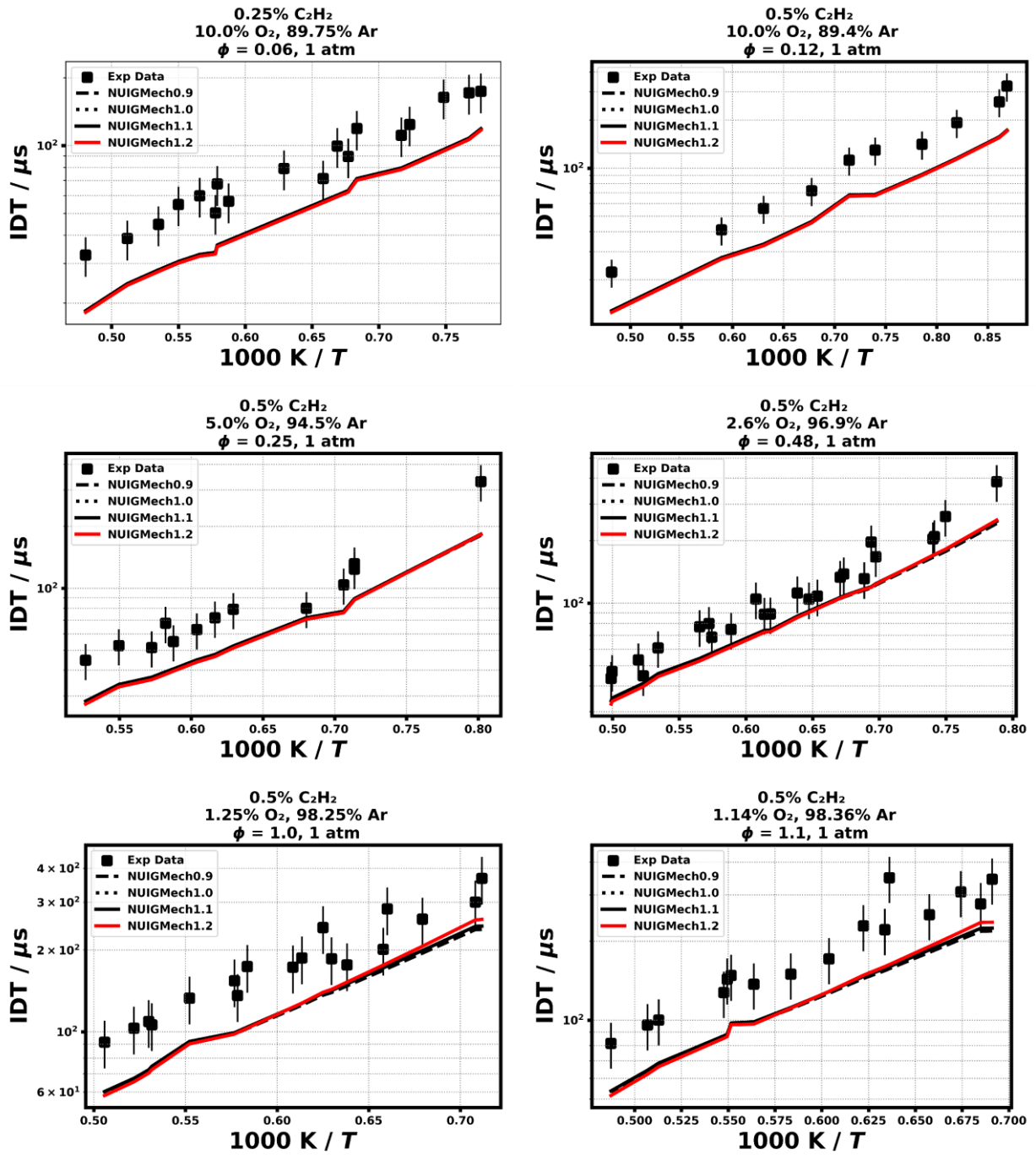
1.1.6 CH₃COCH₃

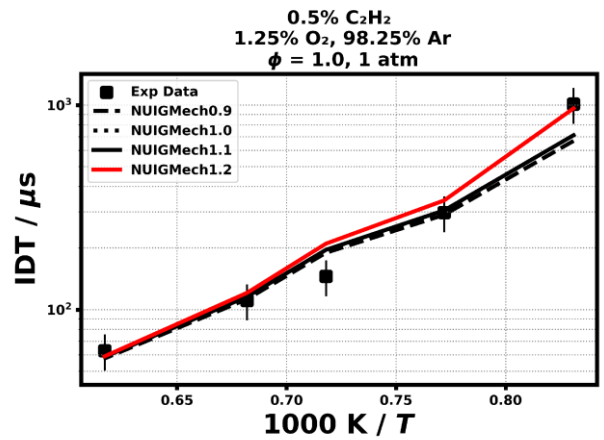
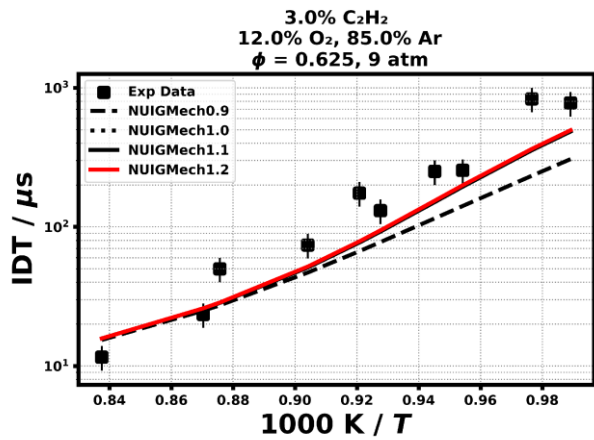
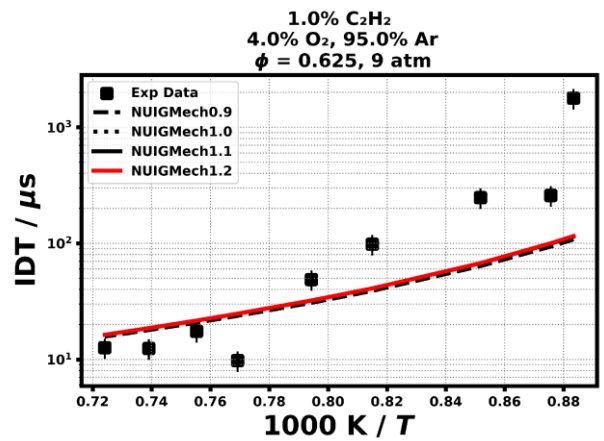
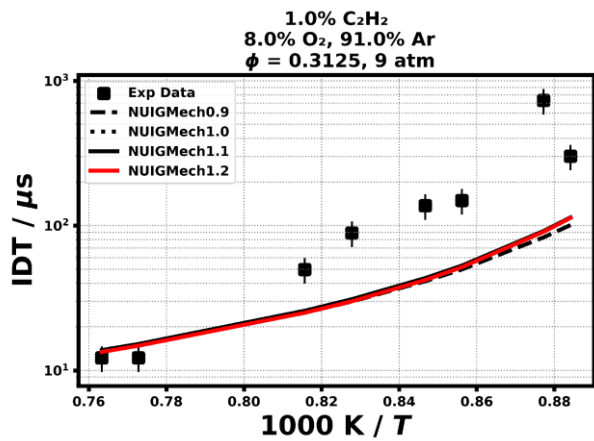
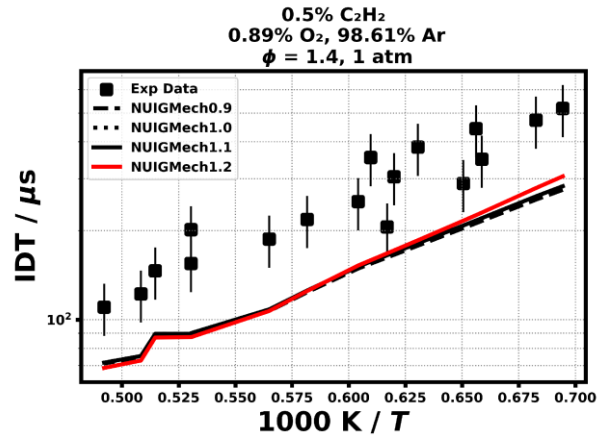
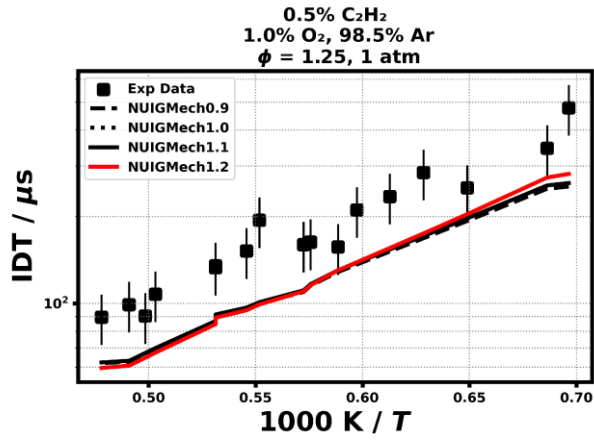


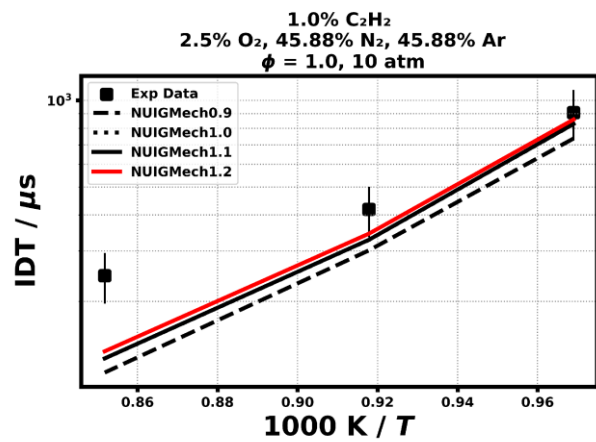
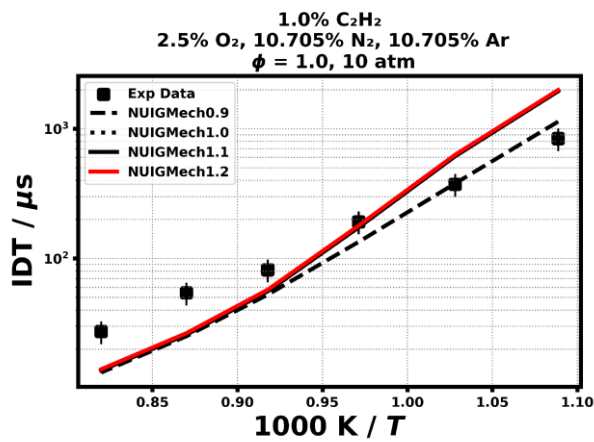
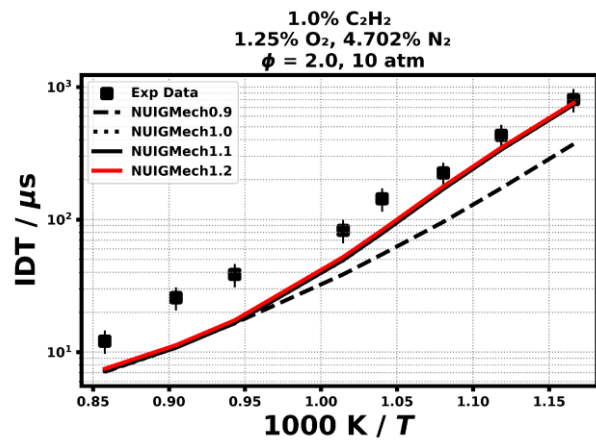
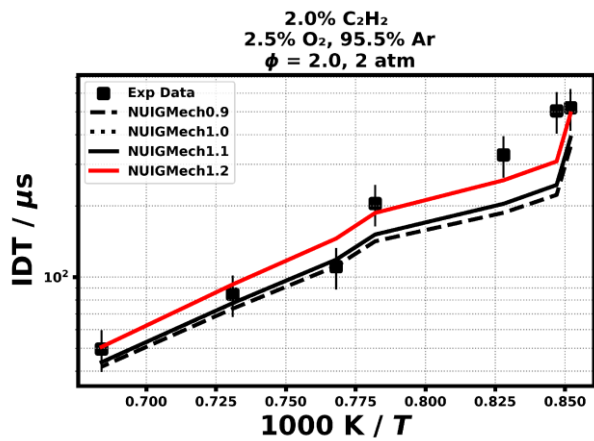
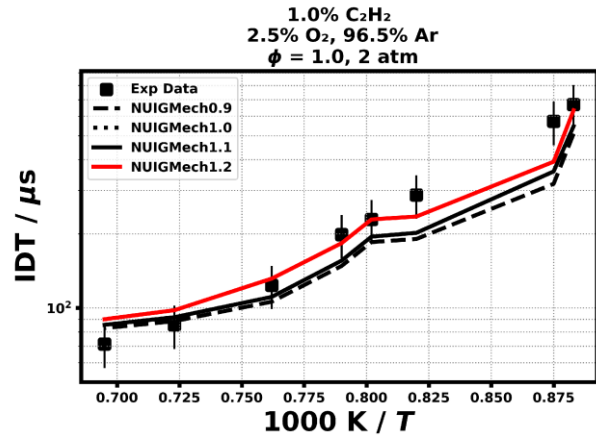
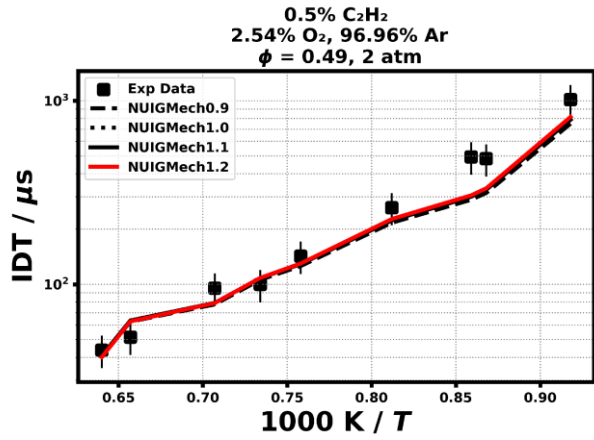
1.1.7 CH₃CHO

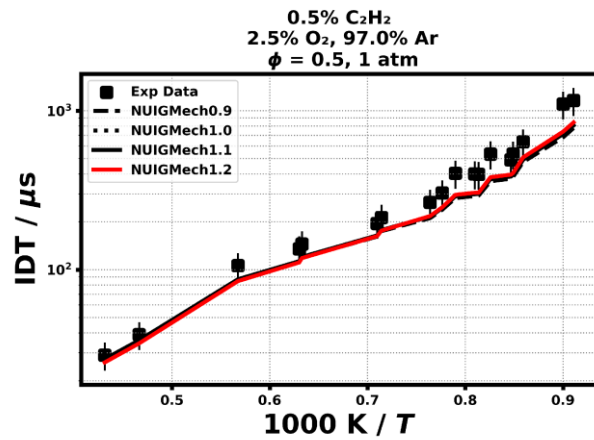
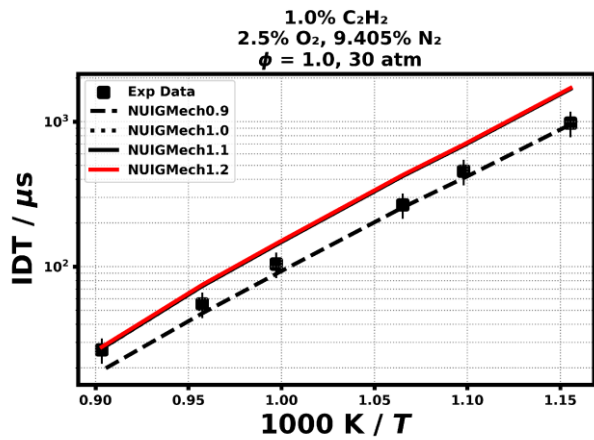
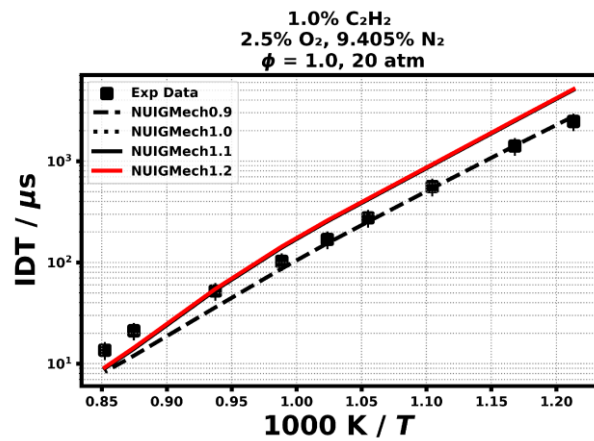
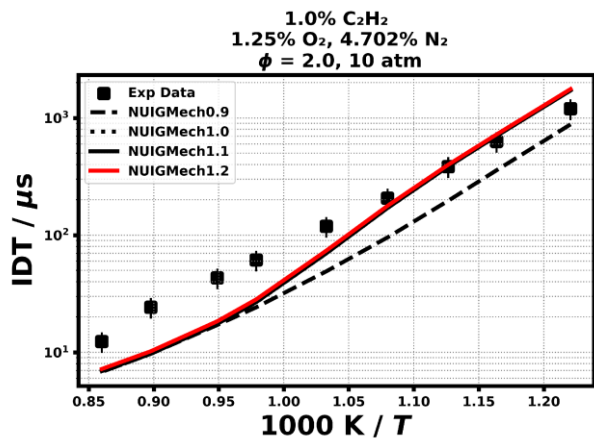
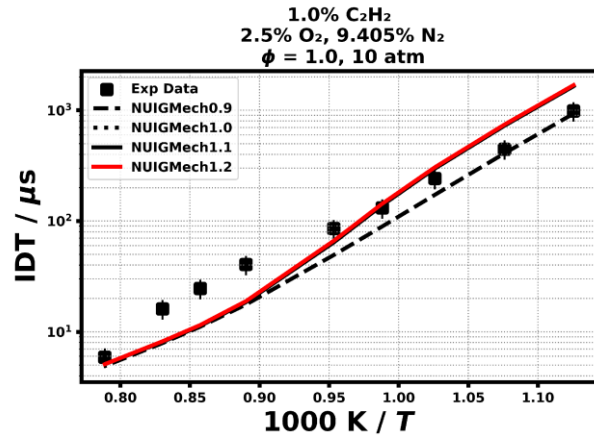
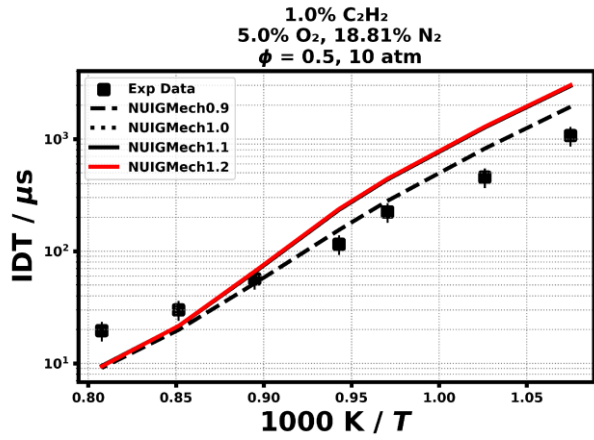


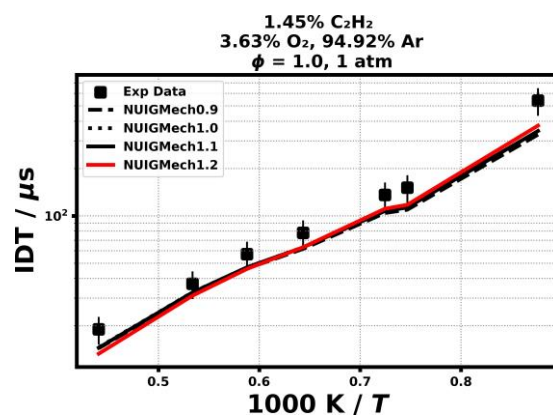
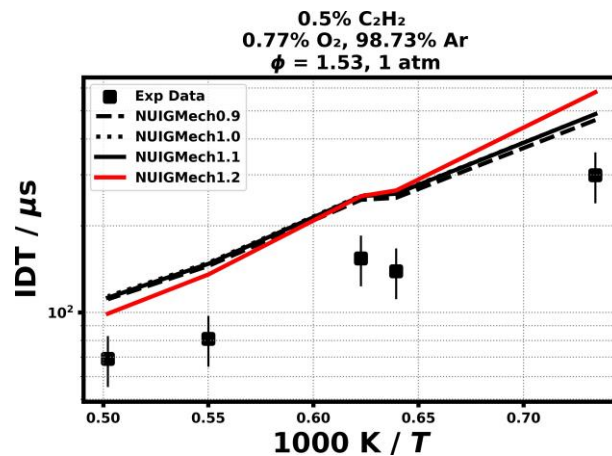
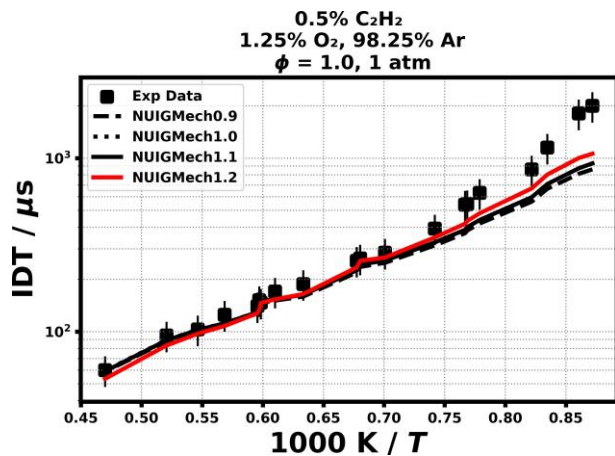
1.1.8 C₂H₂



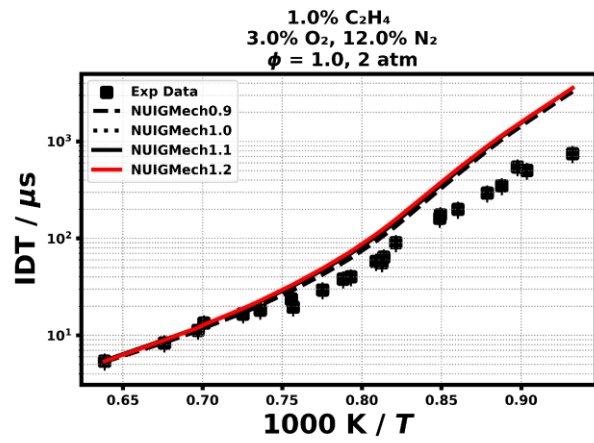
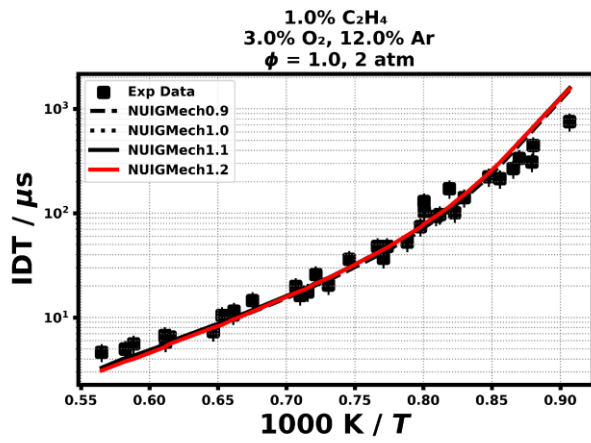
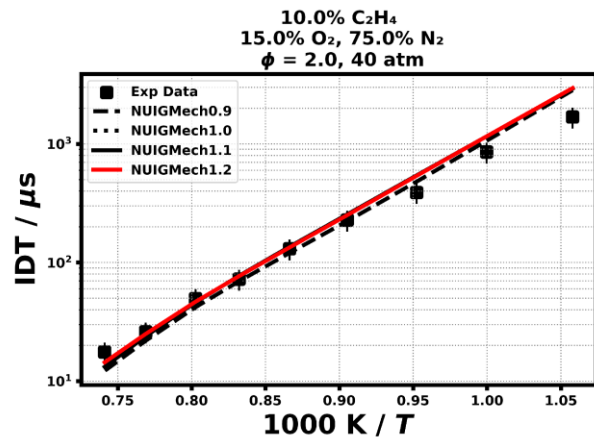
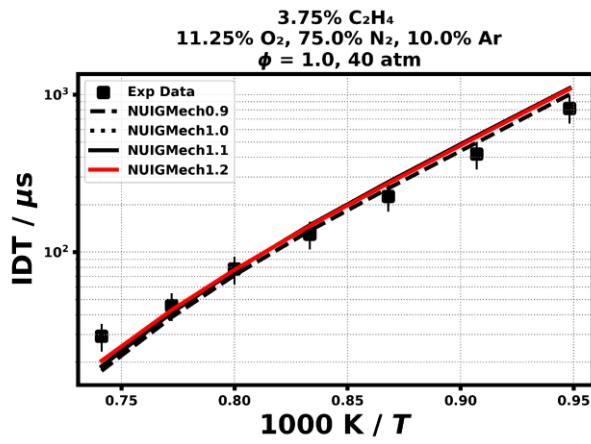
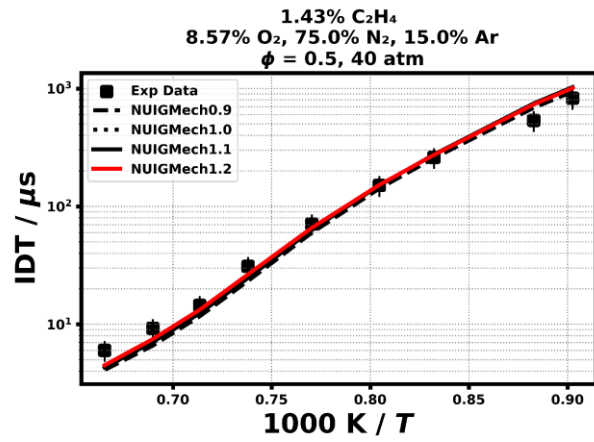
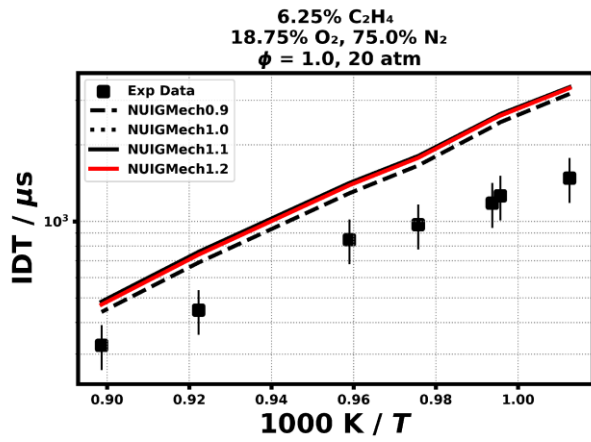


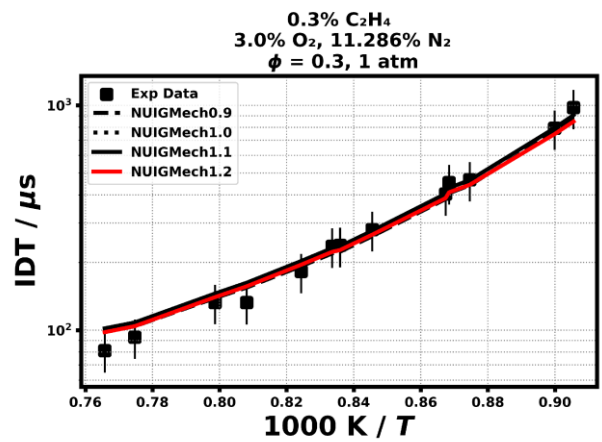
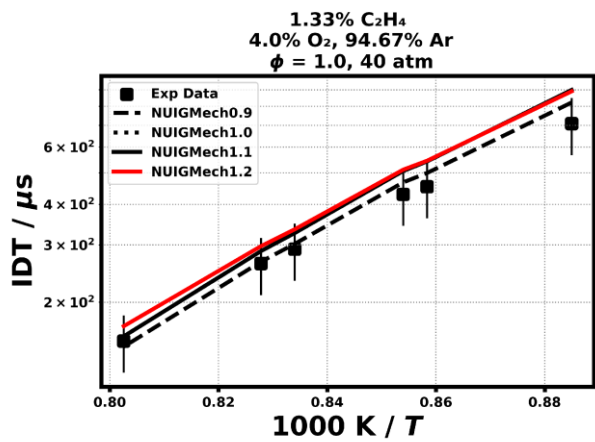
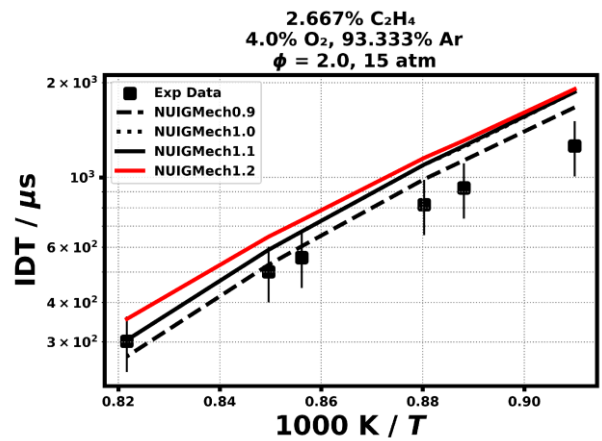
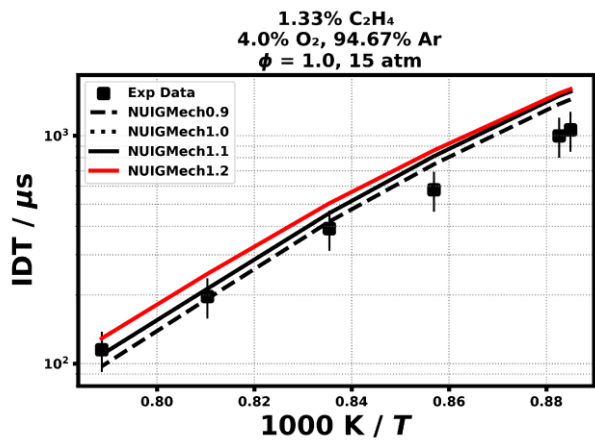
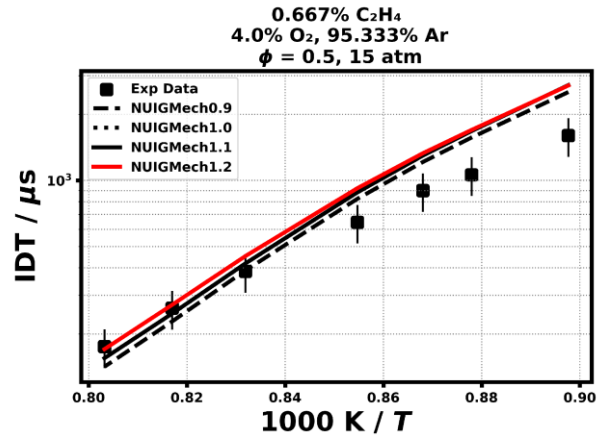
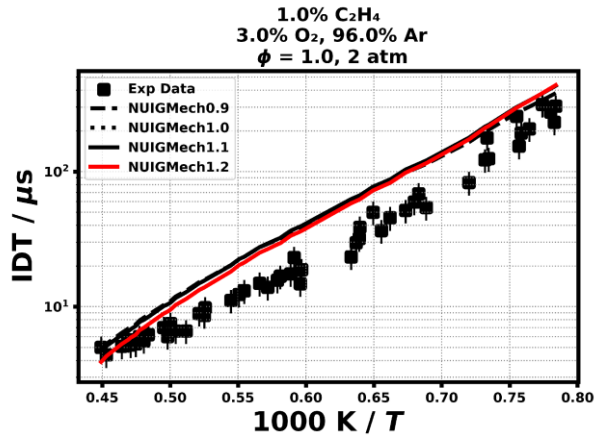


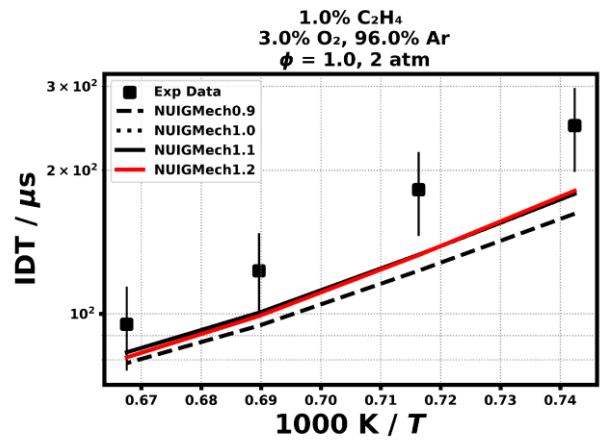
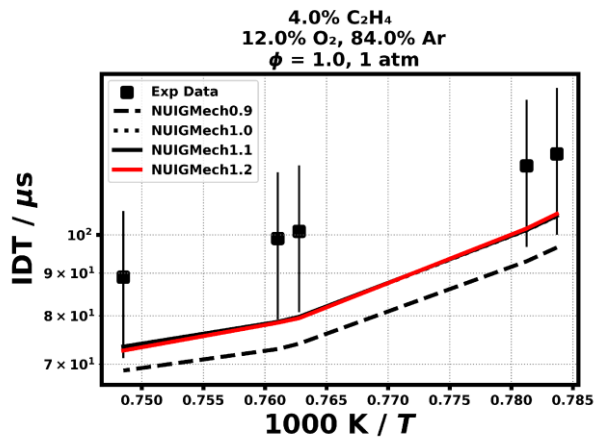
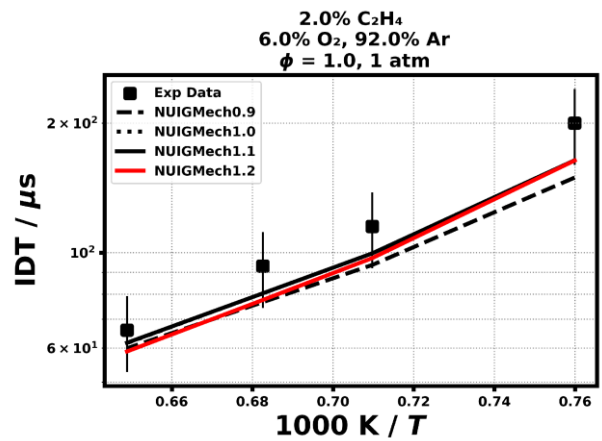
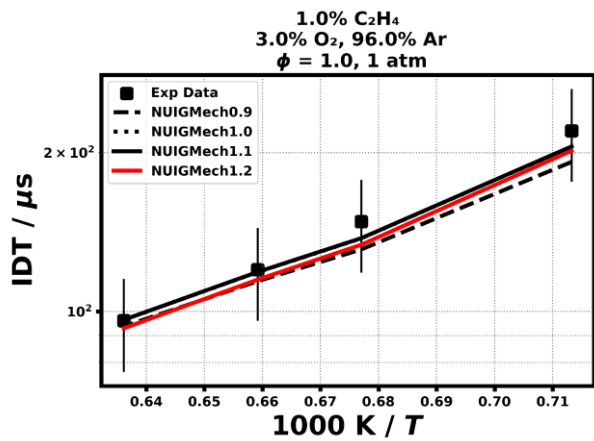
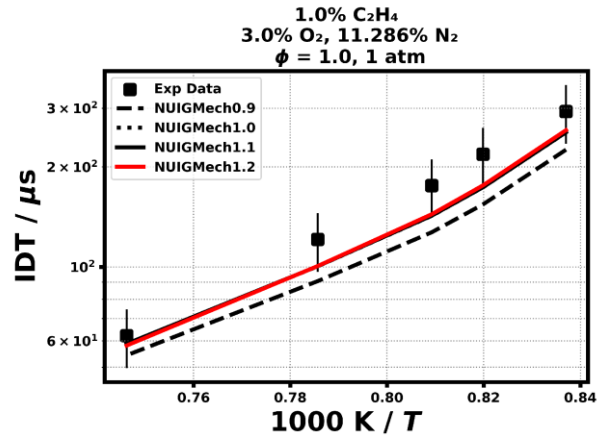
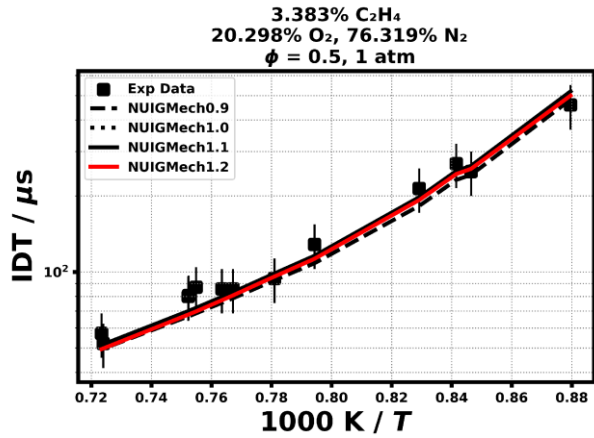


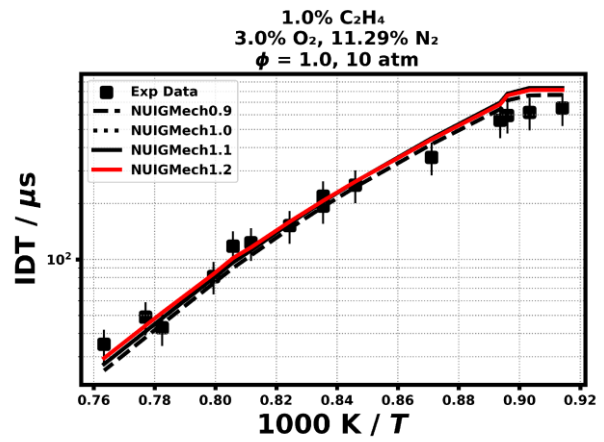
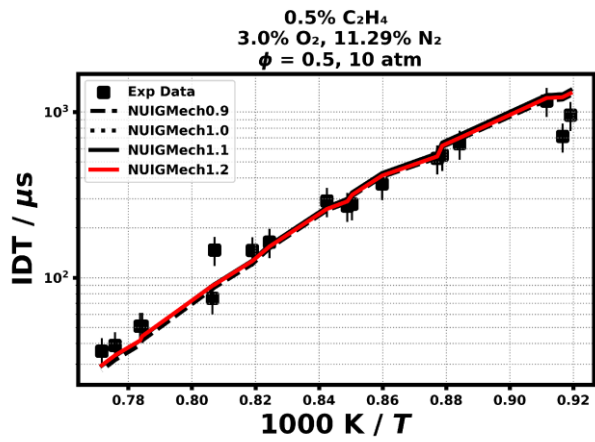
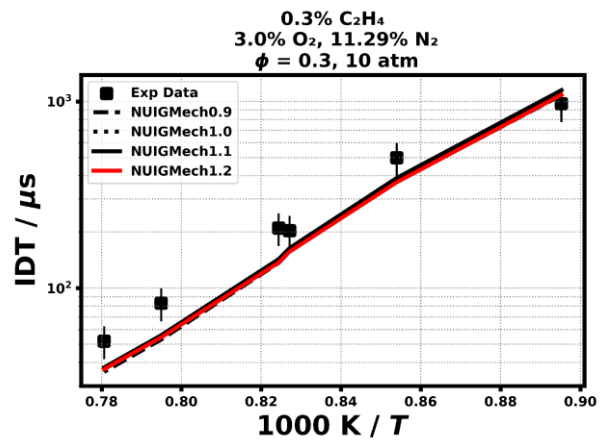
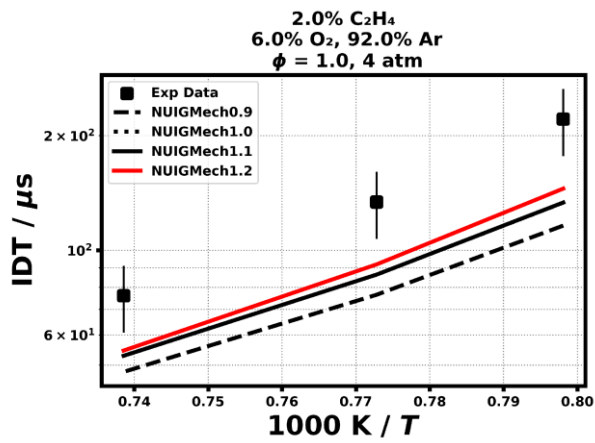
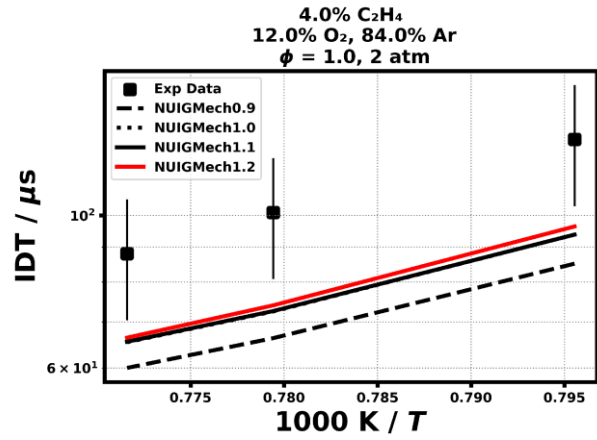
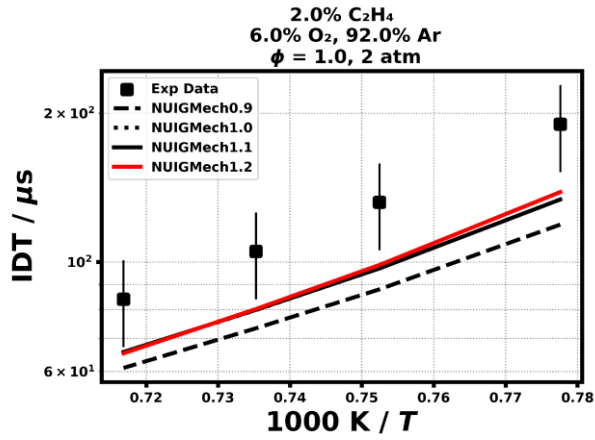


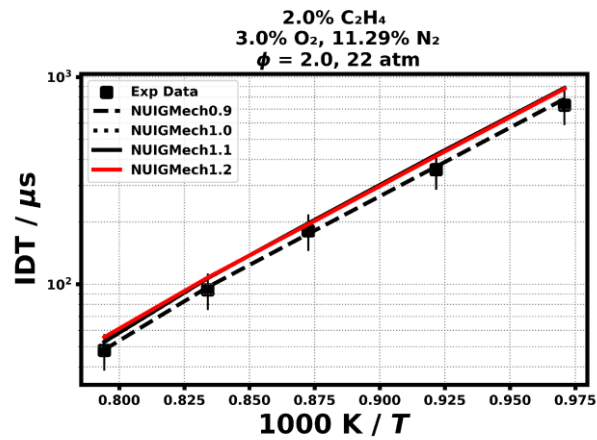
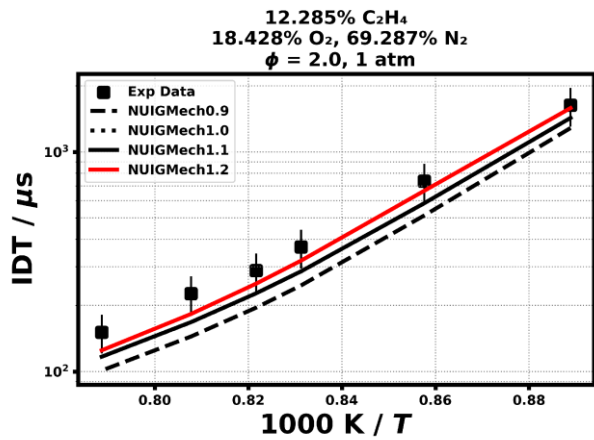
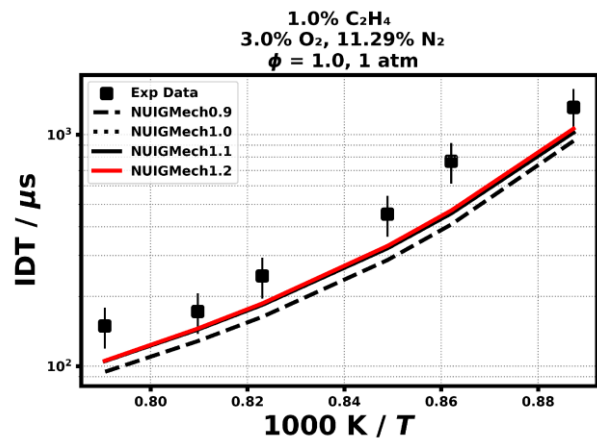
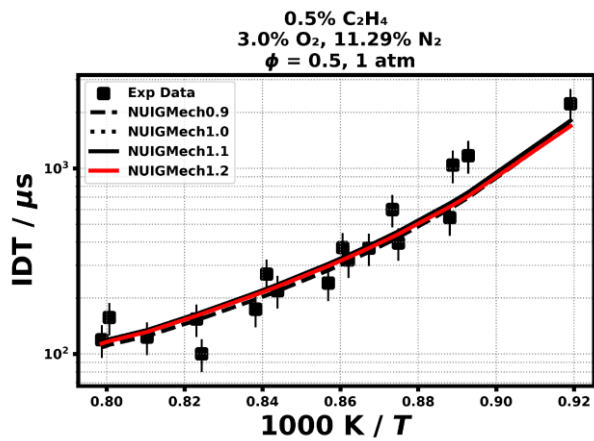
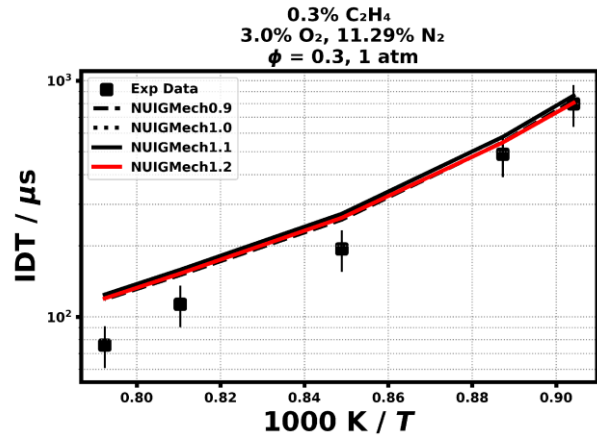
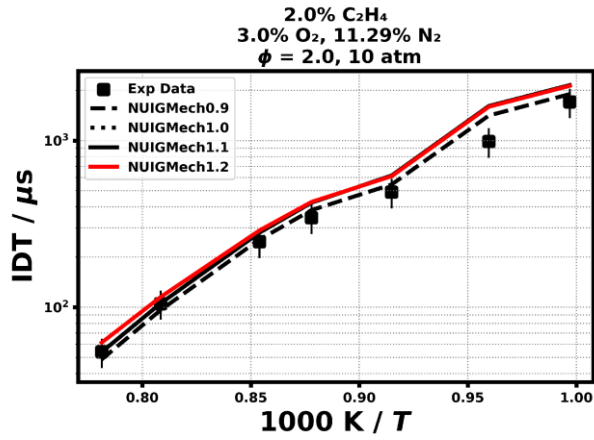
1.1.9 C₂H₄

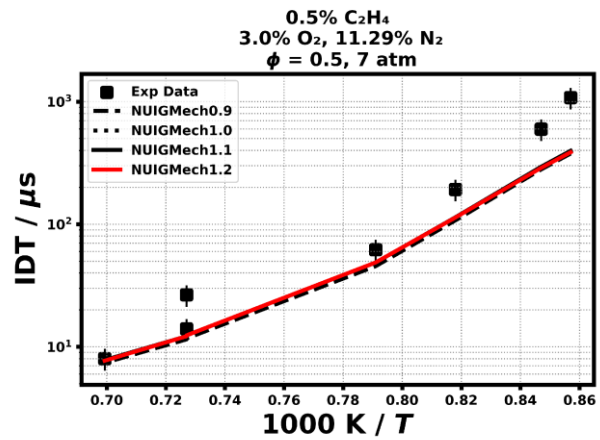
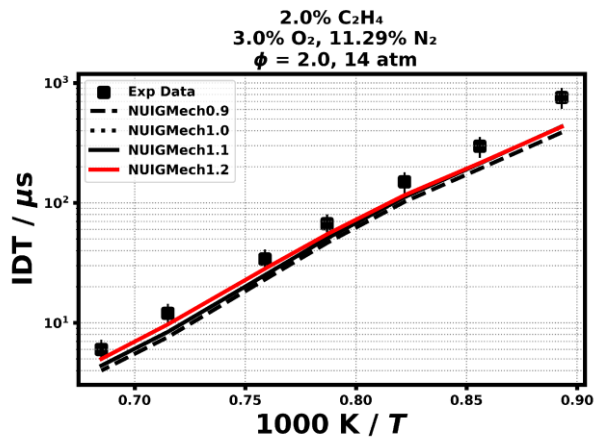
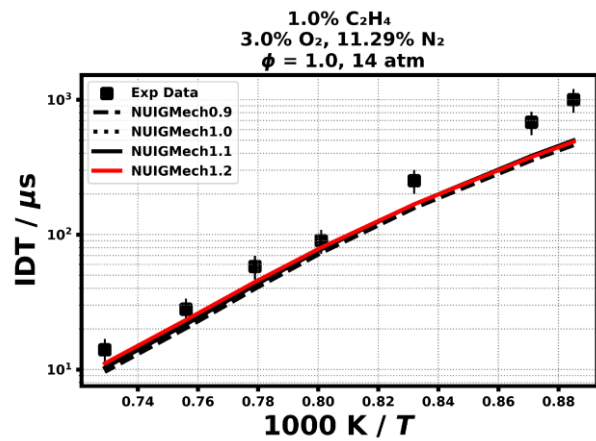
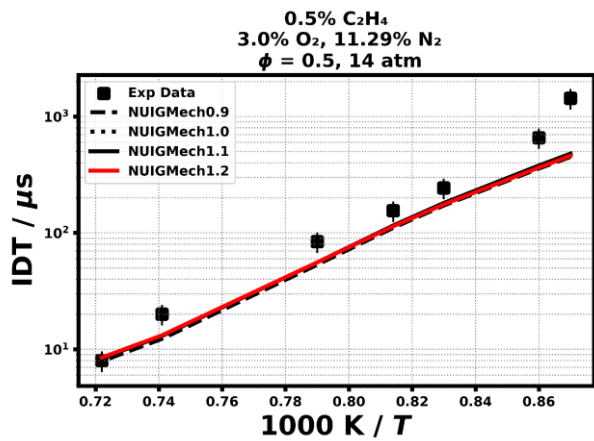
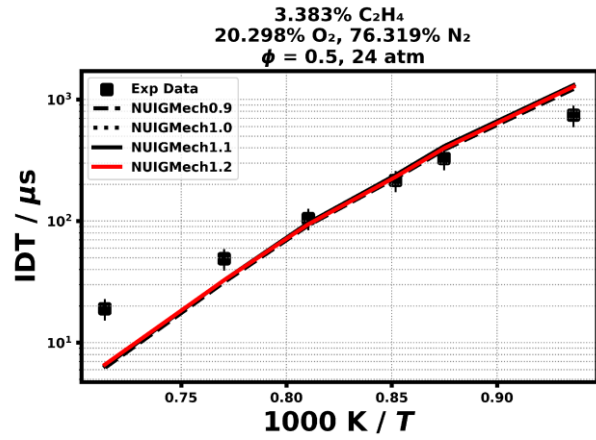
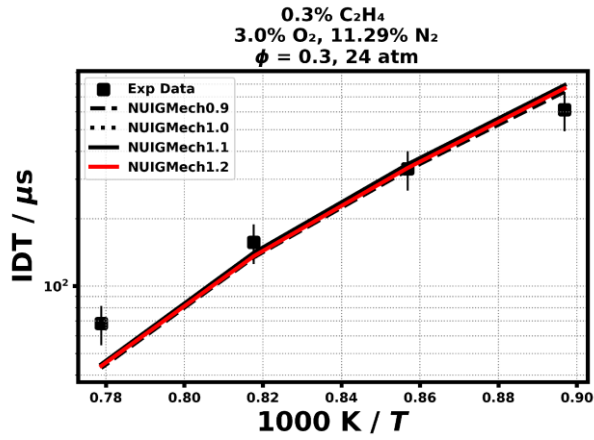


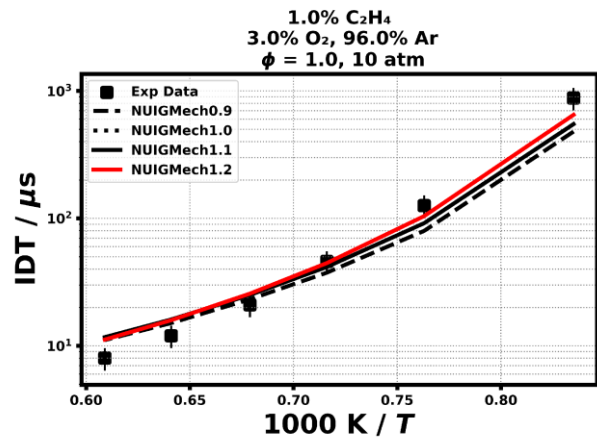
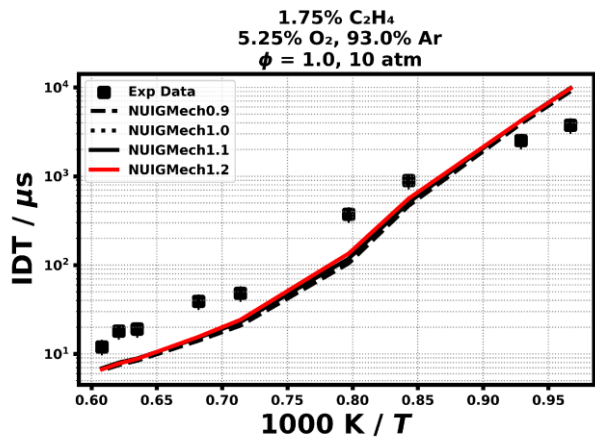
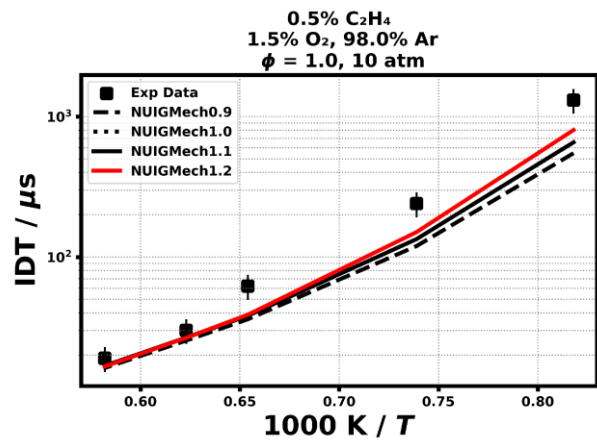
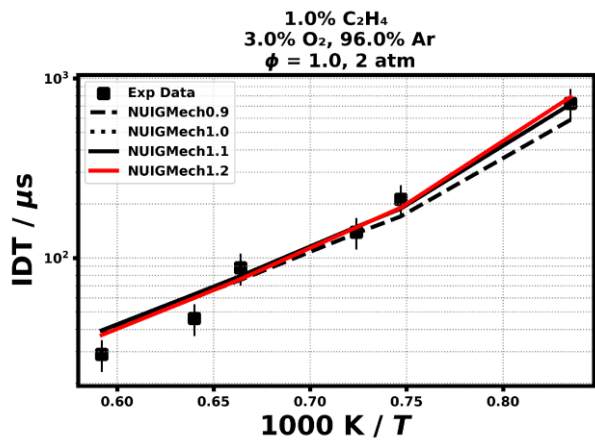
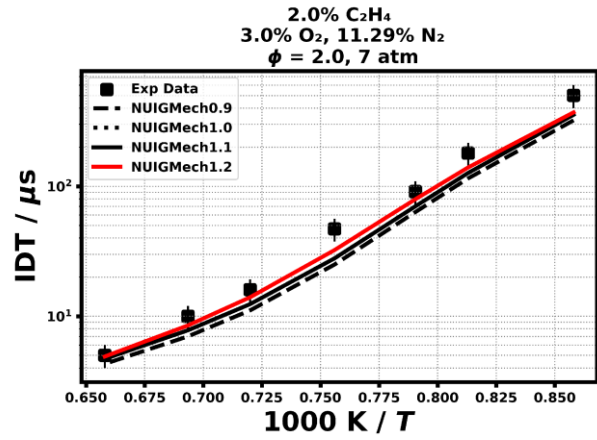
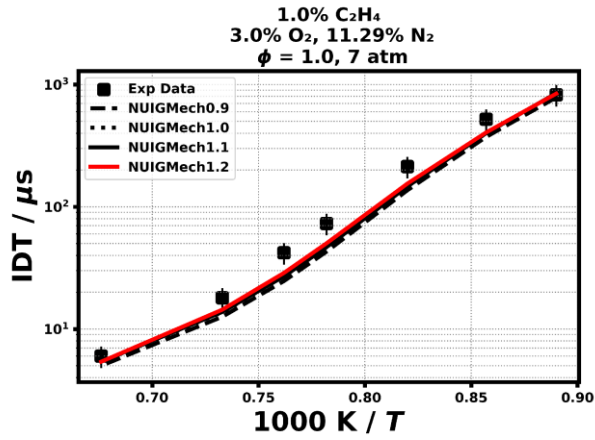


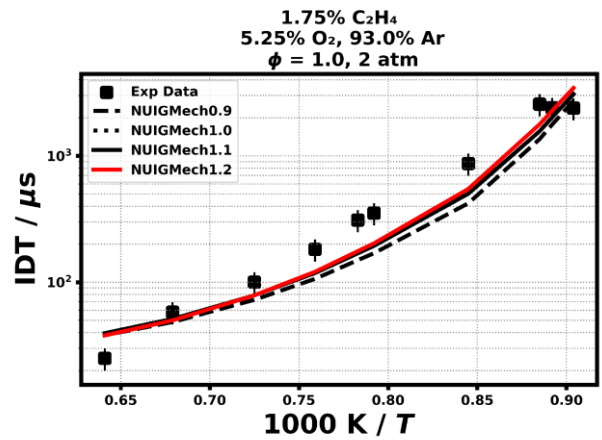
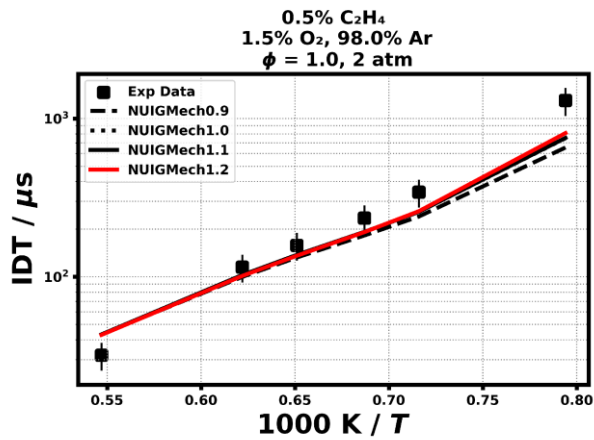
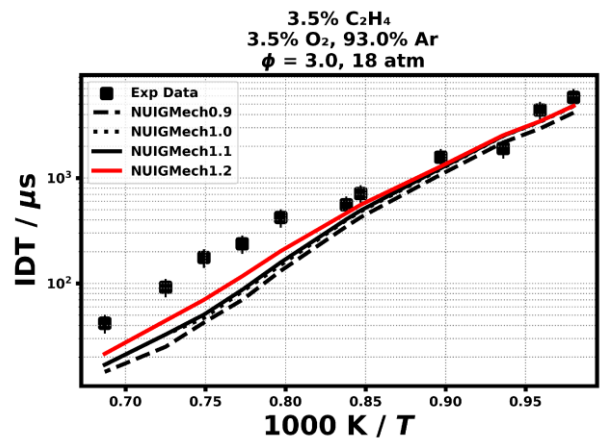
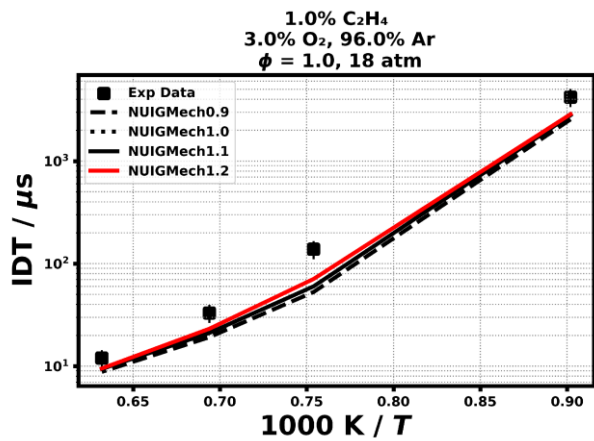
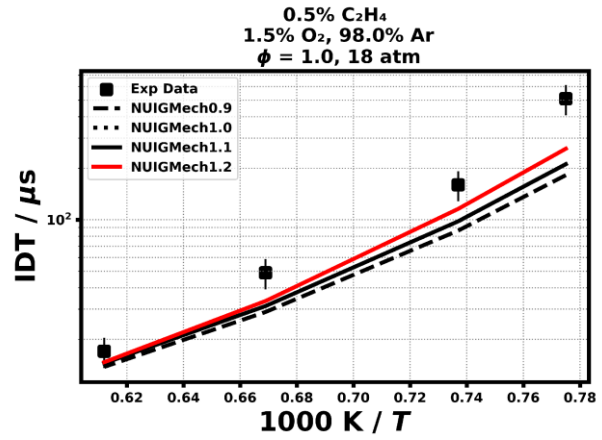
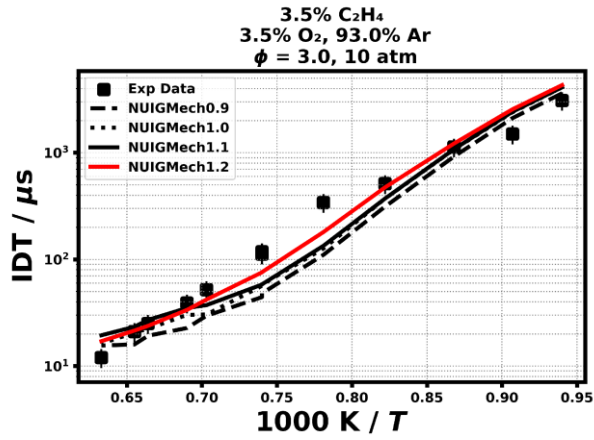


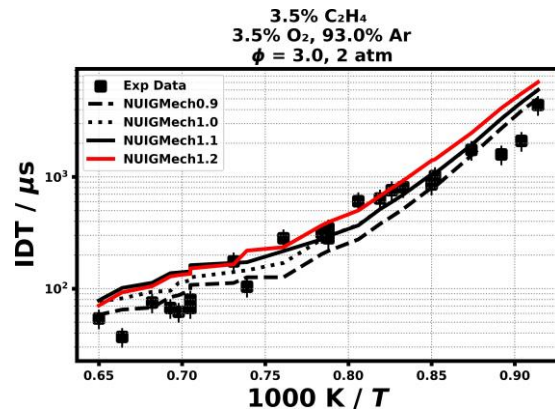




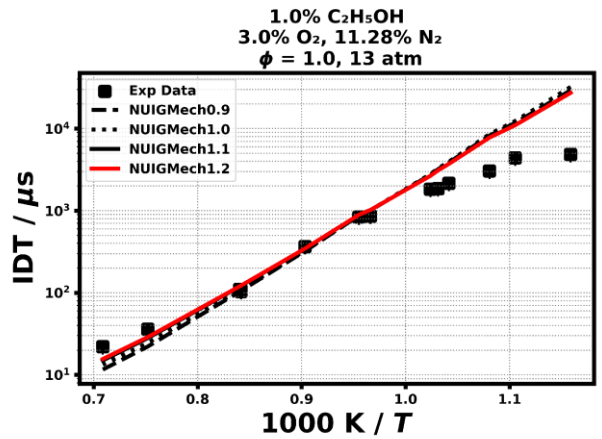
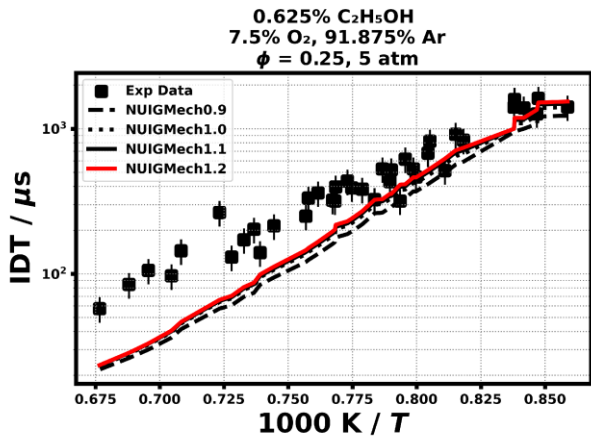
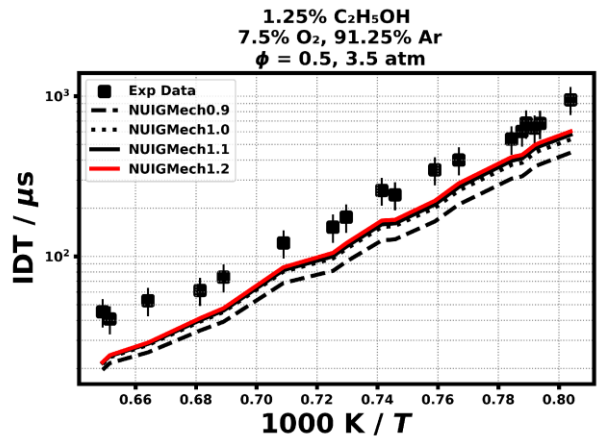
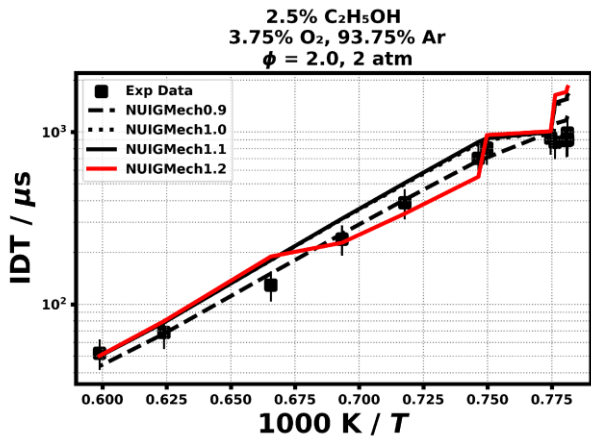
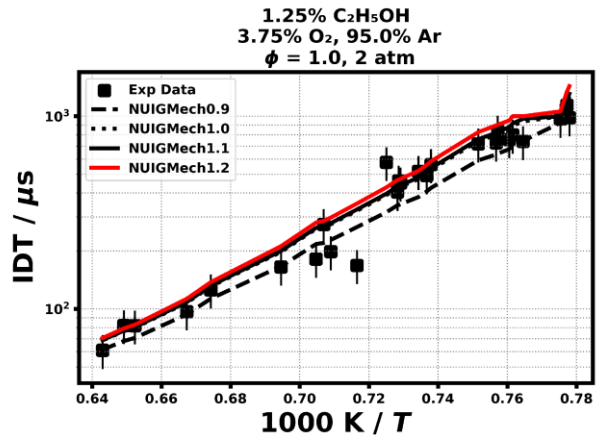
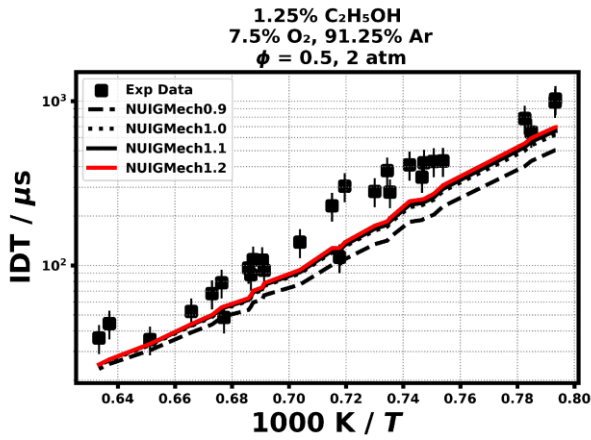


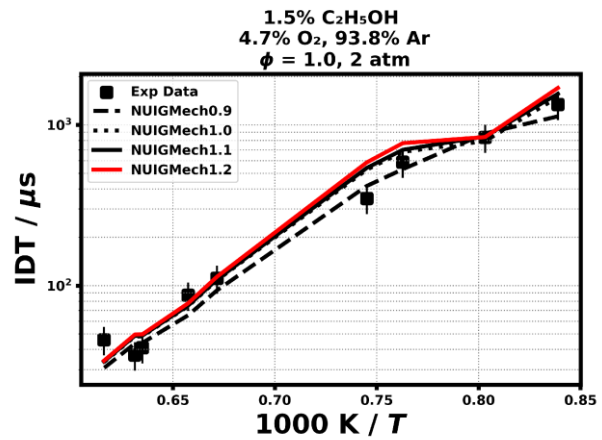
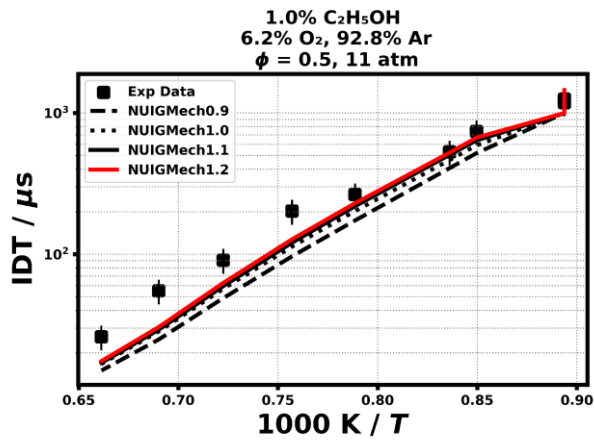
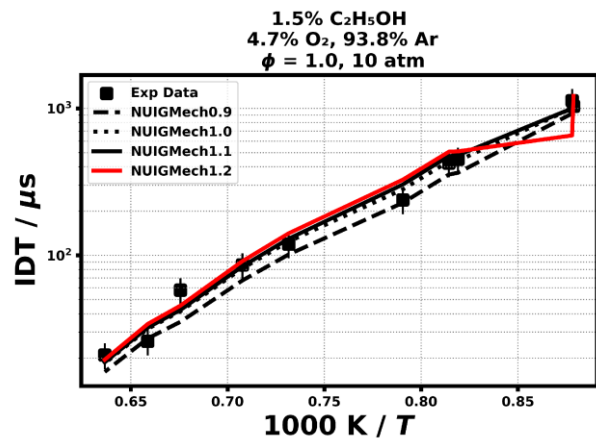
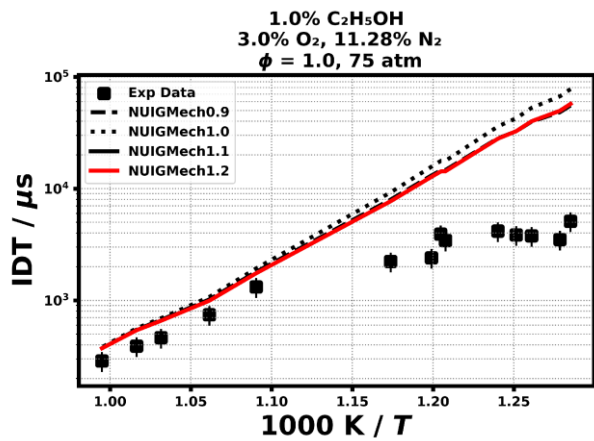
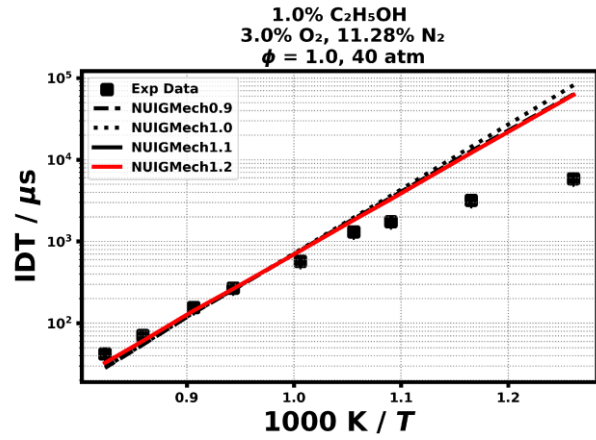
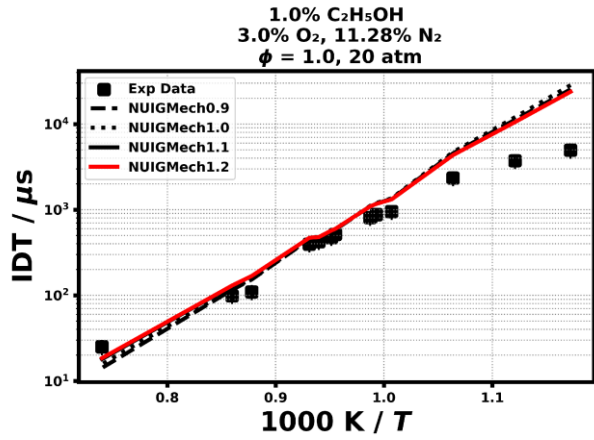


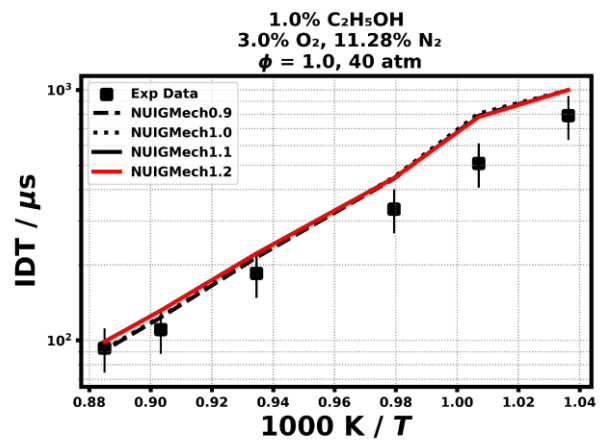
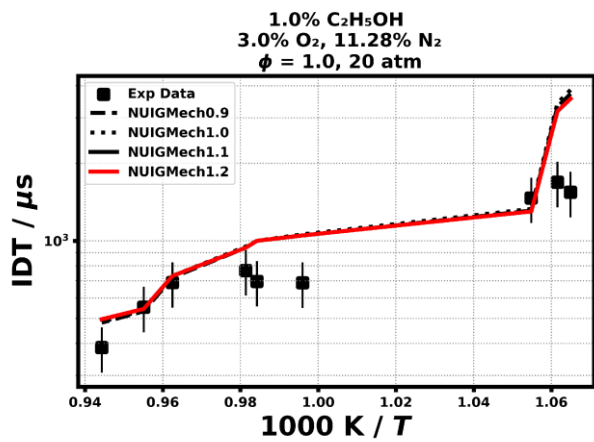
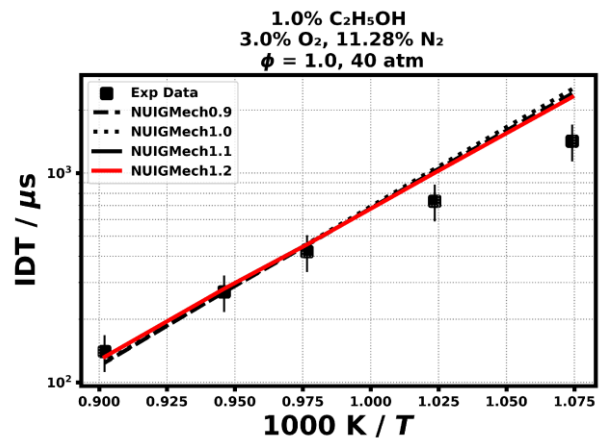
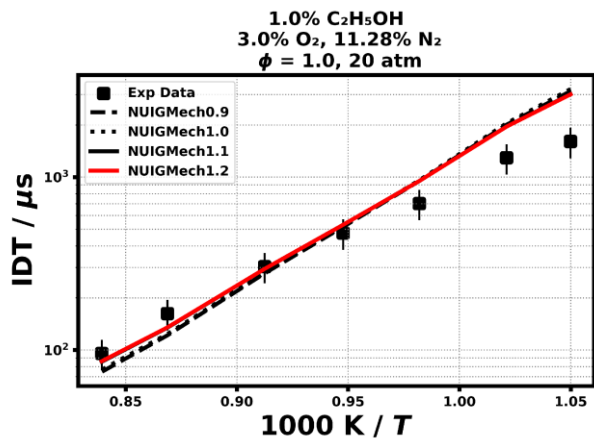
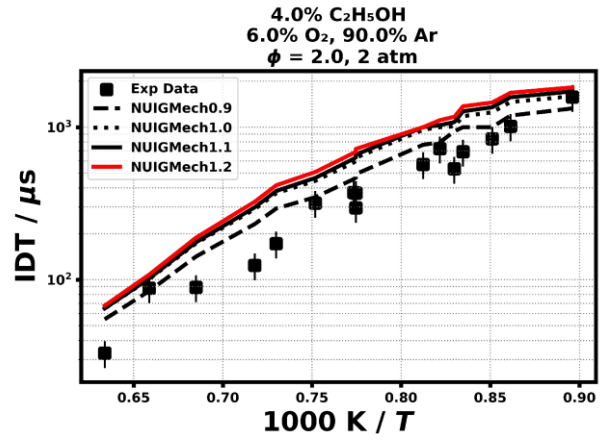
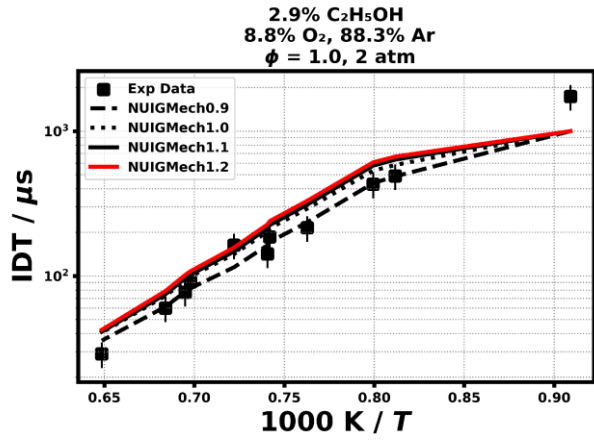


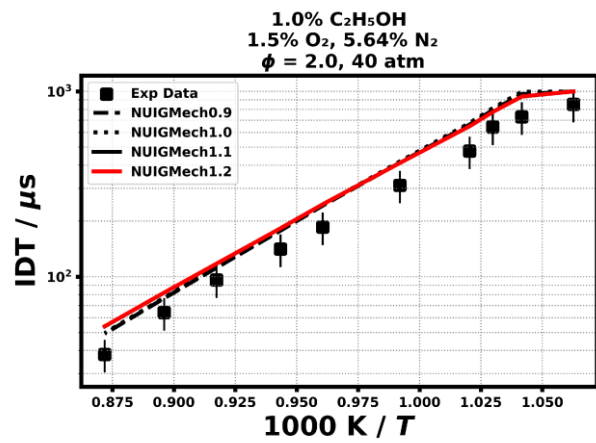
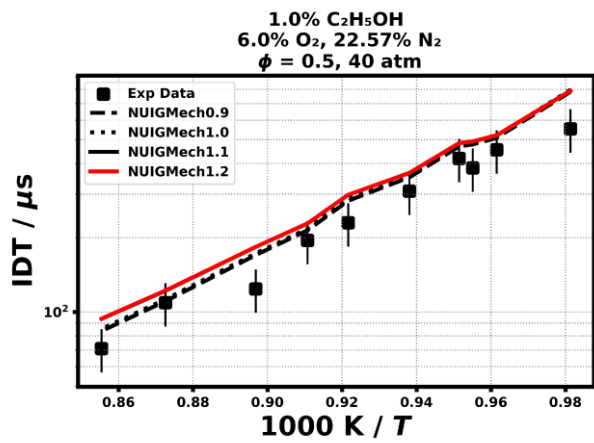
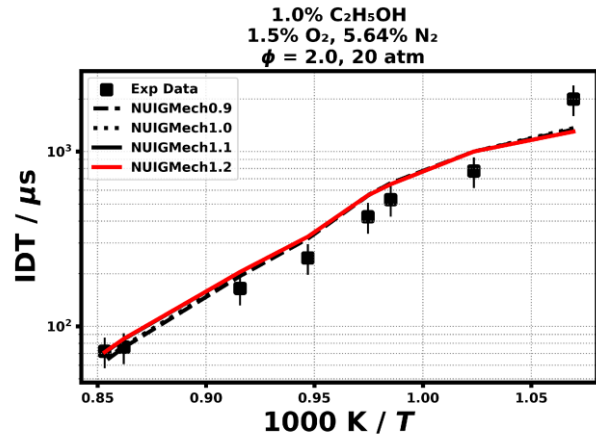
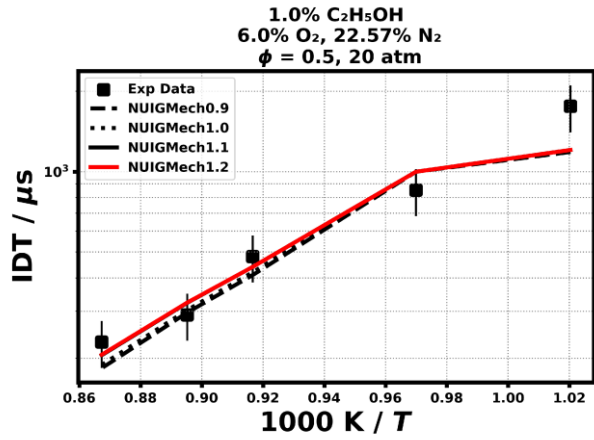


1.1.10 C₂H₅OH

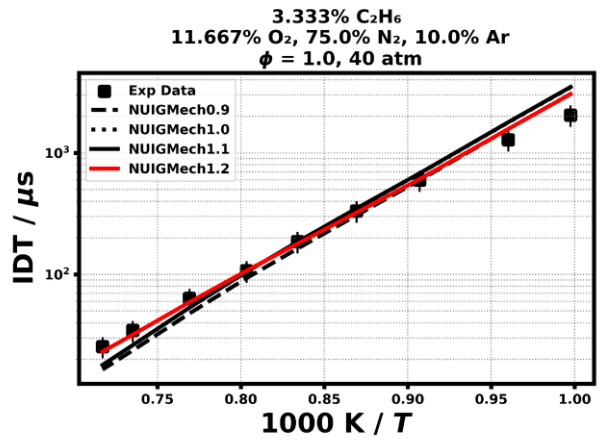
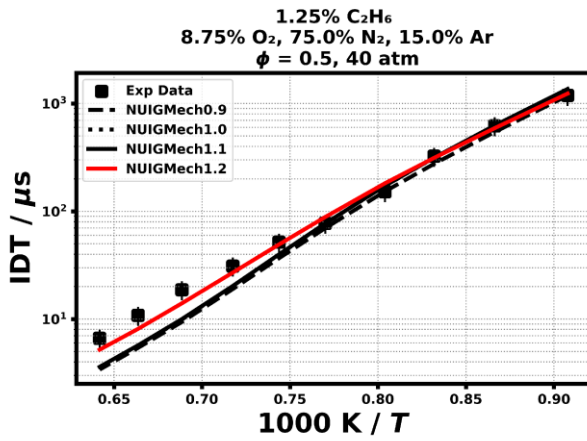
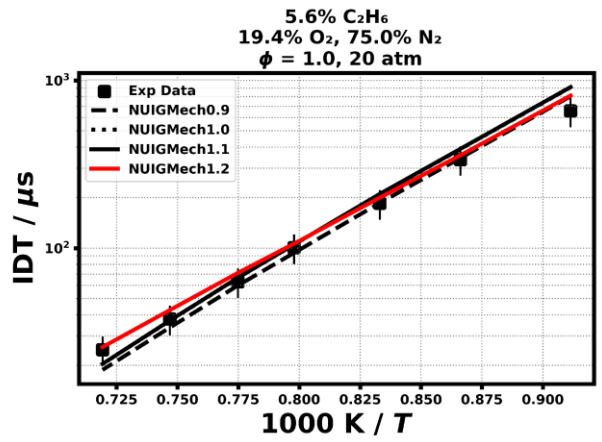
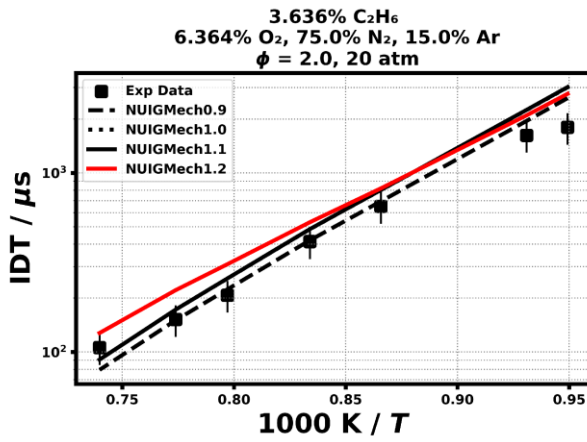
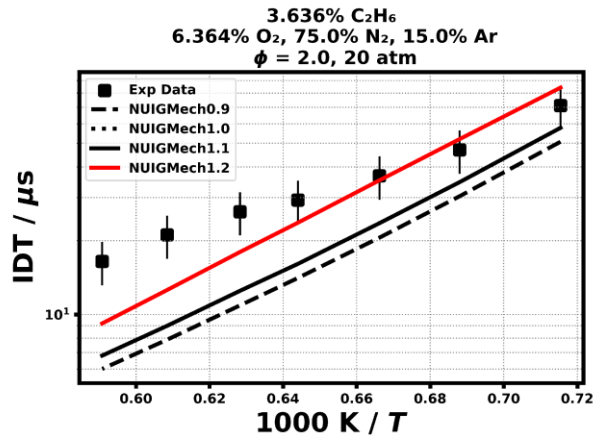
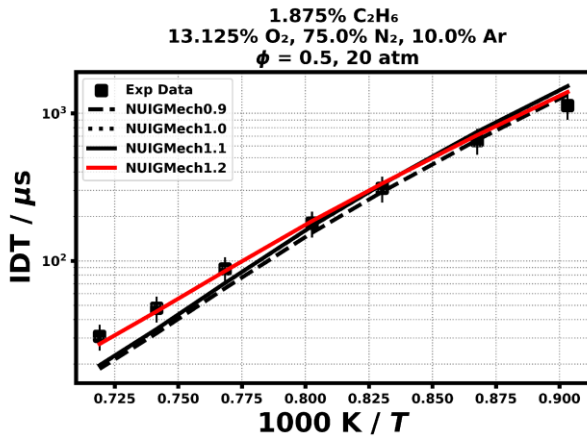


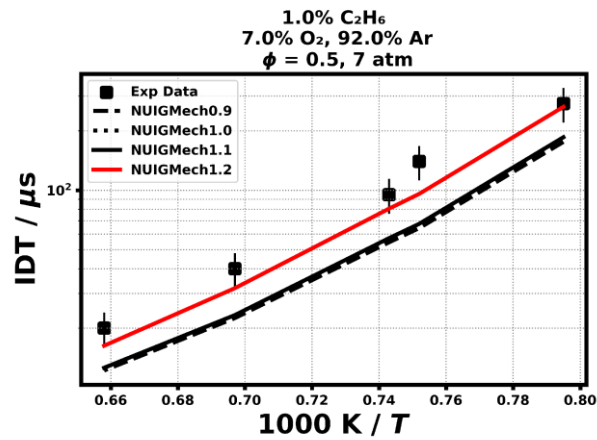
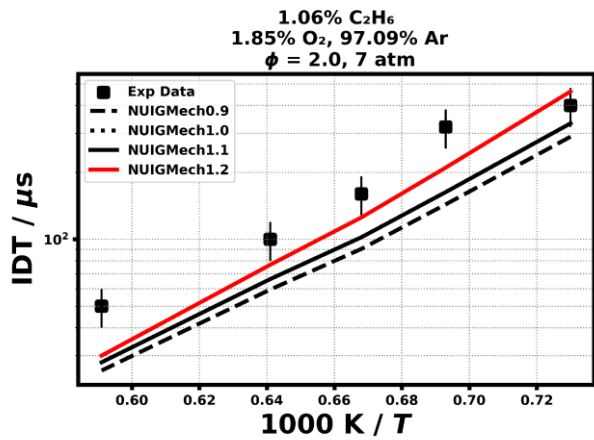
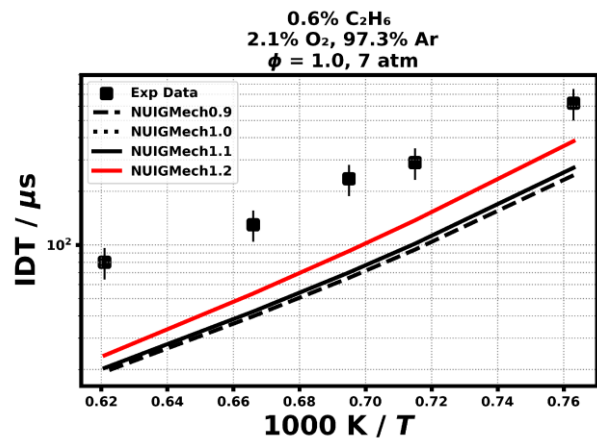
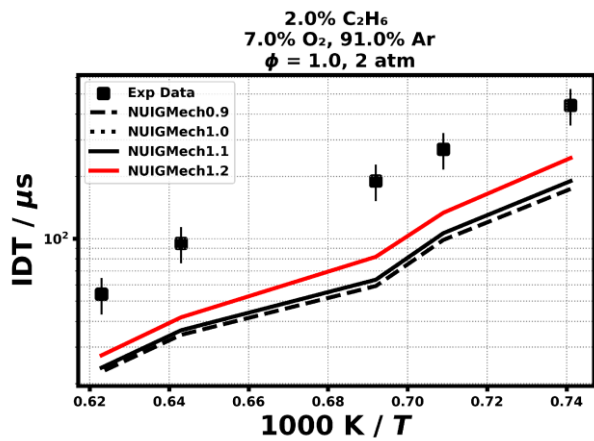
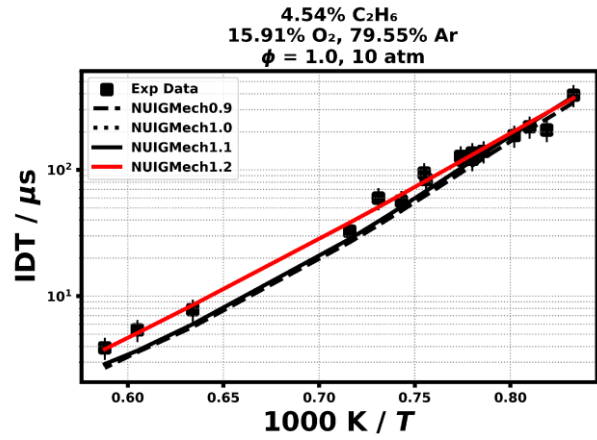
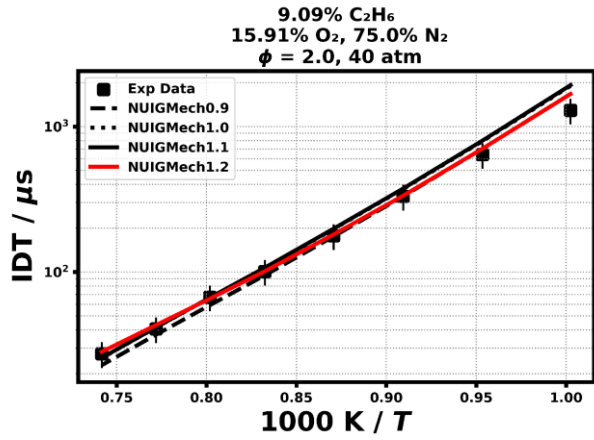


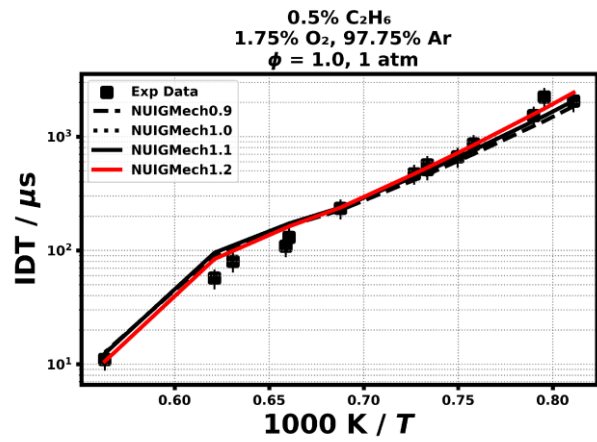
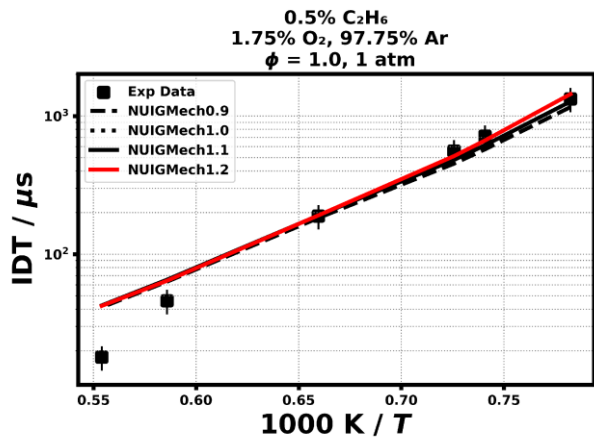
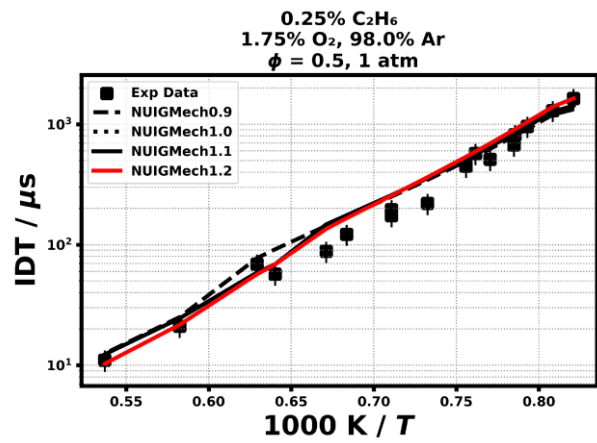
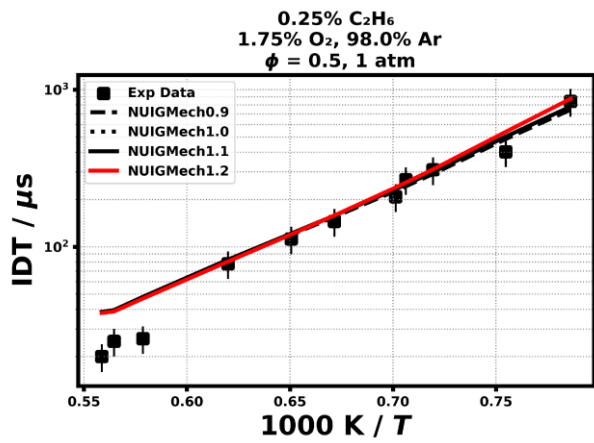
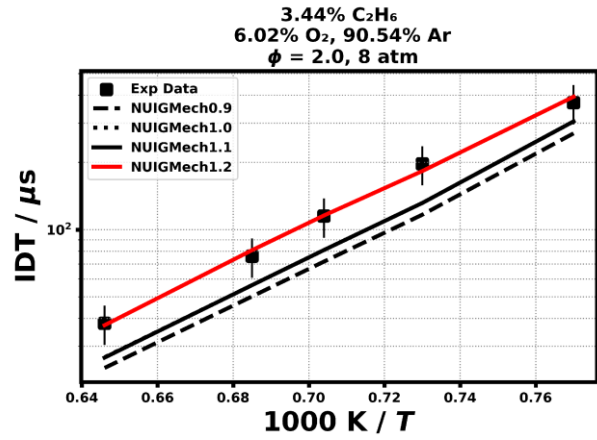
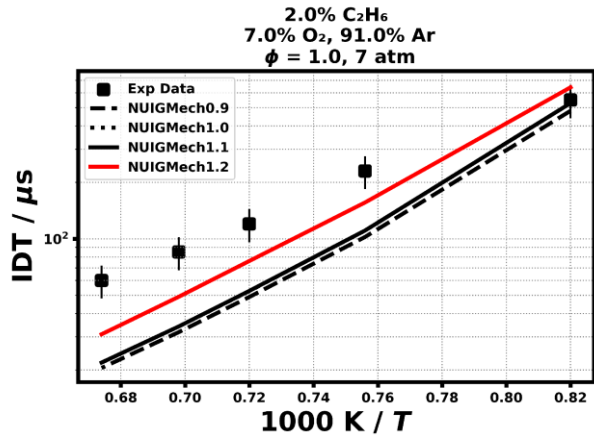


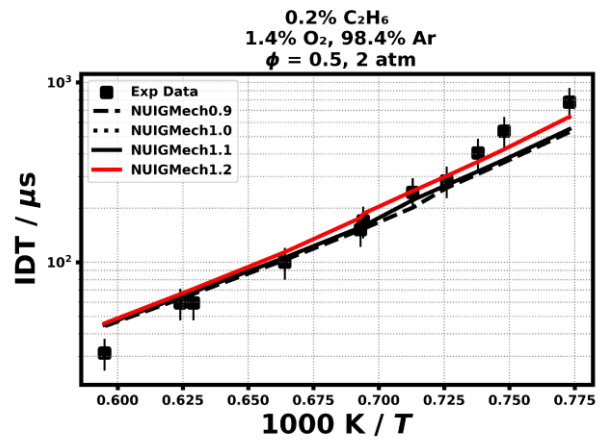
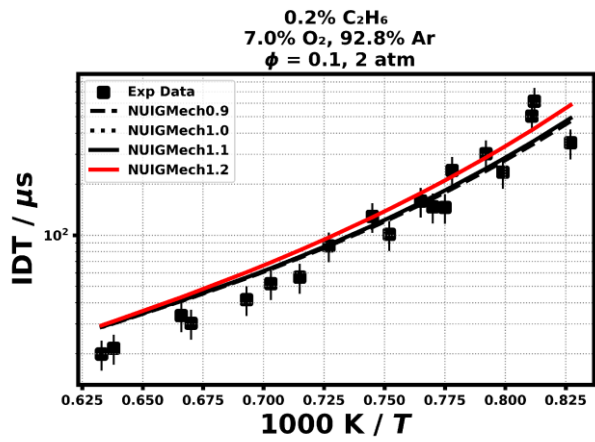
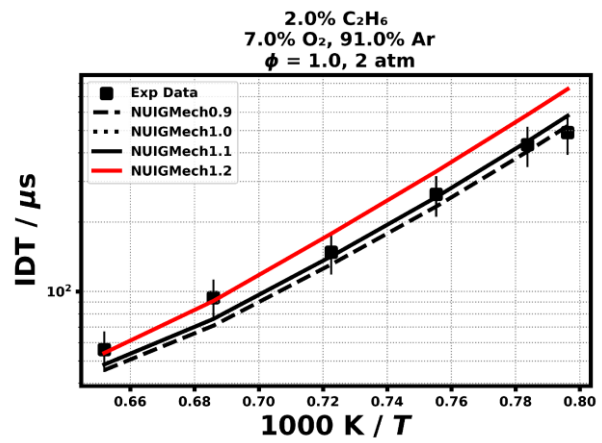
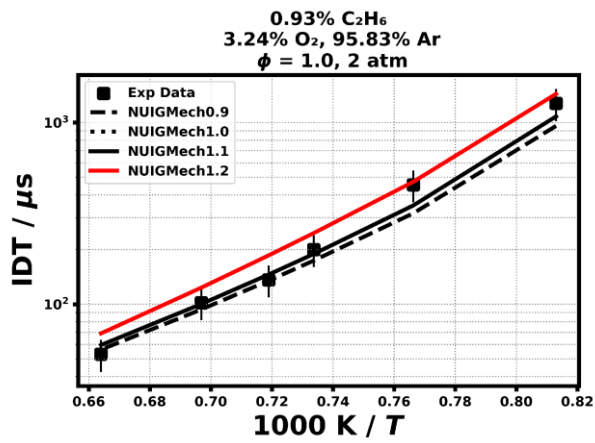
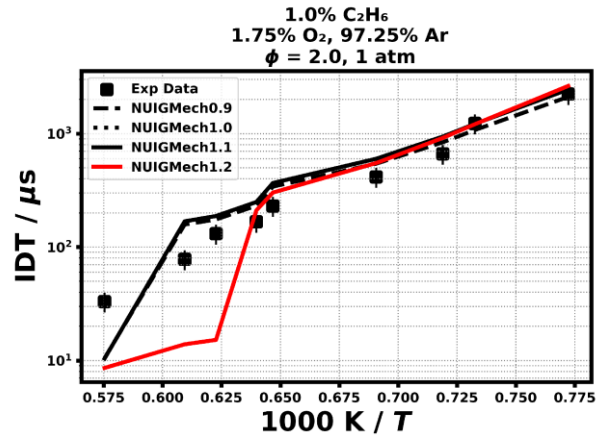
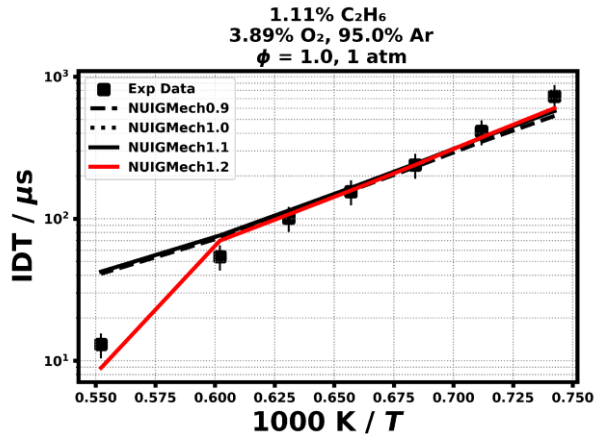


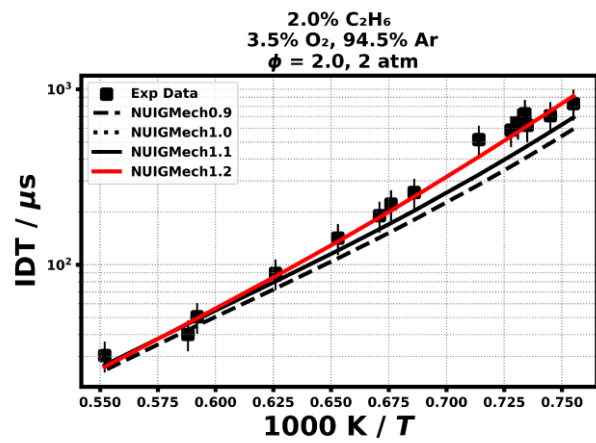
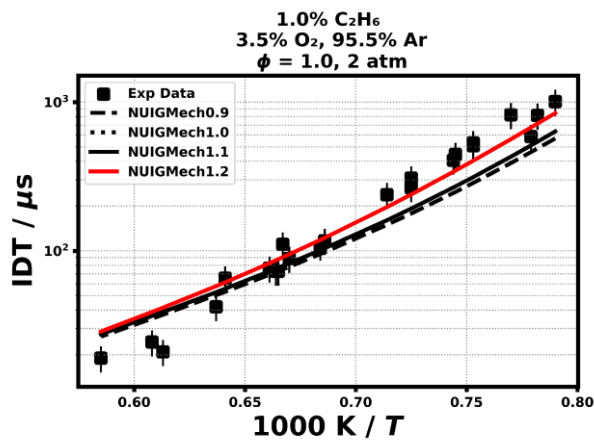
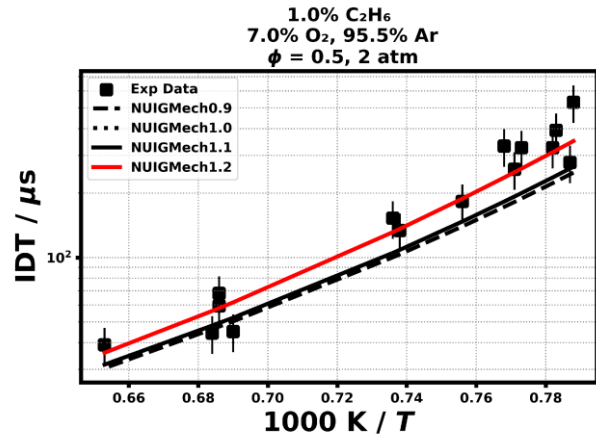
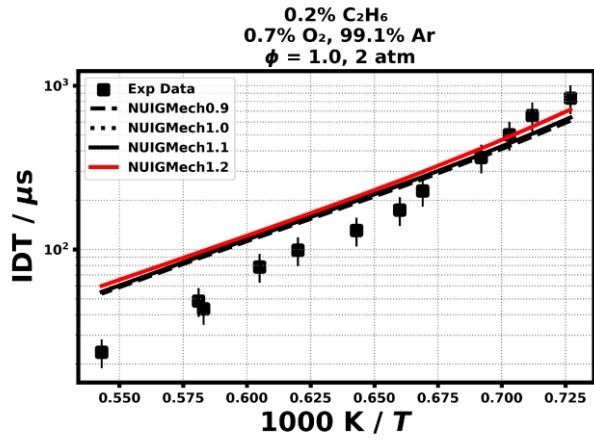
1.1.11 C₂H₆



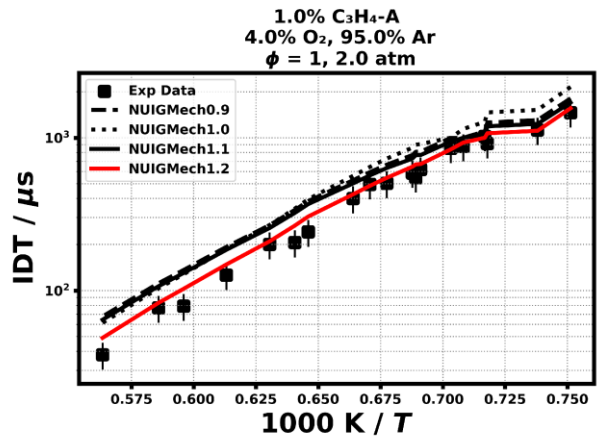
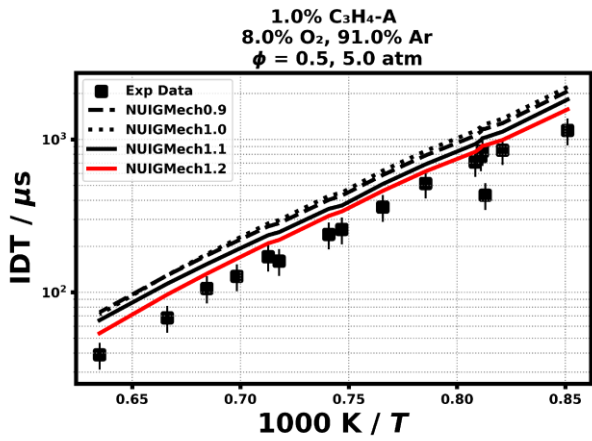
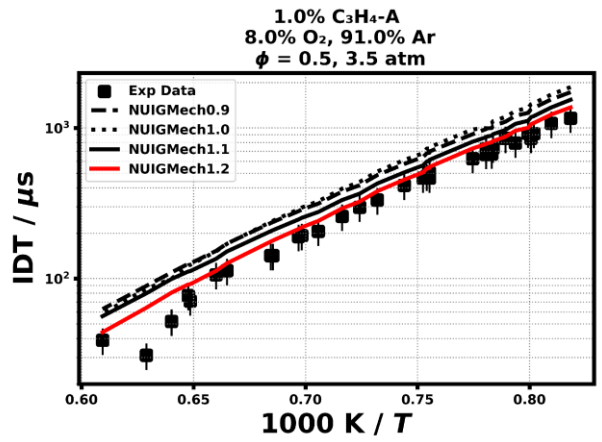
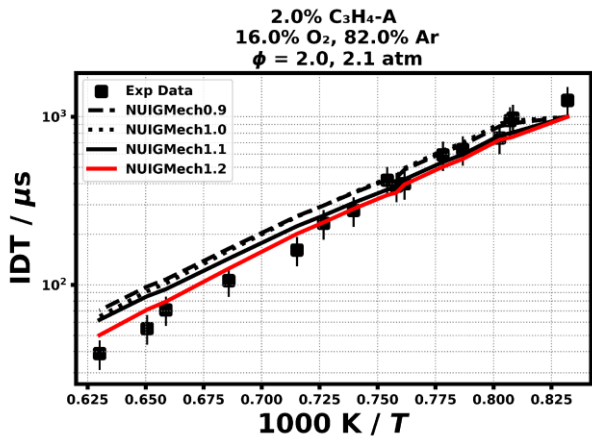
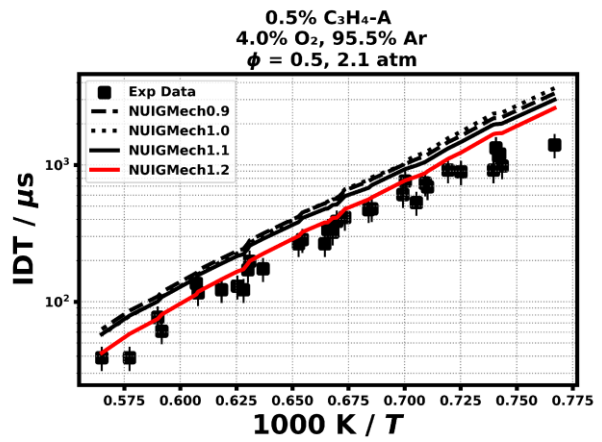
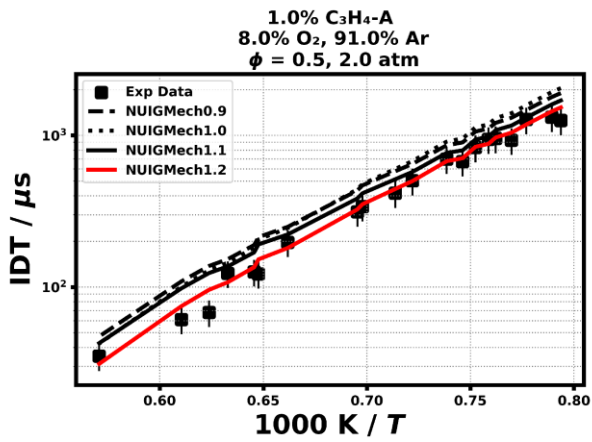


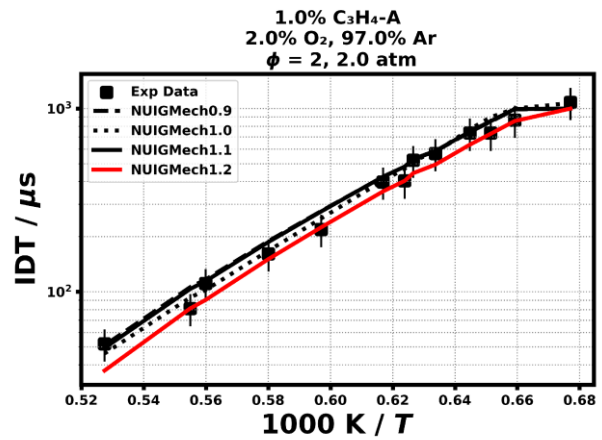
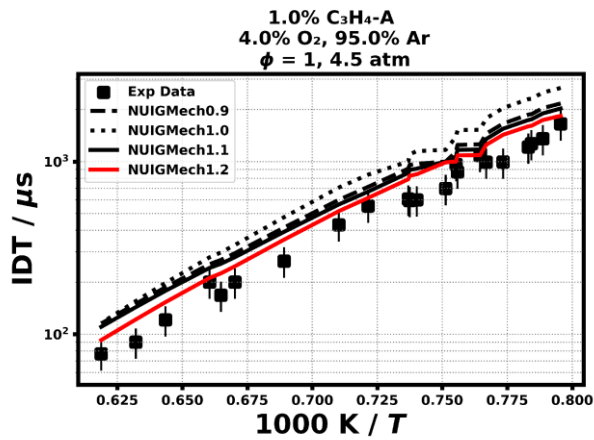
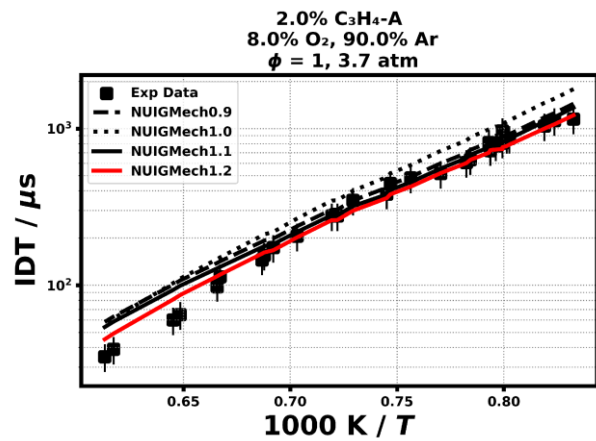
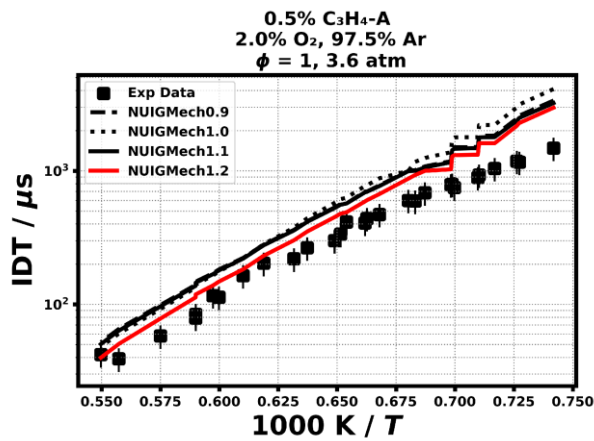
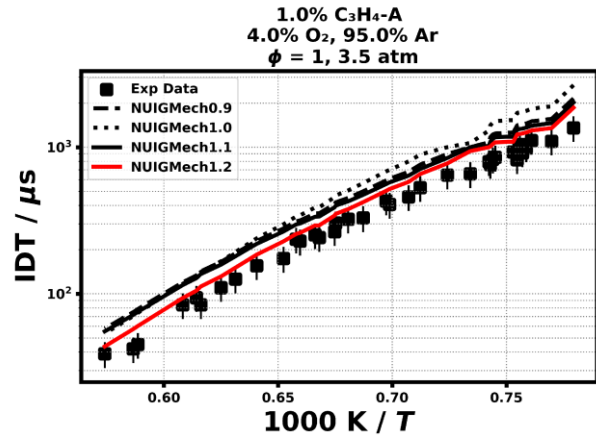
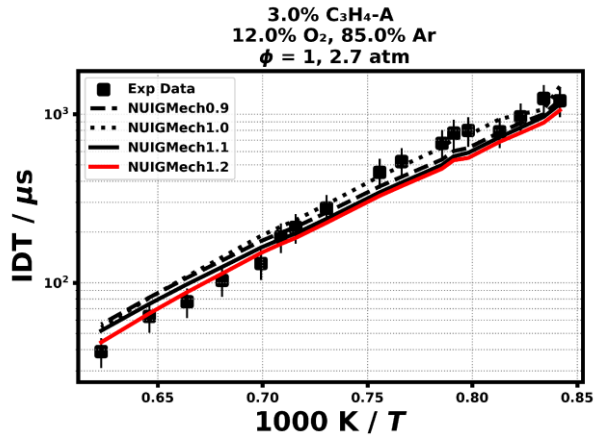


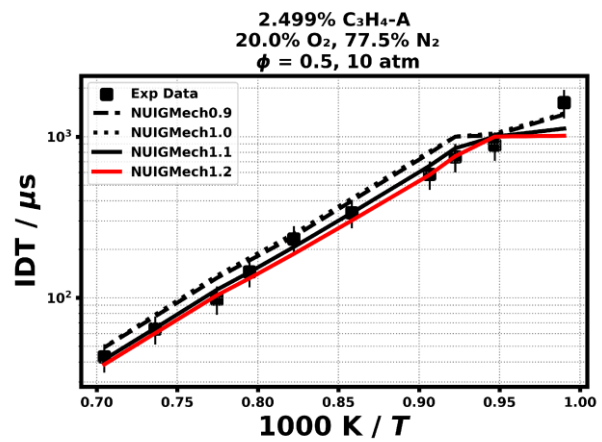
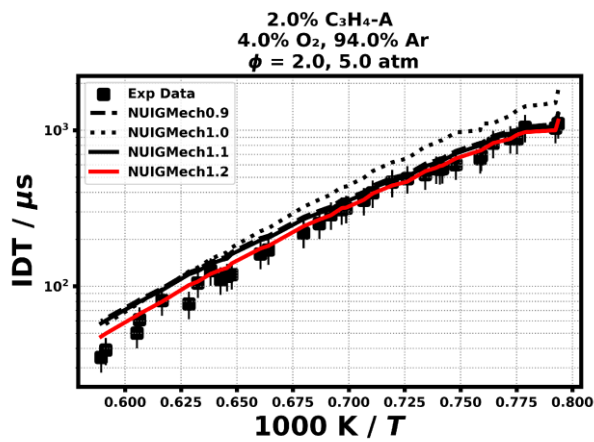
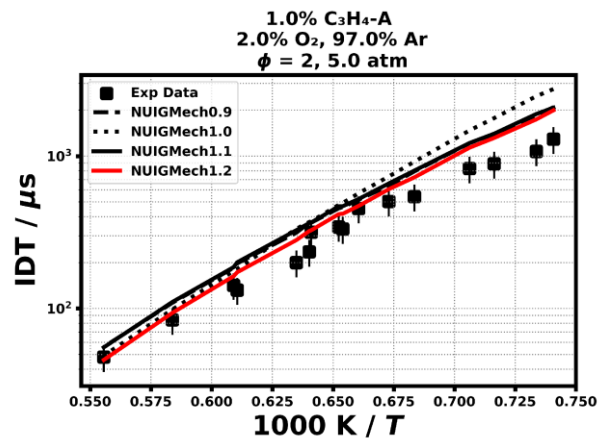
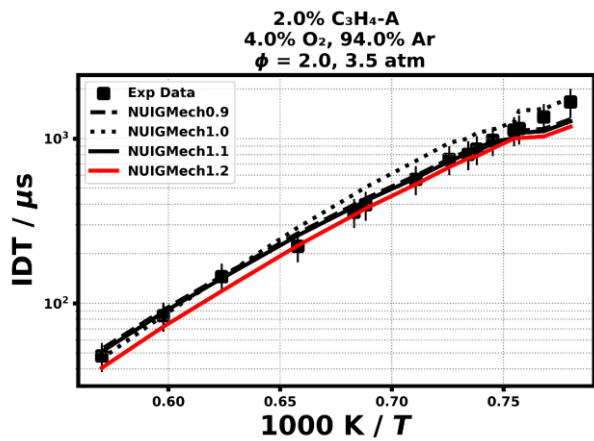
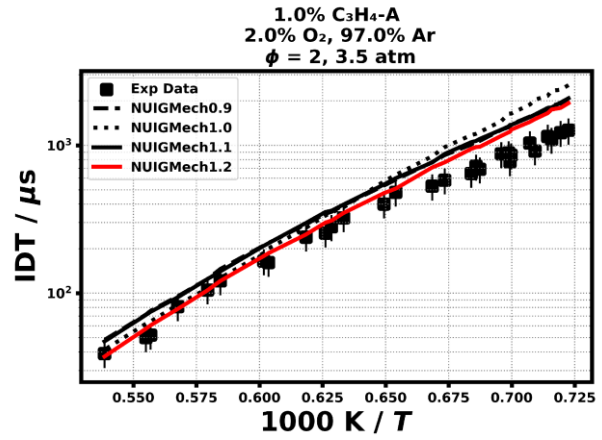
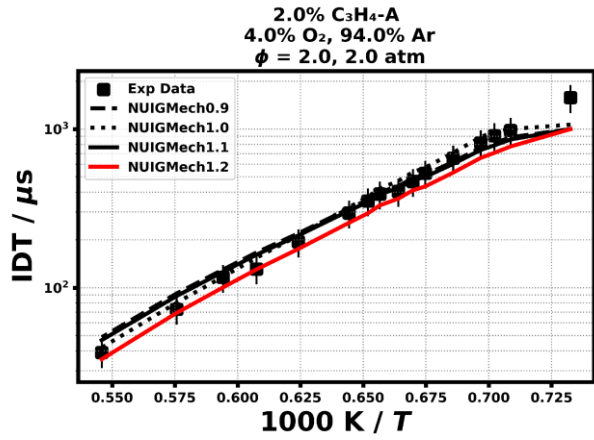


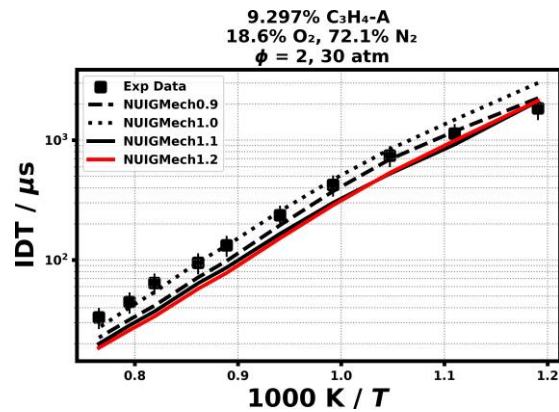
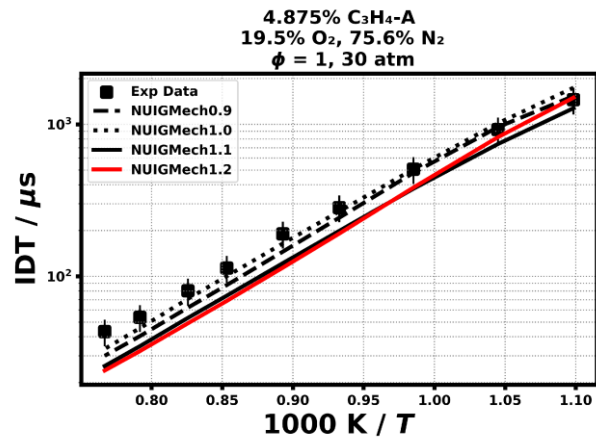
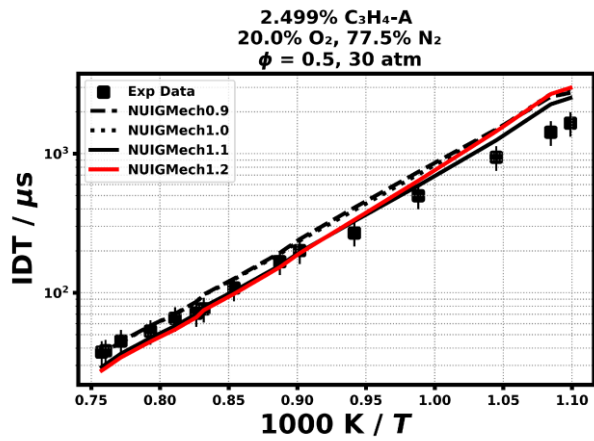
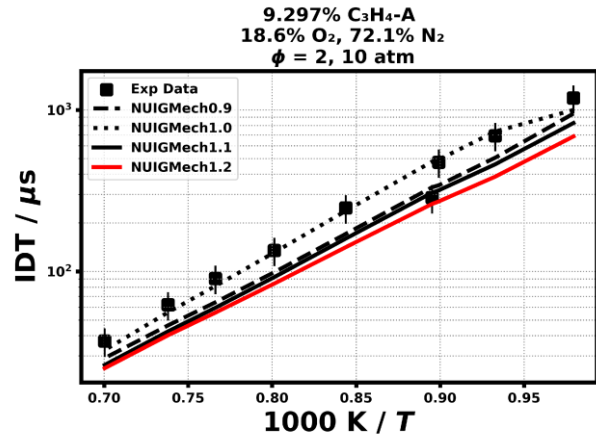
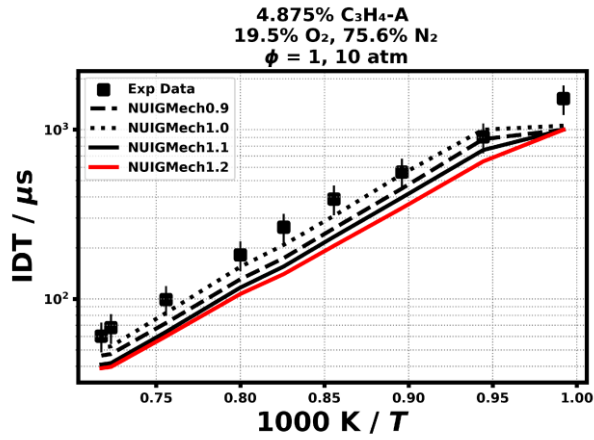


1.1.12 C₃H₄-A

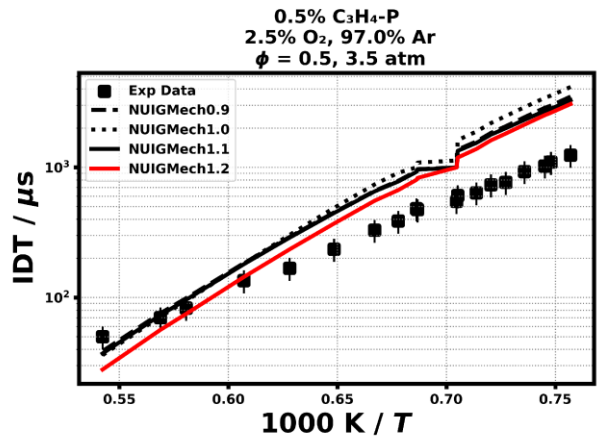
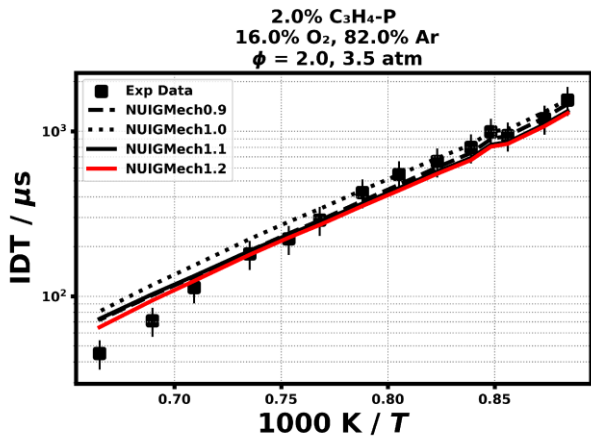
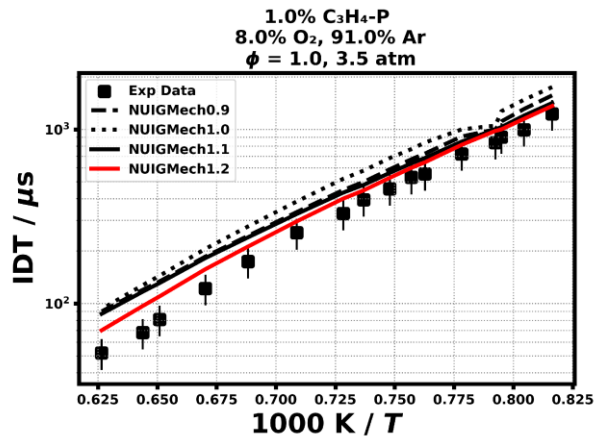
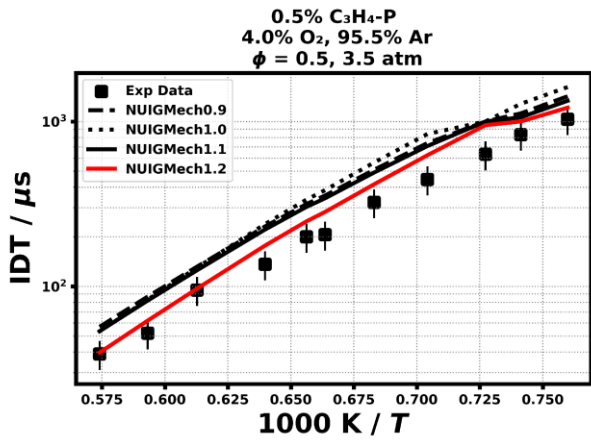
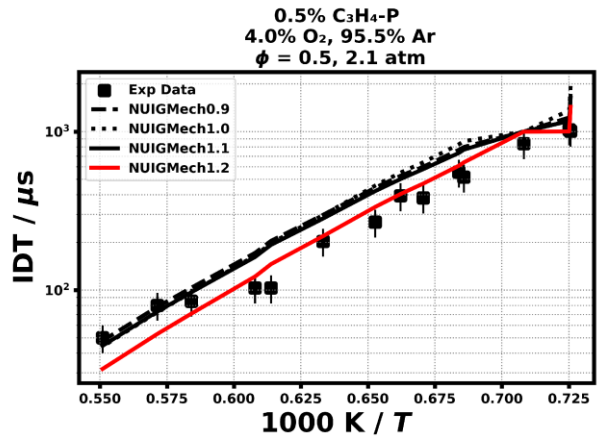
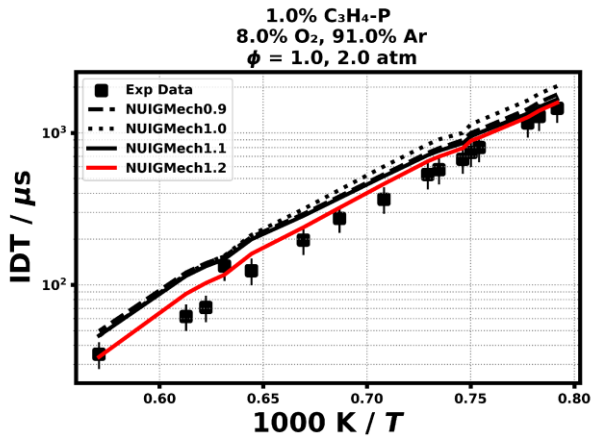


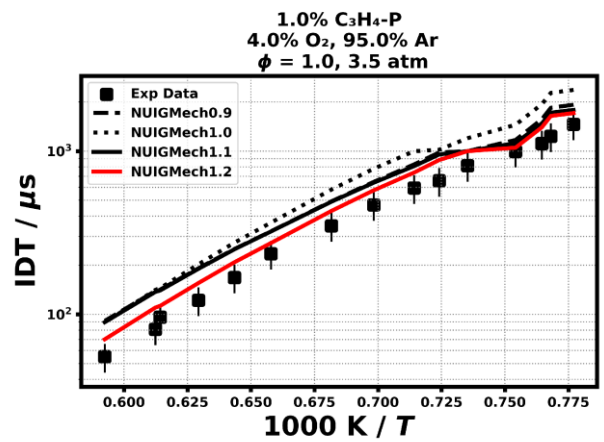
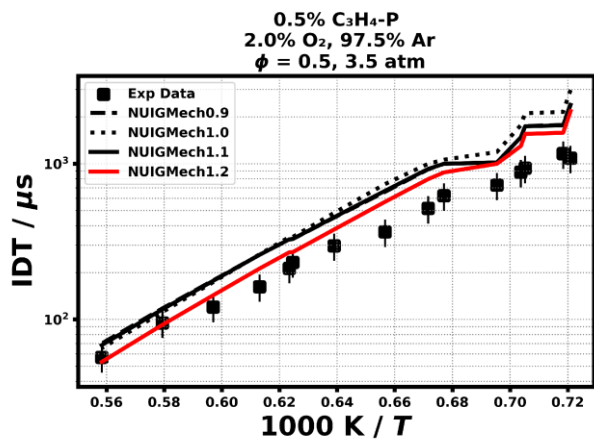
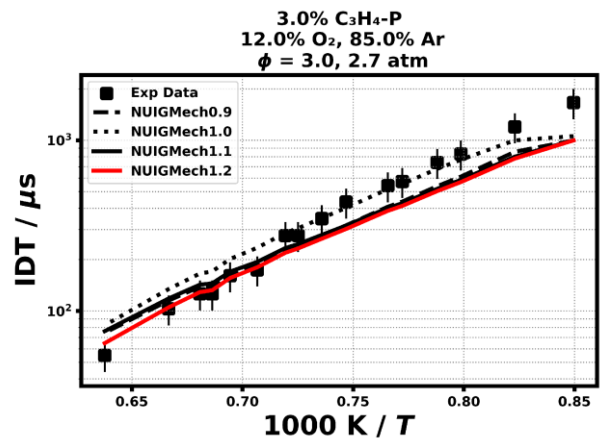
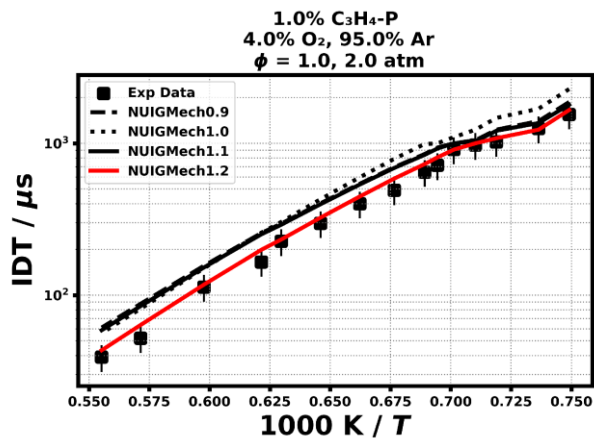
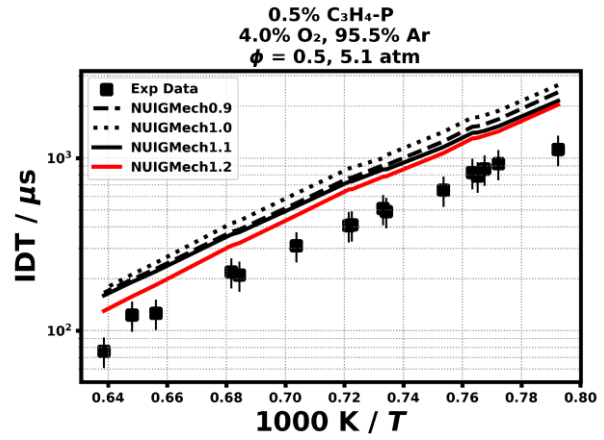
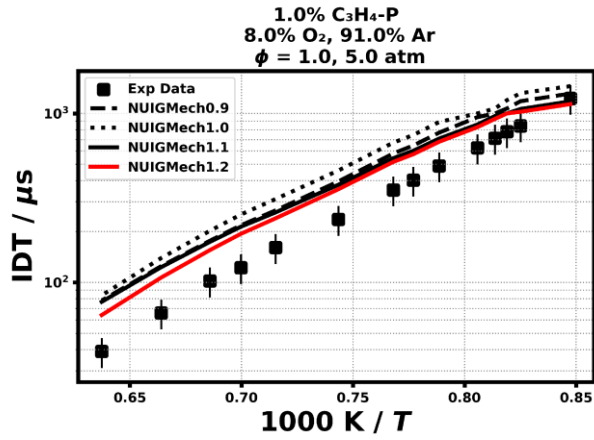


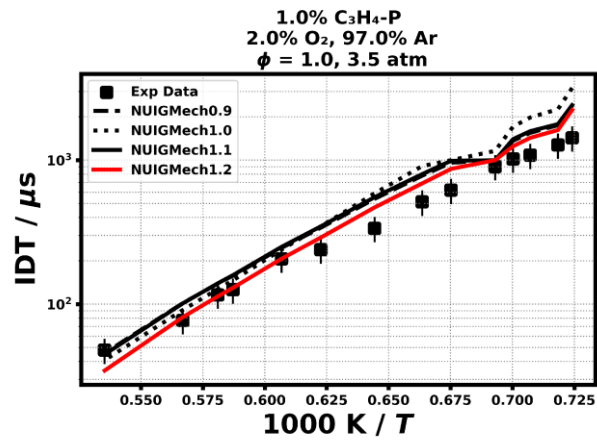
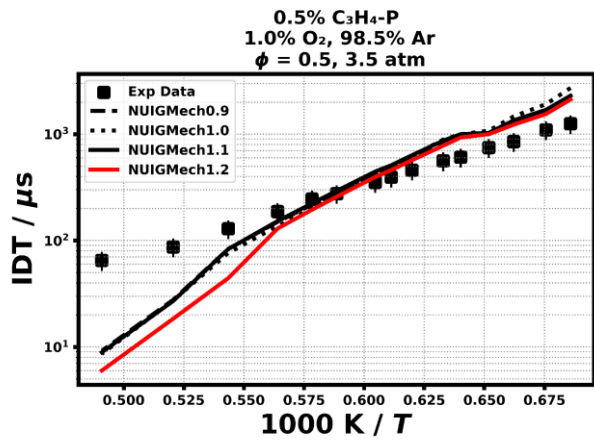
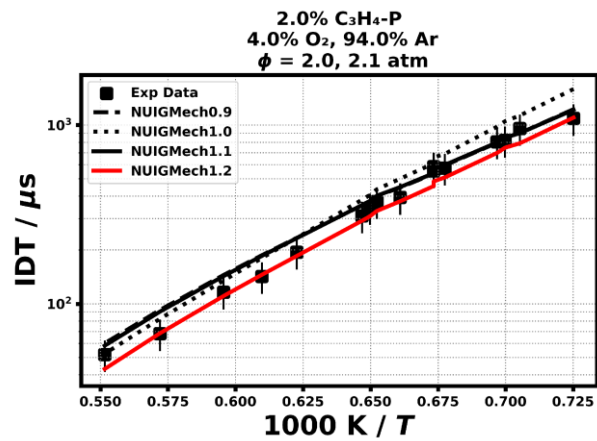
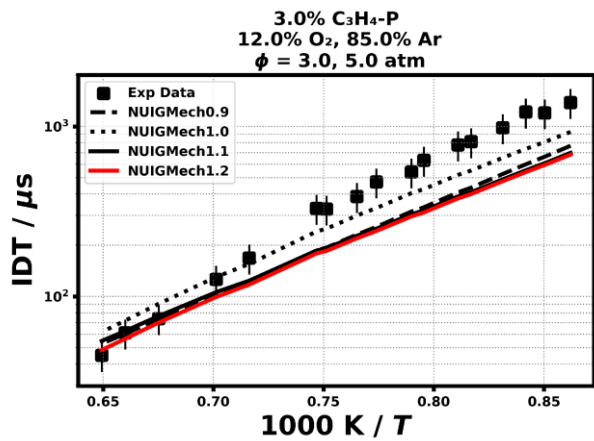
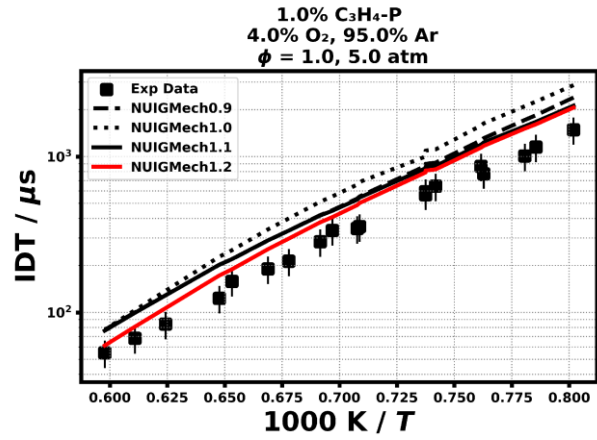
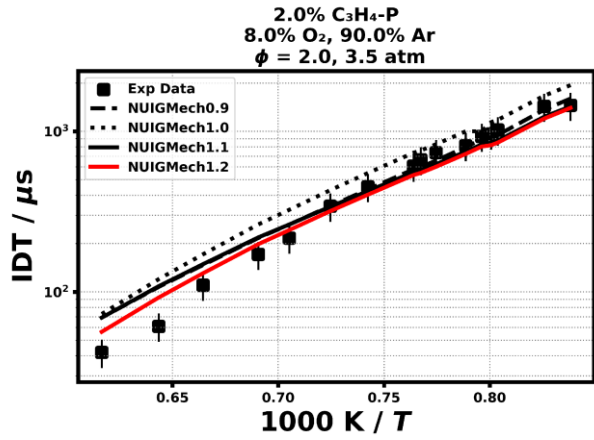


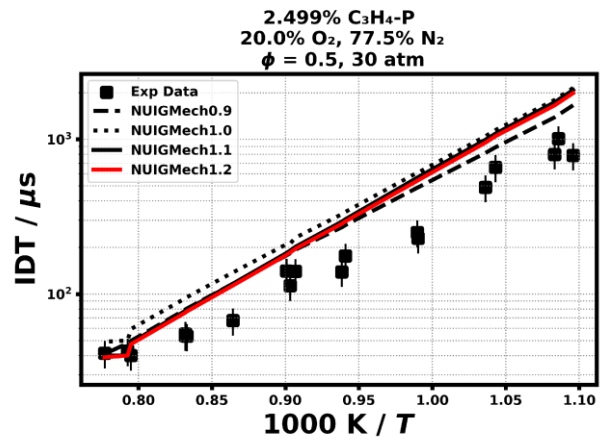
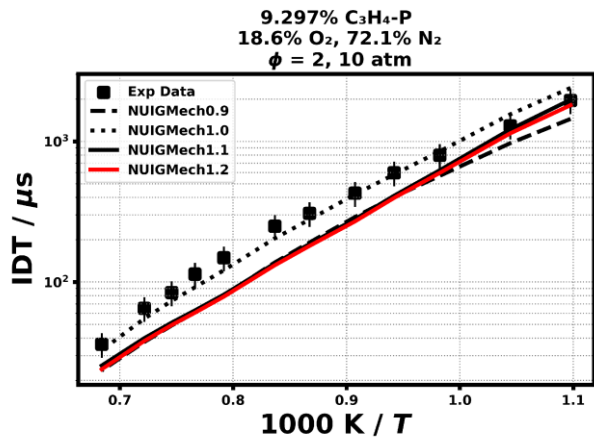
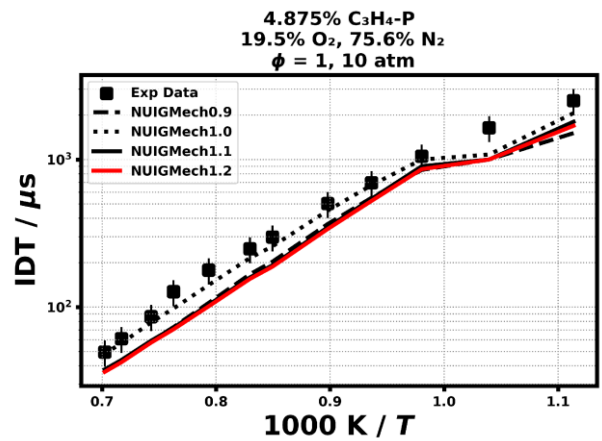
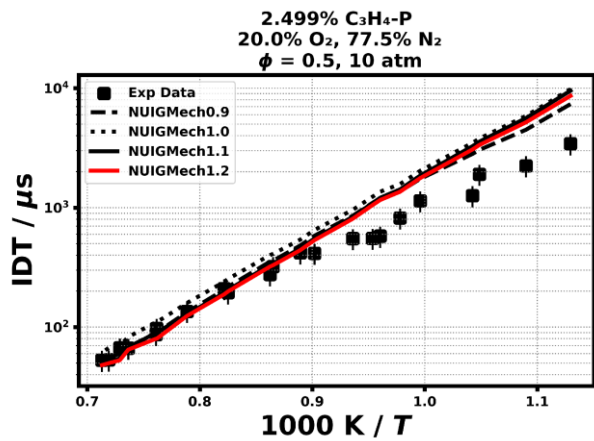
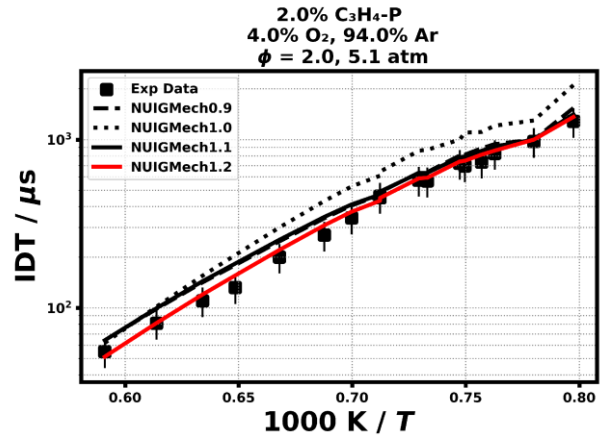
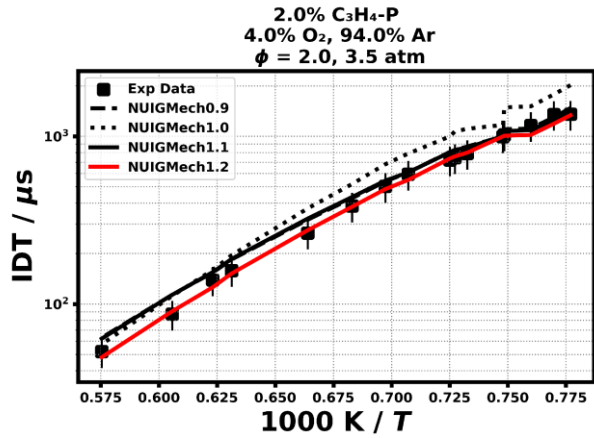


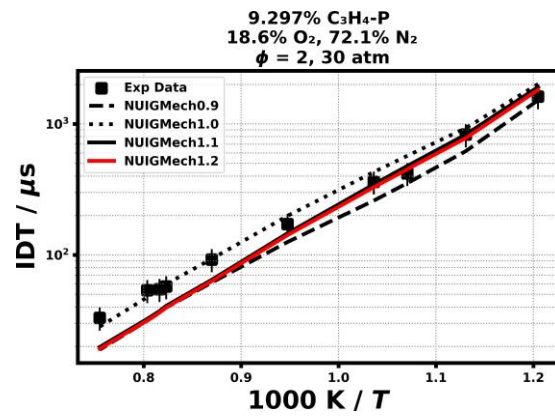
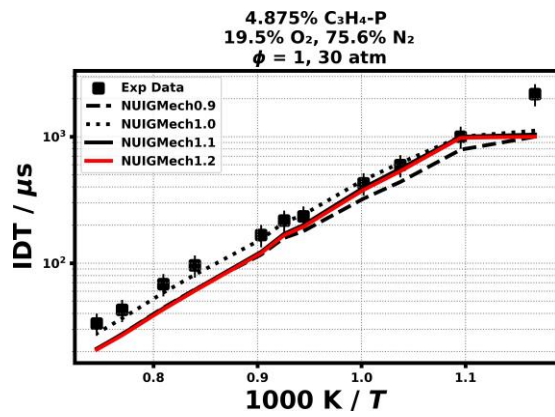
1.1.13 C₃H₄-P



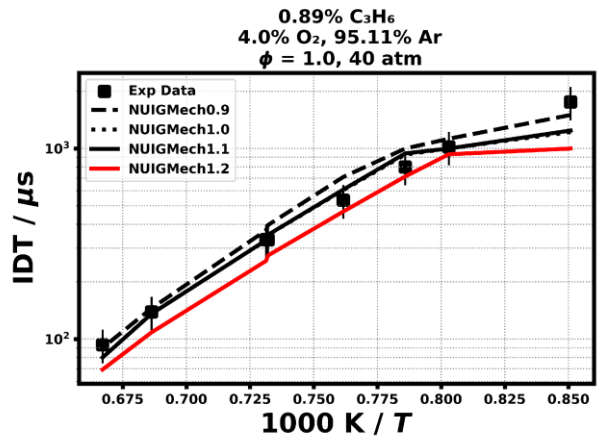
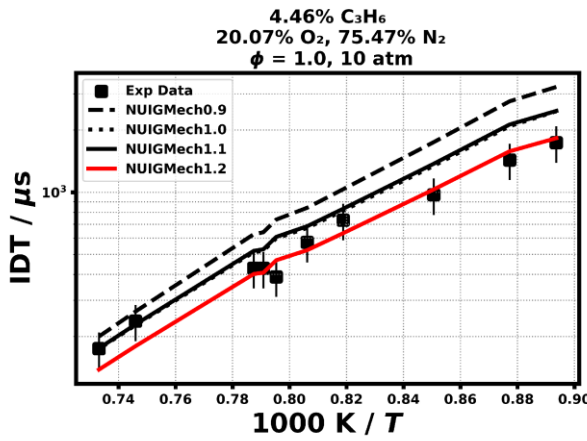
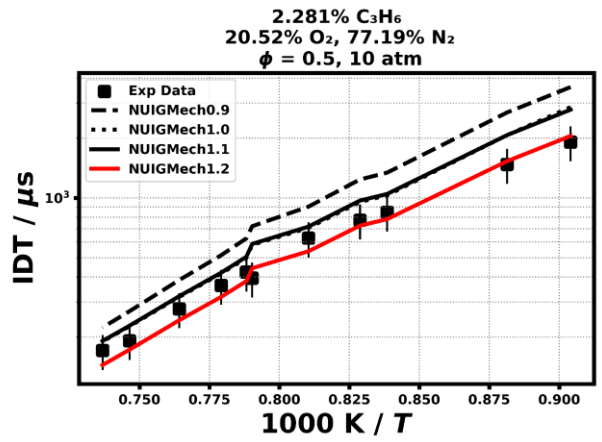
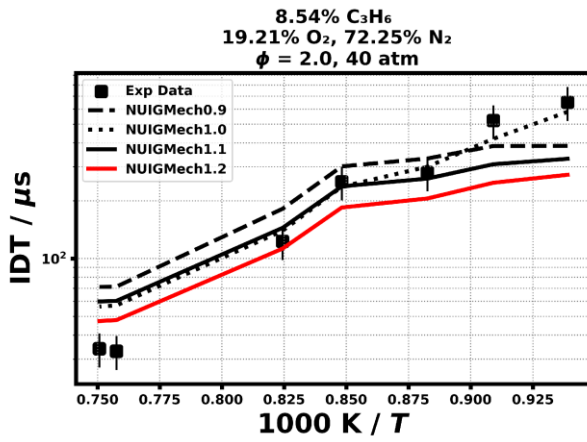
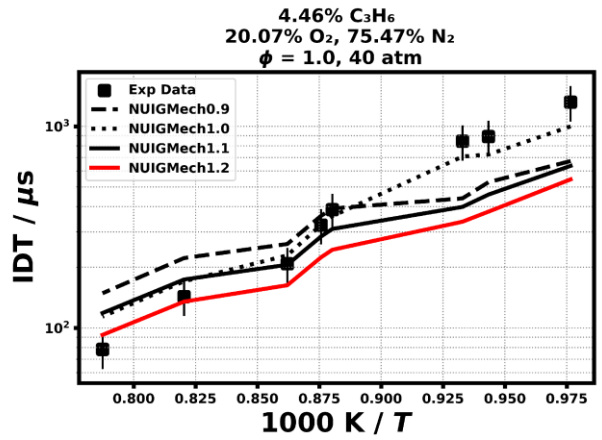
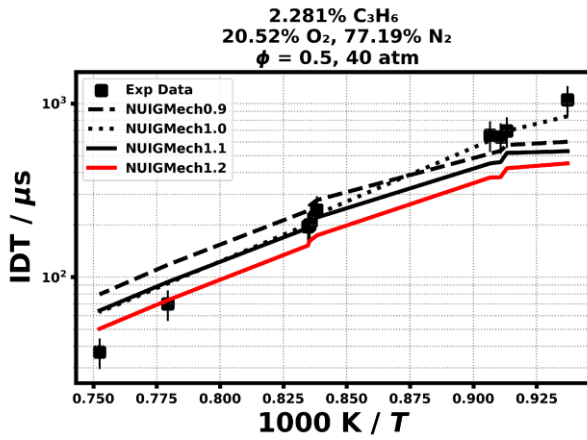


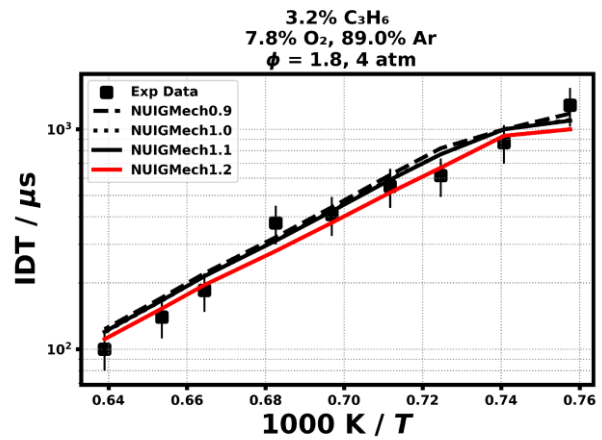
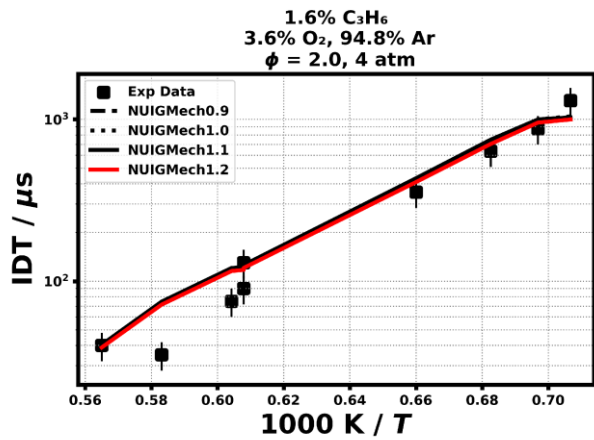
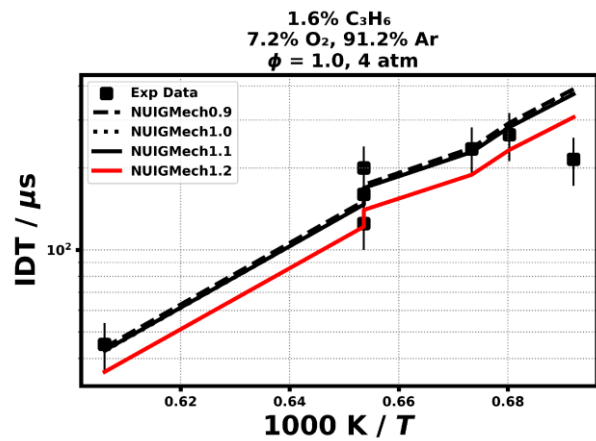
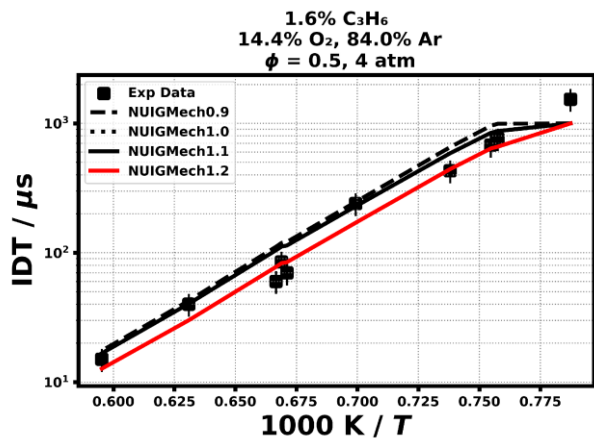
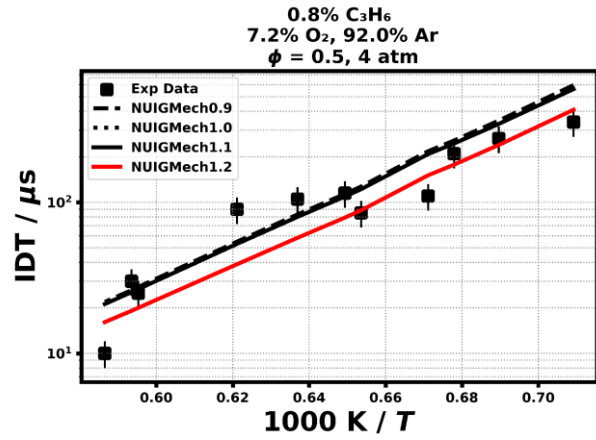
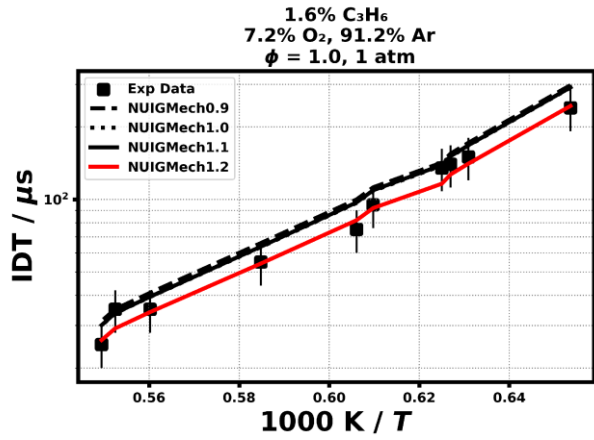


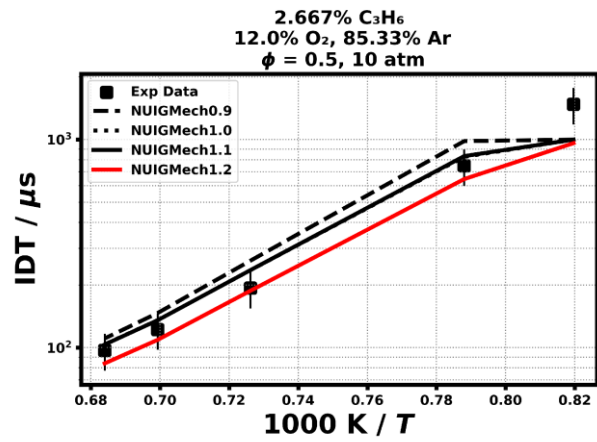
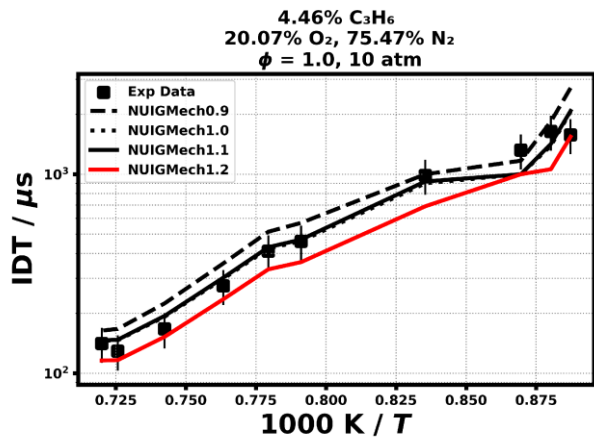
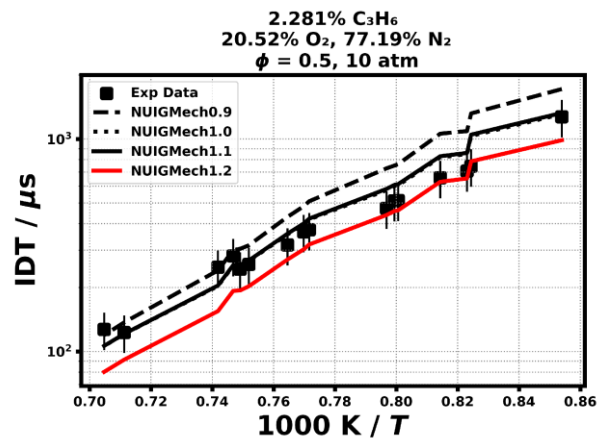
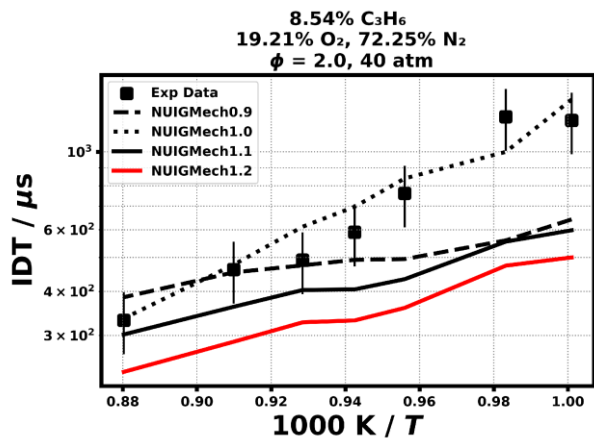
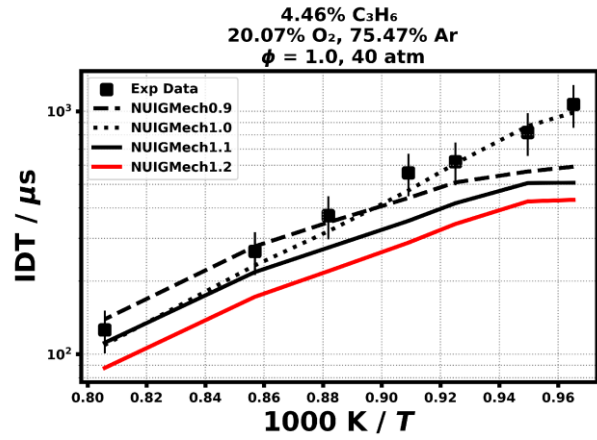
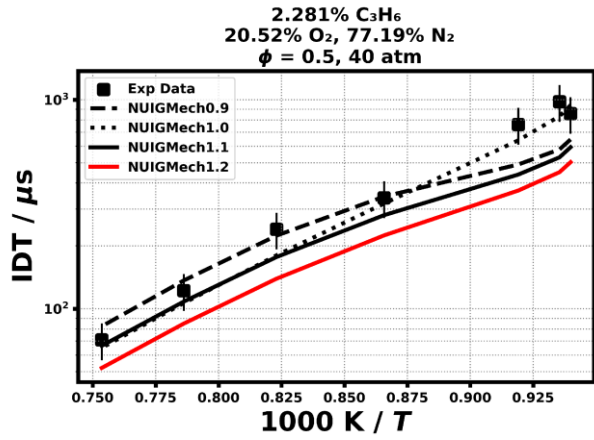


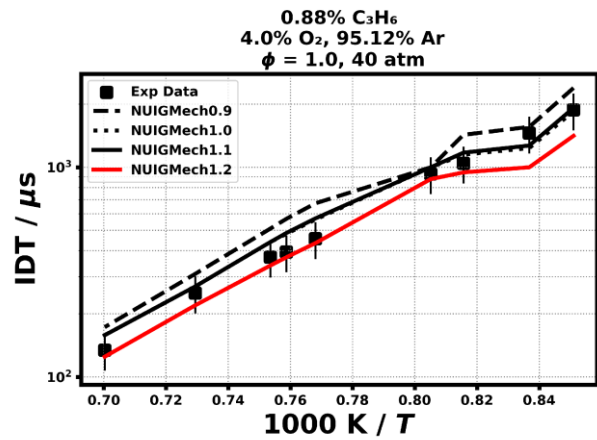
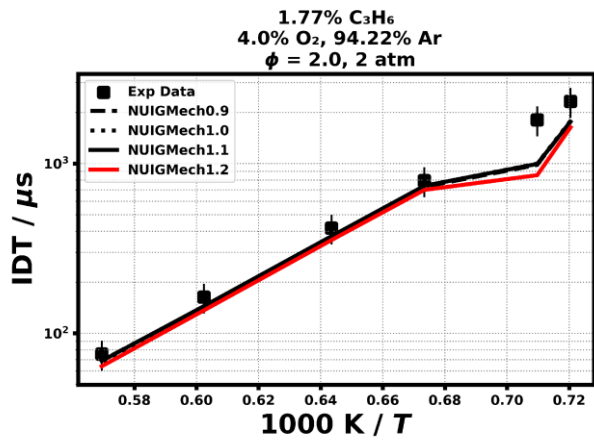
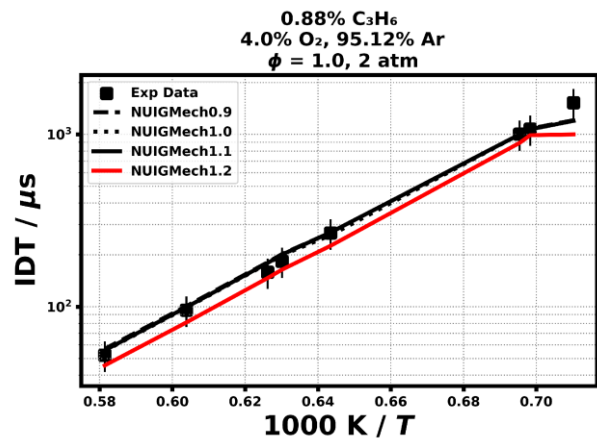
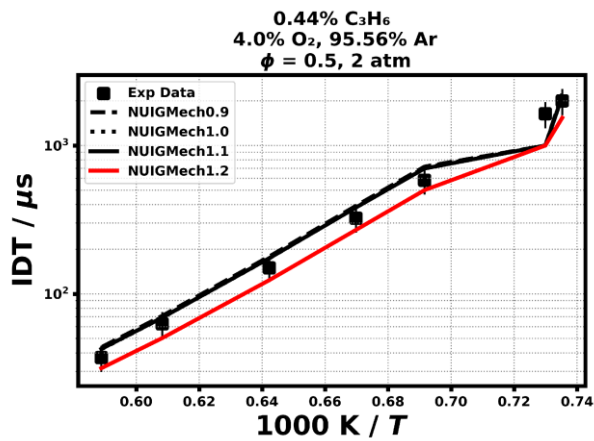
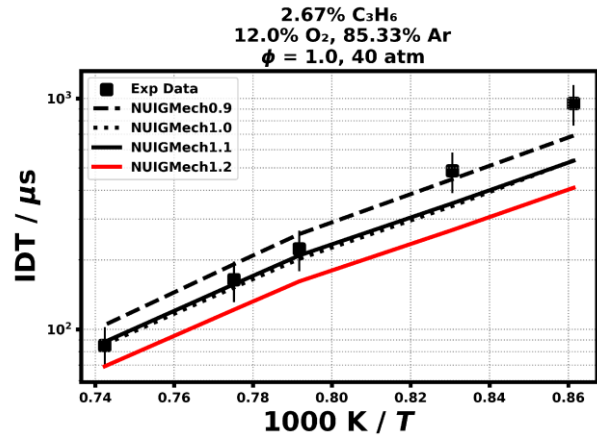
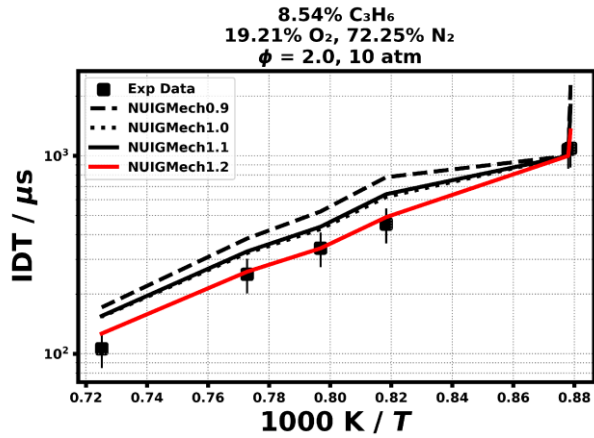


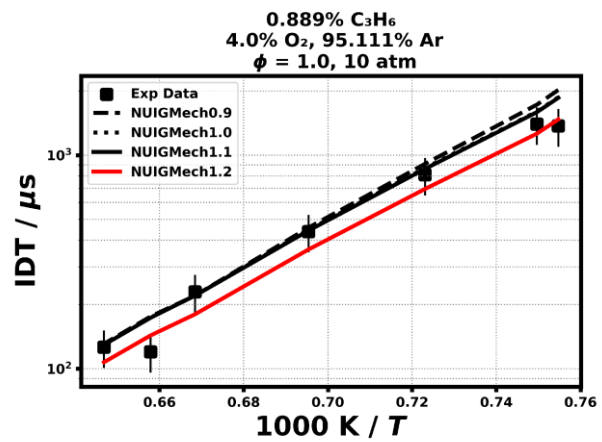
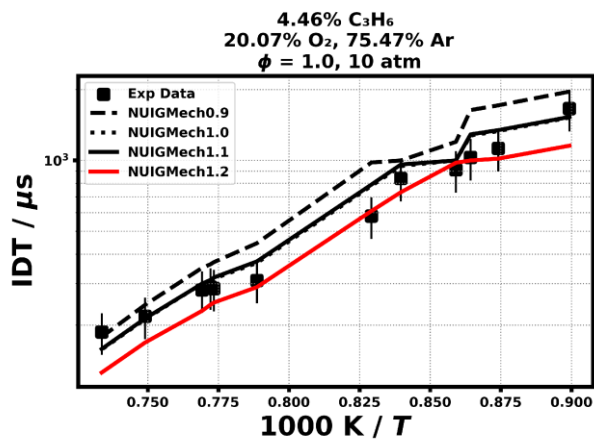
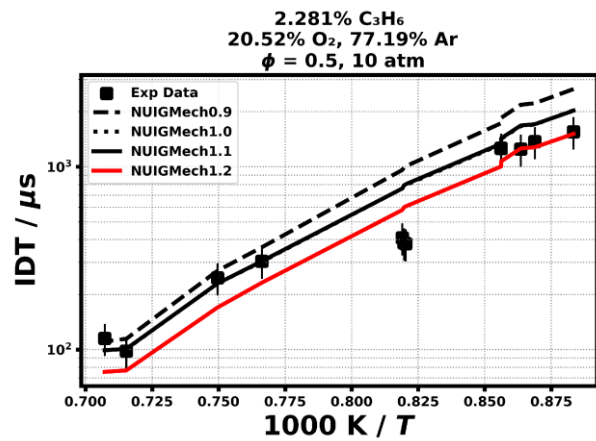
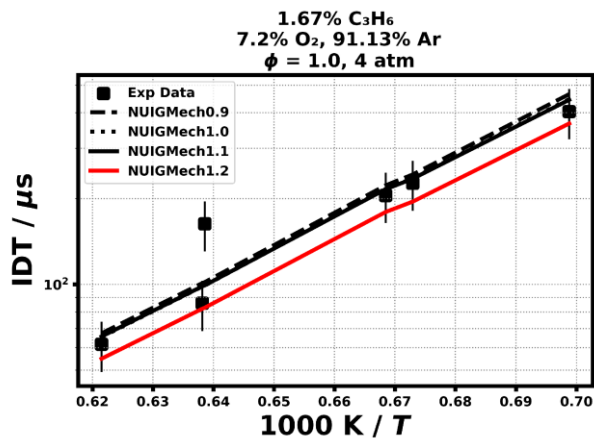
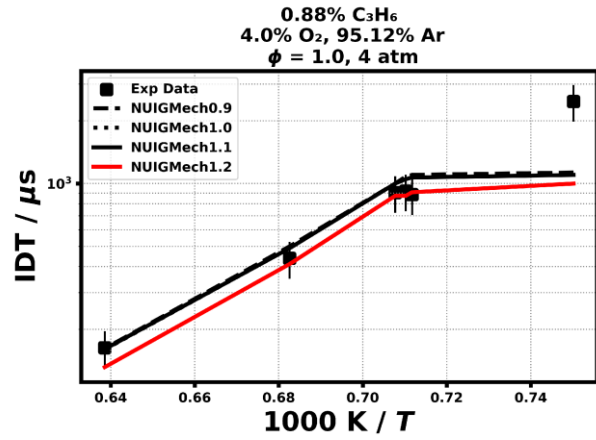
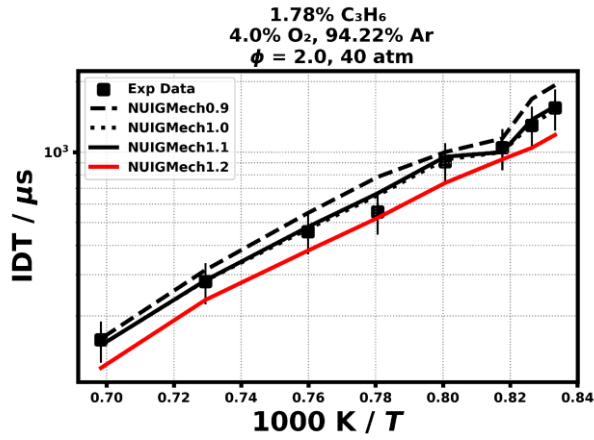
1.1.14 C₃H₆

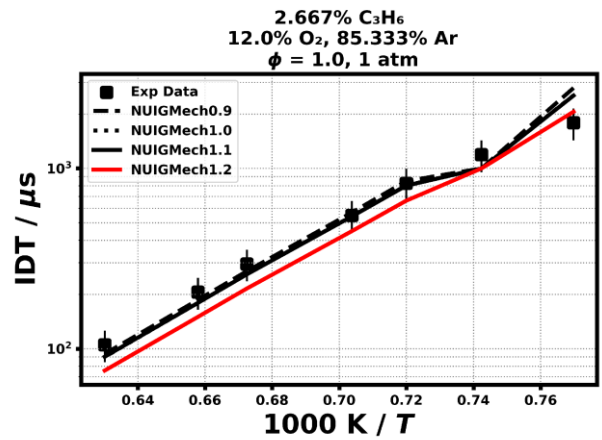
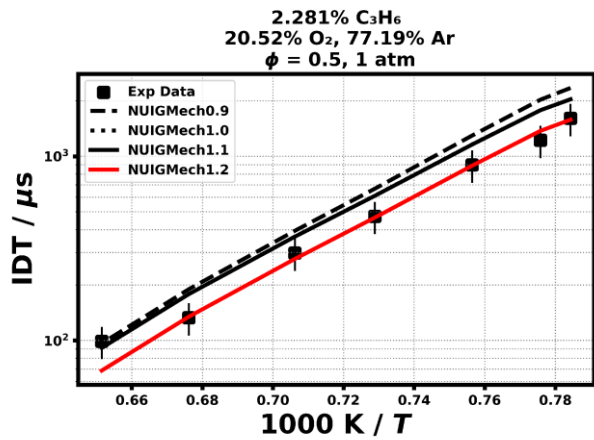
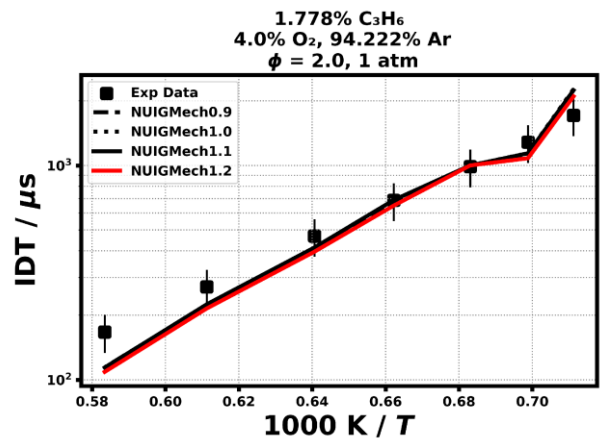
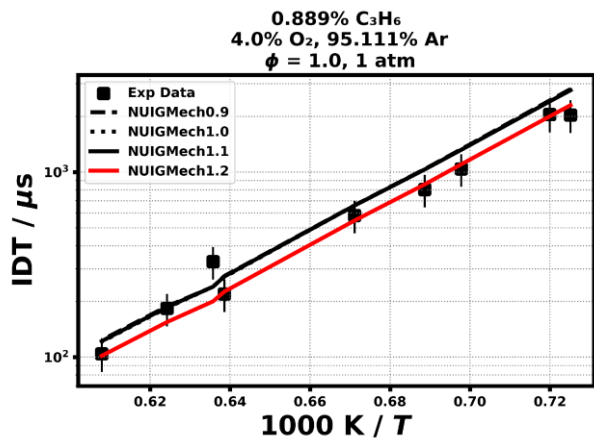
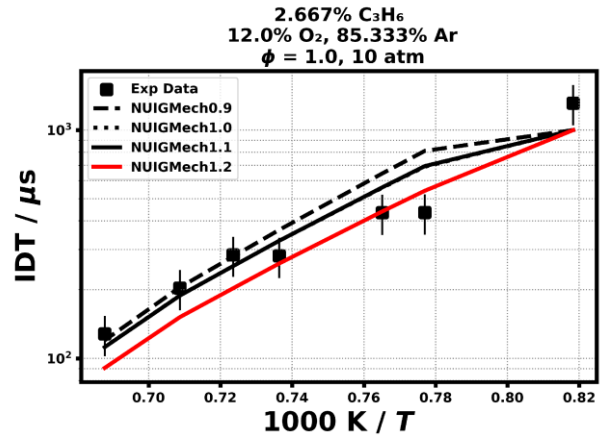
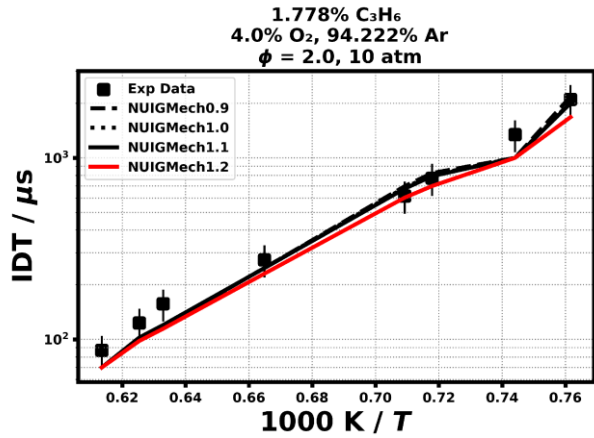




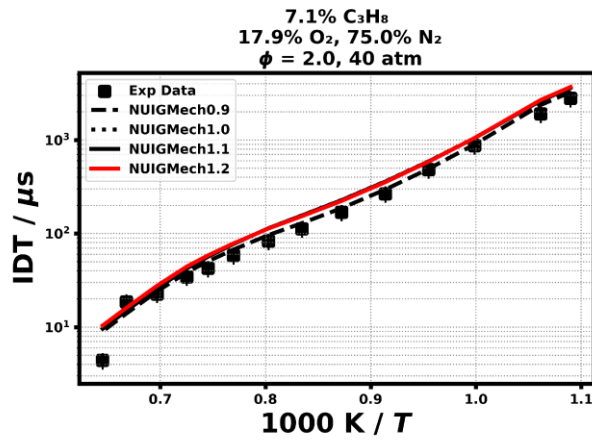
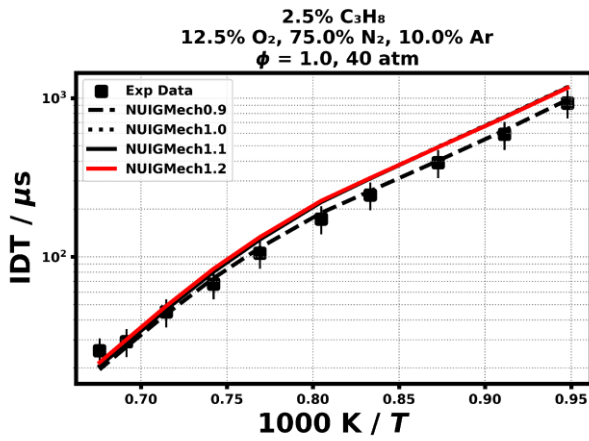
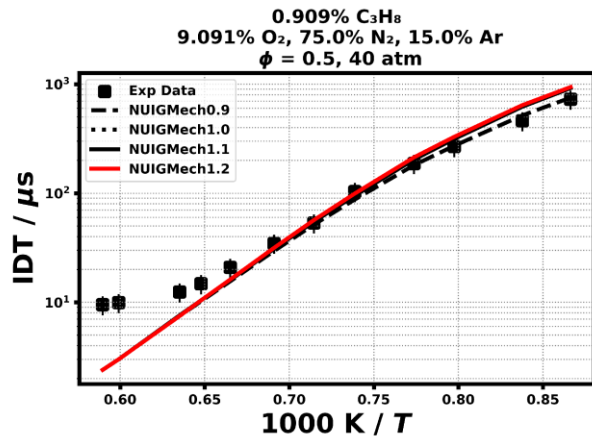
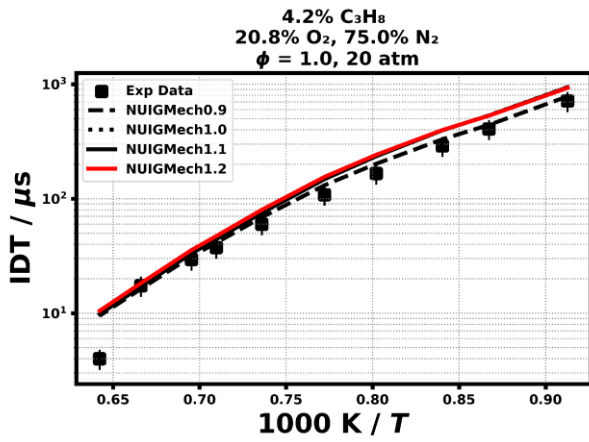
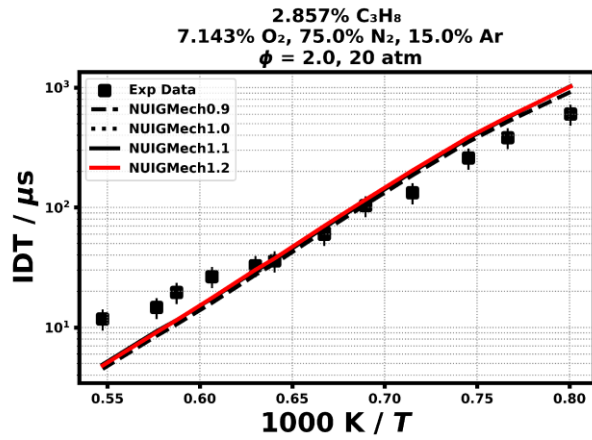
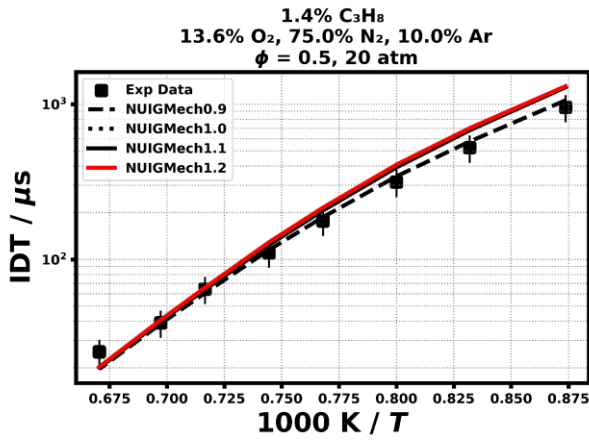


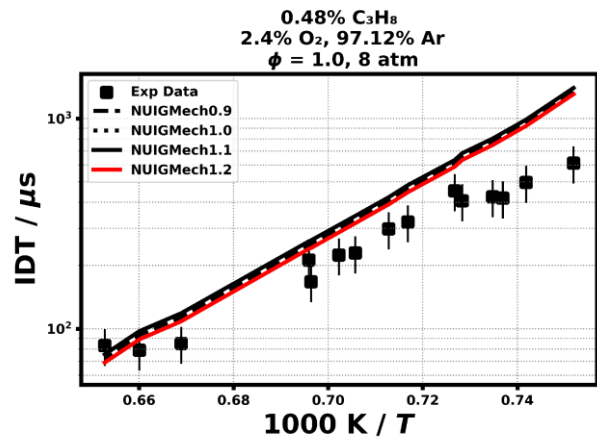
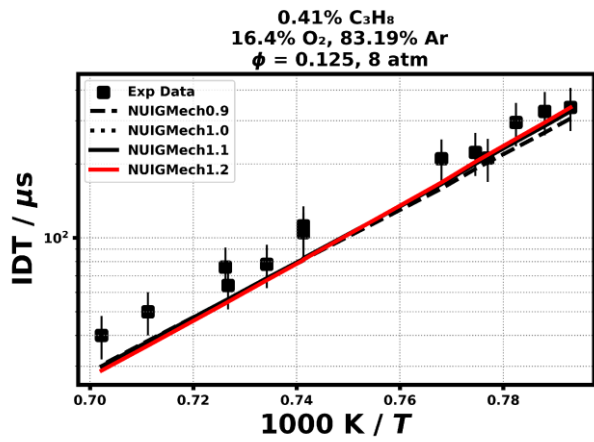
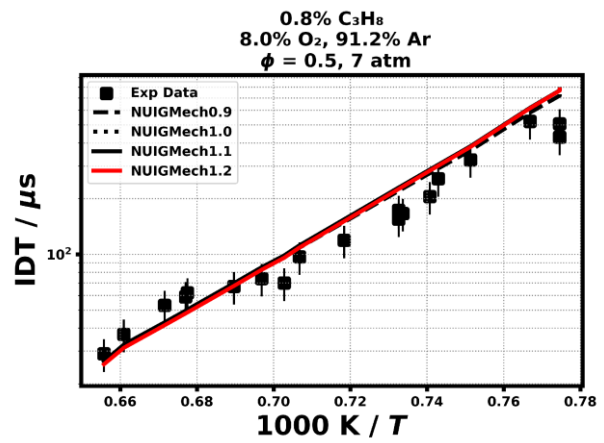
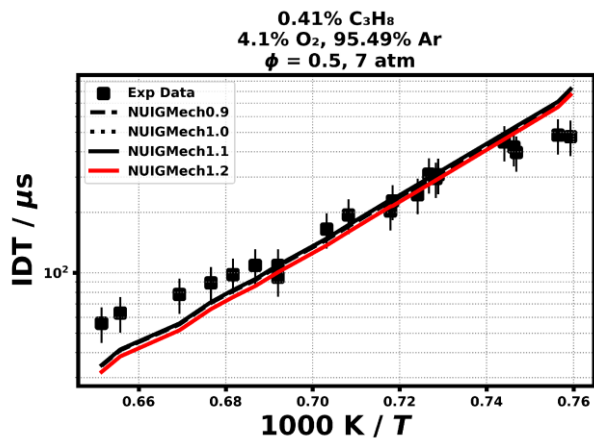
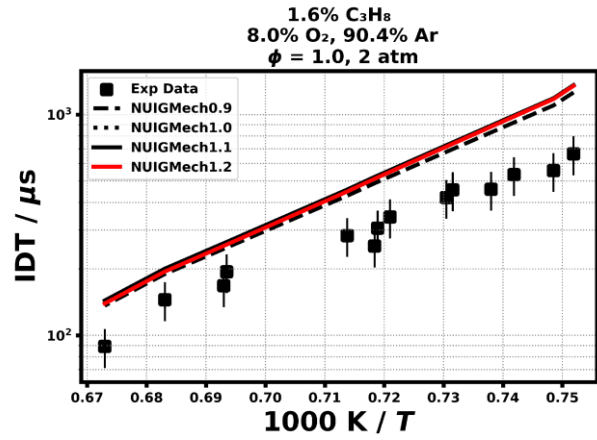
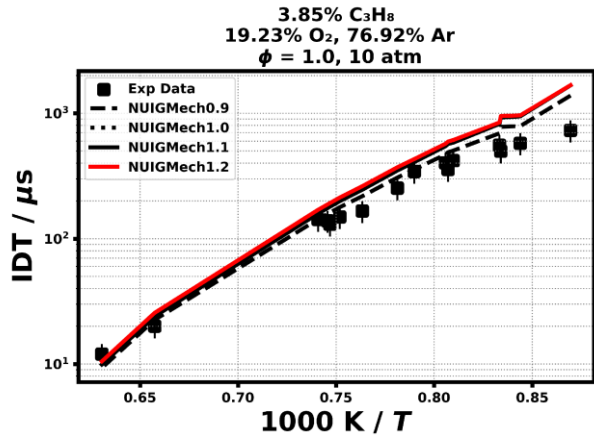


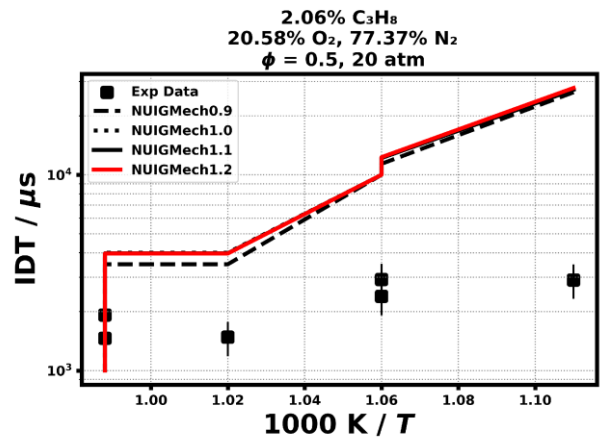
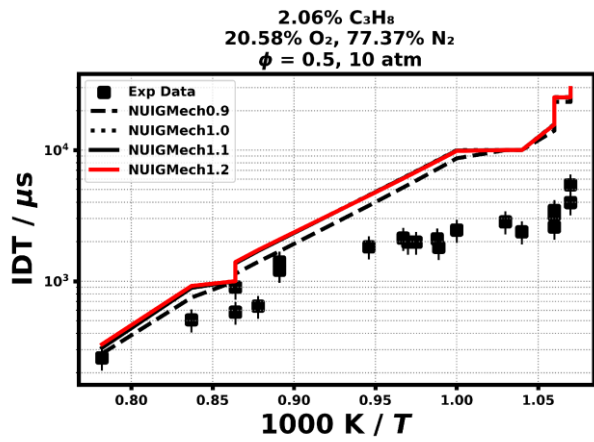
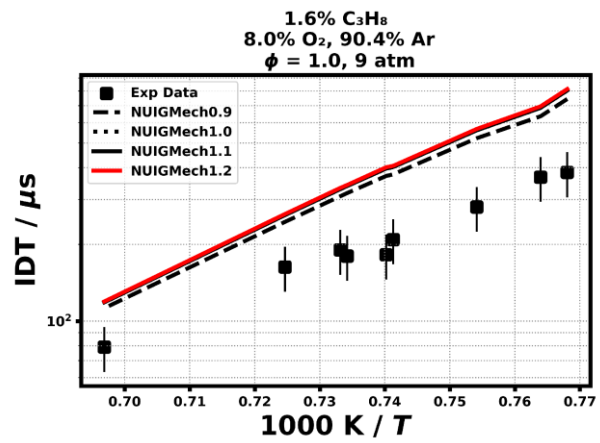
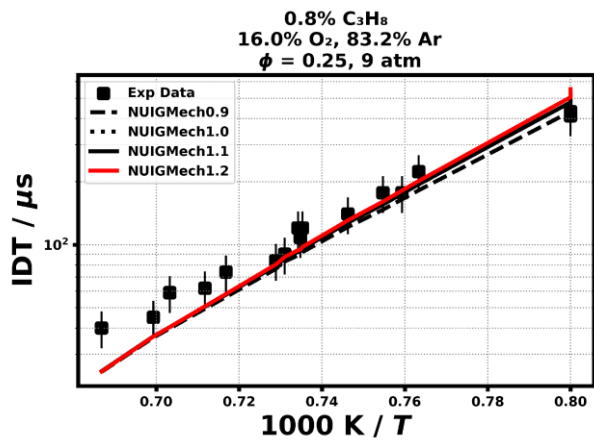
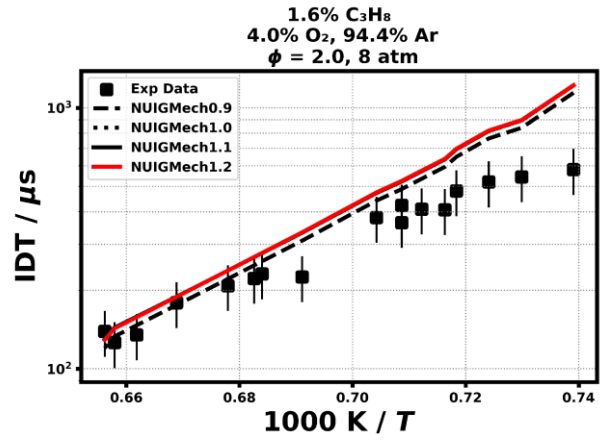
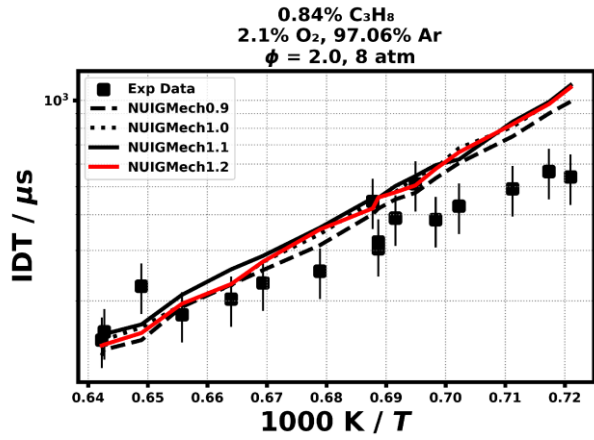


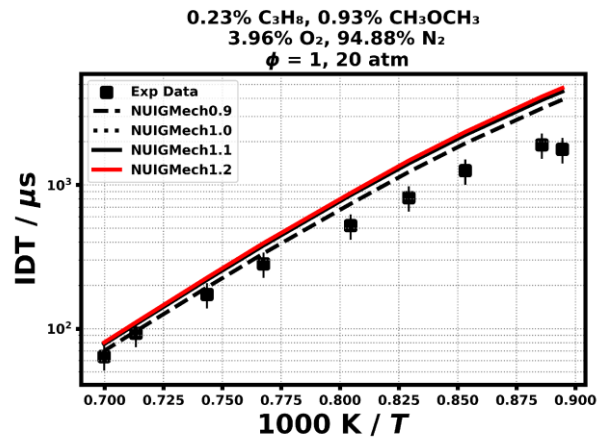
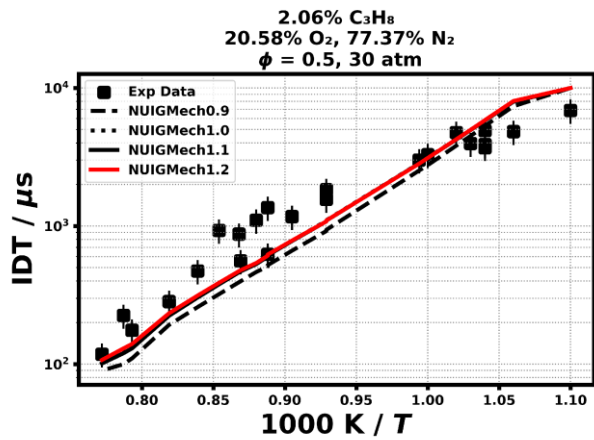
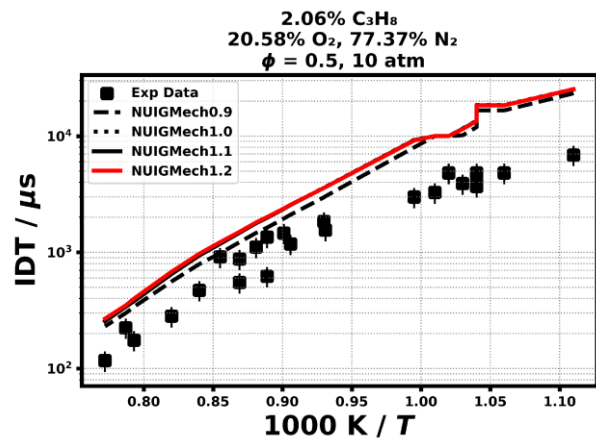
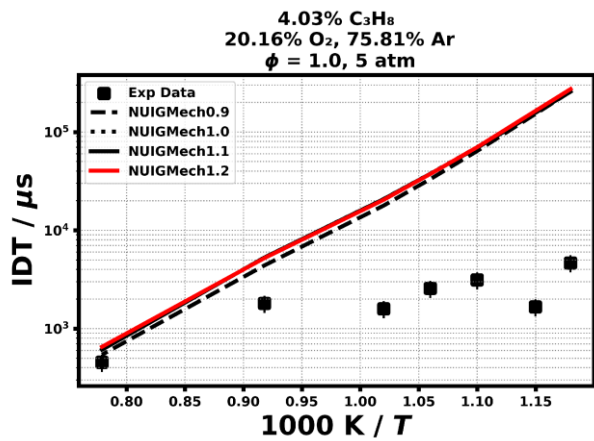
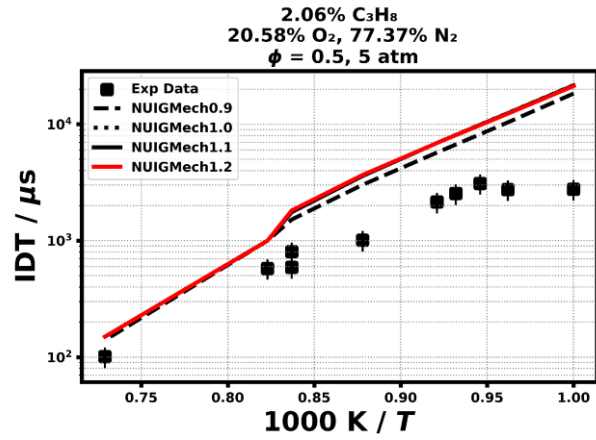
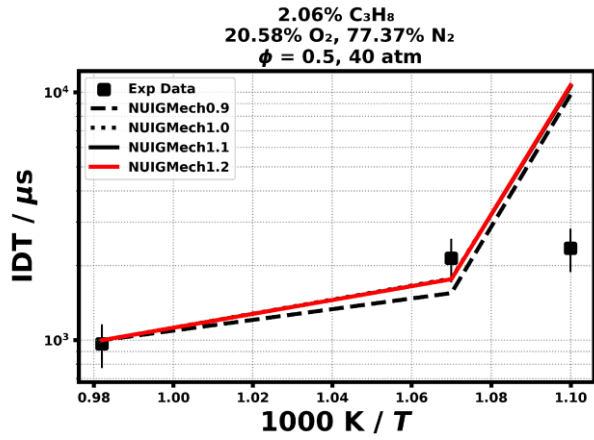


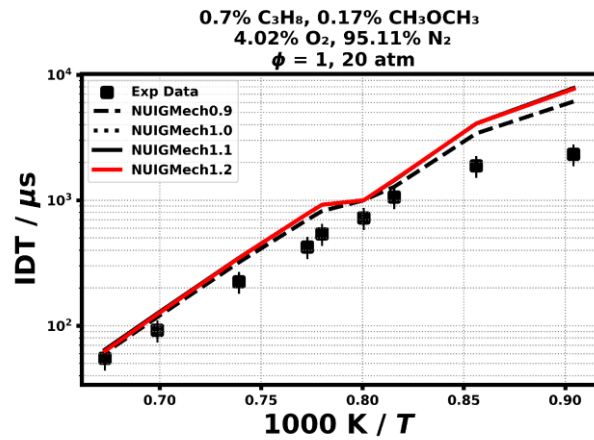
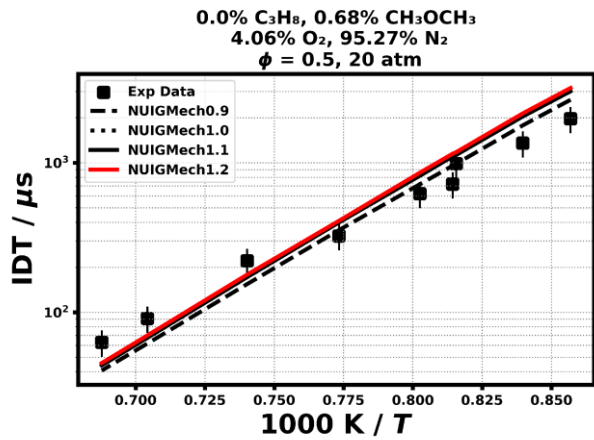
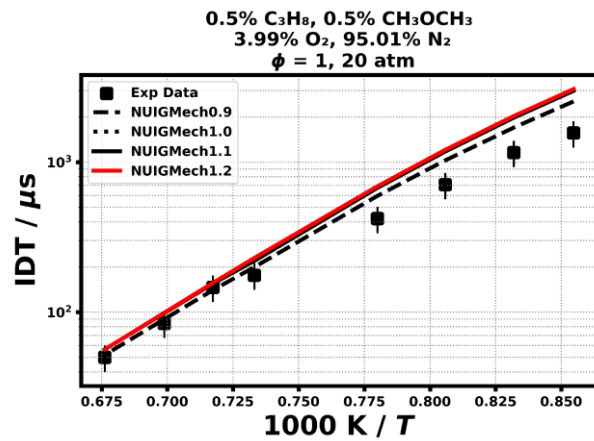
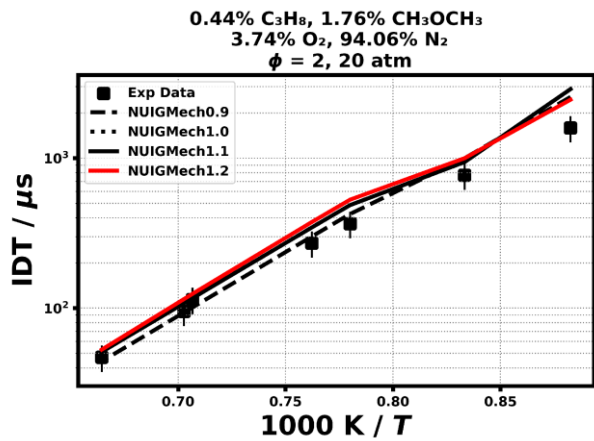
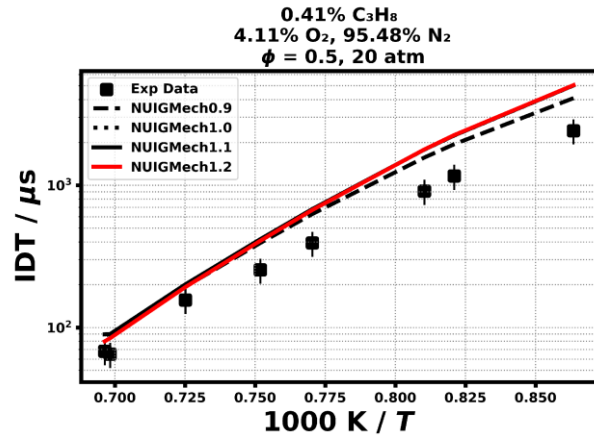
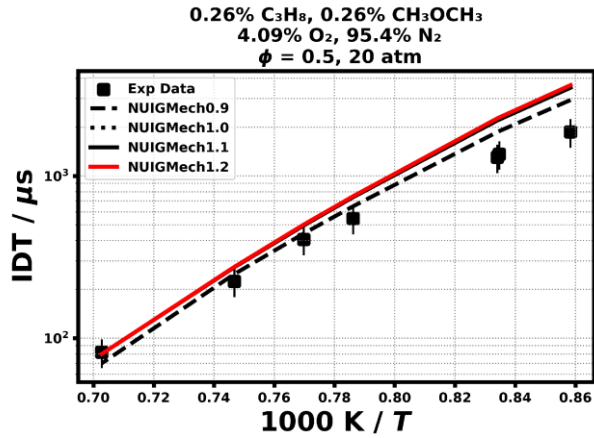
1.1.15 C₃H₈

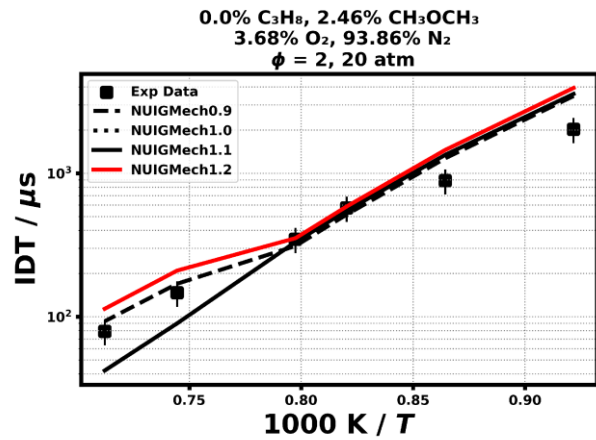
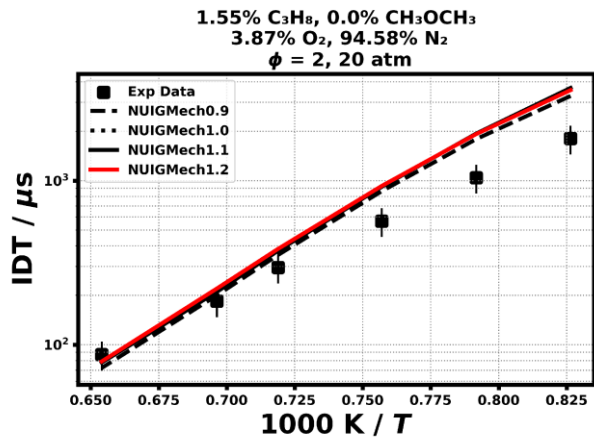
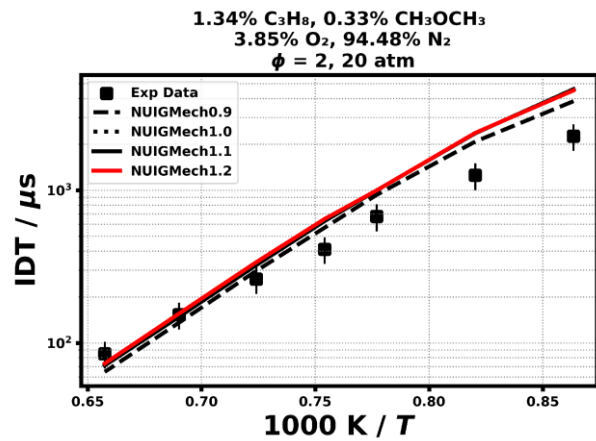
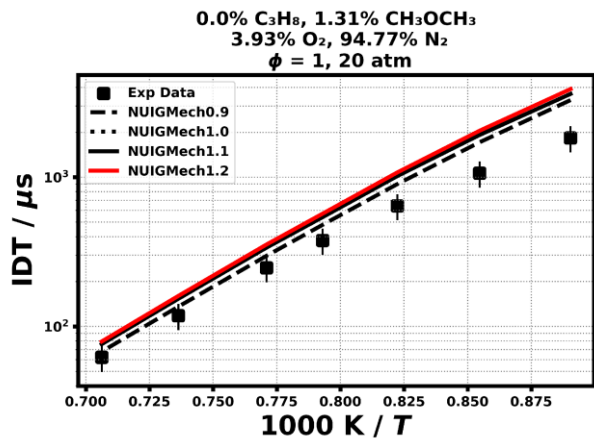
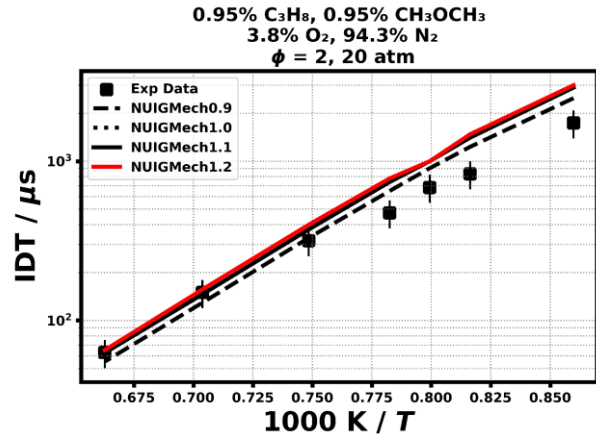
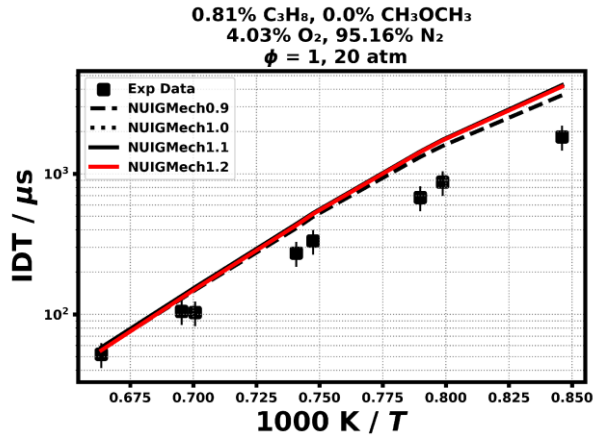


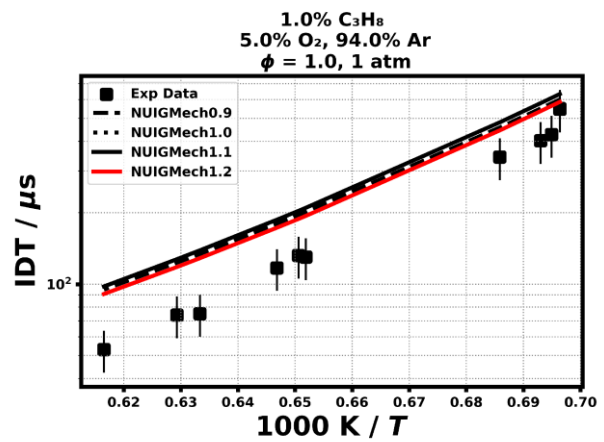
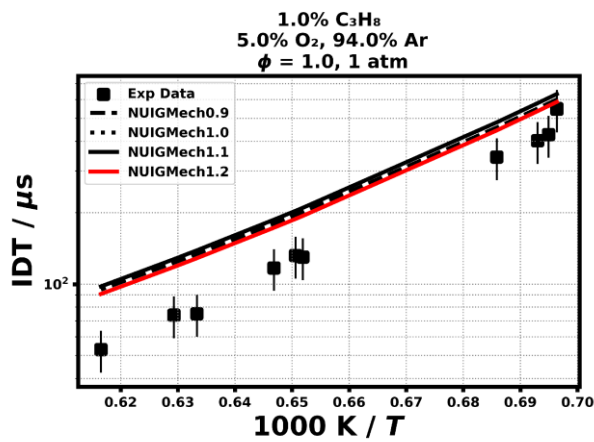
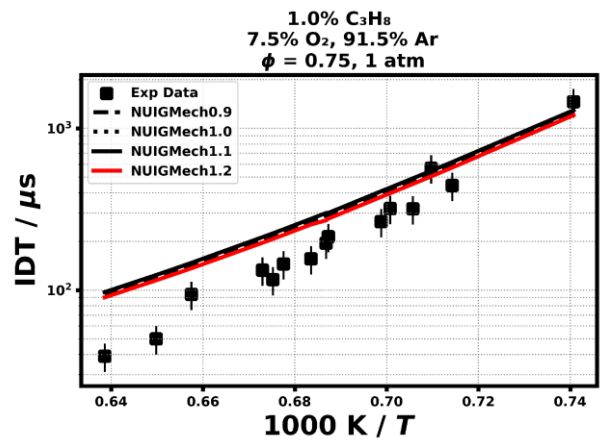
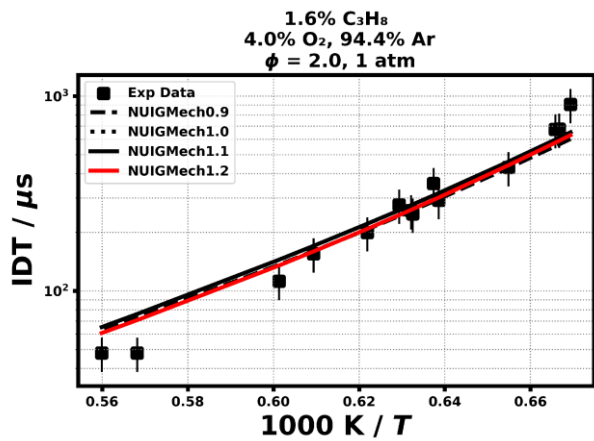
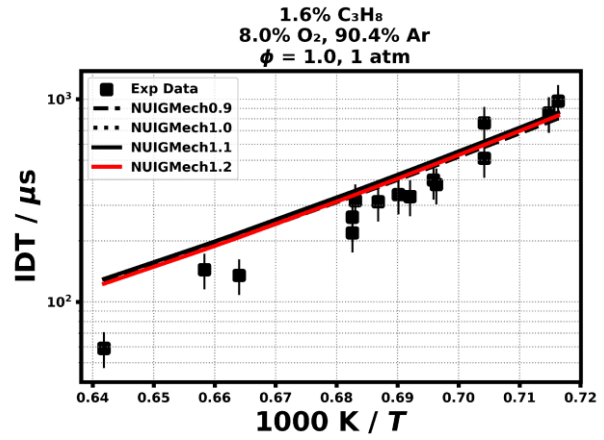
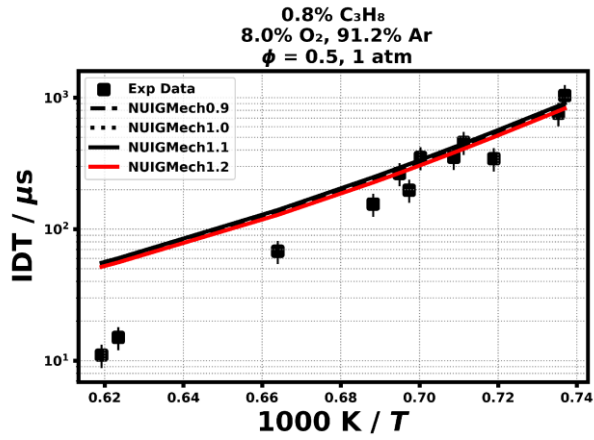


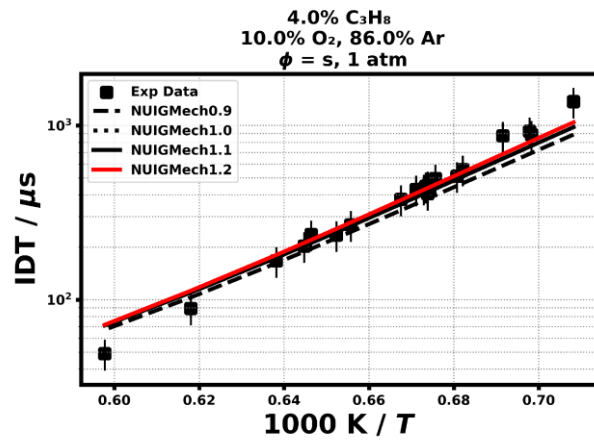
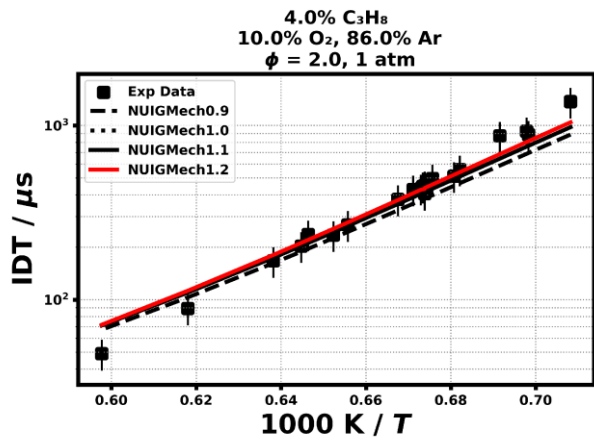
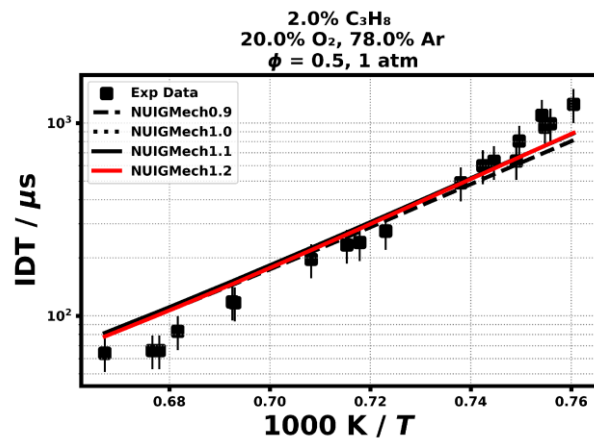
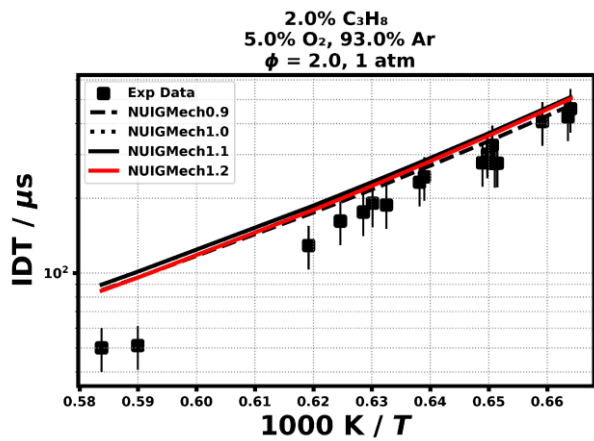
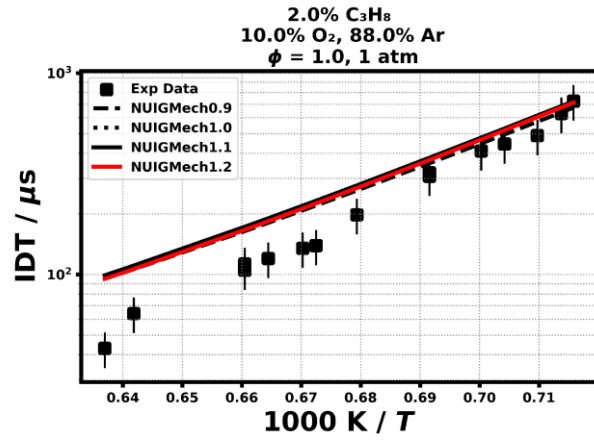
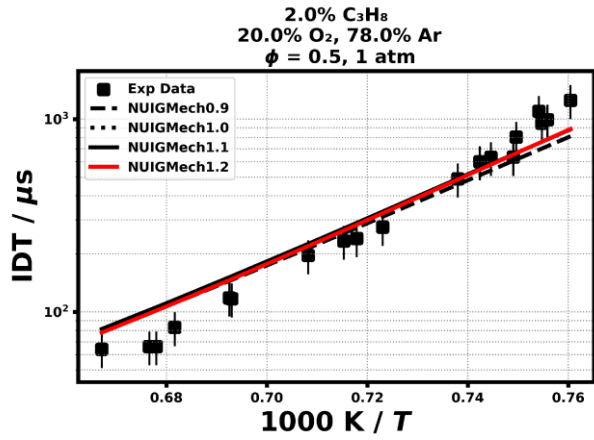




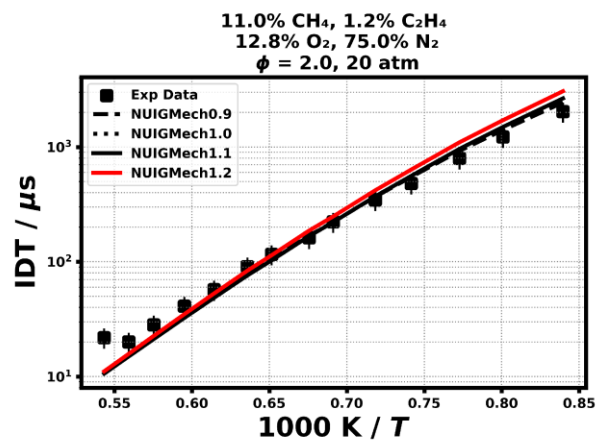
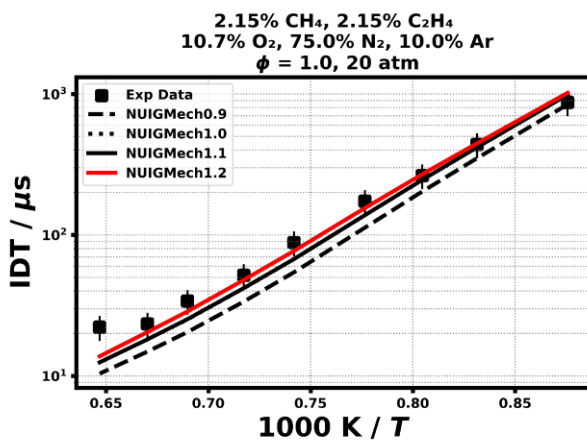
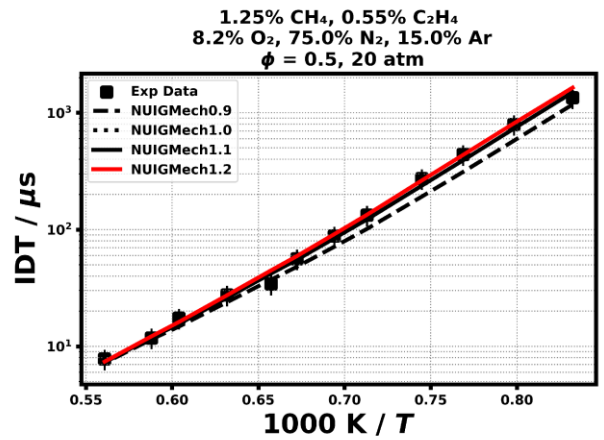
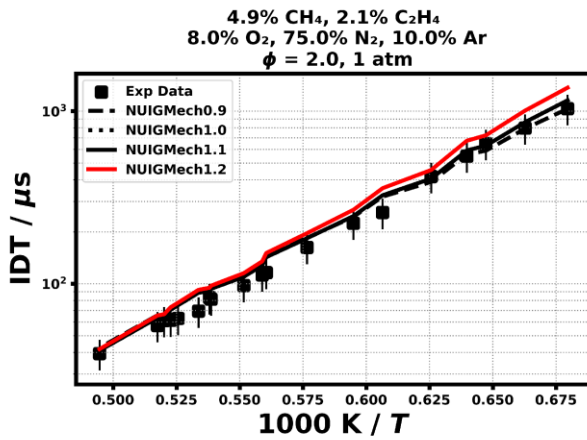
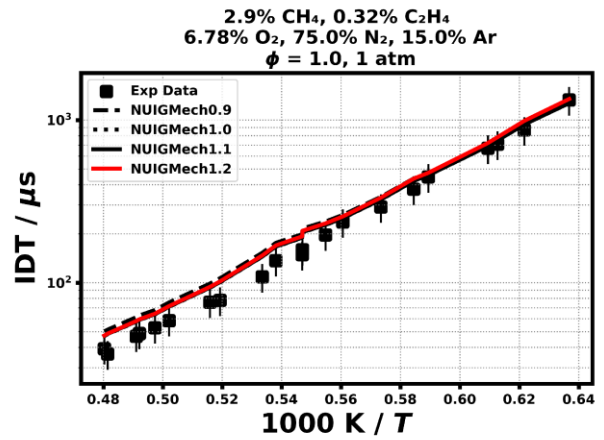
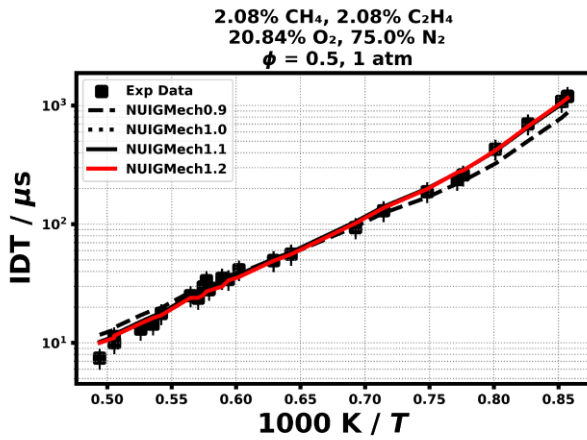


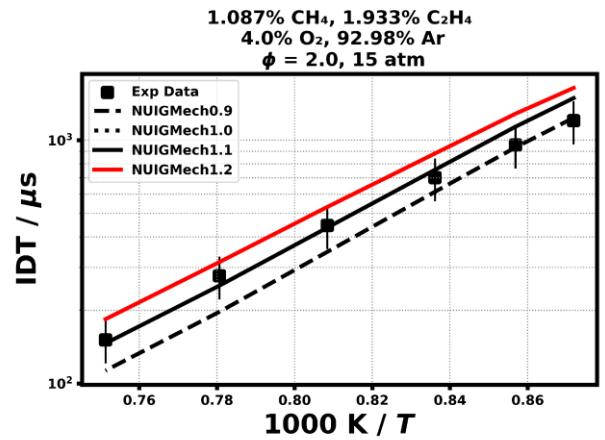
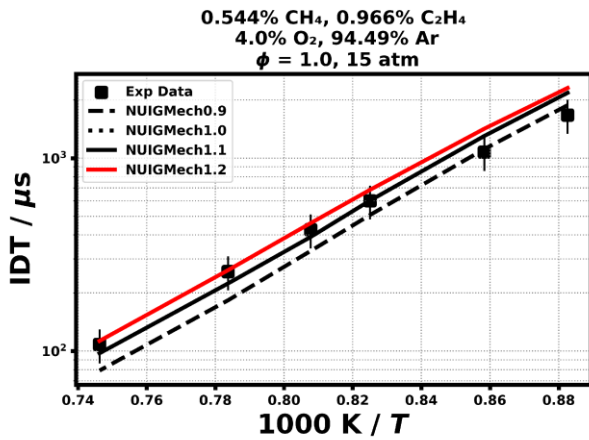
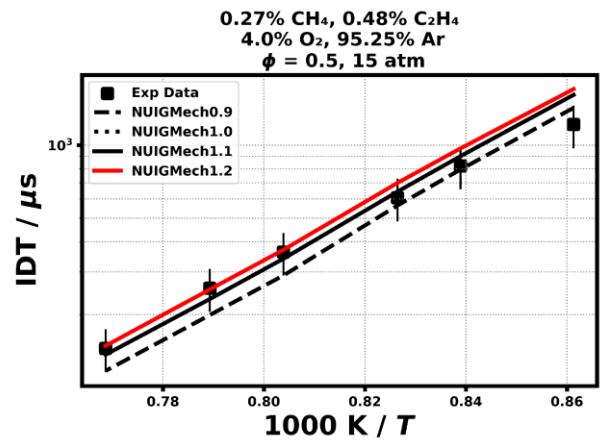
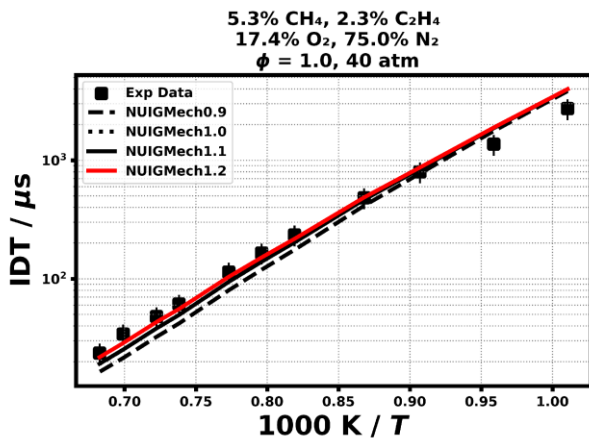
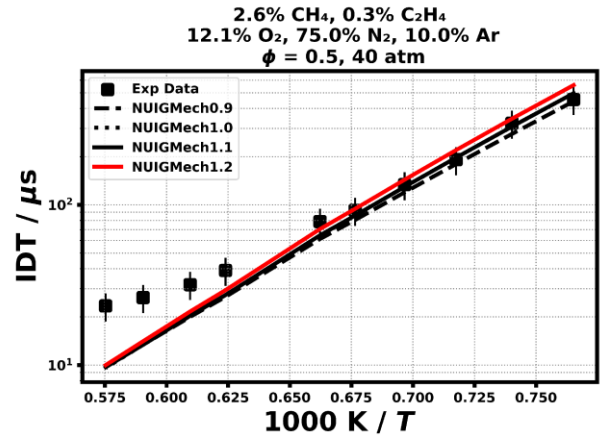
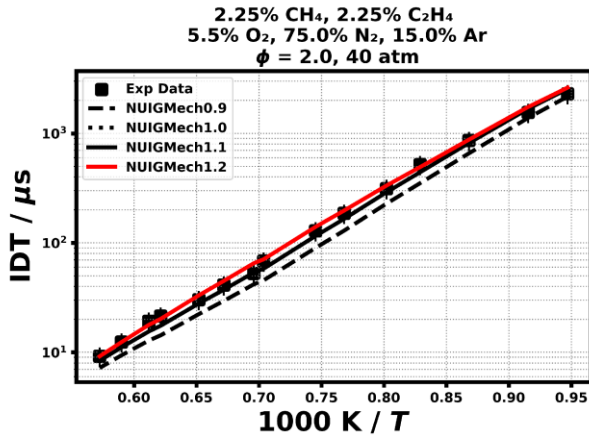




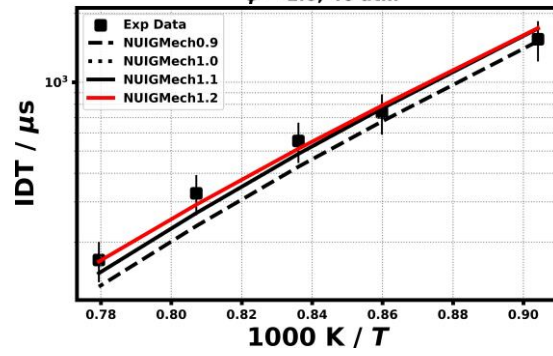


1.1.16 CH₄/C₂H₄

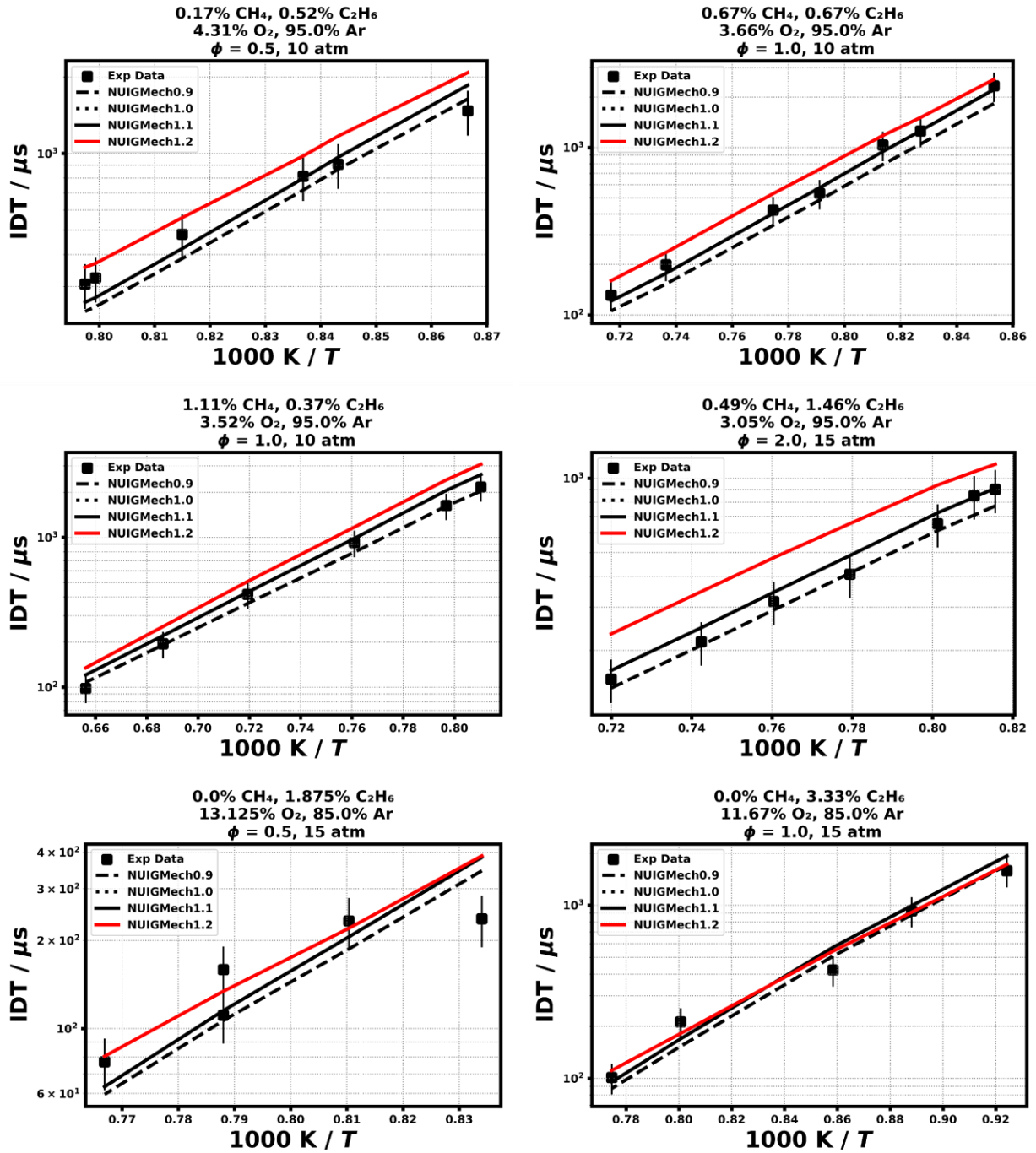


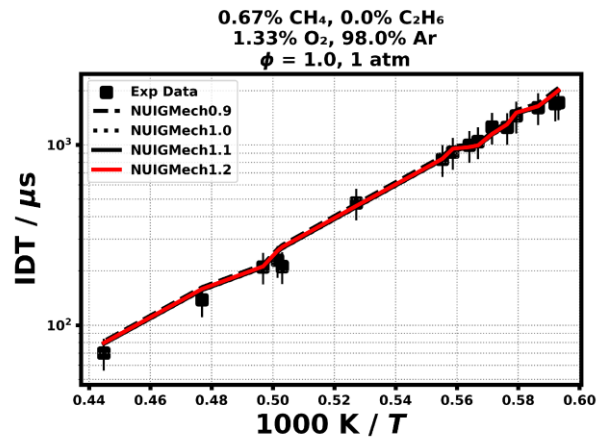
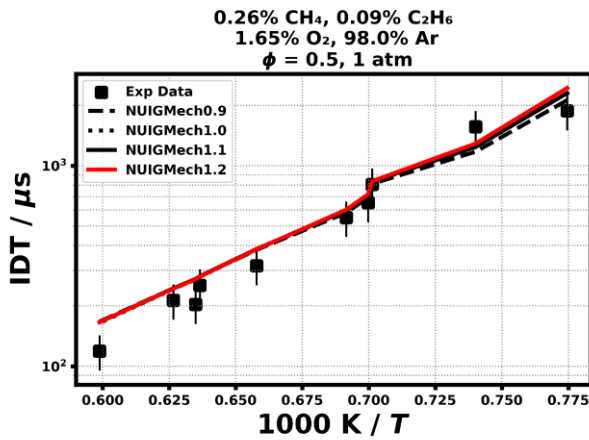
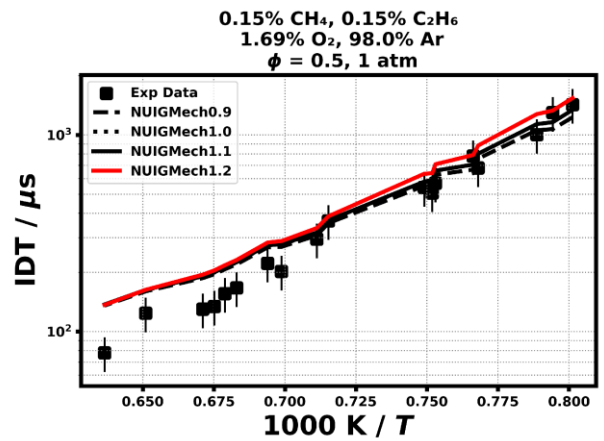
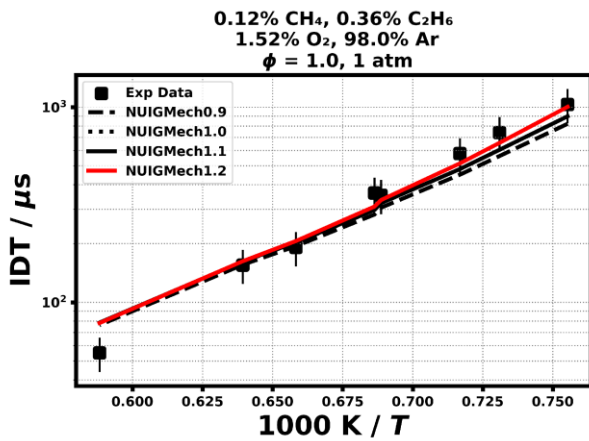
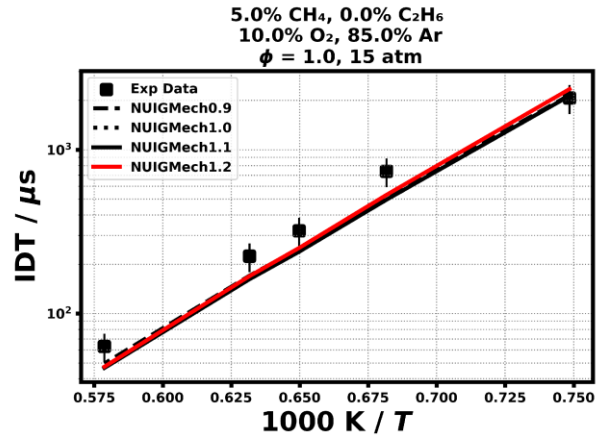
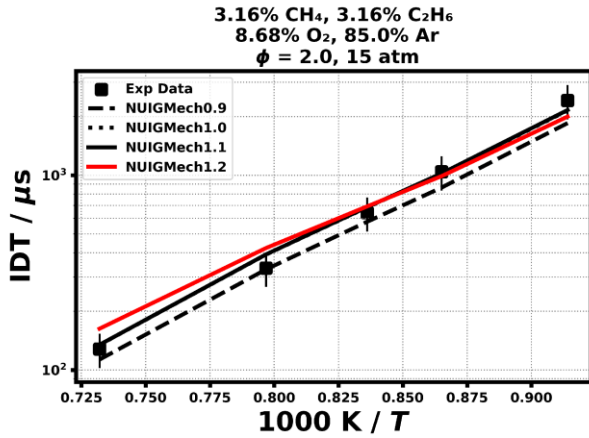


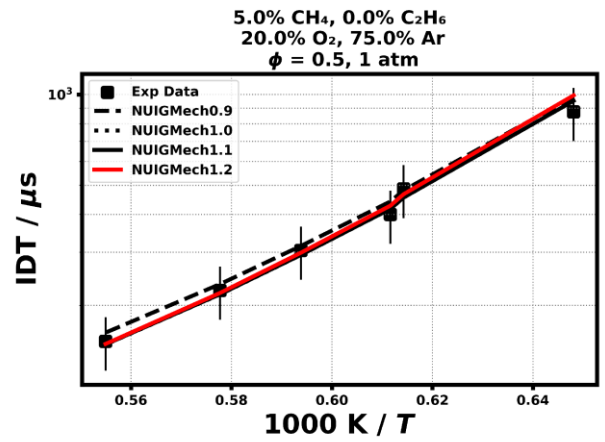
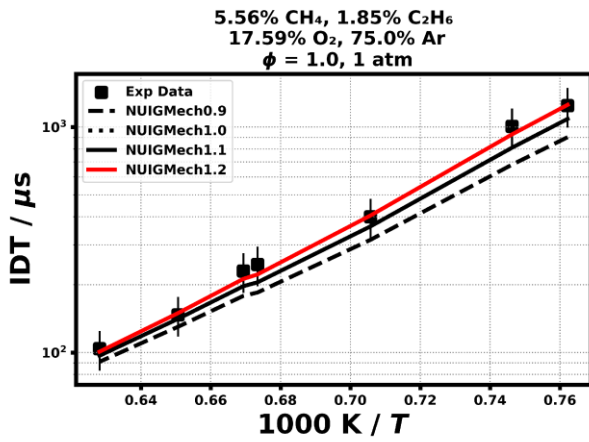
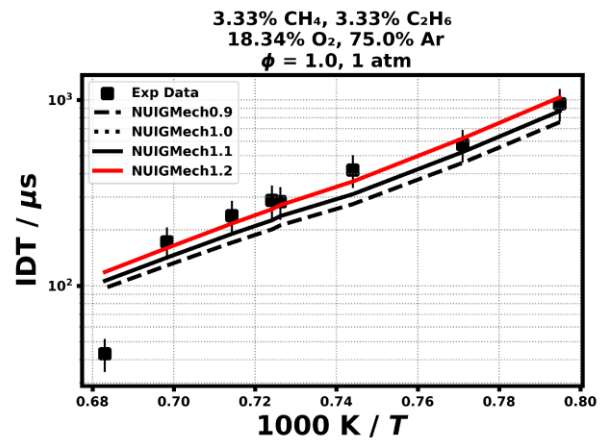
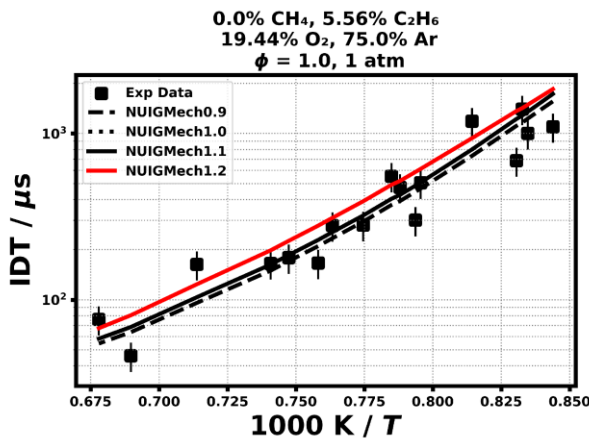
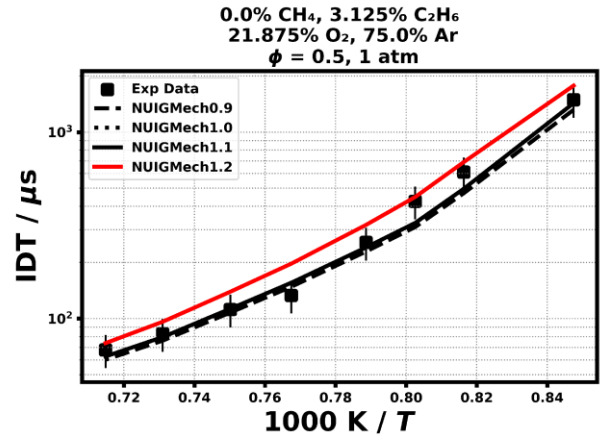
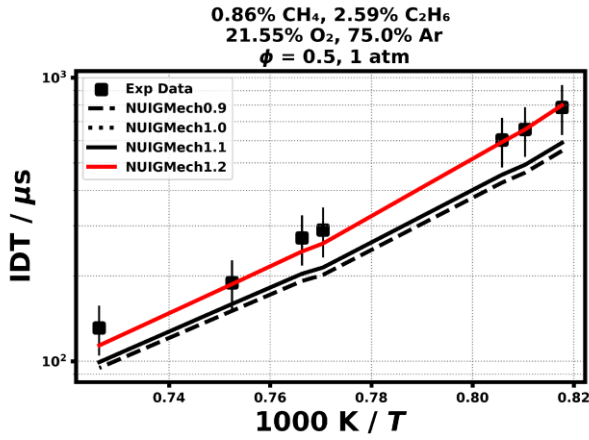
0.544% CH₄, 0.966% C₂H₄
4.0% O₂, 94.49% Ar
 $\phi = 1.0, 40 \text{ atm}$

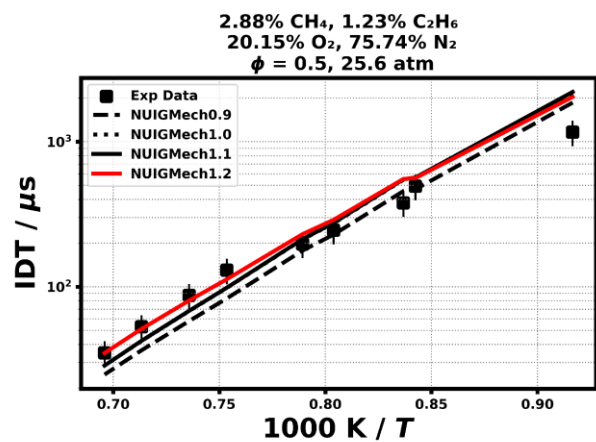
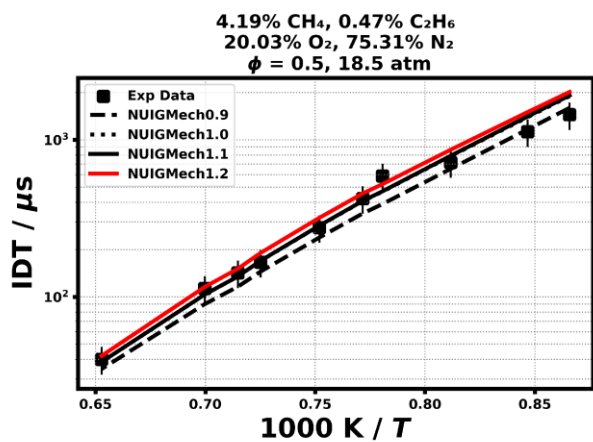
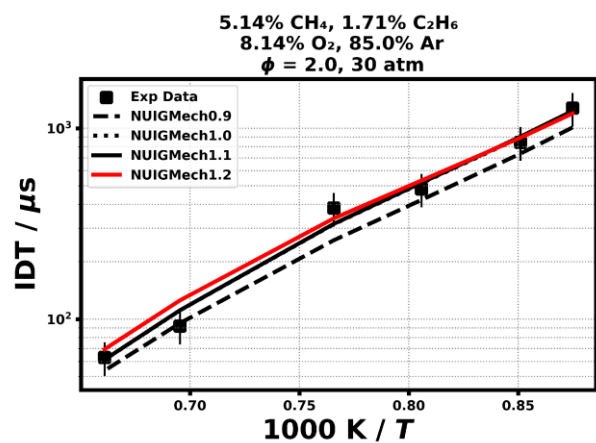
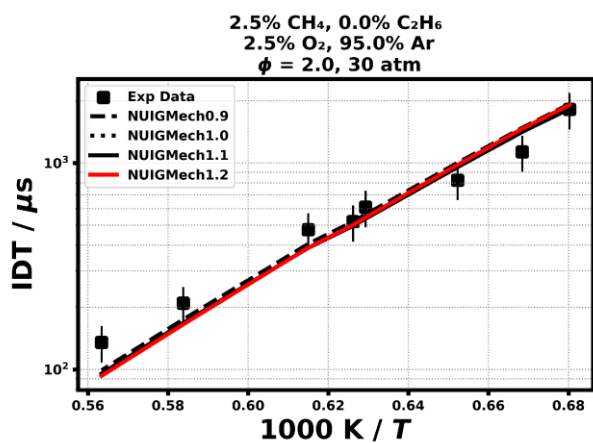
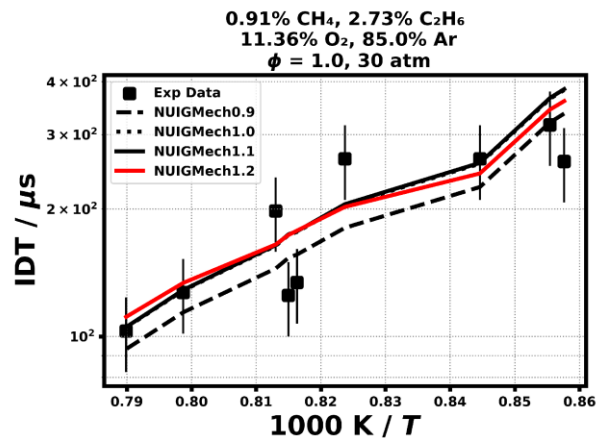
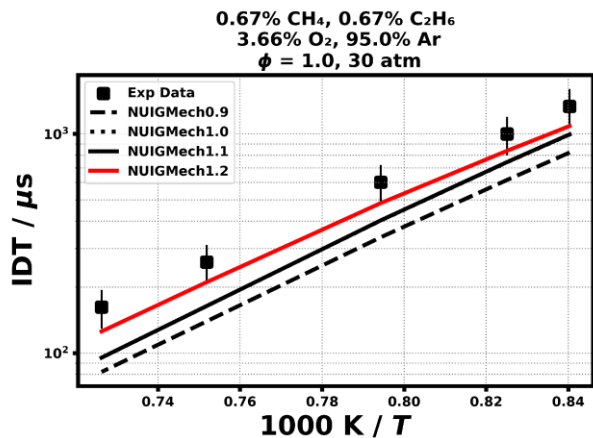


1.1.17 $\text{CH}_4/\text{C}_2\text{H}_6$

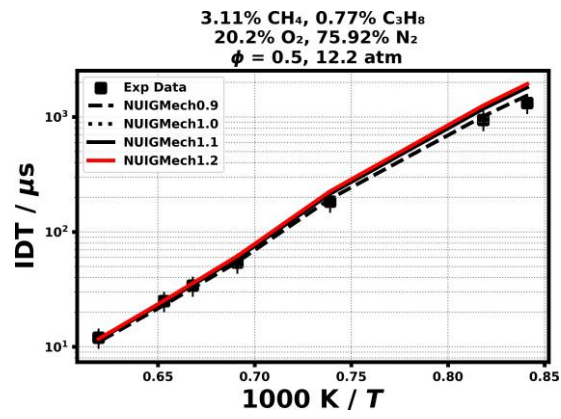




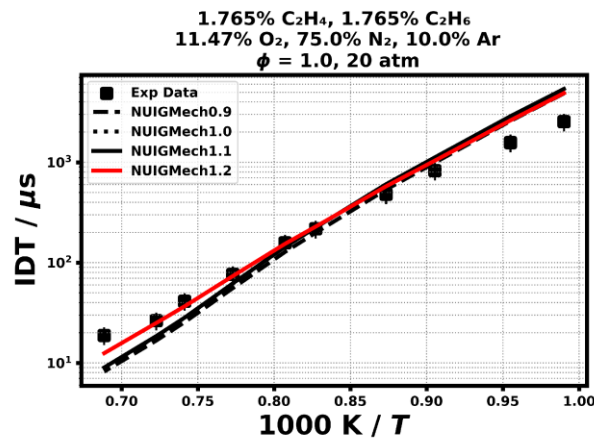
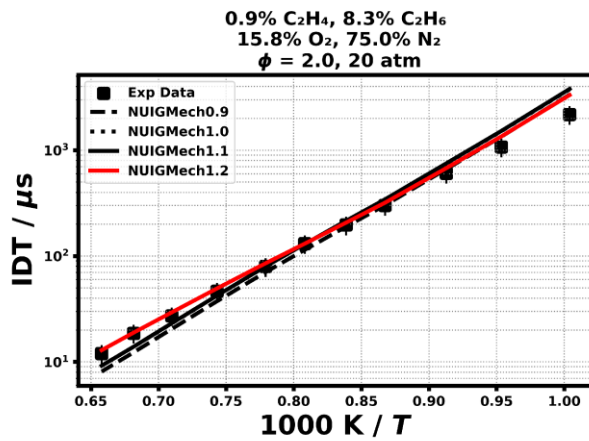
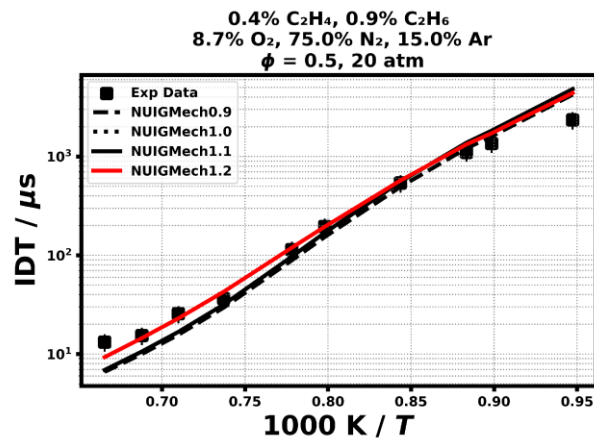
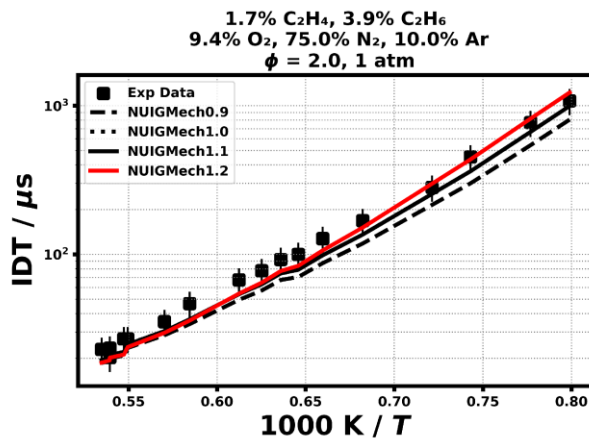
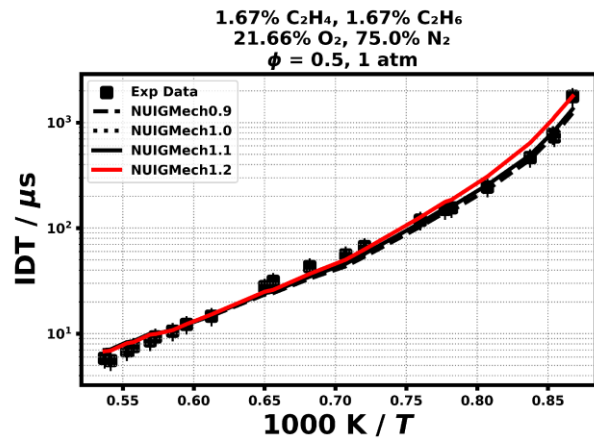
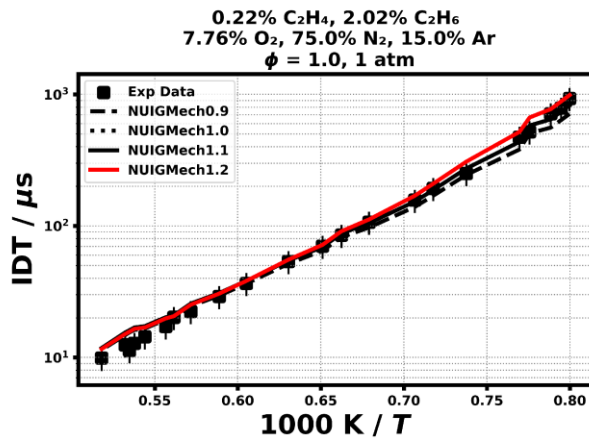


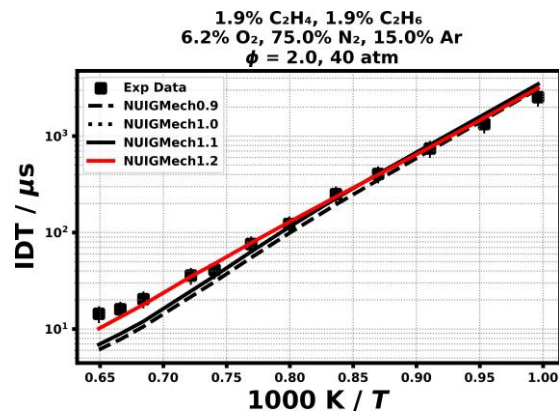
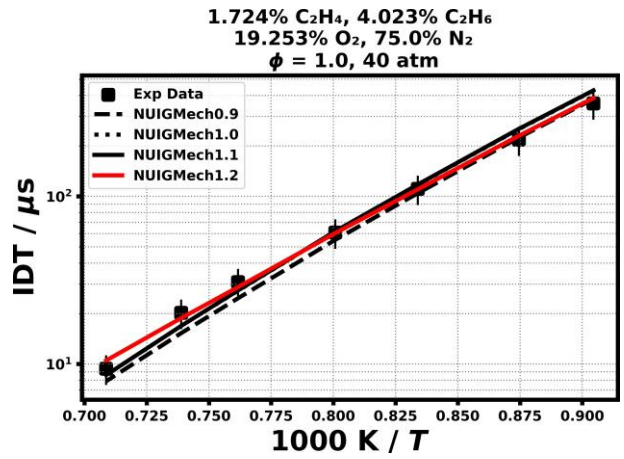
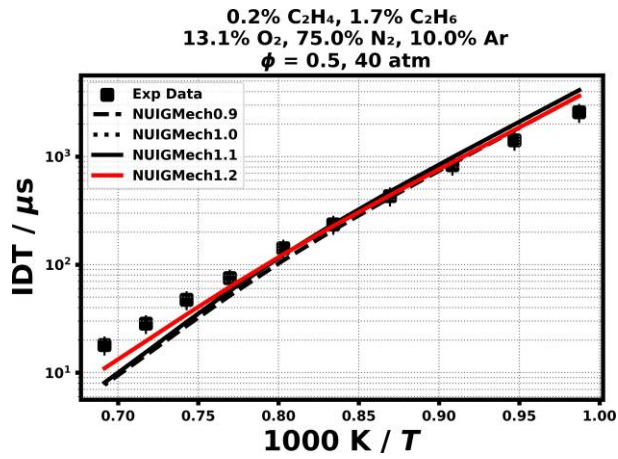


1.1.18 CH₄/C₃H₈

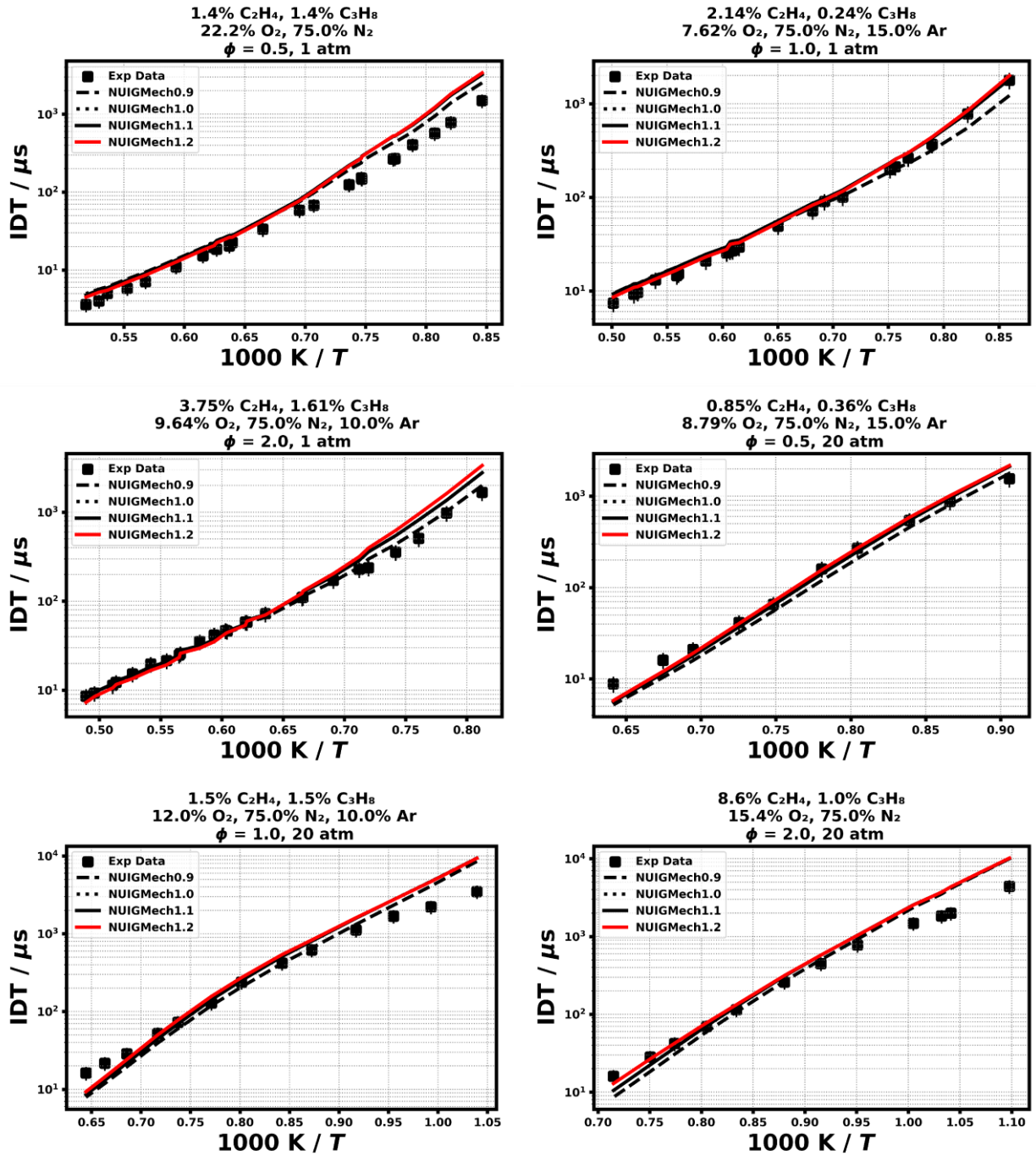


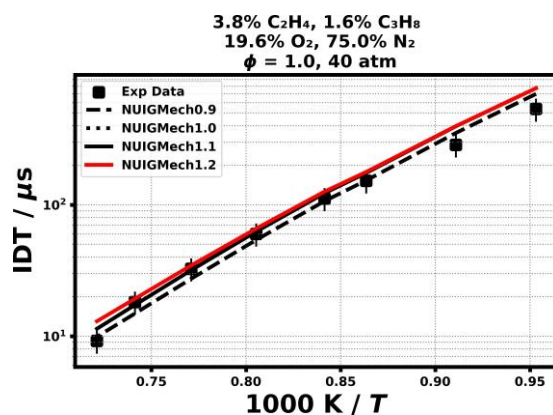
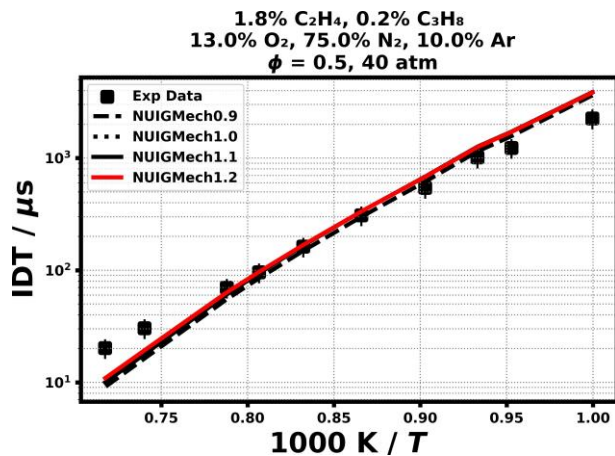
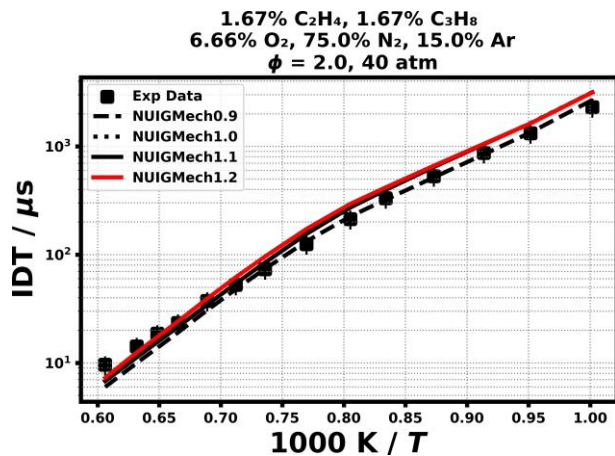
1.1.19 C₂H₄/C₂H₆



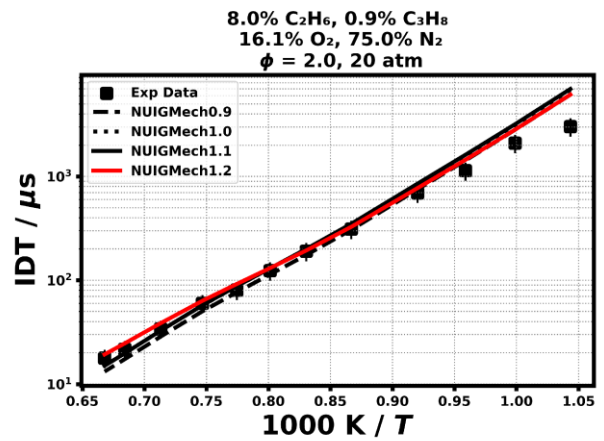
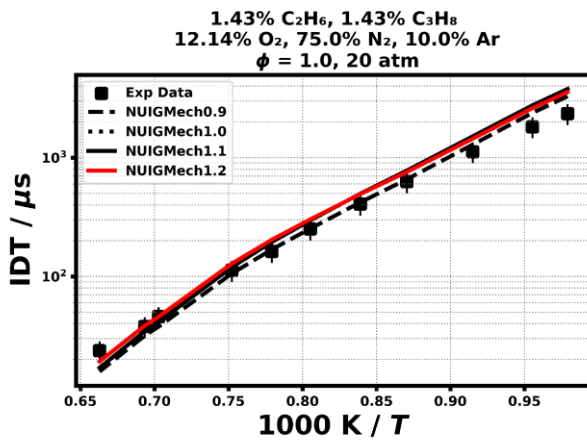
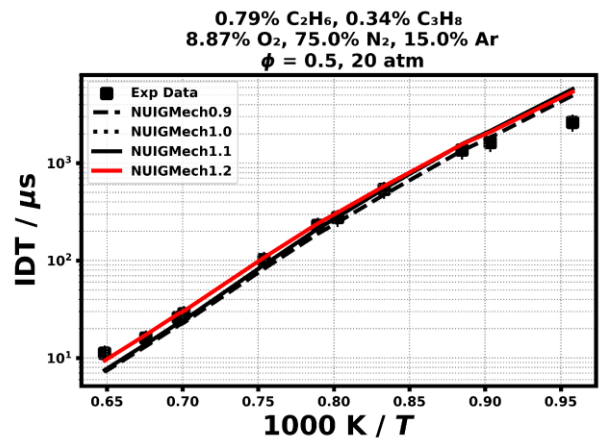
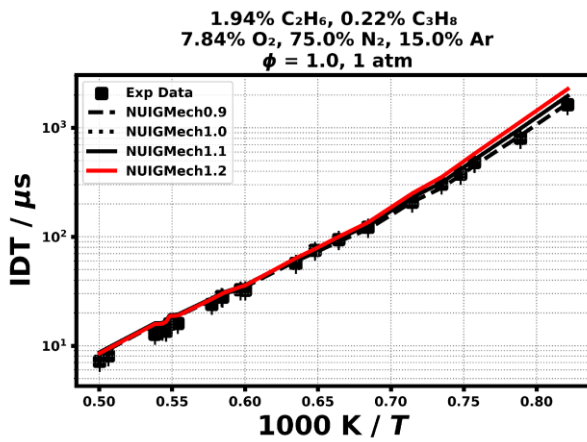
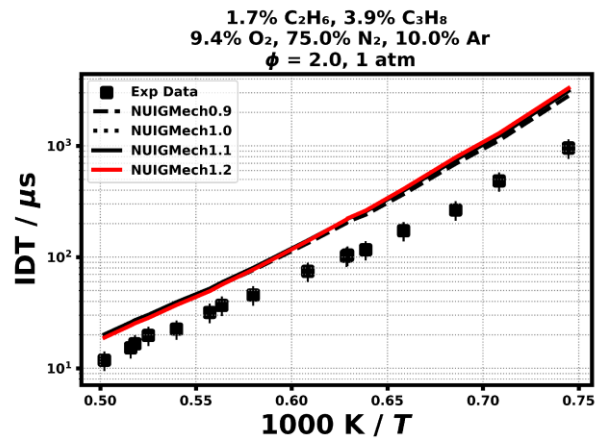
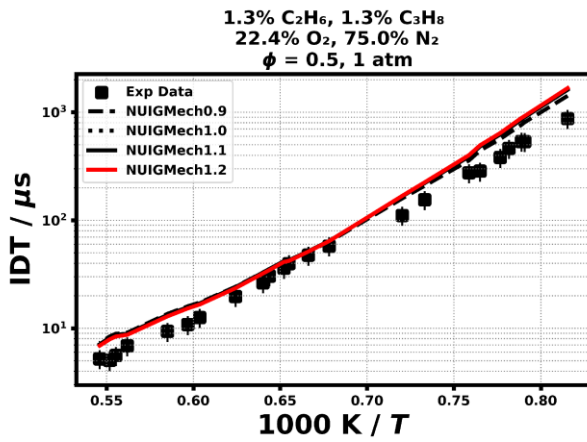


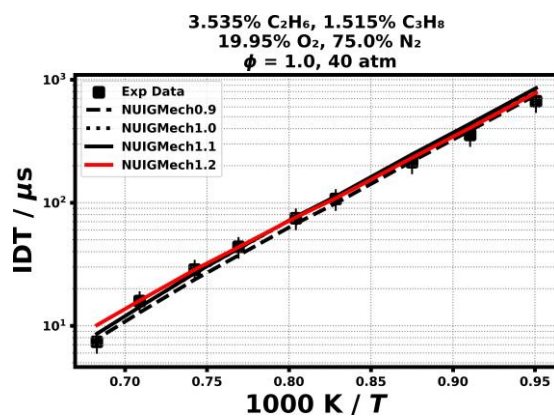
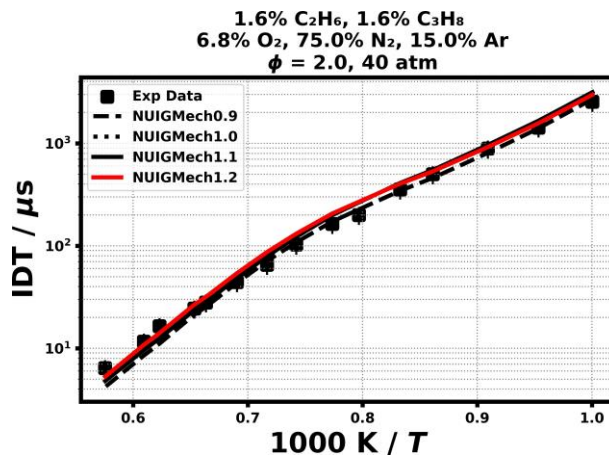
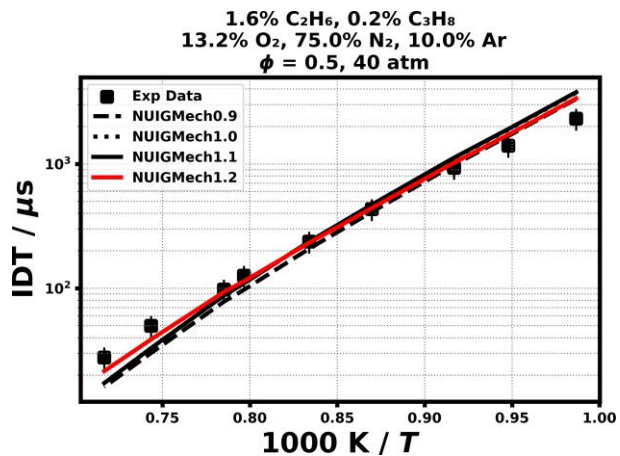
1.1.20 C₂H₄/C₃H₈



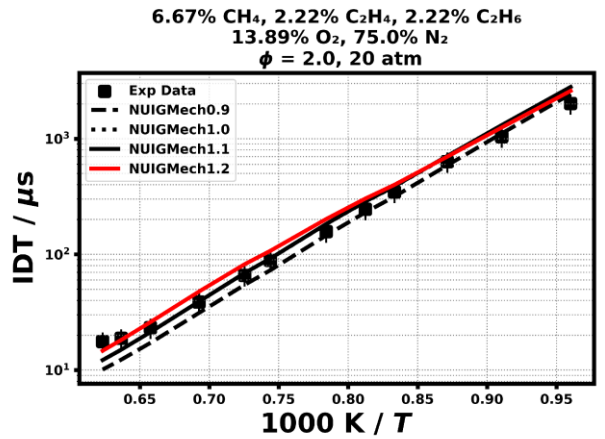
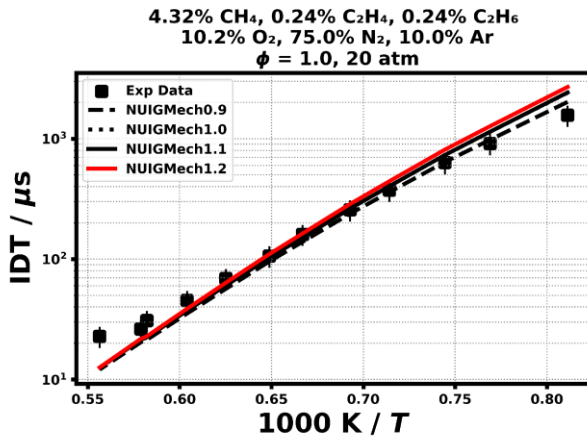
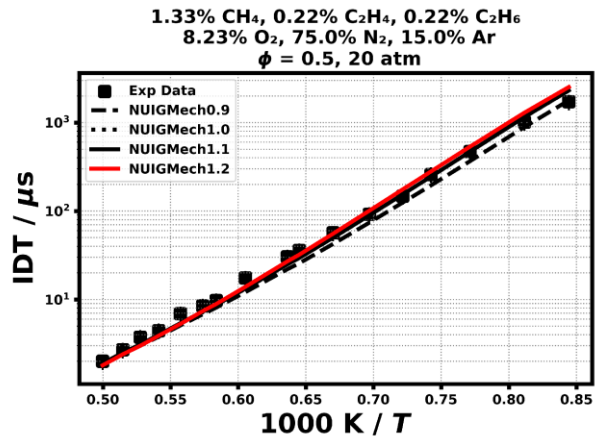
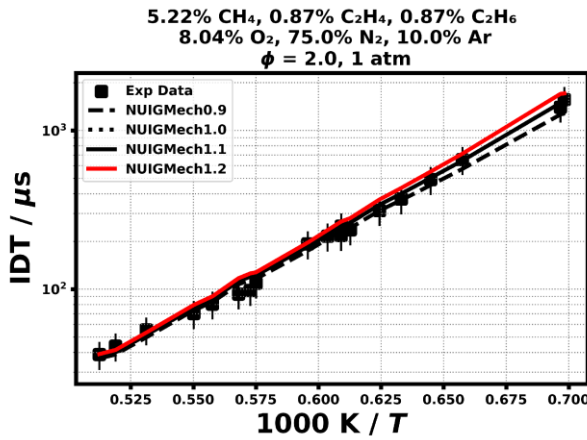
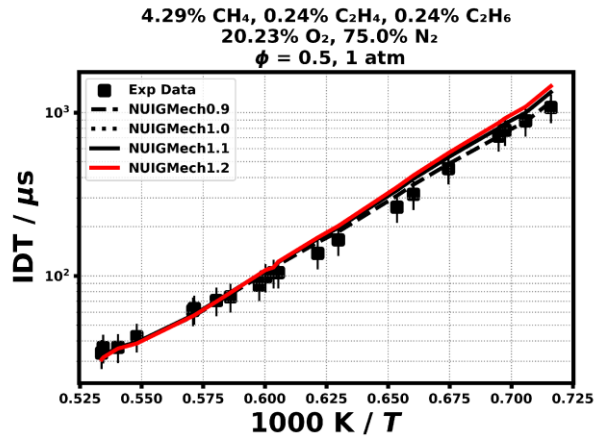
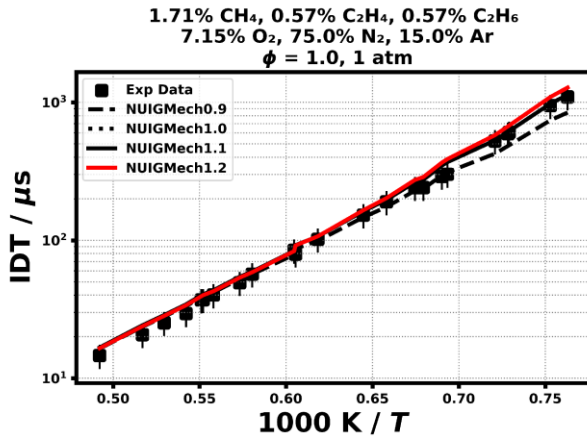


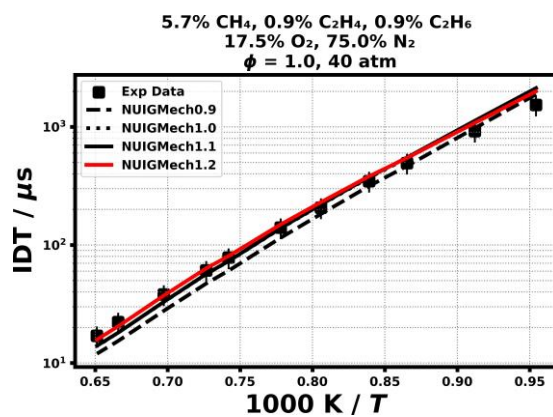
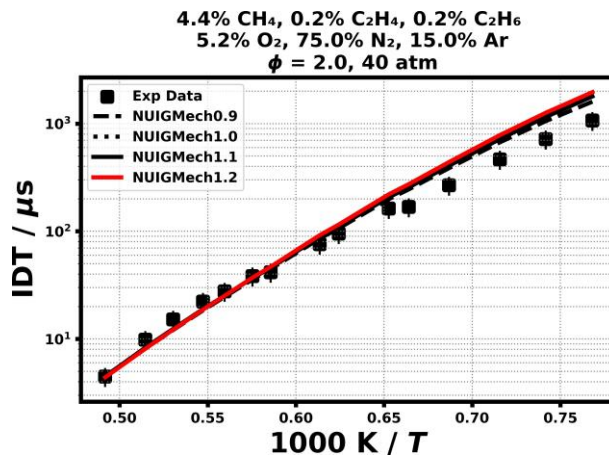
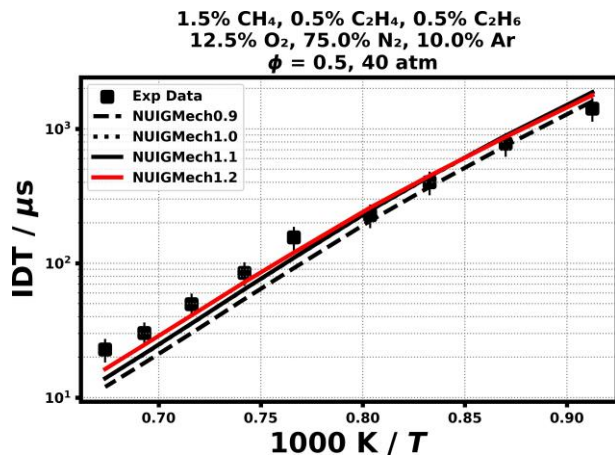
1.1.21 C₂H₆/C₃H₈





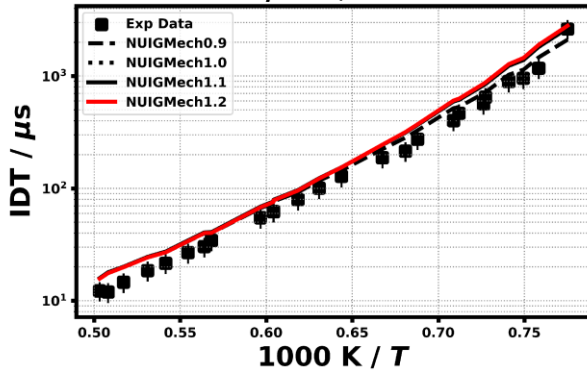
1.1.22 CH₄/C₂H₄/C₂H₆



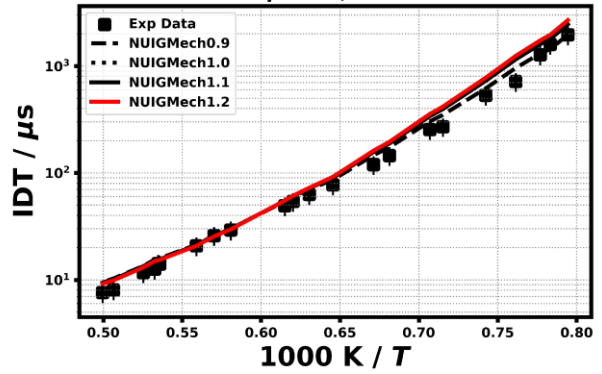


1.1.23 $\text{CH}_4/\text{C}_2\text{H}_4/\text{C}_2\text{H}_6/\text{C}_3\text{H}_8$

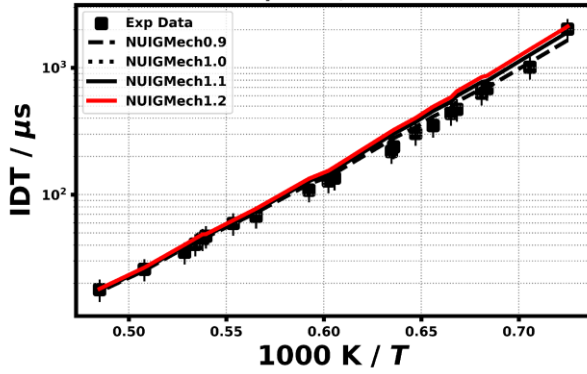
1.63% CH_4 , 0.41% C_2H_4 , 0.41% C_2H_6 , 0.27% C_3H_8
 7.28% O_2 , 75.0% N_2 , 15.0% Ar
 $\phi = 1.0$, 1 atm



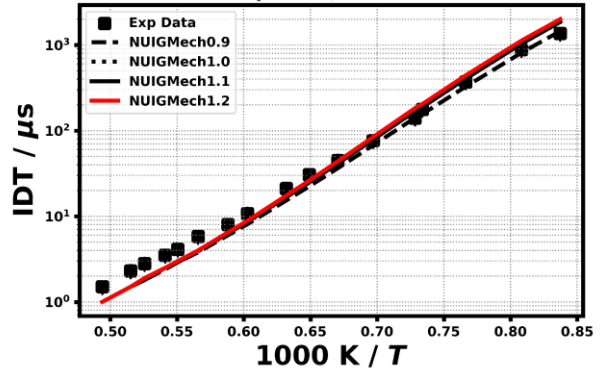
3.51% CH_4 , 0.22% C_2H_4 , 0.44% C_2H_6 , 0.22% C_3H_8
 20.61% O_2 , 75.0% N_2
 $\phi = 0.5$, 1 atm



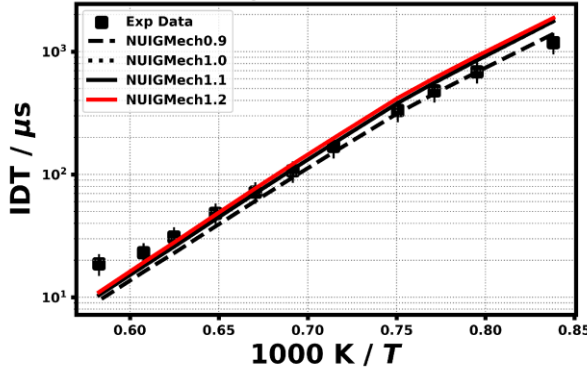
4.62% CH_4 , 0.66% C_2H_4 , 0.66% C_2H_6 , 0.66% C_3H_8
 8.4% O_2 , 75.0% N_2 , 10.0% Ar
 $\phi = 2.0$, 1 atm



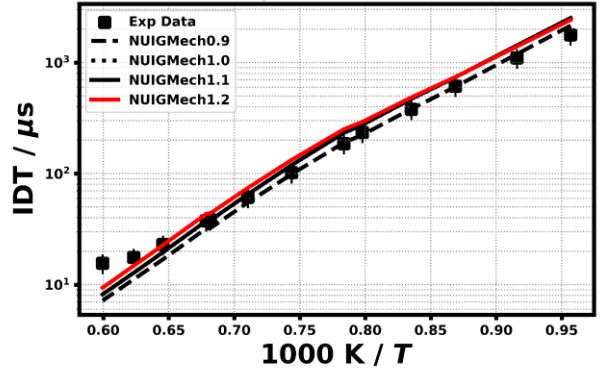
1.147% CH_4 , 0.164% C_2H_4 , 0.164% C_2H_6 , 0.164% C_3H_8
 8.361% O_2 , 90.0% N_2
 $\phi = 0.5$, 20 atm



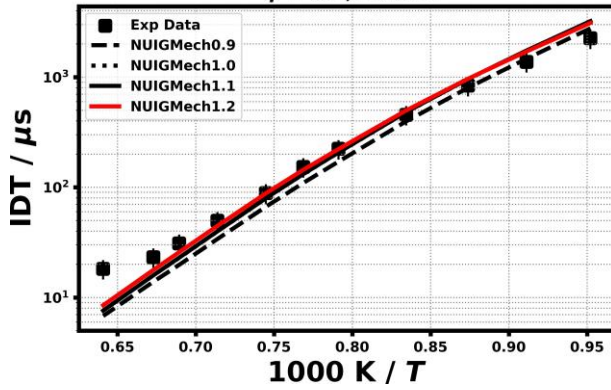
3.582% CH_4 , 0.224% C_2H_4 , 0.448% C_2H_6 , 0.224% C_3H_8
 10.522% O_2 , 85.0% N_2
 $\phi = 1.0$, 20 atm



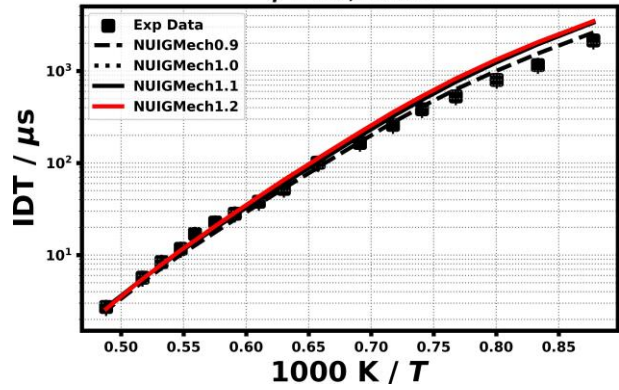
6.42% CH_4 , 1.6% C_2H_4 , 1.6% C_2H_6 , 1.07% C_3H_8
 14.31% O_2 , 75.0% N_2
 $\phi = 2.0$, 20 atm



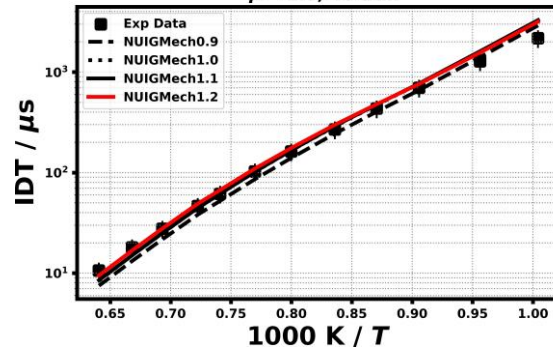
1.41% CH₄, 0.35% C₂H₄, 0.35% C₂H₆, 0.24% C₃H₈
12.65% O₂, 85.0% N₂
 $\phi = 0.5, 40 \text{ atm}$



3.678% CH₄, 0.23% C₂H₄, 0.46% C₂H₆, 0.23% C₃H₈
5.402% O₂, 90.0% N₂
 $\phi = 2.0, 40 \text{ atm}$

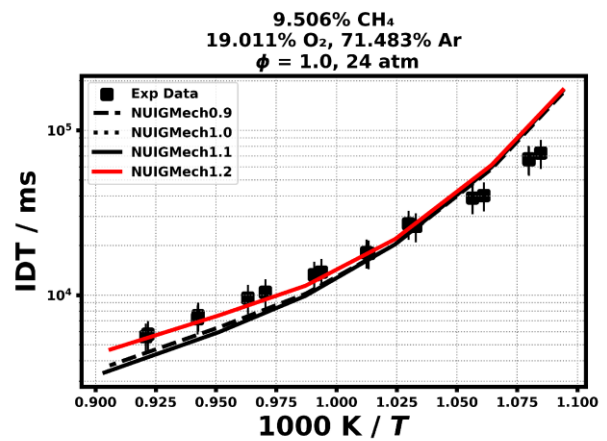
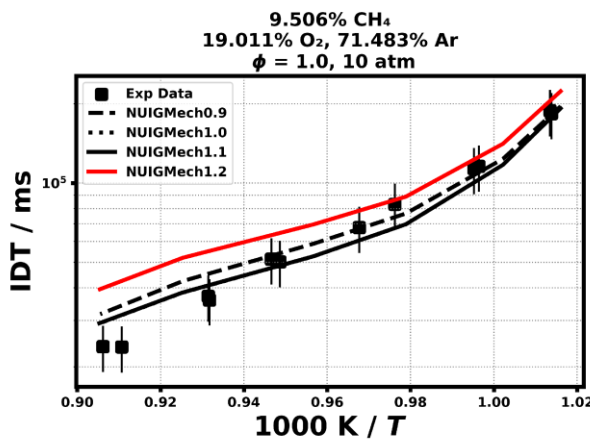
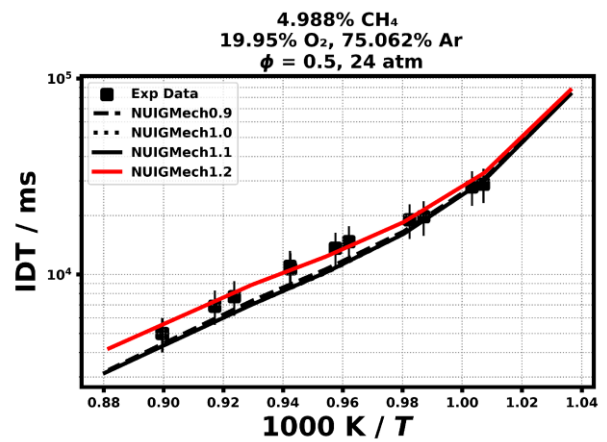
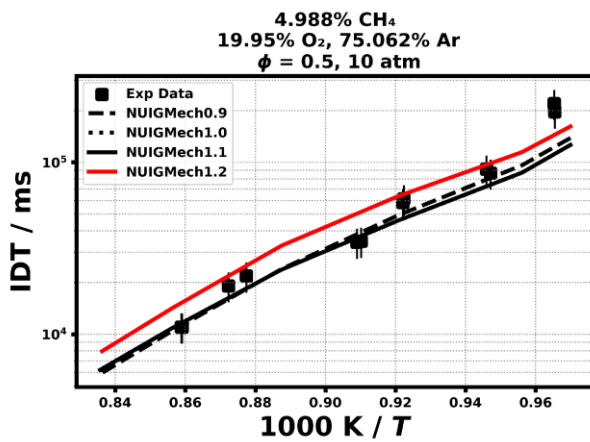
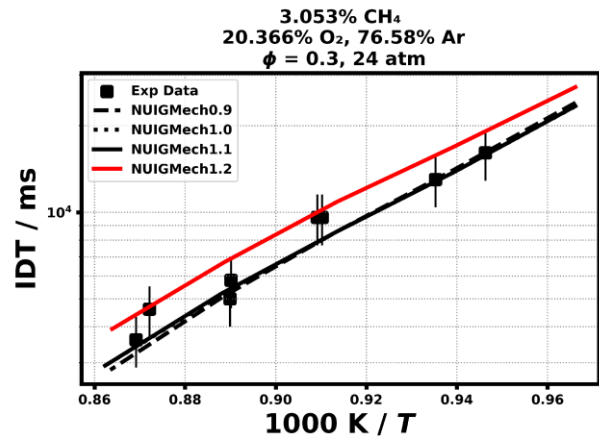
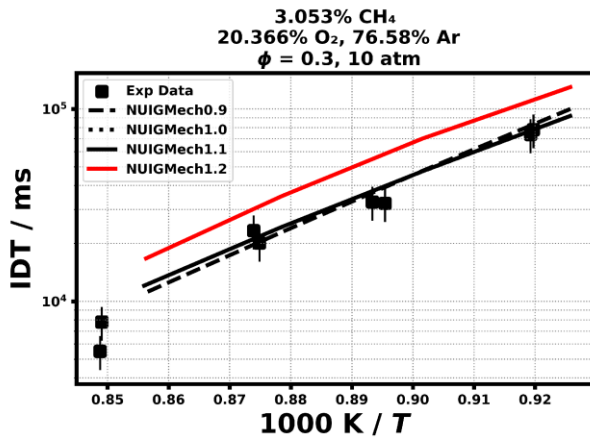


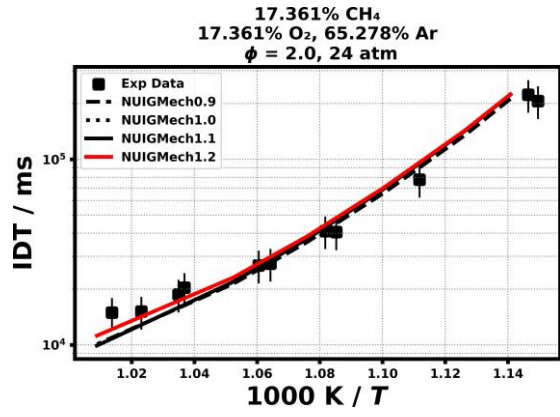
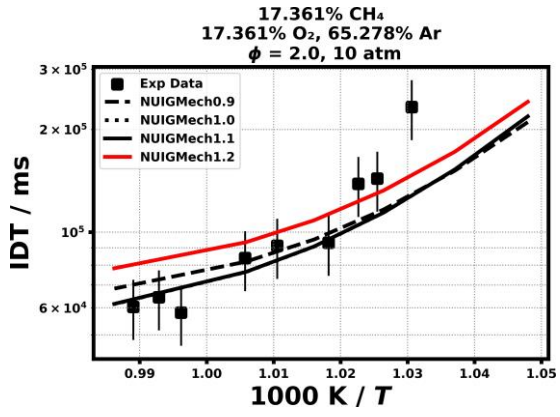
4.93% CH₄, 0.704% C₂H₄, 0.704% C₂H₆, 0.704% C₃H₈
17.958% O₂, 75.0% N₂
 $\phi = 1.0, 40 \text{ atm}$



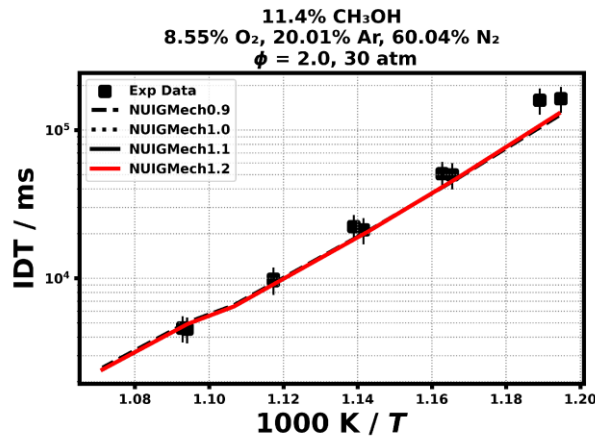
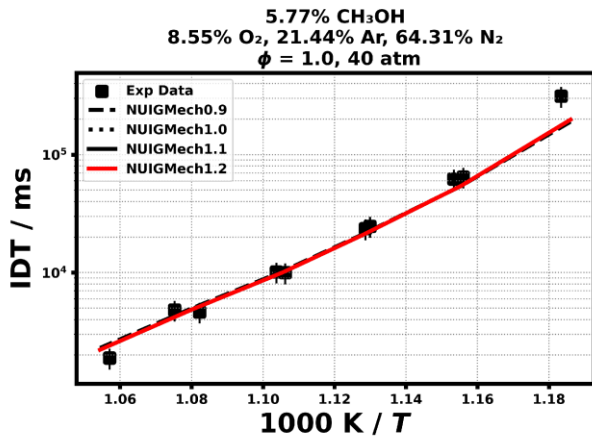
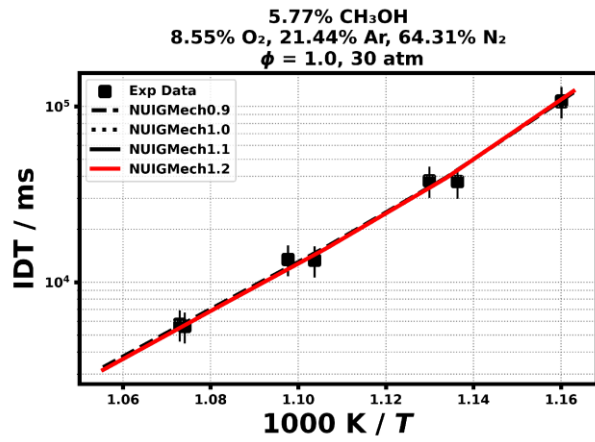
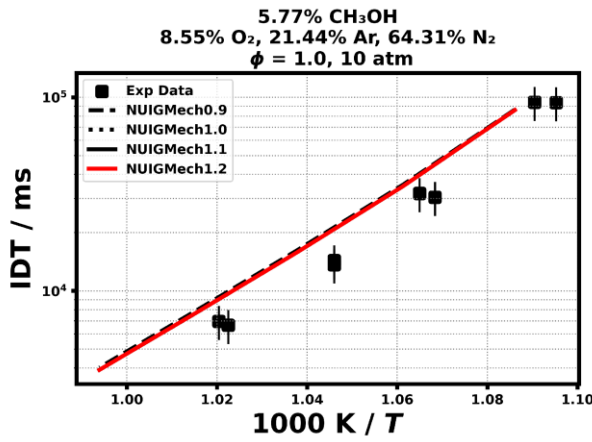
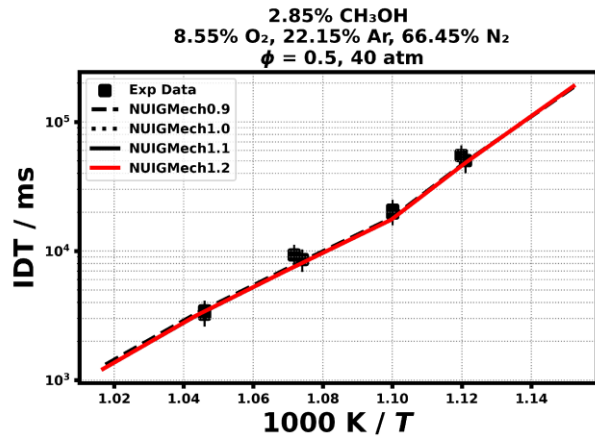
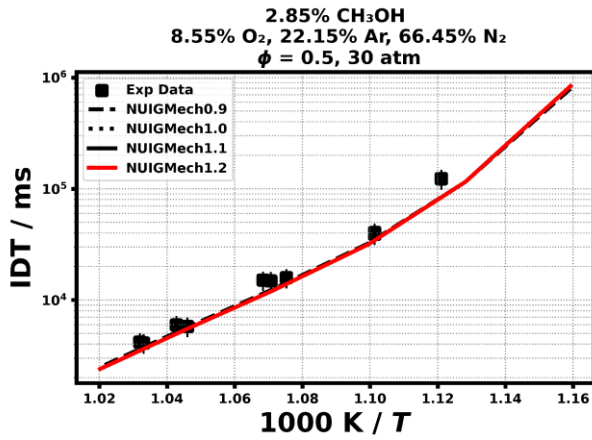
1.2 Rapid Compression Machine

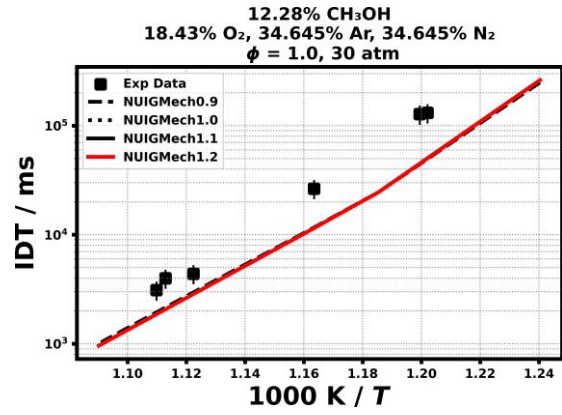
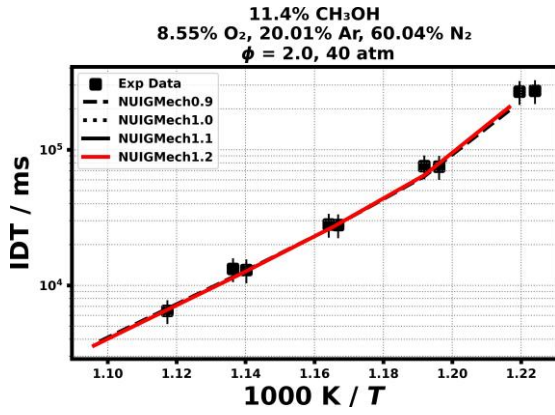
1.2.1 CH₄



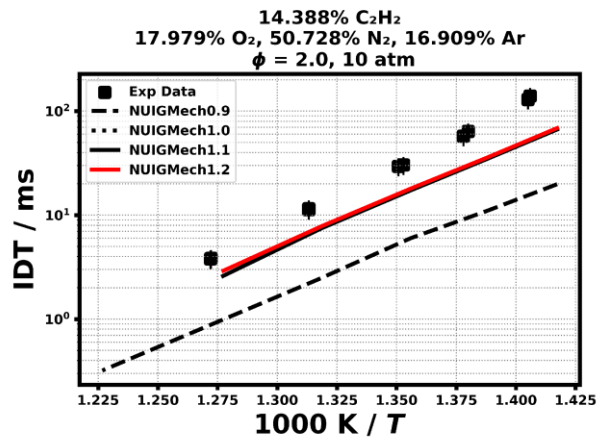
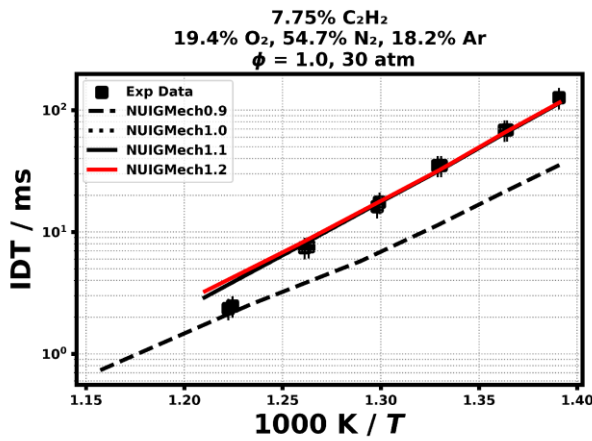
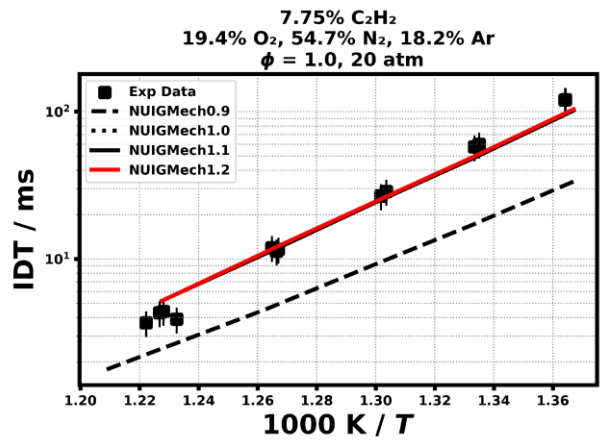
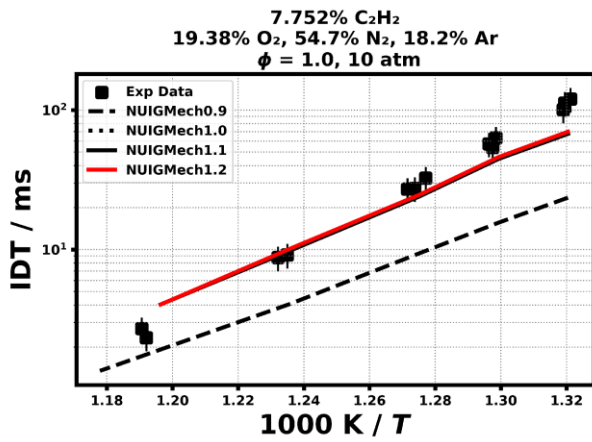
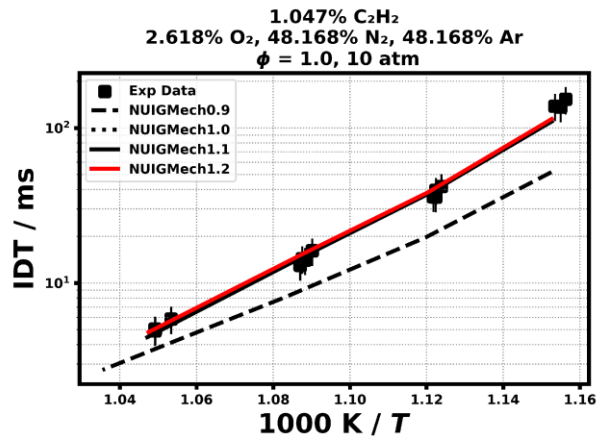
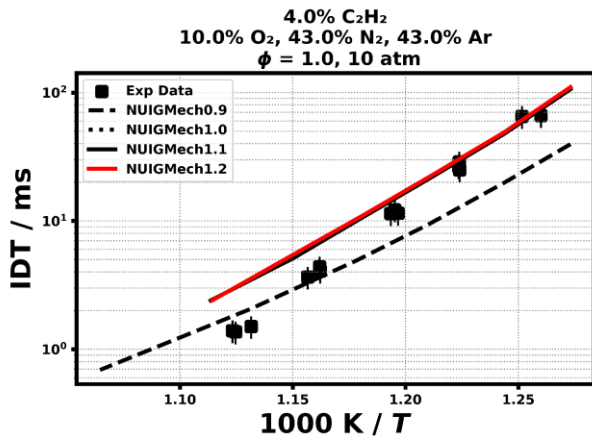


1.2.2 CH₃OH

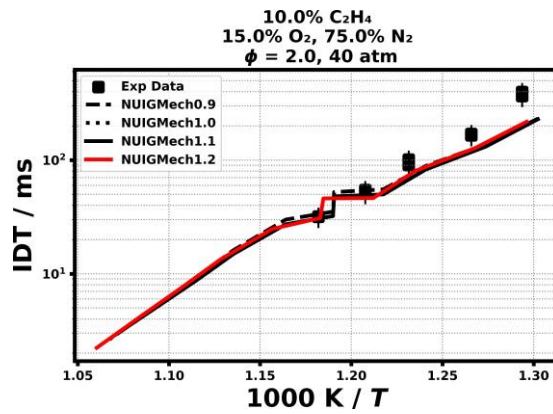
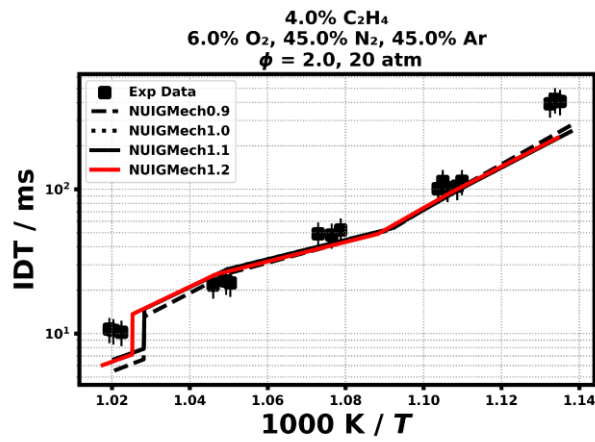
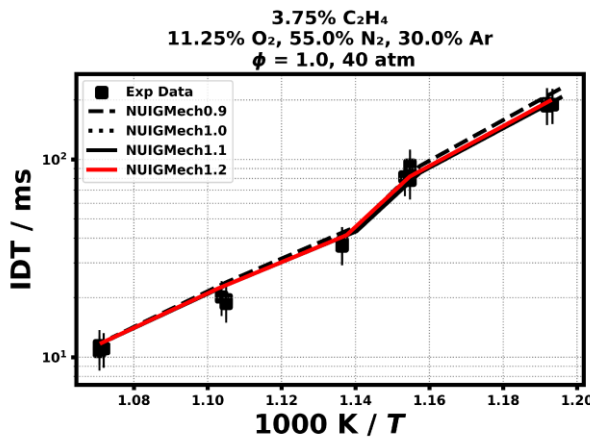
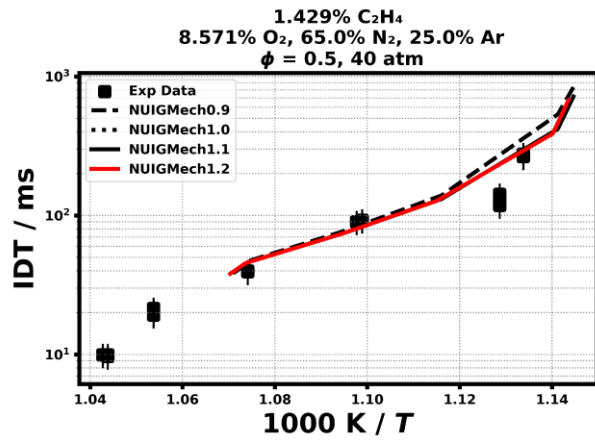
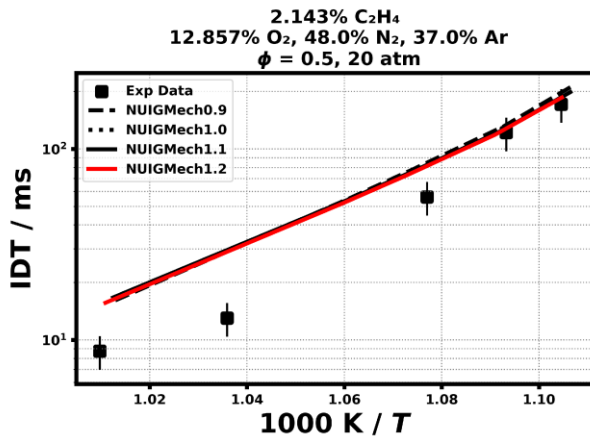




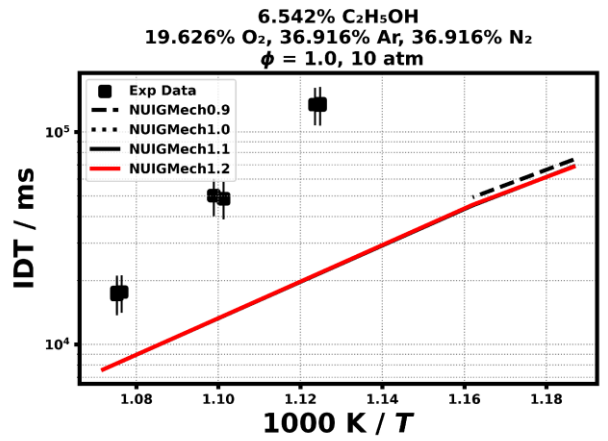
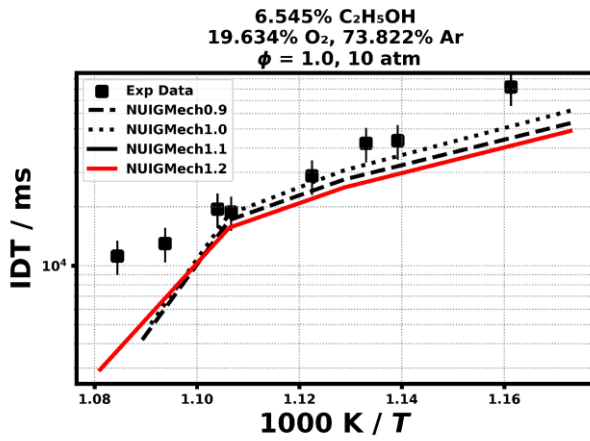
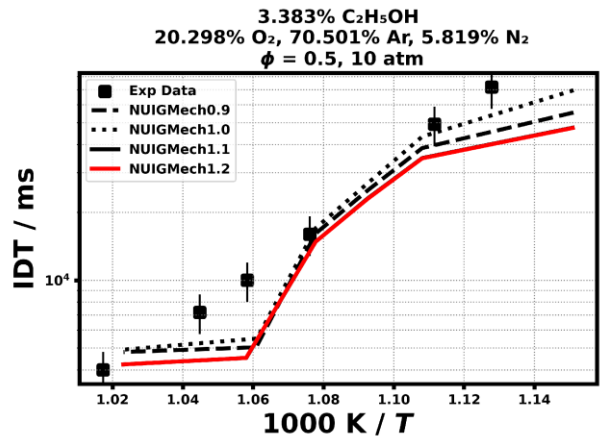
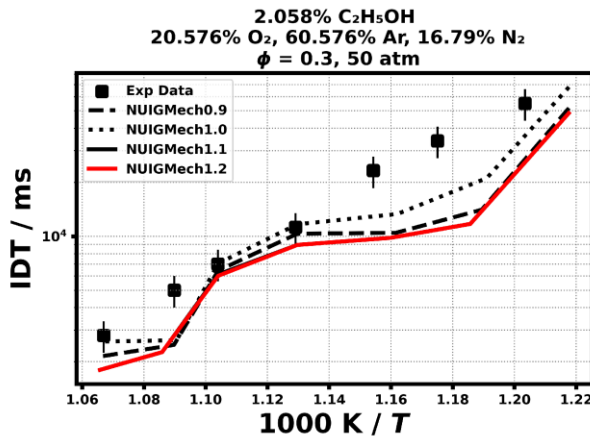
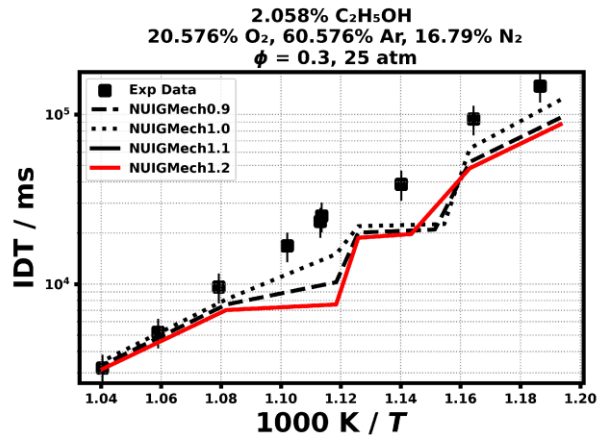
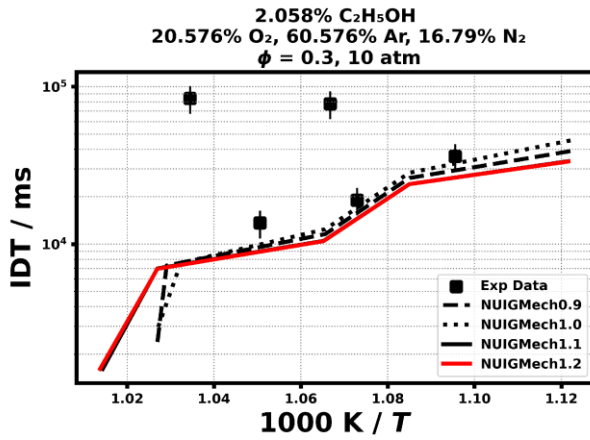
1.2.3 C₂H₂

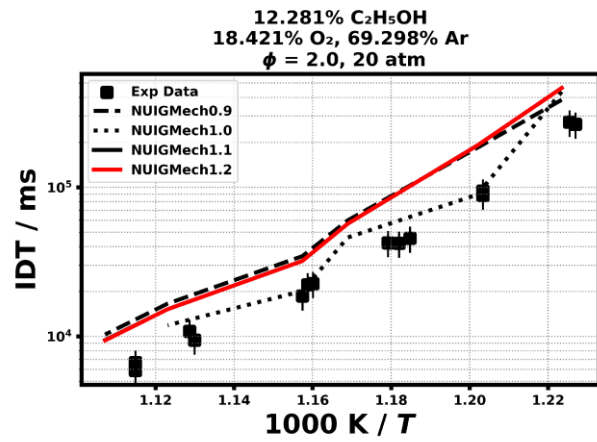
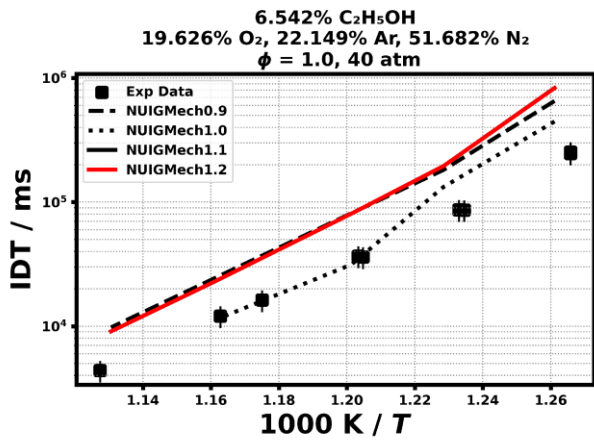
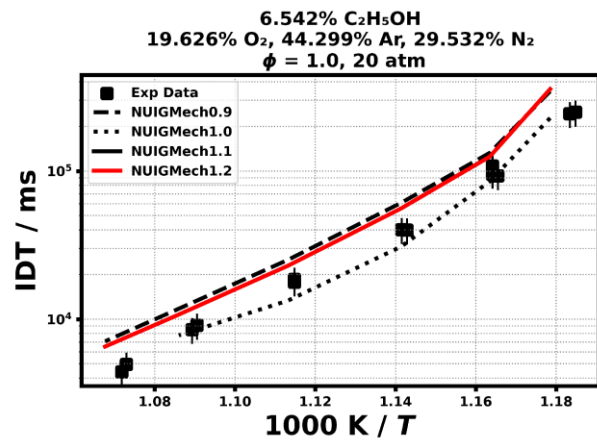
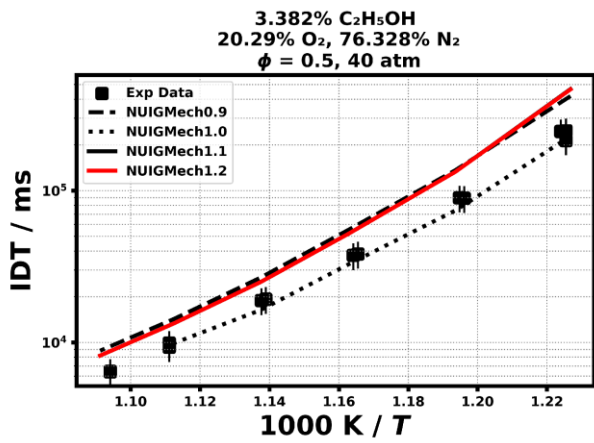
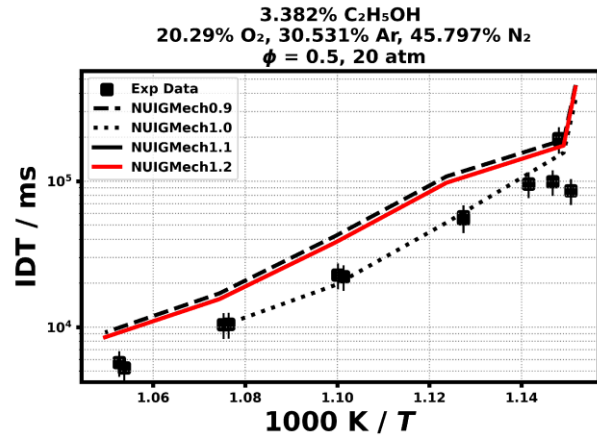
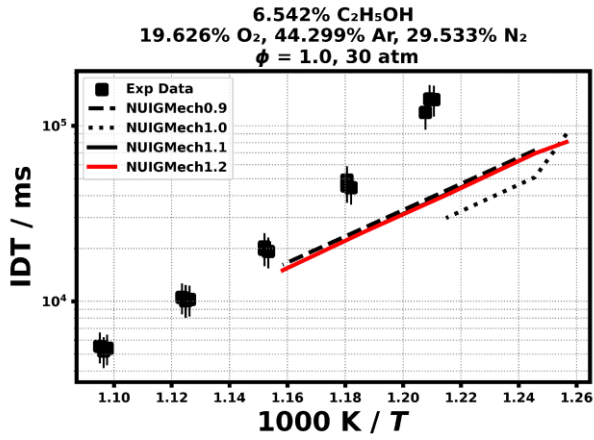


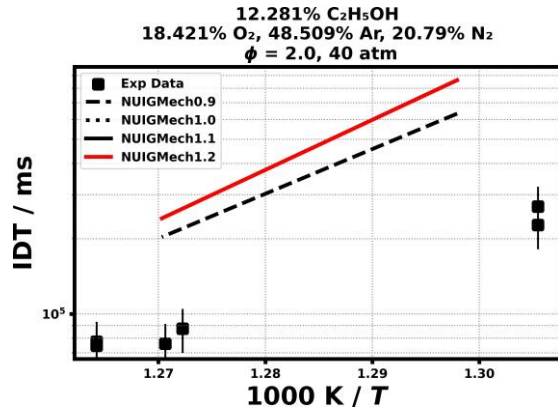
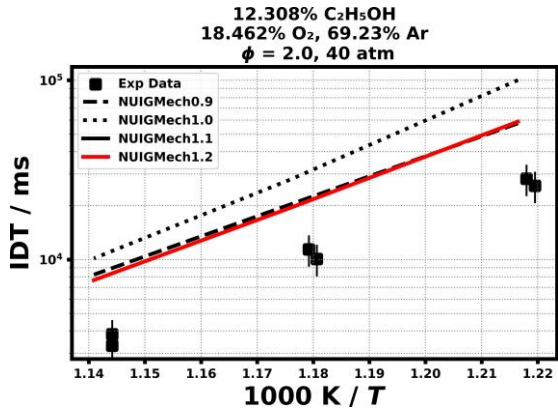
1.2.4 C₂H₄



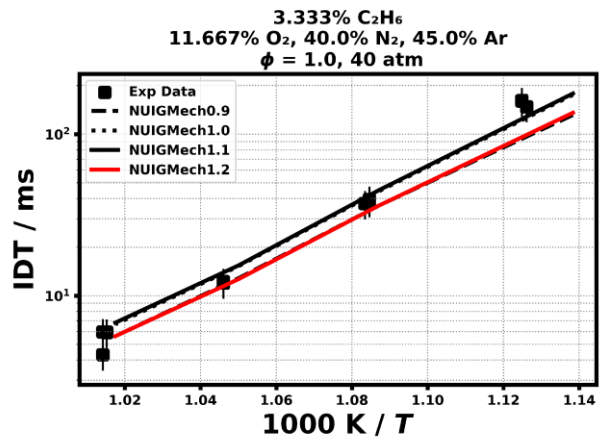
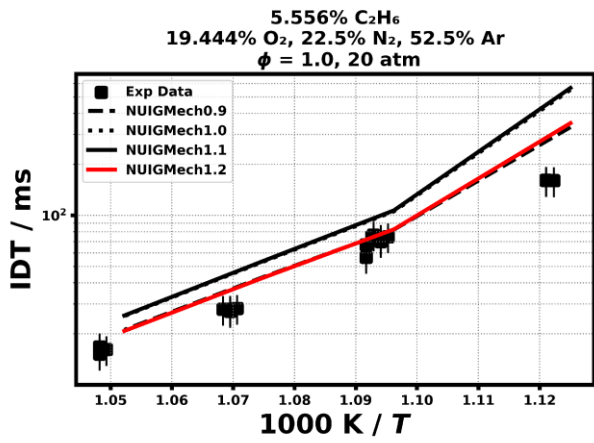
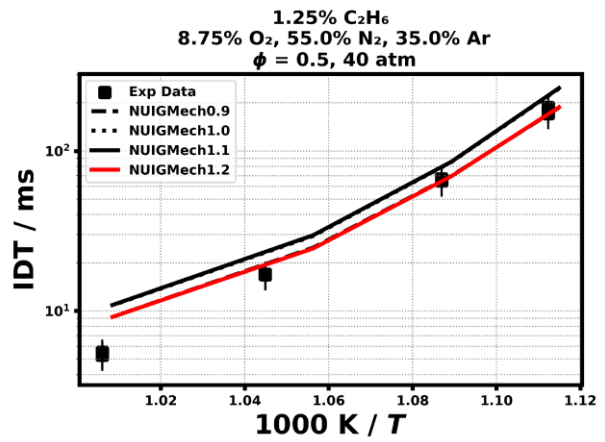
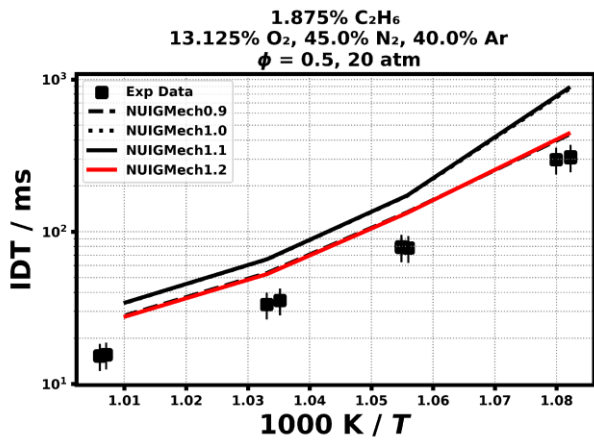
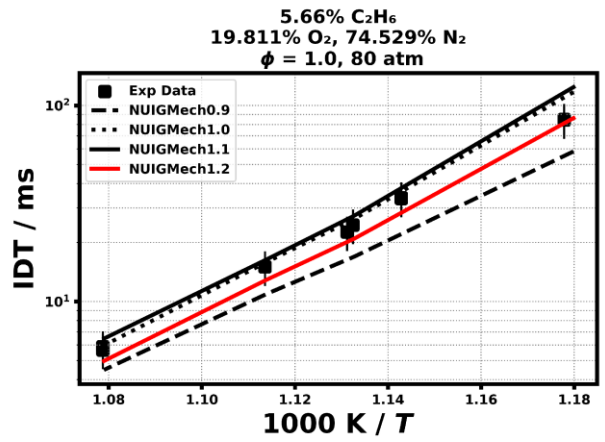
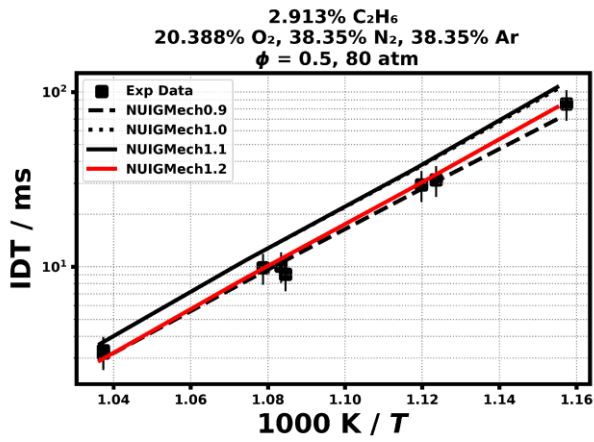
1.2.5 C₂H₅OH

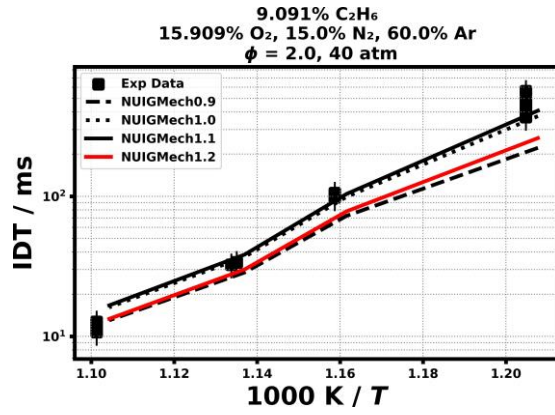
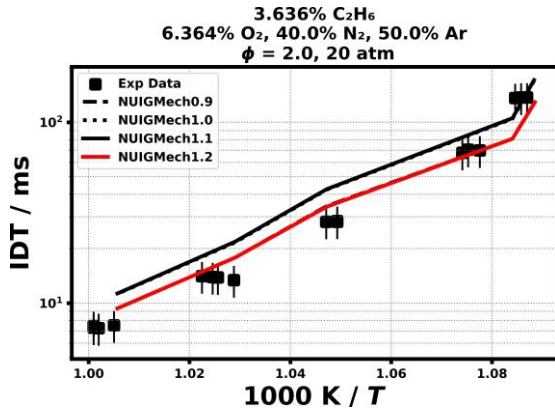




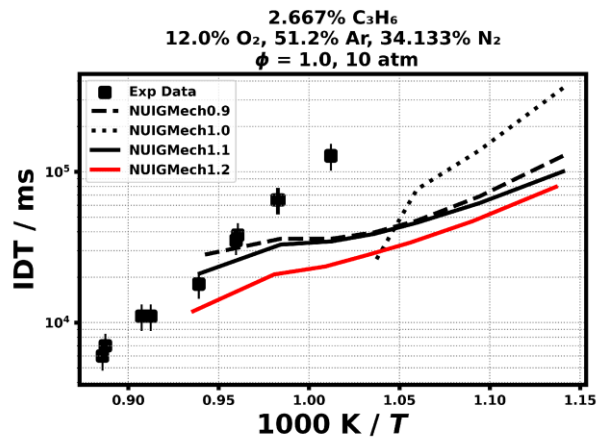
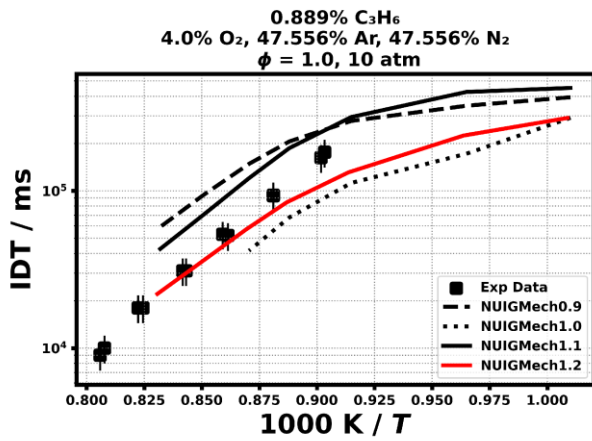
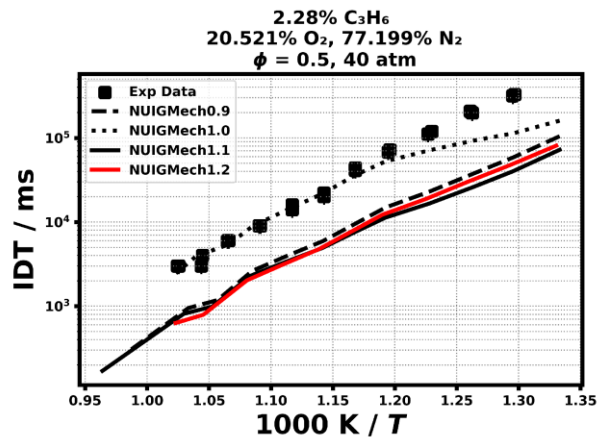
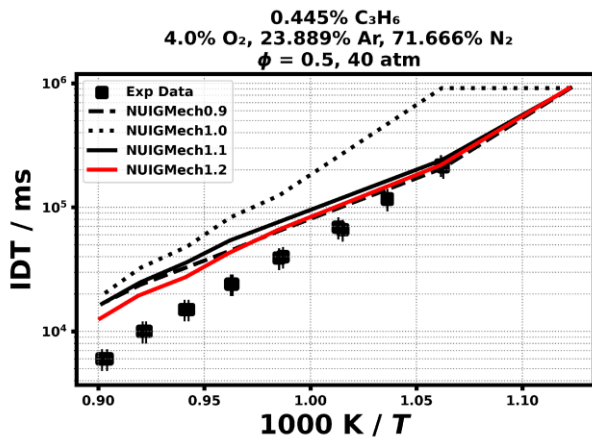
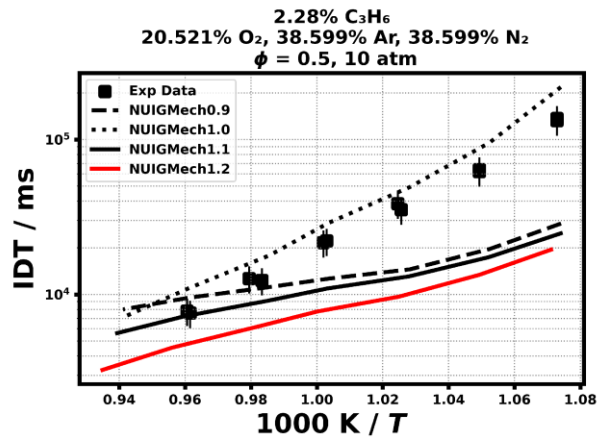
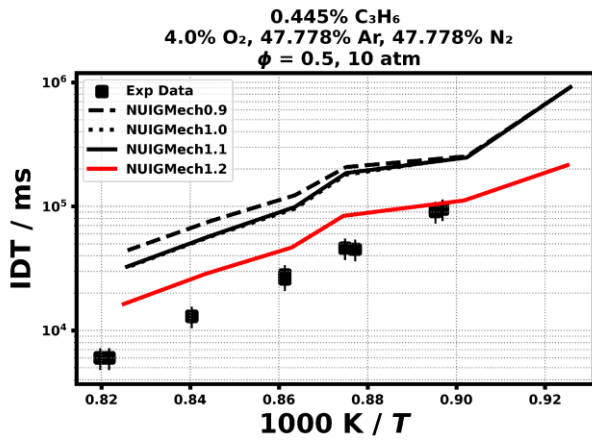


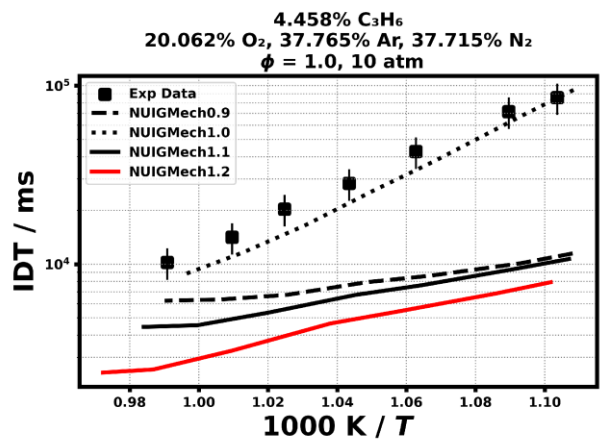
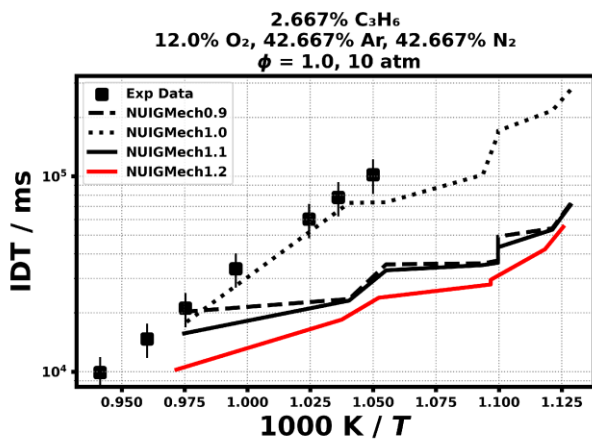
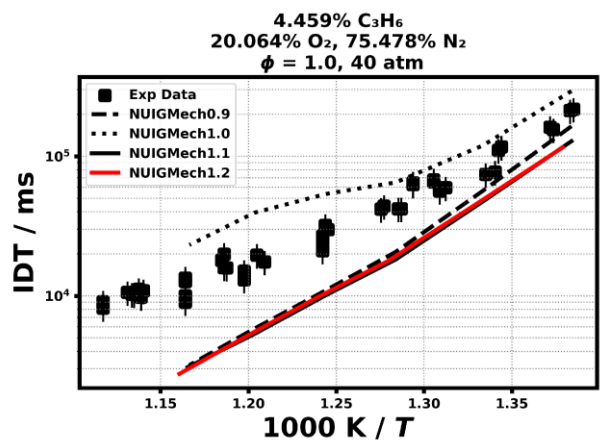
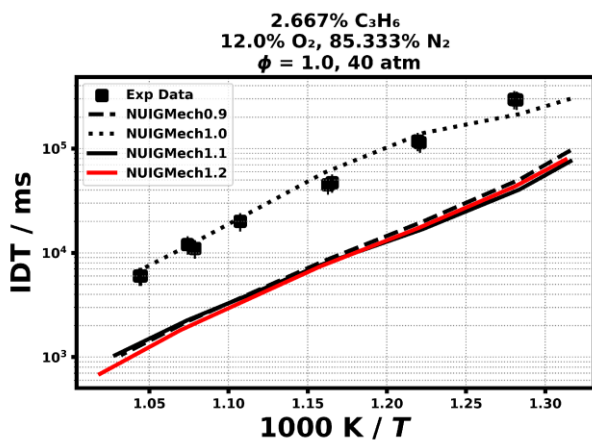
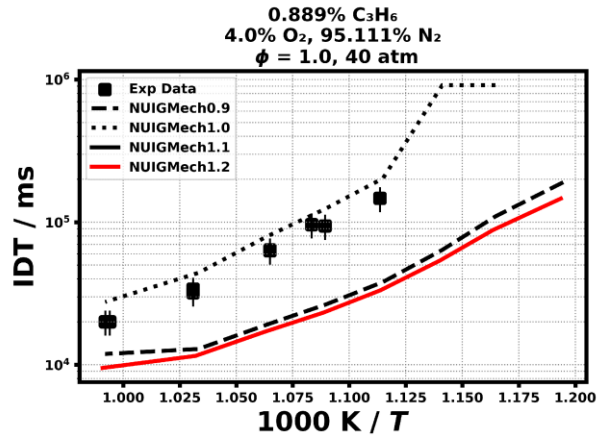
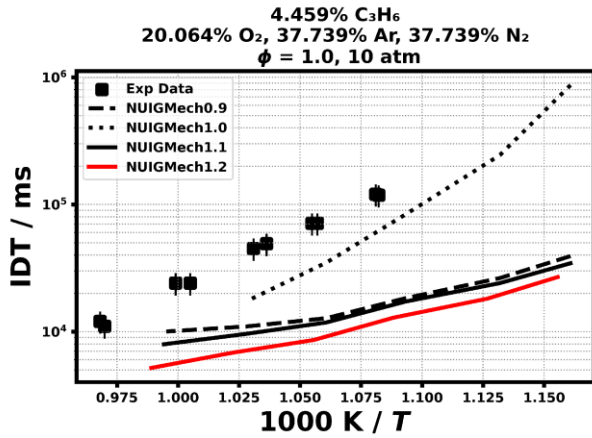
1.2.6 C₂H₆

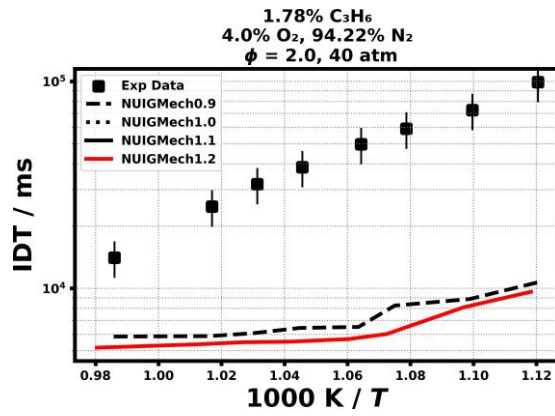
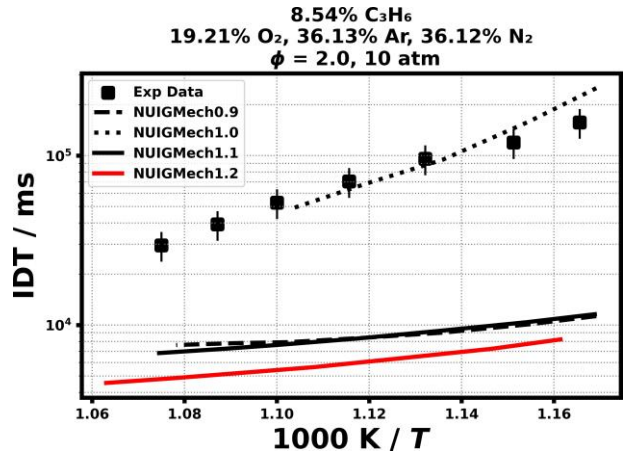
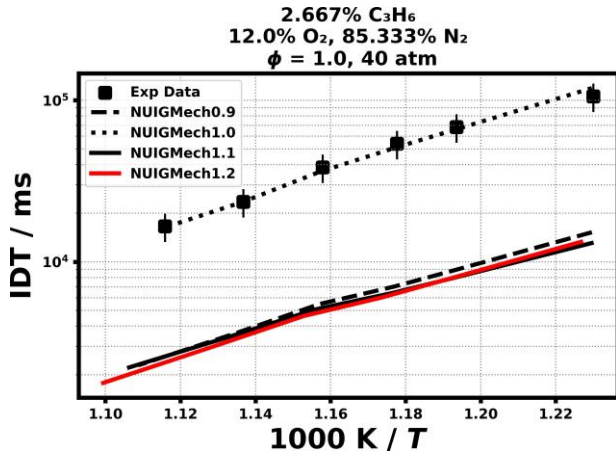




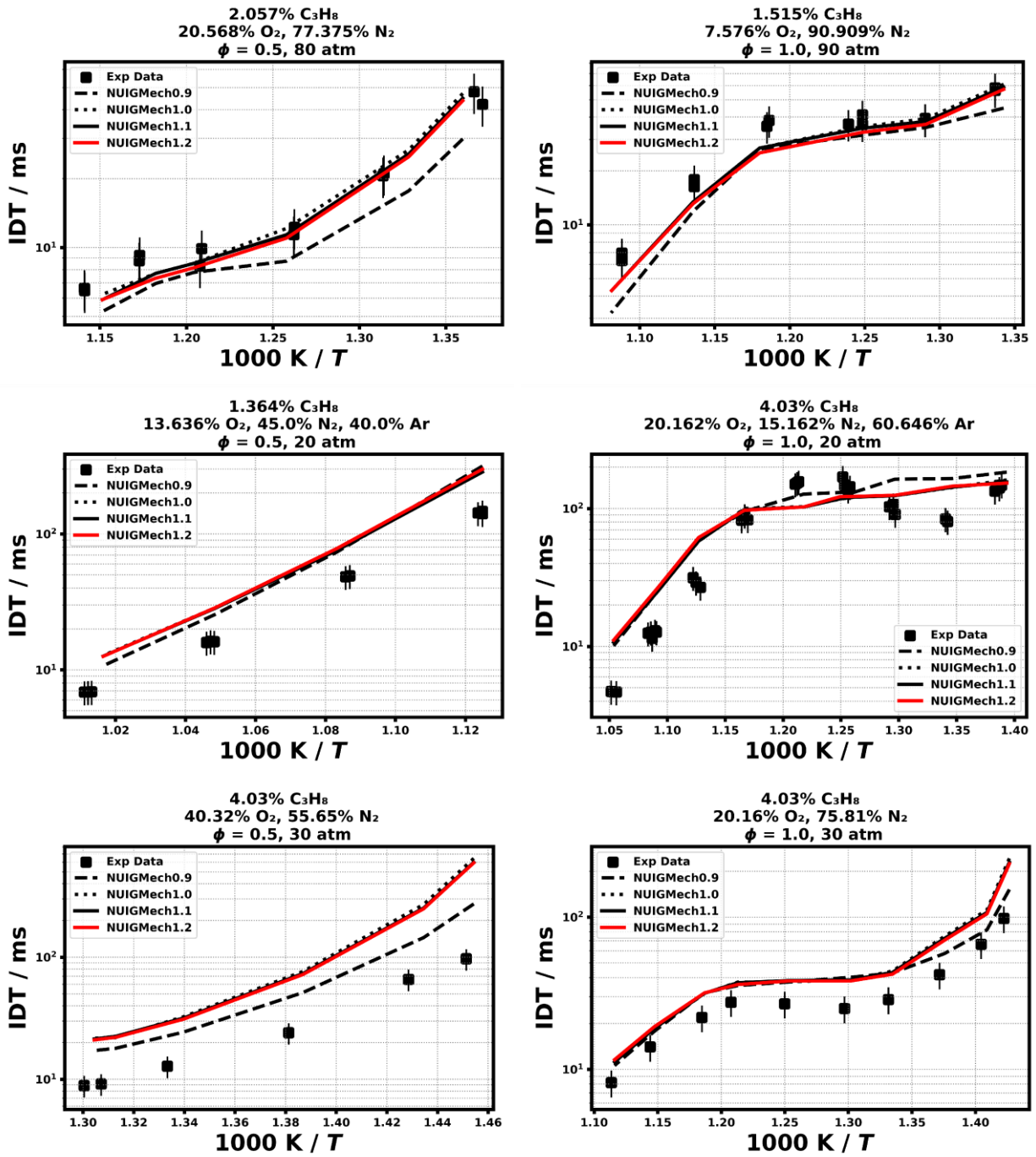
1.2.7 C₃H₆

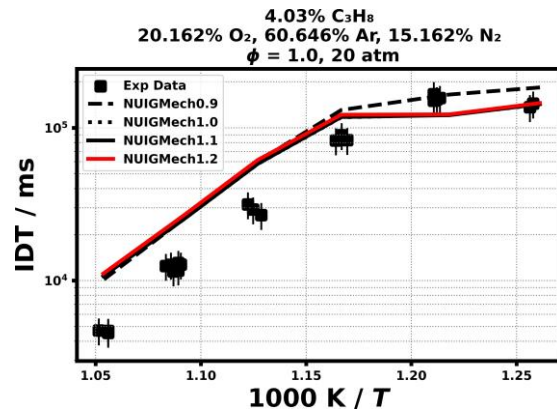




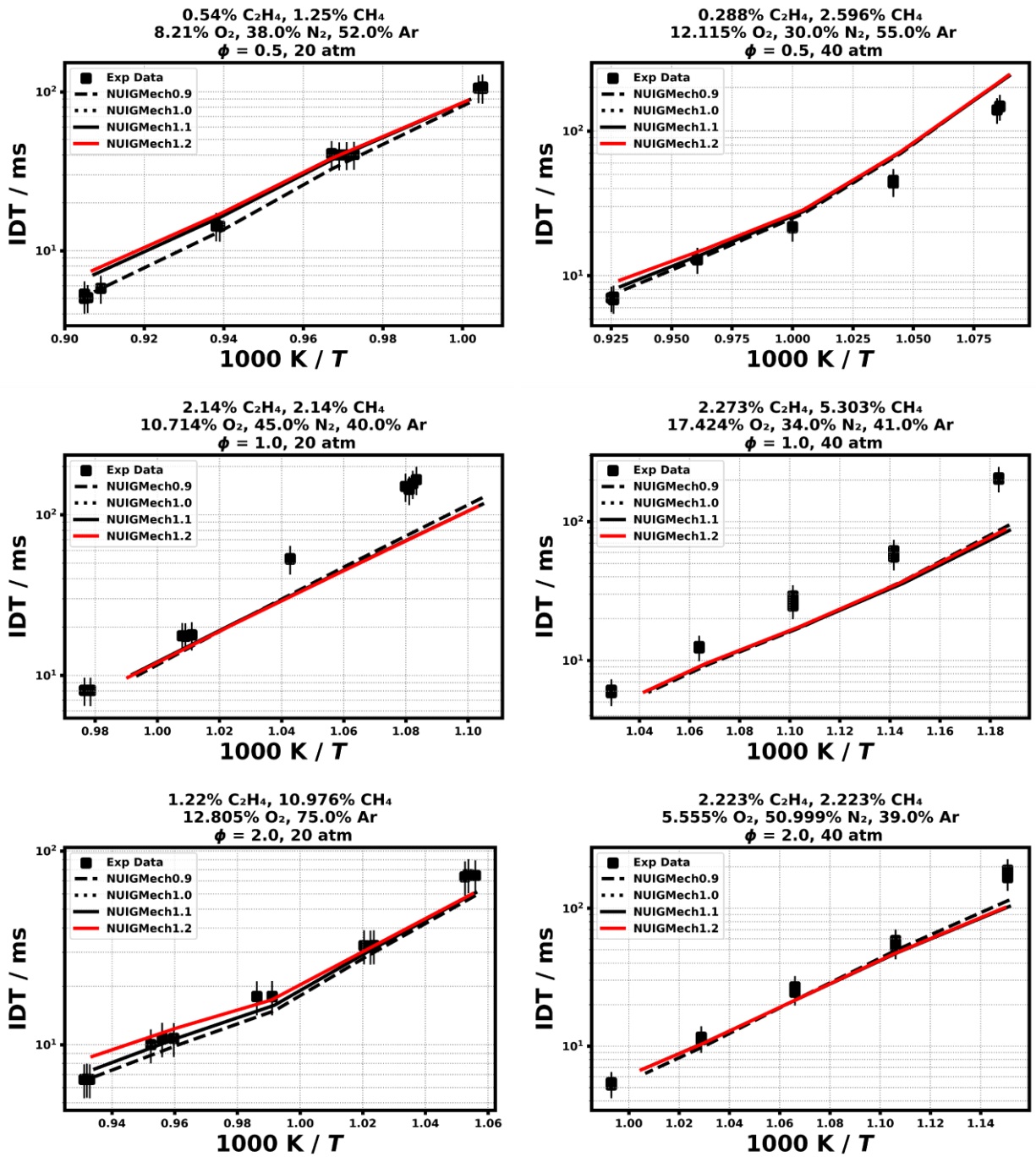


1.2.8 C₃H₈

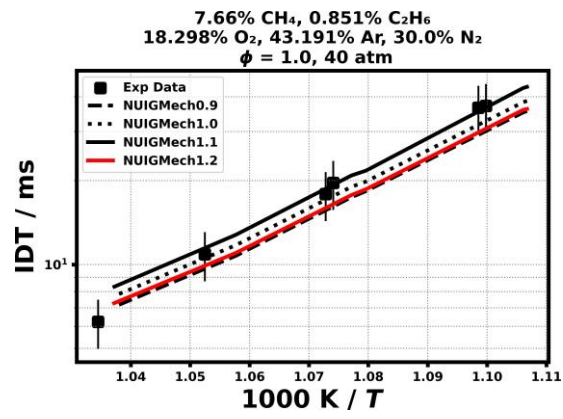




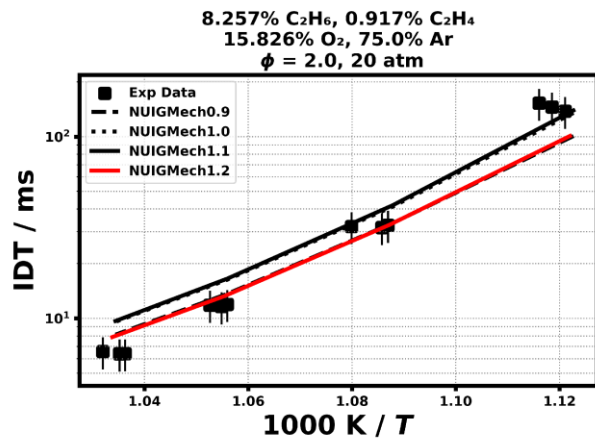
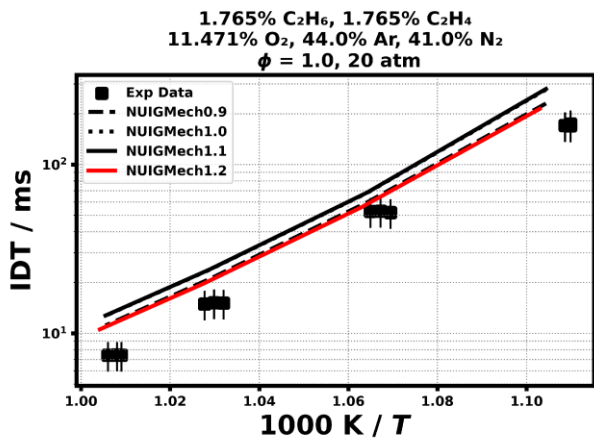
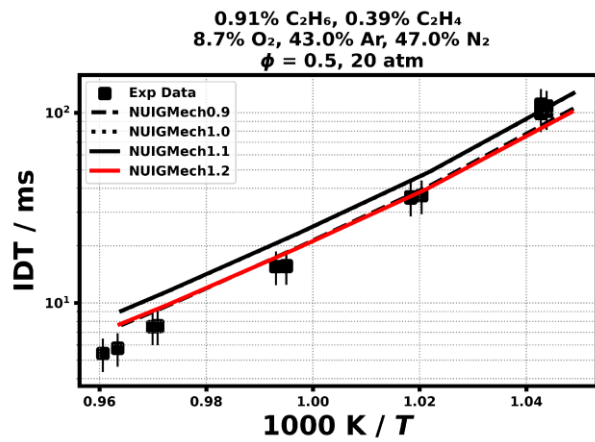
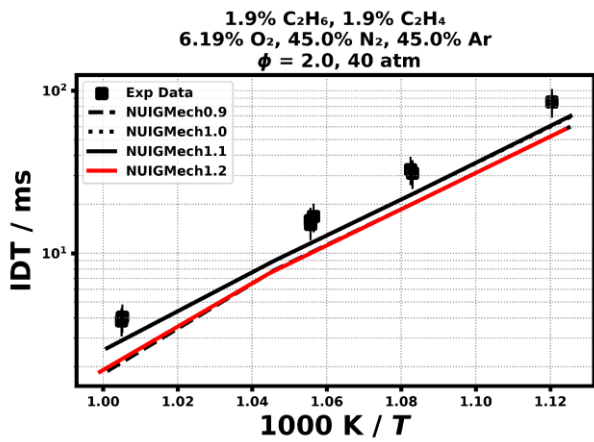
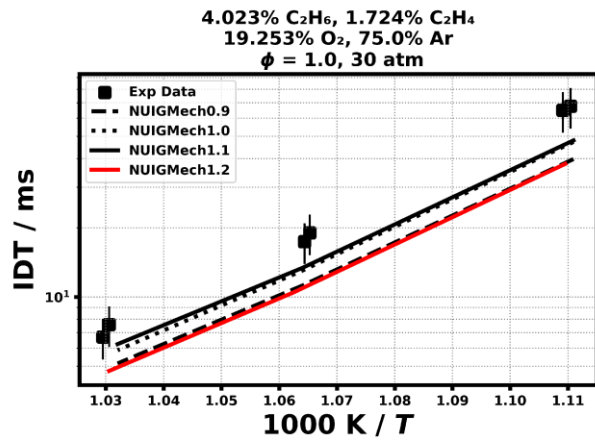
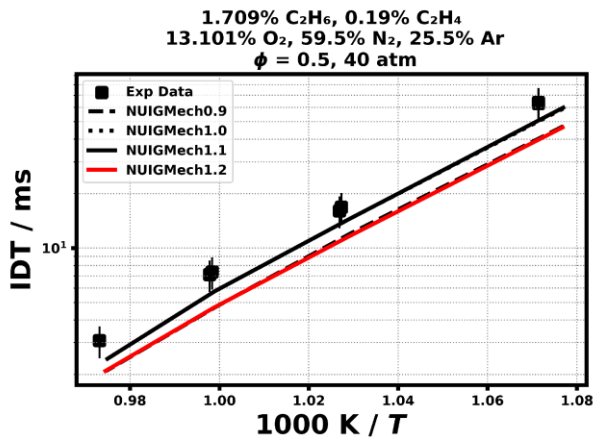
1.2.9 CH₄/C₂H₄



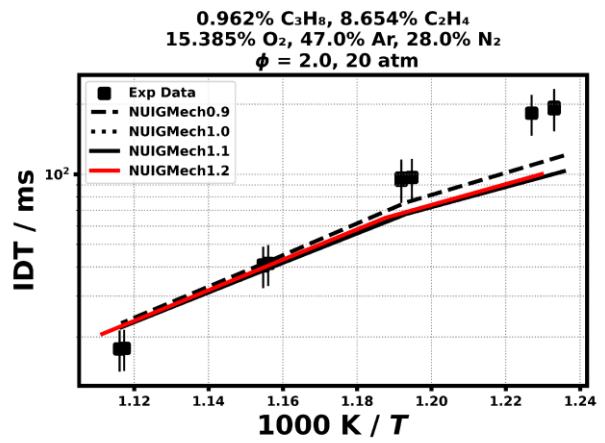
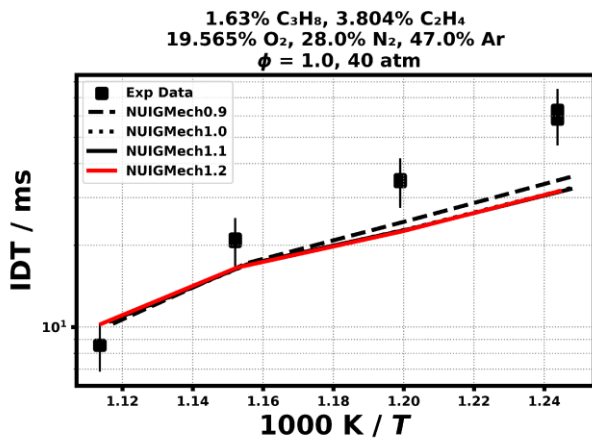
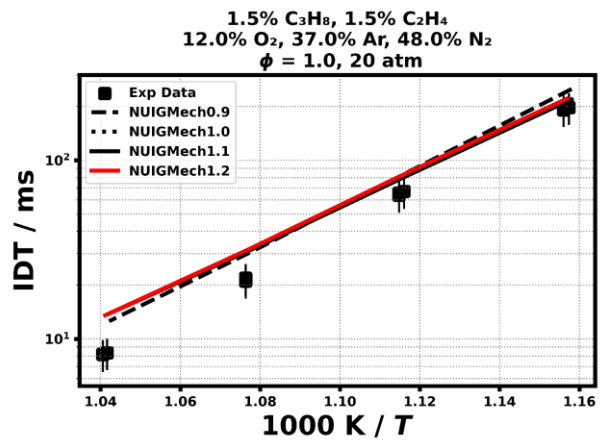
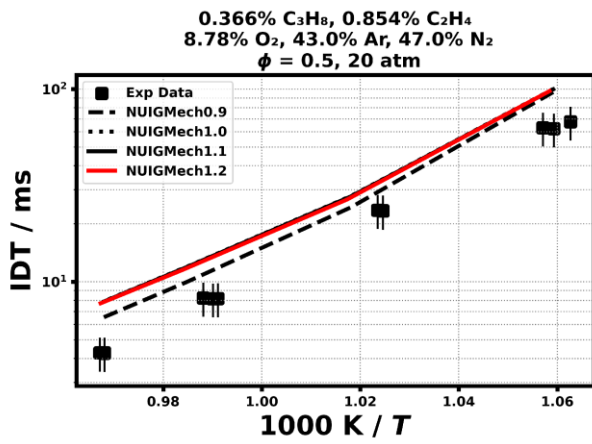
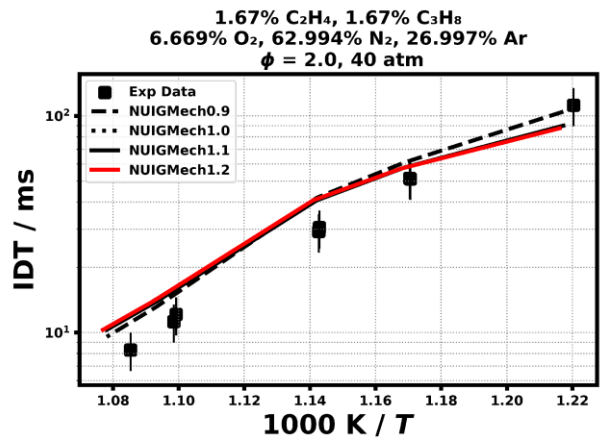
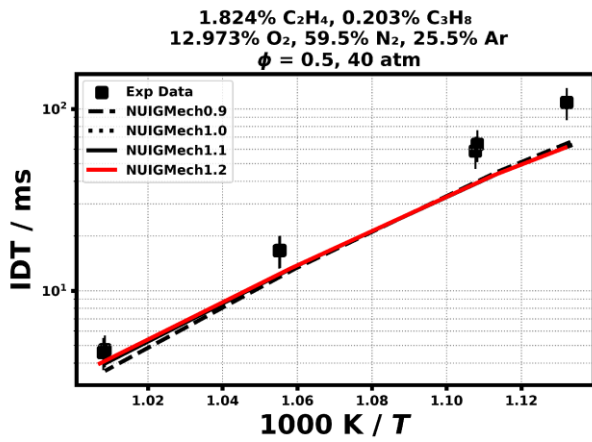
1.2.10 CH₄/C₂H₆



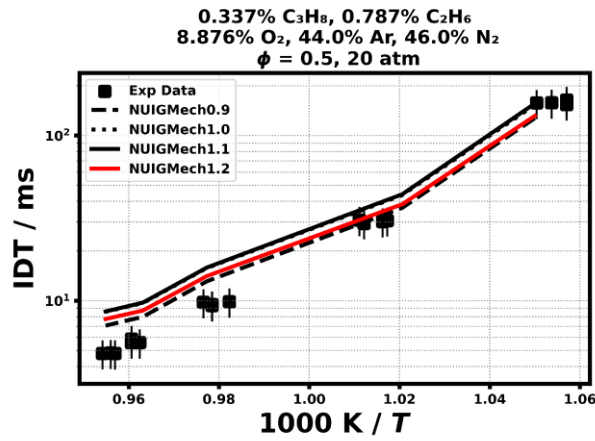
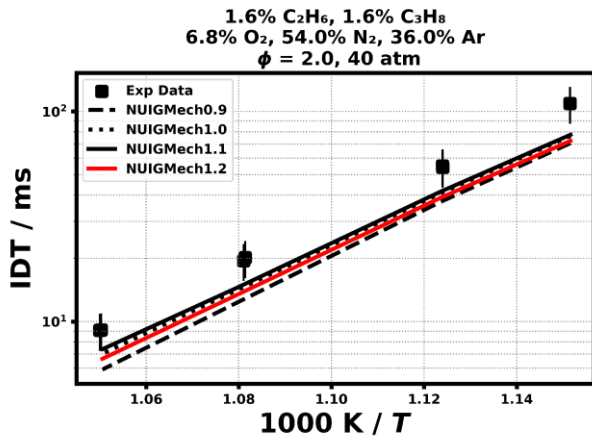
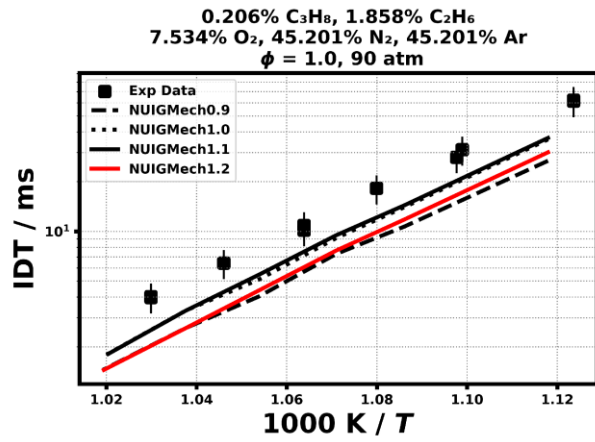
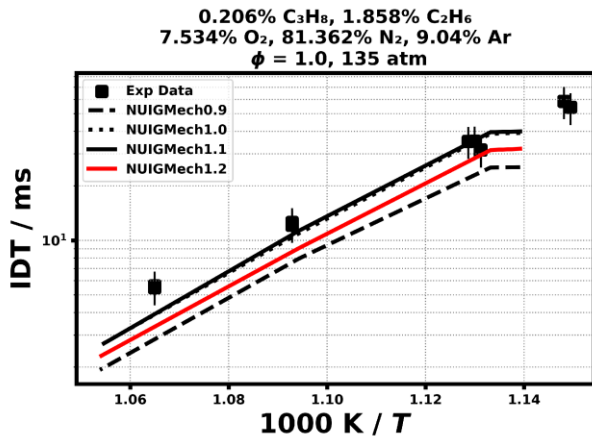
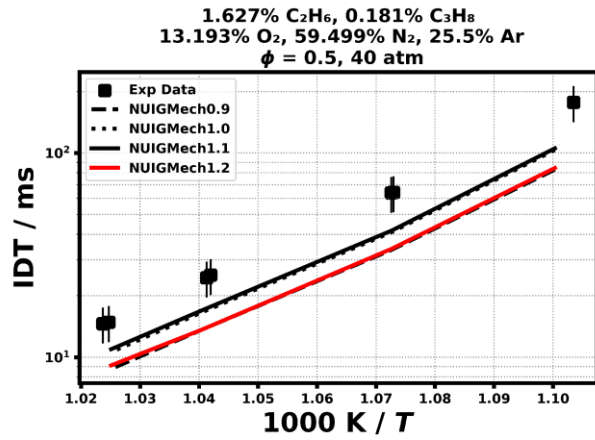
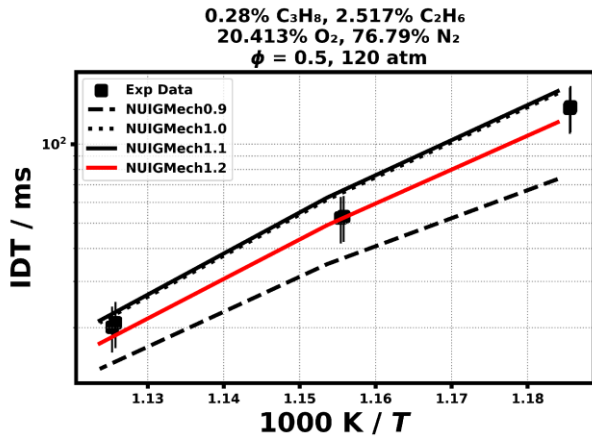
1.2.11 C₂H₄/C₂H₆

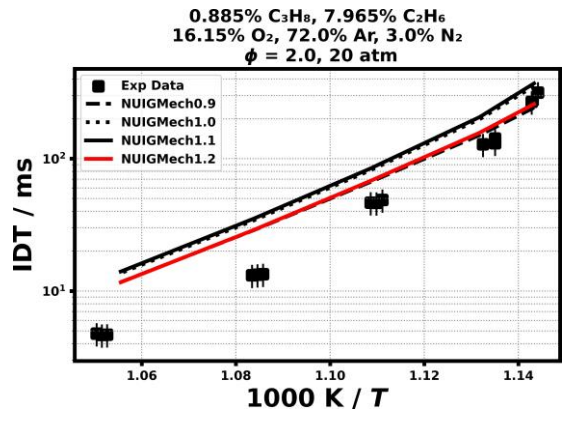
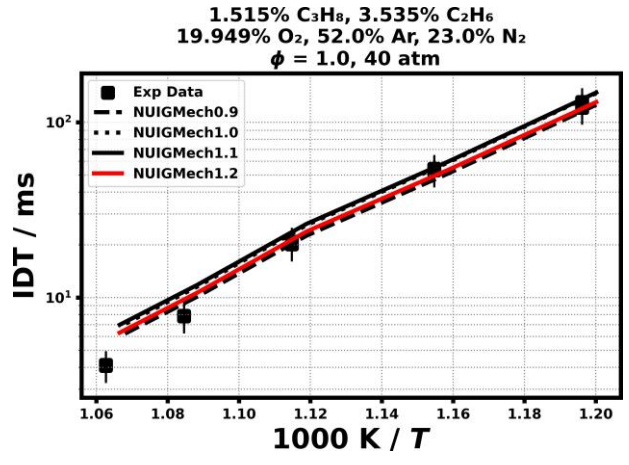
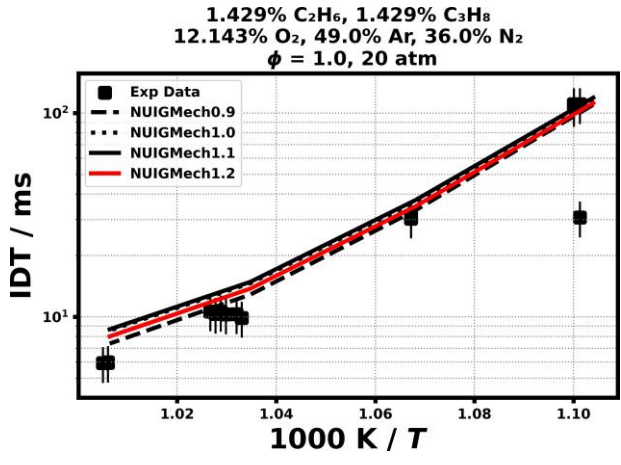


1.2.12 C₂H₄/C₃H₈

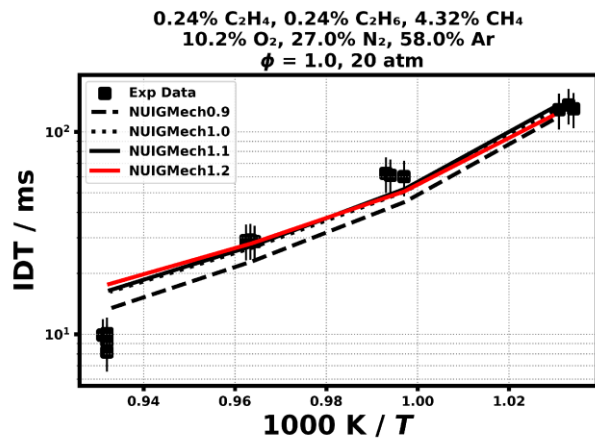
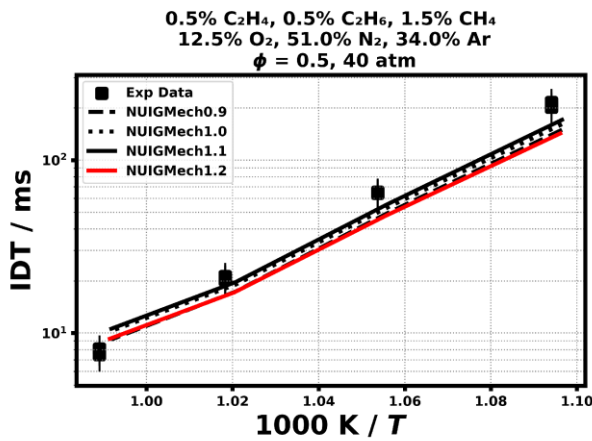
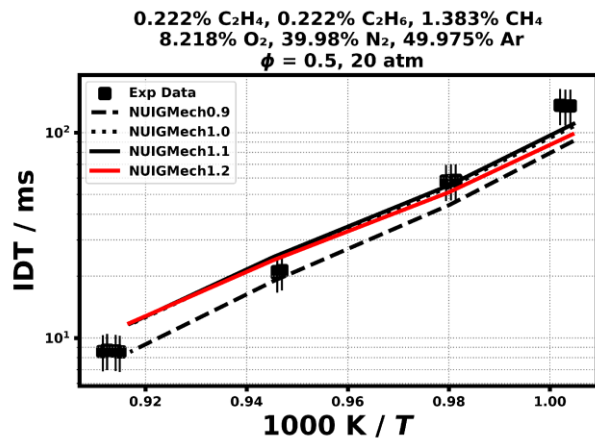
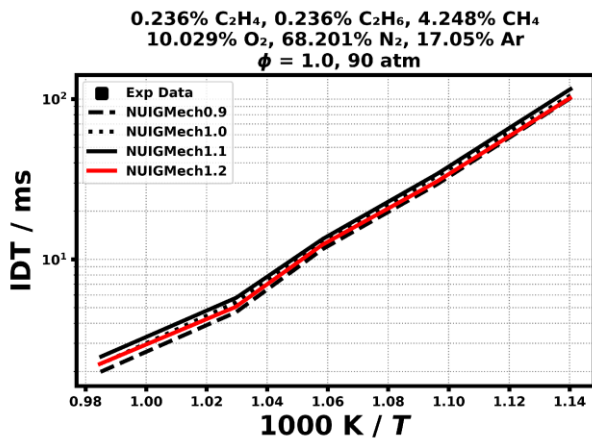
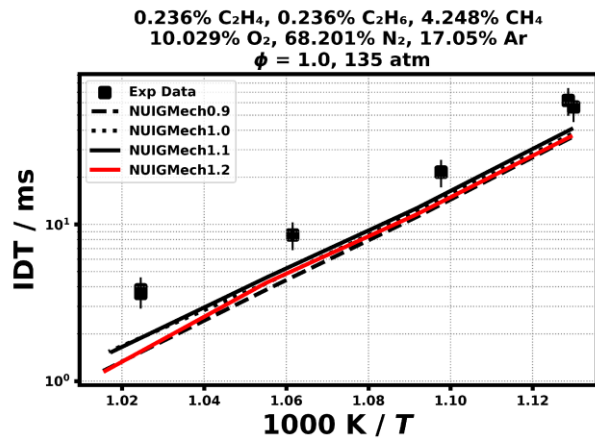
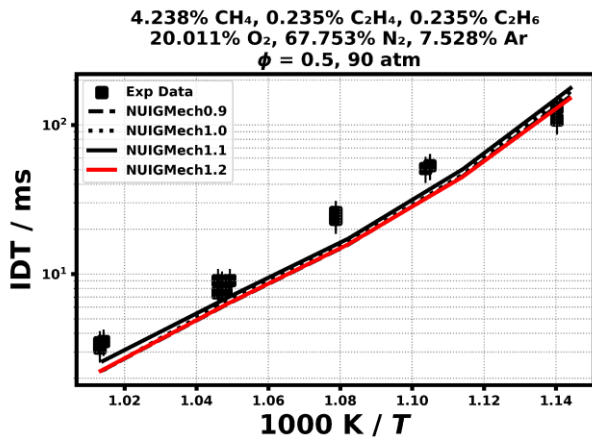


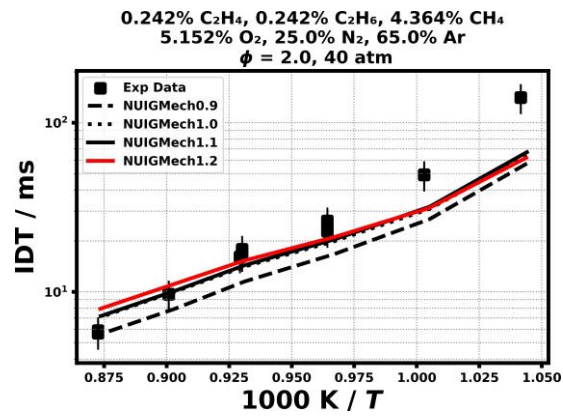
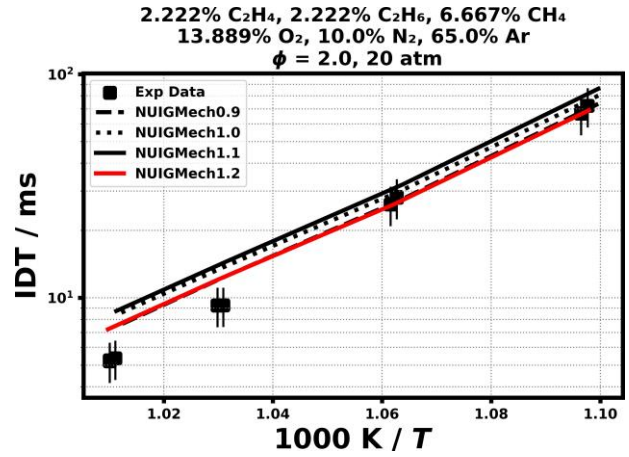
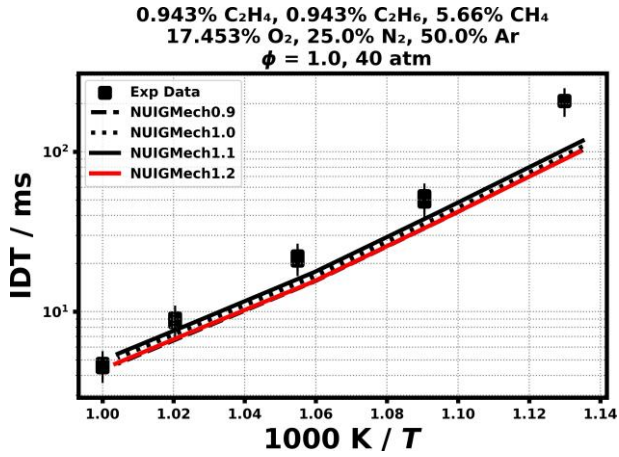
1.2.13 C₂H₆/C₃H₈





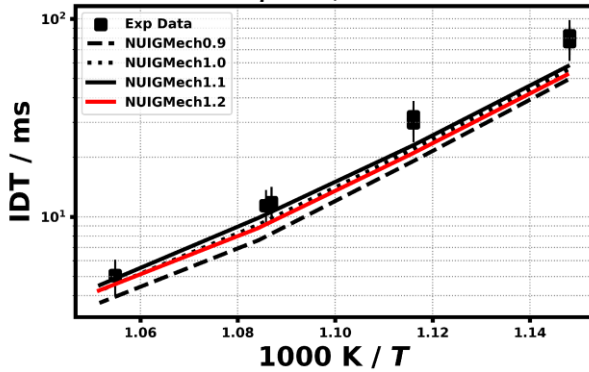
1.2.14 $\text{CH}_4/\text{C}_2\text{H}_4/\text{C}_2\text{H}_6$



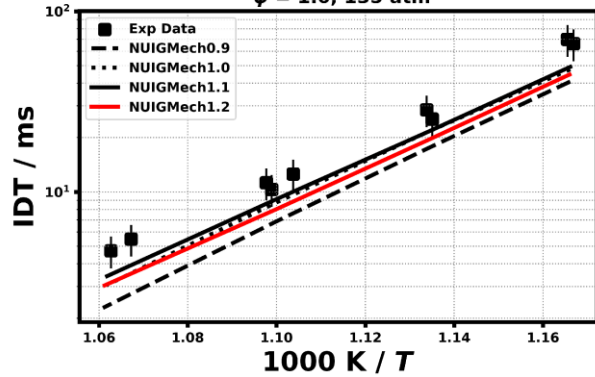


1.2.15 $\text{CH}_4/\text{C}_2\text{H}_4/\text{C}_2\text{H}_6/\text{C}_3\text{H}_8$

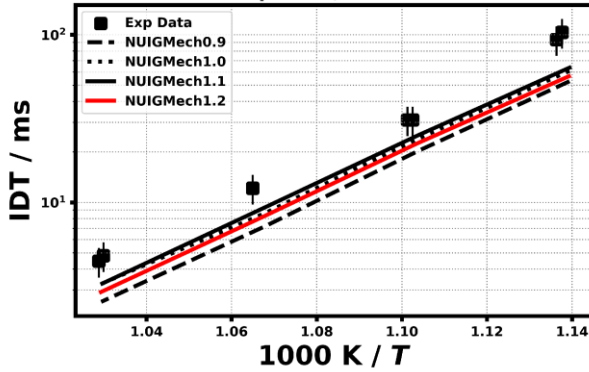
0.214% C_2H_4 , 0.214% C_3H_8 , 0.428% C_2H_6 , 3.422% CH_4 ,
20.102% O_2 , 68.058% N_2 , 7.562% Ar
 $\phi = 0.5$, 90 atm



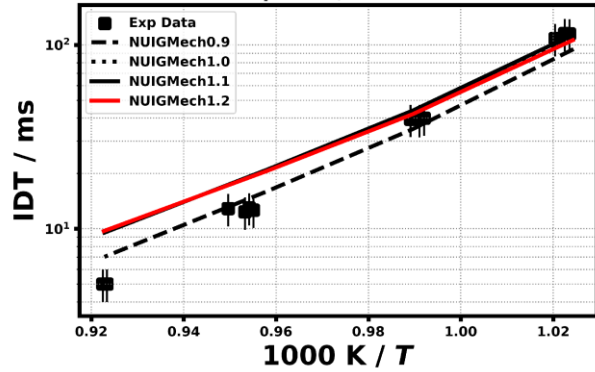
0.214% C_2H_4 , 0.214% C_3H_8 , 0.429% C_2H_6 , 3.43% CH_4 ,
10.075% O_2 , 68.51% N_2 , 17.128% Ar
 $\phi = 1.0$, 135 atm



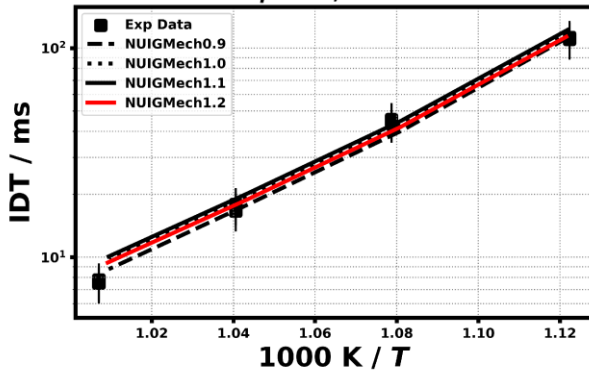
0.214% C_2H_4 , 0.214% C_3H_8 , 0.429% C_2H_6 , 3.43% CH_4 ,
10.075% O_2 , 68.51% N_2 , 17.128% Ar
 $\phi = 1.0$, 90 atm



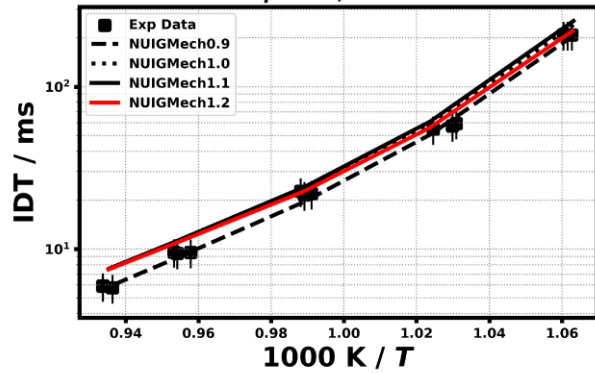
0.164% C_3H_8 , 0.164% C_2H_4 , 0.164% C_2H_6 , 1.148% CH_4 ,
8.361% O_2 , 39.0% N_2 , 51.0% Ar
 $\phi = 0.5$, 20 atm



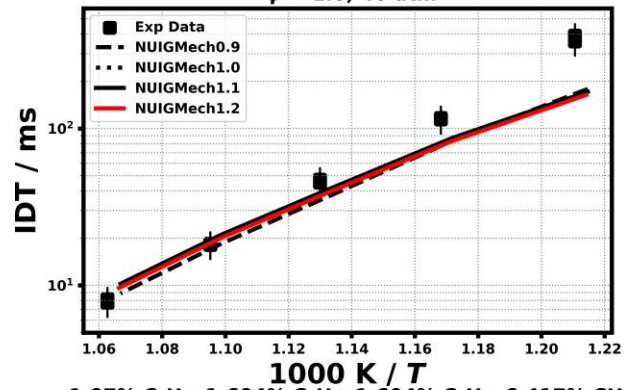
0.236% C_3H_8 , 0.354% C_2H_4 , 0.354% C_2H_6 , 1.417% CH_4 ,
12.638% O_2 , 52.0% N_2 , 33.0% Ar
 $\phi = 0.5$, 40 atm



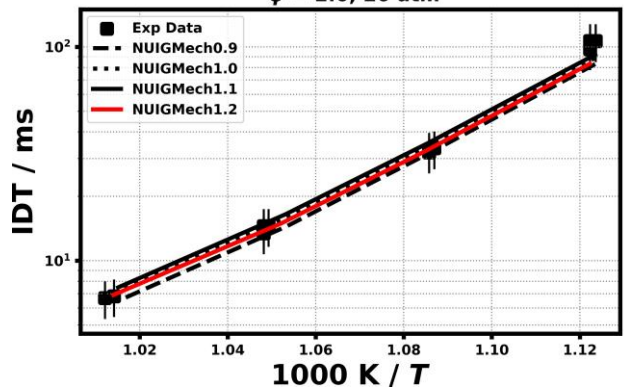
0.224% C_3H_8 , 0.224% C_2H_4 , 0.448% C_2H_6 , 3.582% CH_4 ,
10.522% O_2 , 25.0% N_2 , 60.0% Ar
 $\phi = 1.0$, 20 atm



0.704% C₃H₈, 0.704% C₂H₄, 0.704% C₂H₆, 4.93% CH₄
 17.958% O₂, 37.0% N₂, 38.0% Ar
 $\phi = 1.0$, 40 atm



1.07% C₃H₈, 1.604% C₂H₄, 1.604% C₂H₆, 6.417% CH₄
 14.305% O₂, 8.0% N₂, 67.0% Ar
 $\phi = 2.0$, 20 atm



0.23% C₃H₈, 0.23% C₂H₄, 0.46% C₂H₆, 3.678% CH₄
 5.402% O₂, 40.0% N₂, 50.0% Ar
 $\phi = 2.0$, 40 atm

